hydraulic modeling

SHORT COURSE: "ANALYSIS OF WATERSHEDS AND RIVER SYSTEMS"

SESSION I and II

MAY 28, 1979-JUNE 1, 1979 and JUNE 4, 1979-JUNE 8, 1979

ALL LECTURES will be held in Room A104, Andrew G. Clark Building

MAY 28 AND JUNE 4

8:30-10:00 a.m.	CHAPTER 2:	INTRODUCTION TO WATERSHED AND RIVER ANALYSIS Daryl B. Simons and Ruh-Ming Li
10:30-12:00 N	CHAPTER 3:	PHYSICAL PROCESSES GOVERNING RESPONSE OF WATERSHEDS AND RIVERS Daryl B. Simons, Timothy J. Ward and Ruh-Ming Li
12:00- 1:30 p.m.	LUNCHEON, STUDENT CENTER MAY 28: JUNE 4:	Speaker: Dr. E. V. Richardson, Professor Civil Engineering, CSU, North Ballroom Speaker: Dr. E. V. Richardson, East Ballroom
1:30- 3:00 p.m.	CHAPTER 4:	SEDIMENT TRANSPORT H. W. Shen
3:30- 5:00 p.m.	CHAPTER 5:	ALLUVIAL BED ROUGHNESS H. W. Shen

MAY 29 AND JUNE 5

8:30-10:00 a.m.	CHAPTER 6:	OVERVIEW OF FLOOD ROUTING METHODS Ruh-Ming Li(May 29) and V. Miguel Ponce(June 5)
10:30-12:00 N	CHAPTER 7:	WATER ROUTING AND YIELD FROM WATERSHEDS, PART I Ruh-Ming Li, Daryl B. Simons, and Kenneth G. Eggert
12:00- 1:30 p.m.	BREAK FOR LUNCH	
1:30- 3:00 p.m.	CHAPTER 7:	WATER ROUTING AND YIELD FROM WATERSHEDS, PART II Ruh-Ming Li, Daryl B. Simons, and Kenneth G. Eggert
3:30- 5:00 p.m.	CHAPTER 8:	WATER ROUTING IN RIVERS Yung-Hai Chen
6:00 p.m.	DINNER, STUDENT CENTER MAY 29: JUNE 5:	Speaker: Dr. David Duttweiller, EPA, Athens, Georgia, North Ballroom Speaker: Mr. Lee Mulkey, EPA, Athens, Georgia, East Ballroom

MAY 30 AND JUNE 6

8:30-10:00 a.m.	CHAPTER 9:	STAGE DISCHARGE RELATIONS Robert K. Simons, Ruh-Ming Li, and Daryl B. Simons

10:30-12:00 N	CHAPTER 10:	WATERSHED SEDIMENT YIELD Ruh-Ming Li, Daryl B. Simons, and Timothy J. Ward
12:00- 1:30 p.m.	LUNCHEON, STUDENT CENTER	
	MAY 30:	Speaker: Dr. Stanley A. Schumm, Professor Earth Resources, CSU, North Ballroom
	JUNE 6:	Speaker: Dr. Stanley A. Schumm, North Ballroom
1:30- 3:00 p.m.	CHAPTER 11:	UNSTEADY SEDIMENT ROUTING MODELS IN RIVERS Yung-Hai Chen and Daryl B. Simons
3:30- 5:00 p.m.	CHAPTER 12:	KNOWN DISCHARGE SEDIMENT ROUTING Glenn O. Brown and Ruh-Ming Li

MAY 31 AND JUNE 7

8:30-10:00 a.m.	CHAPTER 13:	LANDSLIDE POTENTIAL DELINEATION Timothy J. Ward, Ruh-Ming Li, and Daryl B. Simons
10:30-12:00 N	CHAPTER 14:	APPLICATION OF KALMAN FILTERING IN WATERSHED AND RIVER ANALYSIS Nguyen Duong
12:00 N	BREAK FOR LUNCH	
1:30- 3:00 p.m.	CHAPTER 15:	HANDHELD CALCULATOR PROGRAMS FOR ANALYSIS Kenneth G. Eggert, Ruh-Ming Li, and Daryl B. Simons
3:30- 5:00 p.m.	CHAPTER 16:	OVERVIEW OF CASE STUDIES AND DATA MANAGEMENT Daryl B. Simons, Ruh-Ming Li, and Nguyen Duong
6:00 p.m.	BANQUET, STUDENT CENTER	
	MAY 31:	Speaker: Dr. Daryl B. Simons, Associate Dean College of Engineering and Professor, Department of Civil Engineering, CSU, North Ballroom
	JUNE 7:	Speaker: Dr. Ross Carder, USDA Forest Service Flagstaff, Arizona, North Ballroom

JUNE 1 AND JUNE 8

8:30-10:00 a.m.	CHAPTER 17:	CANAL AND CHANNEL DESIGN AND RIVER RESPONSE ANALYSIS Daryl B. Simons, Ruh-Ming Li, and Yung-Hai Chen
10:30-12:00 N	CHAPTER 18:	DEGRADATION AND AGGRADATION ANALYSIS Ruh-Ming Li and Daryl B. Simons
12:00- 1:30 p.m.	BREAK FOR LUNCH	
1:30- 3:00 p.m.	CHAPTER 19:	WATERSHED BEST MANAGEMENT ANALYSIS Ruh-Ming Li, Timothy J. Ward, and Daryl B. Simons
3:30- 5:00 p.m.	CHAPTER 20:	LARGE RIVER BASIN ANALYSIS--YAZOO RIVER SEDIMENTATION STUDY Daryl B. Simons and Ruh-Ming Li

NOTE: Underscoring indicates speaker.

CHAPTER 1

GENERAL INTRODUCTION

by

Daryl B. Simons, Associate Dean for Engineering Research and Professor of Civil Engineering, Colorado State University, Fort Collins, Colorado

Ruh-Ming Li, Associate Professor, Department of Civil Engineering, Colorado State University, Fort Collins, Colorado

1.1 OBJECTIVES OF THE SHORT COURSE

The increasing interest in water resource and land-use planning has stimulated the development of particular and general watershed and river system models for predicting response from ecological systems. The models, whether physical process-oriented or conceptual, are intended to be used to estimate physical quantities that describe the major ecosystem responses to precipitation such as water yield, sediment yield, changes of land and river morphology, and transport of pollutants. Methods of estimating water, sediment, and other pollutant transport yields are needed for analyzing the economic feasibility and trade-offs of any proposed water resources or land-use development in watershed and river systems and for predicting possible adverse environmental impacts associated with the proposed development. Colorado State University has been and continues to be actively involved in the development and application of watershed and river mathematical models to solve various real-world problems. The experience and products obtained from efforts over the last ten years by the faculty and staff associated with the Hydraulics Program of the Civil Engineering Department have provided the opportunity to offer a short course with an integrated approach to watershed and river analysis. This short course is designed for individuals dealing with the analysis of watersheds and rivers. Practical applications concerning physical processes will be emphasized.

Specific objectives of the course follow.

1. To provide the opportunity to learn techniques oriented to solving practical problems associated with the analysis of watersheds and rivers.
2. To become acquainted with the physical processes governing the response of watersheds and rivers.
3. To enhance the participant's insight into mathematical modeling techniques related to watershed and river analysis.
4. To demonstrate several levels of integrated methodologies for the analysis of watersheds and rivers, and
5. To provide and utilize documented copies of programmable calculator programs.

1.2 ORGANIZATION

This short course was organized by Drs. Daryl B. Simons and Ruh-Ming Li, Program Directors. Simons and Li were assisted by Ms. Kris Schneider. Faculty and staff of the short course follow:

Dr. Daryl B. Simons, Program Director, Associate Dean of Engineering Research and Director, Engineering Research Center.

Dr. Ruh-Ming Li, Co-Program Director, Associate Professor of Civil Engineering.

Mr. Glenn O. Brown, Research Associate, Department of Civil Engineering.

Dr. Yung-Hai Chen, Assistant Professor of Civil Engineering.

Dr. Nguyen Duong, Research Associate, Department of Civil Engineering.

Mr. Kenneth G. Eggert, Research Associate, Department of Civil Engineering.

Dr. V. Miguel Ponce, Assistant Professor of Civil Engineering.

Dr. Hsieh-Wen Shen, Professor of Civil Engineering.

Mr. Robert K. Simons, Research Associate, Department of Civil Engineering.

Dr. Timothy J. Ward, Assistant Professor of Civil Engineering.

All of the faculty and staff are associated with the Civil Engineering Department of Colorado State University. The group has worked closely together in integrating the various aspects in the analysis and modeling of watersheds and river systems.

Invited luncheon and dinner speakers at the short course include leading experts and administrators from government and university. Invited speakers are:

Dr. D. Ross Carder, Project Leader, USDA Forest Service, Rocky Mountain Forest and Range Experiment Station, Flagstaff, Arizona.

Dr. David Dutweiller, Director, Environmental Research Laboratory, Environmental Protection Agency, Athens, Georgia.

Mr. Lee A. Mulkey, Agricultural Engineer, Environmental Research Laboratory, Environmental Protection Agency, Athens, Georgia.

Dr. Everett V. Richardson, Professor of Civil Engineering, Colorado State University, Fort Collins, Colorado.

Dr. Stanley A. Schumm, Professor of Earth Resources, Colorado State University, Fort Collins, Colorado.

Dr. Daryl B. Simons, Associate Dean, College of Engineering, and Professor of Civil Engineering, Colorado State University, Fort Collins, Colorado.

1.3 CONTENTS OF LECTURES

Since the lectures are oriented to an integrated approach to the analysis of watershed and river systems, the relationship between lectures is emphasized. Some theories and examples will be presented repeatedly from time to time to illustrate the linkage. Outlines of each chapter follow.

Chapter 2 introduces the concept of mathematical modeling and presents a brief assessment of the current state of the art utilized to analyze watershed and river systems, physical processes important to analysis, criteria related to the development of mathematical models for various applications, procedural steps involved in model development, and examples of applications of models to watershed and river systems.

Chapter 3 describes the physical processes governing response from watershed and river systems. Several approaches can be taken in delineating and analyzing physical processes that govern the fluvial system. As a first step, watersheds and rivers can be classified into different groups based on certain physical characteristics. These characteristics are usually a direct result of the physical processes that govern the system and therefore provide an initial view of the controlling phenomena. Once subdivided, watersheds and rivers can be described in terms of the processes that control their responses. After these processes are understood as well as possible, their relative importance can be evaluated. For example, raindrop splash is often an important process in upland watershed erosion, but it has little if any effect on a large river such as the Mississippi. These important physical processes should be considered to determine the qualitative and quantitative response of the system.

Chapter 4 deals with the sediment transport in further detail. This chapter provides the classification of sediment transport, introduces a very important concept for dividing wash load and bed material load. The remainder of this chapter is devoted to a discussion of wash load, bed load and bed material load.

Chapter 5 discusses the resistance to flow for the following four conditions: 1) rigid boundary without rainfall, 2) rigid boundary with rainfall, 3) channel river boundary, and 4) boundary with vegetation. Knowledge of the resistance to flow is the key to successful evaluation of watershed and river response.

Chapter 6 reviews available methods for flood water and sediment routing. Flood routing is defined as the process of tracing by calculation the movement of a flood wave. In general, the problem consists of applying the principles of gradually varied unsteady open channel flow. Two physical characteristics that are useful in describing flood waves are: 2) the rate of travel (flood wave celerity), and 2) the rate of subsidence (flood wave attenuation). The movement of a flood wave is governed by the conservation principles of fluid mechanics. The conservation of mass is expressed by the equation of continuity and the conservation of momentum by the equation of motion.

Several methods of flood routing are described in the remainder of Chapter 6. Owing to the large number of methods available, no attempt is made here to provide a comprehensive treatment. Rather, emphasis is placed on the methods that have a sound theoretical basis. Criteria for the selection of a method to solve a particular type of problem are also given in this chapter.

Chapter 7 discusses water routing and yield simulations. The chapter starts with a description of the spatial representations required by the individual models with different levels of resolution. This section is followed by a description of the physical process components and general layout of the simulators. An important feature of both the high resolution and simplified models is the method used for estimating excess rainfall. This method involves both interception and infiltration processes. The greatest differences between the high resolution and simplified models occur in the water routing methods. Both kinds of models use kinematic wave routing for overland and channel flow. However, the simplified models use the method of characteristics solution to the kinematic wave problem for some or all of the water routing. This analytical solution is presented. The high resolution model uses a numerical solution to the kinematic wave problem for all water routing.

This solution technique is discussed and a discussion of data requirements and parameter estimation techniques is presented.

Chapter 8 describes the one-dimensional water routing models applied to study unsteady flow problems in a simple river system and in a complex river network system. Also, a two-dimensional water routing model is presented. The one-dimensional flow equations assume that the transverse and vertical velocities are low compared to the longitudinal one. In rivers or estuaries where the sections are wide, the one-dimensional assumption is usually invalid. In this case two-dimensional models are used to simulate velocities in the transverse and longitudinal directions. A three-dimensional model can be used when vertical stratification is also important. However, because of its extreme complicity, the practical application of a three-dimensional model is very limited. There are some rivers and estuaries with a complex system of branches, loops and confluences. The flow division among the confluences and the tide effect from downstream complicates the problem. A broad river network system is not only expensive to simulate using two- or three-dimensional models, but the data required are difficult and expensive to obtain. The one-dimensional assumption is the best choice if it does not create serious errors in the solution.

Chapter 9 first presents a dynamic simulation of stage-discharge relationship in rivers utilizing a full-dynamic momentum equation to yield a looped relation and its application to extend the applicability of the kinematic wave flood routing procedure discussed in Chapter 7. Then a comparison of frequency and magnitude of error associated with three models; statistical model, steady flow rigid boundary backwater model, and known discharge sediment routing model, is made.

Chapter 10 discusses types of models for estimating sediment yield from watersheds. One type, physical process simulation models, is discussed in detail, and example applications are presented. The models are used to estimate or predict sediment yields resulting from natural or disturbed watershed lands. They do account for important physical processes such as raindrop splash, overland flow erosion, channel erosion, and movement of the different sediment size fractions. The models presented in this chapter do not account for gully or landslide generated sediment yields. One all-important aspect of model development

and operation is data. Without adequate data, testing and verification of models before application to real situations may produce erroneous results that do not truly represent actual conditions. Understanding model operations and controlling physical processes allow rapid delineation of those data that are erroneous. Model development keeping physical processes and data needs in the forefront can produce realistic, accurate methods for estimating sediment yield from watersheds.

Chapter 11 describes various methods for routing sediment through a channel system considering unsteady flow for both water and sediment. The principal limitation of one-dimensional model is its assumption of one-dimensional flow. In a relatively nonuniform river, only the general pattern of the river geomorphology can be considered. To perform a more detailed study, a two-dimensional model can be applied. The two-dimensional sediment routing model is also presented in this chapter. The advantages and disadvantages of various types of models for unsteady flow routing in rivers are discussed.

Chapter 12 presents a simplified and effective method for routing sediment through a channel system. This method requires the assumption of known discharge in the river system. For determination of long-term river system response, sediment movement through a river system is of primary concern, and detailed information on flood wave movement is of secondary importance. A simple known-discharge uncoupled sediment routing scheme can be utilized to determine aggradation and degradation in a river. The known-discharge, uncoupled sediment routing formulation allowed the development of an extremely fast and efficient model, which makes the long-term simulation of sediment movement possible and practical. The known-discharge formulation requires the user to identify for the mathematical model the water discharge throughout the system for the entire period to be modeled. The water discharge can be determined by either assuming steady flow or by using an unsteady flow routing model (see Chapters 6, 8 and 9). The model computes the water surface profile by assuming gradually varied steady flow. The time increment utilized in the input hydrographs may vary from a few hours to a month or longer, depending on the flow conditions and the required accuracy of the results. The model can accurately simulate unsteady flow profiles if it is coupled

to an acceptable unsteady flow water routing model since it does not linearize the momentum equation.

In Chapter 13, factors controlling landslides and methods used to quantify landslide potential and probability are presented and demonstrated. Use of information supplied in this chapter will provide the reader with a better understanding of a formidable natural hazard.

The aim of Chapter 14 is to give a short introduction to state-space modeling with particular reference to watershed and river channel systems, and discuss the applicability of Kalman filtering techniques to the identification of model parameters and the prediction of system's response. The application of Kalman filtering techniques to watershed and river modeling is relatively new and requires further development.

Chapter 15 presents several hand-held programmable calculator programs for watershed and river analysis. The programs presented implement theory discussed in Chapters 4, 5, 6, 7, 10 and 12. Of course, many of the complex formulations presented in those chapters are inappropriate for use with these calculators. However, as will be shown in this chapter and the case study chapters to follow, a wide range of engineering and prefeasibility studies may be addressed using the material presented in this chapter. The intent of this chapter is to provide a group of programs that may be incorporated into an integrated approach analysis for a preliminary design level.

In the previous chapters (Chapters 2-15), the basic theory and fundamental tools for analysis of watershed and river systems were discussed. The analytical tools for analysis range from simple geomorphic analysis, hand-held calculator analysis, simplified computer models, and complicated computer models. In addition, the data needs for specific models were also presented. In Chapter 16, an overview of some case studies is presented to illustrate types of problems that are often encountered in the analysis of watershed and river systems. General data needs for analysis are discussed and an effective system for data management is presented. Then a general approach to determine the required level of analysis is recommended.

Chapter 17 presents four selected studies specific to the design of channels, canals, floodways, and navigable waterways. The first study presented is a design of channel bank protection associated with

Bijou Creek, Colorado. The second example is a canal design considering a large fluctuation of water and sediment inflow. The third problem is an erosion, sedimentation and debris analysis of proposed Boulder Creek Floodway, Boulder, Colorado, and the last case study is an investigation of the effects of Chippewa River erosion and silt reduction measures. These four examples provide a good overview of hydraulic analysis required for channel design.

Chapter 18 presents four selected studies specific to the degradation and aggradation problems. The first study presented is a degradation analysis below a dam located in the T or C, Williamsburg Watershed, New Mexico. The second study is an erosion and sedimentation analysis of San Juan Creek near Conrock Gravel Pit, Orange County, California. The third example deals with a degradation analysis associated with the pipeline crossings at the Jim River, Alaska, and the fourth example is an analysis of sediment movement in the Muskegon River following the removal of Newaygo Dam. These four examples illustrate an array of degradation and aggradation problems that hydraulic engineers often encounter.

Chapter 19 illustrates case studies involving analysis of watersheds in terms of best management practices. A best management practice, loosely defined, is one that meets social, economic, political, and environmental goals all at once. Since this is usually impractical or impossible, goals must be weighted or modified in order to arrive at the practice that is acceptable to all concerns. In this chapter, model applications showing how management practices can be quantified in terms of water and sediment yields. As an interesting addition, evaluation of a data collection materials using model simulation is also presented. Three model applications to actual watersheds are given. These are 1) Watershed 17 in the Beaver Creek Watershed, Flagstaff, Arizona, 2) an arid, southwest drainage for determining a probable maximum flood, and 3) a generalized planning level model for assessing sediment yield changes in a watershed caused by management activities.

As presented in Chapters 2 through 19, there are many analytical tools available for use in predicting the response of a watershed and river system. One of the shortcomings of most analytical systems devel-

oped to date for analyzing the watershed and river system is that they are too limited in scope. Most watersheds that are subject to planning and legal requirements for water resources management, flood control, and environmental quality are quite large and often encompass complete river basins or sub-basins. Man's activities usually have short- and long-term effects on the environment, and the short-term projects may have prolonged effects. An integral analytical system is required to deal with a large river basin and to predict the response for both short and long terms. Chapter 20 illustrates in detail the analysis of a large basin, the Yazoo River Basin, Mississippi, for the U. S. Army Corps of Engineers.

1.4 ACKNOWLEDGEMENT

Many people provided important and capable assistance to complete the short course text. The organizers and writers would like to extend their appreciation to all those who assisted in this short course and mention a few who were particularly helpful.

Kris Schneider is acknowledged for her capable assistance in managing the short course. Annette Ward, Tammy McFall, Margaret Tilleard, Debbie Price and Barbara Gibbens are recognized for their preliminary editing and proofreading efforts. Technical staff of great service were Arlene Nelson, Head of Technical Typing, and her group; Hanae Akeri, Head of Drafting; and finally Jan Wilson, Margaret Reuss, and Carol Stafford, the three secretaries closest to the everyday problems confronting this effort.

The knowledge, material and methodologies presented in this short course are directly and/or indirectly obtained from long and fruitful association with many sponsoring agencies for research projects. Those of significant contribution are the U. S. Army Corps of Engineers, U. S. Environmental Protection Agency, U. S. Forest Service, U. S. Fish and Wildlife Service, National Science Foundation, and Colorado State University Experiment Station. Individuals who have been particularly helpful include John Henley, Roy Smith, Brien Winkley, Larry Banks, Phil Combs and Don Williams, U. S. Army Corps of Engineers, Vicksburg District; Dennis Cin, Wayne Knott, Robert Northrup, Al Bjorkquist, U. S. Army Corps of Engineers, St. Paul District; Walt Sanders, Bob Swank, Lee Mulkey, Jim Falco, Tom Barnwell and Charlie Smith, Environmental Research Laboratory, U. S. Environmental Protection Agency, Athens, Georgia; Ross Carder, Jim Rogers,

Malchus Baker, Ralph Campbell, Jim Marsh, Nelson Dean, Mike Barton, Eric Siverts, Ron Aygarn, Ed Burrows, Walt Megaham, Lloyd Swift, Fred Swanson and Doug Swanston, Red Ketcham and Bruce Medford, U.S. Forest Service; John Mullins, Division of Ecological Services, U. S. Fish and Wildlife Services, Michael Vanderford, Great River Environmental Action Team, St. Paul, Minnesota; C. T. Yang, U. S. Bureau of Reclamation, Denver, Colorado; Arthur Ezra and Mike Gaus, National Science Foundation; Ray Chamberlain, George Olson, Pat Jordan, Lionel Baldwin, Bill Fead, Bob Hayman, Gary Edelen, Colorado State University.

The developed methodologies and models have been applied to assist in solving many practical problems for the following organizations; Tipton and Kalmbach, Dames and Moore, Engineering Consultants, Inc., Stearns-Roger, URS, Ayleaska Pipeline Company, U. S. Army Corps of Engineers, U. S. Department of Justice, U. S. Environmental Protection Agency, Soil Conservation Service, U. S. Geological Survey, Federal Highway Adminstration, United Nations, World Bank, and other national and international organizations.

CHAPTER 2

INTRODUCTION TO WATERSHED AND RIVER ANALYSIS

by

Daryl B. Simons, Associate Dean for Engineering Research and Professor of Civil Engineering, Colorado State University, Fort Collins, Colorado
Ruh-Ming Li, Associate Professor of Civil Engineering, Colorado State University, Fort Collins, Colorado

2.1 INTRODUCTION

The increasing interest in water resource and land-use planning has stimulated the development of particular and general watershed and river system models for predicting response from ecological systems. The models, whether physical process simulation or conceptual, are intended to be used to estimate physical quantities that describe the major ecosystem responses to precipitation such as water yield, sediment yield, changes of land and river morphology, and transport of pollutants. Methods to estimate water, sediment, and other pollutant transport yields are needed for analyzing the economic feasibility and trade-offs of any proposed water resources or land-use development in watershed and river systems and for predicting possible adverse environmental impacts associated with the proposed development.

A mathematical model is simply a quantitative expression of a process or phenomenon that is being studied. In a conventional method of analysis, a series of manual calculations may be required. With the advancement of numerical techniques and computer technology, a series of tedious computations can be conducted efficiently, repeatedly, and adequately through the formulation and construction of a mathematical model. Utilizing a well developed model, a whole array of "what-if" questions can be answered with minimum requirement of time and effort. Since no process can be completely understood and observed, any mathematical expression of a process will involve some level of uncertainty. This uncertainty can be minimized if the governing physical processes are considered in the analysis and the model is properly designed, calibrated and verified. Model development, verification, and application to the real-world problems requires the consideration of the nature of the problems, physical environment, objective of the study, time, manpower, and money. Since time, manpower, and money always have limited resources, decisions must be made by the model users and developers as to the degree of complexity the model is to have, and the extensiveness of the verifications that are to be performed. According to Overton and Meadows (1976), if a highly complex mathematical representation of the system under study is made, the risk of not representing the system will be minimized but the difficulty of obtaining a meaningful solution will be maximized. Much data will be required, programming effort and

computer time will be large, and the general complexity of the mathematical handling may even render the problem formulation intractable. Further, the resource constraints of time, money, and manpower may be exceeded. Conversely, if a greatly simplified mathematical model without proper examination of physical significance is selected or developed, the risk of not representing the physical system will be maximized but the difficulty in obtaining a solution will be minimized. Figure 2.1 shows the general concept of "trade-offs" considering model complexity. The knowledge of governing physical processes and the sensitivity of system response plays the most important part in deciding an appropriate level of analysis. It is possible to select or develop a model that is simple to use and involves a minimum level of risk if the governing physical processes are emphasized in the analysis.

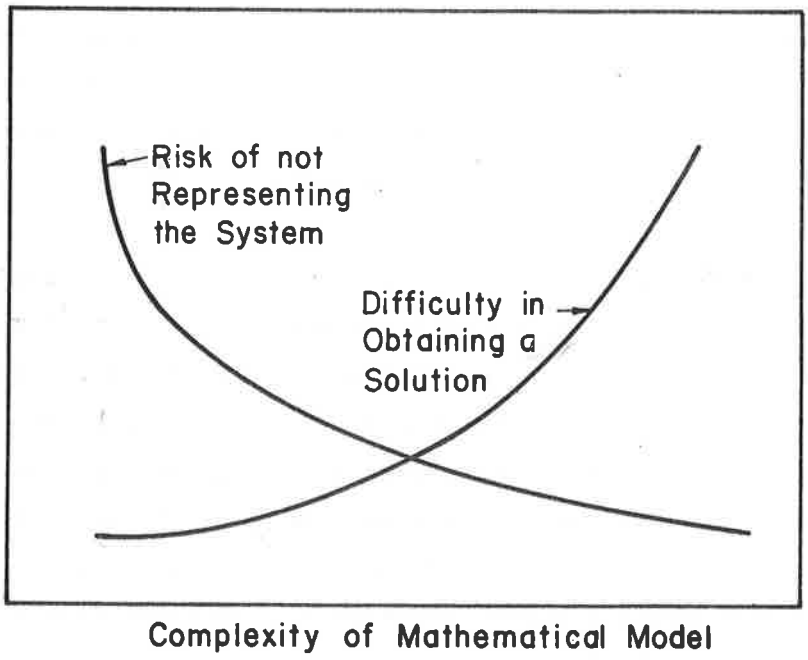

Figure 2.1 The model complexity trade-off diagram (after Overton and Meadows, 1976).

The physical processes governing watershed and river responses are very complicated. Many past studies have utilized a statistical interpretation of observed response data. The unit hydrograph method for water routing, the Universal Soil Loss Equation for soil erosion and the hydraulic equations for stream morphology are examples of these types

of studies. It is often difficult to predict the response of a watershed to various watershed developments or treatments using such methods, because they are based on the assumption of homogeneity in time and space. Mathematically simulating the governing physical process is a more viable way to estimate the time-dependent response of watersheds and river systems to precipitation with varying land use and water resources development. By analyzing basic ecosystem processes and the impact of management activities on specific processes it is possible to predict the cause-effect relationships between management activities and ecosystem response. With the aid of systems analysis techniques, a desirable mix of management activities can then be selected taking into consideration both the environmental and resource goals.

This chapter presents a brief assessment of the current state-of-the-art utilized to analyze watershed and river systems, physical processes important to analysis, criteria related to the development of mathematical models for various applications, procedural steps involved in model development, and examples of applications of models to watershed and river systems.

2.2 CURRENT STATE-OF-THE-ART

Mathematical models used to simulate the effects of management activities on ecosystem responses can be classified as one of three types: regression, "black box" simulation, and physical process simulation. Where models are hybrids of components that fall into two or all three of these categories, they are classified according to the dominant traits of the model as a whole (Simons and Li, 1979).

A general weakness of regression models available for use in water and land resources management, such as the Musgrave approach to soil erosion (U.S. Forest Service, 1976), is that the variables representing water and land uses and conditions are not specific enough to reflect the effects of many individual management activities. In addition, the regression models usually require sufficient observed data to correlate meaningful relations. This is often the most serious drawback for this type of approach. Furthermore, it is very difficult to predict time and space dependent processes using regression equations.

The lumped parameter or "black box" or "simulation programming" type of model interprets input-output relations using oversimplified forms which may or may not have physical significance. All processes related to movement of the water and sediment through the watershed are "lumped" together into several coefficients. The classic example of a lumped parameter model is the rational formula for estimating peak discharge, i.e., $Q = CIA$ where Q is the peak discharge, I is the rainfall input, A is the drainage area, and C is the runoff coefficient which represents the major hydrologic processes. Such a model is easy to use, but has limited physical meaning and can often be inaccurate. In most cases, it is impossible to predict the effects of alternative mixes and sequences of management activities occurring on complex upland watersheds utilizing lumped parameter models. Further, simulation programming models can only be made to represent a particular watershed by calibrating numerous internal model coefficients using water and sediment flow data documented for existing or past vegetation and soil conditions. In the absence of adequate data for calibration of the models for significantly different future vegetation and soil conditions, the predicted future water and sediment flow using simulation programming models must be suspect.

Physical process simulation models, however, avoid the "lumping" of physically significant variables by decomposing components such as infiltration and sediment detachment from raindrop splash. By simulating the selected phenomena into its separate components, each individual process can be analyzed and refined or altered to meet the needs of the user. Consequently, as each process component is upgraded, the model becomes more representative of the physical system. Use of component process models also allows input of variables that have physical significance to the user and the field situation. All of the above characteristics of component process models allow greater flexibility than other types of models. Advantages of physical process component models over other types are numerous. In general, physical process simulation models are superior to regression type models or "black box" type mathematical models. The input variables to process models are physically significant, they indicate system response caused by changing one or more physically significant values. The physical process simulation

models are "dynamic simulation systems." They are not assumed stationary in either time or space and therefore with very little calibration they can be used for predicting the future response of the system in real time and space. Furthermore, because these models are formulated according to physical processes, they are applicable to areas where the governing physical processes are the same.

There are numerous mathematical models available for predicting the response of watershed and river systems. A comprehensive review of nonpoint water quality modeling in wildland management was conducted by the U.S. Forest Service (1976). Herein, a brief review of available component models for predicting system response from watershed and river systems is given.

Physical process simulation models include those models relating to the physical processes such as surface runoff, subsurface flow, raindrop splash erosion, overland flow erosion, channel flow routing, channel bank erosion, degradation and aggradation. Streamflow models have received a great deal of attention in ecosystem modeling. Chapters 7, 8 and 9 describe the water routing models applicable in watershed and river systems. A great deal of research has been conducted on the components within the hydrologic cycle with water as the prime carrier of sediment and pollutants. The research on streamflow and the hydrologic cycle provides the necessary ingredients for advancement of the physical process simulation model for estimating transport of sediment and other pollutants. Determination of resistance to flow is usually the most important item for calibration of streamflow models. The resistance to flow is a function of bed material size, bed form, river stage, temperature, etc. Chapter 5 discusses the resistance to flow in details. It is often difficult to predict the resistance to flow in cobble and boulder bed rivers. Recent studies at Colorado State University by Simons et al. (1978a) further demonstrated the dynamics of flow resistance in mountain rivers. They indicated that the released sediment from upstream watershed or bank erosion during the flood will fill the spaces between the roughness elements, and may cover them completely. Thereafter the cobble channel behaves as a sand bed upper regime channel with a much reduced resistance to flow. A better understanding of resistance to flow for a variety of river and land surface conditions is needed.

Methodologies presented in the literature identify three basic types of mathematical approaches to watershed and river analysis: 1) the analytical solution, 2) the finite difference method, and 3) the finite-element method. Hann and Young (1972) and Simons et al. (1977a) provide a good summary review of finite difference models using both implicit and explicit solution techniques. Chapter 6 summarizes an overview of flood routing techniques. Analytical solutions are usually limited by some simplified assumptions and are applicable to restricted conditions. The finite-element technique has been actively applied recently, especially to the modeling of microscopic flow phenomena. In the finite-element method, the original continuous problem is reduced to a system of ordinary differential equations in time. These can be solved by traditional techniques. Due to the fundamentals of the finite-element formulation, completely arbitrary geometries may be modeled. Thus, spatial programming is not required to fit highly irregular boundaries. In addition, the feature of variable element size can be used to create a fine mesh of elements in areas of high variable gradients in order to obtain the desired accuracy and detail in very sensitive regions. Common boundary conditions are also handled easily by the finite-element method. The major drawback of the finite-element method is the required computer time. This constraint will be less significant in the future as numerical techniques and computer software advancements occur.

Degradation, aggradation and movement of sediment and other pollutants in watersheds and river systems are closely related to water movement. The streamflow and water routing models have received the most intensive study. The ability of the majority of available streamflow and water routing models to relate wildland activities to their unique environments and to account for spatial diversity is not well demonstrated. A model that will predict effects of management activities and represent spatial and temporal variability of both activities and processes is needed.

Existing sediment models in watershed systems deal mainly with surface erosion. No process models exist for unstable channel erosion, nor are any models available for predicting mass wasting and its interaction with channels. Almost all existing surface erosion models are based on either the Musgrave approach or the Universal Soil Loss

Equation (U.S. Forest Service, 1976). These models are difficult to use because they are insensitive to both the spatial and temporal variability of management activities. In 1975, Simons et al. (1975a) developed a numerical model to simulate the physical processes governing sediment movement on small watersheds. Their model can predict the effects of management activities on sediment yield in both time and space. This model is being modified to accommodate unstable channel erosion and deposition, a more complex watershed system, and long-term simulation of response considering interstorm periods. In addition, for coupling the nitrogen, phosphorous, etc., movement with water and sediment, it has been modified to route the sediment considering different sediment sizes (see Li et al., 1977). This is necessary because different sizes of sediment have different uptake rates for different contaminants. Details of the watershed sediment yield models are given in Chapter 10.

It is important to recognize that a river is a dynamic system. An alluvial river is generally continuously changing its position and shape as a consequence of hydraulic forces acting on its bed and banks and as a result of the interaction of these forces with the biological processes of the river environment. These changes may be slow or rapid and may result from natural events or from man's activities. When a river channel is modified locally, the change frequently causes modification of channel characteristics both up and downstream and can be propagated for long distances. Many available river routing models either neglect the dynamic response due to sediment movement or are insensitive to man's activities. In a parallel study completed at Colorado State University by Simons et al. (1975b), a one-dimensional water and sediment routing model was used to simulate the dynamic response of river-bed elevation resulting from operations of locks and dams. Their model can be used to study the short- and long-term impacts of the effects of different operational schemes for the locks and dams, the effects of the pools on the behavior and form of the tributary rivers, the impact of changes in water and sediment inflows on the morphology of the river and adjacent lands, and the impacts of dredging and dredged material disposal on the hydraulic response and sedimentation

in the channel. Chapters 11 and 12 report different methods for sediment routing in rivers.

In a recent study conducted by Simons et al. (1978b) for the U.S. Army Corps of Engineers, Vicksburg District, the sedimentation problems of the Yazoo River Basin were investigated. This is a large and comprehensive mathematical modeling effort. It includes about one-fourth of the State of Mississippi, 27 major rivers, four major reservoirs and many smaller streams and reservoirs. A rather detailed description of the study is presented in Chapter 20. In analyzing a large river system like the Yazoo the development of a data storage and retrieval system is imperative (see Chapter 16).

Sediment transport is one of the most important variables needed for evaluating erosion, sedimentation, and channel morphology. The capacity of a stream to transport sediment depends on hydraulic properties of the stream channel. Such variables as slope, roughness, channel geometry, discharge, velocity, turbulence, fluid properties, and size and gradation of the sediment are closely related to the hydraulic variables controlling the capacity of the stream to carry water, and are subject to mathematical analysis. The total sediment load of a stream is the sum of the bed-material load and the wash load, or bed load and suspended load or measured and unmeasured load.

Because bed material is transported as both suspended load and bed load the different physical laws governing these modes of transport must be incorporated into any method for predicting total transport of bed material. As implied by the definitions, the distinction between bed-material load and wash load is of importance. Bed material is transported at the capacity of the stream and is functionally related to measurable hydraulic variables. Wash load is not usually transported at the capacity of the stream. It depends instead on its availability, and is not functionally related to hydraulic variables. While there is no sharp demarcation between wash load and bed-material load, one rule of thumb assumes that the bed-material load consists of sizes equal to or greater than 0.062 mm, the division between sand and silt. Another reasonable criteria is to choose a sediment size finer than the smallest 10 percent of the bed material as the point of division between wash load and bed-material load.

Sediment particles that constitute the bed-material load are transported either by rolling or sliding along the bed (bed load) or in suspension. Again, there is no sharp distinction between bed load and suspended load. A particle of the bed-material load can move part of the time in contact with the bed and at other times be suspended by the flow. Generally, the amount of bed material moving in contact with the bed of a large sand bed river is only a small percentage of the bed material moving in suspension. These two modes of transport follow different physical laws which must be incorporated into any equation for estimating the bed-material discharge of a river.

Limited quantities of fine material moving as wash load usually will not pose direct problems inhibiting development activities in the riverine environment. However, large concentrations the fine materials can influence are the capacity of a stream to transport bed material through its influence on fluid properties such as viscosity and density, bank stability, growth of aquatic plants, the biomass of the channel, etc.

For a detailed treatment of currently used suspended and bed-material load transport theories refer to Vanoni (1976) and Simons and Sentürk (1977). A systematic approach for selecting a proper sediment transport equation is discussed in Chapter 4. Data on sediment transport in the steep channel systems is generally unavailable due to the extreme difficulty associated with collecting data in the laboratory and field environments. Yet many of the streams in the upland watershed are steep and mountainous channels. Recently, Bathurst et al. (1979) reported a laboratory effort on sediment transport in steep channels with slopes ranging from one to twenty-five percent.

Hydraulic geometry is a general term applied to alluvial channels to denote relationships between discharge, the channel morphology, hydraulics and sediment transport. In self-formed alluvial channels, the morphologic, hydraulic and sedimentation characteristics of the channel are determined by a large variety of factors. In general, these relations apply to channels within a physiographic region and can be derived from data available on gaged rivers. It is understood that hydraulic geometry relations express the integrated effect of all the hydraulic, hydrologic, meteorologic, and geologic variables in a drainage basin.

Geometric relations describing alluvial streams are necessary in river engineering and river modeling. The forerunners of such relations are the regime equations developed to design stable alluvial canals. A generalized version of hydraulic geometry relations was developed by Leopold and Maddock (1953) for different regions in the United States and for different types of rivers. The geometric relations are usually applied to provide an approximation to river response. In addition, Lane's geomorphic response relation stating that the product of the water discharge and slope is proportional to the product of the sediment discharge and the bed-material size (Simons and Sentürk, 1977) is very useful for qualitative analysis of river response (see Chapter 3). For a detailed description of current knowledge on river morphology refer to Schumm (1977) and Simons and Sentürk (1977).

2.3 PHYSICAL PROCESSES IMPORTANT TO THE ANALYSIS

The physical processes governing watershed and river response are very complicated. The two primary inputs to the ecosystem are climatic inputs and man's activities. The climatic inputs include precipitation (rain or snow), solar radiation, air currents and moisture. Man's activities important to watershed and river analysis include weather modification, urban development, watershed management, fire, energy resource acquisition, water resources development, land-use zoning, mining activities, water supply and irrigation, recreational development, the development and operation of transportation systems, the application of fertilizers, herbicides, and pesticides, locks and dam construction and operation, river channelization, river training, transbasin water diversions, timber planting and harvesting, and grazing and browsing. The processes which govern the responses from watersheds and rivers are numerous. The key physical processes are atmospheric, vegetative, ground surface, overland flow, mass wasting, stream, soil, and groundwater processes. The atmospheric processes deal with aerosolization, transport phenomena, diffusion, dispersion, convection, and particle dynamics. The vegetative processes include interception, evaporation, transpiration, nitrogen fixation, litter production, ground cover functions, plant succession, and thermal balance modulation. The ground surface processes account for infiltration, depression storage, evaporation, thermal balance, litter accumulation and decay, and raindrop splash soil

erosion. The overland flow processes involve water flow routing (both surface and subsurface), sediment detachment and transport, pollutant adsorption and transport, rill development and thermal diffusion. The mass wasting processes are important on watersheds having relatively unstable soil. They include mudflows, slides, debris, avalanches, stream bank failure, soil creep, dry ravel, and soil piping. The stream and river processes are of great concern to both engineers and environmentalists, and are often referenced as principal indicators of the impacts of watershed and river basin development. They include water routing, sediment transport, gully development, degradation, aggradation, geomorphology, bank erosion, deltas and fan formulation, pollutant uptake and storage, pollutant transport, dissolved oxygen balance, dissolved solids, and routing of forest litter and debris. The soil processes involve weathering, pollutant storage, nitrate reactions, pollutant adsorption, thermal balance, and water percolation. The groundwater processes include flow movement, pollutant transport, diffusion, dispersion, recharge, heat exchange, nitrogen and phosphorous transport, and dissolved oxygen.

It is important to consider that different variables and physical processes have varying degrees of importance, depending on the purpose of analysis and the size and characteristics of the particular watershed and river ecosystem being analyzed, including the types of climatic conditions, soils, geology, vegetative cover, land-use activities, and water and sediment inflows. In order to determine which of these variables and/or processes must be included in the analysis, it may be necessary to evaluate the importance of many variables and/or processes by sensitivity analyses.

Degradation, aggradation, and movement of pollutants are closely related to water and sediment movement. Therefore, understanding the physical processes related to water and sediment routing is of fundamental importance for effective analysis of watershed and river response. In spite of the complexity of problems involved in water and sediment routing in watershed and river ecosystems, the governing equations are the same. They are the continuity equation of water, the flow momentum equation, the continuity equation of sediment, the flow energy equation, and some supplementary equations such as flow resistance relations,

channel geometry equations, and sediment supply equations. For a detailed discussion of governing physical processes refer to Chapter 3 or the paper by Simons, Ward and Li (1979).

2.4 CRITERIA OF USEFUL MATHEMATICAL MODELS

For all practical purposes, a useful mathematical model for predicting watershed and river system response to potential management actions should meet the following criteria: 1) The temporal resolution should be both short- and long-term. Management practices usually have both short- and long-term effects on our environment, and short-term projects often have prolonged effects. Thus, the temporal resolution should accommodate addressing both short- and long-term response questions. 2) The spatial resolution should be flexible. Specific management plans and activities are very often limited to small watersheds. Most watersheds subject to legal requirements for environmental quality and water resources management are quite large and often encompass complete river basins or sub-basins. As a consequence, the spatial resolution should accommodate both small watersheds and river systems as a whole. 3) The model should be widely applicable. That is, although the model parameters may be area or regionally specific, the model itself should not be area or regionally specific. The only feasible way to develop such a model is to consider the physical significance of the governing processes. Only a physically based model can represent appropriate cause-effect relationships between management practices and ecosystem response in a general way. 4) The model should be sensitive to the desired management activities. That is, it must be possible to explicitly represent management activities and simulate the system response resulting from these activities. For example, if grazing is a desired management activity for evaluating the watershed response, then the model should be formulated to represent the grazing activity through changing model parameters which could be altered according to the intensity of grazing. 5) The uncertainties due to varying climatic and spatial input should be considered. That is, the simulation must consider variations in both mean values and extreme events. This requires a probabilistic approach to describe the stochastic structure of model inputs. 6) The model should be developed within the constraints of available data. Models intended for practical application

should not have requirements for data that are excessively difficult, costly, or time consuming to collect or acquire. If a large quantity of data is required, an effective data storage and retrieval system is necessary. 7) The model should be oriented for use by management personnel. The perspective of the user must be foremost in all model development work. Models intended for use by managers must readily fit into the specific decision-making processes and situations for which they are to be employed, if information resources are to be generated efficiently and used effectively. So, for usable models to be designed and implemented, developers must be in effective communication with target users throughout the development process. Involving users in model design helps insure that the researcher has full knowledge of the decision-making environment, the actual problems managers face, and the user's perception of the situation being modeled. The model will thereby be more relevant and the user will better trust its validity and capabilities. 8) The model should be easily transformed for use at several levels of accuracy and resolution. Models operable at several levels of accuracy and resolution will be required in order to provide the full range of tools needed for land and river management. Providing usable and realistic models and guidelines for professionals operating in the field in many cases will first require developing and testing relatively complex process models. Once the processes involved are thoroughly understood and the sensitive parameters identified, these models can then be regionalized and generalized to provide simplified models and guidelines for field users. 9) The model computer software system should be developed in a modular fashion. Experience has shown that non-modular all-purpose models are expensive to develop, difficult to use and control, and have large data requirements--all of which tend to detract from their field usability. Adopting the modular approach offers an opportunity to build a coordinated nucleus of standardized system components for use in analyzing a wide spectrum of watershed and river systems. This nucleus would be made up of components that provide common storage and retrieval, analysis, and display. Modular systems also have the advantage that individual components can be updated or replaced as needed without disrupting other components of the system. 10) Full model documentation is an important obligation in providing a useful

and viable tool. The documentation should include not only the formulation theory, system flow charts, computer code, and test results, but also ample examples, guidelines, and precautions for users to model implementation, correct use, and pitfalls.

2.5 PROCEDURAL STEPS FOR MODEL DEVELOPMENT

The development of a model for analysis usually involves the following steps: spatial design, temporal design, model formulation, mathematical solution, model calibration, parameter sensitivity analysis, qualitative examination of physical significance, model simplification, regionalization and generalization, validation, testing and refinement under operational field applications and documentation.

The spatial and temporal designs of a simulation model are both important keys to a realistic representation of the time-space structure of a watershed or river system. For example, designing a realistic space structure for the hydrologic analysis of small watersheds would involve devising a systematic means for either the manual or computer-aided determination of hydrologic response units as a function of such attributes as watershed geometry, topography, vegetation distribution, soil distribution, and the like. A computer program for automatically segmenting a watershed and grouping segments into desired response units was developed by Simons and Li (1975). At the time of applying the model in a specific situation, the general spatial and temporal designs must then be made to explicitly fit the watershed or basin being studied, in accordance with the purpose of the analysis. For example, the spatial design of a large river basin would have to consider the nature and location of the river and its tributaries, and the location of all pertinent gaging stations, structures, and confluences. The explicit temporal design would be made using the historic hydrologic record of the basin. This record might include the historic maximum, minimum and mean precipitation, temperature, moisture contents and water flows, river stages, precipitation patterns, flow volumes, and the effect of man's activities, such as reservoir construction, on the hydrologic record. The temporal design is then used to generate the system input for evaluating explicit response of the future system.

After the spatial and temporal designs are completed, the major physical processes governing the system response can be identified. Then, a series of mathematical equations can be assembled to represent the governing processes, constituting the conceptual formulation of the model. The model formulation should be guided by the criteria of a useful mathematical model presented earlier. Successful model formulation requires a blend of theoretical and practical considerations, as the following discussion illustrates.

For simulating the dynamic response of water and river systems, perhaps the most important governing equations include the continuity equation for water, the continuity equation for sediment and the momentum equation (or the energy equation). These three equations can be solved simultaneously or can be approximated by solving the water continuity equation and the momentum equation first and then refined by using the sediment continuity equation. The second approach is usually applicable because the movement of sediment is much slower than that of water. The numerical solution of these three equations can proceed in two directions. Either an attempt can be made to convert the original system of partial differential equations into an equivalent system of ordinary differential equations by using the method of characteristics or one can replace the partial derivatives in the original system with quotients of finite-differences by using the explicit method or the implicit method. Detailed discussions of the water and sediment routing techniques are given in Chapters 6, 7, 8, 9, 10, 11 and 12.

For the flood routing problem, the precise values of the parameters describing flow resistance are usually unknown, but their ranges are known from measured data. However, to pinpoint the parameter values within these ranges which produce the best model response, model calibration is a necessity. The simplest calibration technique is the trial and error method. But except for models that contain parameters with very narrow searching ranges the trial and error procedure is inefficient. So in the mathematical modeling of system responses, the calibration of model parameters often relies on an optimization scheme. There are many optimization techniques available for the purpose of model calibration. However, the usefulness of a particular optimization technique is very dependent on the formulation of the model being

calibrated. For hydrologic model calibration, Rosenbrock's (1960) optimization technique for finding the optimum set of parameters has proven to be the most promising and efficient method.

After development, the sensitivity of model outputs to changes in each model parameter should be examined. This sensitivity analysis facilitates model parameter calibration, identifies data needs, and provides useful information for model simplification. Another important examination is to evaluate the model qualitatively using physical significance as a guide. At this stage, the trends and extremes simulated by the need to model are examined to assure that they are meaningful considering physical significance and field experience.

Simplification is aimed at fostering widespread applications of methods derived from the more complicated process simulation models. In general, the more complicated models explicitly deal with time and space, solving finite difference formulations of the various processes at each time-space point. The simplified model retreats from this approach and averages the processes over both time and space. While the more complex model usually provides the better solution, its main disadvantage is that often it is relatively expensive to use and requires knowledge of computer applications and mathematical formulations and assumptions that are often beyond the capability of the average field user. The limitations of regression type or "black box" models and user restrictions imposed by the more complex physical process models have made necessary the development of simplified physical process component models. Such simplified models can provide the field user with an easy to use, yet reliable methodology for estimating system response (Simons et al., 1977a).

In order to further facilitate application of the model, model parameters may also be regionalized. This can be achieved by extensive application of the model in a particular geographical area, leading to a generalized regional version of the model. An example of regionalization and generalization is given by the Agricultural Research Service (1975).

Model testing, evaluation, refinement, and documentation are continuous processes. As more field data becomes available, the model can be improved so that more accurate predictions are possible.

2.6 EXAMPLE APPLICATIONS

General

Responding to increasing demands for water for human survival, food production, and energy production requires effective tools for analyzing the ecological system response. Mathematical procedures are utilized in a wide variety of water resources planning applications, including flood control, nonpoint source pollution control, water drainage design, river training work, watershed improvement, stream bank erosion control, mine land reclamation, surface mining impacts, maintenance of navigable channel, road construction, pipeline crossing design, canal design, groundwater management, etc.

There are already numerous examples of successful applications of physical process simulation models of various watershed and river systems analysis and planning efforts and interest in utilizing such techniques is steadily increasing. Chapters 16-20 describe some examples of applications to a great detail. The following are brief descriptions of the most significant examples of applications led by the Engineering Research Center, Colorado State University.

Degradation and Aggradation Analysis

Analysis of degradation and aggradation in a gravel stream bed should consider routing of sediment by size fractions, particularly where degradation is of prime concern. The application of models to the routing of sediment by size fractions has been successful. In the analysis of degradation below an emergency spillway in the T or C Williamsburg Watershed, New Mexico, such a technique was applied (Simons and Li, 1978).

The magnitude of scour was determined utilizing a sediment routing procedure that considered the size fractions of bed material. The computational procedure involved the use of a sediment transport equation, the sediment continuity equation, the armoring effect of coarse materials, and the channel geometry equation. Hence, the mathematical model was developed according to physical principles governing water and sediment transport, degradation and armoring processes. Both the local scour immediately below the structure and the general scour pivoting from a downstream control point were evaluated in the analysis. Figure 2.2 shows the time-lapse change of local and general scour. The

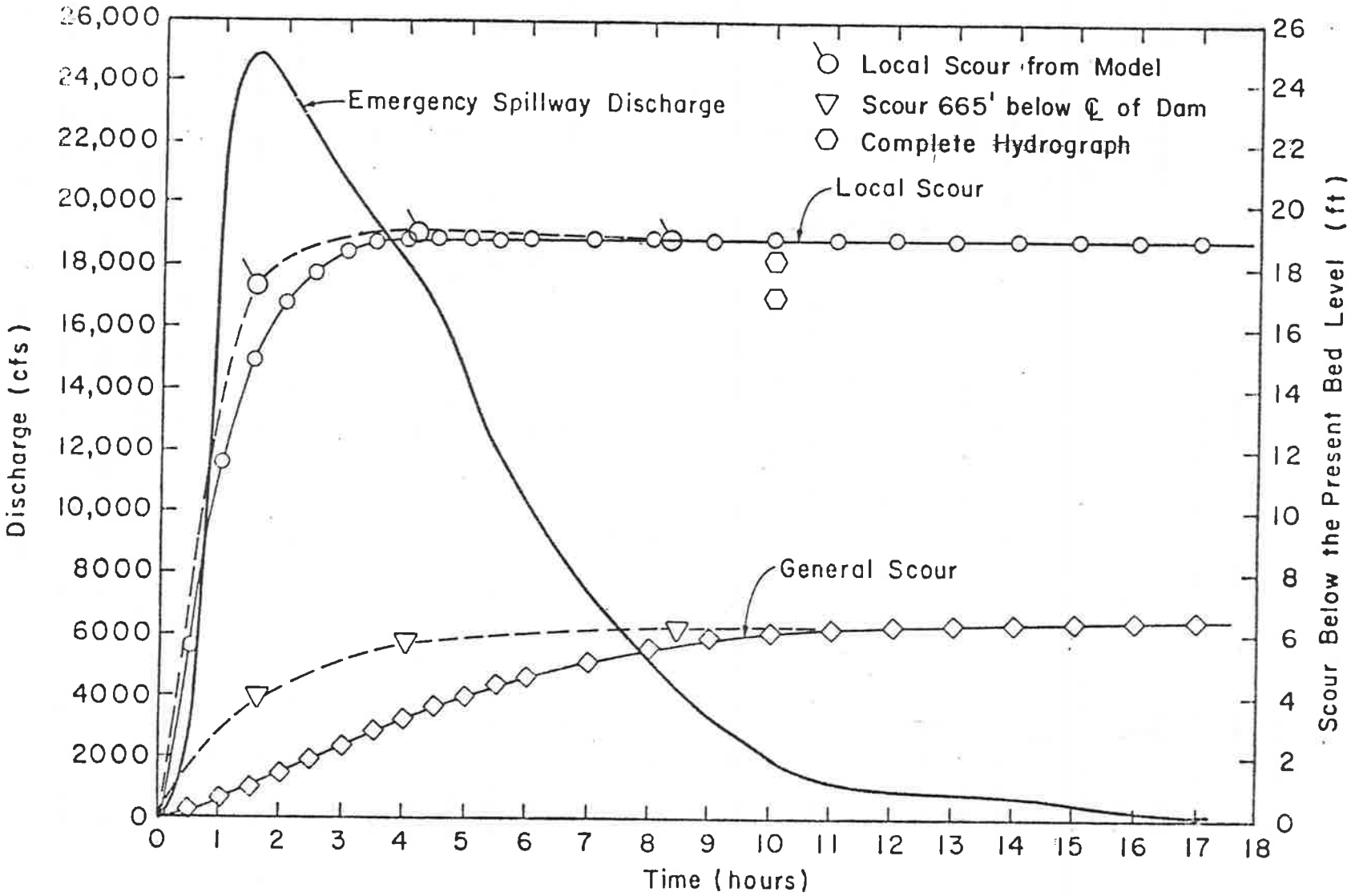

Figure 2.2 Local and general scour with the existing downstream control (6970 ft. from the structure).

local scour depth defined in this study is measured from the present bed level. This local scour depth represents a combination of general scour and local scour according to established definitions. In order to check the applicability of the mathematical model, a large scale physical model (1:30) was utilized by a federal agency to estimate the local and general scour for the design freeboard hydrograph. The results from both totally independent model approaches were extremely close, demonstrating a successful application of the technology of routing sediment by size fractions.

In the analysis of erosion and deposition problems associated with the Conrock gravel mining operation in the San Juan Creek and Bell Canyon of Orange County, California, a mathematical model for routing sediment by size fraction was again applied (Simons and Li, 1978). It provided an estimate of the erosion and deposition response of the stream and gravel pit subject to different hydrologic inputs. Three storms in January, February and March of 1978 induced significant degradation and the data available provided a test for the model. The simulation was made using time steps of four hours. The time lapse changes of elevation at the original gravel pit boundary (Station 16+00) is given in Figure 2.3. The simulation results are excellent when compared with field measurements. One point worth mentioning is that the simulated results of the 1978 storms were predicted utilizing the calibrated sediment transport parameters based on the data from two 1969 storms. The mathematical model was then utilized to evaluate four different alternatives of gravel mining and rehabilitation plans. The above two examples are discussed in detail in Chapter 18.

Water Routing with a Programmable Calculator

The water yield may be obtained by using one of several available methods. These methods fall roughly into two classes: first, the complex watershed model, often involving finite difference representations of physical phenomena, which are designed to be used in a modern digital computer; and second, the simplest empirical schemes such as unit hydrograph for water routing, and basin recharge for infiltration which are practical for hand calculations. The complex models often give accurate predictions of water yield; however, they require the use

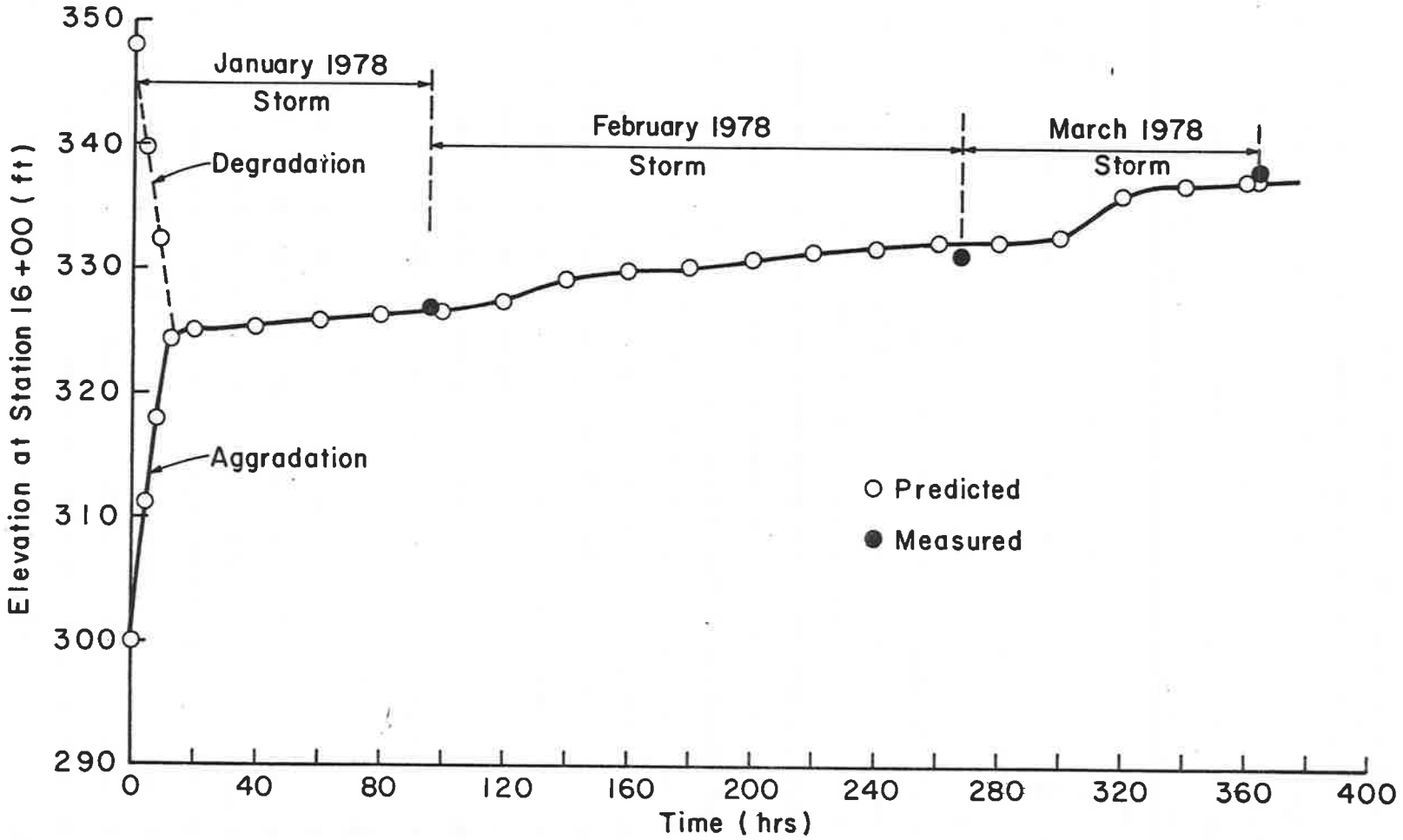

Figure 2.3 Time lapse changes of elevation at the original gravel pit boundary (Station 16+00).

of digital computers and understanding of the complexities of the model. The empirical methods offer a greater utility due to their simplicity, but they are virtually useless when applied to ungaged watersheds. Furthermore, most empirical schemes assume watersheds behave as linear systems. This assumption may be valid for subsurface flow movement, but the flow of surface water and the infiltration process are certainly nonlinear phenomena.

Intuitively, a middle ground which would incorporate some of the advantages of complex physical simulations with the simplicity of the empirical techniques would provide a valuable tool to the practicing hydrologist. The technology of the small programmable calculators has progressed to the point where calculations of considerable complexity may be performed very quickly. In a study performed for the U.S.D.A. Forest Service, a simple watershed model based on physical rather than empirical principles was developed for use in a programmable calculator (Simons et al., 1977).

The developed model is an open-book plane representation of a watershed. It consists of two basic routines. The first routine allows the calculation of infiltration and excess rainfall resulting from an unsteady but spatially uniform storm. The second routine is used to route the excess water from both planes through overland flow to a channel. The same routine can be used again to route the water through the channel. A tabular method for recording intermediate and final results is developed to provide more convenient presentation of calculations. The model is programmed for a Hewlett Packard Model HP-97 (or HP-67) calculator. However, any other programmable calculator with equivalent capacity can be used. The model is tested using rainfall-runoff data from two watersheds at the Agricultural Research Service Research Station located at Hastings, Nebraska. The Hastings watershed is very homogeneous in physical properties and provides a good control for testing the model. Figure 2.4 shows measured and computed runoff at Hastings. Details of hand-held programmable calculator application are given in Chapter 15.

Multiple Watershed Analysis

Legal and environmental concerns often encompass a large area. In order to analyze the total system, a multiple watershed approach is

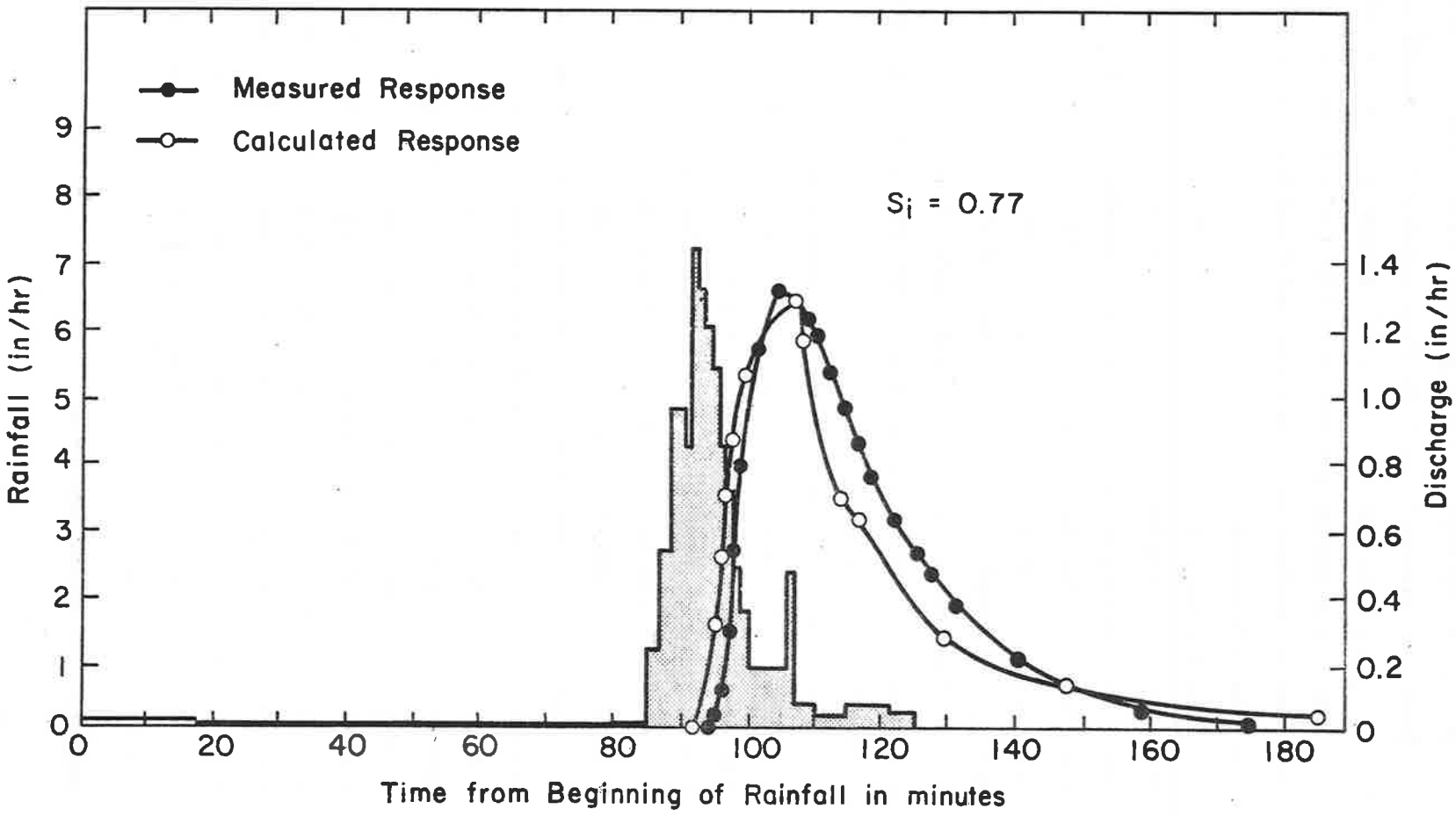

Figure 2.4 Rainfall-runoff response from Watershed 56H, Hastings, Nebraska.

required. The multiple watershed model developed by Simons et al. (1978) subdivides a large watershed into homogeneous response units as dictated by basin geometry and physical characteristics. The system of planes, channels, and subwatersheds developed are designed to represent an entire basin. The hydrographs from each response unit are simulated and then combined to obtain a hydrograph for the entire watershed.

The multiple watershed model was tested by comparing the predicted and measured hydrographs on the Walnut Gulch Watershed in Arizona. The runoff from six square miles was measured by flume number eight in the watershed. Figure 2.5 shows a comparison of recorded and predicted runoff hydrographs at flume eight for four different storm events. Agreement between the measured hydrographs and the simulated hydrographs is satisfactory.

The entire Walnut Gulch Watershed (57.7 square miles) was then modeled for three different storm events utilizing the calibrated parameters based on the data for the six square mile watersheds. The drainage areas (approximately 5.5 square miles) for several stock ponds were not included in the analysis since spillage was assumed to be negligible. The rainfall distributions for the response units were calculated by using an isohyetal map and individual gage records. The comparison of the predicted and recorded hydrograph is shown in Figure 2.6. The agreement between predicted and recorded runoff is good considering the complexity and size of the watershed. Chapter 7 gives more details regarding this multiple watershed model.

Stage-Discharge Relationships

The relationship between stage discharge is very important for the instream flow analysis. Most of the rivers, especially those with flatter channel gradients, have stage-discharge relations that have a hysteresis loop caused by dynamic effects or by other reasons. Simons et al. (1977) presented a new approach to analyze the relation between flow stage and flood discharge. Their method was developed by utilizing a full dynamic equation considering the physical significance. Figure 2.7 shows that the observed and computed stage-discharge relations on the Mississippi River at Tarbert Landing are in close agreement (see Chapter 9).

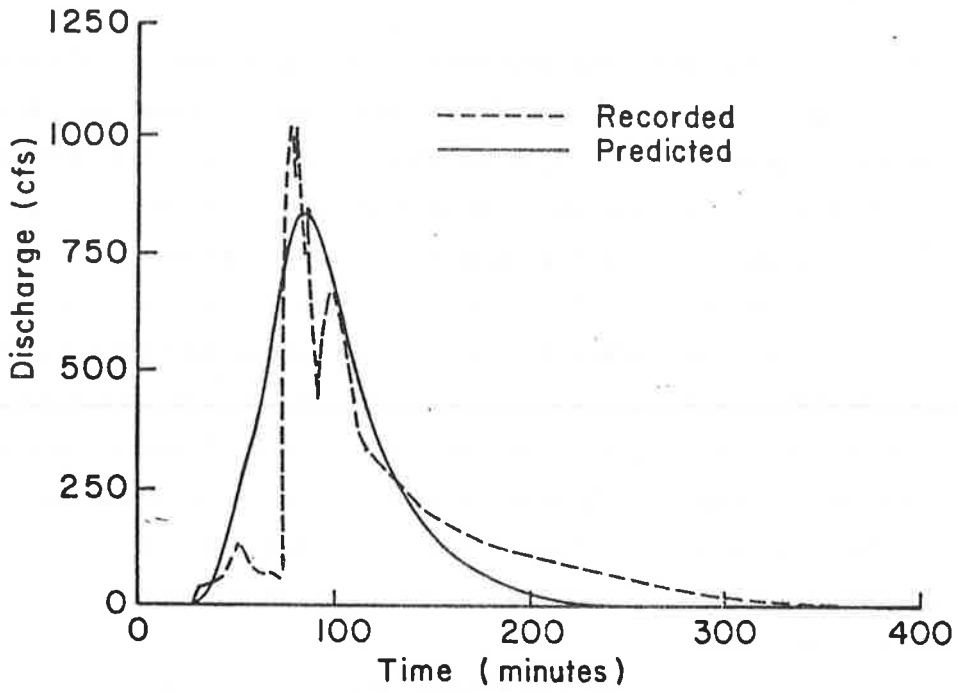

a. Runoff hydrograph for the storm of September 9, 1965, for Walnut Gulch flume #8.

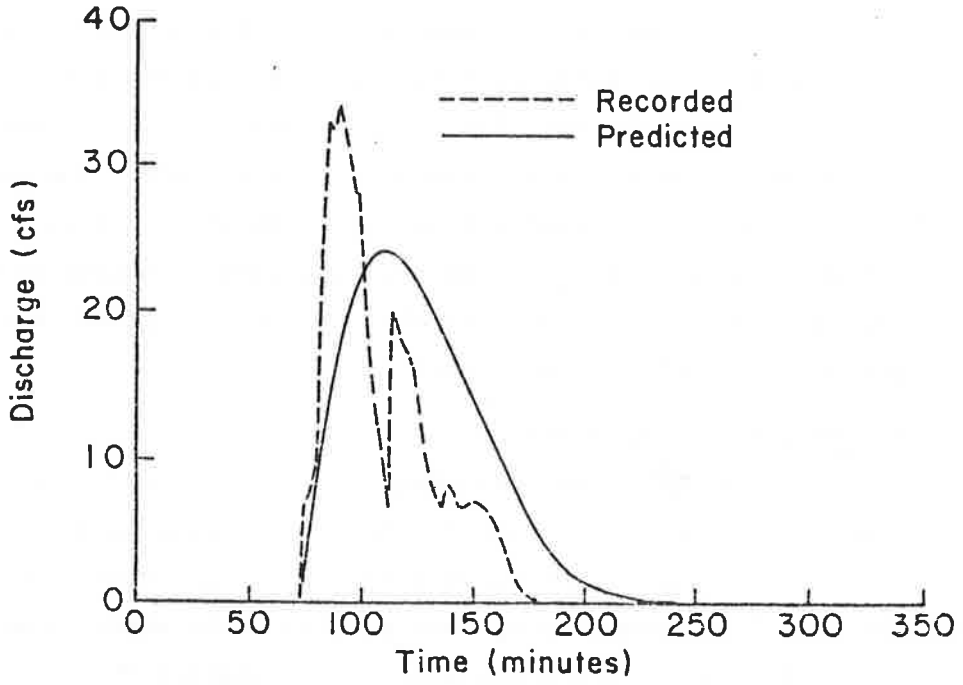

b. Runoff hydrograph for the storm of August 25, 1968, for Walnut Gulch flume #8.

Figure 2.5(a&b) Runoff hydrographs for Walnut Gulch flume #8.

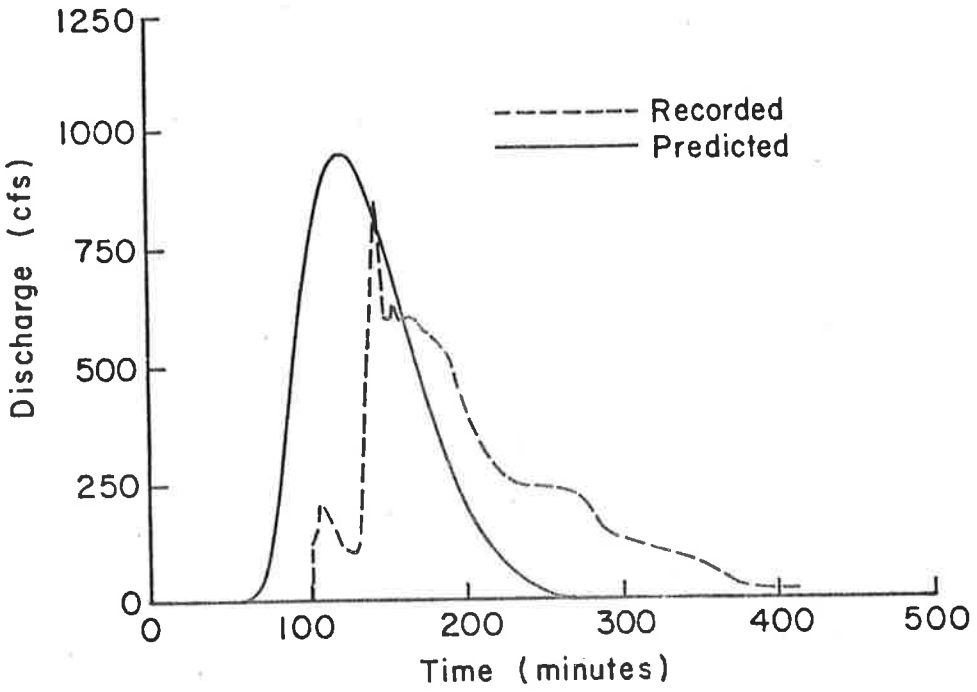

a. Runoff hydrograph for the storm of September 4, 1965, for the entire Walnut Gulch watershed.

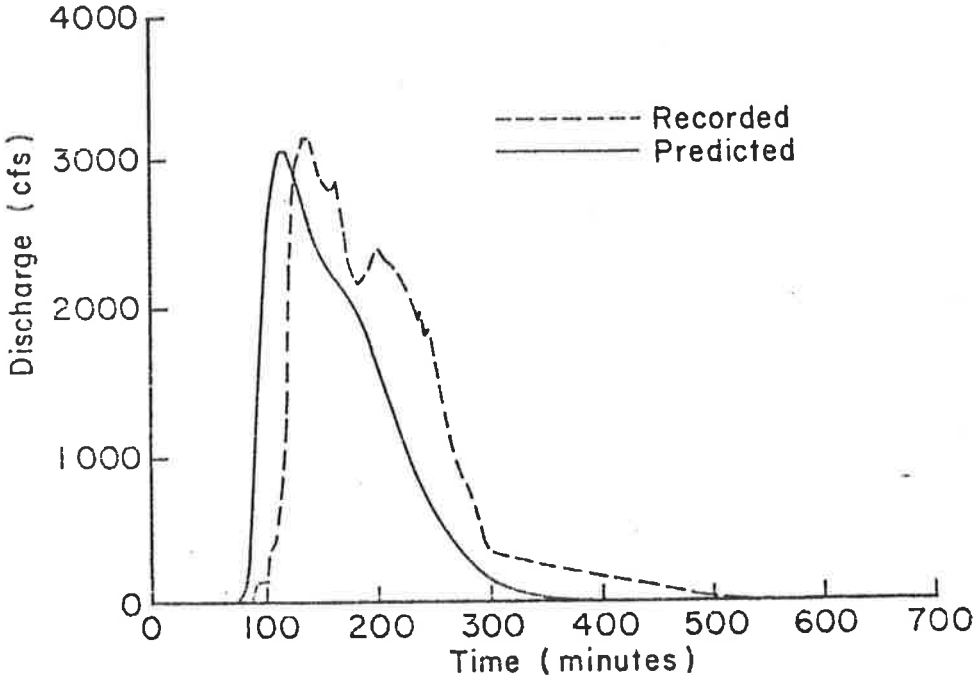

a. Runoff hydrograph for the storm of September 9, 1964, for the entire Walnut Gulch watershed.

Figure 2.6(a&b) Runoff hydrographs for the entire Walnut Gulch watershed.

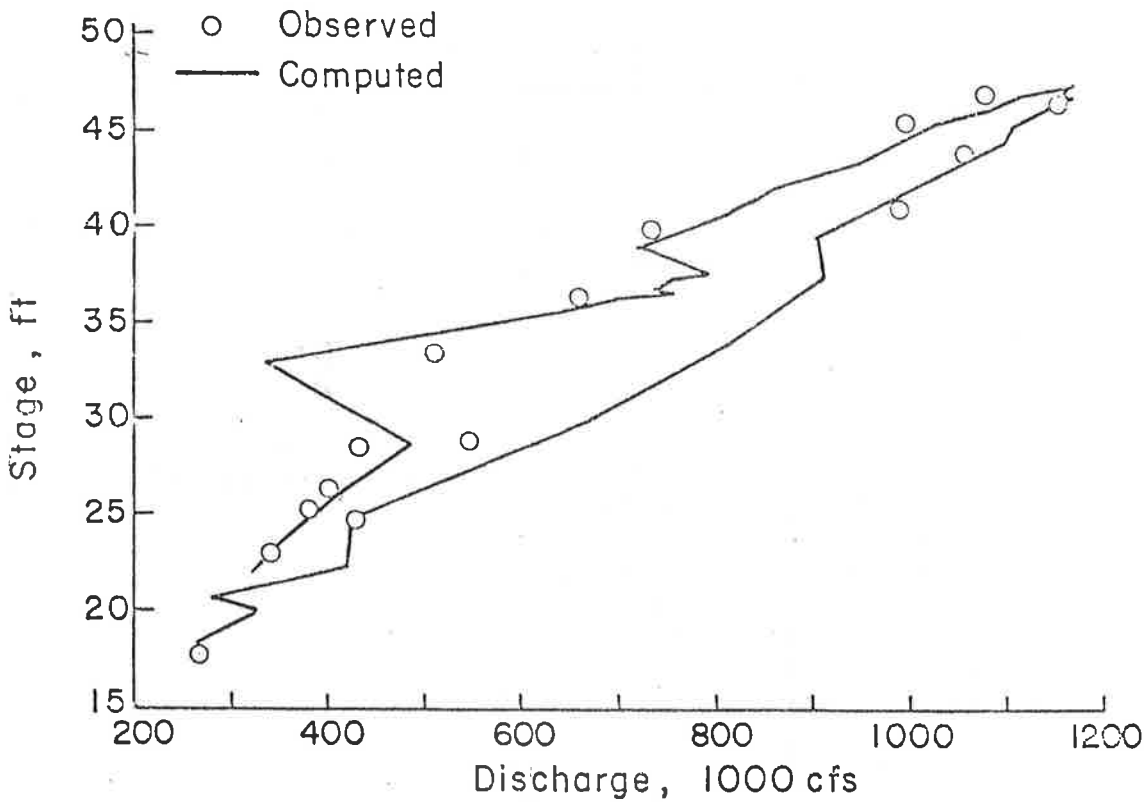

Figure 2.7 Stage-discharge relation for Mississippi River, Tarbert Landing, LA (2/9/66-4/11/66).

Despite the existence of the looped stage-discharge curves, river stage is usually estimated either by statistical stage-discharge relationships or by using backwater simulation models. Frequency and magnitude of error associated with three models were examined by Li et al. (1979). The first model utilized is a statistical stage-discharge relationship. The second model is a steady flow, rigid boundary backwater model, and the third model is a steady flow backwater model with uncoupled sediment routing. The sediment routing model can compute changes in the channel due to aggradation and degradation. For thorough comparison, each model was applied to two case studies. One case involved a relatively stable reach of river, while the other was unstable.

The Yazoo River in Mississippi was selected for study due to the availability of data for that area. Two reaches of the river were carefully analyzed: a stable reach near Locopolis and an unstable reach at the Fort Pemberton cutoff near Greenwood. Historically, the bed elevation in the stable reach has not changed substantially. However, the bed of the unstable reach degraded up to 20 feet during 1973 and 1974. This degradation was caused by the removal of a dam in the cutoff that allowed a large portion of the Yazoo River flow to bypass the Greenwood Bendway. The changing behavior of the river discharge and sediment transport at this unstable reach makes prediction of flood stage from discharge data difficult. This is especially true for models that are based entirely on historical data since they cannot adjust to the new flow conditions. Selection of these two reaches allows evaluation of the reliability of the three models.

All three models were calibrated using the same data. To verify the results of the model's capability, additional computations utilizing data independent of calibration data were made for each model using the calibration results. For comparison purposes, model error is defined as the difference between observed and predicted stage for each day. Figures 2.8 and 2.9 show the relative frequency distribution of verification error for each model, and Table 2.1 lists the statistics of the absolute error for each method.

As indicated in the figures and table, all three methods have approximately the same mean error for Locopolis, but the process models have much lower maximum errors than the stage-discharge relationships.

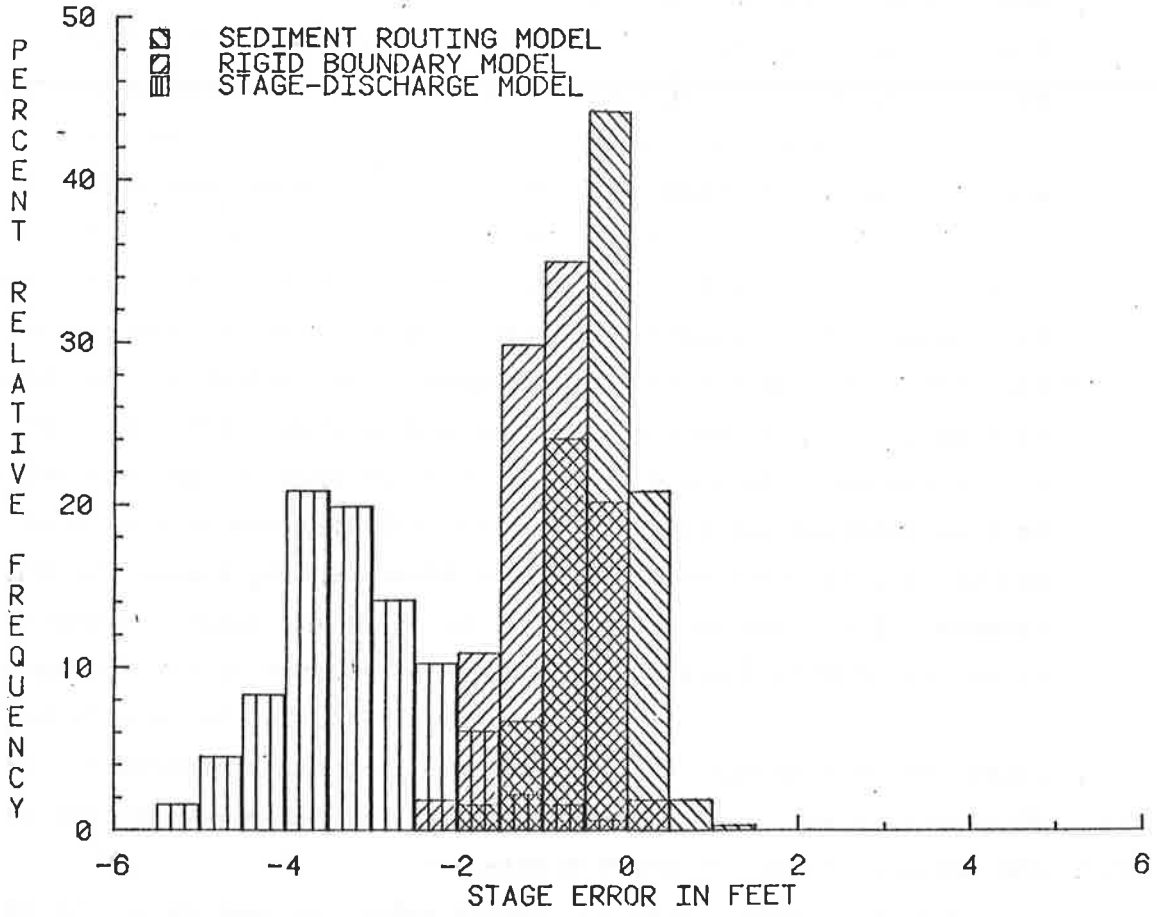

Figure 2.8 Model error frequency at Fort Pemberton.

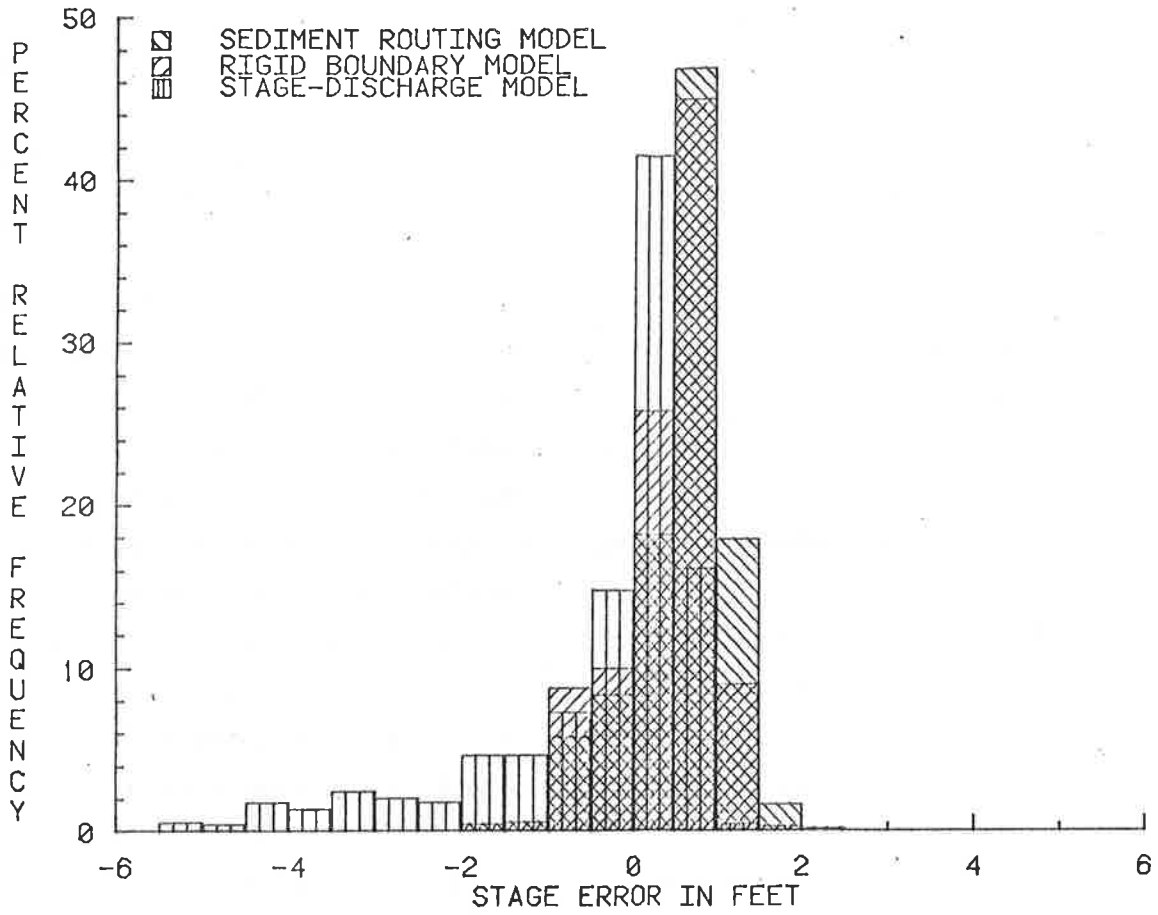

Figure 2.9 Model error frequency at Locopolis.

Table 2.1 Statistics of absolute model errors.

	Error in Feet			
	Calibrated		Verification	
	Mean	Maximum	Mean	Maximum
Stage-Discharge Model				
Fort Pemberton	2.56	10.38	3.47	7.27
Locopolis	0.33	2.56	0.80	5.48
Rigid Boundary Model				
Fort Pemberton	0.90	3.97	0.92	2.39
Locopolis	0.29	2.27	0.62	1.91
Sediment Routing Model				
Fort Pemberton	0.88	3.60	0.45	1.78
Locopolis	0.34	2.12	0.74	2.21

Since there are few channel changes in this reach, the results of the two process models, rigid boundary and movable bed, are essentially the same. At Fort Pemberton the sediment routing model is clearly better than the simple backwater model, assuming a rigid boundary bed, and is superior to the statistical approach because the sediment routing model predicts and adapts to changes in river conditions related to sediment movement and deposition. The stage-discharge and rigid boundary models, however, are based only upon limited historical conditions and cannot adapt to a changing environment.

Statistical prediction of river stage, though easy to apply, should be limited to stable rivers where there are adequate data over the range of flow conditions. The backwater model with rigid boundary assumption should be limited to stable reaches where little change in cross-sectional data occurs. However, since it can account for varying flow conditions, it can be used only where limited stage and discharge data are available. The sediment routing computer model that considers the physical significance of open channel flow and fluvial geomorphology and that computes changes in a river environment is the only feasible approach to predict the response of a river to man's activity, such as implementing a river cutoff, dredging or floodplain encroachment (see Chapter 9).

Road Water and Sediment Yield Using Graphs

Simons et al. (1977) developed a comprehensive mathematical model to predict water and sediment yield from road surfaces for the U.S.D.A.

Forest Service. The mathematical model was used with a large range of input to developed sets of graphs. The graphs related such variables as infiltration rate, soil detachment rate, and rainfall intensity, road gradient, cut and fill slope, sediment discharge and water discharge. These generated graphs can then be used by the forest planner or engineer to quickly estimate water and sediment yield from roadways of different designs. A set of these generated graphs is presented as Figures 2.10, 2.11, 2.12 and 2.13. Using these graphs sediment yield from a roadway can be rapidly estimated as the following example indicates.

Example Water Yield

Given:

Road surface longitudinal gradient: 3 percent
Length: 500 ft
Width: 10 ft
Soil: fine clay, bare soil surface, sediment size is 0.02 mm and porosity is 0.5 (Muren fine clay)
Design Storm: intensity 3 in./hr; duration 30 min
What is the total water yield of the storm:
the procedure follows:

Step 1: From Figure 2.11 with rainfall intensity 3 in./hr and Muren fine clay, one can estimate the ponding time

$$t_p = 8 \text{ min}$$

The ponding time is less than the duration of storm, and surface runoff occurs. Then the duration of excess rainfall is

$$D_e = D_t - t_p = 30 - 8 = 22 \text{ min}$$

where t_p is the ponding time from which runoff begins, D_e is the duration of excess rainfall, and D_t is the duration of storm.

Step 2: From Figure 2.12 with rainfall duration of 30 min and Muren fine clay, the excess rainfall rate

$$I_e = 1.25 \text{ in./hr}$$

where I_e is the excess rainfall rate.

Step 3: The total water yield is

$$Y_w = I_e D_e$$
$$= 1.25 \times 22/60$$
$$= 0.45 \text{ in.}$$

where Y_w is the water yield in depth of water.

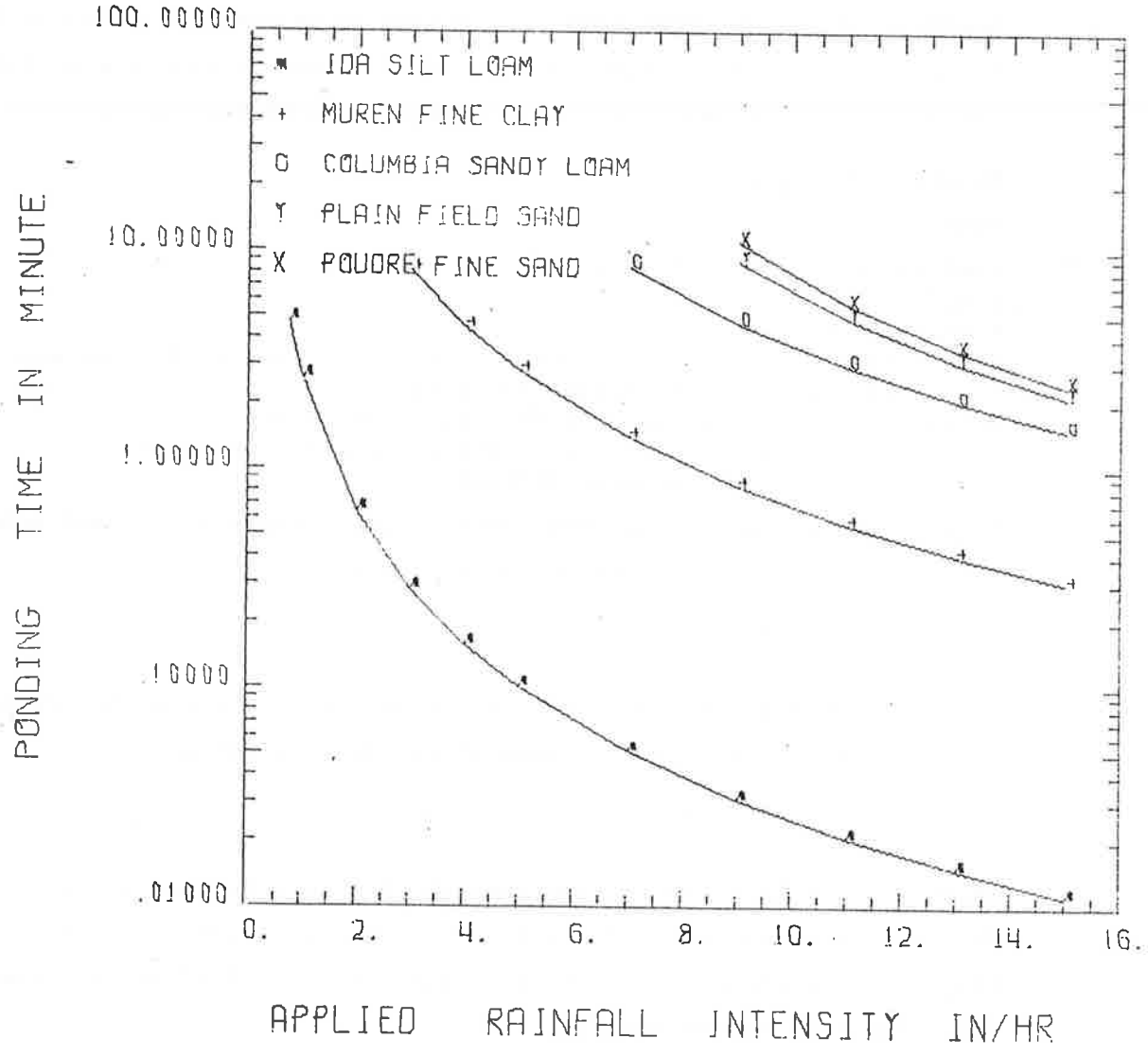

Figure 2.10 Ponding time for different rainfall intensity.

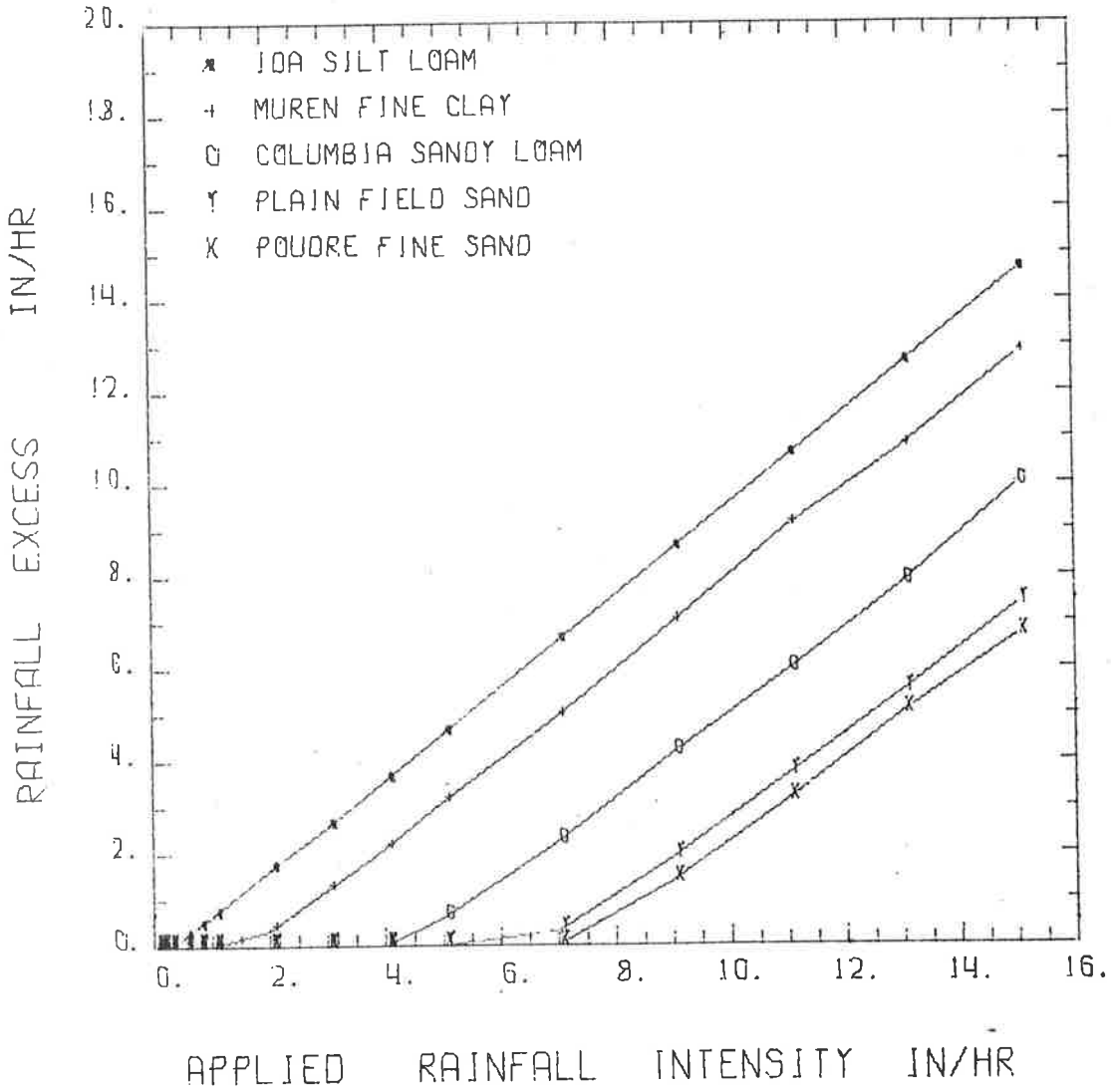

Figure 2.11 Rainfall excess rate versus rainfall intensity for storm duration of 30 minutes.

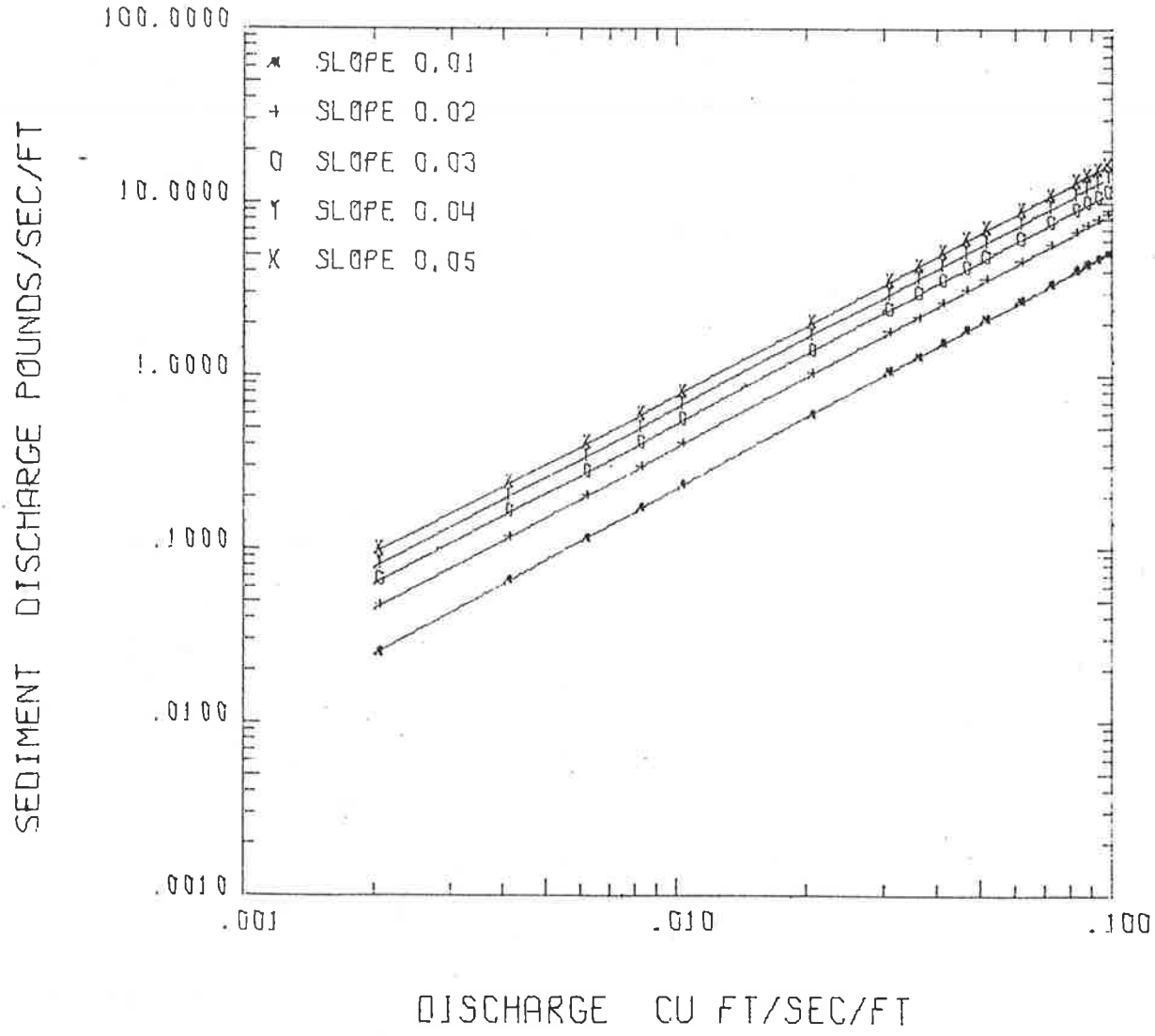

Figure 2.12 Sediment discharge versus water discharge for bare-soil road bed with slopes from 0.01 to 0.05 and for sediment size of 0.02 mm.

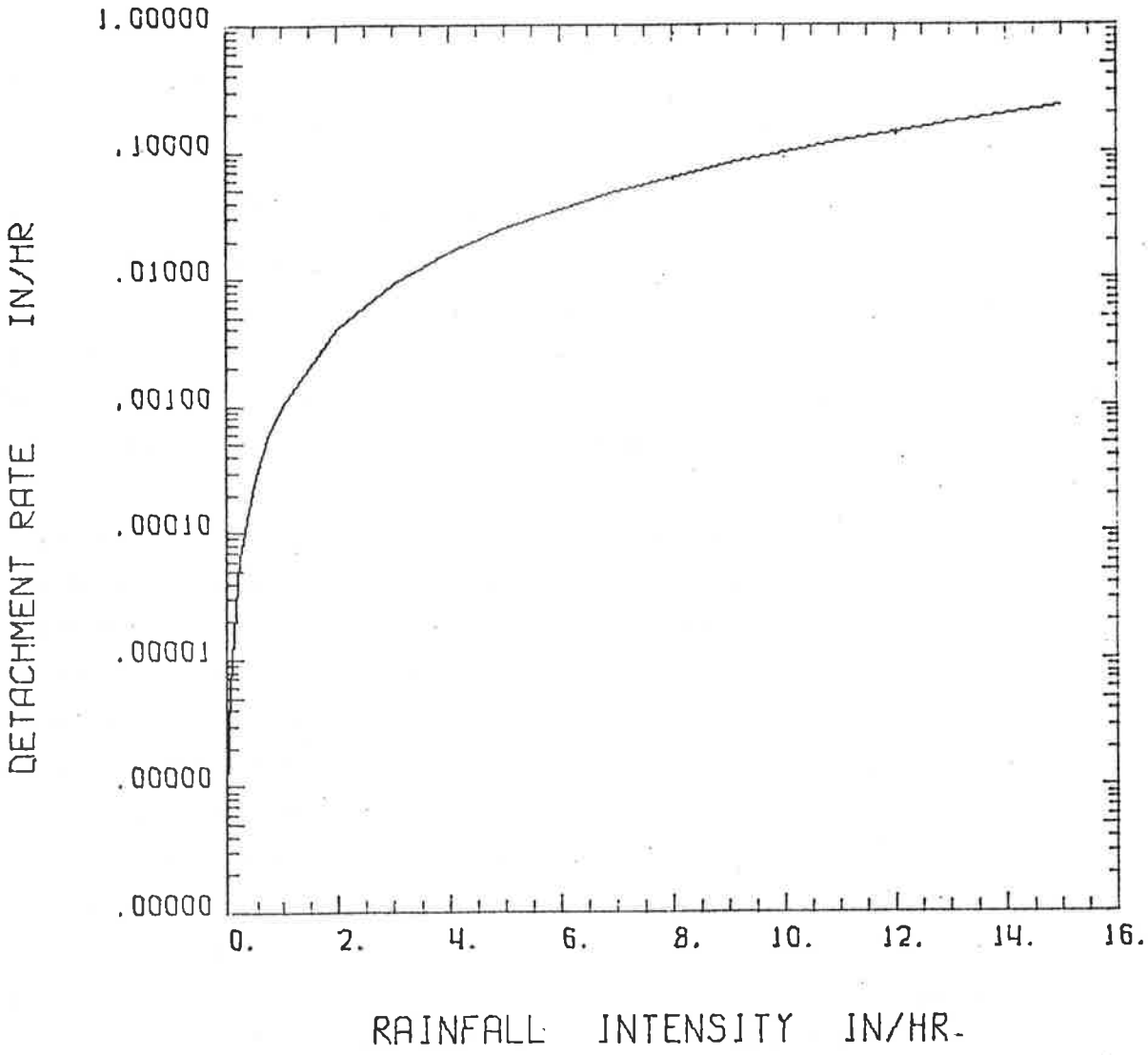

Figure 2.13 Assumed soil detachment by raindrop splash.

Large River Basin Analysis

In a study conducted for the U.S. Army Corps of Engineers, Vicksburg District, the sedimentation problems of the Yazoo River Basin were investigated (Simons et al., 1978). The Yazoo River Basin covers approximately 13,400 square miles in the northwest portion of Mississippi. A system analysis of the main channel and its tributaries was conducted by routing water sediment. The objective was to determine the effectiveness of a proposed system considering flood control, navigation, and the location and analysis of aggradation and degradation sites. Methods of minimizing operation and maintenance problems were also evaluated. This analysis provided a method for evaluating the Upper Yazoo Project and the various design alternatives outlined by the U.S. Army Corps of Engineers.

For analyzing a complicated system like the Yazoo River Basin, different levels of resolution in the analysis are needed to reach different objectives. Two mathematical models were developed to provide the required levels of resolution. One was for simulating flood and sediment movement in a short-time resolution (less than a day) involving the use of an unsteady flow model. This model is particularly useful in predicting flood movement in the Yazoo River system. A second model simulated the sediment movement only and assumed the water hydrographs were known. This simplified model involved use of the discharge synthesized technique and the known discharge uncoupled model for sediment routing. This model can be utilized to evaluate the response of the system using a larger time increment such as one or two days, or even longer. In this study a seven-day time increment for simulation was used since this is the approximate time required for water to travel through the system being analyzed. The closeness of weekly and daily flow statistics further validated the selection of a seven-day time increment for simulation. The primary objective of this study was to identify and analyze sedimentation problems. Consequently, the known discharge model was used extensively in the analysis.

In the Yazoo River Basin, tributaries to the main stem were divided into controlled, uncontrolled, and point source type streams. Controlled tributaries, for example the Yalobusha River, are regulated by large storage reservoirs, including Arkabutla, Sardis, Enid, and Grenada. The controlled tributaries significantly affect the response of the Basin.

Uncontrolled tributaries are generally smaller than controlled ones and do not have large storage reservoirs; however, they are important in analysis. An example of this type of tributary is Big Sand Creek. The third type of tributary is referred to as a point source and is generally smaller than the other two types. Point source tributaries are considered as a point input. The potential impact of sediment inflow from point source tributaries to the main stem is small. However, in order to conserve flow continuity, these tributaries were included in the analysis of the Yazoo system as point source inputs. An example of this type of tributary is Piney Creek.

The computer model developed to analyze the system was a physical process model based on the physical environment. Information provided by the model for the main stem included: water discharge, water level, sediment discharge, and aggradation or degradation of the channel. These outputs were simulated for different development alternatives and operating conditions of the river system, as previously identified. The input required was provided from output of the controlled and uncontrolled tributaries, and other point or nonpoint contributions from tributaries. Input for this type of model consists of water and sediment discharges from primary input sources, and lateral inflows or outflows from land surfaces. Reliable methods are needed to synthesize these required input data if measured data are not available. Because of a limited data base for the analysis, discharges from ungaged tributaries and nonpoint sources were synthesized utilizing watershed area and continuity concepts.

After calibration and verification, the model was utilized to evaluate design alternatives, identify the extent of sedimentation problems in the main stem and principal tributaries, and suggest possible remedies. (Calibration and verification of the known discharge sediment routing model is discussed in Chapter 12.) These alternative study runs were conducted by routing water and sediment through the tributaries and the Yazoo River main stem for a selected hydrograph utilizing the various alternative plans. A total of 15 alternative study runs were made. The alternative study runs included the natural conditions, the effects of land use, the effects of channelization, the effects of

construction scheduling, the various plans for reducing sediment supply from the tributaries, the different dredging schedules, and the proposed navigation channels. Some examples of these applications follow.

Figure 2.14 shows the beginning and final bed profiles after 50 years under natural conditions, that is, conditions with no development. The maximum water surface elevations are the maximum values at each cross section considering the 50-year simulation period. These values do not necessarily occur at the same time for all of the cross sections and may not take place during the period of maximum discharge. The downstream water surface elevations and the long-term sediment movement in the system will dictate local water surface elevations.

Examples of the stage-discharge relationship just below Greenwood Bendway (river mile 162.5) during the first year, 10th year, 30th year, and 47th year are displayed in Figure 2.15. The 47th year was selected because it closely approximated the 1973 flood. These figures indicated that the stage-discharge relationship at the station is consistent with time for the natural conditions.

Plan E, the plan recommended by the U.S. Army Corps of Engineers, was evaluated under the same hydrologic conditions. Figure 2.16 shows the beginning and final bed profiles as well as the maximum water surface elevations along the main stem assuming Plan E conditions and considering 50 years of simulation. This figure clearly indicates that the most critical areas for maintenance problems are the reaches below Abiaca Creek (river mile 140.34) and below the mouth of the P-Q Floodway (river mile 234.65). The maximum water surface levels are generally higher than those under natural conditions for reaches downstream of Money (river mile 192.9). The study shows that deposition rates of Plan E are much larger than those for natural river conditions. The computed average rate of deposition for Plan E decreases with time, which is consistent with changes in hydraulic conditions.

The stage-discharge relationship below Greenwood Bendway (river mile 162.5) for different time periods is shown in Figure 2.17. This figure indicates that the proposed Plan E would increase stage-wise with time due to significant deposition and can only be effective for flood control if maintenance dredging, control of sediment supply from tributaries, or other maintenance methods are implemented.

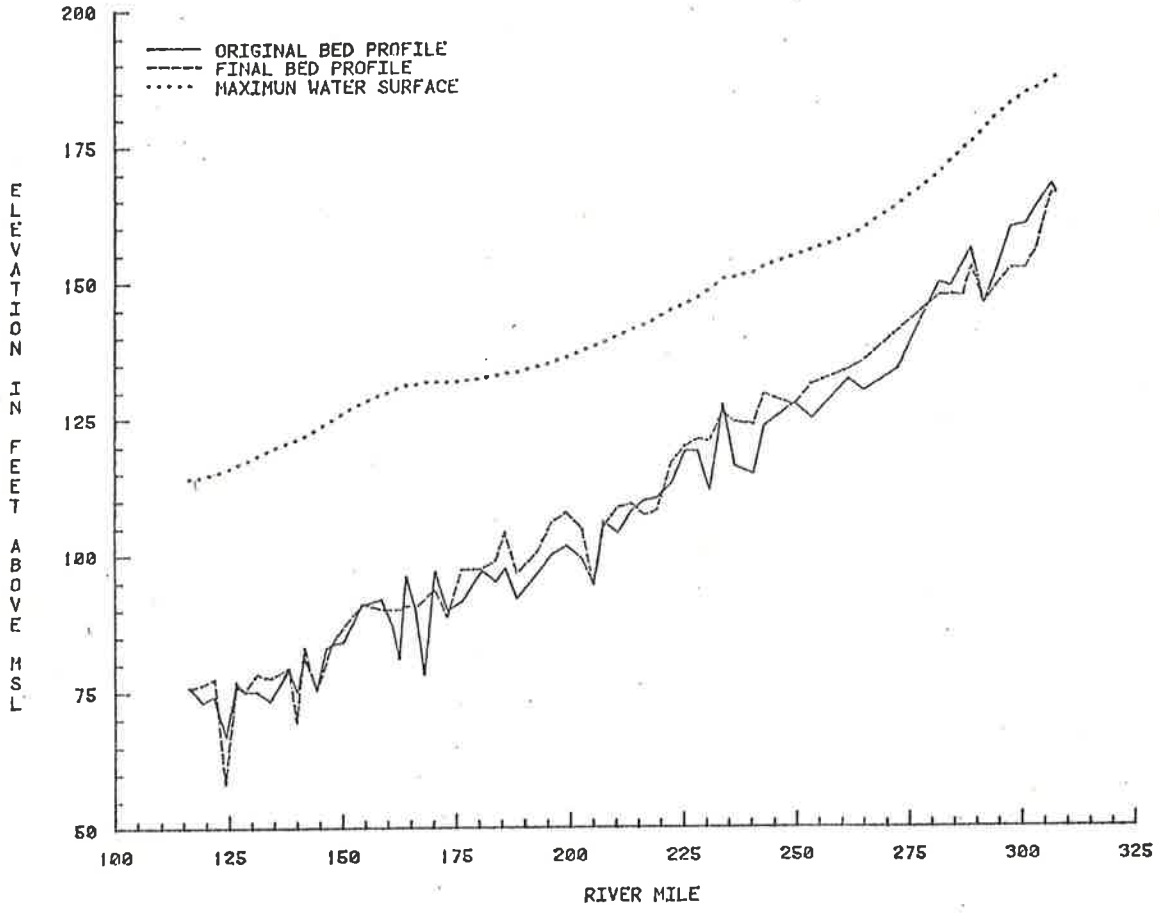

Figure 2.14 Beginning and final bed profiles and maximum water surface elevations for natural conditions (Run No. 1).

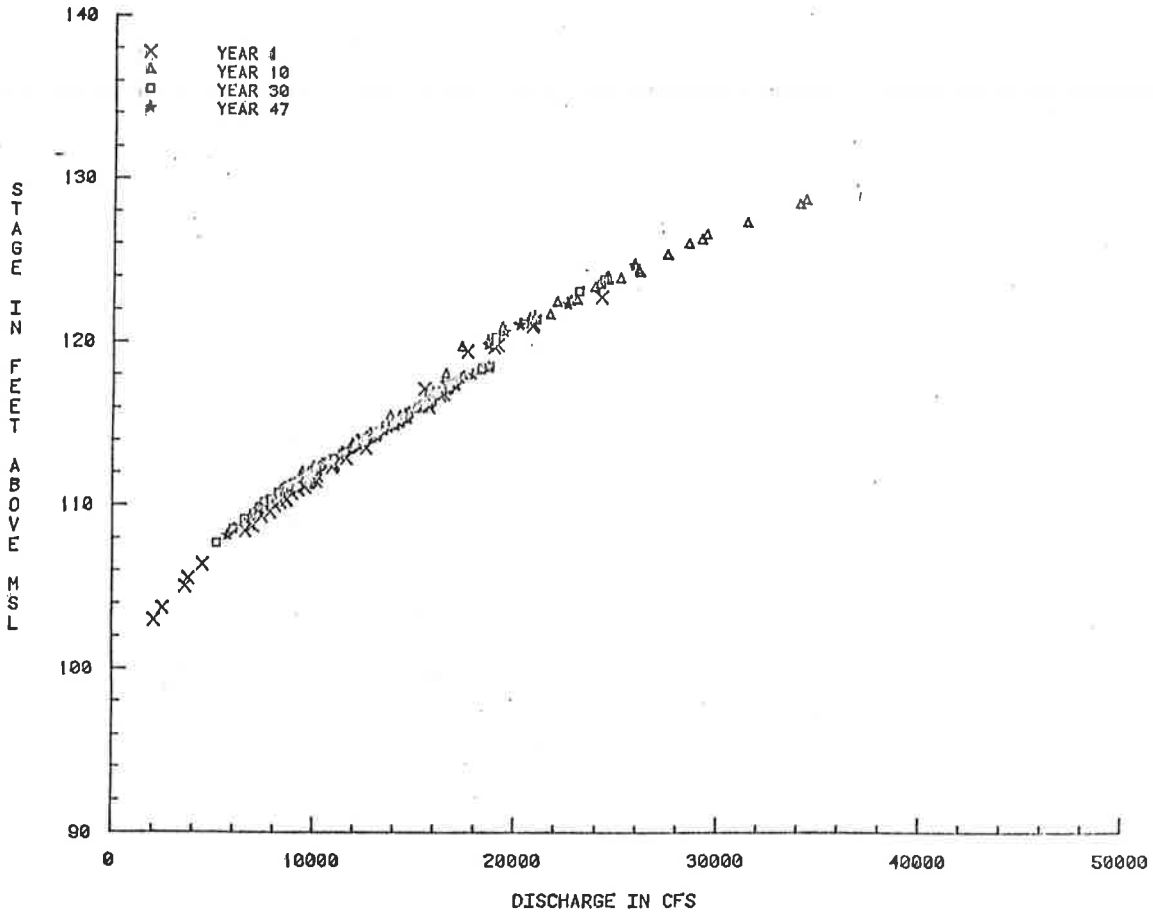

Figure 2.15 Stage-discharge relationship downstream of the Greenwood Bendway (river mile 162.5) for natural conditions.

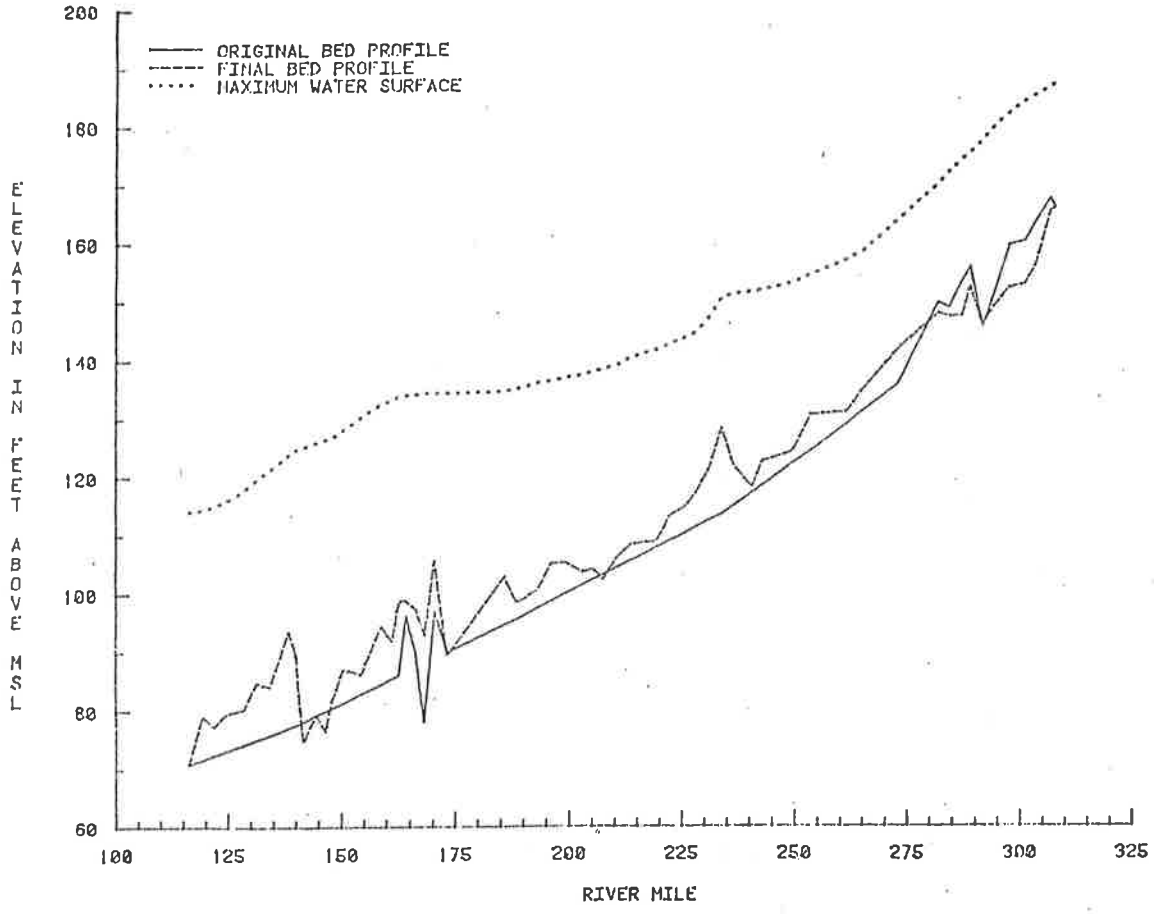

Figure 2.16 Beginning and final bed profiles and maximum water surface elevations for Plan E conditions (Run No. 2).

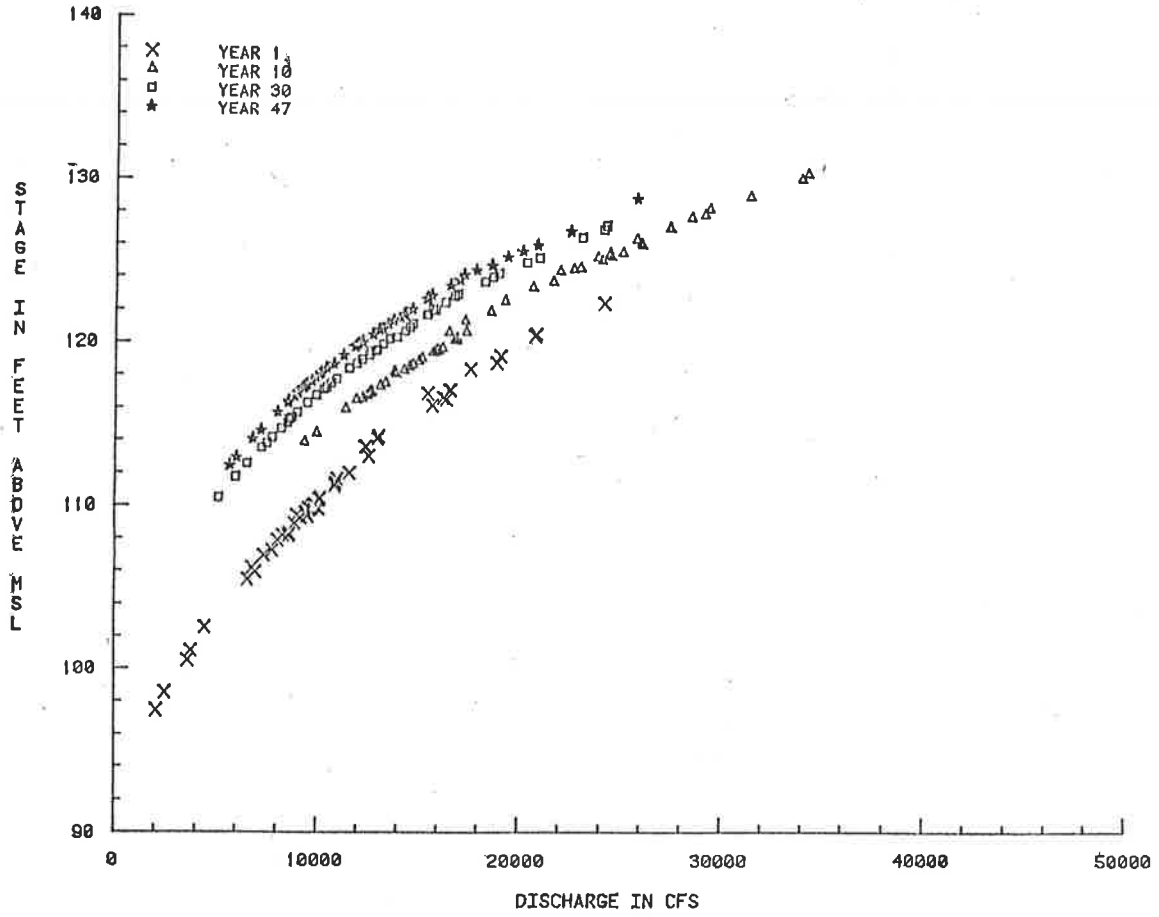

Figure 2.17 Stage-discharge relationship downstream of Greenwood Bendway (river mile 162.5) for Plan E.

Other examples of evaluation of design alternatives utilizing the developed mathematical model are given by Simons et al. (1978) and are also summarized in Chapter 20. The Yazoo Basin sedimentation study represents one of the most complicated river system analyses that has ever been conducted.

2.7 SUMMARY

This chapter presents a brief review of the state-of-the-art of watershed and river system analysis, identifies the important physical processes for analysis, describes the criteria of useful models, and for simulating watershed and river system response for application in water resources planning. Procedural steps for model development are discussed. Finally, brief descriptions of some significant examples of applications are given.

2.8 REFERENCES

Agricultural Research Service, United States Department of Agriculture, "Control of Water Pollution from Cropland," Vol. I-A, Manual for Guideline Development, November, 1975.

Bathurst, J. C., Li, R. M., and Simons, D. B., "Hydraulics of Mountain Rivers," Civil Engineering Department, Colorado State University, Fort Collins, 1979.

Hann, R., Jr. and Young, P., "Mathematical Models of Water Quality Parameters for Rivers and Estuaries," Technical Report No. 45, Water Resources Institute, Texas A and M University, College Station, Texas, 1972.

Leopold, L. B. and Maddock, T., Jr., "The Hydraulic Geometry of Stream Channels and Some Physiographic Implication," U.S. Geological Survey Professional Paper 252, 1953, 57 p.

Li, R. M., Brown, G. O., and Simons, D. B., "Computer Simulation of River Stage," to be presented, 1979 Summer Computer Simulation Conference, Toronto, Canada, July 16-18, 1979.

Li, R. M., Simons, D. B., and Simons, R. K., "A Mathematical Model for Evaluating On-site Soil Erosion," prepared for USDA Forest Service, Rocky Mountain Forest and Range Experiment Station, Flagstaff, Arizona, February, 1977.

Overton, D. E. and Meadows, M. E., Stormwater Modeling, Academic Press, New York, 1976.

Rosenbrock, H. H., "An Automatic Method for Finding the Greatest or Least Value of a Function," The Computer Journal, Vol. 3, 1960, pp. 175-184.

Schumm, S. A., The Fluvial System, Wiley Interscience, 1977, 338 p.

Simons, D. B., Al-Shaikh-Ali, K. S., and Li, R. M., "Flow Resistance in Cobble and Boulder Riverbeds," Paper approved for publication in the H. Hyd. Div., ASCE, 1978a.

Simons, D. B. and Li, R. M., "Watershed Segmentation by a Digital Computer for Mathematical Modeling of Watershed Response," prepared for USDA Forest Service, Rocky Mountain Forest and Range Experiment Station, Flagstaff, Arizona, December, 1975.

Simons, D. B. and Li, R. M., "Degradation Below the Emergency Spillway Chute of the Site 8C, T and C Williamsburg Watershed, New Mexico," prepared for USDA Soil Conservation Service, Albuquerque, New Mexico, March, 1978.

Simons, D. B. and Li, R. M., "Erosion and Sedimentation Analysis of San Juan Creek near Conrock Grand Pit, Orange County, California," prepared for Dames and Moore, Denver, Colorado, June, 1978.

Simons, D. B. and Li, R. M., "Analysis of Watershed and River Systems, In: Modeling of Rivers," H. W. Shen (ed.), John Wiley and Sons, New York, 1979.

Simons, D. B., Li, R. M., Brown, G. O., Chen, Y. H., Ward, T. J., Duong, N., and Ponce, V. M., "Sedimentation Study of the Yazoo River Basin--Phase I General Report," prepared for U.S. Army Corps of Engineers, Vicksburg, Mississippi, June, 1978.

Simons, D. B., Li, R. M., and Eggert, K. G., "Simple Water Routing and Yield Model Using Small Programmable Calculator," prepared for USDA Forest Service, Rocky Mountain Forest and Range Experiment Station, Flagstaff, Arizona, April, 1977.

Simons, D. B., Li, R. M., and Shiao, L. Y., "Formulation of Road Sediment Model," prepared for USDA Forest Service, Rocky Mountain Forest and Range Experiment Station, Flagstaff, Arizona, March, 1977.

Simons, D. B., Li, R. M., and Spronk, B. E., "Storm Water and Sediment Runoff Simulation for a System of Multiple Watersheds," prepared for USDA Forest Service, Rocky Mountain Forest and Range Experiment Station, Flagstaff, Arizona, April, 1978.

Simons, D. B., Li, R. M., and Stevens, M. A., "Development of Models for Predicting Water and Sediment Routing and Yield from Storms on Small Watersheds," prepared for USDA Forest Service, Rocky Mountain Forest and Range Experiment Station, Flagstaff, Arizona, 1975a.

Simons, D. B., Li, R. M., and Ward, T. J., "Simple Procedural Method for Estimating On-Site Soil Erosion," prepared for USDA Forest Service, Rocky Mountain Forest and Range Experiment Station, Flagstaff, Arizona, February, 1977a.

Simons, D. B., Ponce, V. M., Li, R. M., Chen, Y. H., Gessler, J., Ward, T. J., and Duong, N., "Flood Flows, Stages and Damages," CER77-78DBS-VMP-RML-HYC-JG-TJW-ND9, prepared for Land-Use Studies, Colorado State University Experiment Station, November, 1977a.

Simons, D. B., Schumm, S. A., Stevens, M. A., Chen, Y. H., and Lagasse, P. F., "A Geomorphic Study of Pools 24, 25 and 26 in Upper Mississippi and Lower Illinois Rivers," prepared for the Waterways Experiment Station, Vicksburg, Mississippi, 1975b.

Simons, D. B. and Sentürk, F., Sediment Transport Technology, Water Resource Publications, Fort Collins, Colorado, 1977.

Simons, D. B., Ward, T. J., and Li, R. M., "Sediment Sources and Impacts in the Fluvial System, In: Modeling of Rivers," H. W. Shen (ed.), John Wiley and Sons, New York, 1979.

Simons, R. K., Li, R. M., and Simons, D. B., "On Stage-Discharge Relations of Rivers," presented to the 17th Congress of International Association of Hydraulic Research, Baden-Baden, August 15-19, 1977.

U.S. Forest Service, "Non-point Water Quality Modeling in Wildland Management: A State-of-the-Art Assessment," USDA Forest Service Interagency Agreement No. EPA-IAG-05-0660, Washington, D.C., 1976.

Vanoni, V. A., editor, "Sedimentation Engineering," ASCE Manual and Report of Engineering Practice, No. 54, prepared by ASCE Task Committee for the preparation of the Manual on Sedimentation of the Sedimentation Committee of the Hydraulics Division.

CHAPTER 3

PHYSICAL PROCESSES GOVERNING RESPONSE OF WATERSHEDS AND RIVERS

by

Daryl B. Simons, Associate Dean for Engineering Research and Professor of Civil Engineering, Colorado State University, Fort Collins, Colorado.
Timothy J. Ward, Assistant Professor, Department of Civil Engineering, Colorado State University, Fort Collins, Colorado
Ruh-Ming Li, Associate Professor, Department of Civil Engineering, Colorado State University, Fort Collins, Colorado

3.1 INTRODUCTION

Representative descriptions, either written or mathematical, of a natural system rely on understanding the physical processes that govern the system. This holds true for climatologic, hydrologic, hydraulic and biologic systems. Only by recognizing and comprehending the myriad of complex processes can a system be correctly analyzed and the future response of the system be adequately estimated.

The fluvial system, composed of watershed, channels, and those entities that act on and react to them, is a prime example of a highly nonlinear complex system. The fluvial system includes hydrologic, hydraulic, geologic, soil, climatologic, biologic, and man's influences as subsystems or components. Each of these components is governed by physical processes that often affect other components. Because of the overlap and the complex nature of the processes, fluvial system components are often difficult to fully understand. However, current knowledge of the governing physical processes will permit a better depiction of the fluvial system.

In general, two types of forces are common to all components of the fluvial system, those resulting from gravity and those resulting from inertia, friction and cohesion. Gravity is involved in rainfall, infiltration, runoff, sediment movement, mass wasting, weathering, plant growth, and man's activities. Conversely, inertia, friction and/or cohesive forces sometimes undo the actions of gravity by developing flow resistance, landslide stability, and erosion resistance. Because gravity and friction-cohesion forces affect so many processes, their effects can be either positive or negative. For example, although gravity promotes downslope water movement resulting in soil erosion, it also prevents some soil particles from being eroded due to their weight.

Several approaches can be taken in delineating and analyzing physical processes that govern the fluvial system. As a first step, watersheds and rivers can be classified into different groups based on certain physical characteristics. These characteristics are usually a direct result of the physical processes that govern the system and therefore provide an initial view of the controlling phenomena. Once subdivided, watersheds and rivers can be described in terms of the processes that control their response. After these processes are

understood as well as possible, their relative importance can be evaluated. For example, raindrop splash is often an important process in upland watershed erosion, but it has little if any effect on a large river such as the Mississippi. These important physical processes should be considered to determine the qualitative and quantitative response of the system.

3.2 CLASSIFICATION OF WATERSHEDS AND RIVERS

General

Classification of watersheds and rivers is usually based on observable physical characteristics. These characteristics are the result of the governing physical processes (including man's influence) that determine the system configuration.

Classification systems utilize qualitative and quasi-quantitative descriptions. Qualitative descriptions are those that identify easily visualized physical characteristics of the system being described. Examples of these are descriptive terms for rivers such as meandering, straight and braided. Quasi-quantitative descriptions use numerical values to relate qualitative descriptions to one another. For example, a river with a certain degree of sinuosity, slope, and characteristic discharge can be classified as meandering based on the values of these variables. Use of quantitative means of description allows comparisons between areas on a more theoretical and less subjective basis.

Classifications reflect the morphology of the system in question. Although the physical processes controlling watershed and river systems overlap considerably, each has a set of processes that is extremely important. Therefore, classification systems for watersheds and river channels can provide considerable insight into the controlling physical processes.

Watershed Classification

There are many factors which combine to characterize a watershed (Figure 3.1). However, at present there does not seem to be any widely accepted or employed classification system used to categorize upland watersheds. This is largely caused by the wide diversity of watersheds and watershed conditions and the more intense interest in river classification systems. However, as the United States population continues

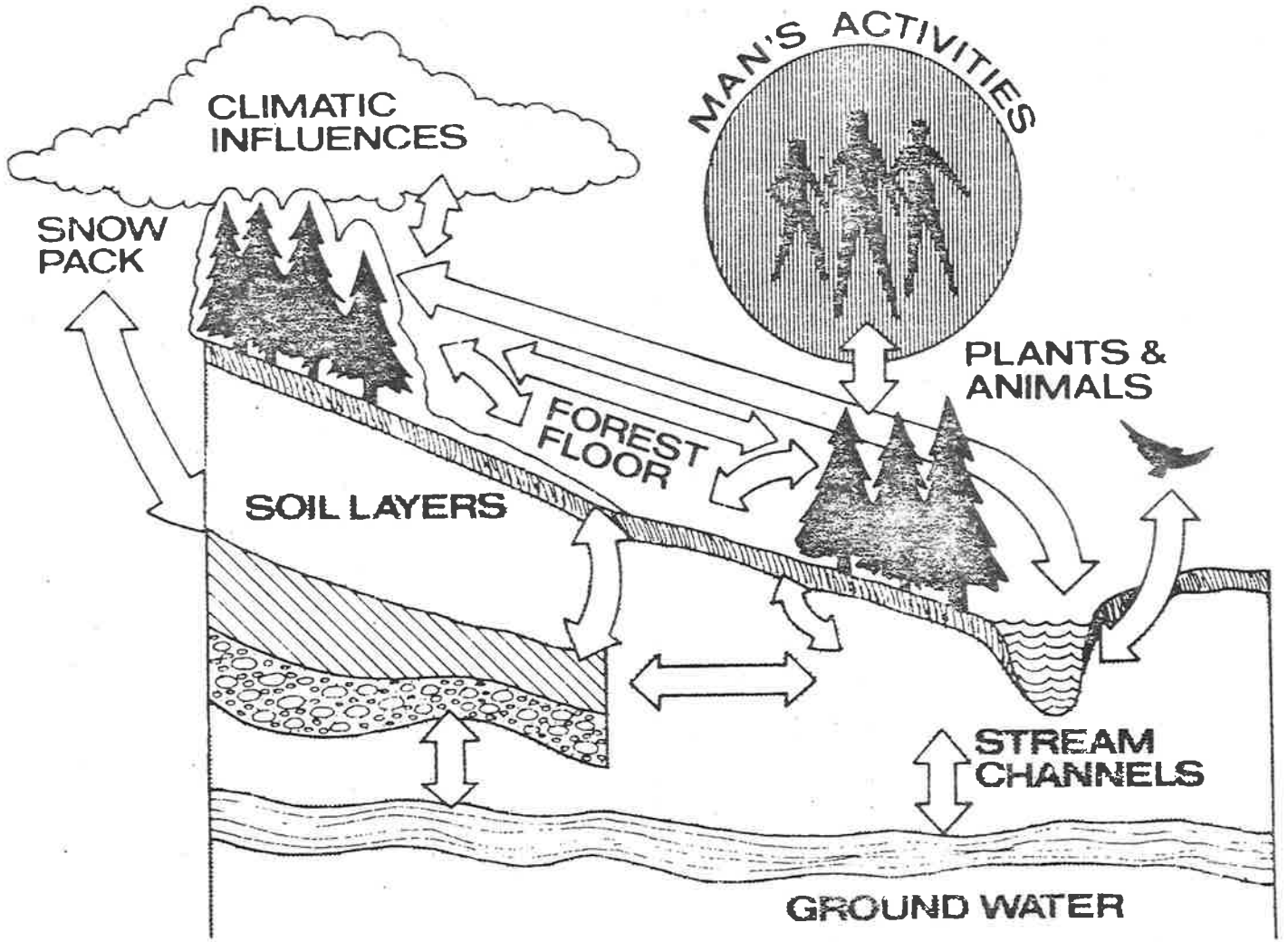

Figure 3.1 Some common factors used for characterizing watersheds.

to expand, and interest continues to increase in environmental issues, more emphasis will be placed on water, mineral resources, timber, energy, recreation, and residential uses on upland watersheds. This will necessitate a better understanding of processes and responses. Such an understanding can be partially attained through better classification schemes.

Research has identified various methods for quantifying watersheds according to morphological measures. Horton (1945) was one of the first to recognize and utilize the relationship between stream order and number and length of streams in that order. In general, drainage area and stream length increase as the stream order increases. But as stream order increases, the number of streams in that order decreases. Qualitatively, this says that a large stream has a large drainage basin and is longer than a small stream. However, "the Horton analysis" of a drainage basin does not provide a quantitative basis for these qualitative observations. Langbein et al. (1947) and Strahler (1952, 1957) developed methods for determining additional watershed indices. Many of the most widely used morphological characteristics and their related measurement techniques have been summarized by Chow (1964). Some of the widely used characteristics are watershed area, stream length, average main stream slope, drainage density (miles of stream per square mile of watershed area), measures of watershed shape such as circularity ratio (ratio of basin area to area of circle with same perimeter as basin), and watershed slope (such as average overland slope or relief ratio which is the total watershed relief divided by the distance from the outlet to the furthest point on the basin divide).

Little more in the way of watershed classification has been utilized beyond morphological measures. However, a watershed cannot be completely described by these measures alone. Indices of soils, geology, vegetation, hydrology, and hydraulics are also needed to more accurately describe the watershed. Pfankuch (1975) and Rosgen (1975) have presented methods for delineating important watershed channel characteristics that can lead to numerical and descriptive classifications of the channels. This is a positive step that should be extended to other parts of the watershed system. For example, a rating system or classification of sediment sources and yields from watersheds would

be helpful in describing this important aspect. Simons, Ward, and Li (1979) have delineated important sources of sediment in watersheds. More effort to establish a quantification scheme is needed.

It is currently possible, using experience gained from years of field inspections and modeling efforts, to develop a framework of watershed classification. This proposed framework, Table 3.1, is based on the primary needs of modeling and quantifying descriptions as determined from past experience.

Table 3.1 Proposed frameworks for classification of watersheds

Key Component	Possible Descriptors
GEOMETRY	Location, area, slope, drainage density, length of streams, channel characteristics
SOIL	Type, distribution, dominant size, erosivity, depth, texture
GEOLOGY	Bedrock and surficial types and distribution, structure, effects on hydrology and soils
VEGETATION	Overstory and understory types and distribution, interception, transpiration, stage of succession
CLIMATE	Precipitation type, seasonal occurrence, duration, frequency, temperature, evaporation
HYDROLOGY	Surface water, groundwater, infiltration interflow, peak discharges, yearly hydrographs, ephemeral or perennial discharge
SEDIMENT YIELD	Sources, erosion and transport mechanisms, sediment hydrograph characteristics
MAN'S INFLUENCE	Degree of development, type of development or construction activity, impacts on other components

As Table 3.1 indicates, there is the possibility for many different combinations of components for watershed classification. However, such a system would provide a common basis for comparison of different watersheds. For example, a watershed may be classified as listed in Table 3.2.

Although Table 3.2 gives fairly general descriptions, it does serve to show the myriad pieces of information needed to fully describe and classify a watershed.

River Classification

In contrast to the lack of a widely used watershed classification systems are the numerous schemes applied to rivers. Davis (1899) first suggested that rivers could be divided into three stages: youth, maturity, and old age. These stages were later subdivided based on the presence or absence of rapids, falls, meanders, oxbow lakes, flood plains, canyons, and other factors. In general with this system, a stream can range from youth to old age as it flows from its watershed to the ocean.

Although this system does not account for spatial variability, it provides an initial common classification language. Thornbury (1969) presented common valley classifications based on their development on the surface of the land. Although not precisely analagous, these patterns are often used for stream classification. These patterns are recognized as antecedent, superposed, consequent, and subsequent. Antecedent streams or valleys antidate structures that they cut across, such as a valley through an updomed area or a fault zone. A superposed stream extends across structures that are older than the stream but were covered by the original stream bed material. Erosion eventually removed this material and superposed the river on the structure. Consequent streams are a result of the initial land slope, while subsequent streams have been shifted from their original consequent courses to ones following weaker belts of rocks.

Schumm (1963, 1971) quantified the stream types by using discharge and type of sediment load (Table 3.3). These two independent variables determine alluvial channel (versus bedrock channels, which are controlled by the rock and its structure) morphology or how the stream will shape its channel.

Table 3.2 Example of a watershed classification using component system proposed in Table 3.1.

Key Component	Selected Descriptors
GEOMETRY	Area = 10 sq. miles Average channel slope = 0.05 Average overland slope = 0.25 Narrow, deep channel; width/depth = 3
SOIL	Gravelly sand loam predominates, sand sizes predominate Moderately erodible (gravel offers protection) Typically 20"-30" deep
GEOLOGY	Granitic rocks - primarily granodiorite. Some basalt flows Major fault in watershed and basalt-granodiorite contact provides zones of groundwater discharge
VEGETATION	Ponderosa pine (second growth) overstory Minimal understory from recent fire Sixty percent canopy cover Forty percent ground cover
CLIMATE	Winter snowfall ≈ 70% of yearly total Spring rain showers ≈ 15% of yearly total Summer thunderstorms ≈ 15% of yearly total Yearly precipitation average ≈ 25 inches Average January minimum temperature = 10^{o} F. Average July maximum temperature = 83^{o} F.
HYDROLOGY	Mixed ground and surface water flow Geologic controls force most of groundwater to surface at basin mouth Ephemeral stream Storm flow controlled by interflow
SEDIMENT YIELD	Primarily surface and rill erosion A few small landslides, little channel erosion Bedload transport of sand size particles
MAN'S INFLUENCE	Increased erosion near an unprotected roadway Some soil disturbance on logged areas

Table 3.3 Classification of alluvial channels.

Mode of Sediment Transport and Type of Channel	Channel Sediment (M) Percent	Bedload (Percentage of Total Load)	Channel Stability		
			Stable (Graded Stream)	Depositing (Excess Load)	Eroding (Deficiency of Load)
Suspended Load	20	3	Stable suspended-load channel. Width-depth ratio less than 10; sinuosity usually greater than 2.0; gradient relatively gentle.	Depositing suspended load channel. Major deposition on banks cause narrowing of channel; initial streambed deposition minor.	Eroding suspended-load channel. Streambed erosion predominant; initial channel widening minor.
Mixed Load	5-20	3-11	Stable mixed-load channel. Width-depth ratio greater than 10; less than 40; sinuosity usually less than 2.0; greater than 1.3; gradient moderate.	Depositing mixed-load channel. Initial major deposition on banks followed by streambed deposition.	Eroding mixed-load channel. Initial streambed erosion followed by channel widening.
Bed Load	5	11	Stable bed load channel. Width-depth ratio greater than 40; sinuosity, usually less than 1.3; gradient relatively steep.	Depositing bed load channel. Streambed deposition and island formation.	Eroding bed load channel. Little streambed erosion; channel widening predominant.

Simons et al. (1975) discusses how rivers, or segments of rivers, can also be generally classified as straight, meandering, braided, or some combination of these (Figure 3.2). Reaches of a river that are

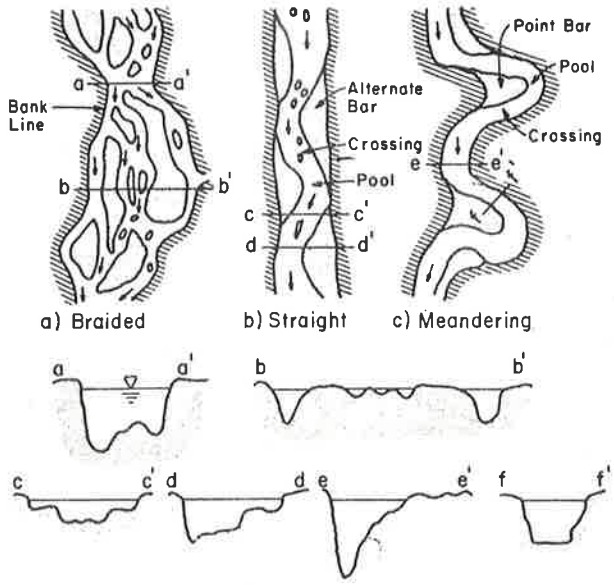

Figure 3.2 Typical river channel patterns (after Simons et al., 1975).

relatively straight over a long distance are generally unstable, as are divided flow reaches and those in which bends are rapidly migrating. Long straight reaches can be created by natural or man-made cutoffs of meander loops when long reaches of sinuous meandering channels with relatively flat slopes are converted to shorter reaches with much steeper slopes. Straight reaches can also be man-induced by contraction works such as dikes and revetment used to reduce or control sinuosity.

A braided channel is relatively wide with poorly defined unstable banks. It is characterized by a steep, shallow water course with multiple channel divisions around alluvial islands. Braiding is one pattern which can maintain quasi-equilibrium among the variables of discharge, sediment load, and transport capacity. Lane (1957) concluded the two primary causes that may be responsible for the braided condition generally are: the stream may be supplied with more sediment than it can now carry, resulting in deposition of part of the load,

and steep slopes which produce a wide shallow channel where bars and islands readily form.

Either one or both factors alone could be responsible for a braided pattern. If the channel is overloaded with sediment, deposition ensues, the bed aggrades, and channel slope increases in an effort to maintain a graded condition. As the channel steepens, the velocity increases, multiple channels develop and cause the overall channel system to braid. The multiple channels, which form when bars of sediment accumulate within the main channel, are generally unstable and change position over time and with stage fluctuations.

Another cause of braiding is easily eroded banks. If the banks are easily eroded, such as sand and gravel banks, the stream widens at high flow and during periods of low flow bars form which may become stabilized by armoring and vegetation, forming islands. In general, a braided channel has a steep slope, a large bed-material load in comparison with its suspended load, and relatively small amounts of silts and clay in the bed and banks. The precise response of a braided stream is difficult to predict because it is unstable, rapidly changes its alignment, carries large quantities of sediment, and is wide and shallow even at flood flow.

A meandering channel is one that consists of alternating bends, giving an S-shaped appearance to the plan view of the river. Lane (1957) concluded that a meandering stream has a channel alignment consisting principally of pronounced bends, the shapes of which have been determined predominantly by the varying nature of the terrain through which the channel passes. The meandering river consists of a series of deep pools in the bends and shallow crossings in the short straight reach connecting the bends. The thalweg flows from a pool through a crossing to the next pool, forming the typical S-curve of a single meander loop.

As shown schematically in Figure 3.2, the pools tend to be somewhat triangular in section with point bars located on the inside of the bend. In the crossing the channel tends to be more rectangular, widths are greater and depths are relatively shallow. During periods of low flow the local slope is steeper and velocities are larger in the crossings than in the pools. At low stages the thalweg is located very close to the outside of the bend. At higher stages, the thalweg tends to

More specifically, the thalweg moves away from the outside of the bend encroaching on the point bar to some degree. In extreme cases, the shifting of the current causes chute channels to develop across the point bar at high stages. In the crossings the channel is relatively shallower than in the pools and the banks may be more subject to erosion.

Because of the physical characteristics of straight, braided, and meandering streams, all natural channel patterns intergrade. Although braiding and meandering patterns are strikingly different, they actually represent extremes in a continuum of channel patterns. On the assumption that the pattern of a stream is determined by the interaction of numerous variables whose range in nature is continuous, it is not surprising that a river may exhibit braiding, straight and meandering forms. Alteration of the controlling parameters in a reach can change the character of a given stream from meandering to braided or vice versa. Studies have quantified this concept of a continuum of channel patterns. Khan (1971) related sinuosity, slope, and channel pattern (Figure 3.3). Any natural or artificial change which alters channel slope such as the cutoff of a meander loop, can result in modifications to the existing river pattern. A cutoff in a meandering channel shortens channel length, i.e., increases slope, tends to move the plotting position of the river to the right on Figure 3.3. This indicates a tendency to evolve from a controllable meandering pattern to a less controllable braided pattern that rapidly varies with

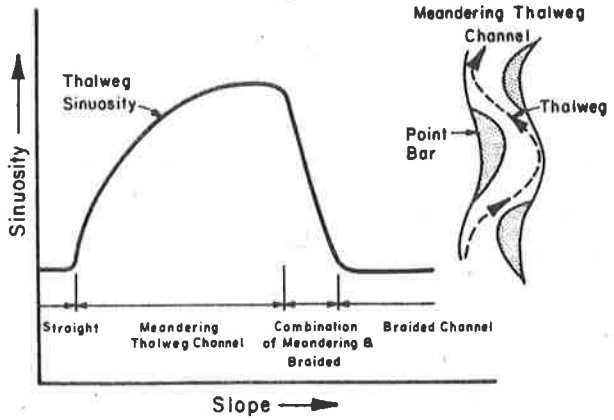

Figure 3.3 Sinuosity vs. slope with constant discharge relative to channel patterns (channel patterns are illustrated in Figure 3.2).

time, has high velocities, is subdivided by sandbars, and carries relatively large quantities of sediment. Conversely, a decrease in slope could change an unstable braided river into a more stable meandering pattern.

Lane (1957) suggested relationships among slope, discharge and channel patterns in meandering and braided streams, and observed that an equation of the form

$$SQ^{\frac{1}{4}} = K \qquad (3\text{-}1)$$

fits a large amount of data from meandering sand streams. Here S is the channel slope, Q is the water discharge, and K is a constant. Figure 3.4 summarizes Lane's results. If a river is meandering, but with a discharge and slope that borders on transitional, a relatively small increase in channel slope could initiate a tendency toward a transitional or braided character.

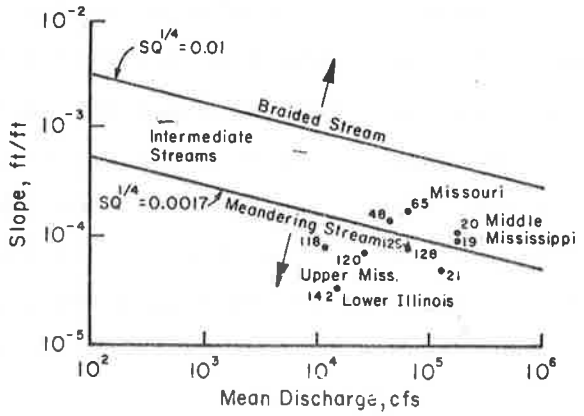

Figure 3.4 Slope-discharge relation for braiding or meandering in sand bed streams (Lane, 1957).

Another classification scheme that uses vegetation pattern, sinuosity, and bank characteristics has been proposed by Culbertson, Young and Brice (1967). Their contribution is summarized in Figure 3.5. Using this approach, a more descriptive classification can be developed.

There are other more complex classification schemes available (such as Garg's, 1972). Many of these have been compiled by Rundquist (1975). However, no matter what classification scheme is used, it should be remembered that the classification only applies to that

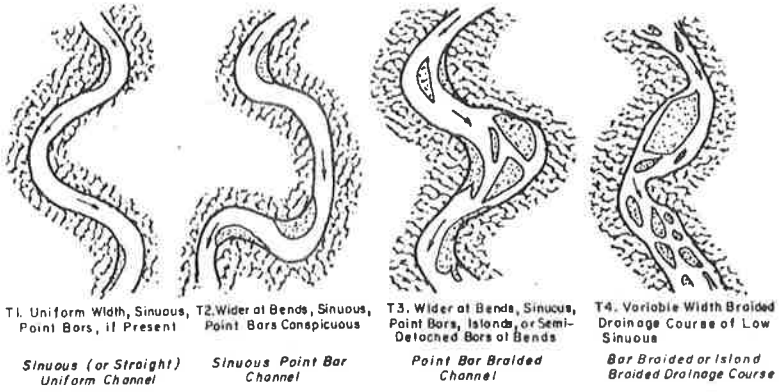

(a) Variability of Unvegetated Channel Width: Channel Pattern at Normal Discharge

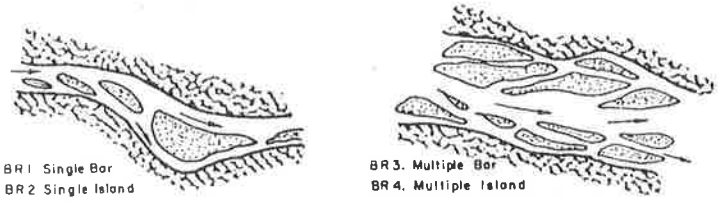

(b) Braiding Patterns

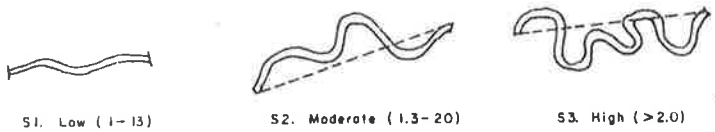

(c) Types of Sinuosities

Figure 3.5 Classification of river channels (after Culbertson et al., 1967).

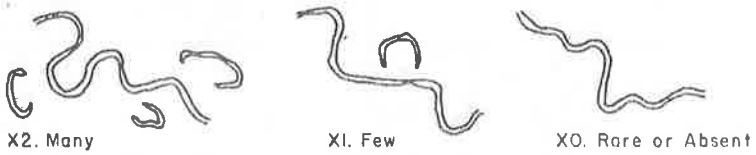

(d) Oxbow Lakes on Floodplain

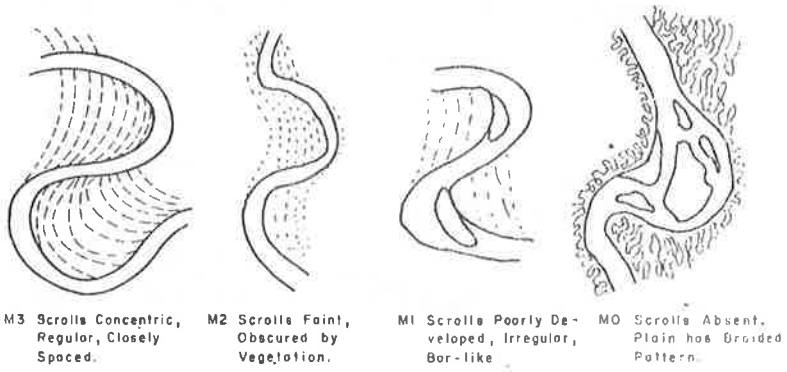

(e) Types of Meander Scroll Formations

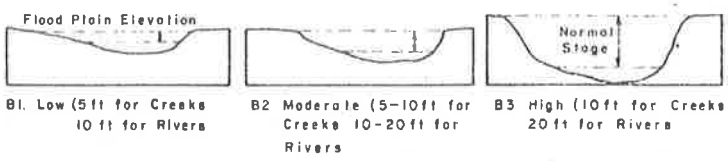

(f) Types of Bank Heights

Figure 3.5 (continued).

L0. No Levees | L1. Levees Mainly on Concave Bank | L2. Levees Well Developed on Both Banks

(g) Types of Natural Levee Formations

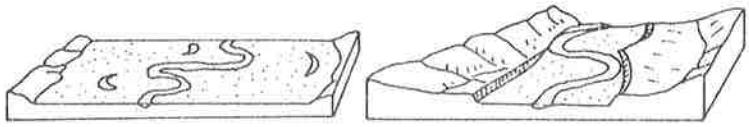

F2. Broad in Relation to Channel Width | F1. Narrow, Confined by Terraces or Valley Sides

(h) Types of Modern Floodplains

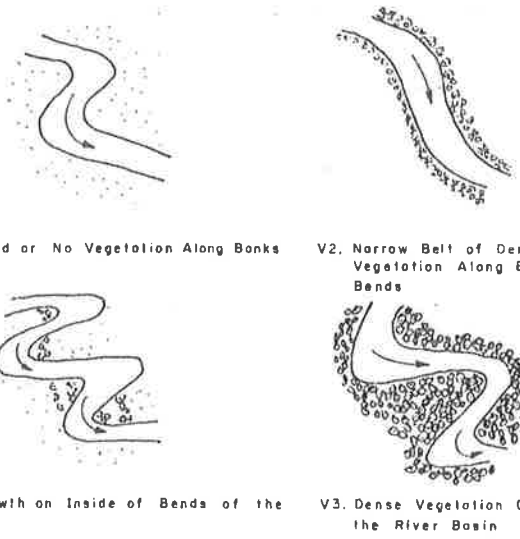

V0. Very Limited or No Vegetation Along Banks | V2. Narrow Belt of Dense Vegetation Along Both Bends

V1. Vegetal Growth on Inside of Bends of the Channel | V3. Dense Vegetation Growth in the River Basin

(i) Types of Vegetal Patterns

Figure 3.5 (continued).

segment of the system being analyzed at the time. Because river channels are very dynamic, the river form can change dramatically from location to location, in turn changing its classification.

Watershed and river channel classification systems are a reflection of the physical processes that govern their observable characteristics. Understanding the physical processes helps consideration of classification as well as determining future response of the system to natural or man-induced changes. Response of the system has been briefly presented in Figures 3.3 and 3.4. However, a more concise understanding of controlling factors is needed before the entire response of the system can be predicted.

3.3 PHYSICAL PROCESSES GOVERNING WATERSHED RESPONSE

The governing physical processes or quantities in watersheds can be divided into seven broad groups of topography, soils, geology, vegetation, climatic conditions, hydrology and hydraulics, and man's influence. These divisions are similar to those presented in Table 3.1. They are reconsidered here as the actual physical processes that govern the response of a watershed. Because all parts of a natural system are interrelated to some degree, there is some overlap between groupings that is not detailed here.

Topography, including land and channel slopes, aspect, and surface and channel geometry, is an expression of the morphological, geologic, and other erosive forces that have acted on the watershed. In turn these forces are modified by the topography they have created. For example, channel slope governs water discharge rate and sediment transport rate. Conversely, the discharge rate and the sediment transport can alter the channel form to produce a new slope. Aspects of land surfaces influence vegetative growth and soil moisture conditions, which in turn affect water yield. Channel and surface geometry affect the depth and velocity of water flow, thus altering sediment transport.

Soils

Watershed soil characteristics depend to a large extent on the parent geologic materials and the predominant weathering processes. For example, a light-colored silaceous type igneous rock will usually

produce more granular materials than an igneous rock containing relatively higher proportions of dark-colored minerals. This is caused by the chemical reactions and the formation of clay materials from the constituent minerals comprising the rocks. Clay minerals, abundance or lack of, affect soil properties, which govern or influence watershed response or other processes. Infiltration is a key example of a process controlled by soil characteristics. In general, sandier, more porous soils have higher infiltration rates than do clayey types. This differentiation will tend to create faster runoff from the clay soils, whereas the sandy soils may not permit (unless saturated) surface runoff. However, the sandy soils may lend themselves more to groundwater or interflow processes because of their rapid drainage characteristics. Soil mineralogy also influences soil moisture relationships, water quality, and vegetation growth. Size of surface soil particles or aggregates determines, given other conditions, the rate of water and wind-produced soil erosion. Soil type is a factor in the major types of sediment sources in watersheds: surface and rill gullies, landslides, and channels (Simons, Ward and Li, 1979). Soil characteristics are important physical quantities that describe watershed response.

Geology

Geology is important because it affects soils, vegetation, topography, and hydrology. Its effects on soils, and in turn on vegetation, have already been mentioned. Erosion-resistant rocks, large-scale erosive forces such as glaciation, and bedrock structure dictate the general topography--ridges, cliffs, plateaus, valleys--and the resultant channel and land surface configuration. Long-term surface adjustments through folding, faulting, isostatic rebound (e.g., rise in land surface after removal of ice), vulcanism, and changes in sea level are all important geologic processes. The effect of geology on hydrology is varied and extensive, resulting from the above mentioned processes and other influences on climate, such as the abrupt rise of the Sierra Nevada Mountains, creating a wet climate to the west and a dry, rain-shadowed climate to the east. Another influence that geology has on watershed hydrology is in helping determine the

relative importance of ground and surface water contributions in a basin. Typically, crystalline igneous terrain, unless highly fractured, is not noted for its sustained baseflow during dry periods. Sedimentary and metamorphic (in some cases) terrains are more often capable of sustaining baseflow. This difference is related to rock type and structure.

Vegetation

Vegetation plays important roles in water balance and soil stability in a watershed. It is well known that vegetation, usually in the form of trees or large brush, is a heavy user of water in watersheds. Through transpiration, interception, and evaporative processes, vegetation can substantially reduce water yield from a watershed. Reduction in the amount of vegetation or introduction of less consumptive types can decrease water use by plants. However, reduction in vegetation may have detrimental effects in that vegetation plays an important part in protecting the soil from erosion. Vegetation can: reduce the amount of water reaching the ground through interception, reduce rainfall intensities by providing an energy-absorbing cover, bind or reinforce surface materials into more erosion-resistant aggregates, reduce landslide hazards through binding and lowering soil water content, reduce overland and channel erosion by providing added roughness which retards water velocity, and provide organic debris for stream channels, creating stairstep configurations, thus lowering flow energy and transport capacity. Trees and large brush also assist in maintaining water quality by shading stream channels.

Climate

Climate and its associated meteorological components are important processes affecting response in a watershed. These components, however, are influenced by topography, vegetation, and geologic features, but to a much lesser extent than they affect these and other watershed processes and quantities. Important climatic or meteorological processes are related to precipitation, temperature, solar radiation, and wind.

Precipitation occurs as a solid, liquid, or aerosol (mist, fog), all of which eventually manifest themselves in the watershed in

liquid form. Snowfall and snowpack present unusual problems in that the melt rate, distribution, sublimation, interception, inter-snow packs and sub-snow packs, waterflow, and wind effects are all long-term processes having lag effects that are complex and not easily delineated. In addition, freeze-thaw effects caused by temperature variations within and external to the snowpack add more complexity to the heat and mass transfer aspects of the pack. Also, little is known about the erosion processes that occur at the snowpack-soil surface interface. Although snow and snowpack processes are important in many watersheds, in governing water yield, runoff hydrographs, and sediment yield, a better understanding of these complex processes are needed. Rainfall, because it is already in liquid form, is more easily understood in terms of its related processes. Of primary importance are volume, time distribution intensity, spatial distribution, and duration. Intensity affects runoff occurrence and soil erosion from raindrop splash, whereas volume, intensity, duration, and spatial duration help determine (along with other processes) the water hydrograph and yield from a storm. Mist or fog, although not recognized as primary sources of runoff, can create antecedent moisture conditions, such as reduced interception or increased soil moisture, that can alter the water balance during subsequent storms.

Temperature not only affects the type of precipitation, but infiltration rate because higher temperature water is less viscous and flows faster through the soil. Temperature also influences snowpack dynamics, vegetation growth, and freeze-thaw phenomena.

Solar radiation is extremely important, but often hard to work with, in understanding the long-term response of a watershed. Fortunately, incoming solar radiation is constant for the time span of most interest to the engineer. Alterations or influences on radiation reaching a soil surface occur from airborne particulates, gases, water vapor, and vegetation. Although important in studying long-term balances, such as water yield, in a watershed, we often neglect solar radiation when examining short-term phenomena such as storm runoff. Solar radiation does influence, to a major extent, most climatic processes, vegetation, snowpack dynamics, and soil-water

balance. Solar radiation and its effects on other processes must be considered in watershed analyses.

Wind is not often given enough attention as being an important process in watersheds. It does, however, affect evaporation, sublimation, snow redistribution, transpiration, rainfall intensity and distribution, wind erosion, vegetation stability, and landslide potential (from vibrating soil caused by wind sway in trees). Wind is usually considered in water balance-energy balance studies, but neglected in short-term rainfall-runoff storm analyses because of its variability.

Hydrology and Hydraulics

Hydrology and hydraulic processes in watersheds are heavily influenced and interrelated with the other important processes. Two important processes should be recognized as belonging to this broad group. These are water flow and sediment transport. Controlling both are gravity, resistance, and other related watershed processes. Water flow is the result of many complex interactions. It can be described by two basic concepts; continuity and momentum. Continuity is a mass balance which means, in general, input minus output is the change in storage of the system. For example, if two inches of rain produces one inch of runoff, then the other inch either is retained in the system or lost to other outputs such as evaporation, transpiration, or regional groundwater flow. The momentum equation is a force balance of inertial, gravity, and frictional components. These two concepts govern the movement of water. Similarly, the movement of sediment is described by the sediment continuity concept. Again this concept, like water continuity, describes the input, output and storage change of sediment in the watershed.

Complementary to these concepts are those dealing with the specifics of water and sediment movement. In steep watersheds, the energy slope in the momentum concept or equation can be assumed equal to the land surface or channel slope. Such an assumption permits major simplifications in descriptive modeling of a watershed. This assumption is permissible because other components in the momentum equation are relatively minor compared to the surface slope. Descriptive relations for infiltration, evapotranspiration, and groundwater flows are also important in organizing and identifying each segment of the water

continuity equation. Sediment transport is usually considered in three parts:

1) bed load - sediment movement primarily along the surface,
2) suspended load - sediment transport primarily in the flow with some contact with the bed, and
3) wash load - fine particles not found in appreciable quantities in the bed material suspended in the flow.

Bed load and suspended load can be described by transport equations as they are usually related to water discharge. Wash load, however, is more dependent on supply conditions. In upland watersheds, the concept of supply and capacity is crucial, as it determines the sediment yield. Typically, transport capacity for small sizes (e.g., wash load) is in excess of supply. Therefore, the yield is related to the supply. Conversely, for large sizes the capacity is much less than the supply (e.g., large cobbles in a mountain stream), therefore capacity controls. More details of sediment yield processes can be found in Chapter 10, water yield processes in Chapters 7 and 8. In general, the hydrology and hydraulics of a watershed are expressions of the other physical processes and accounting on balance concepts. Understanding these processes must be coupled with understanding the other processes.

Man's Influence

Man's influences are not natural physical processes in a strict sense. They do, however, tend to affect other processes to some degree, and in doing so create watershed responses that can be beneficial or deleterious. Although there are many influences, such as dam building, intermountain diversions, removal of vegetation, alteration of hillslopes, road building, energy and mineral resource acquisition, and recreational and agricultural uses, only a simple example will be presented here that encompasses several processes.

Timbering is a well known and long practiced resource acquisition activity in the United States. However, sometimes techniques have been used that alter the natural processes and create adverse impacts. For example, if a watershed is clear-cut, water yield may increase and provide more water for domestic and industrial use because the trees no longer are transpiring the water. However, the increased water yield may result in higher streamflow levels that produce more channel erosion

and instability. At the same time, removal of the vegetation can expose the soil surface to rainfall and snowmelt erosion, thus promoting sediment yield. Increased groundwater levels and lack of vegetative anchoring may lead to higher landslide risk in steep watersheds. Landslides, if they do occur, can produce large quantities of sediment that affect the sediment yields and other activities (refer to Chapter 13). Loss of cover and increased organic debris can have an adverse water quality impact on the stream through increased: sediment, water temperatures and BOD loading.

The above simple example illustrates several key concepts. First, physical processes controlling watershed response are varied, complex, and interrelated. Second, man's influence can have ripple effects as they are passed between processes, and third, understanding of watershed response must encompass several distinct but related subjects.

3.4 PHYSICAL PROCESS VARIABLES AND RIVER MECHANICS GOVERNING CHANNEL RESPONSE

General

In general, the physical process groupings described previously for watersheds are also applicable to stream or river channels. However, the importance of each can be considerably different between the watershed and the channel system. In addition, the specific effects of each element in the broad groups can be quite different for two systems. For example, vegetation in the watershed affects several different processes whereas in the channel it usually affects flow resistance and the stability of river banks and islands.

The major physical processes in an alluvial channel are those related to water discharge, channel slope and shape, geology and soils, sediment transport, vegetative effects, and again, man's influence. As in the watershed, each of these is intertwined in a set of complex relationships. Again bedrock channels have a restricted set of conditions while alluvial channel conditions are more general.

Water discharge is a key process, resulting from other processes, that affects channel shape and sediment transport. Discharge variables of velocity, depth, and flow area are important in analysis of channel response. Coinciding with these are channel shape, channel slope and flow resistance from grains and bed forms. Geology and soils of the

channel bottom and banks help determine the relative erodibility of the system and, therefore, its response to other changes or alterations. Local variations in geology, soils, vegetation and flow rate play important roles in determining bank stability in channels. Sediment transport in channels differs from watersheds because there is often more material available for transport than can be carried. Vegetation is an importnat variable in channel systems. Often, it is bank vegetation that resists erosion during periods of high flow. Similarly, vegetation tends to stabilize interchannel bars and islands thus producing an added resistance in the channel. These banks and bars can substantially alter flow lines and channel movement.

A more complete understanding of the physical processes governing channel response can be attained through a study of important river mechanics concepts, processes and relations. Some of these were previously presented in Section 3.2 and Figures 3.3 and 3.4 as related to channel form. Other important processes and variables follow.

Generalized Hydraulics of Open Channel Flow

General

Fundamentals of rigid boundary open channel flow described in this section have been excerpted from Richardson et al. (1974) and Simons, Lagasse, Chen and Schumm (1975). The open channel flow water surface is not confined and surface configuration, flow pattern and pressure distribution within the flow depend on gravity. In rigid boundary open channel flow, no deformations or movements of the bed and banks are considered. One-dimensional analysis of flow is considered; that is, the direction of velocity and acceleration are large only in one direction and are so small as to be negligible in all other directions.

Open channel flow can be classified as: 1) uniform or nonuniform flow, 2) steady or unsteady flow, 3) laminar or turbulent flow, and 4) tranquil or rapid flow. In uniform flow, the depth and discharge remain constant with respect to space. Also the velocity at a given depth is the same everywhere. In steady flow, no change occurs with respect to time. In laminar flow, the flow field can be characterized by layers of fluid, one layer not mixing with adjacent ones. Turbulent

flow on the other hand is characterized by random fluid motion. Tranquil flow is distinguished from rapid flow by a dimensionless number called the Froude number Fr where $Fr = \frac{V}{\sqrt{gd}}$ and V is average velocity, g is acceleration of gravity, and d is flow depth. If $Fr < 1$, the flow is tranquil; if $Fr > 1$, the flow is rapid, and if $Fr = 1$, the flow is called critical.

Open channel flow can be nonuniform, unsteady, turbulent and rapid at the same time. Because the classifying characteristics are independent, 16 flow types are possible.

Basic Principles

The basic equations of flow in open channels are derived from the three conservation laws. These are: 1) the conservation of mass, 2) the conservation of linear momentum, and 3) the conservation of energy. Conservation of mass means (except for mass-energy interchange) matter can neither be created nor destroyed. The principle of conservation of linear momentum is based on Newton's second law of motion which states that a mass (of fluid) accelerates in the direction of and in porportion to the applied forces on the mass. The principle of conservation of energy is based on the First Law of Thermodynamics.

Much simplification in the analysis of flow problems can result if there is no acceleration of the flow or if the acceleration is primarily in one direction and the accelerations in other directions being negligible. Inaccuracies may occur if small or zero accelerations are assumed when they are not. Concepts presented here assume one-dimensional flow and derivations of the basic equations utilize a control volume. A control volume is an arbitrarily shaped isolated volume in the body of the fluid, through which mass, momentum, and energy can be convected. The control volume may be assumed fixed in space or moving with the fluid. A stream tube is a control volume bounded by streamlines. Fluid containing mass, momentum and energy enters at 1 and leaves at 2 (Figure 3.6). Because steady flow is assumed, there can be no storage within the stream tube. Acting on the stream tube boundaries are the fluid pressures p_1 and p_2 and shear stresses τ.

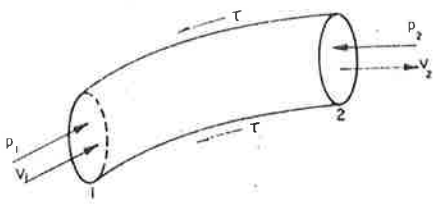

Figure 3.6 A stream tube as a control volume.

Continuity Equation. The principle of conservation of mass is that matter can be neither created nor destroyed. Mathematically for the stream tube the principle can be expressed

$$\rho_1 A_1 V_1 = \rho_2 A_2 V_2 \ , \tag{3-2}$$

where ρ_1 is the mass density of the fluid entering the stream tube with velocity V_1 at Section 1 with cross-section area A_1 and leaving with a mass density ρ_2 and velocity V_2 at Section 2 with area A_2. The velocity vectors V_1 and V_2 are perpendicular to the areas A_1 and A_2. The weight rate of flow is written $\gamma_1 A_1 V_1 = \gamma_2 A_2 V_2$ where γ is the specific weight and is given by $\gamma = \rho g$, where g is the acceleration of gravity.

If the mass density is constant (incompressible flow) then Equation 3-2 becomes the Continuity equation or

$$Q = A_1 V_1 = A_2 V_2 \tag{3-3}$$

where Q is the flow discharge.

Momentum Equation. The conservation of momentum is based on Newton's second law of motion applied to the fluid within the control volume. The equation expressing Newton's second law of motion is

$$F_i = ma_i \tag{3-4}$$

where the left side of the equation is the summation of all external forces acting on the fluid (pressure and shear forces on the boundary) and the right side of the equation includes the product of the mass and the change in velocity (acceleration) either in direction or magnitude that results from the force. It is a vector equation, hence, the subscript i denotes the components of an orthogonal coordinate system.

The momentum equation is derived by writing the Newtonian equation in the differential impulse momentum form

$$d\ F_i dt = d\ M_i \tag{3-5}$$

For steady flow with constant density, integration between Section 1 and 2 yields

$$\Sigma F_i = M_{i2} - M_{i1} \tag{3-6}$$

where ΣF_i is the summation of all forces acting in the i direction on the fluid within the control volume and M_i is the change in momentum between Sections 1 and 2 resulting from the external forces (momentum flux into and out of the control volume) or

$$M_i = \rho \int v_i dQ \tag{3-7}$$

where v_i is the velocity in the i direction. For channel flows it is more convenient to treat average velocities at a cross section, using an integrated momentum flux and a correction coefficient β to account for the velocity variation in the cross section. The momentum term M_i then is

$$M_i = \beta \rho Q V_i \tag{3-8}$$

With these changes, Equation 3-6 for steady, incompressible flow becomes

$$\Sigma F_i = \rho Q[(\beta V_i)_2 - (\beta V_i)_1] \tag{3-9}$$

The coefficient β normally varies from 1 to 1.05 and is often assumed to be unity. In cartesian coordinates with directions x, y, and z, and for $\beta = 1$ Equation 3-9 becomes

$$\Sigma F_x = \rho Q(V_{x_2} - V_{x_1}) \tag{3-10}$$

$$\Sigma F_y = \rho Q(V_{y_2} - V_{y_1}) \tag{3-11}$$

$$\Sigma F_z = \rho Q(V_{z_2} - V_{z_1}) \tag{3-12}$$

Energy Equation. Energy can exist in many forms (light, heat, chemical, mechanical, petrochemicals) and every process of nature involves

conversion of energy from one form to another. In hydraulics the principal forms of energy are:

1) E_K, kinetic energy per unit mass ($V^2/2$),
2) E_p, pressure energy per unit mass (p/ρ),
3) E_e, potential energy per unit mass (gz),
4) E_H, heat energy per unit mass (gH_L), and
5) E_M, mechanical energy per unit mass added by a pump or subtracted by a turbine (gH_m).

Note that z is an elevation above some arbitrary fixed datum. The law of conservation of energy (First Law of Thermodynamics) states that energy can neither be created nor destroyed therefore the above energy forms must sum to a constant or

$$E_K + E_p + E_e + E_H + E_m = \text{Constant} \tag{3-13}$$

or dividing each term by the local gravitational acceleration and substituting gives

$$V^2/2g + p/\gamma + z + H_L + H_m = \text{Constant} \tag{3-14}$$

In this form, the energy within a fluid system is based on unit weights of fluid. The energy equation is a scalar equation and accounts for net efflux of energy from a control volume plus input of energy from outside the control volume minus the energy expended (transferred) from the control volume to its surroundings. As the present development is for a control volume which is a stream tube, and a stream tube becomes a streamline as its cross-sectional area is gradually reduced, Equations 3-13 and 3-14 apply to a streamline. It is convenient also to be able to apply the energy equation to a larger control volume, say one which encompasses an entire channel cross section and a measurable length of the channel. For this control volume, it is more convenient to use an average cross-sectional velocity. In general, the velocity differs for different streamlines in a cross section. Consequently, a kinetic energy correction factor α must be introduced. Thus, Equation 3-14, neglecting mechanical energy input for open channel flow, may be rewritten as

$$\alpha_1 \frac{V_1^2}{2g} + \frac{p_1}{\gamma} + z_1 = \alpha_2 \frac{V_2^2}{2g} + \frac{p_2}{\gamma} + z_2 + H_L \qquad (3\text{-}15)$$

The subscripts 1 and 2 refer to upstream and downstream cross sections of the channel respectively. When $\alpha = 1$ and $H_L = 0$, Equation 3-15 is commonly referred to as the Bernoulli equation which can also be derived from the equation of motion (F = ma). If derived from the equation of motion it is called the Euler equation.

Steady Uniform Flow

Introduction. In steady, uniform open channel flow there are no accelerations, streamlines are straight and parallel and the pressure distribution is hydrostatic. Hydrostatic means that only pressure and fluid weight forces act on the flow. The slope of the water surface S_w, bed surface S_o and the energy grade line S_f are equal to each other and equal to the head loss term in the energy equation divided by the length of reach (Figure 3.7).

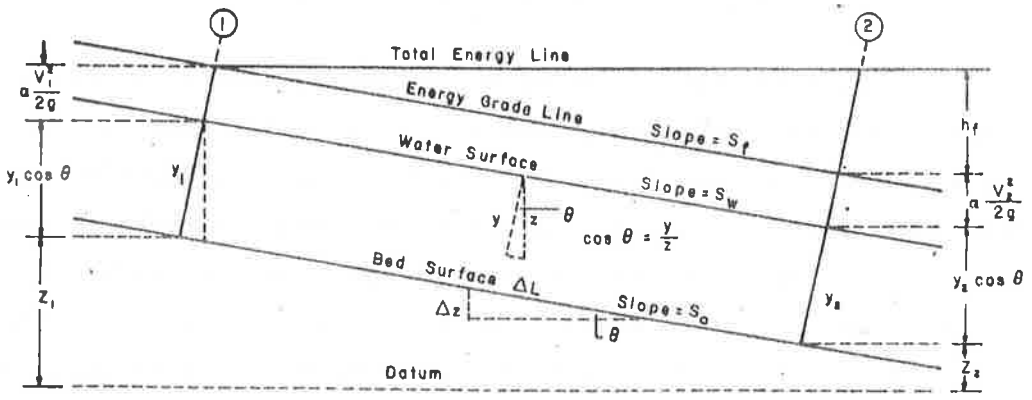

Figure 3.7 Definition sketch for steady uniform flow.

The energy equation from Section 1 to Section 2 can be written

$$z_1 + y_1 \cos\theta + \alpha \frac{V_1^2}{2g} = z_2 + y_2 \cos\theta + \alpha \frac{V_2^2}{2g} + H_L \qquad (3\text{-}16)$$

for most natural channels θ is small and $y \cos\theta \approx y$ and in general $\alpha \approx 1$. The slopes of the bed, water surface and energy grade line are:

$$S_o = \sin \theta = \frac{z_1 - z_2}{L} \tag{3-17}$$

$$S_w = \frac{(z_1+y_1)-(z_2+y_2)}{L} = \frac{z_1 - z_2}{L} \tag{3-18}$$

$$S_f = \frac{H_L}{L} = \frac{z_1 - z_2}{L} \tag{3-19}$$

Steady uniform flow is an idealized concept for open channel flow. However, for many applications the flow is steady and the changes in width, depth or direction (resulting in nonuniform flow) are so small that the flow can be considered uniform. In other cases when changes occur over a long distance, the flow is considered gradually varied flow. However, in other cases the changes are large enough that the accelerations cannot be neglected (rapidly varied flow and flow around bends). Steady, uniform flow is probably the simplest of the flow fields to analyze and provides a framework for analysis of other flow conditions.

Variables of interest for steady uniform flow are 1) the mean velocity V, 2) the discharge Q, 3) the velocity distribution $v(y)$ in the vertical, 4) the head loss H_L through the reach, and 5) the shear stress, both local τ and at the bed τ_o. The variables are interrelated and which variable we determine and how we determine it depends on the data available. For example, if the discharge and cross-sectional area are known, the mean velocity is easily determined for some suitable equation such as Manning's or Chezy's equation.

Empirical Velocity Equations. Because of the difficulties involved in determining the shear and hence the velocity distribution in turbulent flows an empirical approach to determine mean velocities in rivers has generally been utilized. Two such empirical equations are in common use. They are the Manning equation

$$V = \frac{1.486}{n} R^{2/3} S_f^{1/2} \tag{3-20}$$

and the Chezy equation

$$V = CR^{1/2} S_f^{1/2} \tag{3-21}$$

where V is the average velocity in the cross section, n is Manning's roughness coefficient, R is the hydraulic radius equal to the cross-sectional area A divided by the wetted perimeter P, S_f is the energy slope of the channel, and C is Chezy's discharge coefficient. In these equations, the boundary shear stress is expressed implicitly in the roughness coefficient n or in the discharge coefficient C. By equating the velocity determined from Manning's equation with the velocity determined from Chezy's equation, the relation between the coefficients is

$$C = \frac{1.486}{n} R^{1/6} \tag{3-22}$$

If the flow is gradually varied, Manning's and Chezy's equations are used with the energy slope S_f replaced with an average friction slope $S_{f_{ave}}$. The term $S_{f_{ave}}$ is determined by averaging over a short time increment at a station or over a short length increment at an instant of time, or both.

Over many decades sets of values for Manning's n and Chezy's C have been assembled so that an engineer can estimate the appropriate value by knowing the general nature of the channel boundaries. Such values are given by Barnes (1967), Chow (1959), and Simons and Senturk (1977).

Average Boundary Shear Stress. The shear stress at the boundary τ_o for steady uniform flow is determined by applying the conservation of mass and momentum principles. Such an analysis yields

$$\tau_o = \gamma \frac{A}{P} \sin\theta \tag{3-23}$$

The term A/P is called the hydraulic radius R. If the channel slope angle is small

$$\sin\theta \simeq \tan\theta = S_o$$

and the average shear stress on the boundary is

$$\tau_o = \gamma R S_o \tag{3-24}$$

If the flow is gradually varied, the average boundary shear stress is

$$\tau_o = \gamma R S_f \tag{3-25}$$

where S_f is the slope of the energy grade line.

Hydraulics of Steady Flow in Bends

The hydraulics of steady flow in a rigid boundary bend provides the basis for understanding the morphology of alluvial channel bendways. The change in flow direction around bends produces centrifugal forces which result in a higher elevation on the concave (outside) bank than on the convex (inside) bank. The resulting transverse slope can be evaluated using cylindrical coordinates as sketched in Figure 3.8. The

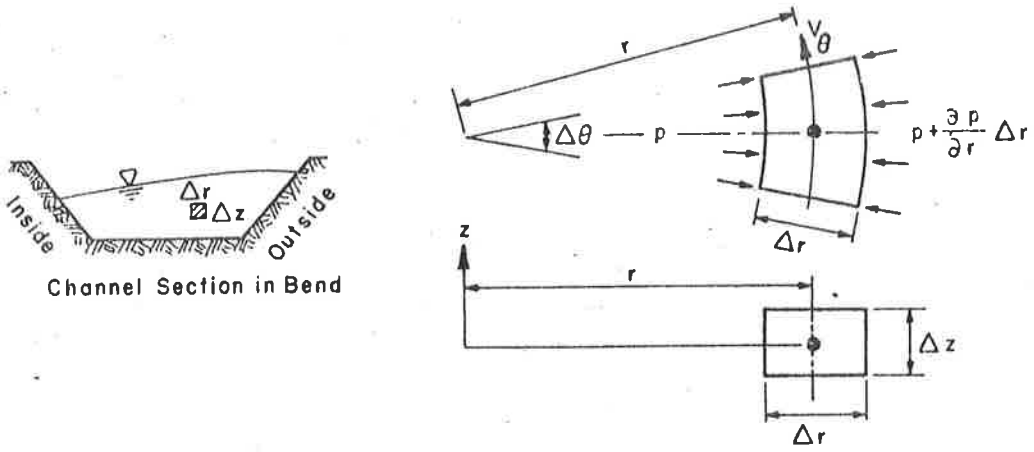

Figure 3.8 Definition sketch of dynamics of flow around a bend.

differential pressure in the radial direction can be obtained by equating radial forces to the product of mass and radial acceleration:

$$[p - (p + \frac{\partial p}{\partial r}\delta r)]r\delta\theta\delta z = -(\rho\delta r\delta z r\delta\theta)\frac{V_\theta^2}{r}$$

$$\frac{1}{\rho}\frac{\partial p}{\partial r} = \frac{V_\theta^2}{r} \tag{3-26}$$

The total superelevation between outer and inner bank is

$$\Delta z = \frac{1}{\rho g}\int_{p_i}^{p_o} dp = \frac{1}{g}\int_{r_i}^{r_o}\frac{V_\theta^2}{r}\,dr \tag{3-27}$$

Assuming that radial and vertical velocities are small compared to the tangential velocities, or $V_\theta \simeq V$, and that the pressure distribution in the bend is hydrostatic, or $p = \gamma h$, yields:

$$\Delta z = \frac{1}{g} \int_{r_i}^{r_o} \frac{V^2}{r} dr \tag{3-28}$$

Equation 3-28 can be solved if the velocity distribution along the radius of the bend is known or assumed. For example, if V is the average velocity, or Q/A, and r equals the radius to the center of the stream, r_c, then

$$\Delta z = \frac{1}{g} \int_{r_i}^{r_o} \frac{V^2}{r_c} dr$$

$$\Delta z = z_o - z_i = \frac{V^2}{g r_c} (r_o - r_i) \tag{3-29}$$

where z_i and r_i are the water surface elevation and radius at the inside of the bend, and z_o and r_o are the same parameters at the outside of the bend.

Additional expressions for superelevation can be obtained by assuming that the velocity distribution approximates that of a free vortex, $V = c/r$, or a forced vortex $V = cr$, or combinations of these. However, Equation 3-29 serves the purpose of illustrating the basic characteristics of flow in bends.

Superelevation in bends produces a transverse velocity distribution which results from an imbalance of radial forces on a fluid particle as it travels around the bend. Radial forces acting in a bend are the centrifugal force mv^2/r and the differential hydrostatic force $\gamma(dz)^2$ caused by the differential superelevation dz of the water surface. The centrifugal force is greater near the surface where the fluid velocity v is greater, and less near the bed where v is smaller. The differential hydrostatic force is uniform throughout the depth of the section. A summation of differential head and centrifugal forces shows an absence of equilibrium in the fluid in the plane of the stream cross

section. This summation indicates the presence of a transverse flow directed toward the concave bank in the upper part of the section and a reverse flow toward the convex bank along the bottom. Transverse currents, superimposed on the longitudinal flow, form the screw-like, helicoidal secondary circulation observed in river bends and laboratory flumes. These transverse currents, with a magnitude of about 15 percent of the average current velocity, have been cited as the primary mechanism for scour and deposition in bends. The heuristic argument has been that in the upper portions of the cross section secondary currents increase bank line erosion on the concave bank, and as they flow along the bottom, sweep heavy concentrations of sediment toward the convex bank where deposition forms point bars.

Steady Gradually Varied Flow

Introduction. In uniform flow, acceleration forces are zero and energy is converted to heat as a result of viscous forces within the flow; there are no changes in cross section or flow direction and the depth (called normal depth) is constant. In steady uniform flow, the slope of the bed, the slope of the water surface and the slope of the energy grade line are all parallel and are equal to the head loss divided by the length of channel in which the loss occurred. Steady gradually varied flow is nonuniform in that changes in depth and velocity take place slowly over large distances. Resistance to flow dominates and acceleration forces are neglected. The study of this type of flow involves: 1) the determination of the general characteristics of the water surface and 2) the elevation of the water surface or depth of flow.

In gradually varied flow, the actual flow depth y is either larger than or smaller than the normal depth y_o and either larger than or smaller than the critical depth y_c. The water surface profiles which are often called backwater curves, depend on the magnitude of the actual depth of flow y in relation to the normal depth y_o and the critical depth y_c. Normal depth y_o is the depth of flow that would exist for uniform flow as determined from the Manning or Chezy equation and the critical depth is the depth of flow when the Froude number equals 1.0. Flow at the critical depth y_c implies that the local flow

velocity V is equal to the velocity of propagation of a small gravity wave $\sqrt{gy}$ on the free surface.

Flow depth can be different from the normal depth because of changes in slope of the bed, changes in cross section, obstruction to flow, and imbalances between gravitational forces accelerating the flow and shear forces retarding the flow.

In working with gradually varied flow, the first step is to determine what type of backwater curve would exist. The second step is to perform the numerical computations.

Classification of Flow Profiles. The classification of flow profiles is obtained by analyzing the change of the various terms in the total head equation in the x-direction. The total head is

$$H_T = \frac{V^2}{2g} + y + z \tag{3-30}$$

or

$$H_T = \frac{Q^2}{2gA^2} + y + z \tag{3-31}$$

Then assuming a wide channel for simplicity

$$\frac{dH_T}{dx} = -\frac{q^2}{gy^3}\frac{dy}{dx} + \frac{dy}{dx} + \frac{dz}{dx} \tag{3-32}$$

where the flow per unit width is

$$q = Vy \tag{3-33}$$

The term $-dH_T/dx$ is the slope of the energy grade line S_f. For short distances and small changes in y the energy gradient can be evaluated using Manning's or Chezy's equation.

When Chezy's equation is used, the expression for dH_T/dx is

$$-\frac{dH_T}{dx} = S_f = \frac{q^2}{C^2y^3} \tag{3-34}$$

The term $-dy/dx$ is the slope of the water surface S_w and $-dz/dx$ is the bed slope S_o. For steady uniform flow, the bed slope is (from Equation 3-21)

$$S_o = \frac{q^2}{C_o^2 y_o^3} \tag{3-35}$$

where the subscript o indicates the steady uniform flow values.

When Equations 3-34 and 3-35 are substituted into Equation 3-32, the familiar form of the gradually varied flow equation results

$$\frac{dy}{dx} = S_o \left\{ \frac{1 - \left(\frac{C_o}{C}\right)^2 \left(\frac{y_o}{y}\right)^3}{1 - \left(\frac{y_c}{y}\right)^3} \right\} \tag{3-36}$$

If Manning's equation is used to evaluate S_f and S_o, Equation 3-36 becomes

$$\frac{dy}{dx} = S_o \left\{ \frac{1 - \left(\frac{n}{n_o}\right)^2 \left(\frac{y_o}{y}\right)^{10/3}}{1 - \left(\frac{y_c}{y}\right)^3} \right\} \tag{3-37}$$

The slope of the water surface $\frac{dy}{dx}$ depends on the slope of the bed S_o, the ratio of the normal depth y_o to the actual depth y and the ratio of the critical depth y_c to the actual depth y. The difference between flow resistance n_o for steady uniform flow and flow resistance n for steady nonuniform flow is small and the ratio is taken as 1.0. With $n = n_o$, there are 12 types of water surface profiles. These are summarized in Table 3.4 and illustrated in Figures 3.9 and 3.10. When y approaches y_c, the assumption that acceleration forces can be neglected no longer holds. Equations 3-36 and 3-37 indicate that $\frac{dy}{dx}$ is perpendicular when y approaches y_c. For sections close to the cross section where the flow is critical (a distance of from 10 to 50 feet) curvilinear flow analysis and experimentation must be used to determine the actual values of y. When analyzing long distances (100 to 1000 feet or longer) one can assume qualitatively that y reaches y_c. In general when the flow is rapid (Fr $\geq$ 1), the flow cannot become tranquil without a hydraulic jump occurring. In contrast, tranquil flow can become rapid (cross the critical depth line).

Table 3.4 Characteristics of water surface profiles.

Class	Bed Slope	Depth	Type	Classification
Mild	$S_o>0$	$y>y_o>y_c$	1	M_1
Mild	$S_o>0$	$y_o>y>y_c$	2	M_2
Mild	$S_o>0$	$y_o>y_c>y$	3	M_3
Critical	$S_o>0$	$y>y_o=y_c$	1	C_1
Critical	$S_o>0$	$y<y=y_c$	3	C_3
Steep	$S_o>0$	$y>y_c>y_o$	1	S_1
Steep	$S_o>0$	$y_c>y>y_o$	2	S_2
Steep	$S_o>0$	$y_c>y_o>y$	3	S_3
Horizontal	$S_o=0$	$y>y_c$	2	H_2
Horizontal	$S_o=0$	$y_c>y$	3	H_3
Adverse	$S_o<0$	$y>y_c$	2	A_2
Adverse	$S_o<0$	$y_c>y$	3	A_3

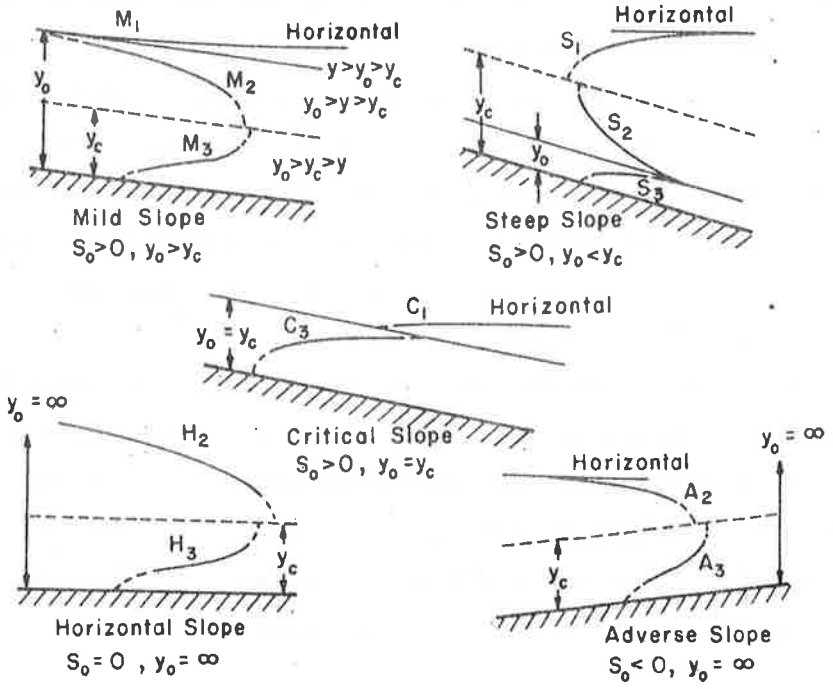

Figure 3.9 Classification of water surface profiles.

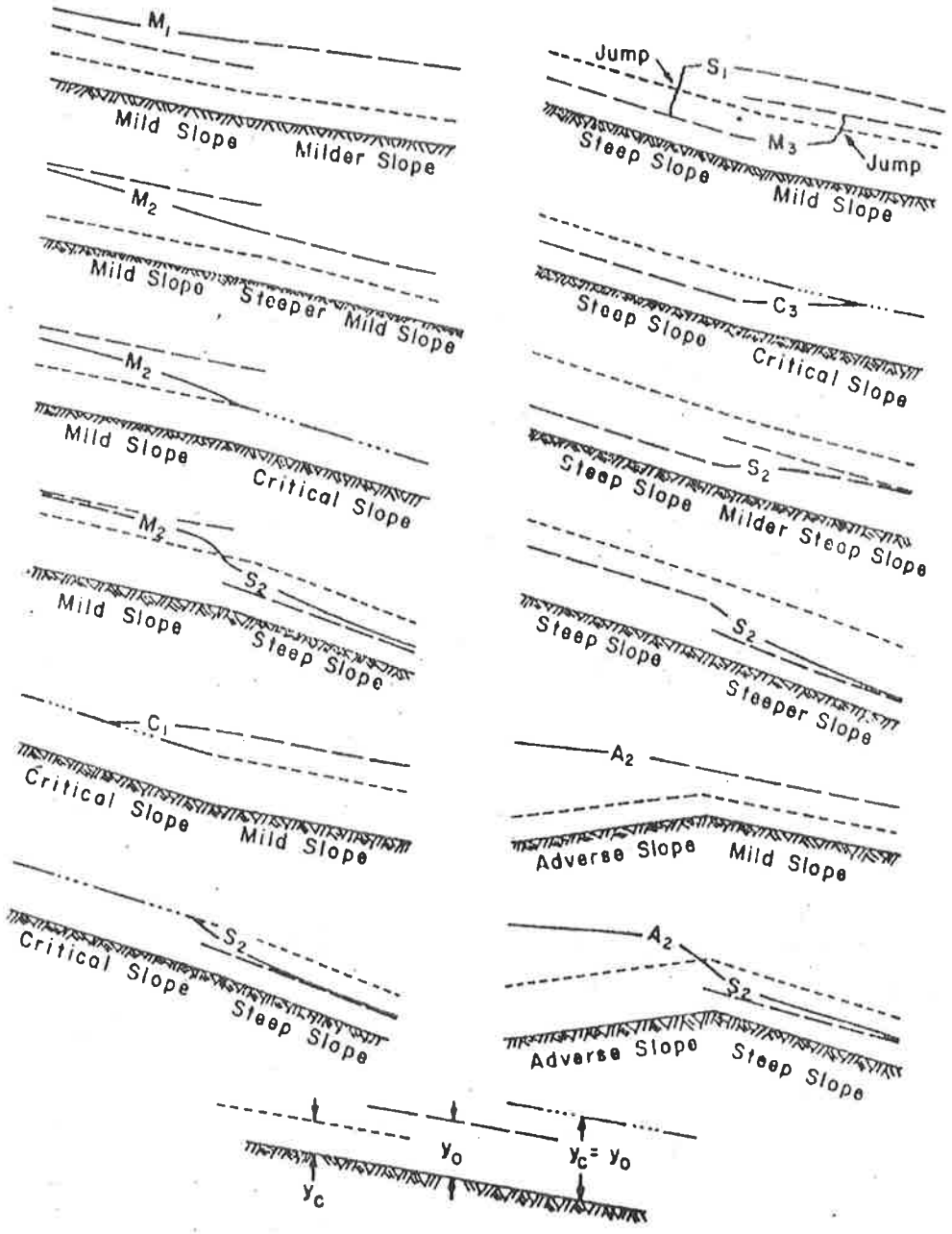

Figure 3.10 Examples of water surface profiles.

When there is a change in cross section or slope at an obstruction to the flow, the qualitative analysis of the flow profile depends on locating the control points, determining the type of curve upstream and downstream of the control points and then sketching the backwater curves. It must be remembered that when flow is rapid ($Fr \geq 1$) the control of the depth is upstream and the backwater calculations proceed in the downstream direction. When flow is tranquil ($Fr < 1$) the depth control is downstream and the computations must proceed upstream. The backwater curves that result from a change in slope of the bed are illustrated in Figure 3.9.

Steady Rapidly Varied Flow

Introduction. Steady flow through relatively short transitions where the flow is uniform before and after the transition can be analyzed using the energy equation. Energy loss due to friction may be neglected; at least as a first approximation. Refinement of the analysis can be made as a second step by including friction loss. For example, the water surface elevation through a transition is determined using the Bernoulli equation and then modified by determining the friction loss effects on velocity and depth in short raches through the transition. Energy losses resulting from separation cannot be neglected and transitions where separation may occur need special treatment which may include model studies. Contracting flows (converging streamlines) are less susceptible to separation than expanding flows. Also, any time a transition changes velocity and depth so that the Froude number approaches unity, problems such as waves and blockage or choking of the flow may occur. If the approaching flow is rapid (supercritical), a hydraulic jump may result.

Transitions are used to contract or expand channel width, to increase or decrease bottom elevation or to change both the width and bottom elevation. The first step in the analysis is to use the energy equation (neglecting any head loss resulting from friction or separation) to determine the depth and velocity changes of the flow through the transition. Further refinement depends on importance of freeboard, whether flow is rapid, and whether flow approaches critical.

The energy equation for flow where bottom elevation is changed by an amount Δz is

$$\frac{V_1^2}{2g} + y_1 = \frac{V_2^2}{2g} + y_2 + \Delta z \tag{3-38}$$

or

$$H_1 = H_2 + \Delta z \tag{3-39}$$

where

$$H = \frac{V^2}{2g} + y \tag{3-40}$$

The term H is called the specific head and is the height of the total head above the channel bed.

In the analysis of flow through transitions, the energy equation gives a numerical solution to the problem but very little descriptive information of the depth variation. Only after the analysis is completed will it be known if the depth will increase or decrease as the fluid passes through the transition or even if the flow is physically possible. On the other hand by investigating the various interrelations between the variables (H, V and y) in the specific head equation the variation of depth through a transition can be predicted.

There are two conditions for analyzing the flow through transitions. In the first condition, the width is constant and the elevation of the stream bed changes; that is, $q = Q/W$ is constant and H and y vary. In the second, the width changes and the elevation of the stream bed (neglecting the slope) is constant; that is, H is constant. These conditions can be qualitatively analyzed using a plot of depth versus specific head, called a specific head diagram.

Specific Head Diagram. For simplicity, the following specific head analysis is done on a unit width of channel so that Equation 3-40 becomes

$$H = \frac{q^2}{2gy^2} + y \tag{3-41}$$

For a given q, Equation 3-41 can be solved for various values of H and y. When y is plotted as a function of H, Figure 3.11 is obtained. There are two possible depths, called alternate depths, for any H larger than a specific minimum. Thus, for specific head larger

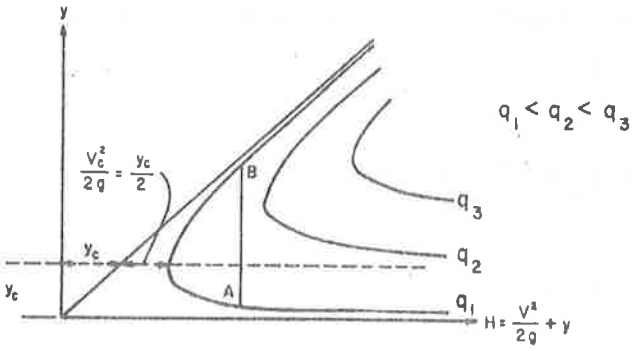

Figure 3.11 Specific head diagram

than the minimum, the given flow may have a large depth and small velocity or small depth and large velocity. Flow cannot occur with specific energy less than the minimum. The single depth of flow at the minimum specific head is called the critical depth y_c and the corresponding velocity, the critical velocity $V_c = q/y_c$. To determine y_c the derivative of H with respect to y is set equal to 0 or

$$\frac{dH}{dy} = -\frac{q^2}{gy^3} + 1 = 0 \tag{3-42}$$

and

$$q = (gy_c^3)^{1/2} \tag{3-43}$$

or

$$y_c = \left(\frac{q^2}{g}\right)^{1/3} = 2\frac{V_c^2}{2g} \tag{3-44}$$

Note that

$$V_c^2 = y_c g \tag{3-45}$$

or

$$\frac{V_c}{\sqrt{gy_c}} = 1 \tag{3-46}$$

But

$$\frac{V}{\sqrt{gy}} = Fr \tag{3-47}$$

Also

$$H_{min} = \frac{V_c^2}{2g} + y_c = \frac{3}{2} y_c \qquad (3\text{-}48)$$

Thus flow at minimum specific energy has a Froude number equal to one. Flows with velocities larger than critical (Fr > 1) are called rapid or supercritical and flows with velocities smaller than critical (Fr < 1) are called tranquil or subcritical. There is a maximum rise in the bed for a given H_1 where the rate of flow is physically possible. If the rise in the bed is increased beyond Δz_{max} for H_{min} then the approaching flow depth y_1 would have to increase (increasing H) or the flow would have to be decreased. Thus, for a given flow in a channel, a rise in the bed level can occur up to a Δz_{max} without causing backwater. Related aspects of steady flow and unsteady flow conditions are presented in more detail in Chapters 6, 7, 8, 9 and 12. The reader is referred to Chow (1959) for further information.

Variables Affecting Alluvial Channels

Because of the large number of interrelated variables that can react simultaneously to natural or imposed changes in a river system, river response to both natural and man-imposed forces is complex and varied in nature, but it is predictable. Simons and Richardson (1966) have detailed the variables affecting alluvial channel geometry and bed roughness, concluding that the nature of these variables is such that, unlike rigid boundary hydraulics problems, it is not possible to isolate and study the role of an individual variable. For example, evaluation of the effects of increasing channel depth on average velocity is hampered because related variables such as flow resistance also respond to the changing depth. Not only will velocity respond to a change in depth, but also the form of bed roughness, shape of the channel cross section and sediment discharge. Position and shape of alternate, middle and point bars can also be expected to change.

Variables that influence alluvial channel flow include velocity, depth, slope of energy grade line, density of water-sediment mixture, apparent viscosity of water-sediment mixture, gravitational constant, representative fall diameter of the bed material, gradation of bed material, density of sediment, shape factor of the particles, shape

factor of the reach of the stream, shape factor of the cross section of the stream, seepage force in the bed of the stream, concentration of bed-material discharge, fine material concentration, and particle terminal fall velocity. Dimensional analysis of these variables verifies the importance of the Froude number ($V\sqrt{gy}$), the Reynolds number ($Vy\rho/\mu$) and a relative roughness parameter (D/y).

Bed Forms and Resistance to Flow

The bed of an alluvial river is not a smooth regular boundary, but is characterized instead by forms that vary in size, shape, and location created by changes in flow, temperature, sediment load, size of bed material and other variables. These bed forms produce a major portion of the flow resistance exhibited by alluvial channels, and in turn feedback by exerting a significant influence on flow parameters such as depth, velocity and sediment transport.

Bed Form without Sediment Movement

If the bed material of a stream moves at one discharge but not at a smaller discharge, the bed configuration at the smaller discharge will be a remnant of the bed configuration formed when sediment was moving. In general, Shields' relation, Figure 3.12, is adequate to define beginning of motion of bed material. In this figure the dimensionless shear stress F_* represented by

$$F_* = \frac{\tau}{(\gamma s-\gamma)D_s} \tag{3-49}$$

where τ is the shear on the bed, γ_s is the unit weight of sediment, γ is unit weight of water, and D is particle size, is related to the boundary Reynolds number R_* as

$$R_* = \frac{U_* D_s}{\nu} \tag{3-50}$$

where U_* is the shear velocity and ν is the kinematic viscosity of water. After the beginning of motion, the bed will become rippled for sand material smaller than 0.6 mm. Dunes will develop for material no coarser than 0.6 mm. Resistance to flow is small for a plane bed without sediment movement and is caused by sand grain roughness. Values of Manning's n range from 0.012 to 0.016 depending on the size of the bed material.

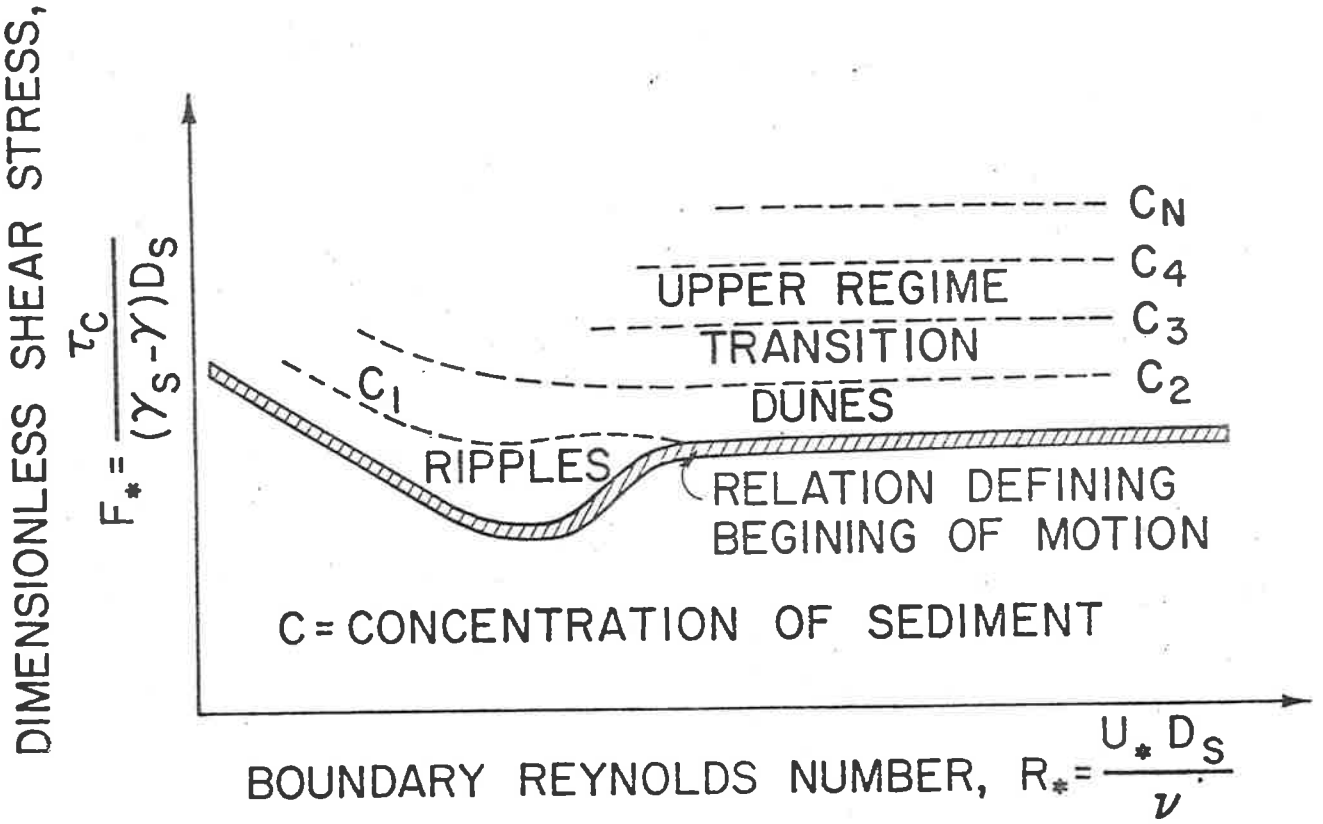

Figure 3.12 Generalized Shield's relation for beginning of motion showing relative bed form positions.

Bed Form with Sediment Movement

Profiles of typical bed forms and their relation to the water surface are shown in Figure 3.13. Using these bed forms as a criteria, flow in alluvial channels can be divided into two regimes separated by a transition zone. These two flow regimes are characterized by similarities in the shape of the bed form, mode of sediment transport, process of energy dissipation, and phase relation between the bed and water surface. These regimes and associated bed forms are:

1. Lower Flow Regime--low stream power
   a. Ripples
   b. Ripples superimposed on dunes
   c. Dunes
2. Transition Zone
3. Upper Flow Regime--high stream power
   a. Plane bed (with sediment movement)
   b. Antidunes
   c. Chutes and pools

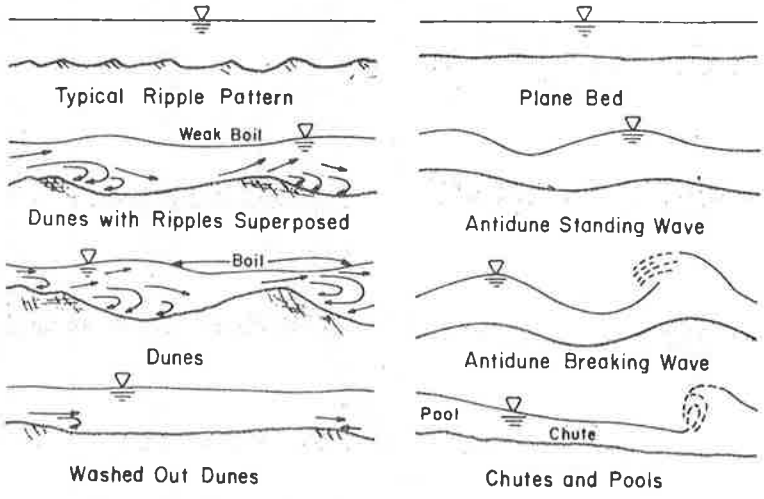

Figure 3.13 Typical bed forms in sand-bed channels (Simons and Richardson, 1966).

Simons and Richardson (1966) used flume and stream data to develop a graphical relation among stream power (τV), median fall diameter and bed form. This relation shown in Figure 3.14 indicates the form of bed roughness that may occur if the depth, slope, velocity, and fall diameter of the bed material are known. Another useful relation (Figure 3.15)

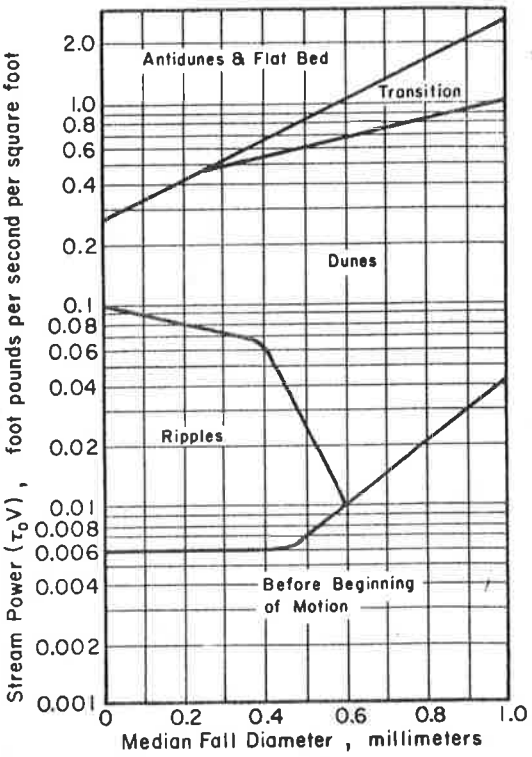

Figure 3.14 Relation of stream power and median fall diameter to form of bed roughness.

schematically shows the effect of bed form on roughness coefficients such as Manning's n. As the bed configuration passes through lower regime to upper regime, Manning's n changes from a typical value of 0.012 to 0.016 for plane bed without sediment motion to values as high as 0.04 for a dune bed. If stream power increases, upper regime plane bed conditions will develop that may produce a decrease in roughness to values as small as 0.010 to 0.015.

In natural streams a large increase in discharge with little or no change in stage is possible as a result of a change in bed configuration from dunes to plane bed. Figure 3.16 shows a break in the depth-discharge relation resulting from this phenomena. Conversely, an increase in depth with constant slope and bed material can change a dune bed to plane bed or antidunes. A decrease in depth can reverse the regime.

Bars

In natural channels other types of bed configurations or forms occur. These bed configurations are generally called bars and are related to the plan form geometry and the width of the channel.

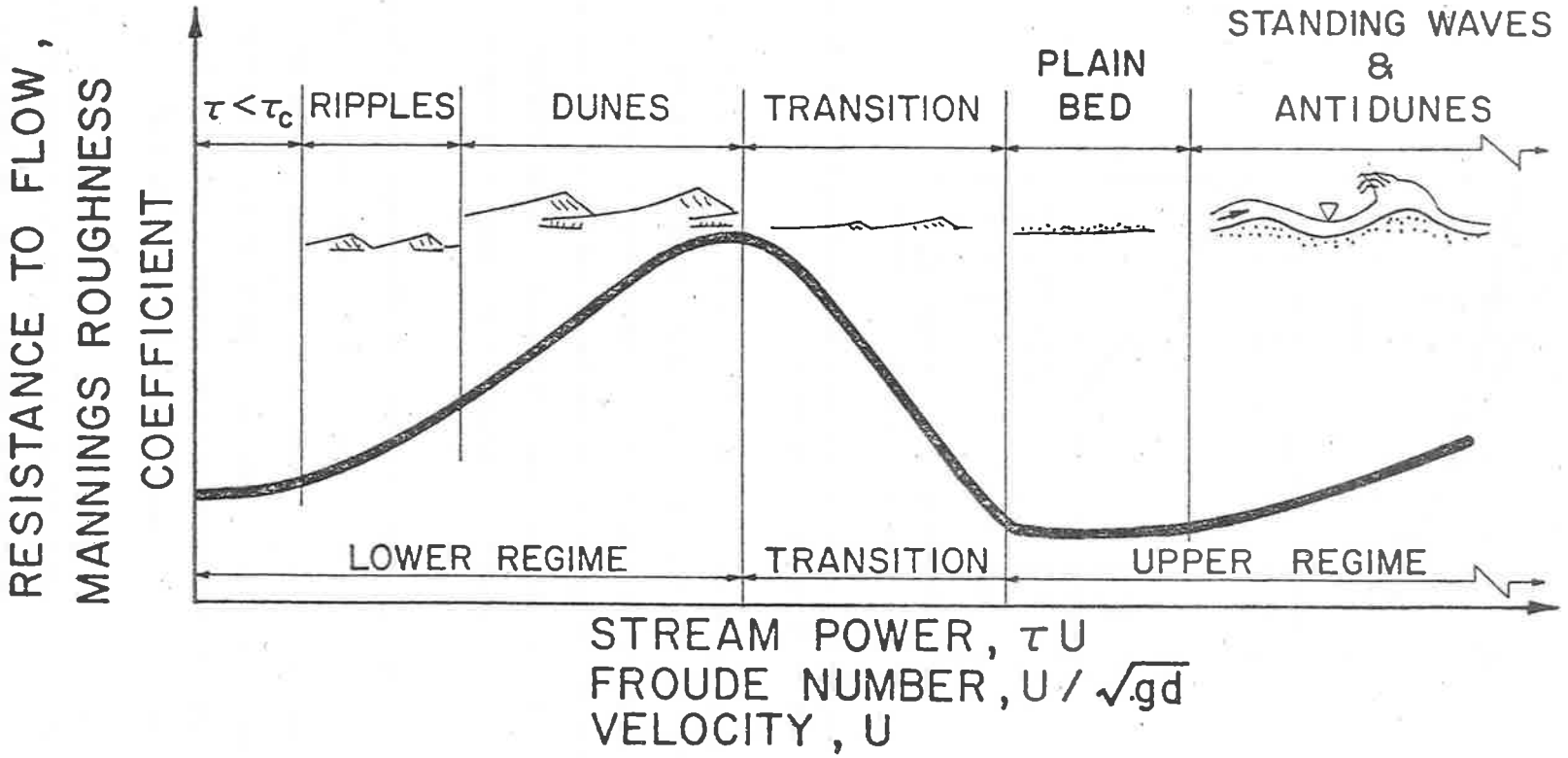

Figure 3.15 Generalized variation of resistance with changing bed forms.

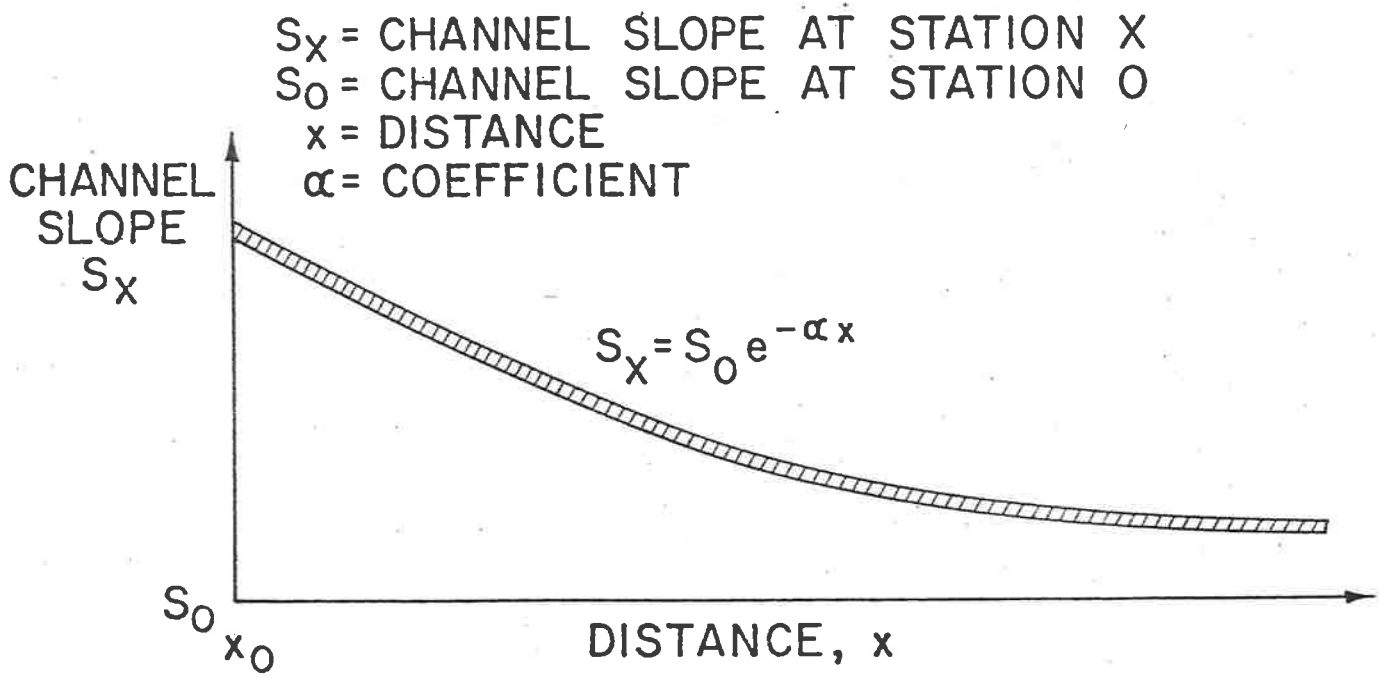

Figure 3.16 Generalized variation of channel slope with distance.

Bars are bed forms having lengths about the same size as the channel width, or greater, and heights comparable to the mean depth of the generating flow. Several different types of bars occur and are classified as:

1. Point Bars which occur adjacent to the convex bank of channel bends. Point bar shape may vary with changing flow conditions, but point bars do not move relative to the bends.
2. Alternate Bars which occur in straighter reaches of channels and tend to be distributed periodically along the reach, with consecutive bars on opposite sides of the channel. Their lateral extent is significantly less than the channel width. Alternate bars slowly move downstream.
3. Transverse Bars (middle bars) which also occur in straight channels. They occupy nearly the full channel width of the producing divided and multiple flow channels. They occur as isolated and as periodic forms along a channel. They also move slowly downstream.
4. Tributary Bars which occur immediately downstream from points of tributary or other lateral inflow into a channel.

Longitudinal sections indicate that bars are approximately triangular with very long gentle upstream slopes and short downstream slopes at approximately the angle of repose. They are similar to dunes in form but much larger. Bars appear as small barren islands during low flows. Portions of the upstream slopes of bars are often covered with ripples and dunes. Bars significantly affect the development of new flow alignments as well as resistance to flow, particularly if these bars are armored.

Hydraulic Geometry

Hydraulic geometry is a general term used to denote relationships between bankful discharge, channel morphology, hydraulics and sediment transport. In natural alluvial channels, the morphologic, hydraulic and sedimentation characteristics of the channel result from a large variety of factors. Generalized hydraulic geometry relations apply to channels within a physiographic region and can be computed from data available for gaged rivers. Hydraulic geometry relations express the integral effect of all hydrologic, meteorologic, vegetative, and geologic variables in a drainage basin.

Hydraulic geometry relations of alluvial streams are necessary for river engineering computations and river modeling. Forerunners of these relations were the regime theory equations of stable alluvial canals. A generalized version of hydraulic geometry relations was developed by Leopold and Maddock (1953) for different regions in the United States and for different types of rivers. Hydraulic geometry relations can be stated as: $W = a\ Q^b$; $y_o = c\ Q^f$; $V = k\ Q^m$; $Q_T = p\ Q^j$; $S = t\ Q^z$; $n = r\ Q^y$, where W is the channel width, y_o is the channel depth, V is the average velocity of flow, Q_T is the total bed-material load, S is the energy gradient, n is the Manning's roughness coefficient, and Q is the discharge defined below. Leopold and Maddock (1953) have shown that in a drainage basin, two types of hydraulic geometry relations can be defined: 1) those relating W, y_o, V and Q_T to the variation of discharge at a station, and 2) those relating these same variables to the discharges of a given frequency of occurrence at various stations on a channel. Because Q_T was not available, they used Q_s the suspended load transport rate. The former relations are called at-station relationships and the latter downstream relationships.

Hydraulic geometry relations were theoretically developed at Colorado State University (Simons and Li, 1975). These relations are almost identical to those proposed by Leopold and Maddock. The at-station relations derived at Colorado State University are:

$$W \sim Q^{0.26} \tag{3-51}$$

$$y_o \sim Q^{0.46} \tag{3-52}$$

$$S \sim Q^{0.00} \tag{3-53}$$

$$V \sim Q^{0.30} \tag{3-54}$$

Equation 3-54 implies that slope is constant at a cross section. This is not precisely true. At low flow the effective channel slope is determined by the thalweg which flows from pool through crossing to pool. At higher stages the thalweg straightens somewhat thus shortening the path of travel and increasing the local slope. In extreme cases river slope approaches the valley slope at flood stage. During high floods flow often cuts across the point bars thus developing chute channels.

This direction of travel verifies the shorter path the water takes and that a steeper channel prevails under this condition.

Similarly, the derived downstream relations for bank-full discharge are:

$$y_b \propto Q_b^{0.46} \tag{3-55}$$

$$W_b \propto Q_b^{0.46} \tag{3-56}$$

$$S \propto Q_b^{-0.46} \tag{3-57}$$

$$V_b \propto Q_b^{0.08} \tag{3-58}$$

where the subscript b indicates the bank-full condition.

Sediment Transport in Alluvial Channels

The sediment in a river almost always originates in the drainage basin. Eroded material is carried into the river and along the river's course by flowing water. Ultimately, this material is deposition in the lower reaches of the river, on the river delta, or, for the finer material, in the sea. This constant displacement of material implies a slow but continuous change in the longitudinal profile of the river, ending eventually in the destruction of the upland region drained by the river. As a result, it must be anticipated that large quantities of sediment will pass through a river system each year.

Longitudinal Stream Profile

The longitudinal profile of a stream shows its slope, or gradient. It is a representation of the ratio of the fall of a stream to its length over a given reach. Because a river channel is often steepest in its upper regions, most river profiles are concave upward. As with other channel characteristics, shape of the profile is a result of a number of interdependent factors, representing a balance between the transport capacity of the stream and the size and quantity of the sediment load supplied.

Shulits (1941), among others, provided an equation describing the concave horizontal profile of a channel in terms of distance along the stream as

$$S_x = S_o e^{-\alpha x} \tag{3-59}$$

where S_x is the slope at any station a distance x downstream of a reference station, S_o is the slope at the reference station, and α is a coefficient of slope reduction (Figure 3.16).

Similarly, grain size of the bed material decreases in a downstream direction. Transport processes reduce the general size of sediment particles by abrasion and hydraulic sorting. Abrasion is size reduction by mechanical actions such as grinding, impact and rubbing, while hydraulic sorting results in differential transport of particles of varying sizes. For sedimentary particles of similar shape, roughness and specific gravity, the end result of these processes is the observed reduction of bed material size along the direction of transport. The change in particle size with distance downstream can be expressed as

$$D_{50x} = D_{50o} e^{-\beta x} \tag{3-60}$$

where D_x is size of bed material at distance x downstream of a reference station, D_o is median size of bed material at the reference station, and β is a wear or sorting coefficient (Figure 3.17). This trend is found in large and small channels.

The longitudinal profile of an alluvial river is dynamic, continually adjusting to changed input conditions of water and sediment discharge. Altered input conditions change the channel geometry, roughness and other parameters including channel gradient.

Sediment Yield

The quantity of sediment delivered to the channel depends on watershed processes discussed in previous sections. The capacity of a stream to transport sediment depends on hydraulic properties of the stream channel. Such variables as slope, roughness, channel geometry, discharge, velocity, turbulence, fluid properties, and size and gradation of the sediment are closely related to the hydraulic variables controlling the capacity of the stream to carry water. The total sediment load of a stream is the sum of the bed-material load and the wash load, the sum of bed load and suspended load, or the sum of measured and unmeasured load.

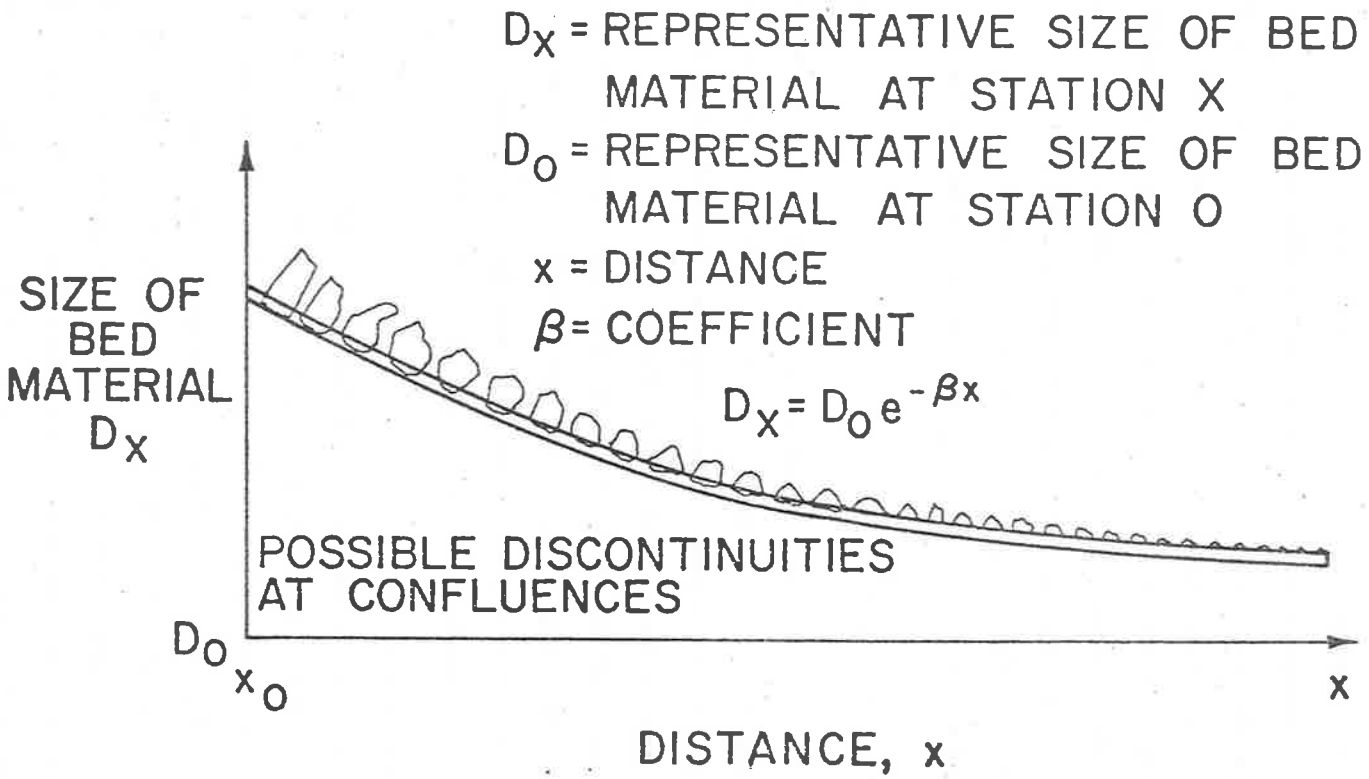

Figure 3.17 Generalized variation of size of bed material size with distance.

Bed-Load Transport

Because bed material is transported as suspended load and bed load, the different physical laws controlling these modes must be incorporated into any method for predicting total transport of bed material. Transport of bed load is usually related to the tractive force or shear on the bed as in the historic Du Boys formula of

$$q_b = K\,\tau_o(\tau_o-\tau_c) \tag{3-61}$$

where q_b is the bed-load discharge per unit width of section per unit time, K is a sediment parameter, τ_o is intensity of bed shear, and τ_c is critical shear at which motion is initiated (Figure 3.12).

Bed-Material Transport

As implied by the above definitions, the distinction between bed-material load and wash load is important and is reiterated here. Bed material is transported at the capacity of the stream and is functionally related to measurable hydraulic variables. Wash load, however, is not transported at the capacity of the stream, depending instead on supply, and is not functionally related to hydraulic variables. While there is no sharp demarcation between wash load and bed-material load, one criteria assumes the bed-material load consists of particle sizes equal to or greater than 0.062 mm, the division between sand and silt. Another reasonable demarcation is to use a sediment size finer than the smallest 10 percent of the bed material as a point of division.

Sediment particles which constitute the bed-material load are transported either by rolling or sliding along the bed (bed load) or in suspension. Again there is no sharp distinction between bed load and suspended load. A particle of the bed-material load may move part of the time in contact with the bed and at other times be suspended by the flow. Generally, the amount of bed material moving in contact with the bed of a large sand bed river is only a small percentage of the bed material moving in suspension.

The fine material moving as wash load usually will not pose direct problems for development activities in the channel system. However, large concentrations of fine material can affect the capacity of a

stream to transport bed material through its influence on fluid properties such as viscosity and density. A more detailed discussion of sediment routing in rivers is given in Chapters 4 and 15.

The processes, variables and mechanics controlling the response of channel systems are varied and complex. It is impossible to consider all of the factors at one time. Therefore an analysis to delineate the most important variables is needed. One way is through use of physical process models and parameter sensitivity tests. Another way is by order of magnitude analyses. The following section presents such an evaluation of important forces in river channels.

3.5 QUALITATIVE ORDER OF MAGNITUDE ANALYSIS OF FORCES ACTING ON A RIVER--AN EXAMPLE

General

Previous sections have primarily dealt with qualitative analyses of the processes and forces acting in watersheds and river channels. In this section, a quasi-quantitative approach is described and applied to a major New England River (Simons, Andrew, Li and Alawady, 1979). This analysis is general in nature and can be applied to other rivers. Through such an analysis a better understanding of the key or important variables can be gained.

Evaluation of Forces

The tractive force method has been utilized to evaluate bank erosion on different rivers. It is an acceptable method and has been used in the design and stability evaluation of alluvial canals. The method used by the U.S. Army Corps of Engineers is limited to straight reaches of channel that are principally affected by shear stresses exerted on the bed and banks by the flowing water. In this example the banks of the channel are subjected to additional forces produced by operation of numerous power dams and their pools. Typical average depth, average velocity, and average sediment transport for natural rivers, upper pools and lower pools are given in Figures 3.18, 3.19 and 3.20, respectively. The definition of a natural river is one that is usually unaffected by backwater caused by a downstream dam. The computed depth is roughly within 10 percent of the normal depth of the river. Figure 3.20 indicates that the sediment-transporting capacity is

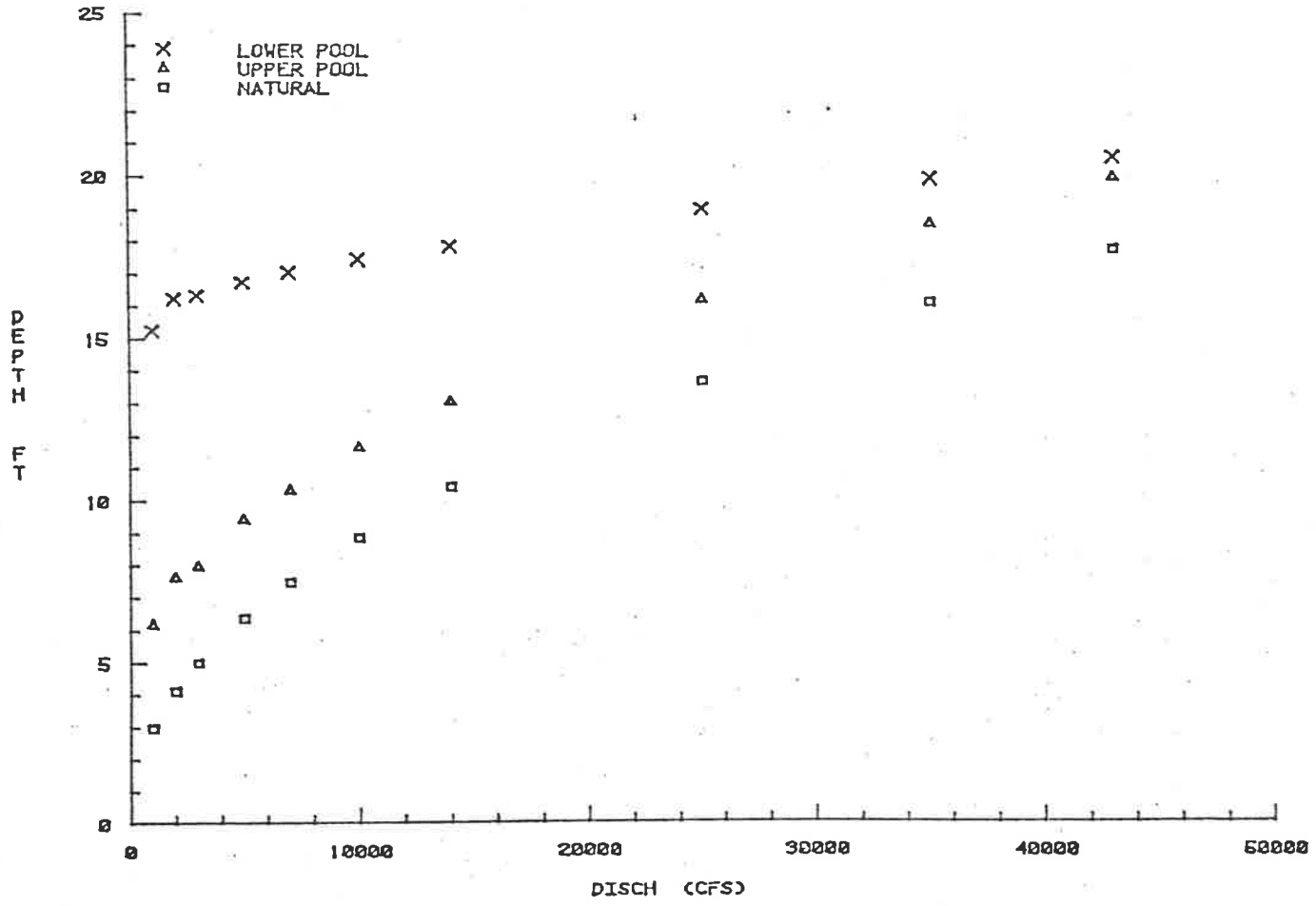

Figure 3.18 Water discharge as compared to depth for typical reaches.

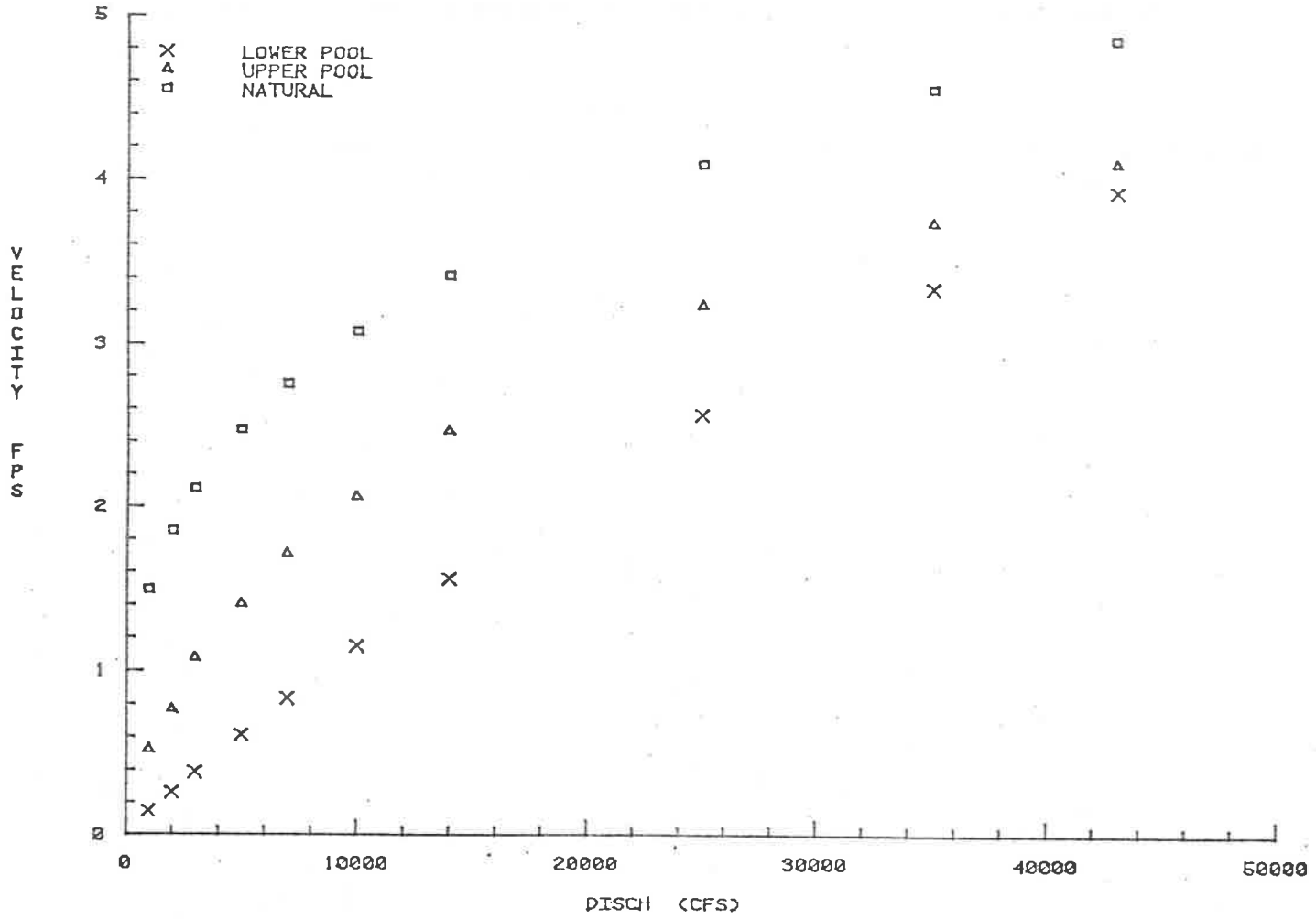

Figure 3.19 Water discharge as compared to velocity for typical reaches.

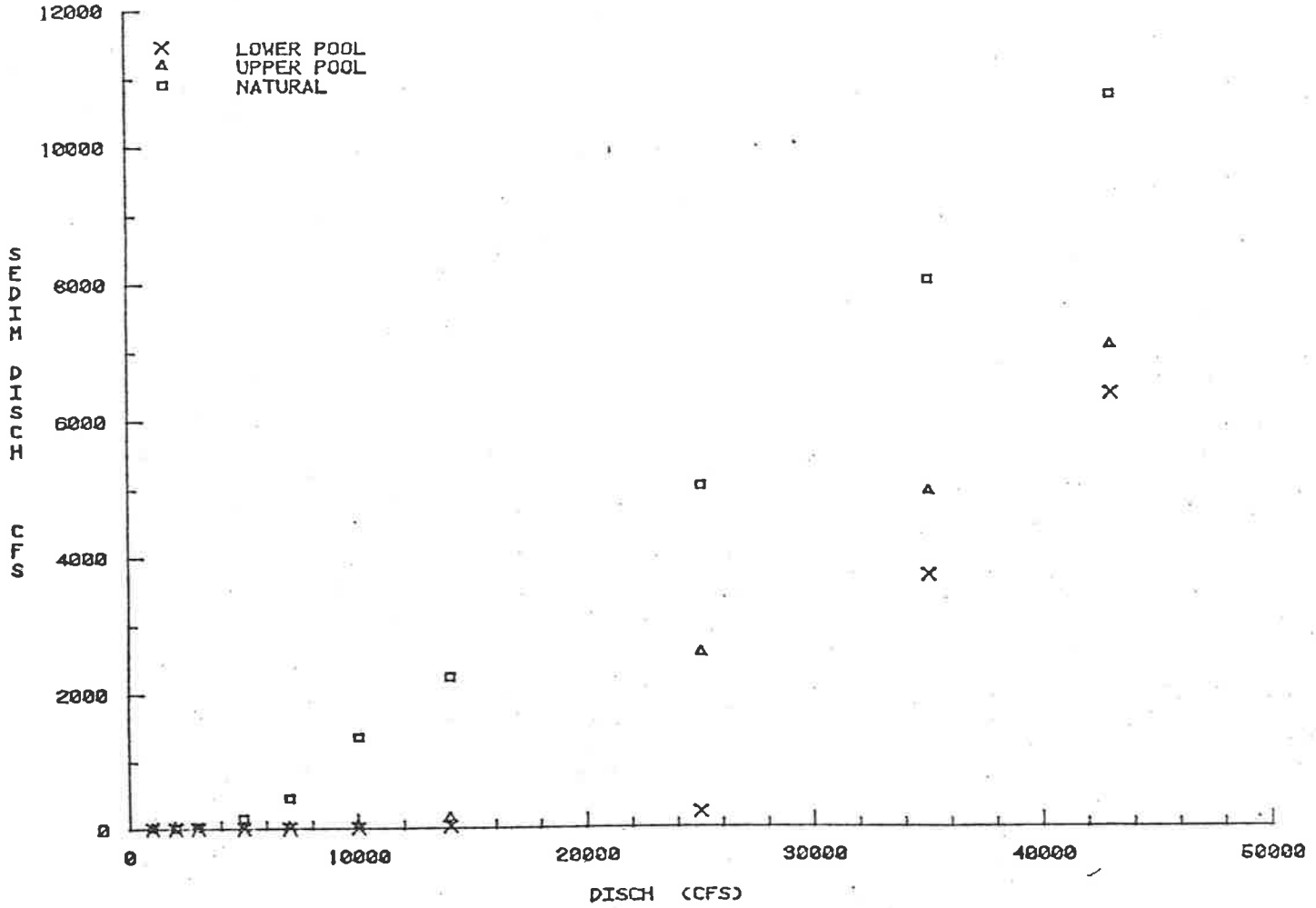

Figure 3.20 Water discharge as compared to sediment discharge for typical reaches.

significantly lower in the pools than in the natural river. These figures were determined using a dam height of 30 feet, a channel bed slope of 0.00029, and a typical channel cross section.

Magnitudes of the forces acting on the river banks can be expressed as a percentage of the tractive force exerted on the bed of the channel by the flowing water. This flowing water tractive force can be approximated by the relation

$$\tau = \gamma dS \tag{3-62}$$

where τ is shear stress, γ is specific weight of the water-sediment mixture, d is depth of flow at the location where the shear stress is to be estimated, and S is slope of energy gradient.

As an alternative, the shear stress acting on the channel boundary can be estimated by the relation

$$\sqrt{\tau/\rho} = \frac{u_1 - u_2}{5.75 \text{ Log } \frac{y_1}{y_2}} \tag{3-63}$$

where ρ is the density of water and u_1, u_2 are the point velocities measured at distances y_1 and y_2 from the boundary of the channel.

For best results, y_1 and y_2 should be as close as possible to the boundary. This relation provides a better approximation of the boundary shear stress in reaches affected by power dams since shear stress is independent of the channel and is sensitive to the velocity distribution.

To estimate the stability of a river channel the critical shear stress which is just sufficient to initiate movement of bed material is first determined. This critical shear stress can be approximated from Shields diagram previously presented in Figure 3.12 if τ at motion is taken as critical shear τ_c. If the shear stress acting on the bed or boundary of the river determined by Equations 3-62 and 3-63 is greater than the critical shear stress τ_c, the bed material will be in motion. If the rate of transport on a segment of the river exceeds the inflow of sediment from upstream or lateral inputs, degradation of the river bed will occur. Aggradation will occur if the converse is true. After estimating shear stress acting on the river bed and the critical shear

stress, the critical shear stress and the actual shear stress acting on the banks exceeds the critical shear stress, bank erosion will result. Consequently, the river bank will be unstable unless protected by vegetation, riprap, or some other stabilization measure. The critical shear stress for the river banks can be estimated utilizing Shields diagram and the computed value of the critical shear stress for the bank material if the material was located on a plane surface instead of a sloping surface. For wide channels the shear stress for the material forming the bank is approximately 0.77 times the shear stress for the same material if it were on the bed of the stream or is

$$\tau_{c_{side}} = 0.77\ \tau_{c_{bed}} \tag{3-64}$$

As an alternative, the ratio of the shear stress acting on the bank or side of a channel τ_s to the shear stress acting on the bed of a channel τ_b can be more accurately determined using the relation

$$\frac{\tau_s}{\tau_b} = K = \cos\theta\sqrt{1 - \frac{\tan^2\theta}{\tan^2\phi}} \tag{3-65}$$

where θ is the angle of bank side slope and ϕ is the angle of repose for the bank material. Banks will be unstable if the tractive force acting on the banks exceeds the critical tractive force for the bank material. The tractive force acting on the river banks can be estimated from Equation 3-65 for determining the critical shear stress on the river bank.

Only the shear stress exerted on the river banks as caused by flowing water was evaluated above. Consequently, it is necessary to add effects of other forces acting on the banks to the tractive force. These additional increments of shear stress can be determined from Table 3.5. For example, the incremental values of shear stress acting on the banks of a natural river with high banks formed of noncohesive material are tabulated in Table 3.6. For these conditions, the total effective tractive force acting on the bank of the river can be estimated by adding the 0.52 γdS from the preceding tabulations taken from Table 3.5 to the shear stress exerted by the flowing water on the banks of the channel. In summary, if this shear stress is 0.77 γdS, then

Table 3.5 Relative magnitudes and duration of erosive forces.

Factors & Variables Causing Bank Erosion	River Condition	Relative Magnitude of Forces		Relative Duration of Forces	Relative Magnitude of Bank Erosion			
		Noncohesive	Stratified		Noncohesive		Stratified	
Shear Stress or Velocity	Natural river	9	8	9	81	1.0	72	1.0
	Natural river with high banks	9	8	9	81	1.0	72	1.0
	Pools; low banks	9	8	7	63	.78	56	.78
	Pools; low banks with vegetation	7	6	6	42	.52	36	.50
	Pools; high banks	8	7	7	56	.69	49	.68
	Pools; high banks with vegetation	6	5	6	36	.44	30	.42
Flood Variation	Natural river	2	2	1	2	.02	2	.03
	Natural river with high banks	2	2	1	2	.02	2	.03
	Pools; low banks	2	2	1	2	.02	2	.03
	Pools; low banks with vegetation	1	1	1	1	.01	1	.01
	Pools; high banks	2	2	1	2	.02	2	.03
	Pools; high banks with vegetation	1	1	1	1	.01	1	.01
Stage Variation	Natural river	3	3	2	6	.07	6	.08
	Natural river with high banks	4	3	2	8	.10	6	.08
	Pools; low banks	3	3	1	3	.04	3	.04
	Pools; low banks with vegetation	2	2	1	2	.02	2	.03
	Pools; high banks	5	4	1	5	.06	4	.06
	Pools; high banks with vegetation	3	3	1	3	.04	3	.04
Pool Fluctuations	Natural river	3	3	2	6	.07	6	.08
	Natural river with high banks	4	3	2	9	.11	6	.08
	Pools; low banks	4	3	3	12	.15	9	.13
	Pools; low banks with vegetation	3	3	3	9	.11	9	.13
	Pools; high banks	5	4	3	15	.19	12	.17
	Pools; high banks with vegetation	4	4	3	12	.15	12	.17
Wind Waves surface erosion & piping	Natural river	2	2	1	2	.02	2	.03
	Natural river with high banks	1	1	1	1	.01	1	.01
	Pools; low banks	3	3	2	6	.07	6	.08
	Pools; low banks with vegetation	2	2	1	2	.02	2	.03
	Pools; high banks	2	2	1	2	.02	2	.03
	Pools; high banks with vegetation	1	1	1	1	.01	1	.01

Table 3.5 (continued)

Factors & Variables Causing Bank Erosion	River Conditions	Relative Magnitude of Forces		Relative Duration of Forces	Relative Magnitude of Bank Erosion			
		Noncohesive	Stratified		Noncohesive		Stratified	
Boat Waves surface erosion & piping	Natural river	2	3	2	4	.05	6	.08
	Natural river with high banks	2	2	2	4	.05	4	.06
	Pools; low banks	3	4	2	6	.07	8	.11
	Pools; low banks with vegetation	3	3	2	6	.07	6	.08
	Pools; high banks	4	5	2	8	.10	10	.14
	Pools; high banks with vegetation	3	4	2	6	.07	8	.11
Freeze-Thaw	Natural river	1	1	1	1	.01	1	.01
	Natural river with high banks	1	1	1	1	.01	1	.01
	Pools; low banks	1	1	1	1	.01	1	.01
	Pools; low banks with vegetation	1	1	1	1	.01	1	.01
	Pools; high banks	1	1	1	1	.01	1	.01
	Pools; high banks with vegetation	1	1	1	1	.01	1	.01
Ice	Natural river	2	2	1	2	.02	2	.03
	Natural river with high banks	3	2	1	3	.04	2	.03
	Pools; low banks	2	2	1	2	.02	2	.03
	Pools; low banks with vegetation	1	1	1	1	.01	1	.01
	Pools; high banks	2	2	1	2	.02	2	.03
	Pools; high banks with vegetation	1	1	1	1	.01	1	.01
Seepage Forces	Natural river	2	3	2	4	.05	6	.08
	Natural river with high banks	3	3	2	6	.07	6	.08
	Pools; low banks	2	3	2	4	.05	6	.08
	Pools; low banks with vegetation	2	3	2	4	.05	6	.08
	Pools; high banks	3	4	2	6	.07	8	.11
	Pools; high banks with vegetation	2	3	2	4	.05	6	.08
Gravitational Forces	Natural river	2	2	2	4	.05	4	.06
	Natural river with high banks	3	4	3	9	.11	12	.17
	Pools; low banks	2	2	2	4	.05	4	.06
	Pools; low banks with vegetation	1	2	1	1	.01	2	.03
	Pools; high banks	3	4	3	9	.11	12	.17
	Pools; high banks with vegetation	2	3	2	4	.05	6	.08

Table 3.6 Example of estimated incremental values of shear stress from different processes.

Variable Causing the Force on the River Bank	Magnitude of Equivalent Shear Stress
flood variation	0.02 γdS
normal stage variation	0.10 γdS
pool fluctuations	0.11 γdS
wind waves	0.01 γdS
boat waves	0.05 γdS
freezing and thawing	0.01 γdS
ice	0.04 γdS
seepage forces	0.07 γdS
gravitational forces	0.11 γdS
	Σ = 0.52 γdS

the total effective shear stress will be 1.29 γdS. If this value exceeds the critical shear stress acting on the banks, erosion of the banks will occur unless protected.

If the bank line is subjected to erosion, the size of riprap required to stabilize the bank line can be estimated from the Shields diagram. In this case the estimated effective shear stress acting on the river bank can be substituted for τ in the relation $\tau/(\gamma_s-\gamma)D_s$. If $R_* > 500$, then

$$\frac{1.29\ \gamma dS}{(\gamma_s-\gamma)D_s} = 0.06 \qquad (3\text{-}66)$$

The median diameter of the required size of riprap can be approximated by solving for D_s. Because the numerator term 1.29 γdS is not a constant but a function of river geometry and the forces acting on the river banks, its value can be approximated for each condition or evaluated as above.

The preceding analysis applies to essentially straight channel reaches but can be extended to apply to outside banks of a river bend by considering the lateral velocity distribution resulting from the geometry of the river bend. This procedure requires an estimate of the

increase in boundary shear stress acting on the outside bank of a river bend. This procedure is illustrated in the following example. The procedure utilizes the relation

$$\Delta' = 0.42\ \Delta\ \frac{d_{max}}{W}\ \frac{\sqrt{g}}{C} \qquad (3\text{-}67)$$

where Δ is the angle of the bend, r_c is the radius of curvature to the centerline of the bend, $C/\sqrt{g}$ is the dimensionless Chezy flow resistance coefficient, d_{max} is maximum depth of flow in the cross section, and W is channel width. To numerically illustrate this procedure, assume that a river bend has the following properties:

$$\Delta = 65°$$

$$r_c = 1500'$$

$$C/\sqrt{g} = 15$$

$$d = 15'$$

$$d_{max} = 18'$$

$$W = 300'$$

$$S = 1.67 \times 10^{-4}$$

From Equation 3-67, the value of Δ' is

$$\Delta' = \frac{(0.42)\ (65)\ (18)}{(300)\ (15)} = 0.11$$

or

$$\Delta' \times 10^2 = 11$$

From Figure 3.21

$$100\ \Delta V'_{max} = 4.1$$

$$X' = 0.43$$

then

$$X' = \frac{2X}{W}$$

where X is equal to the horizontal distance from the centerline of the channel to the point of maximum velocity or

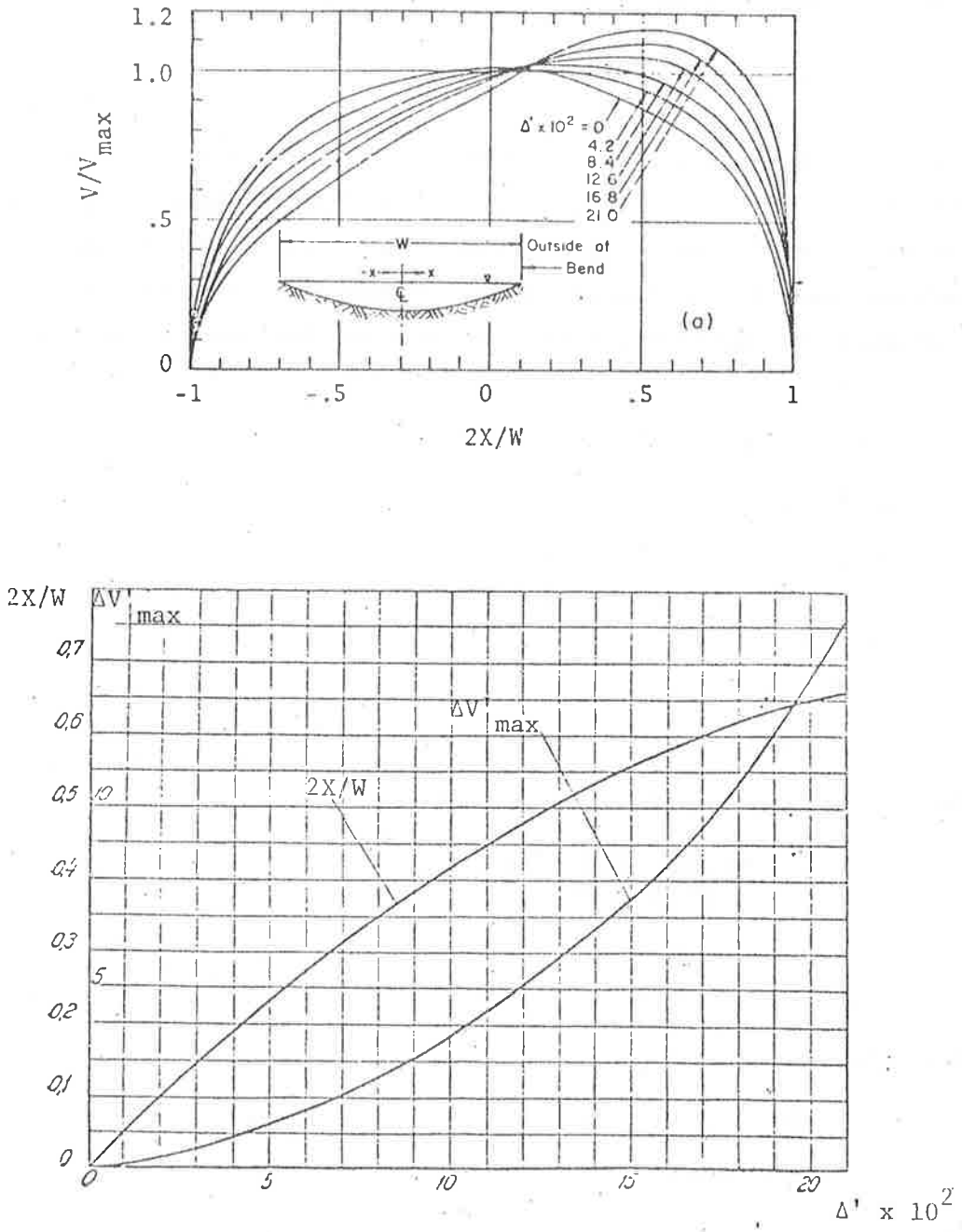

Figure 3.21 Lateral distribution of velocity in a bend (after Karaki, Mahmood, Richardson, Simons and Stevens, 1974).

$$X = \frac{(0.43)\ (300)}{2} = 65'$$

The average velocity in the channel determined by the Chezy equation is

$$V = \frac{C}{\sqrt{g}} \sqrt{g\ RS} \qquad (3\text{-}68)$$

and assuming $R \simeq d$, the average depth gives

$$V = 15 \sqrt{32.2(15)\ (1.67 \times 10^{-4})} = 4.26 \text{ ft/sec}$$

with X' equal to 0.43 and $\Delta' \times 10^2$ equal to 11, Figure 3.21 yields

$$\Delta V' = V/_{V_{max}} = 1.04$$

and

$$V = 1.04\ V_{max} = (1.04)\ (4.26) = 4.43 \text{ ft/sec}$$

Because shear stress is proportional to velocity squared, the ratio of the shear stress in the bend to that in a straight reach is

$$\frac{\tau_{bend}}{\tau_{straight}} = \frac{\overline{4.43}^2}{\overline{4.26}^2} = 1.08$$

For this example, the shear stress in the bend is about 1.1 times that in the straight reach. With this value established, the effect of the other forces acting on the bank can be added to the computed value to determine the total effective shear stress acting on the bank. The stability of the bank can be evaluated, and if riprap is required, it can be sized as described in the preceding paragraphs.

In general, shear stress in the bendway can be evaluated for each case. For more severe conditions, the shear stress acting on the outside bank in the bend way may be as much as 1.5 times that for a straight reach.

Table 3.5 is based on theoretical consideration of causative factors and available data. Further quasi-quantitative uses of Table 3.5 are exemplified below for the river channel evaluated in this study.

A summation of the relative magnitude of bank erosion for different factors causing erosion is determined from Table 3.5 and is given in Table 3.7. This table indicates relative importance of these factors.

Table 3.7 Sum of relative magnitude of bank erosion for different factors.

VARIABLES CAUSING EROSION	SUM OF RELATIVE MAGNITUDE OF BANK EROSION	
	NONCOHESIVE*	STRATIFIED
Shear stress or velocity	359 (1.0)	315 (0.88)
Flood variation	10 (0.03)	10 (0.03)
Stage variation	27 (0.08)	24 (0.07)
Pool fluctuation	63 (0.18)	54 (0.15)
Wind waves, surface erosion and piping	14 (0.04)	14 (0.04)
Boat waves, surface erosion and piping	34 (0.09)	42 (0.12)
Freeze-thaw	6 (0.02)	6 (0.02)
Ice	11 (0.03)	10 (0.03)
Seepage forces	28 (0.08)	36 (0.10)
Gravational forces	31 (0.09)	40 (0.11)

*Values are obtained from summing the relative magnitude of basic erosion for each variable as extracted from Table 3.4.

In decreasing importance they are: shear stress (velocity), pool fluctuation, boat waves, gravitational forces, seepage forces, stage variation, wind waves, ice, flood variation, and freeze-thaw. In general, stratified soil is slightly less susceptible to bank erosion than the noncohesive banks except when considering boat waves, seepage forces, and gravitational forces. Overall, the predominant force causing bank erosion is the shear stress (or velocity).

Analysis of Table 3.5 provides a measure of the relative magnitude of bank erosion for different conditions (Table 3.8). This table demonstrates that a reach with a high bank is more susceptible to erosion, and vegetation is important in stabilizing the bank. Furthermore, the natural river has a higher potential for bank erosion than do the pools. The average sum of relative magnitude of bank erosion for a natural river is 113.75 and that for pools is 84.75. In other words, the natural river is roughly 1.34 times more susceptible to bank erosion than are pools.

Table 3.8 Sum of relative magnitude of bank erosion for different conditions.

	SUM OF RELATIVE MAGNITUDE OF BANK EROSION		
CONDITIONS	NONCOHESIVE*	STRATIFIED	AVERAGE
Natural river	112	107	109.5
Natural river with high banks	124	112	118.0
Pools: low banks	100	97	98.5
Pools: low banks with vegetation	69	66	67.5
Pools: high banks	106	102	104.0
Pools: high banks with vegetation	69	69	69.0

*Values are obtained from summing the relative magnitude of basic erosion for each river condition as extracted from Table 3.4.

The number of erosion sites per mile for the natural river is 1.01 and that for pools is 0.68 (Table 3.9). Therefore, the measured data indicate that the natural river is 1.49 times more susceptible to bank erosion than are pools. This is very close to the theoretical value of 1.34.

Table 3.9 Number of erosion sites per mile for different reaches.

	NATURAL RIVER	POOLS
No. of erosion sites	23.0	82
Total river mile	22.8	121.0
No. of erosion sites per mile	1.01	0.68

Based on the above discussion, the theoretical approach, as presented in Table 3.5, is justified considering physical significance and field observations. However, a further investigation of causative factors is needed to improve the information gap and the developed method.

The use of quasi-quantitative order of magnitude analysis to determine the important processes acting in a channel provides useful information about those variables that are most needed in river response analyses. In the above example, it was found that shear stress was relatively more important to erosion than was other river processes, therefore, this process should be studied in more detail.

In general, river or watershed response analyses must require two preliminary steps. First, controlling processes must be identified and second, the most important processes delineated.

3.6 QUALITATIVE ANALYSIS OF CHANNEL RESPONSE FOR SELECTED EXAMPLES

General

The previous sections have formed a basis for qualitatively analyzing channel response to different activities. This section takes those ideas and introduces some new ones to permit evaluation of selected channel modifications. Many channels have achieved approximate

equilibrium over long reaches. For engineering purposes, such reaches can be considered stable. However, this does not mean significant changes over a short period of time or over a period of several years cannot occur. This is evidenced by streams that contain long reaches that are actively aggrading or degrading as well as stable reaches.

Regardless of the degree of channel stability, man's local activities may produce major changes in river characteristics both locally and throughout an entire reach. Frequently, the result of a river improvement is a greater departure from equilibrium than which originally prevailed. Good design must seek to enhance the natural tendency of the stream toward equilibrium conditions. This requires an understanding of the direction and magnitude of change in channel characteristics caused by the actions of man and nature. This understanding can be obtained by: 1) studying the river in a natural condition, 2) having knowledge of the sediment and water discharge, 3) being able to predict the effects and magnitude of man's future activities, and 4) applying to these a knowledge of geology, soils, hydrology, and hydraulics of alluvial rivers.

Predicting the response to channel development is a very complex task. There are a large number of variables involved in analyses that are interrelated and can respond to changes in a river system and the continual evolution of river form. Channel geometry, bars, and forms of bed roughness all change with changing water and sediment discharges. Because prediction of channel response is necessary, useful methods have been developed to qualitative and quantitative estimate changes in channel systems.

Qualitative Prediction of General River Response

Quantitative prediction of response can be made if all of the required data are known with sufficient accuracy. Usually, however, the data are not sufficient for quantitative estimates, and only qualitative estimates are possible.

Lane (1955) studied the changes in river morphology in response to varying water and sediment discharge. Leopold and Maddock (1953), Schumm (1971), and Santos and Simons (1972) have all investigated channel response to natural and imposed changes. These studies support the following general relationships:

1. Depth of flow y is directly proportional to water discharge Q.
2. Channel width W is directly proportional to both water discharge Q and sediment discharge Q_s.
3. Channel shape, expressed as width to depth W/y ratio is directly related to sediment discharge Q_s.
4. Channel slope S is inversely proportional to water discharge Q and directly proportional to both sediment discharge Q_s and median grain size D_{50}.
5. Sinuosity s is directly proportional to valley slope and inversely proportional to sediment discharge Q_s.
6. Transport of bed material Q_s is directly related to stream power $\tau_o V$ and concentration of fine material C_F, and inversely related to the fall diameter of the bed material D_{50}.

A very useful relation for predicting system response was developed by Simons et al. (1975) establishing a proportionality between bed-material transport and several related parameters.

$$Q_s \sim \frac{(\tau_o V)WC_F}{D_{50}} \tag{3-69}$$

where τ_o is bed shear, V is cross-sectional average velocity, and C_F is concentration of fine material load. Equation 3-69 can be modified by substituting γDS for τ_o, and

$$Q = AV = WDV \tag{3-70}$$

from continuity, yielding

$$Q_s \sim \frac{(\gamma DS)WV}{D_{50}/C_F} = \frac{\gamma QS}{D_{50}/C_F} \tag{3-71}$$

If specific weight γ is assumed constant and concentration of fine material C_F is incorporated in the fall diameter, this relation can be expressed simply as

$$QS \sim Q_s D_{50} \tag{3-72}$$

Equation 3-72 is essentially the relation proposed by Lane (1955), except fall diameter, which includes the effect of temperature on transport, has been substituted for the physical median diameter used by Lane.

Applications of Qualitative Analysis

Equations 3-71 and 3-72 are most useful for qualitative prediction of channel response to natural or imposed changes in a river system. A well-known example is the downstream response of a river to the construction of a dam (Figure 3.22). Aggradation in the reservoir upstream of the dam will result in relatively clear water being released downstream of the dam. That is, Q_s will be reduced to $\bar{Q_s}$ downstream.

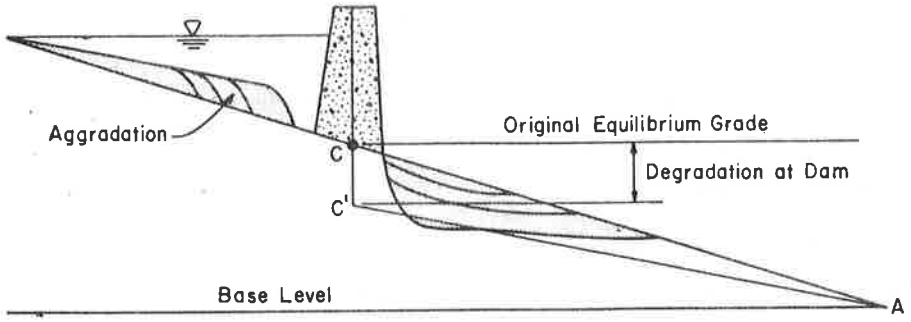

Figure 3.22 Channel adjustment above and below a dam.

Assuming fall diameter and water discharge remain constant, slope must decrease downstream of the dam to balance the proportionality of Equation 3-72

$$\bar{Q_s} D_{50}^{o} \sim Q^{o} \bar{S} \qquad (3\text{-}73)$$

In Figure 3.22 the original channel gradient between the dam and a downstream geologic control (line CA) will be reduced to a new gradient (line C'A) through gradual degradation below the dam. With time, the pool behind the dam will fill and sediment would again be available to the downstream reach. Then, except for local scour, the gradient C'A would increase to the original gradient CA to transport the increase in sediment load. Upstream, the gradient would eventually parallel the original gradient, offset by the height of the dam. Thus, dams with small storage capacity may induce scour and then deposition over a relatively short time period.

Quantitative results in addition to qualitative indications of trends are also of interest. The geomorphic relation $QS \sim Q_s D_{50}$ is only an initial step in analyzing long-term channel response problems. However, this initial step is useful because it warns of possible future difficulties in designing channel improvement and flood protection works and provides a good estimate of response to all types of river development.

Qualitative Analysis Examples of River Response

Consider next several relatively simple situations commonly encountered by engineers, scientists, and geologists in the river environment. Each case is introduced by a sketch which shows the physical situation prior to a selected natural or man-induced change. Below the sketch, some of the major local effects, upstream effects, and downstream effects resulting from natural processes or development activity are given. It is necessary to emphasize that only the gross local, upstream and downstream effects are identified. For more detail on regimes of flow, bed forms, and resistance to flow and their effects on river response, the reader could refer to Simons and Sentürk (1977).

The initial river conditions are sometimes given in terms of storage dams, water diversions, or other works of man. These examples are used in illustrations relating to common experience. For more details refer to Simons et al. (1975). In general, the effect of a storage reservoir is to cause a sudden increase of base level for the upstream section of the river. The result is aggradation of the channel upstream, degradation downstream and a modification of the downstream flow hydrograph. Similar changes in the channel result if the base level is raised by some other mechanism, such as uplift from tectonic activity. The effect of diversions from rivers is to decrease the river discharge downstream of the diversion with or without an overall reduction of the sediment transport. Similarly, changes in water and sediment input to a river reach often occur due to river development projects upstream from the reach under consideration or as a result of natural causes.

Figure 3.23 illustrates the confluence of a tributary stream with the main channel. The average water surface elevation in the main channel acts as the base level for the tributary. It is assumed here that base level in the main channel has been lowered by a natural change

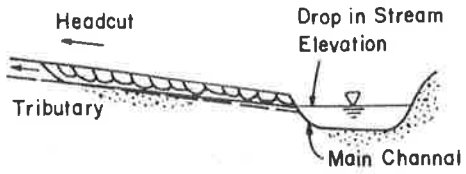

Local Effects	Upstream Effects	Downstream Effects
1. Headcutting	1. Increased velocity	1. Increased transport to main channel
2. General scour	2. Increased bed material transport	2. Aggradation
3. Local scour	3. Unstable channel	3. Increased flood stage
4. Bank instability	4. Possible change of form of river	4. Possible change of form of river
5. High velocities		

Figure 3.23 Lowering of base level for tributary stream (Simons et al., 1975).

in the river environment or by man-induced change such as the lowering of a reservoir level on the main stem. Applying Equation 3-72 to the tributary stream shows that the increase in slope S^+ must be balanced by an increase in sediment transport Q_s^+. Thus, under the new imposed condition, the local gradient of the tributary stream is significantly increased. This increased energy gradient induces headcutting and causes a significant increase in water velocities in the tributary stream. The result is bank instability, possible major changes in the geomorphic characteristics of the tributary stream and increased local and general scour.

Response to the converse situation, raising the base level, can be illustrated by considering river response to construction of a dam (Figure 3.24). Whenever the base level of a channel is raised a pool is created extending a distance upstream depending on the channel gradient and dam height. This results in a "backwater" effect. As the water and sediment being transported by the river encounters this pool, most of the sediments drop out forming a delta-like formation at the head of the pool which slowly advances downstream. The deposition of sediment at the entrance to the pool induces aggradation in the channel upstream. This aggradation may extend many miles upstream after a long

period of time, producing significant changes in river geometry, and increased flood stages by raising the channel bed. Again, Equation 3-72 provides an indication of the response. The decrease in slope $\bar{S}$ must be accompanied by a decrease in transport capacity $\bar{Q}_s$ or $Q_s^{o-} \sim Q_s \bar{D}_{50}^{o}$. It is possible that the river may become sufficiently perched so at some high flow the river could abandon the old channel and adopt a new one.

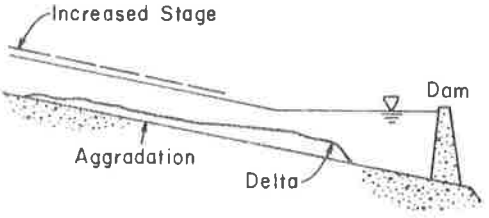

Local Effects	Upstream Effects	Downstream Effects
1. Aggradation of bed	1. See local effects	1. See downstream effects, Fig. 14
2. Loss of waterway capacity	2. Change in base level for tributaries	
3. Change in river geometry	3. Deposition in tributaries near confluences	
4. Increased flood stage	4. Aggradation causing a perched river channel to develop or changing the alignment of the main channel	

Figure 3.24 Raising base level in main channel.

As noted in Figure 3.24, the effects of raising the base level of the main channel include an increase in base level for any tributaries entering the pool formed by the main stem dam. The impact of this change on the tributaries is shown in Figure 3.25.

The change in gradient of the tributary stream in most cases causes significant deposition. This can be seen from Equation 3-72 where a decrease in slope is accompanied by a decrease in sediment transport or

$$Q^{o}\bar{S}^{-} \sim \bar{Q}_s D_{50}^{o}$$

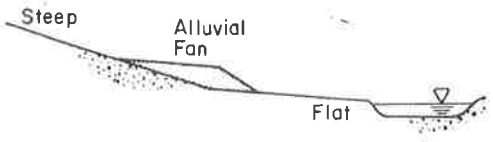

Local Effects	Upstream Effects	Downstream Effects
1. Alluvial fan reduces waterway	1. Erosion of banks	1. Aggradation
2. Channel location is uncertain	2. Unstable channel	2. Flooding
	3. Large transport rate	3. Development of tributary bar in the main channel

Figure 3.25 Raising base level for tributary stream.

assuming constant conditions of water discharge and size of bed material. In this case an alluvial fan develops which in time can divert the river or reduce the waterway. In general, streams on alluvial fans shift laterally so that the future location of the channel is uncertain. A similar situation occurs naturally where a steep tributary stream draining an upland region reaches the flatter floodplain of the parent stream.

The impact of the construction of a dam on the reach upstream of the dam is also outlined in Figure 3.24. Construction of an upstream storage dam provides a desilting basin for the water flowing in the system. In most instances all of the bed-material load coming into a reservoir deposits within the reservoir. Water released from the reservoir is quite clear. The existing river channel is the result of its interaction with normal water-sediment flows over a long period of time. With the sediment-free flows the channel below the dam is too steep and sediments are entrained from the bed and the banks bringing about significant degradation. The channel banks may become unstable due to degradation and there is a possibility that the river, as its profile flattens, may change its plan form (Figure 3.26). Assuming that prior to dam construction the reach below the dam plotted as an intermediate stream (Point 1), the decrease in slope at constant water discharge could move the stream's plotting position to Point 2 in the

meandering region of the chart. In the extreme case, it is possible that the degradation may cause failure of the dam and the release of a flood wave.

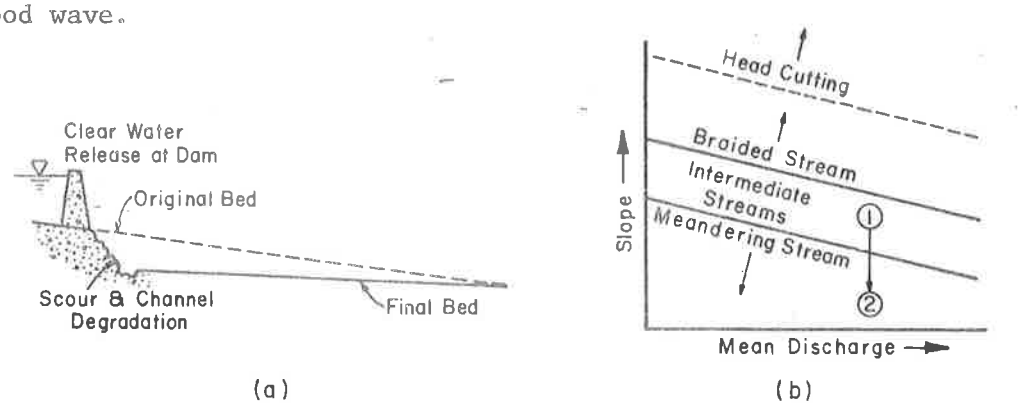

Local Effects	Upstream Effects	Downstream Effects
1. Channel degradation	1. See upstream effects, Fig. 12	1. Degradation
2. Possible change in river form		2. Reduced flood stage
3. Local scour		3. Reduced base level for tributaries, increased velocity and reduced channel stability causing increased sediment transport to main channel
4. Possible bank instability		
5. Possible dam failure		

Figure 3.26 Clear water release below a dam.

Figure 3.27 illustrates a situation where artificial cutoffs have straightened the channel below a given reach. Straightening the channel downstream of Reach A significantly increases the channel slope. This causes higher velocities, increased bed material transport, degradation, and possible headcutting through Reach A. This can result in unstable river banks and a braided stream form. The original plotting position (Point 1) is moved to Point 2 in the braided region by the increase in channel slope. In addition, the straightening of the main channel brings about a drop in base level and any tributary streams flowing into the affected reach of the main channel are subjected to conditions outlined in Figure 3.23.

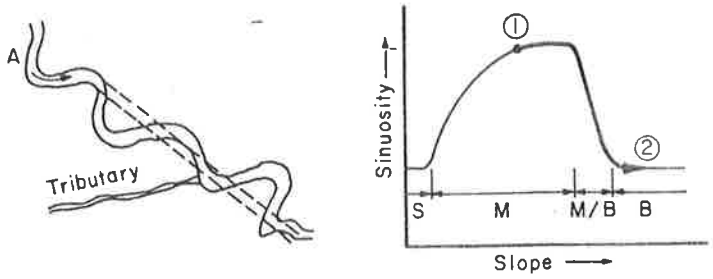

(a) (b)

Local Effects	Upstream Effects	Downstream Effects
1. Steeper slope	1. See local effects	1. Deposition downstream of straightened channel
2. Higher velocity		2. Increased flood stage
3. Increased transport		3. Loss of channel capacity
4. Degradation and possible headcutting		
5. Banks unstable		
6. River may braid		
7. Degradation in tributary		

Figure 3.27 Straightening of a reach by construction of cutoffs.

On the other hand, if the straightened section is designed to transport the sediment loads that the river is capable of carrying both upstream and downstream of the straightened reach, bank stability may not be decreased. Such a channel should not undergo significant change over either short or long periods of time. It is possible to build modified reaches of main channels that do not introduce major adverse responses due to local steepening of the main channel. In order to design a straightened channel so that it behaves essentially as the natural channel in terms of velocities and magnitude of bed-material transport, it is necessary, in general, to build a wider shallower section.

Qualitative Analysis of Response of Large Scale Systems

The simple examples presented above lead into more complex ones for large scale problems or systems. However, it should be noted that the

large scale systems are analyzed by the same procedures as the smaller examples.

Impact of Construction of a Large Dam on a River System Upstream of a Diversion to an Irrigated Area

A particular river system carried significant percentages of fine sediments comprised of silts and clays during the majority of the year. An irrigation diversion system was developed long before there was any construction of dams upstream of the diversion structure (Figure 3.28). The main feeder canal diverts water from the river system to the irrigated area at the diversion structure. Thereafter, it flows around a side hill, comprised of rather permeable materials including sands and gravels, passes through a city area where there is relatively dense development along both sides of the canal, and then continues downstream to serve the distant irrigated area.

A large storage dam was constructed on the river immediately upstream of the diversion structure. The reservoir acts as a desilting basin and water relased below this dam is essentially clear. This clear water flows down the short reach of river channel and is then diverted to the irrigation canal. This release of clear water may cause some degradation immediately downstream of the dam before it enters the canal. There has been some degradation in the main canal and erosion has exposed more permeable bed and bank materials thus increasing seepage losses. There are several major detrimental consequences from the increased seepage losses including 1) a significant decrease in the amount of water that can be delivered to the farm units for irrigation, and 2) the seepage from the canal system has a potential to cause a rise in the water table. The increase in the water table level may cause extensive damage to adjacent buildings by basement flooding.

There are other potentially detrimental factors that can adversely affect the irrigation system. For example, with clear water in the canal system it will be a suitable environment for growth of aquatic plants. With these plants choking the channels, there will be added water losses and it will be difficult to convey required water to the downstream irrigation systems. Therefore, some type of periodic treatment would be required to keep the channels free of vegetation. On the farm units, where land has been irrigated by diversions from head ditches into

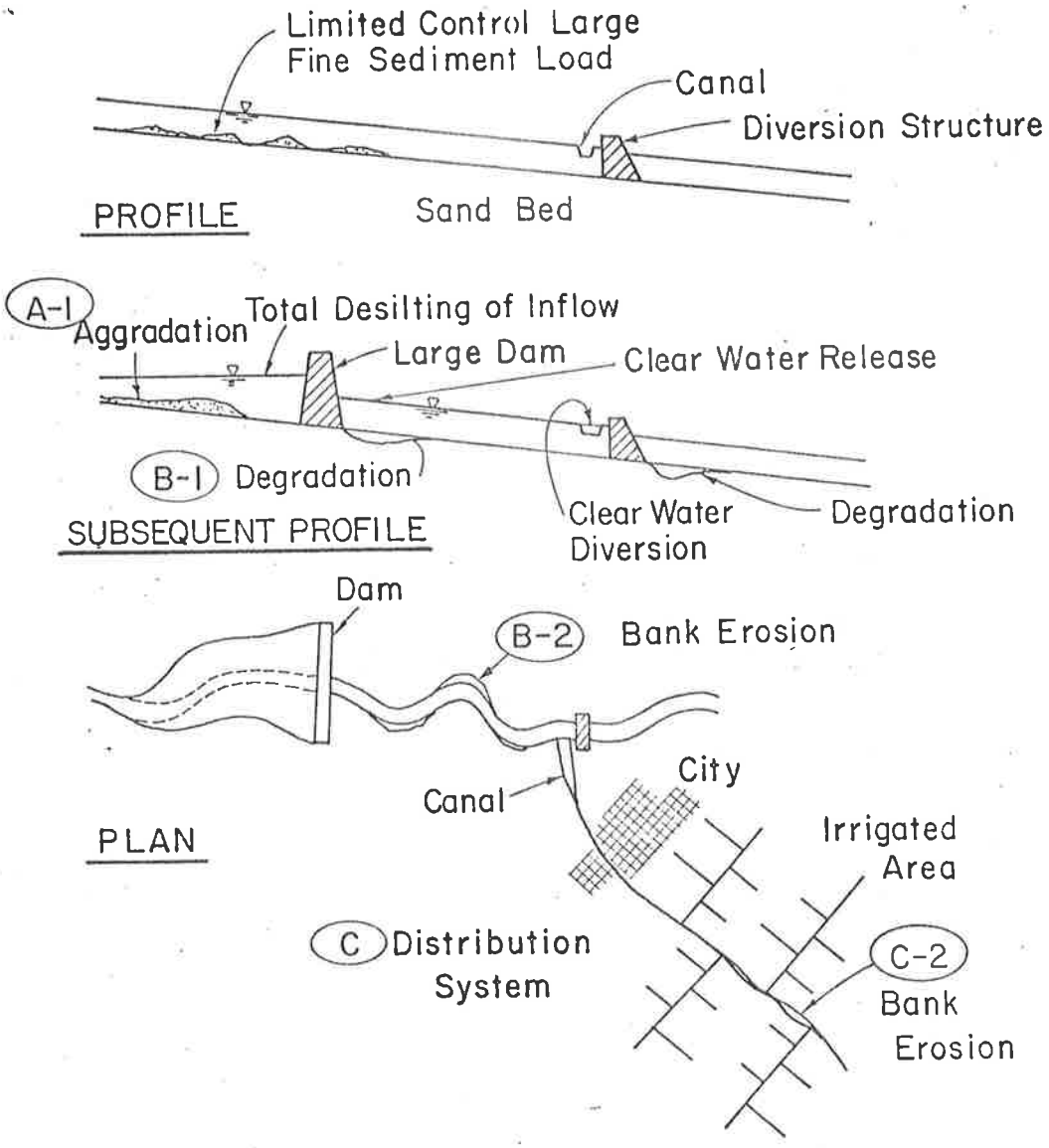

Figure 3.28 Impact of construction of a large dam on a river system upstream of a diversion to an irrigated area.

furrows, the head ditches were designed and spaced so that a fairly efficient application of water could be made with water containing silts and clays. With silt and clay in the water, relatively long runs were possible. If the same lengths of runs are used with clear water there are excess seepage losses and before the water reaches the ends of the furrows, all of it is infiltrated thus building up the groundwater level. This means that the distribution system on the farm units must be dramatically changed. Length of runs may have to be cut in half. This will require more head ditches and more nonproductive space. The numerous ditches may also add to problems of harvesting.

As referred to previously, the clear water tends to scour the banks and degrade the bed of the canal system. If the attack is sufficiently severe, channel stabilization may be required or some type of lining may be required to minimize the losses of water and to provide stability to the system.

The Response of a River System and Intervening Reaches of Channel to the Construction of Major Reservoirs (Simons and Li, 1977)

In the analysis of river systems it is common to find water resources development projects that involve the construction and use of major reservoirs. Such a case is outlined in Figure 3.29. The reservoir, identified as "A", has been constructed on a major river. Reservoir "B", further downstream, is planned for subsequent development. At location "C", there is a city that will be affected by the backwater from reservoir "B". With this general background, the responses of the system to these developments can be considered. Reservoir "A" is large. It stores on the order of 10,000,000 acre feet of water. However, even though it is large, it only stores a small percent of the water that is annually discharged from this watershed, as illustrated by the small inserted hydrograph. This particular hydrograph points out that approximately five times the volume of the reservoir flows down the river system each year. All of the sediment carried into the reservoir is trapped and the quantity of water that is desilted is approximately equal to five times the volume of the reservoir, about 50,000,000 acre feet per year. The sediment load carried by the river ranges from average to large for similar sized rivers. This means that desilting of such a large volume of water causes a large volume of sediment to be

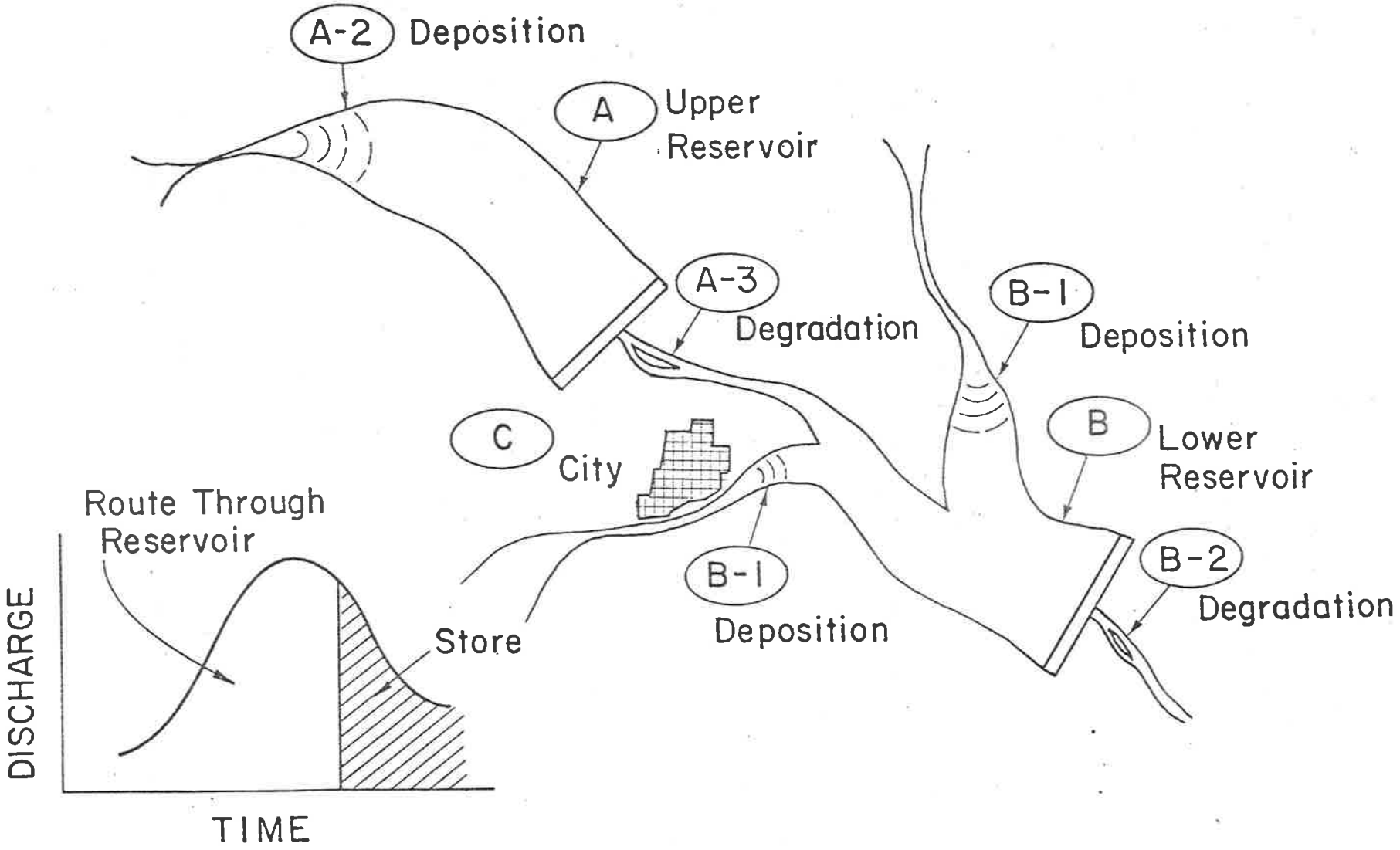

Figure 3.29 The response of a river system and intervening reaches of channel to the construction of major reservoirs.

deposited within reservoir "A" each year. This deposition can significantly decrease the storage capacity of the reservoir for hydropower, irrigation, and flood control in a relatively short time. Furthermore, essentially clear water is released downstream of the dam. The channel is comprised of materials ranging from fine sand, silts, and clays, to coarse gravel. Coarser materials in the bed of the stream will tend to limit the degradation induced downstream of the dam by the release of clear water. It is essential not only to evaluate the rate at which the loss of live storage will occur in the reservoir, and also to document the rate and magnitude of ultimate degradation so that the structure's safety can be adequately considered.

Reservoir "B" is considered next. This particular reservoir has approximately the same storage capacity as reservoir "A". The waters released into this particular reservoir will be essentially clear insofar as the water coming through reservoir "A" is concerned. On the other hand, two other river systems flow into reservoir "B". These are not desilted and, consequently, will carry significant quantities of sediment into the reservoir. Once again it is necessary to consider the rate of loss of live storage as a consequence of inflowing sediments. It should also be recognized that ultimately reservoir "A" will lose its capacity to store sediment and sediments may be discharged from reservoir "A" to reservoir "B". On the other hand, there is the possibility that other reservoirs upstream of reservoir "A" will be constructed. This type of activity can significantly increase the lifetime of reservoirs such as "A" and "B". This is very typical of what has happened to downstream reservoirs due to the construction of upstream reservoirs along the Colorado River.

Because of the importance of sediment in terms of the economics of operation of the reservoirs over long periods of time, an interesting problem with respect to reservoir "B" is to attempt to construct it in such a way that relatively large quantities of sediment can be discharged annually from it instead of being stored within it. This would involve building a large gated structure in such a way that reservoir "B" could essentially run as an open river during those periods of high flow when water could be passed through the system. Then, toward the end of the runoff period, it would be necessary to close the gates in time to

allow filling of the reservoir. With this type of operation it would be necessary to empty the reservoir annually. Otherwise, it would not be possible to pass excess sediments through the reservoir system. Hence, it can be seen that there are many trade-offs that have to be considered when determining the economics of these systems as well as the response of the rivers and impacts that may result.

Location "C" is considered next. Here a city is located on a river discharging into an arm of reservoir "B". The backwater from the reservoir may require construction of flood protection works for the city. In addition, just determining water levels in the vicinity of the city is not adequate. It is necessary to route the water and sediment down the river system into the reservoir to determine the rates of deposition, the location of deposition, and to how these deposits of sediment may increase river stage, aggravate the flooding situation, increase the groundwater level, and perhaps cause other adverse responses..

As the above simple examples and case histories illustate, knowledge of the qualitative responses of a system to changes is important in understanding the quantitative changes. Without this knowledge, a mathematical and aphysical models can be constructed that do not and cannot truly represent the system being studied.

3.6 SUMMARY

A key to mathematical modeling of watershed or channel responses to natural or man-induced changes is through understanding of the important physical processes. These processes can be broadly grouped as topography, soils, geology, vegetation, climate, hydrology and hydraulics, and man's influence. Processes differed somewhat between watershed and channel systems, but they shared a common trait of being interrelated and complex. Identification of physical processes must coincide with determination of the most important ones. This can be done through sensitivity analysis of mathematical models that describe the process or by relative order of magnitude comparisons. Once the processes are understood, they can be used to qualitatively predict system response or can be used to construct more representative mathematical models. The qualitative analysis often provides a check for results obtained from mathematical models (see Chapter 2). Either way knowledge of physical processes is necessary in understanding natural systems.

3.7 REFERENCES

Barnes, H. H. 1967. Roughness Characteristics in Natural Channels. U. S. Geological Survey Water Supply Paper 1849.

Chow, V. T. 1959. Open Channel Hydraulics. McGraw Hill Book Company, New York.

Chow, V. T. 1964. Handbook of Applied Hydrology. McGraw Hill Book Company, New York, 1000+p.

Culbertson, D. M., Young, L. E., and Brice, J. C. 1967. Scour and Fill in Alluvial Channels. U.S. Geological Survey, Open File Report.

Davis, W. M. 1899. The Geographical Cycle. Geographical Journal, Vol. 14, pp. 481-504.

Garg, M. M. 1972. River Classification by Photos and Map. M. S. Thesis, Colorado State University, Fort Collins, 1972.

Horton, R. E. 1945. Erosional Developments of Streams and Their Drainage Basins; Hydrophysical Approach to Quantitative Morphology. Geol. Soc. Am. Bull., Vol. 56.

Khan, Hamidur, R. 1971. Laboratory Studies of Alluvial River Channel Patterns. Ph.D. Dissertation, Civil Engineering Department, Colorado State University, Fort Collins.

Lane, E. W. 1955. The Importance of Fluvial Morphology in Hydraulic Engineering. ASCE Proc., Vol. 81, No. 745, 17 p.

Lane, E. W. 1957. A Study of the Shape of Channels Formed by Natural Streams Flowing in Erodible Material. Missouri River Division Sediment Series No. 9, U.S. Army Engineer Division, Missouri River, Corps of Engineers, Omaha, Nebraska.

Langbein, et al. 1944. Topographic Characteristics of Drainage Basin. U.S. Geological Survey Water Supply Paper 968-C. In Contributions to the Hydrology of the United States.

Leopold, L. B. and Maddock, T., Jr. 1975. The Hydraulic Geometry of Stream Channels and Some Physiographic Implications. U.S. Geological Survey Professional Paper 252, 57 p.

Pfankuch, D. J. 1975. Stream Reach Inventory and Channel Stability Evaluation. U.S. Department of Agriculture Forest Service, Northern Region.

Richardson, E. V., Karaki, S., Mahmood, K., Simons, D. B. and Stevens, M. A. 1975. Highways in the river environment - hydraulic and design considerations. Colorado State University, Fort Collins, Colorado, CER73-74EVR-SK-KM-DBS-MAS49, September (Federal Highway Administration, U.S. Department of Transportation, May 1975).

Rosgen, D. L. 1975. Watershed Response Rating System. In Forest Hydrology, Part II. U.S. Department of Agriculture Forest Service Northern Region, Missoula, Montana.

Rundquist, L. A. 1975. A Classification and Analysis of Natural Rivers. Ph.D. Dissertation, Department of Civil Engineering, Colorado State University, Fort Collins, Colorado.

Schumm, S. A. 1963. A Tentative Classification of Alluvial River Channels. U.S. Geological Survey Circular 477.

Schumm, S. A. 1971. Fluvial Geomorphology: The Historical Perspective. In Chapter 4 of River Mechanics, Vol. I, H. W. Shen, Ed., Fort Collins, Colorado.

Shulits, S. 1941. Rational Equation of River-Bed Profile. Trans., AGU, Vol. 22, pp. 622-630.

Simons, D. B. 1972. River System Response to Proposed Upper Auxiliary Channel, Yazoo Basin, Mississippi. Prepared for U.S. Corps of Engineers, Vicksburg District, Vicksburg, Mississippi, September.

Simons, D. B., Andrew, J., Li, R. M., Alawady, T. 1979. Connecticut River Streambank Erosion Study of Massachusetts, New Hampshire and Vermont. Prepared for U.S. Army Corps of Engineers, Waltham, Massachusetts.

Simons, D. B., Lagasse, P. F., Chen, Y. H. and Schumm, S. A. 1975. The River Environment--A Reference Document. Prepared for U.S. Department of the Interior, Fish and Wildlife Service, Twin Cities, Minnesota.

Simons, D. B. and Li, R. M. 1977. In-Field Estimation of Infiltration Parameters. Colorado State University Report, prepared for USDA Forest Service, Rocky Mountain Forest and Range Experiment Station, Flagstaff, Arizona.

Simons, D. B. and Li, R. M. 1975. Watershed Segmentation by a Digital Computer for Mathematical Modeling of Watershed Response. Prepared for USDA Forest Service, Rocky Mountain Forest and Range Experiment Station, Flagstaff, Arizona, December.

Simons, D. B. and Richardson, E. V. 1966. Resistance to Flow in Alluvial Channels. USGS Professional Paper 422-J.

Simons, D. B. and Senturk, F. 1977. Sediment Transport Technology. Water Resources Publication, Fort Collins, Colorado.

Simons, D. B., Ward, T. J., and Li, R. M. 1979. Sediment Sources and Impacts in the Fluvial System. In Modeling of Rivers, H. W. Shen, Ed., John Wiley and Sons, New York.

Strahler. 1952. Hypsometric (arca-altitude) Analysis of Erosional Topography. Geological Society of America Bulletin, no. 63.

Strahler. 1957. Quantitative Analysis of Watershed Geomorphology. Transactions, American Geophysical Union, Vol. 38, no. 6.

Thornbury 1969. Principles of Geomorphology. 2nd Edition. John Wiley & Sons.

CHAPTER 4

SEDIMENT TRANSPORT

by

H. W. Shen, Professor of Civil Engineering, Colorado State University, Fort Collins, Colorado

CHAPTER 4

4.1 DEFINITION

Total sediment transport can be divided three different ways:

1) By the mechanics of movements. The total sediment transport can be divided into the bed load and the suspended load. Bed load is the movement of sediment particles very close to the beds; most of the time these particles are supported by the sediment bed. The suspended load consists of those sediment particles supported by the moving fluid.

2) By methods of measurement. In this case, total sediment transport consists of the measured load and the unmeasured load. Since bed load is very difficult to measure, the measured load consists entirely of suspended load. It does not include the entire suspended load because we can only measure from the water surface to a distance about 10 centimeters from the top of the bed. Therefore, the measured load is that part of the suspended load which is at least 10 centimeters above the top of the bed. The unmeasured load consists of the entire bed load plus the suspended load within 10 centimeters of the top of the bed.

3) According to the method of calculations. In this case, total sediment transport it is equal to the wash load plus the bed material load. The concepts of wash load and bed material load may not be clear to many geologists and an explanation may be necessary. In general, the wash load is limited by the supply of particles from the watersheds to the stream. The bed material load is entirely determined by the capability of the flow to transport sediments.

The best that a sediment transport equation based on river flow conditions can do is to predict the sediment transport capability of a given flow for a certain sediment mixture. For instance, one may hope to obtain a relationship between transport capability and sediment size for a flow discharge q on a particular river as shown by curve COD in Figure 4.1. One may also plot the available supply of various sediment sizes from the upslope area for the same river discharge q, as indicated by AOD on Figure 4.1. The intersection of these two curves may not be

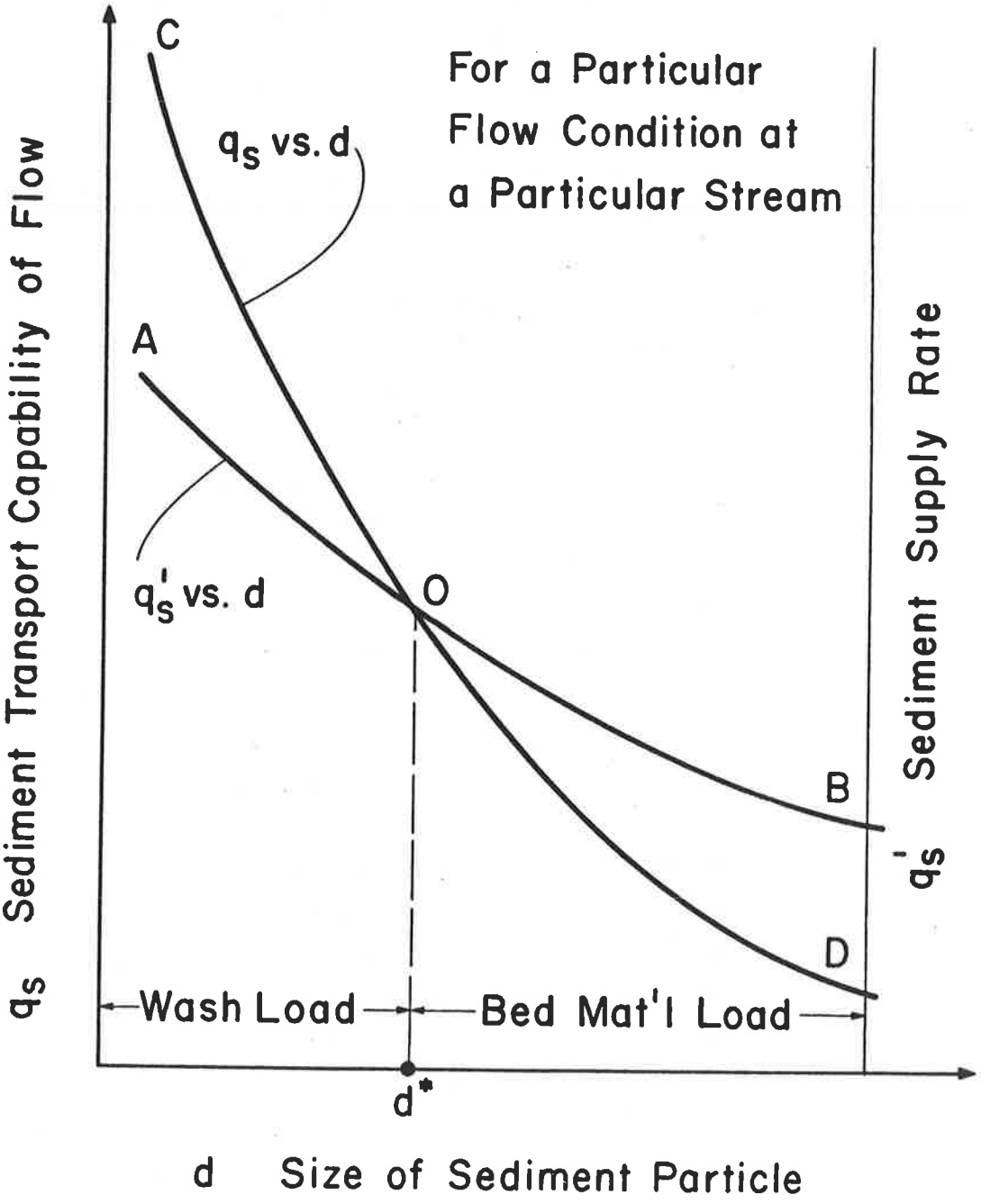

Figure 4.1 Division between wash load and bed material load.

distinct as shown; however, let us assume that they intersect at point O. The sediment size at point O is d_s^*. For sediment sizes larger than or equal to d_s^*, the available supply from the upslope area is equal to or greater than what the river can carry, and therefore deposition of these sizes will occur in the upstream reach; the river's ability to transport these sediment sizes is dictated by its transport capability in the lower reach. One may hope to establish a sediment transport equation, based on the sediment transport capability of the river, that agrees with the actual sediment transport in the lower reach. However, for sediment sizes smaller than d_s^*, the transport capability of the river exceeds the supply from upslope, the actual amount of sediment of this size transported is determined by the rate of upslope supply or production, and not by the capability of the river to transport. Obviously, in order to predict the actual amount of this sediment transported, one must study the upslope erosion rate and not the sediment transport capability of the river. Knowledge of d_s^* is important because for a sediment size equal to or greater than d_s^*, the actual transport rate equals the sediment transport capability and may be determined by a sediment transport equation (based on river flow condition). For sediments smaller than d_s^*, the actual transport rate equals the upslope sediment supply rate, and therefore must be estimated by a different technique. Consequently, the best that a sediment transport equation based on river flow can do is to predict sediment transport rates of sizes equal to and larger than d_s^*.

Wash load is defined as that portion of the sediment load governed by the upslope supply rate, and is considerably less than the sediment transport capability of a river. Wash load size is less than d_s^*, as defined in Figure 4.1. Bed material load is defined as the portion of the sediment load that is governed by the sediment transport capability of a river and is less than or equal to the upslope supply rate. The sizes of sediment in the bed material load is equal to or larger than d_s^*. The sum of the wash load and the bed material load equals the total sediment load.

Since d_s^* is determined by the intersection of the sediment transport capability curve and the available sediment supply from the upslope curve, the value of d_s^* will certainly be changed if either or both of these curves change.

The remainder of this chapter is devoted to a discussion of wash load, bed load and bed material load.

4.2 WASH LOAD

By definition, wash load is that portion of the sediment transport rate which is supplied to the stream from the watershed. Soil erosion formulae must be used to estimate the erosion rate, and thus the supply rate to the stream. Almost all of these equations were obtained after years of data collection from different watersheds.

The U.S. Department of Agriculture began to study soil loss in about 1930, when the first ten Federal-State Cooperative Stations began operation. Thirty-two additional stations were established in the next 25 years. Measurements of precipitation, runoff and soil loss at these 42 stations in 23 states east of the Rocky Mountains were collected continuously for periods of from 5 to 30 more years. The field plots were rectangular to facilitate normal flow row spacing for cultivated units. A "unit plot" 22.1 meters long on a nine percent uniform slope, continuously in bare fallow soil and tilled to break surface crusts was arbitrarily selected to serve as a common reference point for evaluation. The dimensions were chosen because most of the plots in U.S Department of Agriculture erosion studies from 1930 to 1960 were 22.1 meters long and nearly nine percent slope.

Six major factors describing rainfall (R), soil erodibility (K), slope length (L), slope steepness (S), cropping and management (C), and supplemental erosion-control practices such as contouring, terracing, etc. (P) were used to develop the following Universal Soil Loss Equation based on the field data described above and rainfall simulation data by a multiplicative model:

$$\underline{E} = RKLSCP \qquad (4\text{-}1)$$

where $\underline{E}$ is the computed soil loss per unit area, expressed in the units selected for K and for the period selected for R. In practice, these units are usually so selected that they compute $\underline{E}$ in tons per acre per year, but other units can be selected. R, the rainfall and runoff factor, is the number of rainfall erosion index units, plus a factor for runoff from snowmelt or applied water where such runoff is significant. K, the soil erodibility factor, is the soil loss rate per

erosion index unit for a specified soil as measured on a unit plot, which is defined as a 72.6-ft length of uniform 9 percent slope continuously in clean-tilled fallow. L, the slope-length factor, is the ratio of soil loss from the field slope length to that from a 72.6-ft length under identical conditions. S, the slope-steepness factor, is the ratio of soil loss from the field slope gradient to that from a 9 percent slope under otherwise identical conditions. C, the cover and management factor, is the ratio of soil loss from an area with specified cover and management to that from an identical area in tilled continuous fallow. P, the support practice factor, is the ratio of soil loss with a support practice, such as contouring, stripcropping, or terracing, to that with straight-row farming up and down the slope.

Numerical values for each of the six factors were derived from analyses of the assembled research data and from National Weather Service precipitation records. For most conditions in the United States, the approximate values of the factors for any particular site may be obtained from Wischmeier and Smith (1978). Localities or countries where the rainfall characteristics, soil types, topographic features, or farm practices are substantially beyond the range of present U.S. data will find these charts and tables incomplete and perhaps inaccurate for their conditions. However, they will provide guidelines that can reduce the amount of local research needed to develop comparable charts and tables for their conditions. Smith and Wischmeier (1957), Meyer (1971), Wischmeier (1973), and Wischmeier and Smith (1978) gave detailed analyses of recommended values for these factors.

The Universal Soil Loss Equation is designed to predict average annual soil losses on sheet and rill erosion on uplsope areas such as farmland and construction sites. It can be helpful for prediction of contributions from these sources to downstream sediment loads, but its capabilities and limitations for this use must be recognized. It is an erosion equation and is not designed to predict deposition. Its predictions do not include sediment contributions from gully erosion, and it does not include factors to account for sediment losses or gains between the field and the stream or reservoir. These items must be evaluated separately.

Many investigators have also formulated difficult equations to estimate soil erosion from experimental data. Table 4.1 gives a brief summary of some available soil loss equations, where L_o is the plot length in feet, S_o is the bed slope, and S_c and L_c are the values of S_o and L_o at which erosion begins.

Shen and Li (1976) presented a theoretical analysis of these soil loss regression equations. Of the six factors affecting soil erosion, it is impossible at this stage to make a theoretical analysis of the cropping management factor C and the erosion control factor P. It is also difficult to analyze the soil erodibility factor K, because the relationship between soil characteristics and soil erosion loss was not given in a closed form.

Assume that: 1) the overland flow reach is wide and one-dimensional; 2) hydrostatic pressure distribution is valid across the flow depth; 3) the variation of the momentum coefficient β along the direction of flow is negligible; 4) the soil layer is loose and uniform, with fine-sediment size; 5) the sediment concentration is small so the equation of motion for sediment-laden water can be approximated by the equation of motion for water only; 6) the variation of bottom slope S_o is negligible; 7) the rainfall intensity and the infiltration rate are constant and the approximate solutions to the mechanics of steady sheet flow can be developed; 8) the continuity equation for sediment can be expressed as

$$\frac{dq_s}{dx} = p_s \tag{4-2}$$

where q_s is the sediment discharge per unit width of channel and p_s is the fine-sediment pickup rate per unit area; and 9) the rate of fine-sediment pickup is assumed to be a power function of τ, the boundary shear stress of surface runoff. The relation is

$$p_s = a\,\tau_o^b \tag{4-3}$$

where a is a constant describing the erodibility of a specific soil and b is an exponent which, judging from the existing sediment transport equations, is assumed to be 2.0. However, a and b can be determined

Table 4.1 Soil loss equations.

Investigator	Relationship presented
Zingg (1940)	$\underline{E} \alpha L_o^{0.66} S_o^{1.37}$
Musgrave (1947)	$\underline{E} \alpha RKL_o^{0.37} S_o^{1.35} C$
Wischmeier and Smith (1965)	$\underline{E} \alpha RKL_o^{0.5} (0.00076 S_o^2 + 0.0053 S_o + 0.0076) CP$
Meyer and Monke (1965)	$\underline{E} \alpha L^{0.9} S_o^{3.5}$
Meyer (1965)	$\underline{E} \alpha (L_o - L_c)^{1.\sim 1.5}$, $E \alpha (S_o - S_c)^{1.5}$
Meyer and Kramer (1968)	$\underline{E} \alpha L^{0.5} (S_o - S_c)^{1.4}$
Young and Mutchler (1969)	$\underline{E} \alpha L^{1.24} S_o^{0.74}$
Kilinc (1972)	$\underline{E} \alpha L^{1.035} S_o^{1.664}$

by an optimization scheme. Shen and Li found that for a small Reynolds number of the flow

$$\underline{E} = R_k L_o^{0.67} S_o^{1.33} \tag{4-4}$$

and for a large Reynolds number of the flow

$$\underline{E} = R_k L_o^{1.17} S_o^{1.33} \tag{4-5}$$

where R_k is a factor describing the rainfall characteristics, soil erodibility, and fluid properties.

The exponents of slope length and percent slope in the above equations are consistent with the regression equations given in Table 4.1. The analytical results indicate that the exponents of L_o and S_o for most of these empirical equations are reasonable, and that these exponents should be different for different Reynolds numbers.

Although these equations seem to be reasonable, one must be very cautious in using any of them. Erosion of soil in watersheds is an extremely complex matter and there are so many factors involved that these equations can only provide qualitative answers at best.

4.3 BED LOAD

Generally the bed load is small compared to suspended load in the main flow. In most of the canals and rivers in West Pakistan the bed load is only about five percent of the total load, and may even be neglected for computing the total sediment load. If this is the case, why should one even consider bed load? The answer is that although the bed load may be small compared to the total sediment load, it is nevertheless important because it shapes the bed and is a major factor in determining the stability of the channel, the form of the sediment bed surface, etc.

The bed load equation can be classified into the following four categories. From a great deal of practical experience, engineers have found that bed load is a function of the flow velocity, V, and the characteristics of sediment. Thus, the following type of equation is developed:

$$q_B = \text{bed load (rate)} = k_1 V^{k_2} \tag{4-6}$$

They have also found that velocity is much more important than flow depths or slopes or other parameters in the determination of the bed load. However, it was later found that this equation does not satisfy the condition that there is a critical velocity below which no bed load movement would occur. In order to satisfy that condition, engineers have proposed a second equation

$$q_B = k_1 (V-V_c)^{k_2} \tag{4-7}$$

where V_c is defined as the critical velocity below which no sediment transport would occur. This equation does satisfy the initial condition that when $V \leq V_c$, q_B is zero or even negative, which is impossible. Although this equation does satisfy the initial condition for incipient motion, there is no physical reason to believe that if $V > V_c$, q_B should be a function of $V - V_c$ rather than a function of V as indicated in Equation 4-6. In recent decades it has been found that shear stress on the bed may be a better parameter than flow velocity to indicate the bed load rate. Thus, engineers propose the equation

$$q_B = k_1 \tau^{k_2} \tag{4-8}$$

In order to satisfy the initial condition for incipient motion, engineers propose Equation 4-9 where

$$q_B = k_1 (\tau - \tau_c)^{k_2} \tag{4-9}$$

In the above equation τ is the shear stress on the bed and τ_c is the shear stress on the bed for incipient motion. Similar to Equation 4-7, this Equation 4-9 also satisfies the initial condition that when $\tau \leq \tau_c$, q_B is zero or negative, which is impossible. Laursen (1956) reviews several well-known bed load equations as follows:

	Original Form	Reduced Form
DuBoys (Straub)	$q_B = A_1(\tau - \tau_c)$	$= B_1 n^4 \frac{V^4}{d^{2/3}}$
Schoklitsch (Shulits 1935)	$q_B = \frac{A_2}{d_s^{1/2}} S^{3/2}(q - q_c)$	$= B_2 \frac{n^3}{d_s^{1/2}} \frac{V^4}{d}$
Meyer-Peter et al. (1934)	$q_B = (A_3 q^{2/3} S - A_4 D)^{3/2}$	$= B_3 n^3 \frac{V^4}{d}$
Wes (1935)	$q_B = \frac{A_5}{n} (\tau - \tau_c)^m$	$= B_5 n^{2m-1} \frac{V^{2m}}{d^{m/3}}$
Shields (1936)	$q_B = \frac{A_6}{d_s} q\, S(\tau - \tau_c)$	$= B_6 \frac{n^4}{d_s} \frac{V^5}{d^{m/3}}$
Brown-Einstein (1950)	$q_B = \frac{A_7}{d_s^{3/2}} \tau^3$	$= B_7 \frac{n^3}{d_s^{3/2}} \frac{V^6}{d}$
Brown-Kalinske (1950)	$q_B = \frac{A_8}{d_s} \tau^{5/2}$	$= B_8 \frac{n^5}{d_s} \frac{V^5}{d^{5/6}}$

where m, A_1 through A_8 (inclusive) and B_1 through B_8 (inclusive) are constants, n is Manning's roughness, d is the flow depth, and d_s is the sediment size.

Of these equations the one developed by Einstein (1950 probably is the most reliable because it is based on a very comprehensive study and has been most extensively tested. It should also be pointed out that these equations are applicable only to cohesionless material in steady and uniform flow. Another limitation could probably be added--that

these equations are not useful if the ratio between the flow depth and the sediment particles size is too small. A possible improvement over these equations is through the formulation of stochastic bed load. For a general discussion of stochastic bed load models the reader is referred to Shen (1976).

Meyer-Peter and Müller (1948) developed the following equation based on experiments with sand particles of uniform size, sand particles of mixed sizes, natural gravel, ligmite, and baryta:

$$\left(\frac{Q_b}{Q}\right)\left(\frac{K_b}{K_r}\right)^{3/2}\gamma y_o S = B'(\gamma_s - \gamma)D_m + B\left(\frac{\gamma}{g}\right)^{1/3}\left(\frac{\gamma_s - \gamma}{\gamma_s}\right)^{2/3} q_B^{2/3} \qquad (4\text{-}10)$$

where q_B is the bed load rate in weight per unit time and per unit width, Q_b is water discharge quantity determining bed load transport, Q is total water discharge, y_o is the depth of flow, S is the energy slope and B' and B are dimensionless constants. B' has the value 0.047 for sediment transport and 0.034 for the case of no sediment transport. B has a value of 0.25 for sediment transport and is meaningless for no transport, since q_B is zero and the last term drops out. Equation 4-10 is dimensionally homogeneous so that any consistent set of units may be used.

The quantities K_b and K_r are defined by the expressions

$$V = K_b R_b^{2/3} S^{1/2} \qquad (4\text{-}11)$$

and

$$V = K_r R_b^{2/3} S'^{1/2} \qquad (4\text{-}12)$$

where S' is the part of the total slope, S, required to overcome the grain resistance and S-S' is that part of the total slope required to overcome form resistance. Therefore,

$$\frac{K_b}{K_r} = \sqrt{\frac{f_b'}{8}}\ \frac{V}{\sqrt{g\ R_b S}} \qquad (4\text{-}13)$$

where f_b' is the Darcy-Weisbach bed friction factor for the grain roughness. If the boundary is hydraulically rough ($V_* D_{90}/\nu \geq 100$), K_r is given by

$$K_r = \frac{26}{D_{90}^{1/6}} \tag{4-14}$$

in which D_{90} is in meters and K_r is in $m^{1/3}$ sec. The quantity D_m is the effective diameter of the sediment given by

$$D_m = \frac{\sum_i p_i D_i}{100} \tag{4-15}$$

where P_i is the percentage by weight of that fraction of the bed material with geometric mean size, D_i.

The Meyer-Peter and Müller formula (Equation 4-10) is often written in the form

$$q_b = K (\tau - \tau_c)^{3/2} \tag{4-16}$$

where

$$K = \left[\frac{1}{B(\frac{\gamma}{g})^{1/3} (\frac{\gamma_s - \gamma}{\gamma_s})^{2/3}} \right]^{3/2}$$

4.4 SEDIMENT BED MATERIAL LOAD

Rational Approaches

Lane and Kalinske (1941) and Kalinske (1947) probably made the first successful attempts to determine suspended sediment discharge by integrating Equation 4-17 below. They first found the bed load sediment concentration and then, using that as the reference sediment concentration at a certain level, integrated Equation 4-17 to give the total bed material load.

Einstein (1950) also integrated Equation 4-17 to obtain suspended load from bed load.

$$\frac{C_y}{C_a} = \left(\frac{d-y}{y} \quad \frac{a}{d-a}\right)^Z \tag{4-17}$$

where C_y and C_a are suspended sediment concentrations at distances y and a from the top of the bed surface and Z is a function of shear velocity and sediment size. He first determined the bed load for a particular particle size and assumed from experimental evidence that the bed load concentration occurred at two grain diameters from the bed

in order to integrate Equation 4-17 to obtain the suspended load for that size. Einstein gave an example to illustrate the application of his procedure in calculating the total sediment transport rate for Big Sand Creek, Mississippi.

Einstein's procedure, although theoretically sound, does involve many assumptions. Some of these assumptions are necessary if no other data are available. However, if sediment concentration and stream flow can be measured in a river, one may find the total load according to a modified procedure.

Colby and Hembree (1955) proposed a modified Einstein procedure to obtain the total sediment transport rate in a river. The term "modified Einstein procedure" usually gives the false impression that it serves the same purpose as Einstein's procedure. Actually, these two procedures, although based on similar principles, serve entirely different purposes. As stated in the previous paragraph, Einstein's procedure estimates total sediment bed material load for different river discharges based on the channel cross section and a sediment bed sample from a selected river reach with uniform flow. This procedure is mainly for design purposes. The modified Einstein procedure developed by Colby and Hembree only estimates the total sediment load (including wash load) for a given discharge from the measured depth integrated suspended sediment load, the stream flow measurements, the bed material samples, and the water temperature for this discharge at a given cross section.

The major modifications from Einstein's original procedure used in the modified Einstein procedure are:

1. The calculation is based on a measured mean velocity rather than on the slope, and the depth is observed for each velocity.
2. The friction velocity and the corresponding suspended load exponent Z in Equation 4-17 are determined from the observed Z value for a dominant grain size and are assumed to change with the 0.7 power of the settling velocity.
3. A slight change in the hiding factor is introduced.
4. Flow depth replaces the hydraulic radius.
5. The value of Einstein's intensity of bed load transport is arbitrarily divided by a factor of two to fit the data more closely. Since the modified Einstein procedure essentially

estimates the total sediment load from the measured sediment load, it no doubt can give better agreement with field data than the Einstein procedure, which is based on more assumptions and fewer data. Since the modified Einstein procedure relies on depth-integrated suspended sediment samples, it should be more reliable with shallow streams where the sediment concentration variation is less than in deep rivers.

Bishop, Simons, and Richardson (1965) present other modifications of the procedure presented by Einstein (1950).

Toffaleti (1968, 1969) presents a procedure for the analytical determination of sediment transport based on the concepts of Einstein (1950) and Einstein and Chien (1953). First, he establishes that Einstens's ψ versus ϕ curve may be represented by the equivalent expression,

$$\psi = \frac{TA}{V^2} 10^4 d \qquad (4\text{-}18)$$

in which ψ is Einstein's transport parameter, T (unit in length/time^2) is a parameter that includes constants and those components of shear force that are functions of water temperature, A is a dimensionless correction factor to replace Einstein's correction factors for sediment of mixed sizes, V (unit in length/time) is the mean flow velocity, and d (unit in length) is the grain diameter. He divides the flow depth into three zones: the lower zone where the depth of flow is less than R/11.24 (R is the hydraulic radius), the middle zone where the depth is between R/11.24 and R/2.5, and the upper zone, for a depth greater than R/2.5. Toffaleti further states that the G_F, or nucleus load, in tons per day, computed for a 1-foot width in lower zone and assuming the bed is composed entirely of one sand, can be represented by

$$G_F = \frac{0.600}{\left(\frac{TA}{V^2}\right)^{5/3} \left(\frac{d}{0.00058}\right)^{5/3}} \qquad (4\text{-}19)$$

For very fine sand (d_s < 0.00029 feet) the equation would be

$$G_F = \frac{1.905}{\left(\frac{TA}{V}\right)^{5/3}} \qquad (4\text{-}20)$$

The form of Equations 4-14 and 4-20 is based on Equation 4-18. The exact relationships are determined from field data as measured in a large river (the Atchafalaya River). These data were taken over a 20-year period covering a range of discharges of 20,000 cfs to 500,000 cfs. (The above information was obtained by private communication with Toffaleti.) The sediment concentration distribution is expressed as

$$C_y = C_a \left(\frac{R}{y}\right)^Z \tag{4-21}$$

in which C_y is the sediment concentration at y, C_a is the sediment concentration at a level a, and y is the vertical elevation. For his middle zone,

$$Z = \frac{VW}{C_z SR} \tag{4-22}$$

in which W is the fall velocity of the particle, C_z is a temperature correction factor which equals 260.67 - 0.667x (degrees Fahrenheit), and S is the energy or water surface slope. The exponents, Z, of the sediment concentration distribution at the lower and upper zones are, respectively, 0.756 and 1.5 times that of the middle zone.

After knowing G_F and the sediment concentration distribution in the lower zone, one can proceed to determine the sediment concentration at the upper edge of the lower zone. With G_F and the sediment concentration distribution in the middle zone, one can determine the sediment concentration load in the middle zone, and similarly, one can obtain the total sediment load in the upper zone. The summation of the total sediment loads in the three zones is of course the total sediment load in the entire flow depth.

Bagnold (1966) introduced the concept that the sediment transport mechanism is related to the availability and the efficiency of stream power to transport sediments.

Empirical Approaches

Because most of the rational approaches described previously involve rather complex procedures and many questionable assumptions, there is definitely a need to develop a simple relationship between the sediment transport rate and the flow condition, based entirely on available data,

to provide the design engineer with an estimation that is of the correct order of magnitude. In order to achieve a successful empirical approach, one must first select all the important factors involved. It is generally agreed that the flow velocity, the flow depth (or hydraulic radius), the energy slope, the characteristics of the sediment, and the temperature of the fluid are important factors; whether or not all these factors must be included in the analysis is, of course, subject to interpretation.

In making the analysis, one must recognize that the sediment concentration increases much faster than does of flow discharge. There is a generalized rule that sediment transport rate increases with flow velocity to the fourth power at low flow discharges, and increases with flow velocity to the eighth power at high flow discharges. In other words, there is not much hope of finding a single combination of flow and sediment characteristics to describe sediment concentration for all flow conditions. Recognizing this fact, Colby (1964) developed different sediment discharge relationships with flows for 0.1-foot, 1-foot, 10-foot, and 100-foot flow depths; Maddock (1969) provided different sediment discharge relationships with flow for low-, mid-, and high-velocity ranges, and Shen and Hung (1972) constructed a sediment-transport parameter and determined the concentration as a function of this parameter.

Colby (1964) investigated the effect of mean flow velocity, shear, shear velocity computed from mean velocity, stream power of flow, flow depth, viscosity, water temperature, and concentration of fine sediment on the discharge of sand per foot of channel width. He recommended three diagrams. In spite of many inaccuracies in the available data and uncertainties in the graphs, Colby found that "...about 75 percent of the sand discharges that were used to define the relationships were less than twice or more than half of the discharges that were computed from the graphs of average relationship. The agreement of computed and observed discharges of sands for sediment stations whose records were not used to define the graphs seemed to be about as good as that for stations whose records were used." Note that all curves of 100-ft depth, most curves of 10-ft depth and part of the curves of 1.0-ft and 0.1-ft depths for Colby's diagrams are not based on available data and are extrapolated. His curves are given in Figure 4.2 and the corrections for temperature and time suspended sediment are given in Figure 4.3.

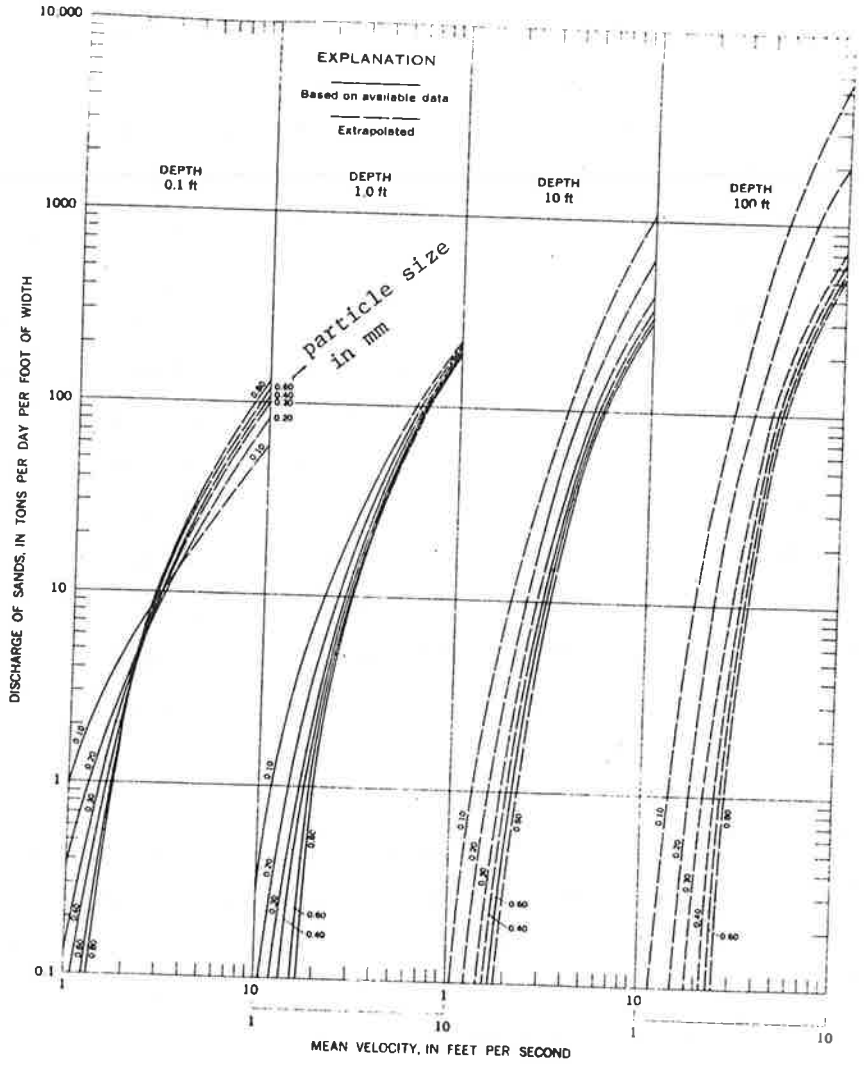

Figure 4.2 Relationship of discharge of sands to mean velocity for six median sizes of bed sands, four depths of flow, and a water temperature of 60°F, after Colby (1964).

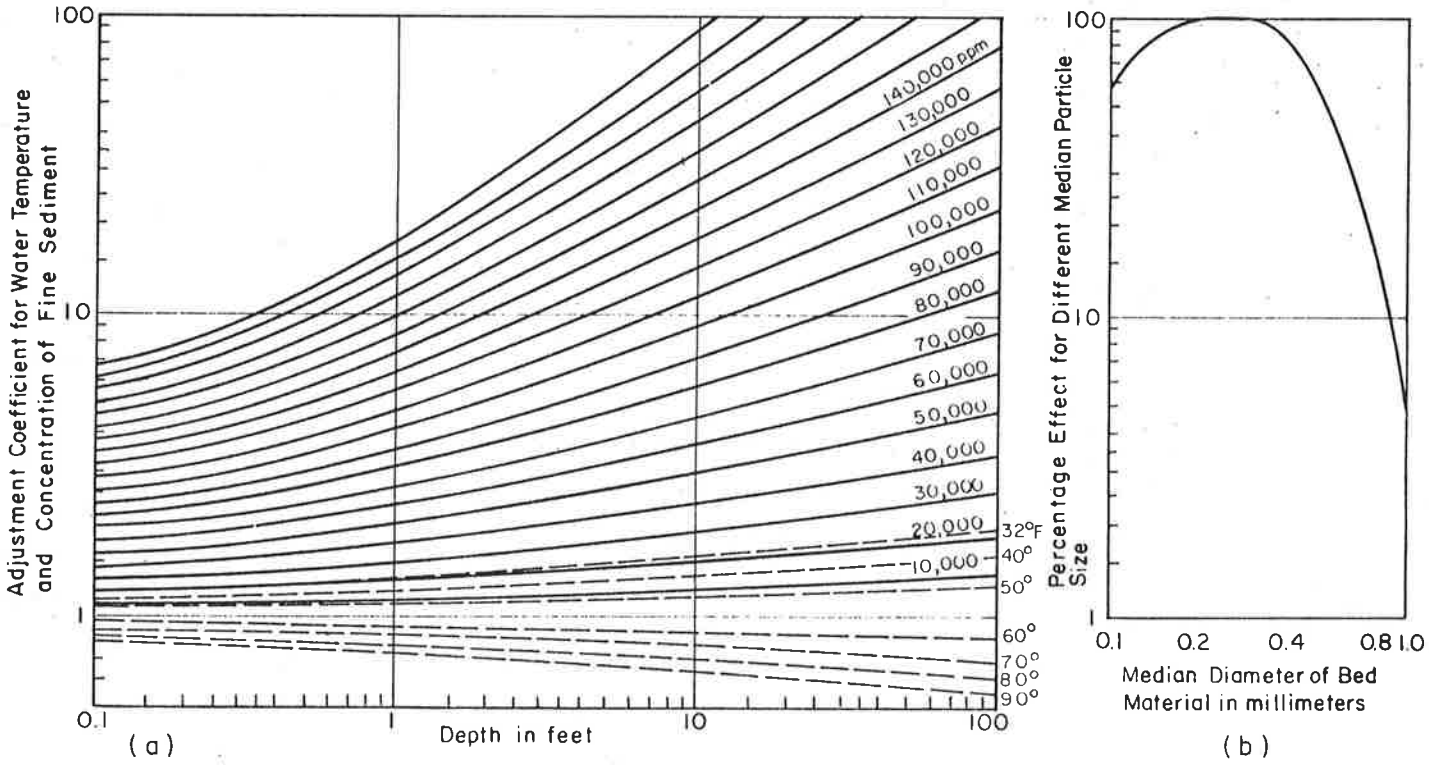

Figure 4.3 Approximate effect of water temperature and concentration of fine sediment on the relationship of discharge of sands to mean velocity, after Colby (1964).

Shen and Hung (1972) began with the assumption that sediment transport is such a complex phenomenon that no single Reynolds number, Froude number, or combination thereof can be found to describe sediment motion under all conditions. They recommended use of a regression method to develop a formula based on all available data for immediate engineering purposes. The disadvantage of this approach is, of course, that the final flow parameter will probably be dimensional, but the approach has merit in that if all previous data are found to correlate well, it is likely that other data within the same range will follow the same trend. They selected the sediment concentration (bed material load) as the dependent variable and the fall velocity of the median sediment particle of the bed sample, the flow velocity, and the flow depth as the independent variables.

Based on available reliable flume data and a few river data, they found that the sediment concentration is a function of $V^{0.57}\ S/w^{0.32}$ where V is the flow velocity in feet per second, S is the energy slope, and w is the fall velocity in feet per second of the median sediment size. Since this is an empirical dimensional equation it is not easy to convert it to cgs units. This curve is shown in Figure 4.4.

Yang (1972) presented another regression equation based on his stream power concept. He found that the sediment concentration C is a function of stream power (product of flow velocity and energy slope), sediment particle size, shear velocity, fall velocity of sediment particle, etc. Table 4.2 gives a comparison of many equations by Yang (1977) based on all data available to him.

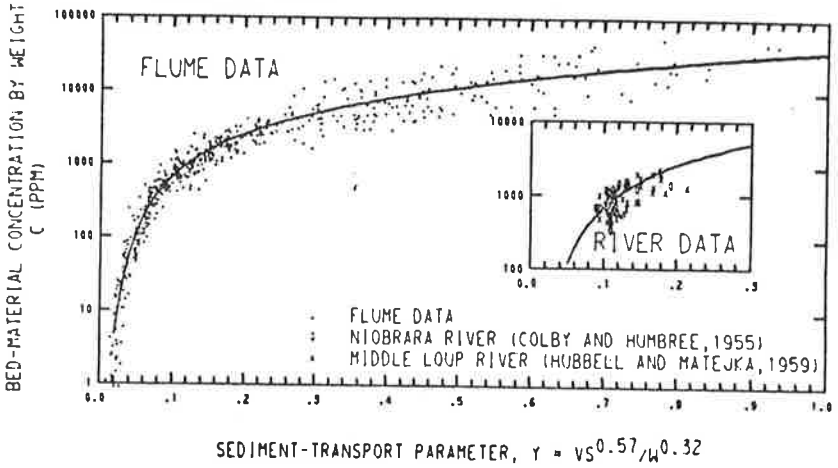

Figure 4.4 Bed-material load vs flow (all primary data).

Table 4.2 Summary of accuracies of different equations.

Equations	Date	Data with Discrepancy Ration Between 1/2 and 2
Yang	1973	91 percent
Shen and Hung[a]	1972	85 percent
Ackers and White	1973	68 percent
Engelund and Hansen	1967	63 percent
Rottner	1959	56 percent
Einstein	1950	46 percent
Bishop et al.	1965	39 percent
Toffaleti	1969	37 percent
Bagnold	1966	22 percent
Meyer-Peter and Müller	1948	10 percent

[a]Should not be applied to large rivers.

4.5 CONCLUSIONS

Because of the tremendous uncertainties, it is difficult to make any final recommendations on the estimation of sediment transport which is, unfortunately, an extremely important problem. However, the following procedures are suggested for analyzing field data:

1. Use the modified Einstein's method (Colby and Hembree, 1955) to estimate the unmeasured suspended load and bed load based on measured data. There is a question on whether Einstein's intensity of bed load transport should be arbitrarily divided by a factor of two.
2. Separate bed material load and wash load and analyze them separately.
3. Decide which available sediment transport equation best agrees with the measured data and use it to estimate the sediment transport load for design flow where actual measurement is not available.
4. If the measured data do not agree with any available sediment transport equation, use a simple power relationship between flow discharge and sediment transport rates. These terms are given as Equations 4-6, 4-7, 4-8, and 4-9.

When no measured data is available, the writer is inclined to:

1. Use Einstein's (1950) procedure if bed load is a significant portion of the total bed material load. Meyer-Peter's (1948) equation should be used if bed load consists of very large-sized material.
2. Use Colby's (1964) method for rivers with flow depth up to about 10 feet; also see 4 below.
3. Use Toffaleti's (1969) method for large rivers.
4. Use methods by either Shen and Hung (1971) or Yang (1972) for reference purposes.

4.6 APPENDIX. SEDIMENT MEASURING EQUIPMENT

Introduction

The most complete set of reports to describe flow- and sediment-measuring equipment were prepared by the U.S. Inter-Agency Committee on Water Resources. Since the U.S. Geological Survey is the official data collection agency for the U.S. government, any problem related to measurements should be related to them. A series of manuals entitled "Techniques of Water Resource Investigations of the United States Geological Survey" can be purchased from the U.S. Printing Office, Superintendent of Documents, Washington, D. C. Section Three of Book A is written on surface water measuring techniques.

Site Selection for Gaging Stations

This is an extremely important item for consideration because the usefulness of this data depends a great deal on choosing the proper sites.

Consideration should be given to the following items:

1. Natural controls or opportunity to install artificial controls so that the relationship between stage and discharge is constant.
2. Accessibility, especially during flood.
3. No backwater so that the relationship between stage and discharge is distinct.
4. Uniform reach so that the effect by secondary currents is not strong.
5. Suitability for installing measuring structures.

Stream Flow Measurements

1. Current meter: A price current meter is the most commonly used method to measure flow velocities. The meter usually consists of six cups and the velocity is measured by noting the number of revolutions in a given time interval. It is a durable piece of equipment. The total flow discharge is the sum of the product of velocity and flow area for each subsection.

2. Dilution techniques: The steady-feed method (continuous source) and the instantaneous source method are used. The steady-feed method is illustrated below.

   As shown in Figure 4.5: a constant injection of tracer $C_1 Q_T$ is introduced at x_1. (C_1 is the tracer concentration at 1 and Q_T is the tracer design). By continuity relationsips between x_1 and x_2

$$Q_T C_1 = (Q + Q_T)C_2 \tag{4-23}$$

   where Q is the flow discharge and C_2 is the concentration of tracer at status x_2. Thus,

$$Q = \frac{Q_T C_1}{C_2} \tag{4-24}$$

   if $Q_T << Q$.

   Thus the flow discharge Q can be obtained if Q_T, C_1 and C_2 are known.

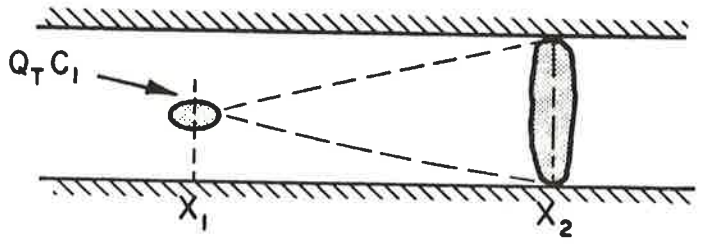

Figure 4.5 Use of dye-dilution method to estimate flow discharge.

The main assumption there is that 1) the total Q at x_1 and x_2 is the same, and 2) C_2 is well mixed in the flow $Q + Q_T$.

The instantaneous source method is to inject a quantity of tracer W at x_1. Since

$$W = \int_0^\infty QCdt \tag{4-25}$$

and the flow discharge Q is approximately constant,

$$Q = \frac{W}{\int_0^\infty cdt} \tag{4-26}$$

3. Other methods: If a stream is relatively narrow, a weir can be constructed for flow measurements. Another method would be to continue the flow discharge from Manning's equation that

$$Q = \frac{1.49}{n} A R^{2/3} S^{1/2} \tag{4-27}$$

where n is the Manning's roughness, A is the estimated flow area, R is the estimated flow depth, and S is the estimated channel bottom slope.

Sediment Discharge

1. Bed load is the most difficult item to measure. There are four methods to measure it and these are listed below according to their relative accuracies.
   A. Bed load sampler. This is useful if the stream bed surface is relatively flat (no dunes or ripples), and if the particles are not too big. The Helly-Smith bed load sampler is a popular instrument.
   B. Turbulent flume. The basic principal here is to stir up the flow so that the bed load is carried in suspension and can be measured as part of the suspended load.
   C. Bed load trap. Measuring the deposit in a trap at the stream bottom is a method that can be used to measure bed load in mountain streams. However, the suspended load deposition in the trap cannot be estimated.

D. Monitor the movements of dunes and other bed forms. Usually this method would overestimate the bed load movement because some sediment in the bed form is stationary even though the entire bed form progresses downstream.

2. Suspended load. All of the standard U.S. sediment-sampling equipment is described in the Inter-Agency Reports. The three commonly used depth integrated samplers are the U.S. DH-48, DH-59 and D-49 Samplers. DH-48 is used in shallow streams. The sampler is calibrated with a 1/4 or 3/16 inch diameter nozzle and can sample to within 3-1/2 inches of the streambed. A standard stream-gaging wading rod is threaded into the top of the sampler body.

The U.S. DH-59 is used with a hand-line suspension in streams that cannot be waded but have flow velocities less than about 6 feet per second. It is similar to the DH-48, except that tail vanes orient this sampler into the flow. The sampler weighs 24 pounds.

The U.S. D-49 sampler has a cast bronze streamlined body and weighs 62 pounds. The hose of the sampler is drilled and tagged for intake nozzles, 1/4, 3/16 and 1/8 inch inside diameter. It is suitable to a flow depth of about 15 feet and up to a flow velocity of about 7 feet per second.

The new P-61 and P-63 point-integrated samplers have replaced the old P-46 and P-50. Maximum sampling depth reaches 150 to 200 feet. All of the samplers are streamlined and cast in bronze, with tail fins to orient the sampler into the flow. They have either a two- or three-position solenoid-activated valves that closes the nozzle, equalize the pressure in the sampler container to avoid an initial surge when sampling starts, and open the sampler nozzle.

3. Bed material size. The size distribution of bed material is an important property of a stream, especially if the bed load or the bed material load is to be estimated by computational methods.

The BMH-53 is designed for shallow streams that can be waded and collects a core 2 inches in diameter and 8 inches

deep. The BM-59 can be used to collect bed material samples from a stream or reservoir at any depth. It is 22 inches long and made of cast steel. When it is supported by a cable, a scoop bucket in the bottom can be set in an open position and when the cable tension is released by resting the sampler on the stream bed, the bucket snaps shut, collecting a sample from the top two inches of the stream bed. The BMH-60 is similar to the BM-59, except it is designed to operate from a handline rather than a cable suspension.

AUTOMATIC SEDIMENT SAMPLER

P-67

Bill Curtis U.S.G.S., Denver

4.7 REFERENCES

Ackers, P. and White, W. R., 1973, "Sediment Transport: New Approach and Analysis," J. Hydraulics Div., ASCE 99, 2041.

Bagnold, R. A., 1966, "An Approach to the Sediment Transport Problem from General Physics," U.S. Geological Survey Professional Paper 422-J.

Bishop, A. A., Simons, D. B., and Richardson, E. V., 1965, "Total Bed-Material Transport," J. Hydraulics Div., ASCE 91, 175.

Brown, C. B., 1950, "Sediment Transportation," Chapter XII of Engineering Hydraulics, ed. Hunter Rouse, John Wiley and Sons, pp. 796-99.

Colby, B. R. and Hembree, C. H., 1955, "Computations of Total Sediment Discharge Niobrara River Near Cody, Nebraska," U.S. Geological Survey Water Supply Paper 1357.

Colby, B. R., 1964, "Discharge of Sands and Mean-velocity Relationships in Sand-bed Streams," U.S. Geological Survey Professional Paper 462-A.

Einstein, H. A., 1950, "The Bedload Function for Sediment Transport in Open Channel Flows," U.S. Department of Agric. Soil Conservation Service, Technical Report No. 1026.

Einstein, H. A. and Chien, N., 1953, "Transport of Sediment Mixtures with Ranges of Grain Size: Missouri River Div. Sediment Series No. 3, U.S. Army Engr. Div., Missouri River, January.

Engelund, F. and Hansen, E., 1967, "A Monograph on Sediment Transport in Alluvial Streams," Danish Technical Press, Copenhagen, Denmark, Revised edition 1972.

Inter-Agency Committee on Water resources, 1940, "A Study of Methods Used in Measurement and Analysis of Sediment Loads in Streams," Report No. 1. Field Practice and Equipment Used in Sampling Suspended Sediment, Washington, U.S. Government Printing Office, 175 p.

_____, 1940, "Equipment for Sampling Bed-load and Bed Material," Report No. 2, 57 p.

_____, 1941, "Analytical Study of Methods of Sampling Suspended Sediment," Report No. 3, 82 p.

_____, 1941, "Methods of analyzing Sediment Samples," Report No. 4, 99 p.

_____, 1941, "Laboratory Investigations of Suspended Sediment Samplers," Report No. 5, 203 p.

_____, 1952, "The Design of Improved Types of Suspended Sediment Samplers, Report No. 6, 103 p.

_____, 1943, "A Study of New Methods for Size Analysis of Suspended Sediment Samples," Report No. 7, 102 p.

_____, 1948, "Measurement of Sediment Discharge of Streams," Report No. 8, 92 p.

_____, 1943, "Density of Sediments Deposited in Reservoirs," Report No. 9, 60 p.

_____, 1953, "Accuracy of Sediment Size Analysis Made by the Bottom Withdrawal Tube Method," Report No. 10, 115 p.

_____, 1957, "The Development and Calibration of the Visual-Accumulation Tube," Report No. 11, 109 p.

_____, 1957, "Some Fundamentals of Particle Size Analysis," Report No. 12, 55 p.

_____, 1961, "The Single-stage Sampler for Suspended Sediment," Report No. 13, 105 p.

_____, 1963, "Determination of Fluvial Sediment Discharge," Report No. 14, 151 p.

Kalinske, A. A., 1947, "The Movement of Sediment as Bed Load in Rivers," Transactions, American Geophysical Union, Vol. 28, pp. 615-620.

Kilinc, M. Y., 1972, "Mechanics of Soil Erosion from Overland Flow Generated by Simulated Rainfall," Dissertation, Department of Civil Engineering, Colorado State University, Fort Collins, Colorado.

Lane, E. W. and Kalinske, A. A., 1941, "Engineering Calculations of Suspended Sediment," Transactions, American Geophysical Union, Vol. 22, pp. 603-607.

Laursen, E. M., 1956, "The Application of Sediment-Transport Mechanics to Stable-Channel Design," Journal of the Hydraulic Div., ASCE, Vol. 82, No. HY4, August 1956, Proc. Paper 1034.

Laursen, E. M., 1958, "The Total Sediment Load of Streams," Journal of Hydraulic Div., ASCE, Vol. 84, No. HY1, February, Proc. Paper 1530, 36 p.

Maddock, T., Jr., 1969, "The Behavior of Straight Open Channels with Movable Beds," U.S. Geological Survey Professional Paper 622-A.

Meyer, L. D., 1965, "Mathematical Relationships Governing Soil Erosion by Water," Journal of Soil and Water Conservation, Vol. 20, No. 4.

Meyer, L. D., 1971, "Soil Erosion by Water on Upland Areas," Chapter 27, Vol. II, River Mechanics, edited by H. W. Shen, Colorado State University, Fort Collins, Colorado.

Meyer, L. D. and Kramer, L. A., 1968 Winter meeting of ASAE, Chicago, Illinois.

Meyer, L. D. and Monke, E. J., 1965, "Mechanics of Soil Erosion by Rainfall and Overland Flow," Transactions, ASAE, Vol. 8, No. 4, pp. 572-580.

Meyer-Peter, E., Favre, H., and Einstein, A., 1934, "Neuere Versuchsresultate über den Geschiebetrieb," Schweizerische Bauzeitung 103.

Meyer-Peter, E. and Müller, R., 1948, "Formula for a Bedload Transport," International Association of Hydraulic Research 2nd Meeting, Stockholm, p. 39.

Musgrave, G. W., 1947, "The Quantitative Evaluation of Factors in Water Erosion, A First Approximation," Journal of Soil and Water Conservation, Vol. 2, No. 3, pp. 133-138.

Rottner, J., 1959, "A Formula for Bed Material Transport," Houille Blanche 4.

Schoklitsch, A., 1934, "Geschiebetrieb und die Geschiebefracht," Wasserkraft Wasserwirtsch, 39.

Shen, H. W., 1976, "Sediment Transport Models," in Stochastic Approaches to Water Resources, Vo. II, H. W. Shen, editor.

Shen, H. W. and Hung, C. S., 1972, "An Engineering Approach to Total Bed Material Load by Regression Analysis," in H. W. Shen (ed.) Proceedings, Sedimentation Symposium, Berkeley, California, p. 14.

Shen, H. W. and Li, R. M., 1976, "Watershed Sediment Yield," in H. W. Shen (ed.) Stochastic Approaches to Water Resources, Vol. II.

Shields, A., 1936, "Application of Similarity Principles and Turbulence Research to Bedload Movement," transl. into English by W. P. Ott and J. C. Van Uchelen at California Institute of Technology, Pasadena, California.

Shulits, S., "The Schoklitsh Bed Formula," Engineering, Vol. 139, June 1935, pp. 644-646, 687.

Smith, D. D. and Wischmeier, W. H., 1957, "Factors Affecting Sheet and Rill Erosion," Transactions, AGU, Vol. 38, pp. 889-896.

Straub, L. G., 1954, "Terminal Report on Transportation Characteristics--Missouri River Sediment," University of Minnesota, St. Anthony Falls Hydraulics Lab., Sediment Series No. 4.

"Studies of River Bed Materials and Their Movement with Special Reference to the Lower Mississippi River," U.S. Waterways Experiment Station (WES) Paper No. 17, Vicksburg, Miss., Jan. 1935.

Toffaleti, F. B., 1968, A Procedure for Computation of the Total River Sand Discharge and Detailed Distribution, Bed to Surface," Tech. Report No. 5, Committee on Channel Stabilization, Corps of Engineers, U.S. Army.

Toffaleti, F. B., 1969, "Definitive Computations of Sand Discharge in Rivers," Journal of the Hydraulic Div., ASCE, Vol. 95, No. HY1, January, Proc. Paper 6350.

Wischmeier, W. H., 1973, "Upslope Erosion Analysis," Chapter 15 in Environmental Impact on Rivers, edited and published by H. W. Shen, Colorado State University, Fort Collins, Colorado.

Wischmeier, W. H. and Smith, D. D., 1965, "Predicting Rainfall-erosion Losses from Cropland East of the Rocky Mountains," Agriculture Handbook, No. 282, USDA.

Wischmeier, W. H. and Smith, D. D., 1978, "Predicting Rainfall Erosion Losses, a Guide to Conservational Planning," U.S. Department of Agriculture, Agriculture Handbook No. 537.

Yang, C. T., 1972, "Unit Stream Power and Sediment Transport," Journal of the Hydraulic Div., ASCE, Vol. 98, No. HY10, October, Proc. Paper 9295, pp. 1805-1826.

Yang, C. T., 1973, "Incipient Motion and Sediment Transport," Journal of the Hydraulics Division, ASCE, Vol. 99, p. 1679.

Yang, C. T., 1977, "The Movement of Sediment in Rivers," Geophysical Surveys, Vol. 3, D. Reidel Publishing Company, Dordrecht-Holland, pp. 39-68.

Young, R. A. and C. K. Mutchler, 1969, "Soil Movement in Irregular Slopes," Water Resources Research, Vol. 5, no. 5, pp. 1084-1089.

Zingg, A. N., 1940, "Degree and Length of Land Slope as it Affects Soil Loss in Runoff," Agricultural Engineering, pp. 59-64.

CHAPTER 5

ALLUVIAL BED ROUGHNESS

by

H. W. Shen, Professor of Civil Engineering, Colorado State University, Fort Collins, Colorado

MANNING'S n

Barnes USGS

5.1 INTRODUCTION

Frictional resistance can be divided into the following four sections: 1) rigid boundary without rainfall, 2) rigid boundary with rainfall, 3) alluvial river boundary, and 4) boundary with vegetation.

5.2 RIGID BOUNDARY WITHOUT RAINFALL

The two best known equations developed and used by hydraulic engineers are the Manning and Chezy equations. Manning's equation is

$$V = \frac{1.49}{n} R^{2/3} S^{1/2} \tag{5-1}$$

and Chezy's equation is

$$V = C\sqrt{RS} \tag{5-2}$$

In the above two equations, V is the average flow velocity, R is the hydraulic radius, S is the energy slope, n is Manning's roughness value, and C is Chezy's roughness value. Many textbooks (Chow, 1959; Henderson, 1966; Barnes, 1967) provide pictures and detailed tables on the approximate n and C values for difficult rigid boundaries. Table 5.1 provides a few commonly used roughness values.

Table 5.1 Resistance parameters for overland flow (after Woolhiser, 1975).

Surface	Laminar Flow	Turbulent Flow	
	k_o	Manning's n	Chezy's C ($ft^{1/2}/sec$)
Concrete or Asphalt	24- 108	.01 -.013	73 -38
Bare Sand	30- 120	.01 -.016	65 -33
Graveled Surface	90- 400	.012-.03	38 -18
Bare Clay-Loam Soil (eroded)	100- 500	.012-.033	36 -16
Sparse Vegetation	1000- 4,000	.053-.13	11 - 5
Short Grass Prairie	3000-10,000	.10 -.20	6.5- 3.6
Bluegrass Sod	7000-40,000	.17 -.48	4.2- 1.8

Strickler (1923) proposed the following formula to relate Manning's n value to median size of the roughness element on the boundary.

$$n = 0.0342\, d_{50}^{1/6} \tag{5-3}$$

where d_{50} is the median size of the roughness element on the boundary in feet.

In laboratory studies, the most popular approach is to use the Darcy-Weisbach friction coefficient and the Moody diagram. The Darcy-Weisbach frictional resistance f is expressed as follows:

$$S = \frac{f}{4R}\frac{V^2}{2g} \tag{5-4}$$

For laminar flow over a smooth surface, the theoretical relationship between the friction factor and Reynolds number ($R_e = VR/\nu$) is

$$f = 24/R_e \tag{5-5}$$

where ν is the kinematic viscosity of the fluid.
For laminar flow over a rough surface, a similar relationship has been observed:

$$f = k_o/R_e \quad ; \quad k_o > 24 \tag{5-6}$$

The values of k_o are given in Table 5.1.

The relationships between f and n and f and C can be derived, respectively, from Equations 5-1 and 5-4 and from Equations 5-2 and 5-4.

$$f = \frac{8gn^2}{1.4^2 R^{1/3}} \tag{5-7}$$

and

$$f = \frac{8g}{C^2} \tag{5-8}$$

Laboratory researchers would prefer to use the Darcy-Weisbach friction coefficient because the variation of f with flow conditions is well tested by Moody's diagram (available in all basic fluid mechanics texts), which was derived from closed conduit studies. However, as shown in Chow (1959), the f and R_e relationship also applies reasonably well for flow through an open channel.

River engineers usually prefer to use either Manning's n values or Chezy's C values because they have more experience with these coefficients. In any case, it must be remembered that normally, for a rigid boundary, if the bed is rougher than the banks and if the channel is reasonably wide, both Manning's n value and Chezy's C value decrease with increasing flow depth.

5.3 RIGID BOUNDARY WITH RAINFALL

The effect of raindrops on flow can be very significant if the flow depth is not too large compared with the raindrop size. Shen and Li (1973a) found that when R_e is smaller than 900, f is a function of both R_e and rainfall intensity; and when R_e is greater than 2000, f is only a function of R_e and is independent of the rainfall intensity. Figure 5.1 shows this effect. For R_e between 900 and 2000, insufficient data is available to define the trend precisely.

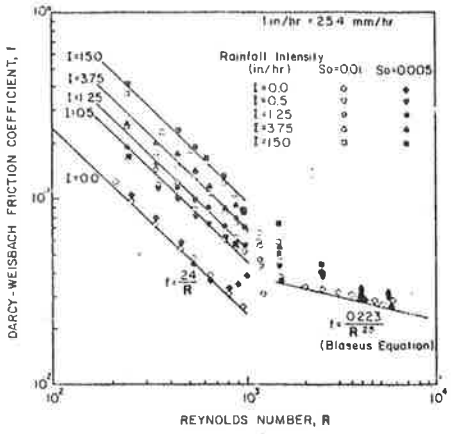

Figure 5.1 Relationship among f, R, I, S_o (after Shen and Li, 1973a; experimental data after Yoon, 1970).

From data collected by Yoon (1970) and Li (1972) from a smooth channel bottom with slope between 0.005 and 0.0108, rainfall intensity between 0.5 and 17.5 in./hr, and Reynolds number between 126 and 12,600, Shen and Li (1973a) found that

$$k = k_o + AI^b \tag{5-9}$$

where $k = fR_e$ and is the parameter including the effect of rainfall, I is rainfall intensity in inches per hour, and A and b are empirical coefficients. For R_e less than 900, A = 27.162 and b = 0.407; for R_e greater than 2000, A = 0.

Izzard (1944) found that A = 5.67 and b = 1.333, and Fawkes (1972) found that A = 10.0 and b = 1.0. These were derived by using fewer experimental data than did Shen and Li (1973a).

Woolhiser (1975) also presented some suggestions on how to derive a given relationship based on experimental data. For laminar flow, the equation for the rising hydrograph is:

$$Q = \frac{8gS_o}{kv} i^m t^m \tag{5-10}$$

where S_o is the bottom channel slope, Q is the flow discharge, t is the time, and m and k are parameters to be determined. Let

$$Q^1 = \frac{Qv}{8gS_o i^m} \tag{5-11}$$

thus

$$\log Q^1 = n \log t - \log k \tag{5-12}$$

If Q^1 and A, obtained from experimental data, are plotted on logarithmic graph paper, m and k can be obtained graphically. Woolhiser (1975) stated that for experimental watersheds or plots that have other than planar geometrics, the rising hydrograph and the equilibrium detention are very complex; therefore, optimization techniques must be utilized for parameter estimation. One objective function that is frequently used and is appropriate for parameter estimates for a single event is

$$F(k, A, b) = \sum_{i=1}^{n} [Q_o(i\Delta t) - Q_c(i\Delta t)]^2 \tag{5-13}$$

where the subscripts o and c refer to observed and computed discharges, respectively, and Δt is a fixed time increment. If a set of n runoff events is available for analysis, the objective function could incorporate the sum of squares of deviations between observed and computed peak rates.

5.4 ALLUVIAL RIVER BOUNDARY

When fluid flows over a movable river bed, the bed surface normally is deformed into various configurations. Einstein (1950) was perhaps the first to separate the total resistance into skin resistance and form resistance. He assumed that

> "On such a bed, friction develops in two distinctly different ways: 1) along the sediment grains of the surface as a rough wall with the representative grain diameter equal to k_s; and, in addition, 2) by separation of the flow from the surface at characteristic points of the ripples or bars. This separation causes wakes to develop on the lee side of the bars, characterized by rollers or permanent eddies of basically stagnant water such as those observed behind most submerged bodies of sufficient size. This flow pattern causes a pressure difference to develop between the front and rear sides of each bar so that part of the flow resistance is transmitted to the wall by this shape resistance, i.e. by normal pressure ..."

He then proceeded to divide the cross-sectional flow area into two parts: one area attributed to the grain resistance and the other area to the shape or form resistance. Through the results of Einstein and Banks (1950), Einstein felt that these two resistances could be added together to obtain the total resistance.

Einstein and Barbarossa (1952) proposed the use of the universal logarithmic velocity relationship, developed for a plane rigid boundary, to estimate the skin resistance. They also found from laboratory and field data that their form resistance, obtained by subtracting skin roughness from total roughness, varied with ψ', an inverse of a Froude number based on flow shear velocity and sediment grain sizes. According to Einstein (1950), ψ' is also an indication of sediment transport rate.

Subsequently, Vanoni and Brooks (1957) developed a graphical solution for the estimation of the skin resistance to facilitate the use of Einstein and Barbarossa's procedure. Shen (1962) found that: 1) Einstein and Barbarossa's form resistance varied with both ψ' and sediment size, and 2) the Reynolds number (based on the fall velocity of the particle and the particle diameter) seems to correlate well with sand, coal, and plastic pellets. Since then, many researchers such as Simons and Richardson (1966), Haynie and Simons (1968), Engelund and Hansen (1967), Lovera and Kennedy (1969), Alam and Kennedy (1969), and Mahmood (1971) have proposed various methods to estimate the skin roughness and the form roughness.

As discussed by Shen (1975), there are many difficulties in using some of the above approaches.

Rigid Boundary Versus Movable Boundary

When fluid flows over a flat rigid boundary, the total resistance contributed by the boundary to the flow occurs at the interface between the two. However, when fluid flows over a flat movable boundary, the total resistance consists of the resistance between the fluid and the top moving layer as well as the resistance existing among the various sediment layers moving at different speeds. Lovera and Kennedy (1969) found that the skin resistance of a movable flat boundary was quite different than that of a flat rigid boundary.

Flat Boundary Versus Curved Boundary

The total skin resistance on a dune or bar with flow separations occurring at its downstream end can be very different from that of a plane rigid boundary. As indicated by Raudkivi (1963) and Mahmood (1971), the flow velocity distribution above ripples and dunes is rather complicated. There is still insufficient information on this aspect.

Mutual Interference of Various Bed Forms

Vanoni (1946) and Vanoni and Nomicos (1959) found that a suspended load concentration of 1.2-3.3 g/1 can reduce the Darcy-Weisbach friction factor for flat beds by about 18%. Simons, Richardson and Haushild (1963) concluded from their experiments that the resistance to flow and bed material transport decreased in the lower flow regime and increased in the upper flow regime when fine sediment was added to the flow.

The effect of suspended sediment load has not been specifically included in the many resistance formulas, although it has been taken care of at least partially by the use of some flow parameters such as ψ'. The presence or the absence of wash load has not been considered in the friction formula.

Effect of Temperature

Straub, Anderson, and Flammer (1958) found from their laboratory experiments that the energy slope (or the frictional resistance) increased by more than 50% when flow temperature decreased from 86°F to 35°F for a mean flow velocity of about 2.2 fps and a flow depth of about 0.23 ft. Franco (1968) determined from his laboratory experiments that the energy gradient increased by about 20% when the temperature decreased from 80°F to 40°F for the same flow depths and flow velocities. Hubbell and Al-Shaikh (1961) and Cunha (1973) presented separate evidence that increasing temperature could either increase or decrease flow resistances for different flow conditions.

Actually, the temperature could affect the flow resistance differently depending on the existing range of flow conditions. It was concluded by Taylor and Vanoni (1972a,b) from their experiments that: 1) in a stream with a rippled bed of fine sand, an increase in water temperature (discharge and depth held constant) may effect either an increase or a reduction in bed roughness and sediment discharge; 2) under certain conditions (unspecified

by Taylor), an increase in water temperature alone can accomplish a change in bed form; and 3) in flows where the Reynolds number (based on the shear velocity and sediment size) is less than 8, the transition from ripples to dunes is accomplished at a lower velocity in a warmer water flow.

As shown in Figure 5.2, Shen, Mellema and Harrison (1977) developed criteria to show the variation of bed forms with water temperature for a constant flow discharge in the Missouri River near Omaha. For instance, in a river flow discharge of 32,500 cubic feet per second, the river bed form changes from dunes to plane bed at a water temperature of about 60°F.

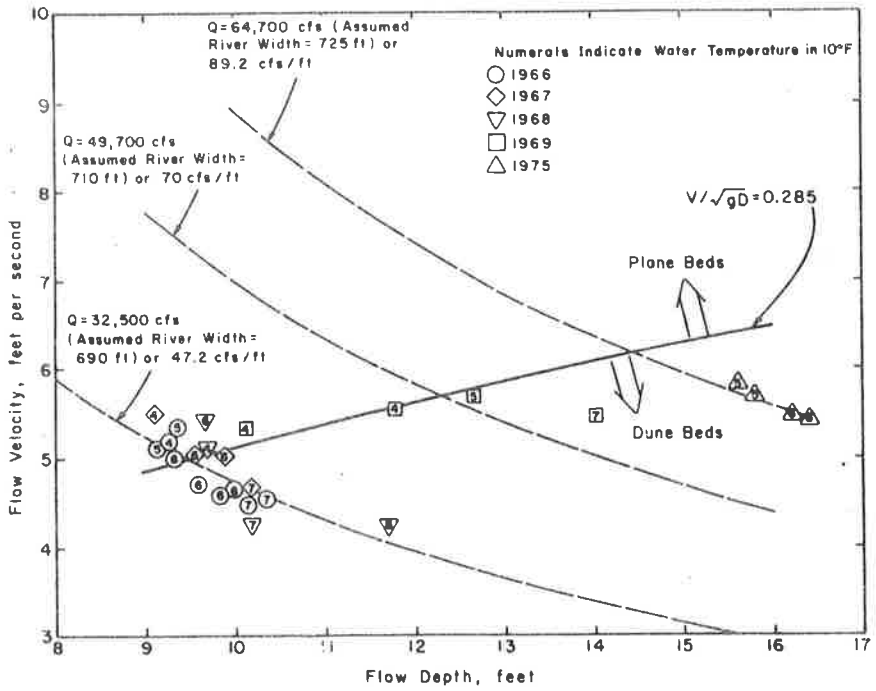

Figure 5.2 Prediction of bed forms of Missouri River near Omaha (after Shen, Mellema and Harrison, 1977).

Porosity of Bed

Munoz and Gelhar (1968) have shown that the friction factor for a porous pipe boundary is much greater than for a rigid boundary. However, for a case with fine sediment, this effect is perhaps small.

Effect of Three-Dimensional Flow

Secondary currents and other variations in the transverse direction may have significant effects on the development of bed configurations.

Characteristics of Time Fluctuation of Boundary Shear Stress

Blinco, Mahmood, and Simons (1973) presented measurements for the time fluctuation of shear stress over a flat rigid boundary. Conceivably, the time variation of shear stress over dunes can be quite different than that for a flat rigid boundary.

Limitation of Flow Depth in Laboratory Flumes

This is an extremely important problem and no conclusive evidence is presently available. Annambhotla, Sayre, and Livesey (1972) and Cheong and Shen (1973) have shown that some statistical properties of alluvial bed forms in field data (collected by Annambhotla, et al.) are quite similar to those obtained from laboratory flumes. If the development of bed forms should be limited by small flow depths or narrow flow depths, or both, the usefulness of laboratory experimental results in the field would be questionable.

There are many other difficulties in addition to the aforementioned. Since there is no known way to correctly estimate the skin resistance of an alluvial channel bed, perhaps the total resistance can be separated into the following three items: 1) "skin resistance" according to whatever procedure is selected; 2) correction of skin resistance due to incorrect procedure used in the first item; and 3) form resistance. The main problem will then be to find a procedure for the estimation of the "skin resistance" so that one can find a way to estimate the sum of the second and third items. Of course, at this stage it appears that if the term in Item 2 can be minimized by selecting the proper procedure to estimate Item 1, the chance of successfully estimating the sum of Items 2 and 3 would improve.

It is obvious from the above discussion that there is no completely acceptable method to describe the variation of alluvial bed form roughness with flow condition. However, the situation is not entirely hopeless and an experienced engineer may make a reasonable estimate according to the following rules (different researchers probably believe in different rules).

For grain roughness, Lovera and Kennedy's (1969) curve as shown in Figure 5.3 for flat-bed flows in alluvial channels is best used only for dunes and flow depths less than about 10 feet. For larger rivers, this estimation appears to be much too great.

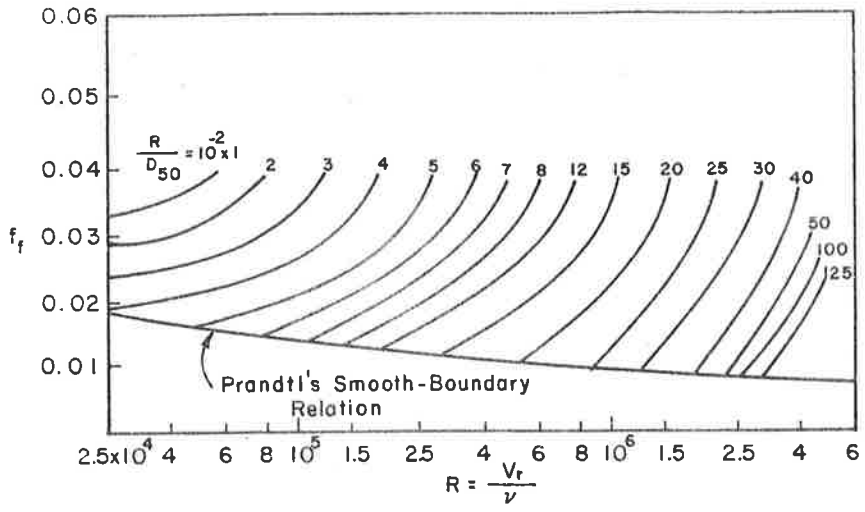

Figure 5.3 Flat-bed friction factor diagram for alluvial streams (after Lovera and Kennedy, 1969).

Einstein's (1950) procedure for calculating grain roughness by the logarithm's velocity distribution is reasonably valid in all cases. For river depths less than 10 feet and for dune beds, Lovera and Kennedy's (1969) curve appears to be slightly better.

Einstein and Barbarossa's (1952) recommended equation for grain roughness is

$$\frac{V}{\sqrt{U_*'}} = 5.75 \log_{10}(12.2) \frac{R_{bx}'}{k_s} \tag{5-14}$$

where U_*' is the boundary shear stress pertaining to grain roughness, R_b' is the hydraulic radius related to grain roughness, k_s is the representative grain roughness, and x is a parameter depending on the ratio between the representative grain roughness and the viscous sublayer thickness. U_*' and R_b' are related by

$$U_*' = \sqrt{gR_b'S_f} \tag{5-15}$$

With known flow conditions, i.e., V, S_f, k_s (which, according to Einstein is approximately the grain size at which 65% of the sediment is finer) and the viscous sublayer thickness, one can calculate the value of either R_b' or U_*' through a trial and error procedure. Vanoni and Brooks (1957) provided a graphical solution of Equation 5-14 without trial and error.

When the flow depth is of the same order of magnitude as the bed material height, the sediment bed material will act as an obstruction to flow rather than as a rough boundary and thus must be dealt with entirely differently. Hartung and Scheuerlein (1967), Judd and Peterson (1969), Scheuerlein (1973), Ashida and Bayozit (1973), Shen and Li (1973), Bathurst (1978), and Bathurst, Li, and Simons (1979) have investigated this problem. Figure 5.4 shows the curve presented by Shen and Li (1973b) for analyzing some previous data. The dimensions of the blocks are given in Figure 5.5.

Bathurst, Li and Simons (1979) stated that the effect of roughness geometry can largely be described by a single parameter, b (the function of effective roughness concentration).

$$b = [1.175 \left(\frac{Y_{50}}{w}\right)^{0.557} \left(\frac{d}{S_{50}}\right)^{0.648 \sigma^{-0.134}}] \qquad (5\text{-}16)$$

where Y_{50} and S_{50} are the respective sizes of the median cross-stream axis and short axis of the bed material, w is the channel width, d is the flow depth and σ is the standard deviation of the median axis of the median sediment size.

For $b < 0.755$, they found that

$$\frac{\bar{V}}{(gdS)^{0.5}} = \left[\frac{0.28}{b} F_r\right]^{\log(0.755/b)} \left[\frac{A_w}{wd}\right] \kappa \qquad (5\text{-}17)$$

when

$$\kappa = 13.434 \left(\frac{w}{Y_{50}}\right)^{0.492} b^{1.025} \left(\frac{w}{Y_{50}}\right)^{0.118} \qquad (5\text{-}18)$$

$\bar{V}$ is average flow velocity, g is the gravitational acceleration, S is the energy slope, F_r is the Froude number of the flow, A_w is the wetted roughness cross-sectional area, w is channel width, and d is the flow depth. Equation 5-9 was based on data collected from a steep stream flume at the Colorado State University. Although the collected data agreed with this equation rather well as shown in Figure 5.6 some earlier data collected by Barnes (1967), Judd and Peterson (1969), Emmett (1972), Virmani (1973), and Bathurst (1978) did not agree with the equation too well. However, it is perhaps the best presently available.

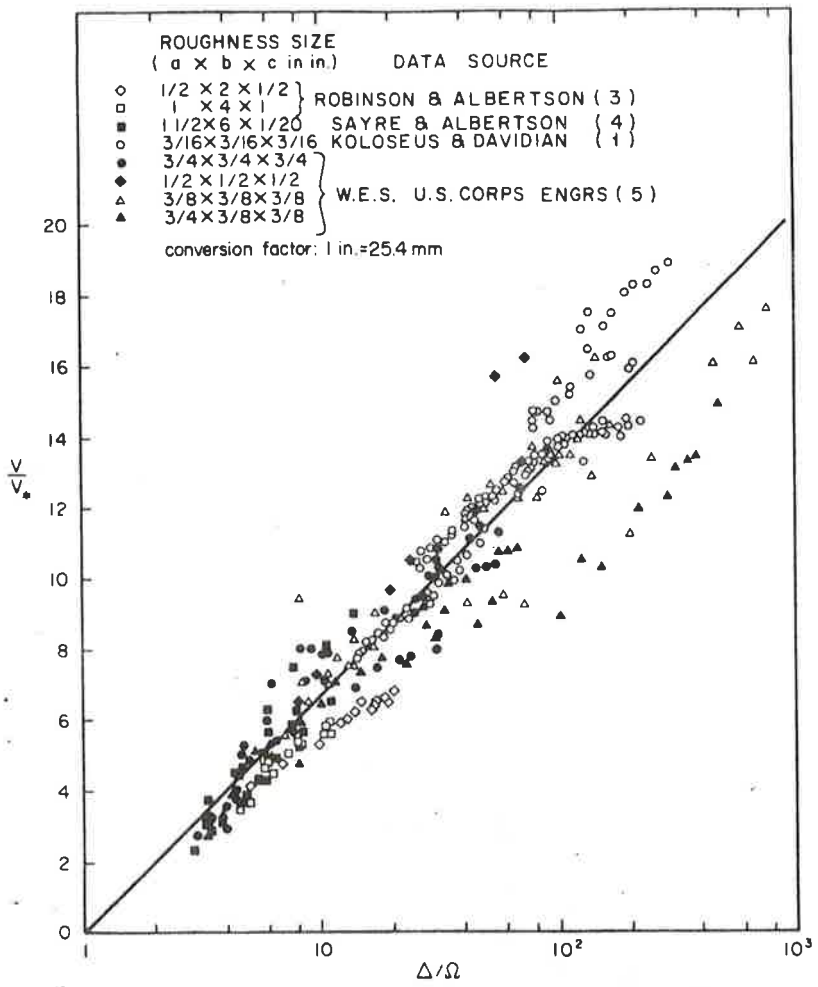

Figure 5.4 V/V_* versus Δ/Ω for rigid roughness elements (after Shen and Li, 1973b).

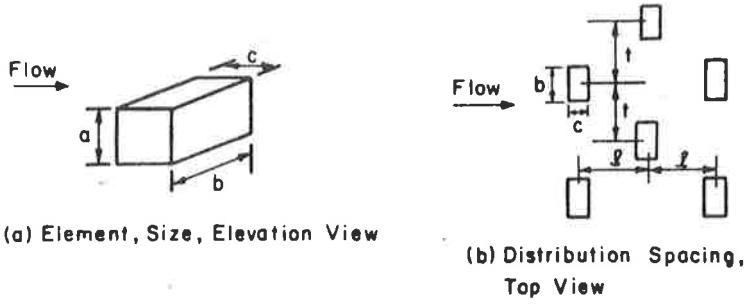

Figure 5.5 Roughness elements (after Shen and Li, 1973b).

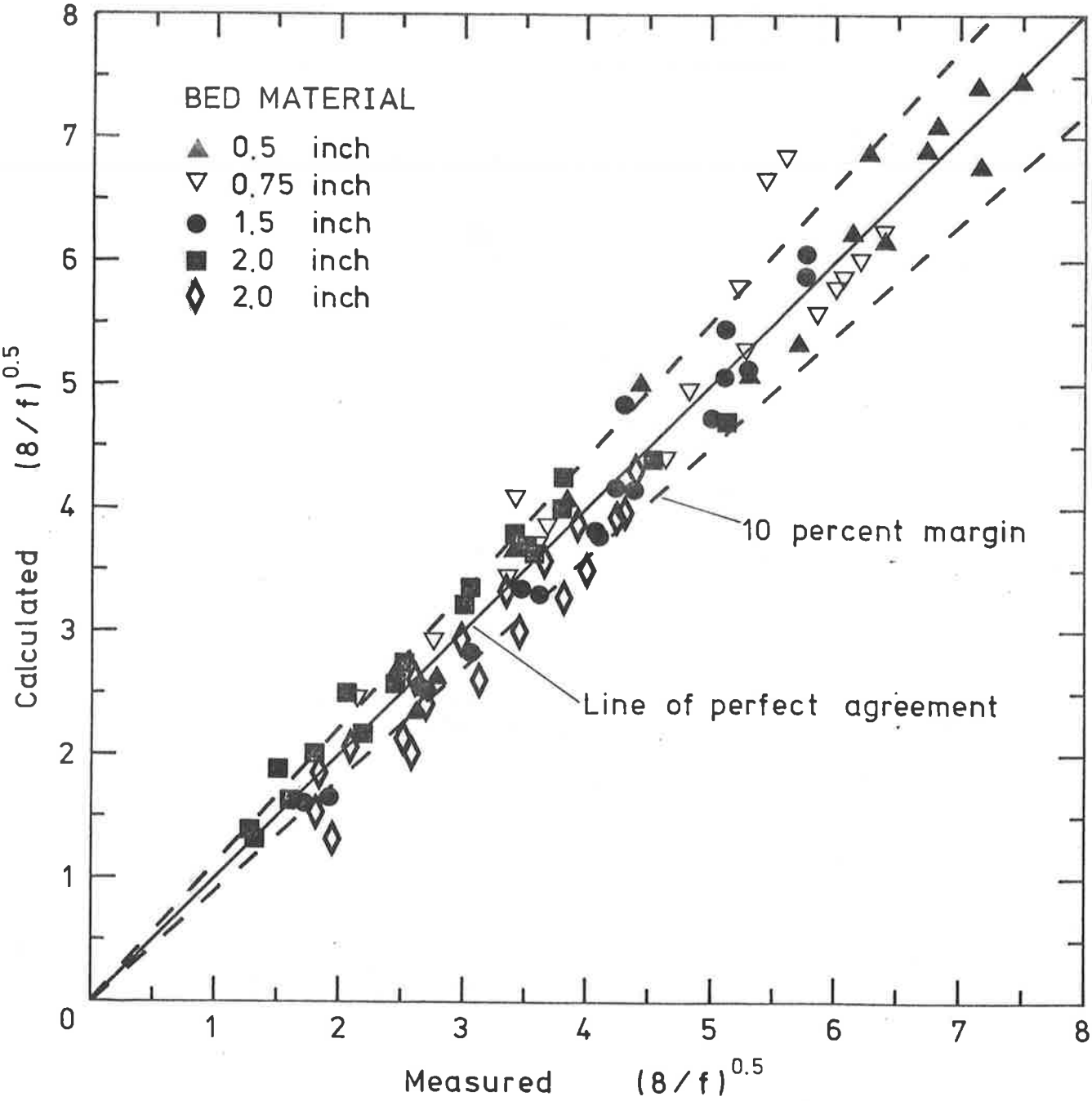

Figure 5.6 Comparison of values of the resistance function calculated using Equation 5-9, with measured values for all the flows over the fixed roughness beds (after Bathurst, Li and Simons, 1979).

For Form Roughness

1. Form roughness in a laboratory flume is usually less than the grain roughness if either Einstein and Barbarossa's (1952) procedure as shown in Figure 5.7 or Lovera and Kennedy's (1969) procedure is used to calculate grain roughness.

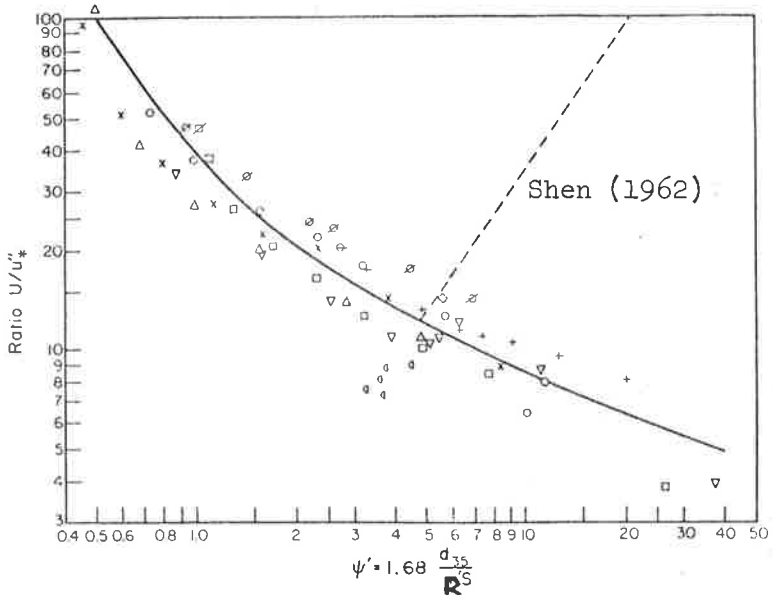

Figure 5.7 Friction loss due to channel irregularities as a function of sediment transport (after Einstein and Barbarossa, 1952).

2. Form roughness in a river can be greater than (up to twice as large as) the grain roughness.

3. For sediment particles less than 0.6 mm in diameter (or Wd/ν less than 100, where W is the fall velocity of the particle, d is the grain size and ν is the kinematic viscosity of fluid), form roughness always decreases with an increase in sediment transport rate.

4. For sediment particles not much greater in diameter than 0.6 mm, form roughness first decreases, then increases with the increase of sediment transport rate. Minimum form roughness occurs when the shear stress is about two and one-half times the critical shear stress for incipient motion.

5. For very large sediment particles ($R/R_s < 10$) the alluvial bed form is almost flat (perhaps with some large- and low-amplitude bars).

6. For sediment particles less than 0.6 mm in diameter, there is a greater tendency to form larger dunes, as suggested by Shen (1962).

7. Einstein and Barbarossa's (1952) procedure is particularly applicable to rivers less than 20 feet deep, with sediment sizes of about 0.2 to 0.3 mm. A recent study by Shen, Mellema and Harrison (1978) indicates this, as shown in Figure 5.8.

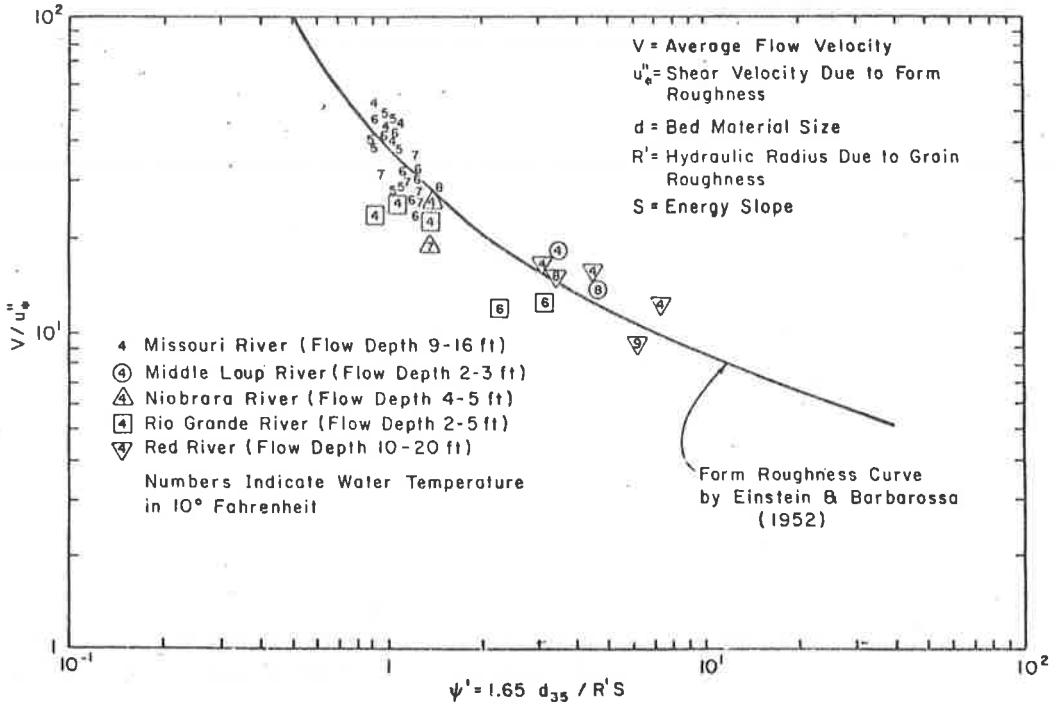

Figure 5.8 Variation of form resistance (after Shen, Mellema and Harrison, 1978).

8. For sediment particles greater than 0.6 mm, the branch of the form roughness curve for $Wd/\nu > 100$ suggested by Shen (1962) is a little better than that proposed by Einstein and Barbarossa.

9. The bed form resistance curve suggested by Alam and Kennedy (1969), as shown in Figure 5.9, is reasonably good for R/d_{50} between 5×10^2 and 5×10^4.

5.5 EFFECT OF VEGETATION ON FLOWS

From a hydraulic viewpoint, the effect of vegetation on flow retardation can be divided into three parts: 1) tall vegetation, such as trees, on the order of flow depth; 2) low vegetation, such as grasses, on the order of normal boundary roughness; and 3) vegetation height on the order of a few percent of full flow depth.

The effects of vegetation on sediment yield in watersheds are numerous; for instance, tall vegetation (a forest) could: 1) intercept

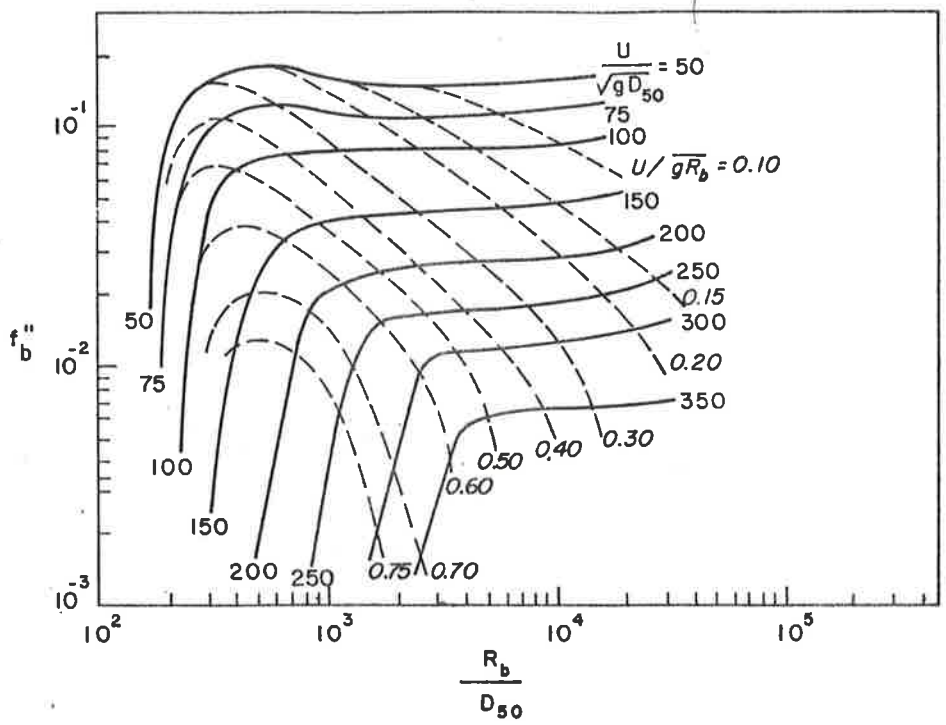

Figure 5.9 Graphical expression of f''_b as function of Froude number and r_b/d_{50} (after Alam and Kennedy, 1969).

solar radiation and affect soil temperature, 2) diminish wind speed and decrease evaporation and wind erosion, 3) induce rainfall, and 4) reduce sediment yield. Vegetation can be used as a rather effective method of reducing sediment yield by: 1) protecting soil from direct rainfall impact, 2) retarding flow rate, 3) increasing soil resistance, and 4) enhancing infiltration and decreasing surface runoff.

Very low vegetation has the same effect as surface roughness, and Manning's n values given by various textbooks such as Chow (1959) would provide reasonable solutions. For slightly taller vegetation (with height varying from zero to full flow depth) there are several comprehensive studies.

Ree and Palmer (1949) summarized their results of the estimates of Manning's n value for various vegetation and hydraulic conditions in Figure 5.10 and Table 5.2.

Kouwen and Unny (1973) found that deflection by vegetation can be described approximately by a simple combination of m (number of roughness limits per square centimeter), E (the modulus of elasticity of the simulated vegetation), I (the second moment of area of its cross section), ρ (the density of the fluid), and u_* (the density shear stress).

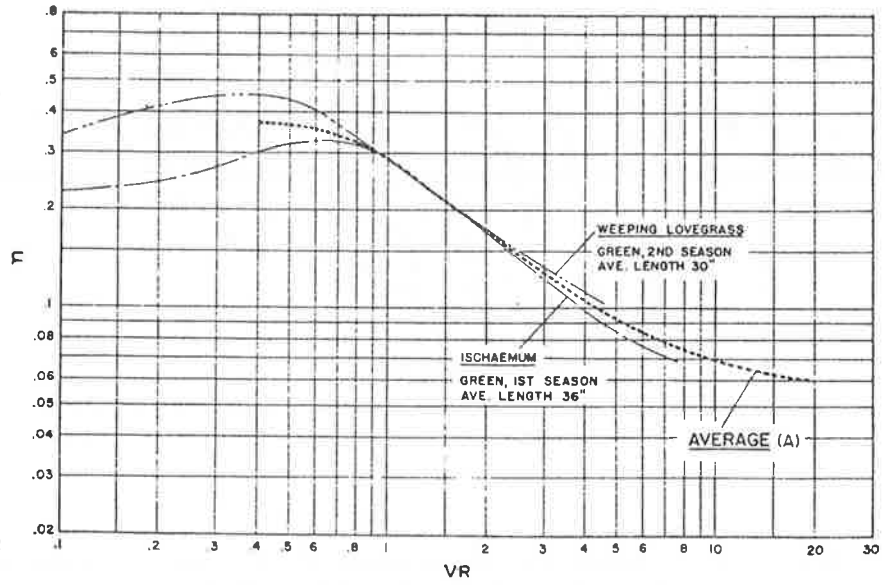

(*a*) Curves for A or very high vegetal retardance.

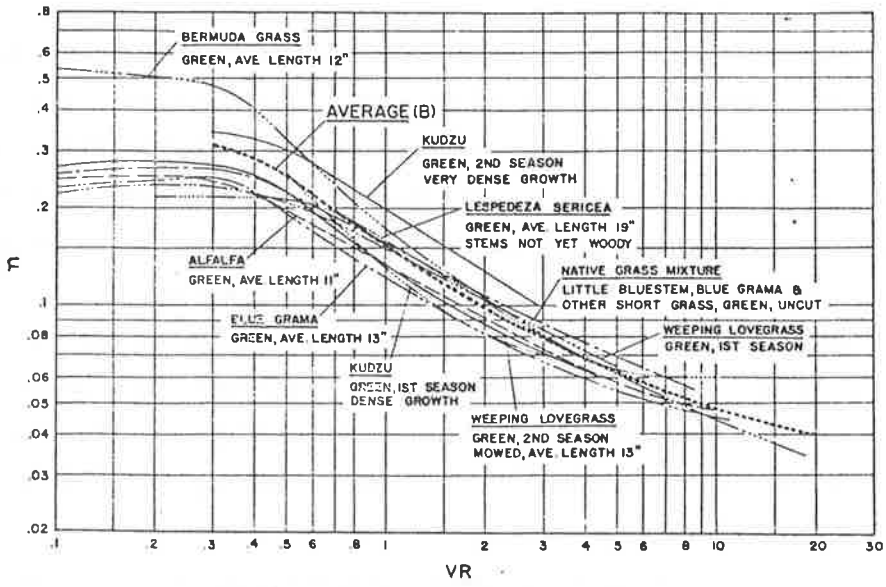

(*b*) Curves for B or high vegetal retardance.

Figure 5.10 Experimental n-VR curves (after Ree and Palmer, 1949).

Table 5.2 Classification of degree of retardance for various kinds of grass (after Ree and Palmer, 1949).

Retardance	Cover	Condition
A Very high	Weeping love grass	Excellent stand, tall (av 30 in.)
	Yellow bluestem ischaemum	Excellent stand, tall (av 36 in.)
B High	Kudzu	Very dense growth, uncut
	Bermuda grass	Good stand, tall (av 12 in.)
	Native grass mixture (little bluestem, blue grama, and other long and short Midwest grasses)	Good stand, unmowed
	Weeping love grass	Good stand, tall (av 24 in.)
	Lespedeza sericea	Good stand, not woody, tall (av. 19 in.)
	Alfalfa	Good stand, uncut (av 11 in.)
	Weeping love grass	Good stand, mowed (av 13 in.)
	Kudzu	Dense growth, uncut
	Blue grama	Good stand, uncut (av 13 in.)
C Moderate	Crab grass	Fair stand, uncut (10 to 48 in.)
	Bermuda grass	Good stand, mowed (av 6 in.)
	Common lespedeza	Good stand, uncut (av 11 in.)
	Grass-legume mixture--summer (orchard grass, redtop, Italian rye grass, and common lespedeza)	Good stand, uncut (6 to 8 in.)
	Centipede grass	Very dense cover (av 6 in.)
	Kentucky bluegrass	Good stand, headed (6 to 12 in.)
D Low	Bermuda grass	Good stand, cut to 2.5 in. height
	Common lespedeza	Excellent stand, uncut (av 15 in.)
	Buffalo grass	Good stand, uncut (3 to 6 in.)
	Grass-legume mixture--fall, spring (orchard grass, redtop, Italian rye grass, and common lespedeza)	Good stand, uncut (4 to 5 in.)
	Lespedeza sericea	After cutting to 2 in. height, very good stand before cutting
E Very Low	Bermuda grass	Good stand, cut to 1.5 in. height
	Bermuda grass	Burned stubble

The relationship between $(mEI/\rho u_*^2)^{1/4}/h$ and k/h is given in Figure 5.11, where k is the deflected roughness height and h is the original roughness height. Series A, B, C, D, and E were conducted with difficult simulated vegetation spacings. Kouwen and Unny (1973) presented two figures (Figures 5.12 and 5.13) to indicate the change with the flow conduits of Manning's n value and the Darcy-Weisbach f value. In these two figures, y_n is the flow depth.

Chen (1976) conducted a series of laboratory experiments in a flume 20 ft wide, 20 ft long and 2 ft deep with Kentucky Blue Grass and hybrid Bermuda Grass. Several channel slopes were used. His results are given in Figure 5.14. He found that the Darcy-Weisbach friction factor f is

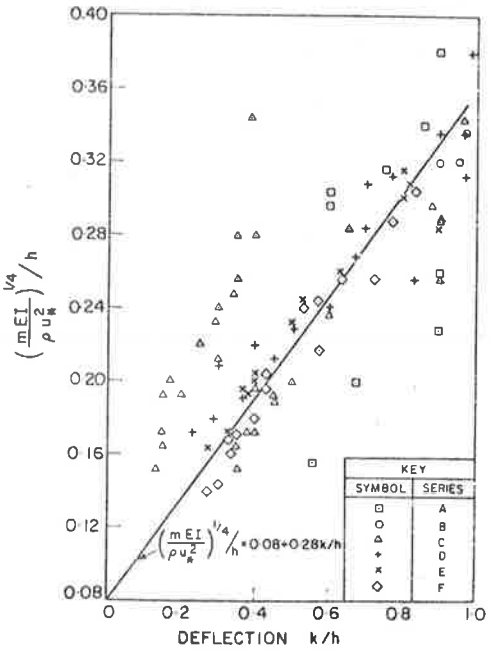

Figure 5.11 Plot of $[mEI/(\rho u_*^2)]^{1/4}/h$ versus deflection k/h (after Kouwen and Unny, 1973).

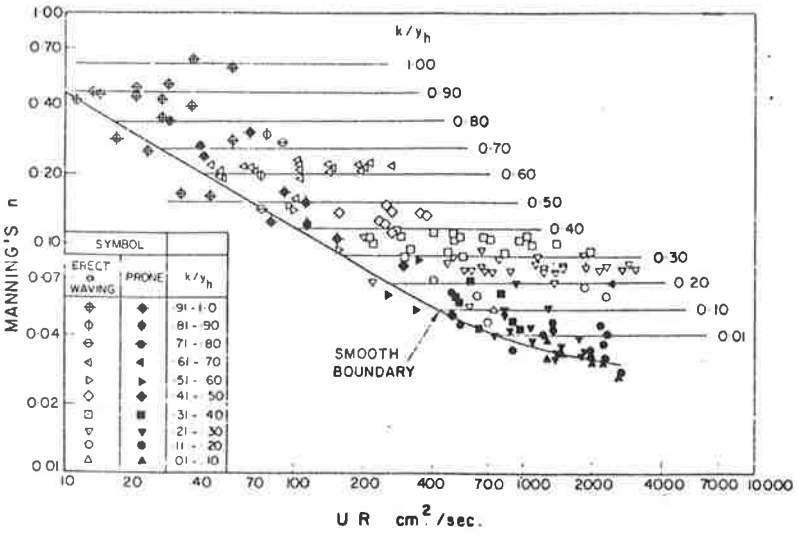

Figure 5.12 Variation of Manning's n as function of UR and k/y_n (after Kouwen and Unny, 1973).

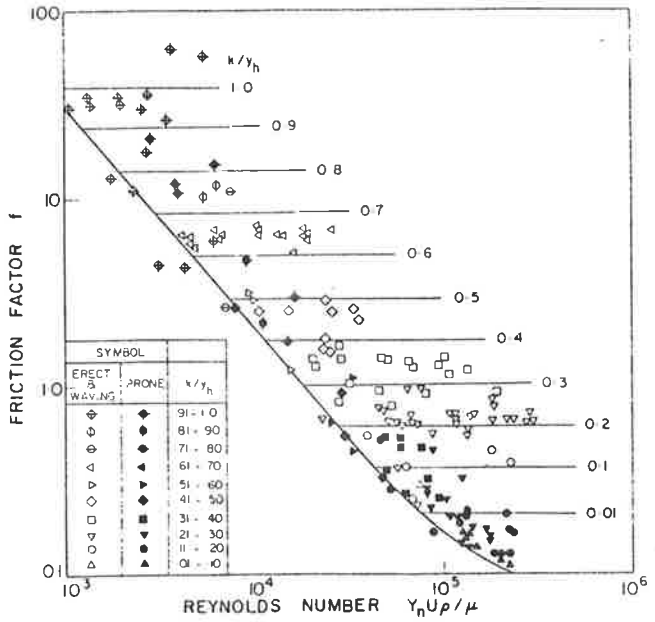

Figure 5.13 Variation of friction factor with relative roughness (after Kouwen and Unny, 1973).

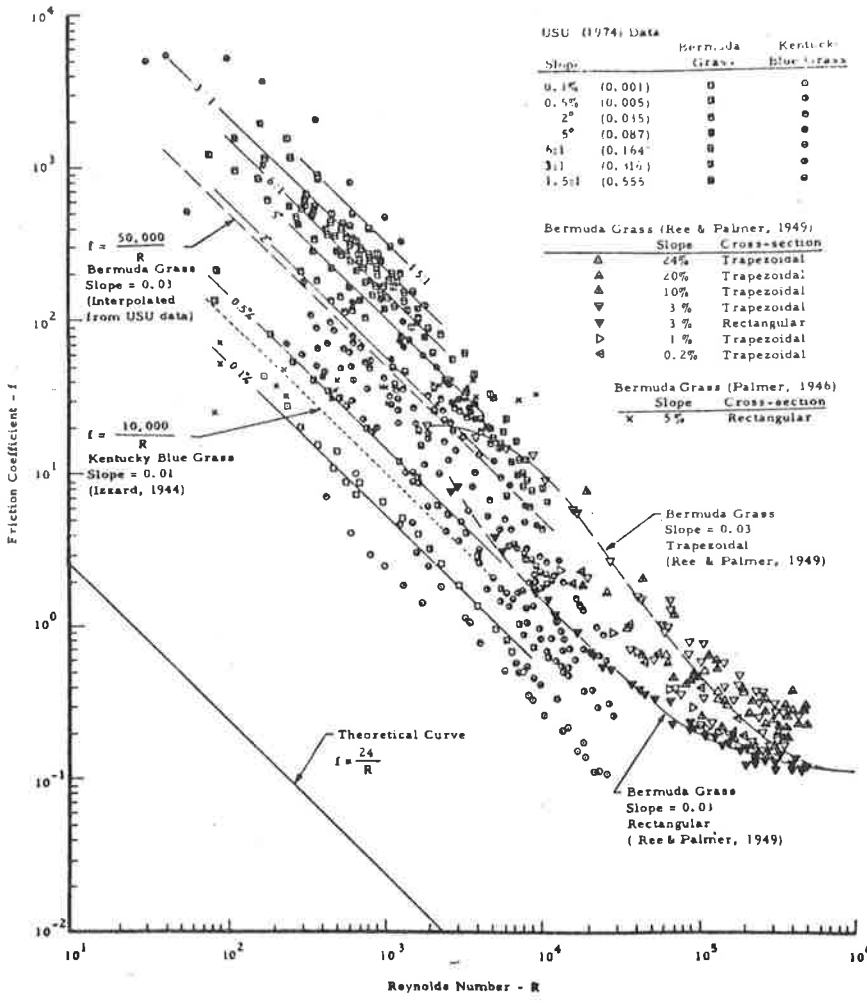

Figure 5.14 Relationships between Darcy-Weisbach friction coefficient and Reynolds number for flow on natural turf surfaces (after Chen, 1976).

a function of both the channel slope and the flow Reynolds number. It is a little strange that the friction factor should be a function of channel slope, and one should not apply his results to cases outside of the experimental range in which these data were collected.

Li and Shen (1973) presented a theoretical analysis of the effect of tall vegetation on flow and sediment. They found that:

1. The different patterns or groupings of tall vegetation have a significant effect on retardation of flow rates and sediment yields.

2. The retardation of flow rate due to tall vegetation with heights of the same order of magnitude as flow depth can be estimated from the present method if the spacing between the tall vegetation stems is at least 6 diameters in the downstream direction and 3 diameters in the transverse direction. The Reynolds number based on the vegetation diameter should be less than 2×10^5, although there is no evidence to indicate that this method will not be applicable for other ranges of Reynolds numbers.

3. Tall vegetation in staggered patterns is much more effective in reducing flow rate than the same amount of tall vegetation in any other pattern. Thus, if the main aim of planting tall vegetation is to reduce flow rates and sediment yield, it should be planted in a staggered pattern.

4. Since it is difficult to harvest tall vegetation in a staggered pattern, the next best thing is to harvest it in rows perpendicular to the flow direction.

5. The average boundary shear stress on the bed is much more sensitive to a change of bottom slope and vegetation size than to the variation of flow discharge and sediment size. The retardation of boundary shear stress on the bed will increase significantly as trees grow. All these effects can be estimated quantitatively by their method.

Petryk and Bosmajian (1975) found that the composite n value for channel roughness and vegetation roughness can be expressed as

$$n = n_p \sqrt{1 + \frac{C_d \, \Sigma A_i}{2g \, AL} \left(\frac{1.49}{n_b}\right)^2 \left(\frac{A}{p}\right)^{4/3}} \qquad (5\text{-}19)$$

where n is Manning's n value for boundary and vegetation effects, n_b is Manning's n value excluding the influence of vegetation, C_d is the drag coefficient of each plant, A_i is the projected area of the i^{th} plant in the upstream direction, A is the cross-sectional area of flow, L is the length of channel being considered, and p is the wetted perimeter. This equation has not been extensively tested.

5.6 CONCLUSIONS

In this chapter, some of the current knowledge on flow resistance is assembled. Although the knowledge is by no means sufficient to define a roughness value with certainty, an experienced specialist usually can derive a reasonable estimate for a given flow condition based on his own experience. Quite often, it is assumed that

$$n = a\, Q^b \tag{5-20}$$

or

$$n = a\, S^b \tag{5-21}$$

and a regression analysis is used to determine the best set of a and b values for a given situation. One must remember that a and b should vary with the variation of flow condition.

5.7 REFERENCES

Alam, A. M. Z., and Kennedy, J. F., 1969. Friction factors for flow in sand bed channels. Journal of the Hydraulics Division, ASCE, Vol. 95, No. HY6, Proc. Paper 6900, November, pp. 1973-1992.

Annambhotla, V. S. S., Sayre, W. W., and Livesey, R. H., 1972. Statistical properties of Missouri River bed forms. Journal of the Waterways, Harbors and Coastal Engineering Division, ASCE, Vol. 98, No. WW4, Proc. Paper 9358, November, pp. 489-510.

Ashida, K., and Bayazit, M., 1973. Initiation of motion and roughness of flows in steep channels. Proceedings of the Fifteenth Congress of the International Association for Hydraulic Research, Istanbul, Turkey, Vol. 1, pp. 475-484.

Barnes, H. H., 1967. Roughness characteristics of natural channels. Water Supply Paper 1849, United States Geological Survey, Department of the Interior, United States Government Printing Office, Washington, D. C.

Bathurst, J. C., 1978. Flow resistance of large-scale roughness. Journal of the Hydraulics Division, ASCE, Vol. 104, No. HY12, Proc. Paper 14239, Dec., pp. 1587-1603.

Bathurst, J. C., Li, R. M., and Simons, D. B., 1979. Hydraulics of mountain rivers. Colorado State University Experiment Station Report CER78-79JCB-RML-DBS55

Blinco, P. H., Mahmood, K., and Simons, D. B., 1973. Stochastic structure of the turbulent boundary shear stress process. Proceedings of the 15th Congress, Vol. 1, International Association for Hydraulic Research, Turkey, pp. 371-380.

Chen, C. L., 1976. Flow resistance in broad shallow grassed channels. Journal of the Hydraulics Division, Proceedings of the ASCE, Vol. 102, No. HY3, March.

Cheong, H. F., and Shen, H. W., 1973. Spectral properties of alluvial bed forms in rivers and flumes. First International Symposium on River Mechanics, Asian Institute of Technology, Bangkok, Thailand, January.

Chow, V. T., 1959. Open-channel Hydraulics. McGraw-Hill Book Company.

Cunha, L. V., 1973. The influence of water temperature on the roughness of alluvial forms. Proceedings of the 15th Congress, Vol. 1, International Association for Hydraulic Research, Turkey, pp. 15-20.

Einstein, H. A., 1950. The bed-load function for sediment transportation in open channel flows. Technical Bulletin 1026, Soil Conservation Service, United States Department of Agriculture, September.

Einstein, H. A., and Banks, R. B., 1950. Fluid resistance of composite roughness. Transactions, American Geophysical Union, Vol. 31, No. 4, August, pp. 603-610.

Einstein, H. A., and Barbarossa, N. L., 1952. River channel roughness. Transactions, ASCE, Vol. 117, Paper No. 2528, pp. 1121-1132.

Emmett, W. W., 1972. The hydraulic geometry of some Alaskan streams south of the Yukon River. Open-File Report, Water Resources Division, Alaska District, United States Geological Survey, Department of the Interior, July.

Engelund, F., and Hansen, E. A., 1967. Monograph on sediment transport in alluvial streams. Teknisk Forlag, Copenhagen, Denmark.

Fawkes, P. E., 1972. Roughness in a model of overland flow. M.S. Thesis, Colorado State University, Fort Collins.

Franco, J. J., 1968. Effects of water temperature on bed load movement. Journal of the Waterways and Harbors Division, ASCE, Vol. 94, No. WW3, Proc. Paper 6083, August, pp. 343-352.

Hartung, F., and Scheuerlein, H., 1967. Macroturbulent flow in steep open channels with high natural roughness. Proceedings of the Twelfth Congress of the International Association for Hydraulic Research, Fort Collins, Colorado, Vol. 1, Sept., pp. 1-8.

Haynie, R. B., and Simons, D. B., 1968. Design of stable channels in alluvial materials. Journal of the Hydraulics Division, ASCE, Vol. 94, No. HY6, Proc. Paper 6217, November, pp. 1399-1420.

Henderson, F. M., 1966. Open-channel Flow. The MacMillan Co., New York.

Hubbell, D. W., and Al-Shaikh Ali, K. S., 1961. Qualitative effects of temperature on flow phenomena in alluvial channels. Professional Paper 424-D, United States Geological Survey.

Izzard, C. F., 1944. The surface profile of overland flow. Transactions, A.G.U., pp. 959-968.

Judd, H. E., and Peterson, D. F., 1969. Hydraulics of large bed element channels. Report No. PRWG 17-6, Utah Water Research Laboratory, Utah State University, Logan, Utah.

Kouwen, N., and Unny, T. E., 1973. Flexible roughness in open channels. Journal of the Hydraulics Division, Proceedings of the ASCE, Vol. 99, No. HY5, May.

Li, R. M., 1972. Sheet flow under simulated rainfall. M.S. Thesis, Colorado State University, Fort Collins.

Li, R. M., and Shen, H. W., 1973. Effect of tall vegetation on flow and sediment. Journal of Hydraulics Division, ASCE, Proc. Paper 9748, Vol. 99, No. HY5, May.

Lovera, F., and Kennedy, J. F., 1969. Friction factors for flat-bed flows in sand channels. Journal of the Hydraulic Division, ASCE, Vol. 95, No. HY4, Proc. Paper 6678, July, pp. 1227-1234.

Mahmood, K., 1971. Flow in sand-bed channels. Water Management Technical Report No. 11, Colorado State University, Fort Collins, Colorado.

Munoz, G. R. J., and Gelahar, L. W., 1968. Turbulent pipe flow with rough and porous walls. Hydrodynamic Laboratory Report 109, Massachusetts Institute of Technology, Cambridge, Massachusetts.

Petryk, S., and Bosmajian, G., III, 1975. Analysis of flow through vegetation. Journal of the Hydraulics Division, Proceedings of the ASCE, Vol. 101, No. HY7, July.

Raudkivi, A. J., 1963. Study of sediment ripple formation. Journal of the Hydraulics Division, ASCE, Vol. 89, No. HY6, Proc. Paper 3692, November, pp. 15-33.

Ree, W. O., and Palmer, V. J., 1949. Flow of water in channels protected by vegetative linings. U.S. Soil Conservation Bulletin No. 967, February, 115 p.

Scheuerlein, H., 1973. The mechanics of flow in steep, rough, open channels. Proceedings of the Fifteenth Congress of the International Association for Hydraulic Research, Istanbul, Turkey, Vol. 1, pp. 457-465.

Shen, H. W., 1962. Development of bed roughness in alluvial channels. Journal of Hydraulics Division, ASCE, Proc. Paper 3113, Vol. 88, No. HY3.

Shen, H. W., 1975. Hans A. Einstein's contributions in sedimentation. Journal of Hydraulics Division, ASCE, Proc. Paper 11290, Vol. 101, No. HY5, May.

Shen, H. W., and Li, R. M., 1973a. Rainfall effect on sheet flow over smooth surface. Journal of Hydraulics Division, ASCE, Proc. Paper 9733, Vol. 99, No. HY5, May.

Shen, H. W., and Li, R. M., 1973b. Analysis of resistance over staggered roughness. Journal of the Hydraulics Division, ASCE, Technical Note, Proc. Paper 10147, No. HY11, November.

Shen, H. W., Mellema, W., and Harrison, A. S., 1977. Analysis of temperature effects on stage-discharge relationship in a Missouri River reach near Omaha. U.S. Army Engineering Division, Missouri River, Omaha, Nebraska, MRD Sediment Series, No. 15, February.

Simons, D. B., and Richardson, E. V., 1966. Resistance to flow in alluvial channels. Professional Paper 422-J, United States Geological Survey.

Simons, D. B., Richardson, E. V., and Haushild, W. H., 1963. Some effects of fine sediment on flow phenomena. Water Supply Paper 1498-G, United States Geological Survey.

Straub, L. B., Anderson, A. G., and Flammer, G. H., 1958. Experiments on the influence of temperature on the sediment load. MRD Sediment Series No. 10, United States Army Engineer Division, Missouri River, Omaha, Nebraska.

Strickler, A., 1923. Beiträge zur Frage der Geschwindigkeitsformel und der Rauhigkeitszahlen für Ströme, Kanäle and geschlossene Leitungen (some contributions to the problem of velocity formula and roughness coefficients for rivers, canals, and closed conduits), Mitteilungen des eidgenössischen Amtes für Wasserwirtschaft, Bern, Switzerland, No. 16.

Taylor, B. D., and Vanoni, V. A., 1972a. Temperature effects in low-transport, flat-bed flows. Journal of the Hydraulics Division, ASCE, Vol. 98, No. HY8, Proc. Paper 9105, August, pp. 1427-1445.

Taylor, B. D., and Vanoni, V. A., 1972b. Temperature effects in high-transport, flat-bed flows. Journal of the Hydraulics Division, ASCE, Vol. 98, No. HY12, Proc. Paper 9456, December, pp. 2191-2206.

Vanoni, V. A., 1946. Transportation of suspended sediment by water. Transactions, ASCE, Vol. 111, Paper No. 2267, pp. 67-102.

Vanoni, V. A., and Brooks, N. H., 1957. Laboratory studies of the roughness and suspended load of alluvial streams. Sedimentation Laboratory No. E-68, California Institute of Technology, Pasadena, California, December.

Vanoni, V. A., and Nomicos, G. N., 1959. Resistance properties of sediment-laden streams. Journal of the Hydraulics Division, ASCE, Vol. 85, No. HY5, Proc. Paper 2020, May, pp. 77-107.

Virmani, J. K., 1973. The relationship between channel forming flows and the cross section shape, slope, and bed materials in large bed element streams. Thesis presented to Utah State University, at Logan, Utah, in partial fulfillment of the requirements for the degree of Doctor of Philosophy.

Woolhiser, D. A., 1975. Simulation of unsteady overland flow. In Unsteady Flow in Open Channels, edited by K. Mahmood and V. Yevjevich, Chapter 12, Vol. II, Water Resources Publications, P.O. Box 303, Fort Collins, Colorado 80522.

Yoon, N. Y., 1970. The effect of rainfall on the mechanics of steady spatially varied sheet flow on a hydraulically smooth boundary. Ph.D. Thesis, Department of Civil Engineering, University of Illinois, Urbana, Illinois.

CHAPTER 6

OVERVIEW OF FLOOD ROUTING METHODS

by

V. Miguel Ponce, Assistant Professor, Department of Civil Engineering, Colorado State University, Fort Collins, Colorado
Ruh-Ming Li, Associate Professor, Department of Civil Engineering, Colorado State University, Fort Collins, Colorado

6.1 INTRODUCTION

Decades ago the behavior of water and sediment in alluvial channels was studied only in a qualitative manner or by highly simplified, statistical methods. With improved knowledge of the movement of water and sediment combined with the availability of high-speed digital computers, mathematical modeling of rivers has attracted increasing attention. Mathematical modeling of rivers usually involves a numerical technique to solve the differential equations for the movement of water and sediment through a river reach. With proper calibration and adjustment of the model, one can eliminate many of the uncertainties involved and develop valuable information on present and future river conditions.

Flood Routing is defined as the process of tracing by calculation the movement of a flood wave. In general, the problem consists of applying the principles of gradually varied unsteady open channel flow.

Two physical characteristics that are useful in describing flood waves are: 1) the rate of travel (flood wave celerity), and 2) the rate of subsidence (flood wave attenuation). The concept of flood wave celerity is closely associated with the work of Kleitz (Lighthill and Whitham, 1955) and Seddon (1900), who formulated the Kleitz-Seddon law for the celerity of a flood wave of long duration. Later, Lighthill and Whitham (1955) embodied the physical basis underlying the Kleitz-Seddon law into what has since been referred to as the kinematic wave theory. Lighthill and Whitham made a clear distinction between the larger, slower moving kinematic flood waves, and the smaller, faster moving dynamic waves. They showed that for a large number of cases of practical interest, the dynamic waves are subordinated to the more permanent kinematic and diffusive waves.

The attenuation of a flood wave can be accomplished by either longitudinal or lateral storage. The attenuation due to lateral storage is exemplified by the subsidence of a flood wave as it passes through a lake or reservoir. In the absence of lateral storage, such as the case of a flood wave moving through a prismatic channel of constant cross section, the wave attenuation is caused by longitudinal storage. The amount of longitudinal storage is directly related to the relative magnitude of the various forces responsible for the wave movement. For

instance, waves controlled primarily by gravity, friction and the pressure gradient will attenuate very slowly; waves in which inertia is also significant will attenuate at a faster rate.

The movement of a flood wave is governed by the conservation principles of fluid mechanics. The conservation of mass is expressed by the equation of continuity and the conservation of momentum by the equation of motion. These two equations constitute a system of partial differential equations for which no complete analytical solution is available. With the advent of the digital computer, numerical solutions are increasingly being used to solve the partial differential equations describing flood movement.

A numerical solution is based on the formulation of an algebraic analog of the partial differential equations. Independent variables (space and time) are represented discretely on the x-t plane such that dependent variables (discharge, velocity, stage) are either known or can be calculated at specified locations of the grid.

The early work on flood routing placed emphasis on specific problems which could be treated by an appropriate simplification of the equations of continuity and motion. For instance, if lateral storage is the predominant physical mechanism, such as in the passage of a flood wave through a lake or reservoir, the routing follows directly from the equation of continuity alone, in effect disregarding the equation of motion. This is the basis of the level pool or Modified Puls reservoir routing method.

For stream channel routing, classical hydrology relied on the storage (or hydrologic) routing methods. These methods are aimed at simplifying the equation of motion by postulating a relationship between inflow, outflow and storage in a channel reach, in lieu of the more complex partial differential equation. A linear algebraic relationship of this type is the basis of the Muskingum method, which has had wide application in engineering practice. The Muskingum method, however, cannot properly be regarded as a storage routing method, since it can be shown to be closely linked to hydraulic routing methods, which do take account of the equation of motion.

The equation of motion expresses the balance of inertia, surface and body forces in a given direction. The inertia forces originate in

the acceleration of the motion, while the surface forces are the longitudinal pressure gradient and the shear resistance along the channel bottom. The body force is the gravitational component along the direction of motion. In flood routing applications, the question of the relative magnitude of these various forces is often raised. If one or more forces are of negligible magnitude as compared with the remaining forces, they can be assumed equal to zero. This gives rise to approximate wave models, which are valid provided the neglected terms do not contribute appreciably to the solution. An important model of this sort is the kinematic wave, which postulates the exact balance of gravity forces and bottom friction, neglecting the pressure gradient and inertia forces. An equally important model is the diffusive wave, which considers the balance of gravity, bottom friction and the pressure gradient, while also neglecting the inertia forces.

Flood routing in natural river channels is subject to an additional degree of freedom imposed by the nonrigid boundary. An imbalance between sediment supply and transport capacity causes aggradation or degradation of the channel bed. Two additional equations are necessary in order to calculate the changes in bed elevation: 1) the equation of sediment continuity, and 2) the equation of sediment motion (sediment transport equation). By solving these two together with the equations describing the water phase (water continuity and motion), a solution for the unsteady flow of water and sediment in natural river channels can be obtained.

Several methods of flood routing are described in the remainder of this chapter. Owing to the large number of methods available no attempt is made here to provide a comprehensive treatment. Rather, emphasis is placed on the methods that have a sound theoretical basis. Criteria for the selection of a method to solve a particular type of problem are given in the last section of this chapter.

6.2 CLASSIFICATION OF FLOOD ROUTING METHODS

The flood routing problem can be stated in the following terms: given a hydraulic system with a specified input discharge hydrograph, find the output discharge hydrograph. The system can be a channel reach, a lake or reservoir, or a combination of channel and reservoir. In the most general case, the system is subject to the laws of unsteady

flow in alluvial channels, which are expressed in terms of three governing equations: 1) the equation of water continuity, 2) the equation of motion, and 3) the equation of sediment continuity. Various simplifications are possible depending on whether certain features of the motion are predominant over others, or if an expedient mathematical solution to a simplified problem is desired. Thus, the neglect of the equation of sediment continuity results in the routing of water waves only. The further neglect of the equation of motion results in the routing of volumes of water, in effect disregarding the force balance.

For the purpose of clarity of presentation, the following classification is advanced:

1. Classification based on the quantity being routed.
   a. Water Routing. This refers to the routing of water waves only. It is governed by the equations of water continuity and motion.
   b. Water and Sediment Routing. This refers to the routing of water and sediment, therefore taking into consideration transient changes in sediment transport. The problem is formulated in terms of the three governing equations.
2. Water Routing: classification based on the predominant physical mechanism.
   a. Mass Balance. This refers to the routing of volumes of water, without considering the momentum balance. The problem is formulated only in terms of the equation of water continuity.
   b. Mass and Momentum Balance. This refers to the routing of water, considering both mass and momentum balance. The problem is formulated in terms of the equations of water continuity and motion. Alternatively, these two equations can be combined to form a second order convection-diffusion equation.

The term Hydrologic (or Storage) Routing is often used in the literature to encompass a large class of routing methods which are primarily based on the storage equation, i.e., the lumped form of the water continuity equation. The term Hydraulic Routing refers to those methods

which are based on a mass and momentum balance. Furthermore, some methods originally regarded as hydrologic have recently been shown to be linked to the more general hydraulic routing methods. The Muskingum method and its variations are a good example of this.

3. Mass and Momentum Balance: classification based on approximations to the equations of motion.
   a. Kinematic Wave Approximation. This method is based on the assumption that the pressure gradient and inertia terms in the equation of motion are negligible as compared with the gravity and bottom friction terms. This assumption leads to the kinematic wave equation, which is an equation of pure convection.
   b. Diffusive Wave Approximation. This method is based on the assumption that the inertia (local and convective) terms of the equation of motion are negligible as compared with the gravity, bottom friction and pressure gradient terms. This assumption leads to the diffusive wave equation, which is an equation describing convection and diffusion.
   c. Dynamic Wave Routing. This method considers the complete equation of motion. It is often referred to as full dynamic routing. It is the most general model for flood routing.

The Muskingum Method with improvement by Cunge (1969) can be shown to be based on a discretization of the convection-diffusion equation. Therefore, it can properly be classified as a diffusive wave model.

4. Water and Sediment Routing: classification based on the method of formulating the problem.
   a. Sequential Routing Method. The equations of water continuity and motion are solved as a first stage, and the changes in bed elevation are calculated by using the sediment continuity equation in a second stage.
   b. Known-Discharge Method. Since the speed of the bed transients is several orders of magnitude smaller than that of the water transients, the water discharge can be assumed steady when modeling bed transients. The problem can be formulated in terms of the sediment continuity equation and the steady water surface profile (backwater) equation.

5. Classification based on the solution technique.

   a. Analytical Routing. The governing equations are solved strictly by analytical means. Examples are the diffusion analogy of Hayami and the linear routing of Dooge.

   b. Numerical Routing. The governing equations are solved by numerical methods, such as: 1) the method of characteristics, 2) the finite difference method, and 3) the finite element method.

6.3 GOVERNING EQUATIONS

The governing equations of gradually varied unsteady alluvial channel flow are: 1) the equation of water continuity, 2) the equation of motion, and 3) the equation of sediment continuity. The first two are often referred to in the literature as the Saint Venant equations, while the third is sometimes called the Exner equation.

The Water Continuity Equation

The equation of water continuity for unsteady open channel flow is

$$\frac{\partial Q}{\partial x} + \frac{\partial A}{\partial t} = q_L \qquad (6\text{-}1)$$

in which Q is the water discharge, A is the flow area, and q_L is the lateral inflow. In the absence of lateral inflow, Equation 6-1 reduces to

$$\frac{\partial Q}{\partial x} + \frac{\partial A}{\partial t} = 0 \qquad (6\text{-}2)$$

Expressed per unit of channel width, Equation 6-2 reduces to

$$\frac{\partial q}{\partial x} + \frac{\partial d}{\partial t} = 0 \qquad (6\text{-}3)$$

in which q is water discharge per unit width, and d is the depth of flow.

Equation 6-3 can also be expressed as

$$d\,\frac{\partial u}{\partial x} + u\,\frac{\partial d}{\partial x} + \frac{\partial d}{\partial t} = 0 \qquad (6\text{-}4)$$

in which the first term is the prism storage, the second term is the wedge storage, and the third term is the rate-of-rise.

The lumped form of the equation of water continuity is obtained by integrating Equation 6-2 over a channel reach or reservoir to yield the storage equation

$$I - O = \frac{dV}{dt} \qquad (6\text{-}5)$$

in which I is the inflow, O is the outflow and V is the storage.

The Equation of Motion

The equation of motion is derived by applying Newton's second law of motion to the force balance in gradually varied unsteady open channel flow. This yields

$$\frac{\partial Q}{\partial t} + \frac{\partial}{\partial x}\left(\frac{Q^2}{A}\right) + gA\frac{\partial y}{\partial x} + gA\,S_f = 0 \qquad (6\text{-}6)$$

in which y is the water surface elevation, g is the acceleration of gravity and S_f is the friction slope. It is most convenient to discuss the Kinematic Wave, Diffusion Wave, and Quasi-Steady Dynamic and Dynamic Wave equations together. Figure 6.1 shows the relationships among these different equations by showing which terms are considered in each formulation.

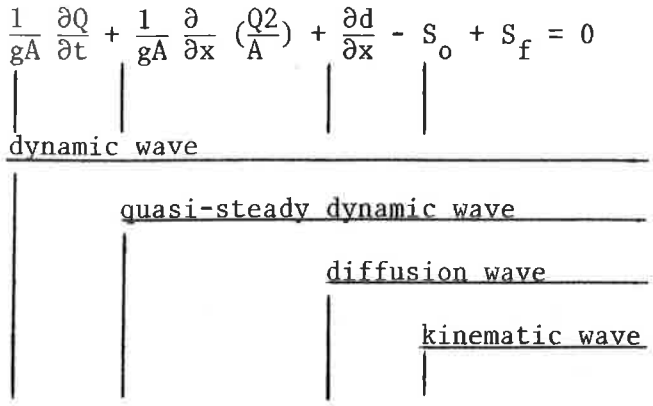

Figure 6.1 Relationship among various equations.

The dynamic wave equation is the full momentum equation (Equation 6-6). If the first term is neglected for quasi-steady flow, a quasi-steady dynamic wave equation is formed. When the first two terms on the left-hand side are neglected, the diffusion wave equation is formed. When the first three terms of the left-hand side are neglected, the kinematic wave equation is formed.

If Equation 6-6 is expressed in terms of per unit width, the equation of motion becomes

$$\frac{\partial}{\partial t}(ud) + \frac{\partial}{\partial x}(u^2 d) + gd\frac{\partial}{\partial x}(z+d) + gd\,S_f = 0 \qquad (6\text{-}7)$$

in which u is mean velocity, d is flow depth, and z is bed elevation.

Equation 6-7 is often used in reduced form. The derivatives are operated to yield

$$d\frac{\partial u}{\partial t} + u\left[\frac{\partial d}{\partial t} + \frac{\partial}{\partial x}(ud)\right] + ud\frac{\partial u}{\partial x} + gd\frac{\partial d}{\partial x} + gd\frac{\partial z}{\partial x} + gdS_f = 0 \quad (6\text{-}8)$$

The terms enclosed in brackets are a statement of the water continuity, without lateral inflow, and equal zero by definition. Furthermore, if $\partial z/\partial x = -S_o$, Equation 6-8 reduces to

$$\frac{1}{g}\frac{\partial u}{\partial t} + \frac{u}{g}\frac{\partial u}{\partial x} + \frac{\partial d}{\partial x} - S_o + S_f = 0 \quad (6\text{-}9)$$

which is the equation of motion in its reduced form. In Equation 6-9, the first two terms are the inertia terms, local and convective, respectively; the third term is the pressure gradient term; the fourth is the gravity (bed slope) term; and the fifth is the bottom friction (friction slope) term. Furthermore, the energy slope S_e can be defined as

$$S_e = \frac{u}{g}\frac{\partial u}{\partial x} + \frac{\partial d}{\partial x} - S_o \quad (6\text{-}10)$$

and the acceleration slope S_a as

$$S_a = \frac{1}{g}\frac{\partial u}{\partial t} \quad (6\text{-}11)$$

from which Equation 6-9 reduces to

$$S_a + S_e + S_f = 0 \quad (6\text{-}12)$$

Assuming for simplicity a Chezy resistance relation of the form

$$Q = CA\,(RS_f)^{1/2} \quad (6\text{-}13)$$

in which C is the Chezy friction coefficient and R is the hydraulic radius, the equation for the looped rating curve is obtained by substituting Equation 6-9 into Equation 6-13 to yield

$$Q = CA\,R\left(S_o - \frac{\partial d}{\partial x} - \frac{u}{g}\frac{\partial u}{\partial x} - \frac{1}{g}\frac{\partial u}{\partial t}\right)^{1/2} \quad (6\text{-}14)$$

The Sediment Continuity Equation

The sediment continuity equation, expressed per unit of channel width is

$$\frac{\partial q_s}{\partial x} + \frac{\partial}{\partial t}(C_s d) + (1\text{-}p)\,\rho_s g\frac{\partial z}{\partial t} = 0 \quad (6\text{-}15)$$

in which q_s is the bed material transport rate, C_s is the spatial bed material concentration, p is the bed porosity, and ρ_s is the mass density of the solids in the channel bed.

6.4 LEVEL POOL ROUTING

The Level Pool Routing method is used to describe the movement of a flood wave as it passes through a lake or reservoir. In such a system,

the water surface is practically horizontal, and the attenuation of the flood wave is predominantly accomplished through lateral storage. The routing procedure follows directly from the lumped form of the water continuity equation (Equation 6-5), by balancing inflow, outflow and volume of storage. A significant role is played by the equation governing the outflow conditions. Through this equation the outflow rate is uniquely determined by the pool level and therefore by the volume of storage.

Defining inflow, outflow and volume of storage as I, O and V, respectively, Equation 6-5 discretized over a time interval Δt is

$$\frac{1}{2}(I_1 + I_2) - \frac{1}{2}(O_1 + O_2) = \frac{V_2 - V_1}{\Delta t} \tag{6-16}$$

in which the subscripts 1 and 2 indicate the start and end of the time interval, respectively. Equation 6-16 can be expressed as

$$\frac{V_2}{\Delta t} + \frac{O_2}{2} = \frac{V_1}{\Delta t} + \frac{O_1}{2} - O_1 + \frac{1}{2}(I_1 + I_2) \tag{6-17}$$

calling

$$N = \frac{V}{\Delta t} + \frac{O}{2} \tag{6-18}$$

Equation 6-17 reduces to

$$N_2 = N_1 - O_1 + \frac{1}{2}(I_1 + I_2) \tag{6-19}$$

in which N is called the storage indication quantity.

The data consists of the inflow hydrograph and a storage-outflow (V-O) relation. The inflow hydrograph is discretized in time to yield a series of I values. By using Equation 6-18, the V-O relation is used to derive an N-O relation. With a known initial value of O, the N-O relation is used to obtain an initial value of N. The calculation then proceeds by a sequence of the following steps: 1) use of Equation 6-19 to calculate a new value of N, and 2) use of the N-O relation to calculate a new value of O corresponding to the new value of N.

6.5 MUSKINGUM METHOD

The Muskingum method and its variations are used to describe the movement of a flood wave through a channel reach. The method was developed in connection with flood control schemes in the Muskingum River Basin, Ohio; hence its name. It is based on the assumption of a linear relationship between inflow I, outflow O, and volume of storage V in a channel reach, of the form

$$V = K[XI + (1-X)\ O] \tag{6-20}$$

in which K and X are the Muskingum parameters. Equation 6-20 leads to (Figure 6-2))

$$Q_{j+1}^{n+1} = C_1\ Q_j^n + C_2\ Q_j^{n+1} + C_3\ Q_{j+1}^n \tag{6-21}$$

from which the outflow discharge at the new time level Q_{j+1}^{n+1} can be calculated from a knowledge of the inflow discharge at the present level

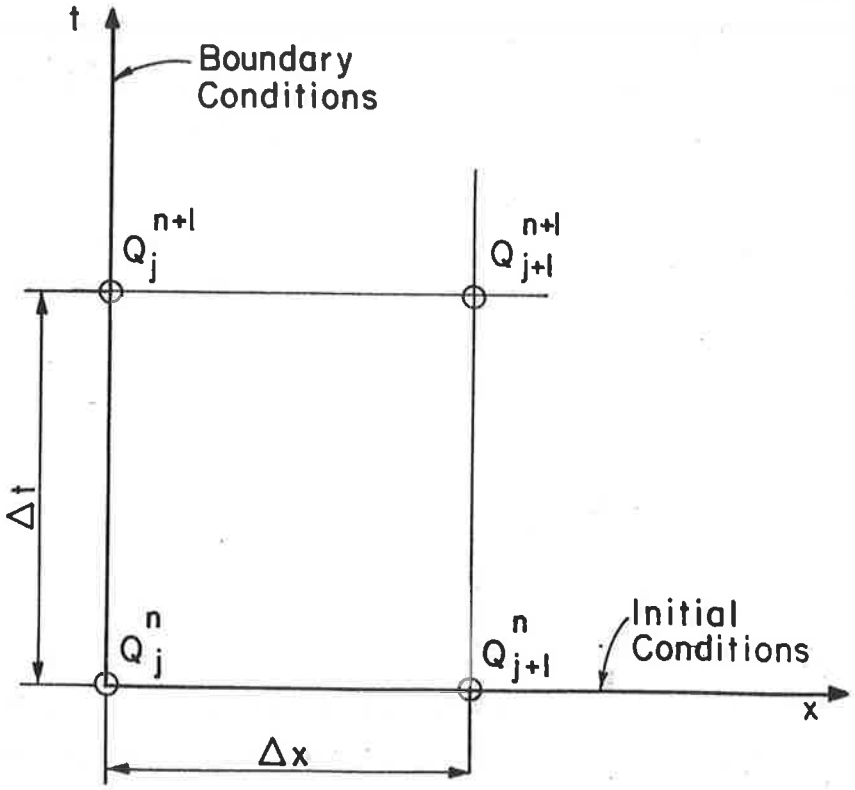

Figure 6.2 Space-time discretization in the Muskingum formulation.

Q_j^n, the inflow discharge at the new time level Q_j^{n+1}, and the outflow discharge at the present level Q_{j+1}^n. The coefficients C_1, C_2 and C_3 are the Muskingum coefficients, defined as

$$C_1 = \frac{2X + \frac{\Delta t}{K}}{2(1-X) + \frac{\Delta t}{K}} \tag{6-22}$$

$$C_2 = \frac{-2X + \frac{\Delta t}{K}}{2(1-X) + \frac{\Delta t}{K}} \tag{6-23}$$

$$C_3 = \frac{2(1-X) - \frac{\Delta t}{K}}{2(1-X) + \frac{\Delta t}{K}} \qquad (6\text{-}24)$$

in which Δt is the time step (also called time interval or routing period).

In the original Muskingum method, the parameters K and X are determined by calibration using measured inflow and outflow hydrographs. The predictive capability of the method has been enhanced by Cunge (1969), who demonstrated the equivalence of the Muskingum formulation and a four-point finite difference analog of the kinematic wave equation. Since the latter cannot account for diffusion effects, Cunge correctly traced the diffusion of the hydrograph as calculated by the Muskingum method to the truncation errors of the first order scheme. By matching the numerical diffusion coefficient of the first order scheme with the physical diffusion coefficient of the convection-diffusion equation (the diffusive wave equation), Cunge further showed that a theoretical basis for the parameter X could be established. Thus, the improved Muskingum method is referred to as the Muskingum-Cunge method.

In the Muskingum-Cunge method, the parameter K is the propagation time of the flood wave, defined as

$$K = \frac{\Delta x}{c} \qquad (6\text{-}25)$$

in which x is the computational reach length and c is the flood wave celerity. The parameter X is a measure of the amount of numerical diffusion, and can be calculated by

$$X = \frac{1}{2}\left(1 - \frac{q}{S_o\, c\Delta x}\right) \qquad (6\text{-}26)$$

in which q is the discharge per unit width and S_o is the channel bed slope. The parameters K and X can either be assumed constant (linear case) or varied with the flow (quasilinear case) (Ponce and Yevjevich, 1978). In the linear case, the accuracy of the simulation improves when the calculation of K and X is based on average values of q and c.

A convenient way of expressing the Muskingum coefficients is obtained by substituting Equations 6-25 and 6-26 into Equations 6-22 to 6-24, to yield

$$C_1 = \frac{1+C-D}{1+C+D} \qquad (6\text{-}27)$$

$$C_2 = \frac{-\ 1+C+D}{1+C+D} \tag{6-28}$$

$$C_3 = \frac{1-C+D}{1+C+D} \tag{6-29}$$

in which

$$C = c\,\frac{\Delta t}{\Delta x} \tag{6-30}$$

is the Courant number, and

$$D = \frac{q}{S_o\ c\Delta x} \tag{6-31}$$

is a cell Reynolds number.

The analogy between the Muskingum formulation and the diffusive wave equation has been demonstrated. Therefore, it follows that both have the same limits of applicability. The applicability of the diffusive wave model was established by Ponce et al. (1978) on theoretical grounds. They showed that the diffusive wave is justified as an approximation to the full dynamic wave provided the following inequality is satisfied

$$TS_o\ (g/d_o)^{1/2} \geq \xi \tag{6-32}$$

in which T is the flood wave duration, S_o is the channel bed slope, d_o the average flow depth, and ξ a real number which is a function of the average Froude number and the required accuracy. For the Froude number in the subcritical range, $\xi = 30$ assures an attenuation error of not more than 5% after an elapsed time T.

Two additional comments regarding the applicability of the Muskingum method are necessary. First, it is clear that while numerically simulating the subsidence of the flood wave, the method is still based on the specification of a steady state rating curve. However, this contradicts the essence of the phenomenon being simulated, since it is a fundamental property of unsteady flow that non-unique discharge-stage relations are generated as a consequence of the flow variability. The error due to this cause can be minimized if inequality Equation 6-32 is satisfied.

Second, the Muskingum method cannot be applied to the cases where there is some type of downstream control. Since the method is based on a kinematic formulation, it can only propagate information in one direction, from upstream to downstream. For the cases with a significant downstream control, a more elaborate method has to be used.

6.6 BACKWATER COMPUTATION

The backwater profile can be described by using Equation 6-6 for a steady state solution. The equation of motion for this case is

$$\frac{\partial}{\partial x}\left(\frac{Q^2}{A}\right) + gA\frac{\partial y}{\partial x} + gA\,S_f = 0. \qquad (6\text{-}33)$$

The steady flow continuity equation is

$$Q = V\,A\ . \qquad (6\text{-}34)$$

Using equations 6-33 and 6-34 in conjunction with the law of resistance such as Chezy's or Manning's equation, the backwater profile can be determined with the proper boundary condition.

6.7 NUMERICAL ROUTING

Numerical Routing refers to flood routing methods that are based on the numerical integration of the governing equations. The numerical integration can proceed along two lines: 1) by the method of characteristics, and 2) by finite difference methods. In the method of characteristics, the two partial differential equations (water continuity and motion) are replaced by four ordinary differential equations, which are solved numerically on a characteristic grid. The intersections of characteristic lines on the x-t plane define the characteristic grid (Figure 6.3).

In the finite difference methods, the functions and their derivatives are expressed in terms of their discrete values on a rectangular grid defined on the x-t plane (Figure 6.4). A finite difference scheme is a formula that expresses a relationship between neighboring values of the dependent variables on the rectangular grid.

Both methods of integration provide sufficiently accurate results when proper care is exercised in their use. The flexibility of the finite difference methods, however, is a definite advantage over the more cumbersome characteristic methods. This is reflected in the current trend to increased use of finite difference methods in flood routing. For this reason, only the finite difference method will be treated here. Extensive accounts of the method of characteristics as applied to flood routing are given by Abbott (1975) and Amein (1966).

The finite difference methods can be of two types: 1) explicit, and 2) implicit. Explicit schemes are those that advance the solution

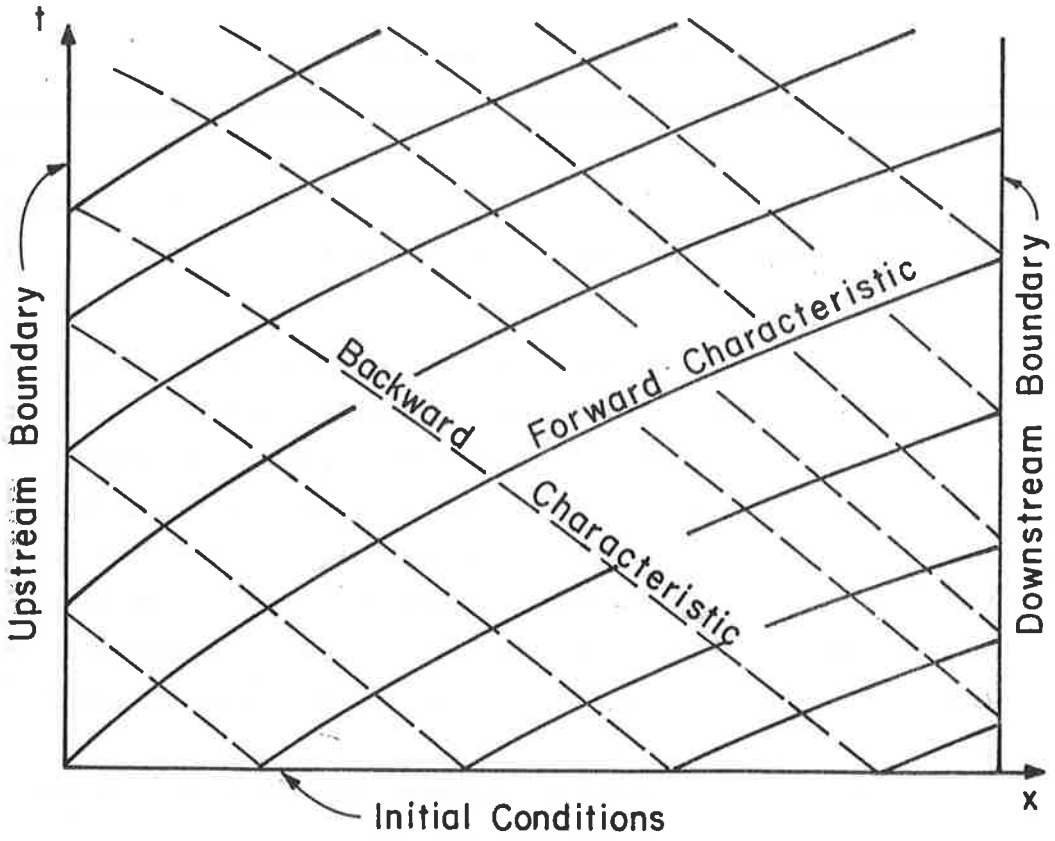

Figure 6.3 Characteristic grid on the x-t plane.

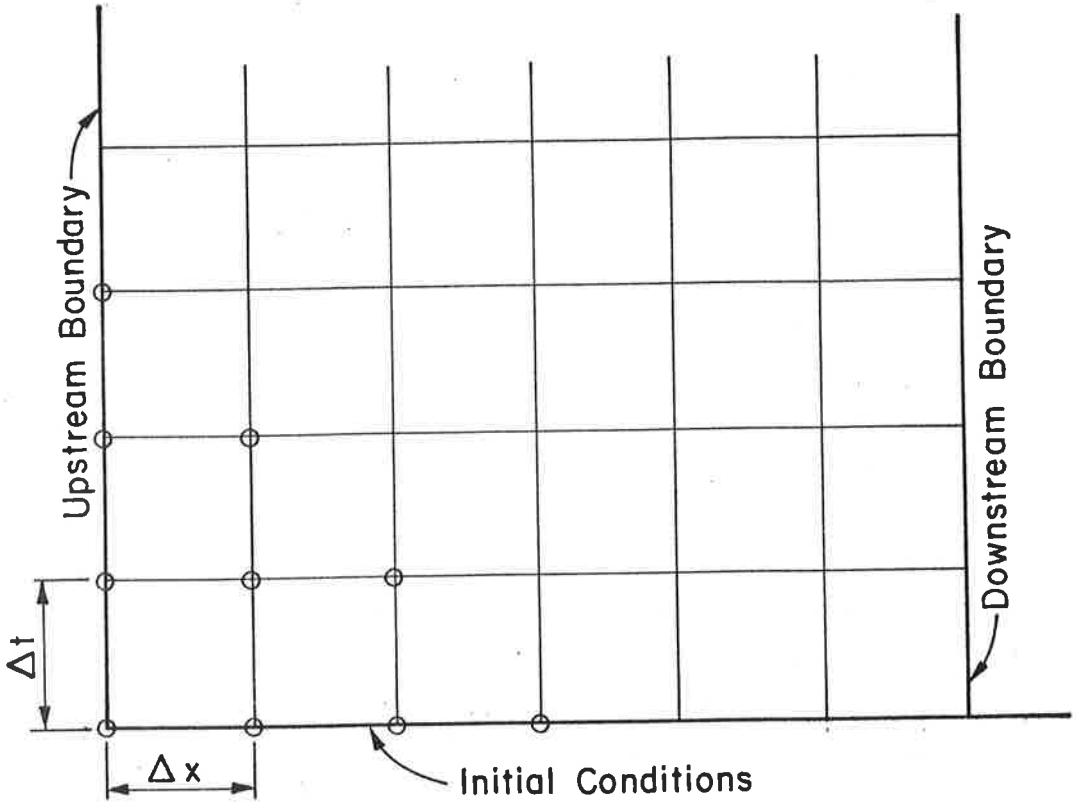

Figure 6.4 Finite difference grid on the x-t plane.

in time by solving for the unknown values of the dependent variables, one grid point at a time. Implicit schemes advance the solution in time by simultaneously solving for the dependent variables at a number of grid points.

Explicit schemes are relatively simple to formulate, but are usually limited to a very small time step by a strict numerical stability criterion. On the other hand, implicit schemes require the inversion of a matrix, but are not subject to the strict stability criterion of explicit schemes. Therefore, in implicit schemes, the size of the time step is primarily based on accuracy considerations. In general, implicit schemes are more efficient in their use of computational resources than their explicit counterparts.

The numerical solutions to the system formed by either the diffusion wave approximation, the quasi-steady dynamic wave or the dynamic wave equation in conjunction with the water continuity equation can proceed in two directions. Either an attempt can be made to convert the original system of partial differential equations into an equivalent system of ordinary differential equations by using the method of characteristics (Chang and Richards, 1971), or one can replace the partial derivatives in the original system with quotients of finite-differences by using the explicit method or the implicit method (Amein, 1968; Amein and Fange, 1970; and Chen, 1973). Amein (1968) found that the implicit method is faster and more accurate than other finite difference methods when applied to flood routing in river systems. Chen (1973) modified Amein and Fang's method to derive an unconditionally stable linear implicit method. These implicit methods require downstream boundary conditions and are usually applicable only in low Froude number flows.

Another group of methods is developed by simplifying the momentum equation. The most common simplified method is the kinematic wave approximation. This method assumes that the friction slope is equal to the channel bed accelerations. The kinematic wave approximation can be solved either by an analytical or a numerical method. Unfortunately, the analytical solution is often restricted for practical applications because of the formulation of kinematic "shockwave." The "shock" is represented by the intersection of characteristics in the space and time characteristic plane (Kibler and Woolhiser, 1970, and Li et al., 1976).

In the analytical solution, water is conceptually routed along a particular characteristic path which is independent of the other characteristic paths. This additional assumption can cause the formation of "shock." Numerical solutions have not been developed under this additional assumption. Normally, numerical solutions provide artificial "damping" and "smoothing" effects. Thus, there is usually no kinematic wave "shock" problem when a numerical solution is used. However, if the dynamic effect is significant, the kinematic wave assumption is no longer valid.

For watershed runoff problems, the dynamic effects are generally negligible, and therefore the kinematic wave approximation is usually limited to the watershed system. Some of the available numerical methods for kinematic wave approximation are given by Kibler and Woolhiser (1970) and Li et al., (1975). The method developed by Li et al., (1975) is unconditionally stable and the simplest one.

Four-Point Implicit Scheme

Of all the implicit schemes for flood routing computations, the four-point scheme of Preissmann (Liggett and Cunge, 1975) has received the most attention. It is based on the following equations (Figure 6.5)

$$f(x,t) = \frac{\theta}{2}\left(f_{j+1}^{n+1} + f_j^{n+1}\right) + \frac{1-\theta}{2}\left(f_{j+1}^{n} + f_j^{n}\right) \tag{6-35}$$

$$\frac{\partial}{\partial x} f(x,t) = \theta \frac{\left(f_{j+1}^{n+1} - f_j^{n+1}\right)}{\Delta x} + (1-\theta)\frac{\left(f_{j+1}^{n} - f_j^{n}\right)}{\Delta x} \tag{6-36}$$

$$\frac{\partial}{\partial t} f(x,t) = \frac{\left(f_{j+1}^{n+1} - f_{j+1}^{n}\right) + \left(f_j^{n+1} - f_j^{n}\right)}{2\Delta t} \tag{6-37}$$

in which $f(x,t)$ is any dependent variable, j is a space index, n is a time index, and θ is a weighting factor introduced in the formulas in order to provide flexibility in the numerical computations. The practical range of the weighting factor is $0.5 \leq \theta \leq 1.0$. While values of θ close to 0.5 may be desirable from an accuracy standpoint, larger values are often needed to numerically smooth out perturbations with wave lengths on the order of $2\Delta x$ which can render the computation unstable. In practice, an optimum compromise between stability and accuracy is sought.

Equations 6-35 to 6-37, when applied to the governing equations for several computational reaches, yield a set of simultaneous nonlinear algebraic equations for the dependent variables at the unknown time level (n+1). Since the equations are nonlinear, two possibilities arise: either they are solved by the Newton-Raphson iterative technique, or they are linearized and solved directly without iteration. If the iterative solution is chosen, the linearized solution can be used as the first guess in order to speed the convergence of the iterative procedure.

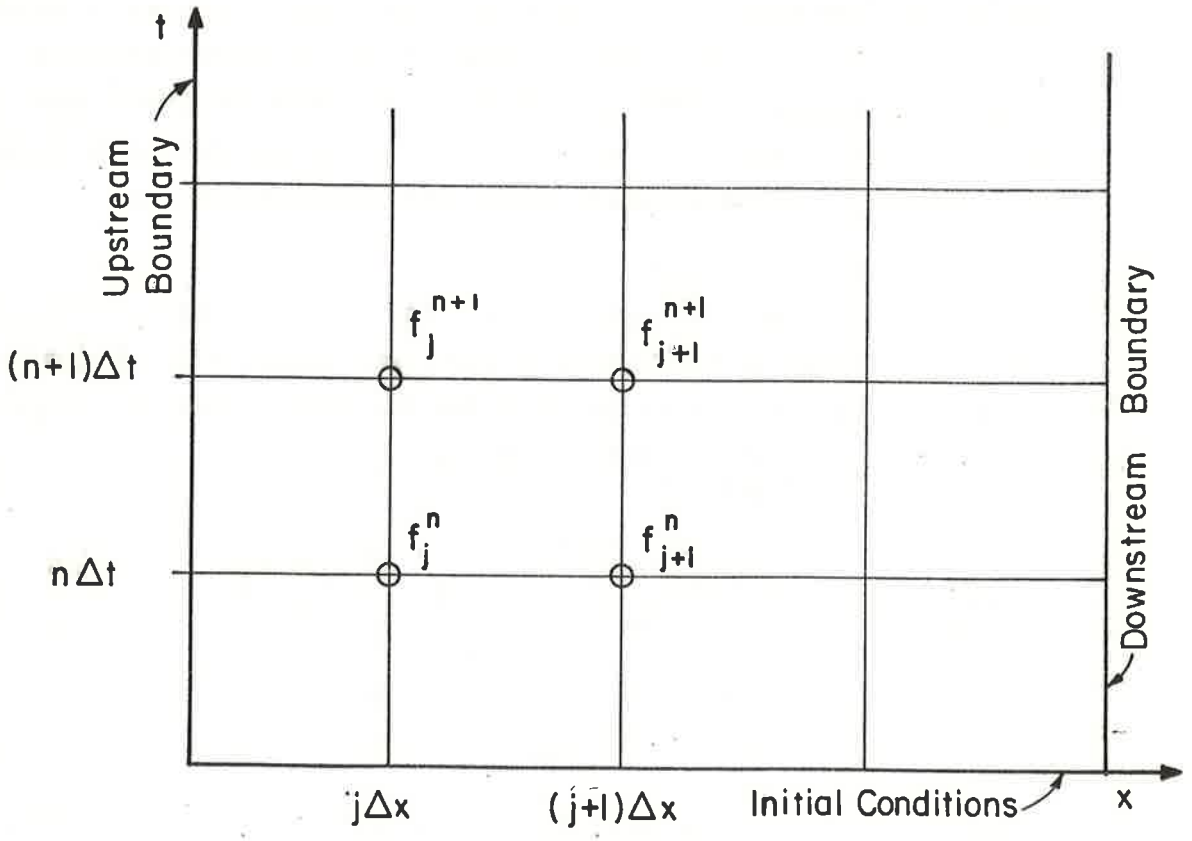

Figure 6.5 Schematic representation of the x-t plane for use in Preissmann's implicit scheme.

The solution of the system of linear algebraic equations can be accomplished by the double sweep technique. This is a recursive type of Gauss elimination process particularly suited for application to banded (tridiagonal or pentadiagonal) matrices. The implicit schemes lend

themselves to this type of solution, thereby reducing computer core requirements and the computational time required for matrix inversion. In the double sweep solution technique, the upstream boundary condition starts the first sweep, from the upstream to the downstream boundary, in which two internal arrays are generated. Then, the downstream boundary condition starts the second sweep, from the downstream to the upstream boundary, in which the dependent variables at time level (n+1) are calculated based on the internal arrays generated by the first sweep.

Backwater Profile Computation

The numerical backwater profile computation is much easier. The most common method is the HEC-2 computer program developed by the U.S. Army Corps of Engineers. In the HEC-2 program, the solution technique employs successive approximations. Results at each cross section are checked to insure they are on the correct side of critical depth. That is, if the boundary value is subcritical flow, the correct side is above critical depth. If the prescribed boundary value is supercritical, all calculated depths will be less than or equal to critical. These details are handled automatically by the computer.

The convergence equations estimate the next trial water surface based on the present and preceding values of trial and computed water surface elevation. Solutions prove to be stable, and they converge to the .01 foot tolerance rapidly in most cases. Occasionally, flows near bank-full will display an oscillation between in-banks and out-of-banks elevations rather than converging. After 20 such trials the program leaves the trial and error loop with the water surface elevation equal to top bank elevation. A note is printed.

The solution of the critical depth equation requires successive approximations, also. Since large amounts of computer time can be consumed in calculating critical depth, an approximation is used to first test the need for critical depth. If calculations are near critical, the full solution is made.

Minor losses may be neglected if zero loss coefficients are prescribed. In any case they are simply added to the friction loss to get total loss.

Flow at bridges is a complex hydraulic process which is approximated by one-dimensional equations and discharge coefficients. Usually, more

than one type of flow exists (i.e., flow beneath the bridge plus flow over the roadway approaches or the roadway). The program can handle very complex situations, but interested readers are referred to HEC-2 "Water Surface Profiles;" HEC Training Document No. 6, "Computation of Water Surface Profiles through Bridges Using HEC-2;" and HEC Technical Paper #20, "Computer Determination of Flow Through Bridges."

Stability, Consistency and Convergence

Finite difference solutions of differential equations have certain numerical properties that characterize them, namely, the properties of stability, consistency and convergence. Stability refers to the ability of the numerical scheme to inhibit error growth. Consistency refers to the property of a scheme to produce a solution that approaches the analytical solution as the discretization is made exceedingly small. Convergence is a measure of the size of the errors introduced in the numerical solution due to an improper discretization.

An unstable numerical model is one in which a certain type of numerical error is allowed to grow unbounded until it eventually spoils the calculations. The causes of instability can usually be traced back to the type of continuum system of equations (elliptic, parabolic, or hyperbolic) and its finite difference analog (explicit or implicit).

Explicit numerical analogs are usually subject to a necessary condition for stability: that the domain of dependence of the difference equation encompass the domain of dependence of the corresponding differential equation (Figure 6.6). This is referred to as the Courant-Friedrichs-Lewy stability condition, and it is expressed by

$$c_e \frac{\Delta t}{\Delta x} \leq 1 \qquad (6\text{-}38)$$

in which c_e is the phase velocity of an elementary wave. This inequality effectively restricts the size of the time step that can be used in practice, often leading to inefficient computation.

In implicit schemes, the domain of dependence of the difference equation constitutes the domain of dependence of the entire solution to the differential equation (Figure 6-7), and thus, the necessary condition is always satisfied. Therefore, implicit schemes allow for the use of larger time steps than those possible with explicit schemes. The size of the time step, however, cannot be set arbitrarily, since there is a

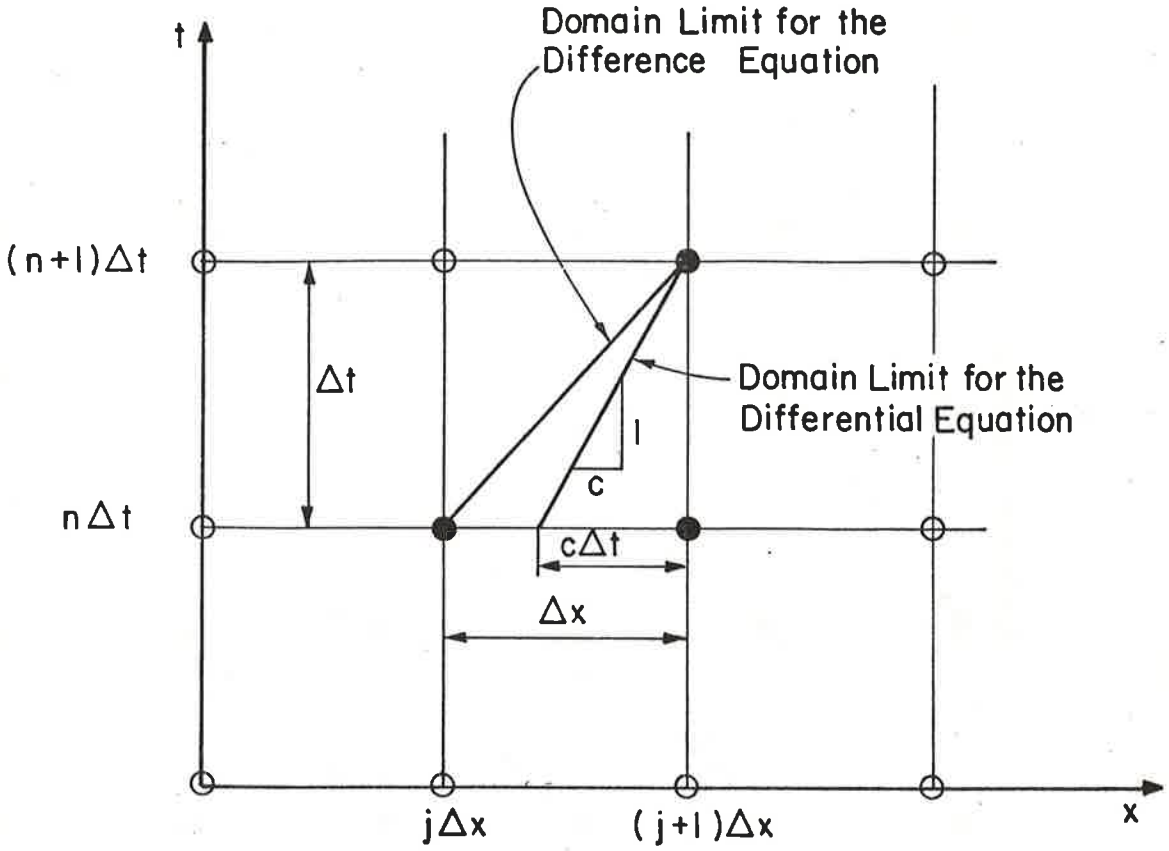

Figure 6.6 Illustration of the necessary condition for stability of explicit schemes (Courant-Friedrichs-Lewy Condition).

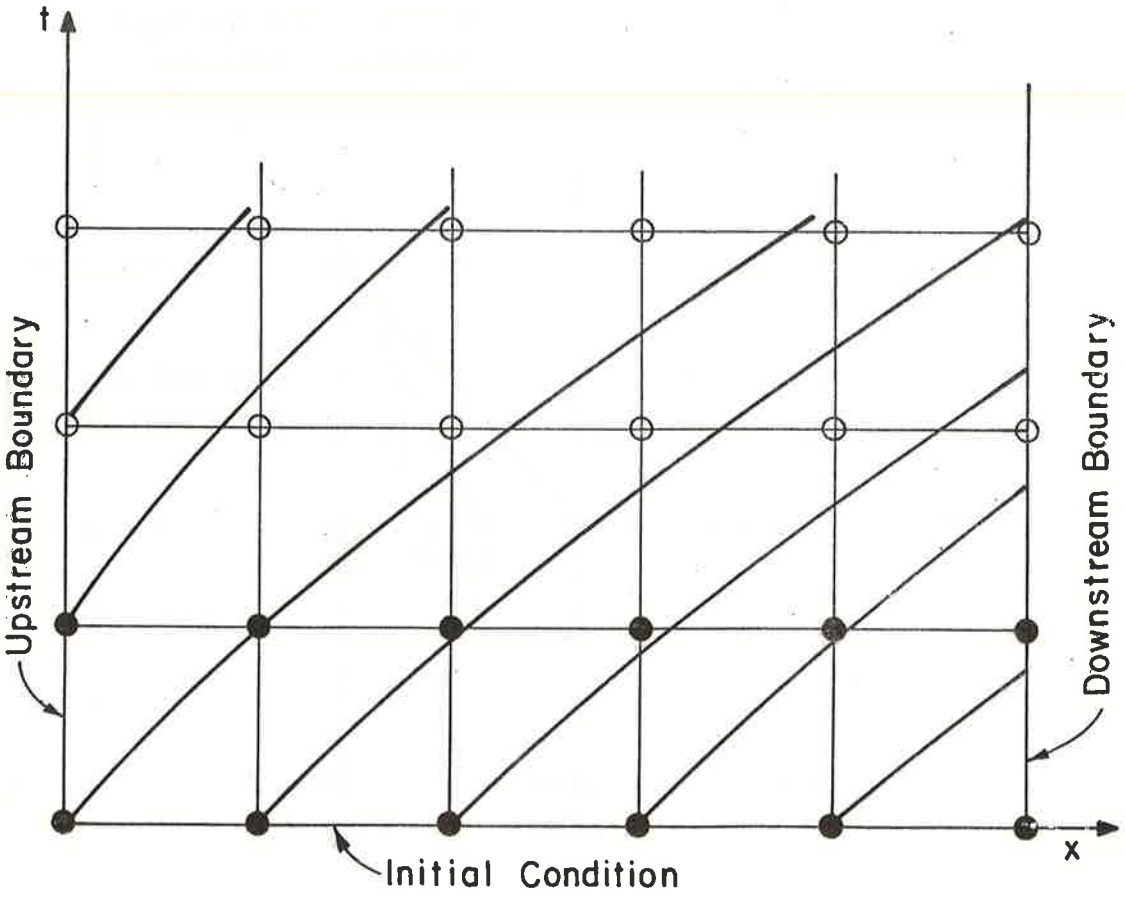

Figure 6.7 Characteristic structure illustrating the stability of implicit schemes being independent of the Courant-Friedrichs-Lewy Condition.

practical upper limit dictated by the grid resolution above which accuracy (convergence) would be considerably impaired.

Implicit schemes are by no means free from stability problems. While the question of stability in explicit schemes is closely related to the Courant-Friedrichs-Lewy necessary condition, the stability of implicit schemes is subject to other complications. Several authors have linked the instability of implicit schemes to roundoff errors (O'Brien et al., 1950), while others attribute it to nonlinear wave interaction (Phillips, 1959). Leaving the question unanswered, it suffices here to say that implicit schemes may also exhibit instabilities, and that the common reference to the "unconditional stability" of implicit schemes is probably an unfortunate choice of words. A more precise description such as "stable regardless of the Courant condition" is proposed.

Consistency refers to the property of a scheme to produce a solution that approaches the analytical solution as the discretization is made exceedingly small. Given a certain consistency condition, a scheme is either consistent with the related differential equation (scheme A and B of Figure 6.8) or inconsistent (scheme C). Convergence, on the other hand, refers to the rate at which the numerical solution approaches the analytical solution. The schematic error portraits shown in Figure 6.8 illustrate the concept of rate of convergence: Scheme A will converge at a faster rate than Scheme B, i.e., when used with comparable grid resolutions, Scheme A will be more accurate than Scheme B. The accuracy of Scheme B can be improved by increasing the grid resolution, but this is at the expense of increased computational effort.

In implicit schemes, convergence is associated with a certain combination of weighting factor and grid resolution. The practical range for the weighting factor is $0.5 \leq \theta \leq 1.0$. In theory, a weighting factor close to 0.5 would be optimum from the convergence standpoint. In practice, however, higher values of θ are needed in order to numerically smooth out perturbations with wavelengths on the order of $2\Delta x$ which can render the computation unstable. Thus, the weighting factor acts as a numerical filter, eliminating the high frequency perturbations which can cause instability. For the filter to function

effectively, it should have a negligible effect on the smaller frequencies of interest. In general, the higher the weighting factor, the higher the grid resolution needed if the numerical filter is to have a negligible effect on the smaller frequencies. Stated in other terms, for a given grid resolution, the higher the weighting factor, the more stable and less rapidly convergent the scheme.

Boundary Conditions

The specifications of the boundary conditions constitute an integral part of the formulation of a numerical model. No scheme, no

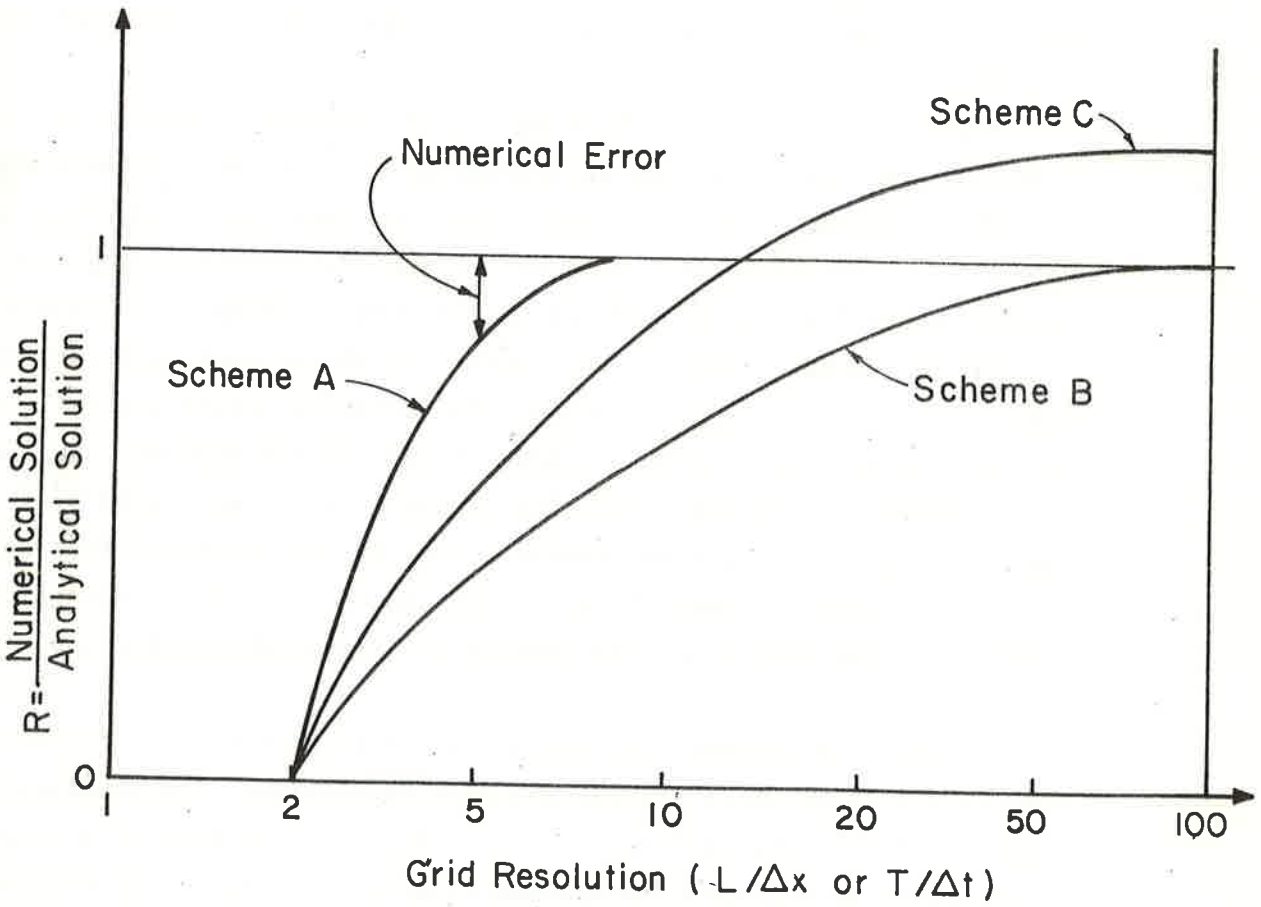

Figure 6.8 Illustration of the concept of consistence and convergence. Schemes A and B are consistent with the differential equation, and Scheme C is inconsistent. Scheme A converges faster than Scheme B.

matter how elaborate, will lead to correct results unless the boundary conditions are properly specified.

Implicit schemes require two boundary conditions, one upstream and one downstream. For instance, discharge can be specified upstream and stage downstream. The stage upstream and discharge downstream are generated by the double sweep solution technique. Often there is no boundary condition available downstream, and a single-valued rating curve is used instead. However, this type of boundary condition contradicts the solution at the boundary, introducing an error which is distributed upstream by the inversion algorithm. A finely balanced numerical scheme will usually become unstable in this situation, but schemes with heavy numerical damping may survive at the expense of accuracy. A viable alternative is to specify the equation for the looped rating curve (or approximations to it) as a way of relating discharge to stage at the downstream boundary.

6.8 THE CHOICE OF A FLOOD ROUTING METHOD

The choice of a flood routing method is based on the systematic evaluation of the following criteria: 1) nature of the problem, 2) input needs, 3) output needs, and 4) utilization of resources.

Nature of the Problem

The nature of a flood routing problem can be categorized into: 1) type of system, 2) type of hydrologic event, and 3) type of boundary control. The system could be a stream channel, a reservoir or lake, or a combination of channel and reservoir. Stream channels are characterized by a finite water surface slope. On the other hand, in reservoir systems the water surface slope can usually be assumed equal to zero. At the channel-reservoir confluence, the backwater effects will effectively reduce the water surface slope to a small but nonetheless finite value.

The hydrologic event could be such that it creates a fast rising, a normal rising, or a slow rising flood wave. In general, the rate-of-rise and duration of the hydrograph are directly related to the size of the contributing watershed, larger watersheds resulting in longer duration hydrographs.

The boundary control could be either: 1) upstream only, or 2) upstream and downstream. Certain stream channel reaches may be subject

to upstream control only. Channel-reservoir and reservoir cases are usually subject to both upstream and downstream control. The routing of tributaries through river junctions may also be subject to downstream control, depending on the relative magnitude of mainstream and tributary flow.

Input Needs

The input needs can comprise one or more of the following: 1) inflow discharge or stage hydrograph, 2) hydraulic data, 3) topographic data, and 4) historic data. The inflow discharge or stage hydrograph has to be properly discretized to minimize errors due to insufficient temporal resolution.

The hydraulic data comprises: 1) discharge-area relations, or 2) Manning's friction coefficient. To achieve greater detail in the simulation, these can be specified at every cross section. Alternatively, average values may be used for a number of cross sections at the cost of reduced accuracy.

The topographic data consists of: 1) wetted perimeter-area relations, 2) stage-area relations, and 3) top width-area relations. In addition, a longitudinal channel bed profile and the distance between adjacent cross sections are also necessary.

The historic data on past floods may be needed for calibration purposes. This is aimed at "fine tuning" the estimation of the hydraulic parameters.

Output Needs

Depending on the problem at hand, the output requirements may comprise one or more of the following: 1) peak discharge and/or peak stage, 2) accurate timing of the hydrograph, 3) hydrograph shape, and 4) definition of the looped rating curve.

Utilization of Resources

An important but sometimes neglected aspect in choosing a flood routing method is that of the expenditure of resources, i.e., the total cost, including manpower training, research and development, and actual computer run costs to achieve a certain objective. The following need to be considered as inputs to a decision regarding utilization of resources: 1) manpower utilization for training, research, development and operation, in man-days or man-months, 2) computer hardware requirements,

such as desktop or main frame, 3) availability of commercial and/or institutional software packages, and 4) actual computational cost, primarily in the case of main frame computers.

Method Selection

As an example of how to select a method most suited to a particular set of conditions, the following four general approaches are examined here: 1) kinematic wave, 2) diffusive wave, 3) dynamic wave, and 4) level pool case. Any flood routing problem of practical importance can be formulated by using at least one of these approaches.

The kinematic wave model is particularly suited for stream routing in steep channels with little or no downstream control. According to Ponce et al. (1978), the kinematic wave model is applicable provided the following inequality is satisfied: $TS_o\, u_o/d_o \geq 171$, in which T is the flood wave duration, S_o is the channel bed slope, u_o is the average mean velocity, and d_o the average flow depth. For a given slope S_o, the slower rising flood waves (larger T) will satisfy the above inequality. In practice, the kinematic wave model is restricted to overland flow cases for which S_o is rather large.

A specific input need in the kinematic wave model is the discharge-area relation, which contains friction and cross-sectional information. Output is usually given in terms of peak discharge, fairly accurate timing of the hydrograph peak, and hydrograph shape. No looped rating curve can be obtained by the kinematic wave model.

The diffusive wave model is well suited for stream channel routing. Its implicit formulation requires the specification of a downstream boundary condition, which can partly account for downstream backwater effects. However, its explicit formulation (Muskingum-Cunge Method) cannot account for a downstream boundary control. According to Ponce et al. (1978), the diffusive wave model is applicable provided the following inequality is satisfied: $TS_o\sqrt{g/d_o} \geq 30$. Most cases of floodwaves in stream channels satisfy this inequality.

The explicit formulation of the diffusive wave model (Muskingum-Cunge Method) requires discharge-area relations as input. The implicit formulation, however, is based on Manning's n values. For the latter, historic data may be needed in order to "fine tune" the friction coefficients. Output is usually given in terms of peak discharge, good

timing of the hydrograph peak, and hydrograph shape. In addition, the implicit formulation will calculate a looped rating curve.

The dynamic wave model is the most general model of unsteady open channel flow waves. Its advantages are readily seen in connection with a channel-reservoir system for which the average surface slope may be too small to satisfy the diffusive model criterion. In addition, the dynamic wave model can take full account of backwater effects, i.e., it has upstream and downstream control. Extensive hydraulic, topographic and historic data are needed in order to successfully operate a dynamic model. Output is usually given in terms of peak discharge, peak stage, accurate timing of the hydrograph peak, hydrograph shape, and a looped rating curve at all cross sections.

The level pool routing method is primarily applicable to cases in which the water surface slope can be assumed to be horizontal, i.e., in reservoir and lake systems. The input requirements comprise the inflow discharge or stage hydrograph, and the relationship between outflow and volume of storage in the reservoir. The output consists of the outflow discharge hydrograph.

After the technical requirements have been assessed, the next step is evaluation of the cost constraints. In general, the more precise the method, the greater are the data collection requirements, the manpower training time, the investment in research and development, and the operational costs. Therefore, the selection of a flood routing method for a particular application is a highly demanding task. Considerable judgment and practical experience are required in order to make an intelligent decision regarding this choice. The information presented in this chapter is intended to provide a reference frame to aid the engineer in the adequate choice of a flood routing method.

6.9 REFERENCES

Abbott, M. 1975. Method of Characteristics. In Unsteady Flow in Open Channels. K. Mahmood and V. Yevjevich, eds., Water Resources Publications, Fort Collins, Colorado.

Amein, M. 1968. An Implicit Method for Numerical Flood Routing. Water Resources Research, AGU, Vol. 4, No. 4, Aug., pp. 719-726.

Amein, M. 1966. Streamflow Routing on Computer by Characteristics. Water Resources Research, Vol. 2, No. 1, pp. 123-130.

Amein, M., and Fang, C. S. 1970. Implicit Flood Routing in Natural Channels. J. Hyd. Div. ASCE, Vol. 96, No. HY12, Proc. Paper 7773, Dec., pp. 2481-2500.

Chang, F. F. M., and Richards, D. L. 1971. Deposition of Sediment in Transient Flow. J. Hyd. Div., ASCE, Vol. 97, No. HY6, Proc. Paper 8191, June, pp. 837-849.

Chen, Y. H. 1973. Mathematical Modeling of Water and Sediment Routing in Natural Channels. Ph.D. dissertation, Civil Eng. Dept., Colorado State University, Fort Collins.

Cunge, J. 1969. On the Subject of a Flood Propagation Computation Method (Muskingum Method). IAHR Journal of Hydraulic Research, Vol. 7, No. 2, pp. 205-230.

Eichert, B. S. and J. Peters. 1970. Computer Determination of Flow Through Bridges. HEC Technical Paper #20, Journal of the Hydraulics Division, ASCE, Vol. 96, No. HY7, July

HEC Training Document No. 6. 1974. Computation of Water Surface Profiles Through Bridges using HEC-2, Draft, June 1974.

HEC-2. Water Surface Profiles. Users Manual. Generalized Computer Program, Users Manual, Hydrologic Engineering Center, U.S. Army Corps of Engineers, Davis, California.

Hydrologic Engineering Center, Corps of Engineers, U. S. Army. 1976. HEC-6 Scour and Deposition in Rivers and Reservoirs. Users Manual.

Kibler, D. F. and Woolhiser, D. A. 1970. The Kinematic Cascade as a Hydrologic Model. Hydrology Paper No. 39, Colorado State University, Fort Collins.

Li, R. M., Simons, D. B., Shiao, L. S., and Chen, Y. H. 1976. Kinematic Wave Approximation for Flood Routing. Rivers '76 Symposium on Inland Waterways for Navigation, Flood Control, and Water Diversions, Colorado State University, Vol. 1, pp. 377-398.

Li, R. M., Simons, D. B., and Stevens, M. A. 1975. Nonlinear Kinematic Wave Approximation for Water Routing. Water Resources Research, Vol. 11, No. 2, April, pp. 245-252.

Liggett, J. A., and Cunge, J. A. 1975. Numerical Methods of Solution of the Unsteady Flow Equations. In Unsteady Flow in Open Channels, K. Mahmood and V. Yevjevich, eds., Water Resources Publications, Fort Collins, Colorado.

Lighthill, M. J., and Whitham, G. B. 1955. On Kinematic Waves, I. Flood Movement in Long Rivers. Proceedings of the Royal Society of London, A229, pp. 281-316.

O'Brien, G. G., Hyman, M. A., and Kaplan, S. 1950. A Study of the Numerical Solution of Partial Differential Equations. Journal of Mathematics and Physics, Vol. 29, No. 4, pp. 231-251.

Phillips, N. A. 1959. An Example of Nonlinear Computational Instability. In Atmosphere and Sea in Motion, Rossby Memorial Volume, B. Bolin, ed., Rockefeller Institute Press, New York.

Ponce, V. M., Li, R. M., and Simons, D. B. 1978. Applicability of Kinematic and Diffusion Models. Journal of the Hydraulics Division, ASCE, Vol. 104, No. HY3, Proc. Paper 13635, March, pp. 353-360.

Ponce, V. M., and Yevjevich, V. 1978. Muskingum-Cunge Method with Variable Parameters. Journal of the Hydraulics Division, ASCE, Vol. 104, No. HY12, Proc. Paper 14199, December, pp. 1663-1667.

Seddon, J. A. 1900. River Hydraulics. Transactions, ASCE, Vol. 43, pp. 179-243.

CHAPTER 7

WATER ROUTING AND YIELD FROM WATERSHEDS

by

Ruh-Ming Li, Associate Professor, Department of Civil Engineering, Colorado State University, Fort Collins, Colorado
Daryl B. Simons, Associate Dean for Engineering Research and Professor of Civil Engineering, Colorado State University, Fort Collins, Colorado
Kenneth G. Eggert, Research Associate, Department of Civil Engineering, Colorado State University, Fort Collins, Colorado

7.1 INTRODUCTION

The management of watersheds and river basins for the optimum benefit of the people in general requires a complete knowledge of the interrelations between ecology and environment. The watershed response to developments, either natural or man-induced, must be anticipated correctly if progress is to be made toward wise use of our natural resources. The increasing interests in predicting watershed response has accelerated the progress in the mathematical modeling of water hydrographs and yields. As will be discussed in Chapter 10, concern for protecting the natural environment has also increased research in the field of predicting watershed sediment yields. Further, degradation, aggradation and movement of sediment and other pollutants in watersheds are closely related to water movement. In fact, no sediment yield can be predicted without the knowledge of water routing and yield. This chapter describes several methodologies for calculating water yield and storm water routing from watersheds being developed at the Engineering Research Center, Colorado State University, under the general direction of Daryl B. Simons and Ruh-Ming Li.

The physical processes governing watershed response are very complicated. Many past studies have utilized a statistical interpretation of observed response data. The unit hydrograph method for water routing and the hydraulic geometry equations for stream morphology are examples of these types of studies. It is often difficult to predict the response of a watershed to various watershed developments or treatments using these methods, because they are based on the assumption of homogeneity in time and space. Mathematical modeling using the governing physical processes may be used as an alternative means of estimating the time-dependent response of watersheds to precipitation with varying vegetative covers and land use. The principal advantage of the mathematical simulation approach is that the parameters that are used to vary watershed response may be physically defined. Such a definition enables the user to predict changes in watershed response arising from alterations in the watershed environment. The principal disadvantage of the simulation approach in comparison to purely statistical methods is size and complexity of simulation models. However, the speed and availability of modern computers largely

answer this problem. In addition, as will be shown in Chapter 15, the availability of inexpensive and powerful hand-held programmable calculators places many sophisticated simulation methods in the hands of both researchers and application-oriented engineers.

Physical process simulation models represent the system being modeled by decomposing it into its respective components. By dividing a system into its respective components, "lumping" of processes or parameters can be avoided. By simulating the selected phenomena through separate components, each individual process can be analyzed and refined or altered to meet the needs of the user. Consequently, as each process component is upgraded, the model becomes more representative of the physical system. Only a limited number of physical process models are presented. However, because they are physical process component models, the processes involved are similar between the models. Differences do exist between some components, making some models more complex or versatile than others. Basically two modeling approaches are described below. Later sections discuss the physical processes used in these models and outline techniques that will enable the user to prepare input data and parameters. The selected water routing approaches are: 1) high resolution watershed storm water routing and yield model, and 2) simplified watershed storm routing and yield models. A number of other approaches are available, but research has shown that these contain the most sensitive physical processes.

The above general approaches share essentially the same basic physical process. The main differences are in the formulation, implementation and degree of detail that may be represented. The high resolution model was first developed by Li (1974) and subsequently published by Simons, Li, and Stevens (1975) and updated by Shiao (1978). The model routes storm runoff water from overland flow surfaces and then through the channel system of a watershed. This is done using mathematical formulations of the water continuity equations and certain assumptions about the flow. This model is termed high resolution because it uses a finite difference solution technique to solve for water discharge at selected times and points on the overland flow surface and channel system. The watershed for this model can be subdivided into numerous overland flow surfaces and the channel represented by several connected segments.

The simplified models in contrast to the high resolution model require a watershed to be represented by a channel and two contributing planes or a combination of two-plane and single plane watersheds connected by a channel system. This much simpler representation of the watershed provides for easier application, but may create problems if the watershed is extremely nonhomogeneous or anisotropic. This model uses an analytic formulation to route water from the overland flow planes (Simons, Li, and Eggert, 1977). Use of the single two-plane one channel model is warranted for watersheds that are fairly homogeneous and are subject to spatial constant rainfall. The combined watershed model may be used for larger, more heterogeneous drainages that may be modeled as a group of differing, yet internally homogeneous, subwatersheds.

The discussion of these routing and yield simulations begins in Section 7.2 with a description of the spatial representations required by the individual methods. This section is followed by a description of the physical process components and general layout of the simulators. An important feature of both the high resolution and simplified models is the method used for estimating excess rainfall. This method involves both interception and infiltration processes. These components are similar in both types of model, and they are described in the fourth section. The greatest differences between the high resolution and simplified models occur in the water routing methods. Both kinds of models use kinematic wave routing for overland and channel flow. However, the simplified models use the method of characteristics solution to the kinematic wave problem for some or all of the water routing. This analytical solution is presented. The high resolution model uses a numerical solution to the kinematic wave problem for all water routing. This solution technique is discussed in Section 7.5. Section 7.6 contains examples of model applications, and Section 7.7 presents a discussion of data requirements and parameter estimation techniques.

All of these methods exist as specific computer programs at Colorado State University; however, the theory presented is not intended as a program description, but rather a general approach that may be used in a variety of watershed simulation problems.

7.2 SPATIAL REPRESENTATION OF WATERSHEDS

Because most watersheds are nonhomogeneous in topography, soils, vegetation, and other features, it is necessary to segment each watershed into units which can be treated as being homogeneous. Similarly, the channel system in a watershed can be represented by one or more segments, each having a characteristic location, shape, slope, and roughness.

The location, area, length, and slope of each watershed unit is usually obtained from the available topographic maps. The following steps can be used in collecting the geometric data from topographic maps. Two types of watershed segmentation are considered. For the high resolution model, the watershed is subdivided into square grids of a selected size (Simons, Li and Ward, 1978). The size of these grids or cells is chosen to conform with the watershed geometry and represent the accuracy of the input data and required output. Node points of the grid system represent sampling points where topographic, soils, and vegetative data are selected. The channel system is represented by straight line segments between node points. The sampled information is computer processed to produce a segmented watershed of overland flow cells with corresponding length, slope, width, and soil and vegetative indices, and a channel system described by lengths, slopes, and locations. Gravity flow logic, cell and channel aspect is used to determine flow directions in the watershed. On a much smaller scale, the slope, lengths, widths and flow directions of roadways can be prepared from maps, construction plans, or field measurements. For the simplified watershed models consisting of planes and channels, a different approach is used to abstract the geometry for model input. This approach can be used on small or large watersheds. On large watersheds multiple sets of two plane-one channel watersheds may be present (Simons, Li, and Spronk, 1978). A method is presented below that is applicable to single watersheds or subdivided watersheds.

Geometric Representation for High Resolution Model

The first problem encountered in numerical modeling of watershed response is to determine representative response units for mathematical computations. Simons and Li (1975) have approached this problem by developing a watershed segmentation program based on a grid system.

The grid size is chosen so that the watershed boundary and channel segments can be approximated by grid lines (Figure 7.1). The overland flow units are the grid units inside the watershed boundary and the channel units are segments of channel between grid intersection points.

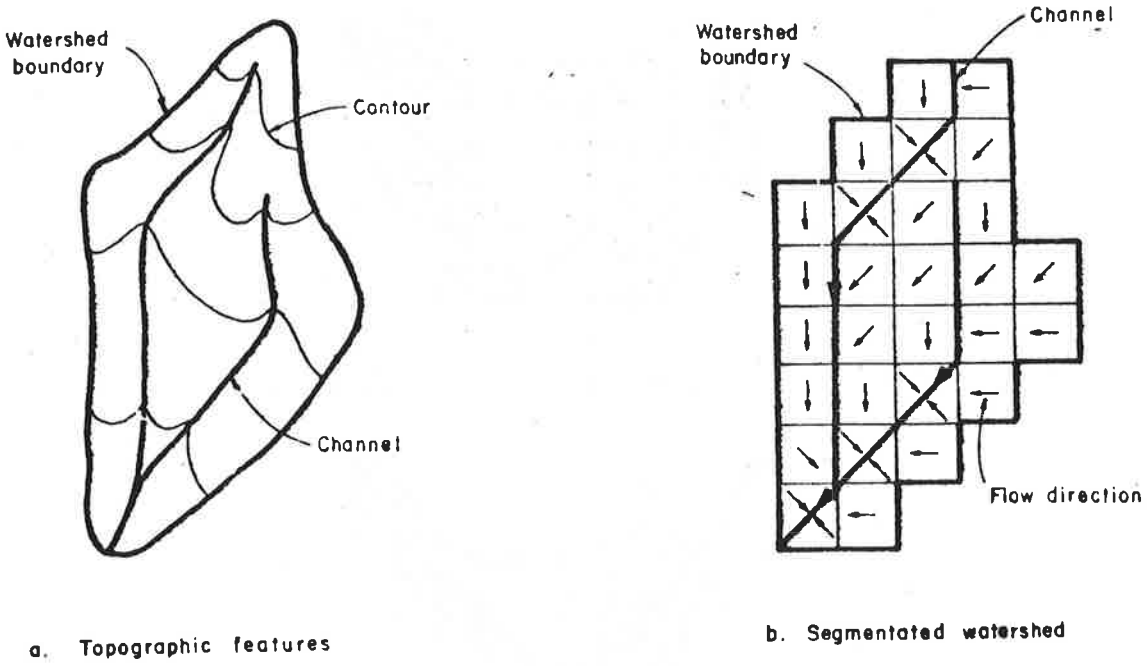

Figure 7.1 Example of watershed segmentation.

From the contour lines, the elevations of the land surface at the grid points are determined (Figure 7.2). These elevations, along with the locations and bed elevation of the stream channel, are input to the developed computer program. In addition to elevation data, vegetation and soil code numbers can be input for each grid point (Figure 7.2). The computer program then performs the following functions:

1. The slope and the slope azimuth of each overland flow unit are computed.

2. It is assumed that the water flows in the opposite direction of the slope gradient to the next overland flow unit or to the adjacent channel. Thus, water cascades from overland unit to overland unit and then into the channel system. The program identifies the cascade sequence (arrows in Figure 7.1).

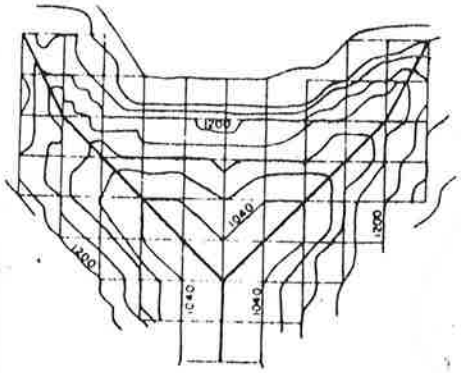

(a) Topographic Map Contour Interval = 40'

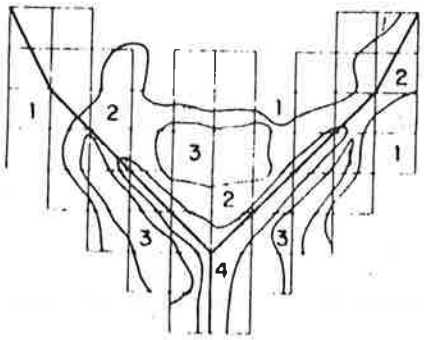

(b) Soils Map Numbers are soil type codes

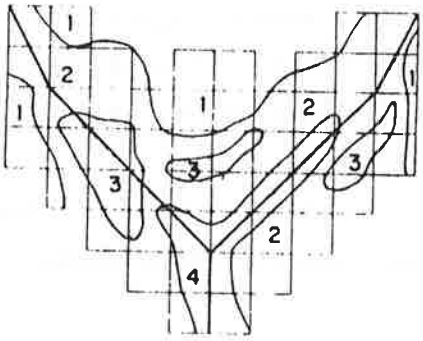

(c) Vegetation Map Numbers are vegetation type codes

Figure 7.2. Input data for hypothetical watershed.

3. The computational sequence for the flow is established by the program. The method employed is simply to follow the logics of gravity flow and flow continuity.

4. If data on the vegetation type, soil type, canopy cover density, and ground cover density are available, the variations of these factors inside a watershed can be established in the program. This is executed by decoding the vegetation and soil codes and assigning previously input parameters to each type code. These parameters may include soil porosity, soil depth, and selected vegetation measures.

In order to save computer storage capacity and processing time in the water and sediment routing computations, an additional computer program to combine small grid units into larger response units is developed. With this treatment, the flow is conceptually routed from overland flow units to channel units and to the selected watershed outlet.

This segmentation method is essential not only in water and sediment routing, but also for introducing the information from snowmelt computations, landslide hazard mapping, forest fire hazard mapping, forest inventory studies, and snow avalanche hazard identification into the routing model. Moreover, if such factors as soil properties, vegetation cover, type of management treatment, or rainfall vary within the watershed, these variations can be handled easily and with the least manual input by segmenting the watershed with a grid system. The developed segmentation method provides input data on watershed geometry and computational sequence required for the simulation model to predict water and sediment routing and yield from small watersheds.

Often the manual determination of the response unit is preferable for non-computer oriented personnel. Such a manual determination should follow the similar logic used in the computer segmentation method. The flow path can be drawn perpendicular to contour lines. The manual determination of hydrologic response unit is subject to the individual's perception and is time-consuming for applications to complicated watersheds. It is recommended that the manual determination be limited in application to small and simple watersheds.

Another characteristic of the channel system that must be numerically defined is the wetted perimeter-flow area relationship for each

channel segment. This relationship is needed for use in water and sediment routing in the channel. The relationship is most often expressed in the power form as

$$P = a_1 A^{b_1} \tag{7-1}$$

where p is the wetted perimeter, A is the flow area, a_1 and b_1 are statistically determined values. Data needed for development of Equation 7-1 are measurements on the channel cross-section. These measurements are the horizontal distance from a datum mark or a bank to a point in the channel and the elevation change between the point and the mark. In a complex application where many stream cross-sections are involved, the values of a_1 and b_1 for each channel segment may be found by a fitting routine contained within the simulation program. As an alternative, a_1 and b_1 may be determined beforehand using a small calculator program such as described in Chapter 15.

Geometric Representation for Simplified Model

The two types of simplified watershed simulation use essentially the same geometric representation. The watershed must be subdivided in such a manner to allow approximation of the land surface by planes that extend to the watershed boundary and one or more interconnecting channels. The simpler of these two models uses an "open-book" representation wherein the watershed is transformed into a single two-planes unit with a central channel. The more complex model uses a number of such units in combination with single planes and interconnecting channel segments.

At Colorado State University these two simplified models have been developed and named ANAWAT and MULTWAT. The former is an acronym for Analytical Watershed Model and is the simpler single open-book representation. The latter name is an acronym for Multiple Watershed Model and is the more complex formulation. These acronyms are only introduced here to simplify later reference to these two model approaches. The basic method of transforming the contour map geometry into planes and channels, however, is the same for both models. This technique is described below for the ANAWAT and then extended for the MULTWAT case. The process is illustrated by Figure 7.3 and presented in a step-by-step form below.

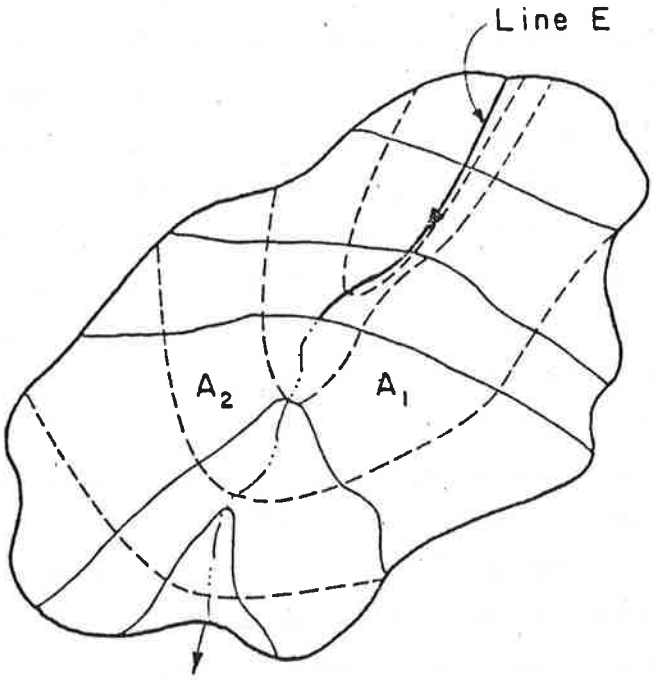

(a) Original Subwatershed Topographic Map

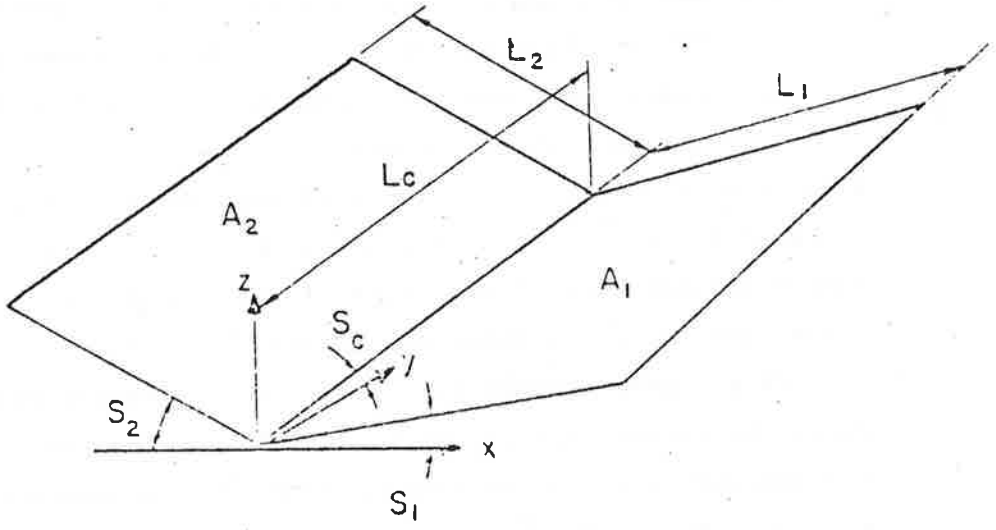

(b) Openbook Plane Representation

Figure 7.3 Geometric representation of a subwatershed unit.

1a. Divide the watershed into units which can be considered homogeneous by using the available topographic, soil type, and vegetation type maps for the watershed. The size of the division is based on the resolution needed and the availability of data.

1b. Divide the watershed using the channel system. This division is often at the user's discretion, but should be based on homogeneity in the channel segment or its contributing side slopes. This homogeneity may be the channel segment gradient or similar soil types on the contributing side slopes.

2. Delineate the main channel in the unit. Extend the channels at least to the last distinct end points. Such as end point is often noted as the last distinct "V" on the a contour line for tributary channels. In small watersheds determining the correct path along which to extend the channel may be difficult. In larger watersheds the extension of the channel may be apparent all the way to the basin boundary. Therefore, the extension of the channel for measurement purposes is arbitrary. A general consideration may be:

(a) Small watersheds - Extend the channel to the last distinct "V" and no further.

(b) Medium sized watersheds - Extend the channel from the last "V" one-half the distance to the watershed boundary.

(c) Large watersheds - Extend the channel from the last "V" to the watershed boundary.

No distinction is made on watershed size as this is a factor that is dictated by experience. In general, however, a small watershed may have a maximum size of one hundred acres, medium would be 100 to 1,000 acres, and large, anything more than 1,000 acres.

If a channel extension is made, the extension must perpendicularly cross the contour elevations to insure that the water is following the shortest path to the channel. Measure the channel segment length.

3. Sketch in the boundaries between contributing side slopes to the different channel segments. The enclosed contributing areas are now the watershed subdivisions. Each channel has a left and right subdivision when looking downstream.

4. Determine the channel segment slope as the ratio of elevation difference at the channel end points to the channel length.

5. Determine the area of the left and right contributing subdivisions by using the channel as the dividing line. For small and medium sized watersheds, an artificial dividing line may need to be constructed as an extension from the assumed channel end point to the watershed boundary. Make sure this division remains perpendicular to the topographic contours.

6. Determine each subdivision width as sum of subdivision area divided by channel length as determined in Step 4.

7. Subdivide the channel into several (5-20) equally spaced sampling points. At each sampling point lay out sampling lines from the channel to the watershed or response unit boundary. Sampling lines are drawn perpendicular to contour lines and represent flow lines that cross equipotential lines in a flow net. The sampling lines are the potential routes water would follow when flowing across the subdivision. Determine the slope as elevation change on the sampling line. Form the product of sampling line length times slope. Sum these products for the sampling lines in each response unit.

8. For small or medium sized watersheds, a single slope sampling line will be extended from the end point of the channel. This sampling line should coincide with the artificial dividing line constructed in Step 6. Because the area above the assumed channel endpoint represents an overland flow plane, it is treated as being equally divided between the two response units. To do this, add the slope-length products for this sampling line to the summed slope-length products for each subdivision. Also add the length of the sampling line to the summed lengths of the sampling lines of each subdivision. These additions will incorporate the effects of this headwater overland flow plane into each of the subdivisions.

9. Determine the average slope of each subdivision as the summed slope-length products for the unit divided by the summed sampling line lengths or

$$\bar{S} = \frac{\sum_{i=1}^{n} S_i \times \ell_i}{\sum_{i=1}^{n} \ell_i} \qquad (7\text{-}2)$$

where $\bar{S}$ is average of overland slope, n is number of sampling lines, S_i is slope of line i, and ℓ_i is length of line i. The consistent step-by-step procedure presented above will provide a digitized watershed amenable to analysis by watershed modeling.

An example of the above procedure is presented below.

Example: Small Watershed (see Figure 7.4)

Area = 4.01 acres

Length of Channel to "V" = 418 feet

Slope of Channel to "V" = 0.108

	(Acres)	Average Width feet	Weighted* Average Slope
Left side	2.64	275.5	0.172
Right side	1.37	142.4	0.205

* includes artificial extension 192.5 feet long with slope of 0.26. Ten sampling lines utilized.

As mentioned earlier, ANAWAT has the capability of simulating the storm water runoff from a single plane or from the "open book" geometry as shown in Figure 7.3. MULTWAT classifies the single plane units as planes and the "open book" units as subwatersheds. Storm water runoff hydrographs from the ANAWAT units serve as inputs to the interconnecting channel units. Water in the channels is routed by using a numerical solution to the nonlinear kinematic wave approximation. A method to account for channel losses due to infiltration is included in the channel routing procedure. The necessity of using a numerical channel routing routine rather than an analytical routine is due to the occurrence of kinematic shock. The analytical solution cannot be applied in situations where kinematic shock occurs.

There are four types of response units in MULTWAT: 1) a single plane ANAWAT unit, 2) an "open book" ANAWAT unit, referred to as a subwatershed, 3) a channel, which is a larger channel interconnecting the other units, and 4) a connection. A connection unit is used when only the lower part of a basin is being modeled and the response of the upstream portion of the basin is input as a hydrograph recorded or simulated at the gaging station dividing the upper and lower parts of the basin. The method of obtaining the size and slope of planes and channels was given above. As an example of the transformation

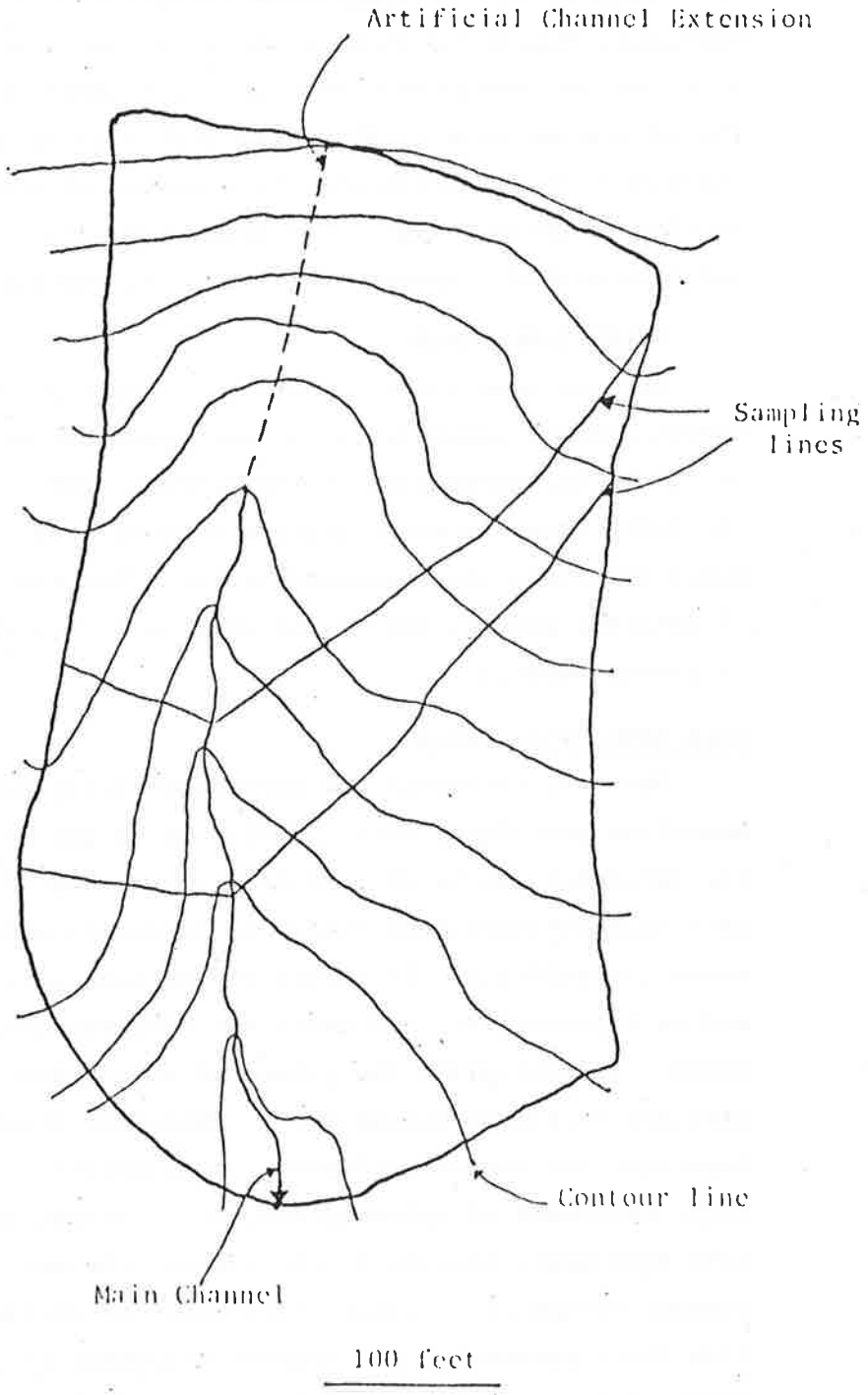

Figure 7.4 Important features for developing a small watershed representative geometry.

of a larger, more heterogeneous watershed into a system of planes and channels, Figure 7.5 shows a map of Walnut Gulch, Arizona, a watershed selected for development and testing of MULTWAT. The boundaries of the planes and subwatersheds are marked to illustrate how a large watershed can be represented by a system of these units interconnected by channel units. Figure 7.6 shows a schematic diagram of Walnut Gulch Watershed, represented by planes, subwatersheds, and channels.

7.3 MODEL COMPONENTS

As mentioned earlier, both the high resolution and simplified models contain essentially the same physical process components; however, the implementation of the process varies considerably due to the differences in water routing methods. The components and basic model structure are presented below. This discussion is a description of existing models, but may be used as a blueprint for the development of similar models.

High Resolution Model

Once the watershed has been numerically defined by the above segmentation procedure, overland flow units and channel flow units in the watershed can be determined. Simons and Li (1975) developed a watershed sediment model which is primarily applicable for surface erosion simulation. It simulates the land surface hydrologic cycle, sediment production, and water and sediment movement on small watersheds. Conceptually, the watershed is divided into an overland flow part and a channel system part. Different physical processes are important for the two different environments. In the overland flow loop, processes of interception, evaporation, infiltration, and overland flow water routing to the nearest channel are simulated. In a channel system loop, water contributed by overland flow is routed. A flow chart presenting the interrelationship of these processes is shown in Figure 7.7. A brief summary of the components is given below. The model described in Figure 7.7 also contains sediment routing and erosion components that were discussed in Chapter 10.

Overland Flow Loop

There are three components in the overland flow loop: interception infiltration, and overland surface water.

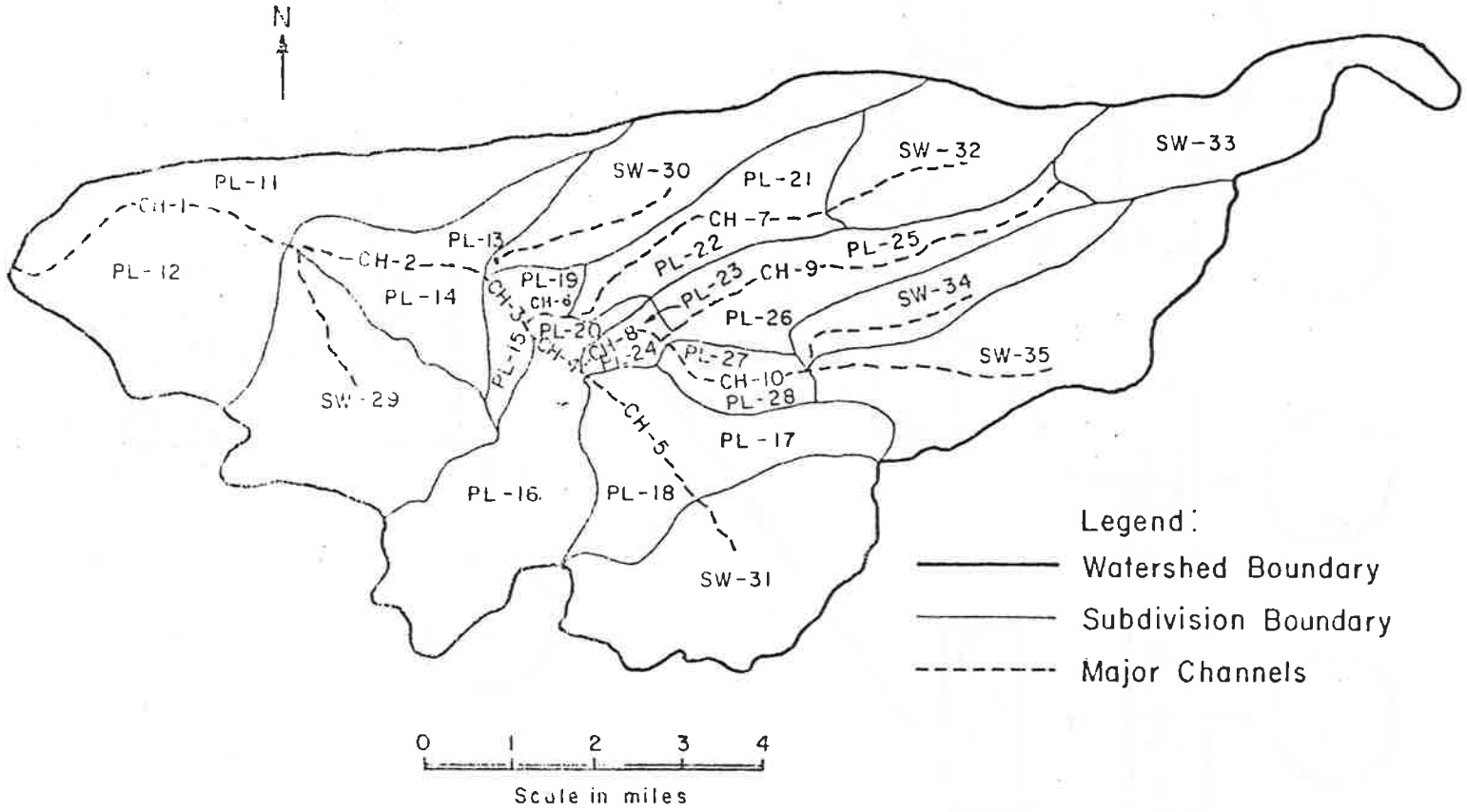

Figure 7.5 Response units for Walnut Gulch, Arizona, watershed.

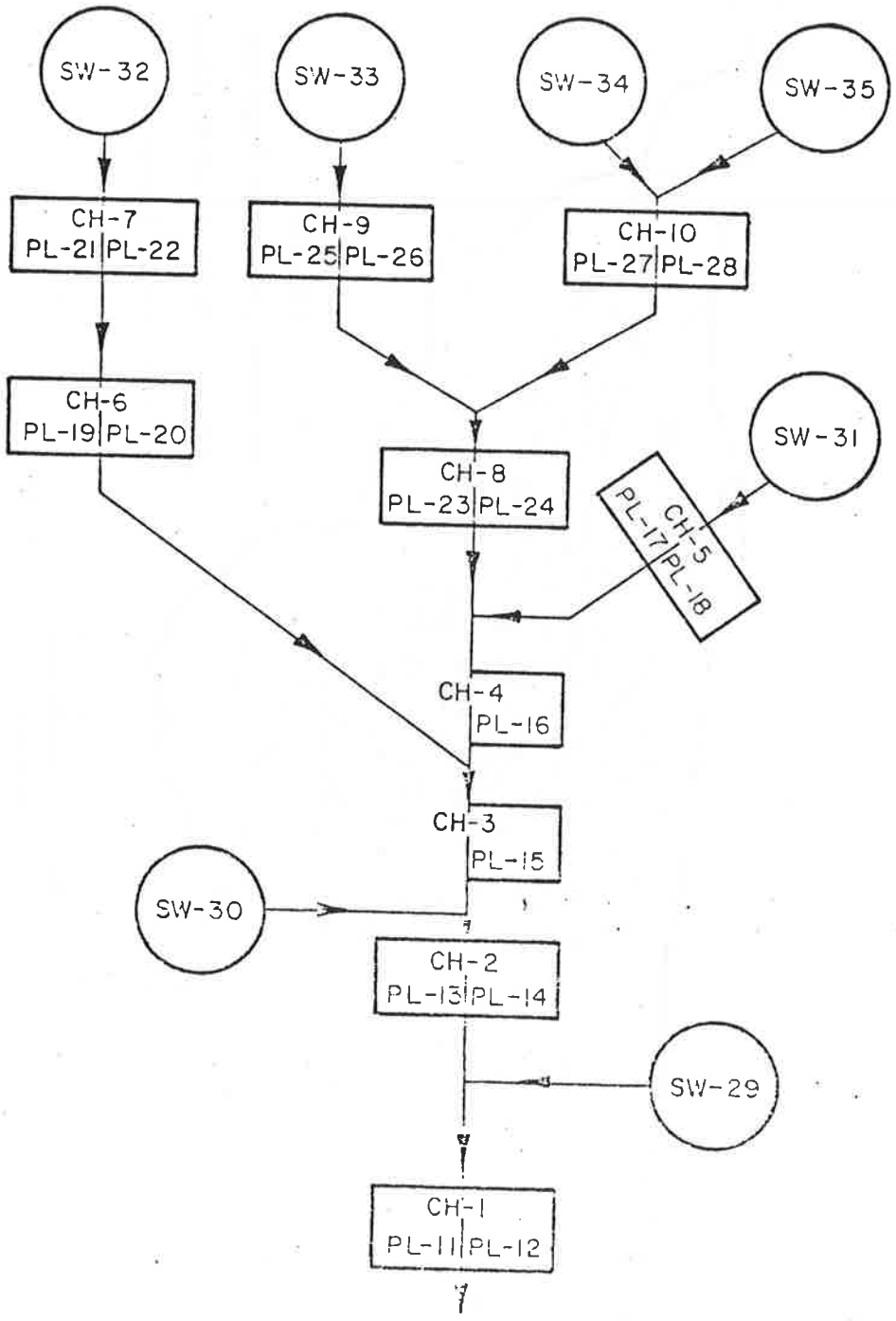

Figure 7.6 Schematic diagram of the Walnut Gulch response units.

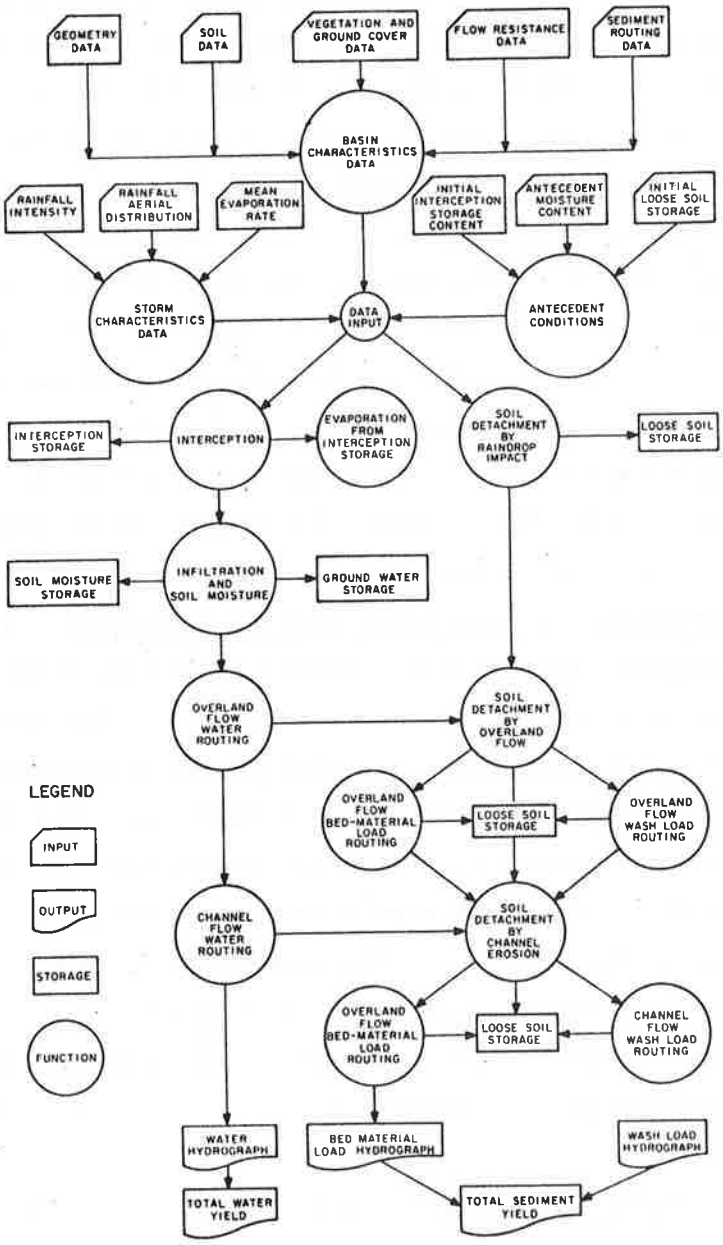

Figure 7.7 Flow chart for the watershed sediment and routing model.

Interception Component. In this component the interception amounts due to the crown and forest floor are computed and the net rainfall is determined from the rainfall input. The interception loss includes the constant interception storage and the continuous evaporation from the interception surfaces. The evaporation is usually negligible during the storm. The interception storage is formulated to be a function of canopy cover density, ground cover density, and vegetation type.

Infiltration Component. This component of the model simulates the process of infiltration. The infiltration rate is computed by an approximation of Darcy's Law assuming that a distinct wetting front exists and is formulated to be a function of saturated hydraulic conductivity, average capillary suction pressure, soil porosity, antecedent moisture content, and moisture content in the wetted zone. Therefore, the rate of rainfall excess can be determined from the net rainfall and infiltration rates.

Overland Surface Water Routing Component. With this component the overland surface water runoff resulting from the mean rainfall excess is routed to the nearest channel. The routing procedure is based on the continuity of water, a momentum equation of kinematic wave approximation, and a set of resistance functions for different hydraulic conditions. The total resistance to flow is assumed to be a sum of the drag resistance due to ground cover and the shear stress acting on the soil bed. The computation is carried out by a nonlinear finite difference scheme developed by Li et al. (1975a) and the computation results include the mean flow depth, bed shear stress and flow discharge at computation points as a function of time and space point.

Channel Water Routing Component. This component of the model routes the water down the creeks in the channel system and computes the hydrograph at the watershed outlet. The lateral water inflows to the channel system are the overland surface water flows. The channel water routing procedure and the finite difference scheme are similar to those used in the overland flow loop.

Simplified Models

The simplified models contain the same physical processes listed above, but these routines are applied to subunits that are in general much larger than those of the high resolution model. In addition, these routines are uncoupled in the sense that they are used to calculate the process response for the entire event on a given unit before passing on to the next physical process. For example, infiltration for the entire storm is calculated before passing the entire rainfall excess function on to overland flow routing. This is as opposed to the time step by time step calculation of the high resolution model. Therefore, some resolution is sacrificed for a gain in computational speed.

The physical processes modeled for each type of unit are shown in Table 7.1. The processes involved in the plane and subwatershed units

Table 7.1 Physical Processes Considered for Each Type of Unit

	Plane	Subwatershed	Channel
Physical Processes Considered	1. Interception	1. Interception	1. Channel Infiltration
	2. Overland Infiltration	2. Overland Infiltration	2. Overland Channel Routing
	3. Analytical Overland Routing	3. Analytical Overland Routing	
		4. Analytical Channel Routing	

are identical except for the analytical channel routing performed for the subwatershed units. The only processes considered for the channel units are numerical routing and channel infiltration.

Much of the rain falling during the first part of a storm is intercepted by the vegetal ground cover. Precipitation intercepted by vegetation or other ground cover eventually evaporates, and the

amount of rainfall reaching the soil surface is less than the recorded amount. The amount of interception loss depends on the percentage of the ground that is covered by canopy and ground cover, and their respective water holding capacities. It is assumed that interception starts at the beginning of a storm and continues until the potential intercepted volume is filled.

A portion of the rainfall reaching the ground moves through the soil surface into the soil. This process is defined as infiltration. The model used to simulate this process is based on the Green and Ampt infiltration equation (Li, Simons and Eggert, 1976).

Using an approximate explicit solution to the Green-Ampt equation for time varying rainfall given by Eggert, Li and Simons (1979), a function for infiltration with respect to time is developed. Thus, the infiltration occurring during a selected time period can be determined if the soil characteristics are known.

An analytical solution to the continuity, momentum, and cross section geometry equations is used to route water in the plane and subwatershed units. The method presented is identical to the routing scheme presented by Simons, Li, and Eggert (1977). However, the routing of water with the conditions of continuous infiltration is developed and incorporated. Due to the assumed "open book" geometry, both overland and channel routing are required. Excess rainfall, the amount of rainfall not intercepted or infiltrated, serves as the input to the overland flow routing scheme. Results of the overland flow routing are then used as the lateral inflow into either a subwatershed or a channel unit.

The partial differential equations for overland flow are solved by the method of characteristics. The characteristic paths along which the solution is valid can be calculated in either the upstream or downstream direction. This allows a user to find the discharge at the downstream boundary for any given time.

A numerical procedure for water routing developed by Li, Simons and Stevens (1975) is used for the channel units. Routing is accomplished by a second-order nonlinear scheme developed to numerically solve the kinematic wave equation. A numerical routing procedure rather than an analytical procedure is used for the channel units

because analytic solutions are restricted by the formation of kinematic shock. Kinematic shock results when characteristic paths intersect. Physically this may be described as a faster moving parcel of water overtaking a slower moving parcel of water as they both travel downstream. Analytic solutions for problems that have kinematic shock display discontinuities in the hydrographs. Due to this restriction, a simple numerical routing procedure is necessary for the channel units.

Stability of a numerical procedure refers to whether the computational errors, due to the finite difference approximation of the partial differential equations, accumulate to an unbounded error. If the errors do not grow unbounded, the procedure is stable. The numerical scheme that is used has proved to be unconditionally stable and can be used with a wide range of time to space increment ratios without loss of significant accuracy. However, the physical significance of the time and space intervals should be considered when selecting their values.

An infiltration routine is combined with the numerical channel routing procedure to account for channel seepage losses. The channel infiltration procedure is similar to the overland infiltration procedure because both are based on the Green-Ampt infiltration equation (1911). The major difference between the two routines is that the depth of the water in the channel situation cannot be neglected as in the overland situation.

This description has listed the components of a MULTWAT model. The same description applies to the simple ANAWAT model up to the numerical channel routing scheme. Since the singel open book representation does not require an upstream inflow to any channel segment, a numerical channel routing is not required.

7.4 EXCESS RAINFALL ESTIMATION

A discussion of excess rainfall determination involves the processes of rainfall interception and infiltration. The formulation of these processes is the same for all of the models discussed in this chapter, so their discussion is combined in this section.

Rainfall Interception

The amount of interception loss depends on the percentage of the ground that is covered by canopy and ground cover, their respective water holding capacities, as well as their initial moisture levels. The total intercepted volume can be written as:

$$V_i = C_c V_c + C_g V_g \qquad (7\text{-}3)$$

in which V_i is the total intercepted volume in depth, C_c is the canopy cover density ($0 \leq C_c \leq 1$), V_c is the potential volume of canopy cover interception in depth, C_g is the ground cover density ($0 \leq C_g \leq 1$), and V_g is the potential volume of ground cover interception in depth. The value of V_i is dependent on the type of vegetation, height of vegetation (related to leaf areas), and the initial moisture level. The value of V_g is a function of forest litter, grass and rock mulch, and the initial moisture level.

As the computations proceed through time, the rainfall is all intercepted until the potential volumes for ground and canopy cover are filled. This would constitute a series of net rainfall rates. Although interception losses are continuous over the storm period, it is assumed that the losses occur during the beginning period of the storm. A more detailed simulation of the interception process is given by Simons et al. (1975).

Infiltration of Unsteady Rainfall

In the determination of storm water runoff, an accurate estimation of storm water runoff is of critical importance. Not only the volume available for runoff, but the time history of the infiltration process is important if hydrographs are to be simulated. Because of its importance and its association with the soil surface, infiltration is one of the model processes most sensitive to man's activities in the watershed. Therefore, it is important that the process be modeled in such a way that parameters are sensitive to watershed development and utilization activities. However, it is equally important that the infiltration routine be time-efficient so that a digital computer simulation will remain economical.

In the past few years several authors--Bouwer, 1969; Li, Stevens and Simons, 1976; Bouwer, 1976; and Morel-Seytoux and Khanji, 1974--have discussed the applicability of the Green-Ampt (1911) equation to

a variety of infiltration problems. In particular, Mein and Larson (1971) applied the equation to natural rainfall. Green and Ampt's formulation is particularly attractive since it is the simplest infiltration equation based on Darcy's Law. However, the method is somewhat more difficult to use than such infiltration equations as Horton's equation, since the Green-Ampt equation is implicit with respect to time. This difficulty is particularly visible in watershed simulation when merging an infiltration routine with a finite difference surface water routing scheme.

Li, Stevens and Simons (1976) proposed a time-explicit solution to the Green-Ampt equation for the case of constant intensity rainfall. Since that time Eggert (1976) has presented a modification of that solution for unsteady rainfall, and Eggert, Li and Simons (1979) have indicated a further extension of the method to layered soils. The models discussed in this section share the time-explicit formulation of the Green-Ampt equation for unsteady rainfall. A version of MULTWAT using layered infiltration has also been developed.

The Green-Ampt infiltration model is a simple, physically based, two-parameter infiltration equation first proposed in 1911. It may be derived by direct application of Darcy's Law under the following assumptions:

1. A distinct piston wetting front exists.
2. The hysteresis effects in the soil properties are negligible.
3. The pressure effect of ponded water is negligible.

A Green-Ampt type equation may be written as

$$\frac{F}{\delta} - \ell n(1 + \frac{F}{\delta}) = \frac{Kt}{\delta} \qquad (7\text{-}4)$$

in which F is the infiltrated volume, K is the hydraulic conductivity of the soil in the wetted zone, t is the time, and δ is the potential head parameter and defined as

$$\delta = (\theta_w - \theta_i)\psi_{ave} \qquad (7\text{-}5)$$

in which θ_w is the moisture content of the soil after wetting, θ_i is the antecedent moisture of content, and ψ_{ave} is the average suction head across the wetting front.

If at any time t the infiltrated volume is $F(t)$, then at some later time $t + \Delta t$

$$F(t + \Delta t) = F(t) + \Delta F \tag{7-6}$$

in which ΔF is the change in infiltrated volume which occurred during the time increment, Δt. An expression for ΔF is obtained from Equation 7-6

$$\Delta F = F(t + \Delta t) - F(t) \tag{7-7}$$

Li et al. (1976a) developed the following method of solving for the infiltration rate. Their derivation yields

$$\frac{\Delta F}{\delta} - \ell n \left[\frac{\delta + F(t) + \Delta F}{\delta + F(t)}\right] = \frac{K}{\delta} \Delta t \tag{7-8}$$

Equation 7-8 is implicit with respect to ΔF. However, the equation is simplified by expanding the logarithmic term in a power series (see Li et al., 1976b).

$$\ell n\left(1 + \frac{\Delta F}{\delta + F}\right) = \ell n\ 1 + \frac{\frac{2\Delta F}{\delta + F}}{2 + \frac{\Delta F}{\delta + F}} + \ldots \tag{7-9}$$

Truncating Equation 7-9 after the second term and substituting into Equation 7-8, one obtains

$$\frac{\Delta F}{\delta} - 2\left[\frac{\frac{\Delta F}{\delta + F}}{2 + \frac{\Delta F}{\delta + F}}\right] = \frac{K}{\delta} \Delta t \tag{7-10}$$

Equation 7-10 is simplified into a quadratic whose solution is (see Li et al., 1976a):

$$\Delta F = -\frac{(2F - K\Delta t)}{2} + \frac{[(2F - K\Delta t)^2 + 8K\Delta t(\delta + F)]^{\frac{1}{2}}}{2} \tag{7-11}$$

Only the positive root of Equation 7-11 has any physical significance. The average infiltration rate, $\bar{f}$, is obtained by dividing ΔF by Δt, or

$$\bar{f} = \frac{\Delta F}{\Delta t} \tag{7-12}$$

After accounting for the interception and infiltration losses, the rainfall excess, i_e, can be determined. A rainfall event is commonly reported as a hyetograph, i.e., a series of net rainfall intensities, I, each lasting for a time increment, Δt. Thus, if the net rainfall intensity is greater than the infiltration rate, the infiltration rate is subtracted from the net rainfall intensity to give the excess rainfall. If the net rainfall intensity is less than the corresponding infiltration rate, the infiltration rate equals the net rainfall intensity, and there is no excess.

Bouwer (1969) and Brakensiek (1970) suggested an application of Green and Ampt equation to layered soils having equal layer thicknesses. Their basic concepts are easily implemented to modify Equation 7-11 to a form allowing calculation of the change of infiltrated volume within a given soil layer. The only additional complication is the increased amount of bookkeeping required to know the location of the wetting front.

Briefly, after Bouwer (1969), the total head loss Δh_T through the soil layers to a wetting front that is assumed to be contained in the $k^{\underline{th}}$ layer may be written as

$$\Delta h_T = \sum_{i=1}^{k-1} \Delta z_i + \ell + \psi_{ave_k} \tag{7-13}$$

where Δz_i is the thickness of the $i^{\underline{th}}$ soil layer above the wetting front, ℓ is the depth of penetration of the wetting front into the $k^{\underline{th}}$ layer below the base of the $k\text{-}1^{\underline{th}}$ layer, and ψ_{ave_k} is the average capillary suction head of the $k^{\underline{th}}$ layer. Additionally, the total head loss may be written in terms of Darcy's Law

$$\Delta h_T = q \left(\sum_{i=1}^{k-1} \frac{\Delta z_i}{K_i} + \frac{\ell}{K_k} \right) \tag{7-14}$$

where q is the Darcian flux which is equal by continuity for all layers behind the wetting front and K_i is the hydraulic conductivity of the $i^{\underline{th}}$ layer. Equating the right hand side of Equations 7-13 and 7-14, solving for q and using analysis similar to the homogeneous soil case, the change in infiltrated volume within the $k^{\underline{th}}$ layer may be expressed as

$$I = \frac{-[2F + K_k(2d_k - \Delta t)] + \{[2I + K_k(2d_k - \Delta t)]^2 + 8K_k\Delta t(F + c_k)\}^{\frac{1}{2}}}{2} \tag{7-15}$$

where

$$c_k = \phi_k \Delta S_k \sum_{i=1}^{k-1} \Delta z_i + \psi_{ave_k} - \sum_{i=1}^{k-1} \phi_i \Delta S_i \Delta z_i$$

$$S_k = S_{w_k} - S_{i_k} \tag{7-16}$$

and

$$d_k = \phi_k \Delta S_k \sum_{i=1}^{k-1} \frac{\Delta z_i}{K_i} - \frac{1}{K_k} \sum_{i=1}^{k-1} \phi_i \Delta S_i \Delta z_i$$

Above S_{w_k} and S_{i_k} are the degree of saturation of the wetted zone behind the wetting front and the initial degree of saturation for the $k^{\underline{th}}$ layer, respectively.

Equation 7-11 for homogeneous soils and Equations 7-15 and 7-16 for layered soils are used to calculate the potential average infiltration rate $\bar{f}$ occurring during the time interval between t and $t + \Delta t$. This calculation is carried out time increment by time increment throughout the event and compared to the corresponding rainfall intensity. If the rainfall intensity is greater than the average inviltration rate, the change in infiltration volume during Δt is ΔF. If the rainfall intensity is less than the average potential rate, the change in infiltration volume during Δt is $r\Delta t$, where r is the current rainfall intensity. Since ΔF for both layered and homogeneous soils is a function of the infiltrated volume at time t, the value of $\bar{f}$ during time increment t to $t + \Delta t$ reflects periods of rainfall control as well as potential infiltration rate control. Therefore, although these methods appear somewhat more involved than Horten's, and similar time-explicit approaches to infiltration calculations, the additional complexity can provide an inherently more accurate description of the infiltration process under unsteady rainfall. Further, these equations and the bookkeeping logic necessary for their use are easily programmed for incorporation into watershed simulations or into the more sophisticated programmable calculations for simple infiltration calculations using Equation 7-11, as will be demonstrated in Chapter 15.

7.5 WATER ROUTING

The largest difference between the high resolution watershed model and the simplified approaches is visible in the water routing methods. The basic theory for both kinds of model is the same; however, the solution techniques used for implementation of the theory are different. The simplified models use an analytical solution to the kinematic wave problem for both overland flow and the unbranched finger-tip channel between the planes of the open book or ANAWAT

watersheds. In the high resolution and the connecting channels of MULTWAT, a numerical water routing scheme is used. Both schemes are based on the theory presented below.

Governing Equations

Water runoff can be described by the equation of continuity, the equation of motion, and equations describing resistance to flow.

Continuity Equation. The equation of continuity for water is

$$\frac{\partial Q}{\partial x} + \frac{\partial A}{\partial t} = q_\ell \tag{7-17}$$

in which Q is the discharge, x is the downslope distance, A is the cross-sectional area of flow, t is the time, and q_ℓ is the lateral inflow or outflow rate per unit length of channel. For overland flow, q_ℓ is the rainfall excess, A is the depth of flow, Q is the discharge per unit width of channel.

Momentum Equation. The momentum equation for a prismatic channel can be expressed as (Henderson, 1966):

$$S_f = S_o - \frac{\partial y}{\partial x} - \frac{1}{gA}\frac{\partial Q}{\partial t} - \frac{1}{gA}\frac{\partial}{\partial x}\left(\frac{Q^2}{A}\right) \tag{7-18}$$

in which S_f is the friction slope, S_o is the channel bed slope, y is the depth of flow, and g is the gravitational acceleration.

The assumption of the kinematic wave approximation is that the friction slope is equal to the channel bed slope. That is, the gradients due to local and convective accelerations are assumed to be negligible and the water surface slope is assumed to be equal to the bed slope. Then the simplified momentum equation is

$$S_o \simeq S_f = f\frac{Q^2}{8gRA^2} \tag{7-19}$$

in which f is the Darcy-Weisbach friction factor and R is the hydraulic radius. By definition,

$$R = \frac{A}{P} \tag{7-20}$$

in which P is the wetted perimeter. Usually the wetted perimeter can be expressed as a power function of the flow area, i.e.,

$$P = a_1 A^{b_1} \tag{7-21}$$

where a_1 and b_1 are constants.

If Manning's equation is used, the simplified momentum equation is

$$S_o \approx S_f = \frac{n^2 Q^2}{2.21\ R^{4/3} A^2} \qquad (7\text{-}22)$$

in which n is Manning's roughness coefficient.

Resistance Equations. In a natural watershed, the form resistance due to the ground cover is a very important component of the resistance to flow. The dependence of flow resistance on the ground cover becomes further complicated depending on whether the ground cover is submerged or not. Rarely is the ground cover submerged in overland flow units. Therefore, in overland flow units, one only needs to consider the resistance caused by flow through the ground cover. In channel flow units, the probability of submerging the ground cover is relatively large. The resistance is then considered as the resistance caused by flow through ground cover and flow over ground cover simultaneously.

Resistance to flow for the overland flow response units is generally expressed as a function of surfacing material, vegetation type and density of vegetation. Palmer (1946), Ree (1949), and Ree and Palmer (1949) conducted a series of experiments in channels with various types of grasses. More recently, Kouwen and Unny (1969), Phelps (1970), Wenzel (1970), Li and Shen (1973), and Chen (1976) carried the experimental studies further. Results indicate a functional relationship between the overall Darcy-Weisbach friction factor and flow characteristics as

$$f = \frac{K_t}{N_r} \qquad (7\text{-}23)$$

in which f is the overall Darcy-Weisbach friction coefficient, N_r is the flow Reynolds number, K_t is a constant describing the overall resistance. According to Chen (1976), this type of relationship can be used for a Reynolds number up to 10^5. This would practically cover all of the possible overland flow conditions on the natural surfaces.

The flow Reynolds number is defined

$$N_r = \frac{QR}{\nu A} \qquad (7\text{-}24)$$

in which ν is the kinematic viscosity of water.

Assuming that the factors describing resistance to flow are independent, the overall resistance can be expressed as

$$f = f_g + f_d \tag{7-25}$$

in which f_g is the Darcy-Weisbach friction factor for grain resistance only which is a function of grain size, flow Reynolds number and rainfall intensity, and f_d is the Darcy-Weisbach friction factor due to form drag resistance which is a function of ground cover density, size of ground cover, drag coefficient, depth of flow and flow Reynolds number. In overland flow cases, the value of f_g can be further assumed as

$$f_g = \frac{K_g}{N_r} \tag{7-26}$$

in which K_g is the parameter describing Darch-Weisbach friction factor for grain resistance only. Laboratory experiments show that K_g is between 30 and 60 (Chow, 1959, and Woolhiser, 1975). It is assumed that K_g is equal to 50 for practical purposes.

The review of literature suggests that the overall flow resistance of overland flow can be assumed as

$$K_t = K_\ell + (K_h - K_\ell)\, C_g^2 \tag{7-27}$$

in which K_ℓ is the parameter describing the minimum resistance ($C_g = 0.0$) and K_h is the parameter describing the maximum resistance ($C_g = 1.0$).

In the channel flow, the Darcy-Weisbach friction factor is often considered as a constant. Sometimes, the Chezy function equation is used in evaluating the overall resistance for overland flow and flow in rivers. By definition,

$$C = \sqrt{\frac{8g}{f}} \tag{7-28}$$

in which C is the Chezy friction factor. Equation 7-28 shows that a constant value of f will give a constant value of C.

Manning's equation is frequently used by hydraulic engineers to describe flow in open channels. The Manning roughness coefficient is usually determined by measurement and can be expressed as a power function of flow discharge, i.e.,

$$n = a_2\, Q^{b_2} \tag{7-29}$$

in which a_2 and b_2 are constant.

Discharge and Flow Area Relation. In general, the cross-sectional area of the flow can be expressed as a power function of discharge

$$A = \alpha Q^{\beta} \tag{7-30}$$

in which α and β are coefficients whose values depend on the shape of the channel, the friction slope, and the roughness of the wetted perimeter.

If the Darcy-Weisbach friction factor is used, the values of α and β can be determined by substituting Equations 7-19, 7-20, 7-21, 7-23 and 7-24 into Equation 7-30. The solutions are

$$\alpha = \left(\frac{K_t \nu a_1^2}{8gS_f} \right)^{1/(3-2b_1)} \tag{7-31}$$

and

$$\beta = \frac{1}{3-2b_1} \tag{7-32}$$

For overland flows or flows in very wide channels, the wetted perimeter is constant so that $b_1 = 0$ and $\beta = 1/3$.

If Manning's equation is applied, the corresponding α and β values are determined from Equations 7-20, 7-21, 7-22, 7-29 and 7-30. The results are:

$$\alpha = \left(\frac{a_1^{4/3} a_2^2}{2.21 S_f} \right)^{3/(10-4b_1)} \tag{7-33}$$

and

$$\beta = \frac{3-3b_2}{5-2b_1} \tag{7-34}$$

If the Chezy friction equation is used, the corresponding α and β values are determined by using Equations 7-19, 7-20, 7-21, 7-28 and 7-30. The values are:

$$\alpha = \left(\frac{a_1}{C^2 S_f} \right)^{1/(3-b_1)} \tag{7-35}$$

$$\beta = \frac{2}{3-b_1} \tag{7-36}$$

For the kinematic wave approximation, the friction slope S_f in Equations 7-31, 7-33 and 7-35 is equal to the bed slope S_o.

The problem of water routing is now a matter of solving Equations 7-17 and 7-30. These two equations can be solved either by an analytical method or a numerical method. The solution techniques follow.

Analytical Solutions

The analytical solutions of Equations 7-17 and 7-30 are available for some special cases (Eagleson, 1970; Kibler and Woolhiser, 1970; Harley et al., 1970; and Li et al., 1975b). For analytical solutions, it is common to express Equation 7-30 in the following form:

$$Q = \alpha' A^{\beta'} \tag{7-37}$$

where

$$\alpha' = \left(\frac{1}{\alpha}\right)^{1/\beta} \tag{7-38}$$

and

$$\beta' = \frac{1}{\beta} \tag{7-39}$$

From Equations 7-17 and 7-37, one obtains

$$\alpha'\beta' A^{\beta'-1} \frac{\partial A}{\partial x} + \frac{\partial A}{\partial x} = q_\ell \tag{7-40}$$

This partial differential equation may be solved by the method of characteristics. The total differential of $A(x,t)$ is given by

$$dA = \frac{\partial A}{\partial t} dt + \frac{\partial A}{\partial x} dx \tag{7-41}$$

Equations 7-40 and 7-41 form a system of two equations in two unknowns, and may be written in matrix form as

$$\begin{bmatrix} \alpha'\beta' A^{\beta'-1} & 1 \\ dx & dt \end{bmatrix} \begin{bmatrix} \frac{\partial A}{\partial x} \\ \frac{\partial A}{\partial t} \end{bmatrix} = \begin{bmatrix} q_\ell \\ dA \end{bmatrix} \tag{7-42}$$

The characteristic paths along which the solution is valid are found by determining the loci of indeterminancy of the solution. These loci are obtained by equating the determinant of the coefficient matrix with zero. The resulting characteristic equation is

$$\frac{dx}{dt} = \alpha'\beta' A^{\beta'-1} \tag{7-43}$$

Integrating Equation 7-43 with respect to time yields

$$x - x_o = \alpha'\beta' \int_{t_o}^{t} A^{\beta'-1}\, dt' \tag{7-44}$$

in which x_o is the initial distance and t_o is the initial time.

The invariants of this solution are found by substituting the right-hand side of Equation 7-42 for each column of the coefficient matrix and equating the determinant of the resulting matrix equal to zero. The invariants are

$$\frac{dA}{dt} = \frac{dQ}{dx} = q_\ell \tag{7-45}$$

or by integrating Equation 7-45

$$A - A_o = \int_{t_o}^{t} q_\ell\, dt' \tag{7-46}$$

or

$$Q - Q_o = \int_{x_o}^{x} q_\ell\, dx' \tag{7-47}$$

in which A_o and Q_o are initial values of area and discharge, respectively. By substituting Equation 7-46 into Equation 7-44, the following expression for the characteristic is obtained.

$$x = x_o + \alpha'\beta' \int_{t_o}^{t} \left[A_o + \int_{t_o}^{\eta} q_\ell(\sigma)\, d\sigma\right]^{\beta'-1} d\eta \tag{7-48}$$

Theoretically, if the functional form of $q_\ell(\sigma)$ is known, then Equation 7-48 will give the characteristics in the x-t plane. Harley et al. (1970) noted that when $q_\ell(\sigma)$ is a histogram, then with reference, Equation 7-46 and 7-48 may be evaluated in pieces.

The procedure as outlined by Harley et al. (1970) is as follows (see Figure 7.8). From any point (x_i, t_i) on characteristic C, the value of x_{i+1} on C corresponding to time t_{i+1} may be calculated by Equation 7-48.

$$x_{i+1} = x_i + \alpha'\beta' \int_{t_i}^{t_{i+1}} \left[A_i + q_{\ell i+1}(\eta - t_i)\right]^{\beta'-1} d\eta \tag{7-49}$$

or

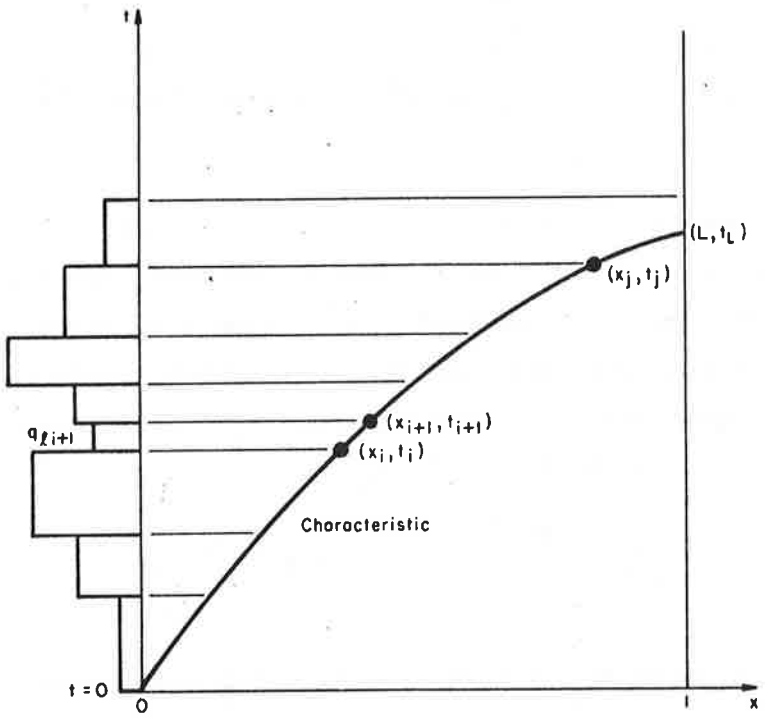

Figure 7.8 Schematic diagram of characteristic path.

$$x_{i+1} = x_i + \frac{\alpha'}{q_{\ell i+1}} \{[A_i + q_{\ell i+1}(t_{i+1} - t_i)]^{\beta'} - A_i^{\beta'}\} \quad (7\text{-}50)$$

for $q_{\ell i+1} \neq 0$, and

$$x_{i+1} = x_i + \alpha'\beta' A_i^{\beta'-1} (t_{i+1} - t_i) \quad (7\text{-}51)$$

for $q_{\ell i+1} = 0$.

From Equation 7-46 one obtains

$$A_{i+1} = A_i + q_{\ell i+1} (t_{i+1} - t_i) \quad (7\text{-}52)$$

For a given plane of length L, values of x_{i+1} are calculated until $x_{i+1} \geq L$. The time of arrival of the characteristic at the downstream boundary, t_L, is found by solving Equation 7-50 or Equation 7-51 for t_L in terms of t_j and x_j.

$$t_L = t_j + \frac{1}{q_{\ell i+1}} \left\{ \left[\frac{q_{\ell i+1}(L - x_j)}{\alpha'} + A_j^{\beta'} \right]^{1/\beta'} - A_j \right\} \quad (7\text{-}53)$$

for $q_{\ell i+1} \neq 0$, and

$$t_L = \frac{L - x_j}{\alpha' \beta' A_j^{\beta'-1}} + t_j \tag{7-54}$$

Then, the discharge at the end of channel or overland flow reach is

$$Q_L = \alpha' A_L^{\beta'} \tag{7-55}$$

Repeating the above solution, it is not difficult to route the water in terms of time and space. However, the timing of the outflow at the downstream boundary, t_L, cannot be predetermined. Li et al. (1975) suggested tracing the characteristic path backward from the downstream boundary for a desired t_L. Their method is simply to solve Equation 7-48 in terms of t_o. Or

$$\frac{L}{\alpha' \beta'} = \int_{t_o}^{t_L} \left[\int_{t_o}^{\eta} q_\ell(\sigma)\, d\sigma \right]^{\beta'-1} d\eta \tag{7-56}$$

As pointed out earlier, the continuity equation for overland flow has the same form as Equation 7-17. That is,

$$\frac{\partial q}{\partial x} + \frac{\partial y}{\partial t} = e \tag{7-57}$$

where q is the overland flow discharge per unit width, y is the depth of overland flow, and e is the excess rainfall intensity. Also, analogous to Equation 7-37,

$$q = \alpha_1 y^{\beta_1} \tag{7-58}$$

where, using the Darcy Weisbach resistance equation for overland flow,

$$\alpha_1 = \frac{K_t \nu}{8 g S_o} \tag{7-59}$$

and

$$\beta_1 = 3 \tag{7-60}$$

Noting that the lateral inflow to the channel between the planes of the open-book watershed, q_ℓ, is simply the sum of the overland flow discharge hydrographs from the two planes, the basis for an ANAWAT watershed model has been established. In fact, the routing of storm water in such a watershed may be accomplished using only the development to this point. In Chapter 15, such a watershed program for small calculators is presented. The overland and channel flow hydrographs

may be determined with great resolution using Equations 7-46, 7-55 and 7-56. However, as examination of Equations 7-53 and 7-54 shows, t_L, the time at which the overland flow hydrograph points are known, is a function of rainfall, geometric and hydraulic parameters. Therefore, if the two planes are dissimilar, the times, t_L, for the two overland flow hydrographs will not correspond, and in order to form the lateral inflow hydrograph to the channel, both overland flow hydrographs must be interpolated onto a common time base. This calculation presents no difficulties, but it is somewhat time-consuming and introduces some error into the lateral inflow hydrograph. When using a programmable calculator method such as will be presented in Chapter 15, this step must be performed; however, a computer provides sufficient storage for a more elegant method.

If $q_\ell(\sigma)$ in Equation 7-56 is in the form of a histogram, Equation 7-56 becomes a polynomial of degree β that may be solved for t_o when t_L is selected. This allows the time points of the overland flow discharge hydrographs to be selected providing for simple addition of the hydrograph points to form the lateral inflow to the channel. Using the notation of Equations 7-57 and 7-58, the method is described below for overland flow.

Since $e(t)$ has the form of a histogram, excess rainfall during the j^{th} time increment $t_j - t_{j-1}$ is constant. In addition, the form of Equation 7-56 may be simplified by noticing the inner integration, i.e., the integration on σ is simply the difference between the cumulative excess at time t_L and the cumulative excess at time t_o. That is,

$$\int_{t_o}^{t_L} e(\sigma)\, d\sigma = E(t_L) - E(t_o) \qquad (7\text{-}61)$$

where E represents the cumulative excess.

With this notation in mind and taking advantage of the histogram form of $e(t)$, Equation 7-61 may be rewritten as

$$\frac{L}{\alpha_1\beta_1} = \int_{t_K}^{t_L} [e_{k+1}\ t' - e_{k+1}\ t_k + E_k - e_{j+1}\ t_o + e_{j+1}\ t_j - Ej]^{\beta_1-1}\ dt'$$

$$+ \sum_{i=j+2}^{k} \int_{t_{i-1}}^{t_i} [e_i\ t' - e_i\ t_{i-1} + E_{i-1} - e_{j+1}\ t_o + e_{j+1}\ t_j - E_j]^{\beta_1-1}\ dt'$$

$$+ \int_{t_o}^{t_{j+1}} [e_{j+1}\ t' - e_{j+1}\ t_j + E_j - e_{j+1}\ t_o + e_{j+1}\ t_j - E_j]^{\beta_1-1}\ dt' \qquad (7\text{-}62)$$

Equation 7-62 consists of nothing more than a series of simple integrations of the form

$$\int (at' + b)^{\beta_1-1}\ dt' = \frac{1}{\alpha_1\beta_1}\ (at' + b)^{\beta_1} \qquad (7\text{-}63)$$

Integrating as in Equation 7-63 and introducing A_i as defined below

$$A_i = -e_i\ t_{i-1} + E_{i-1} + e_{j+1}\ t_j - E_j \qquad (7\text{-}64)$$

Equation 7-62 may be written as:

$$\frac{L}{\alpha_1\beta_1} = \frac{1}{e_{k+1}\beta_1} [e_{k+1}\ t' + A_{k+1} - e_{j+1}\ t_o]^{\beta_1} \Bigg|_{t_k}^{t_L}$$

$$+ \sum_{i=j+2}^{k} \frac{1}{e_1\beta_1} [e_i\ t' + A_i - e_{j+1}\ t_o]^{\beta_1} \Bigg|_{t_{i-1}}^{t_i}$$

$$+ \frac{1}{e_{j+1}\beta_1} [e_{j+1}\ t' - e_{j+1}\ t_o]^{\beta_1} \Bigg|_{t_o}^{t_{j+1}} \qquad (7\text{-}65)$$

Since Equation 7-65 may be explicitly differentiated with respect to t_o, a Newton-Rapson technique provides a simple solution. The subroutine developed uses a second-order routine to speed convergence. The routine proceeds by rewriting Equation 7-65 as

$$f(t_o) = -\frac{L}{\alpha_1\beta_1} + \frac{1}{e_{k+1}\beta_1} [e_{k+1}\ t' + A_{k+1} - e_{j+1}\ t_o]^{\beta_1} \Bigg|_{t_k}^{t_L}$$

$$+ \sum_{i=j+2}^{k} \frac{1}{e_1\beta_1} [e_i t' + A_i - e_{j+1}\ t_o]^{\beta_1} \Bigg|_{t_{i-1}}^{t_i}$$

$$+ \frac{1}{e_{j+1}\beta_1} [e_{j+1}\ t' - e_{j+1}\ t_o]^{\beta_1} \Bigg|_{t_o}^{t_{j+1}} \qquad (7\text{-}66)$$

The first and second derivatives of $f(t_o)$ with respect to t_o are respectively,

$$f'(t_o) = \frac{e_{j+1}}{e_{k+1}} \left\{ [e_{k+1}\, t_L + A_{k+1} - e_{j+1}\, t_o]^{\beta_1 - 1} - [e_{k+1}\, t_k + A_{k+1} - e_{j+1}\, t_o]^{\beta_1 - 1} \right\} + \sum_{i=j+1}^{k} \frac{e_{j+1}}{e_i} \left\{ [e_i\, t_o + A_i - e_{j+1}\, t_o]^{\beta_1 - 1} - [e_i\, t_{i-1} + A_i - e_{j+1}\, t_o]^{\beta_1 - 1} \right\} - [e_{j+1}\, t_{j+1} - e_{j+1}\, t_o]^{\beta_1 - 1} \tag{7-67}$$

and

$$f''(t_o) = \frac{e_{j+1}^2}{e_{k+1}} (\beta_1 - 1) \left\{ [e_{k+1}\, t_L + A_{k+1} - e_{j+1}\, t_o]^{\beta_1 - 2} - [e_{k+1}\, t_k + A_{k+1} - e_{j+1}\, t_o]^{\beta_1 - 2} \right\} + \sum_{i=j+2}^{k} \frac{e_{j+1}^2}{e_i} (\beta_1 - 2) \left\{ [e_i\, t_i + A_i - e_{j+1}\, t_o]^{\beta_1 - 2} - [e_i t_{i-1} + A_i - e_{j+1}\, t_o]^{\beta_1 - 2} \right\} + (\beta_1 - 1)\, (e_{j+1}) [e_{j+1}\, t_{j+1} - e_{j+1}\, t_o]^{\beta_1 - 2} \tag{7-68}$$

The second-order Newton's method is based on truncating a Taylor's series expansion of $f(t_o)$ about a trial value of t_o, defined as t_o^*, after the third term. Thus, $f(t_o)$ is written as

$$f(t_o) \simeq f(t_o^*) - (t_o - t_o^*)\, f'(t_o^*) + \frac{(t_o - t_o^*)^2}{2} f''(t_o^*) \tag{7-69}$$

Roots of $f(t_o)$ are then obtained by setting $f(t_o) = 0$ in Equation 7-69 and solving the resulting quadratic for t_o. This value of t_o becomes the new estimate of the root and iterations continue until

$$\left| \frac{f(t_o^*)}{\frac{L}{\alpha_1 \beta_1}} \right| < \eta \tag{7-70}$$

where η is some arbitrarily small convergence increment.

In this manner, t_o's can be calculated corresponding to selected t_L's. The values of t_o contain some error due to the Newton's method approximation; however this error, unlike the error due to interpolation, may be precisely controlled by the specification of η.

The number of terms in the summation appearing in Equations 7-66, 7-67 and 7-68 are determined by using the histogram of the lateral inflow to subdivide the solution domain. This subdivision is accomplished by calculating the characteristics arising at the beginning of each new histogram element (Figure 7.9). Since the applications for which these routines are intended never exhibit kinematic shock, no

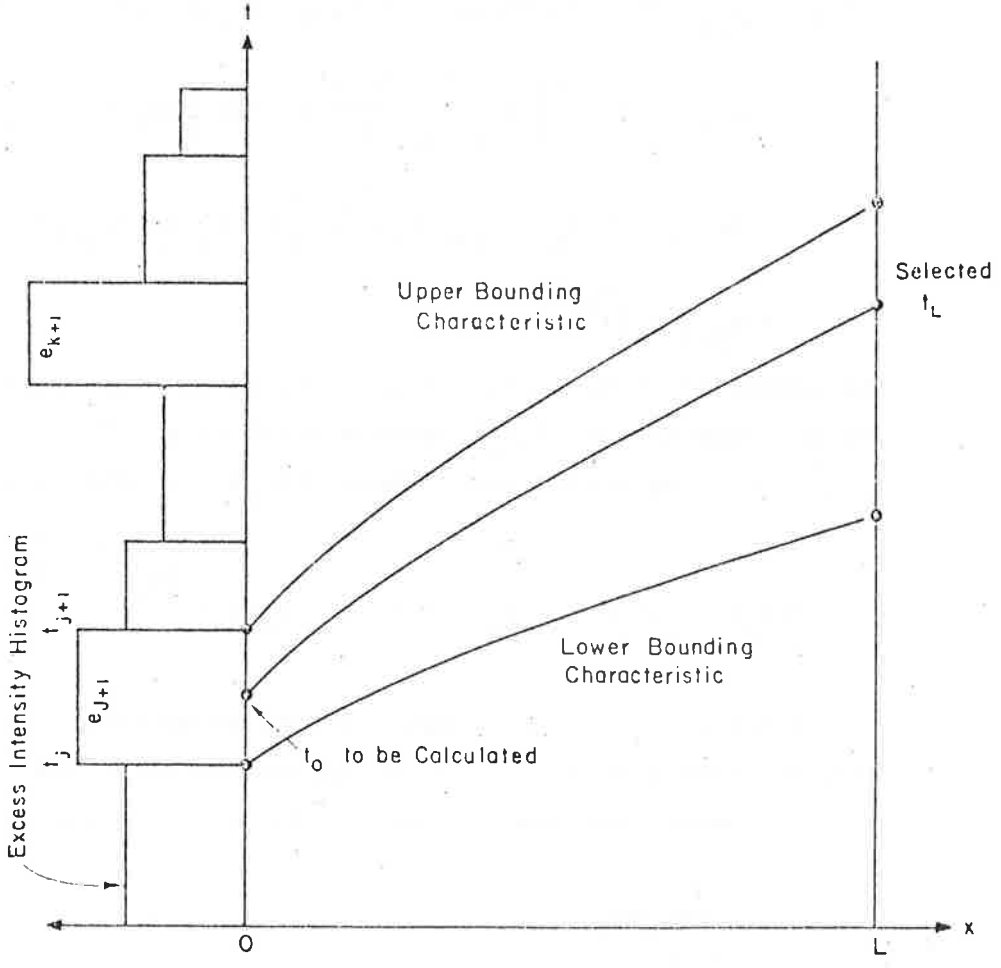

Figure 7.9 Method of characteristics solution domain illustrating upstream calculation of characteristics between bounding characteristics previously calculated in downstream direction.

characteristics in the solution domain intersect. Therefore, the characteristics calculated serve as a minimum set of bounds for those to be calculated by Equation 7-70. The number of terms in Equations 7-66 through 7-68 are immediately known by simply counting the number of histogram units crossed by the regions that are bounded by the characteristics having t_L's on either side of the t_L selected (Figure 7.9). Thus, the values of k and j for a given t_L in Equations 7-66 through 7-68 are known.

This technique provides a rapid means of finding t_o's corresponding to a given t_L. Three iterations of Newton's method have seemed sufficient for $\eta = 0.0001$. Knowing t_o and t_L, the depth may be evaluated at the downstream boundary at time t_L by using Equation 7-46. This depth is used to determine the discharge at the downstream boundary at time t_L by using Equation 7-37 with q and y substituted for Q_ℓ and A, respectively.

For the simplified formulation, in the absence of channel cross-sectional data it may be assumed that the planes meet to form a triangular channel as shown in Figure 7.10. The wetted perimeter of that channel P (Figure 7.10) may be expressed as

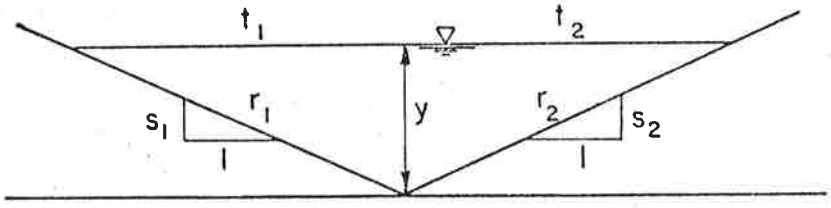

Figure 7.10 Definition sketch of triangular channel.

$$P = \frac{A}{R} = r_1 + r_2 = (y^2 + t_1^2)^{\frac{1}{2}} + (y^2 + t_2^2)^{\frac{1}{2}} \qquad (7\text{-}71)$$

where the subscripts refer to plane 1 and plane 2. Since t_1 and t_2 may be expressed as

$$t_1 = \frac{y}{S_1} \quad ; \quad t_2 = \frac{y}{S_2} \qquad (7\text{-}72)$$

Equation 7-71 may be written

$$P = y \left[\left(1 + \frac{1}{S_1^2} \right)^{\frac{1}{2}} + \left(1 + \frac{1}{S_2^2} \right)^{\frac{1}{2}} \right] \tag{7-73}$$

Referring to Figure 7.10, the cross-section area of the channel may be expressed as

$$A = \frac{1}{2} y \, (t_1 + t_2) \tag{7-74}$$

or

$$A = \frac{1}{2} y^2 \, (\frac{1}{S_1} + \frac{1}{S_2}) \tag{7-75}$$

Solving Equation 7-74 for y and substituting the result into Equation 7-73 yields the following expression for P in terms of A:

$$P = a_1 A^{\frac{1}{2}} \tag{7-76}$$

with

$$a_1 = \left[\frac{2}{\left(\frac{1}{S_1} + \frac{1}{S_2} \right)} \right]^{\frac{1}{2}} \left[\left(1 + \frac{1}{S_1^2} \right)^{\frac{1}{2}} + \left(1 + \frac{1}{S_2^2} \right)^{\frac{1}{2}} \right] \tag{7-77}$$

and

$$b_1 = 1/2 \tag{7-78}$$

The a_1 and b_1 once calculated may then be used to obtain α' and β' by substitution into either Equation 7-55 or 7-56. If channel cross-sectional data is avilable, a_1 and b_1 can be determined.

The above analytical solution is certainly desirable since there is no problem encountered in computational stability and convergence. Unfortunately, this analytical solution is often restricted for practical applications because of the kinematic "shock wave." The "shock" is represented by the intersections of characteristics in the x-t plane. This produces an abrupt increase in flow depth (Kibler and Woolhiser, 1970). An example of the kinematic wave shock is given in Figure 7.11. Li et al. (1976c) gives an in-depth discussion of this limitation. However, for a small watershed with simple geometry having two planes and one channel, the above analytical procedure can be used. Simons et al. (1977a) reported a simple watershed model using small programmable calculations based on the two-planes and one-channel representation of watersheds.

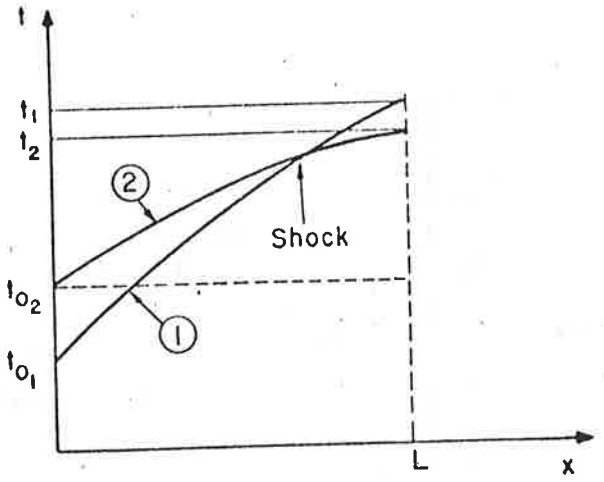

Figure 7.11 Schematic diagram of kinematic-wave shock formation.

Numerical Solution

Li et al. (1977b) and Simons (1977) developed a nonlinear scheme with an iterative procedure to solve a four-point implicit formulation of Equations 7-17 and 7-30. A linear scheme is used to obtain the initial estimate of the unknown discharge for the nonlinear scheme. The linear scheme may be used as is, with no iterations to solve for the unknown discharge, providing accuracy is satisfactory.

Nonlinear Scheme. The finite difference form of Equation 7-17 using quantities at all four points (see Figure 7.12) of the box scheme can be written as

$$\left[\frac{Q_{j+1}^{n+1}-Q_j^{n+1}}{\Delta x}(1-a)+\frac{Q_{j+1}^{n}-Q_j^{n}}{\Delta x}(a)\right]+\left[\frac{A_{j+1}^{n+1}-A_{j+1}^{n}}{\Delta t}(1-b)+\frac{A_j^{n+1}-A_j^{n}}{\Delta t}(b)\right]=\frac{(1-b)q_{\ell\,j+1}^{n+1}+bq_{\ell\,j}^{n+1}+(1-b)q_{\ell\,j+1}^{n}+bq_{\ell\,j}^{n}}{2} \qquad (7\text{-}79)$$

in which Q_j^n is the quantity Q at grid point $x = j\Delta x$, $t = n\Delta t$, where Δx is the space increment and Δt is the time increment. Also, a is the time weighting factor and b is the space weighting factor where $0 \leq a \leq 1$ and $0 \leq b \leq 1$.

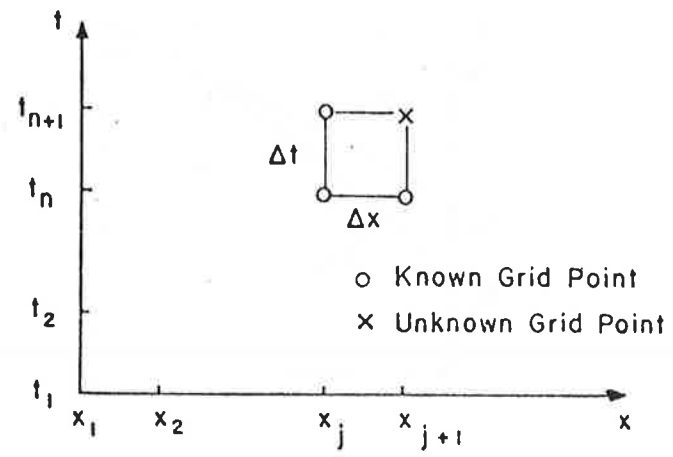

Figure 7.12 Rectangular network in x-t plane.

The unknowns in Equation 7-79 are Q_{j+1}^{n+1} and A_{j+1}^{n+1}, but they are related according to Equation 7-30. With the two equations, the two unknowns may be calculated. The boundary conditions required for this particular formulation are as follows: Q(0,t) and Q(x,0), or in other words, the discharge must be known or assumed along both the space axis [Q(x,0)] and the time axis [Q(0,t)]. No downstream boundary conditions are required. However, if there is a strong downstream control, the kinematic wave approximation no longer applies.

Either Q or A can be selected as the independent variable in the numerical procedure. As customary in backwater computations, the depth of flow (equivalent to A above) is chosen as the independent variable (see Henderson, 1966). However, Q is a better choice for the following reason. From Equation 7-30 one can derive

$$\frac{dA}{A} = \beta \frac{dQ}{d} \tag{7-80}$$

Since the value of β is generally less than 1.0, if the discharge is computed incorrectly, the relative error in the flow area is smaller than the relative error in the discharge. On the other hand, the error in the discharge estimation is magnified if the numerical computations are performed on the flow area. From the physical viewpoint it is more appropriate to consider routing unit volumes of water rather than areas of flow.

From Equation 7-30

$$A_{j+1}^{n+1} = \alpha \ (Q_{j+1}^{n+1})^{\beta} \tag{7-81}$$

$$A_{j}^{n+1} = \alpha \ (Q_{j}^{n+1})^{\beta} \tag{7-82}$$

$$A_{j+1}^{n} = \alpha \ (Q_{j+1}^{n})^{\beta} \tag{7-83}$$

$$A_{j}^{n} = \alpha \ (Q_{j}^{n})^{\beta} \tag{7-84}$$

Equations 7-81 through 7-84 are substituted into Equation 7-79 and rearranged to yield

$$\begin{aligned} &\frac{\Delta t}{\Delta x} Q_{j+1}^{n+1} \ (1-a) + \alpha \ (Q_{j+1}^{n+1})^{\beta} \ (1-b) \\ &= \frac{\Delta t}{\Delta x} \left[Q_{j}^{n+1} \ (1-a) - (Q_{j+1}^{n} - Q_{j}^{n}) \ (a) \right] \\ &+ \alpha \ (Q_{j+1}^{n})^{\beta} \ (1-b) - [\alpha (Q_{j}^{n+1})^{\beta} - \alpha (Q_{j}^{n})^{\beta}] \ (b) \\ &+ \frac{\Delta t}{2} \left[(1-b) q_{\ell}{}_{j+1}^{n+1} + b q_{\ell}{}_{j}^{n+1} + (1-b) q_{\ell}{}_{j+1}^{n} + b q_{\ell}{}_{j}^{n} \right] \end{aligned} \tag{7-85}$$

The right-hand side of Equation 7-85 consists of known quantities and is represented by Ω, i.e.,

$$\begin{aligned} \Omega = &\frac{\Delta t}{\Delta x} \left[Q_{j}^{n+1} (1-a) - (Q_{j+1}^{n} - Q_{j}^{n}) \ (a) \right] + \alpha (Q_{j+1}^{n})^{\beta} (1-b) \\ &- [\alpha (Q_{j}^{n+1})^{\beta} - \alpha (Q_{j}^{n})^{\beta}] (b) \\ &+ \frac{\Delta t}{2} \left[(1-b) q_{\ell}{}_{j+1}^{n+1} + b q_{\ell}{}_{j}^{n+1} + (1-b) q_{\ell}{}_{j+1}^{n} + b q_{\ell}{}_{j}^{n} \right] \end{aligned} \tag{7-86}$$

Let $r = Q_{j+1}^{n+1}$ and $\theta = \frac{\Delta t}{\Delta x}$ so that the left-hand side of Equation 7-85 can be written as

$$f(r) = \theta (1-a) r + \alpha (1-b) r^{\beta} \tag{7-87}$$

The solution to Equation 7-85 is the solution r^* which satisfies the condition

$$f(r^*) = \theta (1-a) r^* + \alpha (1-b) r^{*\beta} = \Omega \tag{7-88}$$

Equation 7-88 is nonlinear in r^*. An approximate solution to this nonlinear equation is obtained by the following iterative technique.

Let r^k be the value of r at the k^{th} iteration. The Taylor series expansion of the function $f(r)$ around r^k is

$$f(r) = f(r^k) + (r-r^k)f'(r^k) + 1/2(r-r^k)^2 f''(r^k) + 1/6(r-r^k)^3 f'''(r^k) + \ldots \quad (7\text{-}89)$$

in which $f'(r^k)$, $f''(r^k)$, and $f'''(r^k)$ are the first, second and third derivatives of the function at r^k.

Dropping terms higher than third order, one obtains

$$f(r) \quad f(r^k) + (r-r^k)f(r^k) + 1/2(r-r^k)^2 f''(f^k) \quad (7\text{-}90)$$

Iteration forces $f(r^{k+1})$ to approach the value of Ω

$$\Omega = f(r^k) + (r^{k+1}-r^k)f'(r^k) + 1/2(r^{k+1}-r^k)^2 f''(r^k) \quad (7\text{-}91)$$

The solution of Equation 7-91 is

$$r^{k+1} = r^k - \frac{f'(r^k)}{f''(r^k)} \pm \left\{ \left[\frac{f'(r^k)}{f''(r^k)} \right]^2 - \frac{2[f(r^k)-\Omega]}{f''(r^k)} \right\}^{1/2} \quad (7\text{-}92$$

in which

$$f(r^k) = \theta(1-a)r^k + \alpha(1-b)(r^k)^\beta \quad (7\text{-}93)$$

$$f'(r^k) = \theta(1-a) + \alpha\beta(1-b)(r^k)^{\beta-1} \quad (7\text{-}94)$$

$$f''(r^k) = \alpha\beta(\beta-1)(1-b)(r^k)^{\beta-2} \quad (7\text{-}95)$$

There are two solutions to Equation 7-92. It is advisable to choose the solution which gives the smaller value of $|f(r^{k+1})-\Omega|$. The iterations are continued until the absolute error $|f(r^{k+1})-\Omega|$ is less than some preassigned tolerance ε

$$|f(r^{k+1})-\Omega| \leq \varepsilon \quad (7\text{-}96)$$

An appropriate value for ε is 0.01Ω.

The initial guess r^o is the key to the speed of convergence to the correct numerical solution. The best way to determine r^o is to use a linear scheme. The linear scheme may be used as the solution instead of going through the iterative, nonlinear scheme when accuracy is of less importance and when computer time is to be conserved.

Linear Scheme. The term $\frac{\partial A}{\partial t}$ in Equation 7-17 can be expressed as

$$\frac{\partial A}{\partial t} = \frac{\partial A}{\partial Q}\frac{\partial Q}{\partial t} \quad (7\text{-}97)$$

and from Equation 7-30

$$\frac{\partial A}{\partial Q} = \alpha\beta Q^{\beta-1} \quad (7\text{-}98)$$

Substitution of Equations 7-97 and 7-98 into 7-17 yields

$$\frac{\partial Q}{\partial x} + \alpha\beta Q^{\beta-1} \frac{\partial Q}{\partial t} = q_\ell \tag{7-99}$$

The finite difference form of Equation 7-99 can be expressed as

$$\frac{Q_{j+1}^{n+1} - Q_j^{n+1}}{\Delta x}(1-a) + \frac{Q_{j+1}^{n} - Q_j^{n}}{\Delta x}(a)$$

$$+ \alpha\beta \left[\frac{Q_j^{n+1} + Q_{j+1}^{n}}{2}\right]^{\beta-1} \left[\frac{Q_{j+1}^{n+1} - Q_{j+1}^{n}}{\Delta t}(1-b) + \frac{Q_j^{n+1} - Q_j^{n}}{\Delta t}(b)\right]$$

$$= \frac{1}{2}\left[(1-b)q_{\ell}{}_{j+1}^{n+1} + bq_{\ell}{}_{j}^{n+1} + (1-b)q_{\ell}{}_{j+1}^{n} + bq_{\ell}{}_{j}^{n}\right] \tag{7-100}$$

Solving for $r^o = Q_{j+1}^{n+1}$,

$$Q_{j+1}^{n+1} = \left[\frac{1-a}{\Delta x} + \alpha\beta\left(\frac{Q_j^{n+1} + Q_{j+1}^{n}}{2}\right)^{\beta-1}\frac{(1-b)}{\Delta t}\right]^{-1}$$

$$\left\{\frac{Q_j^{n+1}}{\Delta x}(1-a) - \frac{Q_{j+1}^{n} - Q_j^{n}}{\Delta x}(a)\right.$$

$$-\alpha\beta\left(\frac{Q_j^{n+1} + Q_{j+1}^{n}}{2}\right)^{\beta-1}\left[-\frac{Q_{j+1}^{n}}{\Delta t}(1-b) + \frac{Q_j^{n+1} - Q_j^{n}}{\Delta t}(b)\right]$$

$$\left. + \frac{1}{2}\left[(1-b)q_{\ell}{}_{j+1}^{n+1} + bq_{\ell}{}_{j}^{n+1} + (1-b)q_{\ell}{}_{j+1}^{n} + bq_{\ell}{}_{j}^{n}\right]\right\} \tag{7-101}$$

Equation 7-101 provides the best estimate for r^o for the non-linear scheme. However, Equation 7-101 is not applicable if both Q_{j+1}^{n} and Q_j^{n+1} are zero. In this case, use $\beta = 1$ in Equation 7-88.

$$r^o = \frac{\Omega}{(1-a)\theta + (1-b)\alpha} \tag{7-102}$$

Li et al. (1977b) proved that the weighting factor a and b must be less than or equal to 1/2 in order to insure stability. When a and b are both zero, this is a fully implicit scheme. This scheme was developed by Li et al. (1975a). When a and b are equal to 1/2, it is a central implicit scheme. The central implicit formulation has been tested using Iwagaki's experiment data (Iwagaki, 1955). Figure 7.13 shows good comparison between experimental and computed results for the three events during different time duration. Li et al. (1975a) successfully applied the fully implicit scheme to a variety of flow conditions.

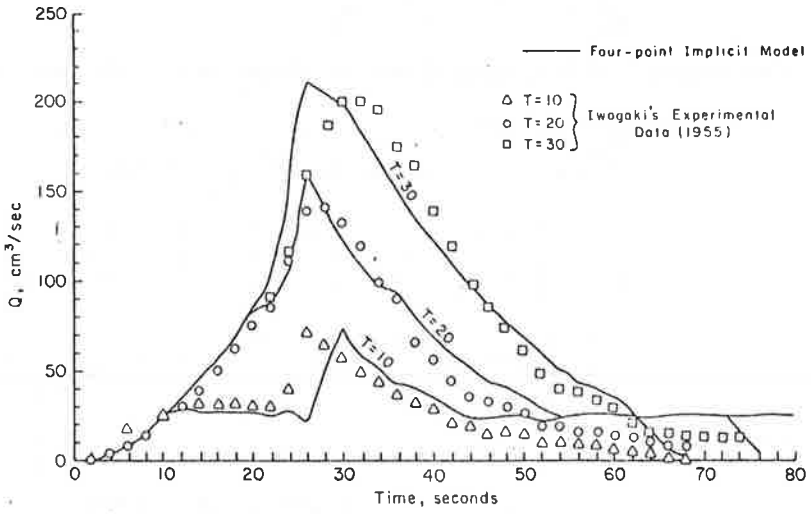

Figure 7.13 Comparison of the discharge hydrographs given by the four-point, central implicit model to Iwagaki's experimental data.

Other available numerical methods for kinematic wave approximation are given by Houghton and Kasahara (1968), Brakensiek (1967), Kibler and Woolhiser (1970), and Singh (1975). However, these methods are much more complicated and sometimes unstable in solution. An extension of the kinematic wave assumption to account for dynamic effects due to the unsteady nonuniform flow encountered in natural channels is presented in Chapter 9.

7.6 EXAMPLE OF APPLICATION

Simplified Models

An example of the application of the single open book model approach is provided by an event on Watershed 17 located in the Coconino National Forest near Flagstaff, Arizona. This watershed has an area of approximately 300 acres. This watershed is an area of heterogeneous topography partially forested in conifers. The modeled event was recorded on September 5, 1970. Figure 7.14 shows measured and calculated runoff. The agreement between measured and calculated runoff appears to be quite good. Some rudimentary calibration of K_w was performed to make the runoff volume agree with the measured volume, but Figure 7.14 represents a substantially uncalibrated result. Resistance for the main channel was guessed to correspond to a Manning's n of about 0.07 as reported by Chow (1959) for a cobble and boulder

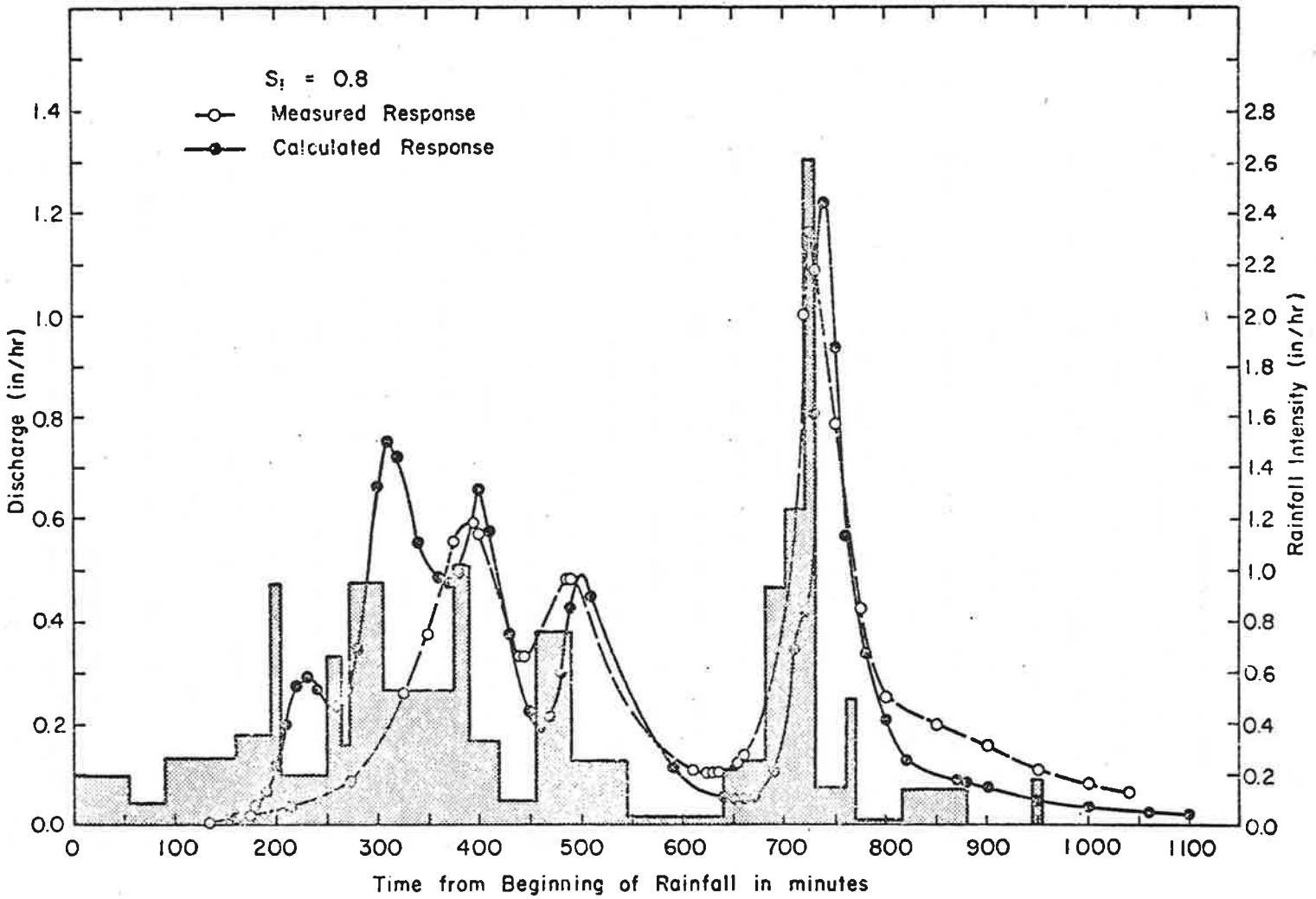

Figure 7.14 Rainfall-runoff response for Watershed 17, Coconino National Forest.

channel. The Manning's n was then converted to the Darcy-Weisbach friction factor.

As an example of application of the MULTWAT method to a large heterogeneous watershed, the model was used to simulate runoff from the Walnut Gulch watershed in southeastern Arizona. The spatial representation of the watershed appears in Figure 7.6 and the watershed map in Figure 7.5. Walnut Gulch is operated by the Agricultural Research Service and surrounds the historic town of Tombstone, Arizona. The study area consists of 57.7 square miles of uncultivated semiarid rangeland. Precipitation is measured with 93 recording rain gages spaced about evenly over the watershed. Runoff from the entire watershed and from nine subwatersheds is calculated from stage records collected at special flow measuring flumes.

The vegetation of Walnut Gulch consists of desert grasses and shrubs, and most of the soils are a gravelly loam. Seventy percent of the annual precipitation of 11.5 inches occurs during high-intensity, short-duration thunderstorms in the late summer months.

The entire Walnut Gulch watershed (57.7 square miles) was modeled for two different storm events. The drainage areas (approximately 5.5 square miles) for several stock ponds were not included in the analysis since spillage was assumed to be negligible. The rainfall distributions for the response units were calculated by using an isohyetal map and individual gage records. United States Geological Survey topographical maps were used to determine the slopes and lengths of the units representing Walnut Gulch. The channel geometry parameters were obtained from a limited number of cross sectional profiles. The comparison of the predicted and recorded hydrograph is shown in Figure 7.15. The agreement between predicted and recorded runoff is good considering the complexity and size of the watershed.

High Resolution Models

Water Routing Component. The high resolution is chiefly characterized by the water routing component. Two more examples of applications of this component are presented.

Natural Channel. A flood hydrograph in the Rio Amana in Venezuela was used to test the applicability of the numerical method of flood routing in a natural channel. Both inflow and outflow hydrographs

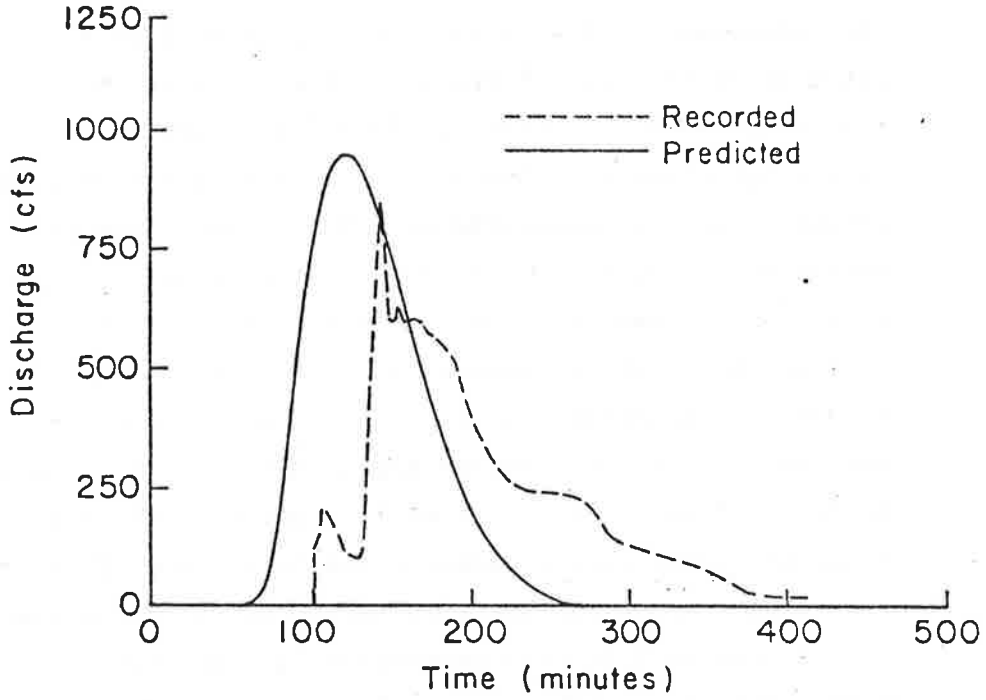

a. Runoff hydrograph for the storm of September 4, 1965, for the entire Walnut Gulch watershed.

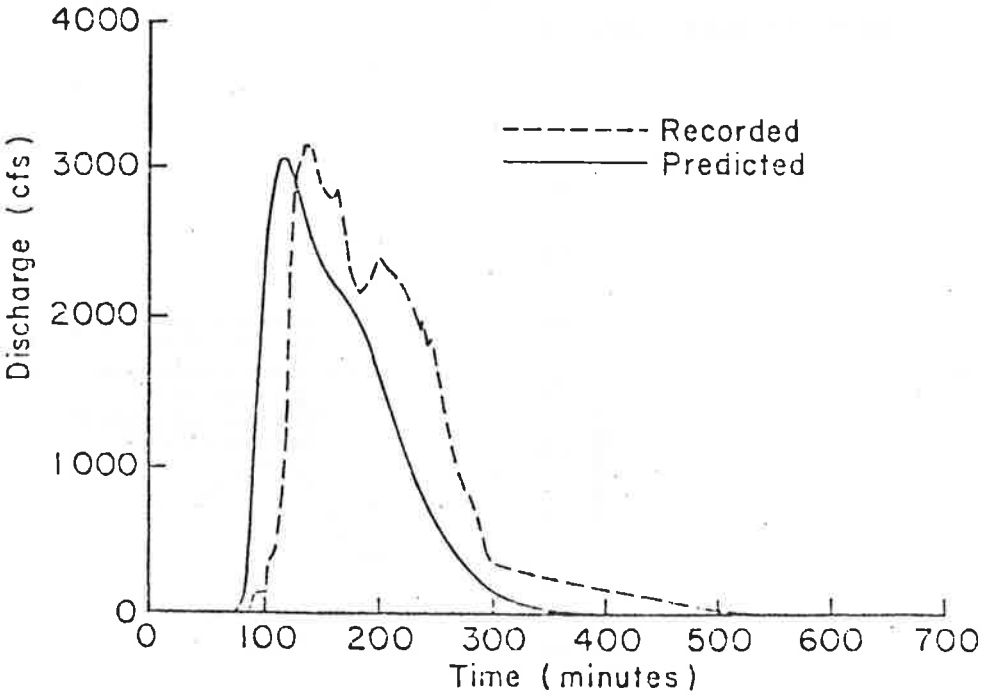

b. Runoff hydrograph for the storm of September 9, 1964, for the entire Walnut Gulch watershed.

Figure 7.15 Runoff hydrographs for the entire Walnut Gulch watershed.

were measured in 1969 in the reach of river between El Tejero and the crossing of the Naturin-Tembledor Road (see Simons et al., 1971a). As described by Simons et al. (1971b), the reach is 47.1 mi long and has an average slope of 0.00146. The bank-full top width at the downstream station is approximately 70 ft. The measured α and β values in A versus Q relation are available at the downstream station. The values are $\alpha = 1.1$ and $\beta = 0.9$. For the reach it has been assumed that β remains a constant and α changes linearly with distance. The estimated value of α at upstream station is 2.5, and the lateral outflow rate was approximately 0.26 $ft^3/s/mi$. The estimated upstream α value is much larger than the downstream value because of larger flow resistance and larger wetted perimeters for the same flow area in the upstream reach than in the downstream reach.

In Figure 7.16 the numerical solutions ($\Delta t = 2h$ and $\Delta t/\Delta x = 0.58$ s/ft) agree with the measured results. The proposed numerical method is applicable in natural channels with steep gradients and slow-rising hydrographs because the kinematic wave approximation is applicable for such channels.

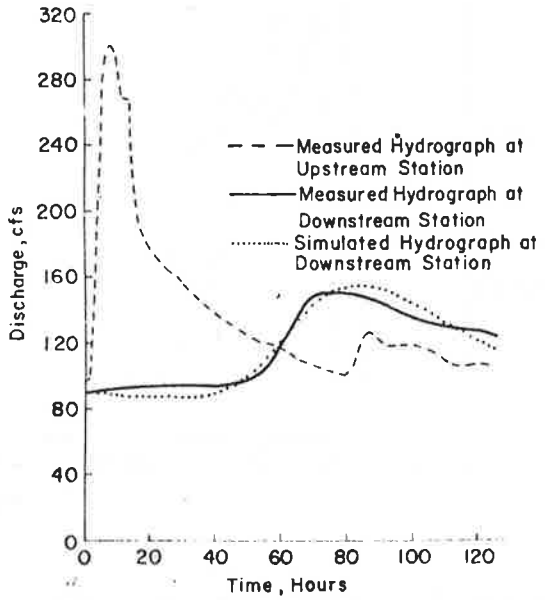

Figure 7.16 Flood routing in the Rio Amana in Venezuela.

Confined Catchment. The numerical model presented herein is valid for channel flows as well as overland flows. A catchment system is formulated by routing the overland flows to channels and then routing the flows through the channels. The numerical solutions for hydrographs from small catchments agree very well with the measured runoff. A comparison of computed and measured hydrographs at the outlet of SPL1 parking lot at Johns Hopkins University is shown in Figure 7.17. The storm used in this analysis is 13SPL1, which was reported by Schaake (1965). The area of the parking lot was 0.39 acre. The catchment area consisted of the overland flow area and V-shaped channels. The lengths of overland flow paths varied from 20 to 36 ft, and the overland slopes varied from 0.0167 to 0.019. The side slopes of V-shaped channels were 1:113. The lengths of these channels varied from 50 to 165 ft, and the channel slopes ranged from 0.0148 to 0.0213. The resistance parameters are estimated as follows: $K_o = 35$ (asphalt surface), $K_r = 27$ (assuming an 8-ft fall to give the terminal velocity for raindrops), and $K_2 = 0.4$ (asphalt surface). In the numerical computations, $\Delta t = 1$ min and $7.3 \leq \Delta t/\Delta x \leq 30$ s/ft.

The agreement between computed and observed hydrographs shown in Figure 7.17 indicates the applicability of the proposed numerical model for time variant inflows and watershed modeling.

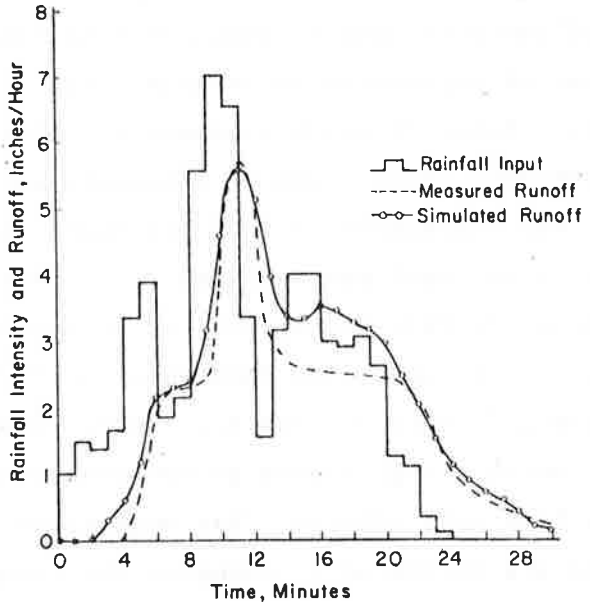

Figure 7.17 Runoff from SPL1 parking area, Johns Hopkins University.

Simons et al. (1975) tested the applicability of their model on the Beaver Creek Watershed, Arizona. Five runoff events in Watershed 1 and one runoff event in Watershed 17 were used.

Watershed 1 is a small drainage catchment with an area of 313.6 acres which has been clear cut. The five storm events in Watershed 1 used in this study area occurred on November 22, 1965, November 24, 1965, November 25, 1965, September 6, 1967, and September 5, 1970. The latter is known as the "Labor Day" storm. This is the same storm presented in Figure 7.14.

An example of the comparison between the simulated and the measured water hydrographs is shown in Figure 7.18. The agreement between the measured and the simulated water hydrographs is, in the most part, satisfactory. Because there is no measured sediment hydrograph, no comparison can be made. Other comparisons on water yield, peak water flow, time to peak water flow, and sediment yield are given respectively in Figures 7.19, 7.20, and 7.21. These figures show that the water routing model simulated the shape, volume, peak flow, and time to peak flow of the six water hydrograph from Watershed 1 and Watershed 17 within approximately 30 percent. Satisfactory results were obtained for different size storms and in different watersheds by using only one set of model parameters. This verifies that the model could be used to synthesize missing data and to predict the response of watersheds to various types of watershed management practices. Also, it has been demonstrated that the model could be used to estimate flood flows from ungaged watersheds.

The transferability of the model is one of the main advantages of this physical process simulation model over the conventional methods such as the Unit Hydrograph and Universal Soil Loss equation. For example, the Labor Day (September 5, 1970) storm produced approximately 2.2 times the surface runoff in Watershed 17 than in Watershed 1.

An important aspect in watershed management is to predict watershed treatment effects. The vegetation treatment effects on water yield are estimated by changing the canopy cover density and the ground cover density in overland flow units. Based on the storms of September 5, 1970, and September 6, 1967, the effects of vegetation treatment on the water yield from Watershed 1 have been evaluated. As

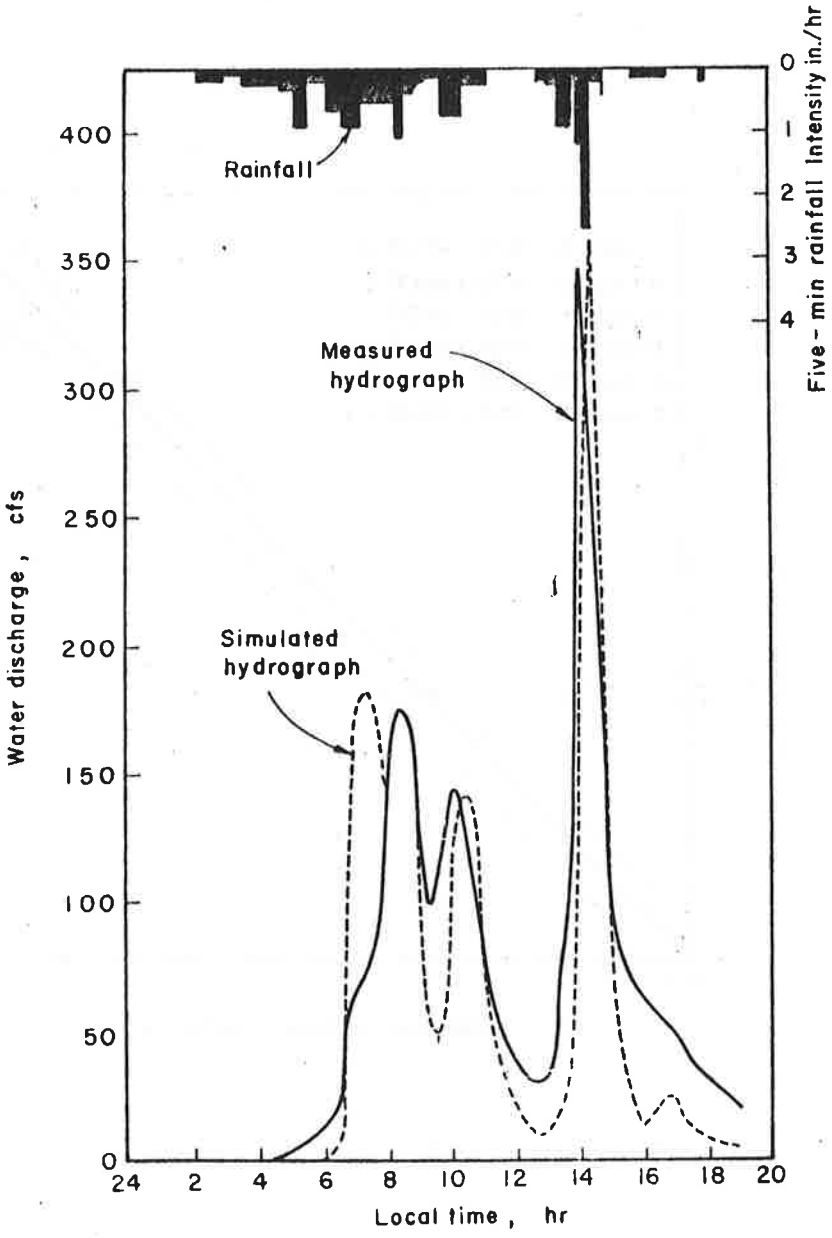

Figure 7.18 Water hydrograph from Watershed 17 for the September 5, 1970, storm (after Simons et al., 1975).

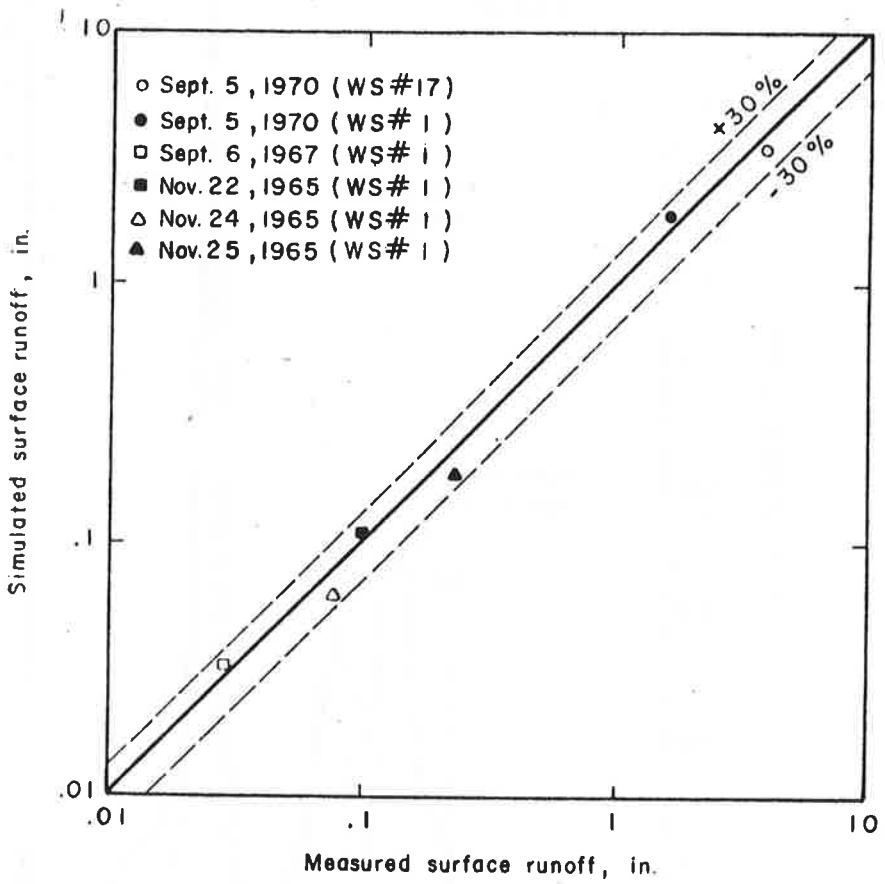

Figure 7.19 Comparison of measured and simulated water yield (after Simons et al., 1975).

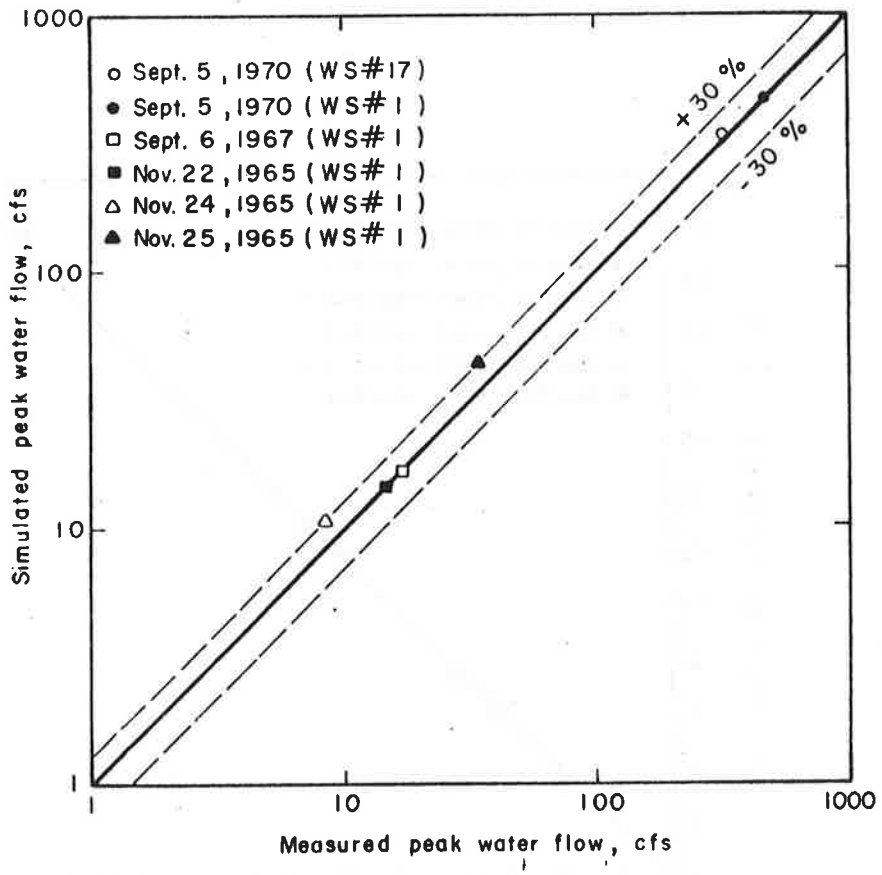

Figure 7.20 Comparison of measured and simulated peak water flows (after Simons et al., 1975).

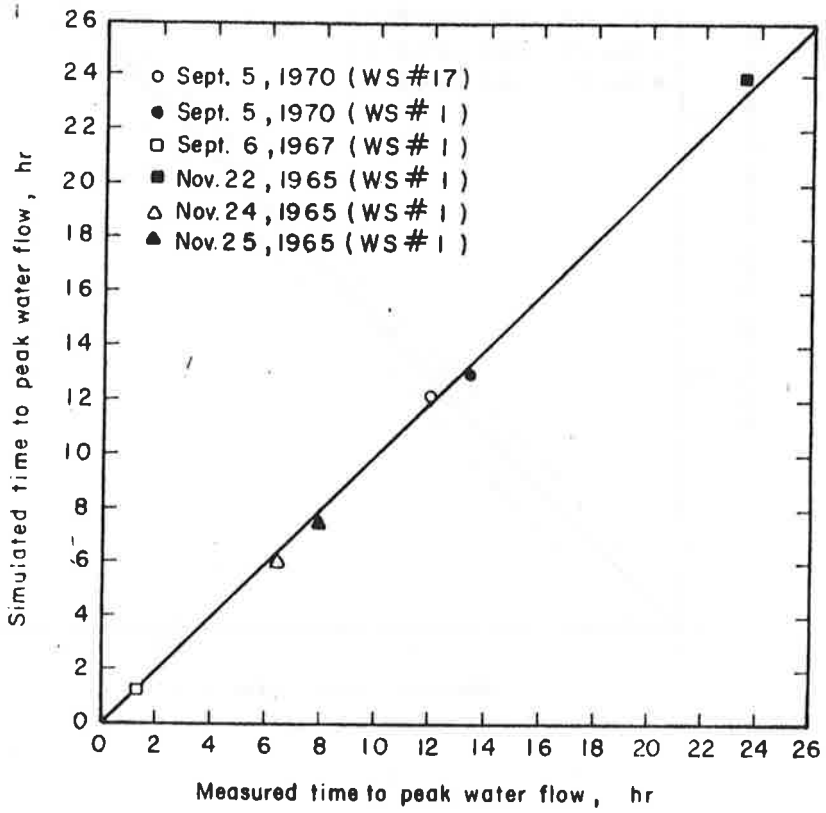

Figure 7.21 Comparison of measured and simulated time to peak water flow (after Simons et al., 1975).

shown in Figures 7.22 and 7.23, for a constant and undisturbed ground cover of 65 percent, water yield and the peak flow rates from these two storms are increased as the canopy cover density is decreased.

The reduction in interception caused by removing the vegetation results in the increase of excess rainfall. These effects are much more pronounced in Watershed 1 for the smaller size of storm than for large storms like the Labor Day storm. The time to peak flow is shortened as the canopy cover is decreased for the small storm, but there is no change in time to peak flow for the large storm.

If a watershed is clear-cut and the forest litter, tree mulch, rocks, etc. are also removed in different degrees, or if the ground cover is seriously destroyed by a burning treatment, the associated response can be estimated by changing the ground cover density in overland flow units. The changes in water yield in Watershed 1 for the storms of September 5, 1970, and September 6, 1967, is shown in Figure 7.25. As the ground cover is decreased, the total surface runoff and peak water flow are increased moderately and the time to peak flow shortened slightly. The effect on water yield is more pronounced for a smaller storm.

7.7 DATA NEEDS

The data needed for mathematical modeling of watershed response are dependent on the type of watershed, the objective of modeling and the type of model utilized. The data requirements summarized below are primarily for studying the major watershed response (water yield, sediment yield, and stream morphology) from small watersheds. The emphasis is made on the input data requirements of the watershed models presented in this chapter. However, additional data for other potential studies related to the watershed response are also identified.

There are two distinct types of data involved in the analysis. They are the model input data, which are specifically required for the model input, and the basic data (raw data), which are directly taken from field measurements. Generally, the model input data are obtained from retrieving and/or analyzing the raw data. The required model input data and basic data, and the supplementary data that are important to watershed study are summarized as follows.

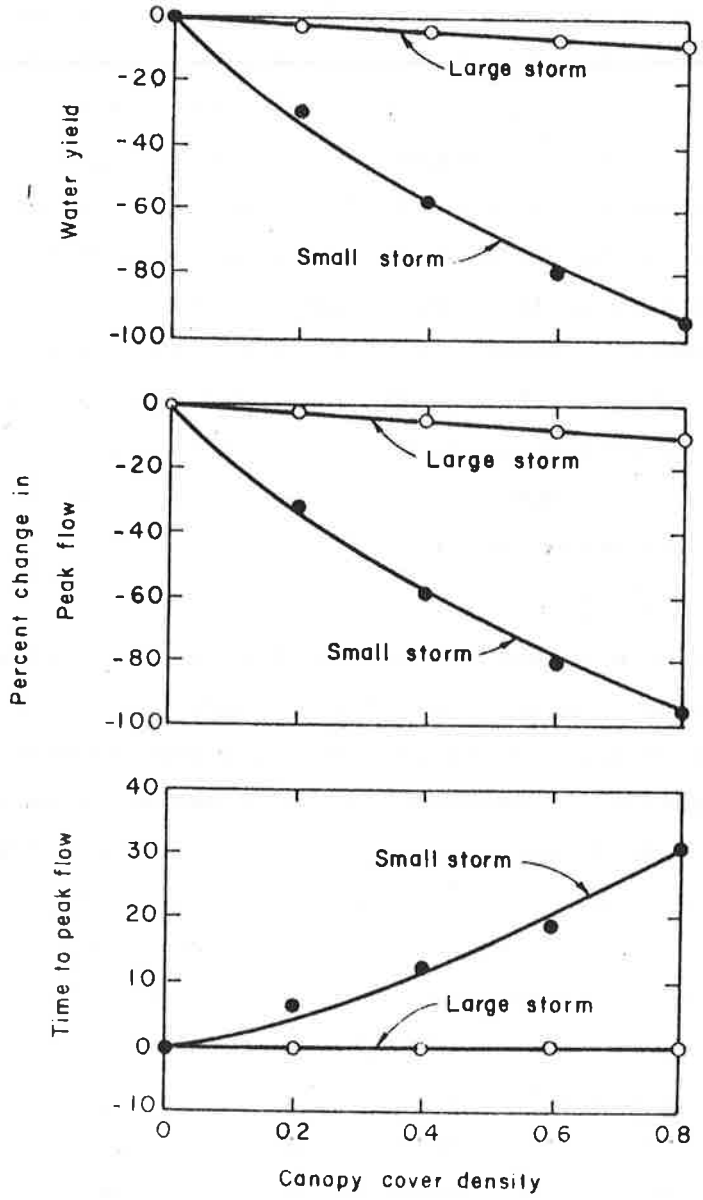

Figure 7.22 Effect of canopy cover density on the water hydrograph from Watershed 1 (after Simons et al., 1975).

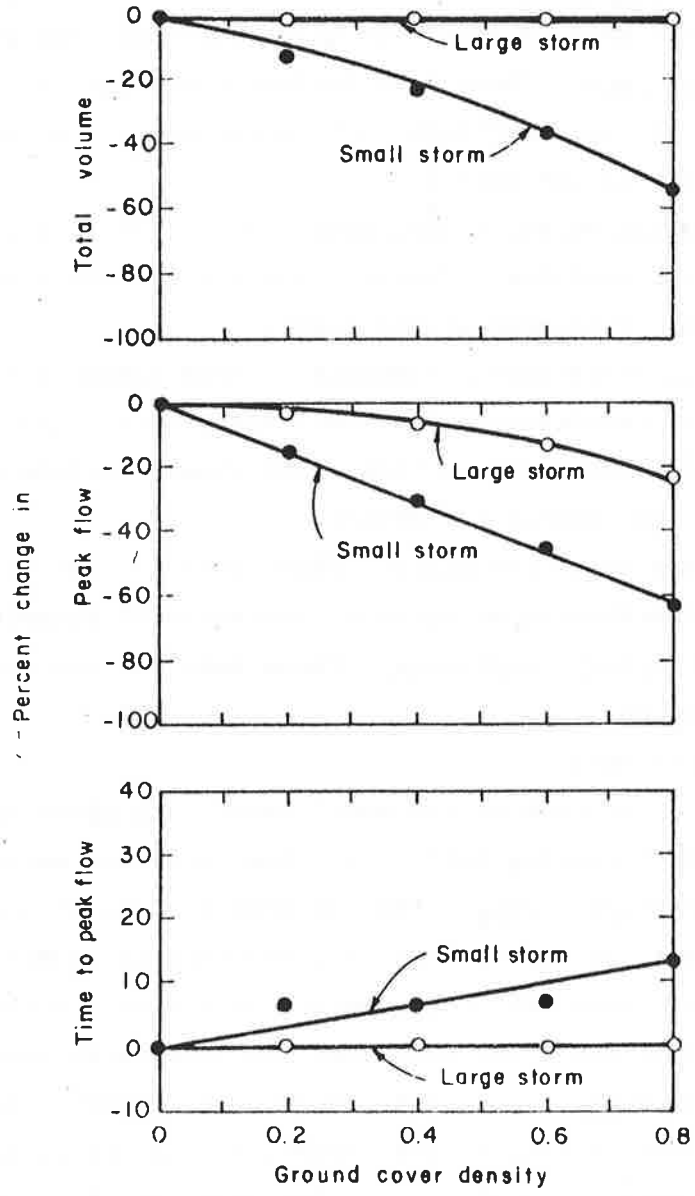

Figure 7.23 Effect of ground cover density on the water hydrograph from Watershed 1 (after Simons et al., 1975).

General

Model Input Data

The input data required for the simulation are different for different models. Described below are those for general purposes.

Geometry Data. These data include slope length, bed slope, wetted perimeter versus flow area relations, and computation sequence.

Soil Data. These data include the saturated hydraulic conductivity, average capillary suction pressure, soil porosity, degree of saturation in the wetted zone.

Vegetation and Ground Cover Data. These data include canopy cover density, ground cover density, the typical interception storage capacity of canopy cover, and ground cover.

Flow Resistance Parameters. These parameters are constants describing grain resistance and overall resistance. The overall resistance parameters for overland flow units should include parameters for both minimum and maximum resistance.

Storm Characteristics. These data include rainfall intensity and areal distribution of rainfall intensity if studying a large watershed.

Antecedent Conditions. These data include antecedent soil moisture content.

Basic Data

In order to have the model input data given in the previous section, the following basic data (raw data) are needed.

Topographic Data. The topographic data include the topography survey map, aerial photographs, and channel geometry survey results. With these data, all the geometry data required for the model input can be determined for both overland flow areas and channels.

Soil Data. These data include soil survey map indicating the aerial distribution of soil types, and saturated hydraulic conductivity, average capillary suction pressure, soil porosity, and degree of saturation in the wetted zone.

Forest Inventory Data. The forest inventory data include total vegetation volume, total litter volume (or litter index), canopy cover density, ground cover density, areal distribution of vegetation type (can be estimated from aerial or color infrared photos), and interception storage capacity ofa typical tree and a unit area of forest

floor. From these forest inventory data, the vegetation and ground cover data for the model input can be easily determined.

Hydraulic Data. The hydraulic data include flow discharge, depth, and velocity. These data are used to estimate the flow resistance parameters to evaluate the performance of the mathematical model.

Climatologic Data. The climatologic data include the rainfall record in either strip charts or hyetographs. The antecedent conditions can only be estimated if the interstorm water balance simulation is available.

Hydrographic Data. The hydrographic data are needed for model calibration and simulation evaluation. These data include the water at the watershed outlet and the resultant channel profiles.

Watershed Management Data. The watershed management data are very important for evaluating the watershed treatment effects. These data include the vegetation treatment data (clear-cut, patch-cut, or burning treatment) and the mechanical treatment data (check dam, logging road, windrow and skid trail, etc.).

Sensitivity of Input Data

Response of model prediction to changes in an input parameter indicate the model's sensitivity to that parameter. Parameters can then be termed sensitive or insensitive depending on the model's response. A common force of sensitivity analyses is through parameter perturbation when one parameter is varied while all the others are held constant. Changes in parameter and model response are then compared. Shiao (1978) used sensitivity analyses to show the response of the high resolution watershed water routing and yield model. Shiao utilized data from four small agricultural watersheds in Georgia and three small forest watersheds in Mississippi. Sensitivity analysis helped him determine the important variables and those that must be carefully calibrated. Although applied to a particular model, the results he presented represent the response of the other models because they all contain the same or similar physical processes and associated parameters.

The variables selected for analysis included ground cover density, canopy cover density, resistance coefficients for both overland and channel flow, the suction parameter, soil permeability or hydraulic conductivity.

The suction parameter is a variable that includes the potential capillary suction head, porosity, and antecedent moisture content of the soil. The total overland flow resistance coefficient is a function of ground cover density and a constant describing the resistance of ground cover density. A change in either ground cover density or the value of the constant will change the total overland flow resistance coefficient. Varying the value of the constant describing the resistance for ground cover density was used instead of ground cover density. The effect of the ground cover density on the resulting water and sediment yield was obtained by evaluating the change in the total overland resistance coefficient.

The interception loss is a function of cover density and the water holding capacity of canopy and ground cover. The channel flow resistance coefficient is comprised of grain and total channel flow resistance. Parameters related to sediment transport are dependent on the sediment transport equation selected for use. The values of these parameters remained constant. The sensitivity of each tested parameter was determined by varying the parameter and monitoring changes in peak discharge, volume, time of the peak discharge and total sediment yield.

Hypothetical rainfall and runoff data and other necessary parameters were assumed for this analysis. One set of rainfall data and two sets of parameters were assigned. These parameters, representing two different watershed responses, are called Case 1 and Case 2. Case 1 showed that the watershed did not store water and had a higher runoff rate. Runoff volume was about 67 percent of the rainfall. Case 2 had a much smaller runoff with runoff volume of only 11 percent of the total rainfall. The influences of parameters on the peak discharge is shown in Figures 7.24 and 7.25.

Two parameters, the suction parameter and soil permeability, greatly influenced peak discharge for Case 1. The influence rate of each parameter to the resulting peak discharge was evaluated by observing the corresponding percent change in each parameter for an assumed variation. For example, a 10 percent increase in peak discharge resulted from decreasing the permeability of the soil by 65 percent and the suction parameter by 210 percent.

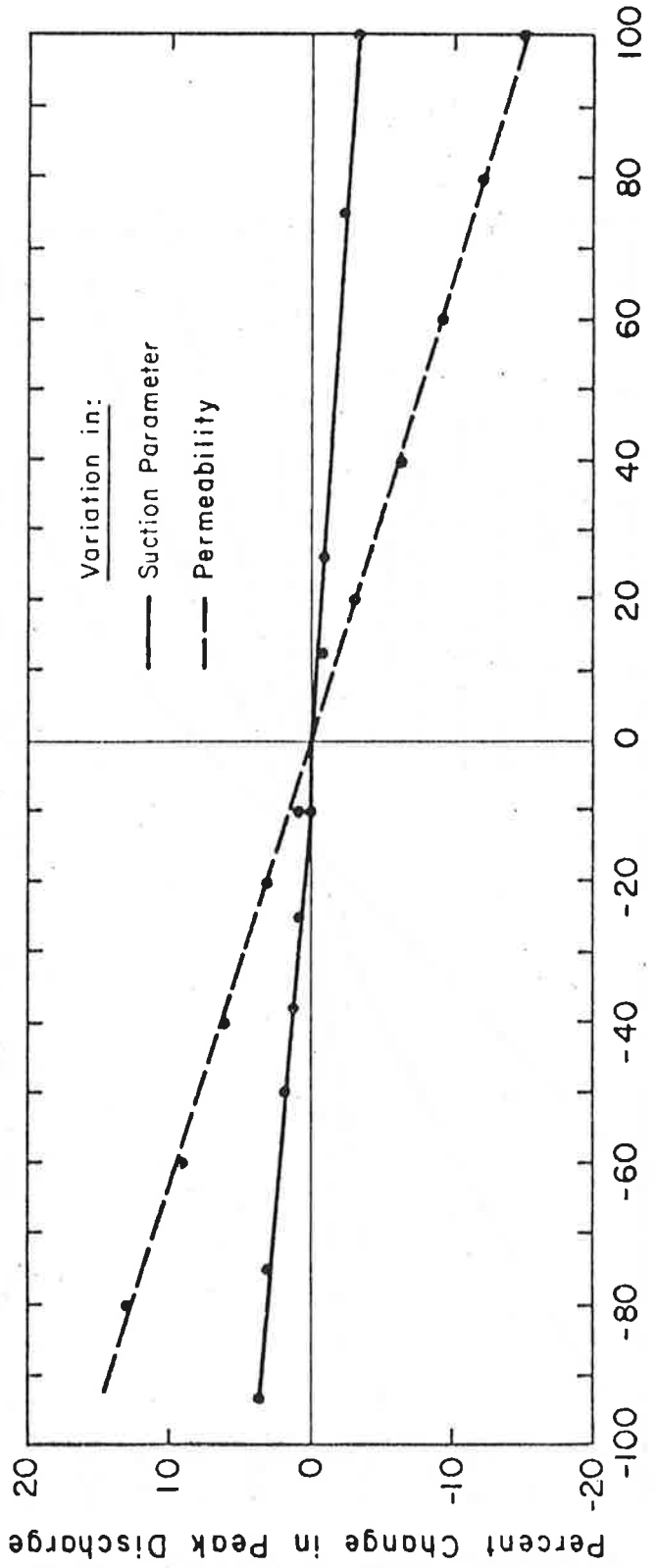

Figure 7.24 Percent change in peak discharge due to change in parameters for Case 1.

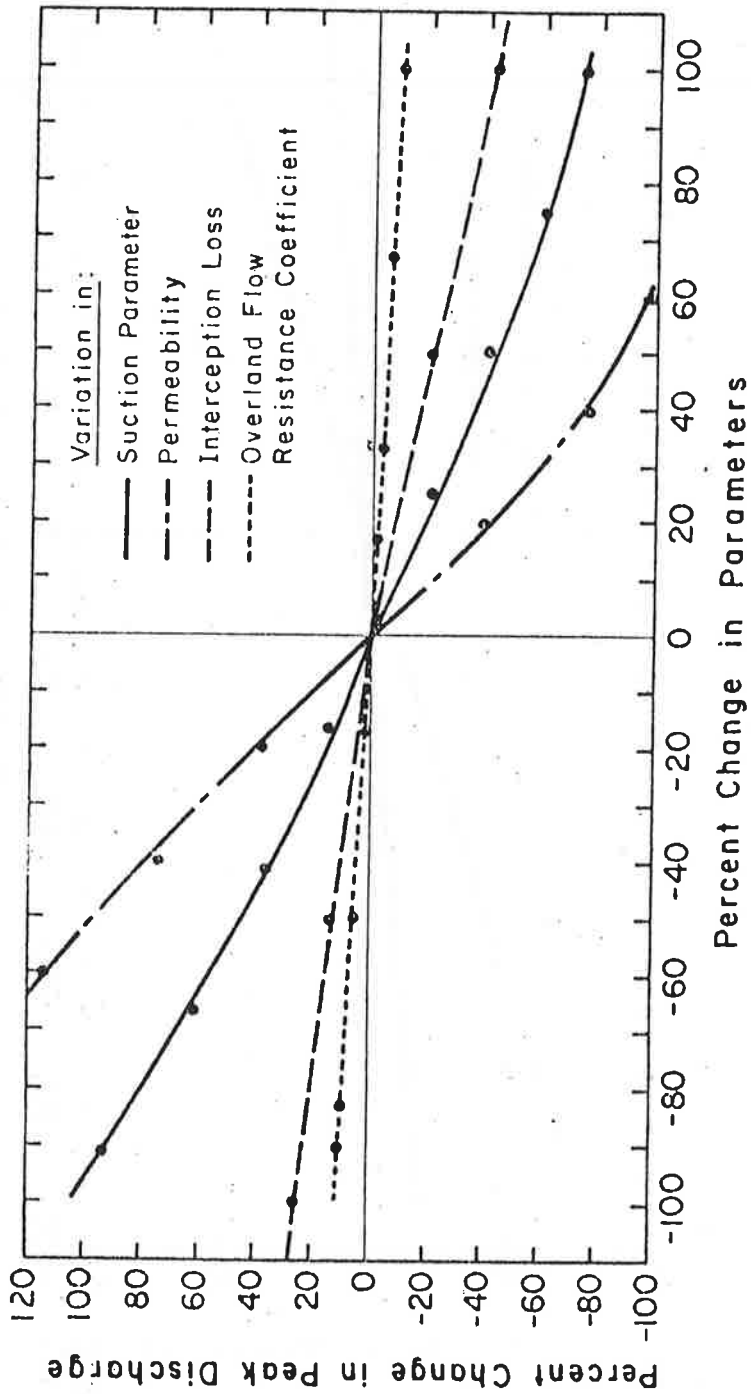

Figure 7.25 Percent change in peak discharge due to change in parameters for Case 2.

In Case 2, however, four parameters, suction parameter, permeability, interception losses, and the overland flow resistance coefficient, influence the resulting peak discharge. A 10 percent increase in peak discharge resulted from decreasing the suction parameter by 14 percent, permeability by 5 percent, interception loss by 40 percent and the overland flow resistance coefficient by 90 percent. The range of variation of parameters for Case 2 is greater than that of Case 1. This indicates that Case 2 is more sensitive to change. However, in both cases, permeability is the dominant factor, and the influence of the overland flow resistance coefficient is small and may be neglected. Similarly, the influence of ground cover density on the resulting peak discharge is small.

The corresponding change in peak discharge, time of the peak discharge, and shape of the hydrograph for both cases for an assumed change in the value of permeability and suction parameter are shown in Figures 7.26 thourgh 7.29. For Case 1, even a 100 percent change in the value of the suction parameter did not change the shape of the hydrograph and the time of peak discharge (Figure 7.26). The change in peak discharge is less than 5 percent. A change in the value of the permeability by 100 percent only changes the peak discharge by 15 percent (Figure 7.27). However, the result for Case 2 is completely different from Case 1 (Figures 7.28 and 7.29). Both suction parameter and permeability exert the greatest influence on the magnitude and time of the peak discharge and the shape of the hydrograph. There is more than a 50 percent change in the value of the peak discharge (Figures 7.28 and 7.29).

A 99 percent change in soil permeability changes the hydrograph shape dramatically. There is more than 100 percent change in peak discharge for a 99 percent decrease in permeability. If the permeability of the soil increases by 100 percent, the resulting runoff is almost zero. This is another indication of the greater sensitivity of Case 2. The resulting percent change in water volume for both cases is shown in Figures 7.30 and 7.31. The influence of the overland flow resistance coefficient to water volume was through an increase or decrease in the detention storage.

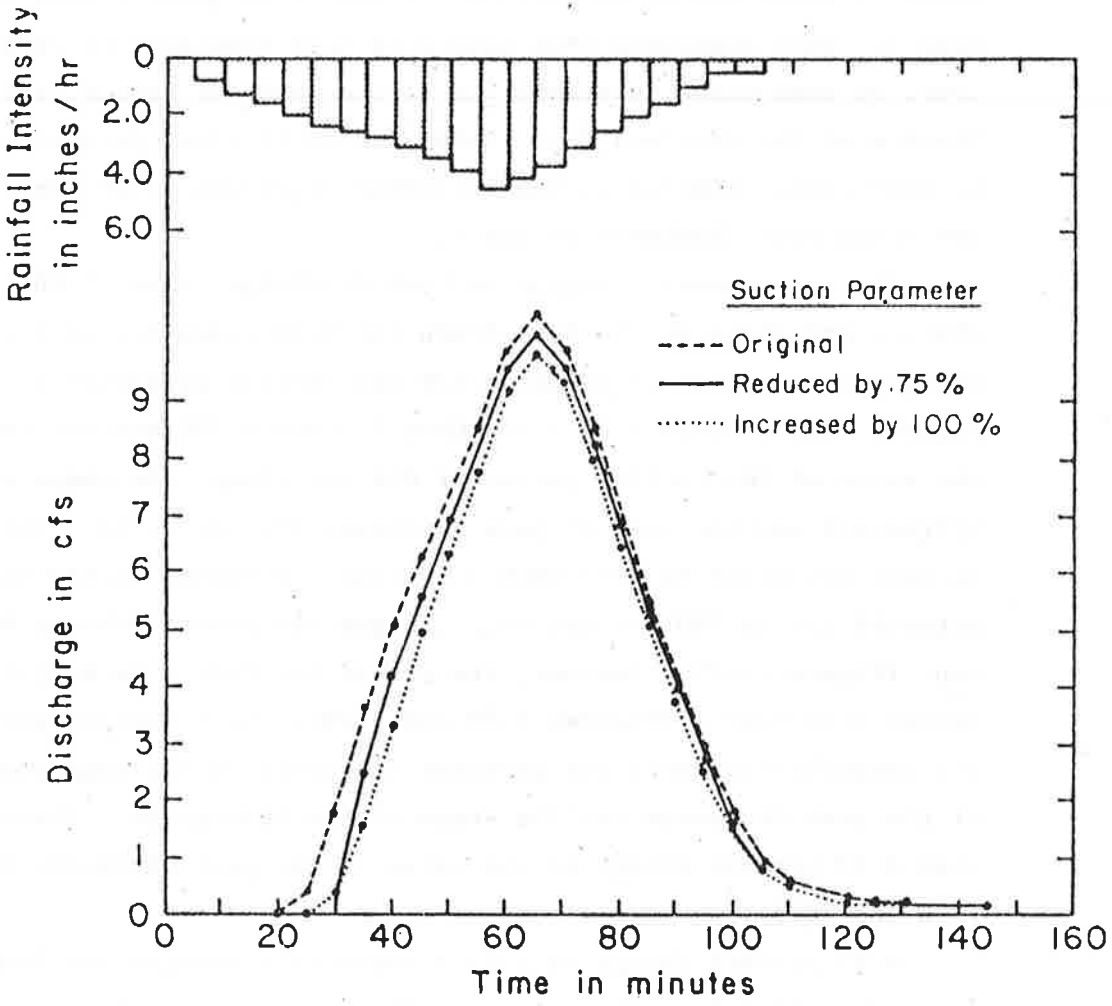

Figure 7.26 Variations in the water hydrograph due to changes in the suction parameter for Case 1.

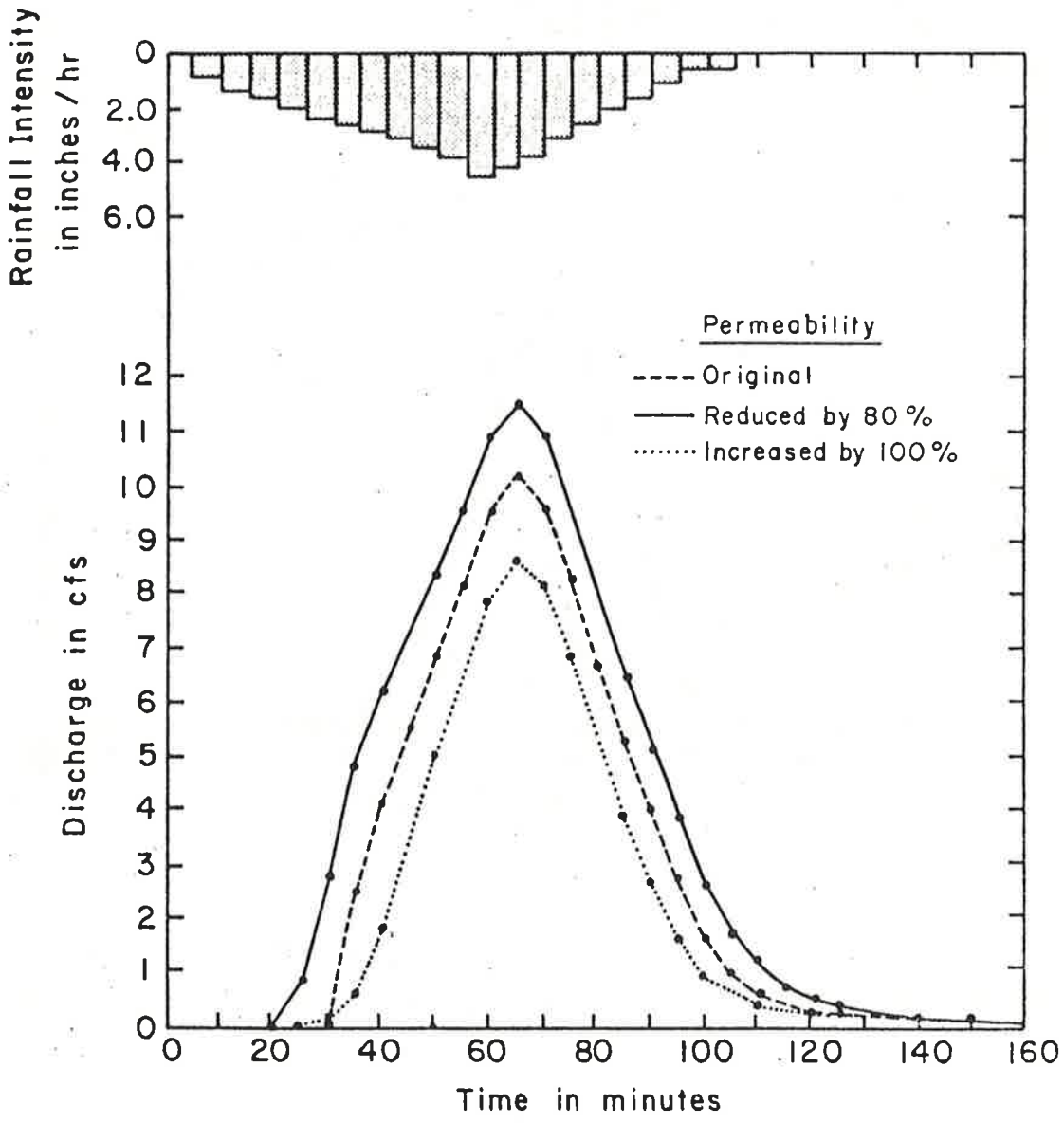

Figure 7.27 Variation in the water hydrograph due to changes in the permeability of the soil for Case 1.

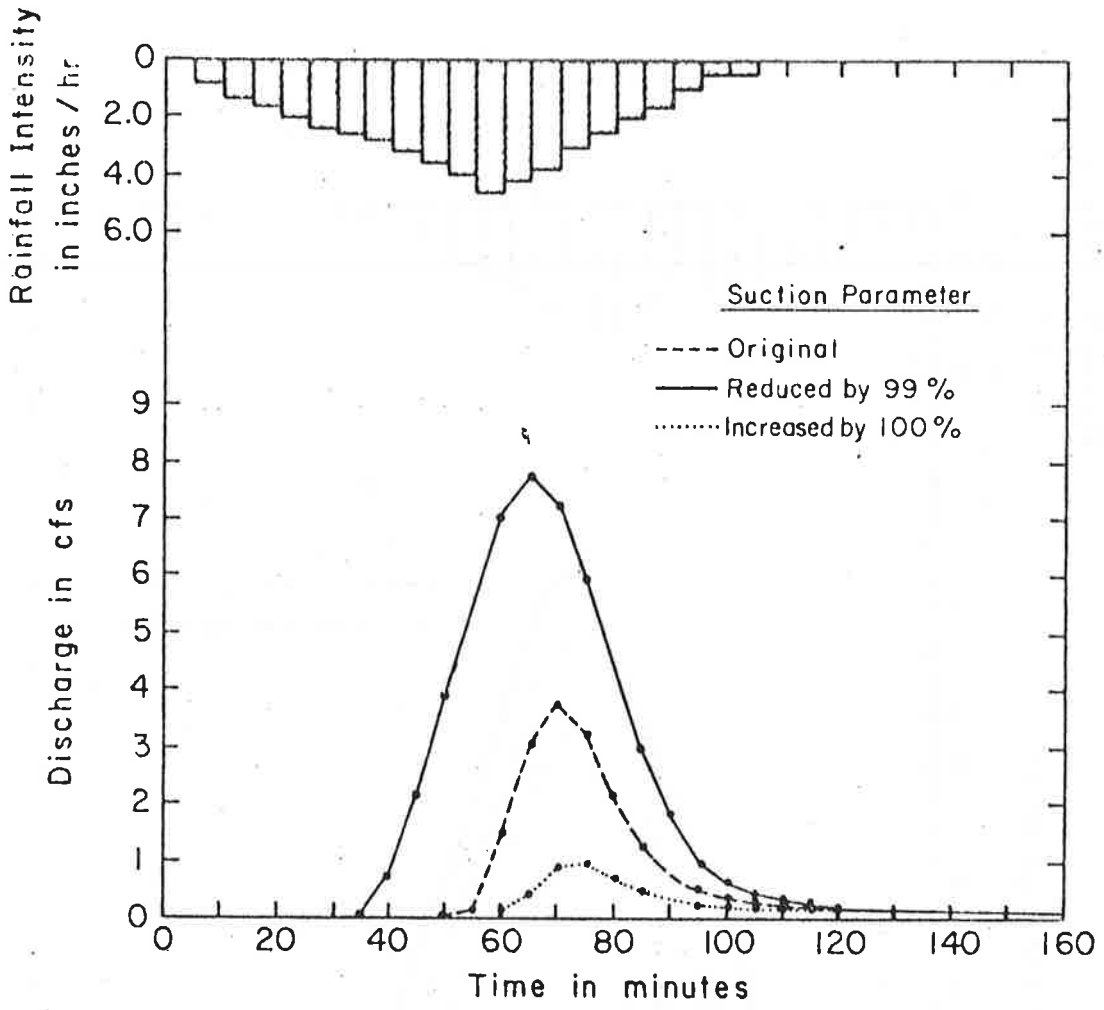

Figure 7.28 Variation in the water hydrograph due to change in the suction parameter for Case 2.

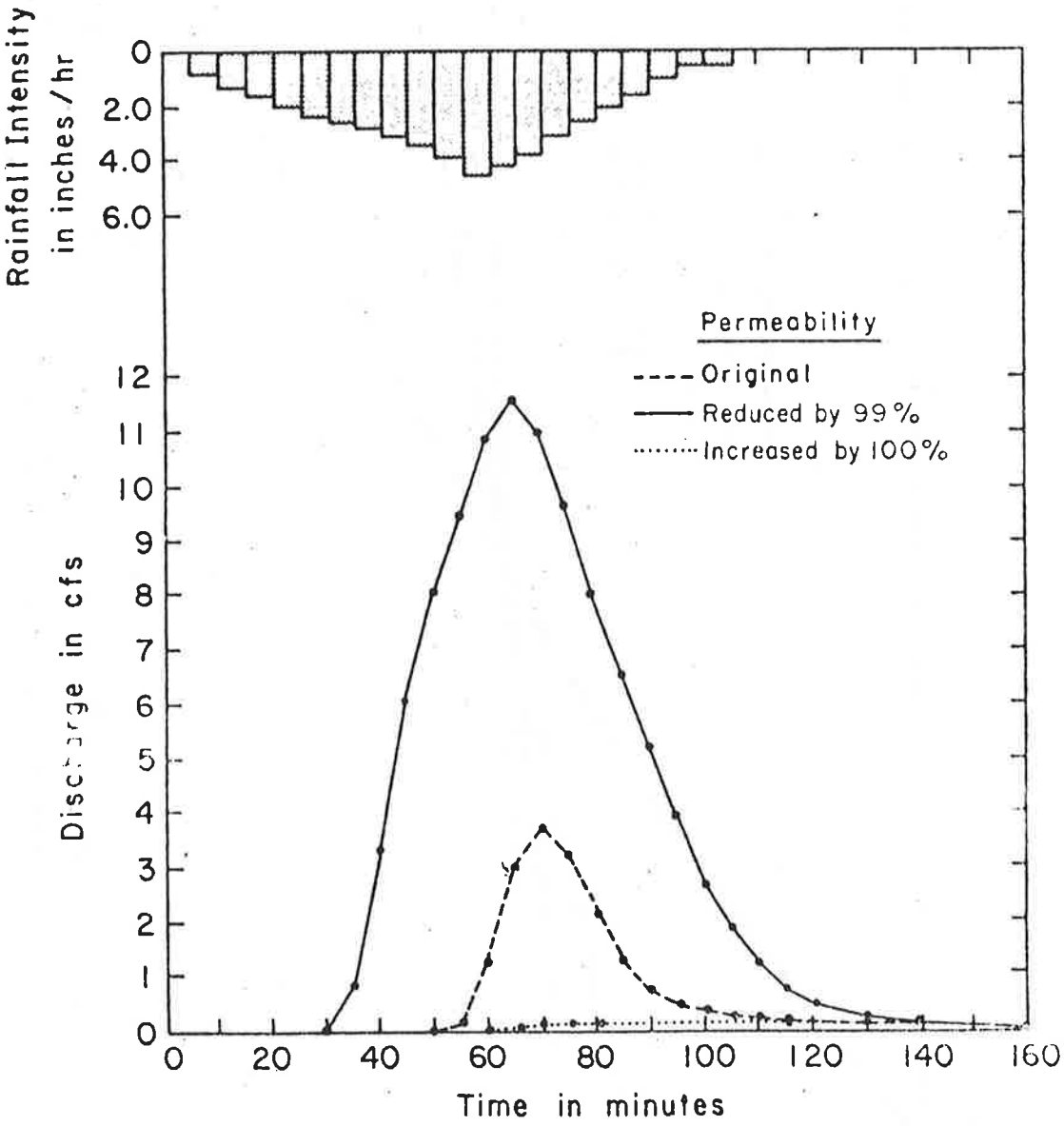

Figure 7.29 Variation in the water hydrograph due to changes in the permeability of the soil.

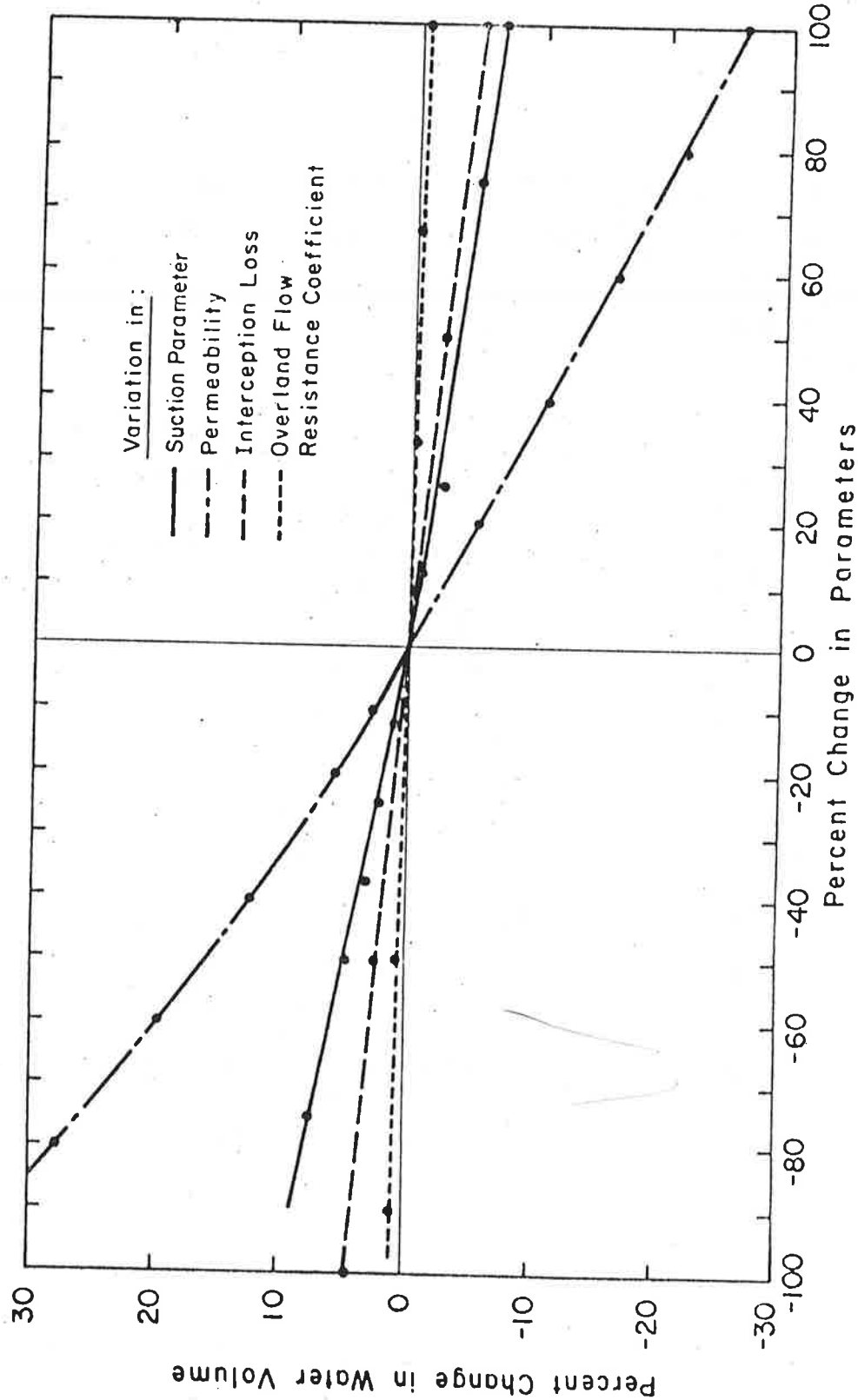

Figure 7.30 Percent change in water volume due to change in parameters for Case 1.

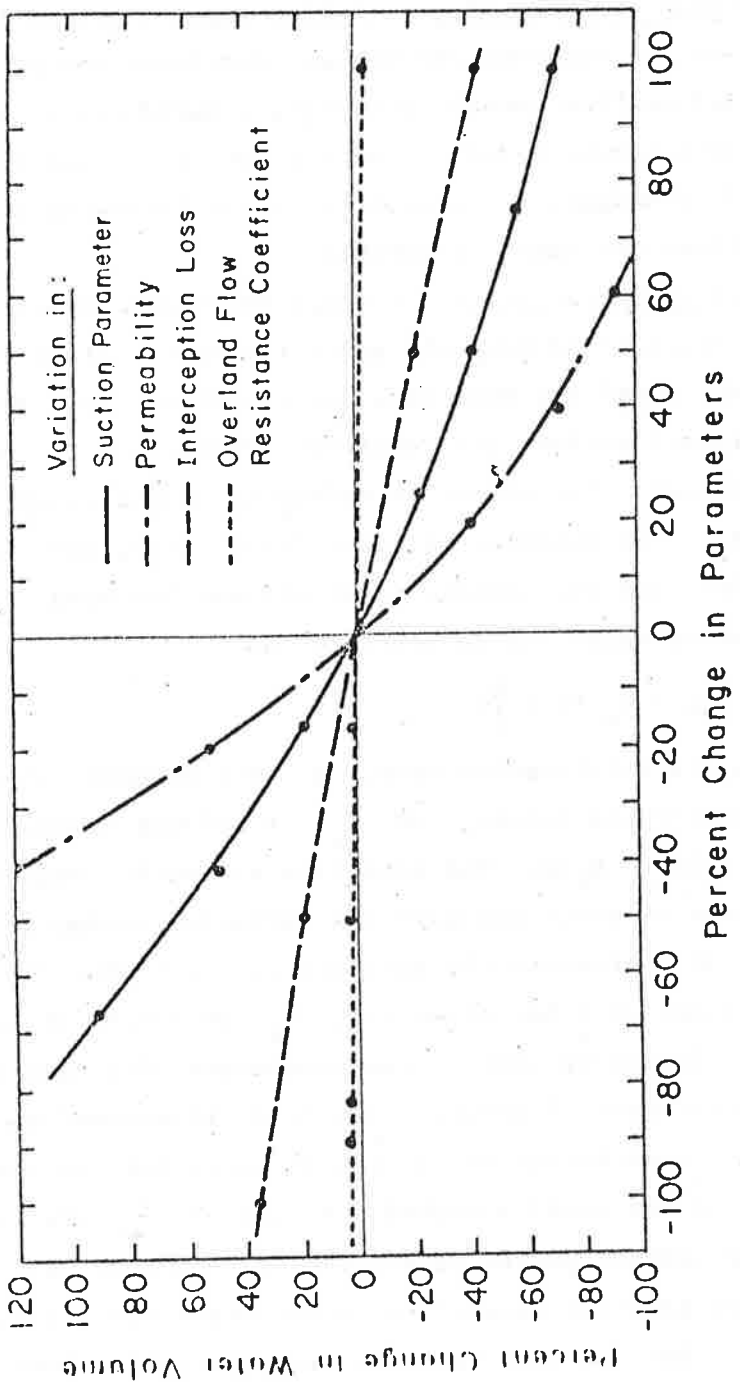

Figure 7.31 Percent change in water volume due to change in parameters for Case 2.

As this analysis indicates, sensitivity analysis is dependent on size of storm, hydrologic and hydraulic conditions, and initial magnitude of the variables.

Methods for Computing or Estimating Model Information

There are numerous and varied techniques for gathering and estimating information needed to operate a mathematical model. Experience has shown how some model parameters can be estimated from scanty data. Selected techniques are presented in the following section for determining these necessary parameters.

Soil Characteristics. Certain hydrologic properties of the soil must be obtained to properly model the infiltration process using the Green-Ampt model and soil size distribution. As a minimum, soil textural classifications are required. Parameters in the infiltration model include: the effect of hydraulic conductivity in the wetted zone, K_w, the porosity ϕ, the final (S_w) and initial (S_i) soil saturation, and the average capillary suction head ψ. The Green-Ampt infiltration model can be rewritten as

$$i = K_w \left(1 + \frac{\Phi}{I}\right) \qquad (7\text{-}103)$$

where i is infiltration rate, Φ is a grouping of soil parameters, I is infiltrated volume, and K_w is defined above. The Φ parameter is $\Phi = \psi (S_w - S_i)\phi$. The effective hydraulic conductivity in the wetted zone is about one-half the hydraulic conductivity normally reported. It represents the infiltration rate when the soil nears saturation. Experience has shown that K_w is a more sensitive parameter than Φ. Therefore some of the parameters that make up Φ can be roughly estimated if needed. Often ϕ is assumed as 0.5 and S_w as 1.0. Better estimates of ϕ can be made, but the improvement in model accuracy is not usually marked. Values of S_w are usually close to 1.0. The initial degree of saturation can be roughly estimated from antecedent rainfall conditions, temperature data, and a knowledge of the soil. Because this value is used for calibration in conjunction with the ψ value, only an intuitive realistic initial estimate is needed. Wet conditions are about 0.8 and greater, and dry is usually below about 0.3 or 0.4. The volumetric water content w is defined as

$$w = nS \tag{7-104}$$

and can be used if water content data are available.

Unfortunately, except for soils which have undergone considerable laboratory study, soil data for values of K_w and $\bar{\psi}$ are simply not available. Since soils are, in general, anisotropic and heterogeneous in their physical properties, conductivity, porosity, and capillary pressures may easily vary by significant amounts over very small areas (Carvallo et al., 1976). Therefore, given the mathematical analysis based on data from one or two extensively studied samples may not be meaningful. Any watershed simulation requires calibration to attempt to compensate for neglected processes and inadequacies in theory. The parameters of this infiltration model, particularly K_w, are prime candidates for such calibration; therefore, good first estimates of K_w and ψ are needed. To this end, the following, admittedly somewhat simplistic, method for estimating K_w and ψ is suggested.

If infiltrometer data are available, the following method can be used to obtain estimates of K_w and Ω:

1) Plot the infiltration rate and infiltrated volume as a function of time. Figure 7.32 shows an example of a plotted infiltrometer data from Walnut Gulch, Arizona.

2) Plot the infiltration rate versus the reciprocal of the infiltrated volume using the curves plotted in Step 1 of the procedure. Figure 7.33 shows the result of plotting this type of curve from data given in Figure 7.32.

3) The curve of infiltration rate as a function of the reciprocal of infiltrated volume is nearly a straight line, at least to the extent that the Green-Ampt equation represents the actual soil performance. If a straight line is fitted to this data, then the y-intercept is K_w, and the slope is ΩK_w. Thus estimates of K_w and Ω can be obtained by measuring the slope and intercept of the line approximating the data. From Figure 7.34, the value of K_w may be estimated as 0.78 inches per minute and Ω as 1.22 inches.

As seen from Figure 7.34, a considerable amount of "noise" exists in this data. This "noise" may be due to a number of causes; for example, bubbling, inhomogeneities in the soil, or even a badly executed

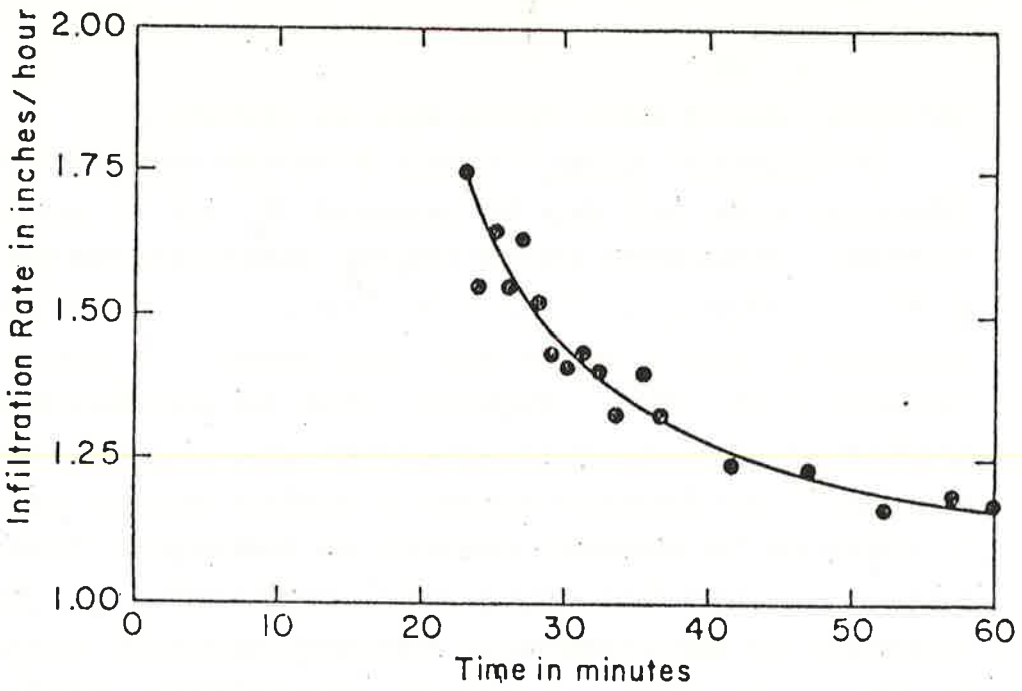

Figure 7-33 Infiltration rate data from Walnut Gulch, Arizona.

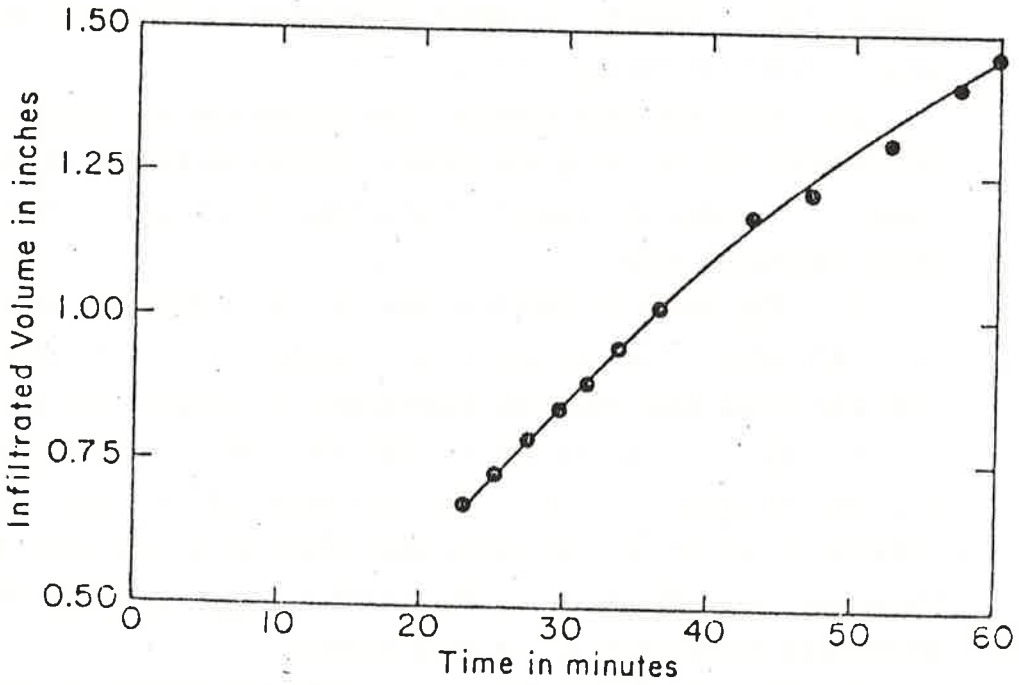

Figure 7-32 Infiltration volume data from Walnut Gulch, Arizona.

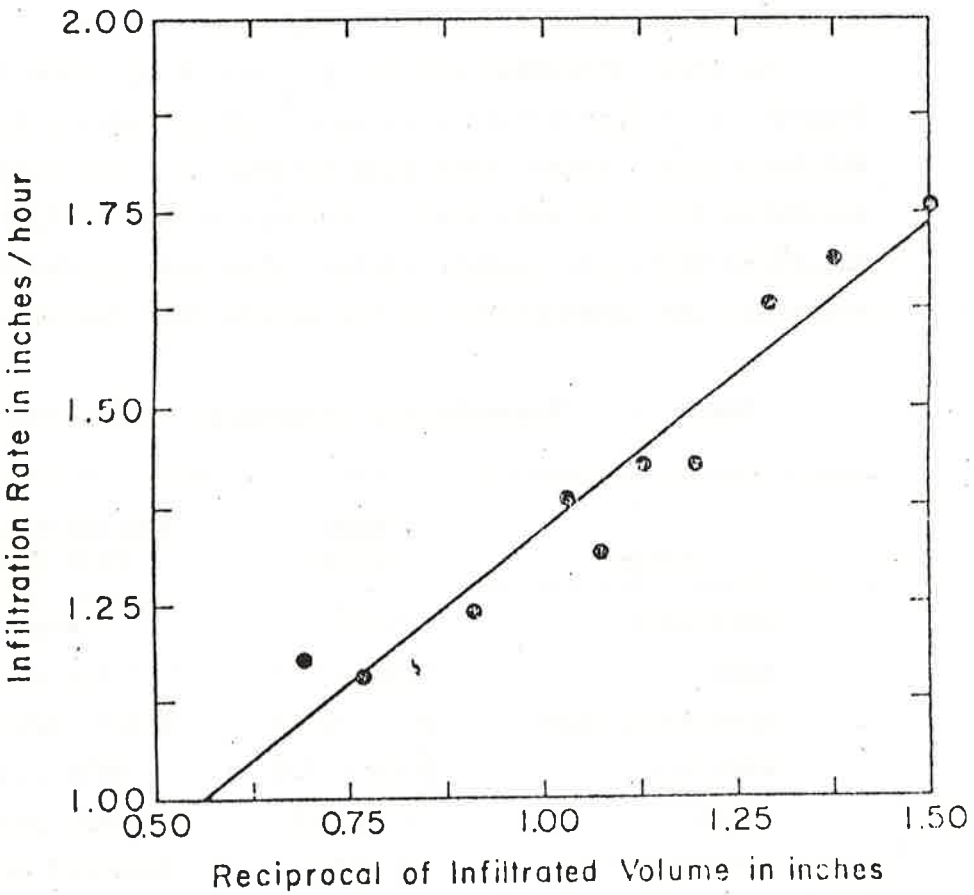

Figure 7.34 Plot of infiltration rate as a function of the reciprocal of infiltrated volume.

infiltrometer experiment. Whatever the cause, the scatter in the data makes fitting a straight line a difficult task.

A more precise estimate of these parameters using the same raw data could be obtained by using optimization techniques such as proposed by Li and Simons (1977). However, the use of these techniques, while more precise, suffers the same criticism as those mentioned earlier considering the wide spatial variability of soil characteristics. Therefore, while certainly not rigorous, the method proposed herein may be more consistent with available field data.

The first approximation of K_w may be obtained from United States Department of Agriculture Soil Conservation Service field profile permeability tests. These tests give a range for the value of hydraulic conductivity for each soil class. Because values in Table 7.2 are saturated hydraulic conductivities, they must be divided by two to represent the conductivity in the wetted zone (Bouwer, 1969).

Table 7.2. Permeability (hydraulic conductivity) classes.

Class	Rate in/hr	Representative Soil Type
very slow	< 0.06	Clay
slow	0.06 - 0.2	Silty clay
moderately slow	0.2 - 0.63	Silty clay loam
moderate	0.63 - 2.0	Silt loam
rapid	2.0 - 6.3	Sandy loam
very rapid	> 6.3	Sand and gravel

Because the hydraulic conductivity depends on texture, porosity and structure, as well as the viscosity of the water, a particular soil type may have different hydraulic conductivities as changes in these characteristics occur. Therefore, it is often difficult to assign conductivity values to each soil type. In general, though, clean sandy soils will have higher conductivities than plastic clay soils.

The range of values for ψ, average capillary suction, for selected types of soils is shown in Table 7.3 (Eggert, 1976). Eggert shows a

relationship between initial saturation and ψ which demonstrates that for a high initial saturation, the value of average capillary suction will be in the lower part of the given range, e.g., capillarity is destroyed. Though only a few soil types are listed in the table, a rough estimate for ψ can be made by associating the soil mixture found in the watershed to the most closely related soil listed in Table 7.3. It is necessary to specify soil types and distribution by use of a soil map so an effective value of ψ for the entire area being investigated can be obtained. Soil maps and textural descriptions can usually be obtained from soil surveys done by the United States Department of Agriculture Soil Conservation Service.

Table 7.3 Average capillary suction for selected types of soil (after Eggert, 1976)

Soil Type	Range of Average Capillary Suction (inches)
Nickel gravel-sand loam	2.0 - 4.5
Ida silt loam	2.0 - 3.5
Poudre fine sand	2.0 - 4.5
Plainfield sand	3.5 - 5.0
Yolo light clay	5.5 - 10.0
Columbia sandy loam	8.0 - 9.5
Guelph loam	8.0 - 13.0
Muren fine clay	15.0 - 20.0

Vegetative Cover

Ground and canopy cover density determines rainfall interception volumes. Ground cover density is also used to compute overland flow resistance. Cover density data can be acquired by on-site inspection or by use of aerial photography. If aerial photography is used, some on-site inspection is also needed for ground truth. Canopy cover and ground cover interception storage values are more difficult to determine. A starting point for estimating interception values is Table 7.4, from Zinke (1967). It is necessary to specify vegetation types and distribution by use of a vegetation map so that realistic interception volumes can be computed. There are tremendous ranges in the reported values making it sometimes difficult to select an appropriate number. Typical values for conifers average about 0.1 inches, and ground cover interception is

Table 7.4 Some interception storage values reported for vegetation in the american literature*

Vegetation Element	Species	Storage Amount (mm)	(in.)
CONIFERS	Abies concolor Lindl.	3.8	0.15*
	Mature	6.6	0.26*
	Pole size	7.6	0.30*
	Abies magnifica A. Murr.	0.8	0.03
	Pinus contorta Dougl.		
	Pinus lambertiana Dougl.	0.3	0.10*
	Pinus ponderosa	3.0	0.12
	Pinus ponderosa laws	0.8-1.3	0.03-0.05
	Second growth	2.3	0.09*
	Mature	2.3	0.09*
	Young(14 ft. high)	0.3	0.01*
	Pinus radiata D. Don	0.3-0.1	0.01-0.04
	Pinus resinosa Ait.	0.8	0.03
	Picea rubens Sar. (30 yr old)	9.1	0.36
	Pinus storbus L.	0.5	0.02
	Tsuga canadensis (L) Carr.	0.8-1.3	0.03-0.05
HARDWOODS	Aesculus californica (Spach) Nutt.		
	Fall and winter	0.8	0.03
	spring and summer	1.3	0.05
	Citrus aurantium L.		0.04
	Mixed hardwoods (Acer, Ulmus, Quercus, Betula)	0.5-1.8	0.02-0.07
	Mixed hardwoods West Virginia		
	Quercus rubra L., Liviodendron tulipifera L., etc.)		
	Summer	0.5	0.02
	Winter	0.2	0.006
	Northern hardwoods	2.0	0.08

Table 7.4 (continued)

Vegetation Element	Species	Storage Amount (mm)	(in.)
	Liquidamber stvraciflua L.	0.8	0.034
	All eastern N. American hardwood data	0.03-1.6	0.001-0.064
SHRUBS	Adenostonma fasciculatum H & A	1.3-1.5	0.05-0.06'
	Baccharis pilularis DC	0.5-1.5	0.02-0.06'
	Ceanothu cuneatus (Hook) Nutt., Arctostaphylos mariposa Dudley	1.5	0.06
	Cercocarpus ledifolius Nutt.	1.0	0.04'
	Photinia aributifolia Lindl.	0.3-1.8	0.01-0.07'
	Quercus dumosa Nutt. Cercocarpus betuloides Nutt. Ceanothus crossifolius	2.0	.0.08
GRASS	Annual grasses-Ca.	1.0-1.5	0.04-0.06'
	Secale cereale L.	1.3	0.05
FOREST FLOOR	Liriodendron tulipfera L., Hicoria spp. Quercus coccinea Muenchh.	1.4	0.057
	Pinus ponderosa laws 20-24 yr	2.3	0.09
	70-80 yr	8.1	0.32
	140-160 yr	11.2	0.44
	Pinus radiata D.Don 5-10 yr	0.5	0.02
	10-15 yr	1.0	0.04
	15-20 yr	1.8	0.07
	25-30 yr	3.6	0.14

*Precipitation as rain unless indicated as snow(*) or artificial sprinkling (').

estimated at about 0.05 to 0.1. The interception depth is computed as the percent of cover times the selected interception value for the vegetative type.

Climatic Data

Two types of climatic data are important in modeling of water and sediment yields. The most important is rainfall data and the other is temperature. Temperature is used to scale the hydraulic conductivity in the soil between various seasons of the year. Because hydraulic conductivity is a function of viscosity as temperature rises so does the conductivity. Therefore, conductivities that represent winter rainfalls will be too low for summer storms. Since this is a scaling procedure, air temperatures themselves are not scaled but the corresponding water viscosities. Because temperature change is such a widespread phenomena, use of temperatures from any nearby similar area is satisfactory.

The measurement of precipitation forms an integral part of watershed modeling. Information on precipitation-amount, intensity, frequency, and duration is essential in determining the water and sediment yield from a watershed. The primary source of quality rainfall data is a network of of recording raingages. This data should consist of gage locations, time of recording, and volume or depth of rain at the recording time. From this information and records from standard raingages, a spatial and temporal description of the storm can be developed from which the rainfall hyetograph for each modeled area is obtained. If gaged records are not available for an area, design storms can be generated from publications such as U. S. Weather Bureau TP40 (Hershfield, 1961), and nondimensional accumulated volume-time curves. These design storms can then be used to drive a model to study watershed or road response to listic input.

Channel and Flow Resistance Information

Channel data includes flow resistance coefficients, channel geometry parameters and channel bed sediment characteristics. Flow resistance is estimated after a visual or photographic inspection of the flow surface.

Overland flow resistance is defined using the Darcy-Weisbach friction factor as

$$f = \frac{k}{Re} \qquad 1\text{-}105$$

where f is the Darcy-Weisbach friction factor, k is an overall flow resistance parameter and Re is the Reynolds number of the overland flow. Reynolds number is the ratio of internal forces to viscous forces in flowing water. Overland flow resistance parameters will vary depending on the flow surface. Suggested values for the upper and lower overall resistance factors are given in Table 7.5 from Woolhiser (1975).

Table 7.5. Overall resistance parameters for overland flow.

Surface	Range of Parameter
Concrete or Asphalt	24 - 108
Bare Sand	30 - 120
Graveled Surface	90 - 400
Bare Clay - Loam Soil (eroded)	100 - 500
Sparse Vegetation	1000 - 4000
Short Grass Prairie	3000 - 10000
Bluegrass Sod	7000 - 40000

A forest floor may have a lower value of 100 for the bare soil surface up to 40,000 for the dense ground cover. Similarly a grain resistance Darcy-Weisbach friction factor is used in the models. A good estimate for the corresponding grain resistance parameter is in the range of 45 to 50.

An estimate of Manning's n value can be used to determine a resistance parameter specifically for channel flow. The channel flow resistance parameter or Darcy-Weisbach friction factor, f, can be related to Mannings n as

$$f = \frac{116\ n^2}{R^{1/3}} \qquad 1\text{-}106$$

where R is the hydraulic radius in feet of the channel flow.

Channel geometry is usually determined by on-site measurements of cross sections. These measurements can be converted to sets of geometric relationships between depth, area, wetted perimeter, and top width. Recently, Simons, Li, and Ward (1978) presented a method for acquiring channel cross section measurements from stream photographs.

7.8 SUMMARY

Presented in this chapter are some of the efforts at Colorado State University related to water routing from watersheds. Details of sediment routing are given in Chapter 10.

Models being developed, used, and improved are based on physical processes and therefore reflect changes in the natural system much more meaningfully than models based on regression analysis. This allows these process models to be widely used and easily transferable if the limitations of each model are recognized.

Computer based process models are a very useful tool in predicting and planning. However, more research is needed to perfect and simplify these models before they are widely accepted.

7.9 REFERENCES

Bouwer, H., "Infiltration of Water into Non-uniform Soil," Journal of the Irrigation and Drainage Division, ASCE, Vol. 95, No. IR4, December 1969, pp. 451-462.

Bouwer, H., "Infiltration into Increasingly Permeable Soils," Journal of the Irrigation and Drainage Division, ASCE, Vol. 102, No. IR1, March 1976, pp. 127-136.

Brakensiek, D. L., "Kinematic Flood Routing," ASAE, Vol. 10, No. 3, pp. 340-343, 1967.

Brakensiek, D. L., Discussion of "Infiltration of Water into Non-uniform Soils," by H. Bouwer, Journal of the Irrigation and Drainage Division, ASCE, Vol. 96, IR3, September 1970, pp. 358-360.

Carvallo, H. O., Cassel, D. K., Hamnand, J. and Bauer, A., "Spatial Variability of Insitu Unsaturated Hydraulic Conductivity of Maddock Sandy Loam," Soil Science, Vol. 121, No. 1, January, 1976.

Chen, C. L., "Flow Resistance in Broad Shallow Greased Channels," Journal of the Hydraulics Division, ASCE, Vol. 102, No. HY3, March, 1976, pp. 307-322.

Chow, V. T., Open Channel Hydraulics, McGraw-Hill Book Company, New York, 1959.

Eagleson, P. S., Dynamic Hydrology, McGraw-Hill, New York, 1970.

Eggert, K. G., "Modeling the Unsteady Infiltration Process," M.S. Thesis, Colorado State University, Fort Collins, Colorado, 1976.

Eggert, K. G., Li, R. M., and Simons, D. B., "Time Explicit Formulation of the Green-Ampt Infiltration Equation," Proceedings of the XVIIIth International Congress of the IHRA in Italy to be held in September 1979.

Green, W. H. and G. A. Ampt, "Studies on Soil Physics part 1: The Flow of Air and Water through Soils," Journal of Agriculture Science, May, 1911.

Harley, B. M., Perkins, F. E., and Eagleson, P. S., "A Modular Distributed Model of Catchment Dynamics," MIT, Department of Civil Engineering, Hydrodynamics Laboratory Report No. 133, June, 1970.

Henderson, F. M., Open Channel Flow, Macmillan, New York, 1966.

Hershfield, M. T., "Rainfall Frequency Atlas of the U.S.," 1961.

Houghton, D. P. and Kasahara, A., "Nonlinear Shallow Fluid Flow over an Isolated Ridge," Communication on Pure and Applied Mathematics, Vol. XXI, 1968.

Iwagaki, Y., "Fundamental Studies on Runoff Analysis by Characteristics," Disaster Prevention Research Institute Bulletin No. 10, Kyoto University, Kyoto, Japan, 1955.

Kibler, D. F. and Woolhiser, D. A., "The Kinematic Cascade as a Hydrologic Model," Hydrology Paper No. 39, Colorado State University, Fort Collins, Colorado, 1970.

Kouwen, N. and Unny, T. E., "Flow Retardance in Vegetated Channels," Journal of Irrigation and Drainage Division, ASCE, Vol. 95, No. IR2, June 1969, pp. 329-342.

Li, R. M., "Mathematical Modeling of Response from Small Watershed," Ph.D. Dissertation, Department of Civil Engineering, Colorado State University, Fort Collins, Colorado, 1974.

Li, R. M. and Shen, H. W., "Effect of Tall Vegetation on Flow and Sediment," Journal of Hydraulics Division, ASCE, Vol. 99, No. HY5, May 1973, pp. 793-814.

Li, R. M. and Simons, D. B., "In-Field Estimation of Infiltration Parameters," Colorado State University Report prepared for United States Department of Agriculture Forest Service, Rocky Mountain Range and Experiment Station, Flagstaff, Arizona, CER76-77, RML-DBS43, August 1977.

Li, R. M., Simons, D. B., and Eggert, K. G., "Process Model of Infiltration and Subsurface Flow Routing," Colorado State University Report, CER76-77RML-DBS-KGE20, prepared for USDA Forest Service, Rocky Mountain Forest and Range Experiment Station, Flagstaff, Arizona, December 1976.

Li, R. M., Simons, D. B., and Eggert, K. G., "Process Model of Infiltration and Subsurface Flow Routing," Colorado State University Report CER76-77RML-DBS-KGE20. Prepared for USDA Forest Service, Rocky Mountain Forest and Range Experiment Station, Flagstaff, Arizona, December 1976a.

Li, R. M., Simons, D. B., Shiao, L. S., and Chen, Y. H., "On Kinematic Wave Approximation for Flood Routing," Rivers 76, Vol. 1, 3rd Annual Symposium on Inland Waterways for Navigation, Flood Control and Water Diversion, Colorado State University, Fort Collins, Colorado, August 1976c, pp. 377-398.

Li, R. M., Simons, R. K., and Simons, D. B., "A Generalized Kinematic Wave Approximation for Flood Routing," paper submitted to Journal of Hydraulic Division, ASCE for possible publication, 1976b.

Li, R. M., Simons, D. B. and Stevens, M. A., "Nonlinear Kinematic Wave Approximation for Water Routing," Water Resources Research, Vol. 11, No. 2, 1975a.

Li, R. M., Simons, D. B., and Stevens, M. A., "On Overland Flow Water Routing," Proceedings of the National Symposium on Urban Hydrology and Sediment Control, Lexington, Kentucky, July 1975b.

Li, R. M., Simons, D. B., and Stevens, M. A., "Nonlinear Kinematic Wave Approximation for Water Routing," Water Resources Research, Vol. 11, No. 2, April 1975.

Li, R. M., Stevens, M. A., and Simons, D. B., "Solutions to Green-Ampt Infiltration Equations," Journal of the Irrigation and Drainage Division, ASCE, Vol. 102, No. IR2, June 1976, pp. 239-248.

Mein, R. G. and Larson, C. L., "Modelling the Infiltration Component of the Rainfall-Runoff Process," Water Resources Research Center, Minneapolis, 1971.

Morel-Seytoux, H. J. and Khanji, J., "Derivation of an Equation of Infiltration," Water Resources Research, Vol. 10, No. 4, August 1974, pp. 795-800.

Palmer, V. J., "Retardance Coefficients for Low Flow in Channels Lined with Vegetation," Trans. AGU, Vol. 27, pp. 187-197, 1946.

Phelps, H. O., "The Friction Coefficient for Shallow Flows over a Simulated Turf Surface," Water Resources Research, Vol. 6, No. 4, August 1970, pp. 1220-1226.

Ree, W. O., "Hydraulic Characteristics of Vegetation for Vegetated Waterways," Agricultural Engineers, Vol. 30, No. 4, pp. 184-189, 1949.

Ree, W. O. and Palmer, V. J., "Flow of Water in Channels Protected by Vegetative Linings," U.S. Soil Conservation Technical Bulletin No. 967, 1949.

Schaake, J. C., Jr., "Synthesis of the Inlet Hydrograph," Tech. Rep. 3, Storm Drainage Project, Johns Hopkins Univ., Baltimore, Md., June 1965.

Simons, D. B. and Li, R. M., "Watershed Segmentation by a Digital Computer for Mathematical Modeling of Watershed Response," Colorado State University Report, CER75-76DBS-RML9, prepared for USDA Forest Service, Rocky Mountain Forest and Range Experiment Station, Flagstaff, Arizona, 1975.

Simons, D. B., Li, R. M., and Eggert, K. G., "Storm Water and Sediment Runoff Simulation for Upland Watersheds Using Analytical Routing Technique," Volume I--Water Routing and Yield, Colorado State University Report CER77-78DBS-RML-DGE16, prepared for USDA Forest Service, Rocky Mountain Forest and Range Experiment Station, Flagstaff, Arizona, April 1977.

Simons, D. B., Li, R. M., and Eggert, K. G., "Simple Water Routing and Yield Model Using a Small Programmable Calculator," Colorado State University Report for USDA Forest Service, Rocky Mountain Forest and Range Experiment Station, Flagstaff, Arizona, CER76-77DBS-RML-KGE52, April, 1977a.

Simons, D. B., Li, R. M. and Spronk, B. E., "Storm Water and Sediment Runoff Simulation for a System of Multiple Watersheds," Vol. I, Water Routing and Yield, Draft Report Prepared for USDA Forest Service, Rocky Mountain Forest and Range Experiment Station, April 1978.

Simons, D. B., Li, R. M., and Stevens, M. A., "Development of Models for Predicting Water and Sediment Routing and Yield from Storms on Small Watershed," USDA Forest Service, Rocky Mountain Forest and Range Experiment Station, August, 1975.

Simons, D. B., Li, R. M., and Ward, T. J., "Estimation of Parameters that Describe Channel Geometry for Watershed Modeling," Colorado State University Draft Report Prepared for USDA Forest Service, Rocky Mountain Forest and Range Experiment Station, Flagstaff, Arizona, December 1978.

Simons, R. K., "A Modified Kinematic Approximation for Water and Sediment Routing," M.S. Thesis, Colorado State University, Fort Collins, Colorado, 1977.

Singh, V. P., "A Distributed Approach to Kinematic Wave Modeling of Watershed Surface Runoff," Proceedings of National Symposium on Urban Hydrology and Sediment Control, July 28-31, University of Kentucky, 1975, pp. 227-236.

Woolhiser, D. A., "Simulation of Unsteady Overland Flow," In Unsteady Flow in Open Channels, edited by K. Mahmood and V. Yevjevich, Water Resources Publications, Fort Collins, Colorado, 1975.

Wenzel, H. G., "The Effects of Raindrops Impact and Surface Roughness on Sheet Flows," WRC Research Report No. 34, University of Illinois, Water Resources Center, Urbana, Illinois, 1970.

Zinke, P. J., "Forest Interception Studies in the United States," Forest Hydrology, W. E. Sopper, Editor, Pergamon Press, Oxford, 1967.

Chapter 8

WATER ROUTING IN RIVERS

Yung H. Chen, Assistant Professor, Department of Civil Engineering
Colorado State University, Fort Collins, Colorado

8.1 INTRODUCTION

The study of flow dynamics in open channel systems is of vital importance in the design of hydraulic structures and water resource systems and in the analyses of river mechanics problems and the development of river control works. Flow in a river system is usually gradually varied and unsteady. In general this type of flow can be simulated by a mathematical model derived from the equations of continuity and momentum, which are expressed as one-dimensional nonlinear partial differential equations. These equations are also called the St. Venant equations.

The analytical solution of these equations is not possible for a complete equation. However, there are some analytical solutions for the simplified form of these equations. When the storage effect is the important phenomenon, only the continuity equation is used. This model is called the Storage Routing. The Kinematic Wave Model takes into account the storage and friction effects of flow using the continuity equation and the momentum equation with the bottom slope equal to the friction slope. The Diffusion Wave Model uses the continuity equation plus the momentum equation with the water surface slope equal to the friction slope. When the two complete St. Venant equations are used it is called the Dynamic Wave Model. The first two models are usually used when the bottom slope is much greater than the other terms of the momentum equation (Henderson, 1968). These methods can not be applied when there are significant backwater effects or inversion flow, as occurs in some rivers near the sea or near the confluence of a tributary of the main river. Ponce et al. (1978) discussed the applicability of Kinematic and Diffusion models by comparing the propagation characteristics of sinusoidal perturbations to the steady uniform flow. They concluded that the important physical characteristics in determining the applicability of the approximate models are the bed slope and wave period and the Diffusion Model has a wider range of application than the Kinematic Model. The simplified solution of the equations is reviewed in Chapter 6. In this chapter, only the solution of the complete St. Venant equations is presented.

The one-dimensional flow equations assume that the transverse and vertical velocities are low compared to the longitudinal one. In rivers or estuaries where the sections are wide, the one-dimensional assumption is usually invalid. In this case two-dimensional models are used to

simulate velocities in the transverse and longitudinal directions. A three-dimensional model can be used when vertical stratification is also important. However, because of its extreme complicity, the practical application of a three-dimensional model is very limited.

There are some rivers and estuaries with a complex system of branches, loops and confluences. The flow division among the confluences and the tide effect from downstream complicates the problem. A broad river network system is not only expensive to simulate utilizing two- or three-dimensional models, but the data required are difficult and expensive to obtain. The one-dimensional assumption is the best choice if it does not create serious errors in the solution.

This chapter describes the one-dimensional water routing models applied to study unsteady flow problems in a simple river system and in a complex river network system. Also a two-dimensional water routing model is presented.

8.2 ONE-DIMENSIONAL WATER ROUTING MODEL OF A SIMPLE RIVER SYSTEM

Basic Equations

One century ago, St. Venant developed the equations for gradually varied unsteady river flow, based on the conservation of mass and the conservation of momentum. The derivation of the one-dimensional version of these equations has been described by Chow (1959), Harleman (1971), Chen (1973), Yen (1973), and Liggett (1975).

The gradually varied unsteady water flow in a river can be described by two equations: the water continuity equation which take into account the continuity of mass flow, and the momentum equation which represents the dynamic effects of the flow. The basic assumptions made in the derivation of the equations are:

1. The channel is sufficiently straight and uniform in the reach so that the flow characteristics may be physically represented by a one-dimensional model.
2. Hydrostatic pressure prevails at every point in the channel.
3. The water surface slope is small.
4. The resistance coefficient is assumed to be the same as that for steady flow in open channels and can be approximated from resistance equations applicable to open channels or from field survey.

The two basic equations derived are:

(1) The flow continuity equation:

$$\frac{\partial Q}{\partial x} + T\frac{\partial y}{\partial t} - q_\ell = 0 \qquad (8\text{-}1)$$

(2) The flow momentum equation:

$$\frac{\partial Q}{\partial t} + \frac{\partial \beta\, Q|V|}{\partial x} + g\,A\frac{\partial y}{\partial x} = \rho g\, A(S_o - S_f + D_\ell) \qquad (8\text{-}2)$$

where x = horizontal distance along the channel

t = time

A_d = volume of sediment deposited on channel bed per unit of length of channel, the value of which is negative when bed erosion occurs

A = water cross-sectional area

Q = flow discharge

q_s = lateral sediment flow per unit length of channel, a positive quantity indicates inflow and a negative value denotes outflow

q_w = lateral water flow per unit length of channel, a positive quantity indicates inflow and a negative value denotes outflow

q_ℓ = lateral flow per unit length of channel, given by $q_s + q_w$

β = momentum coefficient

V = mean flow velocity

T = $\partial A/\partial y$

y = flow depth

g = acceleration of gravity

S_o = bed slope

S_f = friction slope

D_ℓ = dynamic contribution of lateral discharge given by $q_\ell V_\ell/Ag$

V_ℓ = velocity component of lateral inflow in the main flow direction

h = water surface elevation

z = riverbed elevation

Δz = change in riverbed elevation

B = top width

Figure 8.1 is a definition sketch of an alluvial channel. In Equation 8-2 to adequately consider the dynamic effects, an absolute value of velocity $|V|$ is used in the convective acceleration term to preserve the flow vector.

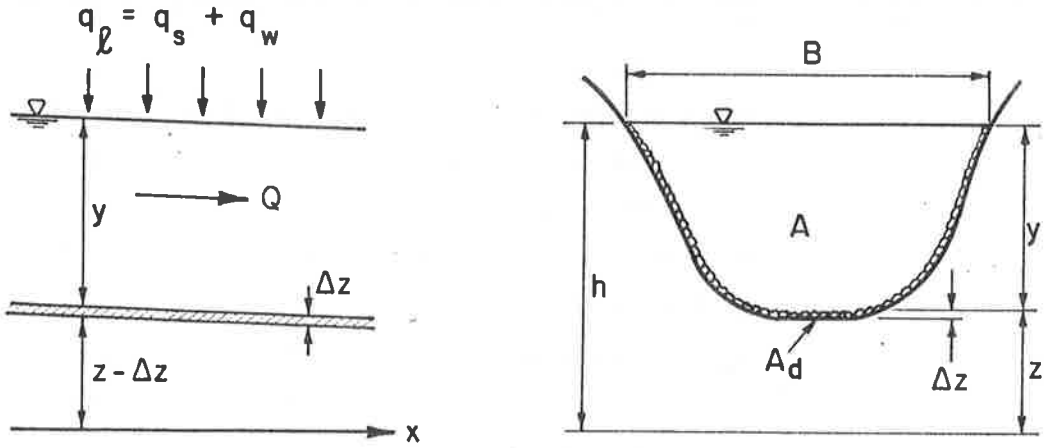

Figure 8.1 Definition sketch of an alluvial channel.

Supplemental Equations

Equations 8-1 and 8-2 contain two basic unknowns: Q and y. The other variables in the equations must be expressed as a function of the two unknowns in order to obtain a solution. These supplementary equations describe the physical properties of the prototype.

1. The geometric properties of cross sections are expressed as a function of stage from the unknown channel geometry.

2. The mean bed slope

$$S_o = -\partial z/\partial x \tag{8-3}$$

in which the bed elevation z is known.

3. The friction slope S_f is a function of flow and channel characteristics. The resistance functions such as Manning's or Chezy's equations can be employed to relate to S_f with the basic unknowns.

That is

$$S_f = \frac{Q|Q|}{K_i^2} \tag{8-4}$$

where K_i = total conveyance for section i at a given stage h_i. Considering a channel with nonuniform cross-sectional shape and resistance, the conveyance for a subsection k (e.g., see Figure 8.2) is defined by

$$K_{ki} = \frac{1.486}{n_{ki}} A_{ki}^{5/3} P_{ki}^{-2/3} \tag{8-5}$$

where A_{ki} and P_{ki} are cross-sectional area and wetted perimeter at subsection k, respectively. The total conveyance is then

$$K_i = \sum_k K_{ki} \tag{8-6}$$

A simplified relation for K_i is

$$K_i = \frac{1.486}{n_i} A_i^{5/3} P_i^{-2/3} \tag{8-7}$$

where n_i, A_i and P_i are overall Manning's roughness coefficient, cross-sectional area and wetted perimeter at section i, respectively.

4. The lateral inflow discharge q_ℓ is considered as known function of time and space.

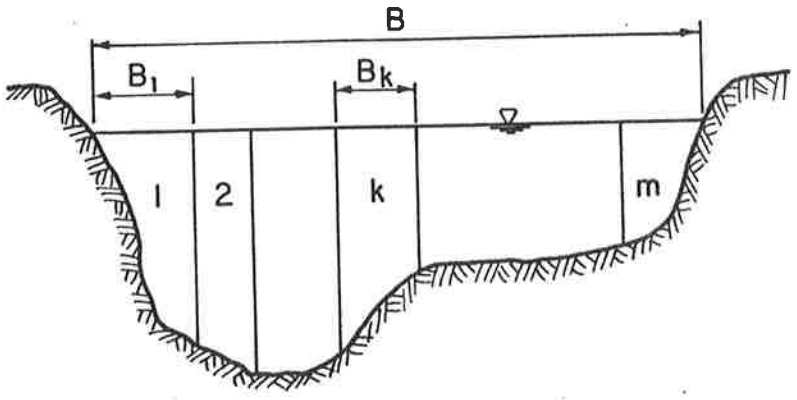

Figure 8.2 Channel elements to calculate the section conveyance of a composite cross section.

Numerical Solution of Basic Equations

The finite-difference numerical solution of Equations 8-1 and 8-2 can proceed in two directions. Either an attempt can be made to convert the original system of partial differential equations into an equivalent system of ordinary differential equations by using the method of characteristics (De Vries, 1965; Amein, 1966; Liggett and Woolhiser, 1967; Wylie, 1970; Chang and Richards, 1971; Chen, 1973), or one can replace the partial derivatives in the original system with quotients of finite-differences by using the explicit method or the implicit method (Preissmann, 1961; Abbott and Ionescu, 1967; Baltzer and Lai, 1968; Ballofet, 1969; Amein and Fang, 1970; Contractor and Wiggert, 1972; Chen, 1973; Vreugdenhill, 1973; Fread, 1976). The finite element method was also used to solve the one-dimensional equation by Gunaratnam and Perkin (1970), Keuning (1976), Cooley and Moin (1976), Partridge and Brebbia (1976).

In general, the finite-difference method is simpler and easier to apply in the one-dimensional modeling than the finite-element model. Therefore, the former method is used in this chapter to solve the unsteady flow equation. The various finite-difference solution techniques frequently used for flood routing pruposes (Chen, 1973; Price, 1974) are:

1. Characteristic equations in explicit or implicit finite-difference form, solved in a curvilinear network of time and distance;
2. Characteristic equations in explicit or implicit finite-difference form, solved in a fixed rectangular time-distance network;
3. The original equations in implicit finite-difference form, solved in a fixed rectangular time-distance grid; and
4. The original equations in explicit finite-difference form, solved in a fixed rectangular time-distance network.

The choice of a numerical technique for a particular case should be made with regard to its accuracy, stability and convenience in use. Accuracy refers to the closeness of the computed values to the actual or true values. Stability problems are usually identified in the computed results as oscillations of the computed values. The basic disadvantage of the explicit method is the requirement of a short time interval which needs high cost of computation. In practical problems, the grid is dictated by channel geometry which makes the solution by the characteristic

method more difficult to achieve. Amein and Fang (1970) found that the implicit method is unconditionally stable and is faster and more accurate than other finite-difference methods when applied to flood routing in open channels. Price (1974) also came up with a similar conclusion after comparing four numerical methods for flood routing. Therefore, the implicit method is used for solving the basic governing equations.

A widely accepted implicit finite-difference scheme to approximate a function $f(x, t)$ and its derivatives of $\partial f/\partial x$ and $\partial f/\partial t$ at Point B in Figure 8.3 is (Preissman, 1960; Richtmyer and Morton, 1967)

$$f_B(x,t) \simeq \lambda \frac{f_i^{j+1} + f_{i+1}^{j+1}}{2} + (1-\lambda) \frac{f_i^j + f_{i+1}^j}{2}$$

$$\left.\frac{\partial f}{\partial x}\right|_B \simeq \lambda \frac{f_{i+1}^{j+1} - f_i^{j+1}}{\Delta x} + (1-\lambda) \frac{f_{i+1}^j - f_i^j}{\Delta x} \qquad (8\text{-}8)$$

and

$$\left.\frac{\partial f}{\partial t}\right|_B \simeq \frac{1}{2} \left\{\frac{f_i^{j+1} - f_i^j}{\Delta t} + \frac{f_{i+1}^{j+1} - f_{i+1}^j}{\Delta t}\right\}$$

where $f_i^j = f(x_i, t^j)$, $f_{i+1}^j = f(x_{i+1}, t^j)$, representing Q , A, T, etc., and $\lambda = \delta t/\Delta t$, δt is the distance of the point B on the time axis from the old time line, $\Delta x = x_{i+1} - x_i$ and $\Delta t = t^{j+1} - t^j$. Equation 8-8 is also named the four-point implicit scheme. Such an approach

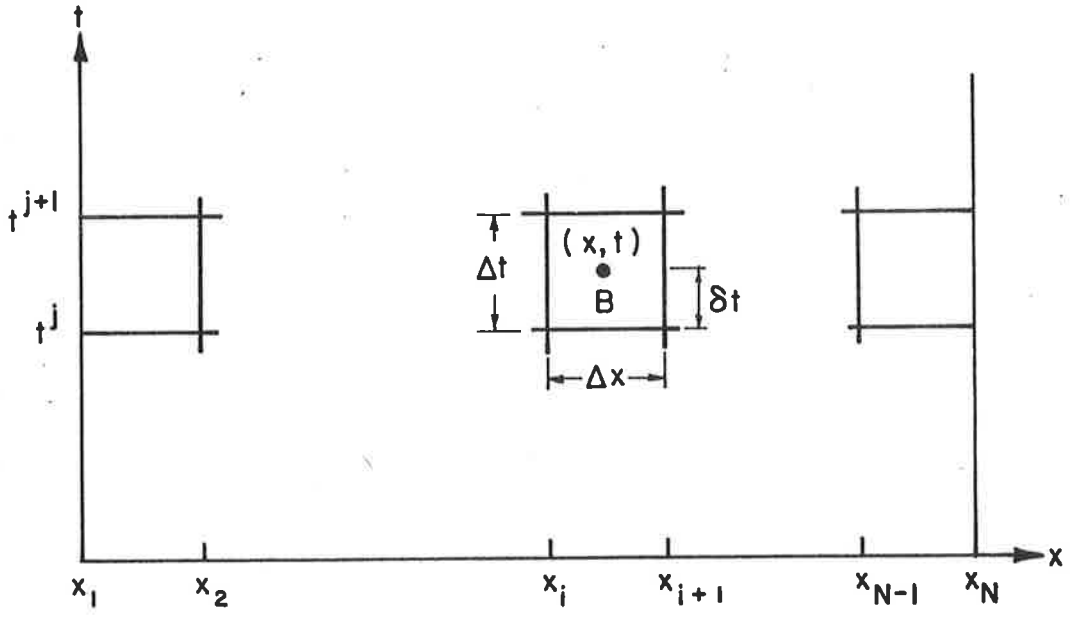

Figure 8.3 Network for the implicit method.

permits the use of varying values of Δt and Δx which may be required to cover the specified points in the x-t network of Figure 8.3. For $\lambda = 1/2$, the scheme is center-implicit; for $\lambda = 1$, the scheme is fully implicit; and for $\lambda = 0$, the scheme is fully explicit. Liggett and Cunge (1975) show that the difference scheme is numerically stable for $1/2 \leq \lambda \leq 1$ and it is always unstable for $\lambda < 1/2$. They recommend the use of λ in the range $0.6 \leq \lambda \leq 1.0$ in order to avoid numerical oscillations. For greater value of λ the solution is less accurate but more stable. Chen (1973) modified Preissmann's (1960) and Amein and Fang's (1970) methods to derive an unconditionally stable and convenient linear implicit method as

$$f \simeq \frac{1}{2} (f_i^j + f_{i+1}^j)$$

$$\frac{\partial f}{\partial x} \simeq \frac{1}{\Delta x} (f_{i+1}^{j+1} - f_i^{j+1}) \qquad (8\text{-}9)$$

and

$$\frac{\partial f}{\partial t} \simeq \frac{1}{2\Delta t} [(f_i^{j+1} - f_i^j) + (f_{i+1}^{j+1} - f_{i+1}^j)]$$

Stability and convergency of numerical schemes will be discussed in a later section.

As the finite-difference approximations (Equation 8-8) are substituted into flow continuity Equation 8-1 and momentum Equation 8-2, the following equations are obtained:

$$\frac{\lambda}{\Delta x} (\Delta Q_{i+1} - \Delta Q_i) + \frac{1}{\Delta x} (Q_{i+1}^j - Q_i^j) + \frac{T_{i+1}}{2\Delta t} \Delta y_{i+1} + \frac{T_i}{2\Delta t} \Delta y_i$$

$$- \frac{1}{2} (q_{\ell_{i+(\frac{1}{2})}}^j + q_{\ell_{i+(\frac{1}{2})}}^{j+1}) = 0 \qquad (8\text{-}10)$$

and

$$\frac{1}{2\Delta t} (\Delta Q_i + \Delta Q_{i+1}) + \frac{\lambda}{\Delta x} [2(\beta |V|)_{i+1}^j \Delta Q_{i+1} - (\beta V |V| T)_{i+1}^j \Delta y_{i+1}$$

$$- 2 (\beta |V|)_i^j \Delta Q_i + (\beta V |V| T)_i^j \Delta y_i] + \frac{1}{\Delta x} [(\beta Q |V|)_{i+1}^j - (\beta Q |V|)_i^j]$$

$$+ \frac{g\lambda}{2\Delta x} [(A_{i+1}^j + A_i^j) + (y_{i+1}^j - y_i^j) T_{i+1}^j] \Delta y_{i+1}$$

$$+ \frac{g\lambda}{2\Delta x} [(y_{i+1}^j - y_i^j) T_i^j - (A_{i+1}^j + A_i^j)] \Delta y_i$$

$$+ \frac{g}{2\Delta x} (A^j_{i+1} + A^j_i) (y^j_{i+1} - y^j_i) = \frac{g}{2\Delta x} (A^j_{i+1} + A^j_i) (z^j_i - z^j_{i+1})$$

$$+ \frac{\lambda g}{2\Delta x} (T^j_i \Delta y_i + T^j_{i+1} \Delta y_{i+1}) (z^j_i - z^j_{i+1})$$

$$- \frac{g\lambda}{4} [(S_{f}{}^j_{i+1} + S_{f}{}^j_i) T^j_{i+1} + (A^j_{i+1} + A^j_i) (\frac{\partial S_f}{\partial y})^j_{i+1}] \Delta y_{i+1}$$

$$- \frac{g\lambda}{4} [(S_{f}{}^j_{i+1} + S_{f}{}^j_i) T^j_i + (A^j_{i+1} + A^j_i) (\frac{\partial S_f}{\partial y})^j_i] \Delta y_i$$

$$- \frac{g\lambda}{4} (A^j_{i+1} + A^j_i) (\frac{\partial S_f}{\partial Q})^j_{i+1} \Delta Q_{i+1} - \frac{g\lambda}{4} (A^j_{i+1} + A^j_i) (\frac{\partial S_f}{\partial Q})^j_i \Delta Q$$

$$- \frac{g}{4} (A^j_{i+1} + A^j_i) (S_{f}{}^j_{i+1} + S_{f}{}^j_i) + \frac{1}{2} [(q_\ell V_\ell)^j_{i+(\frac{1}{2})} + (q_\ell V_\ell)^{j+1}_{i+(\frac{1}{2})}] \quad (8\text{-}11)$$

in which λ is the weighting factor, and

$$\frac{\partial S_f}{\partial Q} \simeq 2 S_f (\frac{1}{Q} + \frac{1}{n} \frac{\partial n}{\partial Q}) \quad (8\text{-}12)$$

and

$$\frac{\partial S_f}{\partial y} \simeq -2 \frac{S_f}{K} \frac{\partial K}{\partial y} \quad (8\text{-}13)$$

Rearranging Equations 8-10 and 8-11 yields:

$$A_i \Delta Q_i + B_i \Delta y_i + C_i \Delta Q_{i+1} + D_i \Delta y_{i+1} = E_i \quad (8\text{-}14)$$

and

$$A'_i \Delta Q_i + B'_i \Delta y_i + C'_i \Delta Q_{i+1} + D'_i \Delta y_{i+1} = E'_i \quad (8\text{-}15)$$

in which the coefficients A, B, C, D, and E are functions of variables evaluated at the time step t^j for $1 \leq i \leq N - 1$ and therefore are known. The expression for the coefficients are given below:

$$\begin{aligned} A_i &= -2\theta\lambda \\ B_i &= T_i \\ C_i &= -A_i \\ D_i &= T_{i+1} \\ E_i &= -2\theta (Q^j_{i+1} - Q^j_i) + \Delta t (q_{\ell}{}^j_{i+(\frac{1}{2})} + q_{\ell}{}^{j+1}_{i+(\frac{1}{2})}) \end{aligned} \quad (8\text{-}16)$$

and

$$A'_i = 1. - 4\theta\lambda\,(\beta|V|)^j_i + \frac{1}{2}K_1K_2\lambda\,(\frac{\partial S_f}{\partial Q})^j_i$$

$$B'_i = 2\theta\lambda\,(\beta V|V|T)^j_i + g\theta\lambda\,(K_3T^j_i - K_2) - g\theta\lambda\,(z^j_i - z^j_{i+1})\,T^j_i$$

$$+ \frac{1}{2}K_1\,\lambda[K_4T^j_i + K_2\,(\frac{\partial S_f}{\partial y})^j_i] \qquad (8\text{-}17)$$

$$C'_i = 1 + 4\theta\lambda\,(\beta|V|)^j_{i+1} + \frac{1}{2}K_1K_2\lambda\,(\frac{\partial S_f}{\partial Q})^j_{i+1}$$

$$D'_i = -2\theta\lambda\,(\beta V|V|T)^j_{i+1} + g\theta\lambda\,(K_2 + K_3\,T^j_{i+1}) - g\theta\lambda\,(z^j_i - z^j_{i+1})\,T^j_{i+1}$$

$$+ \frac{1}{2}K_1\,\lambda[K_4T^j_{i+1} + K_2\,(\frac{\partial S_f}{\partial y})^j_{i+1}]$$

$$E'_i = -2\theta\lambda\,[(\beta Q|V|)^j_{i+1} - (\beta Q|V|)^j_i] - g\theta K_2K_3 + g\theta K_2\,(z^j_i - z^j_{i+1})$$

$$- \frac{1}{2}K_1K_2K_4 + \Delta t\,[q_\ell V_\ell)^j_{i+(\frac{1}{2})} + (q_\ell V_\ell)^{j+1}_{j+(\frac{1}{2})}]$$

in which

$$\theta = \frac{\Delta t}{\Delta x}$$

$$K_1 = g\Delta t$$

$$K_2 = A^j_i + A^j_{i+1}$$

$$K_3 = y^j_{i+1} - y^j_i$$

$$K_4 = S_{f_i}{}^j + S_{f_{i+1}}{}^j$$

Boundary and Initial Conditions

There are two kinds of boundary conditions for one-dimensional water and sediment routing models: (1) exterior boundary conditions, at the ends of the model, and (2) interior boundary conditions.

Exterior Boundary Conditions

The exterior boundary conditions vary with the character of the flow. If the flow is tranquil (subcritical), the water routing solution is possible only when one condition is specified at the downstream end of

the reach. If the flow is supercritical the condition at the downstream boundary is redundant. For this type of flow the conditions cannot influence the upstream situation and the boundary conditions should be specified at the upstream boundary. The exterior boundary conditions are usually of three kinds: 1) the stage hydrograph, 2) the water discharge hydrograph, and 3) the stage-discharge rating curve.

For water routing in a river system at the upstream boundary, it is assumed that the gaging station flood hydrograph provides the flow depth or discharge as a function of time. The relation can be written as

$$C_0' \Delta Q_1 + D_0' \Delta y_1 = E_0' \tag{8-18}$$

in which C_0' or D_0' is usually zero and the other is unity, and E_0' equals $\Delta Q_1(t)$ or $\Delta y_1(t)$.

At the downstream boundary, a depth hydrograph, a discharge hydrograph, or a depth-discharge relationship can be used as a downstream boundary condition if the flow is subcritical. This relationship can be expressed in segment form as

$$A_N \Delta Q_N + B_N \Delta y_N = E_N \tag{8-19}$$

Significant error may be introduced when the relationship $Q = f(h)$ is imposed at the downstream boundary in subcritical flow. This relation is a single-valued function corresponding to the steady flow. The computed results of the unsteady flow in the reach upstream of this condition are biased within the range of the backwater influence. In this case one can try to prolong the reach fictitiously so as to displace the unsatisfactory condition as far downstream as possible.

Interior Boundary Conditions

The interior boundary conditions are all similar. There are always continuity conditions for discharges and another condition usually concerning the water stage or energy balance for water routing. Some examples are given below:

1) Junction of two rivers. The confluence is treated as an internal boundary according to Chen (1973) and Cunge (1975). Assuming a steady state flow condition at the junction as shown in Figure 8.4, the mass conservation of water is satisfied by the following equation:

$$Q_{k3} = Q_{k1} + Q_{k2} \tag{8-20}$$

and the conservation of energy is represented by the equations:

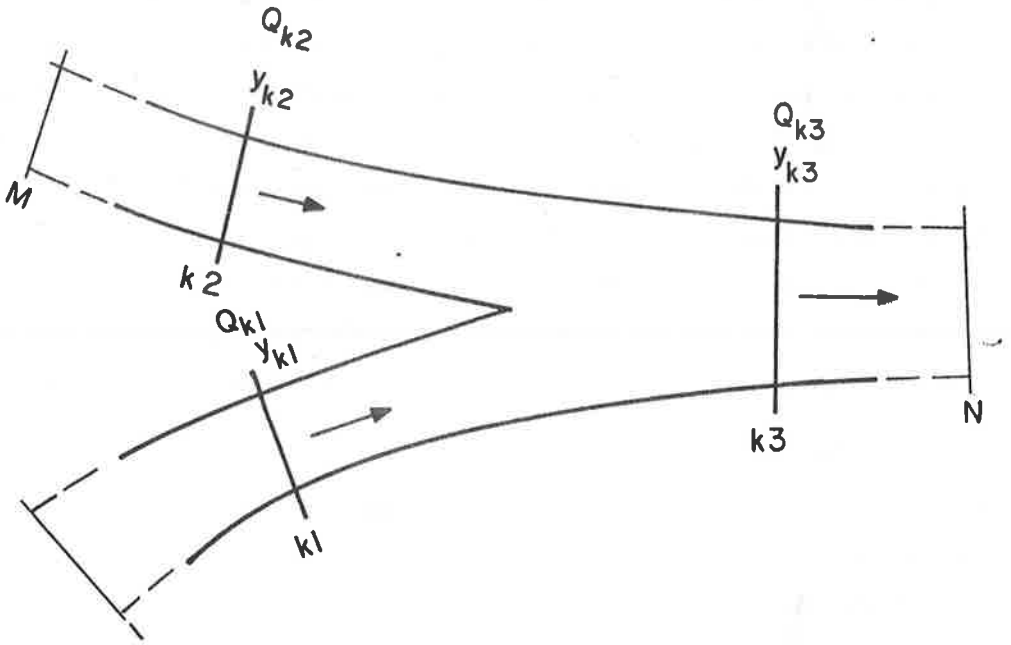

Figure 8.4 Joint sections at a confluence.

$$y_{k1} + z_{k1} + \frac{V_{k1}^2}{2g} = y_{k3} + z_{k3} + \alpha_{13} \frac{V_{k3}^2}{2g} + h_{f_{13}} \qquad (8\text{-}21)$$

$$y_{k2} + z_{k2} + \frac{V_{k2}^2}{2g} = y_{k3} + z_{k3} + \alpha_{23} \frac{V_{k3}^2}{2g} + h_{f_{23}} \qquad (8\text{-}22)$$

where α = correction factor for energy loss

h_f = energy head loss given by the product of the friction slope and the distance between sections

y = water depth

z = bed elevation

V = velocity

Substituting the numerical scheme given by Equation 8-9 to Equations 8-21 and 8-22:

$$z_{k1} + y_{k1}^{j+1} + \frac{1}{2g} \left[2 \left(\frac{V}{A}\right)^j Q^{j+1} - 2 \left(\frac{V^2\, T}{A}\right)^j y^{j+1} - (V^2)^j + 2 \left(\frac{V^2\, Ty}{A}\right)^j\right]_{k1}$$

$$= z_{k3} + y_{k3}^{j+1} + \frac{\alpha_{13}}{2g} \left[2 \left(\frac{V}{A}\right)^j Q^{j+1} - 2 \left(\frac{V^2\, T}{A}\right)^j y^{j+1} - (V^2)^j + 2 \left(\frac{V^2\, Ty}{A}\right)^j\right]_{k3}$$

$$+ \Delta x_{13} \left\{\frac{1}{2} \left(S_{f_{k1}}^j + S_{f_{k3}}^j\right) + \left[\left(\frac{S_f}{Q}\right)^j \left(Q^{j+1} - Q^j\right) - \left(\frac{S_f}{K} \frac{\partial K}{\partial y}\right)^j \left(y^{j+1} - y^j\right)\right]_{k1}\right.$$

$$\left. + \left[\left(\frac{S_f}{Q}\right)^j \left(Q^{j+1} - Q^j\right) - \left(\frac{S_f}{K} \frac{\partial K}{\partial y}\right)^j \left(y^{j+1} - y^j\right)\right]_{k3}\right\} \qquad (8\text{-}23)$$

Equation 8-23 results in

$$C_a\ Q_{k1}^{j+1} + C_b\ y_{k1}^{j+1} + C_c\ Q_{k3}^{j+1} + C_d\ y_{k3}^{j+1} = C_e \tag{8-24}$$

In the same way, Equation 8-22 results in the following equation by the use of the numerical scheme from Equation 8-9

$$C'_a\ Q_{k2}^{j+1} + C'_b\ y_{k2}^{j+1} + C'_c\ Q_{k3}^{j+1} + C'_d\ y_{k3}^{j+1} = C'_e \tag{8-25}$$

where

$$C_a = \left(\frac{V}{Ag}\right)_{k1}^{j} - \Delta x_{13}\left(\frac{S_f}{Q}\right)_{k1}^{j}$$

$$C_b = 1 + \left(\Delta x_{13}\frac{S_f}{K}\frac{\partial K}{\partial y} - \frac{V^2 T}{Ag}\right)_{k1}^{j}$$

$$C_c = -\alpha_{13}\left(\frac{V}{Ag}\right)_{k3}^{j} - \Delta x_{13}\left(\frac{S_f}{Q}\right)_{k3}^{j} \tag{8-26}$$

$$C_d = \alpha_{13}\left(\frac{V^2\ T}{Ag}\right)_{k3}^{j} + \Delta x_{13}\left(\frac{S_f}{K}\frac{\partial K}{\partial y}\right)_{k3}^{j} - 1$$

$$C_e = z_{k3} - z_{k1} - \alpha_{13}\left(\frac{V^2}{2g}\right)_{k3}^{j} + \left(\frac{V^2}{2g}\right)_{k1}^{j} + y_{k3}^{j}(C_d + 1)$$

$$- \frac{1}{2}\left(S_{f_{k1}} + S_{f_{k3}}\right)^{j} \Delta x_{13} + y_{k1}^{j}\ (C_b - 1)$$

The coefficients of Equation 8-25 are the same as above except the index changes. k_2 is used instead of k_1 and "23" instead of "13". Equations 8-21 and 8-22 can be simplified as follows:

$$h_{k1} = h_{k3} \tag{8-27}$$

$$h_{k2} = h_{k3} \tag{8-28}$$

These simplified equations are used when the velocity terms and the energy losses are small at the confluence.

2) Flow over weirs or closing dams (Figure 8.5).

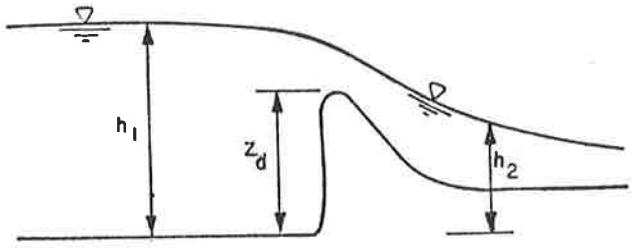

Figure 8.5 Flow over a weir.

To account for the effects of dams, the following equations are utilized to simulate water flowing over a dam:

i) Water continuity equation

$$Q_1 = Q_2 \tag{8-29}$$

ii) Water discharge equation

For free fall flow with $h_2 - z_d < \frac{2}{3}(h_1 - z_d)$

$$Q = C\, A_u\, (h_1 - z_d)^{1/2} \tag{8-30}$$

For submerged flow with $h_2 - z_d \geq \frac{2}{3}(h_1 - z_d)$

$$Q = C\, A_u\, (h_1 - h_2 - S_f\, \Delta x_{12})^{1/2} + Q_F \tag{8-31}$$

in which C = discharge coefficient, determined from an experimental study or from empirical relations such as these given by the USDI Bureau of Reclamation (1973)

A_u = flow cross-sectional area over the dam

S_f = average energy slope

Δx_{12} = distance between Sections 1 and 2

Q_F = overbank flow discharge at the dam

z_d = height of dam crest or gate sill

h = water surface elevation

1 and 2 = sections immediately above and below the dam, respectively.

Equation 8-29 can be written in a standard finite-difference equation form as Equation 8-14 by assigning $A_i = 1$, $B_i = 0$, $C_i = -1$, $D_i = 0$ and $E_i = 0$. By using Taylor's series expansion, Equation 8-30 and 8-31 can be linearized as

$$A_i' Q_1^{j+1} + B_i' y_1^{j+1} + C_i' Q_2^{j+1} + D_i' y_2^{j+1} = E_i' \tag{8-32}$$

in which for Equation 8-30

$$A_i' = 0.5,\ B_i' = [Q_1 \frac{T_u}{A_u} + \frac{Q_1}{2(h_1 - z_d)}]^j$$

$$C_i' = 0.5,\ D_i' = 0 \quad \text{and} \quad E_i' = Q_1^j + B_i' y_1^j \tag{8-33}$$

and for Equation 8-31

$$A_i' = \frac{1}{2}\left(1 + \frac{\Delta x_{12} \bar{S}_f}{h_1 - h_2 - \Delta x_{12} \bar{S}_f} \frac{Q_F}{Q}\right)^j_1$$

$$B_i' = - \left\{ S_1 + S_2 \left[1 + \Delta x_{12} \left(\frac{S_f}{\bar{K}} \frac{\partial K}{\partial y} \right)_1^j \right] + S_3 \right\}$$

$$C_i' = A_i'$$

$$D_i' = - \left\{ S_2 \left[- 1 + \Delta x_{12} \left(\frac{S_f}{\bar{K}} \frac{\partial K}{\partial y} \right)_2^j \right] \right\} \qquad (8\text{-}34)$$

$$E_i' = 2A_i' Q_1^j + B_i' y_1^j + D_i' y_2^j$$

$$S_1 = \left(\frac{Q_m T_u}{A_u} \right)^j$$

$$S_2 = \frac{1}{2} \left(\frac{Q_m}{h_1 - h_2 - \Delta x_{12} \bar{S}_f} \right)^j$$

$$S_3 = \frac{5}{3} \left(\frac{Q_f}{h_1 - z_F} \right)^j$$

3) Flow through control gates. The governing equations are:

i) Water continuity equation

$$Q_1 = Q_2 \qquad (8\text{-}35)$$

ii) Water discharge equation

For free fall flow through a gated dam

$$Q = C L a \sqrt{h_1 - z_d - a} \qquad (8\text{-}36)$$

For submerged flow through a gated dam

$$Q = C L a \sqrt{h_1 - h_2} \qquad (8\text{-}37)$$

where a = height of the gate opening

L = effective width of the gate

By using Taylor's series expansion, Equations 8-36 and 8-37 can be linearized to the standardized form of

$$A_i' Q_1^{j+1} + B_i' y_1^{j+1} + C_i' Q_2^{j+1} + C_i' y_2^{j+1} = E_i' \qquad (8\text{-}38)$$

in which for Equation 8-36

$$A'_i = \frac{1}{2}\ , \quad B' = -\left[\frac{Q}{2(h_1 - z_d - a)}\right]^j \tag{8-39}$$

$$C'_i = \frac{1}{2}\ , \quad D'_i = 0\ , \text{ and } \quad E'_i = Q^j \left(\frac{a^{j+1}}{a^j}\right) + B'_i\ (a^{j+1} - a^j + y_1^j)$$

and for Equation 8-37

$$A'_i = \frac{1}{2}\ , \quad B'_i = -\frac{1}{2}\left(\frac{Q}{h_1 - h_2}\right)^j$$

$$C'_i = \frac{1}{2}\ , \quad D'_i = \frac{1}{2}\left(\frac{Q}{h_1 - h_2}\right)^j\ , \text{ and} \tag{8-40}$$

$$E'_i = Q^j \left(\frac{a^{j+1}}{a^j}\right) + B'_i\ y_1^j + D'_i\ y_2^j$$

4) Storage basin. In some rivers there are storage basins linked to the channel as shown in Figure 8.6. They contribute only to the storage effect and the continuity equation should take this volume into account.

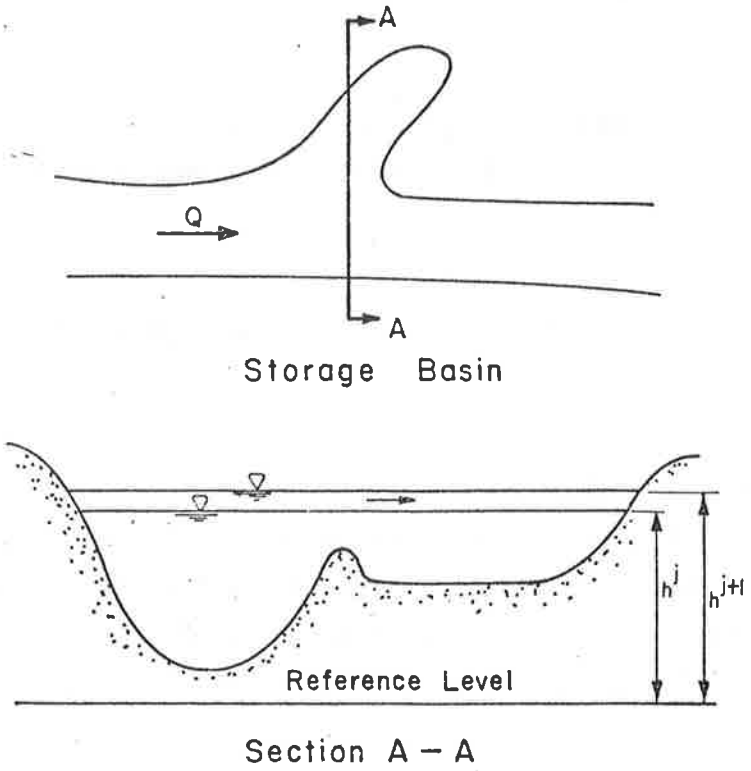

Figure 8.6 Storage basin as an interior boundary.

The volume lost by the river reach in Δt is

$$\frac{dV_F}{dt} = \frac{dV_F}{dy}\frac{dy}{dt} \tag{8-41}$$

Where V_F is the storage basin volume. Using a numerical approximation

$$\frac{dV_F}{dt} = \left(\frac{dV_F}{dy}\right)^j \frac{\Delta y}{\Delta t} \tag{8-42}$$

The function $V_F = f(y)$ is obtained from the maps. Equation 8-42 can be substituted for $(q_\ell \Delta x)$ in Equation 8-10. When this storage basin has dynamic effects on the flow, it can be assumed to be a flood area with more roughness than the normal river roughness.

5) Dead end. When there is a channel with a dead end, the section at that end may have the condition of $Q = 0$ at the dead end.

Initial Condition

In order to proceed to the calculations it is necessary to specify the level and discharge at all the sections in the initial time step. Usually these values are not known and one needs to estimate them. However, the initial values at the boundary are known and by using the program with about 50 or less time steps, and holding the boundaries constant, the steady state condition for the initial boundaries is reached. Another way is to interpolate the levels, making the discharges constant when there are no confluences nor lateral inflows. In case of confluences, adequate knwoledge of the system is required to specify these values by inspection. A third way is to solve the steady momentum equation using a backwater computation method.

Normally, in this type of equation, after some time steps, different initial conditions converge to the same solution. Baltzer and Lai (1968) showed the convergence to the same solution using different values of initial discharge.

Solution of Linear System of Basic Equations

There are N - 1 pairs of equations in the form of Equations 8-14 and 8-15, yielding 2(N - 1) equations. With the addition of two boundary conditions, Equations 8-18 and 8-19, the system of equations constitutes 2N linear algebraic equations in 2N unknowns. The coefficient matrix of this linear system of equations is a sparse diagonal matrix

(band matrix). This type of system can be solved efficiently by the double-sweep algorithm, which takes into account only the non-zero coefficients and is more accurate and use less storage and computer time than the methods which utilize the full matrix.

The following linear relationship can be shown to exist between the two unknowns at a given computation section:

$$\Delta Q_i = S_i \Delta y_i + T_i \tag{8-43}$$

If Equation 8-43 is substituted into Equations 8-14 and 8-15, the following equations result when written in terms of Δy_i:

$$\Delta y_i = (E'_i - A_i T_i - B_i \Delta Q_{i+1} - D_i \Delta y_{i+1})/(C_i + A_i S_i) \tag{8-44}$$

$$\Delta y_i = (E_i - A'_i T_i - B'_i \Delta Q_{i+1} - D'_i \Delta y_{i+1})/(C'_i + A'_i S_i) \tag{8-45}$$

The right-hand sides of Equation 8-44 and 8-45 can be equated, which after rearranging yields the following:

$$\Delta Q_{i+1} = \frac{D_i U_i - D'_i}{V_i} \Delta y_{i+1} + \frac{E'_i - A'_i T_i - U_i (E_i - A_i T_i)}{V_i} \tag{8-46}$$

where

$$U_i = (C'_i + A'_i S_i)/(C_i + A_i S_i) \tag{8-47}$$

$$V_i = B'_i - U_i B_i \tag{8-48}$$

Equation 8-46 is in the same form as Equation 8-43, and its coefficients are therefore defined by:

$$S_{i+1} = \frac{D_i U_i - D'_i}{V_i} \tag{8-49}$$

$$T_{i+1} = \frac{E'_i - A'_i T_i - U_i (E_i - A_i T_i)}{V_i} \tag{8-50}$$

Since the upstream boundary condition supplies S_1 and T_1, Equations 8-49 and 8-50 can be used as recursive formulas to calculate S_i and T_i for $i = 2,\ldots,N$. This would complete the forward sweep.

At the downstream boundary, the following equation exists

$$\Delta Q_N = S_N \Delta y_N + T_N \tag{8-51}$$

where S_N and T_N are known from the forward sweep. Equations 8-19 and 8-50 can be combined to solve for the unknowns at the downstream boundary. These solutions are:

$$\Delta y_N = \frac{E_N - A_N T_N}{A_N S_N + B_N} \tag{8-52}$$

$$\Delta Q_N = S_N \Delta y_N + T_N \tag{8-53}$$

Now the backward sweep begins with the calculation of the unknowns at the first cross section upstream of the downstream boundary. First, either Equation 8-44 or 8-45 with $i = N - 1$ is used to calculate Δy_{N-1}. Then Equation 8-43 is used to calculate ΔQ_{N-1}. This two-step procedure is continued for each cross section upstream to the upstream boundary. The backward sweep and the solution are now complete.

If there are interior boundaries in the river system, the double-sweep solution scheme may have to be modified. For the cases of flow over weirs or through gates, the finite difference equations, Equation 8-29 and 8-32 (or Equations 8-35 and 8-38) can be directly substituted for Equation 8-14 and 8-15 without changing the solution scheme. For the exception that during the backward sweep for computing the unknowns, it is better to interrupt the backward sweep across dams to use the original discharge equation 8-30 (or 8-31, 8-36, 8-37) for computing the stage immediately upstream of dams.

If a river confluence is considered, the following procedure is utilized (see Figure 8.4):

1) Define the exterior boundary conditions at each end of the river system, i.e., at Sections 1, M, and N.
2) Use the forward sweep from Section 1 to k1 and from Sections M to k2. This will result in two equations in the form of Equation 8-51.
3) Combining these two equations with Equation 8-20, 8-25 and 8-26 yields six unknowns in five equations. Then an equation in the form of Equation 8-18 can be derived. This equation is utilized as a starting equation to proceed the forward sweep to the downstream boundary Section N.

4) The backward sweep for the solution of unknowns start from Section N backward to Section k3 to compute the unknowns in the reach k3 - N. Then by using the confluence equations, derived from Step 3, the unknowns at Sections k2 and k1 can be computed. The backward sweep is then proceeded from k1 to 1 and from k2 to M to solve for all the unknowns.

Stability and Accuracy

A finite difference procedure for calculating time-dependent phenomena is considered stable when small numerical errors of truncation and round-off inevitably introduced at time t_o are not amplified during successive applications of the procedure, and at subsequent time t have not grown so large as to obscure the valid part of the solution. In practical computational experience, instability of a process for calculating unsteady open-channel flows shows up as wildly oscillating values of the dependent variables with respect to t and x. In practice, this means that limitations in the maximum size of the space and time intervals must be imposed to the numerical scheme in order to avoid stability problems.

Implicit methods of finite differences are generally regarded as unconditionally stable, the maximum size of the time step being limited only by accuracy requirements (Fread, 1974; Liggett and Cunge, 1975; Ponce et al., 1978). On the other hand, explicit methods are limited in the maximum size of the time step by a strict stability criterion called the Courant condition,

$$\Delta t \leq \frac{\Delta x}{c} \tag{8-54}$$

where c is the celerity of the small gravity wave given by $c = \sqrt{gy} + V$, V is the mean flow velocity, and Δx and Δt are the space and time increments.

Accuracy is the degree of difference between observed real-life data (such as measured hydrographs) and computed results. Unfortunately, however, true values are not available since the equations in consideration are analytically unsolvable and the field or laboratory measurements may be subject to uncertainties just as great as those in the mathematical model solutions. Liggett and Cunge (1975) point out that there might

be several reasons for discrepancy between a mathematical model and the prototype such as:

1) Inaccurate simplifications and approximations in the basic equations fail to simulate the complexity of the prototype.

2) Insufficiently accurate measuring techniques, e.g., surveying errors, badly located gages, etc.

3) Insufficient data, e.g., unknown tributary discharges, exchange of discharge with underground water, etc.

4) Phenomena which are not taken into account, e.g., infiltration into the dried-up soil at the beginning of a flood, variation of roughness coefficients with vegetation, etc.

5) Poor schematization of topographic features.

An estimate of accuracy, often used in numerical schemes, is introduced by the concept of convergence. Convergence refers to the ability of a numerical scheme to reproduce the terms of the differential equation without introducig extraneous terms that impair the accuracy of the solution. In theory, the numerical solution converges to the analytical solution as Δt and Δx tend to zero. In practice, however, Δx and Δt equal to zero is an impossibility. Therefore, when using mathematical models it is necessary to introduce the concept of degree of convergence. This concept refers to the approximation of the numerical solution to the analytical solution.

Since the flow equations 8-1 and 8-2 are analytically unsolvable, the best measure of convergence of a particular numerical scheme is to check against a simplified problem which has an analytical solution. Price (1974) used this approach to compare results from four of the more important numerical methods for flood routing with exact analytical solutions for the monoclinal wave. He found that the Preissmann type implicit scheme is the most efficient method for flood routing problems, and the optimum accuracy is obtained when the finite difference time step is chosen approximately equal to the space step divided by the kinematic wave speed

$$\Delta t = \frac{\Delta x}{c_k} \tag{8-55}$$

in which the kinematic wave speed is given by $c_k = 1.5\ V$.

The importance of the Courant criterion in numerical modeling is apparent when the similarity of Equations 8-54 and 8-55 is recognized. In explicit schemes, the Courant number cannot exceed one for stability reasons, i.e., $c\,\Delta t/\Delta x \leq 1$. In implicit schemes, no limitations of stability are imposed and the Courant number can take values greater than one depending on the spatial resolution and the accuracy requirements. In addition, there is a definite computational advantage of the implicit over the explicit scheme because the explicit Courant condition is based on the celerity of small disturbances while the implicit Courant "condition" (Equation 8-55) is based on the flood wave celerity (Ponce et al., 1978). This means that for a comparable degree of accuracy, the implicit time step can be many times larger than the explicit time step. Liggett and Cunge (1975) also obtained the same conclusion. They applied the Preissmann implicit scheme of finite differences to a highly simplified set of linear differential equations with a known Fourier series analytical solution, and showed that each component of the series obtained by the numerical method is characterized by its damping factor and its celerity, and that the convergence criterion is a function of the Fourier series component wavelengths and also of the ratio $\Delta t/\Delta x$. They reported better accuracy for the implicit scheme than for other well-known explicit schemes of finite differences.

Application of the One-Dimensional Mathematical Models

Introduction

The procedure of applying the one-dimensional water routing model to study river problems is summarized. More detailed information is given by Chen (1973) and by Cunge (1975).

1. Planning and selection of models. There are a large number of different mathematical models available. A model which is efficient and is able to accomplish the objectives of the study should be adopted. Therefore, the advantages, disadvantages and limitations of various models should be realized.

2. Construction of the mathematical model.

    a. Select a series of computational points (channel cross sections) to simulate the water course in such a way that the points represent all important topographical and hydraulical features of the study reach. As a rule of

thumb, the computational points may be chosen at all irregular sections and/or interesting locations. These computational points are a function of the model and its study objectives. For example, when computing river bed changes in the Mississippi River the distance between the points was varied from 0.5 to 4 miles. The model itself was 200 miles long. To study a local problem such as dredging the space increment was reduced to as small as 0.07 miles by introducing additional sections in the modeled river reach.

b. Evaluate the physical features at each section (computational point) by defining the supplemental relations as described in the section titled "Supplemental Equations."

Some guidelines are given in that section and also below:

(i) The area and top width of the cross section is computed for different water levels in the section and tabulated starting with the zero depth. Thus, a tabulated or fitted function which represents the cross-sectional geometry is built. This geometric function can be computed either directly in the water routing computer program or determined separately and then input into the computer program. When there are cross-sectional geometries measured between the computational points, the representative channel geometry at the computation points may be obtained by averaging these cross-sectional geometries. This case is especially true when simplified routing methods are used or computational points are far apart from each other. A method developed by Simons, et al. (1971), can be used to determine the geometry of the representative section. The method is physically correct and easy to apply.

The volume of water within the reach can be approximated as

$$V = \frac{1}{2} \sum_{i=1}^{m-1} (A_i + A_{i+1})(L_{i+1} - L_i) \qquad (8\text{-}56)$$

where A_i is the cross-sectional area of the water passage at a distance L_i downstream along the water course from some

arbitrary reference point and m is the number of cross sections describing the reach.

The length of the river reach is

$$L = L_m - L_1 \tag{8-57}$$

The average cross-sectional area is the volume divided by the length of the reach or

$$A = \frac{\sum_{i=1}^{m-1} (A_i + A_{i+1})(L_{i+1} - L_i)}{2(L_m - L_1)} \tag{8-58}$$

Similarly, the average wetted perimeter of the reach is

$$P = \frac{\sum_{i=1}^{m-1} (P_i + P_{i+1})(L_{i+1} - L_i)}{2(L_m - L_1)} \tag{8-59}$$

and the average top width is

$$T = \frac{\sum_{i=1}^{m-1} (T_i + T_{i+1})(L_{i+1} - L_i)}{2(L_m - L_1)} \tag{8-60}$$

(ii) The conveyance factor, using Manning's equation is easily defined as a function of water level for the given section as shown in Figure 8.2:

$$K = \sum_{k=1}^{M} K_k \quad \text{with} \quad K_k = \frac{1.486}{n_k} A_k R_k^{2/3}$$

Thus, it is possible to construct the function representative of the hydraulic characteristics of a given section $K = K(y)$. Again, sometimes the analytic, often a polynomial or power function is used instead of the tabulated one. On many occasions it may be difficult to obtain a good approximation of the function $K(y)$ by any fitting procedure.

(iii) The lateral inflow discharges can be evaluated from field data, empirical relations and/or theories. For example, water yield inflowing to rivers from watersheds can be determined from methods described in Chapter 7.

3. Calibration of the mathematical model. It is desired to reproduce the historical flow characteristics and geomorphic changes in the study reach to insure existence of similarity between the mathematical model and the modeled river reach such that the model can be used to predict future changes. The important features to be simulated include:

The water discharges and water surface profiles, where the hydrographs need to be discretized according to variation rate of the hydrographs and computation time steps. Usually, for water routing a time step varying from minutes to hours is used.

Efforts should be made to modify the resistance function and at each section until the known historical changes are reproduced.

4. Operation of the mathematical model. The calibrated mathematical model can be operated to forecast floods and predict the river responses to changes. It is necessary to check the calculated results with the principles of river mechanics. If the results make sense, confidence in the model is reinforced.

5. Evaluation of development plans. By comparing the river responses to various development plans obtained from operation of the mathematical model, the feasible plans can be identifed and their corresponding effects can be determined.

6. Improving the mathematical model. The mathematical model should be updated using the new measured data and/or improved theories. This process is designed to:

a. Verify the applicability of the mathematical model.

b. Refine the model for predicting future responses of the river basin to development.

c. Finalize a methodology for assessing watershed and river response to water resources control and development.

7. Documentation of the mathematical model and the model results.

A flow chart is given in Figure 8.7 to show the principal programming steps. Some application examples are presented in the following sections.

Study of Pools 24, 25, and 26 in the Upper Mississippi and Lower Illinois Rivers (Simons, et al., 1975; Chen and Simons, 1975)

Description of study reach

A mathematical model was constructed to cover the Upper Mississippi River from above Lock and Dam 22 (River mile 304.8) to St. Louis (River mile 179.6), the lower Illinois River from River mile 80 to the mouth of

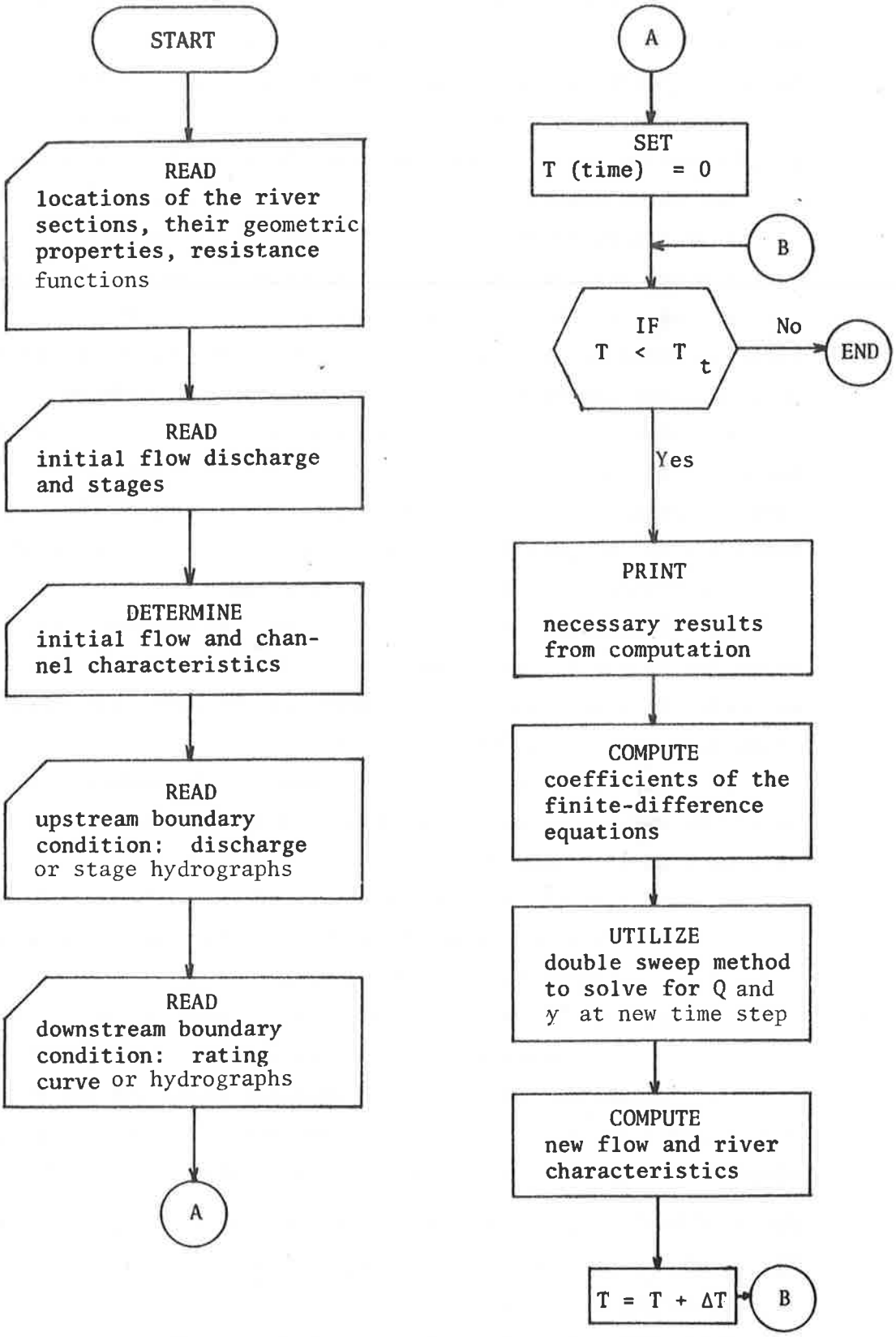

Figure 8.7 Flow chart of the one-dimensional mathematical model.

the Illinois River, and the Lower Missouri River below Hermann (River mile 98) (see Figure 8.8). The effects of locks and dams and the interactions between the Mississippi River and its main tributaries on the geomorphology of rivers and adjacent lands were considered. The model can be used to study the impacts of different operation schemes for the locks and dams, the effects of the pools on the behavior and form of the tributary rivers, the impact of change in the delivery of sediment and water to the study reach on the morphology of the river and adjacent lands, and the impacts of dredging and dredged material disposal on the hydraulic response and sedimentation patterns in the main channel.

Objectives of the Study

The model permits an analysis of future hydraulic and geomorphic change. What will Pools 24, 25, and 26 in the Upper Mississippi and Lower Illinois Rivers look like 50 years from now? Will the flood stage increase? Will the side channels fill the sediment? Will the riverbed aggrade making the maintenance of the 9-foot channel project more expensive? Are there any viable alternatives to the present-day operations that would enhance the environmental aspects of the pools and at the same time maintain the navigation channel? The mathematical model was applied to answer these and other questions relative to the Pool 24, 25, and 26 reach. Only the water routing model component and results are presented in this chapter.

Construction and Calibration of the Model

The water routing component of the mathematical model was constructed and calibrated using the following information: 1) hydrographic maps of the river reach, and 2) hydrographs of stage and flow discharge. The model was formulated using the basic equations, Equation 8-1 and 8-2, coupled with the interior conditions simulating the interaction between the Upper Mississippi River and its tributaries (Equations 8-20 to 8-21). Also, Equations 8-35 and 8-37 were utilized to simulate water flowing through the locks and dams. These equations were solved by the double sweep method after evaluating the supplemental relations as follows. From the hydrographic maps, one can evaluate the geometric properties of the river reach by tabulating cross-sectional areas and top widths versus stage at each selected computation point. The spatial increment

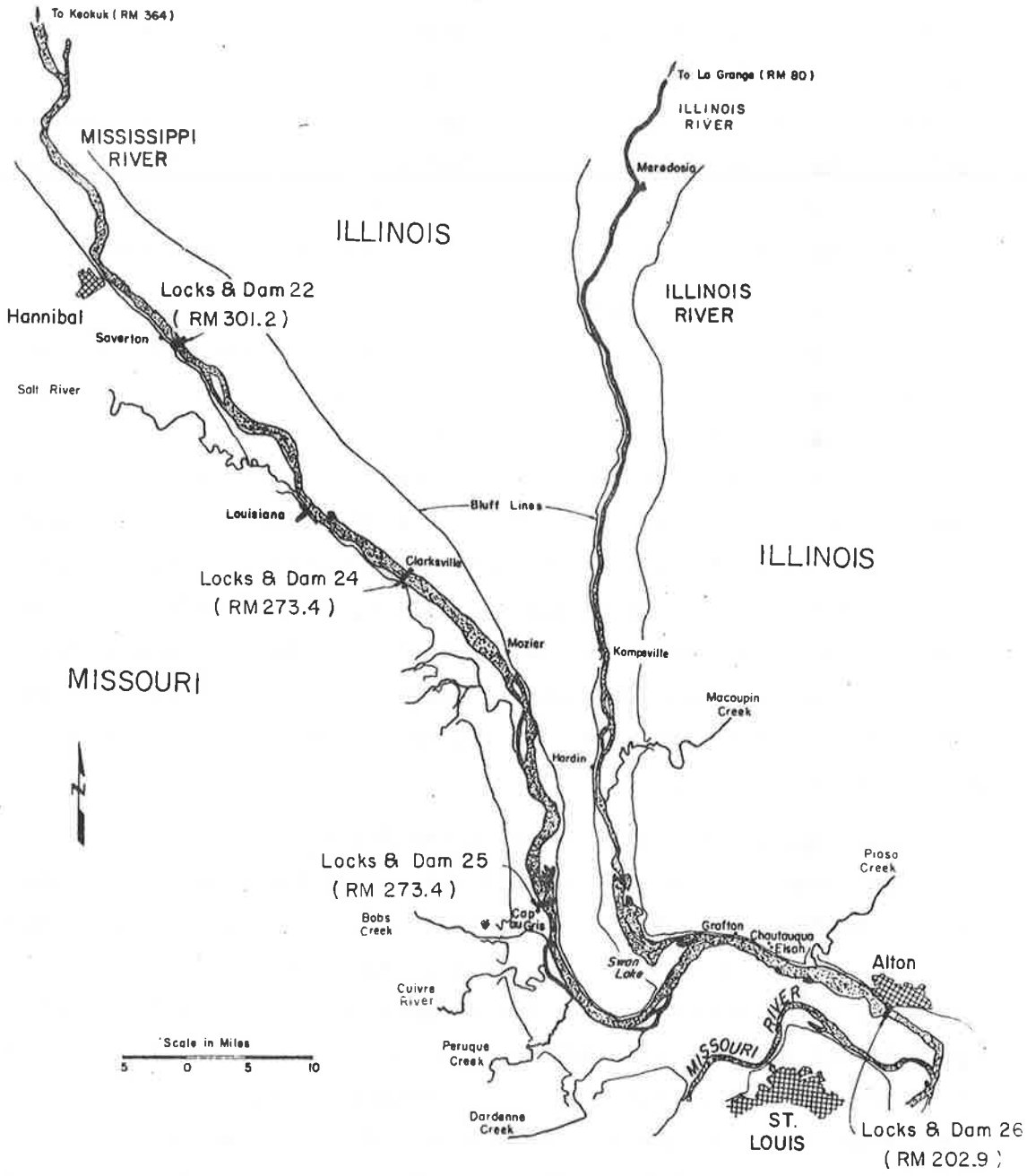

Figure 8.8 Index map of Pools 24, 25, and 26 in the Upper Mississippi and Lower Illinois River.

Δx varied from 0.4 mile at a lock and dam to 20 miles in the Missouri River. The relations for q_ℓ and S_f can be evaluated from the stage and discharge hydrographs. In this study, q_ℓ was assumed negligible. Initial Manning's roughness coefficients were obtained from solving the steady momentum equation for a given water discharge and stage profile. The S_f relation was modified until the mathematical model reproduced faithfully the observed changes in water surface profiles.

The calculated and verified 1965 and 1967 water surface profiles are compared with the measured stages in Figure 8.9 through 8.12. The size of time step Δt varied from 0.5 day to 5 days. These figures show an agreement between the measured and calculated values.

The backwater effects of the Mississippi River on the Lower Illinois River and of the Missouri River on the Mississippi River have been well simulated. This indicates that the mathematical model as calibrated was as good as the available field information, and could be employed to study the river's response to future development.

General Model Operations

The calibrated mathematical model was employed to assess the impacts of factors considered in this study. Typical results of routing a one-year hydrograph through the modeled river reach are given in Figures 8.13 and 8.14. The water-surface profile in the Upper Mississippi River for $Q = 28{,}000$ cfs at 24 days is shown in Figure 8.13a. To maintain the normal pool levels, the control gates were lowered close to the gate sills. As the flow increases, the pool stage was lowered at the dam by gradually opening the gates to maintain the level at the control stations within the prescribed control limits as shown in Figure 8.13b. As inflow continues to increase, the gates were opened further to increase the outflow until the gates were above the water surface as shown in Figure 8.13c. With the passage of flood flow the gates were then partially lowered into the water as required to restore the pool as shown in Figure 8.13d.

During the same flood routing, the water surface profiles in the Lower Illinois River were determined and some results are shown in Figure 8.14. The dashed line in Figure 8.14 depicts the water surface profile without the backwater effect from Pool 26. Because of the regulation of Pool 26, the stage in the Illinois River near the confluence

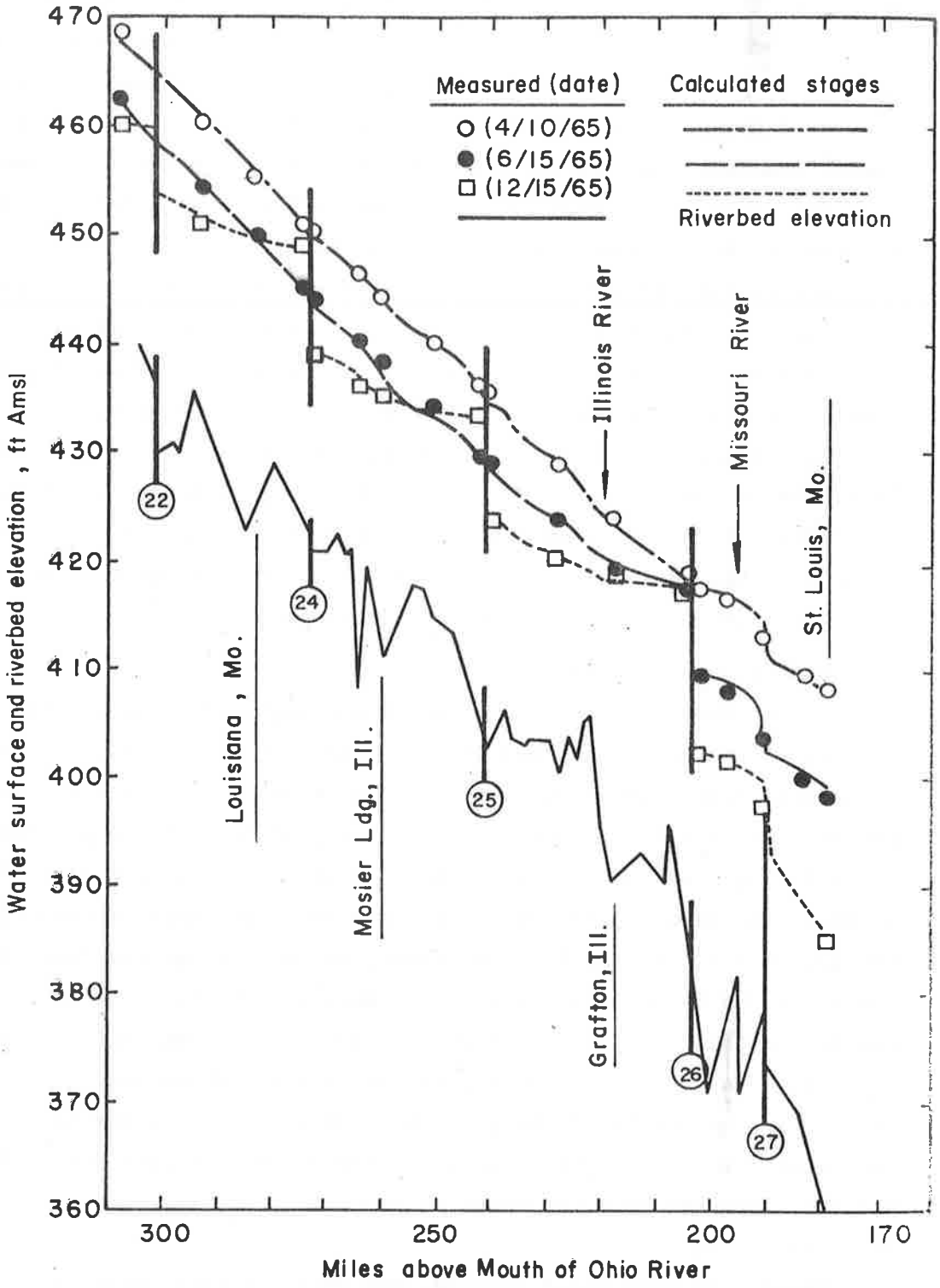

Figure 8.9 Mathematical model reproduction of 1965 water surface profile in the Upper Mississippi River.

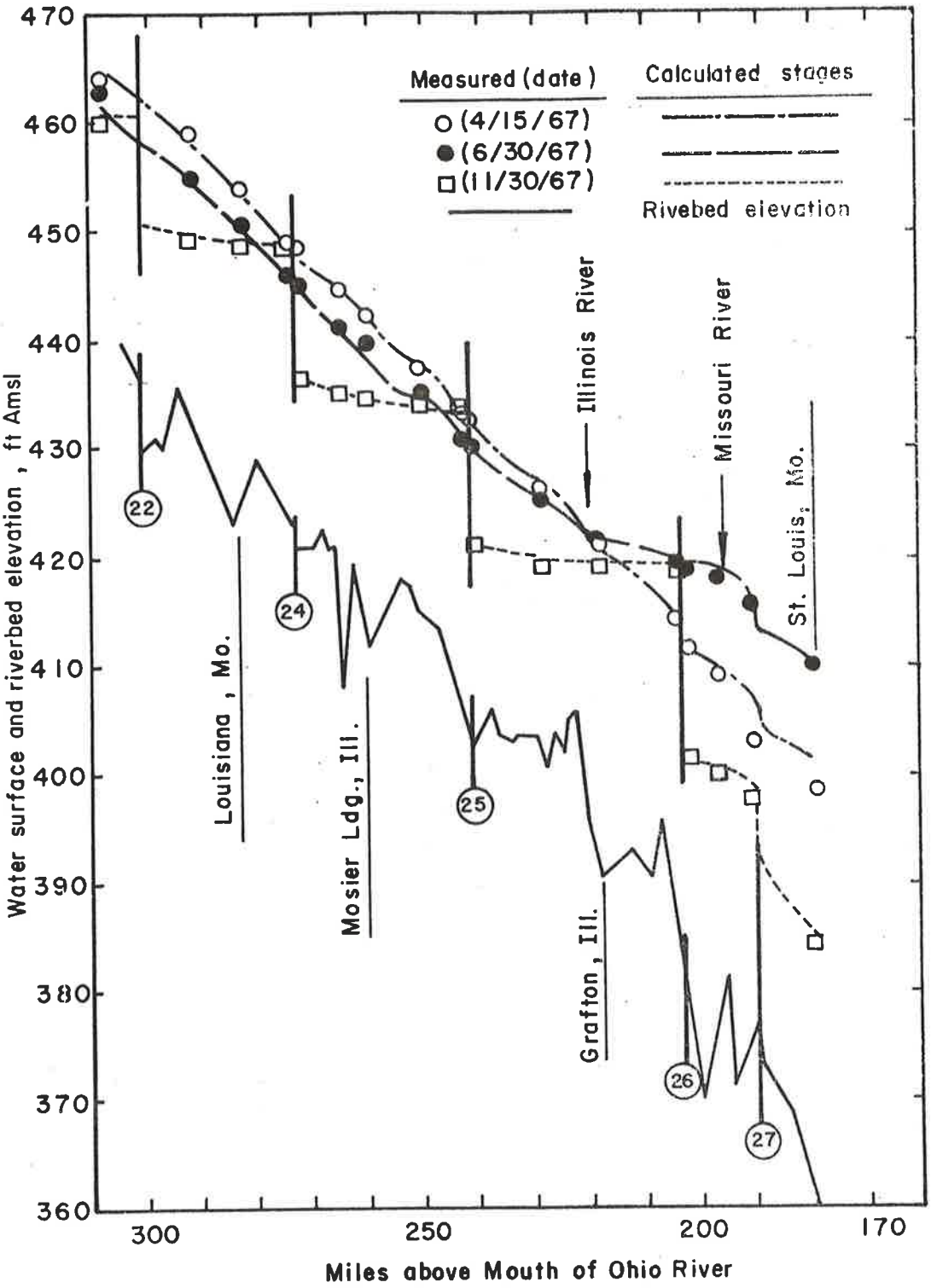

Figure 8.10 Mathematical model reproduction of 1967 water surface profile in the Upper Mississippi River.

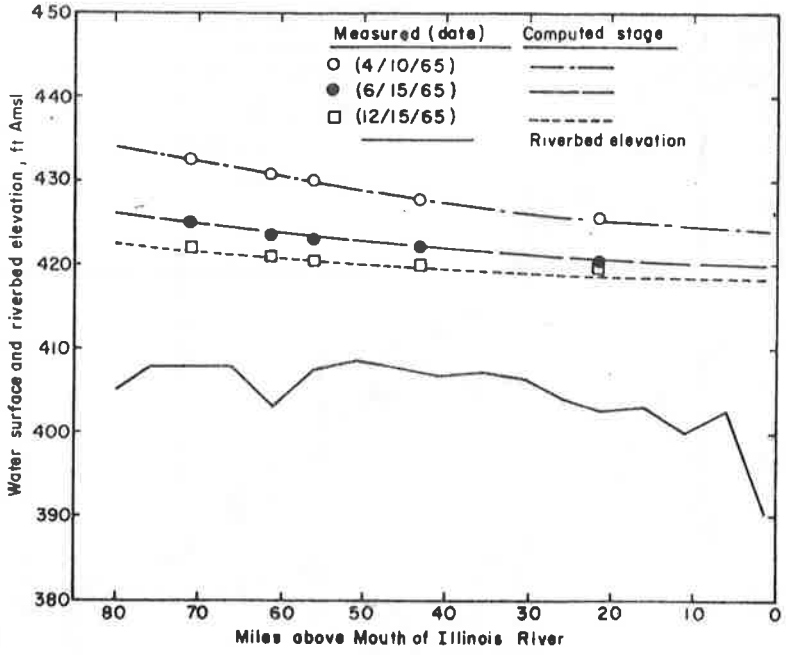

Figure 8.11 Mathematical model reproduction of 1965 water surface profile in the Lower Illinois River.

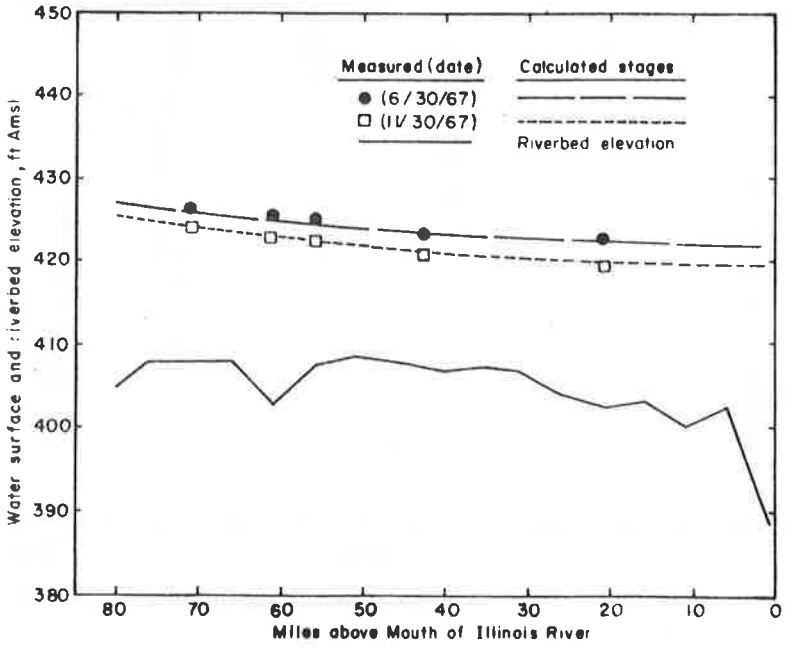

Figure 8.12 Mathematical model reproduction of 1967 water sruface profile in the Lower Illinois River.

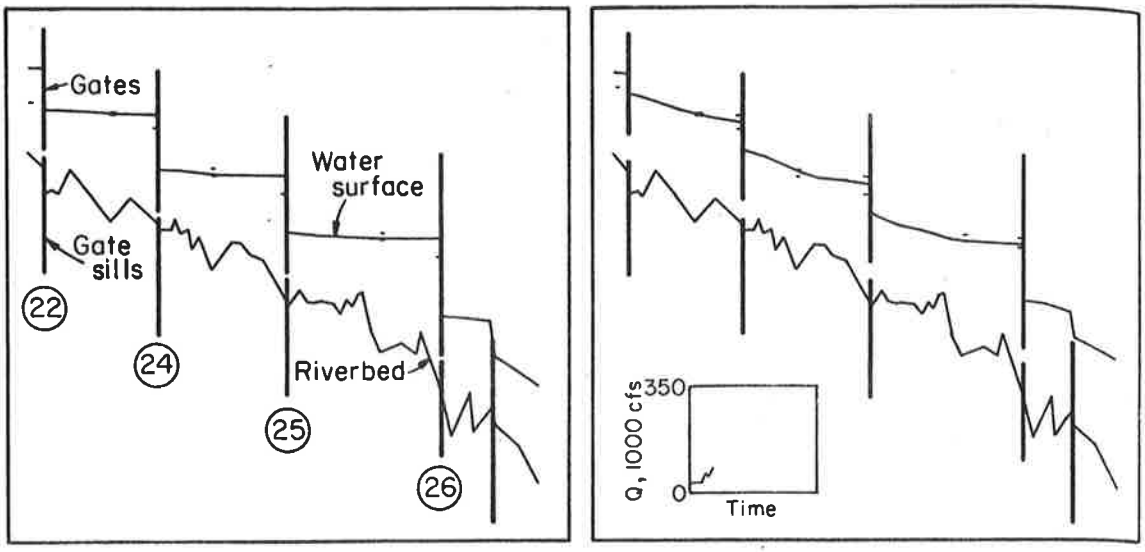

a. Normal pool stages with control gates lowered close to gate sills
Q=28,000 cfs at Dam 22, 24 days

b. Pool stages lowered to maintain control station levels
Q=81,000 cfs at Dam 22, 63 days

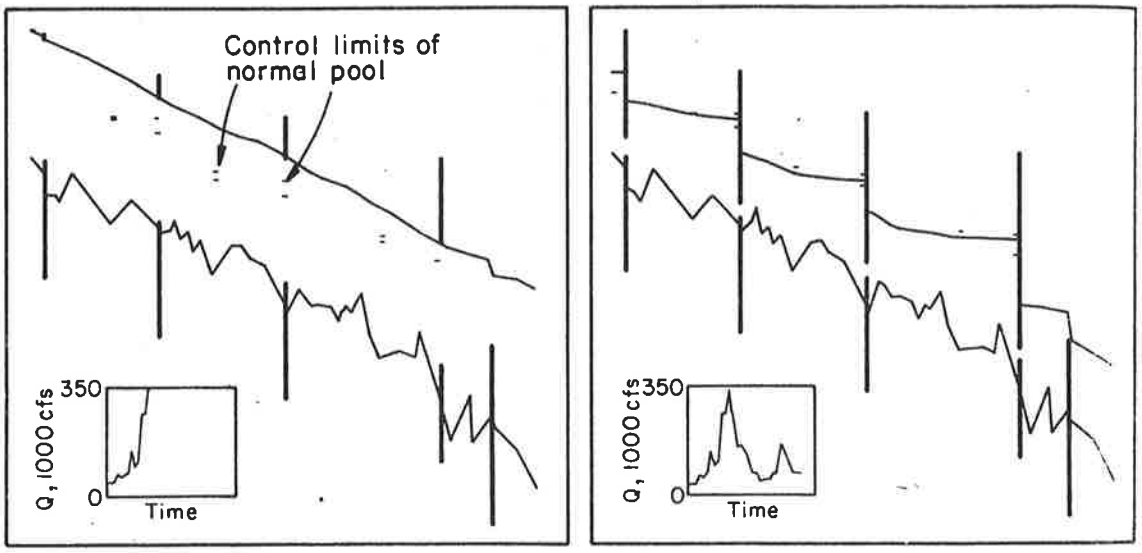

c. Gates entirely out of water at flood crest
Q=339,000 cfs at Dam 22, 117 days

d. Gates partially lowered to restore pools after flood recedes
Q=54,000 cfs at Dam 22, 324 days

Figure 8.13 Water surface profiles in the Upper Mississippi River during a flood routing.

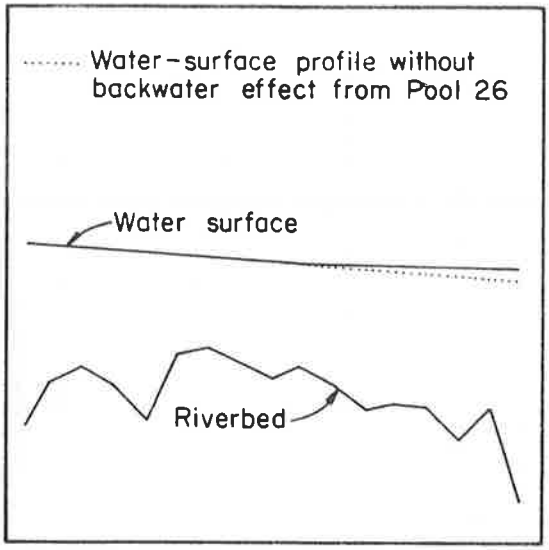

a. Q = 10,000 cfs in the Illinois River, Q = 28,000 cfs in the Mississippi River, 0 days

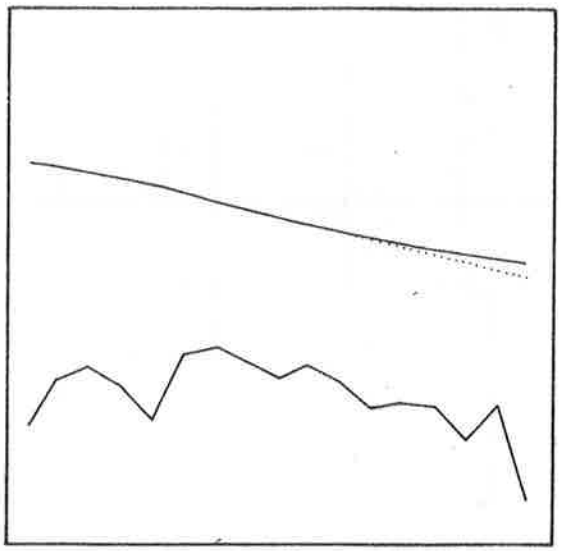

b. Q = 35,000 cfs in the Illinois River, Q = 86,000 cfs in the Mississippi River, 84 days

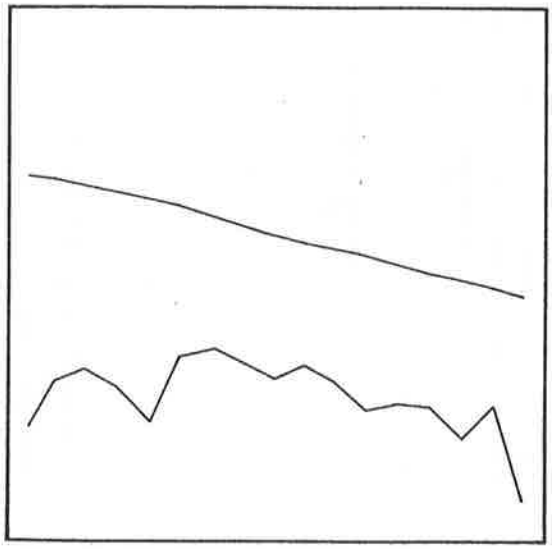

c. Q = 32,000 cfs in the Illinois River, Q = 96,000 cfs in the Mississippi River, 90 days

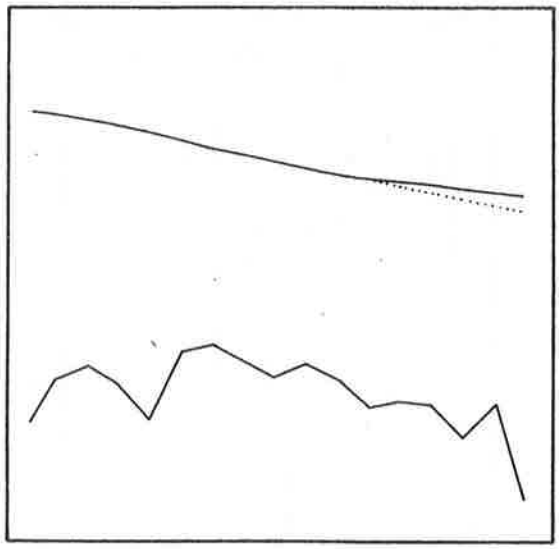

d. Q = 50,000 cfs in the Illinois River, Q = 299,000 cfs in the Mississippi River, 114 days

Figure 8.14 Water surface profiles in the Lower Illinois River during a flood routing.

was raised, increasing the flood stage, reducing the flow velocity and causing changes in river morphology.

The developed mathematical model coupled with a sediment routing model component was utilized to predict the hydraulic and geomorphic changes in Pools 24, 25 and 26 in the Upper Mississippi River and in the Lower Illinois River in the next 50 years.

Study of Unsteady Flow in a Urban Stormwater Runoff and Combined Sewer

The city and county of San Francisco is designing and constructing an extensive wet weather pollution control program by mainly using an automatic, real-time computer controlled stormwater runoff and combined sewer system. The computer control system involves nonlinear partial differential equations for routing storm flows, stochastic rainfall input, and a multitude of variables for integrated city-wide optimized control. The model developed here has been utilized to simulate the dynamic unsteady flow routing in the system. The mathematical model covered the sewer system as shown in Figure 8.15 with a spatial increment Δx of 500 ft in a pipe reach and 10 ft at transition regions, surge tanks or control gates. The basic equations 8-1 and 8-2 were used in the mathematical model except one modification. When the sewer becomes full, the top width T becomes zero. Assuming that the water hammer generated is insignificant, we have

$$\frac{\partial Q}{\partial x} = q_\ell \tag{8-61}$$

For the sections across a surge tank,

$$q_\ell = \frac{A_s \, \Delta y}{\Delta x \, \Delta t} \tag{8-62}$$

where A_s is the cross-sectional area of the surge tank. The equations used to describe the external and interior boundary condition in a river systems are also applicable to simulate gates, junctions, valves, etc. installed in the sewer system.

The mathematical model was verified using a physical model, which only covered a portion of the sewer system, extending from just above the Columbus Street surge tank on the Marina side to just above the Sansome Street inflow on the Embarcadero side. The effect of the remainder of the tunnnel system is approximated by two bypass valves, one at each side of the scale model.

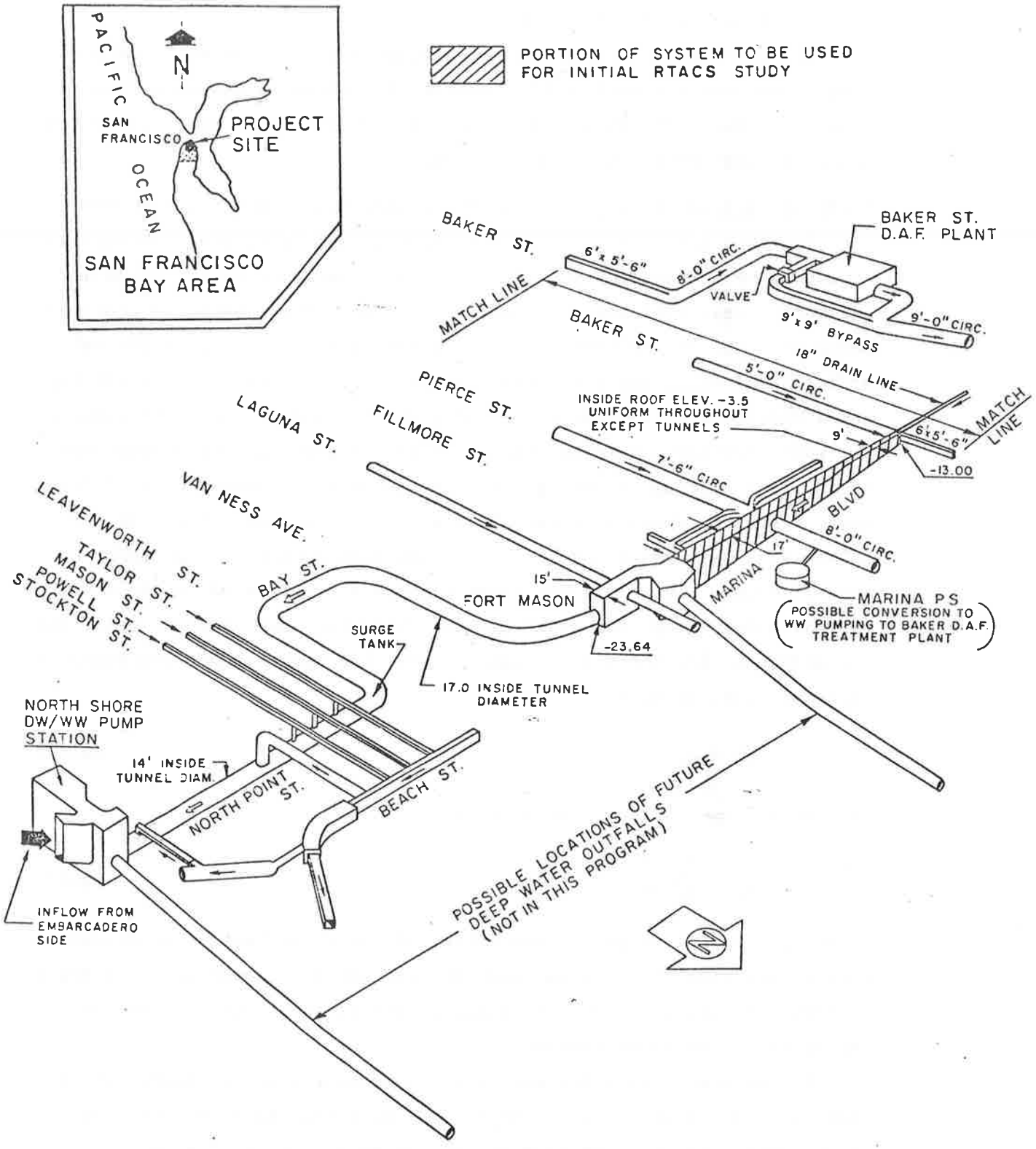

Figure 8.15 North point portion of the San Francisco north shore outfalls consolidation project (design not final).

A five year design storm as shown in Figure 8.16 was routing through both the physical model and the mathematical model. The mathematical model routing time was 2 hours with a time increment of 3 minutes. A comparison between the computed and measured results is shown in Figure 8.17. The computer model results show less of the surge and wave phenomena than the physical model tests. The mathematical mdel is based on the gradually varied unsteady flow equations, which exclude accurate considerations of traveling boxes and surges. Also the finite different scheme which linearizes the unsteady flow equations introducing linearization errors.

8.3 ONE-DIMENSIONAL MATHEMATICAL MODEL OF A RIVER NETWORK SYSTEM

Introduction

There are some rivers and estuaries with a complex system of branches, loops, and confluences. Here the flow division among the confluences and the tide effect from downstream complicates the problem. The one-dimensional mathematical model developed in Section 8.2 is not applicable to study a river network system, because it only considers the hydraulic behavior in a river channel with at most a confluence jointing a tributary to a main channel. Harleman (1971) used a finite-element method for the hydrodynamic equations on a one-dimensional model for transient water quality in an estuary network. Yen and Akan (1976) used an overlapping concept with a form-point implicit scheme for flood routing through junctions. Kenning (1976) applied the finite element method in combination with Gallerkin's principle to the unsteady equations for one-dimensional flow in a channel connected with the sea. These methods are based on some simplified approaches to study a river network. To study the hydraulic and water quality problems in the Jacui Delta, located near Orto Alegre, Brazil, Tucci (1978) developed an unsteady flow model for a river network system based on the complete Saint Venant equations. His method is presented in this section with some minor changes on the formulation of finite difference equations.

Theoretical and Numerical Methods

The basic unsteady flow Equations 8-1 and 8-2, the confluence Equations 8-20, 8-21 and 8-22 and the dam Equations 8-29 and 8-30 (or Equations 8-31, 8-36, 8-37) are all applicable in modeling a river network system. As the finite-difference approximations (Equation 8-8)

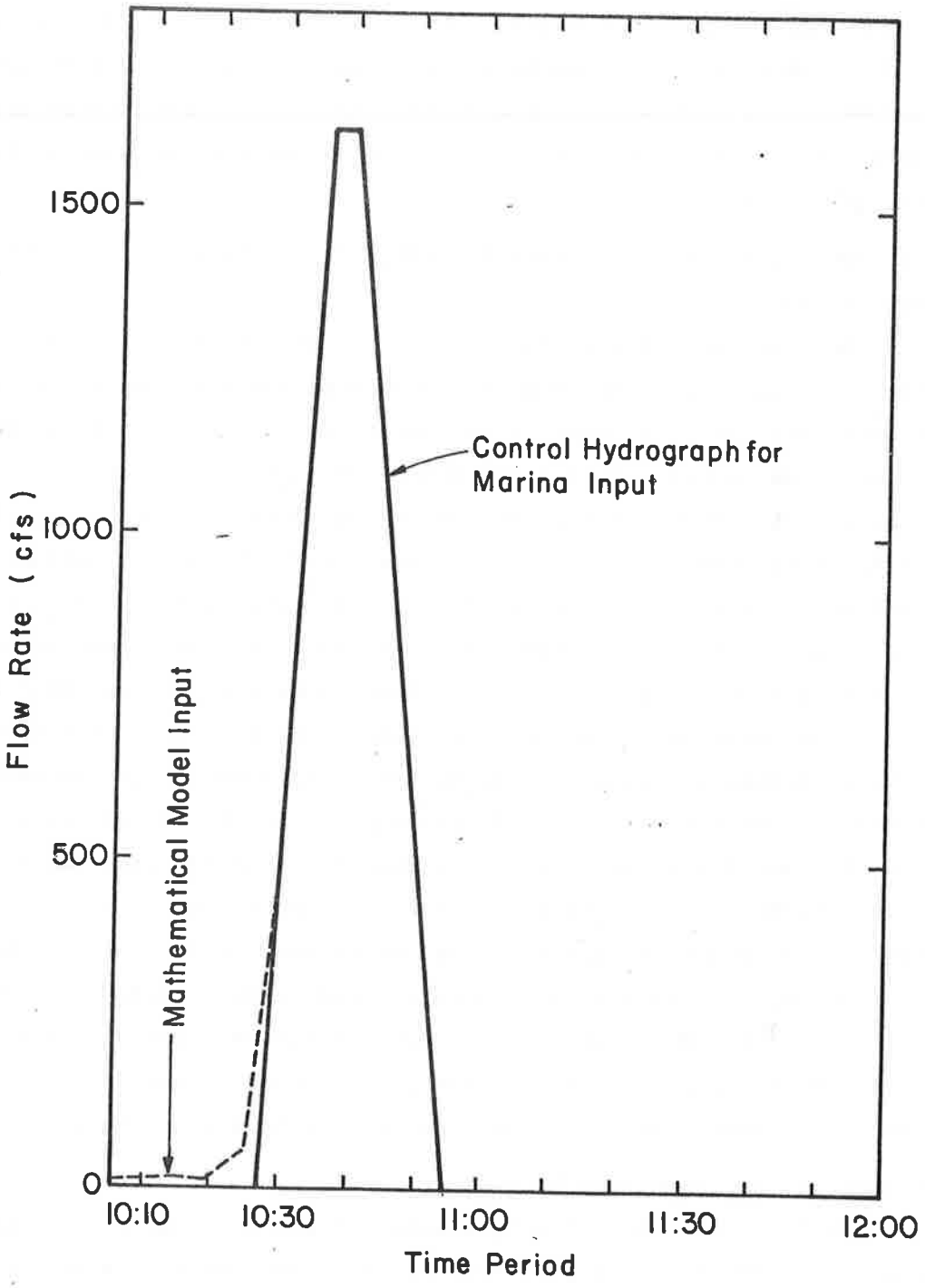

Figure 8.16 Five year design storm - Marina hydrograph.

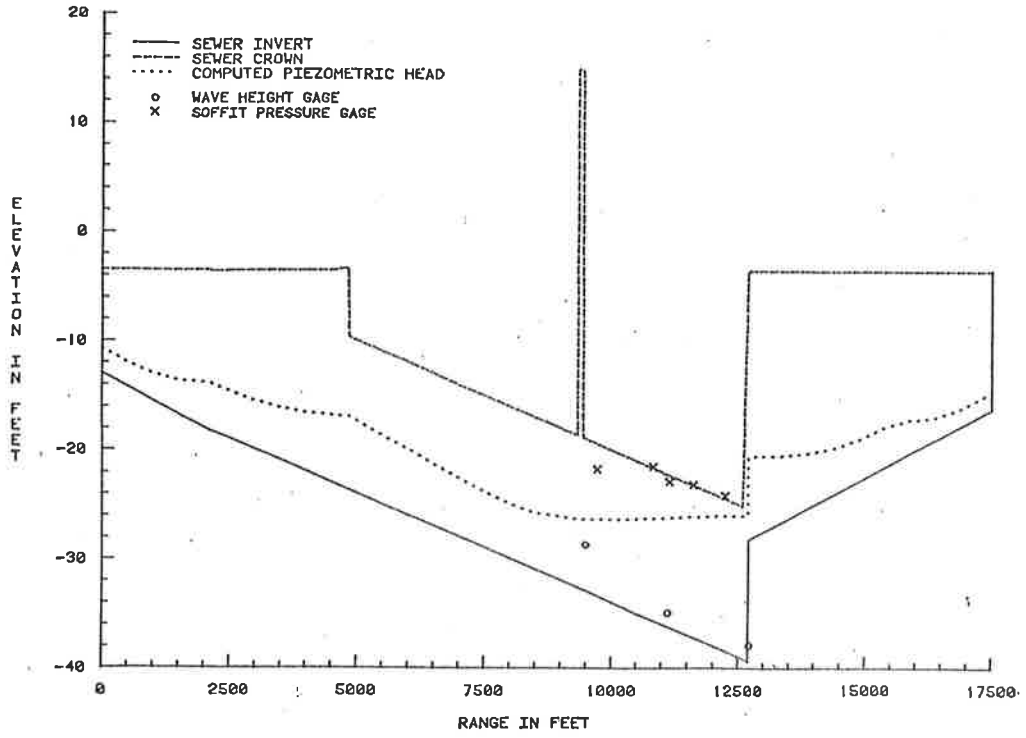

Figure 8.17a San Francisco NSOC Project, profile view--time = 8 minutes.

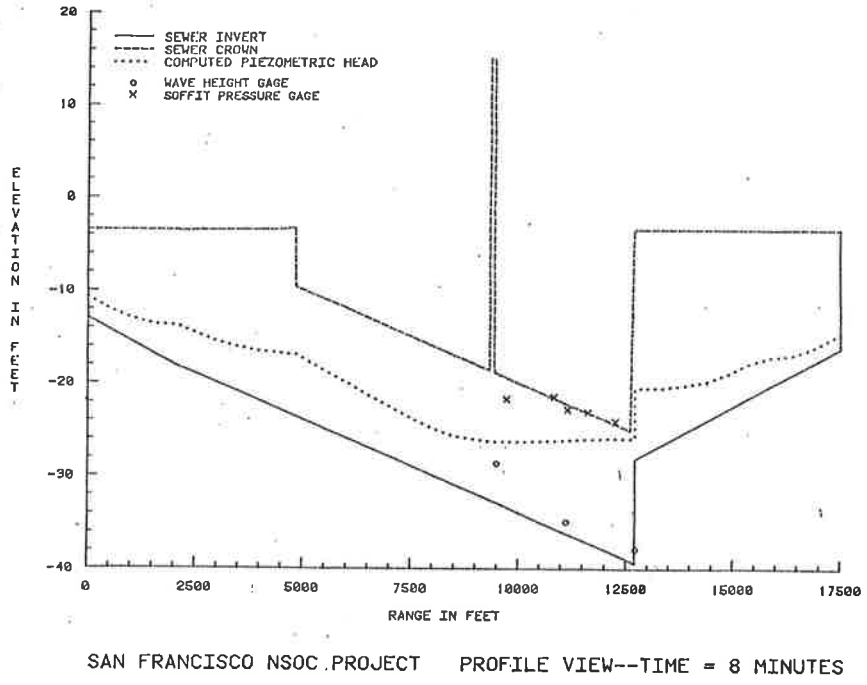

Figure 8.17b San Francisco NSOC Project, profile view--time = 11 minutes.

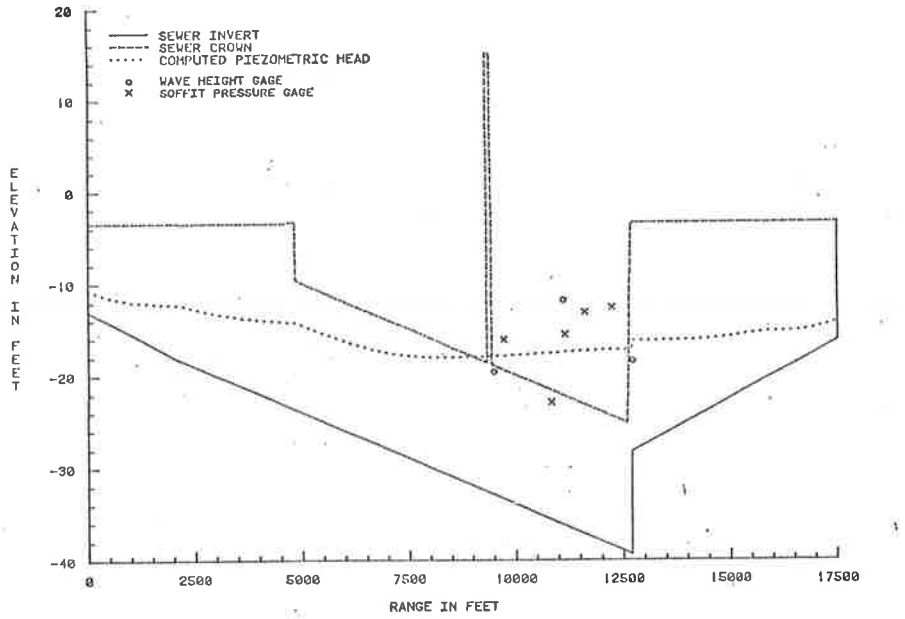

Figure 8.17c San Francisco NSCO Project, profile view--time = 14 minutes.

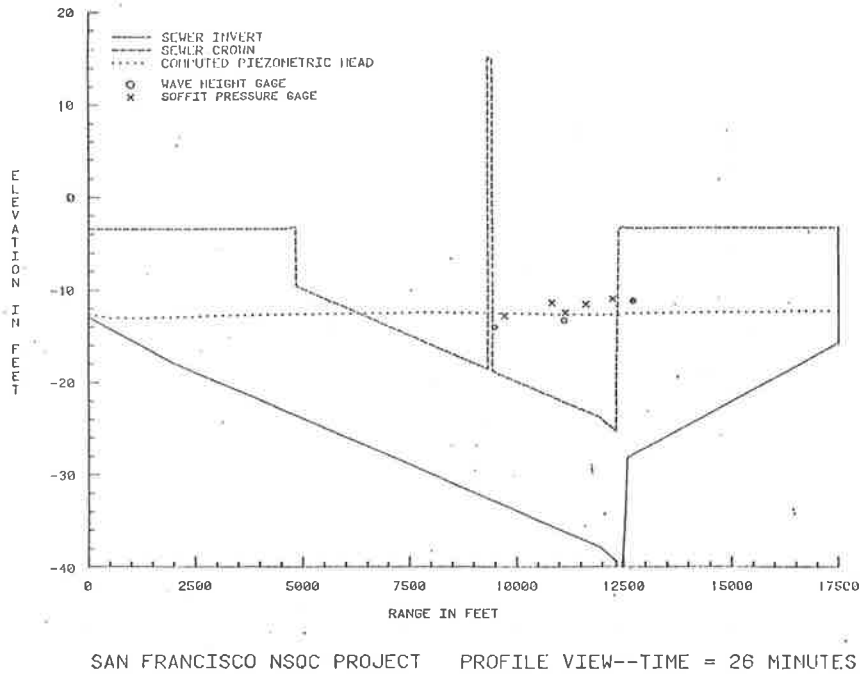

Figure 8.17d San Francisco NSOC Project, profile view--time = 26 minutes.

are substituted into these equations, the finite-difference Equations 8-14, 8-15, 8-20, 8-24, 8-25, 8-29 and 8-32 are derived. Tucci (1978) used Equation 8-9 for the finite-difference approximations and derived slightly different relations for the coefficients of the finite-difference equations.

Using Equation 8-14 and 8-15 for each reach, Equation 8-20, 8-24 and 8-25 for each confluence, and Equation 8-29 and 8-32 for each dam, there will be 2(N-1) equations (if there are only two exterior boundaries), where N is the number of sections. In matrix notation the system of equations

$$\underline{F}\ \underline{X} = \underline{E} \tag{8-63}$$

where

$$\underline{F} = \begin{bmatrix}
A_1 & B_1 & C_1 & D_1 & & & & & & & & \\
A'_1 & B'_1 & C'_1 & D'_1 & & & & & & & & \\
 & & A_2 & B_2 & C_2 & D_2 & & & & & & \\
 & & A'_2 & B'_2 & C'_2 & D'_2 & & & & & & \\
 & & \cdots & \cdots & \cdots & \cdots & & & & & & \\
 & & & & 1 & 1 & & -1 & & & & \\
 & & & C_{ai} & C_{bi} & & C_{ci} & C_{di} & & & & \\
 & & & & C'_{ai} & C'_{bi} & C'_{ci} & C'_{di} & & & & \\
 & & & & & & \cdots & \cdots & \cdots & & & \\
 & & & & & & & & A_{N-1} & B_{N-1} & C_N & D_N \\
 & & & & & & & & A'_{N-1} & B'_{N-1} & C'_N & D'_N
\end{bmatrix}$$

$$\underline{X} = \begin{bmatrix} Q_1^{j+1} \\ y_1^{j+1} \\ \cdot \\ \cdot \\ Q_i^{j+1} \\ y_i^{j+1} \\ \cdot \\ \cdot \\ Q_N^{j+1} \\ y_N^{j+1} \end{bmatrix} \quad ; \quad \underline{E} = \begin{bmatrix} E_1 \\ E_1' \\ \cdot \\ \cdot \\ 0 \\ C_{ei} \\ C_{ei}' \\ \cdot \\ E_N \\ E_N' \end{bmatrix}$$

The specification of the boundaries gives two more equations. This results in the equal number of equations and unknowns, thereby permitting the equations to be solved simultaneously. For instance, in the system in Figure 8.18b, there are four reaches which gives eight equations, two confluences which give six equations and the boundaries with two more equations. There are sixteen unknowns (8 sections) and sixteen equations.

The linear system of equations (8-63) needs to be solved at each time step. The coefficient matrix $\underline{F}$ for a river without confluences can be easily transformed into a banded matrix. In this situation the double sweep method or other method which takes into account only the non-zero coefficients can be used to solve the system of equations. These methods are more accurate and use less storage and computer time than the methods which utilize the full matrix.

In a river network the matrix $\underline{F}$ is a sparse non-banded matrix (Figure 8.18b). In order to solve a system of linear equations when the coefficient matrix is sparse, Vreugdenhill (1973) recommended an iterative method known as the Gauss-Seidal iterative method. This method requires only the storage of non-zero elements of the matrix and their positions in the matrix. The solution at time t is used as the initial guess for beginning the iteration at time step $t + \Delta t$. In this way the initial guess is usually good and computer time is saved, as fewer iterations are required for convergence. The convergence condition for the Gauss-Seidel iterative

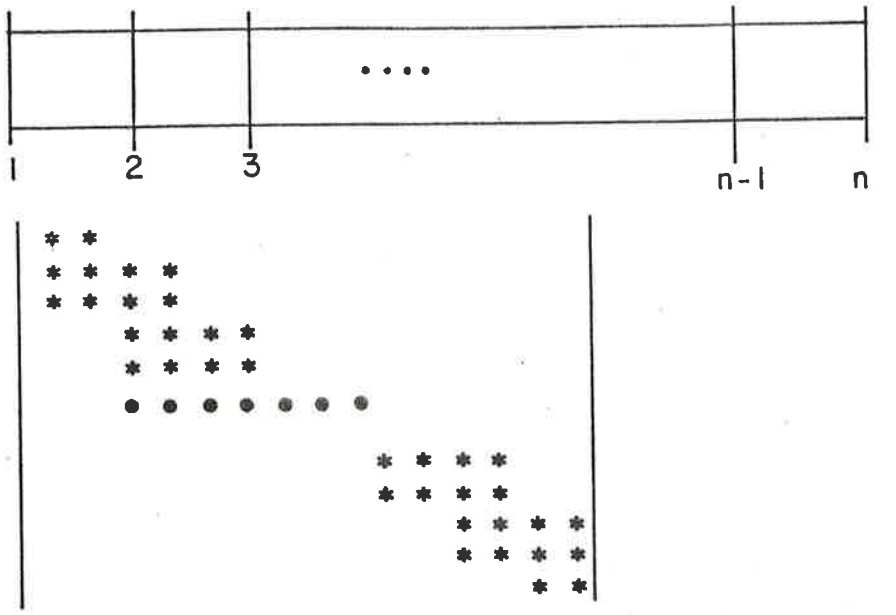

a. Matrix F for a River Reach

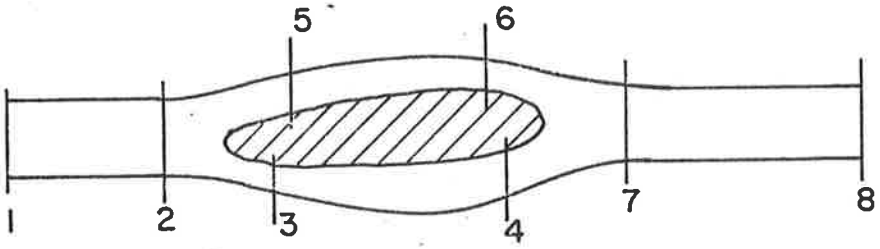

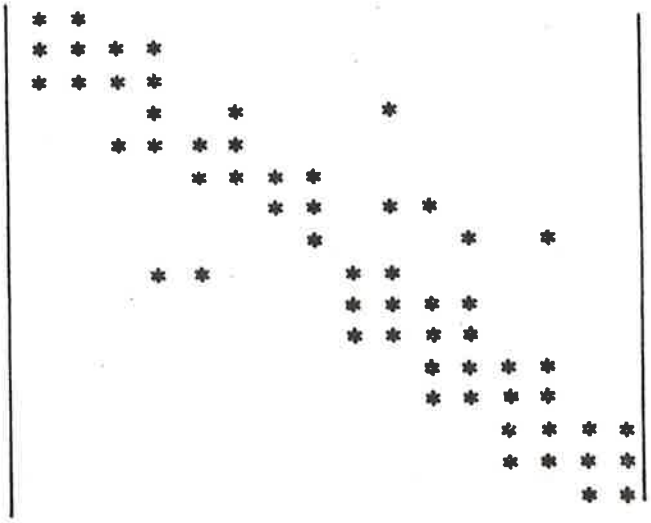

b. Matrix F for a River with Confluence

* Nonzero Elements

Figure 8.18 Matrix $\underline{F}$ for a river reach and for a river with a confluence.

method is that matrix $\underline{F}$ should be positive definite. This method was used in some examples and it was found that convergence did not always occur.

A direct method to solve these equations is the Gauss elimination procedure. The following system of equations

$$\begin{aligned} a_{11}x_1 + a_{12}x_2 + \ldots + a_{1N-1}x_{N-1} + a_{1N}x_N &= b_1 \\ a_{21}x_1 + a_{22}x_2 + \ldots + a_{2N-1}x_{N-1} + a_{2N}x_N &= b_2 \\ \cdots\cdots\cdots\cdots\cdots\cdots\cdots\cdots\cdots\cdots & \\ a_{N1}x_1 + a_{N2}x_2 + \ldots + a_{NN-1}x_{N-1} + a_{NN}x_N &= b_N \end{aligned} \tag{8-64}$$

is solved by transforming the matrix of coefficients in a upper triangle matrix by

$$j = 1, 2, \ldots N-1; \quad i = j, \ldots N;$$

$$b_i^j = b_i^{j-1} - B_j^{j-1} \frac{a_{1,j}^{j-1}}{a_{i,i}^{j-1}}$$

and

$$k = j, 1, \ldots, n$$

$$a_{i,k}^j = a_{i,k}^{j-1} - a_{j,k}^{j-1} \frac{a_{i,j}^{j-1}}{a_{j,j}^{j-1}} \tag{8-65}$$

Using backward substitution the unknown values are calculated by

$$x_i = \frac{(b_i - \sum_{m=n}^{i-1} x_m a_{i,m})}{a_{i,i}} \tag{8-66}$$

The matrix $\underline{F}$ has no more than four non-zero elements in each row, but has many zero elements. If one stores all elements the solution will be less accurate and too expensive. For instance 50 sections would use 10,000 words of storage where only about 2 percent are non-zero elements.

Bathe and Wilson (1976) developed a method called Skyline for Gauss elimination procedure to minimize the storage of the procedure. Their method is designed for solving symmetric matrices resulting from finite element formulations. Since the matrix $\underline{F}$ is not symmetric, Tucci

(1978) modified the Skyline scheme to solve Equation 8-63. His method is adopted in this study. Tucci's method used four one-dimenstional arrays to store the information contained in matrix F. A numerical example is shown in Figure 8.19. The coefficients are stored sequentially in a vector. Each diagonal element is followed by all elements in the column of the matrix above that element, then all elements in the row to the left of the diagonal taking in the inverted L shape ("⌟") shown in Figure 8.19a which extends upwards and to the left as far as the last non-zero element in each direction.

In Figure 8.19c, vector AA(I) shows the storage sequence of coefficients for matrix F in Figure 8.19b. Vector IDIAG(I) gives the positions of each diagonal element in AA(I). Vector IHIGH(I) gives the number of column elements above each diagonal element including the diagonal element. Vector IR(I) gives the number of row elements to the left of each diagonal element excluding the diagonal element. The method uses Equations 8-65 and 8-66 but with a different index since the coefficients are stored in another way.

The flowchart of Figure 8-20 shows the solution using this storage scheme. This method is useful when the matrix is almost banded with a few sparse elements, as it is in this case of river network. For instance, in the Jacui Delta system with 19 confluences and 64 sections, modeled by Tucci (1978), the full matrix would use 16,384 words for storage. This storage scheme uses 1,587 words and in a Cyber 171 computer it takes 1.0 second of Central Processor (CP) time to solve the system of 128 equations by 128 unknowns in each time step.

The section numbering procedure should be done in order to minimize the storage and calculations. The unknowns are numbered based on the section number. In the reach or confluence equations which the section numbers are not continuous integer numbers, zero values will appear among the non-zero values in the coefficient matrix. This increases the matrix band and in consequence the storage and calculation. The minimization can be done by numbering the sections in a crescent (or decrescent) order and when there are confluences by minimizing the difference between the section numbers of the reaches and confluences. Some suggestions to do that are: (1) the number of the sections should be given in crescent order from upstream towards downstream, and (2) for short loop an alternate numbering is a good procedure.

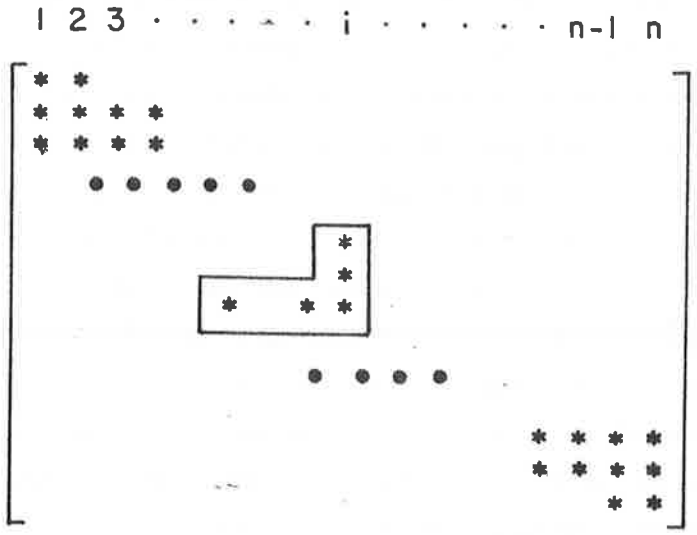

a. Diagonal Element

$$\begin{bmatrix} 1 & -2 & & & \\ & 5 & & 6 & \\ & & 7 & & \\ & 3 & & 4 & & 4 \\ & & & 2 & 1 & \\ & & & & & 6 \end{bmatrix}$$

b. Example Matrix F

AA(I)

$$\begin{bmatrix} 1 \\ 5 \\ -2 \\ 7 \\ 4 \\ 0 \\ 6 \\ 0 \\ 3 \\ 1 \\ 2 \\ 6 \\ 0 \\ 4 \end{bmatrix}$$

IDIAG(I)

$$\begin{bmatrix} 1 \\ 2 \\ 4 \\ 5 \\ 10 \\ 12 \end{bmatrix}$$

IHIGH(I)

$$\begin{bmatrix} 1 \\ 2 \\ 1 \\ 3 \\ 1 \\ 3 \end{bmatrix}$$

IR(I)

$$\begin{bmatrix} 0 \\ 0 \\ 0 \\ 2 \\ 1 \\ 0 \end{bmatrix}$$

c. Definition of the Arrays for the Example in b

Figure 8.19 Storage scheme for the Gauss elimination procedure.

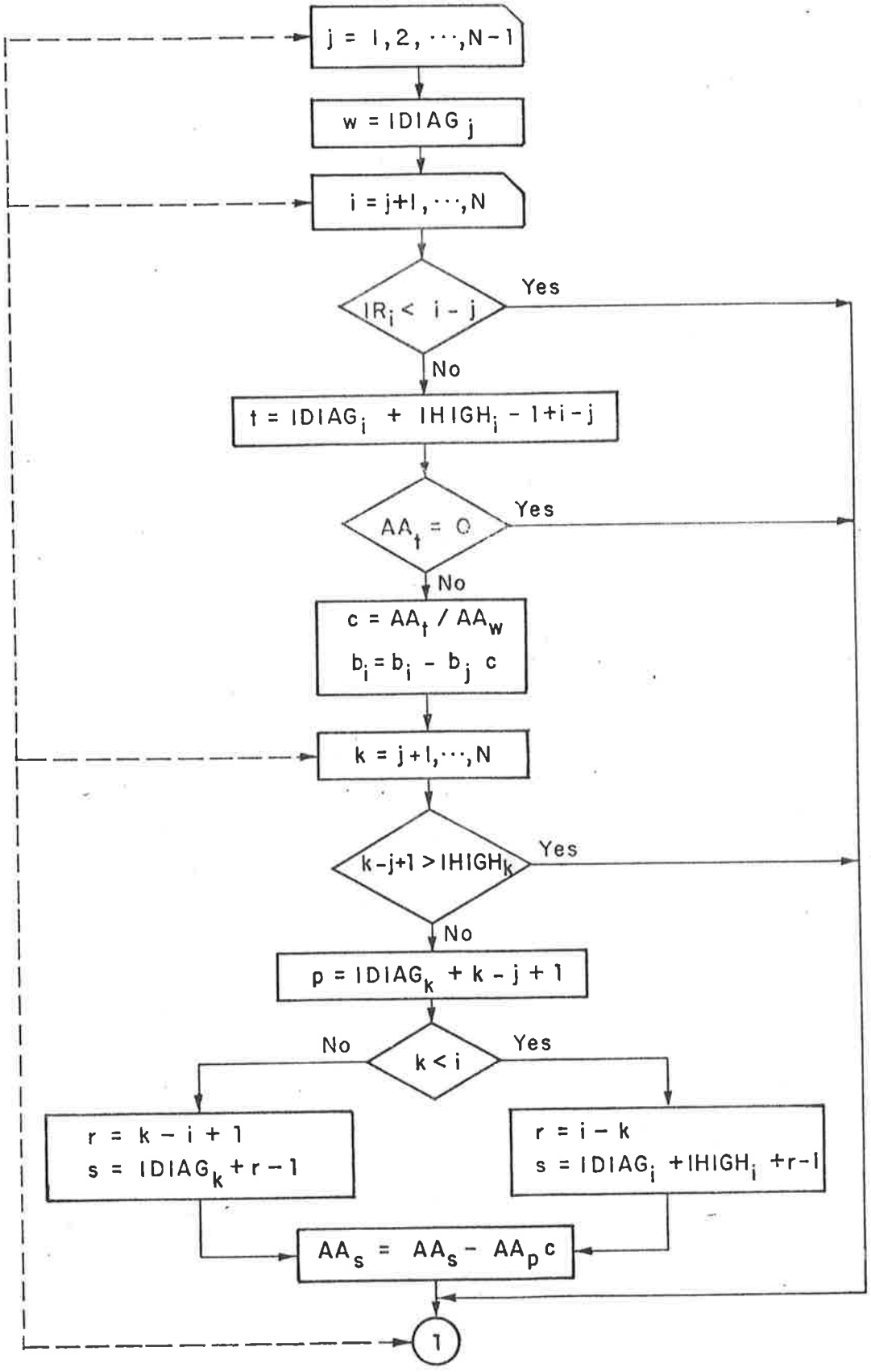

Figure 8.20 Flowchart for the storage scheme.

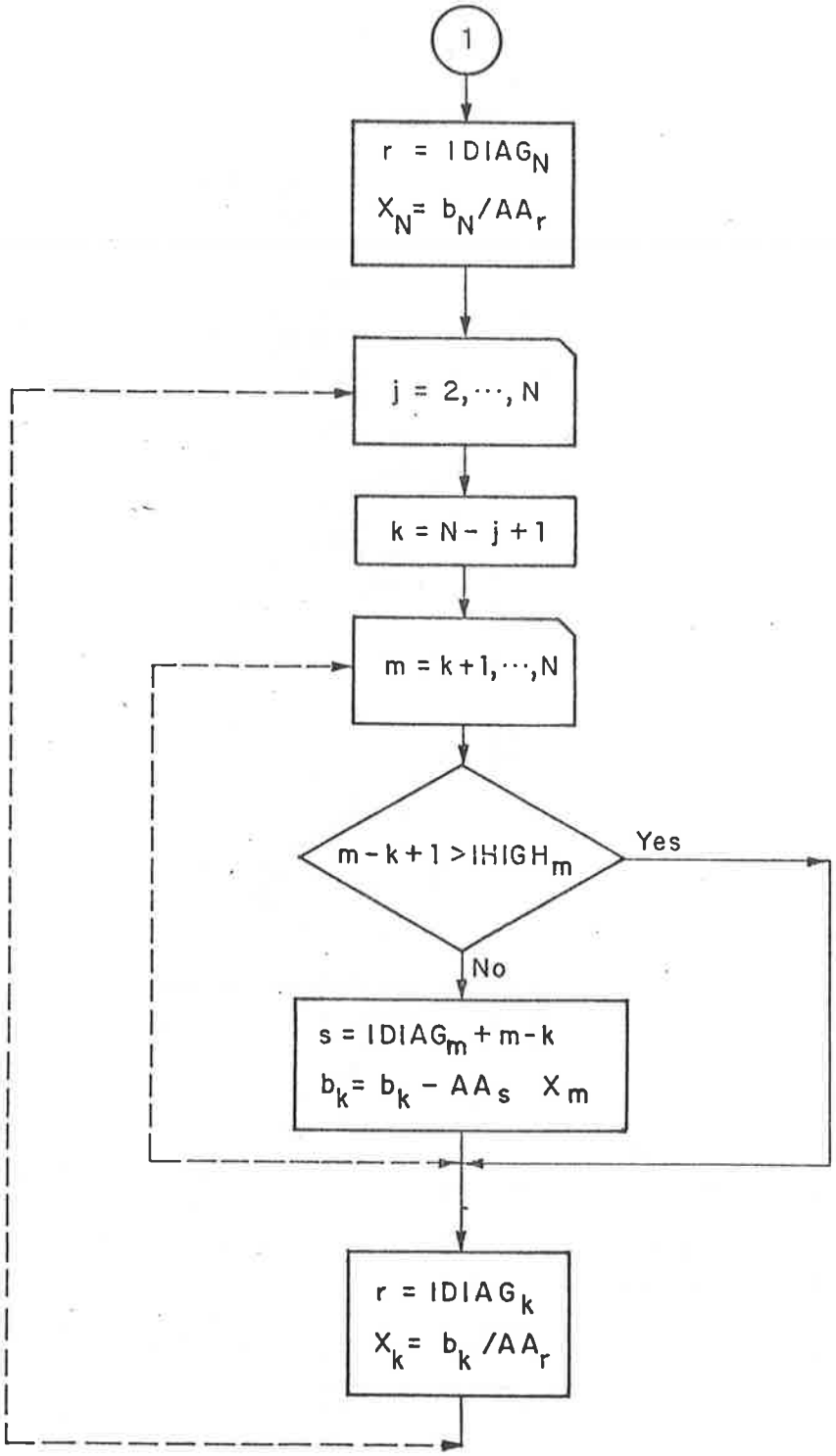

Figure 8.20 Continued.

Application of the Model

The system tested in this study was the Jacui Delta, a small delta located in the south of Brazil in the state of Rio Grande do Sul. Four rivers flow into this delta; they include the Gravatai, the Sinos, the Cai and the Jacui. The total watershed area at section F in Figure 8.21 is about 100,000 km^2 in size, which represents one third of the state. The Jacui River is the main stream. Its watershed at section M makes up about 80% of the total watershed. The Jacui Delta is a complex system of branches, confluences and storage basins; its area is only 42 km^2. The distance between the confluences is small (small islands), the widths are large (about 1000 m) in the main channels and the slope is small. Below the downstream section the rivers form a series of large lakes that are linked together until they reach the Atlantic Ocean. The delta is about 250 km away from the ocean. On the eastern side of the delta there is a harbor and Porto Alegre, which is the capital of the State, a city of about 1.2 million people.

The water level in this delta shows a cyclic variation with an amplitude of about 30 cm within a 24 hour time period. This cyclic variation is sometimes altered by wind effects and floods. In the dry season when the flow is low, a flow inversion can occur due to the backwater effects from the lakes.

The discharges were recorded at seven sections as shown in Figure 8.21. The record of discharge available in those sections is for 24 hours (12 noon of April 27, 1977 to 12 noon of April 28, 1977). The discharges were recorded at time intervals of 3 hours, but conditions were bad and errors were incurred. Only four or five verticals were measured at each cross section. The important sections were between 800 and 1200 meters wide. The vertical position of measurement from time to time was difficult to hold since the velocity was high for this size of river. Some records are missing at sections M, J, and R.

There is a 1940 hydrographic survey map available for the study area. The map was used as a reference to locate the sections for a new survey map measured in 1977. In most of the sections in the model a new cross-sectional geometry was available. In the event that a new geometry did not exist, the old geometry was used.

Figure 8.21 shows that 64 sections were used in the model to represent the river system. These sections were chosen taking into

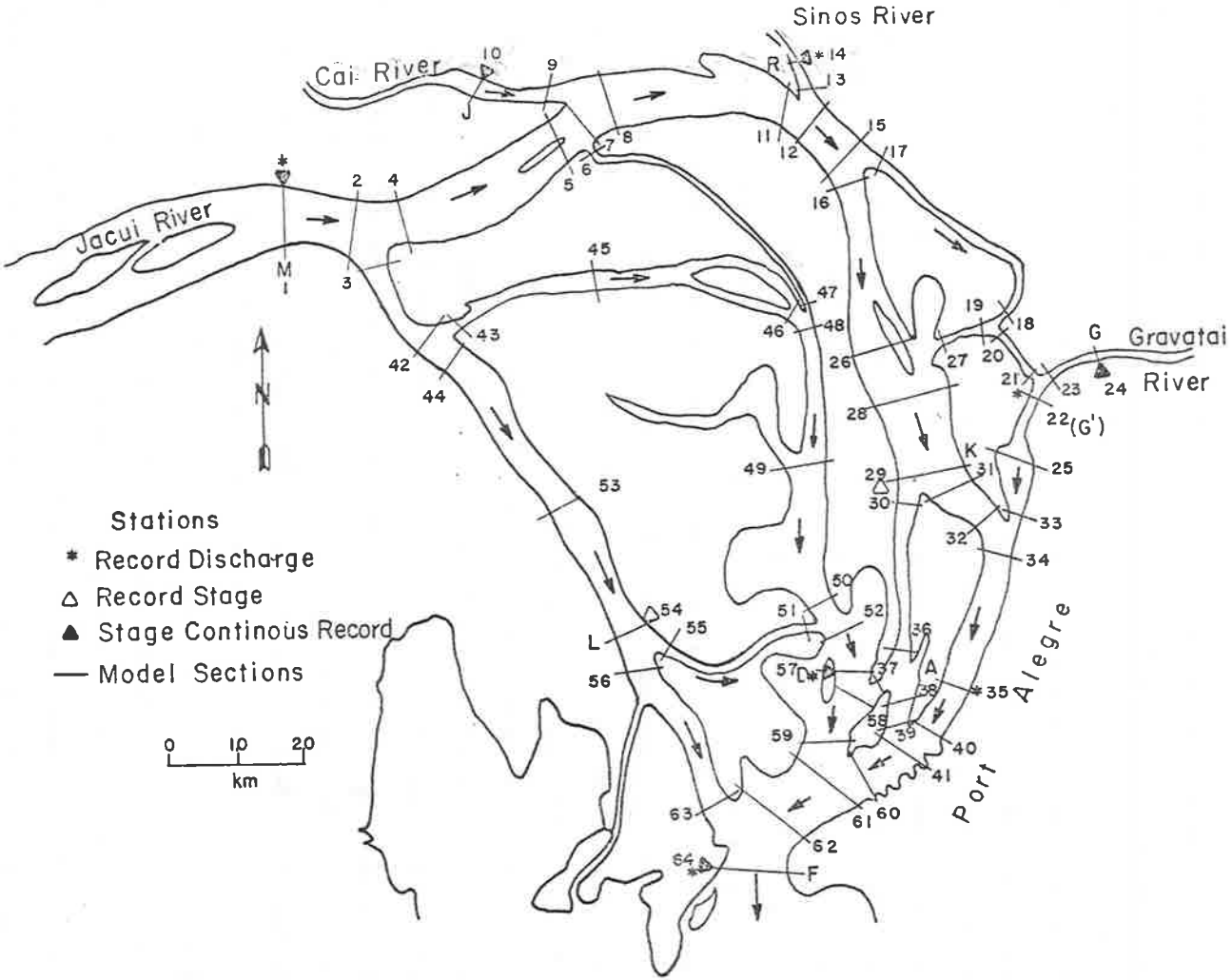

Figure 8.21 Jacui Delta map.

account the cross section changes and confluence criteria. However, the distance between the confluences is often short which implies that the distance between the sections is small.

Model Calibration and Verification

Data used for the parameter adjustment was from 12 noon of April 27, 1977 to 12 noon of April 28, 1977. The boundary conditions used in this calibration were the discharges at sections M, J. R and G and the stage at section F. The initial conditions for all sections were calculated by assuming an arbitrary initial condition for all sections and running the program, holding the boundary values constant. After about 30 time steps the steady state condition was reached.

The parameters of the model which are important in the flow division at the confluences and in the adjustment of the discharges and stages, are the cross-section area, hydraulic radius, Manning's roughness coefficient (n) and the loss coefficient at the confluences (α). Normally the area and hydraulic radius are defined by the data from the maps. The Manning's roughness coefficient has to be estimated for each cross section or, in some situations, for each stage in these cross sections. A practical procedure is to record the discharge in a section and also record the stage of the section and of another nearby section in order to calculate the water surface slope. Using Manning's equation, it is possible to estimate Manning's n. In the Jacui Delta there are limited data available to estimate these values. The procedure used here was to try to adjust the calculated stages and discharges to the recorded ones.

The roughness coefficient has much effect on the water surface elevations and discharge distributions. In a river without a confluence, for the same input hydrograph, the stage increases with Manning's n. When the river system is such as that of the Jacui Delta with confluences, the relationship among the variables and this parameter is more complex. When Manning's n increases in the confluence section, and in the respective branch, less flow comes through this branch and instead of the increases in stage it can decrease. The adjustment turns out to be complex when there are many junctions, as in the Jacui Delta.

The procedure here was to adjust the stages and discharges of the main branches using the data at sections L (also Section 54), D(57),

A(35), and K(29) in Figure 8.21. The main flow division is among sections 2, 3, and 4. The secondary branches could not be adjusted since there was no data and the n values were estimated. The values of α were used in the adjustment. The variables are not sensitive to these parameters. It has a direct effect on the flow division. Increasing α decreases the flow.

Recorded and calculated values at some sections are shown in Figure 8.22 and 8.23. The differences in the levels were on the order of 1.0 cm in most of the sections. The difference in the discharges was on the order of 8%. Since the errors assumed in the record of these discharges are greater than that, refinement would be a waste of time. Unfortunately the period of recorded discharge did not show a critical situation with inversion flow and great variation in level. The levels during this period were above the seasonal normal. More information needs to be obtained in the secondary branches as most of the pollution is carried by small streams. A period in the dry season must be chosen to measure the discharges and stages.

After the parameters were found by adjustment using a period of 24 hours, model verification was required to determine whether the parameters were sufficiently reliable for use in another simulation period other than adjustment. A 48-hour period was chosen for verification when the stage variation is of about 0.65 m. In this case it was only possible to verify the stages because the discharges were not available. The configuration, geometry data, parameters and time step were the same as those used in the model adjustment. The boundaries used were the levels at Sections F and M as shown in Figure 8.21. The recorded stages used in the verification were only from Sections L and D. The results at Sections D and L are shown in Figure 8.24 and 8.25. The solution of the mathematical model shows good agreement with the recorded values.

The limitations of the model are the one-dimensional assumption and the steady solution at the confluence. This limitation is only important when the velocity and energy losses are high which usually occur in small streams. The advantages of the developed model are in handling a broad and complex river network system with minimal computer cost, and in using complete one-dimensional partial differential equations.

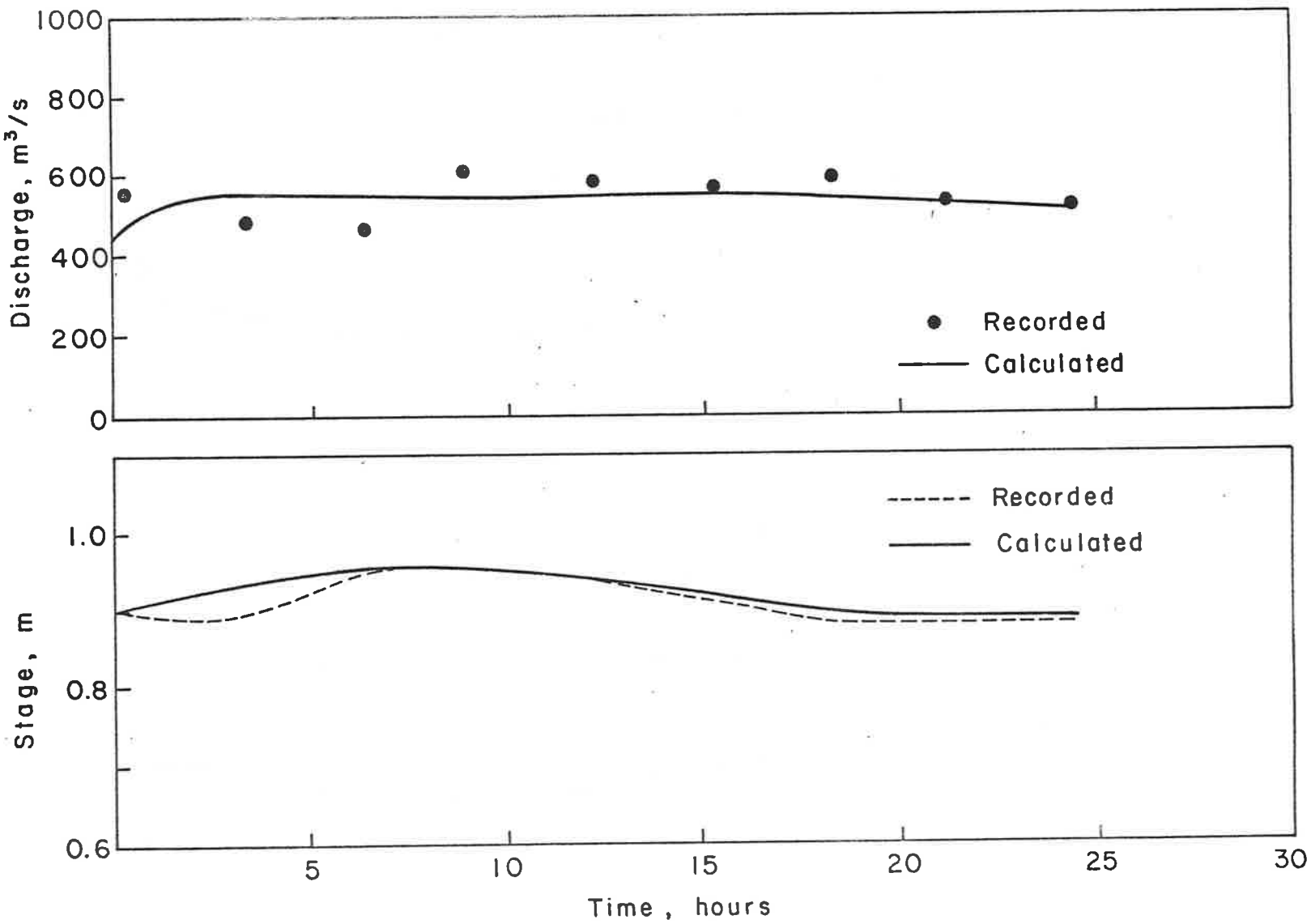

Figure 8.22 Calculated and recorded values at Section A for the adjustment period.

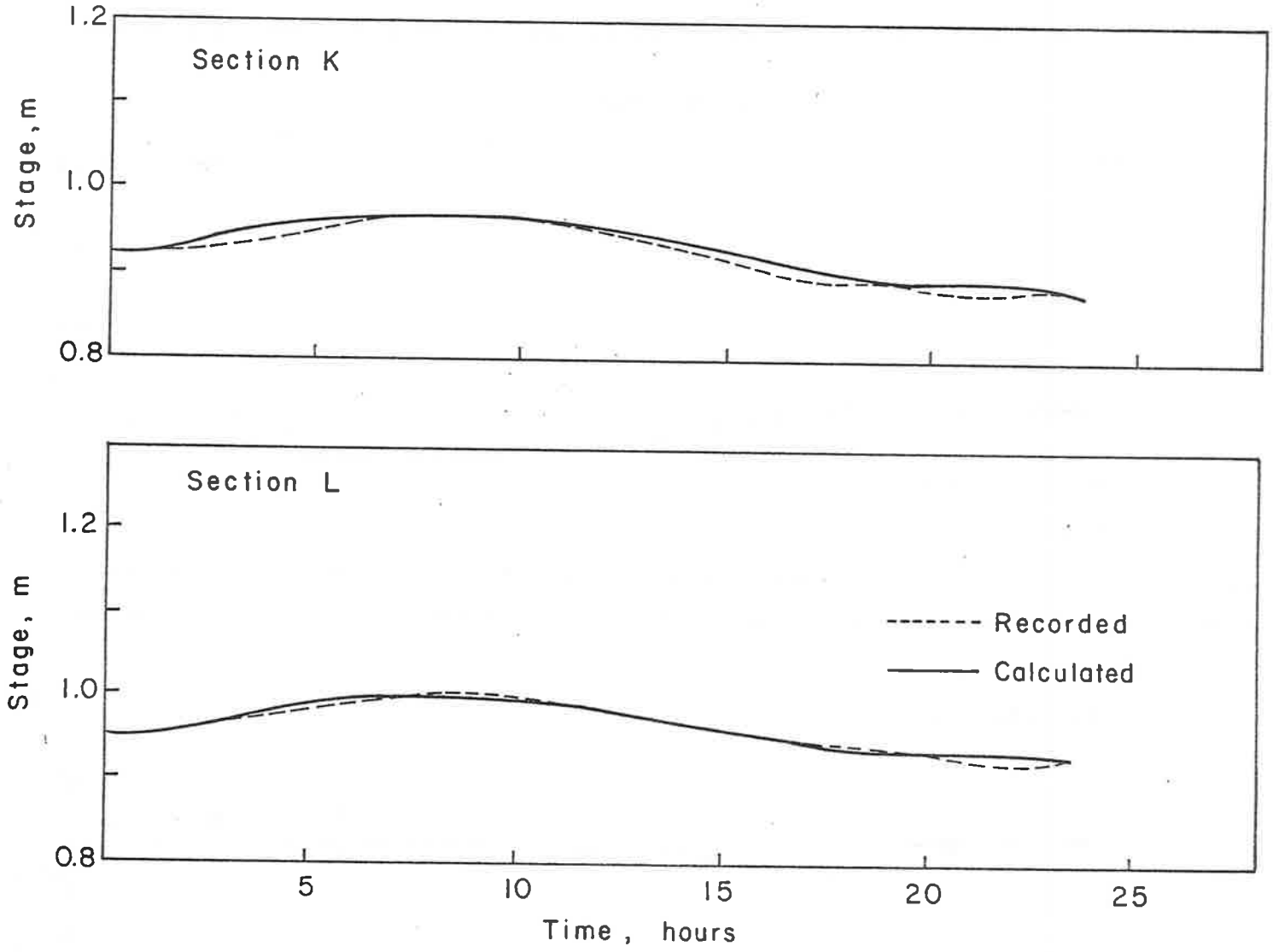

Figure 8.23 Calculated and recorded levels at Sections K and L during the adjustment period.

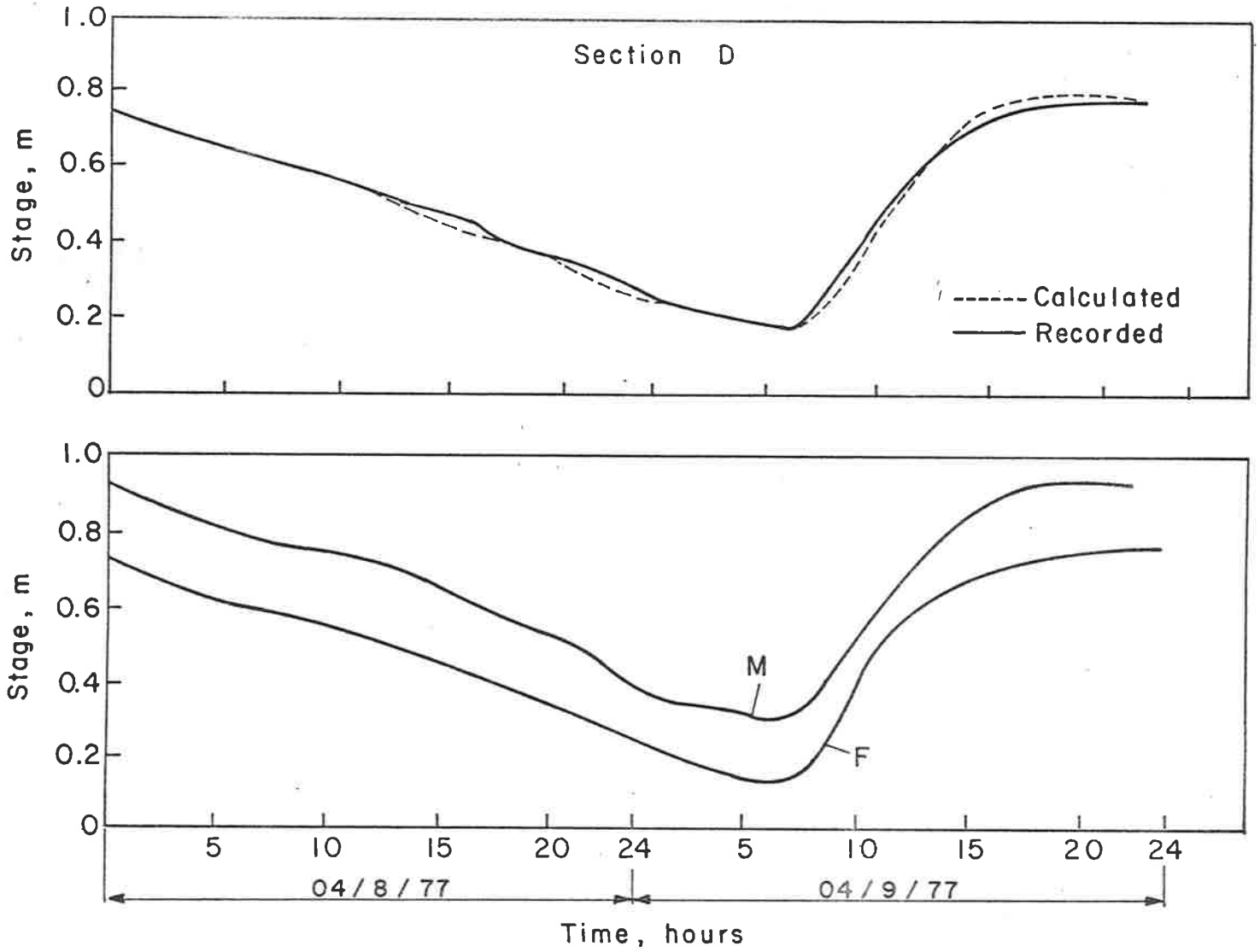

Figure 8.24 Recorded level at Section M, F and D and calculated level at Section D during verification period.

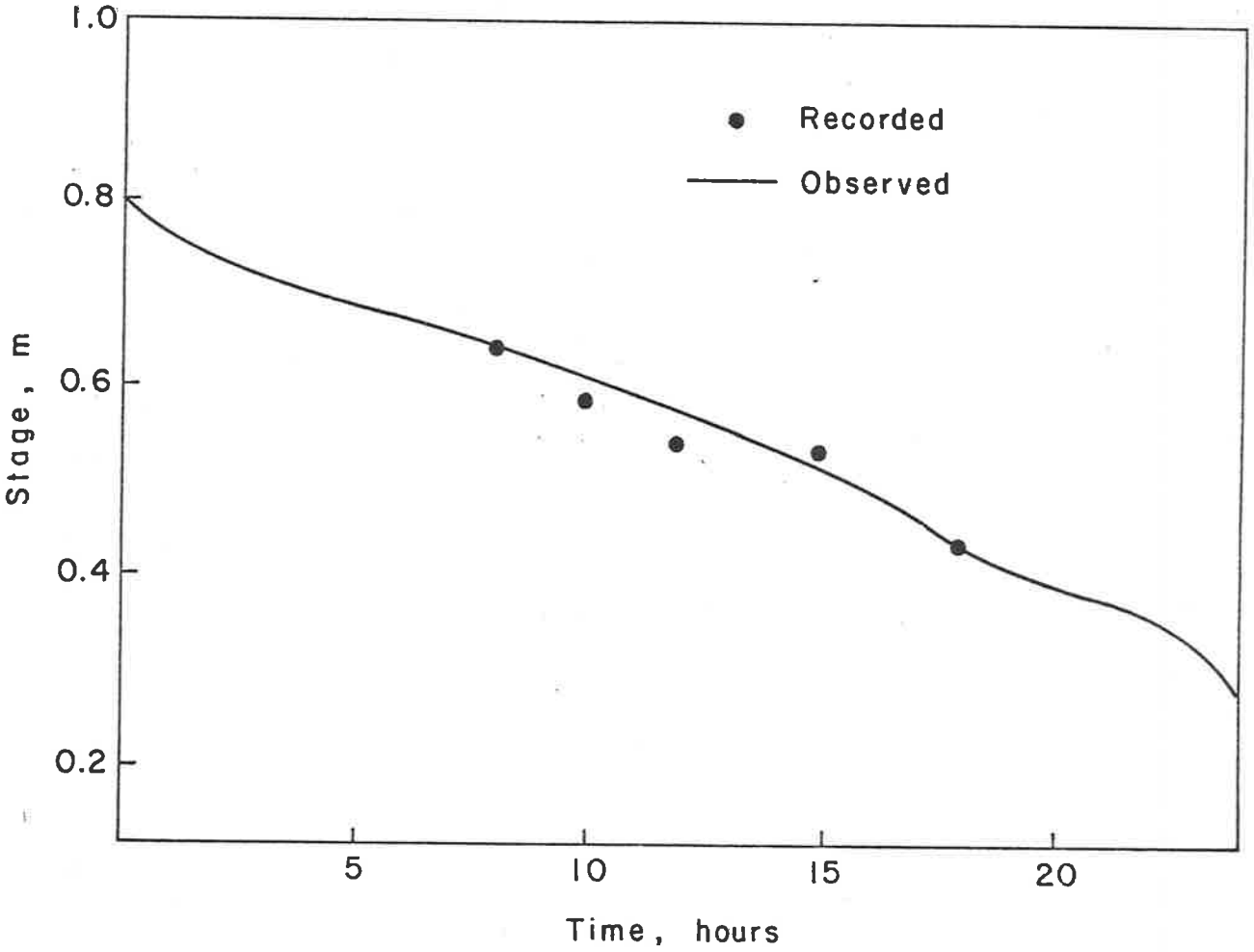

Figure 8.25 Recorded and calculated levels at Section L during April 8, 1977.

8.4 TWO-DIMENSIONAL WATER ROUTING MODEL

Introduction

In many instances, such as flow in estuaries, in highly irregular channels, on floodplains, etc., the flow is predominantly two-dimensional. That is, the flow velocity in both the longitudinal and transverse directions are comparable. As stated above, the one-dimensional model can only determine general trends in nonuniform channels. If more detailed information is to be obtained, a two-dimensional mathematical model can be utilized. Colorado State University is developing a two-dimensional water and sediment routing model, specifically designed for applications to river routing. This model is briefly presented in the following sections. The model is subjected to futher modifications and refinement.

Basic Equations

Flow in an alluvial river is governed by the conservation laws, which state the conservation of mass and momentum quantities. In two-phase flow the conservation of water mass can be expressed analytically by the water continuity equation. Momentum, a vector quantity, has to be conserved in any direction. In cartesian coordinates, the momentum balance is expressed along three orthogonal space directions.

In open channel flow, an expedient approximation to the three-dimensional flow problem is the assumption of bidimensionality along two perpendicular horizontal directions, averaging flow properties in the vertical direction. The pressure distribution along a vertical is assumed hydrostatic, and only time-averaged turbulent flow motions are taken into account in the main flow. However, the simulation of secondary flow patterns, such as large eddies, requires that the effective stresses in vertical planes be taken into account in the two-dimensional analog of the three-dimensional flow problem. No conclusive theory has yet been formulated to evaluate the effective stresses, although simplified approximations have shown to be promising from a practical standpoint.

The equation of water continuity in two horizontal space coordinates is:

$$\frac{\partial q_x}{\partial x} + \frac{\partial q_y}{\partial y} + \frac{\partial d}{\partial t} = 0 \qquad (8\text{-}67)$$

where

q_x = the unit-width water discharge in the x-direction

q_y = the unit-width water discharge in the y-direction

d = the depth of flow

x and y = horizontal space variables

and t = the time variable.

The momentum equations for two-dimensional horizontal flow can be obtained by vertical integration of Reynolds' equations for turbulent flow in three dimensions. Taking into account the boundary conditions at the bottom and at the surface, they yield

$$\frac{\partial}{\partial t}(q_x) + \frac{\partial}{\partial x}\left(\frac{q_x|q_x|}{d}\right) + \frac{\partial}{\partial y}\left(\frac{q_x|q_y|}{d}\right) - f_g q_y + \frac{g}{2}\frac{\partial}{\partial x}(d^2) + gd\frac{\partial z}{\partial x} - \frac{1}{\rho}(\tau_{wx} - \tau_{bx}) - \frac{1}{\rho}\frac{\partial}{\partial x}(d\,\tau_{xx}) - \frac{1}{\rho}\frac{\partial}{\partial y}(d\,\tau_{xy}) = 0 \qquad (8\text{-}68)$$

$$\frac{\partial}{\partial t}(q_y) + \frac{\partial}{\partial x}\left(\frac{|q_x|\,q_y}{d}\right) + \frac{\partial}{\partial y}\left(\frac{q_y|q_y|}{d}\right) + f_g q_x + \frac{g}{2}\frac{\partial}{\partial y}(d^2) + gd\frac{\partial z}{\partial y} - \frac{1}{\rho}(\tau_{wy} - \tau_{by}) - \frac{1}{\rho}\frac{\partial}{\partial x}(d\,\tau_{xy}) - \frac{1}{\rho}\frac{\partial}{\partial y}(d\,\tau_{yy}) = 0 \qquad (8\text{-}69)$$

where

$q_x = ud$

$q_y = vd$

u = the depth-integrated velocity in the x-direction

v = the depth-integrated velocity in the y-direction

f_g = the geostrophic parameter

ρ = the mass density of the water

τ_{wx} and τ_{wy} = the components of surface shear stress due to wind

τ_{bx} and τ_{by} = the components of bottom shear stress

τ_{xx}, τ_{xy} and τ_{yx} = the effective stresses in vertical planes,

and all other terms are as defined previously.

Equations 8-67, 8-68 and 8-69 are the governing equations of the two-dimensional water flow problem. In river flow, the influence of the geostrophic term is usually small, and f_g is made equal to zero. Likewise, the surface shear stresses are small as compared to the bottom shear stresses, and are usually neglected.

Supplemental Equations

The three basic equations contain three basic unknowns: q_x, q_y, and d. The other variables in the equations must be expressed as a function of the three unknowns in order to obtain a solution. Supplemental equations for the bottom shear stress and the effective stresses in vertical planes are needed in order to make the system of governing equations amenable to a mathematical solution.

The usual assumption regarding bottom stress τ_b is that its magnitude is the same as that corresponding to steady uniform flow, and that its direction is the same as that of the depth-averaged velocity. For any direction

$$\tau_{bw} = f \rho w^2 \tag{8-70}$$

where τ_{bw} is the bottom stress in the direction of the depth-averaged velocity w, and f is a dimensionless friction factor defined as

$$f = \frac{g}{C^2} \quad \text{or} \quad f = \frac{gn^2}{(1.486)^2 d^{1/3}} \tag{8-71}$$

where C is the Chezy coefficient, and n is Manning's roughness coefficient.

The depth-averaged velocity w is resolved along two perpendicular horizontal coordinates such that

$$w = (u^2 + v^2)^{1/2} \tag{8-72}$$

In two horizontal space dimensions, the resistance equations are expressed as

$$\tau_{bx} = f \rho uw \tag{8-73}$$

$$\tau_{by} = f \rho vw \tag{8-74}$$

where τ_{bx} and τ_{by} are the bottom shear stresses along the x and y directions, respectively.

In the two-dimensional flow problem, computational convenience dictates that the eddy viscosity term be substituted for the terms accounting for the effective stresses in vertical planes of Equation 8-68 and 8-69. The eddy viscosity term for the x-momentum equation is

$$- \varepsilon d\left(\frac{\partial^2 u}{\partial x^2} + \frac{\partial^2 v}{\partial y^2}\right) \tag{8-75}$$

and for the y-momentum

$$- \varepsilon d\left(\frac{\partial^2 v}{\partial x^2} + \frac{\partial^2 v}{\partial y^2}\right) \tag{8-76}$$

where ε is the coefficient of eddy viscosity.

As a first approximation, the coefficient of eddy viscosity can be related to the mean flow properties by (Vreugdenhil, 1973)

$$\varepsilon = \varepsilon_q (q_x^2 + q_y^2)^{1/2} \tag{8-77}$$

where ε_q is a dimensionless eddy viscosity coefficient, approximately equal to $6\sqrt{f}$.

The eddy viscosity terms, Equation 8-75 and 8-76, although approximations of the effective stress terms, have far-reaching consequences in that they enable the two-dimensional treatment of the predominantly three-dimensional features of the flow phenomena, with the computational advantages associated with it.

Numerical Solution Method

Equations 8-67, 8-68 and 8-69 are the conservation equations governing the water flow in river. Their solution can be carried out by use of a finite-difference scheme that approximates the functions and their partial derivations in terms of their values in a tridimensional orthogonal time-space grid system, or by use of a finite-element scheme to approximate the solution by discretizing a solution domain with a finite number of points at which values of variables are obtained.

Finite-difference solutions to problems involving various forms of the shallow water equations have been obtained by Leendertse (1967, 1970); Leendertse and Gritton (1971); Abbott, Danesgaard and Rodenhuis (1973); Apelt, Gont and Szewezyki (1974) and many other researchers. Finite-element solutions for similar problems have also bee represented

by several authors including Taylor and Davis (1973); Connor and Wang (1974); Brebbia and Partridge (1976); Partridge and Brebbia (1976); and Brebbia and Connor (1976). Most of their solutions have dealt with bays or estuaries where the discretization in space can be fairly coarse. Generally speaking the larger the space grid dimension the larger the time step that can be used. Even so the problem of limited length of time step has continued to restrict the time span of solution because of the computational costs. This aspect has been the subject of much recent research for finite-difference and finite-element methods. The length of time step in the transient integration of the equations is of particular significance in the study of river problems since changes in the channel bed, which are of major concern, tend to occur much more slowly than changes in the water surface. In addition, flood waves in rivers often have periods of several days and in some cases weeks. Detailed description of the numerical formulation of the two-dimensional mathematical models of a river system and their applications is given by Simons et al. (1977, 1979). Only conceptual designs of numerical methods are described below.

The finite-difference solution scheme formulated in a multioperational mode. A review of the available literature (Leendertse, 1967; Abbott and Cunge, 1975; Abbott, Danesgaard and Rodenhuis, 1973) indicated that an alternating direction-implicit finite-difference formulation could be used as a basis for the model. The principle of the solution method is to use several operations to advance the values of the dependent variables to a new time step. In the first operation, the water continuity equation and the momentum equation in the x-direction are solved simultaneously, resulted in the values of water discharge q_x and depth d being advanced to time level $(n + 1/2)$. Variables q_y and z are taken at the known time level n. This operation is performed one row at a time, for as many rows as required by the boundary configuration.

In the second step, the water continuity equation and the momentum equation in the y-direction are solved simultaneously, resulting in the values of water discharge q_y and depth d being advanced to time level $(n + 1)$. Variables q_x and z are taken at the known time levels $(n + 1/2)$ and n, respectively. This operation is performed one column at a time, for as many columns as required by the boundary configuration.

Figue 8.26 shows a schematic illustration of the locations where the various dependent variables are calculated in the time domain.

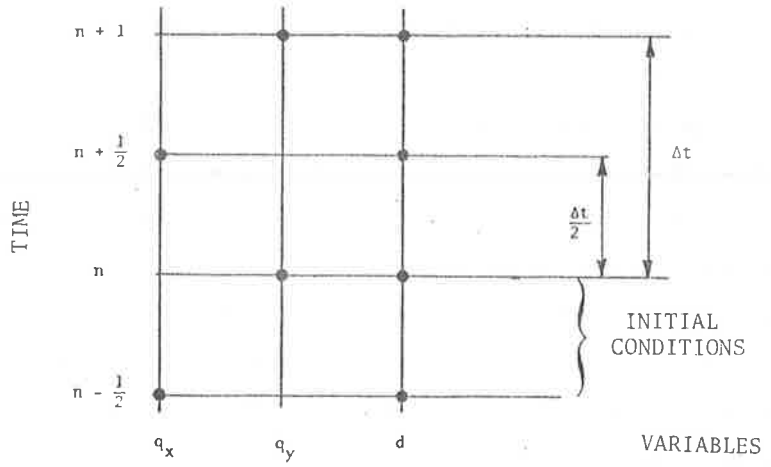

Figure 8.26 Variable location in the time domain.

These dependent variables q_x , q_y and d are defined on a space-staggered grid system to reduce the number of unknowns to be solved. That is, they are defined only at their respective subgrids as shown in Figure 8.27. This grid system is designed so that the multioperation solution method can be effectively applied to compute the unknown variables. This figure also shows two types of boundary conditions specified in the two-dimensional space-staggered system: (1) open boundary and (2) closed boundary. In an open boundary, the water discharge and depth are allowed to vary in time. In a closed boundary, the water discharge component perpendicular to the boundary is set equal to zero. A river configuration can be described by this two-dimensional grid system as shown in Figure 8.28. Some approximations need to be made along the closed boundaries. It is possible to describe the river configuration to a better degree using an orthogonal curvilinear grid system, and then transform this system into a cartesian coordinate. The equations are then solved on this transformed coordinate (Wanstrath et al., 1976). However, the formulation of the computation processes is quite complex. Also, within-river boundaries such as islands cannot be transformed. These limitations restrict the applicabilities of the coordinate transformation method.

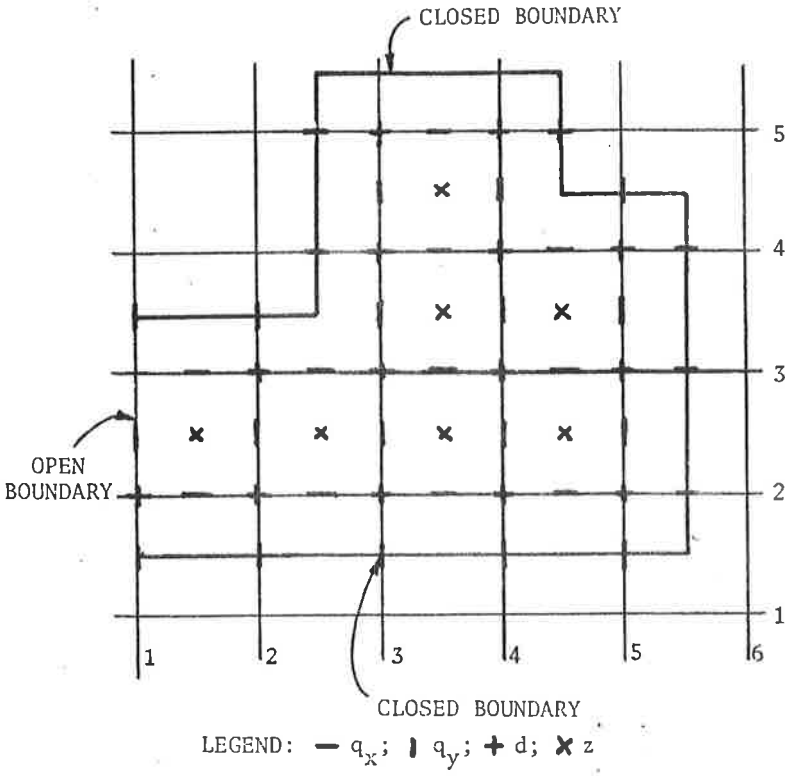

Figure 8.27 The open boundary and closed boundary in the space-staggered grid.

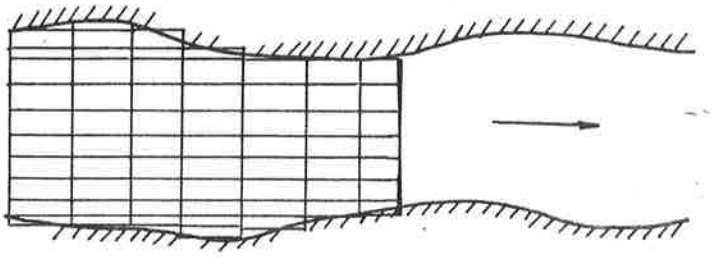

Figure 8.28 Finite-difference grids describing a river reach.

Application of the Two-Dimensional Water Routing Model to Study Pool 4 in the Upper Mississippi River and Lower Chippewa River

The developed two-dimensional mathematical model has been applied to model Pool 4 at the confluence of the Upper Mississippi River and Lower Chippewa River. The model includes water and sediment routing

components. The sediment routing component will be described in Chapter 11. This mathematical model of Pool 4 is used to predict hydraulic and geomorphic changes in the Lower Pool 4 reach and the lower end of the Chippewa River caused by various development activities and thus to identify successful development projects in the study reach that meet the goals of navigation, flood control, recreation, conservation of resources, and preservation or enhancement of the environment.

The mathematical model developed in this study has been calibrated using the following two sources of data: 1) limited field data for Pool 4, Mississippi River, available from previous one-dimensional mathematical model studies, and 2) laboratory data collected by the University of Minnesota in their recently completed physical model study of Pool 4, Mississippi River (horizontal length scale = 1:200 and vertical length scale = 1:40). The Pool 4 river reach used in the calibration of the mathematical model described in this chapter is the same as that used in the University of Minnesota physical model studies (see Figure 8.29). The model calibration based on the results of the physical model study is described below.

The data collected in steady state runs No. 1 of the physical model study (University of Minnesota) was used for the calibration of the two-dimensional water routing model developed in this study. This run was carried out to simulate the two-dimensional flow patterns in the study reach, under the following steady flow conditions: prototype water discharge in the Mississippi River immediately downstream of Lake Pepin, 19,000 cfs (intermediate flow); water discharge in the Chippewa River upstream of its confluence with the Mississippi River, 30,000 cfs (high flow). The following physical and numerical parameters were used in this run:

Bottom friction $f_r = 0.005$ (approximately equivalent to Manning's n = 0.017)

Space step in x-direction $x = 1$ ft

Space step in y-direction $y = 0.5$ ft

Weighting factor $\delta = 0.70$ (This value of weighting factor provides enough dissipation to counteract local unstable tendencies of the numerical model).

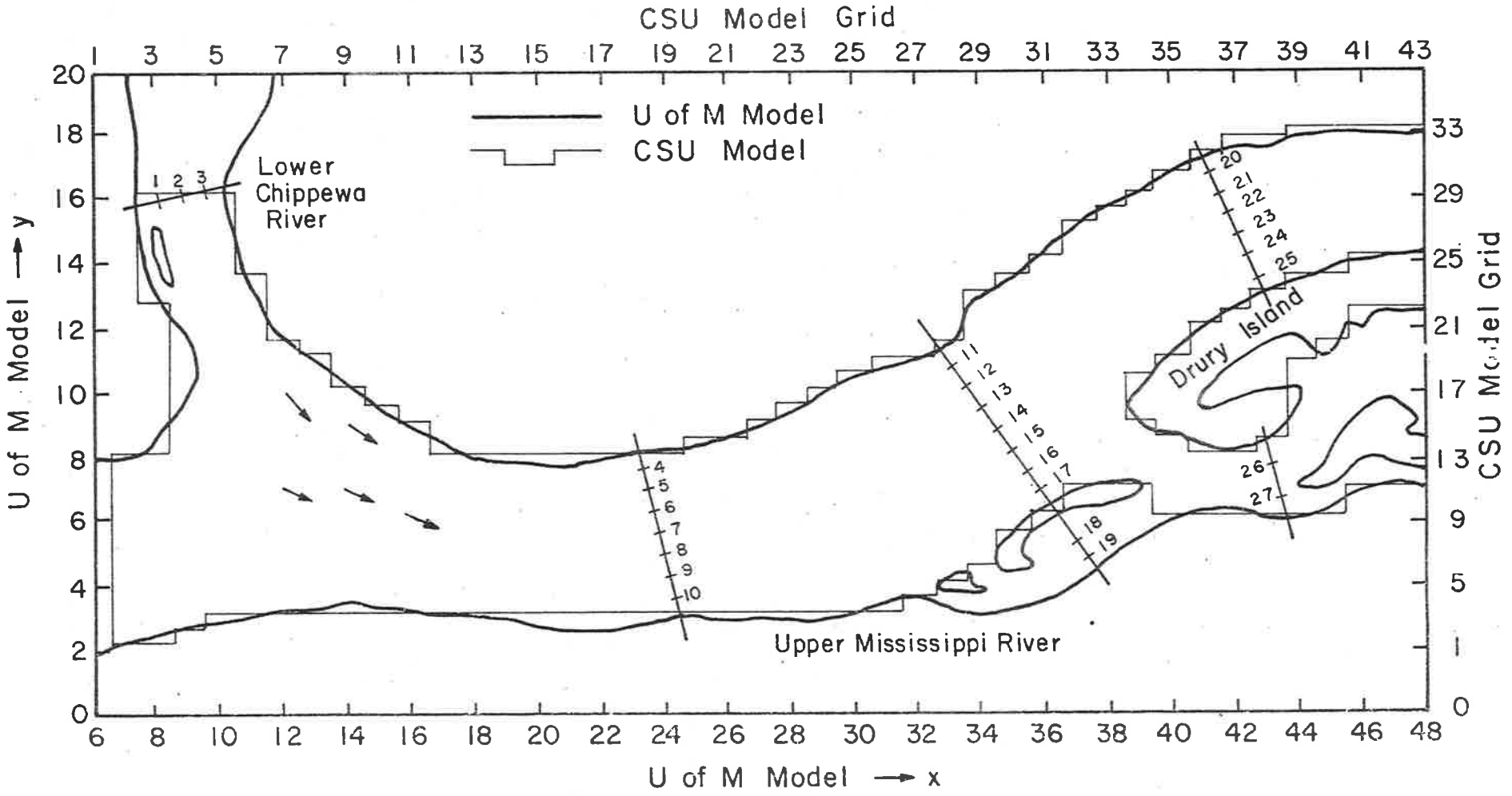

Figure 8.29 General layout of the University of Minnesota physical model and the Colorado State University mathematical model.

The mathematical model simulation was started from a "could start", i.e., the initial conditions were: a) zero for the volumetric fluxes q_x and q_y (discharge per unit width), and b) pool level equal to 1.38 ft for the stage throughout the model. The open boundary conditions where discharge was specified was gradually increased from zero flux to the steady state values corresponding to the physical model (0.69 cfs for the Mississippi River and 1.10 cfs for the Chippewa River). The simulation was continued until the steady state condition was reached throughout the model.

Figure 8.30 shows the results of the calibration run, depicting the overall agreement between calculated and measured values of water discharge (discharge vectors are shown at the scale of 0.5 cfs/ft per feet of physical model dimensions). Figures 8.31 and 8.32 show the comparison between computed and measured velocities and flow depths at the measuring locations shown in Figure 8.29. The agreement between predicted and measured depth and discharge distributions is good. However, more field data is required to verify the mathematical model.

8.5 SUMMARY AND CONCLUSIONS

Mathematical models for water routing in rivers have been described in this chapter. The developed models have been successfully applied to study various types of water related problems in rivers. It is not the intention to present all the models available in hte literature. Instead, the chapter presents some useful models that have been tested and verified.

The models presented include one-dimensional model of a simple river system, one-dimensional model of a river network system and two-dimensional models. These models are based on the conservation laws: water continuity equation and momentum equation. In general, a one-dimensional water routing model is adequate to study flood movement and water related problems, and to predict hydraulic responses to development in a relatively uniform river. The one-dimensional model of a river netowrk system is very useful in the simulation of a river system where islands, meander loops and tributaries are connected to the main channel. For a highly irregular river reach, the one-dimensional model can only determine general hydraulic patterns. If a river reach has significant flow in both longitudinal and transverse directions, detailed knowledge of

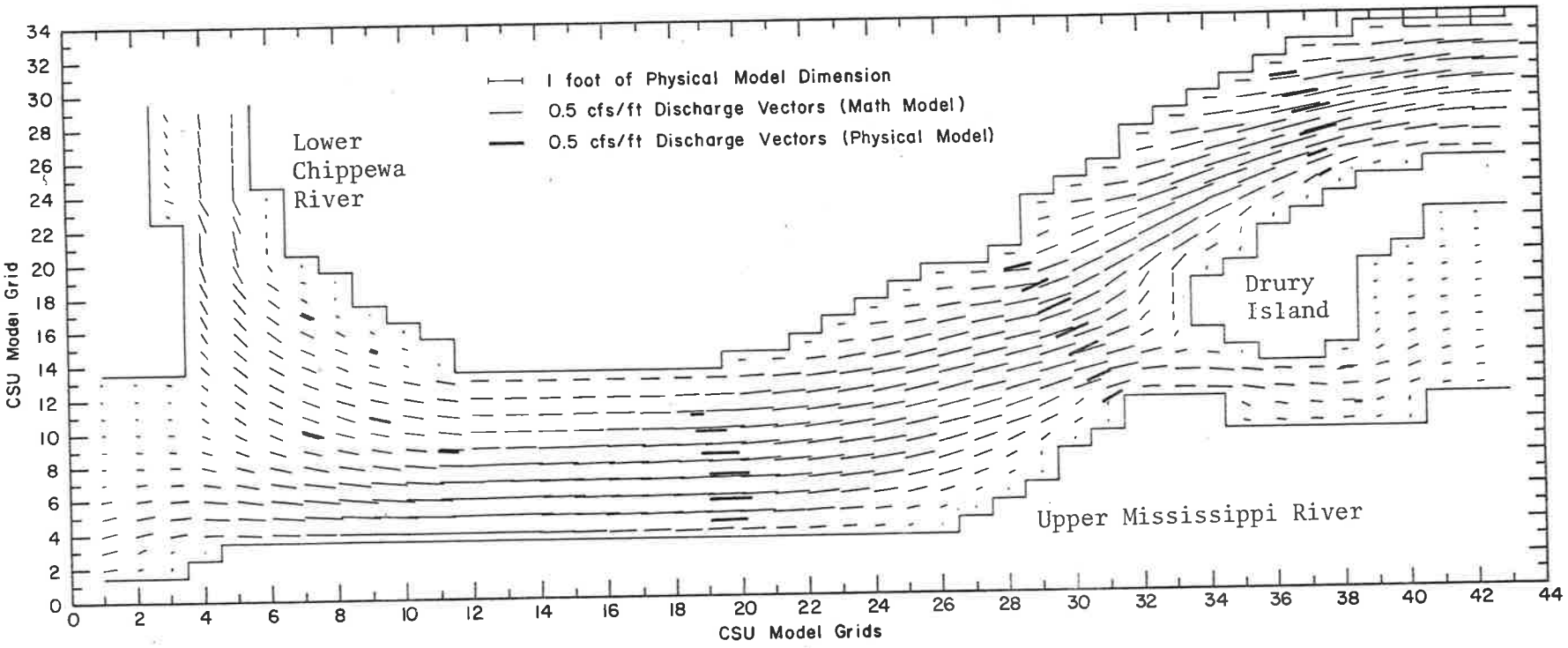

Figure 8.30 Measured and calculated water discharge patterns in the Pool 4 two-dimensional mathematical model.

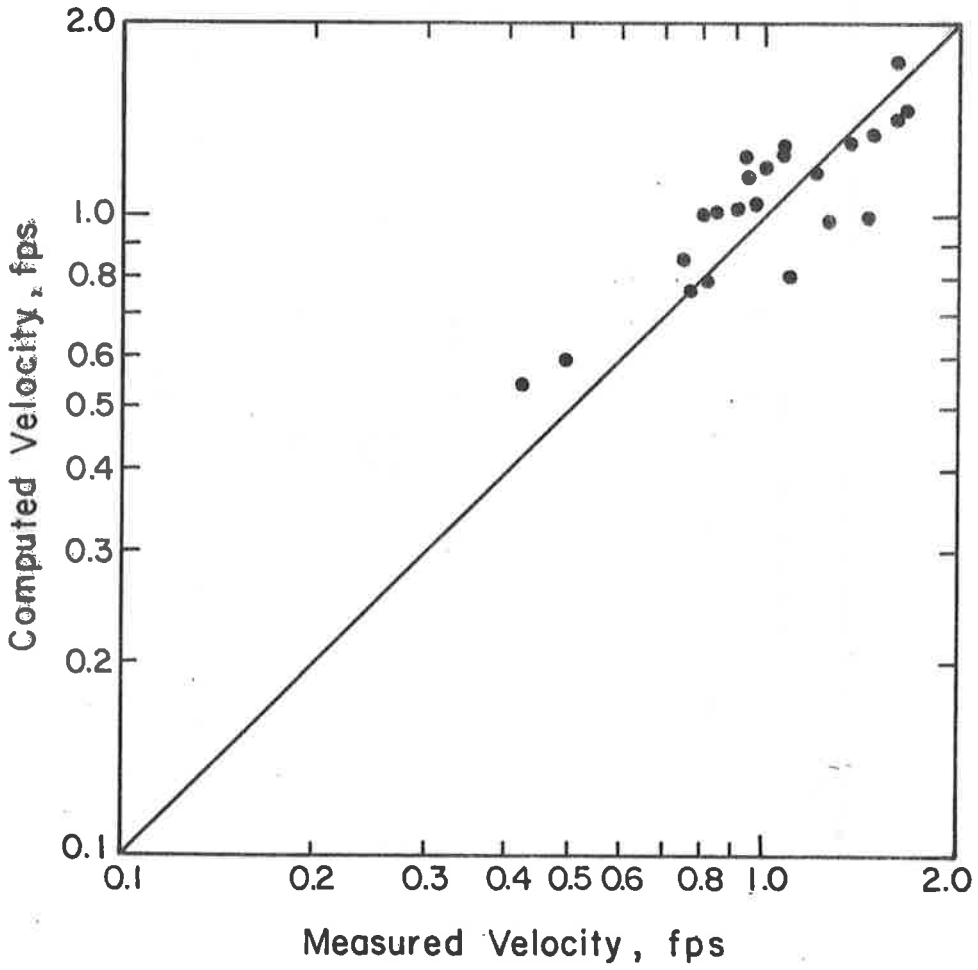

Figure 8.31 Comparison between computed and measured velocities at measurement stations.

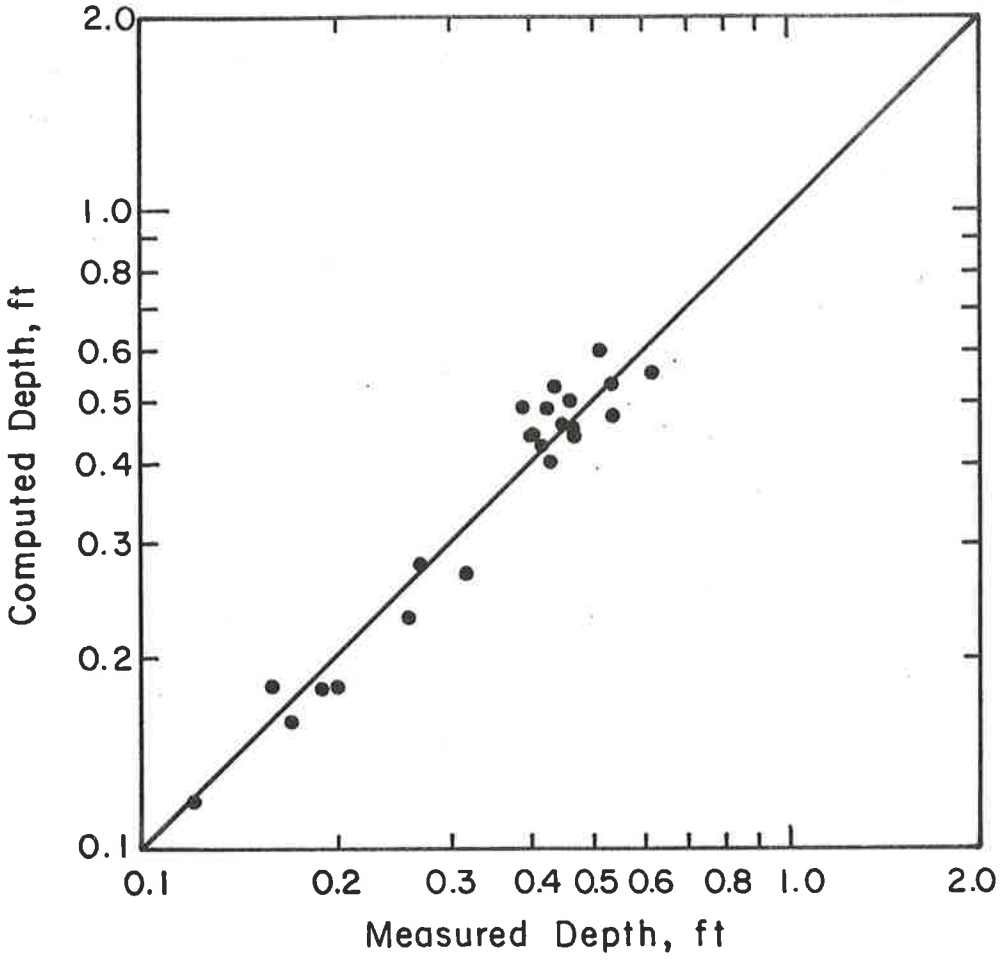

Figure 8.32 Comparison between computed and measured depths at measurement stations.

water movement can only be obtained from a two-dimensional or even only from a three-dimensional model.

It is apparent that the model complexities and computational efficiencies depend on the number of governing equations being solved in the dominative direction(s). A relatively simple model that can provide adequate information is always desired. This requires some engineering judgment and experience with mathematical modeling. Also, on some occasions unreasonable results may be obtained due to wrong data input and/or limitation of models. The computed results from a model need to be carefully interpreted using basic principles of river mechanics.

8.6 REFERENCES

Abbott, M. B., Danesgaards, A., and Rodenhuis, G. S., 1973. System 21 "Jupiter", a design system for two-dimensional nearly horizontal flows. Journal of Hydraulic Research, Vol. 11, No. 1, p.. 1-28.

Abbott, M. B., and Ionescu, F., 1967. On the numerical computation of nearly horizontal flows. Journal of Hydraulic Research, Vol. 5, No. 2, pp. 98-117.

Amein, M., 1966. Streamflow routing on computer by characteristics. Water Resources Research, American Geophy. Union, Vol. 2, No. 1, pp. 123-130.

Amein, M., and Fang, C. S., 1970. Implicit flood routing in natural channels. Journal of the Hydraulics Division, ASCE, Vol. 96, No. HY12, pp. 2481-2500.

Apelt, C. J., and Gout, J. J., 1974. Numerical modeling of tidal phenomena in bays and estuaries with inter-tidal flats. Proceedings 5th Australas Conference on Hyraulics and Fluid Mechanics, Christchurch, New Zealand.

Balloffet, A., 1969. One-dimensional analysis of floods and tides in open channels. Journal of Hydraulics Division, ASCE, Vol. 96, No. HY4, pp. 1429-1451.

Baltzer, R. A., and Lai, C., 1968. Computer simulation of unsteady flow in waterways. Journal of Hydraulics Division, ASCE, Vol. 95, No. HY4, pp. 1559-1575.

Bathe, K., and Wilson, E. L., 1976. Numerical methods in finite element analysis. Prentice-Hall, Inc., Englewood Cliffs, New Jersey.

Brebbia, C. A., and Connor, J. J., 1976. Introduction to finite element techniques for fluid flow. Butterworths, London, England.

Brebbia, C. A., and Partridge, P. W., 1976. Finite element simulation of water circulation in the North Sea. Applied Math MOdeling, Vol. 1, No. 2, September, pp. 101-107.

Chang, F. F. M., and Richards, D. L., 1971. Deposition of sediment in transient flow. Journal of the Hydraulics Division, ASCE, Vol. 97, No. HY6, Proc. Paper 8191, June, pp. 837-849.

Chen, Y. H., 1973. Mathematical modeling of water and sediment routing in natural channels. Ph.D. diss., Department of Civil Engineering, Colorado State University, Fort Collins, Colorado.

Chen, Y. H., and Simons, D. B., 1975. Mathematical modeling of alluvial channels. Symposium on Modeling Techniques, ASCE, Vol. 1, September 3-5, pp. 466-483.

Chow, V. T., 1959. Open channel hydraulics. McGraw-Hill Book Co., New York.

Cooley, R., and Moin, S. A. Finite element solution of St. Venant equations. ASCE Journal of Hydraulics Division, Vol. 102, No. HY6, pp. 759-775.

Connor, J. J., and Wang, J., 1974. Finite element modeling of hydrodynamic circulation. Numerical Methods in Fluid Dynamics, C. A. Brebbia and J. J. Connor, eds., Peutech Press, London, England, pp. 355-387.

Contractor, D. N., and Wiggert, J. M., 1972. Numerical studies of unsteady flow in the James River. Bulletin 51, Water Resources Research Center, Virginia Polytechnic Institute and State University, Blacksburg, Virginia.

Cunge, J. A., 1975. Applied mathematical modeling of open channel flow. Chapter 10 of Unsteady Flow in Open Channels, K. Mahmood and V. Yevjevich, eds., Water Resources Pub., Fort Collins, Colorado.

DeVries, M., 1965. Considerations about non-steady bed-load-transport in open channels. Proceedings of the Eleventh Congress of the International Association for Hydraulic Research, Vol. 3, No. 3.8, Leningrad, U.S.S.R.

Fread, D. L., 1974. Numerical properties of implicit four-point finite difference equations of unsteady flow. NOAA Technical Memorandum NWS HYDRO-18.

Fread, D. K., 1976. Flood routing in meandering rivers with flood plains. Rivers 76.

Gunaratnam, D. J., and Perkins, F. E., 1970. Numerical solution of unsteady flows in open channels. Hydrodynamic Lab. Report, No. 127, Dept. of Civil Engineering, MIT.

Harleman, D. R. F., 1971. One-dimensional models. Chapter III of Estuarine Modeling; An Assessment, EPA.

Henderson, F. A., 1966. Open channel flow. MacMillan Co., New York.

Keuning, D. H., 1976. Application of finite element method to open channel flow. ASCE Journal of Hydraulics Division, Vol. 102, No. HY4, pp. 459-467.

Leendertse, J. J., 1967. Aspects of a computational model for long period water-wave propagation. Memorandum RM-5294-PR, The Rand Corporation, Santa Monica, California, May.

Leendertse, J. J., 1970. A water quality simulation model for well-mixed estuaries and coastal seas: Principles of computation. Memorandum RM-6230-RC, Vol. 1, The Rand Corporation, Santa Monica, California, February.

Leendertse, J. J., and Girtton, E. C., 1971. A water quality simulation model for well-mixed estuaries and coastal seas: Computational procedures. Memorandum R-708-NYC, Vol. 2, The New York City Rand Institute, New York, New York, July.

Li, R. M., 1977. An uncoupled-steady water and sediment routing model. Unpublished report, Colorado State University, Engineering Research Center, Fort Collins, Colorado.

Liggett, J. A., 1975. Basic equations of unsteady flow. Chapter 2 of Unsteady Flow in Open Channels, K. Mahmood and V. Yevjevich, eds., Vol. 1, Water Resources Pub., Fort Collins, Colorado.

Liggett, J. A., and Cunge, J. A., 1975. Numerical methods of solution of the unsteady flow equations. Chapter 4, Vol. 1, Unsteady Flow in Open Channel, Water Resources Publications, Fort Collins, Colorado.

Liggett, J. A., and Woolhiser, D. A., 1967. Difference solutions of the shallow-water equations. Journal of the Engineering Mechanics Division, ASCE, Vol. 93, No. EM2, Proc. Paper 5189, pp. 39-71.

Partridge, P. W., and Brebbia, C. A., 1976. Quadratic finite-elements in shallow water problems. Journal of Hydraulic Division, ASCE, Vol. 102, No. HY9, September, pp. 1299-1313.

Ponce, V. M., Indlekofer, H., and Simons, D. B., 1978. The convergence of implicit bed transient models. Approved for publication in the Journal of Hydraulics Division, ASCE.

Ponce, V. M., Indlekofer, H., and Simons, D. B., 1978. Convergence of four point implicit water wave models, ASCE Journal of Hydraulics Division, Vol. 104, No. HY7, pp. 947-958.

Ponce, V. M., Li, R. M., and Simons, D. B., 1978. Applicability of kinematic and diffusion models. ASCE Journal of Hydraulics Division, Vol. 104, No. HY3, pp. 353-360.

Preissmann, A., 1960. Propagation des intumescences dan les cannaux et rivieres. 1st Congres de l'Assoc. Francaise de Calcul, Grenoble, printed 1961, p. 433-442.

Price, R. K., 1974. Comparison of four numerical methods for flood routing. Journal of the Hydraulic Division, ASCE, Vol. 100, No. HY7, pp. 879-899.

Richtmyer, R. D., and Morton, K. W., 1967. Solution of the implicit equations. Difference Methods for Initial Value Problems, Interscience Publishers, New York.

Simons, D. B., Chen, Y. H., and Ponce, V. M., 1979. A two-dimensional water and sediment routing model in river basins. Progress Report, Prepared for the U.S. Fish and Wildlife Service, Twin Cities, Minnesota.

Simons, D. B., Richardson, E. V., Stevens, M. A., Duke, J. H., and Duke, V. S., 1971. Geometric and hydraulic properties of the rivers. Venezuelan International Meteorological and Hydrological Experiment (VIMHEX), Hydrology Report, Vol. III, Colorado State University Report CER70-71DBS-EVR-MAS-JHD-VCD36, Fort Collins, Colorado.

Simons, D. B., Schumm, S. A., Stevens, M. A., Chen, Y. H., and Lagasse, P. F., 1975. A geomorphic study of Pools 24, 25, and 26 in Upper Mississippi and Lower Illinois Rivers. Colorado State University, Report No. CER75-76-DBS-SAS-MAS-YHC-PFL8, prepared for the Waterways Experiment Station, Vicksburg, Mississippi.

Simons, D. B., Volker, R. E., and Chen, Y. H., 1977. A two-dimensional reiver flow model based on a finite-element method. Progress Report, Engineering Research Center, Colorado State University, Fort Collins, Colorado.

Taylor, C., and Davis, J. M., 1973. Finite element numerical modeling of flow and dispersion in estuaries. Proceedings International Symposium on River Mechanics, Asian Institute of Technology, Bangkok, Thailand, Vol. 3, January, pp. 465-476.

Tucci, C. E. M., 1978. Hydraulic and water quality model for a river network. Ph.D. disseration, Department of Civil Engineering, Colorado State University, Fort Collins, Colorado.

U.S.D.I. Bureau of Reclamatin, 1973. Design of small dams. 2nd Edition, A Water Resources Technical Publication, U.S. Government Printing Office, Washington, D. C.

Vreugdenhil, C. B., 1973. Secondary flow computations. Publication No. 1973, Delft Hydraulics Laboratory, Delft, The Netherlands, November.

Wanstrath, J. J., and Whitaker, R. E., Reid, R. O., and Vastano, A. C., 1976. Storm surfe simulation in transformed coordinates. Technical Report No. 76-3, U.S. Army, Corps of Engineers, Coastal Engineering Research Center, Fort Belvoir, Virginia.

Wylie, E. B., 1970. Unsteady free-surface flow computation, ASCE Journal Hydraulics Division, Vol. 96, No. HY11, Proc. paper 7683, pp. 2241-2251.

Yen, B. C., 1973, Open channel flow equations revisited. ASCE Journal of Engineering Mechanics Division, Vol. 99, No. EM5 pp. 979-1009.

Yen, B. C., and Akan, A. O., 1976. Flood routing through river junctions. Rivers 76.

CHAPTER 9

STAGE DISCHARGE RELATIONS

by

Robert K. Simons, Research Associate of Civil Engineering, Colorado State University, Fort Collins, Colorado

Ruh-Ming Li, Associate Professor of Civil Engineering, Colorado State University, Fort Collins, Colorado

Daryl B. Simons, Associate Dean for Engineering Research and Professor of Civil Engineering, Colorado State University, Fort Collins, Colorado

9.1 INTRODUCTION

Accurate prediction of the river stage for a given discharge is a primary consideration in hydraulic engineering. Prediction of stage for a given discharge is necessary for analysis of flood control, flood-damage mitigation, sediment transport, navigation, and water quality. River stage can be predicted either by statistical stage-discharge relationships or by using deterministic physical process models. Available physical process simulation models to relate stage and discharge relationship include 1) normal depth determination utilizing Manning's equation or other resistance to flow equations, 2) steady flow rigid-boundary backwater profile model, 3) rigid-boundary unsteady flow model, 4) steady flow backwater profile model with uncoupled sediment routing procedure (known discharge sediment routing model), and 5) unsteady flow water and sediment routing model. Normal calculation is presented in Chapter 3 and 15. Backwater profile determination is given in Chapters 3 and 12. Known discharge sediment routing is reported in Chapter 12. A complicated unsteady flow water routing was given in Chapter 8 and the unsteady flow water and sediment routing in rivers will be presented in Chapter 11. This chapter first presents a dynamic simulation of stage-discharge relationships in rivers utilizing a full-dynamic momentum equation to yield a looped relation and its application to extend the applicability of the kinematic wave flood routing procedure discussed in Chapter 7. Then a comparison of frequency and magnitude of error associated with three models; statistical model, steady flow rigid boundary backwater model, and known discharge sediment routing model is made.

As mentioned earlier, the hydraulic engineer is frequently concerned with the determination of flood discharges at a given location along a river from the corresponding stages or vice versa. The relationship between stage and discharge is usually called a discharge rating curve. In general a discharge rating curve is obtained by making several discharge measurements and then plotting the observed stage versus the measured discharge. However, experience indicates that measurements of stage and discharge do not necessarily form a one to one relationship. Many rivers, especially those with a flatter gradient, display a hysteresis loop in the stage discharge relationship due to dynamic effects or other

reasons. Therefore it is difficult to obtain a meaningful discharge rating curve from statistical analysis.

Many authors report several reasons for deviations from a single-value rating curve (see Fread, 1973; Simons and Richardson, 1961). Among the more significant reasons are: 1) scour and fill, 2) alluvial bedform changes, 3) backwater effects, and 4) variable energy slope due to unsteady, nonuniform flow (dynamic effects). The determination of the friction slope due to dynamic effects considering accelerations associated with unsteady, nonuniform flow will be treated in this chapter. The models are developed to convert from a discharge hydrograph to the stage hydrograph and vice-versa, considering dynamic effects. In addition other reasons such as backwater effects and sediment movement will be discussed in the latter part of the chapter.

The stage-discharge relation plays an important role in river modeling. Stages may differ by 5 or more feet for the same discharge due to dynamic effect on some streams. The effect of rising and falling of flood on stage-discharge relation has to be examined for most of the river. In addition, a kinematic water routing technique was modified to include the other terms of the full dynamic momentum equation.

9.2 SOLUTION OF THE FULL DYNAMIC MOMENTUM EQUATION TO DESCRIBE THE STAGE-DISCHARGE RELATION

The full dynamic momentum equation can be written as (see Henderson, 1966)

$$S_f = S_o - \frac{\partial y}{\partial x} - \frac{1}{gA}\frac{\partial Q^2/A}{\partial x} - \frac{1}{gA}\frac{\partial Q}{\partial t} \qquad (9\text{-}1)$$

in which S_f is the friction slope, S_o is the channel bed slope, y is the depth of flow, x is the downstream distance, g is the gravitational acceleration, A is the cross-sectional area of flow, Q is the discharge, and t is the time. Each term of Equation 9-1 can be solved in terms of the known input hydrograph.

9.3 CONVERSION FROM DISCHARGE TO STAGE

When a discharge hydrograph is known, often the stage hydrograph is desired. One may wish to know how high the water will rise during a flood. For this case a model is formulated to convert a single discharge hydrograph to the corresponding stage hydrograph considering dynamic effects.

The Manning's equation is used to relate discharge to hydraulic parameters.

$$Q = \frac{1.486}{n} AR^{2/3} S_f^{1/2} \tag{9-2}$$

The hydraulic radius, R is defined as A/P in which P is the wetted perimeter. The wetted perimeter can be written as a power function of flow area

$$P = a_1 A^{b_1} \tag{9-3}$$

in which a_1 and b_1 are constants. Therefore, Manning's equation may be written as

$$Q = \left[\frac{1.486}{na_1^{2/3}}\right] A^{(5-2b_1)/3} S_f^{1/2} \tag{9-4}$$

or

$$A = \left[\frac{na_1^{2/3}}{1.486}\right]^{3/(5-2b_1)} (S_f^{-1/2})^{3/(5-2b_1)} Q^{3/(5-2b_1)} \tag{9-5}$$

Often Manning's n varies with discharge and can be written in a power relation

$$n = a_3 Q^{b_3} \tag{9-6}$$

Next, each of the terms in Equation 9-1 are expressed in terms of the known input hydrograph.

The water surface slope, $\partial y/\partial x$, may be determined as follows. The depth of flow can be expressed as a power function of the flow area.

$$y = a_4 A^{b_4} \tag{9-7}$$

in which a_4 and b_4 are constants.

By taking the partial derivative of Equation 9-7 with respect to x one obtains

$$\frac{\partial y}{\partial x} = a_4 b_4 A^{b_4 - 1} \frac{\partial A}{\partial x} \tag{9-8}$$

An expression for $\partial A/\partial x$ is found by taking the partial derivative of Equation 9-5 with respect to x.

$$\frac{\partial A}{\partial x} = \left\{\left(\frac{na_1^{2/3}}{1.486}\right)^{3/(5-2b_1)} (S_f^{-1/2})^{3/(5-2b_1)} \left(\frac{3}{5-2b_1}\right) Q^{(-2+2b_1)/(5-2b_1)}\right\} \frac{\partial Q}{\partial x} \tag{9-9}$$

Next, the term $\partial Q/\partial x$ is expressed in terms of the input discharge hydrograph through the continuity equation for the case of no lateral inflow or outflow (see Chow, 1959).

$$\frac{\partial Q}{\partial x} + \frac{\partial A}{\partial t} = 0 \tag{9-10}$$

The partial derivative of the flow area with respect to time is determined using Equation 9-5.

$$\frac{\partial Q}{\partial x} = -\frac{\partial A}{\partial t} = -\left[\frac{na_1^{2/3}}{1.486}\right]^{3/(5-2b_1)} (S_f^{-1/2})^{3/(5-2b_1)} \left(\frac{3}{5-2b_1}\right) Q^{(-2+2b_1)/(5-2b_1)} \frac{\partial Q}{\partial t} \tag{9-11}$$

This expression is now substituted into Equation 9-9 which is then related to the water surface slope using Equation 9-8. The resultant expression for the water surface slope is

$$\frac{\partial y}{\partial x} = a_4 b_4 A^{b_4 - 1} \left(\frac{1.486}{na_1^{2/3}}\right)^{-6/(5-2b_1)} \left(\frac{3}{5-2b_1}\right)^2 Q^{(-4+4b_1)/(5-2b_1)} S_f^{-3/(5-2b_1)} \frac{\partial Q}{\partial t} \tag{9-12}$$

The next term in the full dynamic momentum equation (Equation 9-1) to be found is the convective acceleration term, $1/(gA)\ \partial Q^2/A/\partial x$. Using Equation 9-4 an expression for $\partial Q^2/A/\partial x$ is derived.

$$\frac{\partial Q^2/A}{\partial x} = \left(\frac{1.486}{na_1^{2/3}}\right)^2 \frac{7-4b_1}{3} S_f A^{(4-4b_1)/3} \frac{\partial A}{\partial x} \tag{9-13}$$

The term $\partial A/\partial x$ is given in Equation 9-9.

From Equation 9-10 one obtains

$$\frac{\partial Q}{\partial x} = -\frac{\partial A}{\partial t} \tag{9-14}$$

The term $\partial A/\partial t$ is found by taking the partial derivative of Equation 9-5 with respect to time.

$$\frac{\partial A}{\partial t} = \left\{\left[\frac{na_1^{2/3}}{1.486}\right]^{3/(5-2b_1)} (S_f^{-1/2})^{3/(5-2b_1)} \left(\frac{3}{5-2b_1}\right) Q^{(-2+2b_1)/(5-2b_1)}\right\} \frac{\partial Q}{\partial t} \tag{9-15}$$

Substitution of Equation 9-15 into Equation 9-14 and then substitution of the resulting expression into Equation 9-9 and finally substitution of this result into Equation 9-13 gives the desired equation.

$$\frac{\partial Q^2/A}{\partial x} = -\left(\frac{7-4b_1}{3}\right)\left(\frac{3}{5-2b_1}\right)^2 \frac{\partial Q}{\partial t} \tag{9-16}$$

The final term of the full dynamic momentum equation is the local acceleration, $\partial Q/\partial t$. This term is known since the input hydrograph $Q(o,t)$ is given.

$$\frac{\partial Q}{\partial t} \approx \frac{\Delta Q}{\Delta t} \tag{9-17}$$

Expressions for all of the terms in the full dynamic momentum equation, Equation 9-1, have been derived and are substituted into Equation 9-1.

$$S_f = S_o - \frac{\partial y}{\partial x} - \frac{1}{gA}\frac{\partial Q^2/A}{\partial x} - \frac{1}{gA}\frac{\partial Q}{\partial t} \tag{9-18}$$

$$S_f = S_o + a_4 b_4 A^{b_4 - 1}\left(\frac{1.486}{n a_1^{2/3}}\right)^{-6/(5-2b_1)}\left(\frac{3}{5-2b_1}\right)^2 Q^{(-4+4b_1)/(5-2b_1)}$$

$$S_f^{-3/(5-2b_1)}\frac{\partial Q}{\partial t} + \frac{1}{gA}\left(\frac{7-4b_1}{3}\right)\left(\frac{3}{5-2b_1}\right)^2 \frac{\partial Q}{\partial t} - \frac{1}{gA}\frac{\partial Q}{\partial t} \tag{9-19}$$

Before Equation 9-19 can be solved for S_f, the area term in the factor $1/(gA)$ and in the water surface slope term are converted to discharge through Equation 9-5.

$$S_f - S_o - a_4 b_4\left(\frac{1.486}{n a_1^{2/3}}\right)^{(-3-3b_4)/(5-2b_1)}\left(\frac{3}{5-2b_1}\right)^2 Q^{(-7+4b_1+3b_4)/(5-2b_1)}$$

$$S_f^{(-3-3b_4)/(10-4b_1)}\frac{\partial Q}{\partial t} + \frac{1}{g}\frac{\partial Q}{\partial t}\left[1 - \left(\frac{7-4b_1}{3}\right)\left(\frac{3}{5-2b_1}\right)^2\right]$$

$$\left\{\left(\frac{n a_1^{2/3}}{1.486}\right)^{-3/(5-2b_1)} Q^{-3/(5-2b_1)} S_f^{\frac{1}{2}(3/(5-2b_1))}\right\} = 0 \tag{9-20}$$

This equation can be solved by the well known Newton-Raphson technique.

Once the friction slope has been determined the depth may be related to the known discharge. First, the flow area is calculated from the discharge by Equation 9-5 and then the depth of flow is related to the cross-sectional area of flow by a power function given in Equation 9-7.

9.4 CONVERSION FROM STAGE TO DISCHARGE

Generally the stage hydrograph is known and the corresponding discharge hydrograph is desired. A method is shown below for converting a stage hydrograph to the corresponding discharge hydrograph with dynamic effects. The formulation is similar to the previous section. The known input is now y expressed as a function of time and hence the partial derivative of y with respect to time is $\frac{\partial y}{\partial t} \approx \frac{\Delta y}{\Delta t}$. Again each term in the full dynamic momentum equation is expressed as a function of the known inputs.

Using Equation 9-7, and assuming lateral inflow is zero, the continuity equation may be written as (Note: $(1/b_4-1)$ does not equal $1/(b_4-1)$).

$$\frac{\partial Q}{\partial x} + (1/b_4)a_4^{-1/b_4} y^{(1/b_4-1)} \frac{\partial y}{\partial t} = 0 \qquad (9\text{-}21)$$

By taking the partial derivative of Equation 9-4 with respect to x and utilizing Equation 9-7

$$\frac{\partial Q}{\partial x} = \left(\frac{1.486}{na_1^{2/3}}\right) S_f^{1/2} \left(\frac{5-2b_1}{3}\right) A^{(2-2b_1)/3} (1/b_4)a_4^{-1/b_4} y^{(1/b_4-1)} \frac{\partial y}{\partial x}$$

This expression is then substituted into the continuity equation, Equation 9-21 yielding

$$\frac{\partial y}{\partial x} = - \frac{\partial y}{\partial t} \left(\frac{1.486}{na_1^{2/3}}\right)^{-1} S_f^{-1/2} \left(\frac{3}{5-2b_1}\right) A^{-(2-2b_1)/3} \qquad (9\text{-}23)$$

Next, the convective acceleration term $(1/gA \frac{\partial Q^2/A}{\partial x})$ is put in terms of the known input data. The term $\frac{\partial Q^2/A}{\partial x}$ was defined in Equation 9-13. The term $\partial A/\partial x$ can be related to the water surface slope

$$\frac{\partial A}{\partial x} = (1/b_4)a_4^{-1/b_4} y^{(1/b_4-1)} \frac{\partial y}{\partial x} \qquad (9\text{-}24)$$

The water surface slope was previously derived in Equation 9-23. This expression is then substituted into Equation 9-24 which is in turn substituted into Equation 9-13.

$$\frac{\partial Q^2/A}{\partial x} = -\left[(1/b_4)a_4^{-1/b_4}\, y^{(1/b_4-1)}\right]\left(\frac{1.486}{na_1^{2/3}}\right)\left(\frac{7-4b_1}{5-2b_1}\right) A^{(2-2b_1)/3} S_f^{1/2}\, \frac{\partial y}{\partial t} \tag{9-25}$$

The local acceleration term is determined by taking the partial derivative of Equation 9-4 with respect to time and using Equation 9-7.

$$\frac{\partial Q}{\partial t} = \left[(1/b_4)a_4^{-1/b_4}\, y^{(1/b_4-1)}\right]\left(\frac{1.486}{na_1^{2/3}}\right)\left(\frac{5-2b_1}{3}\right) S_f^{1/2}\, A^{(2-2b_1)/3}\, \frac{\partial y}{\partial t} \tag{9-26}$$

Again, the expressions describing the water surface slope and local and convective accelerations are substituted into the full dynamic momentum equation, Equation 9-1. The terms involving A are converted to y through Equation 9-7.

$$S_f = S_o + \left(\frac{1.486}{na_1^{2/3}}\right)^{-1} \frac{3}{5-2b_1}\left[a_4^{-1/b_4}\, y^{1/b_4}\right]^{-(2-2b_1)/3} S_f^{-1/2}\, \frac{\partial y}{\partial t}$$

$$+ \frac{1}{g}\left[(1/b_4)a_4^{-1/b_4}\, y^{(1/b_4-1)}\right]\left(\frac{1.486}{na_1^{2/3}}\right)\left(\frac{7-4b_1}{5-2b_1}\right)\left[a_1^{-1/b_4}\, y^{1/b_4}\right]^{(-1-2b_1)/3}$$

$$S_f^{1/2} - \frac{1}{g}\left[(1/b_4)a_4^{-1/b_4}\, y^{(1/b_4-1)}\right]\left(\frac{1.486}{na_1^{2/3}}\right)\left(\frac{5-2b_1}{3}\right)$$

$$\left[a_4^{-1/b_4}\, y^{1/b_4}\right]^{(-1-2b_1)/3} S_f^{1/2}\, \frac{\partial y}{\partial t} \tag{9-27}$$

After multiplying $S_f^{1/2}$ and letting $Z^2 = S_f$ one obtains a cubic equation.

$$Z^3 + Z^2\, \frac{1}{g}\left[(1/b_4)a_4^{-1/b_4}\, y^{(1/b_4-1)}\right]\left(\frac{1.486}{na_1^{2/3}}\right)\left[a_4^{-1/b_4}\, y^{1/b_4}\right]^{(-1-2b_1)/3}$$

$$\frac{\partial y}{\partial t}\left[\frac{5-2b_1}{3} - \frac{7-4b_1}{5-2b_1}\right] - ZS_o - \left(\frac{1.486}{na_1^{2/3}}\right)^{-1}\left(\frac{3}{5-2b_1}\right)$$

$$\left[a_4^{-1/b_4}\, y^{(1/b_4)}\right]^{-(2-2b_1)/3} \frac{\partial y}{\partial t} = 0 \tag{9-28}$$

This equation may be solved using a routine which solves a third order polynomial. The value obtained for Z is then squared in order to determine the friction slope, S_f.

Once the friction slope has been determined and knowing the depth, the corresponding value for discharge can be calculated. The flow area is calculated using Equation 9-7 and the discharge is calculated using Equation 9-4.

9.5 TEST RESULTS OF DYNAMIC STAGE-DISCHARGE RELATION

In order to validate the model an observed stage hydrograph is read into the model to calculate a discharge hydrograph which is then checked against observed discharges. Fread (1973) gave data of this type and two sets of data are run through the model developed in this paper.

Figure 9-1 shows an observed stage hydrograph on the Mississippi River at Red River Landing which is input to the model. The simulated discharge hydrograph is compared to the observed discharge hydrograph in Figure 9-2. The simulated and observed stage-discharge relation is shown in Figure 9-3. For the rising limb of a floodwave the friction slope is larger than the bedslope and hence the corresponding stages are smaller. During the falling limb of a floodwave the friction slope is smaller than the bedslope and hence the corresponding stages are larger. This hysteresis loop is due to dynamic effects. Also, shown in Figure 9-1 is the simulated stage hydrograph which uses the simulated discharge hydrograph as input. Thus the applicability of both the stage to discharge model and the discharge to stage model is established.

A stage hydrograph on the Mississippi River at Tarbert Landing was used as input to the model as further verification. Figure 9-4 shows the comparison of simulated and observed discharge hydrographs. Figure 9-5 shows that the comparison of simulated and observed data agree closely.

9.6 EXTENSION OF KINEMATIC WATER ROUTING TO INCLUDE THE FULL DYNAMIC MOMENTUM EQUATION

Flood management is described by the equation of continuity, the momentum equation and equations describing flow resistance. A kinematic water routing formulation is extended to include the full dynamic momentum equation. The water routing technique is second-order and nonlinear (see Li, et al. 1975, Simons 1977 and Chapter 7).

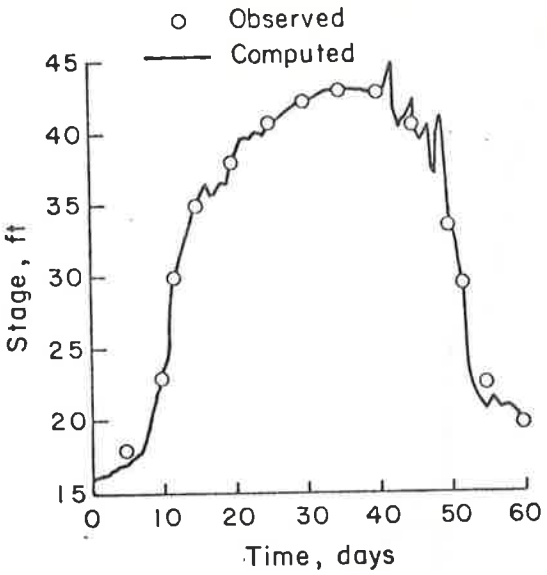

Figure 9-1. Stage hydrograph, Mississippi River at Red River Landing, LA. (3/11/63-5/13/63).

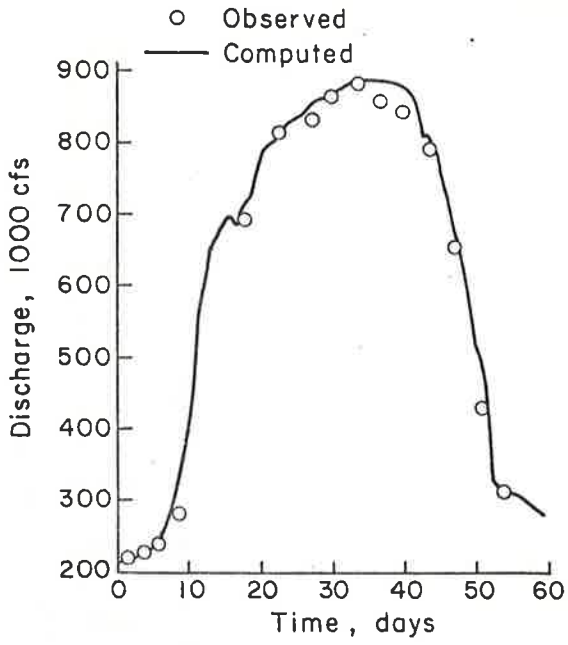

Figure 9-2. Discharge hydrograph for Mississippi River, Red River Landing, LA. (3/11/63-5/13/63).

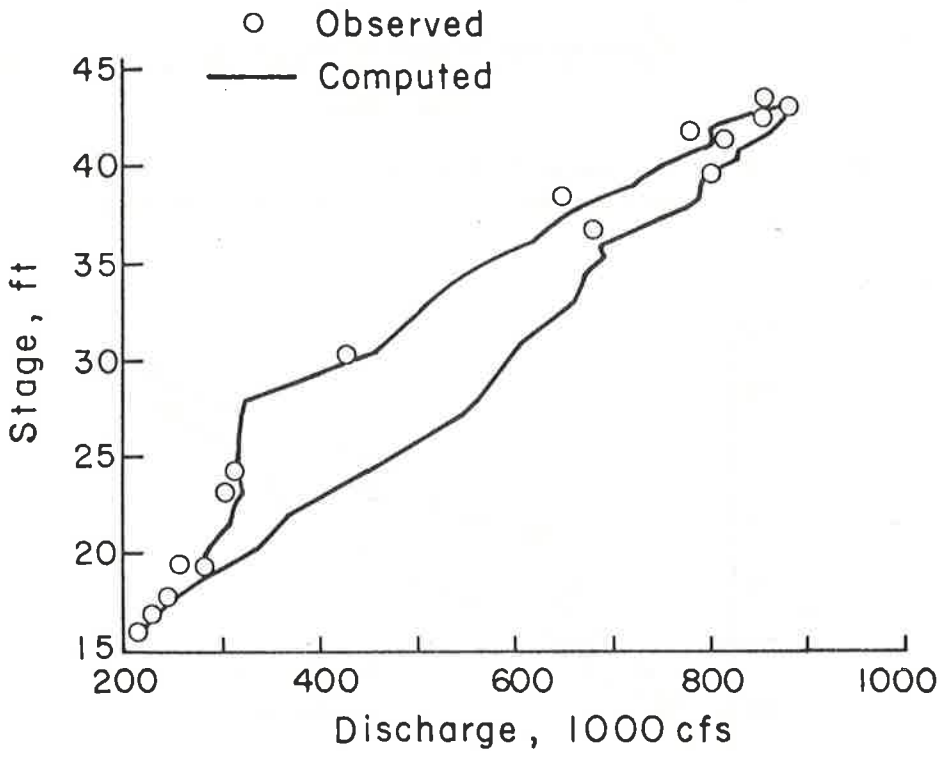

Figure 9.3 Stage-discharge relation for Mississippr River, Red River Landing, LA (3/1163-5/13/63).

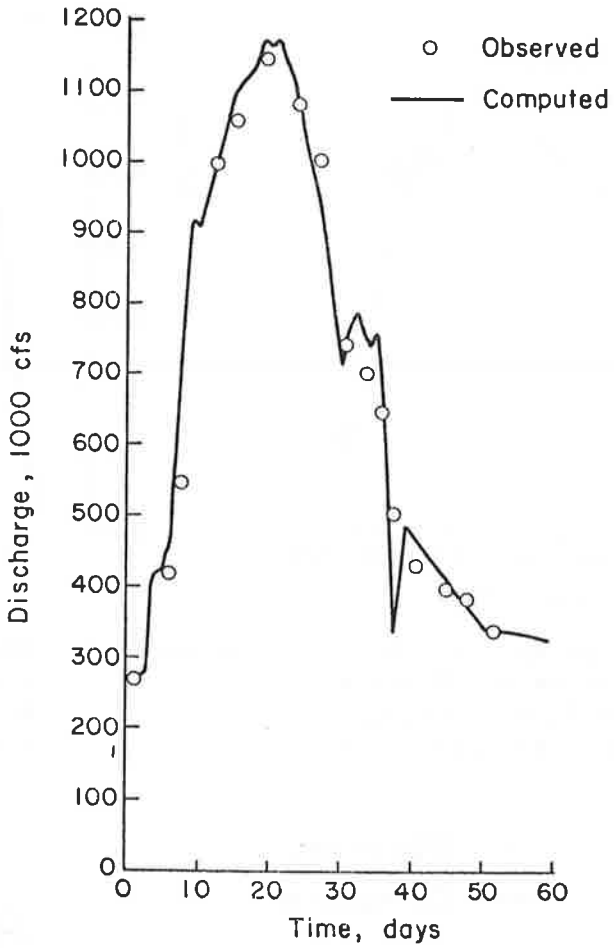

Figure 9-4 Discharge hydrograph for Mississippi River, Tarbert Landing, LA (2/9/66-4/11/66).

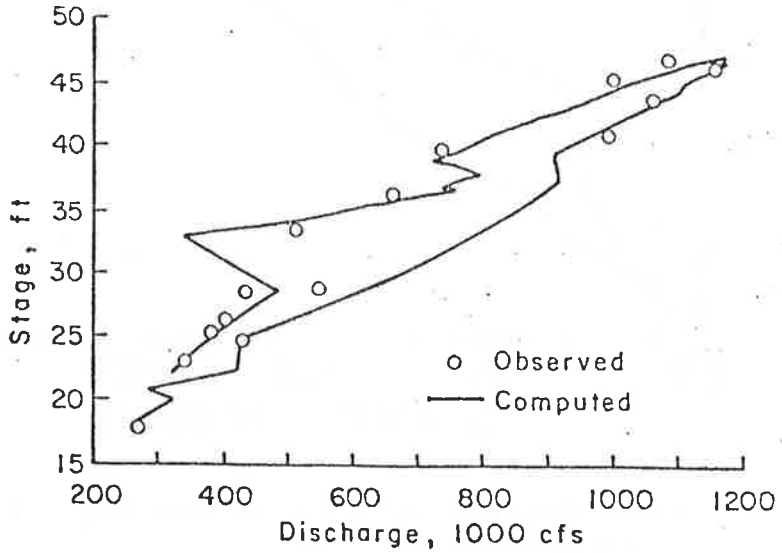

Figure 9.5 Stage-discharge relation for Mississippi River, Tarbert Landing, LA (2/9/66-4/11/66).

The previous section showed how dynamic effects can be accounted for in the stage-discharge relationship. These developments can now be directly applied to water routing by extending a second-order, nonlinear model (Chapter 7). This model may now be applied under two forms of the momentum equation. The two are:

1. Kinematic-wave assumption

$$S_f = S_o$$

2. Full dynamic wave assumption

$$S_f = S_o - \frac{\partial y}{\partial x} - \frac{1}{g\bar{A}} \frac{\partial Q^2/A}{\partial x} - \frac{1}{g\bar{A}} \frac{\partial Q}{\partial t}$$

The friction slope can now be calculated using the previous derivations. Then the value of friction slope, accounting for dynamic effects, can be applied in the relationship between discharge and flow area in the water routing program. A brief development of the water routing formulation follows.

9.7 GOVERNING EQUATIONS FOR MODIFIED KINEMATIC WAVE ROUTING

Flood movement in rivers is described by the equation of continuity, the equation of motion, and equations describing flow resistance. These equations used in the nonlinear, four-point routing scheme are described below.

Continuity Equation

The continuity equation for water can be expressed as

$$\frac{\partial Q}{\partial x} + \frac{\partial A}{\partial t} = q_\ell \qquad (9\text{-}29)$$

where Q is the discharge, x is the down slope distance, A is the cross-sectional area of flow, t is the time, and q_ℓ is the lateral inflow rate per unit length of channel.

Momentum Equation

Under the kinematic wave assumption, the gradient due to local and convective acceleration, and the water surface slope are assumed to be negligible. Thus

$$S_o \simeq S_f = \frac{(n^2 Q^2)}{(2.21\ R^{4/3} A^2)} \qquad (9\text{-}30)$$

where S_o is the bed slope, S_f is the friction slope, n is Manning's roughness coefficient, and R is the hydraulic radius. In the modified kinematic wave approximation the full dynamic momentum equation is substituted using a solution of the previously developed expressions for S_f. By definition

$$R = A/P \tag{9-31}$$

in which P is the wetted perimeter. Usually the wetted perimeter can be expressed as a power function of area

$$P = a_1 A^{b_1} \tag{9-32}$$

Hydraulic engineers frequently use Manning's equation to describe flow in open channels. The Manning's roughness coefficient is determined by measurement or is estimated and can be expressed as a power function of discharge

$$n = a_3 Q^{b_3} \tag{9-33}$$

in which a_3 and b_3 are constants.

Discharge and Flow Area Relation

The flow cross-sectional area can be expressed as a power function of discharge

$$A = \alpha Q^{\beta} \tag{9-34}$$

in which α and β are coefficients whose values depend on channel shape, roughness and slope.

If Manning's equation is used to describe the flow α and β are determined from Equations 9-30, 9-31, 9-32, 9-33.

$$\alpha = \left[\frac{a_1^{4/3} a_3^2}{2.21\ S_f}\right]^{[3/(10-4b_1)]} \tag{9-35}$$

$$\beta = (3+3b_3)/(5-2b_1) \tag{9-36}$$

9.8 NUMERICAL SCHEME

A nonlinear scheme with an iterative procedure is developed to solve a four-point implicit formulation of Equations 9-29 and 9-34. A linear scheme is used to obtain the initial estimate of the unknown discharge for the nonlinear scheme. The linear scheme may be used as is, with no iterations to solve for the unknown discharge if the accuracy is satisfied (see Chapter 7).

Nonlinear Scheme

The finite difference form of Equation 9-29 using quantities at all four points (see Figure 9-6) of the box scheme can be written as

$$\left[\frac{Q_{j+1}^{n+1} - Q_j^{n+j}}{\Delta x}(1-a) + \frac{Q_{j+1}^{n} - Q_j^{n}}{\Delta x}(a)\right] + \left[\frac{A_{j+1}^{n+1} - A_{j+1}^{n}}{\Delta t}(1-b)\ \frac{A_j^{n+1} - A_j^{n}}{\Delta t}(b)\right]$$

$$= \frac{q_{\ell}{}_{j+1}^{n+1} + q_{\ell}{}_{j+1}^{n} + q_{\ell}{}_{j}^{n+1} + q_{\ell}{}_{j}^{n}}{4} \qquad (9\text{-}37)$$

in which Q_j^n is the quantity Q at grid point $x = j\Delta x$, $t = n\Delta t$, where Δx is the space increment and Δt is the time increment. Also, a is the space weighting factor and b is the time weighting factor where $0 \leq a \leq 1$ and $0 \leq b \leq 1$.

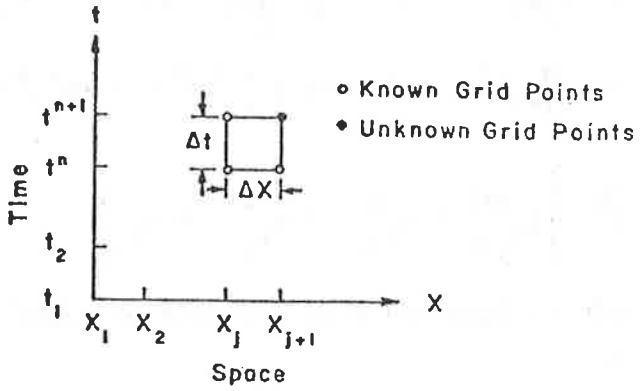

Figure 9-6. Rectangular network in the space-time plane.

The unknowns in Equation 9-37 are Q_{j+1}^{n+1}, and A_{j+1}^{n+1} but they are related according to Equation 9-34. With the two equations the two unknowns may be calculated. The boundary conditions required for this particular formulation are as follows: $Q(0,t)$ and $Q(x,0)$ or in

other words, the discharge must be known or assumed along both the space axis [Q(x,0)] and the time axis [Q(0,t)]. No downstream boundary conditions are required. However, if there is a strong downstream control the kinematic wave approximation no longer applies.

Either Q or A may be selected as the independent variable in the numerical procedure. As customary in backwater computations the depth of flow (equivalent to A) is chosen as the independent variable (see Henderson, 1966), but Li et al. (1975) shows that Q is a better choice.

From Equation 9-34

$$A_{j+1}^{n+1} = \alpha \, (Q_{j+1}^{n+1})^{\beta} \tag{9-38}$$

$$A_{j}^{n+1} = \alpha \, (Q_{j}^{n+1})^{\beta} \tag{9-39}$$

$$A_{j+1}^{n} = \alpha \, (Q_{j+1}^{n})^{\beta} \tag{9-40}$$

$$A_{j}^{n} = \alpha \, (Q_{j}^{n})^{\beta} \tag{9-41}$$

Equations 9-38 through 9-41 are substituted into Equation 9-37 and rearranged to yield

$$\begin{aligned} \frac{\Delta t}{\Delta x} Q_{j+1}^{n+1} \, (1\text{-}a) + \alpha \, (Q_{j+1}^{n+1})^{\beta} \, (1\text{-}b) = \frac{\Delta t}{\Delta x} \Big\{ & Q_{j}^{n+1} \, (1\text{-}a) - [Q_{j+1}^{n} - Q_{j}^{n}] \, (a) \Big\} \\ & + \alpha \, (Q_{j+1}^{n})^{\beta} \, (1\text{-}b) - [\alpha \, (Q_{j}^{n+1})^{\beta} - \alpha \, (Q_{j}^{n})^{\beta}] \, (b) \\ & + \frac{\Delta t}{4} \Big\{ q_{\ell}{}_{j+1}^{n+1} + q_{\ell}{}_{j+1}^{n} + q_{\ell}{}_{j}^{n+1} + q_{\ell}{}_{j}^{n} \Big\} \end{aligned} \tag{9-42}$$

The right-hand side of Equation 9-42 consists of known quantities and is represented by Ω.

$$\begin{aligned} \Omega = \frac{\Delta t}{\Delta t} \Big\{ Q_{j}^{n+1} \, (1\text{-}a) - [Q_{j+1}^{n} - Q_{j}^{n}] \, (a) \Big\} + \alpha \, (Q_{j+1}^{n})^{\beta} \, (1\text{-}b) \\ - [\alpha \, (Q_{j}^{n+1})^{\beta} - \alpha \, (Q_{j}^{n})^{\beta}] \, (b) + \frac{\Delta t}{4} \Big\{ q_{\ell}{}_{j+1}^{n+1} + q_{\ell}{}_{j}^{n+1} + q_{\ell}{}_{j+1}^{n} + q_{\ell}{}_{j}^{n} \Big\} \end{aligned} \tag{9-43}$$

Let $r = Q_{j+1}^{n+1}$ and $\theta = \frac{\Delta t}{\Delta x}$ so that the left hand side of Equation 9-42 can be written as

$$f(r) = \theta \, (1\text{-}a) \, r + \alpha \, (1\text{-}b) \, r^{\beta} \tag{9-44}$$

The solution to Equation 9-42 is the solution r^* which satisfies the condition

$$f(r^*) = \theta\ (1-a)\ r^* + \alpha\ (1-b)\ r^{*\beta} = \Omega \tag{9-45}$$

Equation 9-45 is nonlinear in r^*. An approximate solution to this nonlinear equation is obtained by the following iterative technique.

Let r^k be the value of r at the kth iteration. The Taylor series expansion of the function $f(r)$ around r^k is

$$f(r) = f(r^k) + (r-r^k)\ f'(r^k) + 1/2(r-r^k)^2\ f''(r^k) + 1/6(r-r^k)^3\ f'''(r^k) \tag{9-46}$$

in which $f'(r^k)$, $f''(r^k)$, and $f'''(r^k)$ are the first, second and third derivatives of the function at r^k.

Dropping terms higher than third order one obtains

$$f(r)\ \ f(r^k) + (r-r^k)\ f(r^k) + 1/2(r-r^k)^2\ f''(r^k) \tag{9-47}$$

Iteration forces $f(r^{k+1})$ to approach the value of Ω

$$\Omega = f(r^k) + (r^{k+1} - r^k)\ f'(r^k) + 1/2(r^{k+1} - r^k)^2\ f''(r^k) \tag{9-48}$$

The solution of Equation 9-48 is

$$r^{k+1} = r^k - \frac{f'(r^k)}{f''(r^k)} \pm \left\{\left[\frac{f'(r^k)}{f''(r^k)}\right]^2 - \frac{2[f(r^k)-\Omega]}{f''(r^k)}\right\}^{1/2} \tag{9-49}$$

in which

$$f(r^k) = \theta(1-a)\ r^k + \alpha(1-b)\ (r^k)^\beta \tag{9-50}$$

$$f'(r^k) = \theta(1-a) + \alpha\beta(1-b)\ (r^k)^{\beta-1} \tag{9-51}$$

$$f''(r^k) = \alpha\beta(\beta-1)\ (1-b)\ (r^k)^{\beta-2} \tag{9-52}$$

There are two solutions to Equation 9-49. It is advisable to choose the solution which gives the smaller value of $|f(r^{k+1})-\Omega|$. The iterations are continued until the absolute error $|f(r^{k+1})-\Omega|$ is less than some preassigned tolerance ε

$$f(r^{k+1})-\Omega \leq \varepsilon \tag{9-53}$$

An appropriate value for ε is 0.01 Ω.

The initial guess r° is the key to the speed of convergence to the correct numerical solution. The best way to determine r° is to use a linear scheme. The linear scheme may be used as the solution instead of going through the iterative, nonlinear scheme when accuracy is of less importance and when computer time is to be conserved.

Linear Scheme

The term $\frac{\partial A}{\partial t}$ in Equation 9-29 can be expressed as,

$$\frac{\partial A}{\partial t} = \frac{\partial A}{\partial Q}\frac{\partial Q}{\partial t} \tag{9-54}$$

and from Equation 9-34

$$\frac{\partial A}{\partial Q} = \alpha\beta Q^{\beta-1} \tag{9-55}$$

Substitution of Equation 9-54 and 9-55 into 9-29 yields

$$\frac{\partial Q}{\partial x} + \alpha\beta Q^{\beta-1}\frac{\partial Q}{\partial t} = q_\ell \tag{9-56}$$

The finite difference form of Equation 9-56 can be expressed as

$$\frac{Q_{j+1}^{n+1} - Q_j^{n+1}}{\Delta x}(1-a) + \frac{Q_{j+1}^{n} - Q_j^{n}}{\Delta x}(a)$$

$$+ \alpha\beta\left[\frac{Q_j^{n+1} + Q_{j+1}^{n}}{2}\right]^{\beta-1}\left[\frac{Q_{j+1}^{n+1} - Q_{j+1}^{n}}{\Delta t}(1-b) + \frac{Q_j^{n+1} - Q_j^{n}}{\Delta t}(b)\right]$$

$$= 1/4\left[q_{\ell}{}_{j+1}^{n+1} + q_{\ell}{}_{j}^{n+1} + q_{\ell}{}_{j+1}^{n} + q_{\ell}{}_{j}^{n}\right] \tag{9-57}$$

Solving for $r^o = Q_{j+1}^{n+1}$,

$$Q_{j+1}^{n+1} = \left[\frac{1-a}{\Delta x} + \alpha\beta\left(\frac{Q_j^{n+1} + Q_{j+1}^{n}}{2}\right)^{\beta-1}\frac{(1-a)}{\Delta t}\right]^{-1}\left\{\frac{Q_j^{n+1}}{\Delta x}(1-a) - \frac{Q_{j+1}^{n} - Q_j^{n}}{\Delta x}(a)\right.$$

$$-\alpha\beta\left(\frac{Q_j^{n+1} + Q_{j+1}^{n}}{2}\right)^{\beta-1} - \left[\frac{Q_{j+1}^{n}}{\Delta t}(1-b) + \frac{Q_j^{n+1} - Q_j^{n}}{\Delta t}(b)\right]$$

$$\left. + 1/4\left[q_{\ell}{}_{j+1}^{n+1} + q_{\ell}{}_{j}^{n+1} + q_{\ell}{}_{j+1}^{n} + q_{\ell}{}_{j}^{n}\right]\right\} \tag{9-58}$$

Equation 9-58 provides the best estimate r^o for the nonlinear scheme. However, Equation 9-58 is not applicable if both Q_{j+1}^{n} and Q_j^{n+1} are zero. In this case, use $\beta=1$ in Equation 9-44

$$\Omega/[(1-a)\,\theta + (1-b)\,\alpha] \tag{9-59}$$

The solution technique has been shown to be stable for a and b less than or equal to 1/2 (see Simons, 1977).

The flow routing technique uses either the kinematic or full dynamic assumptions. For each space and time step, the full dynamic momentum equation is solved for the friction slope (S_f). The value for S_f is then used to relate the flow depth, velocity area and discharge in Manning's equation. After S_f is determined for each time and space step the continuity equation is solved using the finite-difference technique described herein.

The water routing model now has the option of solving a problem under either the kinematic wave assumption or the full dynamic assumption.

9.9 A COMPARISON OF KINEMATIC AND FULL DYNAMIC APPROXIMATIONS

In order to compare the kinematic and full dynamic approximations an example problem is chosen. Y. H. Chen (1973) gives a numerical solution to a hypothetical problem involving a channel of unit width, constant resistance to flow and sinusoidal input discharge hydrograph. This model is dynamic and is known to work well on flatter slopes (see Chapter 8). First the models are run with identical input data and $\frac{\Delta t}{\Delta x}$ ratios over a wide range of slopes to show when the kinematic wave approximation is no longer valid. Figure 9-7 shows the output hydrographs at a distance of nine miles downstream.

The comparison shows that on slopes ranging from about .0007 (3.7 ft/mile) on up the kinematic wave approximation is adequate when estimating the discharge hydrograph. For bed slopes flatter than about .0007 the dynamic effects are no longer insignificant and the kinematic wave approximation is no longer valid.

Next the dynamic wave model developed in this chapter is compared with Chen's dynamic model using a similar problem. In this hypothetical case the bed slope is 0.0001 or 0.528 ft/mile which is a fairly small channel gradient. The input discharge hydrograph is a sine wave lasting 20 hours $q(o,t) = 25 + 35 \sin(\pi/20)$. Figure 9-8 shows the discharge hydrographs at a distance of 6 miles downstream. The two models give close results.

Figure 9-9 shows the hysteresis loop in the stage-discharge relationship due to dynamic effects. Also shown is the single valued relationship given by the kinematic wave approximation. In the rising

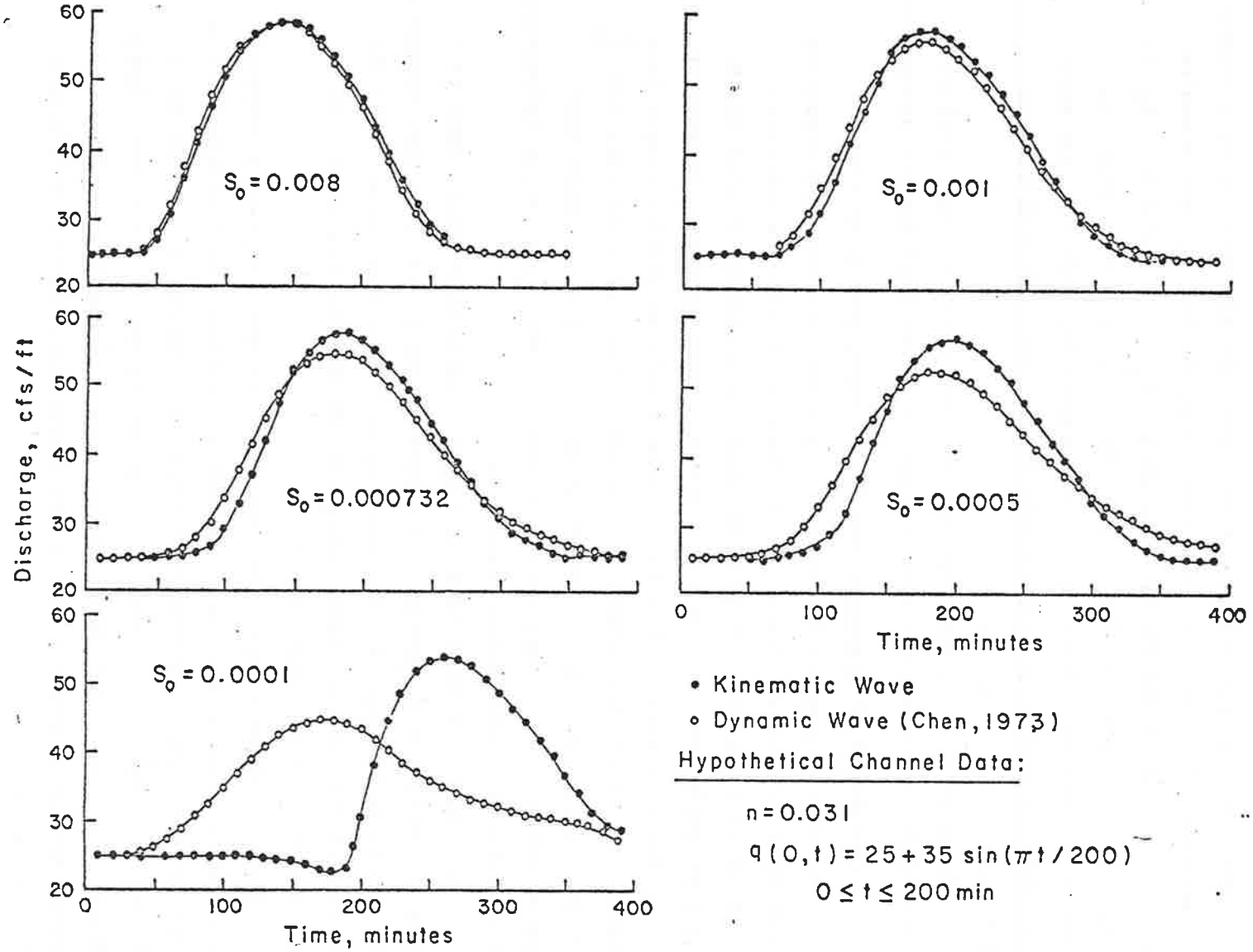

Figure 9.7 Comparison of kinematic and dynamic models on various slopes at a distance nine miles downstream.

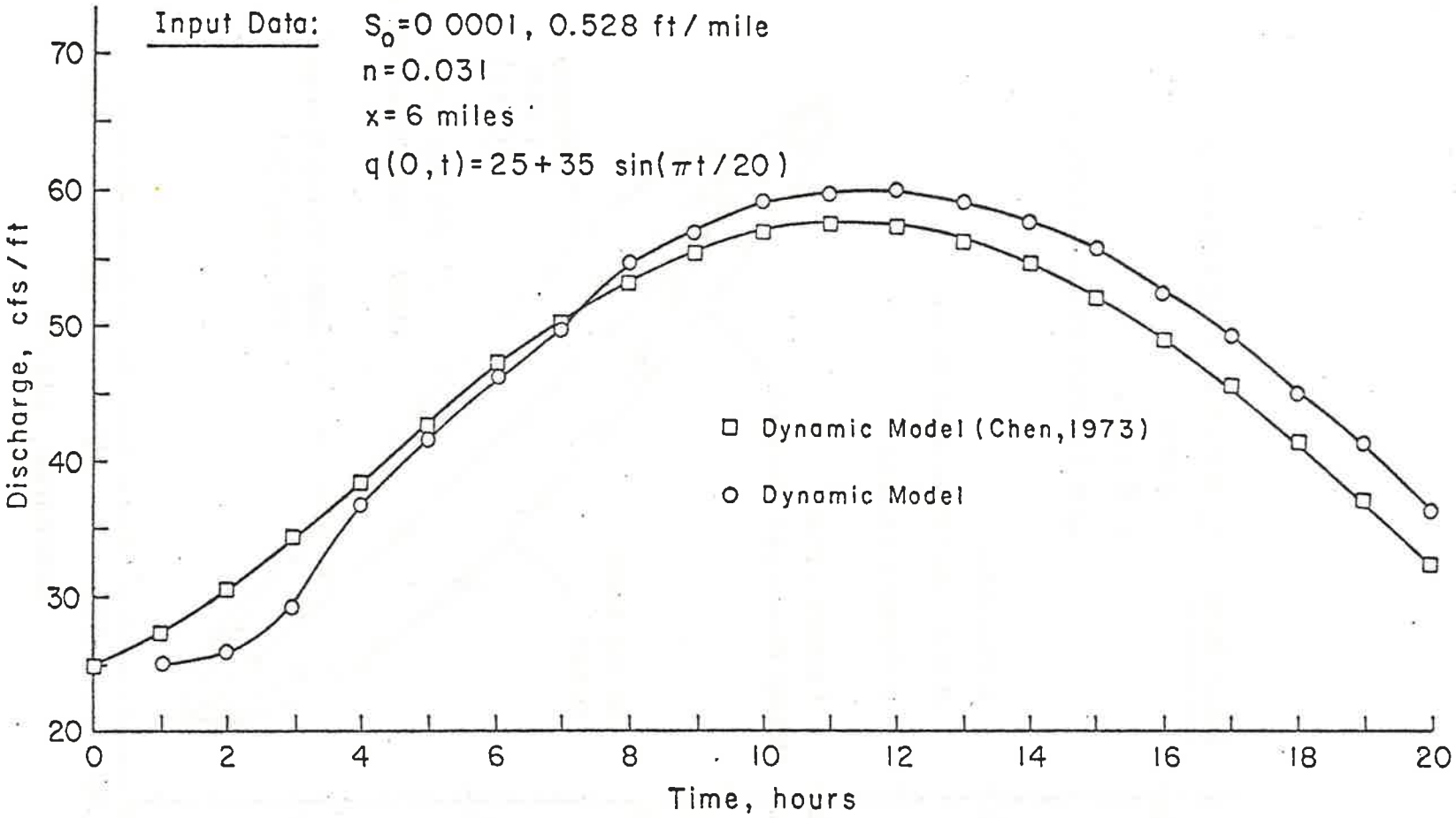

Figure 9.8 Comparison of discharge hydrographs given by dynamic models.

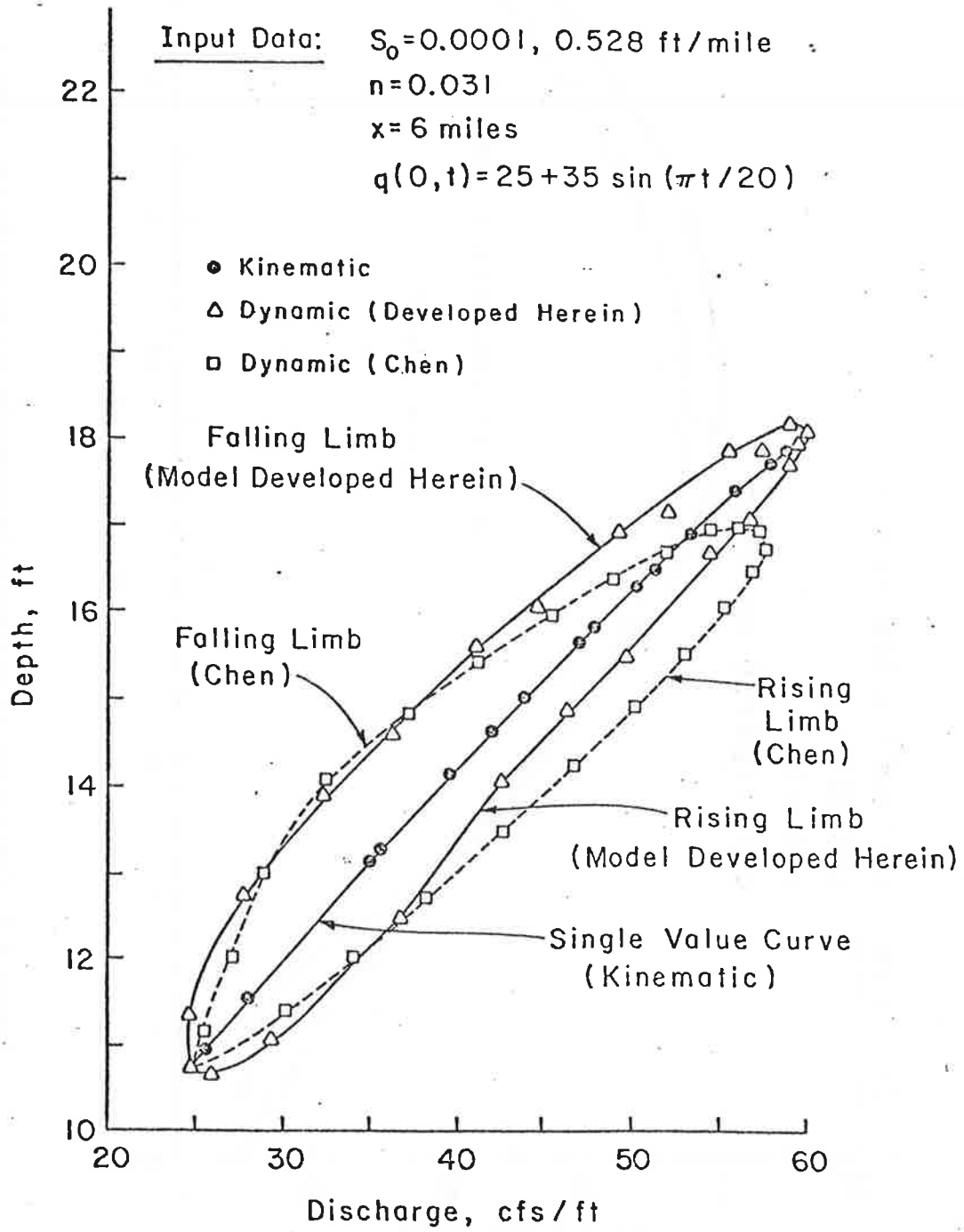

Figure 9.9 Comparison of stage-discharge relationships given by dynamic models.

limb the friction slope is larger than the bed slope and therefore the stages are smaller. In the recession limb the friction slope becomes less than the bed slope and the corresponding stages are larger. The maximum difference in stage between the rising limb and the falling limb is about 2 feet (~ 14 percent of the stage given by the single valued curve at that point). The dynamic effect on stage-discharge relationships can be significant when dealing with channels having relatively flat gradients.

9.10 APPLICATION PROCEDURE OF MODIFIED KINEMATIC WAVE APPROXIMATION FOR FLOOD ROUTING IN RIVER

In order to apply a water routing model several types of input data are required:

1. geometry (cross-section and slope)
2. Upstream discharge or stage hydrograph
3. Lateral inflow data
4. Flow resistance data

After collecting the data it must be put into a useful form that the flow model was designed to accept. A brief account of the data preparation follows.

Geometry

The model requires cross-section geometry and slope data. The slope data is either surveyed or taken from a reliable contour map if the slope is large enough.

A small computer program is used to process the cross-section information. The z,y point pairs (z being the distance across the channel and y the vertical distance) are read into the program. At each y or at some specified number of horizontal lines the cross-sectional area and wetted perimeter are calculated using simple geometry. Now the program has a table of depths, areas and wetted perimeters. The water-routing program uses the power relations $P = a_1 A^{b}1$ and $y = a_4 A^{b}4$. To obtain the desired coefficients and exponents the problem is converted using logrithms

$$\ln P = a_1 + b_1 \ln A \qquad (9\text{-}60)$$

and

$$\ln y = a_4 + b_4 \ln A \tag{9-61}$$

Knowing various values of P and A, a_1 and b_1 are found using linear regression. Likewise knowing Y and A, a_4 and b_4 are again determined using linear regression. Values of a_1, b_1, a_4 and b_4 are read into the model for each cross-section along with the x distances and bed slopes.

Upstream Hydrograph

The upstream hydrogaph (x=0) provides the unsteady flow input to the flow model. The water-routing model uses the discharge hydrograph. Often, only the stage hydrograph is known. In this case the stage hydrograph is converted to dishcarge using the proceedure given in the section describing stage-discharge relations.

Another boundary condition for the flow model is the discharge at time = 0 at all cross-sections. This may be assumed to be the initial upstream discharge, or if it is known at each point it may be read in.

Lateral Inflow

If lateral inflow (or outflow) is known to exist in any significant quantity through the stream reach being modeled it must be read as input. Often this lateral inflow is negligible and can be ignored but if not it must be known or estimated by some means.

Flow Resistance Data

For the channel flow model Manning's equation is used to relate the area and discharge. The program uses a power relation for Manning's n

$$n = a_3 Q^{b_3} \tag{9-62}$$

when n is constant b_3 is set to zero and a_3 is equal to n.

Manning's n may be estimated but where stage-discharge data is available n may be more accurately determined. Since the geometry is known (S_o, A, y, etc.) one can again use linear regression to find a_3 and b_3.

$$\ln n = a_3 + b_3 \ln Q \tag{9-63}$$

The values of a_3 and b_3 are again read into the model at all cross-sections where such information is available. Where unavailable Manning's n is estimated.

Application of these techniques to water routing problems gives good results in numerous cases. As an example, this modified kinematic routing method is tested on a large river of the Yazoo Basin, Mississippi. A flood hydrograph is routed on the Tallahatchie River from Swan Lake to Money in Mississippi. The two stations are 26.2 miles apart. The geometry is described by a cross-section survey taken in 1970. Using observed stage discharge curves at Swan Lake and Money, as well as the bed slope, Manning's equation is computed as a power function of discharge. The input discharge hydrograph (at Swan Lake) is shown in Figure 9.10. Observed and computed stages at Money are compared in Figure 9.11. The error is within acceptable limits. The observed and computed discharges at Money are compared in Figure 9.10 for the second half of the flood when discharges were measured. The computed and observed stage-discharge relation is plotted in Figure 9.12 showing the significance of the dynamic effect due to the unsteady flow accelerations.

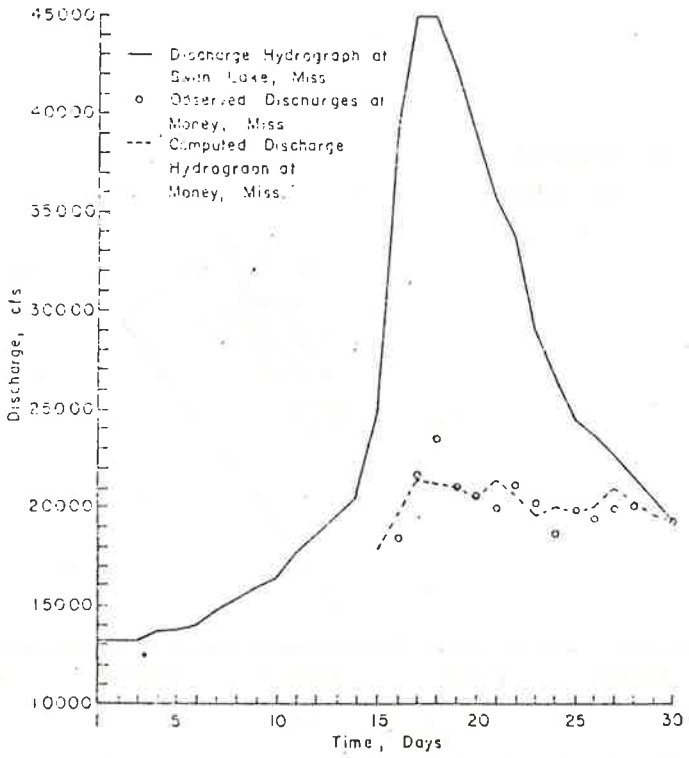

Figure 9.10 Discharge hydrographs on the Tallahatchie River.

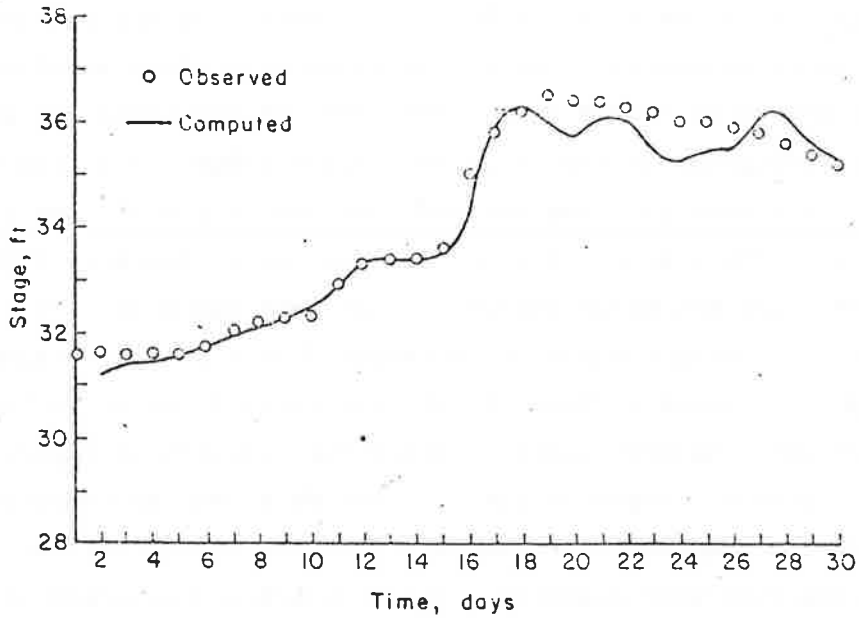

Figure 9-11 Stage hydrograph on the Tallahatchie River at Money, Mississippi.

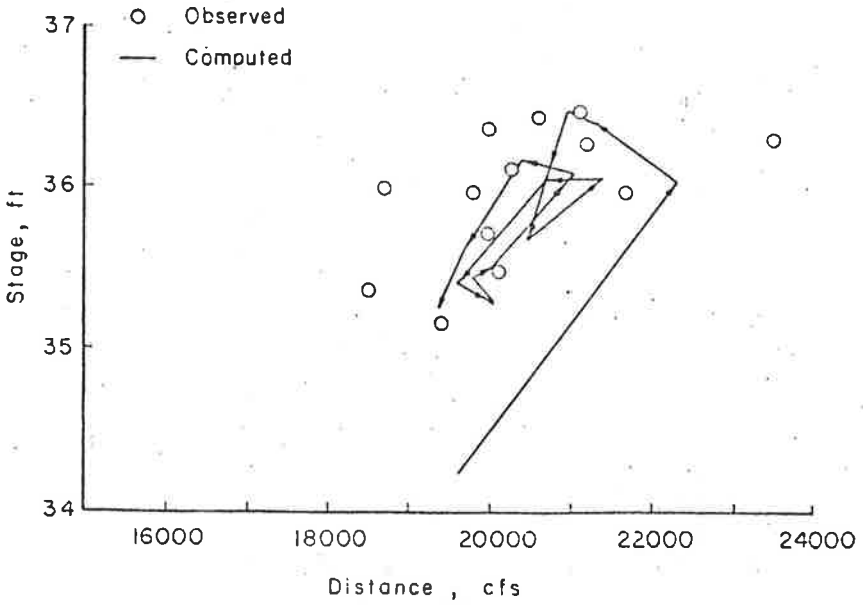

Figure 9.12 Stage-discharge relationship on the Tallahatchie River at Money, Mississippi.

9.11 A COMPARISON OF STATISTICAL, BACKWATER PROFILE AND KNOWN DISCHARGE SEDIMENT ROUTING MODELS

Besides the dynamic effects, the stage-discharge relation is often affected by the backwater and/or sediment movement. In this sediment, frequency and magnitude of error associated with three models are examined. This evaluation was conducted by Li, Brown, and Simons (1979). The first model utilized is a statistical stage-discharge relationship. The second model is a steady flow rigid boundary backwater model, and the third model is a steady flow backwater model with uncoupled sediment routing. The sediment routing model can compute changes in the channel due to aggradation and degradation. For thorough comparison, each model was applied to two case studies. One case involved a relatively stable reach of river, while the other was unstable. All three models are relatively accurate for the stable reach. However, the sediment routing model that considers the physical processes of open channel flow and fluvial geomorphology is the only feasible approach to predict the response of an active river.

Case Studies

The Yazoo River in Mississippi was selected for study due to the availability of data for that area. Two reaches of the river were carefully analyzed: a stable reach near Locopolis and an unstable reach at the Fort Pemberton cutoff near Greenwood. Historically, the bed elevation in the stable reach has not changed substantially. However, the bed of the unstable reach degraded up to 20 feet during 1973 and 1974. This degradation was caused by the removal of a dam in the cutoff that allowed a large portion of the Yazoo River flow to bypass the Greenwood Bendway. The changing behavior of the river discharge and sediment transport at this unstable reach makes prediction of flood stage from discharge data difficult. This is especially true for models that are based entirely on historical data since they cannot adjust to the new flow conditions. Selection of these two reaches allow evaluation of the realiability of the three models.

Description of Models

Stage-Discharge Relationship Model

The relationship between stage and discharge is called a discharge rating curve. Generally, a discharge rating curve is obtained by making several discharge measurements and then plotting the observed stage compared with the measured discharge. In reality, experience indicates that measurements of stage and discharge do not form a one-to-one relationship. Many rivers, especially those with a flatter gradient, display by hysteresis loop in the stage-discharge relationship due in part to dynamic effects and changing bed forms (1). Since these relationships can normally only be determined using water and sediment routing models, the following relation is commonly used to determine the stages at a given location along the river from the corresponding discharges

$$q = \alpha' y^{\beta'} \tag{9-64}$$

where Q = discharge, y = stage, and α' and β' are time-invariant coefficients. The unknown coefficients α' and β' were estimated by least-squares regression techniques based on historical records.

Rigid Boundary Backwater Model (See Chapter 12)

A known discharge model developed by the authors was used in this study. Characteristic features of this model follow.

Known Discharge. This model assumes that during any one time period, water dishcarge is constant along a reach of river, except where lateral inflows occur, i.e., a steady flow is assumed. Although a model of this type cannot predict the dynamic effects that an unsteady flow model can, it requires considerably less computer time. Also, the model is able to calculate flood stages, and provide a practical method to evaluate water surface profiles over long time periods. The time increments on the input hydrographs vary from a few hours to a month or longer, depending on the flow conditions and the desired accuracy of the results. In this study, a time increment of one day was used.

River Geometry. The only river geometry data required by the model are digitized channel cross sections and the river distance between cross sections. The model uses the digitized channel cross sections to determine geometric equations that define conveyance, width, and area of channel as a function of water depth.

Backwater Calcualtions. The backwater curve is determined by starting at a known downstream water surface elevation and calculating the upstream water surface elevation using a first-order Newton-Raphson approximation to solve the total head equation at each successive cross section. For a rigid boundary model the cross-sectional shape is assumed to be unaltered during the simulation.

Sediment Routing Model

In addition, a sediment routing capability is added to the backwater model described above. Additional features of this model are:

Uncoupled Routing. Water and sediment routing are uncoupled, making the bed profile constant during one time increment. Changes in the bed profile due to sediment movement are made at the end of the time increment.

Sediment Transport. The bed material sediment transport at each cross section was calculated using a transport equation derived from river sediment discharge measurements.

Since both process models are used the same backwater calculations, any difference in results is due solely to the higher level of physical processes modeled considering sediment movement.

Calibration of Models

Calibration Data

All three models were calibrated using the same data. In the unstable Fort Pemberton reach, the calibration period was from April 12, 1973 to February 23, 1974 (318 days). In the stable Locopolis reach, the calibration period was from Januray 1, 1971 to December 31, 1972 (731 days). The calibration data included observed discharges and stages at Fort Pemberton and Locopolis. The sediment routing model also utilized the observed bed elevations at Fort Pemberton.

Stage-Discharge Relationship

Measured discharge and observed stage data from the two test reaches for the specified times were used to estimate the unknown parameters, α' and β', that minimized the mean-square-error of the estimates. Regression constants and the coefficient correlation, R, are as follows:

Unstable Reach: $\alpha' = 1783.77782$, $\beta' = 0.75383$, $R = 0.901$

Stable Reach: $\alpha' = 0.28715$, $\beta' = 3.14017$, $R = 0.991$

It is clear that the stage-discharge relationship is very easy to calibrate and use.

Rigid Boundary Backwater Model

The river stage computed by this rigid boundary model was calibrated by adjusting the estimated channel roughness coefficient, Manning's n. Manning's n was calibrated by multiplying a constant with the estimated n value for the main channel and overbanks. The model was then run with flow data from the calibration periods and error between the observed and computed water surface was determined. The process was repeated with different values of the constant until no reduction in error resulted.

Manning's n for the Fort Pemberton reach was determined to be 0.031. At the Locopolis reach it was necessary to allow Manning's n to vary with discharge, since there appeared to be large differences in head loss in the reach at different flow levels. The calibrated Manning's n varies as a power function of discharge, and is about 0.018 for the extreme high flow and approximately 0.040 for the low flow. These values are reasonable considering the hydraulics of the fluvial system.

Sediment Routing Model

The sediment routing model was calibrated at Fort Pemberton by adjusting both Manning's n and sediment input into the cutoff. Sediment input had to be calculated because a weir, a low submerged dam, is located at the upstream end of the cutoff. This weir traps sediment upstream. Sediment input was adjusted until the computed bed elevation at four sections directly downstream of the weir matched as closely as possible the observed bed changes. Figure 9-13 shows a plot of observed and computed bed elevations at the four locations. As indicated, the computed bed profile for February 23, 1974 closely matches the observed bed profile. The calibrated Manning's n had a value of 0.030, which is only 3-1/3 percent lower than the value obtained from the backwater curve model.

In the Swan Lake-Locopolis reach, there was not enough cross-sectional data to calibrate the sediment transport; therefore, only Manning's n

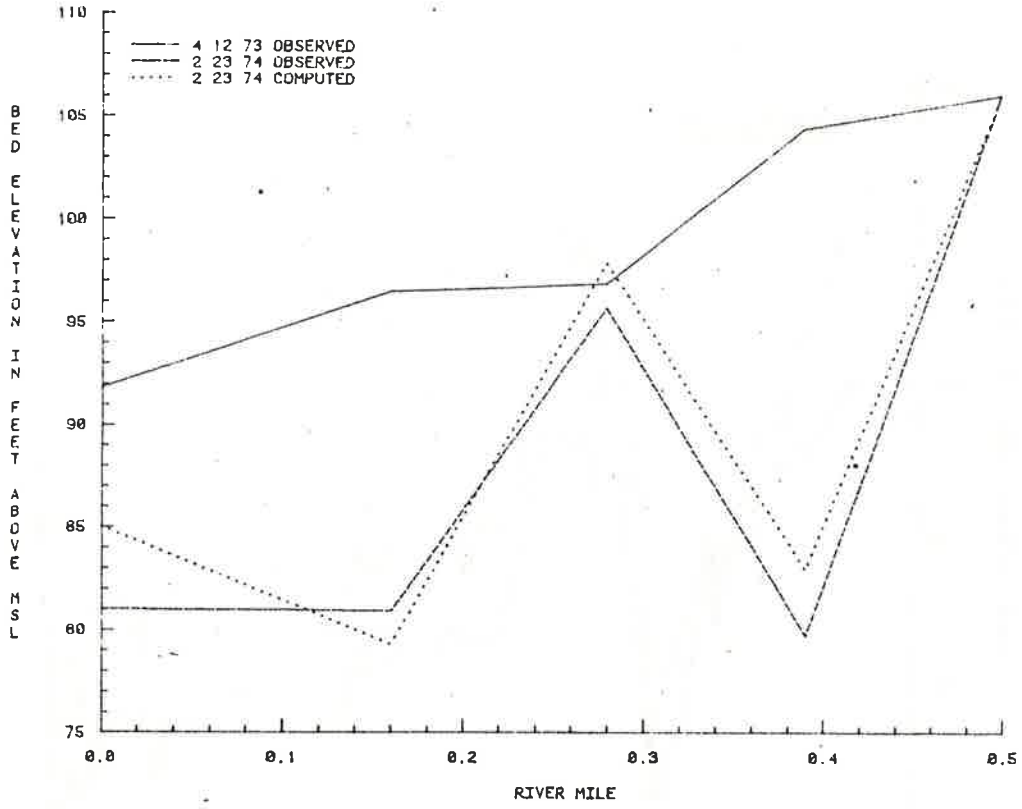

Figure 9.13 Observed and computed bed elevation at Fort Pemberton (1 foot = 0.305 m).

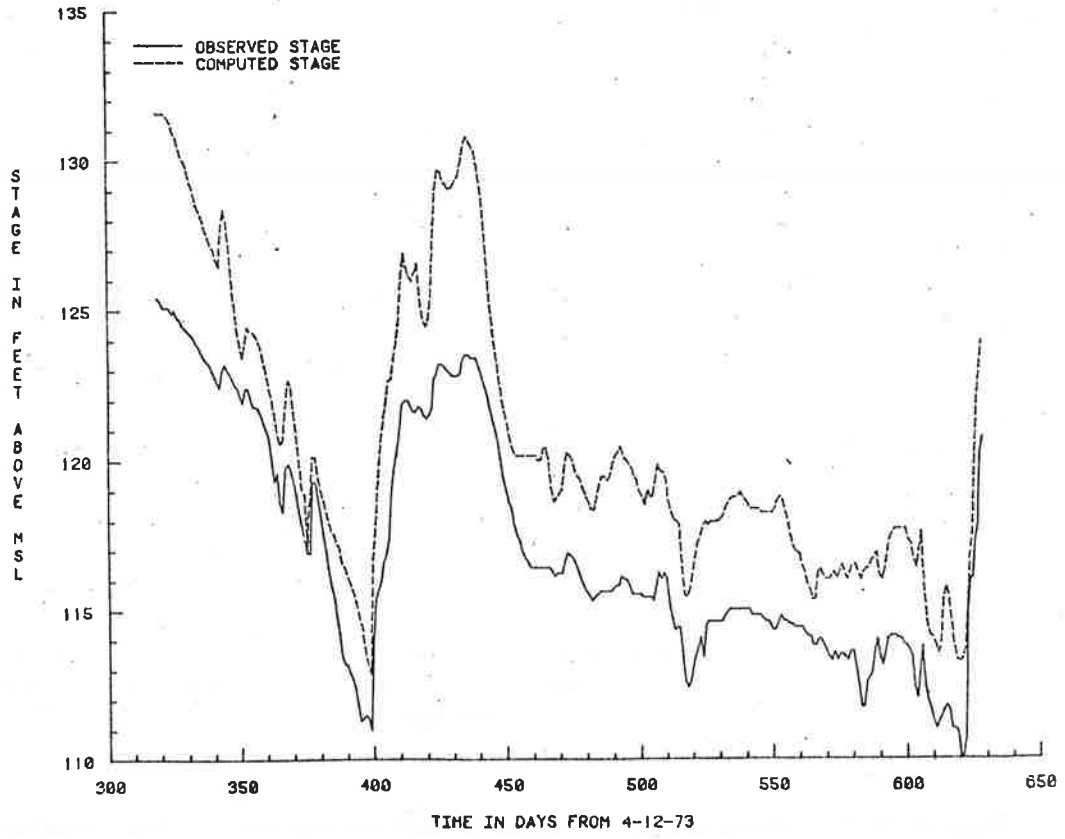

Figure 9.14 Statistical model verification at Fort Pemberton.

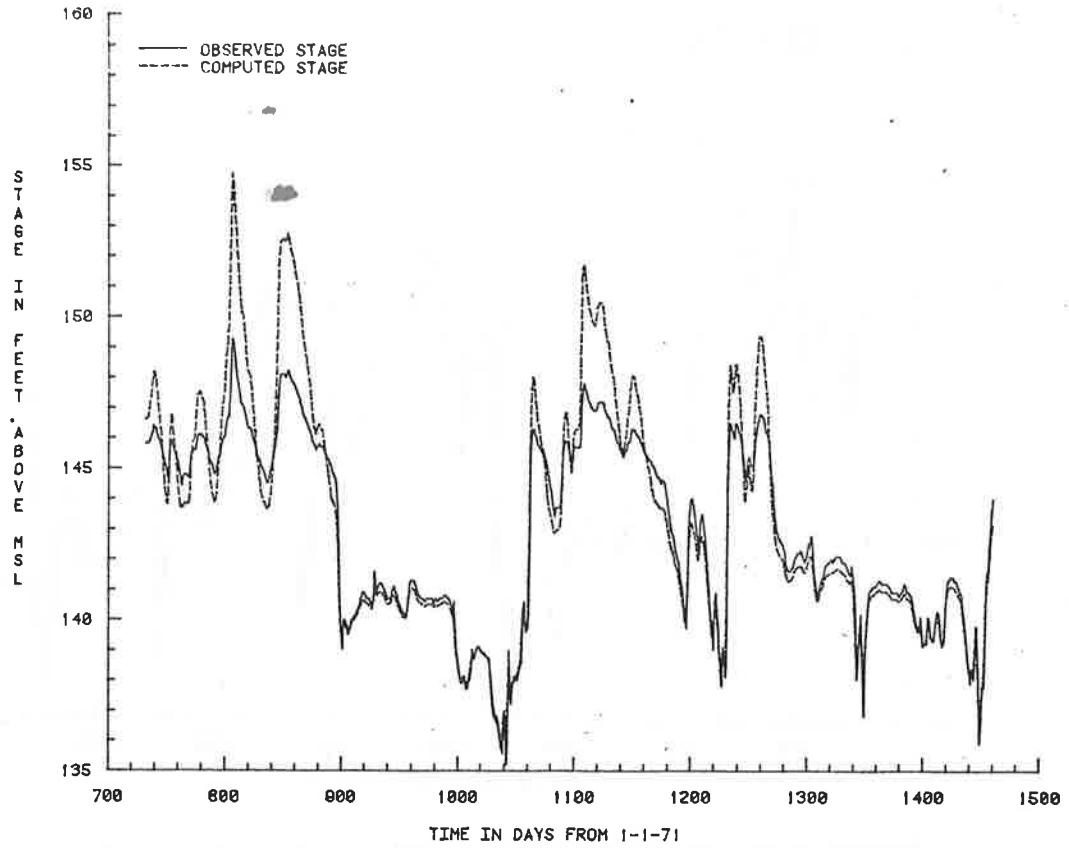

Figure 9.15 Statistical model verification at Locopolis (1 foot = 0.305 m).

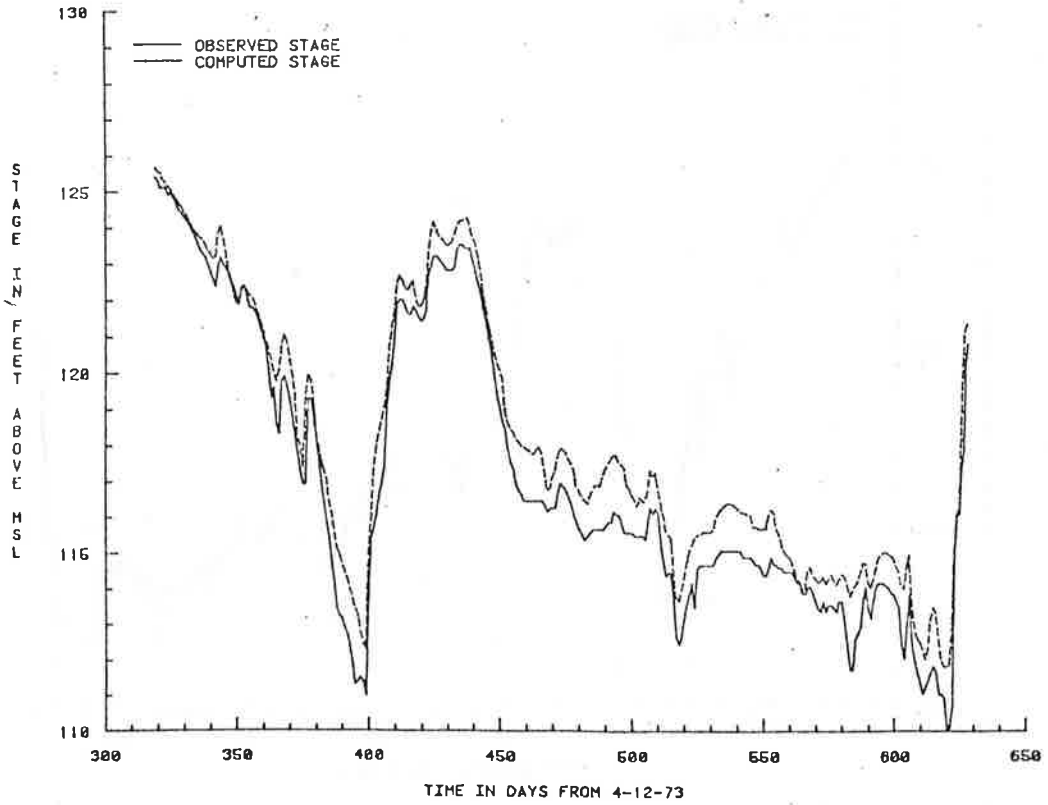

Figure 9.16 Rigid boundary model verification at Fort Pemberton (1 foot = 305 m).

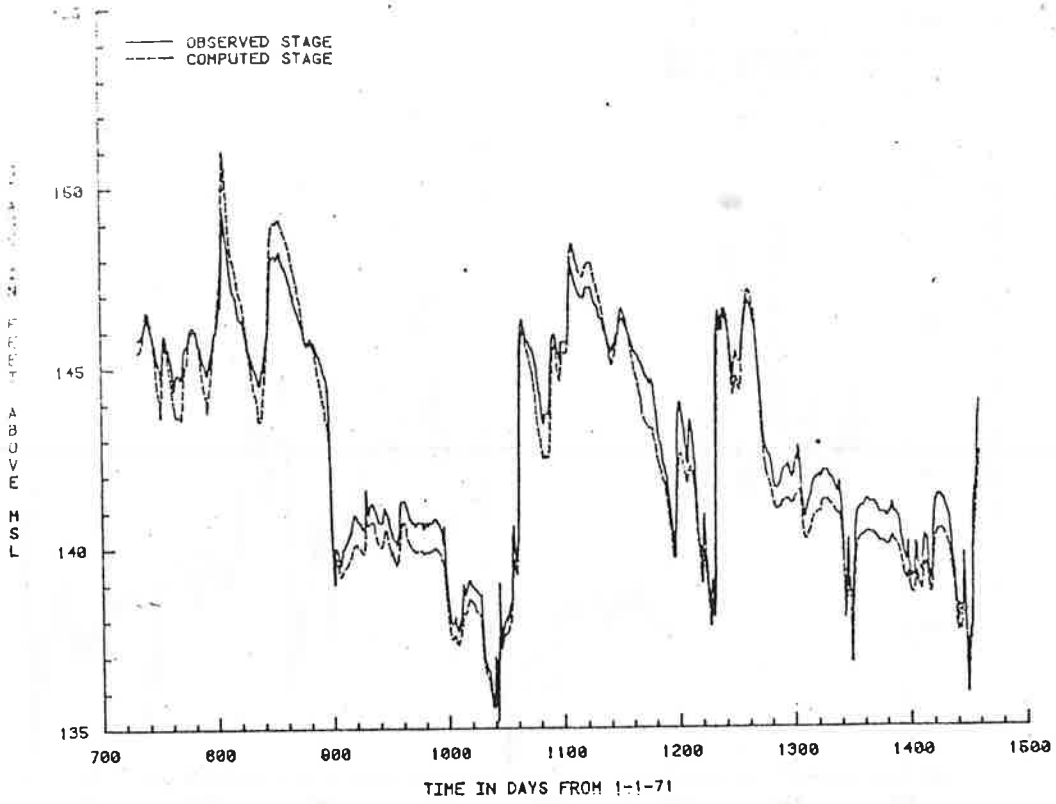

Figure 9.17 Rigid boundary model verification at Locopolis (1 foot = 305 m).

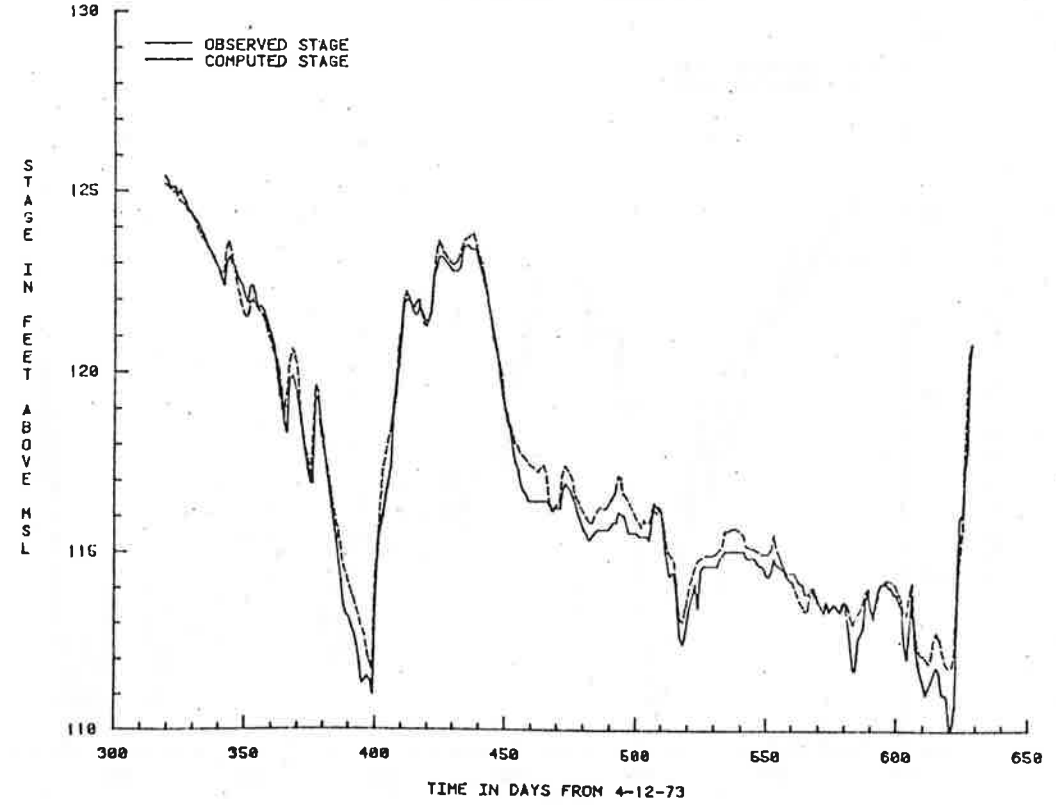

Figure 9.18 Sediment routing model verification at Fort Pemberton (1 foot = 0.305 m).

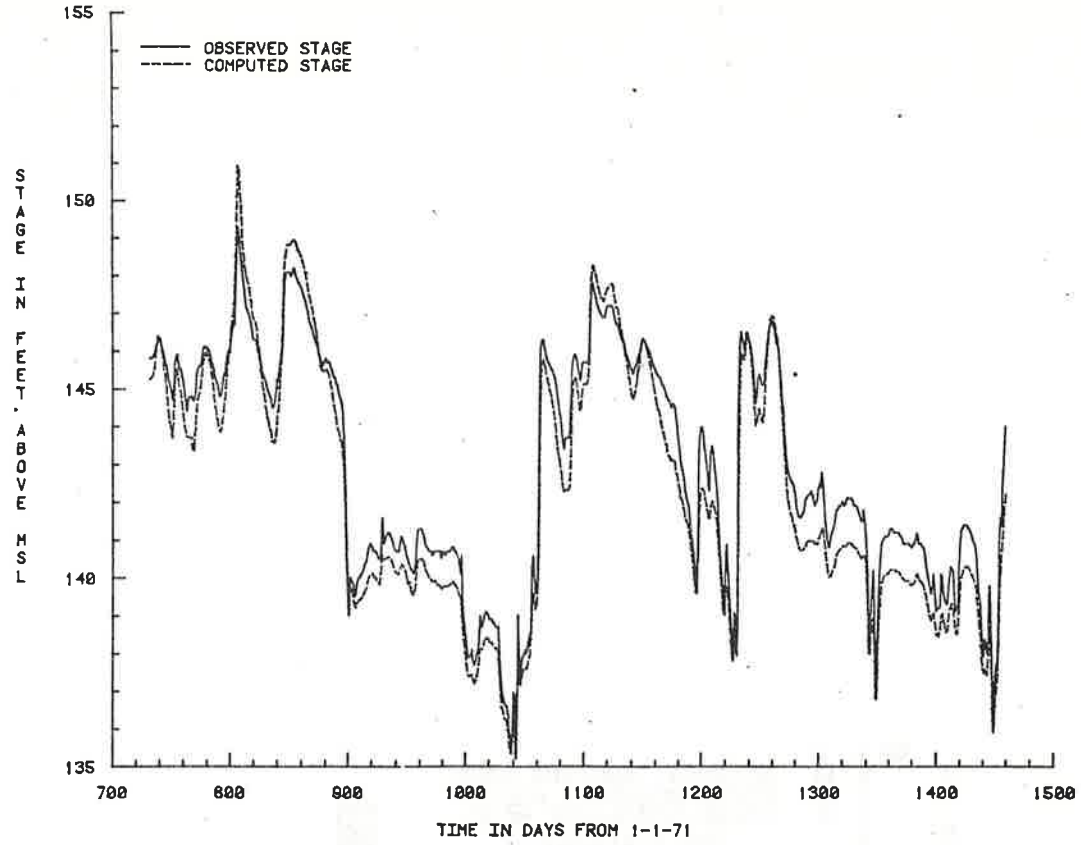

Figure 9.19 Sediment routing model verification at Locopolis (1 foot = 0.305 m).

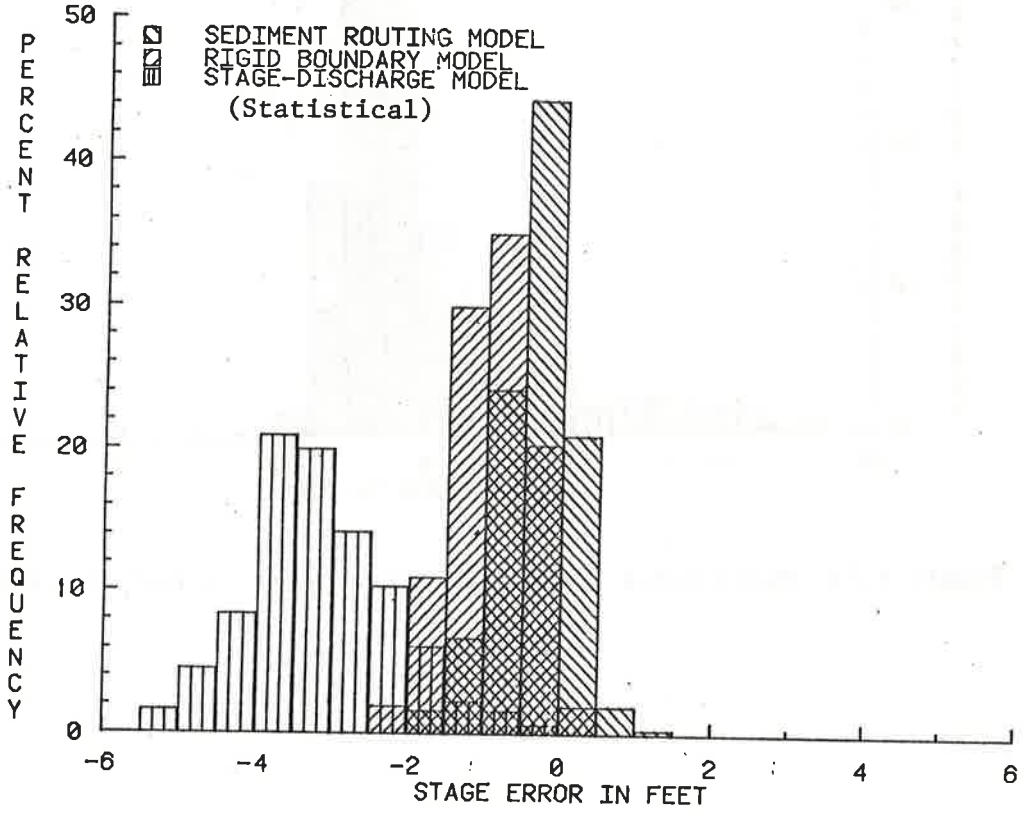

Figure 9.20 Model error frequency at Fort Pemberton (1 foot = 0.305 m).

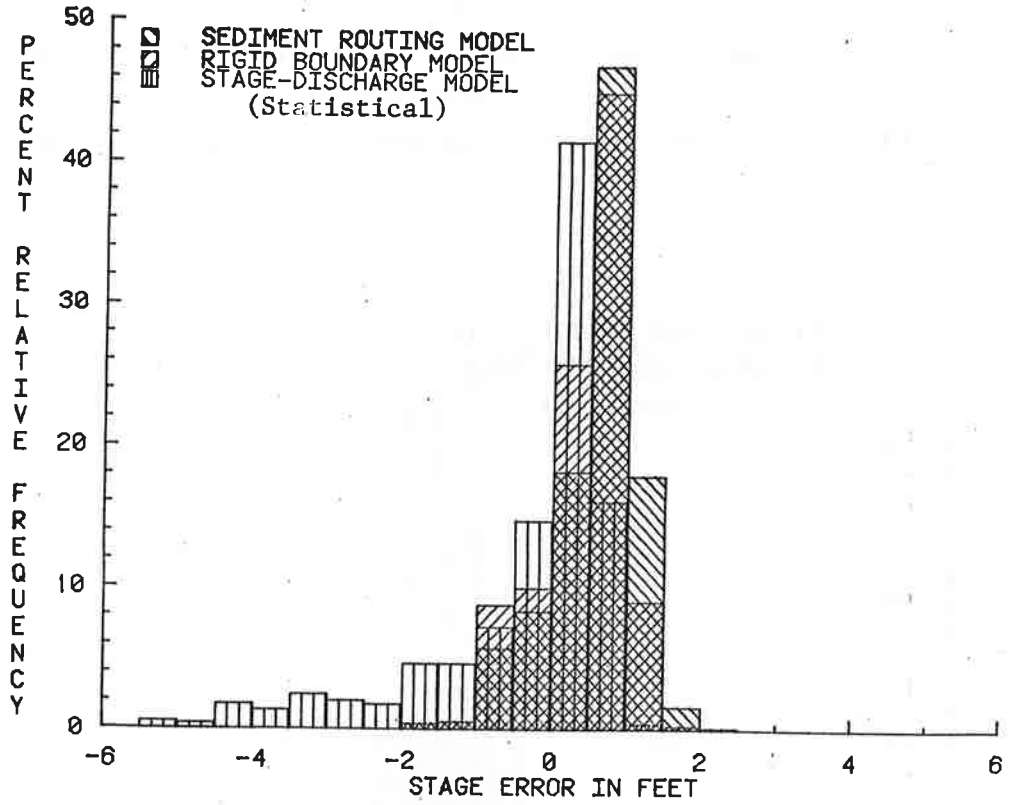

Figure 9.21 Model error frequency at Locopolis (1 foot = 0.305 m).

was calibrated with the sediment transport at its normal value. Again, in this reach the n value changed only slightly from the backwater model, varying from 0.042 at low flows to 0.02 at extreme high flows.

Inference can be made from the above description that calibration of the physical process models requires significantly more data and effort to develop and calibrate than the statistical stage-discharge model. However, once the physical process model is developed and calibrated, less data is actually required for the application.

Verification of Models

To verify the results of the calibration, an additional run utilizing each model was made for each reach using the calibration results. These runs were made for the periods immediately following the calibration period. At Fort Pemberton, the verification time period was from February 24, 1974 to December 31, 1974 (311 days). At Locopolis, the time period was from January 1, 1973 to December 31, 1974 (730 days). Figures 9.14 through 9.19 show plots of the measured and computed stage at Fort Pemberton and Locopolis for the verification period.

Comparison of Methods

For comparison purposes, model error is defined as the difference between observed and predicted stage for each day. Figures 9.20 and 9.21 show the relative frequency distribution of error for the verification periods and Table 9.1 lists the statistics of the absolute error for each method.

Table 9.1 Statistics of absolute model errors.

	Error in Feet			
	Calibrated		Verification	
	Mean	Maximum	Mean	Maximum
Stage-Discharge Model				
Fort Pemberton	2.56	10.38	3.47	7.27
Locopolis	0.33	2.56	0.80	5.48
Rigid Boundary Model				
Fort Pemberton	0.90	3.97	0.92	2.39
Locopolis	0.29	2.27	0.62	1.91
Sediment Routing Model				
Fort Pemberton	0.88	3.60	0.45	1.78
Locopolis	0.34	2.12	0.74	2.21

As indicated in the figures and table, all three methods have approximately the same mean error for Locopolis, but the process models have much lower maximum errors than the stage-discharge statistical relationships. Since there are few channel changes in this reach, the results of the two process models, rigid boundary and moveable bed, are essentially the same. At Fort Pemberton the sediment routing model is clearly better than the simple backwater model, assuming a rigid boundary bed, and is superior to the statistical approach because the sediment routing model predicts and adapts to changes in river conditions related to sediment movement and deposition. The stage-discharge statistical and rigid boundary models, however, are based only upon limited historical conditions and cannot adapt to a changing environment.

Computer central processor times on the Cyber 172 at Colorado State University, required for one run on both test reaches, were 10, 140 and 240 seconds for the stage discharge, backwater, and sediment routing models, respectively. While the stage-discharge model needed to be run once, the process models required several runs to calibrate.

9.12 SUMMARY AND CONCLUSIONS

Using the full momentum equation and the continuity equation a mathematical model which converts stage to discharge or vice versa has been developed. The model simulates the dynamic relation which exists between stage and discharge due to the effect of variable friction slope caused by changing discharge. The frequency observed hysteresis loop in stage discharge. The frequently observed hysteresis loop in stage discharge relationships was accurately reproduced in the two test cases. Required input consists of either a stage or discharge hydrograph, channel slope, cross-sectional properties and Manning's n. The model can successfully simulate the dynamic relation between stage and discharge at locations where significant scour, fill and/or bedform changes are negligible. The application of the derived relation to extend the applicability of the kinematic wave approximation has been successful.

Statistical prediction of river stage, though easy to apply, should be limited to stable rivers where there are adequate data over the range of flow conditions. The backwater model with rigid boundary assumption

should be limited to stable reaches where little change in cross-sectional data occurs. However, since it can account for varying flow conditions, it can be used where only limited stage and discharge data are available. The sediment routing computer model that considers the physical significance of open channel flow and fluvial geomorphology and that computes changes in a river environment is the only feasible approach to predict the response of a river to man's activity, such as implementing a river cutoff or dredging.

9.12 REFERENCES

Chen, Y. H., "Mathematical Modeling of Water and Sediment Routing in Natural Channels," Ph.D. Dissertation, Colorado State University, Fort Collins, Colorado, 1973.

Chow, V. T., Open Channel Hydraulics, McGraw-Hill, 1959.

Fread, D. L., "A Dynamic Model of Stage-Discharge Relations Affected by Changing Discharge," NOAA Technical Memorandum NWS Hydro 16, November 1973.

Henderson, F. M., Open Channel Flow, Macmillan, London, 1966.

Li, R. M., "Mathematical Modeling of Response from Small Watersheds," Ph.D. Dissertation, Department of Civil Engineering, Colorado State University, Fort Collins, Colorado, 1974.

Li, R. M., G. O. Brown and D. B. Simons, "Computer Simulation of River Stages," Colorado State University, Fort Collins, prepared for Summer Computer Simulation Conference in Toronto, Canada, 1979.

Li, R. M., D. B. Simons, and M. A. Stevens, "Nonlinear Kinematic Wave Approximation for Water Routing," Water Resources Research, Vol. 11, No. 2, 1975.

Simons, D. B., R. M. Li, G. O. Brown, Y. H. Chen, T. J. Ward, N. Duong, and V. M. Ponce, "Sedimentation Study of the Yazoo River Basin, Phase I General Report," prepared for U.S. Army Corps of Engineers, Vicksburg District, Vicksburg, Mississippi, 1978.

Simons, D. B. and Richardson, E. V., "Studies of Flow in Alluvial Channels--Basis Data from Flume Experiments," Department of Civil Engineering, Colorado State University, Fort Collins, Colorado, 1961.

Simons, R. K., "A Modified Kinematic Approximation for Water and Sediment Routing," M.S. Thesis, Department of Civil Engineering, Colorado State University, Fort Collins, Colorado, 1977.

CHAPTER 10

WATERSHED SEDIMENT YIELD

by

Ruh-Ming Li, Associate Professor, Department of Civil Engineering, Colorado State University, Fort Collins, Colorado
Daryl B. Simons, Associate Dean for Engineering Research and Professor of Civil Engineering, Colorado State University, Fort Collins, Colorado
Timothy J. Ward, Assistant Professor of Civil Engineering, Colorado State University, Fort Collins, Colorado

10.1 INTRODUCTION

Increased demands on the natural resources has produced beneficial and adverse impacts in different watershed systems. In watersheds, activities such as timbering, road building, mining, and agricultural uses have sometimes created adverse impacts on soil and water systems. Assessment of these impacts often demands quantitative as well as qualitative evaluations. One such evaluation is the sediment yield or change in sediment yield brought about by such activities. The qualitative response of the system can be deduced from knowledge of the controlling physical processes and the influence of the specific activity on those processes (refer to Chapter 3). Quantitative response, such as changes in sediment yield per acre, require some type of mathematical expression or model. Such an expression should relate measures of key physical processes to the sediment yield. In this manner, the model or expression would be sensitive to changes in controlling processes and reflect quantifiable natural or man-induced changes in the system.

This chapter discusses types of models for estimating sediment yield from watersheds. One type, physical process simulation models, is discussed in detail, and example applications are presented. The models are used to estimate or predict sediment yields resulting from natural or disturbed watershed lands. They do account for important physical processes such as raindrop splash, overland flow erosion, channel erosion, and movement of the different sediment size fractions. The models presented in this chapter do not account for gully or landslide generated sediment yields. Landslides, however, are discussed in Chapter 13. One all important aspect of model development and operation is data. Without adequate data, testing and verification of models before application to real situations may produce erroneous results that do not truly represent actual conditions. The old axiom "garbage in, garbage out" strangely applies when otherwise representative models are supplied with incorrect data. Understanding model operations and controlling physical processes allows rapid delineation of those data that are erroneous. Model development keeping physical processes and data needs in the forefront can produce realistic, accurate methods for estimating sediment yield from watersheds.

10.2 CURRENT APPROACHES

General

There are numerous qualitative and quantitative approaches available for estimating sediment yield from watersheds. The most useful types are those that can accurately quantitize yields for short and long time spans, and are sensitive to the management activities and changes in the soil-water system. These restrictions require the use of certain levels of mathematical models for estimating sediment yields. Only by using mathematical models can a system be effectively accurately quantitized.

Types of Mathematical Models

Numerous approaches can be used to determine sediment yield from natural or disturbed land surfaces. Of interest are those approaches that utilize mathematical models. One category of mathematical models is the "black box," or lumped parameter model. Another category is based on regression equations as typified by the Universal Soil Loss Equation. Both types interpret input-output relations using simplified forms that may or may not have physical significance. Processes related to the movement of water and sediment through the watershed are grouped into coefficients. A classic example is the rational formula for estimating peak discharge, i.e., $Q = CiA$ where Q is peak discharge, i is rainfall input, A is the drainage area, and C is the runoff coefficient that represents all hydrologic processes. Although the lumped parameter and regression models are often used, the parameters may not accurately represent observable physical characteristics. Another disadvantage is that some models do not consider the physical environment as dynamic with respect to time and location.

Another approach is through the use of stochastic models. If rainfall events, watershed response and runoff events are stochastic, i.e., probabilistic in nature, the processes of sediment yield are also stochastic. However, the stochastic models are difficult to apply (Shen and Li, 1976), and do not readily show the response of a watershed undergoing changes as a result of various land use activities. Most hypotheses used in stochastic models have not been tested by field data. Woolhiser and Blinco (1975) indicated that knowledge in applying stochastic models to sediment yield from watersheds is primitive. Stochastic models are not considered in this chapter.

Another type of model is the physical process simulation model. In this type of model the governing processes controlling sediment yield are formulated and analyzed separately to provide model sensitivity to land management alternatives. This type of model will be discussed in detail in this Chapter.

Regression Models

Among all available methods used to estimate sediment yield, regression models are perhaps the simplest to use. Validity of regression models is dependent on data availability. Application of regression models is substantially restricted if there is insufficient data.

Musgrave (1947) analyzed soil loss measurement for approximately 40,000 storms occurring on fractional plots in the United States. Results of his study indicated that

$$A_s = I^{1.75} K L^{0.35} S^{1.35} C_g \qquad (10\text{-}1)$$

where A_s is the annual soil loss per unit area, I is the maximum 30 minute intensity with a return period of two years, K is the numerical value that is proportional to the soil erodibility, L is the slope length, S is the percent slope and C_g is the ground cover.

This equation is usually applicable to long-term average soil losses for an extensive area. In order to extend the Musgrave equation to estimate the short-term rates of soil loss for localized areas, extensive data collection and analyses were made by Wischmeier and Smith (1960). Their efforts led to the development of a more refined soil loss equation called the "Universal Soil Loss Equation" (USLE). Since then, the USLE has been applied to all types of watersheds. The USLE is perhaps the most comprehensive and popular regression model to estimate soil loss. It is discussed in the following segments of this chapter.

Williams and Berndt (1972) recognized the application of the Universal Soil Loss Equation as limited to soil loss and developed a different procedure for computing sediment yields from watersheds. They introduced a runoff factor instead of rainfall energy into the Universal Soil Loss Equation to estimate the soil loss and a delivery ratio to estimate the sediment yield. Later Williams (1975) used the modified Universal Soil Loss Equation combined with a decay function to estimate sediment yield from watersheds. The modified Universal Soil Loss Equation is

$$A_s \simeq 95\ (Q_v \cdot q_p)^{0.56}\ K\ LS\ CP \qquad (10\text{-}2)$$

where Q_v is runoff volume in acre-ft and q_p is the peak flow rate in cubic feet per second. The decay functions is

$$A_s \simeq A_o\ e^{-Bt}\ d_s \qquad (10\text{-}3)$$

where A_o is the sediment yield in the upstream section, B is the routing coefficient, t is the travel time between sections, d_s is the soil particle diameter. Although promising, in that it uses more easily understood physical quantities, this storm basis method is subject to some of the same drawbacks as the original USLE.

Meyer and Monke (1965) studied the relationships between runoff erosion and various factors such as slope steepness, slope length and particle size in an indoor laboratory. They analyzed measured data with a multiple regression technique resulting in

$$A_r \simeq L^{1.9}\ S^{3.5}\ d_s^{-0.5} \qquad (10\text{-}4)$$

where A_r is the runoff erosion rate. However, during the study they found that these variables interacted with one another, therefore, further studies were necessary to evaluate the influence of each of these variables to runoff erosion.

Kilinc and Richardson (1973) studied the mechanics of soil erosion by simulated rianfall. Factors considered important in their study were Reynolds number, slope, stream power and discharge. Results showed that stream power was the most important factor in predicting sediment discharge for their study. The model derived from regression analysis can be written as

$$q_s = 2.104\ ((\tau_o - \tau_c)\ \bar{u})^{1.584} \qquad (10\text{-}5)$$

where q_s is sediment discharge in pounds per second per foot, τ_o is boundary shear stress, τ_c is critical shear stress and $\bar{u}$ is mean velocity. All of the described regression models were either developed using experimental data or tested against a particular watershed where data were collected and analyzed. In most cases, these equations are specific for a particular study area or laboratory condition where the data were collected.

Universal Soil Loss Equation

The most widely used of these regression models is the Universal Soil Loss Equation (USLE). The U.S. Department of Agriculture began to study soil loss about 1930 when the first ten Federal-State Cooperative Stations began operation. Thirty-two additional stations were established in the next 25 years. Measurements of precipitation, runoff and soil loss of these 42 stations in 23 states (east of the Rocky Mountains) were collected continuously for periods of from 5 to 30 or more years. The field plots were rectangular to facilitate typical flow row spacings for cultivated units. A plot 72.6 feet long on a nine percent uniform slope in bare fallow soil and tilled to break surface crusts was abritrarily selected to serve as a common reference for evaluation.

Six major factors to describe rainfall (R), soil erodibility (K), slope-length (L), slope steepness (S), cropping and management (C), and supplemental erosion-control practices such as contouring or terracing (P), were used to develop the Universal Soil Loss Equation. This model is based on field data collected from the plots described above and from rainfall simulation data. The USLE model is

$$\underline{E} = R\ K\ L\ S\ C\ P \qquad (10\text{-}6)$$

where L, S, C and P are all dimensionless. The computed soil loss $\underline{E}$ has the time period of R and soil loss dimension of K. Smith and Wischmeier (1957), Meyer (1971), and Wischmeier (1973) provide detailed descriptions of this equation and its terms.

The rainfall factor R is dependent on the parameter, EI, and product of kinetic energy of the storm times maximum 30-minute rainfall intensity. Maximum 30-minute intensity is twice the greatest amount of recorded rainfall in any 30 consecutive minutes, and the storm energy E was computed from a relationship between E and rainfall intensity. An iso-erodent map to indicate the values of R for nearly all locations in the 37 states east of the Rocky Mountains was developed by Wischmeier and Smith (1965) based on data collected by the U.S. Weather Bureau.

In general, the R factor must be predicted on a probability basis. Frequency distributions of annual, seasonal or annual-maximum storm EI values follow the log-normal type of curve that is typical of much hydrological data.

The soil erodibility factor K was found by Wischmeier et al. (1971), to be a function of percent of silt, percent of coarse sand, soil structure, permeability of soil, and percent of organic matter. Their soil erodibility nomograph is shown in Figure 10.1.

The slope length factor L was defined as the ratio of soil loss from a particular slope length to that from a 72.6-foot plot length with all other conditions the same. Slope length has been defined as the distance from the point of origin of overland flow to the point where either the slope decreases to the extent that deposition begins or the runoff water enters a well defined channel (Smith and Wischmeier, 1957). The effect of slope length on soil loss is primarily a result of increased potential due to a greater accumulation of runoff on the longer slopes.

The slope steepness factor S was found by Smith and Wischmeier (1957) to be a function of the actual slope steepness. The cropping-management factor C was defined as the ratio of soil loss from land cropped under specific conditions to the corresponding loss from tilled, continuously fallow ground. The factor ranging from about zero to 1.0, depends on type of vegetation cover, crop season and other management techniques. According to Wischmeier and Smith (1965) continuous corn is 63 percent as erodible as continuous fallow during the first month after seeding, but it is only 26 percent as erodible as fallow when matured. Small grains are approximately 50 percent as erodible as continuous fallow during the first month after seeding, but are only about 5 percent as erodible near maturity. Wischmeier and Smith (1965) presented a table to show the relative erodibilities of several crops (corn, grain, grass) for different crop sequences and yield levels at various stages of crop growth.

The erosion-control practice factor P accounts for the effect of conservation practices such as contouring, strip-cropping and terracing on erosion. It is valuable as the ratio of soil loss using one of these practices to the loss using straight row farming up and down the slope. Terracing is generally the most effective conservation practice for decreasing soil erosion.

Wischmeier (1972) presented a method including graphical aids graphs for determining the cover and management factor (cropping-management factor). C can be divided into three distinct types of

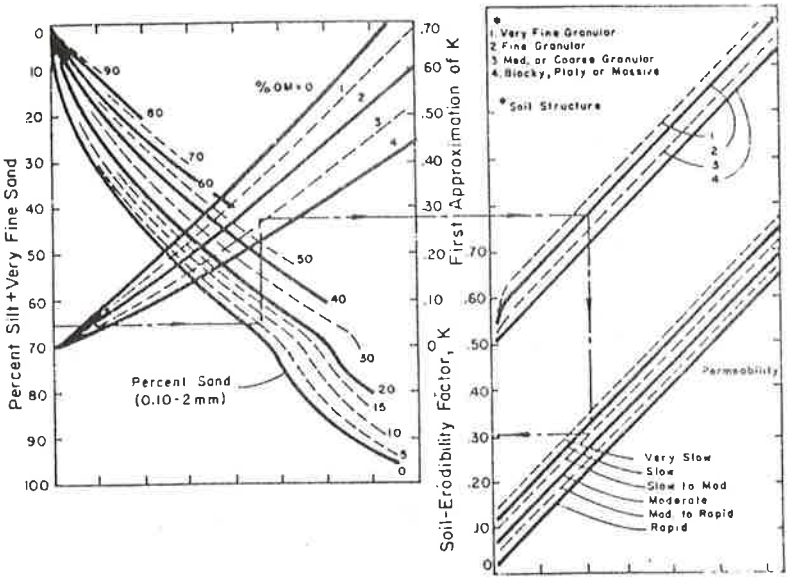

Figure 10.1 Soil erodibility nomograph used to determine Factor K for specific topsoils or subsoil horizons. Solutions are in tons per acre (from Wischmeier et al., 1971).

effects as follows: 1) Type I--effects of canopy cover, 2) Type II--effects of mulch or close-growing vegetation in direct contact with the soil surface, and 3) Type III--tillage and residual effects of the land-use.

Type I. Canopy Cover

Leaves and branches that do not directly contact the soil are effective only as canopy cover. A canopy can intercept the falling raindrops, but waterdrops falling from the canopy may regain an appreciable velocity, although not the terminal velocities of free-falling raindrops. Therefore, the canopy cover reduces rainfall erosivity by reducing its impact energy at the soil surface. The amount of reduction depends on the height and density of the canopy. Figure 10.2 shows the canopy factor as a function of the height and density of the canopy. The canopy factors for various percentages of cover at heights of 0.5, 1, 2, and 4 meters may be obtained directly from this graph.

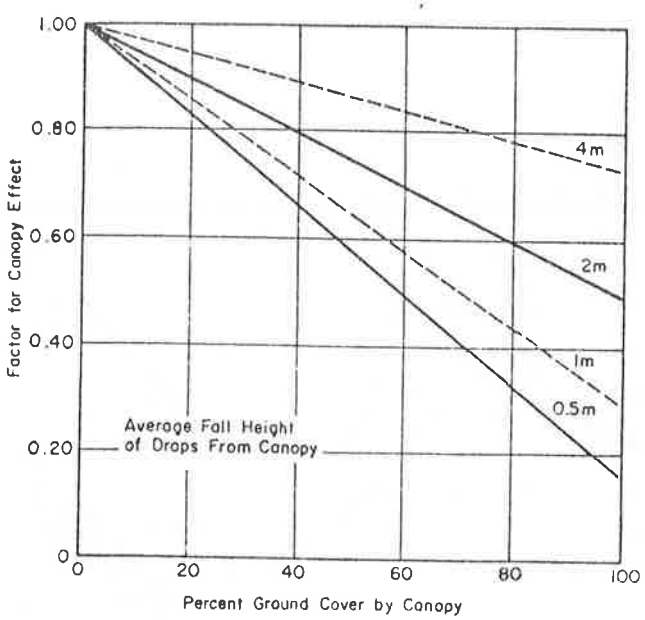

Figure 10.2 Influence of vegetal canopy on effective-EI. (After Wischmeier, 1972).

Type II. Mulch and Close-Growing Vegetation

A mulch at the soil atmosphere interface is much more effective than an equivalent percentage of canopy cover. Because the intercepted raindrops have no remaining fall-height to the ground, their impact on the soil surface is eliminated. A mulch that makes a good contact with the ground also reduces the runoff velocity. The reduction in velocity greatly reduces the potential of the runoff to detach and transport soil material.

Substantial rainulator data are not available on the erosion-reducing effectivness of various amounts and types of mulches used on cropland and construction sites. Extrapolation of these data to other mulches and close-covers, such as those associated with range or woodland, is facilitated by expressing them on the basis of "percent surface cover" rather than tons of mulch per acre. This conversion, and a preliminary summarization of the data, are reflected in the relationship curve shown in Figure 10.3.

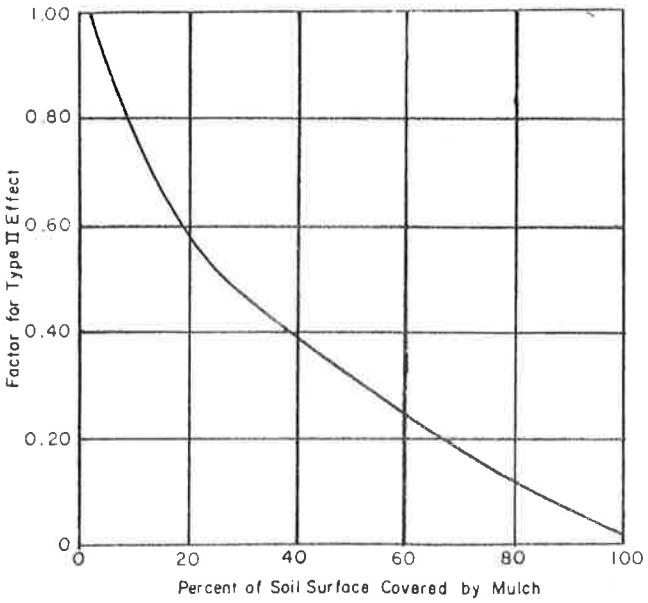

Figure 10.3 Effect of plant residues or close-growing stems at the soil surface (after Wischmeier, 1972).

Type III. Residual Effects of the Land Use

This category includes residual effects of the land use on soil structure, organic-matter content and soil density; effects of tillage, or lack of tillage, on surface roughness and porosity; roots and subsurface stems, biological effects and probably other factors. This factor can be evaluated from Figure 10.4 by knowing the percent of root network in the topsoil relative to a good rotation meadow. This percent of root network is often a difficult value to estimate. This overall C factor can be evaluated by the produce of the three subfactors, i.e., the product of the three subfactors, i.e., the product of the Type I, II, and III subfactors.

Although widely used, the USLE approach has some important limitations. Until recently, the approach was most applicable for estimating long term soil yields.

Wischmeier (1973) discussed confidence in the equation's predictions. As previously indicated, some of the terms in the soil loss equation are themselves functions of several significant parameters and must be derived by separate formulas and subroutines. Therefore, the complete equation could not be derived as a single least-squares fit to the

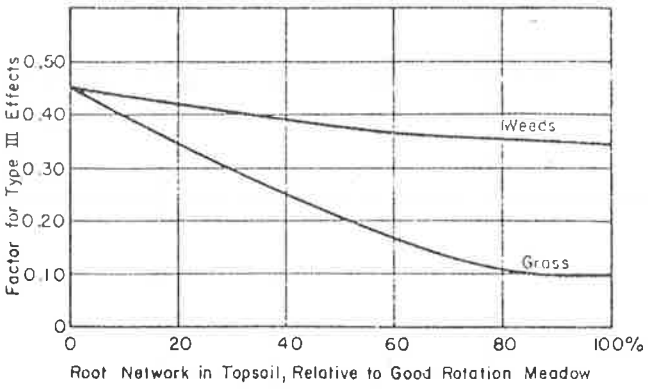

Figure 10.4 Type III effects on undisturbed land areas (after Wischmeier, 1972).

10,000 plot-years of basic data, and overall statistical confidence limits could not be computed by the usual analysis of variance technique. He did, however, obtain and indication of confidence limits by using the equation and the published isoerodent map, EI distribution curves, slope effect chart and soil-loss-ratio table to predict long term average annual soil losses on 189 plots for which he had a total of about 2300 plot-years of soil loss records. The 189 individual plot predictions deviated from the corresponding measured soil losses by an average of 1.4 tons per acre per year, which is about 12 percent of the 11.3-ton overall-average soil loss for the sample. About 84 percent of the deviations were within two tons per year, but the variance indicated that about five percent of such predictions may be in error by as much as 4.6 tons, or 40 percent of the average soil loss for the sample plots.

There is strong evidence of 20- to 22-year cycles in rainfall patterns. The iso-erodent map and EI distribution curves were derived from 22 year long rainfall records, which represent full cycles and therefore can be used to predict long term average losses. Thus the predicted values in the foregoing comparison are long-time averages while the actual data with which they were compared represent specific

time periods, some as short as five years. Since cyclical changes in rainfall patterns tend to be geographically widespred, and most of the short term locational studies in the sample were approximately concurrent, the effects of deviations from long term average rainfall and seasonal distribution of erosive rainstorms would not have averaged out. For the 2300 plot-years in the sample, the equation overpredicted by an average of 0.4 ton per acre per year. Of the 88 deviations of one ton or more, 59 were from comparisons representing less than half of the normal rainfall cycle. Therefore, use of the USLE for short term comparisons may be in error.

Confidence bands on predictions by the equation are the narrowest for silt, silt loam, and loam soils and for uniform slopes of from five to twelve percent, lengths not exceeding 400 feet, and consistent cropping systems that are directly represented by lines in the soil-loss-ratio graph. Beyond these limits significant extrapolation errors become more likely, but the predictions are believed to have sufficient accuracy for most applications over a much wider range of conditions. The equation's accuracy for predicting long-term average soil loss for a given situation is limited by lack of available data to evaluate its individual terms rather than by the model itself. Therefore, the overall attainable prediction accuracy is continuously improving as research provides data for accurate evaluation of the factors over a wider range of conditions.

The Universal Soil Loss Equation is designed to predict average annual soil losses by sheet and rill erosion on upslope areas such as farmland and construction sites. It can be helpful for prediction of contributions from these sources to downstream sediment loads, but its capabilities and limitations for this use must be recognized. It is an erosion equation and is not designed to predict deposition. Its predictions do not include sediment contributions from gully erosion or landslides, and it does not include factors to account for sediment losses or gains between the field and the stream or reservoir. These items must be evaluated separately.

Another problem with the USLE, or other types of regression models, is their dependence on large amounts of data for development. As previously mentioned, approximately 10,000 plot-years of data from the central and eastern United States were used to develop the equation. However, in

the semi-arid west and many watersheds collection of this amount of data may take centuries. This is controlled by the number of rainfall events that occur over an area in a year and the number of data collection sites, both of which are limited in the west and most other forested watersheds. In addition, the tree growth is a long and slow process and its effect on water and sediment yield is prolonged. It is difficult to collect a large amount of data for the wildland conditions. Another drawback to regression type equations, as previously mentioned, is their relative stationarity in time and space. This means that the data are restricted to a certain collection period at selected locations and do not necessarily represent long term variations in the system being studied. Therefore, use of regression equations to predict sediment yields outside the range of their data base can be unwarranted.

10.3 BASIC SEDIMENT ROUTING AND YIELD EQUATIONS

General

Sediment yield from watersheds is governed by the general physical processes cited in Chapter 3. The governing equations and methods of solution for water routing were discussed in Chapter 7. In addition to the continuity equation for water and momentum equation, additional equations are refined for sediment routing. Of primary importance is the sediment continuity equation and corresponding sediment transport formulae. Another basic principle is that sediment yield is directly proportional to either transport or supply. In general, if supply is greater than transport capacity, the transport capacity controls yield and vice-versa. Sediment supply is considered to be from raindrop impact detachment and flow detachment. The basic equations are applicable, to overland and channel flow. Another important aspect is the use of the sediment continuity equation to keep account of aggradation or degradation of the land or channel surface. In all models, sediment yield is considered for the individual size fractions.

Sediment Continuity Equation

The sediment continuity equation can be expressed as

$$\frac{\partial G_s}{\partial x} + \frac{\partial CA}{\partial t} + (1-\lambda)\frac{\partial PZ}{\partial t} = g_s \qquad (10\text{-}8)$$

in which

$$C = \frac{G_s}{Q} \qquad (10\text{-}9)$$

and G_s is the total sediment transport rate by volume per unit time, C is the sediment concentration by volume, Z is the depth of loose soil, λ is the soil porosity, and g_s is the lateral sediment inflow.

Sediment load can be considered for different sizes, and the continuity equation can be divided into N parts or

$$\frac{\partial G_{si}}{\partial x} + \frac{\partial C_i A}{\partial t} + (1-\lambda)\frac{\partial P Z_i}{\partial t} = g_{si} \qquad (10\text{-}10)$$

$$i = 1, \ldots, N$$

in which i is the size fraction index and N is the number of size fractions and

$$C_i = \frac{G_{si}}{Q} \qquad (10\text{-}11)$$

$$C = \sum_{i=1}^{N} C_i \qquad (10\text{-}12)$$

and

$$Z = \sum_{i=1}^{N} Z_i \qquad (10\text{-}13)$$

Sediment Transport Equations

Sediment transport equations are used to determine the sediment transport capacity for a specific set of flow conditions. Different transport capacities can be expected for different sediment sizes. For each sediment size, the transport rate includes the bed-load transport rate and the suspended load transport rate. The following equations are adopted to determine the sediment transport capacity for each size.

The Meyer-Peter, Müller equation is a simple and commonly used bed-load transport equation (see USBR, 1960). It is

$$q_b = \frac{12.85}{\sqrt{\rho}\,\gamma_s}(\tau - \tau_c)^{1.5} \qquad (10\text{-}14)$$

in which

$$\tau_c = \delta_s(\gamma_s - \gamma)d_s \qquad (10\text{-}15)$$

In equations 10-14 and 10-15 q_b is the bed-load transport rate in volume per unit width for a specific size of sediment, τ_c is the critical tractive force, ρ is the density of water, γ_s is the specific weight of sediment, γ is the specific weight of water, d_s is the size of sediment and δ_s is a constant dependent on flow conditions. Gessler (1965) shows that δ_s should be 0.047 for most flow conditions. If rilling develops on the overland flow surface, the value of δ_s should be lower.

It is not necessary to use the Meyer-Peter, Müller equation but an equation should be chosen which is applicable to the field condition. Other bed-load transport equations follow a similar form as Equation 10-14 (Chapter 4). According to Shen (1971), the general bed-load function can be expressed in the following functional form of

$$q_b = a_4 (\tau_o - \tau_c)^{b_4} \tag{10-16}$$

in which a_4 and b_4 are constants.

The flow discharge Q and flow area A are determined by the water routing procedures described in Chapter 7. The corresponding value of τ_o is computed as follows. The mean velocity is, in general,

$$V = Q/A \tag{10-17}$$

The boundary shear stress acting on the grain is

$$\tau_o = \frac{1}{8} \rho f_o V^2 = \frac{1}{8} \rho \frac{K_o}{N_r} V^2 \tag{10-18}$$

where ρ is the density of the flowing water, f_o is the Darcy-Weisbach friction factor, K_o is flow resistance related to grain, and N_r is the flow Reynolds number.

The sediment concentration profile which relates the sediment concentration with depth above the bed (Einstein, 1950) can be written as

$$\frac{C_\xi}{C_a} = \left(\frac{R-\xi}{\xi} \frac{a'}{R-a'}\right)^w \tag{10-19}$$

in which C_ξ is the sediment concentration at the distance ξ from the bed, C_a is the known concentration at a distance a' above the bed, and w is a parameter defined as

$$w = \frac{V_s}{\kappa U_*} \tag{10-20}$$

In Equation 10-20, V_s is the settling velocity of the sediment particles, κ is the Karman constant (assumed 0.4), and U_* is the shear velocity of the flow defined as

$$U_* = \left(\frac{\tau_*}{\rho}\right)^{1/2} \tag{10-21}$$

Note that

$$\tau_* = \frac{1}{8} f\rho V^2 \tag{10-22}$$

where f is the overall Darcy-Weisbach resistance factor.

A logarithmic velocity profile is commonly adopted to describe velocity distribution in turbulent flows. A useful equation is

$$\frac{u_\xi}{U_*} = B + 2.5 \ln \left(\frac{\xi}{\eta_s}\right) \tag{10-23}$$

in which u_ξ is the point mean velocity at the distance ξ from the bed, B is a constant dependent on roughness, and η_s is the roughness height.

The integral of suspended load above the a' level in the flow is obtained by combining Equations 10-19 and 10-23 or

$$q_s = \int_{a'}^{R} u_\xi C_\xi \xi = C_a U_* \int_{a'}^{R} \left[B + 2.5 \ln\left(\frac{\xi}{\eta_s}\right)\right]\left(\frac{R-\xi}{\xi}\frac{a'}{R-a'}\right)^W d\xi \tag{10-24}$$

Let

$$\sigma = \frac{\xi}{R} \tag{10-25}$$

and

$$G = \frac{a'}{R} \tag{10-26}$$

The equation becomes

$$q_s = \int_{a'}^{R} u_\xi C_\xi d\xi = C_a U_* \int_{a'}^{R} \left[B + 2.5 \ln\left(\frac{\xi}{\eta_s}\right)\right]\left(\frac{R-\xi}{\xi}\frac{a'}{R-a'}\right)^W d\xi \tag{10-27}$$

According to Einstein (1950), the concentration near the "bed layer" C_a is related to the bed-load transport rate q_b by the expression

$$q_b = 11.6\ C_a U_* a' \tag{10-28}$$

in which a' is defined as the thickness of the bed layer which is twice the size of sediment or $2d_s$.

The average flow velocity V is defined by the equation

$$V = \frac{\int_0^R u_\xi d\xi}{\int_0^R d\xi} \tag{10-29}$$

Using Equation 10-23 yields

$$\frac{V}{U_*} = B + 2.5\ \ell n\ (\frac{R}{\eta_s}) - 2.5 \tag{10-30}$$

Einstein (1950) defined the two integrals in Equation 10-27 as

$$I_1 = \int_G^1 (\frac{1-\sigma}{\sigma})^w\ d\sigma \tag{10-31}$$

and

$$I_2 = \int_G^1 (\frac{1-\sigma}{\sigma})^w\ \ell n\sigma\ d\sigma \tag{10-32}$$

The integrals I_1 and I_2 cannot be integrated in closed form for most values of w so a numerical integration is necessary. An efficient numerical method of determining I_1 and I_2 was developed by Li (1974).

The substitution of Equations 10-28, 10-30, 10-31, and 10-32 into 10-27 yields

$$q_s = \frac{q_b}{11.6} \frac{G^{w-1}}{(1-G)^w} [(\frac{V}{U_*} + 2.5)\ I_1 + 2.5\ I_2] \tag{10-33}$$

The total load per unit width of channel is

$$q_t = q_b + q_s \tag{10-34}$$

Equation 10-34 gives the total load per unit width of channel for a uniform size of sediment in the bed. When considering the transport by

different sizes and the entire width of channel, the sediment transport capacity of the ith size fraction of a sediment mixture would be

$$G_{ci} = P\ P_{ai}\ q_t \tag{10-35}$$

in which G_{ci} is the sediment transport capacity for the ith size, and F_{ai} is the adjusted fraction of the ith size sediment as determined in the next section.

Equations for Sediment Supply

The sediment supply rate is another determining factor in the actual sediment yield. Simons et al. (1975) stated that the sediment supply depends on the initial depth of loose soil left from previous storms, the amount of soil detachment by raindrop impact, and the amount of soil detachment by flow.

Soil Detachment by Raindrop Impact

Raindrop impact is a primary source of kinetic energy for detaching soil from any unprotected land surface. Ellison (1944) made a comprehensive study about the raindrop splash. Law and Parson (1943), Young and Wiersma (1973) and Mutchler (1967) greatly contributed to the study on detachment by raindrop impact. The conclusion drawn from these studies is that soil detachment is a function of erosivity of rainfall and the erodibility of the soil particles. The erosivity is directly related to the energy produced by raindrop impact and is generally formulated as a power function of rainfall intensity, size of droplet, cover condition, and terminal velocity of the drop. More recently, Carter et al., (1974) reported energy produced by raindrop impact is also a function of air temperature, season of the year, and storm duration. The potential rate of soil detachment by raindrop impact is assumed as a power function of rainfall intensity as given by Meyer (1971a) or

$$D_r = a_5 I^{b_5} \left(1 - \frac{Z_w}{Z_m}\right)(1-C_g)(1-C_c) \tag{10-36}$$

in which I is the rainfall intensity, a_5 is a parameter depending on soil characteristics and b_5 is a constant ($b_5 \cong 2.0$, see Meyer, 1971). The term Z_w is the depth of water plus the loose soil depth. The term Z_m is the depth of water plus the loose soil depth. The term Z_m is the maximum penetration depth of raindrop splash. According to Mutchler

and Young (1975), Z_m can be equal to three times the median raindrop size. The median raindrop size is often expressed as a power function of rainfall intensity. Therefore, Z_m can be written as

$$Z_m = 3(2.231^{0.182}) \tag{10-37}$$

in which Z_m is in millimeters.

Equation 10-36 is valid when Z_w is less than Z_m. When the depth of loose soils plus the water depth is greater than Z_m, D_r is zero, or

$$D_r = 0, \text{ if } Z_w > Z_m \tag{10-38}$$

If the tree branches are high, the drops from leaves can regain terminal velocity and erosive potential. However, the ground cover under trees us usually extensive which protects the surface. The canopy cover density, C_g, in Equation 10-36 should be that portion which effectively protects the soil surface from raindrop impact.

The potential rate of loose soil detachment, D_r, is expressed in units of depth per unit time. Thus, the amount of loose soil available for transport from rain drop splash is

$$Z_i = F_i \, D_r \, \Delta t \tag{10-39}$$

where Z_i is the depth of loose soil available and F_i is the original percentage of sediment size in a given size fraction i.

The percentage in each size fraction on the surface changes over time due to armoring or lagging of the non-eroded sizes. Water transports the smaller sediment sizes more easily and leaves the larger size fractions behind. Thus, the percentages of surface material need adjustment each time step. If the total loose soil depth is greater than D_a (the thickness of the armor layer), the adjusted percentages, F_{ai} can be written as

$$F_{ai} = \frac{Z_i}{Z} \tag{10-40}$$

If the total loose soil depth Z is less than D_a, then the adjusted percentages must account for the layer of undisturbed soil which is distributed according to the original percentages plus the loose soil which covers it or as

$$F_{ai} = \frac{1}{D_a} [Z_i + F_i \, (D_a - Z)] \tag{10-41}$$

The thickness of the armor layer can be determined as the maximum size of particles in motion. It is usually assumed that D_{84} (the size of sediment for which 84 percent of the sample is finer by weight) is the representative size of the armor layer.

Soil Detachment by Surface Runoff

The amount of soil detached by surface runoff is determined by comparing the total sediment transport capacity to the total available amount of loose soil. The total sediment transport capacity is

$$G_c = \sum_{i=1}^{N} G_{ci} \tag{10-42}$$

By substituting the total sediment transport capacity G_c into the transport rate in Equation 10-8, the total potential change in loose soil can be determined as

$$\Delta Z^p = \frac{\partial Z}{\partial t} \Delta t \tag{10-43}$$

where ΔZ^p is change in loose soil.

If $\Delta Z^p \geq -Z$, the loose soil storage is enough for transport and no detachment of soil by surface runoff is expected. Soil is detached if $\Delta Z_p \leq -Z$ and the amount of detachment is

$$D = D_f[\Delta Z^p + Z] \tag{10-44}$$

in which D is the total amount of runoff detached soil and D_f is defined as a detachment coefficient runoff with values ranging from 0.0 to 1.0 depending on soil erodibility. As an example, if the flow were over a nonerodible surface, the value for D_f would be zero. In a river where the riverbed is always loose, D_f would be unity.

The new amount of loose soil should be further modified as

$$Z_{Ti} = Z_i + D\ F_i \tag{10-45}$$

in which Z_{Ti} is the total amount for size fraction i.

Numerical Procedure for Sediment Routing

The following numerical procedure for sediment routing is used to couple the equations governing sediment motion with the water routing procedure in Chapter 7.

The sediment transport capacity is determined by Equation 10-35 for a given sediment size for the flow conditions obtained by water routing. The potential sediment load concentration for a given sediment size i is then

$$C_i^p = \frac{G_{ci}}{Q} \tag{10-46}$$

Using the same finite difference approximation as that in the water routing procedure (see Chapter 7) the potential change in loose soil storage for a given sediment size is determined by utilizing Equations 10-10 and 10-46. That is

$$\Delta z_i^p = \frac{1}{(1-\lambda)p} \{\theta[G_{si_j}^{n+1} - C_i^p Q_{j+1}^{n+1})(1-a) + (G_{s_i}^n - G_{si_j}^n)a]$$

$$- [(C_i^p A_{j+1}^{n+1} - C_{i_{j+1}}^n A_{j+1}^n)(1-b) + (C_{i_j}^{n+1} A_j^{n+1} - C_{i_j}^n A_j^n)b]$$

$$+ \frac{\Delta t}{2} [(1-b)g_{si_{j+1}}^{n+1} + bg_{si_j}^{n+1} + (1-b)g_{si_{j+1}}^n + bg_{si_j}^n]\} \tag{10-47}$$

The sediment transport rate is dependent on both the available supply of sediment and the transporting capacity of the flow. If $\Delta Z_i^p \geq -Z_i$, the availability is greater than the transporting capacity. Consequently, the bed-material load transport rate is equal to its transporting capacity or

$$C_{i_{j+i}}^{n+1} = C_i^p \tag{10-48}$$

and the actual change in Z_i is

$$\Delta Z_i = \Delta Z_i^p \tag{10-49}$$

If $\Delta Z_i^p < -Z_i$, the availability of material is less than the transporting capacity. The transport rate is limited by the availability of loose soil and the bed material concentration is therefore,

$$C_{i_{j+1}}^{n+1} = \{(1-\lambda)pZ_i + \frac{\Delta t}{2}[(1-b)g_{si_{j+1}}^{n+1} + bg_{si_j}^{n+1}$$

$$+ (1-b)g_{si_{j+1}}^{n} + bg_{si_j}^{n}] + \theta[gsi_j^{n+1}(1-a)-(G_{si_{j+1}}^{n} - G_{si_j}^{n})a]$$

$$+ C_{i_{j+1}}^{n} A_{j+1}^{n}(1-b)-(C_{i_j}^{n+1}A_j^{n+1}-C_{i_j}^{n}A_j^{n})b\} /.[A_{j+1}^{n+1}(1-b)+\theta Q_{j+1}^{n+1}(1-a)] \quad (10\text{-}50)$$

and

$$\Delta Z_i = Z_i \quad (10\text{-}51)$$

The sediment transport rate G_{si} is determined by

$$G_{si_{j+1}}^{n+1} = C_{i_{j+1}}^{n+1} Q_{j+1}^{n+1} \quad (10\text{-}52)$$

and the amount of loose soil available at the next time increment is

$$Z_{i_{k+1}} = Z_{i_k} + \Delta Z_i \quad (10\text{-}53)$$

where k designates the time period. If the finite difference scheme weighting factors a and b are zero the above sediment routing scheme becomes identical to that reported by Simons et al., (1975). The main concept for determining the actual sediment transport rate follows the paper by Shen (1971) and is depicted in Figure 10.5. This figure indicates that the actual sediment transport rate for a particle size is determined by the smaller of the following two quantities: transporting capacity or the availability considering all sources of supply. Usually, the transport rates of smaller particle size are controlled by the supply and the transport rates for the coarser particles are dictated by their transporting capacities.

The above equations indicate the key physical processes that must be considered in sediment routing and yield. If the models are simplified or altered in any manner the general physical processes remain the same except that minor adjustments are made to account for the simplifying assumptions or other alterations. The following sections briefly describe various sediment routing and yield physical process models. Similarities and differences for each model type are presented along with limited examples.

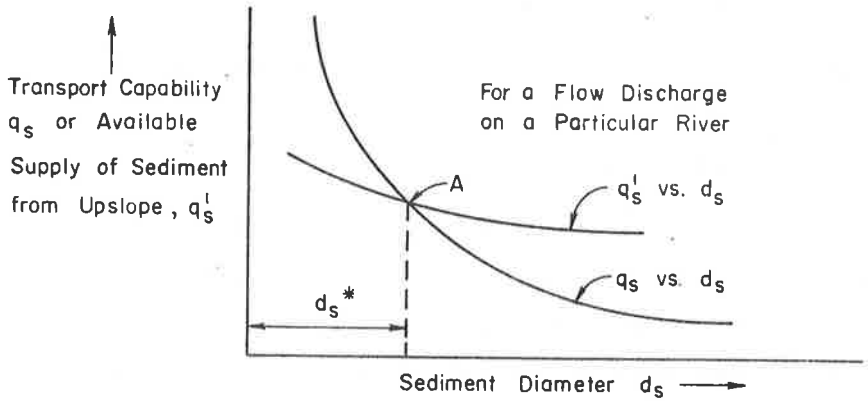

Figure 10.5 Concept of controlling sediment transport rates (after Shen, 1971).

10.4 COMPLEX WATERSHED AND ON-SITE SOIL EROSION MODELS

General

These models utilize the finite difference approach for water (Chapter 7) and sediment (Section 10.3) for simulating sediment yield from land surfaces. The watershed model uses input from a segmented watershed to route sediment over a cascade-of-planes set of land surfaces into channel units. The sediment is then routed through the channel loop to the watershed outlet. Sediment continuity and aggradation-degradation on the land surfaces and in the channel is employed. The on-site erosion model uses the same basic equations except it only considers sediment yield from the land surface. Therefore, it can be considered as a part of the larger watershed model. In the complex on-site model (complex referring to formulation and treatment of watershed geometry) the land surface can be subdivided into segments of homogeneous slope. Water and sediment is routed from segment to segment as in the watershed model then to an outlet or final downslope point. This model is easier to use for smaller areas that require a detailed investigation than is the entire watershed model. Both models are most useful in determining sediment yields from complex watersheds or land surfaces. The following presents some applications of these complex models.

Complex Watershed Sediment Yield Model

Beaver Creek Watersheds, Arizona

Simons et al. (1975) have tested the applicability of the complex watershed model (WASED) on the Beaver Creek Watershed, Arizona. Five runoff events in experimental Watershed 1 and one runoff event in experimental Watershed 17 were used.

Watershed 1 is a small drainage catchment with an area of 313.6 acres which has been cleared of trees. The five storm events modeled for Watershed 1 occurred on November 22, 1965, November 24, 1965, November 25, 1965, September 6, 1967, and September 5, 1970. The latter is known as the "Labor Day" storm which is one of the largest on record. Watershed 17 has an area of 287.4 acres. The only storm available for testing is the "Labor Day" storm.

A comparison between model simulated and measured water hydrographs is shown in Chapter 7. The agreement between the measured and the

simulated water hydrographs was satisfactory. Because there was no measured sediment hydrograph, no comparison could be made. Comparisons of simulated and measured sediment yields are given in Figure 10.6. This figure shows that the water and sediment routing model simulated the sediment yield from Watershed 1 and Watershed 17 within approximately 30 percent. Satisfactory results were obtained for different size storms and in different watersheds by using only one set of model parameters. This verifies that the model could be used to synthesize missing data and to predict the response of watersheds to various types of watershed management practices. The model could be used to estimate flood flows and corresponding sediment yields from ungaged watersheds.

The transferability of the physical process model is one of its main advantages over conventional methods such as the Unit Hydrograph and Universal Soil Loss Equation. The "Labor Day" storm produced approximately 2.2 times more surface runoff in Watershed 17 than in Watershed 1, but only about 0.4 times more yield of sediment. There was more surface runoff and less sediment yield in Watershed 17 because it is longer and narrower and its average slope is less than in Watershed 1.

The computed sediment hydrographs for the large "Labor Day" storm and for a small storm (November 22, 1965) on Watershed 1 are given in Figures 10.7 and 10.8. The shapes of sediment and water hydrographs are similar for the large storm but different for the small storm. For the small storm tested, the peak of the sediment hydrograph occurs earlier than that of the water hydrograph because the sediment supply rate is greater in the early stage of surface runoff. This effect is not significant for a larger storm.

An important task of watershed management is to predict results of selected treatment effects. Vegetation treatment effects on sediment yields are estimated by changing the canopy cover density and the ground cover density of overland flow units. The effects of vegetation treatment on the water and sediment yields from Watershed 1 were evaluated based on the storms of September 5, 1970 and September 6, 1967. As shown in Figure 10.9 for a constant and undisturbed ground cover of 65 percent, sediment yield and the peak flow rates and timing from these two storms are increased as the canopy cover density is decreased.

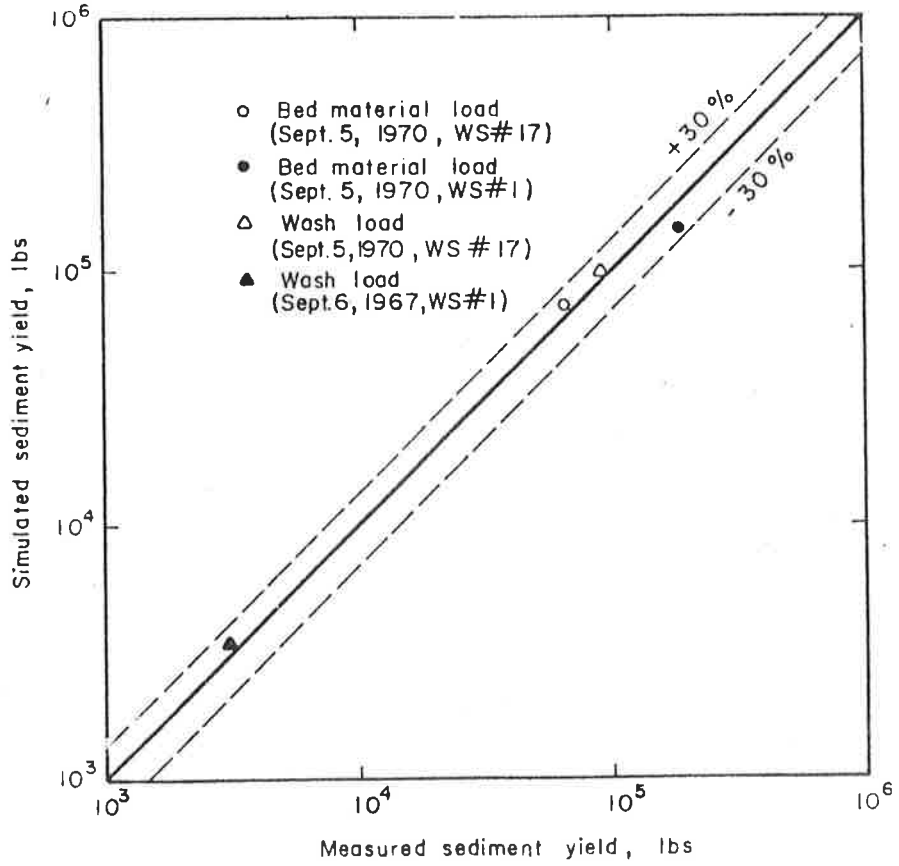

Figure 10.6 Comparison of measured and simulated sediment yields (after Simons et al., 1975).

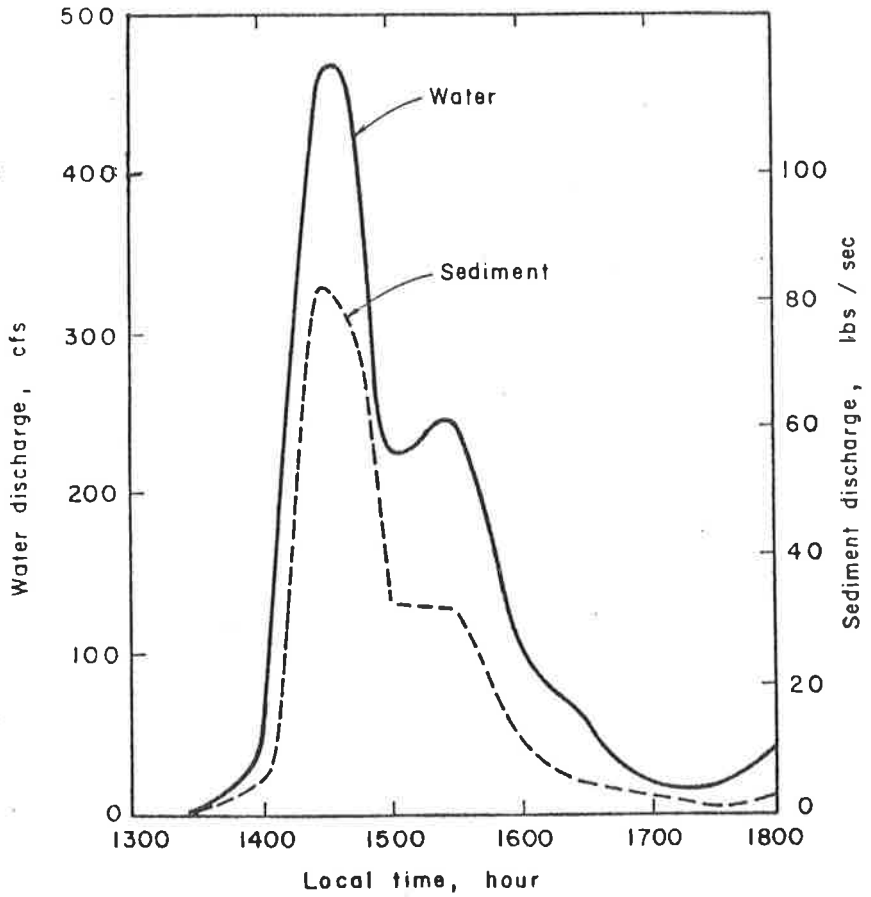

Figure 10.7 Computed hydrographs for the September 5, 1970 storm on Watershed 1 (after Simons et al., 1975).

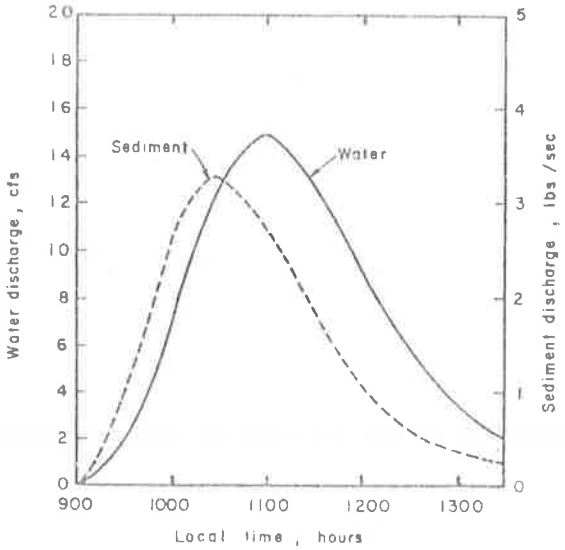

Figure 10.8 Computed hydrographs for the November 22, 1965 storm on Watershed 1 (after Simons et al., 1975).

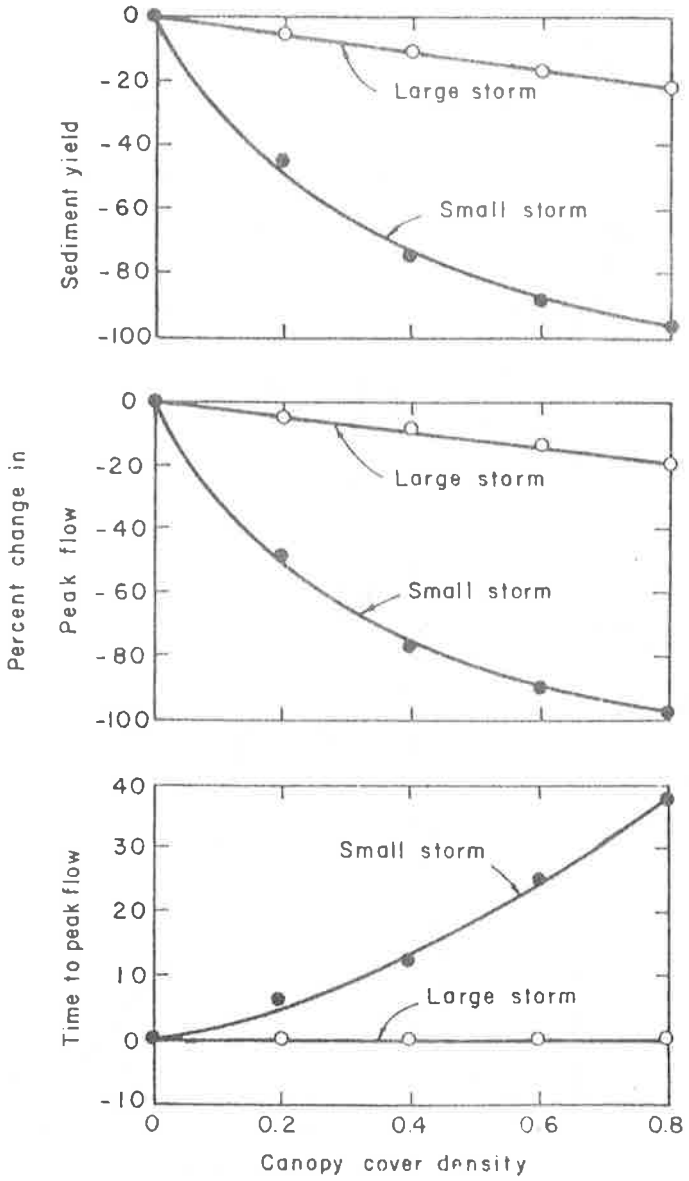

Figure 10.9 Effect of canopy cover density on the sediment hydrograph from Watershed 1 (after Simons et al., 1975).

The reduction in interception caused by removing the vegetation results in the increase of excess rainfall and raindrop soil detachment. These effects are much more pronounced in Watershed 1 for the smaller size of storm than for large storms like the Labor Day storm.

If a watershed is clear-cut and the forest litter, small brush, grass, and rocks are also removed to different degrees, or if the ground cover is seriously destroyed by a burning treatment, the associated response can be estimated by changing the ground cover density in overland flow units. Changes in sediment yields for Watershed 1 from the storms of September 5, 1970 and September 6, 1967 are shown in Figure 10.10. As the ground cover is decreased, the sediment yield and peak sediment flow are increased greatly and the time to peak flow shortened slightly. The effect on water yield is more pronounced for a smaller storm but nearly the same effects on sediment yield are obtained for both small and large storms.

Ground cover density is an important factor in controlling sediment yield. If a watershed is subjected to the clear-cut treatment, but there is a proper management of ground cover, the sediment yield may not be significantly increased.

Pine-Hardwood Watersheds, Oxford, Mississippi

The complex watershed model has been tested on three upland watersheds in Mississippi (Shiao, 1978). These watersheds are located near Oxford, Mississippi and are about three to five acres in size.
Section 10.6 presents more detail in one of the watersheds. The watersheds are administered by the U.S. Department of Agriculture, Forest Service, Forest Hydrology Laboratory in Oxford. Data collection is conducted in cooperation with the Yazoo-Tallahatchie Flood Prevention Project.

The residual soils of the watersheds are derived from Coastal Plain geologic materials. The upper slopes are covered with sandy-loam grading into subsurface sands. A weak fragipan underlies most of the upper slope. Moderate internal drainage exists on the upper slopes grading to well drained sands near midslope. Lower slopes and the south ridge consist of silt and clay loams. At depths of three to ten feet an impermeable fragipan layer exists causing perched water tables. The clay loams of the Wilcox series underlying this fragipan plus root channels create a complex subsurface flow system.

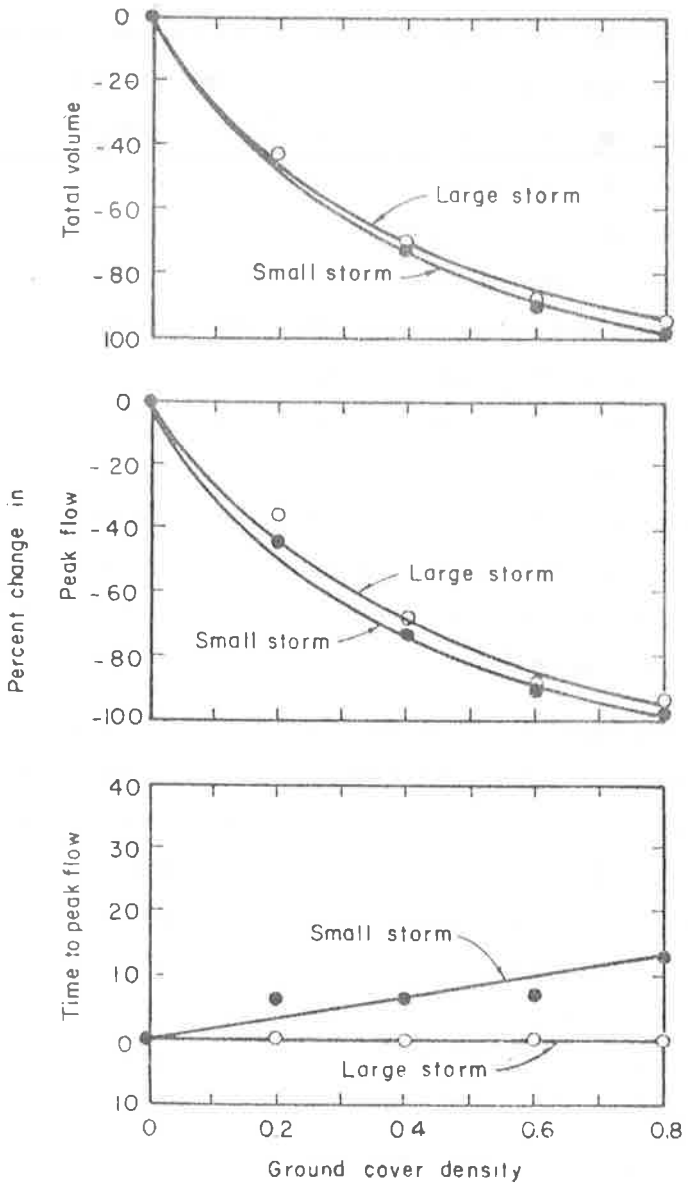

Figure 10.10 Effect of ground cover density on the sediment yield from Watershed 1 (after Simons et al., 1975).

Vegetation consists of 80 to 100 percent canopy cover of small to medium sized pines and hardwoods, and shrubs. It was estimated that most soil loss would come from channel, gully, and rill erosion and not from overland flow.

Five storms with volumes all over 2 inches were chosen for analyses, providing 15 watershed-event pairs. The simulated sediment yields are compared with the measured yields in Figure 10.11. As this figure indicates, most of the simulated yields are within $\pm$ 20 percent of the measured values. Shiao (1978) fitted a simple regression model of the form

$$E = a'(Q_p V)^{b'} \tag{10-54}$$

where E is sediment yield, Q_p is peak water discharge, V is water yield, and a' and b' are coefficients to demonstrate the differences between the physical process model and the regression model which is similar to that shown by Williams (1975) for the first term. Although the regression coefficient attained a correlation of 0.85, it still overpredicted sediment yield by 200 percent in one case while the most error of the simulation model was an 80 percent overprediction. This simple comparison further demonstrates the applicability of the physical process model over the regression model. Shiao (1978) also applied the model to agricultural watersheds.

Agricultural Watersheds near Watkinsville, Georgia

Four small experimental agricultural watersheds, designated as PI, PII, PIII and PIV, and located in the Southern Piedmont physiographic region (Figure 10.12) near Watkinsville, Georgia, were selected for this study. They range in size from about three up to seven acres. These watersheds were established in 1971 under a cooperative program between the Environmental Protection Agency and the Agriculture Research Service to study pesticide and nutrient transport. Data collected in these watersheds include rainfall, runoff, sediment discharge, pesticides, and nutrients.

Watersheds PI and PII utilize no conservation practice. However, a grassed waterway was established in Watershed PI in October 1974 but no tillage practices have occurred since then. Parallel terracing, commonly used in the Piedmont region, and the grassed waterway were used

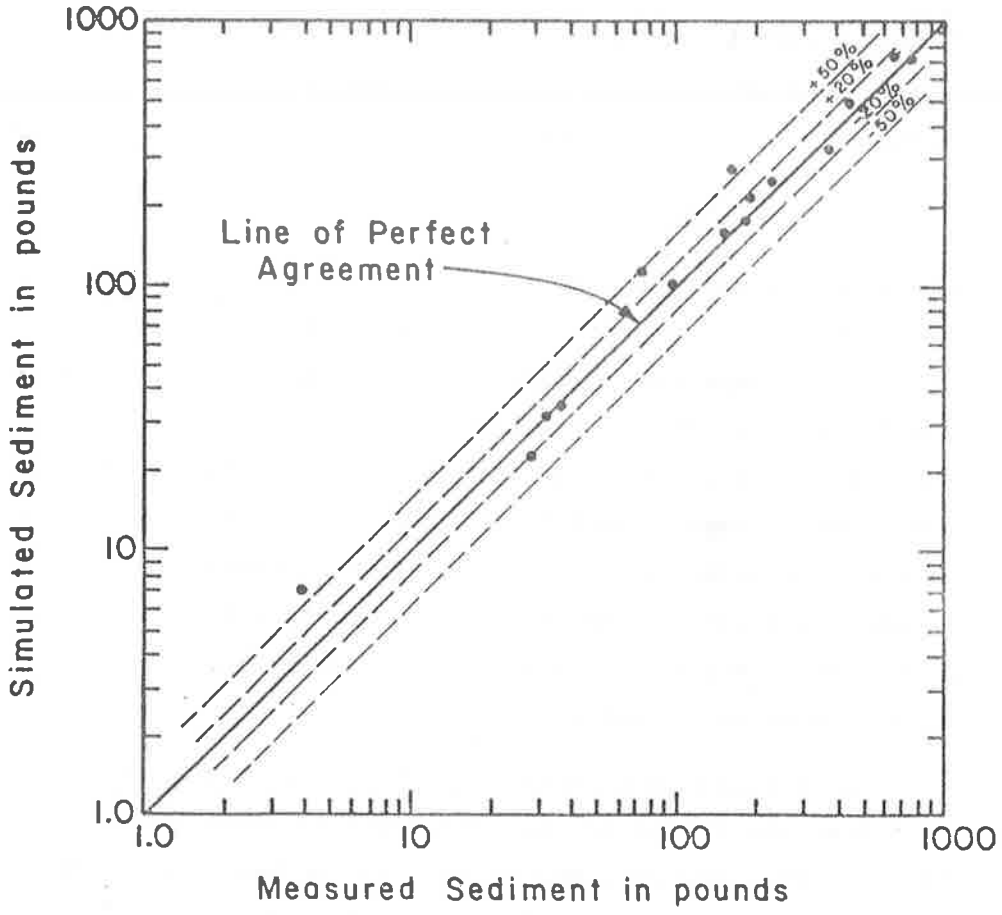

Figure 10.11 A comparison of the simulated and the measured sediment for watersheds at Oxford, Mississippi (from Shiao, 1978).

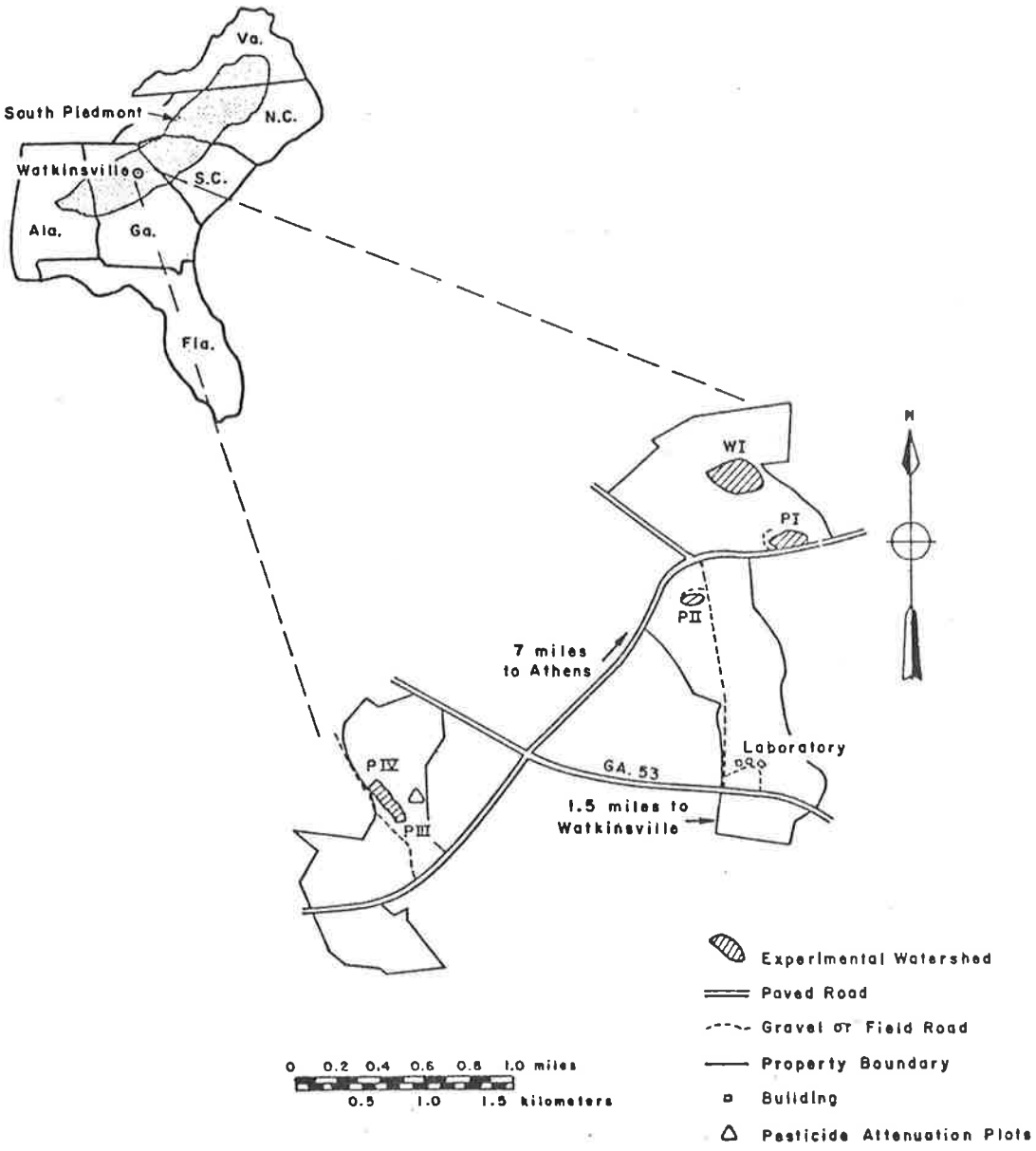

Figure 10.12 Location map for watersheds at Watkinsville, Georgia (from Shiao, 1978).

in Watersheds PIII and PIV to control soil erosion. All watersheds were row cropped with either soybeans, corn or grain sorghum. Winter rye and barley were planted in Watersheds PIII, PIV and PI to provide protective cover against winter storms. Because the data collection material is new, there was not complete information for all watersheds or for all times simultaneously. Eight storms were chosen for analyses, all from 1974. Of these eight, three storms have complete information at all four watersheds. A total of 22 watershed-storm pairs were simulated. Results, as shown in Figure 10.13, indicate that in most cases the model simulated within about ± 20 percent for sediment yield. Simulated yields beyond these ranges can partially be attributed to suspected but unconfirmed data errors. Comparison with a regression equation approach outlined in the previous example showed that the regression equation overpredicted in over half of the cases by 50 percent or more.

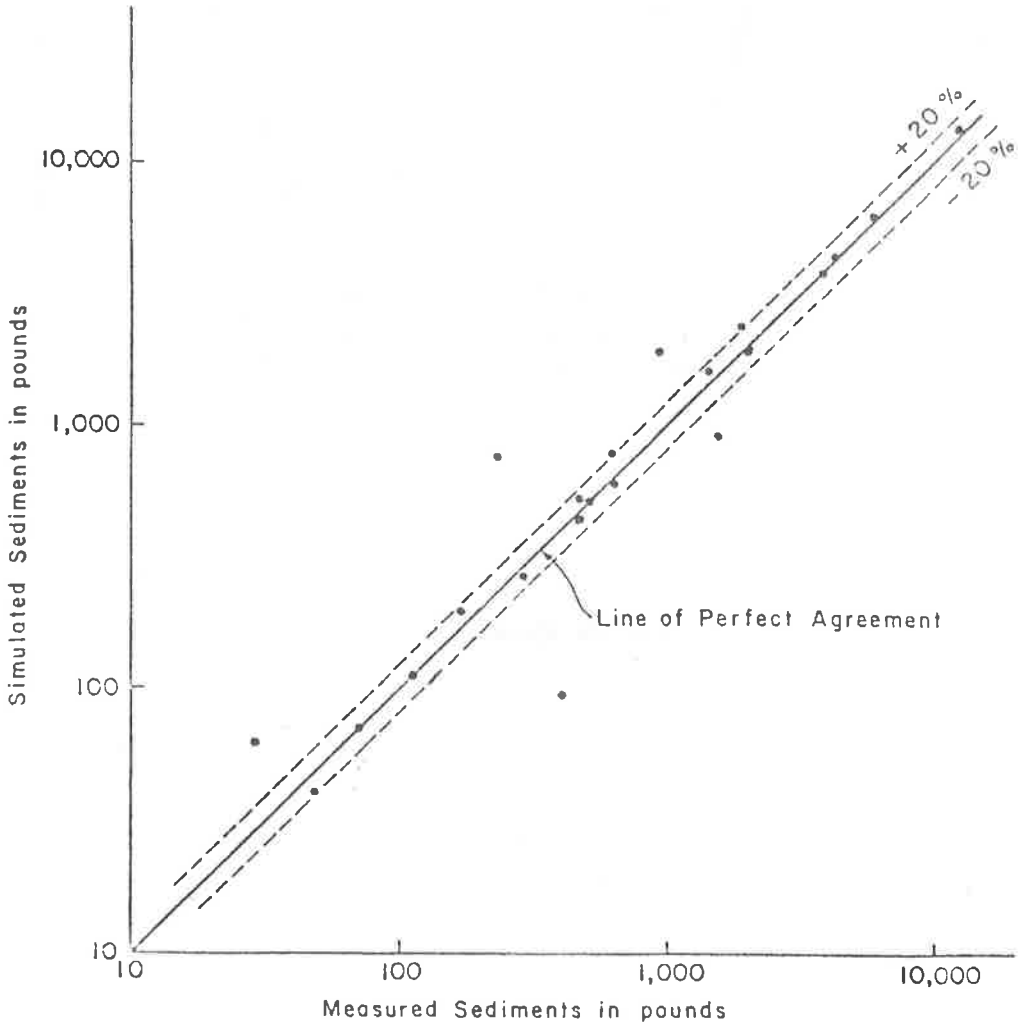

Figure 10.13 Comparison of the simulated and measured sediments for watersheds at Watkinsville, Georgia (from Shiao, 1978).

Complex On-Site Soil Erosion Model

Li et al. (1977c) applied the complex water and sediment routing scheme to evaluate on-site soil erosion for mine spoils on the Edna Mine in the Yampa Coal Field of Routt County, Colorado, Van Lieu (1976). Figure 10.14 shows good agreement of measured and computed water and sediment yields. The sediment hydrographs for run number 1 are plotted in Figure 10.15. Simulation results are acceptable considering the small measured discharge rates. Figure 10.16 gives the original sediment size distribution curve for the mine spoil plot. The size distribution curve of the transported material is shifted to the left showing an armoring effect because larger size fractions are not transported and thus the size distribution curve is expected to shift. The measured and simulated size distributions agree very well.

The second set of data tested was collected by Kilinc (1972). The data was from a hand placed soil plot of adjustable slope in an artificial rainfall facility at Colorado State University. Figure 10.17 is a comparison of observed and simulated sediment yields. Simulated results agree reasonably well except for those runs with the lowest rainfall intensity (1.25 in./hr). Errors at the lowest rainfall intensity may be due to a consistantly high percentage of the infiltrated volume

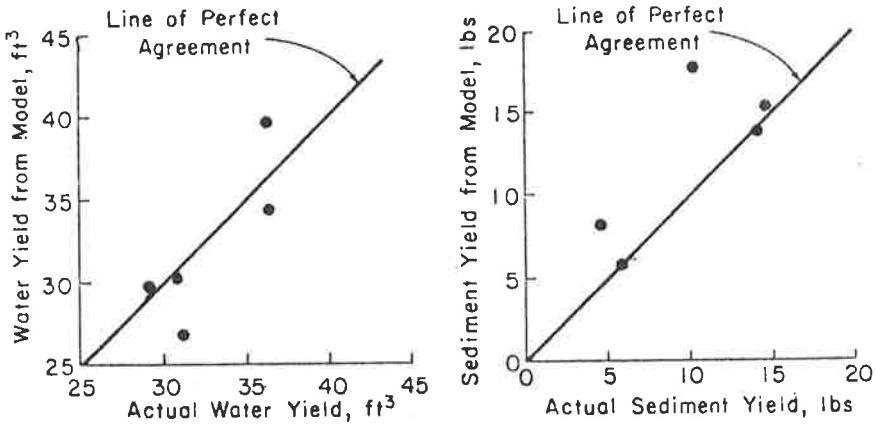

Figure 10.14 Comparison of measured and simulated water and sediment yields of Edna Mine soil plot.

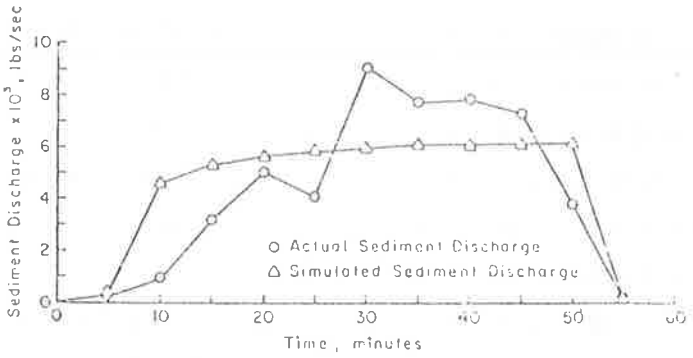

Figure 10.15 Comparison of measured and simulated sediment hydrographs for run number 1 of Edna Mine soil plot.

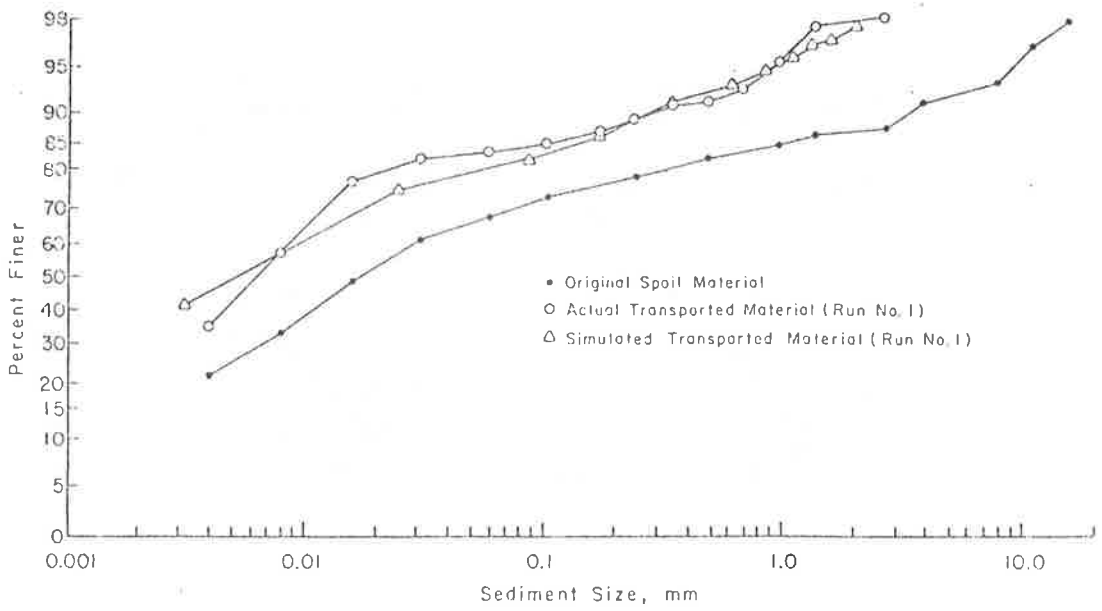

Figure 10.16 Comparison of sediment size distribution curves for run number 1 of Edna Mine soil plot.

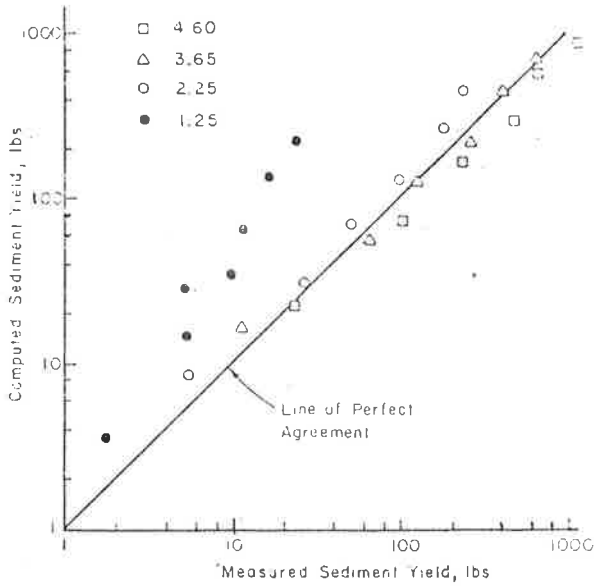

Figure 10.17 Comparison of observed and simulated sediment yields using Kilinc's data.

(21 percent to 40 percent of rainfall) in these runs. Relatively small errors in the infiltration prediction will result in a significant error in sediment estimation. Another source of error may be due to uneven slope profiles. Figure 10.18 is a comparison of measured and simulated sediment concentrations during a 60 minute rainfall duration. Rainfall intensity was 3.65 in./hr, and all slopes were used for comparison. The simulated results agree well with the measured data.

The numerical finite difference sediment routing and yield models are ideal for describing sediment movement in complex watersheds or over land surfaces. In some cases, however, such complete detail is not needed as simplifying assumptions about the geometry of the runoff surfaces can be made. These considerations have lead to simplification of the watershed geometry or the physical process formulations in order to provide easier to use but as accurate a methodology for estimating sediment yields. Both on-site and watershed models have been developed. These are described in the following sections.

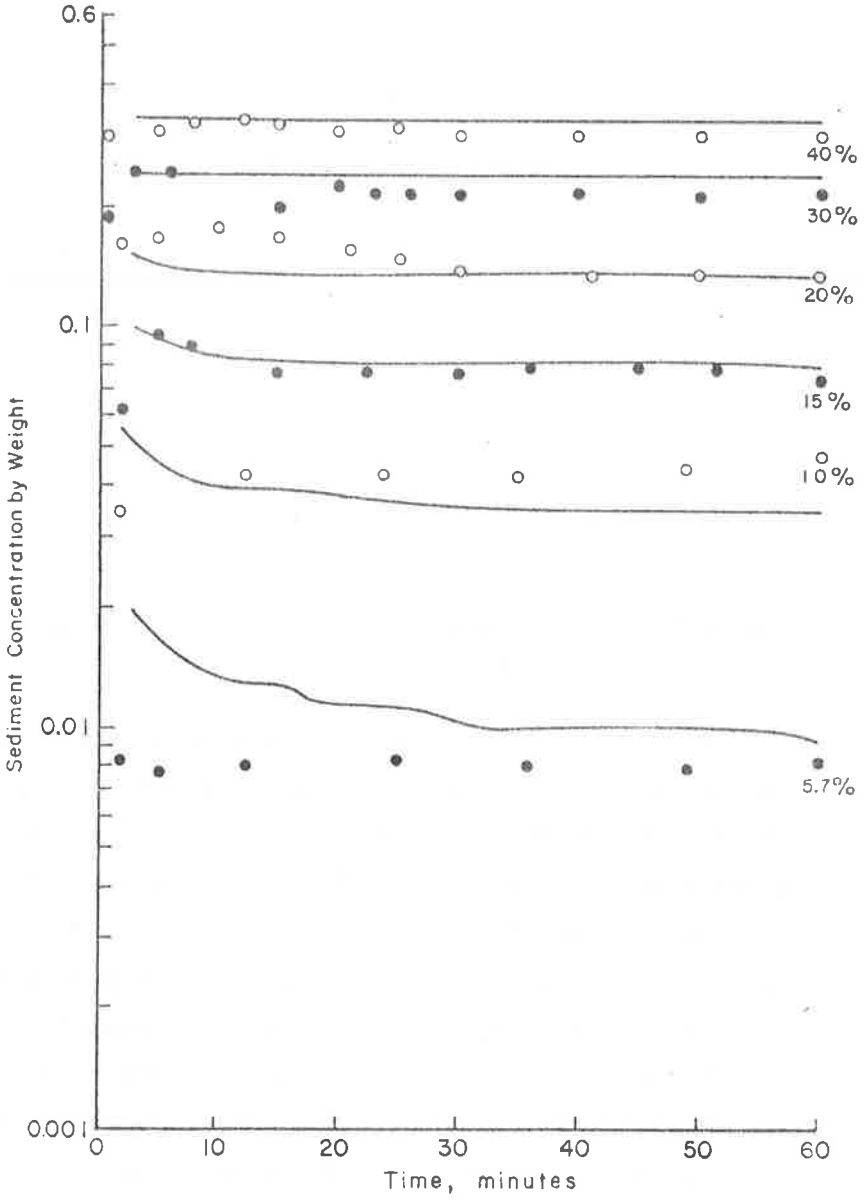

Figure 10.18 Comparison of measured and simulated sediment concentrations (kilinc's data, rainfall intensity = 3.65 in./hr).

10.5 SIMPLE METHOD FOR ESTIMATING ON-SITE SEDIMENT YIELD

General

A simplified model for estimating sediment yield was developed by Simons, Li and Ward (1977) to aid in assessing sediment yields from sites subject to erosion. This model (SIMSED) is most applicable to small planar areas such as roadways, mine spoils, or construction sites.

Simplifying assumptions in the model include surface geometry, rainfall input, raindrop detachment, and outflow hydrograph. Physical processes on the time and space are integrated for the assumed runoff period. Because the primary mover of sediment is water, this model, and the other models described in Chapter 10 incorporate hydrologic components in their formulations (see Chapter 7). Although not the focus of this section on on-site sediment yields, the hydrologic component is necessary to delineate some of the simplifying assumptions.

Basic Concepts and Equations

Erosion, water runoff, and sediment yield are common hydraulic and hydrologic phenomena governed by complex physical processes. Mathematical models can be constructed that accurately simulate these processes in time and space. However, such models are often as complex and difficult to understand and use as the process system they simulate. Model simplification can reduce complexity, and if simplification maintains the basic physical processes, the model may not lose significant accuracy. This is the basis for the simplified on-site water and sediment yield model. The following paragraphs describe the physical processes considered in the simplified model and how they are linked to provide a realistic representation of natural phenomena. These processes include interception losses, infiltration, water runoff, sediment runoff, and erosion by raindrop splash and overland flow.

Assumptions

In order to develop this simplified procedure, several assumptions are made: 1) the design storms can be represented by a constant intensity and duration, 2) flow reaches maximum discharge instantaneously, 3) sediment yield can be approximated by examining the overall sediment availability during the storm and the total sediment transport capacity for the whole runoff period, 4) the armoring effect of any water layer or

loose soil is negligible, and 5) the land surface is homogeneous and isotropic. Generally, these assumptions give an overestimation of sediment yields.

Interception Losses

A certain volume of rainfall is intercepted and stored by canopy and ground cover. In the simplified and complex on-site erosion models, the volume of rainfall intercepted by vegetation is estimated for both canopy and ground cover. The total intercepted volume as presented in Chapter 7 is:

$$V_i = C_c V_c + C_g V_g \qquad (10\text{-}55)$$

where V_i is the total intercepted volume in depth, C_c is the canopy cover density, V_c is the potential volume of canopy cover interception, C_g is the ground cover density, and V_g is the potential volume of ground cover interception.

The length of rainfall time needed to satisfy interception losses is determined by dividing V_i by the constant rainfall intensity i. This interception loss time is then subtracted from the total storm duration to give the length of time of effective rainfall or

$$D_e = D_t - V_i/i \qquad (10\text{-}56)$$

where D_e is the effective rainfall duration and D_t is the total storm duration. Although interception losses are continuous over the storm period, it is assumed that such losses occur at storm initiation Figure 10.19.

Infiltration Losses

The next rainfall losses considered are from soil infiltration processes. These processes determine the volume of water available for runoff from the land surface. The time to ponding or determination of the beginning of runoff and the volume of infiltrated water are the most important infiltration characteristics. Under a constant rainfall with steady soil parameters, the time of ponding can be found by (Mein and Larson, 1971)

$$t_p = \frac{\alpha}{i(\frac{i}{\beta} - 1)} \qquad (10\text{-}57)$$

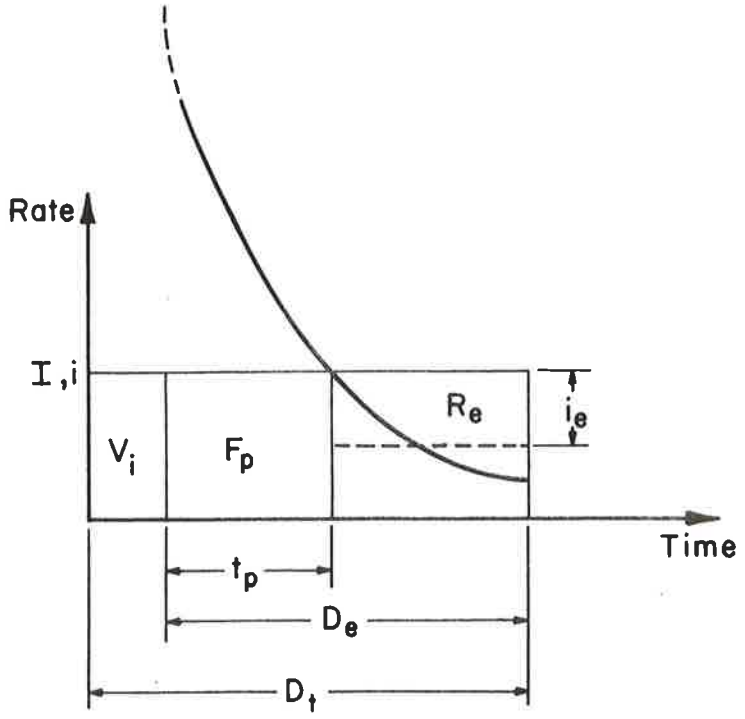

Figure 10.19 Definition sketch for hydrologic processes.

were t_p is the time to ponding since the beginning of effective rainfall, α is the soil parameter equal to $\phi(S_w - S_i)\Psi_{ave}$, ϕ is soil porosity, S_w is the degree of saturation in the wetted zone, S_i is the degree of saturation at the antecedent moisture condition, Ψ_{ave} is the average capillary suction pressure, and β is hydraulic conductivity in the wetted zone which is approximately one-half of the saturated hydraulic conductivity. If $i \leq \beta$, runoff will not occur. In the simplified model, the constant rainfall assumption allows the following infiltration formulation:

The volume of infiltration can be expressed as (Mein and Larson, 1971)

$$F - \alpha \ell n \left(1 + \frac{F}{\alpha}\right) = C_1 \tag{10-58}$$

with

$$C_1 = \beta(D_e - t_p) + F_p - \alpha \ell n \left(1 + \frac{F_p}{\alpha}\right) \tag{10-59}$$

and

$$F_p = it_p \tag{10-60}$$

where F is the accumulated infiltration and F_p is the accumulated infiltration prior to ponding.

Equation 10-58 is a nonlinear implicit equation, therefore, the approximate solution is (Li et al., 1976)

$$F_1 \simeq \frac{1}{2}[C_1 + \sqrt{C_1(C_1 + 8\alpha)}]$$

where F_1 is the first approximation of F. Because the error resulting from this approximation could range up to eight percent, unacceptable results may be obtained when the amount of rainfall excess is small. Another formulation can be utilized to yield a better approximation, i.e., (Li et al., 1976).

$$F_2 = \alpha\left[(1 + \frac{F_1}{\alpha}) \left(\frac{F_1}{\alpha}\right)^2 + 2\left[\frac{C_1}{\alpha} - \frac{F_1}{\alpha} + \ln\left(1 + \frac{F_1}{\alpha}\right)\right] \cdot \left(\frac{F_1}{\alpha}\right)^2\right] \quad (10\text{-}62)$$

which has an error consistently less than 0.003 percent.

Runoff Determination

Once the infiltration volume is determined, the average rainfall excess rate and the total runoff volume can be calculated.

The rainfall excess rate can be determined by

$$i_e = i - \frac{Re}{D_e - t_p} = i - \frac{F_2 - F_p}{D_e - tp} \quad (10\text{-}63)$$

where i_e is the rainfall excess rate.

The runoff rate q at the end of the overland flow plot is

$$q = \int_0^L i_e dx = i_e L \quad (10\text{-}64)$$

where L is the length of the plot

The total water yield volume is

$$Y_w = W \int_0^{D_e - t_p} dt = Wq(D_e - t_p) \quad (10\text{-}65)$$

where Y_w is the water yield in volume and W is the width of overland plot.

Sediment Transport Capacity

After the runoff rate q is known, the sediment transport capacity can be calculated. This is accomplished after completing several intermediate steps. First, overall flow resistance is computed by

$$K_g = K_\ell + (K_h - K_\ell)\ C_g^2 \qquad (10\text{-}66)$$

where K_g is the parameter describing the overall flow resistance associated with cover effects, K_ℓ is the parameter describing the minimum resistance for the area ($C_g = 0$), K_h is the parameter describing the maximum resistance for the area ($C_g = 1.0$), and C_g is the ground cover. An increase in C_g produces a rapid increase in K_g as shown in Figure 10.20.

Both q and K_g are used to find the average flow depth as

$$y = \left(\frac{qK_g v}{8gS}\right)^{1/3} \qquad (10\text{-}67)$$

where y is the flow depth, v is the kinematic viscosity of water, g is the acceleration of gravity, and S is the slope of the ground surface.

The mean flow velocity is

$$V = \frac{q}{y} \qquad (10\text{-}68)$$

The flow parameters calculated above are used to determine sediment transport capacity. The procedure for determining the sediment transport capacity given by Simons et al., (1975) is used in the model and has been previously described in Section 10.3. Important differences are that there is no accounting for aggradation-degradation and sediment discharge is computed based on the average discharge and not at each time step.

The sediment transport rate for a level of discharge q (discharge per unit width) can be determined by using the Meyer-Peter, Müller and Einstein procedures presented in Section 10.3. The transport rate by size fractions is

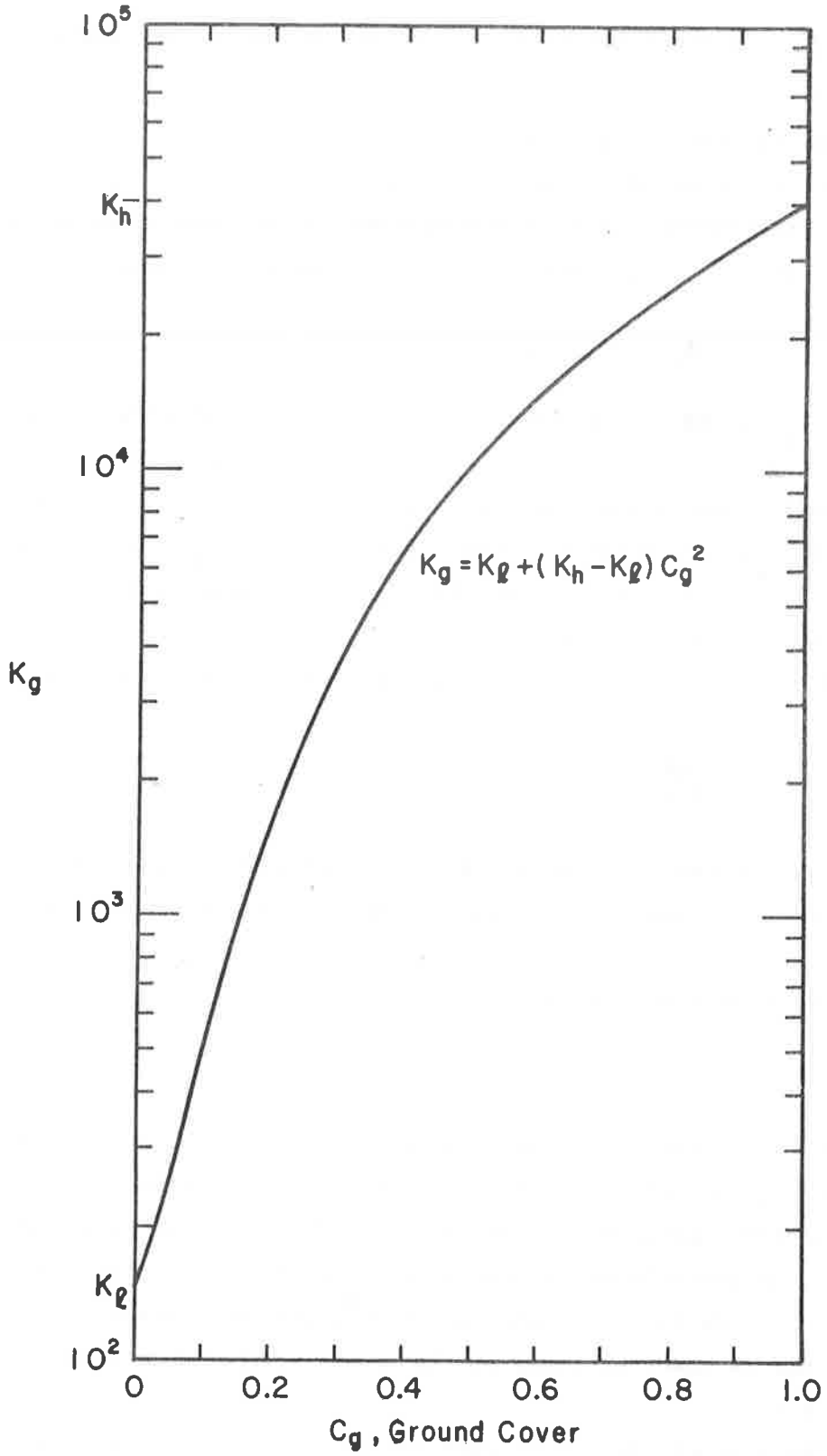

Figure 10.20 Assumed type of variation of overall resistance with ground cover change.

$$q_t = \sum_{i=1}^{N} q_{ti} F_i \qquad (10\text{-}69)$$

in which q_{ti} is determined by using Equation 10-34.

The potential transport capacity can then be found as

$$\Psi_t = \frac{W}{\gamma_s} \int_0^{D_e - t_p} q_t \, dt$$

or
$$\Psi_t = \frac{q_t (D_e - t_p) W}{\gamma_s} \qquad (10\text{-}70)$$

where Ψ_t is the nonporous volume of potential transport.

Determination of Sediment Supply

The potential sediment transport represents the capacity of the system. The supply of sediment comes from two mechanisms, detachment by raindrop splash and detachment by overland flow. The raindrop splash detachment can be formulated as

$$\Psi_r = D_r \, LW(1 - \lambda) \qquad (10\text{-}71)$$

where Ψ_r is the nonporous volume of detached material by raindrop splash. The value of D_r was determined in Equation 10-36. In the simplified model, however, the protecting effects of loose soil and water are neglected.

Sediment supply by overland flow detachment is determined

$$\Psi_f = D_f(\Psi_t - \Psi_r) \qquad (10\text{-}72)$$

where Ψ_f is detachment by overland flow, and D_f is the flow detachment coefficient which must be calibrated. The value of D_f is generally larger for this simplified model than the complicated simulation.

If $\Psi_t < \Psi_r$ then there is no overland flow detachment because the transport rate is limited by the transporting capacity. The total available sediment supply, Ψ_a, is then

$$\Psi_a = \Psi_r + \Psi_f \qquad (10\text{-}73)$$

Determination of Controlling Process

Sediment yield is controlled by either supply or transport capacity (see Figure 10.5). If supply is greater than capacity, capacity controls and vice versa. As particle size changes, so does the capacity and supply. Therefore, supply and capacity must be compared for each particle size. The individual capacity or potential yield is given as

$$\Psi_{ti} = \frac{q_{ti} F_i (D_t - t_p) W}{\gamma_s} \tag{10-74}$$

where Ψ_{ti} is the individual demand for the particle size. The available supply is

$$\Psi_{ai} = F_i \Psi_a \tag{10-75}$$

where Ψ_{ai} is the available supply for the ith particle size. Values of Ψ_{ti} and Ψ_{ai} can be compared. If Ψ_{ti} is greater than Ψ_{ai} then supply controls, if Ψ_{ai} is greater than Ψ_{ti} then capacity controls or

$$\Psi_{yi} = \Psi_{ai} \text{ if } \Psi_{ti} > \Psi_{ai} \tag{10-76}$$

$$\Psi_{yi} = \Psi_{ti} \text{ if } \Psi_{ti} < \Psi_{ai} \tag{10-77}$$

where Ψ_{yi} is the volume yield for the particle size fraction. The total yield will then be

$$Y_s = \gamma_s \sum_{i=1}^{N} \Psi_{yi} \tag{10-78}$$

where Y_s is the sediment yield by weight.

Model Linkage

By linking the different physical processes described above, a simplified yet accurate method for determining water and sediment yield from a selected site can be developed. The conceptual linkage used in the computer model is shown in Figure 10.21. Each process is divided from the others as a separate component that can be substituted or altered to represent the area studied.

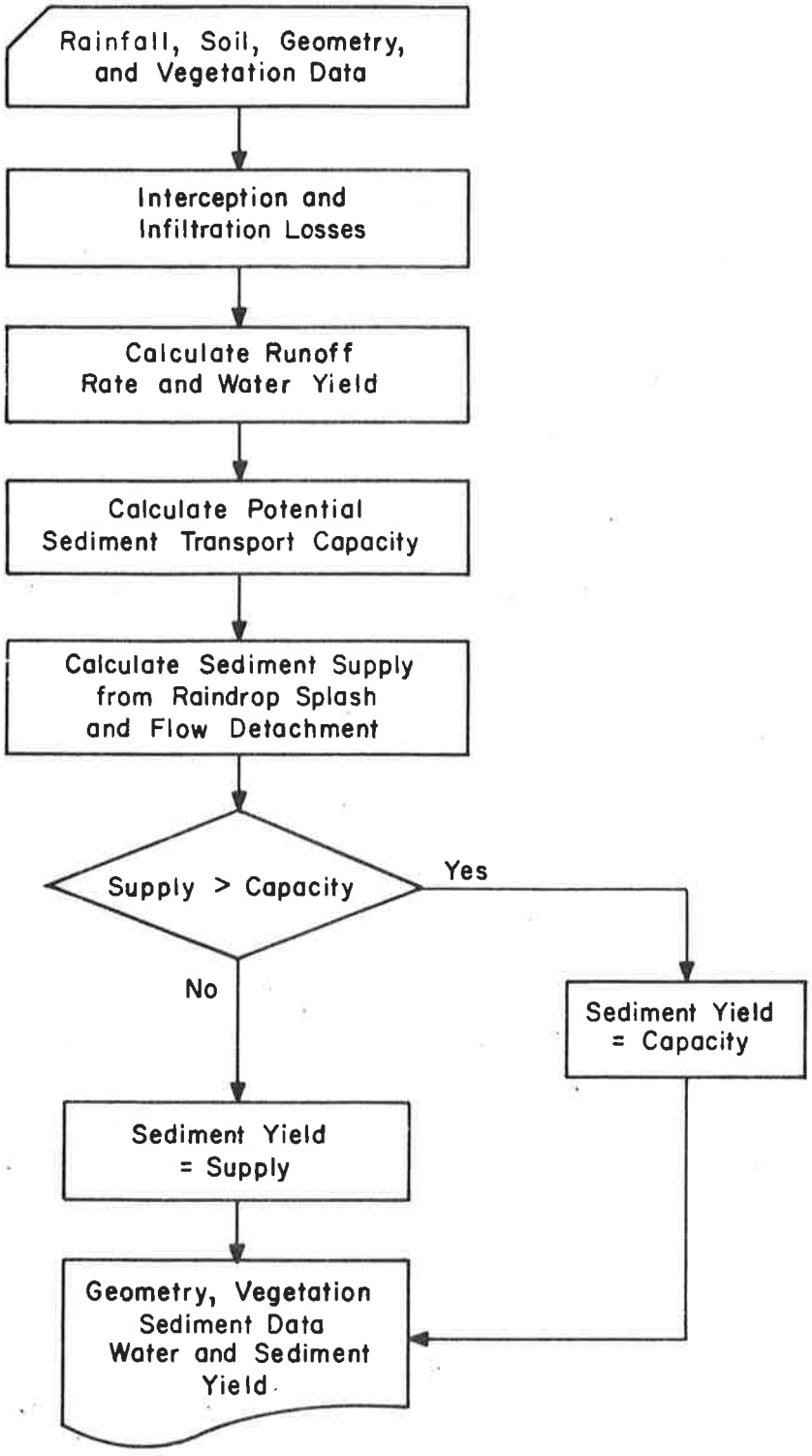

Figure 10.21 Flow chart of conceptual linkage of model components.

Comparison of Simplified and Complex Model Simulations

Simulations of sediment yields for the five runs using Van Liew's data (1976) that was introduced in Section 10.4 were generated by a complex on-site water and sediment routing model (Section 10.4) and the simplified model.

Comparison of the simplified and complex models is quite good (Figure 10.22). This is expected as the simplified model closely simulated the physical processes. Similar close comparisons were obtained by Simons and Li (1976) from simplified and complex model simulations for several hypothetical cases. These results further indicate the applicability of the simplified model.

The computer time required to simulate using the complex model is on the order of 10-15 times more than the simplified model. This time savings alone negates any improvement in accuracy obtained by the complex model for these simple cases. For larger or more complicated planes or watersheds and routing application, however, the complex simulation model is superior to the simplified model because of its time-space routing structure.

Use of Simplified On-Site Model

The use of the on-site model is restricted because of the simplifications involved in formulation. Primary limitations are that the rainfall is of constant intensity and that the hydrograph quickly reaches equilibrium or steady discharge. This second limitation requires that the plot or erosion site be relatively small or have a very short time of concentration. These restrictions are often met in designing or assessing roadway construction practices or mine spoil erosion. The simplified on-site model can provide realistic estimates of sediment and water yields from planar surfaces and indicate the necessity for more complex approaches.

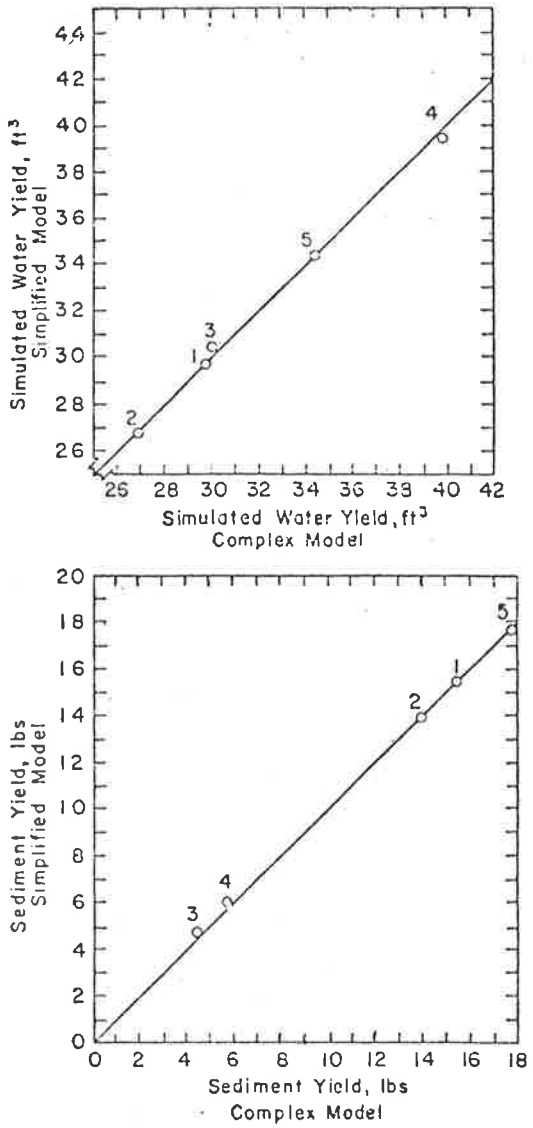

Figure 10.22 Simplified versus complex model simulations for on-site soil erosion.

10.6 SIMPLE SINGLE AND MULTIPLE WATERSHED SEDIMENT ROUTING AND YIELD MODELS

General

Combining the concepts of the simplified on-site sediment yield model and the analytical single and multiple water watershed models described in Chapter 7, has permitted development of a rapid method for estimating sediment yield from land and channel systems that are bigger and more complicated than what can be considered in the on-site model (Simons, Li, Shiao and Eggert, 1977; Simons, Li, and Spronk, 1978). These systems still can be described by a simple geometric representation (two planes, one channel) to avoid the cascade of planes land surface routing in the complex model.

Sediment yield is determined by comparing the transport capacity for a runoff increment with the supply for the increment from both raindrop detachment and overland flow. The method for estimating sediment transport capacity and supply is identical to the simplified on-site erosion model. In this model, however, there are several runoff increments that must be considered. Sediment yield for each size fraction during the increment is the smaller of available supply or transport capacity.

Channel sediment yield is calculated in a different fashion because of timing problems with the water routing technique used in the model. At each time increment the channel transport capacity at the outlet is computed. The total transport capacity for the runoff period is compared to the total sediment supply from lateral inflows and channel detachment. The smaller of the two is the yield. Again these yields are based on size fractions. A time incremented comparison of capacity and yield for the channel is not possible because lateral inflow time lags between inflow points and the channel outlet are not available. The major drawback to this model is that it cannot accurately keep track of sediment yield at incremental times in the channel, but can only consider the entire runoff period. However, if water and sediment are assumed to move in phase with one another, it is possible to redistribute the sediment yield by water volume in the time increment back into a synthetic sediment hydrograph. As indicated in Section 10.4 such an in-phase distribution may not be realistic for small storms but appears adequate for large storms. This redistribution is needed where multiple

watersheds and numerical channel routing are linked to permit correct time sequencing of sediment discharge.

For large watersheds or watersheds that are rather heterogeneous and cannot be truly represented by a homogeneous two-plane and one channel system, a mixed type model is required. The multiple watershed model solves the problem of big or heterogeneous watersheds by combining analytical and numerical routing techniques (Li, Simons, Fullerton, Eggert and Spronk, 1979). In this approach, sediment is supplied to the main channel from two plane-one channel tributary and subwatersheds, as previously described, and from single plane surfaces adjacent to the stream. Subwatershed and lateral sediment inputs are routed through the channel system using the numerical techniques employed in the more complex watershed models (see Sections 10.3 and 10.4). This approach is required to permit use of unsteady lateral and point source inflows.

For both the single watershed and the multiple watershed models are limited by certain assumptions in their formulations. These assumptions are (see Chapter 7):

1. Watersheds or subwatersheds may be represented by an "open book" approximation,
2. Soil characteristics are isotropic and homogeneous.
3. Canopy cover and ground cover are homogeneous.
4. Rainstorm events are spatially homogeneous and cover the entire plane or subwatershed unit.
5. Evaporation processes are neglected for a single runoff event.
6. Streams within the watershed are ephemeral and the movement of subsurface flow and groundwater flow are negligible.
7. The kinematic-wave approximation for flow routing is valid; i.e., the gradients due to local and convective accelerations are negligible and the water surface slope is nearly equal to the bed slope.
8. Water and sediment simulation is based on a single storm.

These assumptions are similar to those used in formulation of the other models described in this chapter and do not create insurmountable problems in simulation. Use of the simplified geometry watershed sediment yield models avoids considering complex topography and numerous computations for the cascade of planes but still retains its physical reality.

Model Applications

Single Two Plane-One Channel Watershed

Oxford, Mississippi Watershed. The two plane-one channel model (SEDWAT) was tested on a pine-hardwood watershed near Oxford, Mississippi (Simons, Li, Shiao and Eggert, 1977). The general characteristic of these pine-hardwood watersheds are described in Section 10.4. For this application, watershed III was selected as the test site. Drainage area of watershed III (PHIII) is 4.01 acres (Figure 10.23). Other geometric information is presented in Table 10.1.

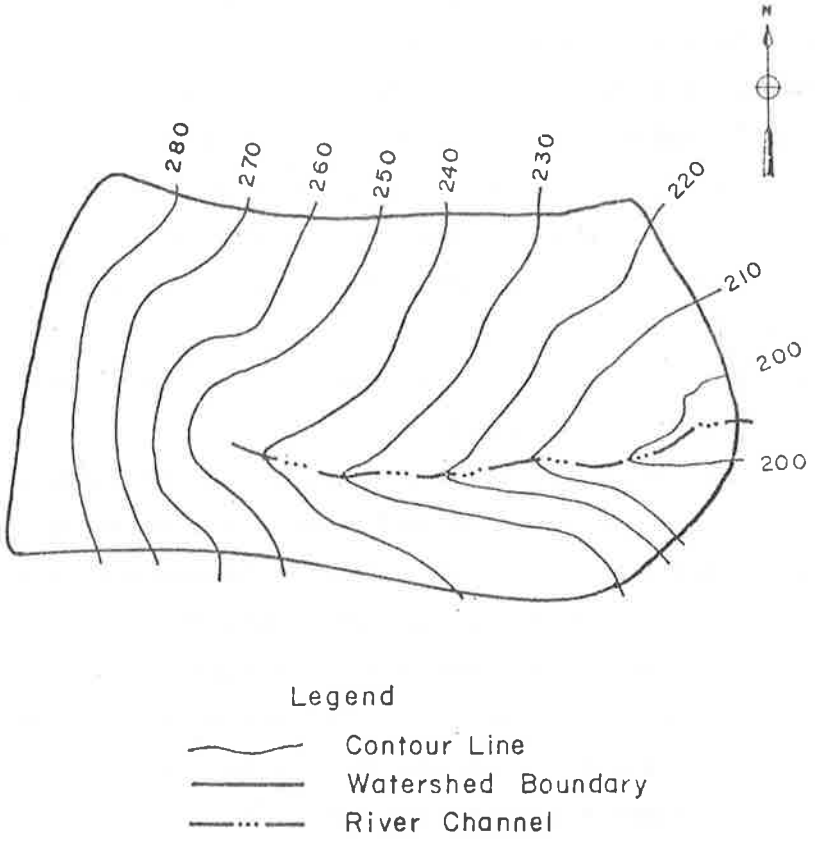

Figure 10.23 Topographic map of upland pine-hardwood watershed III.

Table 10.1 Geometric information for pine-hardwood watershed III.

Left Side:	length	= 275.5
	slope	= .172
Right Side:	length	= 142.2
	slope	= .205
Channel:	length	= 418.0
	slope	= .108

Area = 4.01 acres

Although 17 years of data exist from PHIII, data from only 11 storms was available at the time this analysis was completed. Of these 11 storms only 5 were considered for the study. These storms were: August 15, 1964; May 6, 1967; August 2, 1967; November 27, 1968, and April 1, 1970. All storms except August 1964, were also used in the testing of the complex model (Section 10.4). The April 1970 and the August 1964 storms were chosen for prediction and the rest were used for calibration purposes. The results of the simulations are presented in Figure 10.24 for the sediment yields. The April 1970 storm was underpredicted by about one percent and the August 1964 storm was over-predicted by about one percent. These results indicate the excellent simulation capabilities of this simplified geometry approach.

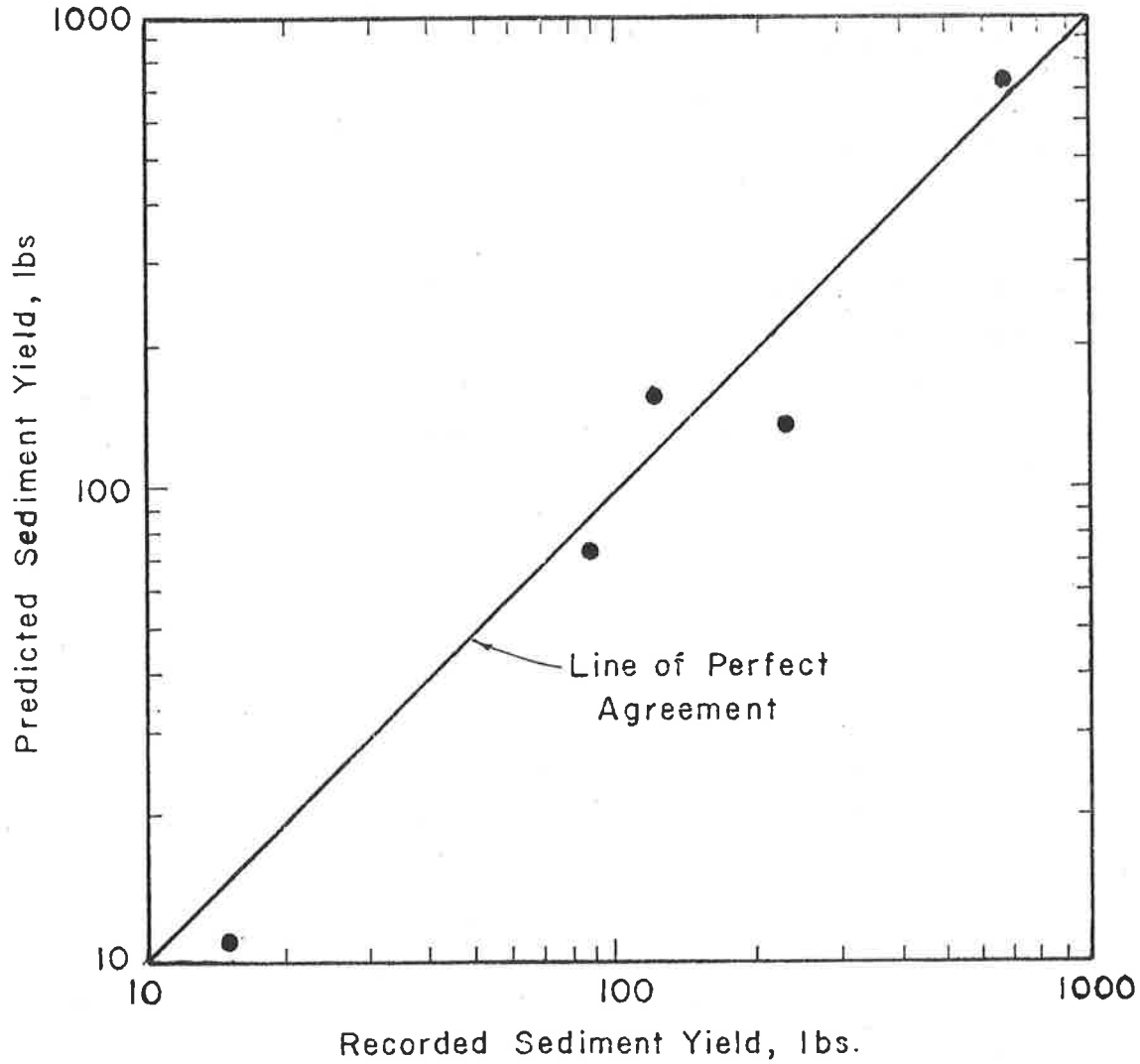

Figure 10.24 Comparison of recorded and predicted sediment yield for pine-hardwood watershed III.

Multiple Plane-Multiple Channel Simplified Model. Extension of the concepts of two plane-one channel watershed sediment yield modeling has lead to the development of a model that simulates a complex watershed consisting of simple subwatersheds linked by channels. Although the water routing and yield components of the model (MULTSED) have been applied to selected watersheds, the sediment portion has not been completely tested for a large watershed. Li et al. (1979) did, however, apply it to watersheds P-3 and P-4 near Watkinsville, Georgia. This area was previously described in Section 10.4.

Seven storms were modeled. Each watershed was subdivided into two one channel-two plane subwatersheds in order to test model linkage. The results of the simulations are shown in Figure 10.25 in comparison with recorded values . As this comparison indicates, the sediment yield model (MULTSED) is a promising approach for analyzing sediment yield from watersheds of complex geometry. Its use is particularly evident in terms of analyzing those watersheds that have heterogeneous properties or are just too difficult to model in a less simple form.

Use of simple watershed models is a needed step in order to reduce complexity of simulation approaches. These two models are a step in the right direction.

A key concept that was employed in this model application, and in others, is the change in hydraulic conductivity through changes in temperature (see Chapter 7). The hydraulic conductivity can be formulated as

$$K = \frac{kg}{\nu} \tag{10-79}$$

where K is the hydraulic conductivity, k is the intrinsic permeability, g is acceleration of gravity, and ν is the kinematic viscosity of water. Changes in temperature affect ν, lower temperatures increase ν and decrease K and increasing temperatures will decrease ν and increase K. The intrinsic permeability is a function of the soil particle size and packing so it can be affected by compaction. Changes in K from changes in temperature can be quite marked. For example, the reduction in viscosity from 40°F to 80°F is about 45 percent. This in turn increases the hydraulic conductivity by about 80 percent. Such a change has severe affects on infiltration, runoff and subsequent erosion and sediment yield. This small example shows the need for fully

evaluating the controlling water yield processes in order to correctly determine the sediment yield processes.

Another application of SEDWAT is presented in Chapter 19. In that example watershed response, water and sediment yields, to management activities will be discussed.

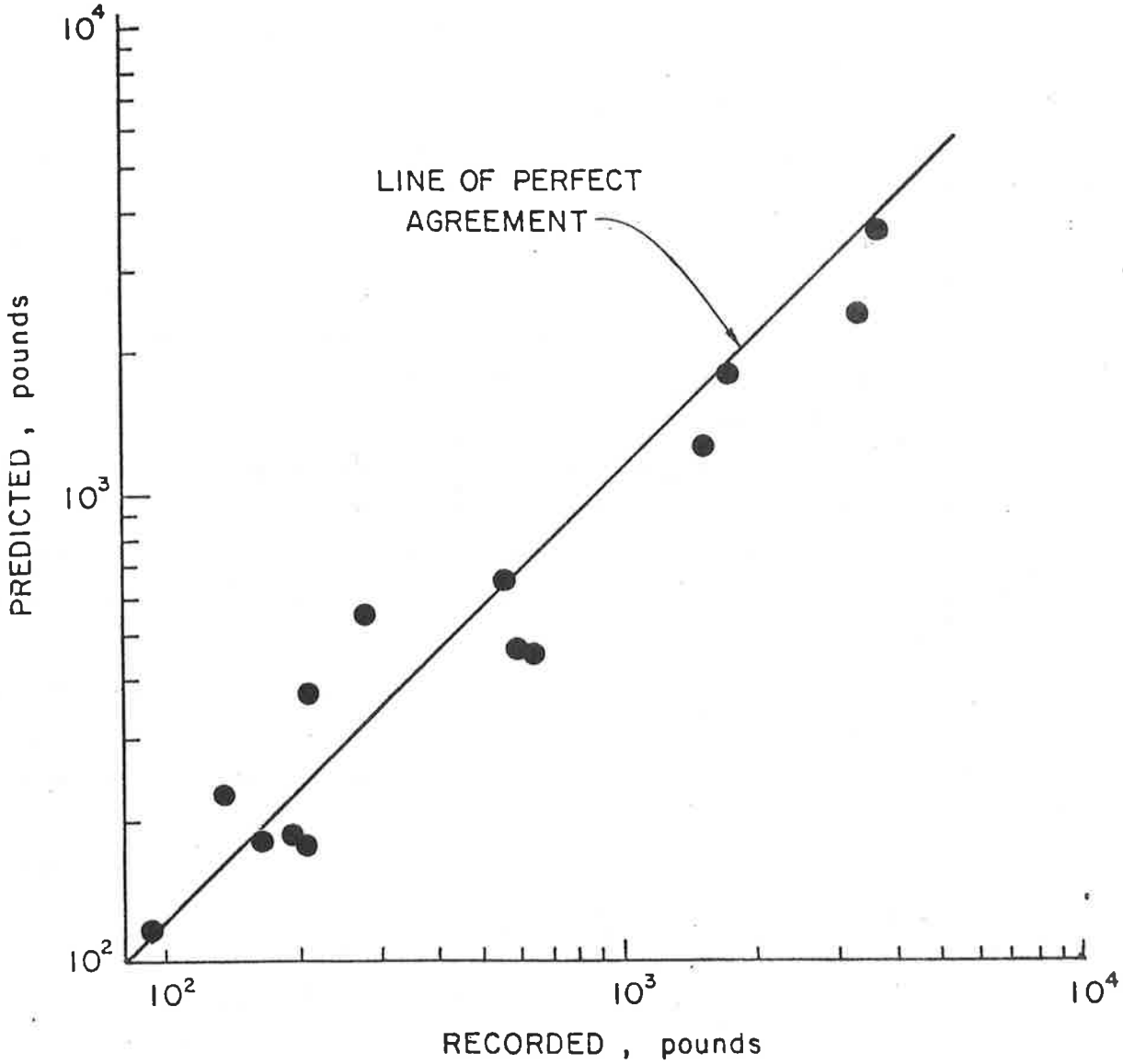

Figure 10.25 Comparison of simulated and recorded sediment yields for Watkinsville, Georgia watershed.

10.7 MANAGEMENT LEVEL PLANNING MODEL

Sometimes it is necessary to link two different models to produce the simulation characteristics that are desired for project objectives. One time would be linkage of models when hydrologic inputs for one portion are not compatible with another and cannot be shared, such as routing techniques used in MULTSED described above. A third would be when a generalized planning approach requiring accurate but low key methods are needed. Recently, such a model (LACP) has been developed for the Roosevelt-Arapahoe National Forest in Colorado. This model is intended for use as a planning level aid for estimating annual sediment yields from fourth order or smaller watersheds that are subjected to natural and man-induced changes in the system. The model is composed of four distinct submodels. In general one submodel is used to keep track of soil moisture for the rainfall season. Another uses the complex watershed model to route sediment from the land surface to the channel system. The channel model uses simple continuity to determine aggradation-degradation and sediment transport for each channel segment, and one small model interfaces data between the overland flow and channel models. The four basic components are connected through data file transfers (Figure 10.26). Table 10.2 lists the programs and data files shown in Figure 10.26.

Data preparation is a key task in watershed modeling. This includes digitization of the watershed segments that can be numerically processed by the computer. This task is conducted using program WASEG which was previously developed by Simons and Li (1975). The watershed is segmented into overland flow cells (40 acres in size for this application) and straight line channel reaches. Information on topography, soil type, and vegetation type at each node point in the watershed is processed to provide representative geometric, soils, and vegetative properties for the overland flow cells and the channels. Soil and vegetation information is further processed to provide a more complete input file to the different components of the planning model.

Program MOIST (MOISTure Balance) computes a simple monthly moisture balance based on incoming precipitation, runoff, infiltration, and evapotranspiration. Output from MOIST is used to provide antecedent soil moisture conditions to LNDSRF (LaND SuRFace) which computes sediment

Table 10.2 Programs and files for overall planning model.

I. Program Files	
MOIST	Simple moisture balance
LNDSRF	Land surface erosion and channel loading
SEDYIE	Reformats and reorganizes land surface erosion output
CHANL	Channel transport and aggradation and degradation
II. Data Files	
DATA18	Input for MOIST
DATA6	Output from MOIST, input for LNDSRF
DATA1, DATA2, DATA3, DATA4, DATA5, DATA7	input for LNDSRF
DLAT8, RESULT2, RESULT3	output from LNDSRF
DPAR1, DCOE2, DS4, DQ3, DCOMP5, DLAT6	input for CHANL
DVSDV7	output from CHANL

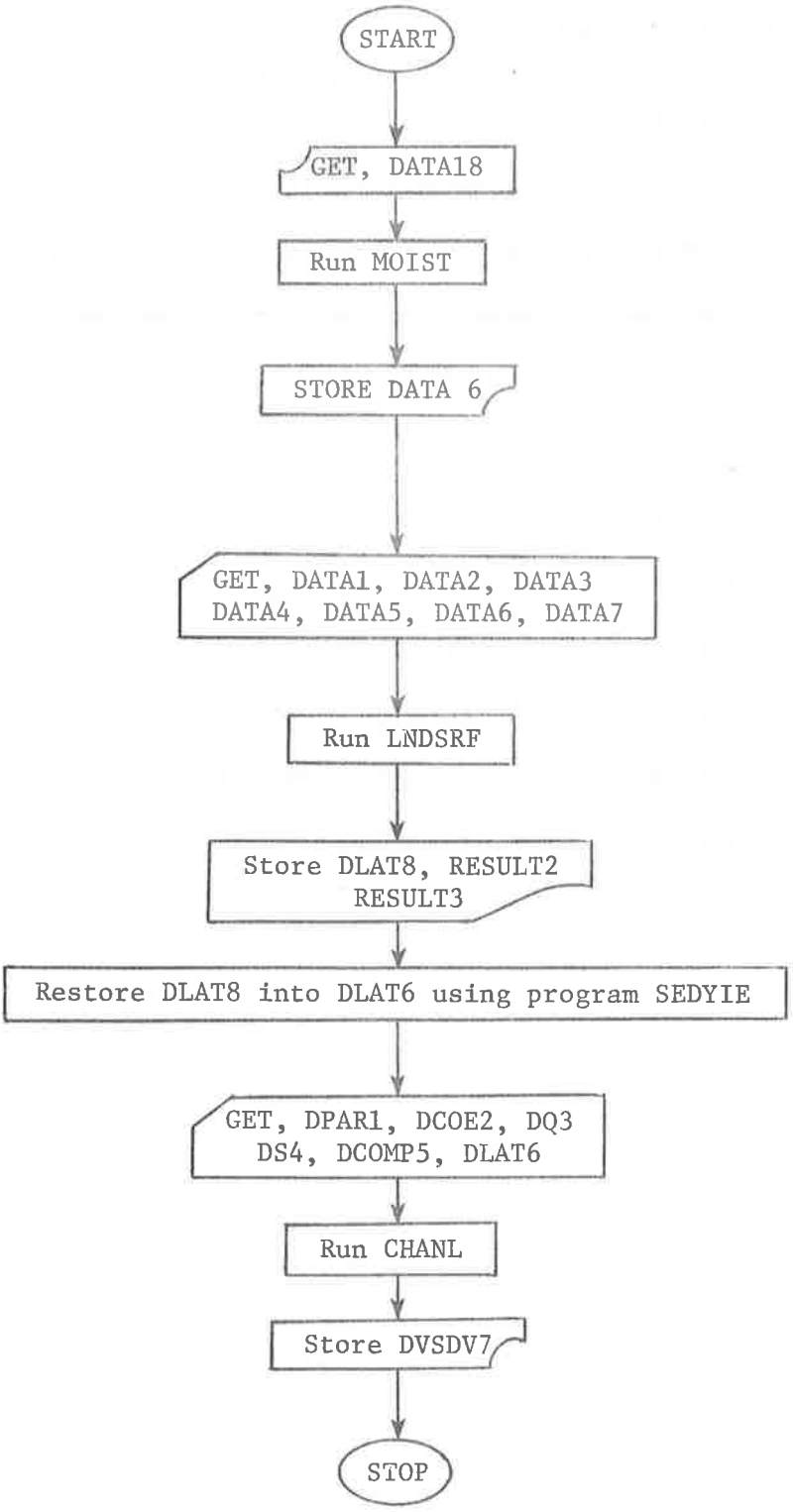

Figure 10.26 Flow chart for planning model.

yield during a rainfall season (approximately May to October) to the stream channel. The land surface erosion model considers processes of interception, infiltration, overland flow, sediment detachment from raindrop splash and overland flow, sediment transport, and vegetation and management effects on water and sediment yield. Only rainfall storms are considered to produce sediment supply to the stream channels. Elevation effects on rainfall volume and air temperature are considered. Water is routed over a cascade of planes or contributing overland flow cells established by program WASEG from topography and gravity flow logic. The simplified on-site soil erosion model developed by Simons, Li and Ward (1977) was modified to estimate the sediment yield from the planes contributing to the channel. Sediment and water yields to the channel are stored for further use. The sediment yields are classified by size fractions.

Information from LNDSRF is then processed and reformatted by program SEDYIE (SEDiment YIEld) for use in program CHANL (CHANneL). Program CHANL determines the transport from each channel segment considering streamflow, sediment supply from upstream channels and adjacent land surfaces, and aggradation and degradation in the channel segment. Streamflow hydrographs are provided by the user (not simulated in the model) at selected sites in the watershed. These hydrographs are reapportioned to the individual channel segments based on a contributing area proration of the flow so that each segment has an individual hydrograph. The hydrographs are six-day average discharge or 61 values per year. Starting at the furthest upstream channel, the model sums the sediment supply to the stream as provided by LNDSRF. Special provision is made in the model to consider inflows to these upstream channels from connected watersheds or diversions. This allows joining of several small areas together to produce a larger watershed. Transport capacity is computed using the water discharge, stream cross-sectional geometry at the outlet end of the channel segment, slope of the channel, and Meyer-Peter, Müller and Einstein procedures. Cross-sectional geometry, bed material distribution, flow resistance coefficients, and sediment transport parameters are based on channel-type classification. Use of channel-type classification is a new approach that will require more effort to adequately relate channel parameters to type. Channel type is used in this study as it applies to

Cabin Creek and is not substantiated at this time for use in other watersheds.

Sediment yield from the channel segment is a balance of transport capacity and sediment supply. Yield is determined by size fractions and involves sediment contributed from upstream channel supply, contributing overland flow supply, and supply from the channel segment. Supply from the channel segment examines that fraction available from the active portion of the channel and from the channel banks above some preselected flow depth. This depth coincides with a characteristic channel flow that may be represented by the bank-full discharge. The actual sediment yield is controlled by either the supply or the channel transport capacity, depending on the size of sediment. In general, fine sediment sizes are controlled by supply, whereas the layer size (usually bed material) is controlled by the transporting capacity (see Figure 10.5).

Once the necessary information has been supplied to the different input data files, the planning model can be run. The different files and component models are linked by control statements to provide efficient operation of the overall planning model. Sequencing of the models permits simplification of several models into a single operation package. Complete program listings and example best management practices applications to the Cabin Creek watershed will be presented in Chapter 19.

The model is intended for use as a management planning aid and not a research tool. This is evidenced by the simplifications and decoupling of the land surface and channel systems. However, the model can provide realistic responses to a number of land use practice scenarios. This will provide the forest planner with valuable information used to judge certain impacts.

10.8 COMPLEX AND SIMPLIFIED YIELD MODELING FOR ROADWAYS

General

Knowledge and experience in modeling watershed water and sediment yields have allowed application to watershed road systems. A road prism or cross section can be considered as a miniature watershed consisting of overland flow surfaces, (cut and fill slopes and road surfaces), ditches, and culverts. Such a system is amendable to complex and simplified modeling. In addition, because roadways present a significant design obstacle when sediment catch is involved, design aids are needed by the lay technicians not familiar with computer modeling. One method for collecting the needed information to develop design aids is through a site studies. Another way is through generation by the most applicable computer models.

Roads are subject to the same physical processes as other land surfaces, therefore, they respond much like other surfaces. Significant differences do occur because man has influenced development to ground cover, drainage systems, compaction, slope, and flow distance to a greater degree. However, each of these can be analyzed using the appropriate model. Only one minor difference between the road and watershed models exists for culvert flow. In the road models a generalized sediment transport equaion for conveyance systems is used (Graf and Acaroglu, 1968).

Models and Applications

Complex Model

Following the same procedures outlined for the complex models (Chapter 7 and Section 10.4) Simons, Li, and Shiao (1977) developed a model (ROSED) for estimating water and sediment yield for different road locations and at different times. The utility of the model was demonstrated by some hypothetical examples commonly found in forested roads. Roadway prism Types A, B, and C were considered as shown in Figure 20.27. Type A road prism has only overland flow units. Type B road prism has overland flow, ditch flow and culvert flow units, and Type C road prism is essentially the same as Type B, layout, except the flow direction of the road surface is different. Table 10.3 gives a summary of the geometry for the road prism. For simplicity, a uniform

Table 10.3 Dimensions of selected road prisms in Figure 10.27.

		Type A	Type B	Type C
Cut and Fill Slope	Length	100 ft	100 ft	100 ft
	Width	100 ft	100 ft	100 ft
	Slope	0.316 (3:1 horizontal to vertical)	0.316 (3:1 horizontal to vertical)	0.316 (3:1 horizontal to vertical)
Road Surface	Length	100 ft	100 ft	100 ft
	Width	40 ft	40 ft	40 ft
	Slope	0.10	0.10	0.10
Ditch	Side Slope	-	3.0	3.0
	Longitudinal Slope	-	0.15	0.15
	Length	-	100 ft	100 ft
Culvert	Diameter	-	3.0 ft	3.0 ft
	Slope	-	0.25	0.25
	Length	-	140 ft	140 ft

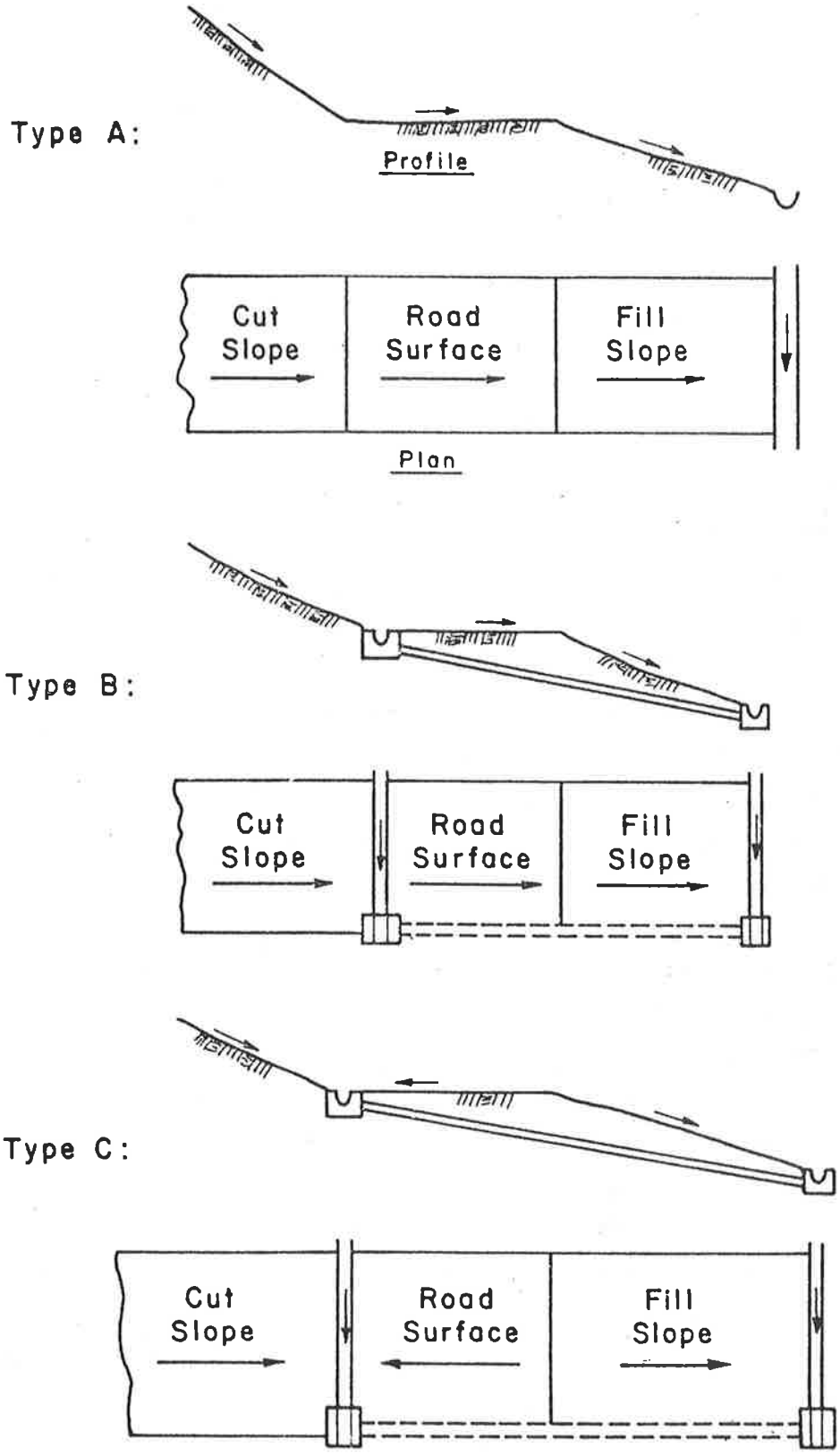

Figure 10.27 Typical road prism.

intensity rainstorm with the intensity of 3.0 in./hr. and the duration of 55 minutes is used for all of the tested conditions.

The amounts of simulated sediment yield at the outlet were found to vary substantially with the flow conditions, physiographic characteristics of cut or fill slopes, and the ground cover conditions. In order to demonstrate the variations of sediment yield due to these factors, five hypothetical cases are studied. Table 10.4 summarizes the simulated results. The water discharge hydrograph at the outlet is the same for all three types of road prism. However, the amount of simulated sediment yield varies substantially from case to case.

Case 1 has no cover for all flow units. For Case 2, the road surface is paved with gravel while both cut and fill slopes have no cover. In Case 3, there is 30 percent ground cover for cut and fill slopes and no cover for the road surface. Case 4 has a paved road surface with gravel. The cover conditions on both cut and fill slopes are the same as in Case 3. In Case 5, the ground cover condition for both cut and fill slopes is increased to about 100 percent, and the road surface is paved with gravel. It is worthwhile to note that the simulation results seem to agree well with physical reality. For all cases, Type A produces the largest amount of sediment as expected. This is because the outslope design of Type A prism will provide the highest degree of runoff concentration, this usually causes severe soil erosion if no control measures, such as grass or gravel paving, are implemented. Other interesting points are that Type B will yield more sediment than Type C if the fill slope is not protected by ground cover, and the trend is reversed when the fill slope is protected by grass. This is because Type B will provide a larger runoff rate and cause more erosion on the fill slope if the surface is not protected as assumed in Cases 1 and 2. If the fill slope is protected by grass as in Cases 3, 4, and 5, the flow on the slope is substantially retarded. In these cases, part of the sediment eroded in the road surface is trapped in the fill slope because of the low transport capacity. Thus, the Type B prism will produce a smaller amount of sediment if the fill slope is protected.

To test the effect of ground cover on the sediment yield, different percents of ground cover are used for the Type C road prism. Figure 10.28 gives the variation of sediment yield versus ground cover density in

Table 10.4 Simulated sediment yield in pounds from three types and five cases.

Case No.	Type A	Type B	Type C
1	16,300	11,630	9,630
2	14,440	11,150	9,150
3	2,790	1,320	1,466
4	1,520	982	990
5	456	241	439

Note: Case 1 = No ground cover.

Case 2 = No ground cover on the cut and fill slopes. Road surface is paved with gravel.

Case 3 = 30% ground cover on cut and fill slope. No ground cover on road surface.

Case 4 = 30% ground cover on the cut and fill slopes and the road surface is paved with gravel.

Case 5 = Close to 100% ground cover on the cut and fill slopes. The road surface is paved with gravel.

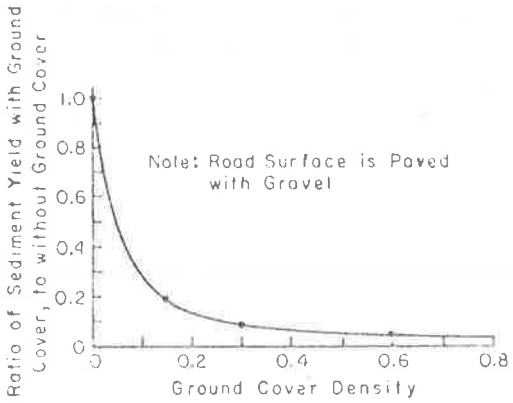

Figure 10.28 Variation of sediment yield versus ground cover density.

terms of percentage. The result indicates that the reduction in sediment yield tends to reach an equilibrium value when ground cover reaches about 60 percent.

The spacing of cross drains is an important factor in the design of a road system. Figure 10.29 shows a power function relationship between the spacing of cross drains and the sediment yield. Note that Figure 10.29 gives the ratio of sediment yield to that of 100 ft cross drain spacing. In general, the total sediment yield at an outlet will increase as cross drain spacing increases due to enlargement of the total area.

The side slopes such as cut or fill slopes are also important factors in determining the total sediment yield. Let the sediment yield from a 5:1 (horizontal to vertical) slope be a base value. The ratios of sediment yields from other slopes to that of 5:1 slope are given in Figure 10.30. For this example case, the total sediment yield will increase about 25 percent when the side slope is increased to 2:1.

The above examples indicate that the model has the potential for use in evaluating the alternatives of road designs or maintenance practices.

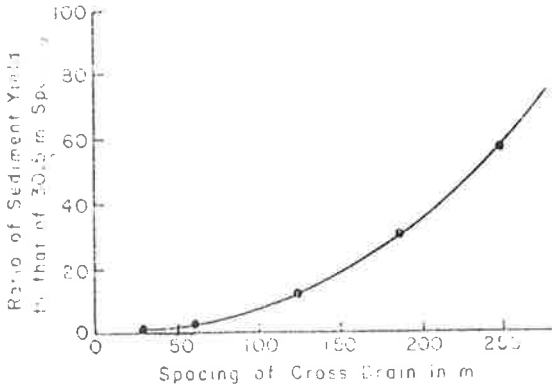

Figure 10.29 Spacing of cross drain in feet.

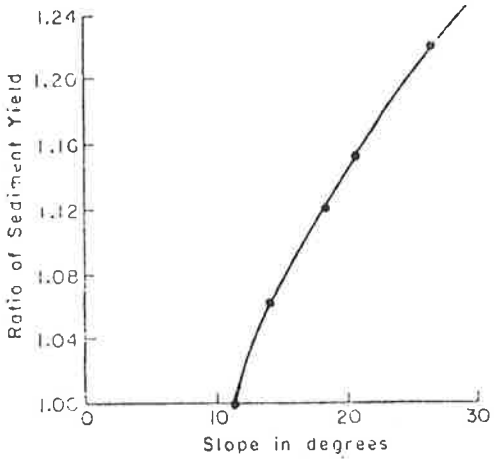

Figure 10.30 Sediment yield versus side slope.

Simplified Model

Simons, Li, Ward, and Shiao (1978) developed a simplified water and sediment yield model (SIRSED) for roadways. The model connects simplified one plane geometries (Section 10.5) together to produce a system that is dependent on the water and sediment that moves from one prism component to another during storm runoff. In general, each section is considered independent with respect to the others in terms of water routing. However, water yield and subsequently erosion are

closely related and must be accounted for in computations. In essence, the model keeps track of the incoming and outgoing yields for the storm period. Application of the model to the three types of road prisms already discussed shows that the model is a rapid method of estimating sediment yields. Comparison with complex model simulation, Figure 10.31, shows that the simplified model is very close to the complex model.

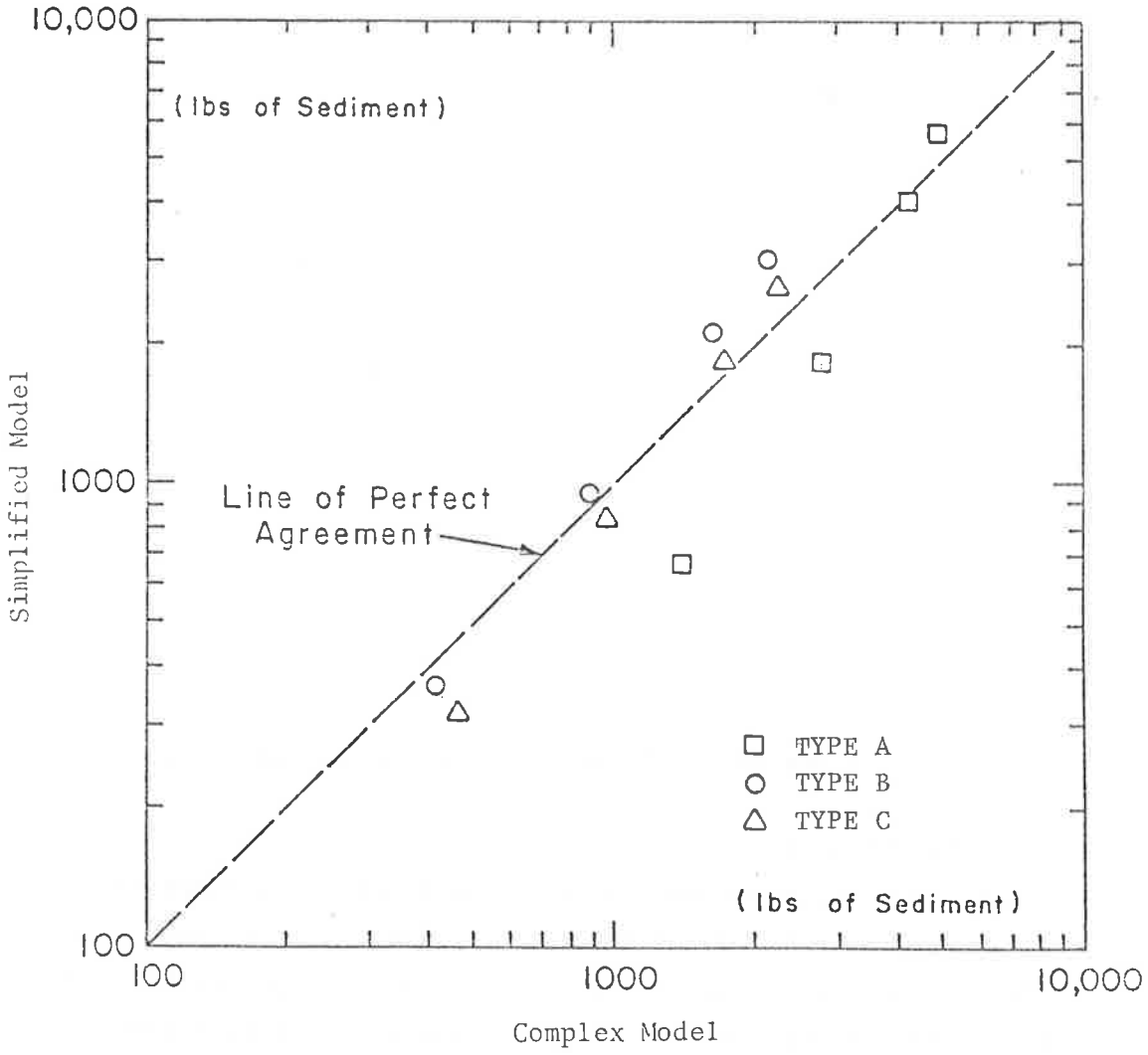

Figure 10.31 Comparison of the simulated sediment yields using the simplified and complex models.

Figure 10.31 shows increasingly better agreement between sediment yield from Type A through Type C. Better agreement is produced for Type C than for Type A because the effective slope over which the water was routed in Type A is longer than the flow distance in Type C. Because of this increased distance, time lag caused by routing water will be greater and the attenuation of peak and extension of flow duration greater. Generally, the longer the slope over which a given input must flow, the longer and flatter is the outflow hydrograph. Whereas the simplified model compresses a more intense runoff into the same outflow time period by raising the average outflow rate, the complex routing model more accurately spreads volume over a longer time period. The complex model usually has slightly higher peak water and sediment outflow rates.

Road Sediment Procedural Guide

Outgrowths from development of the road sediment models have been the generation of a qualitative procedural guide consisting of a series of graphs. These graphs were generated utilizing a reformulated road sediment model (ROSETA). The graphs relate such variables as infiltration rate and soil detachment rate with rainfall intensity and road gradient, cut and fill slope inclination; water discharge with sediment discharge ground cover conditions are also included. Generated graphs can be used by the forest planner or engineer to quickly estimate water and sediment yield from roadways of different designs. Because both the road sediment models and the procedural guide have not been validated, the present procedures should only be used to assess the relative amounts of sediment production considering different design alternatives or cases. A set of generated graphs is presented as Figures 10.32, 10.33, 10.34, and 10.35. Using these graphs sediment yield from a roadway can be rapidly estimated as indicated by the following example (see Simons et al., 1976).

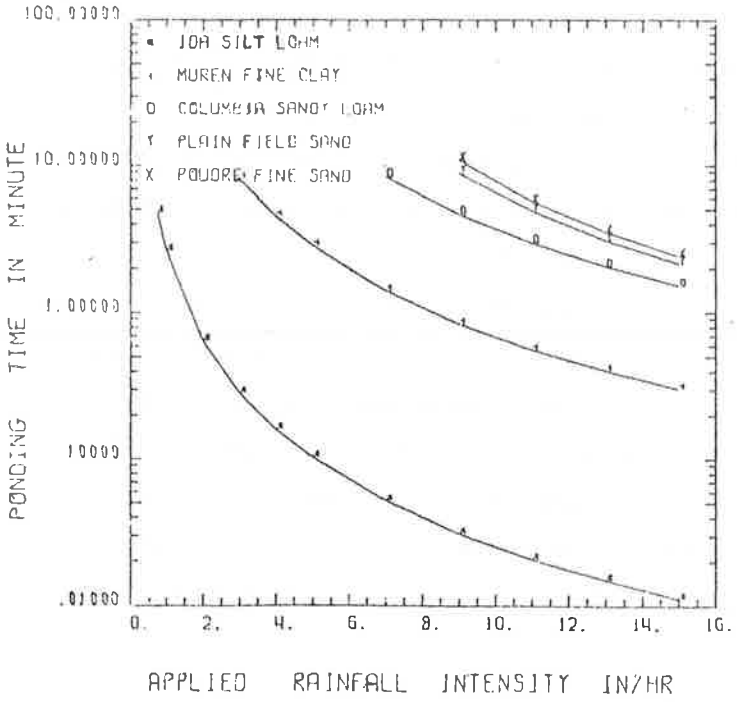

Figure 10.32 Ponding time for different rainfall intensity.

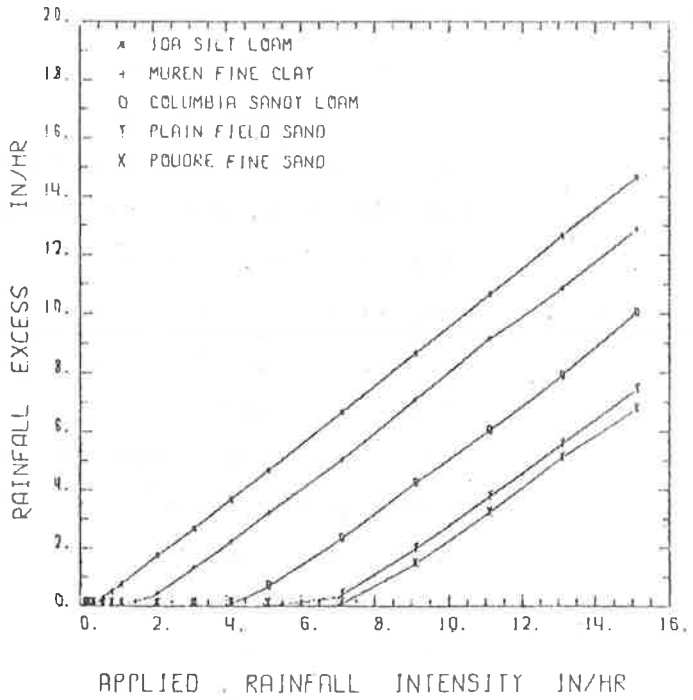

Figure 10.33 Rainfall excess rate versus rainfall intensity for storm duration of 30 minutes.

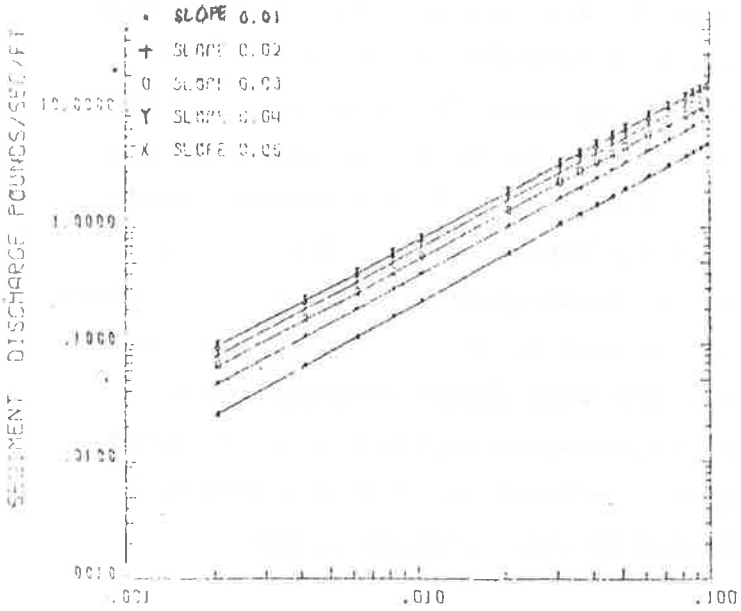

Figure 10.34 Sediment discharge versus water discharge for bare-soil road bed with slopes from 0.01 to 0.05 and for sediment size of 0.02 mm.

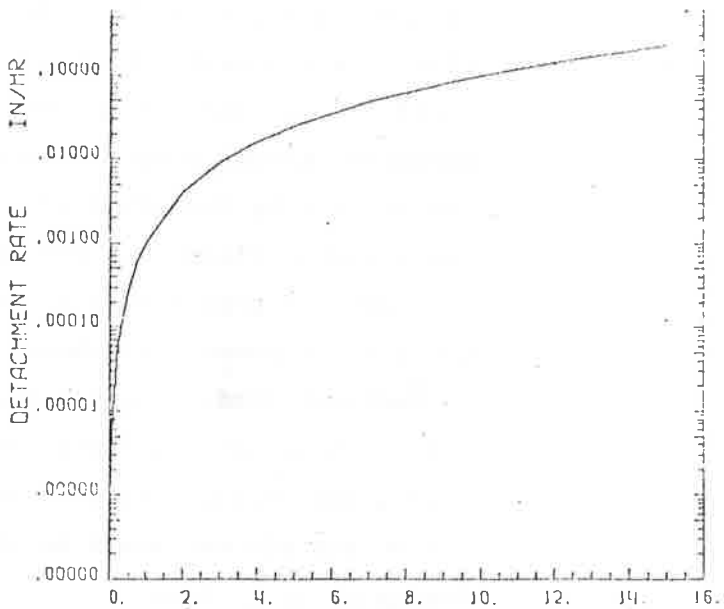

Figure 10.35 Assumed soil detachment by raindrop splash.

Example I. Water Yield

Given:

Road surface longitudinal gradient: 3 percent

Length: 500 ft

Width: 10 ft

Soil: fine clay, bare soil surface, sediment size is 0.02 mm and porosity is 0.5 (Muren fine clay)

Design Storm: intensity 3 in./hr; duration 30 min

What is the total water yield of the storm?

The procedure follows:

Step 1: From Figure 10.32 with rainfall intensity 3 in./hr and Muren fine clay one can estimate the ponding time:

$$t_p = 8 \text{ min}$$

The ponding time is less than the duration of storm, and surface runoff occurs. Then the duration of excess rainfall is

$$D_e = D_t - t_p = 30 - 8$$

$$= 22 \text{ min}$$

Where t_p is the ponding time from which runoff begins, D_e is the duration of excess rainfall, and D_t is the duration of storm.

Step 2: From Figure 10.33 with rainfall duration of 30 min and Muren fine clay the excess rainfall rate:

$$I_e = 1.25 \text{ in./hr}$$

Where I_e is the excess rainfall rate.

Step 3: The total water yield is

$$Y_w = I_e D_e$$

$$= 1.25 \times 22/60$$

$$= 0.46 \text{ in.}$$

Where Y_w is the water yield in depth of water.

Example II. Sediment Yield from Bare-Soil Road Surface

What would be the sediment yield of the storm using the data given in Example I?

Step 1: Determine the duration of excess rainfall and excess rainfall rate as those in Example I.

Step 2: The maximum discharge per unit width of road is

$$q = I_e L = 1.25 \times 500/43{,}200$$
$$= 0.0144 \text{ ft}^3/\text{sec/ft}$$

Where q is the discharge per unit width of road, L is the length of road, or cross drain spacing, and 43,200 is a conversion factor from inches per hour to feet per second.

Step 3: With slope $S_o = 0.03$, $q = 0.0144 \text{ ft}^3/\text{sec/ft}$ and sediment size $d_s = 0.02$ mm, Figure 10.34 shows that

$$q_t = 0.88 \text{ lb/sec/ft}$$

Where q_t is the sediment transport rate per unit width of the road and S_o is the road gradient.

Step 4: The total transport capacity for the entire width of road surface G_c is

$$G_c = q_t \quad W = 0.88 \times 10$$
$$= 8.8 \text{ lb/sec}$$

Where W is the width of road surface.

Step 5: The total potential transport capacity for the storm expressed as volume is

$$\forall_t = G_c \, D_e/\gamma_s$$
$$= 8.8 \times 22 \times 60/165$$
$$= 70.4 \text{ ft}^3$$

Where γ_s is the specific weight of sediment, which is assumed to be 165 lb/ft^3 for our purposes.

Step 6: From Figure 10.35 the volume of loose soil available from raindrop impact detachment during the storm can be estimated by

$$\forall_r = D_r \, D_t \, A_s \, (1-\gamma)$$
$$= 0.009 \times 30/60 \times 1/12 \times 500 \times 10 \times 0.5$$
$$= 0.94 \text{ ft}^3$$

Where $\forall_r$ is the available loose soil by raindrop splash in volume, D_r is the raindrop-splash soil detachment rate, A_s is the area, and n is the porosity of soil.

Step 7: Determine the volume of loose soil available from runoff detachment by comparing $\forall_t$ and $\forall_r$.

Because $\forall_r < \forall_t$, the transport capacity is greater than the availability, soil detachment by runoff occurs with the amount

$$\forall_f = D_f(\forall_t - \forall_r)$$
$$= 0.06 \times (70.4 - 0.94)$$
$$= 4.17 \text{ ft}^3$$

Where $\forall_f$ is the available loose soil by runoff detachment, D_f is the overall runoff detachment coefficient. For clay and silt, D_f is assumed to be 0.06.

Step 8: Determine the total volume of loose soil available for transport during the storm by

$$\forall_a = \forall_r + \forall_f$$
$$= 0.94 + 4.17$$
$$= 5.11 \text{ ft}^3$$

Where $\forall_r$ is the total available loose soil in volume.

Step 9: Determine the amount of soil erosion or sediment yield from road surface by comparing $\forall_t$ and $\forall_a$.

Because $\forall_a < \forall_t$, the availability of loose soil determines the yield. The sediment yield is

$$Y_s = \forall_a = 5.11 \text{ ft}^3$$
$$= 843 \text{ lb}$$

This simple example illustrates the type of useful product that can be generated using a computer-based physical simulation model.

In addition to the example shown here, the model can also estimate sediment yield from cut and fill road slopes with or without vegetative erosion control treatment. The use of computer-based models to develop field user guides, such as those presented above, is an attractive use for transferring the information from the research level to the practicing level.

10.9 DATA NEEDS SPECIFIC TO SEDIMENT YIELD MODELING

Numerous pieces of information are required for operation of computer models. Sometimes the data is available and adequate. Many times, however, it is neither, thus requiring techniques for filling in information gaps. Some of the important data types, and techniques for obtaining them, are presented below.

In addition to the hydrologic characteristics of the area (Chapter 7) is the sediment information needed for modeling. Three types of sediment data are needed to model the sediment yield. These are size analysis, detachment coefficients and a sediment transport coefficient.

Sediment size data should be on-site size distributions and transported material distributions. Use of both distributions helps in model calibration to confirm that the model is transporting the correct size fractions from the correct sediment supply. Size distributions are obtained from sieve analyses of duplicate samples. Common size breakdowns are given in Table 10.5. The particle size distribution for the in situ soil is needed to determine the resultant sediment transport. If it is unavailable, an estimate of the D_{50} sediment size is needed. Some information may be available for USDA Soil Conservation Service Reports or State soil surveys. Textural classification is one crude

Table 10.5 Common size breakdowns for sand, silt and clays.

	size in mm	
Class	Rouse, 1951	Typical Soil Conservation Service Reporting
very coarse sand	2-1	2-1
coarse sand	1-.5	1-.5
medium sand	.5-.25	.5-.25
fine sand	.25-.125	.25-.10
very fine sand	.125-.062	.10-.05
coarse silt	.062-.031	.05
medium silt	.031-.016	to
fine silt	.016-.008	
very fine silt	.008-.004	.002
coarse clay	.004-.002	less than
medium clay	.002-.001	.002
fine clay	.001-.0005	
very fine clay	.0005-.0024	

method for estimating a D_{50} sediment size and aggradation or size distribution. This requires use of a clay-silt-sand chart (Figure 10.36). Entering the chart with a textural class name, a point is selected in a central part of the class name polygon. The corresponding percent sand, percent silt, and percent clay values are used to plot a gradation curve. In Figure 10.36 the silt percent is the difference between 100 percent and the sum of sand and clay percentages. The percents are plotted as 100 percent finer than 2 mm (coarse sand), silt percent plus clay percent finer than 0.05 mm (silt), and clay percent finer than 0.002 mm (clay). The gradation curve consisting of three points (sand, silt and clay) can be described for mathematical purposes by D_{50} and G, the gradation coefficient. The gradation coefficient is defined as

$$G = \frac{1}{2}\left(\frac{D_{84.1}}{D_{50}} + \frac{D_{50}}{D_{15.9}}\right) \tag{10-80}$$

where $D_{84.1}$ and $D_{15.9}$ are the sizes at which 84.1 and 15.9 percent of the sample is finer (Simons and Sentürk, 1977). An example illustrates this point. If a soil is classified as a clay loam it may be, from Figure 10.36, 31 percent sand and 32 percent clay which indicates 37 percent silt. The corresponding gradation curve is shown in Figure 10.37. A practical lower limit, below which particles are very small, is 0.00024 mm. This size is the lower limit on clay sizes (Simons and Sentürk, 1977). In this example, the gradation is equal to 8.1 (reasonable for watershed) because $D_{15.9}$ equals 0.0014 mm, D_{50} equals .0097 mm, and $D_{84.1}$ equals 0.09 mm. Using the D_{50} and G values, a computed gradation curve can be developed as shown in Figure 10.37. The computed distribution can be found by three points, $D_{15.9}$, D_{50} and $D_{84.1}$. If D_{50} is known then

$$D_{84.1} \approx D_{50} \cdot G \tag{10-81}$$

and

$$D_{15.9} \approx \frac{D_{50}}{G} \tag{10-82}$$

Comparison of the synthetic and assumed (from textural classification) distribution shows that the computed curve may be off for the smaller and larger fractions. This discrepancy is reasonable as the techniques

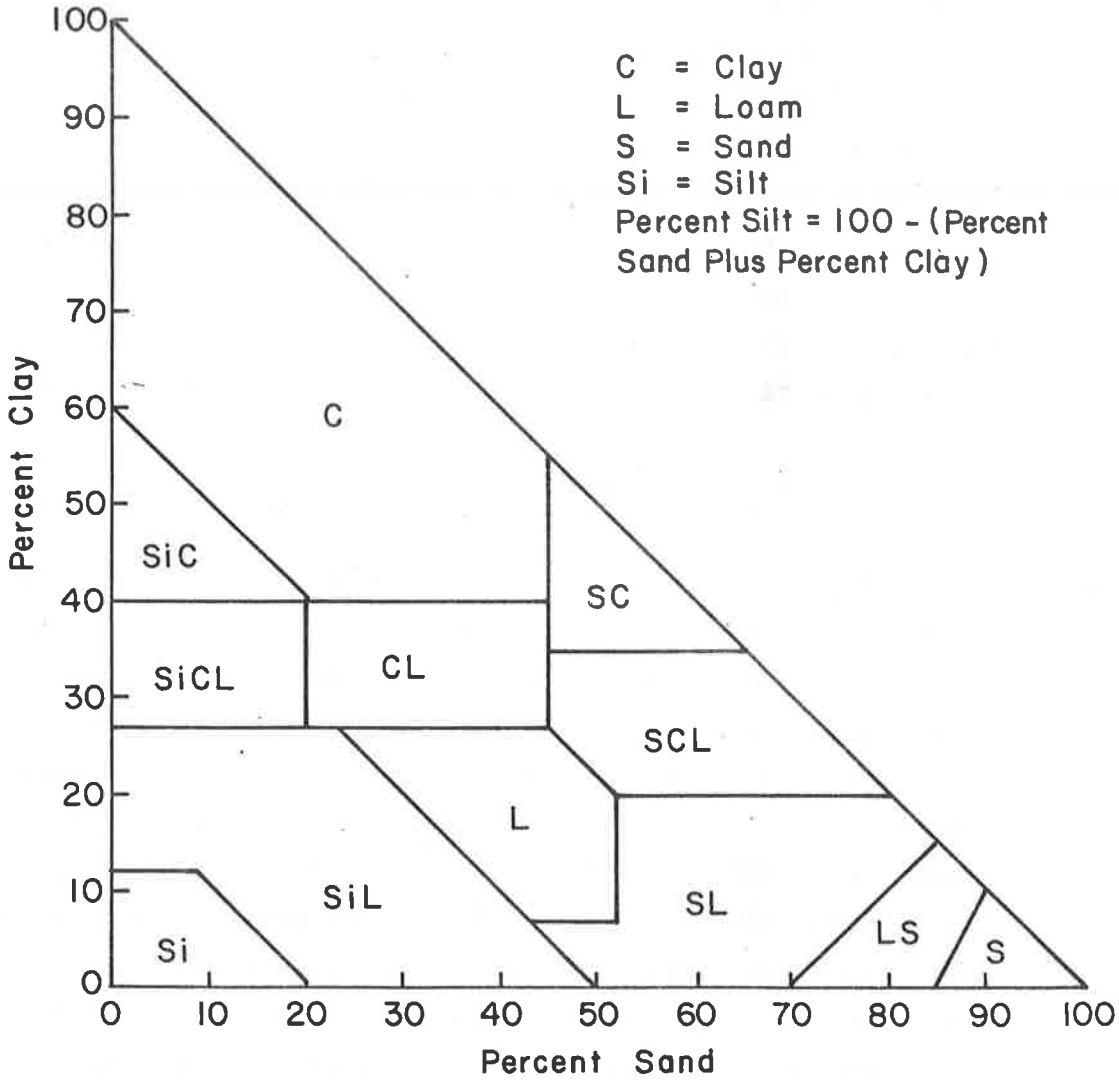

Figure 10.36 Soil textural classification graph for estimating size fractions.

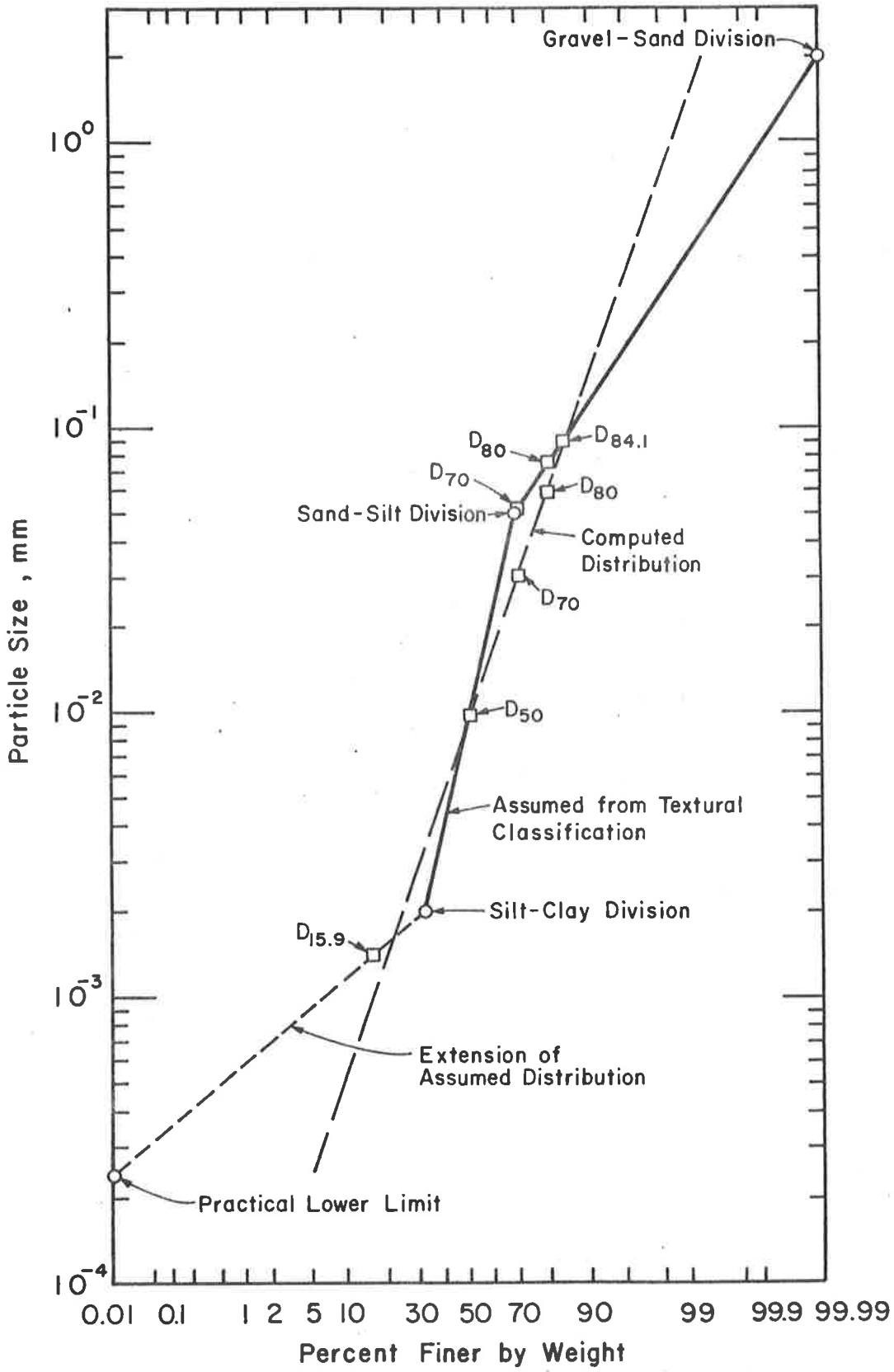

Figure 10.37 Assumed and computed size distributions derived from soil texture classification.

are applicable to soil samples that have lognormal size distributions (Simons and Sentürk, 1977). If the sample does not closely follow such a distribution then deviations at the large and small size fractions may be expected. Therefore, if actual or assumed distributions are available, they should be used in preference to any computed type. If a computed type is used, possible errors must be recognized. Although a crude approximation, it does provide an initial estimate of the size distribution. If more than one textural name is used to represent a soil type then the constructed gradation curves must be composited.

Once a size distribution has been chosen, it is necessary, if desired, to subdivide the distribution into representative size fractions. A rough estimate of transport using the D_{50} size is possible, but because the models are formulated for different size fractions, more information is gained if multiple size fractions are employed. The size distribution may be subdivided into numerous representative values, five to twenty, which are often employed. For example, if the sample in the previous discussion (Figure 10.37) is to be subdivided into ten representative fractions of 10 percent each then the following computations are required. The representative size is computed as

$$\overline{D}_i = \sqrt{D_i \times D_{i-1}} \tag{10-83}$$

where $\overline{D}_i$ is the geometric mean or representative size of the fraction, D_i is the upper limit size of the fraction, and D_{i-1} is the lower limit size of the fraction. From Figure 10.37, the representative size for the D_{80} fraction of 10 percent (i.e., D_{70} to D_{80}) is 0.062 mm because D_{80} is 0.075 mm and D_{70} is 0.052 mm. As a comparison, the computed gradation curve suggests a value of 0.042 mm for this size fraction (D_{70} = 0.03 mm and D_{80} = 0.06 mm). The representative size of 0.062 mm is used in transport computations and the size fraction of 10 percent is used to modify the total transport rate. Although this is a rather crude approach, it does provide a method for developing useful model inputs from sparse data. Actual sieve samples of the transported materials would provide a check of the model and the assumed input distribution by noting if the transported material is equal to or finer than the on-site material. If it is not, an explanation is necessary.

In addition to on-site soil samples and size distributions, other soil information includes soil detachment coefficients for raindrop splash and for overland flow. These two coefficients are used in determining sediment supply. Raindrop splash and overland flow detachment coefficients are initially estimated but are often subsequently calibrated. The rainfall splash detachment coefficient, a_1, is a function of soil type, soil structure, moisture conditions, and cohesion. Moldenhauer and Long (1964) have studied the raindrop splash detachment resulting from simulated rainfall striking a soil target 7.6 cm in diameter. The amount of soil splash resulting from these targets has been replotted with rainfall intensity for several soil types. Figure 10.38 is a replotting of the fitted lines presented by Moldenhauer and Long (1964) as related to the square of the rainfall intensity. Although approximate in nature, the corresponding a_1 values do allow a first estimate of the raindrop splash detachment coefficient for several soil types. The values suggested here are based only on one experiment and should be used with caution as other influences such as cohesion may decrease these values by a factor of 10 or even 100. From previous experience, a factor of at least 10 is recommended for the reduction. Because the raindrop splash detachment coefficient is usually insensitive in the models for many applications, a value of around 0.001 is often adequate for use.

The runoff detachment coefficient, D_f, is also difficult to estimate and often needs to be calibrated. One tentative approach for estimation of the D_f value uses the erosivity index K from the Universal Soil Loss Equation. Knowing the soil particle size distribution, percent organic material, soil texture, and permeability rate, a K can be determined from Figure 10.1. Once K is selected a value of D_f can be estimated from

$$D_f \simeq \frac{K(D_s)^2}{0.63} \tag{10-84}$$

where D_s is the representative sediment size in millimeter. This technique is best when several sediment sizes are being used to estimate sediment yield. If only one representative size is used, the D_f value should be increased on the order of 3-5 times.

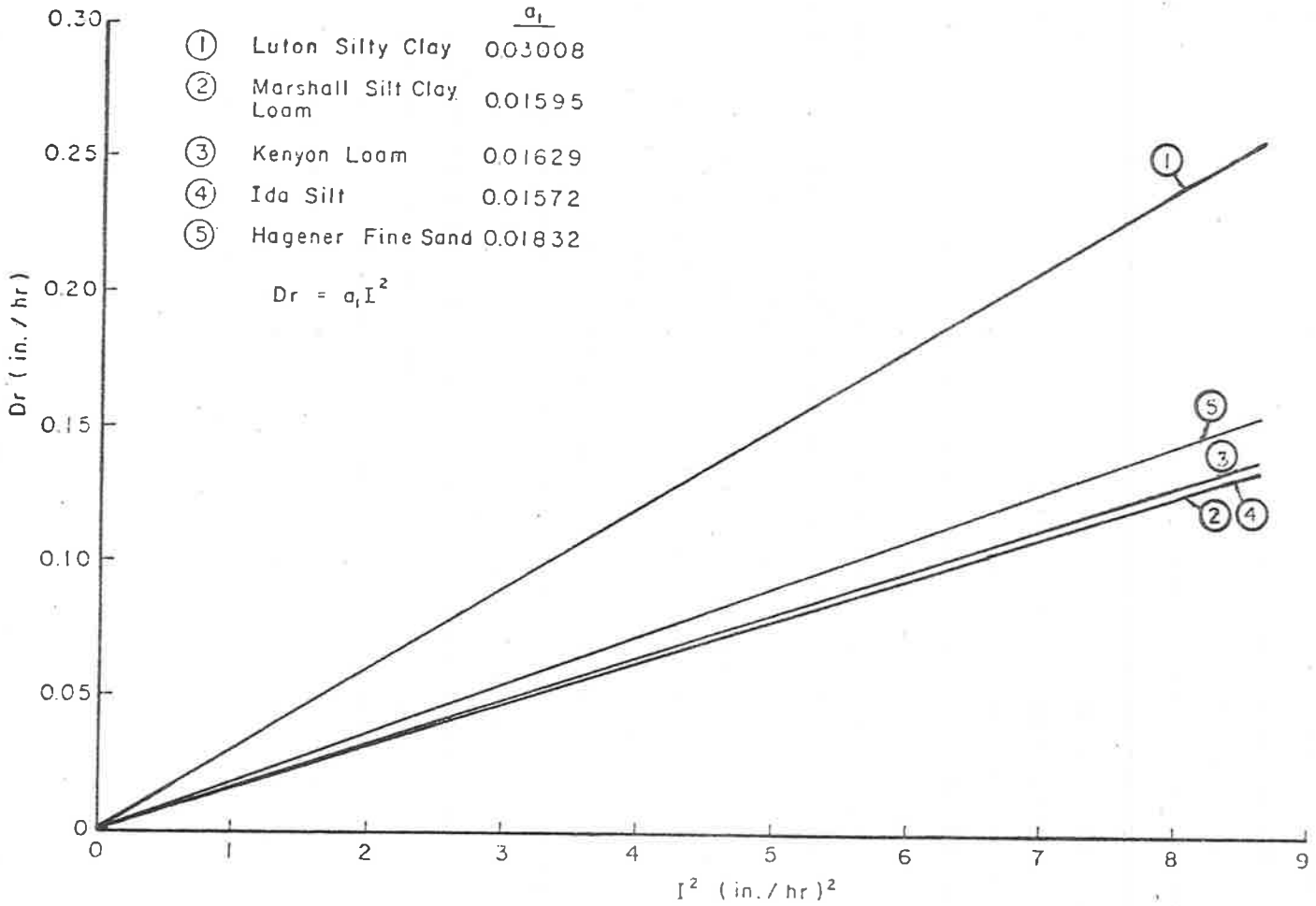

Figure 10.38 Soil detachment rate versus rainfall intensity squared.

An example of this approach for determining D_f can be developed from Figure 10.37. If D_{50} of 0.0097 mm is used as the representative size, and silt plus very fine sand is about 54 percent, organic material is chosen at a realistic value of two percent, sand (.1-2 mm) is about 16 percent, soil structure is fine granular, and permeability (hydraulic conductivity) is slow to moderate, the correesponding value of K from Figure 10.1 is about 0.28. This yields a D_f of 0.00004. This value may be increased or decreased but provides a realistic starting point for model adjustment. It should be noted that D_f ranges from 0 to 1, therefore if D_f is computed to be greater than 1 it should be reduced to 1.0. The last coefficient needed in sediment transport is the dimensionless critical shear stress parameter δ. This coefficient dictates which sediment sizes will be transported, a lower δ value increases transport of larger, previously stable, particle sizes. Values of δ range between about 0.01 and 0.06. A good first estimate is 0.047 (Gessler, 1965). If rilling develops δ should be lower because the flow is more concentrated and more erosive. The δ value can be calibrated by comparing the simulated transport material size distribution and the measured distribution. The value of δ is then adjusted to match these distributions as best as possible. Sometimes it is necessary to subdivide the larger and smaller fractions of the on-site distribution to provide a better fit.

In all cases where parameters are properly chosen, computer simulation results will provide realistic estimates of sediment yield. When field data is available, model parameters should be calibrated using the observed response. In this manner the system will feedback and provide the user with better future estimates of input parameters.

10.10 SUMMARY

This chapter has presented current techniques and selected specific models used for estimating sediment yield from watersheds, small sites, and roadways. The physical process type models are strongly advocated because they are responsive to management activities, are transferable between areas (if the limitations on each model are respected), and can be easily updated or changed. Models for different levels of analysis were discussed. The physical process models are more useful than regression models for severak key reasons. However, further research is needed in order to provide potential users with easy to understand and apply methodologies.

10.11 REFERENCES

Bennett, J. P., "Concepts of Mathematical Modeling of Sediment Yield," Water Resources Research, Vol. 10, No. 3, June, 1974, pp. 485-492.

Carter, C. E., Greet, J. D., Braud, H. J., and Floyd, J. M., "Raindrop Characteristics in South Central United States," Trans. ASAE, 1974, pp. 1033-1037.

Chow, V. T., Handbook of Applied Hydrology, McGraw-Hill Book Company, New York, N.Y., 1964.

Crawford, N. H. and Linsley, R. K., "Digital Simulation in Hydrology - Stanford Watershed Model," Stanford University, Department of Civil Engineering Technical Report No. 39, 1966.

David, W. P. and Beer, C. E., "Simulation of Soil Erosion - Part 1. Development of a Mathematical Erosion Model," Trans. ASAE, 1975, pp. 126-129, 133.

Einstein, A. H., "The Bed Load Function for Sediment Transportation in Open Channel Flows," United States Department of Agriculture Technical Bulletin, No. 1026, 1950.

Ellison, W. D., "Studies of Raindrop Erosion," Agricultural Engineering, May, 1944, pp. 181-182.

Fleming, G., "Sediment Erosion-Transport-Deposition Simulation, State of the Art," Present and Prospective Technology for Predicting Sediment Yields and Sources, ARS-S-40, Agriculture Research Service, United States Department of Agriculture, 1975.

Foster, G. R. and Mayer, L. D., "A Closed-Farm Soil Erosion for Upland Areas," Sedimentation, Edited by H. W. Shen, Water Resource Publication, Fort Collins, Colorado, 1972b.

Foster, G. R. and Mayer, L. D., "Mathematical Simulation of Upland Erosion by Fundamental Erosion Mechanics," Present and Prospective Technology for Predicting Sediment Yields and Sources, Agriculture Research Service, U.S. Department of Agriculture, ARS-S-40, June, 1975, pp. 190-207.

Foster, G. R. and Meyer, L. D., "Transport of Soil Particles by Shallow Flow," Trans. ASAE, 1972a, pp. 99-102.

Graf, W. H., and Acaroglu, E. R., "Sediment Transport in Conveyance Systems (Part 1)," Bulletin of the International Association of Scientific Hydrology," June, 1968, pp. 20-39.

Gessler, J., "The Beginning of Bedload-Movement of Mixtures Investigated as Natural Armoring in Channels," (Translated by Prych, E. A., W. M. Keck Laboratory of Hydraulics and Water Resources, CIT), 1965.

Hjelmfelt, A. T., Piest, R. P., and Saxton, K. E., "Mathematical Modeling of Erosion on Upland Areas," 16th Congress of International Association for Hydraulic Research, Vol. 2, 1975, pp. 40-47.

Kilinc, M. Y., "Mechanics of Soil Erosion from Overland Flow Generated by Simulated Rainfall," Ph.D. Dissertation presented to Colorado State University, Fort Collins, Colorado, 1972.

Kilinc, M. and Richardson, E. V., "Mechanics of Soil Erosion from Overland Flow Generated by Simulated Rainfall," Hydrology Paper No. 63, Colorado State University, Fort Collins, Colorado, 1973.

Law, J. Q. and Parson, D. A., "The Relation of Raindrop Size to Intensity," Trans., AGU, Vol. 24, 1943, pp. 452-459.

Li, R. M., "Mathematical Modeling of Response from Small Watershed," Ph.D. Dissertation, Department of Civil Engineering, Colorado State University, Fort Collins, Colorado, 1974.

Li, R. M., Fullerton, T. J., Eggert, K. G., and Spronk, B. E., "Simulation of Water Runoff and Sediment Yield from a System of Multiple Watersheds," IAHR Paper, Cagliari, Italy, 1979.

Li, R. M., Simons, R. K., and Shiao, L. Y., "Mathematical Modeling of On-Site Soil Erosion," presented at International Symposium on Urban Hydrology, Hydraulics, and Sediment Control, Lexington, Kentucky, July, 1977c.

Li, R. M., Stevens, M. A., and Simons, D. B., "Solution to Green-Ampt Infiltration Equation," Journal of Irrigation and Drainage Division, ASCE, Vol. 102, No. IR2, June, 1976, pp. 239-248.

Mein, R. G. and Larson, C. L., "Modeling Infiltration during a Steady Rain," Water Resources Research, Vol. 9, No. 2, April 1973.

Meyer, L. D., "Soil Erosion by Water on Upland Areas," Chapter 27, Vol. II, River Mechanics edited by H. W. Shen, Colorado State University, Fort Collins, Colorado, 1971.

Meyer, D. L. and Monke, E. J., "Mechanics of Soil Erosion by Rainfall and Overland Flow," Trans. ASAE, 1965, pp. 572-577, 580.

Meyer, L. D. and Wischmeier, W. H., "Mathematical Simulation of the Process of Soil Erosion by Water," Trans. ASAE, 1969, pp. 756-758, 762.

Moldenhauer, W. E. and Long, D. C., "Influence of Rainfall Energy on Soil Loss and Infiltration Rates: 1. Effects over a Range of Texture," Soil Science Society of America, Proceedings, 1964, pp. 813-817.

Musgrave, G. W., "The Quantitative Evaluation of Factors in Water Erosion: A First Approximation," Journal of Soil Water Conservation, Vol. 2, No. 3, July, 1947, pp. 133-138.

Mutchler, C. K., "Parameters for Describing Raindrop Splash," Journal of Soil and Water Conservation, May-June, 1967, pp. 91-94.

Mutchler, C. K. and Young, R. A., "Soil Detachment by Raindrops," Proceedings of the Sediment-Yields Workshops, Oxford, Mississippi, USDA, ARS-S-40, June 1975, pp. 113-117.

Negev, M., "A Sediment Model on a Digital Computer," Department of Civil Engineering, Stanford University, Technical Report No. 76, 1967.

Onstad, C. A. and Foster, G. R., "Erosion Modeling on a Watershed," Trans. ASAE, 1975, pp. 288-292.

Onstad, C. A., Piest, R. F., and Saxton, K. E., "Watershed Erosion Model Validation for Southwest Iowa," Proceedings of Third Federal Inter-Agency Sedimentation Conference, Sedimentation Committee, Water Resources Council, 1976.

Reese, A. J., "Simplified Small Watershed Sediment and Water Yield Modeling," Master's Thesis, Colorado State University, Fort Collins, Colorado, 1977.

Shen, H. W., "Wash Load and Bed Load. Chapter 11, River Mechanics edited and published by H. W. Shen, Colorado State University, Fort Collins, Colorado.

Shen, H. W. and Li, R. M., "Watershed Sediment Yield Model," Chapter 21, Stochastic Application to Water Resources, edited by H. W. Shen, Water Resources Publication Company, Fort Collins, Colorado, 1976.

Shiao, L. Y., "Water and Sediment Yield from Small Watersheds," Ph.D. Dissertation, Colorado State University, Fort Collins, Colorado, Spring, 1978.

Simons, D. B. and Li, R. M., "Watershed Segmentation by a Digital Computer for Mathematical Modeling of Watershed Response," USDA, Forest Service, Rocky Mountain Forest and Range Experiment Station, December, 1975.

Simons, D. B. and Li, R. M., "Procedure for Estimating Model Parameters of a Mathematical Model," USDA, Forest Service, Rocky Mountain Forest and Range Experiment Station, April, 1976.

Simons, D. B., Li, R. M., and Shiao, L. Y., "Formulation of Road Sediment Model," USDA, Forest Service, Rocky Mountain Forest and Range Experiment Station, 1977.

Simons, D. B., Li, R. M., and Spronk, B. E., "Storm Water and Sediment Runoff Simulation for a System of Multiple Watersheds," Vol. I, Water Routing and Yield, draft report prepared for USDA Forest Service, Rocky Mountain Forest and Range Experiment Station, April, 1978.

Simons, D. B., Li, R. M., and Stevens, M. A., "Development of Models for Predicting Water and Sediment Routing and Yield from Storms on Small Watersheds," prepared for USDA Forest Service, Rocky Mountain Forest and Range Experiment Station, Flagstaff, Arizona, 1975.

Simons, D. B., Li, R. M., and Ward, T. J., "Estimation of Parameters that Describe Channel Geometry for Watershed Modeling," USDA, Forest Service, Rocky Mountain Forest and Range Experiment Station, December, 1977.

Simons, D. B., Li, R. M., Ward, T. J., and Shiao, L. Y., "Simple Road Sediment Yield Model," prepared for USDA Forest Service, Rocky Mountain Forest and Range Experiment Station, Flagstaff, Arizona, 1978.

Simons, D. B. and Sentürk, F., Sediment Transport Technology, Water Resources Publication, Fort Collins, Colorado, 1977.

Smerdon, E. T. and Beasley, R. P., "Critical Tractive Forces in Cohesive Soils," Agricultural Engineering, January, 1961, pp. 26-29.

Smith, R. E., "Simulating Erosion Dynamics with a Deterministric Distributed Watershed Model," Proceedings of the Third Federal Inter-agency Sedimentation Conference, Sedimentation Committee, Water Resources Council, 1976.

Smith, D. D. and Wischmeier, W. H., "Factors Affecting Sheet and Rill Erosion," Trans. AGU, Vol. 38, 1957, pp. 889-896.

USBR, "Investigation of Meyer-Peter, Müller Bedload Formulas," Sedimentation Section, Hydrology Branch, Division of Project Investigations, U.S. Department of the Interior, Bureau of Reclamation, June, 1960.

Van Liew, M. W., "Sediment Production from Short Test Plots in Mine Spoils," M.S. Thesis, Colorado State University, Fort Collins, Colorado, 1976.

Williams, J. R., "Sediment Yield Prediction with Universal Equation Using Runoff Energy Factor," Paper presented at the Sediment Yield Workshop, USDA Sed. Lab., Oxford, Mississippi, 1972.

Williams, J. R., "Sediment-Yield Prediction with Universal Equation Using Runoff Energy Factor," in Present and Prospective Technology for Predicting Sediment Yields and Sources, U.S. Department of Agriculture and the Texas Agricultural Experiment Station, Texas A&M University, June, 1975.

Williams, J. R., "Sediment Routing for Agricultural Watersheds," Water Resources Bulletin, Vol. 11, No. 5, October, 1975, pp. 965-974.

Williams, J. R. and Berndt, H. D., "Sediment Yield Computed with Universal Equation," Journal of Hydraulics Division, ASCE, Vol. 98, No. HY12, December, 1972, pp. 2087-2097.

Wischmeier, W. H., "Estimating the Cover and Management Factor for Undisturbed Areas," Paper presented at the Sediment Yield Workshop, USDA Sed. Lab., Oxford, Mississippi, 1972.

Wischmeier, W. H., "Upslope Erosion Analysis," Chapter 15, Environmental Impact on Rivers, edited and published by H. W. Shen, Colorado State University, Fort Collins, Colorado, 1973.

Wischmeier, W. H., Johnson, C. B., and Cross, B. V., "A Soil-Erodibiility Nomograph for Farmland and Construction Sites," Journal of Soil and Water Conservation, Vol. 26, No. 5, 1971, pp. 189-193.

Wischmeier, W. H. and Smith, D. D., "Predicting Rainfall-Erosion Losses from Cropland East of the Rocky Mountains," Agriculture Handbook, No. 282, ARS, USDA, 1960.

Wischmeier, W. H. and Smith, D. D., "Predicting Rainfall-Erosion Losses from Cropland East of the Rocky Mountains, Agriculture Handbook, No. 282, USDA, 1965.

Woolhiser, D. A. and Blinco, P. H., "Watershed Sediment Yield - A Stochastic Approach. Present and Prospect Technology for Predicting Sediment Yields and Sources," Agriculture Research Service, U.S. Department of Agriculture, ARS-S-40, June, 1975, pp. 264-273.

Yalin, M. S., "An Expression of Bed-Load Transportation," Journal of Hydraulics Division, ASCE, Vol. 89, No. HY3, May, 1963, pp. 221-250.

Yang, C. T., "Unit Stream Power and Sediment Transport," Journal of Hydraulics Division, ASCE, Vol. 98, No. HY10, 1972, pp. 1805-1825.

Young, R. A. and Wiersma, J. L., "The Role of Rainfall Impact on Soil Detachment and Transport," Water Resources Research, Vol. 9, 1973, pp. 1629-1636.

Chapter 11

UNSTEADY SEDIMENT ROUTING IN RIVERS

Yung H. Chen, Assistant Professor, Department of Civil Engineering, Colorado State University, Fort Collins, Colorado

Daryl B. Simons, Associate Dean for Engineering Research and Professor of Civil Engineering, Colorado State University, Fort Collins, Colorado

11.1 INTRODUCTION

Many problems in water resources systems, river mechanics and hydraulic structures are directly related to the transport of material by flow. In general, the flows in natural and man-made systems are time-variant. Therefore the related transport phenomena are also time variant. However, even when the flows are steady or nearly steady, the transport phenomena may be unsteady. Examples are river systems that have not achieved equilibrium conditions after an initial disturbance.

In solving the unsteady transport problems analytical solutions are usually not available, and numerical methods using iteration are used. A number of numerical solution techniques are available such as those reported by DeVries (1965), Chang and Richards (1971), Chen (1973), and U.S. Army Corps of Engineers (1976). These methods include the water and sediment routing components. The unsteady water routing model has been presented in Chapter 8. This chapter will describe one-dimensional sediment routing models in rivers combining with water routing techniques, applied to study responses of rivers to development.

The principal limitation of one-dimensional model is its assumption of one-dimensional flow. In a relatively nonuniform river, only the general pattern of the river geomorphology can be considered. To perform a more detailed study, a two-dimensional model can be applied. A two-dimensional sediment routing model is also presented in this chapter. The advantages and disadvantages of various types of models for unsteady flow routing in rivers are discussed.

11.2 ONE-DIMENSIONAL SEDIMENT ROUTING MODEL OF A SIMPLE RIVER SYSTEM

Basic Equations

In solving the unsteady flow problems in rivers, the unsteady flow of sediment-laden water is formulated with one-dimensional partial differential equations representing the continuity of mass for sediment, the continuity of mass for sediment-laden water and the equation of motion for sediment-laden water. If a river is relatively stable and only flood propagation is of interest, then the latter two equations can be used for simulating flood wave movement as described in Chapter 8. These three basic equations for describing the unsteady flow of sediment-laden water are:

(1) The sediment continuity equation:

$$\frac{\partial Q_s}{\partial x} + p \frac{\partial A_d}{\partial t} - q_s = 0 \qquad (11\text{-}1)$$

(2) The flow continutiy equation:

$$\frac{\partial Q}{\partial x} + T \frac{\partial y}{\partial t} + T \frac{\partial z}{\partial t} - q_\ell = 0 \qquad (11\text{-}2)$$

(3) The flow momentum equation:

$$\frac{\partial Q}{\partial t} + \frac{\partial \beta\, Q\, V}{\partial x} + g\, A \frac{\partial y}{\partial x} = \rho g\, A(S_o - S_f + D_\ell) \qquad (11\text{-}3)$$

where x = horizontal distance along the channel

t = time

Q_s = sediment discharge in volume of sediment per unit time

p = volume of sediment in a unit volume of bed layer given by ρ_b/ρ_s

ρ_b = bulk density of sediment forming the bed

ρ_s = density of sediment

A_d = volume of sediment deposited on channel bed per unit of length of channel, the value of which is negative when bed erosion occurs

A = water cross-sectional area

Q = flow discharge

q_s = lateral sediment flow per unit length of channel, a positive quantity indicates inflow and a negative value denotes outflow

q_w = lateral water flow per unit length of channel, a positive quantity indicates inflow and a negative value denotes outflow

q_ℓ = lateral flow per unit length of channel, given by $q_s + q_w$

β = momentum coefficient

V = mean flow velocity

T = $\partial A/\partial y$

y = flow depth

g = acceleration of gravity

S_o = bed slope

S_f = friction slope

D_ℓ = dynamic contribution of lateral discharge given by $q_\ell V_\ell / Ag$

V_ℓ = velocity component of lateral inflow in the main flow direction

h = water surface elevation

z = riverbed elevation

Δz = change in riverbed elevation

B = top width

Figure 11.1 is a definition sketch of an alluvial channel. In Equation 11-3 to adequately consider the dynamic effects, an absolute value of velocity V is used in the convective acceleration term to preserve the flow vector. Equations 11-2 and 11-3 are the same equations used for unsteady water routing as described in Chapter 8.

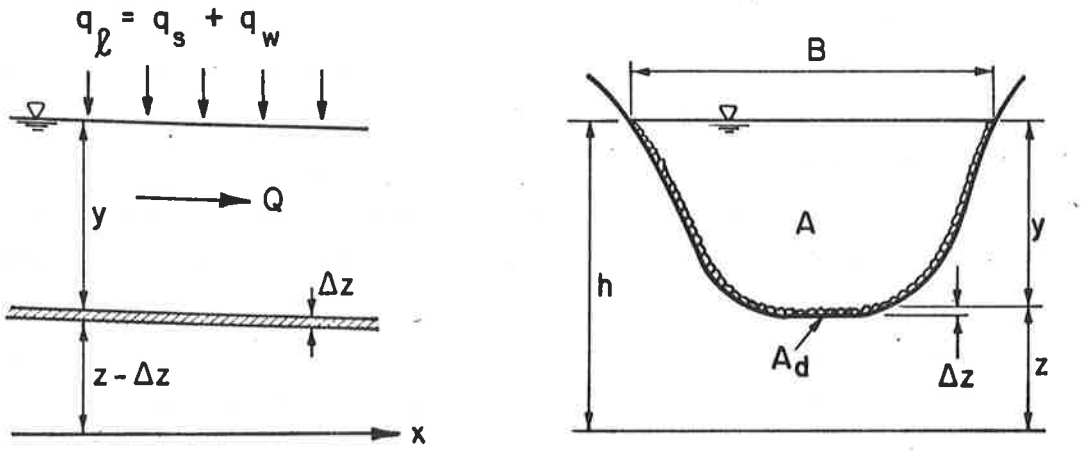

Figure 11.1 Definition sketch of an alluvial channel.

Supplemental Equations

The three equations contain three basic unknowns: Q, y, and A_d. The other variables in the equations must be expressed as a function of the three unknowns in order to obtain a solution. These supplementary equations describe the physical properties of the prototype.

1. The geometric properties of cross sections are expressed as a function of stage from known channel geometries. The geometries will vary with time as the sediment routing proceeds.

2. The mean bed slope

$$S_o = -\partial z/\partial x \qquad (11\text{-}4)$$

in which the initial bed elevation z is known and the change in S_o is related to the change in the bed elevations.

3. The friction slope S_f is a function of flow and channel characteristics. The resistance functions such as Manning's or Chezy's equations can be employed to relate to S_f with the basic unknowns as given in Equation 8-4.

4. The lateral inflow discharges q_ℓ and q_s are considered as known functions of time and space.

5. The sediment discharge can be estimated from the field surveys or from the available theories. Shen (1971) suggested the following procedure for analyzing field data: (a) use the modified Einsteain method (Colby and Hembree, 1955) to estimate the unmeasured suspended load and bed load based on measured data, (b) separate the bed material load from the wash load and analyze them separately, (c) decide which available sediment transport equations best agree with the measured data and use it to estimate the transport load for the given flow conditions. When no measured data are available, Shen suggested: (a) use Einstein's (1950) procedure if bed load is a significant portion of the total bed-material load, (b) use Colby's (1964) method for rivers with flow depth less than or about 10 feet, (c) use Toffaleti's (1969) method for large rivers. For mathematical modeling, it may be more efficient to relate the sediment discharge to the water velocity and depth as a power function.

The first four supplemental relations are required for water routing as described in Chapter 8.

Numerical Solution of Basic Equations

Four different methods of numerical solutions can be used to solve the three basic equations. They are (1) the complete solution, (2) the uncoupled unsteady solution, (3) the known discharge solution, and (4) the uncoupled steady solution.

Complete Solution

As the expressions of the finite-difference approximations Equation 8-9 are substituted into the basic Equations 11-1, 11-2 and 11-3 by assuming $\partial A_d/\partial z = \partial A/\partial y = T$ and $Q_s^{j+1} = Q_s^j + (\partial Q_s/\partial Q)^j \Delta Q + (\partial Q_s/\partial y)^j \Delta y + (\partial Q_s/\partial z)^j \Delta z$, the sediment continuity equation 11-1 becomes.

$$\frac{1}{\Delta x}\left[Q_{s}{}^{j}_{i+1} + \left(\frac{\partial Q_s}{\partial Q}\right)^{j}_{i+1}\Delta Q_{i+1} + \left(\frac{\partial Q_s}{\partial y}\right)^{j}_{i+1}\Delta y_{i+1} + \left(\frac{\partial Q_s}{\partial z}\right)^{j}_{i+1}\Delta z_{i+1} - Q^{j}_{s_i}\right.$$

$$\left. - \left(\frac{\partial Q_s}{\partial Q}\right)^{j}_{i}\Delta Q_i - \left(\frac{\partial Q_s}{\partial y}\right)^{j}_{i}\Delta y_i - \left(\frac{\partial Q_s}{\partial z}\right)^{j}_{i}\Delta z_i\right] + \frac{p}{4\Delta t}\left(T^{j}_{i} + T^{j}_{i+1}\right)\left(\Delta z_i + \Delta z_{i+1}\right)$$

$$+ \frac{1}{4\Delta t}\left[\left(\frac{1}{V}\right)^{j}_{i} + \left(\frac{1}{V}\right)^{j}_{i+1}\right]\left(\Delta Q_{s_i} + \Delta Q_{s_{i+1}}\right) - \frac{1}{2}\left[\left(\frac{Q_s}{AV^2}\right)^{j}_{i} + \left(\frac{Q_s}{AV^2}\right)^{j}_{i+1}\right]$$

$$\left\{\frac{1}{2\Delta t}\left(\Delta Q_i + \Delta Q_{i+1}\right) - \frac{1}{4\Delta t}\left[(VT)^{j}_{i} + (VT)^{j}_{i+1}\right]\left(\Delta y_i + \Delta y_{i+1}\right)\right\}$$

$$= \frac{1}{2}\left(q^{j}_{s_{i+(\frac{1}{2})}} + q^{j+1}_{s_{i+(\frac{1}{2})}}\right) \qquad (11\text{-}5)$$

where Δx is the distance between sections i and (i+1), Δt is the time increment from t^j to t^{j+1}, and Δ indicates the difference between the values at t^{j+1} and at t^j. Rearranging Equation 11-5, the following equation is obtained

$$A_i Q^{j+1}_i + B_i y^{j+1}_i + C_i z^{j+1}_i + D_i Q^{j+1}_{i+1} + E_i y^{j+1}_{i+1} + F_i z^{j+1}_{i+1} = G_i \qquad (11\text{-}6)$$

The coefficients in Equation 11-6 are expressed as:

$$A_i = \left(\frac{\partial Q_s}{\partial Q}\right)^{j}_{i} S_2 - S_3$$

$$B_i = \left(\frac{\partial Q_s}{\partial y}\right)^{j}_{i} S_2 + S_4$$

$$C_i = \left(\frac{\partial Q_s}{\partial z}\right)^{j}_{i} S_2 + S_5 \qquad (11\text{-}7)$$

$$D_i = \left(\frac{\partial Q_s}{\partial Q}\right)^{j}_{i+1} S_6 - S_3$$

$$E_i = \left(\frac{\partial Q_s}{\partial y}\right)^{j}_{i+1} S_6 + S_4$$

$$F_i = \left(\frac{\partial Q_s}{\partial z}\right)^{j}_{i+1} S_6 + S_5$$

and

$$G_i = 2\Delta t[q^j_{s_{i+(\frac{1}{2})}} + q^{j+1}_{s_{i+(\frac{1}{2})}}] - 4\theta(Q^j_{s_{i+1}} - Q^j_{s_i}) + A_i Q^j_i + B_i y^j_i$$

$$+ C_i z^j_i + D_i Q^j_{i+1} + E_i y^j_{i+1} + F_i z^j_{i+1}$$

where $\theta = \frac{\Delta t}{\Delta x}$

$$S_1 = (\frac{1}{V})^j_i + (\frac{1}{V})^j_{i+1}$$

$$S_2 = -4\theta + S_1$$

$$S_3 = (\frac{C_s}{V})^j_i + (\frac{C_s}{V})^j_{i+1}$$

$$S_4 = (C_s T)^j_i + (C_s T)^j_{i+1}$$

$$S_5 = p(T^j_i + T^j_{i+1})$$

The discretization of the continuity equation 11-2 yields

$$\frac{1}{\Delta x}(Q^{j+1}_{i+1} - Q^{j+1}_i) + \frac{1}{4\Delta t}(T^j_i + T^j_{i+1})(y^{j+1}_i - y^j_i + y^{j+1}_{i+1} - y^j_{i+1})$$

$$+ \frac{1}{4\Delta t}(T^j_i + T^j_{i+1})(z^{j+1}_i - z^j_i + z^{j+1}_{i+1} - z^j_{i+1}) = \frac{1}{2}[q^j_{\ell_{i+(\frac{1}{2})}} + q^{j+1}_{\ell_{i+(\frac{1}{2})}}] \qquad (11\text{-}8)$$

Let

$$S_7 = T^j_i + T^j_{i+1}$$

$$S_8 = y^j_i + y^j_{i+1} + z^j_i + z^j_{i+1}$$

$$A'_i = -4\theta$$

$$B'_i = S_7$$

$$C'_i = S_7 \qquad (11\text{-}9)$$

$$D'_i = 4\theta$$

$$E_i' = S_7$$

$$F_i' = S_7$$

and $$G_i' = 2\Delta t[q^j_{\ell_{i+(\frac{1}{2})}} + q^{j+1}_{\ell_{i+(\frac{1}{2})}}] + S_7 S_8$$

Equation 11-8 becomes

$$A_i' Q_i^{j+1} + B_i' y_i^{j+1} + C_i' z_i^{j+1} + D_i' Q_{i+1}^{j+1} + E_i' y_{i+1}^{j+1} + F_i' z_{i+1}^{j+1} = G_i' \qquad (11\text{-}10)$$

Applying the finite-difference approximations, the terms in Equation (11-3) can be approximated by using the finite-difference Equations (8-9):

$$\frac{\partial Q}{\partial t} \simeq \frac{1}{2\Delta t} \{Q_i^{j+1} - Q_i^j + Q_{i+1}^{j+1} - Q_{i+1}^j\}$$

$$\frac{\partial \beta Q|V|}{\partial x} \simeq \frac{1}{\Delta x} \{(\beta|V|)^j_{i+1} Q_{i+1}^{j+1} - (\beta|V|)^j_i Q_i^{j+1}\}$$

$$gA \frac{\partial y}{\partial x} \simeq g(A)^j_{i+(\frac{1}{2})} \frac{1}{\Delta x} \{y_{i+1}^{j+1} - y_i^{j+1}\}$$

$$gAS_o \simeq g(A)^j_{i+(\frac{1}{2})} \frac{1}{\Delta x} \{z_i^{j+1} - z_{i+1}^{j+1}\} \qquad (11\text{-}11)$$

$$gAS_f \simeq g\{\frac{1}{2} [2A \frac{S_f}{Q} (Q^{j+1} - Q^j) - 2A \frac{S_f}{K} \frac{\partial K}{\partial y} (y^{j+1} - y^j)$$

$$- 2A \frac{S_f}{K} \frac{\partial K}{\partial z} (z^{j+1} - z^j) + S_f T(y^{j+1} - y^j)]_i$$

$$+ \frac{1}{2} [2A \frac{S_f}{Q} (Q^{j+1} - Q^j) - 2A \frac{S_f}{K} \frac{\partial K}{\partial y} (y^{j+1} - y^j)$$

$$- 2A \frac{S_f}{K} \frac{\partial K}{\partial z} (z^{j+1} - z^j) + S_f T(y^{j+1} - y^j)]_{i+1}$$

$$+ \frac{1}{2} [(AS_f)^j_i + (AS_f)^j_{i+1}]\}$$

and

$$q_\ell V_\ell \simeq \frac{1}{2} [(q_\ell V_\ell)^j_{i+(\frac{1}{2})} + (q_\ell V_\ell)^{j+1}_{i+(\frac{1}{2})}]$$

Substituting Equation 11-11 to Equation 11-3 and rearranging the resulting equation, the following equation is obtained:

$$A''_i Q_i^{j+1} + B''_i y_i^{j+1} + C''_i z_i^{j+1} + D''_i Q_{i+1}^{j+1} + E''_i y_{i+1}^{j+1} + F''_i z_{i+1}^{j+1} = G'' \qquad (11\text{-}12)$$

The coefficients in Equation 11-12 are formulated as:

$$A''_i = (1 + 2S_{17}) - S_{10}$$

$$B''_i = -\left[S_{13} + S_{14}\left(\frac{\partial K}{\partial y}\right)_i^j - S_{19}\right]$$

$$C''_i = -S_{16} - S_{14}\left(\frac{\partial K}{\partial z}\right)_i^j$$

$$D''_i = (1 + 2S_{18}) - S_{11} \qquad (11\text{-}13)$$

$$E''_i = S_{13} - S_{15}\left(\frac{\partial K}{\partial y}\right)_{i+1}^j + S_{20}$$

$$F''_i = S_{16} - S_{15}\left(\frac{\partial K}{\partial z}\right)_{i+1}^j$$

and

$$G''_i = (Q)_i^j (1 + S_{17}) + (Q)_{i+1}^j (1 + S_{18})$$

$$- S_{14}\left[\left(\frac{\partial K}{\partial y} y + \frac{\partial K}{\partial z} z\right)_i^j\right] + S_{19} y_i^j$$

$$- S_{15}\left[\left(\frac{\partial K}{\partial y} y + \frac{\partial K}{\partial z} z\right)_{i+1}^j\right] + S_{20} y_{i+1}^j$$

$$+ \Delta t\left[(q_\ell V_\ell)_{i+(\frac{1}{2})}^j + (q_\ell V_\ell)_{i+(\frac{1}{2})}^{j+1}\right]$$

where $\theta = \Delta t/\Delta x$

$$S_9 = g\Delta t$$

$$S_{10} = 2\theta(\beta|V|)_i^j$$

$$S_{11} = 2\theta(\beta|V|)_{i+1}^j$$

$$S_{12} = \theta[(\beta V|V|T)_i^j + (\beta V|V|T)_{i+1}^j]$$

$$S_{13} = \theta g[A_i^j + A_{i+1}^j]$$

$$S_{14} = 2S_9[AS_f/K]_i^j$$

$$S_{15} = 2S_9[AS_f/K]_{i+1}^j$$

$$S_{16} = \theta g[A_i^j + A_{i+1}^j]$$

$$S_{17} = S_9(S_f/V)_i^j$$

$$S_{18} = S_9(S_f/V)_{i+1}^j$$

$$S_{19} = S_9(S_f T)_i^j$$

$$S_{20} = S_9(S_f T)_{i+1}^j$$

To assure the stability of the scheme, the friction slope, S_f, is taken on the time line t^{j+1} (Streloff, 1970). The complete solution method was developed and used by Chen and Simons (1974) and Simons, et al. (1975).

There are six unknowns in Equations 11-6, 11-10, and 11-12 at the time step t^{j+1}, which cause the system to be indeterminate. However, three unknowns are common for any two neighboring rectangular grids. Consequently, (N-1) sets of equations contain 3N unknowns. Three additional equations supplied by the boundary conditions make this system of equations mathematically determinable. The boundary conditions may be any of the following relations: (1) the stage hydrograph, (2) the flow discharge hydrograph, (3) the sediment discharge hydrograph, (4) the depth-discharge rating curve, or (5) the known bed elevations at the controlled boundary section.

If two upstream boundary conditions and one downstream boundary condition are given, they can be linearized in the forms

$$D_0'Q_1 + E_0'y_1 + F_0'z_1 = G_0' \qquad (11\text{-}14)$$

$$D_0''Q_1 + E_0''y_1 + F_0''z_1 = G_0'' \qquad (11\text{-}15)$$

and

$$A_N Q_N + B_N y_N + C_N z_N = G_N \qquad (11\text{-}16)$$

The boundary conditions are discussed in more detail in the section titled "Boundition Conditions" forthcoming. Equations 11-6, 11-10, 11-12, 11-14, 11-15 and 11-16 constitute a system of 3N linear algebraic equations in 3N unknowns. Any of the standard methods, such as the Gaussian elimination method or the matrix inversion method can be used for its solution. A double-sweep method similar to that described in Section 8.2 is applied.

The recurrence equations to compute the values of coefficients during the "Forward Sweep" are:

1) Define initial values of

(a) $g_{1,1} = D'_0$, $h_{1,1} = E'_0$, $k_{1,1} = F'_0$, and $\ell_{1,1} = G'_0$

(b) $g_{2,1} = D''_0$, $h_{2,1} = E''_0$, $k_{2,1} = F''_0$, and $\ell_{2,1} = G''_0$

2) Compute

$$m_i = \frac{\ell_{1,i}g_{2,i} - \ell_{2,i}g_{1,i}}{h_{1,i}g_{2,i} - h_{2,i}g_{1,i}} \tag{11-17}$$

$$n_i = -\frac{k_{1,i}g_{2,i} - k_{2,i}g_{1,i}}{h_{1,i}g_{2,i} - h_{2,i}g_{1,i}} \tag{11-18}$$

$$p_i = \frac{\ell_{1,i}h_{2,i} - \ell_{2,i}h_{1,i}}{g_{1,i}h_{2,i} - g_{2,i}h_{1,i}} \tag{11-19}$$

$$q_i = -\frac{k_{1,i}h_{2,i} - k_{2,i}h_{1,i}}{g_{1,i}h_{2,i} - g_{2,i}h_{1,i}} \tag{11-20}$$

$$s_i = k_{1,i} = A_i q_i + B_i n_i + C_i \tag{11-21}$$

$$K2 = A'_i q_i + B'_i n_i + C'_i \tag{11-22}$$

$$K_3 = A''_i q_i + B''_i n_i + C''_i \tag{11-23}$$

$$t_i = k_{4,i} = G_i - A_i p_i - B_i m_i \tag{11-24}$$

$$g_{1,i+1} = D_i K_2 - D'_i k_{1,i} \tag{11-25}$$

$$h_{1,i+1} = E_i K_2 - E_i' k_{1,i} \tag{11-26}$$

$$k_{1,i+1} \quad F_i K_2 - F_i' k_{1,i} \tag{11-27}$$

$$\ell_{1,i+1} = k_{4,i} K_2 - (G_i' - A_i' p_i - B_i' m_i) k_{1,i} \tag{11-28}$$

$$g_{2,i+1} = D_i' K_3 - D_i'' K_2 \tag{11-29}$$

$$h_{2,i+1} = E_i' K_3 - E_i'' K_2 \tag{11-30}$$

$$k_{2,i+1} = F_i' K_3 - F_i'' K_2 \tag{11-31}$$

$$\ell_{2,i+1} = (G_i' - A_i' p_i - B_i' m_i) K_3 - (G_i'' - A_i'' p_i - B_i'' m_i) K_2 \tag{11-32}$$

where i increases from 1 to N and N is the total number of the computational sections. At $i=N$, the computation must stop at Equation 11-20 to complete the "Forward Sweep."

The recurrence equations to compute the values of the unknown variables during "Backward Sweep" are:

1) At the last computational section,

$$z_N = \frac{G_N - A_N p_N - B_N m_N}{C_N + A_N q_N + B_N n_N} \tag{11-33}$$

2) $$Q_i = m_i + n_i z_i \tag{11-34}$$

$$y_i = p_i + q_i z_i \tag{11-35}$$

$$z_{i-1} = \frac{1}{k_{1,i-1}} (k_{4,i-1} - D_{i-1} Q_i - E_{i-1} y_i - F_{i-1} z_i) \tag{11-36}$$

3) Repeat step 2 from i = N to 1, but neglect Equation 11-36 when i=1.

After the flow conditions at each node section on the time line t^{j+1} is computed by solving Equation 11-1, 11-2 and 11-3 numerically by using the double sweep method described above, the computation is moved to the next time step.

The change of sediment area over a time step from t^j to t^{j+1} is given by

$$\Delta A_d = T(z^{j+1} - z^j) \tag{11-37}$$

in which ΔA_d is assumed to be uniformly distributed over the unit width when formulating the finite-difference equations. However, a certain distribution of ΔA_d can be assumed from theoretical or empirical information. A discussion of the method for distributing ΔA_d over a cross section is given in the section titled "Sediment Distribution Function" forthcoming.

Uncoupled Unsteady Solution

If the change in the sediment area A_d within a short period of time is much smaller than in the cross-sectional area A, the solution obtained by solving Equations 11-1, 11-2, and 11-3 simultaneously can be approximated by solving the flow continuity Equation 11-2 and the flow momentum Equation 11-3 first. The solution is then refined by using the sediment continuity Equation 11-1.

Let it be assumed that the effects of changes in A_d and S_o on the propagation of a flood wave within a time step are negligible; then Equations 11-2 and 11-3 can be written in finite-difference form applying Equation 8-8 or 8-9 as

$$A_i\Delta Q_i + B_i\Delta y_i + C_i\Delta Q_{i+1} + D_i\Delta y_{i+1} = E_i \tag{11-38}$$

and

$$A'_i\Delta Q_i + B'_i\Delta y_i + C'_i\Delta Q_{i+1} + D'_i\Delta y_{i+1} = E'_i \tag{11-39}$$

in which Δ denotes the change in values from t^j to t^{j+1} and the values of coefficients in the equations are known. The solution of Equations 11-38 and 11-39 for unsteady water routing has been described in Chapter 8.

After the flow conditions at each node section on the time line t^{j+1} are computed based on a water routing method, there values are used for computing the sediment load Q_s^{j+1} from the sediment transport function. These computed sediment loads are then used to estimate the changes in the riverbed elevations or sediment areas by applying the finite-difference approximation of Equation 11-1 as follows:

$$\frac{1}{2\Delta x_{i-(\frac{1}{2})}} \left[(Q^{j}_{s_i} - Q^{j}_{s_{i-1}}) + (Q^{j+1}_{s_i} - Q^{j+1}_{s_{i-1}}) \right] + \frac{p}{\Delta t} \Delta A_{d_{i-(\frac{1}{2})}}$$

$$- \frac{1}{2} \left[q^{j}_{s_{i-(\frac{1}{2})}} + q^{j+1}_{s_{i-(\frac{1}{2})}} \right] = 0 \qquad (11\text{-}40)$$

in which $\Delta A_{d_{i-(\frac{1}{2})}}$ is the net deposited volume of sediment in Δt per unit length of channel bed between sections (i-1) and i; $q_{s_{i-(\frac{1}{2})}}$ is the lateral sediment inflow between sections (i-1) and i, and $\Delta x_{i-(\frac{1}{2})}$ is the distance between sections (i-1) and i.

The expression for $\Delta A_{d_{i-(\frac{1}{2})}}$ is obtained by rearranging Equation 11-40. Similarly, a relation for $\Delta A_{d_{i+(\frac{1}{2})}}$ can be obtained. Then the values of ΔA_{d_i} at the interior sections can be estimated from

$$\Delta A_{d_i} = \frac{1}{2} \left[\Delta A_{d_{i-(\frac{1}{2})}} + \Delta A_{d_{i+(\frac{1}{2})}} \right]$$

$$= \frac{\Delta t}{4p} \left\{ \left[q^{j}_{s_{i-(\frac{1}{2})}} + q^{j+1}_{s_{i-(\frac{1}{2})}} + q^{j}_{s_{i+(\frac{1}{2})}} + q^{j+1}_{s_{i+(\frac{1}{2})}} \right] \right.$$

$$- \frac{1}{\Delta x_{i-(\frac{1}{2})}} \left[(Q^{j}_{s_i} - Q^{j}_{s_{i-1}}) + (Q^{j+1}_{s_i} - Q^{j+1}_{s_{i-1}}) \right]$$

$$\left. - \frac{1}{\Delta x_{i+(\frac{1}{2})}} \left[(Q^{j}_{s_{i+1}} - Q^{j}_{s_i}) + (Q^{j+1}_{s_{i+1}} - Q^{j+1}_{s_i}) \right] \right\} \qquad (11\text{-}41)$$

At the upstream boundary, let $Q^{j}_{s_o}$ denote the inflow sediment discharge upstream of the reach at time step t^j. This value can be estimated from the inflow sediment discharge hydrograph. If this hydrograph is not available, $Q^{j}_{s_o}$ is assumed equal to $Q^{j}_{s_1}$. Assuming $\Delta A_{d_1} \approx A_{d_{1+(\frac{1}{2})}}$ at the upstream boundary then

$$\Delta A_{d_1} = \frac{1}{2p} \{\Delta t[q_s^j{}_{1+(\frac{1}{2})} + q_s^{j+1}{}_{1+(\frac{1}{2})}]$$

$$- \frac{\Delta t}{\Delta x}{}_{1+(\frac{1}{2})} [(Q_{s_2}^j - Q_{s_o}^j) + (Q_{s_2}^{j+1} - Q_{s_o}^{j+1})]\} \qquad (11\text{-}42)$$

At the downstream boundary, it is assumed that $\Delta A_{d_N} \approx \Delta A_{d}{}_{N-(\frac{1}{2})}$.

Then ΔA_{d_N} can be estimated from Equation 11-40.

Chang and Hill (1976) determined the value of ΔA_{d_i} by assuming

$$\Delta A_{d_i} \approx \Delta A_{d}{}_{i-(\frac{1}{2})} \qquad (11\text{-}43)$$

This assumption simplifies the formulation and calibration of the model. Nevertheless, the conservation of sediment mass is not well satisfied as Equation (11-41).

After ΔA_{d_i} is obtained for each computational section, the change in bed elevation can be determined from a sediment distribution function described in a later section forthcoming.

Known Discharge Solution

For many practical cases the celerities of disturbance at the water level are much larger than those at the bed. It can be assumed that the flow is quasi-steady for the geomorphic computations, and the flow discharge in a channel reach is known. The number of basic unknowns can then be reduced to two, namely, A_d and y. These unknowns can be evaluated by solving the sediment continuity Equation 11-1 and the flow momentum Equation 11-3, where in Equation 11-3 $\partial Q/\partial t$ is known. Equations 11-1 and 11-3 written in finite-difference form are

$$A_i \Delta y_i + B_i \Delta y_{i+1} + C_i \Delta z_i + D_i \Delta z_{i+1} = E_i \qquad (11\text{-}44)$$

and

$$A_i' \Delta y_i + B_i' \Delta y_{i+1} + C_i' \Delta z_i + D_i' \Delta z_{i+1} = E_i' \qquad (11\text{-}45)$$

in which the values of coefficients are known. The system of linear equations obtained by assembling Equations 11-44, 11-45 and the boundary conditions is similar to that for the uncoupled solution and can be solved by using the same double sweep method. The two boundary conditions may be: (1) the sediment discharge hydrograph, (2) the known stage, or (3) the known bed elevation at the controlled boundary section. This method was used by Cunge and Perdreau (1973), Chen and Simons (1974), and Mahmood and Ponce (1976) to study sediment movement in open channels by approximating the actual discharge hydrograph using a step function (e.g., A-B-C-D in Figure 11-2). Owens (1977) modified the method of approximating the hydrograph with a view to better simulate the unsteady flow effect (e.g., E-f in Figure 11-2).

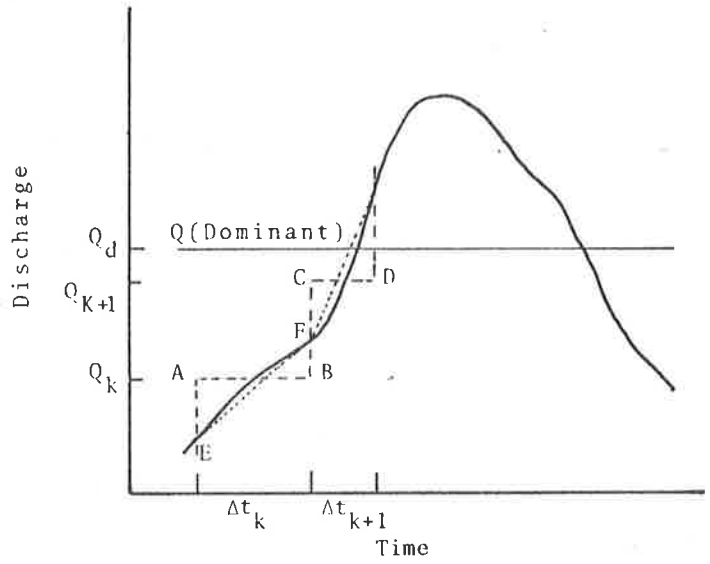

Figure 11.2 Simulation of unsteady flow hydrograph.

Uncoupled Steady Solution

Let it be assumed that the effects of changes in A_d and S_o on the flow conditions within a time step are negligible. Also, let it be assumed that the flow is quasi-steady for the geomorphic computations and the flow discharge in a channel reach is know. Then the solution

of Equations 11-1, 11-2, and 11-3 can be approximated by solving Equation 11-3 for a given known discharge to compute the water surface profile, and then solve Equation 11-1 uncoupled to determine sediment movement. This approximation has been used by Chang and Hill (1976), the Army Corps of Engineers (1976), and recently by Li (1977). More detail will be presented in Chapter 12.

Discussion of the Four Types of Numerical Solution Methods

The four types of methods can be categorized into two groups: coupled method (complete solution and known discharge solution) and uncoupled method (unsteady solution and steady solution). The advantage of the coupled method is its better consideration of the continuous interaction of the hydraulic and sediment transport phases than the uncoupled method. This clearly makes better physical sense. Also, the coupled method can generally be used with a longer time increment. However, the formulation of the complete solution method is the most complex one among the four methods. The known-discharge solution is developed solely for sediment routing.

The uncoupled method is simpler to formulate than the coupled method. However, in the uncoupled solutions, the length of a time increment is restricted in that the bed elevation changes over one time increment must be so small that they do not significantly affect the solution of the hydraulic variables that have been determined in the first step of the uncoupled procedure. Also, the sediment routing scheme is an explicit scheme which has a stability limitation of time increment. The stability criteria will be discussed in a forthcoming section "Stability and Accuracy."

Since the numerical testing and comparison of coupled and uncoupled solutions are not well known, it is suggested that for a stable channel where the channel changes are very mild, the uncoupled method can be applied. In this case, the uncoupled-unsteady method can be used for water and sediment routing. For sediment routing only, the uncoupled-steady method can be used.

If the channel is quite active, the coupled method is preferable. For both water and sediment routing, the complete solution method is desirable, while the known discharge solution can be utilized when only the sediment routing is interested.

Sediment Distribution Function

The erosion and/or deposition on a channel cross section is a two-dimensional process. The one-dimensional mathematical model can only compute cross-sectional area changes but not specifically the changes in cross-sectional shapes. It is necessary to properly distribute the computed area changes over each cross section in order to obtain realistic changes in bed elevations. Several researchers (e.g., Chen, 1973; the Corps of Engineers, 1976) assumed a uniform distribution of bed changes. In some cases this assumption is not adequate. To improve the accuracy of the sediment routing model some nonuniform distributions of scour or deposition on the bed have been developed.

Chang and Hill (1976) distributed the area changes according to the effective shear stress $\tau-\tau_c$ where τ is the actual bed shear and τ_c is the shear stress at incipient motion of the bed material. If over a time increment their uncoupled-steady solution indicates scour, the scour depth in each subsection is calculated using the following formula:

$$\Delta z_{ki} = \frac{(\tau-\tau_c)_{ki}}{\sum_{k=1}^{M} (\tau-\tau_c)_{ki} T_{ki}} \Delta A_{d_i} \qquad (11\text{-}46)$$

where ΔA_{d_i} is the scoured area, M is the number of subsections in Section i, and Δz_{ki}, $(\tau-\tau_c)_{ki}$, and T_{ki} are the bed elevation change, effective shear stress and top width of subsection k at Section i, respectively (see Figure 8.2). If the computed results indicate deposition, the sediment is assumed to deposit on horizontal layers in the lower part(s) of the cross section. It should be emphasized that this scheme for distributing the bed elevation change is not based on an empirical or theoretical law, but instead on the author's experience and knowledge. The model was able to reproduce fairly well the scour and deposition measured in a flooded prototype drainage canal.

To further simplify the sediment distribution process, it appears to be feasible to use a single relation to distribute both the erosion and deposition. Owens (1977) suggested the use of the following simplified relation:

$$\frac{\Delta A_{d_{ki}}}{\Delta A_{d_i}} = \left(\frac{K_{ki}}{\Sigma K_{ki}}\right)^M \qquad (11\text{-}47)$$

where M is a constant exponent and K_{ki} is the conveyance of subsection k at Section i defined by Equation 8-5. The validity of this simplified method was checked preliminarily by field data from Greenwood Bend in the Yazoo River. It is found that this method is valid in a river reach where the channel alignment is reasonably smooth (see Figure 11-3). If the river reach encounters an abrupt change in channel alignment such as the presence of dikes, then both scour and deposition could occur simultaneously in different subsections at a given cross section. In this case, the suggested simplified method is not valid.

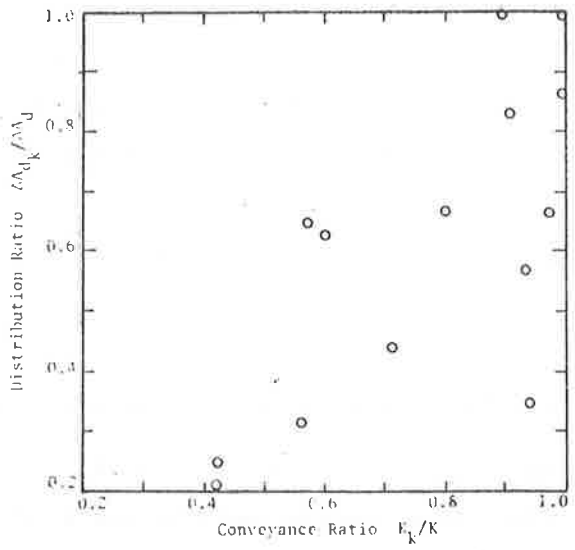

Figure 11.3 Verification of the simplified sediment distribution function using the field data in Greenwood Bend.

Exterior Boundary Conditions

The exterior boundary conditions are usually of five kinds: (1) the stage hydrograph; (2) the water discharge hydrograph; (3) the sediment discharge hydrograph; (4) the depth-discharge rating curve; and (5) the known bed elevations at a controlled boundary section. Conditions (1), (2), and (4) are for water routing, while conditions (3) and (5) are for sediment routing. In general, two boundary conditions are required for water routing and one condition is required for sediment routing. The required boundary conditions for water routing has been described in detail in Chapter 8.

For a sediment discharge hydrograph $Q_s = f(t)$, a linearization process is imposed to linearize the known sediment discharge inflow to a form of Equation 11-14 as follows:

$$Q_s^{j+1} = Q_s^j + (\frac{\partial Q_s}{\partial Q})^j (Q^{j+1} - Q^j) + (\frac{\partial Q_s}{\partial y})^j (y^{j+1} - y^j)$$

$$+ (\frac{\partial Q_s}{\partial z})^j (z^{j+1} - z^j) = f(t^{j+1}) \qquad (11\text{-}48)$$

Equation 11-48 can be rearranged as

$$(\frac{\partial Q_s}{\partial Q})^j Q^{j+1} + (\frac{\partial Q_s}{\partial y})^j y^{j+1} + (\frac{\partial Q_s}{\partial z})^j z^{j+1} = f(t^{j+1})$$

$$- Q_s^j + (\frac{\partial Q_s}{\partial Q} Q)^j + (\frac{\partial Q_s}{\partial y} y)^j + (\frac{\partial Q_s}{\partial z} z^j) \qquad (11\text{-}49)$$

where the superscripts j and $j+1$ indicate that the variables are evaluated at the time t^j and t^{j+1}, respectively. Those variables evaluated at time t^j are all known. Comparing Equation 11-14 with Equation 11-49, the coefficients in Equation 11-14 can be formulated.

Equation 11-49 is used in the coupled method (i.e., complete solution and known discharge solution). For the uncoupled method, the original sediment discharge hydrograph is used for sediment routing. In summary, for a subcritical flow, the complete solution method requires two upstream boundary conditions (on water and sediment, respectively) and one downstream boundary condition (on water). For uncoupled-unsteady method, one upstream and one downstream boundary condition is required for water routing. A boundary condition related to sediment is then used to route sediment. For known-discharge method, the inflow water discharge hydrograph is used to determine the water discharge in the study reach. Then an upstream boundary condition (on sediment) and a downstream boundary condition (on water) are used for the coupled sediment routing. Finally, for the uncoupled-steady method, again the inflow water discharge hydrograph is used to determine the water discharge in the study reach. Then a downstream boundary condition (on water) is used to determine the water surface profile for a given discharge. Thereafter, a boundary condition related to sediment is used for sediment routing.

Interior Boundary Conditions

The coupled solution for water and sediment routing with interior boundaries becomes quite complicated. In this case, the uncoupled solution method is usually utilized. The interior boundary condition for water routing has been described in Chapter 8. In this section, only the sediment routing conditions are presented. The sediment continuity Equation 11-1 is discretized using a backward finite-difference approximation as

$$\Delta A_{d_i} = \frac{\Delta t}{2p} \left[q_{s_{i-(\frac{1}{2})}}^{j} + q_{s_{i-(\frac{1}{2})}}^{j+1} \right] - \frac{1}{\Delta x} \left[(Q_{s_i}^{j} - Q_{s_{i-1}}^{j}) + (Q_{s_i}^{j+1} - Q_{s_{i-1}}^{j+1}) \right] \quad (11\text{-}50)$$

When the sediment discharge Q_s is computed from a sediment transport function by substituting the hydraulic conditions determined from the water routing, the bed area changes can be determined from Equation 11-50.

1) Junction of two rivers. At a confluence as shown in Figure 11.4, where two channels join together, the sediment inflow at the upstream section of a reach $Q_{s_{i-1}}$ is replaced by the sum of $Q_{s_{k1}}$ and $Q_{s_{k2}}$ and Δx is replaced by the sum of Δx_{13} the distance between Sections k_1 and k3 and the distance between Section k2 and k3 Δx_{23}. Then the value of $\Delta A_{d_{k3}}$ can be determined from Equation 11-50. For the case shown in Figure 11-4b where a channel splits into two separate channels, the division of sediment discharge is assumed to be proportional to the water discharge ratio multiplied by a correction factor. That is for the branched channel k_1,

$$Q_{s_{i-1}} = \alpha \frac{Q_{k1}}{Q_{k3}} Q_{s_{k3}} \quad (11\text{-}51)$$

where α is a correction factor, and for channel k_2,

$$Q_{s_{i-1}} = Q_{s_{k3}} \left(1 - \alpha \frac{Q_{k1}}{Q_{k3}}\right) \quad (11\text{-}52)$$

Substituting Equations 11-51 and 11-52 into Equation 11-50, then $\Delta A_{d_{k1}}$ and $\Delta A_{d_{k2}}$ can be determined.

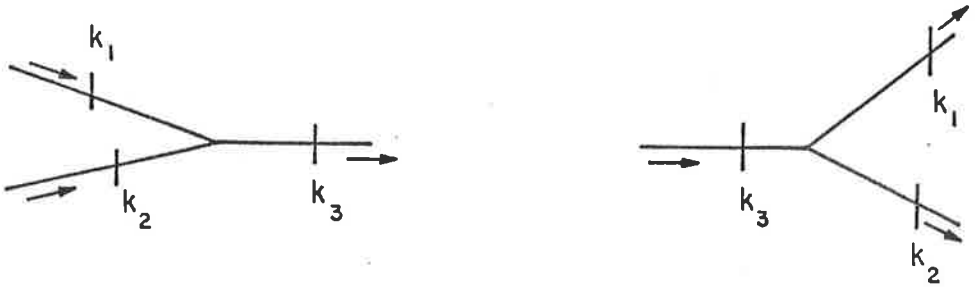

a. k_3 (−) b. k_3 (+)

Figure 11.4 Computer program notation for the confluence equations.

2) Flow over a weir or through a control gate. The sediment concentration distribution upstream of the dam is assumed to follow an equilibrium, O'Brien-Christiansen distribution (O'Brien, 1933)

$$C_\xi = C_a \exp(-\omega \int_a^\xi \frac{d\xi}{\varepsilon_s}) \tag{11-53}$$

where C_a is a concentration of sediment with fall velocity ω at level $\xi = a$ above the bed, and ε_s is mass transfer coefficient (see Figure 11-5). By assuming a constant eddy coefficient,

$$\varepsilon_s = \bar{\varepsilon}_s = \frac{1}{15} U_* y \tag{11-54}$$

where U_* is the shear velocity and y is the depth. The vertical sediment concentration at an elevation ξ above the riverbed is then

$$C_\xi = C_a \exp[-\frac{15\omega}{U_*} \frac{\xi - a}{y}] \tag{11-55}$$

The mean sediment concentration over the dam is

$$\bar{C} = \frac{C_o}{y - z_d} \int_{z_d}^{y} \exp\left[-\frac{15\omega}{U_*} \frac{\xi - a}{y}\right] d\xi$$

$$= \frac{C_o}{y - z_d} \left\{ -\frac{U_* y}{15\omega} \left[\exp(-\frac{15\omega}{U_*}) - \exp(-\frac{15\omega}{U_*} \frac{z_d}{y})\right] \right\} \tag{11-56}$$

where C_o is the sediment concentration on the riverbed and z_d is the elevation of dam crest. The value of C_o can be determined from

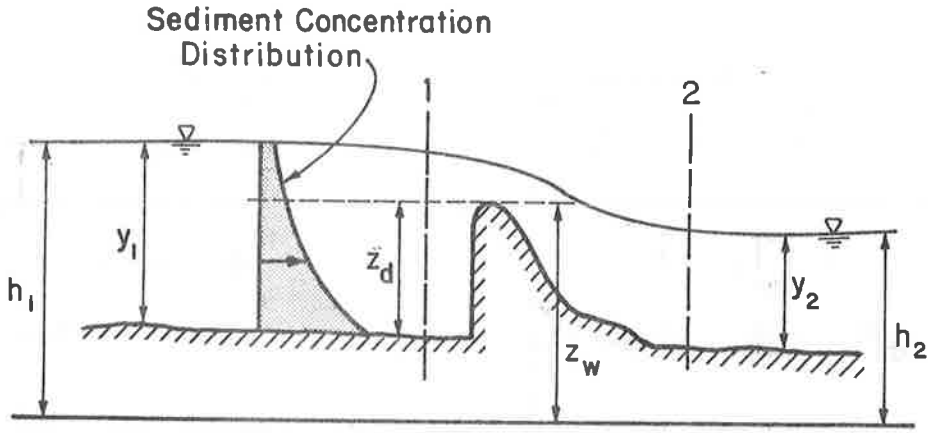

Figure 11.5 Sediment-laden water over a weir.

$$C_o = \frac{15\ C_s \omega}{[1-\exp\ (-\frac{15\omega}{U_*})]\ U_*} \tag{11-57}$$

where C_s is the mean sediment concentration over the cross section and can be determined from the sediment transport function applicable to the study reach. The sediment discharge over the closing dam is then

$$Q_s = Q\ \bar{C} \tag{11-58}$$

This sediment discharge can be substituted for $Q_{s_{i-1}}$ into Equation 11-50 to determine the bed area change immediately below dam.

Sediment Sorting

Studies of river bed material have shown that the size of particles forming the bed of rivers gradually decrease in size in the downstream direction. The principal causes of particle size reduction are abrasion of the particles, hydraulic sorting, and chemical weathering. A size reduction relationship is usually expressed as an exponential function such as:

$$D = D_o\ e^{-\alpha L} \tag{11-59}$$

in which D represents the size of particles at some distance L downstream of a reference station, D_o is the size of bed material at the reference station, and α is the sorting coefficient.

In a sand bed river, the bed material has a similar transport mode and the sediment movement can be simulated by routing bed materials of a representative size. However, in a gravel river with a high percentage of sand, the transport modes of bed materials are significantly different. Also, the bed material size distribution in a river may be changed by construction of hydraulic structures such as dikes, dams, etc., and in turn affects the sediment transport and river stability. To better assess the geomorphic changes under these conditions, the sediment routing can be conducted for each individual size fraction. It means that the sediment transport function for each individual size must be obtained. Then by applying the sediment continuity equation repeatedly to each sediment fraction, the riverbed changes can be obtained. The total change is equal to the sum of values obtained per each fraction.

Since the bed material changes as sediment moves and the transport capacity for a given size depends on the fraction of bed material composed of that size, it is required to recalculate the bed material size distributions in the routing process if these distributions change significantly. There are a number of methods for determining the new size fractions such as those proposed by U.S. Army Corps of Engineers (1976), Lopez (1978), Hales et al. (1970). More detail will be given in Chapter 18.

Stability and Accuracy

The stability and accuracy of the water routing method has been described in Chapter 8. The coupled methods of water and sediment routing are unconditionally stable. However the uncoupled methods which use an explicit finite difference approximation of the sediment continuity equation, should satisfy the Courant criterion to insure the stability of the scheme. The value of $\Delta x/\Delta t$ should be larger than the riverbed wave celerity. Lopez (1978) provided a procedure to determine this bed wave celerity.

Consider a simplified form of the sediment continuity equation:

$$\frac{\partial Q_s}{\partial x} + \frac{\partial A_d}{\partial t} = 0 \qquad (11\text{-}60)$$

in which the lateral flow and the variation of suspended sediment concentration with time have been neglected.

Assuming that A_d is a unique function of Q_s we can write:

$$\frac{\partial A_d}{\partial t} = \frac{dA_d}{dQ_s} \frac{\partial Q_s}{\partial t} \tag{11-61}$$

Substituting Equation 11-61 into Equation 11-60:

$$\frac{dQ_s}{dA_d} \frac{\partial Q_s}{\partial x} + \frac{\partial Q_s}{\partial t} = 0 \tag{11-62}$$

which is a nonlinear equation since dQ_s/dA_d is itself a function of Q_s.

The celerity of bed waves can be represented by

$$\frac{dx}{dt} = \frac{dQ_s}{dA_d} \tag{11-63}$$

which describes a positive characteristic direction in the x-t plane indicating that any perturbation on the bed can only be propagated downstream.

An expression for the celerity can be obtained by assuming that the sediment discharge is a power function of the velocity

$$Q_s = mV^n \, T \simeq m \frac{Q^n}{(h-z)^n} T^{1-n} \tag{11-64}$$

in which T is the cross-section top width, D is the hydraulic depth, and m and n are constants which can be obtained by calibration or from the available equilibrium data. Its derivative with respect to z is

$$\frac{\partial Q_s}{\partial z} \simeq mV^n \, T \frac{n}{y} = \frac{nQ_s}{y} \tag{11-65}$$

where it was assumed that $\partial Q/\partial z = \partial h/\partial z = \partial T/\partial z = 0$. Since

$$\frac{\partial Q_s}{\partial A_d} = \frac{1}{T} \frac{\partial Q_s}{\partial z} \tag{11-66}$$

we have

$$\frac{\partial Q_s}{\partial A_d} \simeq \frac{nQ_s}{Ty} \tag{11-67}$$

Equation 11-67 gives the celerity of the small bed waves indicating that it is proportional to the sediment discharge Q_s and inversely proportional to the flow depth y.

Equation 11-67 is adjusted by carrying out some test runs with the numerical model. A bed wave of trapezoidal shape was imposed as initial condition on the channel bed and its velocity of propagation was determined for different initial flow conditions. It was found that the model celerity c_m and the theoretical celerity c_c computed from Equation 11-67 have a relation: $c_m = 2.33\ c_c^{0.96}$. Equation 11-67 then takes the form:

$$c_m = 2.33\ \left(\frac{nQ_s}{Ty}\right)^{0.96} \tag{11-68}$$

Application of the Mathematical Model

The procedure of applying the one-dimensional water and sediment model to study river problems follows closely the procedure for water routing described in Chapter 8, except that the sediment transport relations at each computational section and lateral sediment inflows should be provided. During the model calibration, the historical cross-sectional area and bed elevation changes and sediment load discharges should be reproduced by altering the sediment transport relations. Also, it may be advantageous to input the original cross-sectional geometries of the computational sections in the model. In this way, the cross-sectional geometries and conveyances can be determined directly from the cross-sectional properties. Then the computed cross-sectional changes can be distributed on the cross-sectional points using a sediment distribution function similar to Equation 11-47. However, if the number of the computational sections is large, this method becomes tedious and time consuming. A combination of this method for computing Δz and tabulated or fitted relations for computing A, T, and K may be a good alternative.

Sand Wave Propagation in a Laboratory Flume (Chen and Simons, 1974). An experiment was conducted in a 1.961-ft wide and 60-ft long flume to study the mechanics of degradation

and aggredation. The experiment was started from the condition of incipient motion with a constant water discharge of 0.5 cfs. Sediment was supplied at the upstream end of the flume at a constant rate of 0.0337 lb/sec to cause aggradation. A mathematical model was constructed using the flow and flume characteristics to simulate the propagation of the sand wave.

The supplementary relations derived for the mathematical model were:

1. The geometric properties of cross section are
   $T = \partial A/\partial y = B = 1.961$ ft and $A = Ty$.
2. The Manning's equation is employed to evaluate the friction slope with the Manning's roughness coefficient equal to 0.0185.
3. The sediment discharge is calculated from

$$c_s = KV^m y^n \tag{11-69}$$

   and

$$Q_s = C_s Q \tag{11-70}$$

   in which $K = 0.0000302$, $m = 3$, and $n = -1$ are so chosen that the calculated results closely fit the measured data.
4. The sediment volume ratio p is found to be 0.59.

The complete solution method and the known discharge model were applied to simulate the propagation of sand wave in the flume. The calculated bed elevations for upstream boundary conditions of $Q = 0.5$ cfs and $Q_s = 0.0337$ lb/sec and downstream boundary condition of $h = 0.939$ ft are plotted on Figure 11.6 and are compared with the measured values. The calculated results are in good agreement with the measured bed elevations especially near the wave front. This indicates that the mathematical model is useful to study sediment transport phenomena.

11.3 ONE-DIMENSIONAL SEDIMENT ROUTING MODEL OF A RIVER NETWORK SYSTEM

Model Procedure

Water and sediment movement in rivers and estuaries with branches, loops and confluences is complicated by the flow division among the junctions and tidal effects from downstream. The water routing model of a river network system descirbed in Section 8.3 can be used to determine the water wave propagation in a river network. This water routing model can be combined with the sediment continuity equation discretized at a junction (Equations 11-50 through 11-52) to study water and sediment

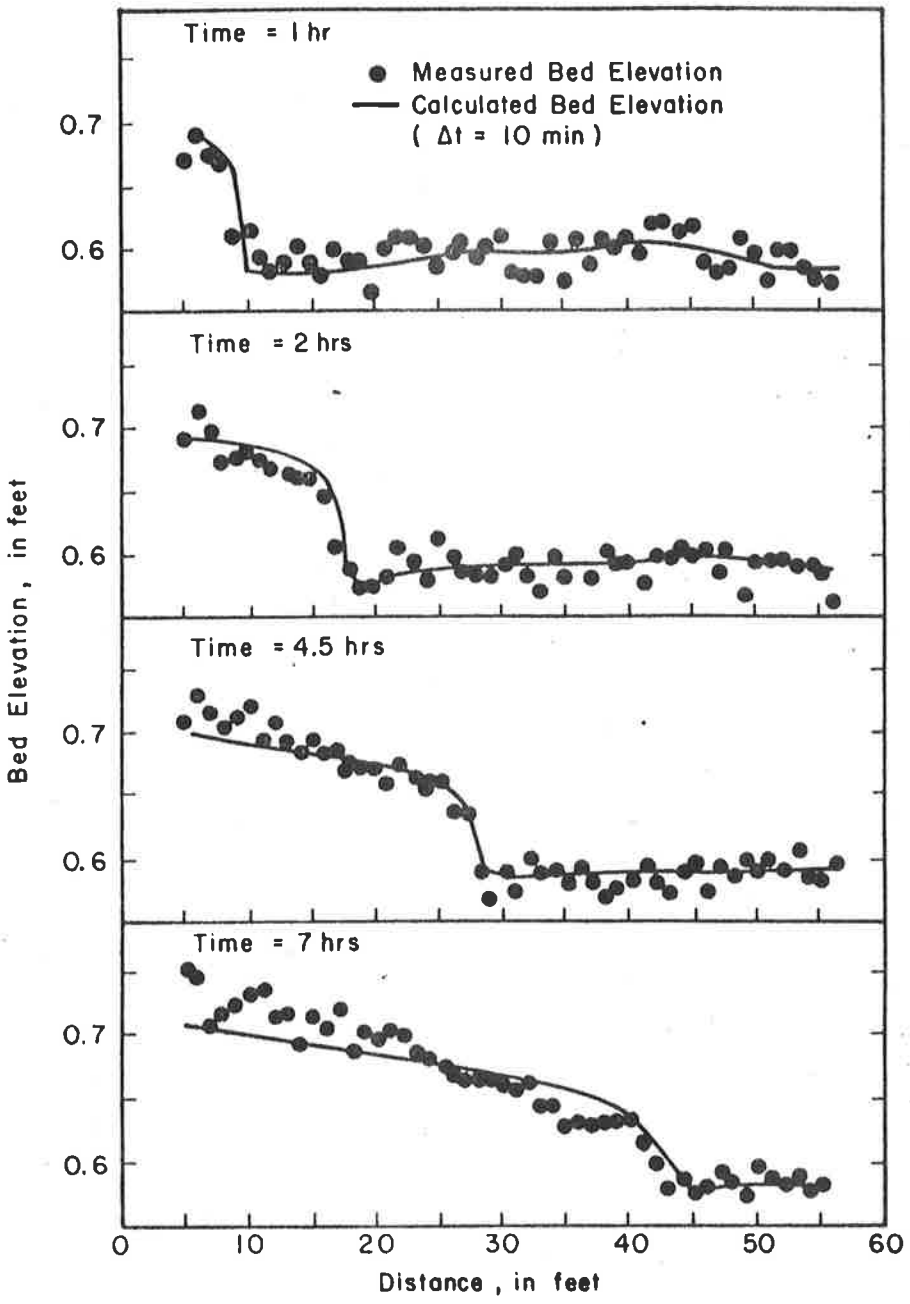

Figure 11.6 Propagation of sand wave in a rectangular flume.

related problems in a river network system. The application of this water and sediment routing model is described in the following application example.

Water and Sediment Routing of the Chippewa River Network System

Description of the Study Reach and Objective of the Study (Simons and Chen, 1979)

Erosion and sedimentation have long been recognized as severe problems along the Chippewa River, especially in the lower reaches below Eau Claire (Figure 11.7). River banks composed of sand and fine gravel are being eroded and transported by the Chippewa flow, resulting in some loss of floodplain. Much of the sediment is ultimately transported to the Mississippi River, its side channels and backwater areas. The amount of sediment delivered exceeds the transport capacity of the Mississippi River, causing aggradation and affecting river environment. It is necessary to periodically dredge the deposits of excess sediment from the Mississippi River to provide adequate water depth for navigation.

To reduce the erosion and sedimentation in the Chippewa River and associated problems in the Upper Mississippi River system a one-dimensional mathematical model was developed for analyzing hydraulics, sediment transport and river morphology to access the impacts of various alternatives on the physical environment of the Lower Chippewa River and Pool 4 in the Upper Mississippi River.

Construction and Calibration of the Mathematical Model

The mathematical model of the river system being studied includes the Lower Chippewa River from Eau Claire (mile 55.7) to the mouth of the Chippewa River (confluence with the Upper Mississippi River). The river reach was divided into 50 sections with space increments ranging from 0.1 miles near channel junctions to 3.1 miles near Eau Claire. The locations of these sections are shown in Figure 11-8. Using the available data including the discharge hydrographs, stage hydrographs, hydrographic survey maps, dredging data and sediment data including bed material size distributions, suspended load and bed load, the following supplemental relations were evaluated at all 50 sections in the modeled river reach:

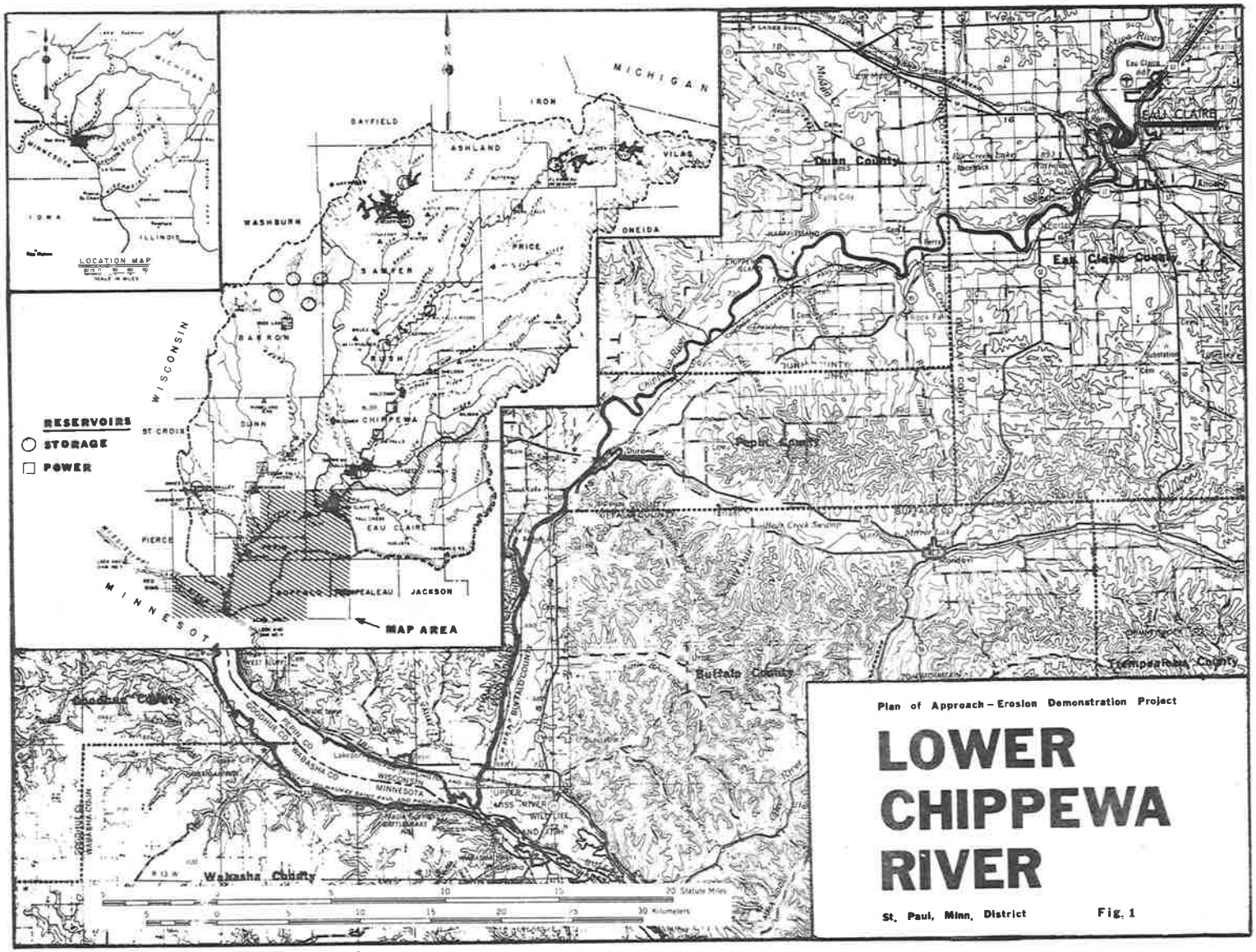

Figure 11.7 Pool 4 in the Upper Mississippi River and the Lower Chippewa River.

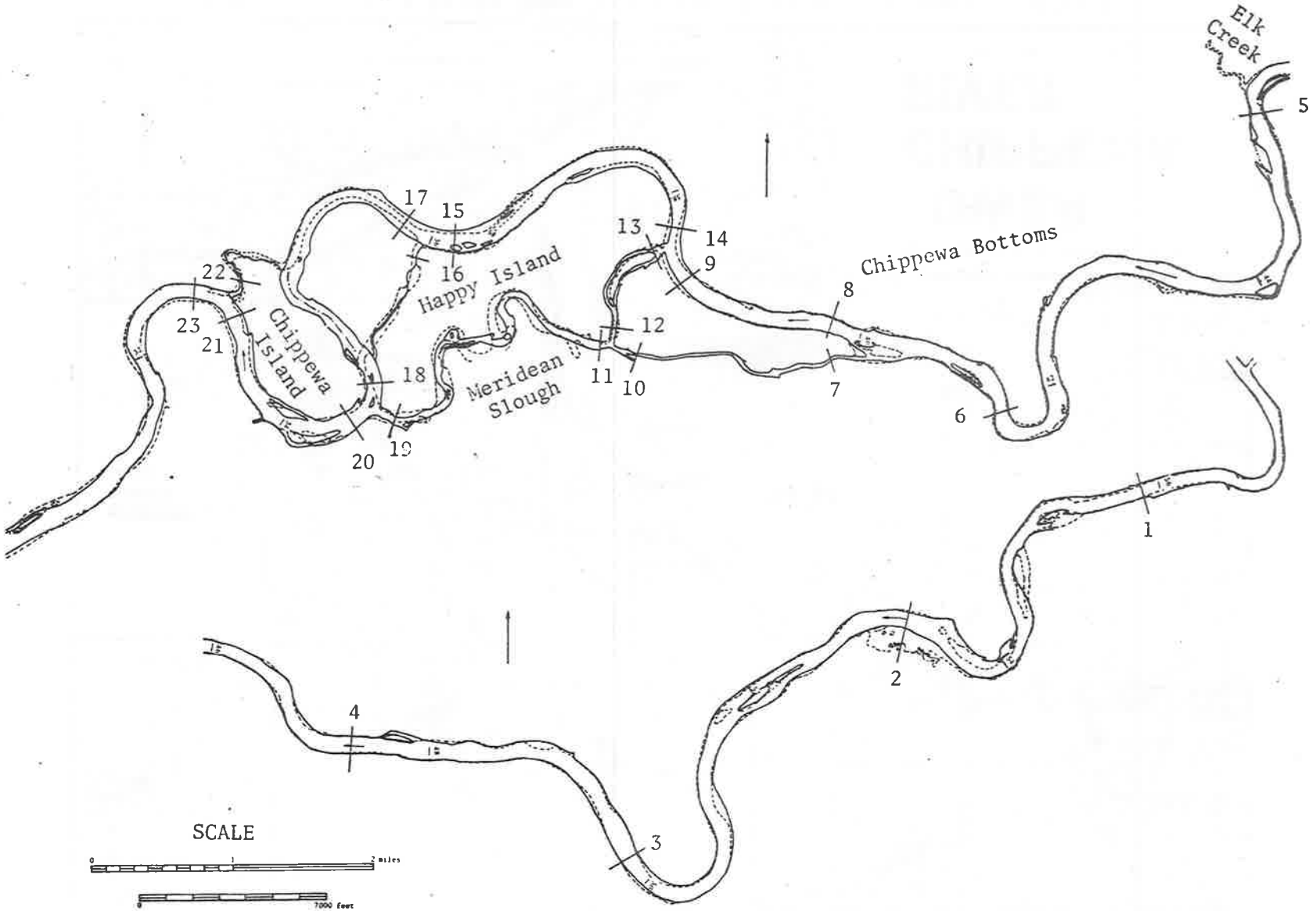

Figure 11.8 Index map of the Lower Chippewa River model.

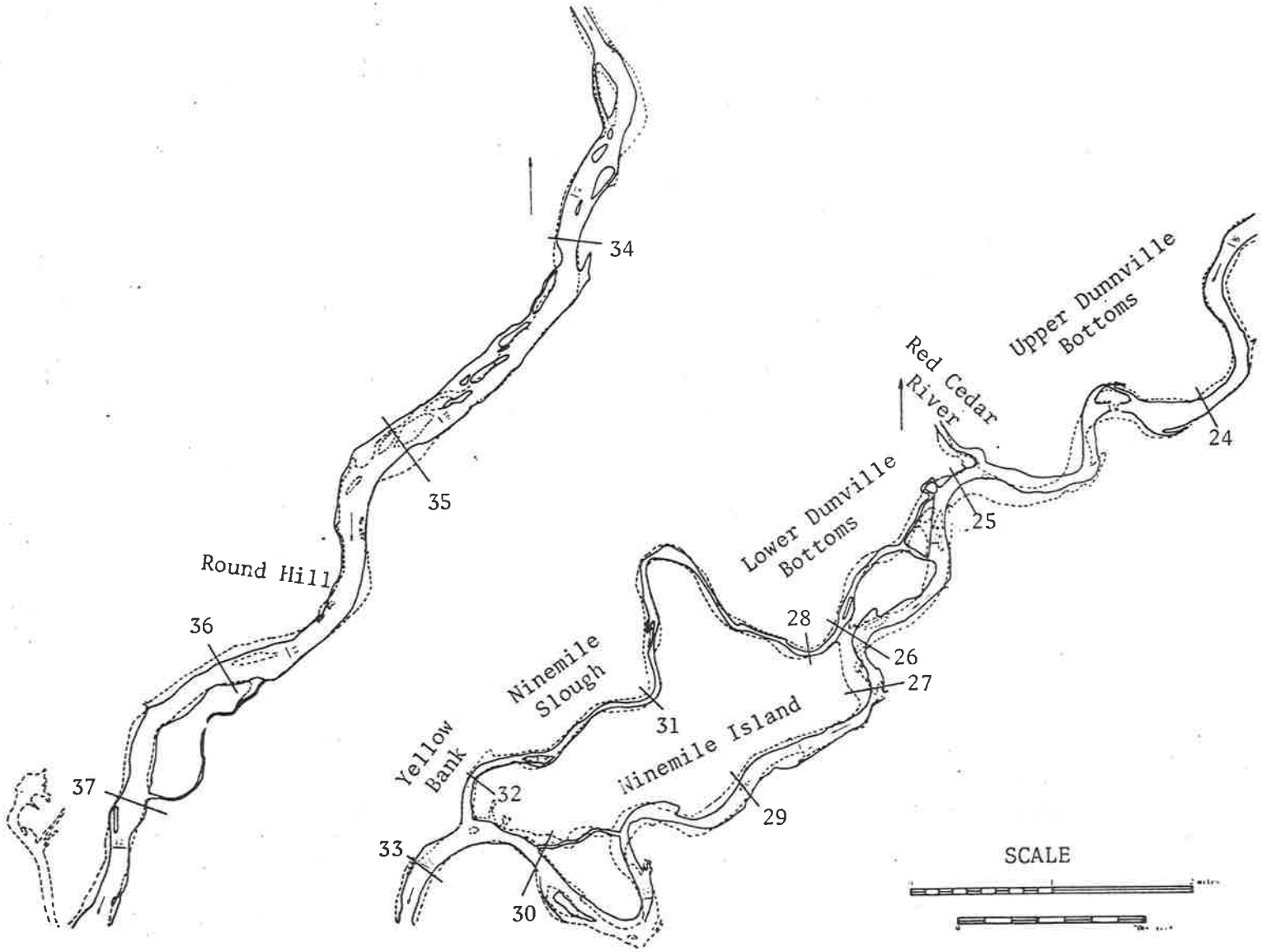

Figure 11.8 (continued)

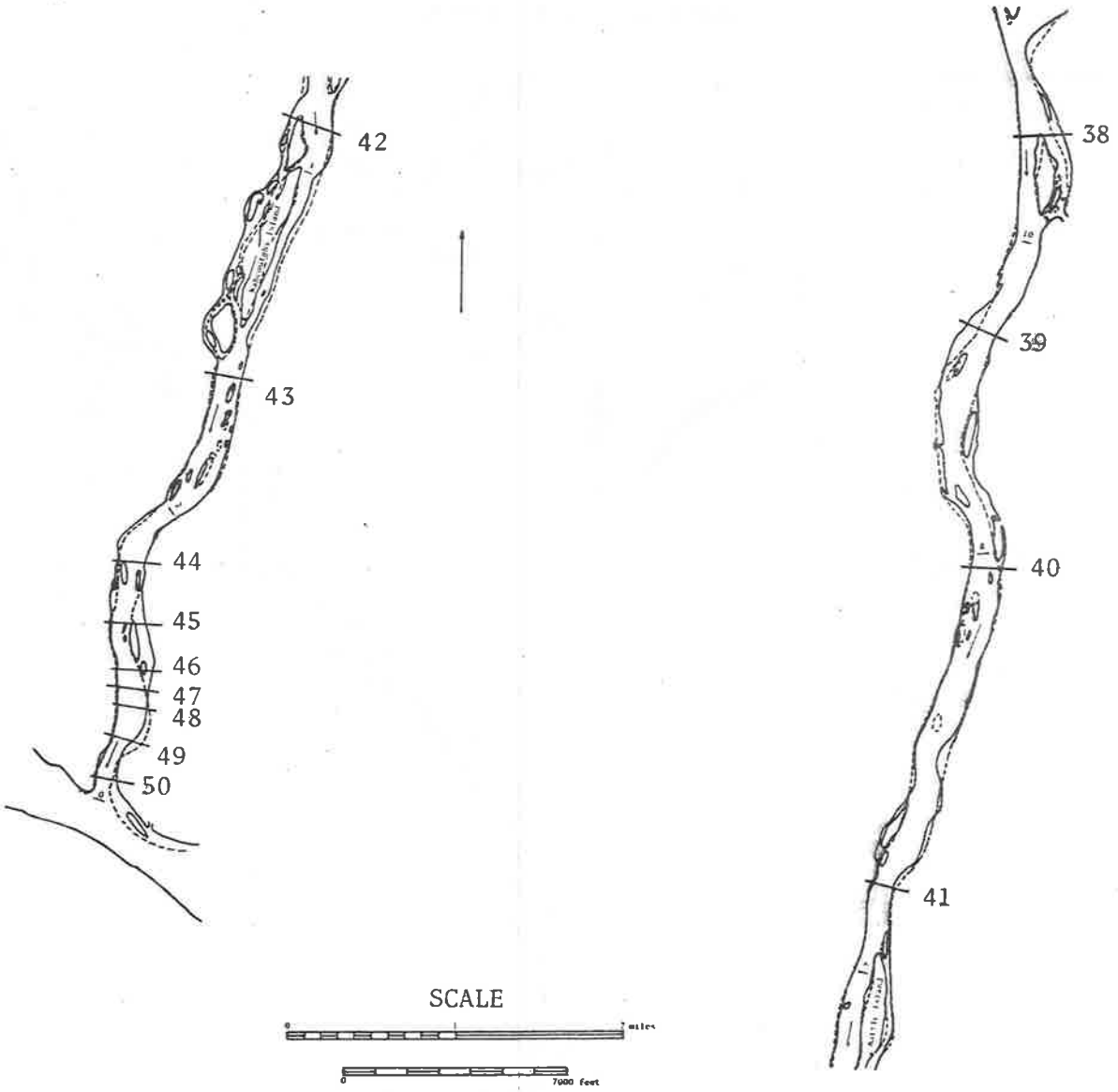

Figure 11.8 (continued)

1) The cross-sectional shapes of the river sections were obtained from the hydrographical surveys. These shapes were digitized and input to the computer program. Then the cross-sectional areas, top widths, hydraulic depths were computed in the computer program.

2) Manning's equation was employed to relate the friction slope to the flow and channel characteristics. Manning's roughness coefficients were determined from the steady water surface profiles for given discharges, where the stage-discharge relationships were assessed from the stage and the discharge hydrographs measured or computed at the gaging stations in the river reach being studied. In general Manning's coefficients decrease with increase in discharges. Their values vary from 0.060 with low flow to 0.028 with high flow.

3) Sediment discharge is related to the flow and channel characteristics by a sediment transport function. By fitting the available data at Caryville, Durand and near Pepin and applying Toffalleti's (1969) and Yang's (1973) methods for a medium sediment size of 0.53 mm, the following relation was established:

$$C_s = a_1 \left[\left(\frac{V}{\omega} - a_2\right) S_f\right]^{a_3} \qquad (11\text{-}71)$$

where C_s = mean concentration of bed-material load on a volume basis, obtained by rearranging and converting Yang's equation a_1 = empirical coefficient equal to 0.0314 to 0.0419, ω = fall velocity equal to 0.23 ft/sec, S_f = energy slope, $a_2 = V_{cr}/\omega = 2.4$, where V_{cr} is the critical velocity at which incipient motion of particles occurs, and a_3 = empirical exponent equal to 1.25. Equation 11-71 obtained an estimate of about 500,000 tons per year of sediment load in the Lower Chippewa River in an average year.

4) The lateral water inflow $(q_\ell \Delta x)$ between Sections 24 and 25 was equal to the inflow discharge from the Red Cedar River measured at Menomonie, Wisconsin. The lateral flows q_ℓ entering the other reaches were assumed negligible. The lateral sediment inflow in cfs/ft was computed by

$$q_s = 3.31 \times 10^{-7} (q_\ell \Delta x)^{1.62}/\Delta x \qquad (11\text{-}72)$$

This equation was derived using Equation 11-71 for a given cross section

and bed slope in the Red Cedar River. For the lateral outflow, the sediment outflow was assumed equal to zero.

5) The discharge coefficient for closing dams C in Equation 8-30 and 8-31 was evaluated based on the design charts prepared by the USDI Bureau of Reclamation (1973). The relation used for determining C is

C = 3.8 for free flow

C = 7.0 for submerged flow

The sediment discharge over the closing dam was estimated from Equation 11-58 where C_s was determined from Equation 11-71.

When the discharge hydrographs were routed through the modeled river reach, the flow discharge, velocity, water surface and riverbed elevations, sediment discharge, and changes in cross-sectional shapes at each section were calculated for each time step. The size of the time step varied from 6 hours to two days depending on the rate of change in flow discharge. A larger time step was used when the rate of change was small.

The calculated flow discharges, water surface and riverbed elevations and bankfull cross-sectional areas were compared with measured data. Calibrations continued through a number of trials. Efforts were made to modify Manning's roughness coefficients and the empirical coefficients in the sediment transport equation at each section until the known historical changes were reproduced.

The calculated 1965 and 1971 discharge and stage hydrographs are compared with the measured hydrographs in Figures 11.9 through 11.11. These figures show an agreement between the measured and calculated values. Some differences were caused by neglecting ice jam effects in the Chippewa River near Durand, because these effects on geomorphic changes in the study reach were generally small.

To simulate the geomorphic changes in the Chippewa River and the sediment transport from the Chippewa River to the Mississippi River, the model was calibrated to reproduce the filling process of the 1965 dredged cut made in the Chippewa River near the mouth. This dredged cut served as a sediment trap to temporarily reduce the Chippewa sediment inflow to the Mississippi River and thereby to reduce sedimentation

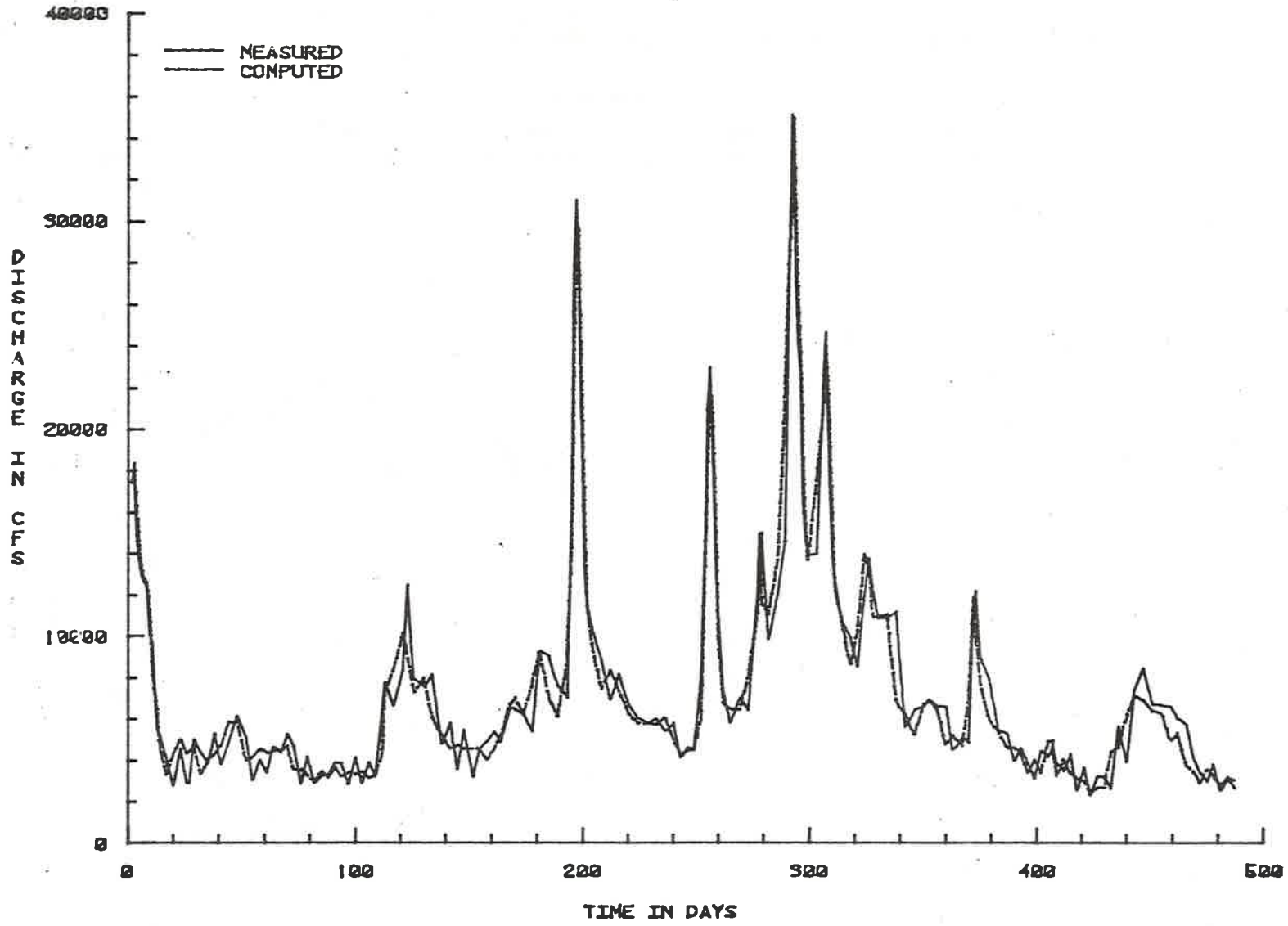

Figure 11.9 Computed and measured discharge in the lower Chippewa River at Durand (Start June 1, 1965).

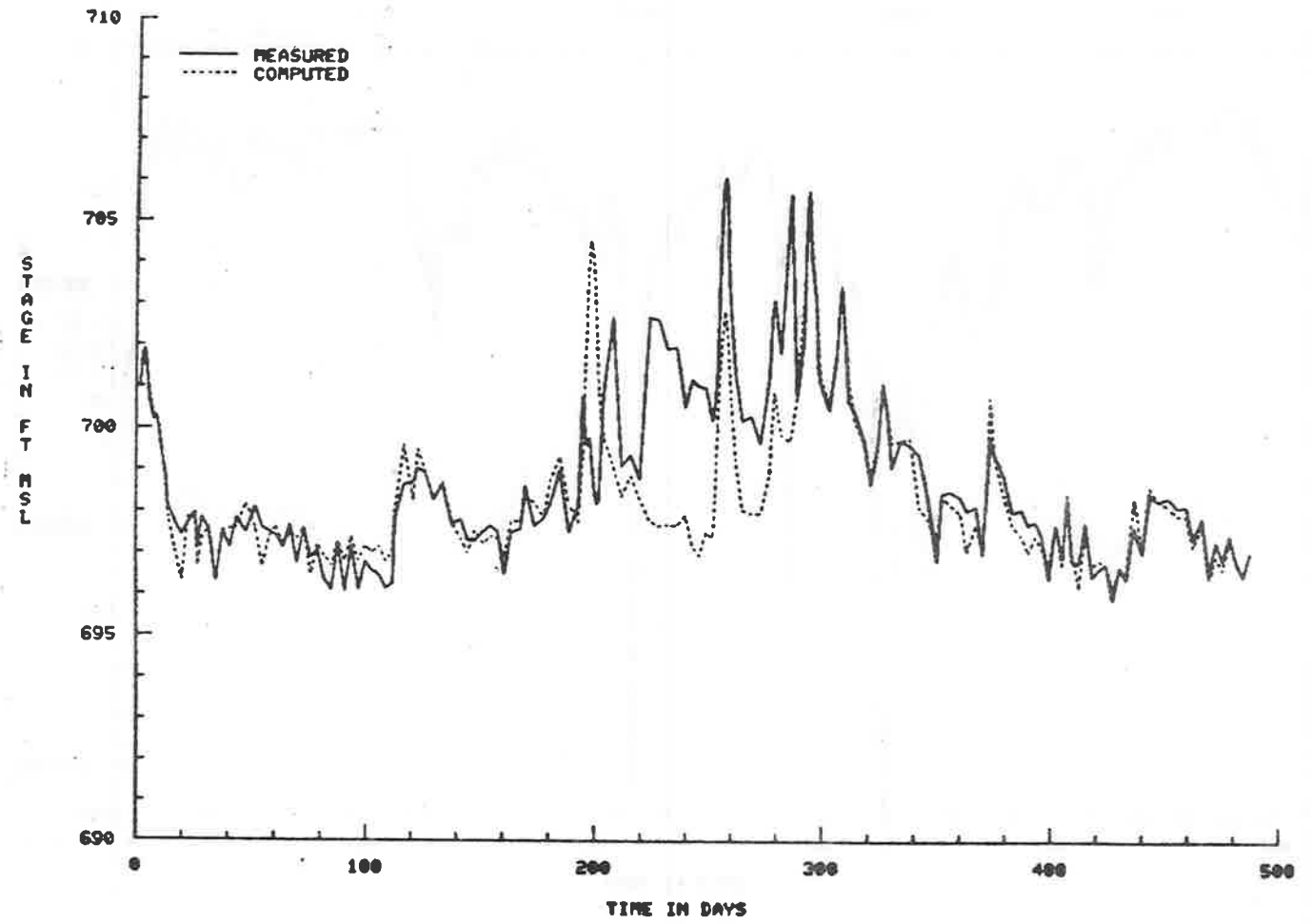

Figure 11.10 Computed and measured stage in the Lower Chippewa River at Durand (Start June 1, 1965).

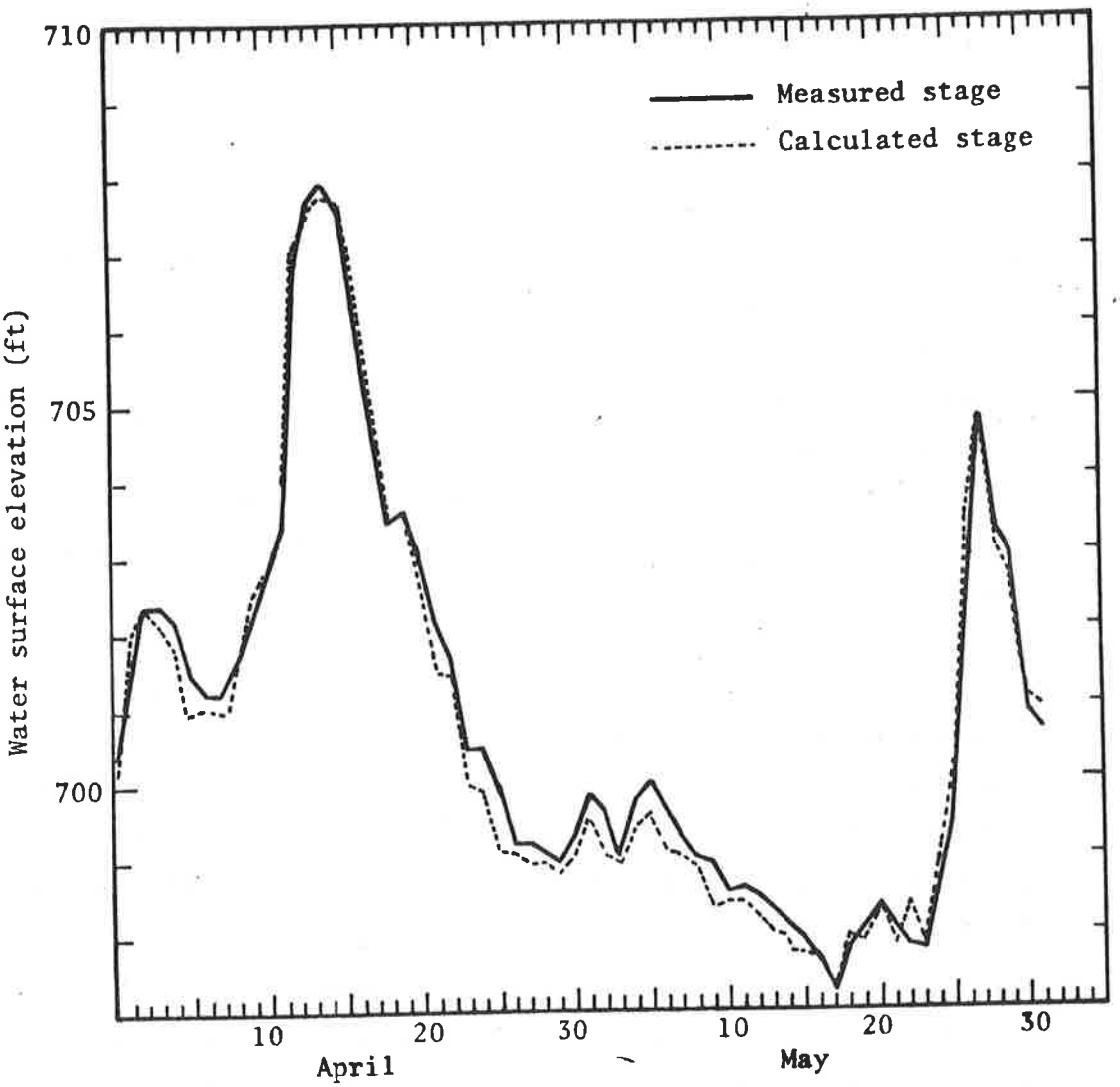

Figure 11.11 Mathematical model reproduction of 1971 stage hydrograph in the Chippewa River at Durand.

problems. Figure 11.12 shows a good agreement between the measured and calculated bankfull cross-sectional areas as well as the mean riverbed elevations (average of the riverbed elevations in the deepest 400 ft width of river channel). This indicates that the modeled Chippewa River can carry adequate sediment load into the Mississippi River and the mathematical model can thus be used to study the effect of changes in the Chippewa geomorphology on the Mississippi River. Also, the changes between cross sections in the branched channel reaches measured in November 1976 and in May 1978 are compared with the calculated results as shown in Table 11.1. The agreement is fair. It should be pointed out that very little water and sediment data in the branched channel reaches are available. A better prediction of the river geomorphic changes in the branched channel reaches can be obtained if additional water and sediment data are available. Since the calculated flow hydraulics and trends of geomorphic changes agree reasonably with the measured values, it was concluded that the mathematical model as calibrated was as good as the available field data and could be employed to study the river's response to future development. To improve the model predictability, the model should be verified and updated whenever additional data are available.

Application of the Chippewa Mathematical Model

The cases studied using the Chippewa network mathematical model to predict physical changes in the next 50 years include:

1) Continue the without-project (natural) condition.

2) Dredge a sedimentation trap at the lower end of the Chippewa River.

3) Construct a low-head dam at the lower end of the Chippewa River.

4) Construct a series of low dams on the Chippewa River Basin.

5) Establish streambank erosion controls on the Chippewa River Basin.

6) Combine the sedimentation trap at the lower end of the Chippewa River with the streambank erosion controls.

7) Combine the low-head dam at the lower end of the Chippewa River with the streambank erosion controls.

Some interesting results are presented. For Simulation (1) without-project condition, a 50-year series of flow was routed through

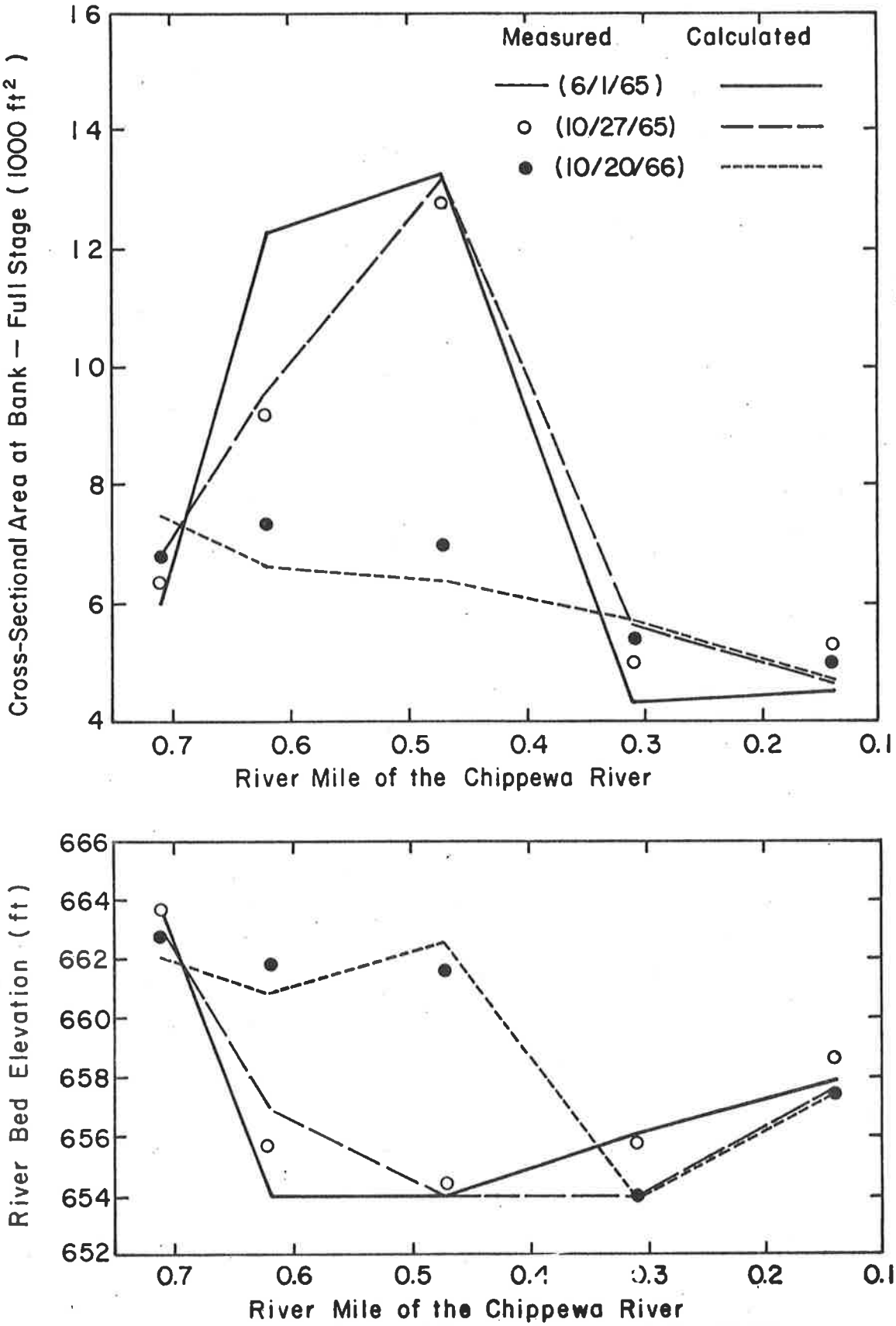

Figure 11.12 Mathematical model reproduction of the filling process of the 1965 dredged cut in the Lower Chippewa River.

Table 11.1 Calibration of model to simulate geometric changes.

Survey Section	River Mile	Model Section (in Figure 11.8)	Bankfull Cross-Sectional Area (ft^2)			Bed Elevation (ft)		
			Nov. 1976	May, 1978 (changes)		Nov. 1976	May, 1978 (changes)	
				Measured	Computed		Measured	Computed
2	20.6	30	5,000	- 100	- 730	697.0	+ 0.5	+ 1.3
		32	3,030	+ 60	- 370	697.0	0.0	+ 0.9
3	23.5	29	4,180	+ 730	+1,090	701.8	- 0.3	- 2.3
		31	2,390	+ 550	+ 400	700.5	- 3.0	- 1.4
9	37.5	11	5,390	- 100	- 190	726.5	0.0	+ 0.4
		14	6,290	- 340	+ 400	725.5	+ 0.3	- 0.6

the model. Because of the increase in channel dimension due to erosion, the sediment inflow from the Chippewa River to the Mississippi River would decrease with time. Figure 11.13 shows the computed reduction of sediment rate with time determined from the mathematical model. For example, the sediment inflow rate would reduce by 10 percent if an annual hydrograph with a recurrence interval of 5 year occurred 10 years later. The overall sediment inflow from the Chippewa River to the Mississippi River would reduce by 12 percent in the next 50 years.

For Simulation (2), the river reach near the lower end of the Chippewa River was dredged to form a sedimentation trap to reduce sediment supply to the Mississippi River. Three dredged cuts having a mean width of 500 ft, a length of 2,100 ft and depths of 3 ft, 6 ft, and 9 ft, respectively, were investigated. It was found that the 3 ft dredged cut was filled up after routing a 2-year annual hydrograph as shown in Figure 11.14. To obtain a generalized relation, the ratios of the weight of the dredged material to the annual sediment loads were plotted against the trap efficiencies of dredged cuts (the ratio of reduced sediment load to the normal annual sediment load). These are shown in Figure 11.15. The figure shows that the annual reduction in the sediment supply from the Chippewa River to the Mississippi River would approximately equal the weight of the dredged material from the sedimentation trap. If the amount of dredged material was larger than the annual sediment load, the dredged cut would be partially filled after a year and the remaining portion could still reduce the sediment supply rate. The sedimentation trap would require redredging periodically to maintain its effectiveness. The reduction in the Chippewa sediment would reduce the dredging requirement in Pool 4 and downstream pools. However, the effect would not occur immediately in the downstream reaches. The elapsed time before the alternatives would become effective can be estimated from Figure 11.16.

Two cases of low-head dams were investigated for Simulation (4). All the dams were designed to block about 50 percent of the bankfull cross-sectional areas. For Case 1 of Simulation (4), three low-head dams were installed at the locations as shown in Figure 11.17. Dam 1 would raise the water surface behind the dam, trapping sediment and reducing the ability of the Chippewa River to erode its banks near the

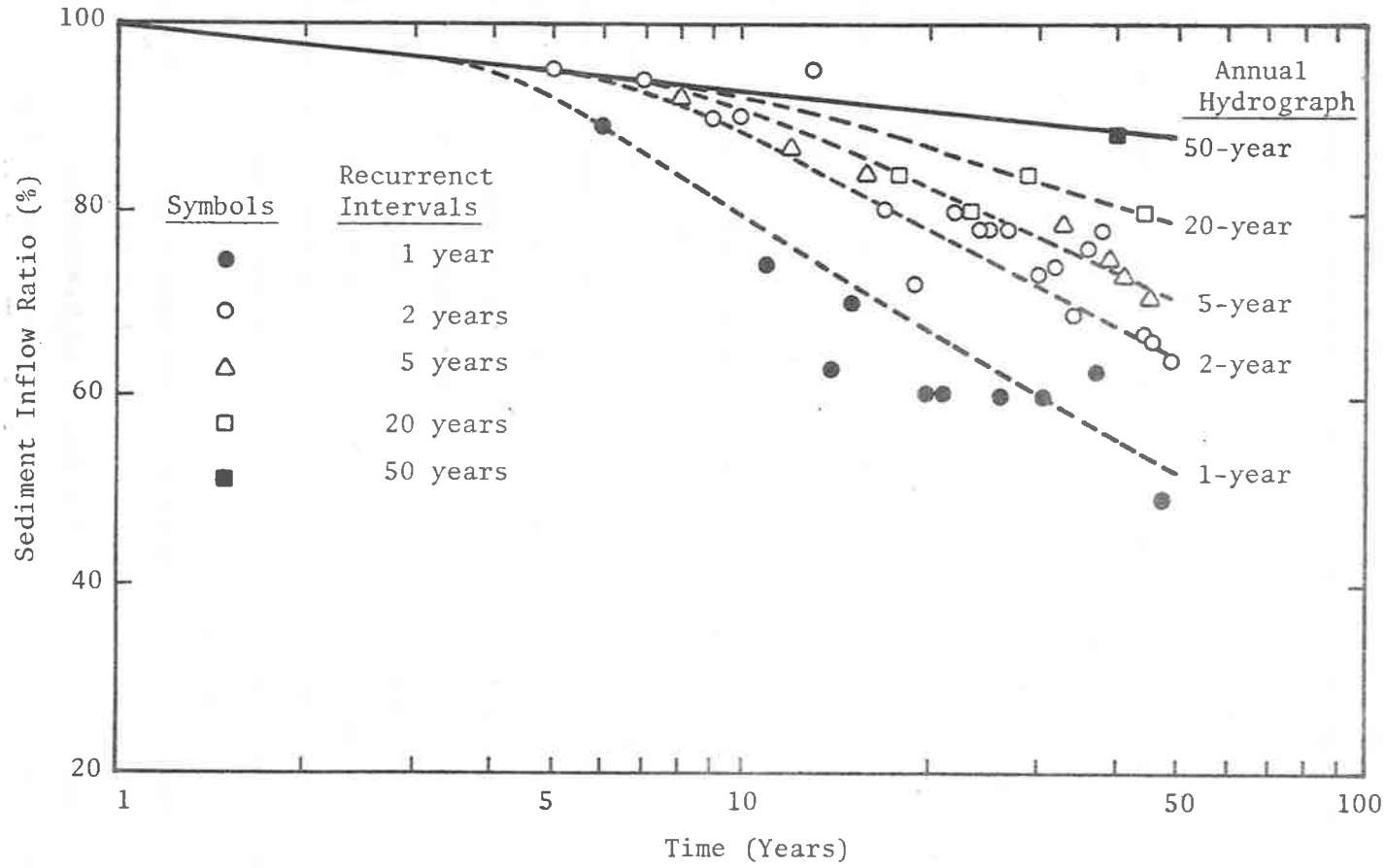

Figure 11.13 Reduction in the sediment inflow from the Chippewa River to the Mississippi River (without project condition).

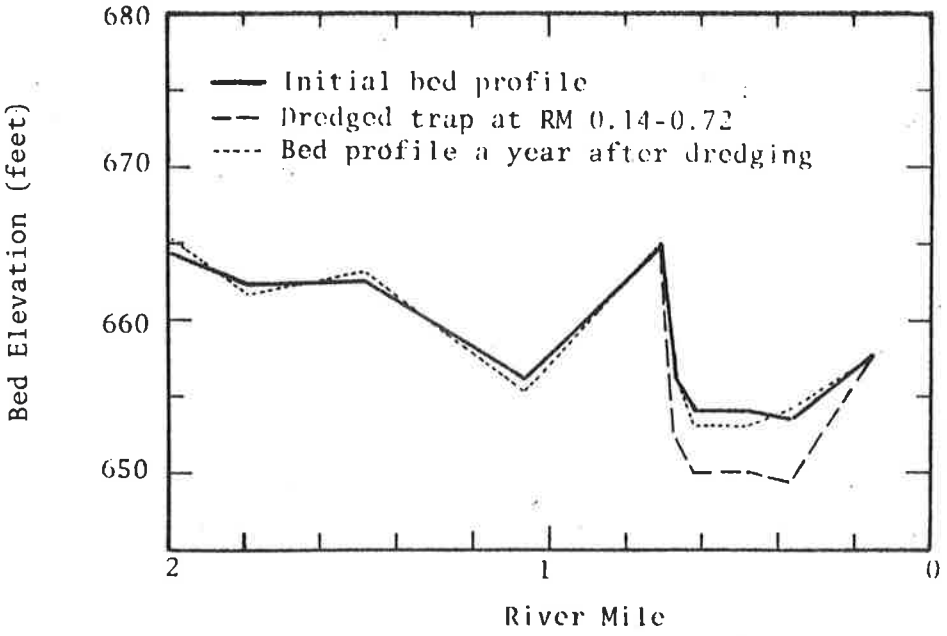

Figure 11.14 Bed elevation changes in the Chippewa River near the dredged sedimentation trap.

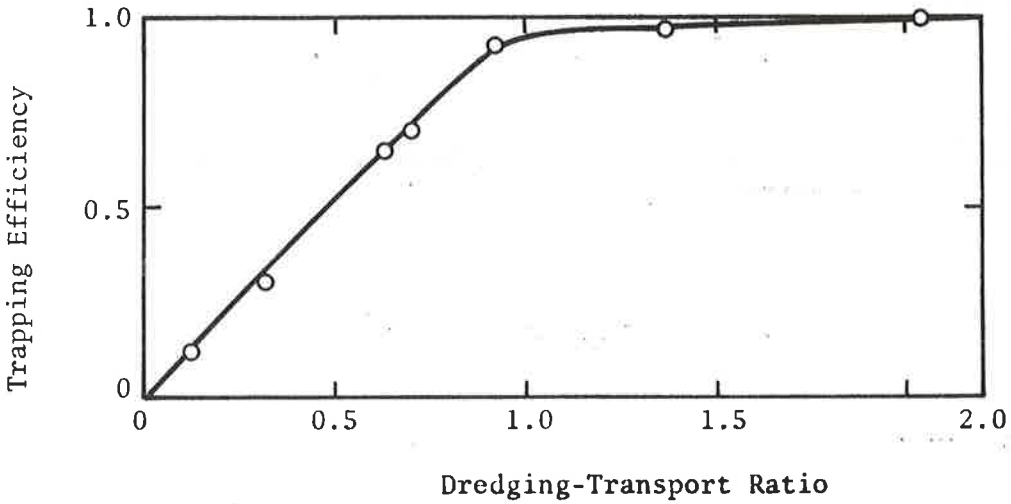

Figure 11.15 Trapping efficiencies of dredged sedimentation traps.

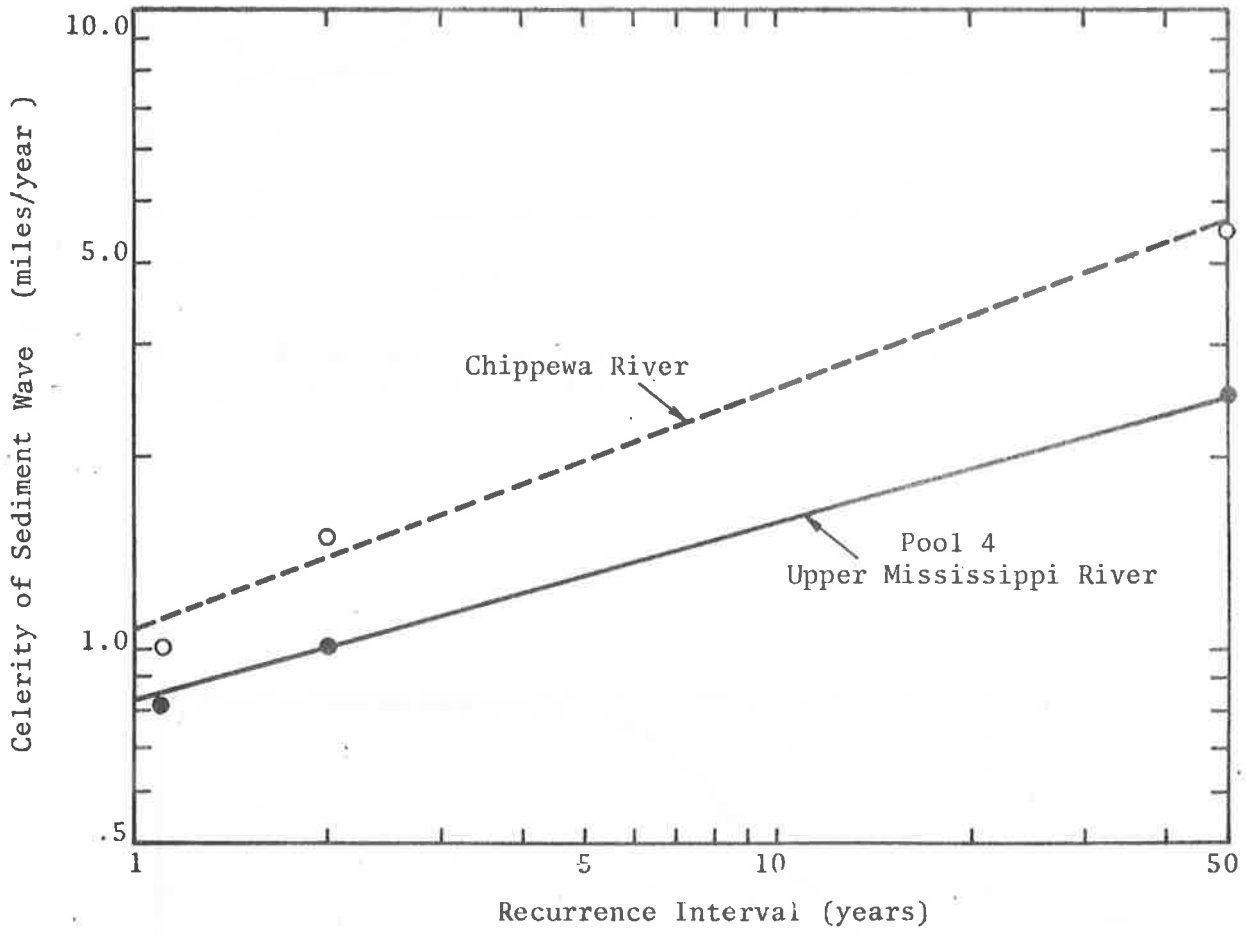

Figure 11.16 Celerities of sediment waves providing the affected distances by alternative measures in a period of time.

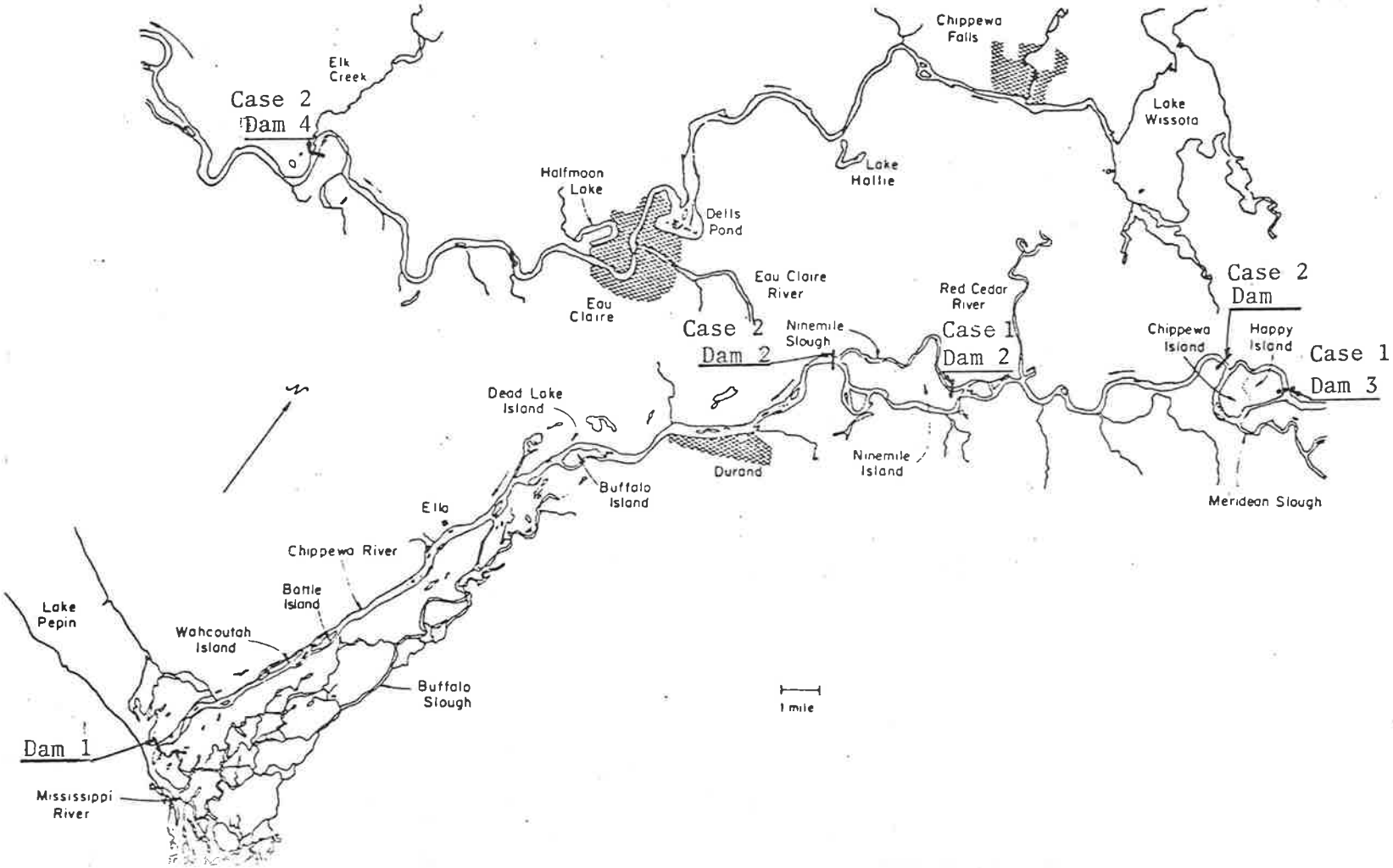

Figure 11.17 Location of Alternative 3: Construct a series of low head dams.

lower end. Dams 2 and 3 would divert excessive flow to the left channels as shown in Figure 11.18, and thereby reduce erosion of the high banks along the righ channels. The computational sections where dams are located are given in Figure 11.8. The left channels would enlarge due to erosion by the extra water discharge diverted by Dams 2 and 3 as shown in Figure 11.19. This increase in channel dimensions would in turn further increase the water discharge and eventually the left channels would become the main channel. For Case 2 of Simulation (4), four low-head dams were installed at the locations as shown in Figure 11.17. The predicted water surface and bed profiles with and without project conditions after 40 years are plotted in Figure 11.20. Because of erosion and deposition sequence caused by the Case 2 dams, the channel slope would be reduced by 20 percent. This in turn would reduce bank erosion and sediment transport. The dams would raise river stage by about 2-3 ft during an average flood condition (Q = 36,000 cfs). These increases in flood stages would inundate an additional 2,430 acres of the Lower Chippewa floodplain.

Other alternative measures can be studied by changing the control statements in the model and operating the model under suitable boundary conditions. The model results can be used to evaluate different alternative measures. This simple and economic methodology of mathematical modeling is very valuable for planning and decision making.

11.4 TWO-DIMENSIONAL SEDIMENT ROUTING MODEL

Introduction

In some cases, such as flow in estuaries, the flow velocity in both the longitudinal and transverse directions are comparable. Then the one-dimensional model can only provide general trends. If more detailed information is to be obtained, a two-dimensional mathematical model can be utilized. Colorado State University is developing a two-dimensional water and sediment routing model. The model is based on the uncoupled-unsteady approach by performing water routing to obtain hydraulic characteristics of flow and then utilizing sediment continuity equations to determine the geomorphic changes. The water routing component of the

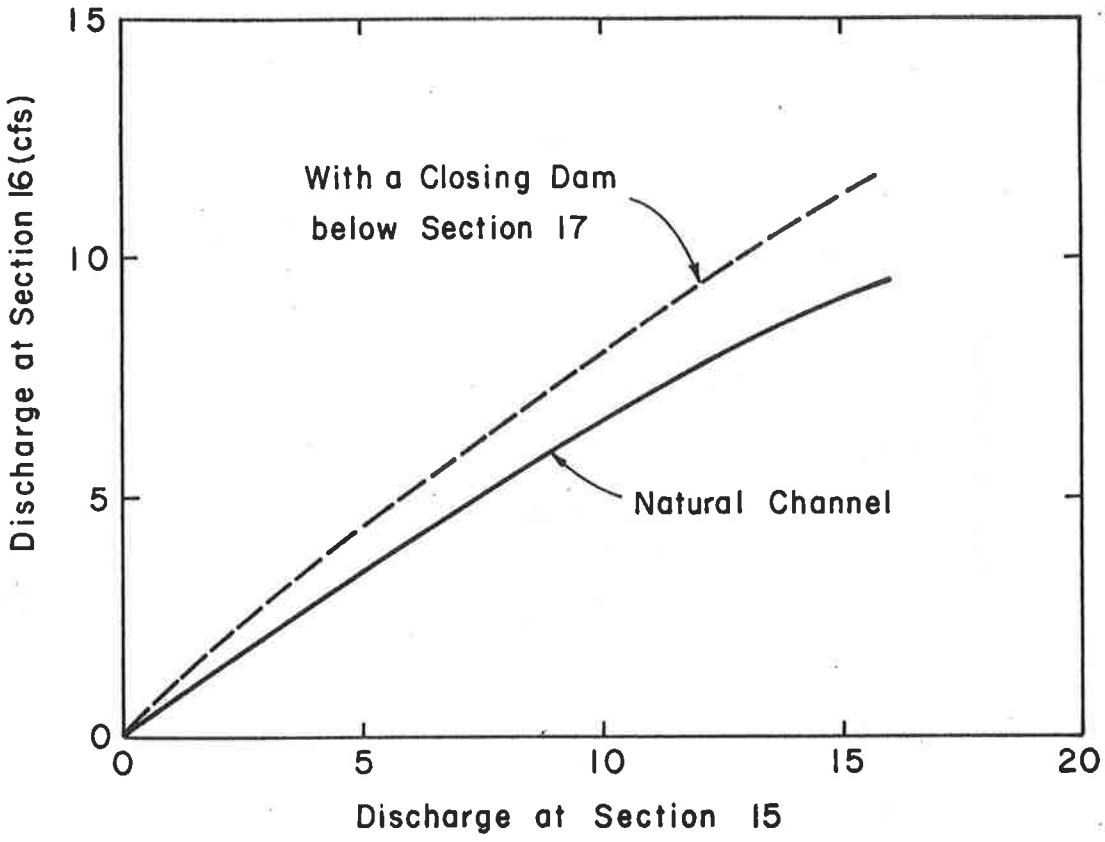

Figure 11.18 Discharge distribution in the branched channels along Happy Island.

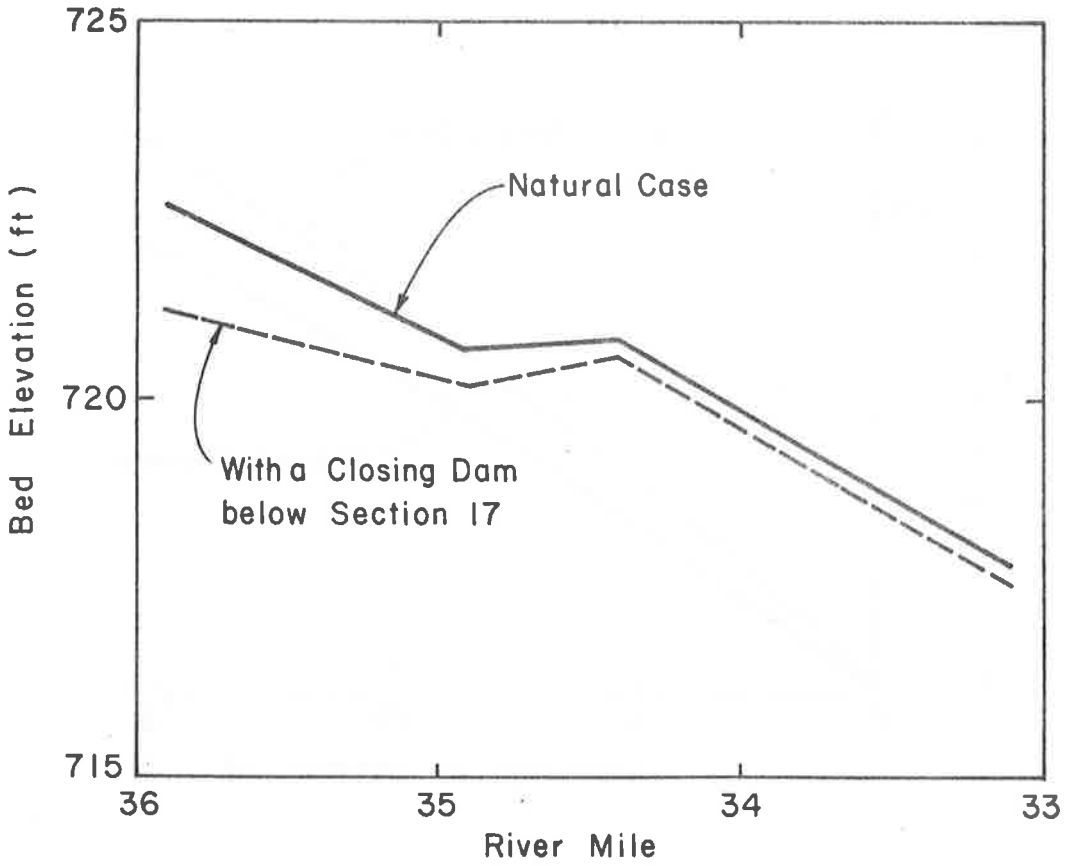

Figure 11.19 New bed profiles in the channel (Sections 16-18-20-21) across Happy Island after routing a 5-year annual hydrograph.

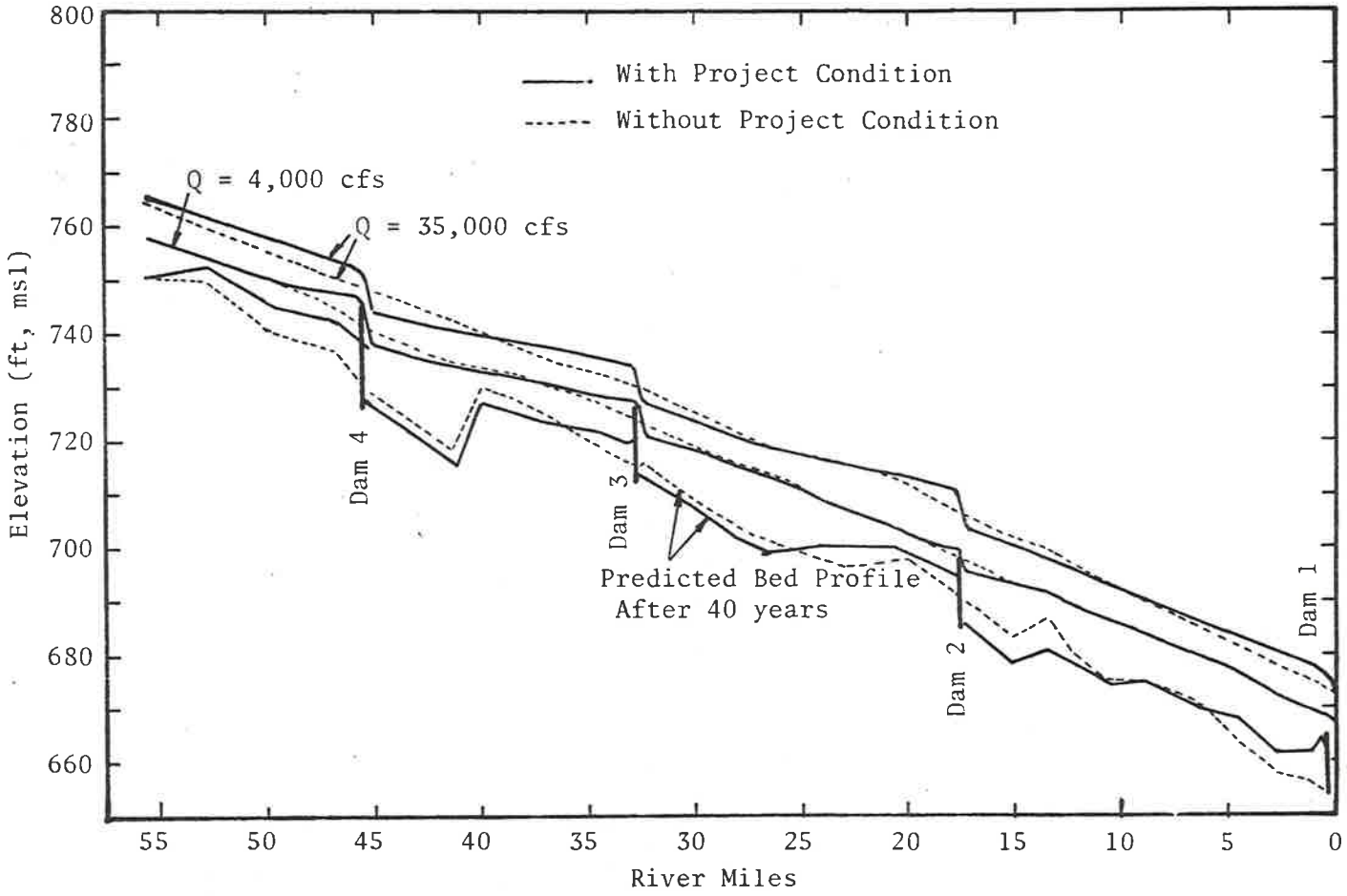

Figure 11.20 Water surface and bed profiles for the without project condition and with Case 2 series dams after 40 years.

two-dimensional model has been described in Chapter 8. In the following sections, the two-dimensional sediment routing method and an application example will be presented.

Theoretical Background for Sediment Routing

The sediment routing method is based on a two-dimensional sediment continuity equation:

$$\frac{\partial g_x}{\partial x} + \frac{\partial g_y}{\partial y} + \gamma_s \frac{\partial z}{\partial t} = 0 \qquad (11\text{-}73)$$

where

g_x = the unit-width bed material transport rate in the x-direction

g_y = the unit-width bed material transport rate in the y-direction

z = the elevation of the channel bed, with reference to an arbitrary datum, and

γ_s = the unit weight of the material deposited in the channel bed.

The bed material transport rate is expressed in units of weight per unit of time, per unit of width. The unit weight of the bed deposit is expressed as:

$$\gamma_s = (1 - \lambda)\ \rho_s g \qquad (11\text{-}74)$$

where λ is the bed porosity

ρ_s is the mass density of sediment

and g is the acceleration of gravity.

The bed material transport is a vector quantity. Therefore, a model for its prediction should be capable of being resolved into two perpendicular horizontal directions. For this reasons, a simple model based on an empirical power function of mean velocity is preferred over the more sophisticated phenomenological models. Furthermore, its simplicity allows for a considerable speed in the transport aspect of the computations, a significant asset of a two-dimensional numerical model where the coefficient and inversion algorithms may take large amounts of computational time.

The selected bed material transport function is of the form

$$g_w = C_g\ \rho\ w^m \qquad (11\text{-}75)$$

where g_w is the bed material transport rate per unit width in the direction of the velocity w (averaged in the vertical), and C_g and

m are an empirical coefficient and exponent, respectively. Equation 11-75 is resolved along two perpendicular directions according to

$$g_x = C_g \rho \, uw^{m-1} \tag{11-76}$$

$$g_y = C_g \rho \, vw^{m-1} \tag{11-77}$$

where u and v are the velocities (averaged in the vertical) in the x and y directions, respectively.

Numerical Solution for Sediment Routing

The water routing component in the two-dimensional model enables the calculation of the unit-width water discharge in the x-direction q_x, in the y-direction q_y and depth d at new time levels. The next step is to calculate the bed level z for the new hydraulic conditions. This is accomplished by the use of an explicit finite difference scheme.

The sediment continuity equation is

$$\frac{\partial g_x}{\partial x} + \frac{\partial g_y}{\partial y} + (1 - \lambda) \rho_s g \frac{\partial z}{\partial t} = 0 \tag{11-78}$$

The terms in Equation 11-78 can be discretized as follows (see Figure 11.21).

If $g_x > 0$,

$$\frac{\partial g_x}{\partial x} = \frac{g_{x_{j+1,\,k+1}}^{n+(\frac{1}{2})} - g_{x_{j,\,k+1}}^{n+(\frac{1}{2})}}{\Delta x} \tag{11-79}$$

If $g_x < 0$,

$$\frac{\partial g_x}{\partial x} = \frac{g_{x_{j,\,k+1}}^{n+(\frac{1}{2})} - g_{x_{j-1,\,k+1}}^{n+(\frac{1}{2})}}{\Delta x} \tag{11-80}$$

If $g_y > 0$,

$$\frac{\partial g_y}{\partial y} = \frac{g_{y_{j+1,\,k+1}}^{n+(\frac{1}{2})} - g_{y_{j+1,\,k}}^{n+(\frac{1}{2})}}{\Delta y} \tag{11-81}$$

If $g_y < 0$,

$$\frac{\partial g_y}{\partial y} = \frac{g_{y_{j+1,\,k}}^{n+(\frac{1}{2})} - g_{y_{j+1,\,k-1}}^{n+(\frac{1}{2})}}{\Delta y} \tag{11-82}$$

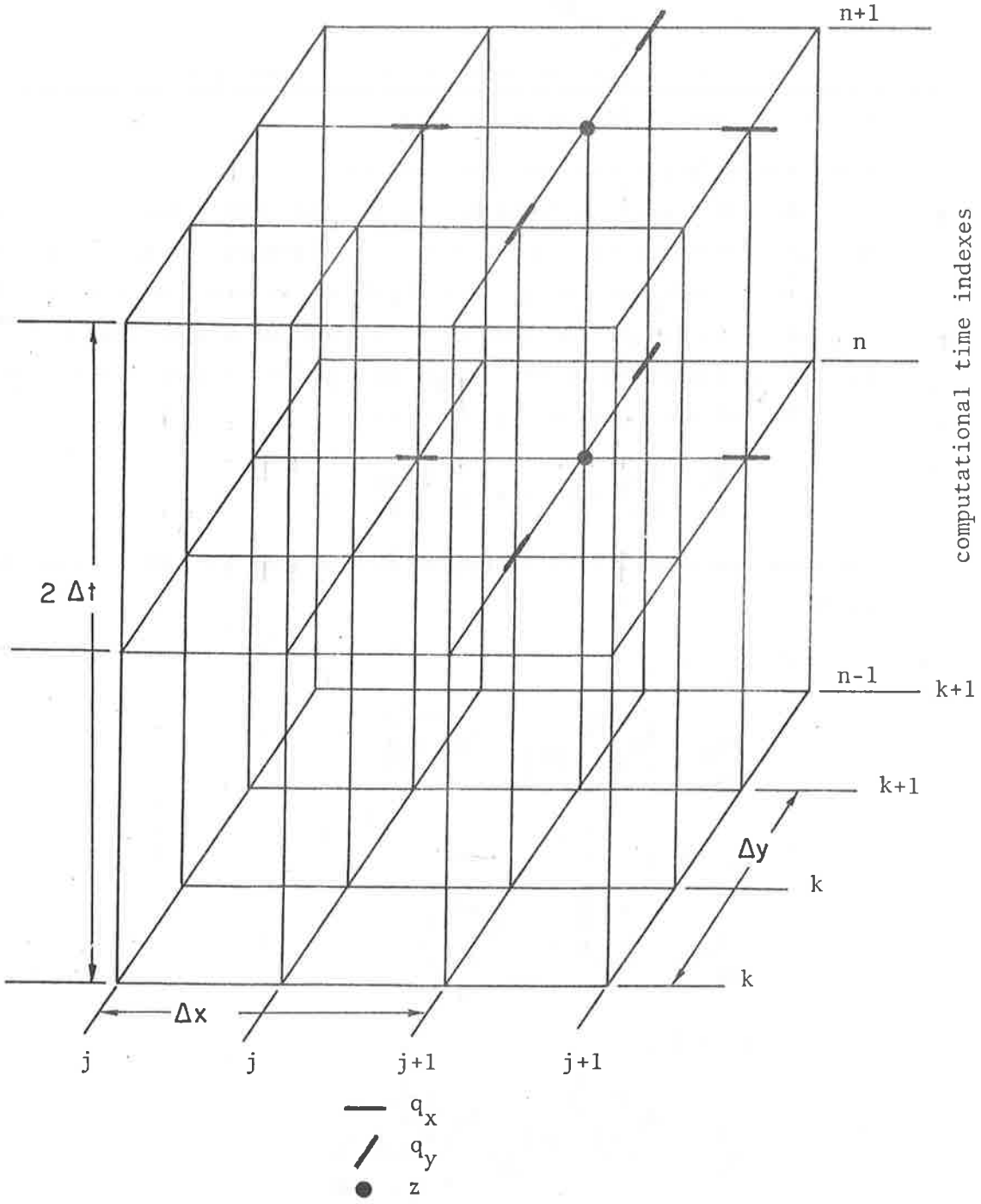

Figure 11.21 Variable location in the discretization of the sediment continuity equation.

Substituting adequate discretized relations into Equation 11-78 yields:

$$z^{n+1}_{j+1,\ k+1} = z^{n}_{j+1,\ k+1} - C_z \qquad (11\text{-}83)$$

where

$$C_z = \frac{\Delta t\ [\frac{\partial g_x}{\partial x} + \frac{\partial g_y}{\partial y}]}{(1 - \lambda)\ \rho_s\ g}$$

Bed material transport rates g_x and g_y are calculated based on Equations 11-76 and 11-77.

Application of the Mathematical Model to Pool 4 in the Upper Mississippi River and Lower Chippewa River

The developed two-dimensional mathematical model has been applied to study Pool 4 at the confluence of the Upper Mississippi River and Lower Chippewa River. The model simulates water and sediment movement in the study reach and is utilized to predict hydraulic and geomorphic changes in the study area caused by various development activities and thus to identify feasible development projects.

The calibration of water routing component of the Pool 4 model has been described in Chapter 8. To calibrate the sediment routing model component, Run No. 5 of the physical model of the same study area conducted by University of Minnesota was used. This run employed water discharges of 19,000 cfs (intermediate flow) in the Upper Mississippi River and of 30,000 cfs (high flow) in the Lower Chippewa River, which are the same conditions used for calibration of water routing component in Chapter 8. In addition, a dredged cut was made immediately upstream of Drury Island (see Figure 11.22). The mathematical model was calibrated to reproduce the filling of this dredge cut in the physical model. Some comparison between the measured and computed results is given in Figure 11.23. The agreement is fair. Calibration of the mathematical model could be improved by modifying the sediment transport functions and riverbed roughness coefficients.

Concluding Remarks

Two-dimensional water and sediment routing models are applied when detailed knowledge of water and sediment movement and bed elevation changes in a river reach due to passage of flood waves is required, and

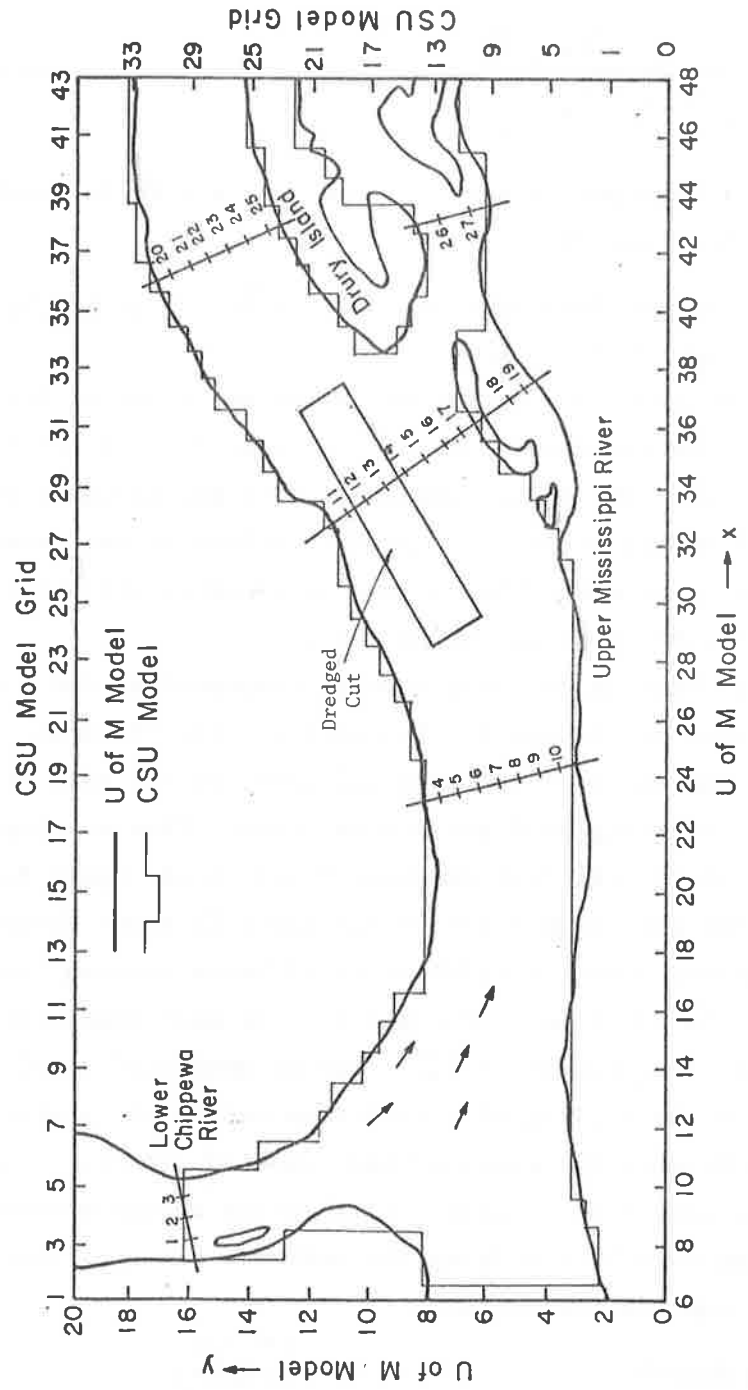

Figure 11.22 The model research of Pool 4 in the Upper Mississippi River and Lower Chippewa River with a dredge and cut.

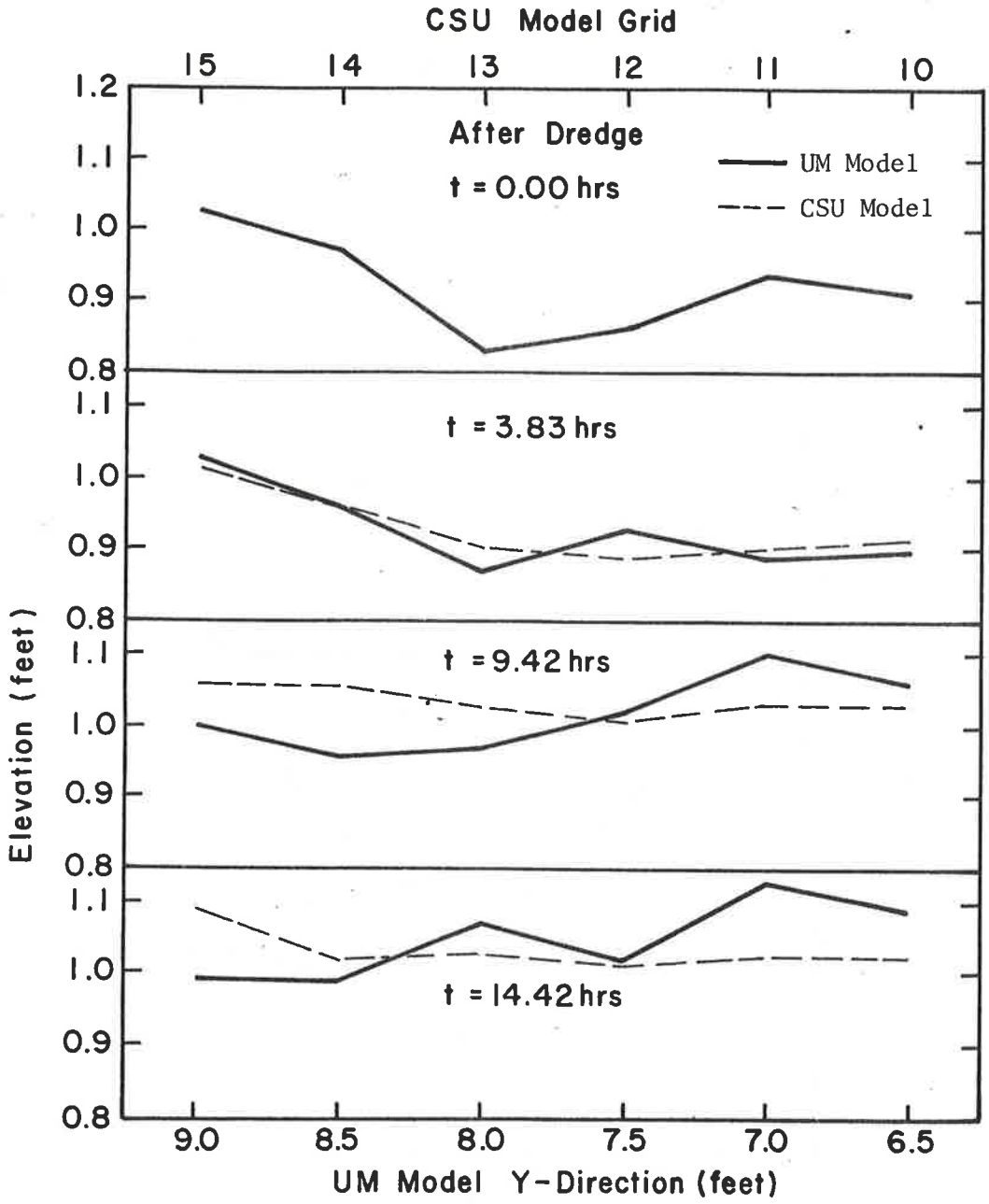

Figure 11.23a Comparison between the measured and computed bed elevations at x = 29 feet, UM model (x = 24, CSU model grid).

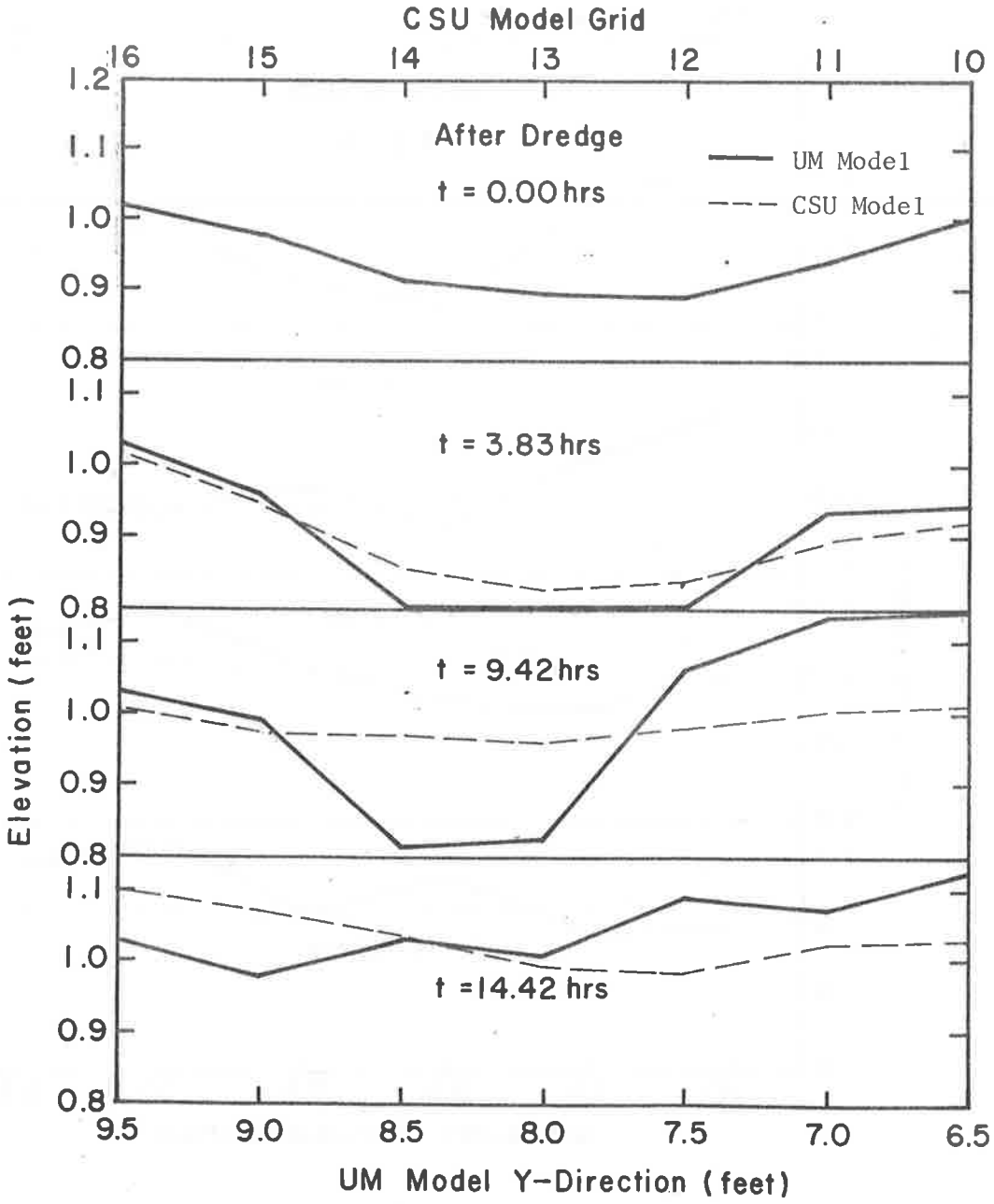

Figure 11.23b Comparison between the measured and computed bed elevations at x = 30 feet, UM model (x = 25, CSU model grid).

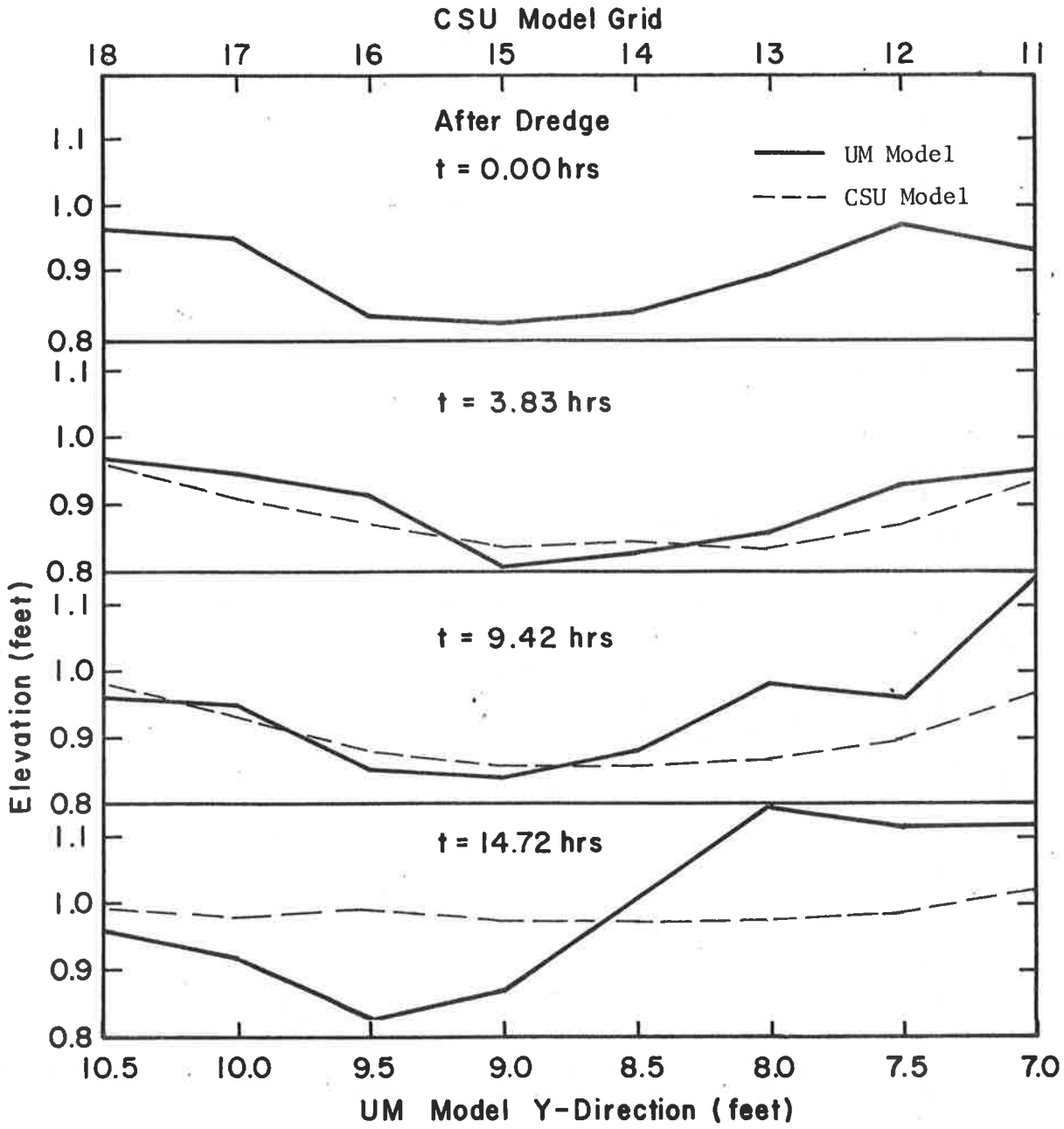

Figure 11.23c Comparison between the measured and computed bed elevations at x = 32 feet, UM model (x = 27, CSU model grid).

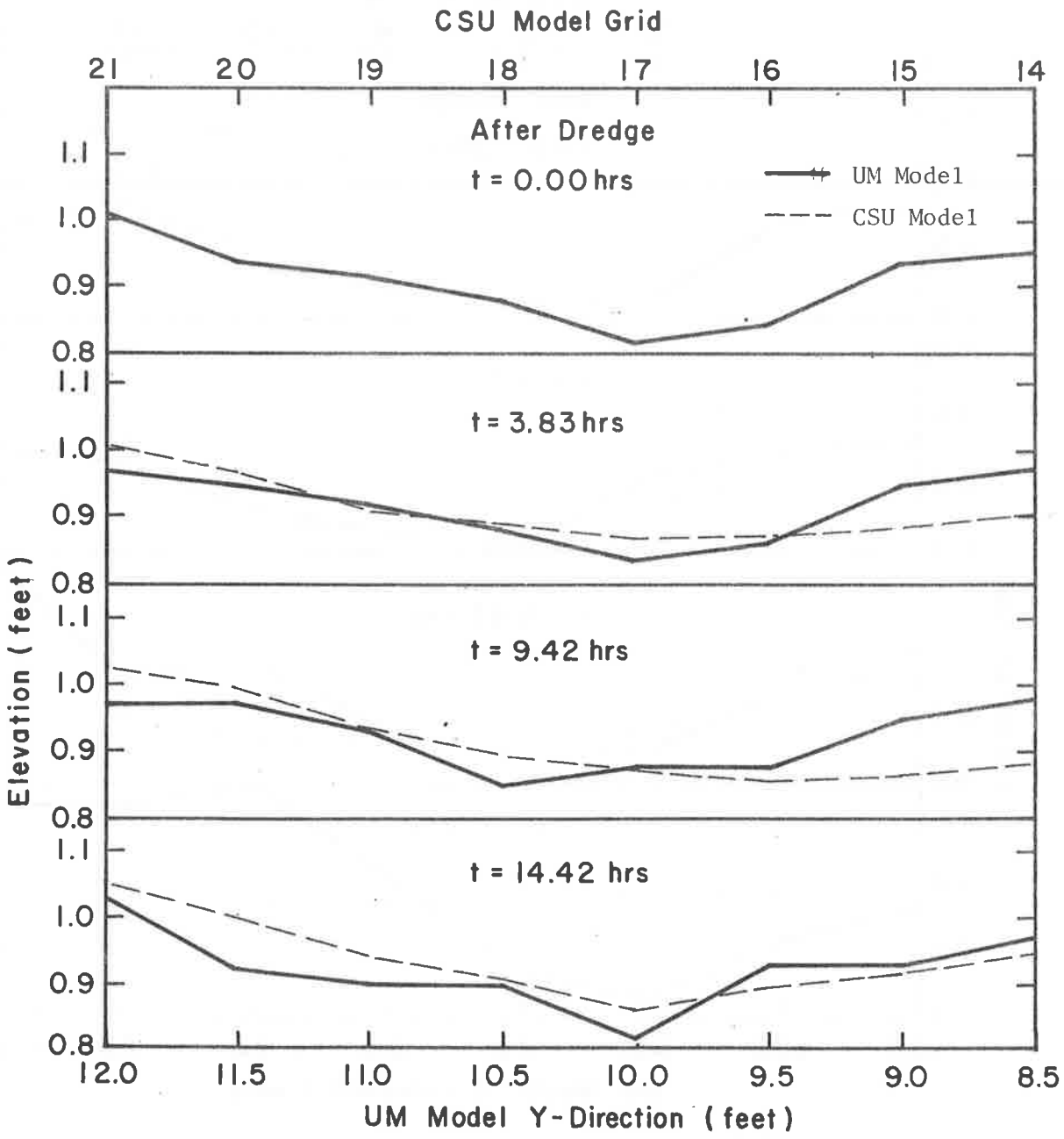

Figure 11.23d Comparison between the measured and computed bed elevations at x = 32 feet, UM model (x = 29, CSU model grid).

when the boundary geometry is complex. For example, with a midstream island or with irregular banklines the one-dimensional approach cannot reflect the detailed flow patterns occurring.

Again, four types of methods can be applied to develop the two-dimensional water and sediment routing models. They are the complete solution, the uncoupled-unsteady solution, the known discharge solution, and the uncoupled-steady solution. The numerical solutions on which these models are based can be categorized into finite-difference and finite-element methods as presented in Chapter 8.

In general, the finite-element method can better represent the irregular configuration of a water course. Therefore, its computed results are generally more reliable near the boundaries than the finite-difference method. However, the computer time required by the finite-element method currently used to determine the unknown variables at one time step is much larger than that required by the finite-difference method. Recent research related to the finite-element method has been concentrated on increasing the time step length and improving the efficiency of matrix solution. Until these problems can be solved, the application of finite-element methods to study two-dimensional unsteady river problems is not practical.

Colorado state University is developing various types of two-dimensional river models and testing their efficiencies and applicabilities. At present, an unsteady-uncoupled finite-difference model and a complete finite-element model are under testing. The former method has been applied to simulate the flow patterns in a physical model. The testing result is promising. After further testing, this and other models will be applied to study water and sediment related problems in Pool 4 in the Upper Mississippi River. The model can be easily modified to study other river systems.

11.5 SUMMARY AND CONCLUSIONS

Mathematical models for water and sediment routing in rivers have been described in this chapter with the major portion of water routing model component described in Chapter 8. The developed models have been successfully applied to study various types of water and sediment related

problems in rivers. It is not the intention to present all the models available in the literature. Instead, the chapter presents some useful models that have been tested and verified.

The models presented include one-dimensional models, and two-dimensional models. These models are based on the conservation laws: sediment continuity, water continuity and momentum equations. Considering types of governing equations used for model formulations, the models can be subcategorized into four types of solution models. They are: (1) complete solution: solve all the governing equations simultaneously, (2) uncoupled-unsteady solution: solve the water continuity and momentum equations for routing water first and then solve the sediment continuity equation explicitly for sediment routing, (3) known-discharge solution: assuming the water discharge in the river reach is known, solve the momentum and sediment continuity equations simultaneously for routing sediment, (4) uncoupled-steady solution: assuming the water discharge is steady and is known in the river reach, solve the momentum equation to determine the water surface profile and corresponding flow conditions and then solve the sediment equation uncoupled to determine bed elevation changes. As discussed in the section titled, "Discussion of the Four Types of Numerical Solution Methods," each solution method has its advantage and disadvantage, and should be used properly considering its applicability and limitations.

In general, a one-dimensional water and sediment routing model is adequate to study water and sediment related problems and to predict river responses to development in a relatively uniform river. Changes in the cross-sectional geometries at the computational sections can be determined from properly distributing the computed changes in cross-sectional area to subsections at a cross section. These computational sections are generally located at irregular points in a study reach and at particularly interesting points. To study water and sediment related problems in a complex river network system with connected loops, branches and confluences, a one-dimensional model of a river network system has been developed.

For a highly irregular or a broad river reach where both the longitudinal and transverse velocities are comparable, a one-dimensional

model can only determine general river patterns and changes to development. To obtain more detailed information, a two-dimensional mathematical model can be utilized. However, the two-dimensional model is much more complicated than the one-dimensional model. It is apparent that a relatively simple model that can provide adequate information is always desired. This requires some engineering judgment and experience with mathematical modeling. To obtain meaningful and accurate results from a mathematical model, the model should be carefully calibrated, operated, and its results carefully interpretted.

11.6 REFERENCES

Chang, F. F. M., and Richards, D. L., 1971. Deposition of sediment in transient flow. Journal of the Hydraulics Division, ASCE, Vol. 97, No. HY6, Proc. Paper 8191, June, pp. 837-849.

Chang, H. H., and Hill, J. C., 1976. Computer modeling of erodible flood channels and deltas. Journal of the Hydraulics Division, ASCE, Vol. 102, No. HY10, Proc. Paper 12485, October, pp. 1461-1478.

Chen, Y. H., 1973. Mathematical modeling of water and sediment routing in natural channels. Ph.D. Dissertation, Department of Civil Engineering, Colorado State University, Fort Collins, Colorado.

Chen, Y. H., and Simons, D. B., 1974. Routing of water and sediment in canals and rivers. Proceedings, Contribution of Irrigation and Drainage to the World Food Supply Specialty Conference, ASCE, August 14-16, pp. 121-146.

Colby, B. R., 1964. Discharge of sands and mean-velocity relationships in sand-bed streams. U.S. Geological Survey Professional Paper, 462-A.

Colby, B. R., and Hembree, C. H., 1955. Computation of total sediment discharge Niobrara River near Cody, Nebraska. U.S. Geological Survey Water Supply Paper, 1357.

Dass, P., 1975. Water and sediment routing in nonuniform channels. Disseration presented to the Department of Civil Engineering, Colorado State University, Fort Collins, Colorado, in partial fulfillment of the requirements for the degree of Doctor of Philosophy.

DeVries, M., 1965. Considerations about non-steady bed load transport in open channels. Proceedings of the Eleventh Congress of the International Association for Hydraulic Research, Vol. 3, No. 3.8, Leningrad, U.S.S.R.

Einstein, H. A., 1950. The bed load function for sediment transportation in open channel flows. U.S. Department of Agriculture, Technical Bulletin, No. 1026.

Li, R. M., 1977. An uncoupled-steady water and sediment routing model. Unpublished report, Colorado State University, Engineering Research Center, Fort Collins, Colorado.

Lopez, S. J. L., 1978. Mathematical modeling of sediment deposition in reservoirs. Ph.D. Dissertation, Department of Civil Engineering, Colorado State University, Fort Collins, Colorado.

O'Brien, M. P., 1933. Review of the theory of turbulent flow and its relation to sediment transport. Transactions, American Geophy. Union.

Owens, E. M., 1977. One-dimensional sediment routing in rivers. M.S. Thesis, Department of Civil Engineering, Colorado State University, Fort Collins, Colorado.

Shen, H. W., 1971. Total sediment load. River Mechanics, Edited by H. W. Shen, Vol. 1, Chapter 13, Water Resources Publications, Fort Collins, Colorado.

Simons, D. B., and Chen, Y. H., 1979. A mathematical model of the Lower Chippewa River network system. Prepared for the U.S. Army Engineer District, St. Paul, Minnesota, Colorado State University, Fort Collins, Colorado.

Simons, D. B., Schumm, S. A., Stevens, M. A., Chen, Y. H., and Lagasse, P. F., 1975. A geomorphic study of pools 24, 25, and 26 in Upper Mississippi and Lower Illinois Rivers. Colorado State University, Report No. CER75-76-DBS-SAS-MAS-YHC-PFL8, prepared for the Waterways Experiment Station, Vicksburg, Mississippi.

Streloff, T., 1970. Numerical solution of Saint-Venant equations. Journal of the Hydraulics Division, ASCE, Vol. 96, No. HY1, Proceedings Paper 7043, January, pp. 223-252.

Toffaletti, F. B., 1969. Definitive computation of sand discharge in rivers. Journal of the Hydraulics Division, ASCE, Vol. 95, No. HY1, Proc. Paper 6350, January, pp. 225-248.

U. S. Army Corps of Engineers, 1976. HEC-6, Scour and deposition in rivers and reservoirs, users manual. Hydrologic Engineering Center, Computer Program 723-G2-L2470, Davis, California.

Yang, C. T., 1973. Incipient motion and sediment transport. Journal of the Hydraulics Division, ASCE, Vol. 99, No. HY10, October.

CHAPTER 12

KNOWN DISCHARGE SEDIMENT ROUTING

by

Glenn O. Brown, Research Associate, Department of Civil Engineering,
Colorado State University, Fort Collins, Colorado

Ruh-Ming Li, Associate Professor, Department of Civil Engineering,
Colorado State University, Fort Collins, Colorado

12.1 INTRODUCTION

A problem of increasing importance for the water resources planning and the environmental impact analysis is to determine the response of a river system to man's activities. Many rivers have been and continue to be, developed for navigation, recreation, and environmental enhancement. Rivers are dynamic ecological systems; the short- and long-term response must be determined in order to evaluate the various development alternatives and to prevent potential disaster associated with man's activities.

A river response can be determined by either physical or mathematical physical process models. Physical models are limited by size and cannot model large systems and long periods of time. There are several process models presently in use such as RIVER (Chen, 1975) and HEC-6 (Hydrologic Engineering Center, 1976). While mathematical models do not have a size limitation, because of computer costs they are usually limited to simulation periods of a year or two. Because of the complex problem involved in the large basin analysis, it was necessary to develop a new model, KUWASER for the United States Army Corps of Engineers, Vicksburg District, in the sedimentation study of the Yazoo River Basin (see Chapter 20).

For determination of long-term river system response, sediment movement through a river system is of primary concern, and detailed information on flood wave movement is of secondary importance. A simple known-discharge uncoupled sediment routing scheme is utilized in the model to determine aggradation and degradation in a river. The known discharge, uncoupled sediment routing formulation allowed the development of an extremely fast and efficient model, which makes the long-term simulation of sediment movement possible and practical.

The known-discharge formulation requires the user to identify for the mathematical model the water discharge throughout the system for the entire period to be modeled. The water discharge can be determined by either assuming steady flow or by using an unsteady flow routing model (see Chapter 6, 8 and 9). The model computes the water surface profile by assuming gradually varied steady flow. The time increment utilized in the input hydrographs may vary from a few hours to a month or longer, depending on the flow conditions and the required accuracy of the results. The model can accurately simulate unsteady flow profiles if it

is coupled to an acceptable unsteady flow water routing model since it does not linearize the momentum equation. Most routing programs presently used, such as HEC-6, utilize a trial and error standard step method to calculate the backwater curve. KUWASER differs from these models. It utilizes channel geometry relationships in an analytical, first order Newton's approximation to solve for the backwater curve. This method is proven more efficient than the trial and error algorithm.

The model can include backwater calculations and sediment routing of the mainstem and multiple tributaries. With this feature it is possible to determine the response of the tributaries to changes on the mainstem, such as channel improvement, realignment, or dredging. The response of the mainstem river to tributary modifications can also be determined. Therefore, the most efficient tributary management procedures can be determined to delineate the mainstem sedimentation problems.

Since the sediment routing is uncoupled, the water surface profile computations and sediment routing are solved sequentially, i.e., the water surface profile is computed for the current time period assuming a fixed bed and the sediment routing is performed at the end of the time period. Any channel changes due to aggradation or degradation are determined before the start of the next time period.

To save computer time, cross section geometry is not changed every time period to reflect the increase or decrease of sediment volume at the cross sections due to sediment routing. Only after a significant amount of sediment has been aggraded or degraded at a cross section, is the channel geometry modified. When the bed elevation has changed more than a threshold value (for example, one foot), the amount of degradation or aggradation sediment volume is distributed through the cross section and new channel geometry relationships are calculated which reflect changes in the hydraulic properties of the channel. The model uses a method which relates the change in bed elevation at a point to the flow conveyance above the point. This method predicts more accurately the location of aggradation or degradation in the cross section and estimates channel response more adequately than a conventional one-dimensional model.

Unlike other models, KUWASER was developed according to the modularity concept. The model consists of linked components that represent a

specific physical process or function. This modularity allows a greater flexibility for updating and improving the various components of the model. The mathematical model is compatible with the data storage and retrieval system described in Chapter 16. This feature makes it very simple to obtain and format all required data to operate the model.

The following describes the theory and application of the developed model. A more detailed description is given by Brown (1979). In addition, other models using the known discharge formulation are briefly discussed.

12.2 WATER SURFACE PROFILE COMPUTATIONS

General

The water surface profile is computed assuming one dimensional, spatially varied, steady flow. This implies the following assumptions: 1) the hydraulic characteristics of flow remain constant for the time interval under consideration; 2) the flow streamlines are practically parallel, i.e., a hydrostatic pressure distribution prevails over the channel section, and 3) the secondary flow (lateral or cross-stream) is negligible when compared to the longitudinal flow. A further assumption is that the frictional loss at a section is the same as for uniform flow having the same velocity and hydraulic radius. In addition to the above basic assumptions, other assumptions will be made and stated when required, the most important being that the slope of the channel is so small that the depth of flow is the same whether the vertical or normal to the channel bottom.

Dynamic equations for spatially varied flow can be obtained for three different approaches. These approaches are: 1) momentum, 2) total head, and 3) energy. While the water surface profiles computed by each method are identical, the derived equations themselves are only identical for the special conditions of steady, uniform flow. The following is a brief derivation of the dynamic equation for spatially varied flow from the total head equation and a comparison with results obtained from the momentum and energy approaches. Yen and Wenzel (1970) and Li (1972) contain completed derivations and additional discussion.

Dynamic Equation of Spatially Varied Flow

Continuity Equation

Figure 12.1 shown an incremental length dx of an open channel with a spatially varied flow profile. The continuity equation for the increment is

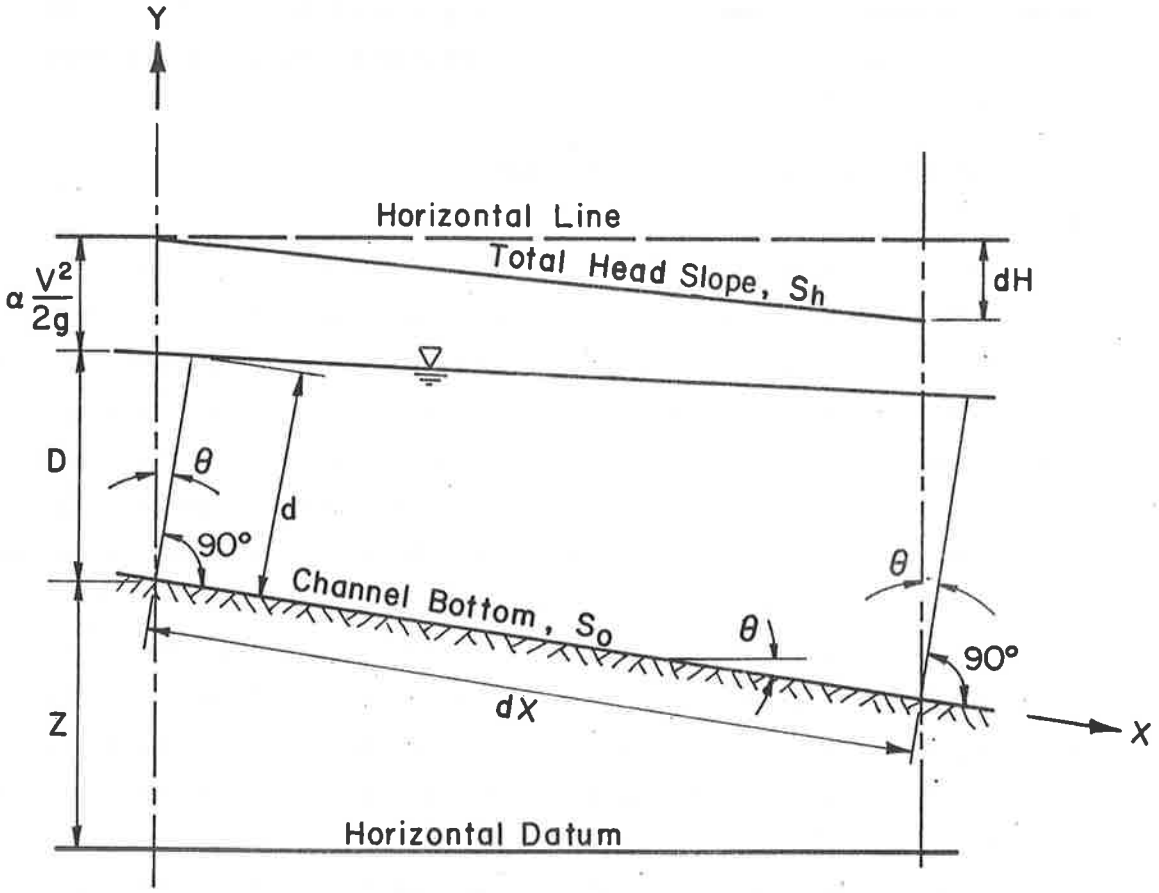

Figure 12.1 Incremental length of channel.

$$\frac{dQ}{dx} = q \tag{12-1}$$

where Q is the channel discharge and q is the lateral inflow per unit channel length. Considering the incompressibility of water, $Q = VA$ and

$$\frac{d(VA)}{dx} = q \tag{12-2}$$

The total hydraulic head above a selected datum at the upstream section is given by

$$H = Z + d \cos \theta + \alpha \frac{V^2}{2g} \tag{12-3}$$

where H is the total head, Z is the elevation of the channel bottom above the datum, d is the depth of flow; θ is the bottom slope angle; α is the velocity head correction factor, and g is the acceleration of gravity. By taking the bottom of the channel as the z axis and differentiating Equation 12-3 with respect to x, the following equation is obtained:

$$\frac{dH}{dx} = \frac{dZ}{dx} + \cos \theta \frac{dd}{dx} + \frac{d}{dx} \left(\alpha \frac{V^2}{2g}\right) \tag{12-4}$$

The total head slope S_h can then be expressed as

$$S_h = - \frac{dH}{dx} \tag{12-5}$$

and the bed slope, S_o can be expressed as

$$S_o = - \frac{dZ}{dx} \tag{12-6}$$

Substituting Equations 12-5 and 12-6 into Equation 12-4 and solving for dd/dx yields

$$\frac{dd}{dx} = \frac{1}{\cos\theta} \left[(S_o - S_h - \frac{d}{dx} \left(\alpha \frac{V^2}{2g}\right)\right] \tag{12-7}$$

which is the general differential equation for spatially varied steady flow derived with the total head. It represents the slope of the water surface with respect to the channel bottom. In most cases the angle θ is small so that $\cos \theta \tilde{\approx} 1$, and $d \tilde{\approx} D$. Placing these approximations into Equation 12-7 results in

$$\frac{dD}{dx} = S_o - S_h - \frac{d}{dx} \left(\alpha_2 \frac{V^2}{2g}\right) \tag{12-8}$$

where D is the depth of flow measured vertically from the bed (see Figure 12.1).

For comparison with the spatially varied flow equation obtained by other methods, Equation 12-8 must be rearranged. Breaking down Equation 12-8 into separate terms yields

$$\frac{dD}{dx} = S_o - S_h - \frac{V^2}{2g}\frac{d\alpha}{dx} - \frac{\alpha V}{g}\frac{dV}{dx} \tag{12-9}$$

From Equation 12-2

$$\frac{AdV}{dx} + \frac{VdA}{dx} = q \tag{12-10}$$

$$\frac{dV}{dx} = \frac{1}{A}\left(q - \frac{VdA}{dx}\right) \tag{12-11}$$

Combining Equation 12-9 and 12-11 and assuming $d\alpha/dx = 0$, results in

$$\frac{dD}{dx} = S_o - S_h - \frac{\alpha V q}{gA} + \frac{\alpha V^2}{gA}\frac{dA}{dx} \tag{12-12}$$

Assuming a unit width channel, $A = D$, and $dA/dx = dD/dx$, placing these terms in Equation 12-12 yields

$$\frac{dD}{dx} = \frac{S_o - S_h - \frac{\alpha V q}{gD}}{1 - \frac{\alpha V^2}{gD}} \tag{12-13}$$

which is the common form of the spatially varied flow equation obtained from the total head equation.

Using control volumes the following equations can be obtained from the momentum and energy equations, respectively.

$$\frac{dD}{dx} = \frac{S_o - S_f - \frac{2\beta V q}{gD}}{1 - \beta\frac{V^2}{gD}} \tag{12-14}$$

$$\frac{dD}{dx} = \frac{S_o - S_e + \frac{q}{Q}\left(\frac{U^2 - 3\alpha V^2}{2g}\right)}{1 - \alpha\frac{V^2}{gD}} \tag{12-15}$$

where S_f is the friction slope, β is the momentum correction factor, S_e is the energy slope, and U is the lateral inflow velocity. The two slopes are devined by

$$S_f = \frac{\tau}{\gamma D} \tag{12-16}$$

$$S_e = - \frac{1}{\gamma Q dt} \frac{dE}{dx} \tag{12-17}$$

where τ is the boundary shear stress and E is the total energy of flow, and t is time.

It should be noted that in Equation 12-15 the only energy terms considered are velocity head, elevation, and flow depth. Other forms of energy such as temperature have been neglected.

Comparison Between Approaches

The momentum and energy approaches have much in common. They both are derived using control volumes. The momentum approaches based on Newton's 2nd law, equates the change in the momentum flux through the volume to the external forces acting on it while the energy approach, based on Newton's 3rd law, equates the change in the energy flux through the volume to the internal energy losses. An important difference is that the momentum equation is a vector relationship while the energy equation is a scalar. Vectors do not appear in Equation 12-14 since only one-dimensional flow is considered. Another difference is that the two approaches handle the lateral inflow differently. The momentum approach considers total momentum of the lateral inflow, while the energy equation considers the differences in the lateral and main channel energy (velocity head). Examination of Equations 12-14 and 12-15 show that even without lateral inflow (gradually varied flow) the two relationships are not equal since the correction factors α and β are generally not equal. The correction factors (and therefore the friction slope S_f and the energy slope S_e) are only equal for uniform flow.

The total head approach based on potential energy is quite different from the energy or momentum approaches. It equates the change in hydraulic head which is a partial measure of energy, to the head loss in the system. Neither external forces or internal losses are considered. Since the total head equation is based on potential energy it is similar to the energy equation, but the two apporaches are only equal if there is

no lateral inflow. The total head equation cannot easily handle energy entering or leaving the system, such as introduced by pumps or turbines, while the energy equation can account for these other sources and sinks by adding additional terms.

Since the water surface slope, dD/dx is the same, the differences between the energy, head, and friction slope can be determined by combining equations 12-13, 12-14, and 12-15.

$$S_h = \frac{(1 - \alpha \frac{V^2}{gD}) S_f + (\alpha - \beta) \frac{V^2}{gD} S_o + (2\beta - \alpha) \frac{Vq}{gD} - \frac{\alpha\beta V^3 q}{g^2 D^2}}{1 - \beta \frac{V^2}{gD}} \qquad (12\text{-}18)$$

$$S_e = S_h + \frac{\alpha V q}{gD} + \frac{q}{Q} \left(\frac{U^2 - \alpha V^2}{2g}\right) \qquad (12\text{-}19)$$

Manning's Equation

The friction slope is evaluated using the empirical Manning's equation

$$S_f = \left(\frac{Qn}{1.49A\ R^{2/3}}\right)^2 \qquad \text{(English units)} \qquad (12\text{-}20)$$

where R is the hydraulic radius of flow and n is the Manning's coefficient of channel roughness.

Manning's equation was developed for uniform steady flow, as such using Equation 12-20 for spatially varied flow produces errors, but the errors are believed to be small compared with those ordinarily incurred in the use of a uniform-flow formula and in the selection of the roughness coefficient (Chow 1959).

The Manning's n value for alluvial streams is not constant but is a function of discharge (see Simons and Sentürk, 1977; and Chapter 9). While there are fairly exact methods of determining the channel roughness, in mathematical modeling Manning's n-value is usually made a simple function of discharge, $n = a_n Q^{b_n}$ where a_n and b_n are empirically determined coefficients.

The channel conveyance is defined by

$$K = \frac{1.49}{n} A\ R^{2/3} \qquad (12\text{-}21)$$

where K is the conveyance. Combining Equations 12-20 and 12-21 yields

$$S_f = \left(\frac{Q}{K}\right)^2 \qquad (12\text{-}22)$$

Chow (1959) presents additional spatially and gradually varied flow theory.

Standard Step Method

The mathematical model uses the finite difference standard step method to solve for the water surface profile. The computations are carried upstream cross section by cross section from a known water surface and the depth of flow at each cross section is determined. Figure 12.2 shows a typical channel reach. Becuase of difficulties with the momentum and energy equations, caused by non-prismatic channels the total head approach is used. The total head and head loss between the two cross sections are equated

$$Z_2 + D_2 + \alpha_2 \frac{V_2^2}{2g} = Z_1 + D_1 + \alpha_1 \frac{V_1^2}{2g} + H_\ell + H_{\ell v} \qquad (12\text{-}23)$$

where H_ℓ is the friction loss and may be written as:

$$H_\ell = S_f \, \Delta X \qquad (12\text{-}24)$$

where ΔX is the horizontal distance between cross sections, and $H_{\ell v}$ is the loss due to all other factors. $H_{\ell v}$ is nominally referred to as the eddy loss. No rational method is available to evaluate eddy losses. The eddy loss depends mainly on the velocity head change and may be expressed as a part of it or $H_{\ell v} = C_e \, [(\alpha_2 V_2^2 - \alpha_1 V_1^2)/2g]$, where C_e is a coefficient. The average of channel conveyance at the two cross sections is used to compute the friction loss. Thus combining Equations 12-22 and 12-24 results in

$$H_\ell = \Delta X \left[\frac{Q_2}{(K_1 + K_2)/2}\right]^2 \qquad (12\text{-}25)$$

The continuity equation can be written

$$Q = VA \; . \qquad (12\text{-}26)$$

The total head at the downstream cross section, H_1 is known and is determined by

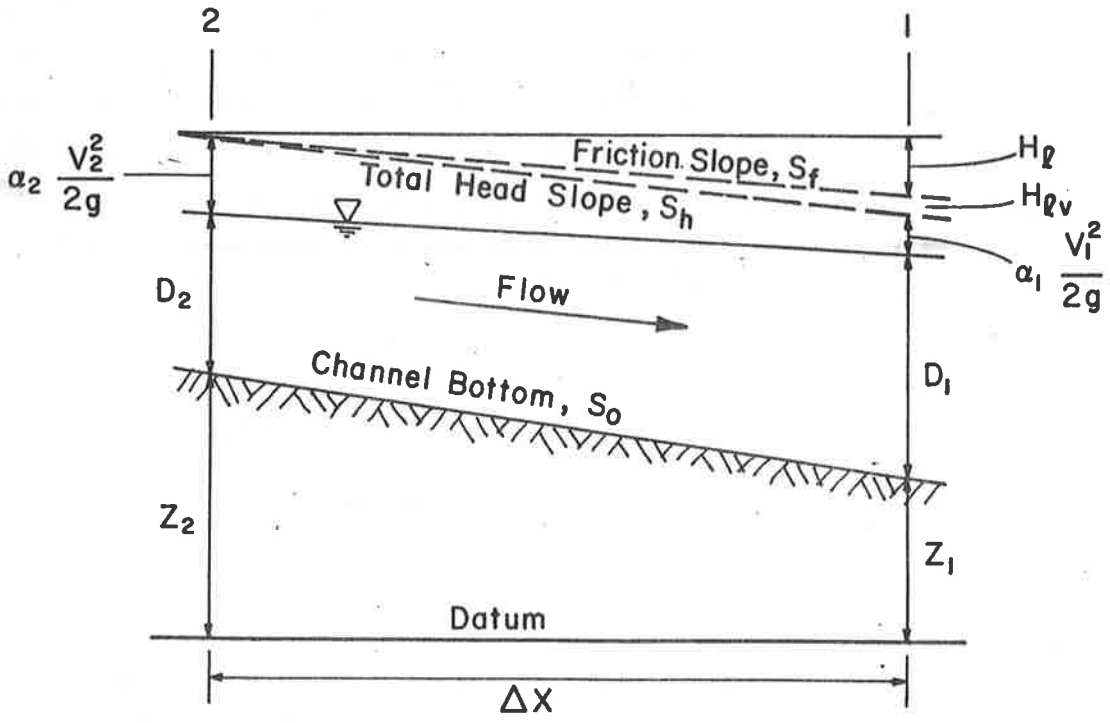

Figure 12.2 Channel reach for standard step method.

$$H_1 = Z_1 + D_1 + \alpha_1 \frac{V_1^2}{2g} \qquad (12\text{-}27)$$

Combining Equations 12-20, 12-25, 12-26 and 12-27 yields

$$\alpha_2 \left(\frac{Q_2}{A_2}\right)^2 \frac{1}{2g} + D_2 + Z_2 - \Delta X \left[\frac{Q_2}{(K_1 + K_2)/2}\right]^2 - C_e \left(\frac{\alpha_2 V_2^2 - \alpha_1 V_1^2}{2g}\right) - H_1 = 0 \qquad (12\text{-}28)$$

By starting at a known downstream water surface and proceeding upstream one cross section at a time, the water surface profile is computed.

Computation of Hydraulic Properties

The solution of Equation 12-15 requires the determination of the channel hydraulic properties, area, conveyance, etc., at various depths. In the backwater computations the hydraulic properties are computed with relationships developed using the digitized channel geometry.

Coordinate Points

Channel cross sections are defined by (x,z) sets of coordinates. Figure 12.3 shows a typical cross section. To allow for different Manning's n-values across the section three subdivisions are made: Right Over Bank, Main Channel, and Left Over Bank. The subsections are divided by the two stations D_{lob} and D_{rob}. The Manning n-value at each coordinate point is determined by its location.

Area

The area of flow for a given water surface elevation is computed by summing incremental areas between consecutive coordinates of the cross section. Figure 12.4 illustrates the technique. The total area of flow is the summation of the increment areas, a_i.

$$A = \sum_{i=1}^{N} a_i \qquad (12\text{-}29)$$

where N is the total number of cross section incremental areas. The incremental areas are computed by

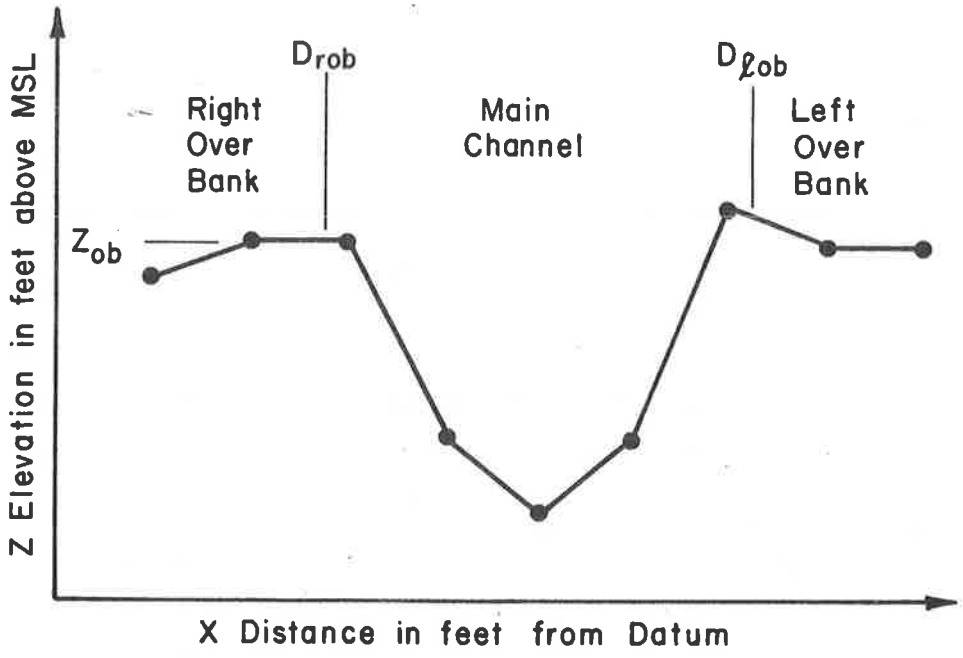

Figure 12.3 Typical channel cross section with subdivisions.

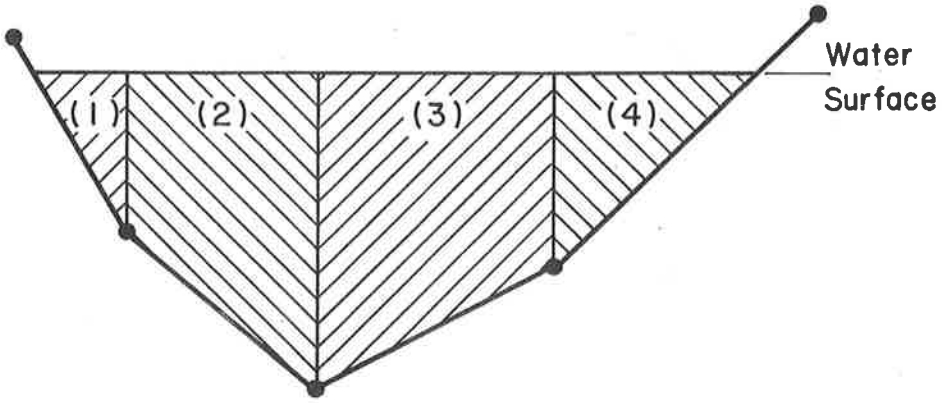

Figure 12.4 Incremental areas in a cross section.

$$a_i = x_b D_a \tag{12-30}$$

where X_b is defined in Figure 12.5 and D_a is defined as:

$$D_a = \frac{1}{2} (D'_1 + D'_2) \tag{12-31}$$

where D'_1 and D'_2 are defined in Figure 12.5. If the water surface intercepts the cross section between coordinate points as shown by increment 4 in Figure 12.4, straight line interpolation between the points is used to compute the triangular area. If the water surface is above a coordinate end point (first or last points), the area of flow is determined by extending a vertical line to the water surface from the end point as shown in Figure 12.6.

In many rivers, especially those with small gradients, man-made or natural levees reduce the area of flow until they are topped. Overbank flow area is not considered until the water surface exceeds the elevation Z_{ob} that is shown in Figure 12.3.

Wetted Perimeter

The wetted perimeter p_i is the length of the cross section below the water surface and is also computed in increments by

$$p_i = \sqrt{X_b^2 + Z_b^2} \tag{12-32}$$

where Z_b is defined in Figure 12.3.

Hydraulic Radius

The incremental hydraulic radius, r_i, is calculated by

$$r_i = \frac{a_i}{p_i} \tag{12-33}$$

Conveyance

The total cross section conveyance is computed by summing the incremental conveyance

$$K = \sum_{i=1}^{N} k_i \tag{12-34}$$

where k_i is the incremental conveyance and is computed by

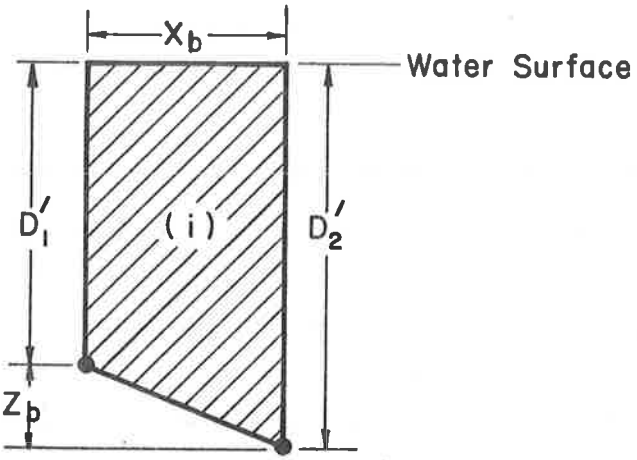

Figure 12.5 Incremental cross section area.

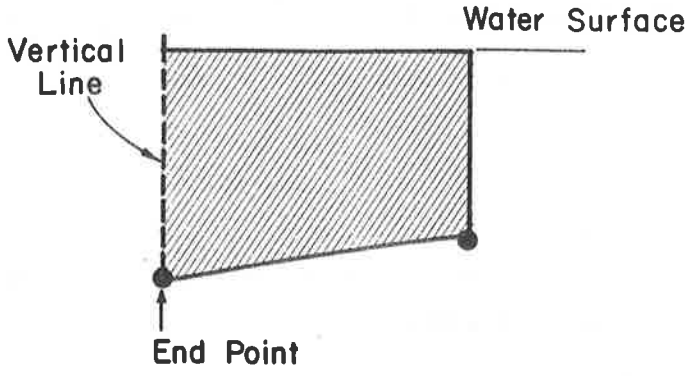

Figure 12.6 Flow area at end of cross section.

$$k_i = \frac{1.49}{n_{a_i}} a_i r_i^{2/3} \quad (12\text{-}35)$$

where n_{a_i} is the average Manning's n value at the two coordinate points which define the increment.

Alpha

Alpha, the velocity distribution factor, is used here to account for the distribution of flow across the cross section and not the vertical shape of the velocity profile. Alpha is calculated by:

$$\alpha = \frac{\sum_{i=1}^{N} \left(\frac{k_i^3}{a_i^2}\right)}{K^3/A^2} \quad (12\text{-}36)$$

Effective Depth and Effective Width. Two conveyance weighed parameters, effective depth, D_e, and effective width, W_e, are used in the sediment transport calculations and are calculated as follows:

$$D_e = \frac{\sum_{i=1}^{N} \frac{D_{a_i}^{5/3} a_i}{n_{a_i}}}{\sum_{i=1}^{N} \frac{D_{a_i}^{2/3} a_i}{n_{a_i}}} \quad (12\text{-}37)$$

$$W_e = \frac{\sum_{i=1}^{N} D_{a_i}^{2/3} a_i}{D_e^{5/3}} \quad (12\text{-}38)$$

The effective depth and effective width values are not used in the water surface profile calculations.

Channel Hydraulic Property Relationship. Hydraulic property relationships are computed which relate area of flow, conveyance, alpha, effective depth, and effective width to the thalweg depth. Two separate sets are calculated: one set for main channel flow and a second for overbank flow. The hydraulic property relations are:

Main Channel Flow ($D \leq Z_{ob}$)

$$W_e = a_1 D^{b_1} \quad (12\text{-}39)$$

$$D_e = a_2 D^{b_2} \quad (12\text{-}40)$$

$$A = a_3 D^{b_3} \quad (12\text{-}41)$$

$$K = a_4 D^{b_4} \quad (12\text{-}42)$$

$$\alpha = a_5 D^{b_5} \quad (12\text{-}43)$$

Overbank Flow ($D > Z_{ob}$)

$$W_e = a_6 D^{b_6} \quad (12\text{-}44)$$

$$D_e = a_7 D^{b_7} \quad (12\text{-}45)$$

$$A = a_8 D^{b_8} \quad (12\text{-}46)$$

$$K = a_9 D^{b_9} \quad (12\text{-}47)$$

$$\alpha = a_{10} D^{b_{10}} \quad (12\text{-}48)$$

where D is the thalweg depth and a_1 to a_{10} and b_1 to b_{10} are computed coefficients. The overbank relationship includes both the overbank and main channel flow for depths greater than Z_{ob}.

The coefficients of the hydraulic properties relations are determined by 1) calculating the hydraulic properties of each cross section for ten evenly spaced incremental depths of flow in the main channel and for ten increments of depths above the overbank elevation, Z_{ob}. Then 2) coefficients of the relations are computed by a least squares regression. To maintain continuity in the backwater computation, the overbank relations for area and conveyance are forced to have the same value as the main channel relations at the overbank elevation.

Newton-Raphson Solution for the Total Head Equation

The model solves the equation of spatially varied steady flow by using an analytical first order Newton-Raphson (N-R) method to give

successive approximations in the standard step calculation. Combining Equations 12-28, 12-41, 12-42 and 12-43 yields the spatially varied flow equation as a sole function of D_2

$$(1 - C_e) \frac{a_5}{a_3^2} \frac{Q_2^2}{2g} D_2^{(b_5 - 2b_3)} + D_2 - \frac{4\Delta X\, Q_2^2}{(K_1^2 + 2K_1 a_4 D_2^{b_4} + a_4^2 D_2^{2b_4})} + Z_2 - H_1 = 0 \qquad (12\text{-}49)$$

From the Taylor series expansion of an arbitrary function $F(\psi)$, the first order N-R approximation to $F(\psi)$ can be obtained by

$$\psi^* = \psi_0 - \frac{F(\psi_0)}{F'(\psi_0)} \qquad (12\text{-}50)$$

where ψ^* is the root of $F(\psi)$ and ψ_0 is the estimate of ψ^*. When applying Equation 12-36 to the solution of the backwater equation ψ is the depth of flow, D_2 at the upstream cross section, and $F(\psi)$ is the total head equation evaluated at that location as computed by Equation 12-49. For the N-R solution the first derivative of the total head equation must be obtained.

Differentiating Equation 12-49 with respect to D_2 yields:

$$(1 - C_e) \frac{Q_2^2}{2g} \left(\frac{a_5}{a_3^2}\right) (b_5 - 2b_3) D_2^{(b_5 - 2b_3 - 1)} + 1 + \frac{4\Delta X Q_2^2 \left[2K_1 a_4 b_4 D_2^{(b_4-1)} + a_4^2 2b_4 D_2^{(2b_4-1)}\right]}{(K_1^2 + 2K_1 a_4 D_2^{b_4} + a_4^2 D_2^{2b_4})^2} \qquad (12\text{-}51)$$

Equation 12-51 is $F'(\psi)$ in the first order N-R. When Equation 12-49 is evaluated at depths other than its roots, the equation is not equal to zero, but is instead equal to the error in the total head. Figure 12.7 is a qualitative plot of Equation 12-49. The shape of the curve can be verified by consideration of Equation 12-28. As the depth approaches zero the area of flow goes to zero and the velocity goes to infinity. With a large velocity the velocity head term dominates the equation and causes a large positive error. Conversely, as the depth

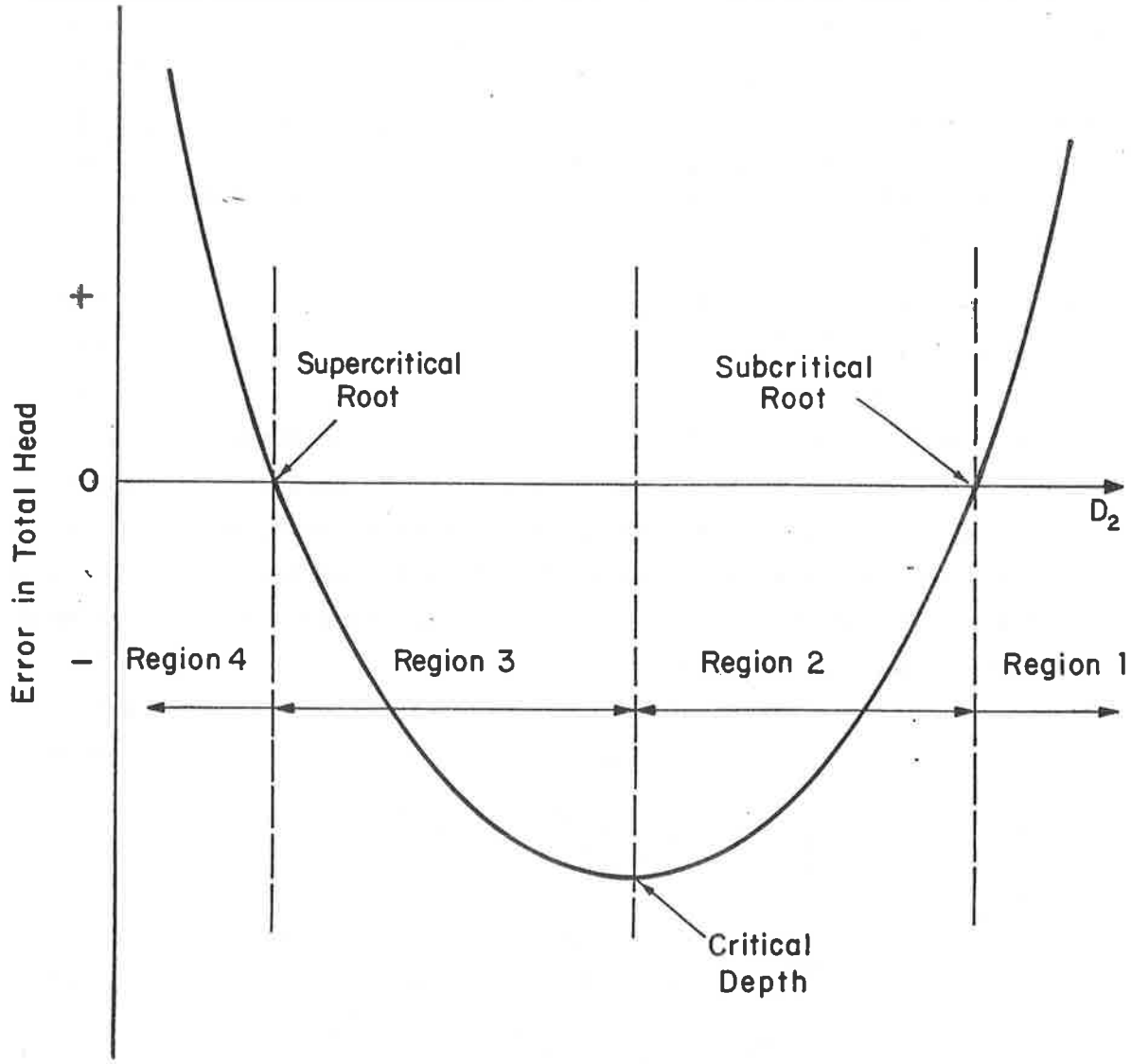

Figure 12.7 Error in total head equation as a function of depth of flow.

becomes large the depth itself dominates, and again the error becomes large and positive. At critical depth the specific head is at a minimum and the error will be negative.

Care must be taken in using Equation 12-50. If the total head equation is not perfectly convex it may take many interactions to converge to a root. Also, if the initial guess is on the supercritical side of the curve, the N-R method will drive the solution to the supercritical root, even though the flow may be subcritical. By using simple logic the convergence of the N-R method can be greatly improved.

The curve in Figure 12.7 can be broken into four different regions by the signs of the error and first derivative. These regions are:

1. error positive, first derivative negative,
2. error negative, first derivative negative,
3. error negative, first derivative positive, and
4. error positive, first derivative positive.

In the computer program simple logic statements can detect which region the estimate of D_2 is in.

In most applications the subcritical root is desired, and logic in the computer program insures it will be found. If the estimate is in region 1 or 2 the N-R method will find the subcritical root, but if it is in regions 3 or 4, the N-R method must be forced to the subcritical root. In region 3, simply taking the negative of the first derivative forces the solution to the subcritical root. In region 4, a new estimate must be determined by computing critical depth and adding a constant to insure that the new estimate of D_2 is in region 1 or 2.

12.3 SEDIMENT ROUTING

General

Once the backwater profile is determined for a given time period, sediment is routed through the system. Sediment routing is accomplished in three separate steps. The first step is the calculation of the sediment transport at each cross section in the river, which requires knowledge of the velocity, depth, and width of flow that is obtained by the backwater calculations. The second step is the routing of the sediment to determine the change in cross section area due to sediment movement. The third step is the distribution of the change in area change through the cross section to obtain a new channel geometry.

Sediment Transport

In the mathematical simulation of stream bed aggradation-degradation, the conventional algorithms for calculating sediment transport such as Einstein's procedure require large amounts of computer time. This excessive use of computer time makes these methods impractical. It is also difficult to calibrate the conventional methods to observed data. Because of these reasons, empirical relationships are often used in mathematical modeling. In the Sedimentation Study of the Yazoo River Basin a relationship of the following form was used:

$$Q_s = 4.48 \times 10^{-6} V^{3.16} D_e^{0.94} W_e \qquad (12\text{-}52)$$

where Q_s is the bed material sediment transport in cfs. While this equation is not applicable to other rivers, it fits data for the Yazoo River Basin. The coefficients in Equation 12-52 were determined by: 1) taking suspended sediment measurements, 2) applying the Modified Einstein procedure to obtain the bed material load, and 3) using standard least squares regression to obtain the coefficients.

It is important to note that Equation 12-52 is only for the bed material load. In most cases the wash load is supply limited and all wash load entering a system will pass through it. An exception to this would occur when sedimentation behind a large dam was of interest. In this case, calculation of the wash load would be required. It is also interesting to note in Equation 12-52 that the bed material size does not enter into sediment calculations. This is caused by the limited range of data from which the equation was derived. In cases when there is insignificant data to develop relationships such as Equation 12-52, Colby's and Meyer-Peter, Mueller's methods have been used with success at a minimal cost in computer time.

Sediment Routing

The channel aggradation-degradation is determined by solving the sediment continuity equation.

$$\frac{\partial Q_s}{\partial x} + (1 - \rho) \frac{\partial A_b}{\partial t} = q_{s\ell} \qquad (12\text{-}53)$$

where A_b is the cross sectional area of the bed, $q_{s\ell}$ is the lateral tributary sediment inflow and ρ is the porosity that is the volume

of voids per unit volume of sediment in place. The first term in Equation 12-53 represents the change in sediment transport along the river, while the second term represents the change in bed area with time. A negative value of the second term signified degradation while a positive value signifies aggradation.

Figure 12.8 shows a typical sediment routing condition. Equation 12-53 is solved by a two step finite difference algorithm. The first step is the calculation of the change in sediment volume between each cross section. The change in volume is computed by:

$$\Delta V_i = (Qs_i - Qs_{i-1} + q_{s\ell_i})dt \qquad (12\text{-}54)$$

where ΔV_i is the change in sediment volume between sections i and i-1. The second step in the sediment routing is the determination of the change in area at each cross section, which requires knowledge of the location of sediment erosion or deposition between the cross sections. Modeling of sediment dispersion is required to compute exactly where in the reach between sections the sediment is eroded or deposited. Unfortunately, modeling of sediment dispersion requires excessive amounts of computer time, and considerable effort to calibrate. For these reasons an empirical distribution based on physical reasoning is used. A triangular distribution weighted downstream as shown in Figure 12.8, is used. One-quarter of the volume is deposited or eroded in the upstream half of the segment between sections, while three-quarters of the volume is deposited or eroded in the downstream half. This simply places more weight of sediment transport rate at the downstream section for determining the degradation and aggradation. With this assumption the change in bed area at a section is then equal to

$$\Delta A_{b_i} = (1 - \rho) \frac{\frac{1}{4}\Delta V_{i-1} + \frac{3}{4}\Delta V_i}{\frac{1}{2}(\Delta X_i + \Delta X_{i-1})} \qquad (12\text{-}55)$$

where ΔA_{b_i} is the change in bed area at the cross section. The physical significance of the triangular distribution can be seen if Equation 12-54 (neglecting lateral sediment inflow) is substituted into Equation 12-55.

$$\Delta A_{b_i} = (1 - \rho) \frac{\frac{1}{4}(Q_{s_i} - Q_{s_{i-1}}) + \frac{3}{4}(Q_{s_{i+1}} - Q_{s_i})}{\frac{1}{2}(\Delta X_{i-1} + \Delta X_i)} dt \qquad (12\text{-}56)$$

$$\Delta A_{b_i} = (1 - \rho) \frac{(\frac{3}{2} Q_{s_{i+1}} - Q_{s_i} - \frac{1}{2} Q_{s_{i-1}})}{\Delta X_{i-1} + \Delta X_i} dt \qquad (12\text{-}57)$$

The multiplying factor for sediment inflow, $Q_{s_{i+1}}$ is positive and the factor for the outflow $Q_{s_{i-1}}$ is negative as can be expected. The important fact to notice is that the multiplying factor for the sediment transport at the cross section is negative. This is physically logical. If the upstream and downstream transport is held constant, a reduction in the sediment transport at the section would cause the section to aggrade while an increase in the transport would cause it to degrade.

Distribution of Erosion and Deposition Across the Cross Section

Once the change in area at a cross section is computed the area must be distributed across the section to determine the new channel geometry. One method of distribution would be to raise or lower the whole cross section a uniform amount, as shown in Figure 12.9. This method is unrealistic because it changes the overbanks as much as the main channel regardless of flow conditions. A method which relates the change in bed elevation at a point to the hydraulic property of conveyance is used in the model. This method as shown in Figure 12.10 is considered appropriate because conveyance is directly related to velocity and sediment transport.

A qualitative analysis was performed to test the validity of the sediment distribution scheme based on conveyance (which is directly related to depth if Manning's roughness is the same across the whole cross-section). Three cross sections were taken from the Greenwood Bendway of the Yazoo River. At several points in each cross section the percent of maximum depth of flow, and the percent of maximum change in bed elevation (from February 2 to February 18, 1977) were determined. The results are plotted on Figure 12.11. As one can see, the change in bed elevation is roughly proportional to the depth. The sediment distribution method based on the hydraulic properties at each point in the cross section more accurately represent the natural cross sectional changes.

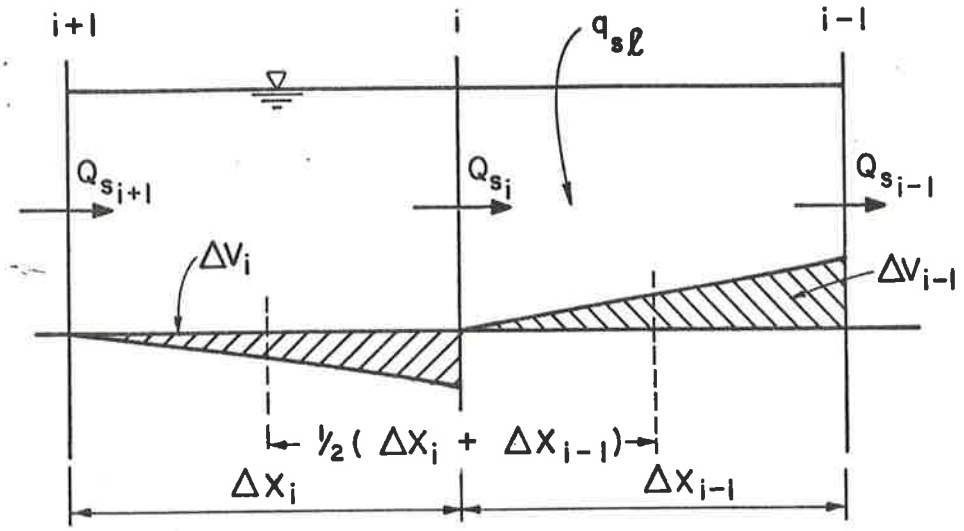

Figure 12.8 Finite difference sediment routing scheme.

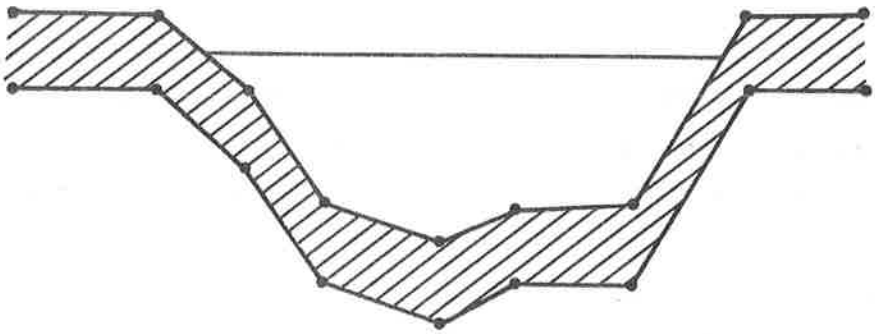

Figure 12.9 Uniform sediment distribution.

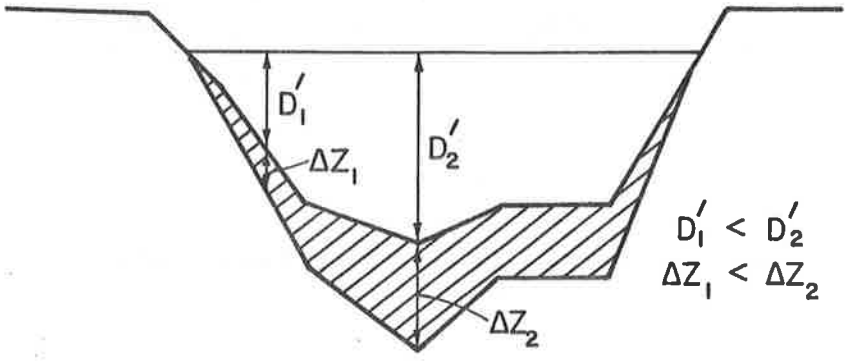

Figure 12.10 Sediment distribution based on depth of flow.

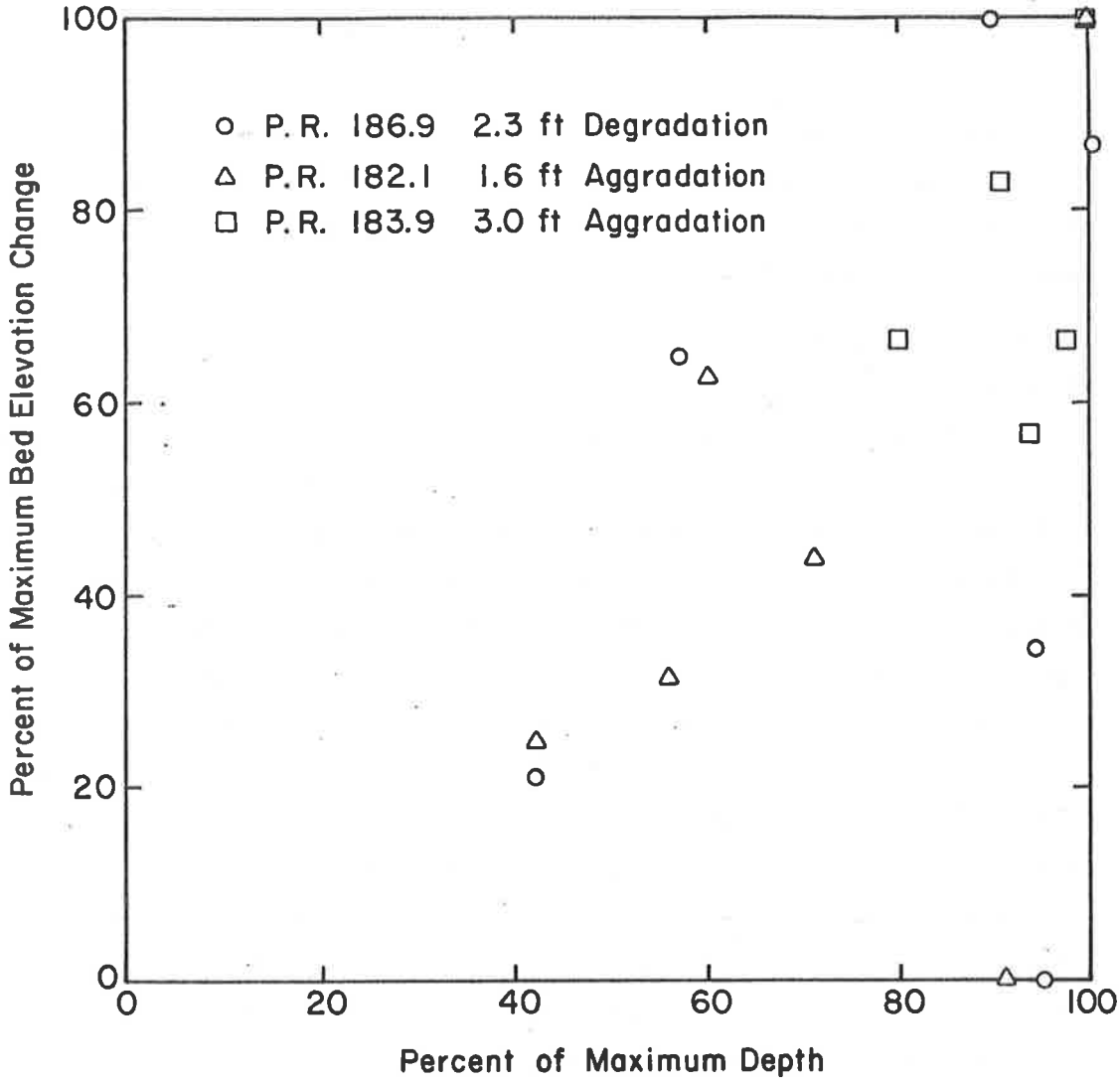

Figure 12.11 Percent bed elevation change vs. percent of maximum depth.

The model computes change in elevation for each cross section point by

$$\Delta Z_j = \frac{k_i + k_{i+1}}{K} \quad \frac{\Delta A_{b_i}}{x_{j+1} - x_{j-1}} \tag{12-58}$$

where ΔZ_j is the change in elevation for point (j), k_i and k_{i+1} are the conveyance of the incremental areas to the right and left of the point, and x_{j+1} and x_{j-1} are the horizontal coordinates of the cross section points adjacent to (j).

To save computer time the sediment is not distributed at a cross section until a significant change in cross section area has occurred. This threshold can be determined according to the physical environment and the objective of study.

12.4 DATA REQUIREMENT

General

Spatial and temporal designs are necessary to provide a realistic representation of the space-time structure for the simulation model. Information on the river and its tributaries, their location, and the location of all pertinent gaging stations, structures and confluences allow the spatial design of a large river basin to be developed. The spatial design should also consider the purposes of the study. The temporal design of a system can be made using the historic hydrologic records of the watershed or river basin. The records should include water flows, river stages, flow volumes, and the effect of man's activities, such as reservoir construction, on the hydrologic record. The temporal design must be compatable with the spatial design. Therefore, only those records pertinent to areas and river reaches included in the spatial design need be analyzed. The temporal design would be used to generate the system input for evaluating the future response of the system. An example of spatial and temporal design is presented in Chapter 20.

Spatial Design

The spatial design is the model's representation of the physical system. Required data for the model are:

1) digitized channel cross sections with over bank stations and Manning's n values;

2) river distance between cross sections;

3) tributary locations; and

4) locations of any structures.

In addition historic cross section measurements are necessary to calibrate the model.

Temporal Design

The temporal design is the model's representation of the water and sediment input to the river system. The temporal design can be made using the historic hydrologic records. Required data for the model are:

1) water discharge at each cross section location;

2) tributary water discharge;

3) tributary sediment discharge or rating curve (for point source tributaries only);

4) downstream stage control hydrograph or rating curve.

In addition, historic stages and discharges throughout the system are necessary to calibrate the model.

12.5 ADDITIONAL KNOWN-DISCHARGE MODELS

General

In the preceeding sections the discussion has been limited to the program KUWASER developed by the authors. While KUWASER has proven its ability in the Sedimentation Study of the Yazoo River Basin, it is by no means the only useful model which utilizes the known-discharge formulation. Three models, HEC-2, HEC-6, and Li's San Juan Creek Model have been selected to show the range of models which can be used to determine channel erosion and deposition.

HEC-2

HEC-2 (Hydrologic Engineering Center, 1976) is a water surface profile program which has become the standard program used in determining flood profiles in the United States. It uses the known-discharge formulation and solves the total head equation by a trial and error standard step method. The program has provisions for detailed analysis of flow effects caused by bridges, weirs, and other hydraulic structures. An important difference HEC-2 has with KUWASER is that HEC-2 uses the actual digitized cross sections to determine the hydraulic properties used in the water surface profile computations. HEC-2 data requirements are comparable with KUWASER.

HEC-2 does not have provisions for sediment routing, but in some cases when stream bed aggradataion-degradation can have drastic effects on the flood profile, there are legal or technical constants requiring the use of HEC-2. When this occurs HEC-2 can be combined with a sediment routing model. Simons and Li (1979) performed a study on Boulder Creek, Colorado which used this procedure (see Chapter 17). HEC-2 was used to compute the water surface profile and cross section hydraulic properties for one discharge. This information was then fed to a sediment routing model which calculated sediment transport and the aggradation-degradation at each cross section. The new cross sections were then fed back to HEC-2 and the process was repeated for the next discharge.

The sediment routing model used in Boulder Creek study utilized the Meyer-Peter, Mueller sediment transport equation and divided the bed into two layers so that armouring effect can be considered.

HEC-6

HEC-6 (Hydrologic Engineering Center, 1976) is a known discharge sediment routing model developed by William A. Thomas. The movable-boundary problem is simplified into one involving only a movable bed in the channel. The horizontal location of the channel banks is considered fixed, and the flood plain on each of the channels is considered as having a fixed ground surface.

In the backwater computations the total head equation is solved by a trial and error standard step method. The friction loss is calculated by Manning's equation, and expansion and contraction losses are included if the respective loss coefficients are specified.

Sediment mixtures are classified by grain-size fraction according to the American Geophysical Union scale. The program transports five fractions of gravel, from very fine (2 mm) to very coarse (64 mm), and five fractions of sand from very fine (0.0625 mm) to very coarse (2 mm).

Three options are available for calculating transport capacity: Toffaleti's application of Einstein's bedload function, Laursen's relationship as modified by Madden for large rivers, or a special relationship developed for the particular study and specified as transport capacity per unit of width versus the water depth-energy slope product.

Transport capacity is calculated at each cross section by using hydraulic data obtained during the calculation of water-surface profiles

(e.g., width, depth, slope, and velocity of flow) and the gradation of bed material for that cross section.

The data requirement for HEC-2 are similar to KUWASER's.

San Juan Model

Simons and Li (1978) develop a known-discharge, sediment routing model to analyze the aggradation and degradation in the San Juan Creek, California. Chapter 17 contains additional information on this model. The developed model is able to simulate to a high degree the development and distruction of the bed armor layer by dividing the bed into two layers. Each layer has its own sediment gradation. The active top layer supplies material for sediment transport and as such controls the transport. The bottom inactive layer supplies material to the top layer as the stream bed degrades. The top layer armors as fine materials are transported away more rapidly than they are replaced by the inflowing sediment layer. The San Juan model uses channel reaches of uniform width as its basic geometry data instead of channel sections. The model computes the water surface profile with the kinematic wave assumption, which is valid for steep slope streams such as San Juan Creek.

12.6 MODEL APPLICATION

General

In a study conducted for the U.S. Army Corps of Engineers, Vicksburg District, the sedimentation problems of the Yazoo River Basin were investigated (Simons, et. al., 1978). The Yazoo River Basin covers approximately 13,400 square miles in the northwest portion of Mississippi. A system analysis of the main channel and its triburaties was conducted by routing water and sediment. The objective was to determine the effectiveness of a proposed system considering flood control, navigation, and the location of aggradation and degradation problems. Methods of minimizing operation and maintenance problems were also evaluated. This analysis provided a method for evaluating the Upper Yazoo Project and the various design alternatives outlined by the U.S. Army Corps of Engineers. In this study a seven-day time increment for simulation was used since this is the approximate time required for water to travel through the system being analyzed. The closeness of weekly and daily flow statistics further validated the selection of a seven-day time

increment for simulation. The primary objective of this study was to identify and analyze sedimentation problems. Consequently, the known discharge model was used extensively in the analysis.

In the Yazoo River Basin, tributaries to the main stem were divided into controlled, uncontrolled, and point source type streams. Controlled tributaries, for example the Yalobusha River, are regulated by large storage reservoirs, including Arkabutla, Sardis, Enid, and Grenada. The controlled tributaries significantly affect the response of the Basin. Uncontrolled tributaries are generally smaller than controlled ones and do not have large storage reservoirs; however, they are important in analysis. An example of this type of tributary is Big Sand Creek. The third type of tributary is referred to as a point source and is generally smaller than the other two types. Point source tributaries are considered as a point input. The potential impact of sediment inflow from point source tributaries to the main stem is small. However, in order to conserve flow continuity, these tributaries were included in the analysis of the Yazoo system as point source inputs. An example of this type of tributary is Piney Creek. Because of a limited data base for the analysis, discharges from ungaged tributaries and nonpoint sources were synthesized utilizing watershed area and continuity concepts.

Calibration

The model was calibrated at Ft. Pemberton Cutoff. This particular reach is quite unstable and experienced a 20-ft degradation during the 1973 and 1974 floods. The model was calibrated for Manning's roughness coefficient from the period of April 12, 1973 to February 23, 1974 (318 days). The model was then run for the same time period, with the sediment transport in the river set to its measured value. Figure 12.12 shows a plot of the observed and computed stage hydrographs for the calibration. The calibration is excellent. Figure 12.13 provides the comparison of observed and computed bed elevations at the four cross-sections in the Cutoff. As indicated, the computed bed profile for February 23, 1974 closely matches the observed bed profile. In addition, Figure 12.14 shows the simulated change in cross-sectional shape is fairly close to the measured change.

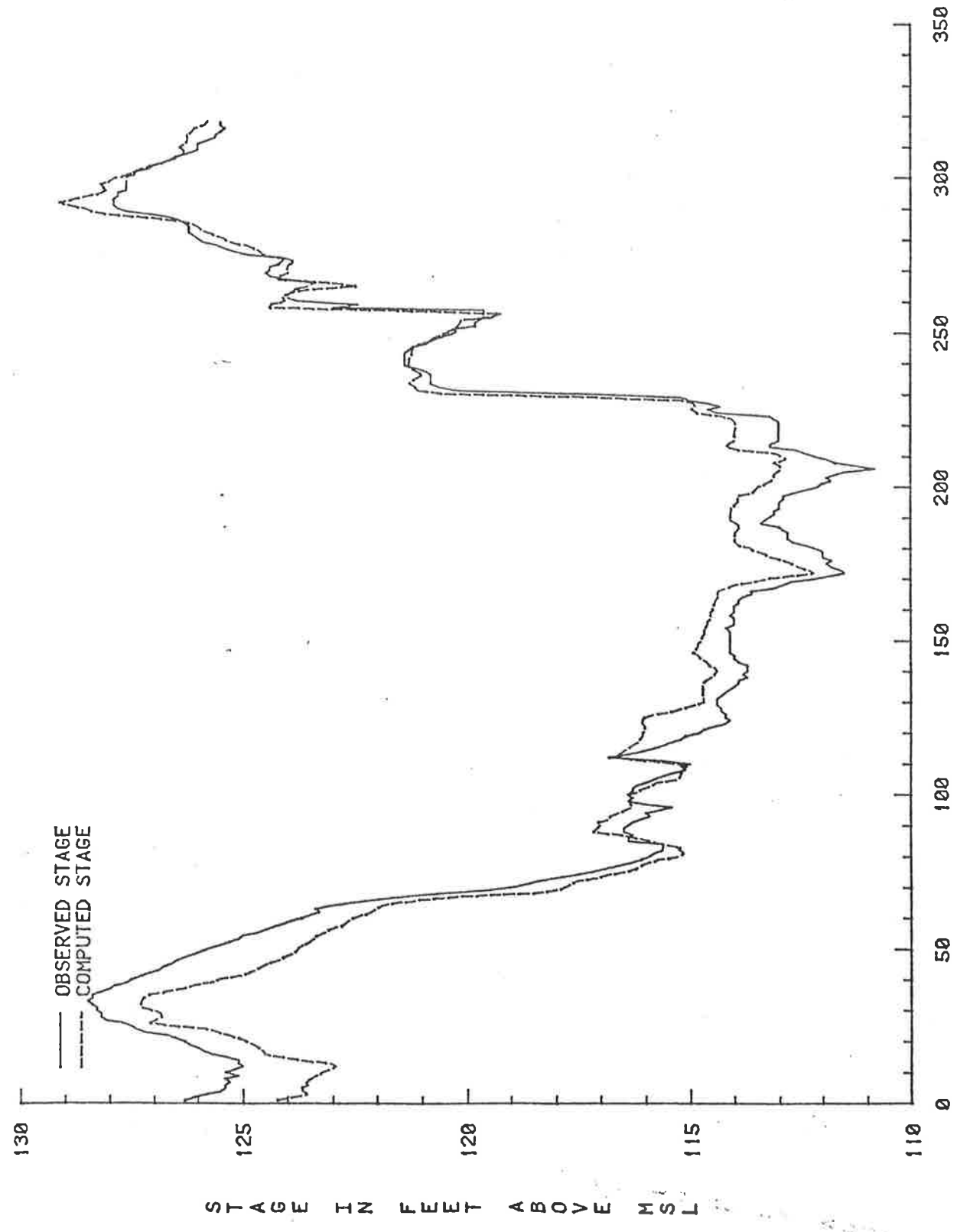

Figure 12.12 Known discharge model calibration at Fort Pemberton.

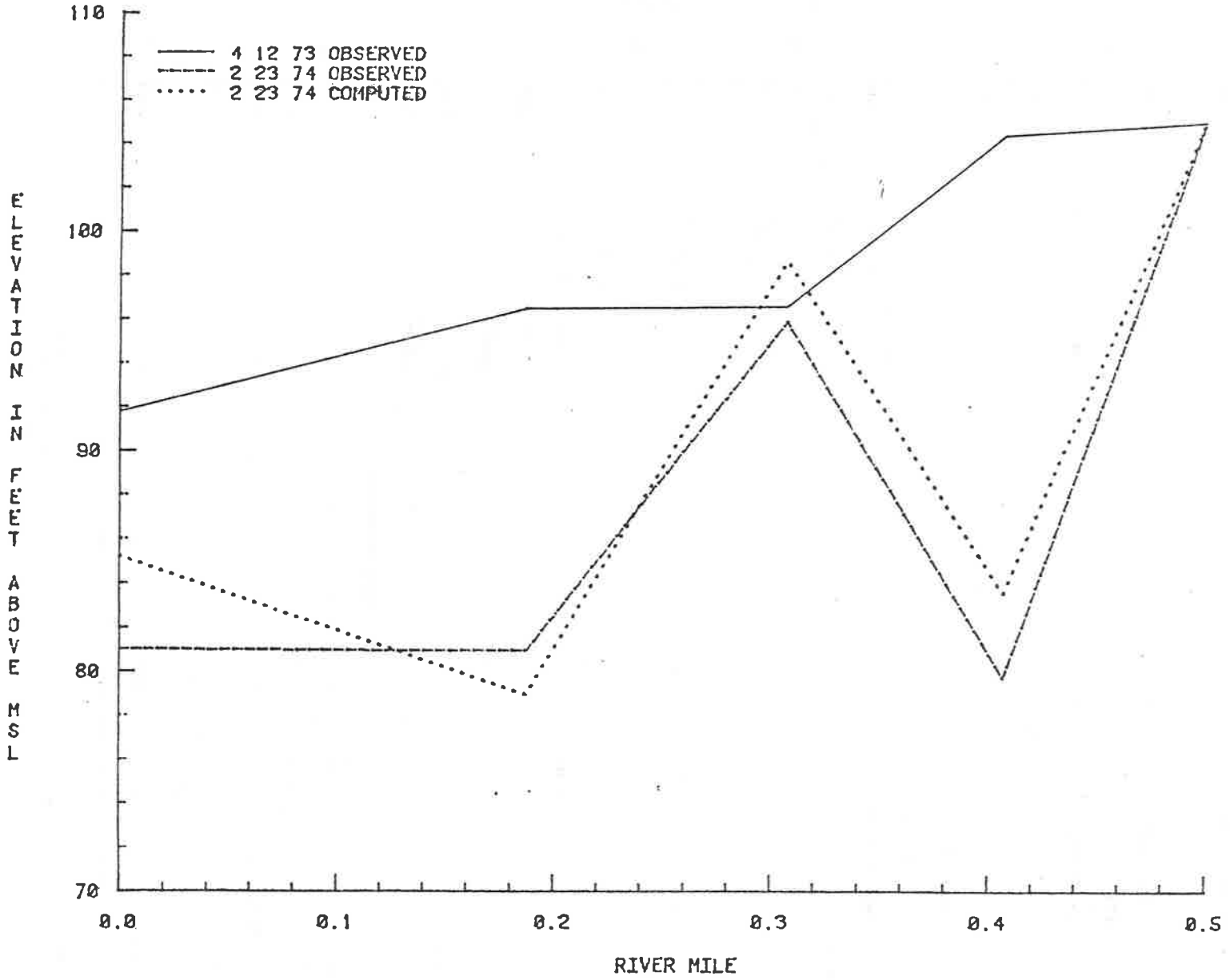

Figure 12.13 Known discharge model calibration of bed elevation at Fort Pemberton.

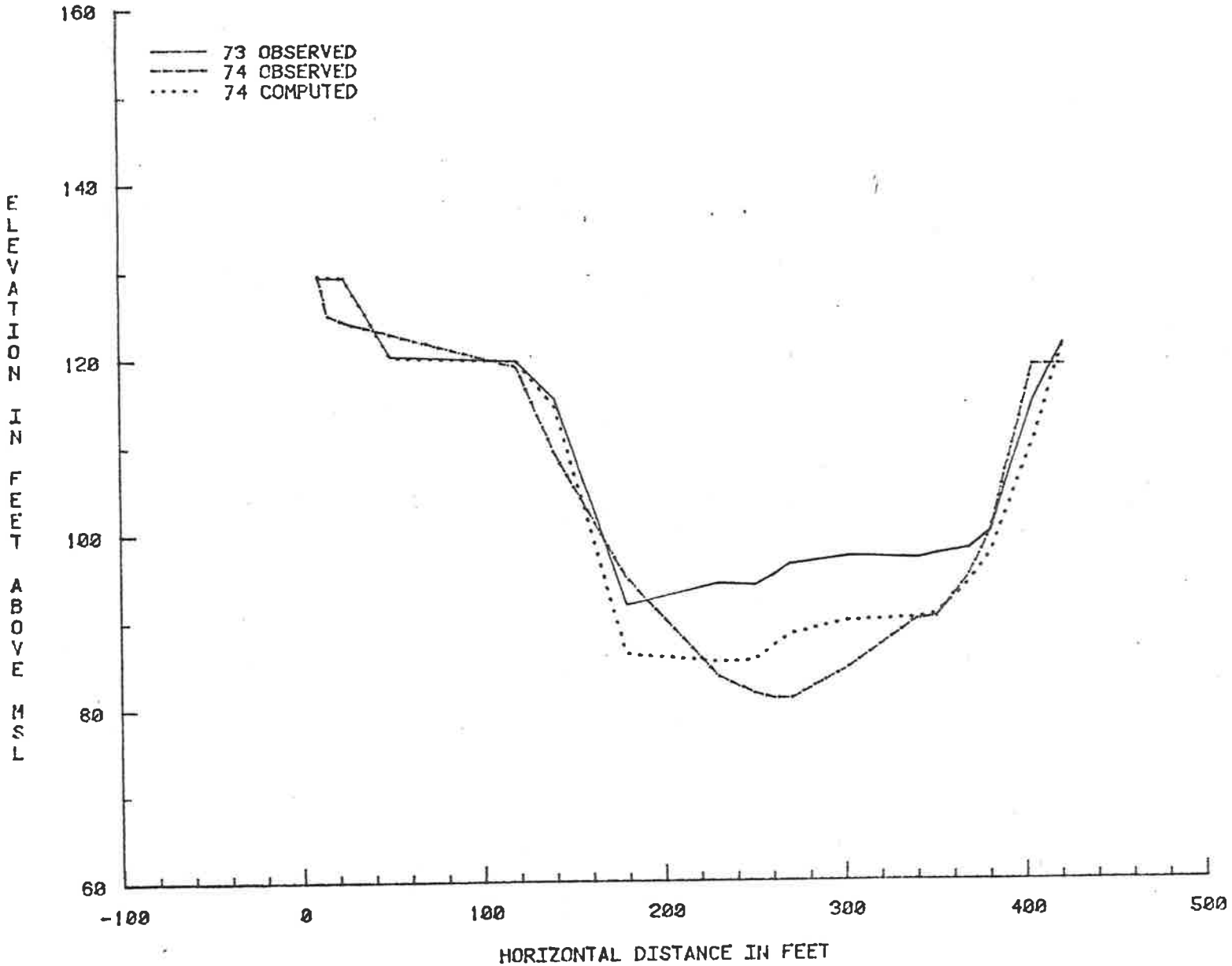

Figure 12.14 Comparison between computed and measured cross sections at Fort Pemberton using the known discharge model (P.R. 162.5).

Verification

To verify the applicability of the model, an additional run was made for time periods immediately following the calibration time. At Ft. Pemberton, the verification time was from February 24, 1974 to December 31, 1974 (311 days). The results of stage prediction are shown in Figure 12.15. The verification results are excellent. The average error between the computed and measured stage for the verification period was 1.10 ft with a maximum error of 2.48 ft.

Long Term Simulation

After calibration, the model was utilized to evaluate design alternatives, to identify the extent of sedimentation problems in the main stem and principal tributaries, and to suggest possible remedies. These alternative study runs were conducted by routing water and sediment through the tributaries and the Yazoo River main stem for a selected hydrograph utilizing the various alternative plans. A total of 15 alternative study runs were made. The alternative study runs included the natural conditions, the effects of land use, the effects of channelization, the effects of construction scheduling, the various plans for reducing sediment supply from the tributaries, the different dredging schedules, and the proposed navigation channels. Examples of these applications follow.

Figure 12.16 shows the beginning and final bed profile after 50 years under natural conditions, that is, conditions with no development. The maximum water surface elevations are the maximum values at each cross section considering the 50-year simulation period. These values do not necessarily occur at the same time for all of the cross sections and may not take place during the period of maximum discharge. The downstream water surface elevations and the long-term sediment movement in the system will dictate local water surface elevations.

Examples of the stage-discharge relationship just below Greenwood Bendway (river mile 162.5) during the first year, 10th year, 30th year, and 47th year are displayed in Figure 12.17. The 47th year was selected because it closely approximated the 1973 flood. These figures indicated that the stage-discharge relationship at the station is consistent with time for the natural conditions.

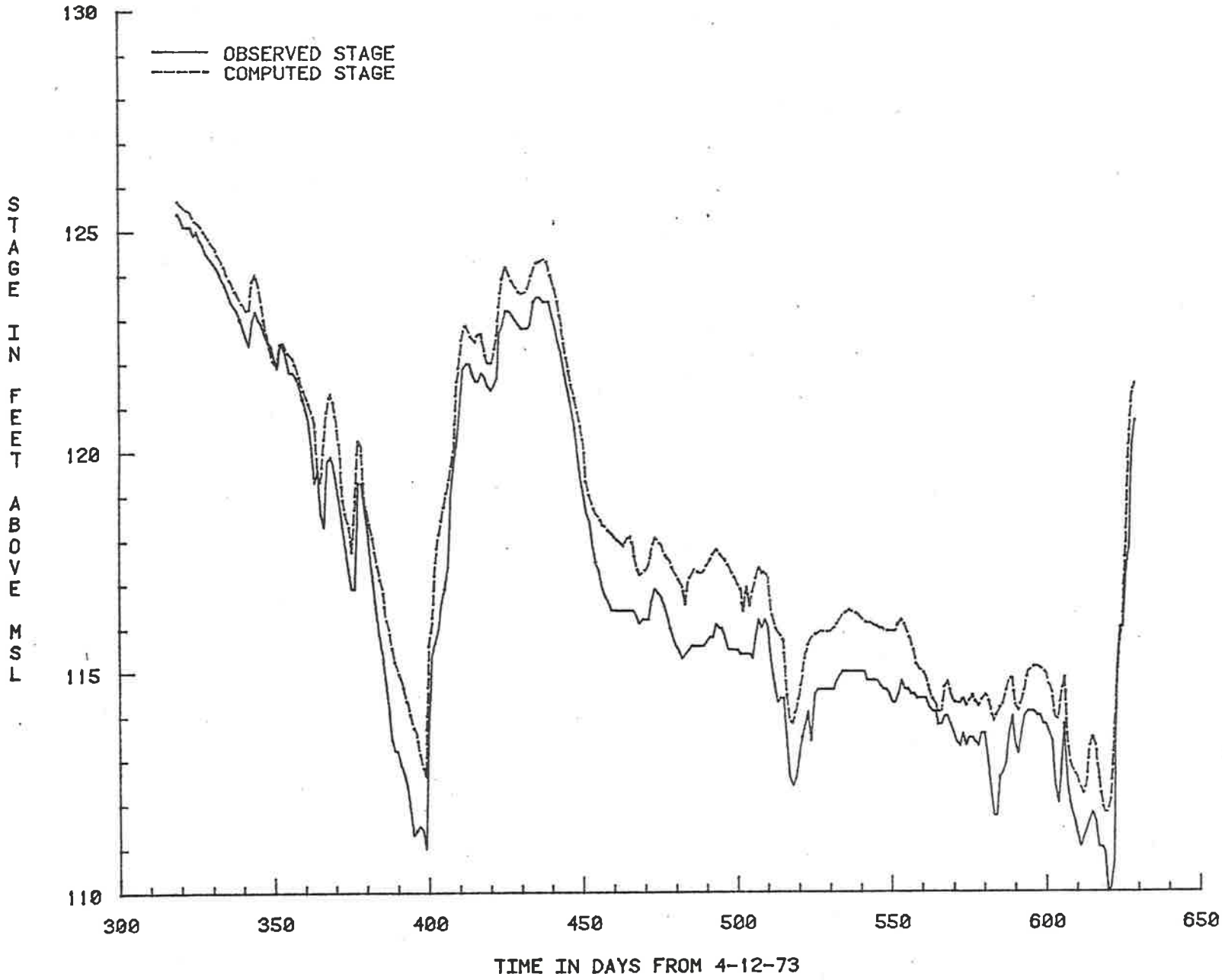

Figure 12.15 Known discharge model verification at Fort Pemberton.

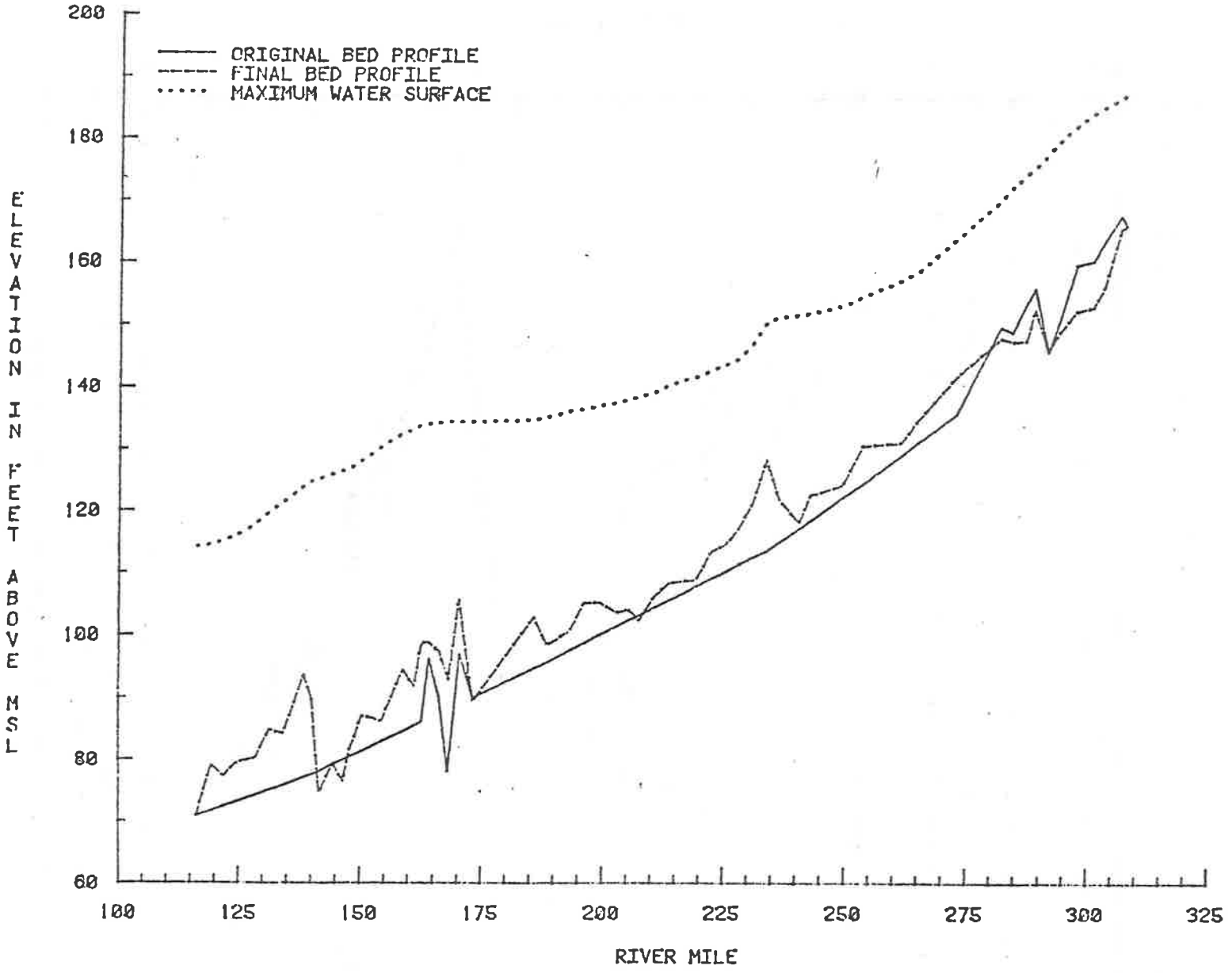

Figure 12.16 Beginning and final bed profiles and maximum water surface elevations for natural conditions (Run No. 1).

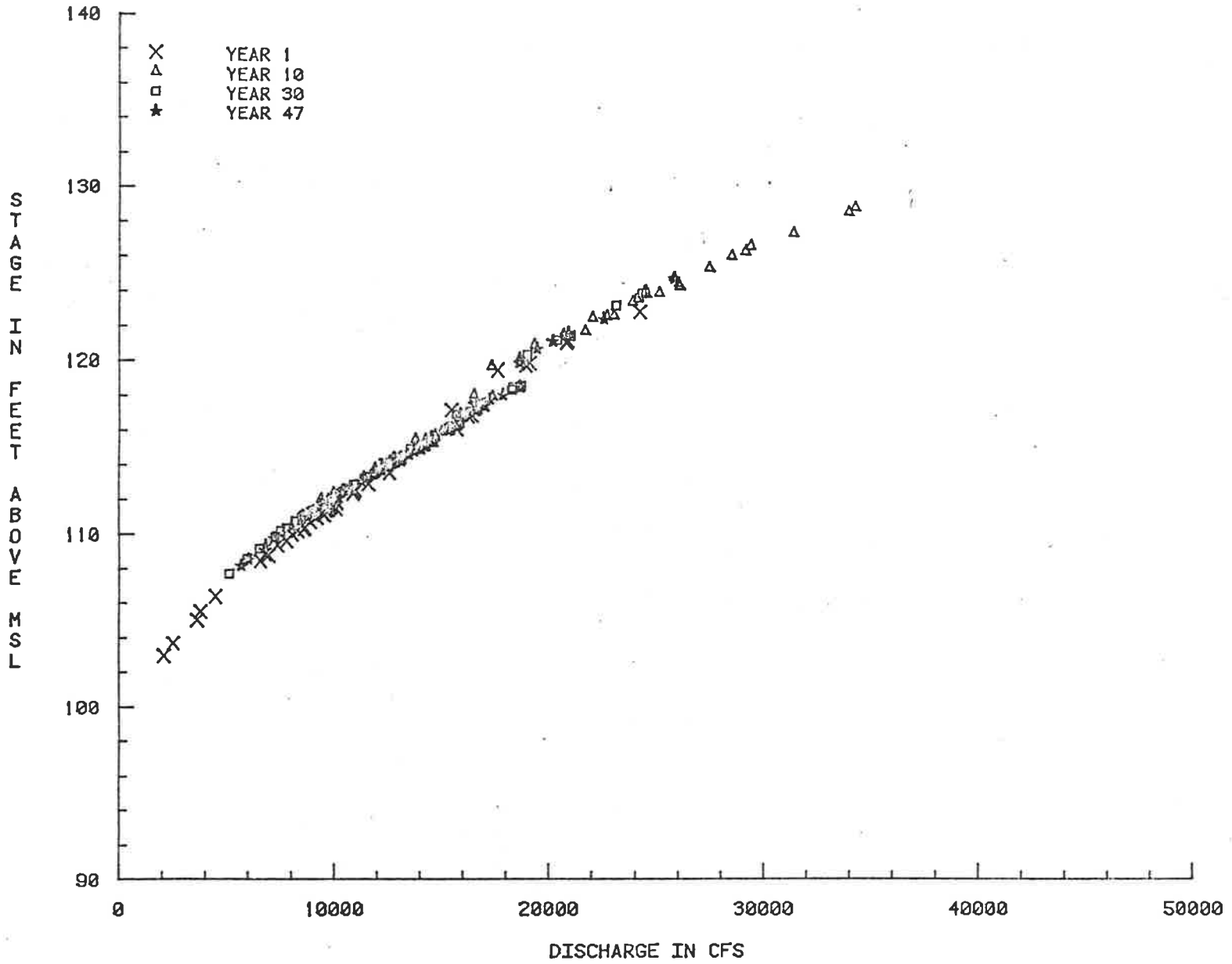

Figure 12.17 Stage discharge relationship downstream of the Greenwood Bendway (river mile 162.5) for natural conditions.

Plan E, the plan recommended by the U.S. Army Corps of Engineers, was evaluated under the same hydrologic conditions. Figure 12.18 shows the beginning and final bed profiles as well as the maximum water surface elevations along the main stem assuming Plan E conditions and considering 50 years simulation. This figure clearly indicates that the most critical areas for maintenance problems are the reaches below Abiaca Creek (river mile 140.34) and below the mouth of the P-Q Floodway (river mile 234.65). The maximum water surface levels are generally higher than those under natural conditions for reaches downstream of Money (river mile 192.9). The study shows that deposition rates of Plan E are much larger than those for natural river conditions. The computed average rate of deposition for Plan E decreases with time, which is consistent with changes in hydraulic conditions.

The stage-discharge relationship below Greenwood Bendway (river mile 162.5) for different time periods is shown in Figure 12.19. This figure indicates that the proposed Plan E would increase stage-wise with time due to significant deposition and can only be effective for flood control if maintenance dredging, control of sediment supply from tributaries, or other maintenance methods are implemented.

Other examples of evaluation of design alternatives utilizing the developed mathematical model are present in Chapter 20. The Yazoo Basin sedimentation study represents one of the most complicated river system analyses that has ever been conducted.

12.7 SUMMARY

This chapter has summarized the theory and application of the known-discharge, uncoupled water and sediment routing model KUWASER. The model incorporates several features which make it unique among existing models. These features include, 1) analytical Newton-Raphson solution to the backwater curve, 2) weighted distribution of the sediment erosion; deposition across the cross section, 3) ability to route water and sediment through an entire river basin, 4) data format compatibility with a data base package and 5) minimal computer time requirements which makes it practical to model large systems for long-time periods.

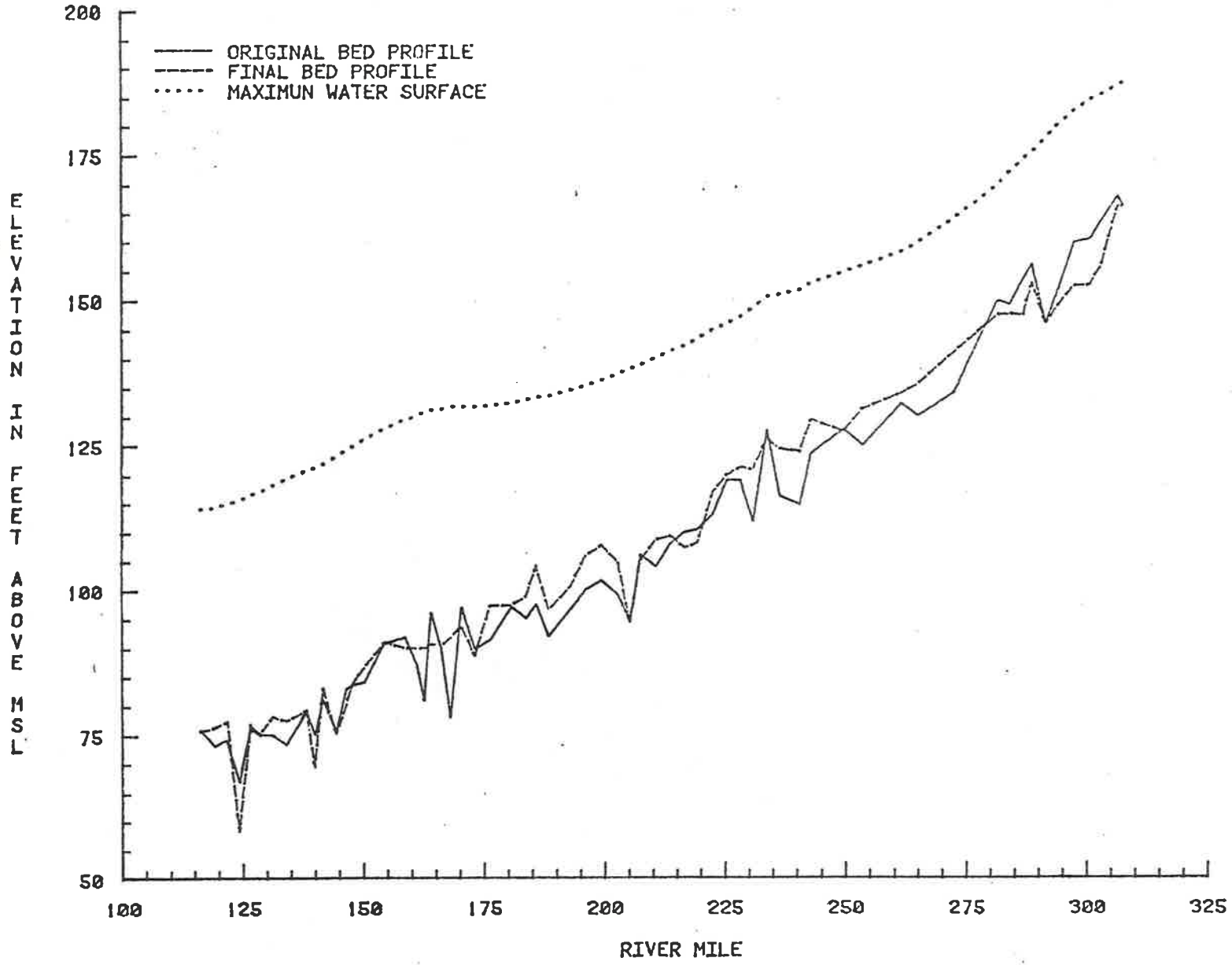

Figure 12.18 Beginning and final bed profiles and maximum water surface elevations for Plan E conditions (Run No. 2).

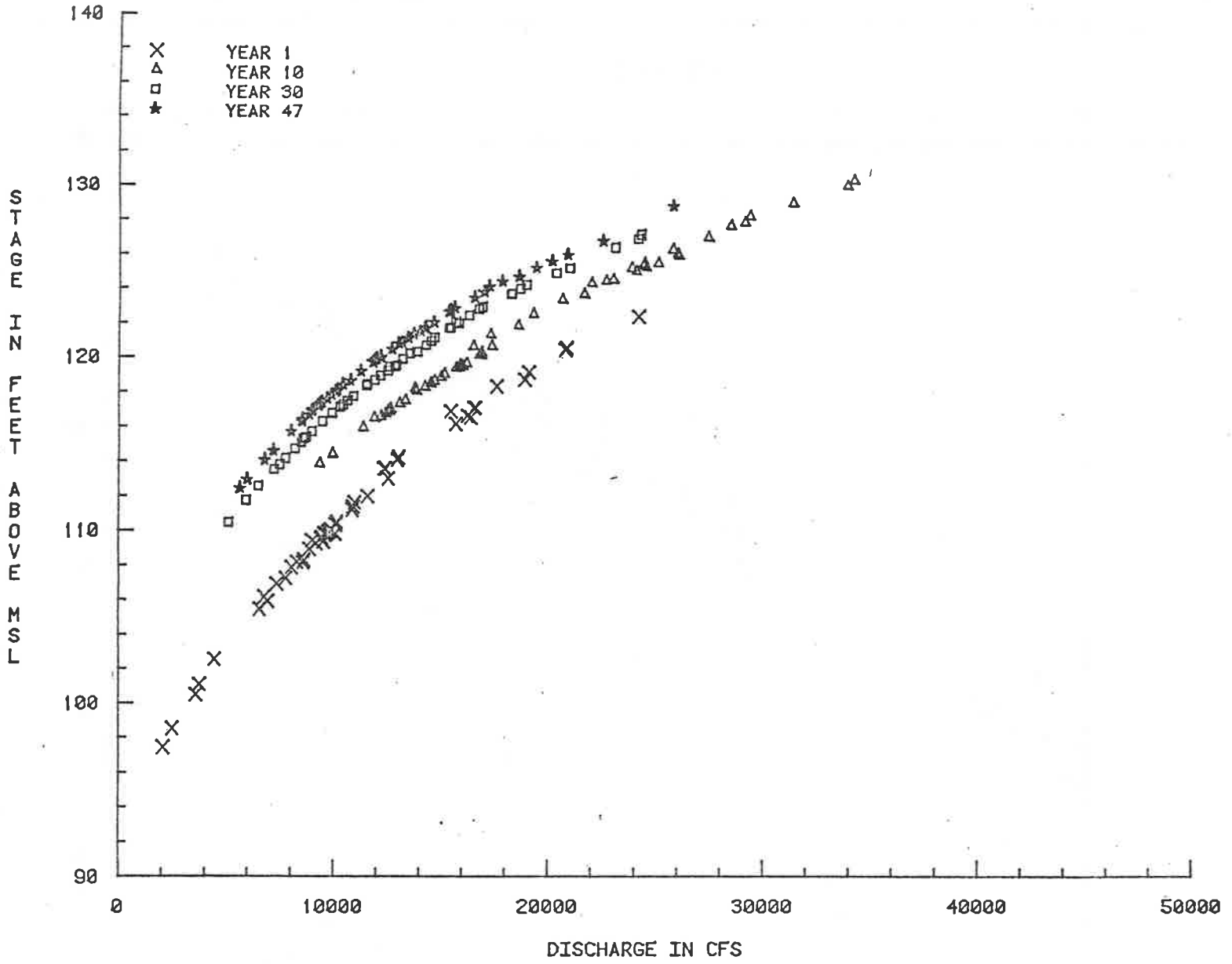

Figure 12.19 Stage discharge relationship downstream of Greenwood Bendway (river mile 162.5) for Plan E.

12.8 LIST OF SYMBOLS

A	area of flow
A_b	bed area
a_i	incremental flow area
a_n	coefficient of Manning's n-value relationship
$a_1 - a_{10}$	coefficients of hydraulic property relationships
b_n	coefficient of Manning's n-value relationship
$b_1 - b_{10}$	coefficients of hydraulic property relationships
C_e	coefficient of eddy loss
D	vertical depth of flow
D_a	average depth for incremental area
D_e	effective depth
D_{lob}	left over bank station
D_{rob}	right over bank station
D'	depth of coordinate point
d	depth of flow normal to the bed
E	energy of flow
g	acceleration of gravity
H	total hydraulic head
H_ℓ	friction head loss
$H_{\ell v}$	eddy head loss
K	flow conveyance
k_i	incremental conveyance
N	number of cross section area increments
n	Manning's n-value
n_{a_i}	average Manning's n-value
p_i	incremental wetted perimeter

Q	water discharge
q	lateral discharge
Q_s	sediment transport
$q_{s\ell}$	lateral sediment inflow
R	hydraulic radius of flow
r_i	incremental hydraulic radius
S_e	energy slope
S_f	friction slope
S_h	head slope
S_o	bed slope
S_w	water surface slope
t	time
U	lateral inflow velocity
V	mean flow velocity
W_e	effective width
X_b	width of incremental area
x	distance along channel bottom
Z	channel bottom elevation
Z_b	change in depth for incremental area
Z_{ob}	over bank elevation
α	velocity head correction factor
β	momentum correction factor
ΔA_b	change in bed area
ΔV	change in sediment volume between crosss sections
ΔX	horizontal distance between cross sections
γ	specific weight of fluid
ρ	sediment deposit porosity

θ	bed angle to horizontal
ψ	arbitrary variable
τ	bed shear stress

12.9 REFERENCES

1. Brown, G. O., 1979, Master's Thesis in preparation, Department of Civil Engineering, Colorado State University, Fort Collins, Colorado.

2. Chen, Y. H., 1973, Mathematical Modeling of Water and Sediment Routing in Natural Channels: Dissertation (Ph.D), Department of Civil Engineering, Colorado State University, Fort Collins, Colorado.

3. Chow, V. T., 1959, Open-Channel Hydraulics, McGraw-Hill Book Co., New York, New York.

4. Hydrologic Engineering Center, 1973, HEC-2 Water Surface Profiles, User's Manual, U.S. Corps of Engineers.

5. Hydrologic Engineering Center, 1976, HEC-6 Scour and Deposition in River and Reservoirs, Users Manual, U.S. Army Corps of Engineers.

6. Li, R. M., 1972, Sheet Flow Under Simulated Rainfall, Thesis (M.S.) Department of Civil Engineering, Colorado State University, Fort Collins, Colorado.

7. Simons, D. B., and Li, R. M., 1978, Erosion and Sedimentation Analysis of San Juan Creek Near Conroch Grand Pit, Orange County, California, Prepared for Dames and Moore, Denver, Colorado, June.

8. Simons, D. B., and Li, R. M., 1979, Erosion and Sedimentation Analysis of Boulder Creek, Colorado, Prepared for URS Company, Denver, Colorado, March.

9. Simons, D. B., and Sentürk, 1977, Sediment Transport Technology, Water Resources Publications, Fort Collins, Colorado.

10. Simons, D. B., Li, R. M., Brown, G. O., Chen, Y. H., Ward, T. J., Duong, N., and Ponce, V. M., 1978, Sedimentation Study of the Yazoo River Basin, Phase I, General Report, Department of Civil Engineering, CER77-78DBS-RML-GOB-YHC-TJW-ND-VMP48, Colorado State University, Fort Collins, Colorado.

11. Yen, B. C., and Wenzel, H. G., Jr., Dynamic Equations for Steady Spatially Varied Flow, Jour. Hydr. Div., ASCE, Vol. 96, No. HY3, March, pp. 801-814.

CHAPTER 13

LANDSLIDE POTENTIAL DELINEATION

by

Timothy J. Ward, Assistant Professor, Department of Civil Engineering, Colorado State University, Fort Collins, Colorado

Ruh-Ming Li, Associate Professor, Department of Civil Engineering, Colorado State University, Fort Collins, Colorado

Daryl B. Simons, Associate Dean for Engineering Research and Professor of Civil Engineering, Colorado State University, Fort Collins, Colorado

13.1 INTRODUCTION

Landslides are the downslope movement of rock, soil, and/or organic material. When landslides occur in populated areas, widespread destruction and loss of human life may ensue. In this chapter, factors controlling landslides and methods used to quantify landslide potential and probability are presented and demonstrated. Use of information supplied in this chapter will provide the reader with a better understanding of a formidable natural hazard.

Classification of Landslides

Classification

There are several landslide classification systems. However, the scheme proposed by Varnes (1958) is one of the most popular and is suggested for use. This system, shown in Table 13.1, accounts for materials, form, and rate of movement. There are three primary types of landslides with a fourth type, complex landslides, being composed of a combination of the other three primary types. Most landslides are the complex type. The three primary types are slides, falls or flows. Slides are commonly translational (Figure 13.1) or rotational (slump), (Figure 13.2). This type of landslide usually occurs along a well-defined failure plane and the material acts as a single or multiple well-defined unit. Falls (Figure 13.3) occur with movement primarily through the air and often act as discrete units such as large rocks or soil aggregates. Flows (Figure 13.4) on the other hand are unconsolidated in nature and act as extremely viscous fluid. Flows may be wet or dry depending on the water content of the moving material.

Useful Definitions

In addition to the primary types of landslides there are specific terms used to define the individual parts of a slide type landslide. These are shown in Figure 13.2 and defined below (Varnes, 1958; Rogers, et al., 1974).

Main scarp - steep undisturbed ground surface above the highest part of the slide, resulting from downward movement of slide material.

Minor scarp - steep surfaces in slide material resulting from differential movement within the body of the slide.

Crown - in-place material just above the main scarp.

Table 13.1 Classification of landslides (after Varnes, 1958).

Type of Movement	Type of Material			
	Bedrock		Soils	
			Granular	Plastic
Falls	Rockfall		Soilfall	
Few Units	Rotational	Planar		
Slides	Slump	Block-Glide	Slump, Block-Glide	
Many Units		Rockslide	Debris Slide	Failure by Lateral Spreading
	All Unconsolidated			
	Rock Fragments	Sand or Silt	Mixed	Mostly Plastic
Flows — Dry	Rockfall-Avalanche	Sand Run	Loess Flow	
Flows			Debris Avalanche	
Flows — Wet				Earthflow
Flows — Wet		Sand or Silt Flow	Debris Flow	Mudflow
Complex	Combinations of Materials or Type of Movement			

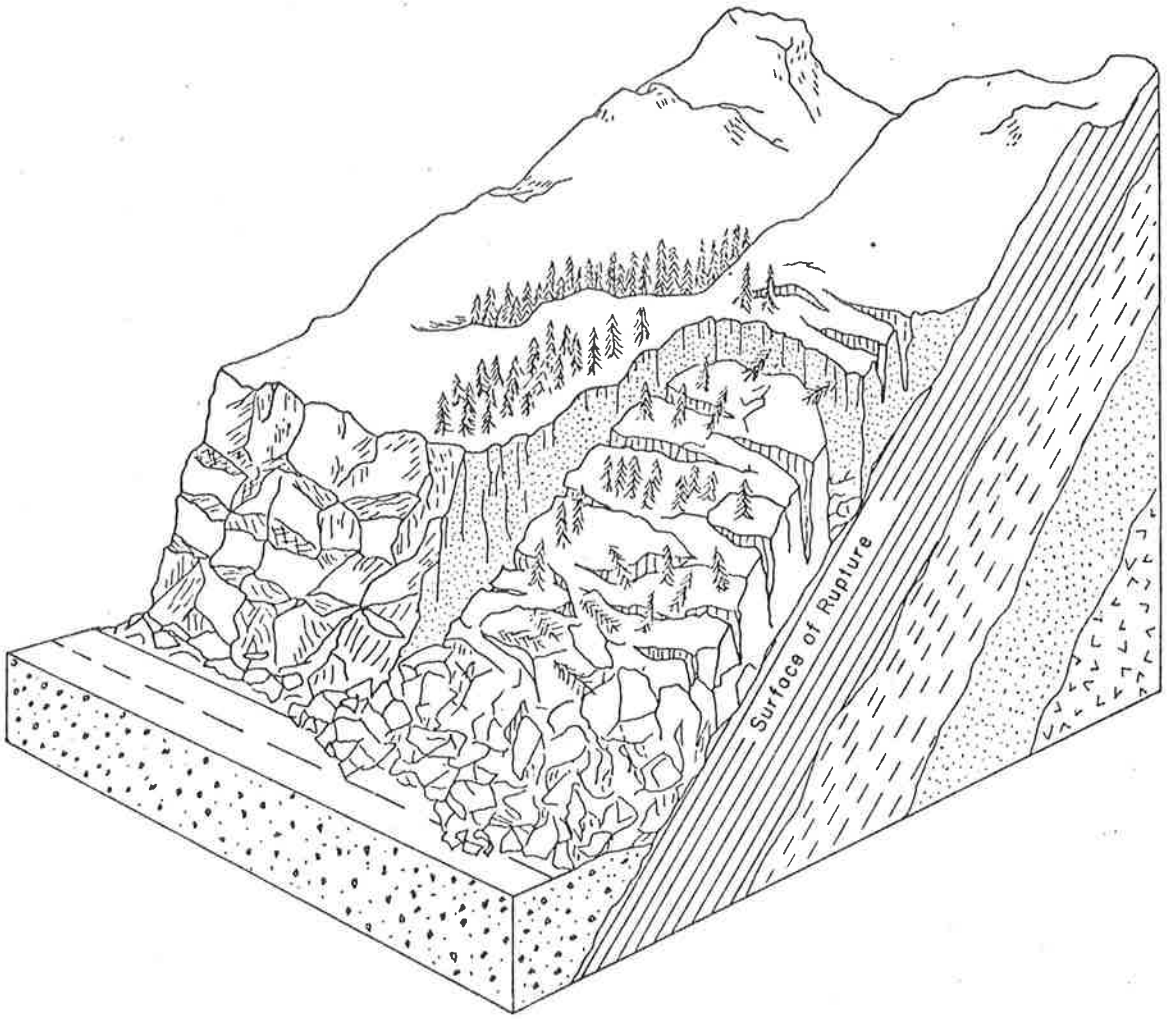

Figure 13.1 Translational slide-type landslide (from Rogers et al., 1974).

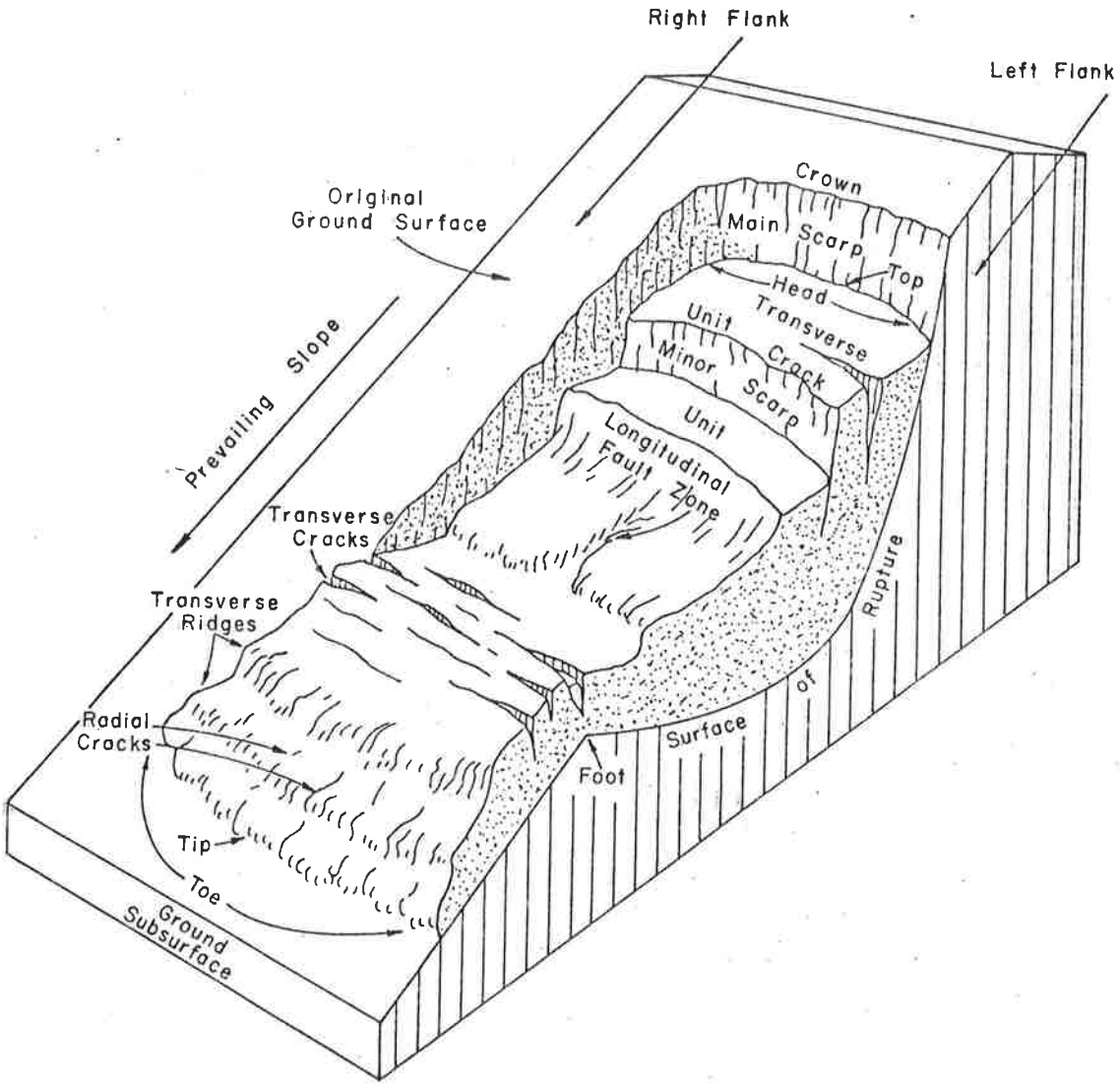

Figure 13.2 Rotational slide-type landslide (from Varnes, 1958; Rogers et al., 1974).

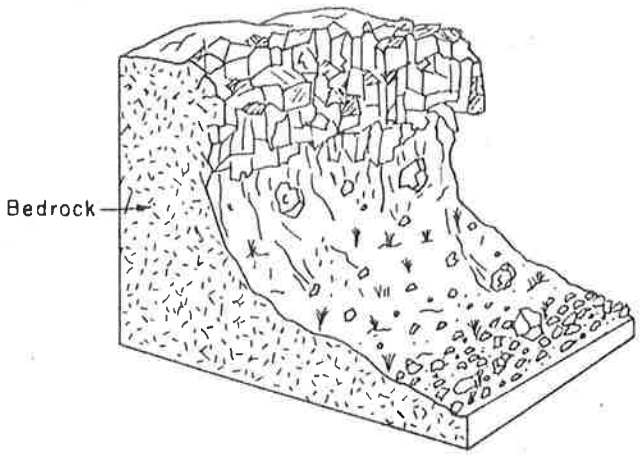

Figure 13.3 Fall-type landslide-rockfall.

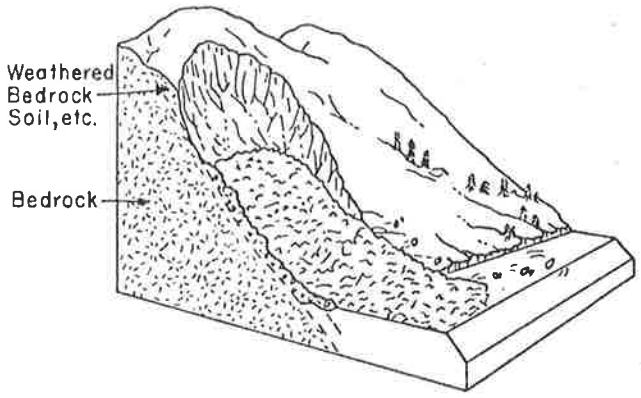

Figure 13.4 Flow-type landslide-debris avalanche (after Varnes, 1958).

Head - uppermost part of the slide material along the contact between the main scarp and the slide material.

Transverse cracks - tension cracks more or less perpendicular to the direction of slide movement, generally resulting from downward and outward movement of slide material over a hump in the rupture surface.

Radial cracks - tension cracks resulting from lateral spreading of unconfined slide material.

Tip - furthest forward extension of slide material.

Toe - furthest forward margin of slide material.

Foot - contact between original ground surface, and the lowermost extension of surface of rupture.

Surface of rupture - projection of main scarp surface beneath the slide mass.

Right flank - right extent of slide as viewed from the crown, looking down onto the slide.

Left flank - left extent of slide as viewed from the crown, looking down onto the slide.

Prevailing slope - direction of predominant ground surface slope in undisturbed area.

Original ground surface - undisturbed ground surface surrounding disturbed slide area.

Longitudinal fault zone - faulting resulting from differential forward progress of downward moving slide material.

Transverse ridges - rolling surface caused by differential movement of slide mass with downslope portion moving slower than upslope portion.

Although most common to slide type landslides, some parts of a slide, as shown in Figure 13.3, can be recognized in flows, such as the toe, tip, and transverse ridges (Johnson, 1970). In this chapter, slide type landslides, particularly translational slides (Figure 13.1) are considered. Further details with respect to landslide nomenclature are provided by Varnes (1958) and Rogers, et al., (1974).

Need for Delineation of Landslides

As population increases, more land development will occur in hilly or mountainous terrain where landslides may occur. In the United States, landslides rank fourth behind expansive soil, riverine flooding, and tornados for causing measureable damage (J. H. Wiggins Co., 1978).

Characteristically the areas of highest losses are the populous states of California, Pennsylvania, New York, Ohio, Maryland and Illinois. These states are located in one or the other of four recognized areas of high landslide occurrence: The Pacific Coast States, the Upper Ohio River Valley, the Appalachian Mountains, and the Rocky Mountains. By the year 2000, national losses from landslides are estimated to be about 830 million dollars (J. H. Wiggins Co., 1978). California losses between 1970 and 2000 are estimated at about 9.9 billion dollars (California Division of Mines and Geology, 1973). Landslides not only affect urban, suburban or mountain dwellers, and dwellings, but also cause impacts on other scenic and biologic systems (Table 13.2).

There are many aspects of landslides that can be investigated or analyzed to provide methods for avoiding, preventing, or correcting landslide hazards. The most efficient approach would be to determine where landslides may occur in order to avoid or prepare for this occurrence. This approach is often termed landslide potential delineation. Landslide potential delineation uses characteristic factors such as steep slopes known to produce landslides to determine where landslides may occur. Complementary to potential delineation is landslide probability. Landslide producing factors are quite variable and can be considered as having a wide range of values for a given location. The variation must be considered when delineating the landslide potential of an area.

Factors Influencing Landsliding

Cleveland (1971) presented landslide producing factors that could be used on a regional basis for delineating landslides. Simons and Ward (1976) have divided landslide controlling factors into two broad groups: static factors and dynamic factors. Static factors are those physical quantities that have little variation in real time and include: 1) slope characteristics, 2) geologic characteristics, 3) soil characteristics, and 4) vegetation characteristics. Dynamic factors are variable in real time and include: 1) hydrologic characteristics, 2) man-induced characteristics, and 3) miscellaneous characteristics.

Slope characteristics include inclination and aspect. Slope inclination is a significant factor in determining stability, however, it is not the only factor. Because slope angle is the result of many factors such as erosional processes and strength of the earth materials, it can be used as an indicator of stability. There are certain limits

Table 13.2 Effects of landslides.

Site	Effects
Tunnels	Closure of tunnel portals by debris
Roadways	Covering road with debris
	Roadway sliding downslope on slide mass
Houses	Debris sliding into houses
	Houses destroyed by ground movements of slide mass
	Access to houses isolated by sliding
Dams and Reservoirs	Overtopping waves produced by slide mass entering reservoir
	Filling of reservoir by slide mass reducing useable volume
Water Channels	Stoppage of flow in waterway
	Increased sediment loading
	Flooding caused by slide dam backup of water
	Floods from failure of slide dam
	Changes in river form
	Loss of canals built on unstable slopes
Utilities	Breakage of gas and water lines
	Burying and breakage of telephone and power lines
Forests	Loss of trees and other vegetation
	Loss of wildlife habitat
Aesthetic	Scarring of hillsides
	Creation of unproductive hummocky terrain

within which landslides often occur. Blanc and Cleveland (1968) suggest a lower limit of 10° in their study, while Radburch and Crowther (1970) suggest 15° as a lower limit. An upper limit may be near 35°, about the angle of repose for most earth materials. Slopes with inclinations less than the lower limit have small forces acting to produce landslides while slopes with inclinations above the upper limit lack a landslide material supply since it is continually being eroded. Slopes between these limits are subject to an ever changing continuum of forces. Slope aspect affects stability through changes in soil moisture and vegetation. Olson (1974) in Colorado and Beaty (1956) and Radburch and Weiler (1963) in California noted that north and east facing slopes usually showed more landslide activity. Usually, north and east facing slopes (in the northern hemisphere) are wetter than south facing slopes because less solar radiation reaches the ground. Increased vegetative growth tends to affect increases in soil moisture if the vegetation is a beneficial type.

Geologic characteristics that are important to slope stability are rock strength and structure. Rock strength is a result of mineral composition, grain size and shape, porosity and permeability, and the type of binding agent in the rock. In general, fine grained nonporous rocks composed of strong, weather resistant grains and binding agents will be stronger than other types. Rock structure influences slope stability on two scales. On the microscale, structure affects rock strength through cleavage planes, foliations, fractures, or grouping of weak materials. Similarly on the macroscale, the integrity of rock masses can be decreased by fractures, jointing, bedding planes, or strata of weaker rocks.

Important soil characteristics are those that influence soil shear strength. These include soil type, porosity and permeability, and soil depth. Clay is prevalent in many landslides. Clay chemistry is such that changing environmental conditions can either beneficially or adversely affect the clay structure and thus the soil strength. Changes of strength can, in time, lead to landsliding. Porosity and permeability control the buildup of pore pressure and level of soil moisture, and they also control shear resistance. Soil depth is important since shallow soils are less susceptible to sliding. Fife (1971) found that

soils at least one and one-half feet thick were sufficient to cause soil slips when subject to other influences. Swanston (1967, 1969) reported data showing debris avalanches in soil at least one foot thick. This is probably a minimum depth.

Vegetation plays an extremely important role in landslide occurrence. Gray (1970, 1978) and the Building Research Advisory Board (1974) indicate that vegetation enhances slope stability by 1) dissipating rainfall energy in the vegetative canopy, 2) lowering soil moisture levels, 3) anchoring surface materials to underlying strata with roots, and 4) binding surface materials together.

Vegetative canopy is composed of trees, brush, grasses, and other small plants. The areal distribution and type of canopy affects the rainfall intensity and the volume of water reaching the ground. Areas with high canopy cover will be less likely to be subject to raindrop impact and rapid saturation; thereby lessening the possibility of mass erosion.

Vegetation can significantly lower soil moisture content through transpiration (Perpich et al., 1965; Hammer and Thompson, 1966). As soil moisture is lowered, water pore pressures and chemical weathering decrease leaving shear strength intact.

According to Rahn (1969), vegetation makes surface materials more resistant to gravitational forces by joining the materials into larger units and anchoring these units to underlying strata. In all cases, the type of vegetation and areal distribution are important measures influencing how effective vegetative cover is in enhancing stability. Plant types that develop deep extensive root systems, deplete soil moisture by transpiration, and possess foliage that dissipates rainfall enhancing slope stability.

There are some deleterious effects from vegetation. Trees can produce a surcharge load on the slope and transmit shear loads during windstorms (Brown and Sheu, 1975). Grasses and other shallow rooted undergrowth can detain water on slopes, allowing more infiltration with resultant deleterious effects. Root systems cause discontinuities in soil layers that disrupt the soil structure and provide large infiltration channels (Gaiser, 1952). When vegetation dies or is killed, the decaying root systems make a smaller and smaller contribution to soil

stability (Bethlahmy, 1962; Gray, 1970; O'Loughlin, 1974; Brown and Sheu, 1975; Burroughs and Thomas, undated). Despite this, vegetation generally enhances slope stability.

Dynamic factors vary rapidly in real time. These factors fall into three major groupings: hydrologic, man induced, and miscellaneous. Because dynamic factors can vary in time, it is often difficult to quantify the influence a dynamic factor has on slope stability (Thomson, 1971; Vandre, 1975). The relationship between dynamic factors and static factors must be understood in order to ascertain their effects on slope stability (Cleveland, 1971; Simons and Ward, 1976).

Hydrologic factors include precipitation, surface flow, and subsurface flow or soil moisture. Soil moisture and groundwater occurrence are the most important hydrologic factors with regards to slope stability (Simons and Ward, 1976; Nilsen and Turner, 1975).

Soil moisture weathers earth materials, alters strength, and produces pore water pressures. Pore water pressures produced by soil moisture or groundwater can decrease the resistance of the earth materials to sliding. Simultaneously, the increase in the unit weight of the soil usually increases the tendency for the earth materials to slide.

Man-induced factors include those that decrease landslide resistance, increase the failure forces, or a combination of the two (Simons and Ward, 1976). Placement of fill on the head of a slope is a common factor in man-induced landslide occurrences. Oversteeping slopes, removing vegetation, and altering the hydrologic systems are also common factors. Landslide literature is filled with case histories of man upsetting the balance between forces (Kiersch, 1964); Wahlstrom and Nichols, 1969; Williams and Armstrong, 1970, Bolt et al., 1975).

Miscellaneous factors include seismic vibration and fires. Seismic vibration can be caused by blasting, heavy machinery operation, sonic booms, or earthquakes (Conlon, 1966; Seed and Wilson, 1967; Voight, 1973). Seismic vibrations produce horizontal acceleration of slope materials that increase horizontal stresses (Okamota, 1973). Seismic vibrations can also alter the physical properties of the slope materials by compaction or fragmentation, or the production of liquefaction phenomena (Youd, 1973; Martin et al., 1975).

Generally, landslides resulting from the effects of fires are probably more prevalent than seismic triggered landslides but are not as widely noticed or reported. Fires remove vegetation and alter slope materials. When the rainy season returns, the slope materials are not as resistive to erosion or sliding. This situation can produce numerous landslides and mud flows (Woolley, 1946; De Bano et al., 1967; Cleveland, 1973; Hay, 1975). Landslides subsequent to fires are probably more prevalent that seismic produced landslides since not all landslide regions are subject to seismic disturbance but all are usually subject to fire.

Two types of factors affecting slope stability exist. Static factors are physical quantities relatively constant in real time. Dynamic factors are harder to quantify since they can vary in real time. Because dynamic factors alter static factors, static factors are measured perferentially to dynamic factors. This enables delineation of potential landslide areas on the basis of variables that can be measured and can be altered by dynamic factors.

13.2 CURRENT APPROACHES

There are many approaches to landslide potential delineation. These approaches include on-ground monitoring, remote sensing techniques, factor overlay methods, statistical models, and geotechnical process models.

On-ground monitoring consists of utilizing installed measuring devices such as strain gages and down hole tilt meters. This type of approach is extremely useful for checking suspected landslide zones but is limited in aerial coverage because of cost of installation and maintenance. Chang (1971) summarized many of these techniques. Takada (1968) and Takeychi (1971) provided two examples of applications of different methods.

Remote sensing coupled with pattern recognition techniques provide a means for surveying large areas. In this approach, remotely sensed data, particularly aerial photography such as black and white, color infrared, and multiban spectral, can be analyzed for features distinctive of landslide hazards (Liang and Belcher, 1958; Poole, 1969, 1972; McKean, 1977). This analysis, a type of the more general pattern recognition, can be quite effective if landslide hazards are manifested in surface

characteristics that can be photographed. However, it is not always the situation since landslides often result from deep seated factors not visible on the ground surface.

The most common delineation method concurrently in use is factor overlay or a combination of landslide producing elements. Krynine and Judd (1957) noted that landslides occur in a regional framework, or that certain factors common to a region contribute to landsliding. Baker and Chieruzzi (1959) expanded this concept to develop a physiographic classification of landslide hazards based on topography, erosional development, and associated rock types. Blanc and Cleveland (1968) were two of the first to attempt delineating landslides by use of selected factors. Evans and Gray (1971) presented a methodology for mud slide risk delineation in Southern Ventura County, California. Cleveland (1971) summarized and presented those factors important in regional landslide prediction. His factors include precipitation, rock strength, vegetation effects, slope, and stream pattern. The approaches described by Nilsen and Brabb (1973) and the Building Research Advisory Board (1974) follow this systematic methodology using landslide factors. In this approach, certain factors related to landslide occurrence are individually delineated. For example, if landslides occur where steep slopes, weak earth materials, and water are all coincident, then these factors should be used as slope stability indicators. Areas where factors coincide can then be classified as a hazard potential. Simons and Ward (1976) summarized this approach as the factor overlay method or set theory approach to hazard delineation as presented in Figure 13.5. Although not explicitly stated in delineation schemes, this idea is the basis for most techniques.

The factor overlay approach is conceptually correct since it recognizes that landslides are a combination of different factors. However, this approach is subjective and nonsensitive to dynamic inputs. Subjectivity results from a lack of defined guidelines for developing and weighting various factors. Nonsensitivity occurs because static factors are usually considered while dynamic factors, such as groundwater fluctuations, are excluded. Factor overlay can be improved if standardized guidelines are developed, dynamic factors are incorporated,

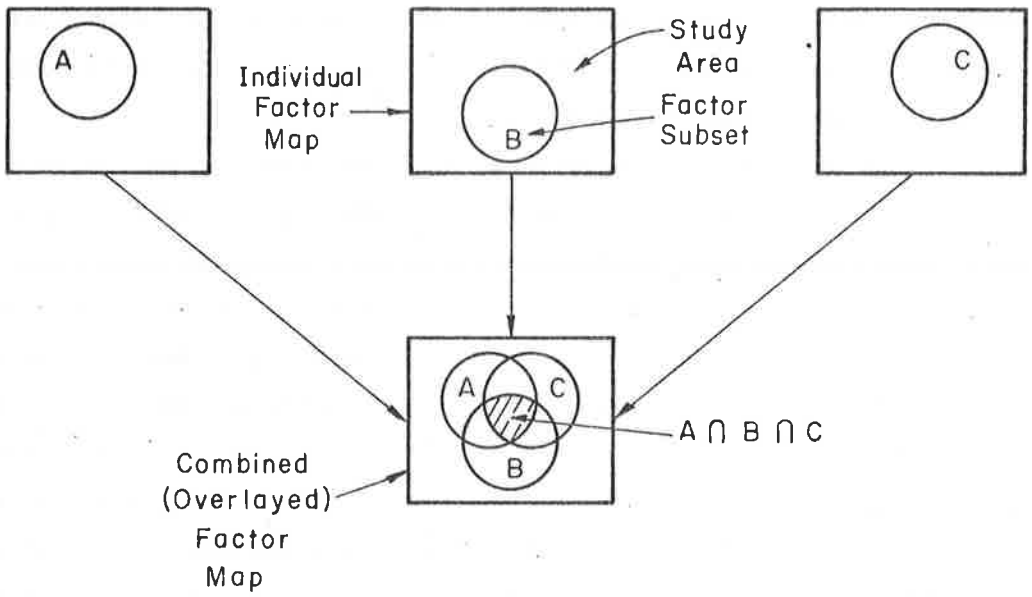

Potential	Set
High	$A \cap B \cap C$
Medium	$A \cap B$; $B \cap C$; $A \cap C$; A; B; C
Low	$\overline{A \cup B \cup C}$ (i.e. not in A, B, or C)

$\cap$ - Intersection of Subsets
$\cup$ - Union of Subsets

Figure 13.5 Set theory approach to landslide potential classification (from Simons and Ward, 1976).

and realistic weighting functions are used. Simons and Ward (1976) presented a numerical approach to the factor overlay technique that may help quantify the relative importance of each factor.

Another method of potential delineation is use of empirically developed models. These models, developed through statistical analyses of measurable data, attempt to provide a numerical value related to slope stability. Multiple regression and discriminant function analyses are common techniques for developing such relationships (Jones, Embody and Peterson, 1961; Waltz, 1971). Empirically derived relationships have a major drawback since they require large amounts of data to develop the equations. Such data is usually temporally and spatially static. Temporally static implies the developed relationship is applicable to a limited time span during which data was collected and, therefore, does

not represent changing conditions. Spatially static implies the method is applicable to a limited area and transfer to other areas may not be warranted.

A final type of landslide hazard delineation methodology is based on geotechnical models. Geotechnical models are derived from observed natural phenomena and basic laws of physics, and are representative of the physical process being studied. Geotechnical models of slope stability relate the forces acting on the hill slope. One set of forces, predominanted by gravity, acts to move earth materials downslope. The other set of forces, predominated by the shear strength of the earth materials, resists the driving gravity forces. When driving forces exceed resisting forces, a landslide occurs. Geotechnical models have been developed and modified to account for primary factors in landslide occurrence such as soil strength, groundwater influences, vegetative effects, and slope inclination. Because geotechnical models represent actual field conditions they can be used to analyze the response of a hill slope to temporally and spatially varying factors. Simplifying assumptions can yield a method for determining the probability of a landslide. Because of the ability to account for several temporally and spatially varying contributing factors in a nonsubjective, physically meaningful manner, geotechnical models are promising methods for landslide potential delineation.

13.3 FACTOR OF SAFETY DELINEATION MODEL

Model Selection

The analysis presented in this chapter is applicable to translational or planar types of landslides in soil masses. Rock masses require a more complex analysis because of their response to the geometry of failure planes, and are not considered here.

Various types of slope stability models exist. Two basic types are the infinite slope and finite slope models, each derived by a different set of assumptions (Lambe and Whitman, 1969). Common to both types is the formation of a factor of safety equation that consists of a ratio of resisting to driving forces of

$$FS = \frac{R}{D} \tag{13-1}$$

where FS = factor of safety; R = resistive forces; and D = driving forces.

Resistive forces are related to soil strength and vegetative parameters while the primary driving force is the downslope weight of the soil mass. If resistance is less than the driving force, then the factor of safety is less than one indicating failure.

The infinite slope model of slope stability is primarily applicable to failure occurring along planar type surfaces such as translational slides. The model presented in this paper consolidates and refines ideas presented by several researchers (Brown and Sheu, 1975; O'Loughlin, 1974; Simons, Ward, and Li, 1976; Swanson, et al., 1973). These developments were further studied by Ward (1976) to yield the model's present form. Because finite slope formulations also relate the same resisting and driving force elements, the model can estimate the failure potential for other landslide types such as rotational slumps.

Derivation of Model Equations

Derivation of the equations of static equilibrium for an infinite slope is relatively easy (Brown and Shen, 1975; Lambe and Whitman, 1969; O'Loughlin, 1974). The derivation presented here is similar to those given by previous authors but with changes in the formulation and simplification of the basic model. An idealized infinite slope consisting of a single soil type with isotropic properties resting on a bedrock interface is shown in Figure 13.6. This situation is similar to residual soil slopes found in forested watersheds and most hilly or mountainous terrain.

The shear strength of a soil can be represented by the Coulomb equation of

$$\tau = \bar{c} + \bar{\sigma} \tan \bar{\phi} \qquad (13\text{-}2)$$

where τ = shear strength; $\bar{c}$ = effective cohesion intercept; $\bar{\sigma}$ = effective normal stress; and $\bar{\phi}$ = effective angle of internal friction.

Equation 13-2 is applicable to drained soil strength conditions and represents resisting forces contributed by the soil mass. Components of $\bar{c}$ and $\bar{\phi}$ (hereafter, the overbar will be dropped) are intrinsic strength characteristics of soil and represent interaction of soil factors.

Analysis of Figure 13.6 aids evaluation of $\bar{\sigma}$. Normal stress on plane A' - B' located at a distance, Z, above the bedrock surface in the soil mass can be easily solved if the plane is assumed parallel to

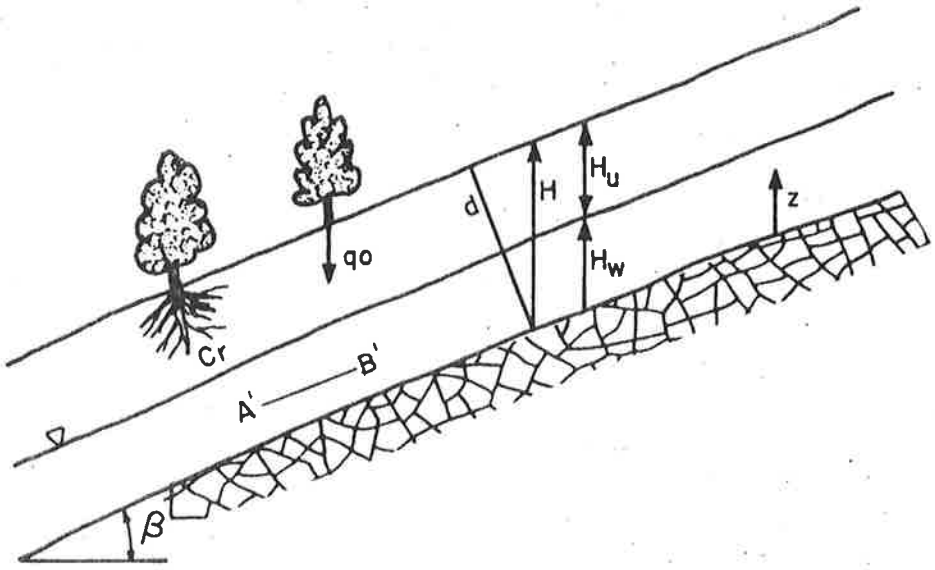

Figure 13.6 Idealized infinite slope.

soil and bedrock surfaces and is located between $Z = 0$ and $Z = H_w$. The total normal stress, σ, on this plane can be written as

$$\sigma = \sum_{i=1}^{n} \gamma_i \Delta z_i \qquad (13\text{-}3)$$

where γ_i = unit weight of layer i ; and Δz_i = thickness of layer i .

In this case $n = 2$ for the saturated and unsaturated soils but can be expanded to a multilayer case. However, in many residual soils, assumption of a single soil type is often valid (Lumb, 1970). The geometry and other important factors can be used to evaluate σ. The normal stress on plane A' - B' is composed of stresses from soil weight and tree surcharge. Soil weight per area component is $(H_u \cos \beta \gamma)$ for the soil above water table level and $[(H_w-Z) \cos \beta \gamma sat]$ for soil below water table level. Normal force per area supplied by tree surcharge is $(qo \cos \beta)$. Assuming the contact surface as a unit squared the area enables the normal stress to be written as

$$\sigma = [qo \cos \beta + (H_w-Z) \cos \beta \gamma sat + H_u \cos \beta \gamma] \cos \beta \qquad (13\text{-}4)$$

In Equation 13-4 the area upon which the normal force acts is defined as $\cos \beta$ times a unit area. Since $H_u = H - H_w$, Equation 13-4 can be converted to

$$\sigma = H \cos^2 \beta \, [qo/H + \gamma sat \, (M-Z^*) + \gamma \, (1-M)] \qquad (13\text{-}5)$$

where $M = \frac{H_w}{H}$ = relative groundwater height and $Z^* = \frac{Z}{H}$ = relative position from bedrock surface.

Because groundwater is present, the buoyancy effect of pore water pressures must be considered in Equation 13-4. From the effective stress concept the relationship between total and effective normal stress in soil mass components is

$$\bar{\sigma} = \sigma - u \qquad (13\text{-}6)$$

where u = the pore water pressure. Hydrostatic pressure can be formulated as

$$u = H(M-Z^*) \, (\cos^2\beta)\gamma_w \qquad (13\text{-}7)$$

Combining and simplifying Equations 13-5, 13-6, and 13-7 yields

$$\bar{\sigma} = H\cos^2\beta \, [qo/H + (\gamma_{sat} - \gamma_w) \, (M-Z^*) + \gamma(1-M)] \qquad (13\text{-}8)$$

Consequently, the shear resistance equation becomes

$$\tau = c + H\cos^2\beta\ [qo/H + (\gamma_{sat} - \gamma_w)\ (M-Z^*) + \gamma(1-M)]\ \tan\phi \qquad (13\text{-}9)$$

The cohesion term, c , in Equation 13-9 has two components in forested watersheds--soil cohesion and tree root cohesion. Gray (1970) described several ways that vegetation enhances slope stability. One of these is anchoring soil to underlaying strata. Endo and Tsuruta (1968) and O'Loughlin (1974) showed that anchoring can be represented in the FS equation as a cohesion term, Cr. The cohesion term, c , can then be replaced by terms for soil cohesion, Cs , and root cohesion, Cr.

A similar analysis can be made for shear stress induced on the plane. Shear stress is composed of loads resulting from the weight of the soil mass, tree surcharge, and wind shear in trees imparted to the soil mass. Seismic loading is not considered. Because air flow usually conforms to ground surfaces or treetops, adverse wind shear will be directed downslope parallel to the failure plane. Downslope components of tree and soil loadings are used except when groundwater flow is assumed parallel to the failure plane; then pore water pressure does not enter shear force computation. Shear stress can then be represented as

$$\tau' = H\sin\beta\cos\beta\ [\frac{qo}{H} + \frac{T_{sw}}{H\sin\beta\cos\beta} + \gamma sat\ (M-Z^*) + \gamma(1-M)] \qquad (13\text{-}10)$$

If τ = overall shear resistance and τ' = overall shear stress, the factor of safety equation can be written as

$$FS = \frac{R}{D} = \frac{\tau}{\tau'} \qquad (13\text{-}11)$$

Substituting shear strength (Equation 13-9) and shear stress (Equation 13-10) into Equation 13-11 yields a factor of safety equation of

$$FS = \frac{Cs+Cr+H\cos^2\beta\{(\frac{qo}{H}) + (\gamma_{sat} - \gamma_w)\ (M-Z^*) + \gamma(1-M)\}\ \tan\phi}{H\{(\frac{qo}{H}) + (Tsw/H\sin\beta\cos\beta)+\gamma_{sat}(M-Z^*)+\gamma(1-M)\}\sin\beta\cos\beta} \qquad (13\text{-}12)$$

Parameters in Equation 13-12 can be placed into nondimensional groups as

$$FS = \frac{\frac{2(Cs+Cr)}{\gamma_w H \sin 2\beta} + \left[\frac{qo}{\gamma_w H} + \left(\frac{\gamma_{sat}}{\gamma_w} - 1\right)(M-Z^*) + \frac{\gamma}{\gamma_w}(1-M)\right]\frac{\tan\phi}{\tan\beta}}{\frac{qo}{\gamma_w H} + \frac{2Tsw}{\gamma_w H \sin 2\beta} + \left(\frac{\gamma_{sat}}{\gamma_w}\right)(M-Z^*) + \frac{\gamma}{\gamma_w}(1-M)} \qquad (13\text{-}13)$$

As Equation 13-13 shows, the basic model contains variables for four factors present in a forested area. Representing soil factors are γ , γsat , Cs , and ϕ ; all controlled by soil type, while H = a measure of soil depth. Topography is included as slope inclination, β . Vegetative factors are qo , Cr , and Tsw . Finally, a dynamic factor for relative groundwater level is included as M . This basic equation is used to derive a more simplified form.

Using sensitivity and order of magnitude analysis techniques, Ward (1976) showed the factor of safety (Equation 13-13) could be reduced to an accurate, simpler form by determining that certain variables were relatively unimportant and others could be assumed as constants. Relative depth, Z^* , was set at zero for the worst case. Wind shear, Tsw , was determined insignificant in magnitude, and soil mass and tree loading terms had little effect on the sensitivity of the equation. Soil and tree loading could have either positive or negative effects on slope stability depending on other factors. The simplified infinite slope factor of safety model used in this study for estimating landslide potential is then

$$FS = \frac{\frac{2(Cs + Cr)}{\gamma_w H \sin 2\beta} + \frac{qo}{\gamma_w H} + \frac{\gamma_{sat}}{\gamma_w} - 1 \quad M + \frac{\gamma}{\gamma_w}(1-M) \quad \frac{\tan\phi}{\tan\beta}}{\frac{qo}{\gamma_w H} + \frac{\gamma_{sat}}{\gamma_w} \quad M + \frac{\gamma}{\gamma_w}(1-M)} \qquad (13\text{-}14)$$

Equation 13-14 defines the landslide potential of a slope in terms of a factor of safety value. For relative rankings of hazards, limits of factor of safety values can be established considering possible errors in the variables. Relative errors in factor of safety values can be approximately 20 to 30 percent (Ward, 1976), comparable to results of others (Feld, 1965; Singh, 1971). A realistic set of relative hazard levels is given in Table 13.3, column 2. Although other limits could be selected, these values were considered most appropriate for the cases under examination.

Table 13.3 Model classification of landslide potential and probability.

Classification (1)	Landslide Potential FS (2)	Landslide Probability P[FS < 1] (3)
High	< 1.2	> 60%
Medium	1.2-1.7	30-60%
Low	> 1.7	< 30%

Derivation of Probability Delineation

Soil root strength parameters are highly variable or uncertain. Other parameters such as soil depth, slope angle, unit weight of soil, and groundwater depth can be estimated and set at some conservative value. If groundwater level, M, is assumed at a steady state, and H, β, and γ are known, the factor of safety equation can be simplified to

$$FS = L_1(Cs) + L_1(Cr) + L_2(\tan\phi) \tag{13-15}$$

where

$$L_1 = \frac{2}{\gamma_w H \sin 2\beta \left[\left(\frac{qo}{\gamma_w H}\right) + \left(\frac{\gamma_{sat}}{\gamma_w}\right)M + \left(\frac{\gamma}{\gamma_w}\right)(1-M)\right]} \tag{13-16}$$

and

$$L_2 = \frac{\left(\frac{qo}{\gamma_w H}\right) + \left(\frac{\gamma_{sat}}{\gamma_w} - 1\right)M + \left(\frac{\gamma}{\gamma_w}\right)(1-M)}{\left[\left(\frac{qo}{\gamma_w H}\right) + \left(\frac{\gamma_{sat}}{\gamma_w}\right)M + \frac{\gamma}{\gamma_w}(1-M)\right]\tan\beta} \tag{13-17}$$

If Equation 13-14 is rewritten in terms of random variables, it becomes

$$S = L_1X + L_1Y + L_2Z \tag{13-18}$$

where S, X, Y, and Z are the random variables. The expected value, $E[\cdot]$, or the mean of a linear equation such as Equation 13-18 is (Benjamin and Cornell, 1970)

$$E[S] = L_1 E[X] + L_1E[Y] + L_2E[Z] \tag{13-19}$$

If the strength parameters are considered independent (Holtz and Krizek, 1971; Lamb, 1970), the variance, $Var[\cdot]$, or standard deviation squared becomes

$$Var[S] = E[(S - E[S])^2] \tag{13-20}$$

or

$$Var[S] = E[S^2 - 2E[S]S + E^2[S]] \tag{13-21}$$

Following the form of Equation 13-19, Equation 13-21 becomes

$$Var[S] = E[S^2] - 2E[S] \cdot E[S] + E^2[S] \tag{13-22}$$

because

$$E[E[S]] = E[S].$$

Equation 13-22 reduces to

$$\mathrm{Var}[S] = E[S^2] - E^2[S] \tag{13-23}$$

The term S^2 is defined as

$$S^2 = L_1^2 [X^2 + 2XY + Y^2] + L_1 L_2 2Z[X + Y] + L_2^2 Z^2 \tag{13-24}$$

Substitution of Equation 13-24 into Equation 13-23 yields

$$\mathrm{VAR}[S] = L_1^2 [E[X^2] + 2E[X]E[Y] + E[Y^2]] + 2L_1 L_2 E[Z] [E[X] + E[Y]] + L_2^2 E[Z^2] - E^2[S] \tag{13-25}$$

Following the form of Equation 13-22, the substitution for $E[X^2]$ can be made as

$$E[X^2] = \mathrm{Var}[X] + E^2[X] \tag{13-26}$$

Similar substitutions are made for Y and Z yielding

$$\mathrm{Var}[S] = L_1^2[\mathrm{Var}[X] + E^2[X] + 2E[X]E[Y] + \mathrm{Var}[Y] + E^2[Y]] + 2L_1 L_2 E[Z] [[E[X] + E[Y]] + L_2^2 [\mathrm{Var}[Z] + E^2[Z]] - E^2[S] \tag{13-27}$$

The mean and variance computed from Equations 13-9 and 13-26 can be used to estimate failure probability. This is written as

$$P[FS \leq 1] = p \tag{13-28}$$

where p = probability of failure and $P[FS \leq 1]$ = cumulative probability that FS is less than or equal to one. A reasonable distribution of failure probabilities is a normal or Gaussian distribution. Making this choice allows computation of the failure of probability. First, a nondimensional variate, U, is computed as

$$U = \frac{1 - \overline{FS}}{(\mathrm{Var}\ [FS])^{1/2}} \tag{13-29}$$

The value of U is used to compute cumulative failure, p, as

$$p \cong 0.4\ U \quad \text{if} \quad U \leq 0.13 \tag{13-30}$$

or

$$p \cong -0.01314 + 0.49494\ U - 0.15804\ U^2 + 0.01661\ U^3 \quad \text{if} \quad U > 0.13 \tag{13-31}$$

Equations 13-29 and 13-30 are approximations with errors less than one percent.

From U and B the failure probability is found as

$$P[FS \leq 1] = 0.5 + p \text{ if } U > 0 \quad (13\text{-}32)$$

$$P[FS \leq 1] = 0.5 - p \text{ if } U < 0 \quad (13\text{-}33)$$

$$P[FS \leq 1] = 0.5 \text{ if } U = 0 \quad (13\text{-}34)$$

Similar to potential rankings, probabilities can be grouped into three hazard classes, as shown in Table 13.1, column 3. These limits can be modified depending upon the case under examination.

The means and variances of Cs , Cr , and tan ϕ must be known or estimated to find failure probability. Usually this type of information is not available to the engineer without extensive measurements. Ward (1976) and Ward et al., (1978) suggest that input variables be assumed as uniformly distributed random values. With this assumption, the mean of a random number is found as

$$E[X] = \frac{X_a + X_b}{2} \quad (13\text{-}35)$$

and the variance as

$$\text{Var } [X] = \frac{(X_b - X_a)^2}{12} \quad (13\text{-}36)$$

where X_a and X_b = lower and upper limits on the variable X.

Ward, Li, and Simons (1978) used Monte Carlo generation techniques to demonstrate that the assumption of a uniform distribution provided a more conservative estimate or overestimate of failure probability. Another appealing aspect of the uniform distribution assumption is that a range of values can be chosen as the input. Ward (1976) presented tentative sets of ranges for Cs , ϕ, and Cr based on the Uniform Soil Classification and vegetative characteristics (Table 13.4). These values are guidelines and are subject to modification by the user.

Tree root cohesion represents the tensile and shear resistance of the roots may vary significantly. Although Table 13.5 indicates values up to 250 psf, Burroughs and Thomas (undated) suggest tree root strengths of 2856 psf for Douglas fir growing in Tyee sandstone basins. However, tree roots are only effective if the failure surface intersects them. In deep seated slides, the failure surface is often below the roots. In instances of planar type landslides, the roots are effective only if

Table 13.4 Estimates of values for soil classification, Cs, and angle of internal friction, ϕ, based on United Soil Classification System.

Unified Soil Classification (1)	Cs Values, in pounds per square foot (tentative values) (2)	ϕ Values (°), in degrees (extracted from Moore (1969)) (3)
GW Well graded gravels	---	38.3
GP Poorly graded gravels	---	36.5
GM Silty gravels	0-50	33.8
GC Clayey gravels	0-100	31.0
SW Well graded sands	---	37.6-39.0
SP Poorly graded sands	---	35.8-37.2
SM Silty sands	0-50	30.6-36.1
SC Clayey sands	0-100	27.9-33.8
ML Inorganic silts and very fine sands	0-100	30.1-33.4
CL Inorganic clays of low to medium plasticity	0-400	26.6-30.1
OL Organic silts and organic silt-clays of low plasticity	0-200	---
MH Inorganic silts	0-200	22.9-27.5
CH Inorganic clays of high plasticity	0-500	14.6-23.8
OH Organic clays of medium to high plasticity	0-400	---
PT Peat and other highly organic soils	---	---

Table 13.5 Estimates of Cr, values for root cohesion, based on vegetation characteristics (tentative).

Vegetation Characteristics (1)	Range of Cr Values, in pounds per square foot (2)
Well developed forest stands: forest area > 75% of total area	40-125 (extreme at 250)
Forest-brush mixtures: forest area 50-75% of total	20-80
Brush-forest-grass mixtures: forest area 25-50% of total	0-60
Grass-brush mixtures: forest area < 25% of total	0-40
Grass	0

they connect the soil mass to the underlying stable strata. Although considered as a beneficial influence to slope stability, tree roots only enhance stability under certain conditions.

Model Sensitivity

An important aspect of any mathematical model is its sensitivity to various input variables. Often it is desirable to know how accurately an input must be measured or the effect changing the value of a variable on a model's output. Ward (1976) used partial differentiation of the factor of safety equation to demonstrate model response to changes in each input variable.

Under certain conditions, an increase in the value of an input variable can produce positive, negative, or no change in the FS value. These types of relationships occur for γ , γ_{sat} , qo , and H . The soil depth measure, H , usually has a negative influence on FS except for a dry cohesionless slope where $FS = \frac{\tan\phi}{\tan\beta}$. It can be demonstrated mathematically that increasing γ , γ_{sat} , and qo may beneficially effect slope stability under certain conditions. Mathematically, this would occur when

$$Cs + Cr < \gamma_w H_w \tan\phi \cos^2\beta \qquad (13\text{-}37)$$

Theoretically, when conditions exist that satisfy this inequality, uniform loading of a slope should increase stability. This result suggests that in some cases forests aid stability by adding a uniform load to the soil. The relative importance of each variable can be graphically displayed through numerical computation of FS values using different variable values. For a selected set of conditions, some inputs have a linear effect on FS values while others, notably H and β , have strong nonlinear effects. Graphs are useful for showing the relative importance of each variable as compared to others (Figure 13.7). Although this figure is for a selected set of values, computations for other input sets show the same relative shapes. Sometimes Cs and Cr reverse their relative importance and qo , not shown, becomes slightly more important. In most cases, γ has only a slight affect as do γ_{sat} and qo. These three variables have smaller effects for reasons previously explained but also because they are included in the numerator (resisting force) and denominator (driving force) of Equation 13-14. This type of

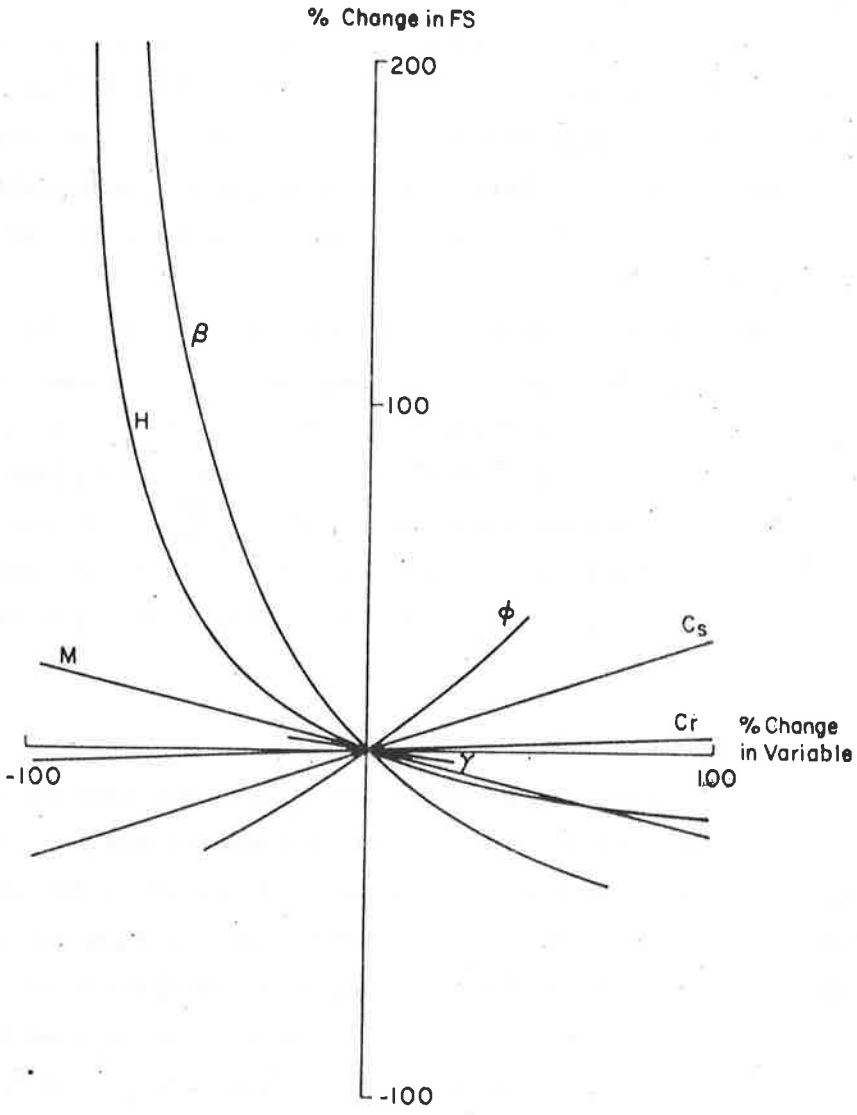

Figure 13.7 Percent change in factor of safety, FS, as compared to percent change in variable.

analysis is important in studying a new area since it indicates which input variables are most important to measure and what variable changes most affect stability.

13.4 COMPUTER MAPPING OF WATERSHED LANDSLIDE HAZARDS

Background

The landslide potential and probability model together with a realistic range of input values allows analysis of slope stability. Such an approach is adequate for small areas but large areas require computer-based models to process extensive quantities of input data and simulate short- and long-term changes. Another desirable feature of computer-based system response models is the ability to process and utilize information from remote sensing sources.

In the landslide mapping model, watersheds are segmented and digitized for analysis using a watershed segmentation model developed by Simons and Li (1975). With this model, a grid system subdivides the watershed into square or rectangle response units, also called cells. Cell size depends on the accuracy required for the output data, size of the area to be mapped, quality of input data, use of the output, and whether mapping will reflect land-use changes.

Data input is fairly general. A cell size is selected and the corresponding grid is overlayed on the raw data maps (Figure 13.8). Some maps are composed entirely of code numbers that designate various characteristics. For example, if the raw data shows vegetation, code number 1 may indicate high root strength while number 2 may indicate low root strength. Code data input at the grid line intersections or nodes allows assignation of values to the respective variables. This procedure is followed for vegetation and soil but other data such as elevation or canopy density (the relative amount of vegetation) are input as raw numbers and are not coded. With data input and stored, the segmentation model computes several useful quantities. Elevation data is used to compute slope inclination and aspect of the cell. Slope aspect indicates the direction the cell slopes; that is, the direction of landslide movement in the cell. The watershed segmentation program organizes data on a cell-by-cell basis for the watershed. The organized, coded, and averaged values are then output to a mass storage device or permanent file where they are accessed by the landslide hazard mapping program.

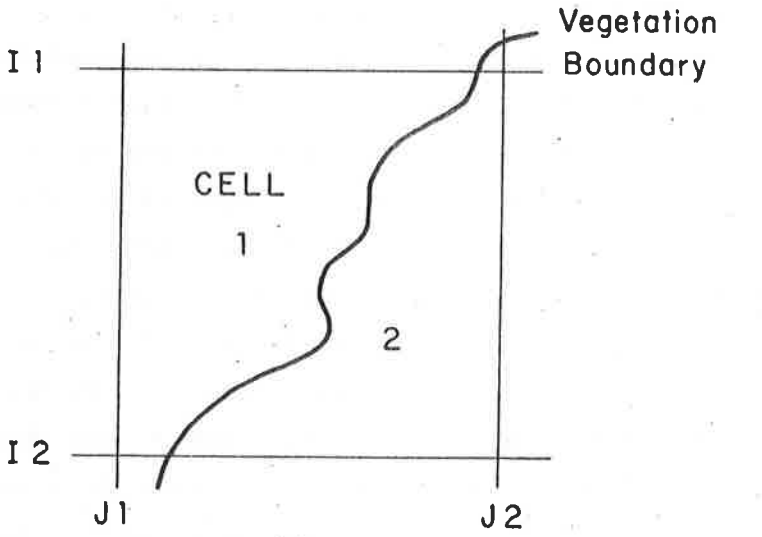

Figure 13.8 Input format to segmentation model.

Landslide Hazard Mapping

Output from the segmentation model (WASEG) is input to the landslide hazard mapping program (LSMAP). In the basic version, LSMAP requires input from program WASEG and the user. A more detailed version incorporates WASEG, LSMAP, and gray map printing routines into a method for delineating landslide hazards as well as other watershed characteristics.

Program LSMAP analyzes the watershed on a cell-by-cell basis. Soil and root strength values and soil depths are averaged for each cell. Consequently, the factor of safety is based on the averaged values for each cell, rather than the average of the factors of safety at each node point.

The landslide hazard mapping model presented here can provide a rapid means of assessing the impacts of various land-use changes on slope stability. An application using actual field data is presented in the following section.

13.5 APPLICATION OF MODEL

Site Selection

A heavily forested, landslide-prone watershed was selected for analysis. The selected watershed is located in the H. J. Andrews Experimental Forest about 50 miles east of Eugene, Oregon on the western edge of the Cascade Range and is shown in the topographic map supplied by Fred Swanson, USDA Forest Service, Oregon State University (Figure 13.9). Watershed 2 with an area of approximately 149 acres is located in the southwest corner of the Experimental Forest. Elevations in the area range from about 1730 to 3500 feet above mean sea level with slopes often in excess of 80 percent.

Vegetation of the watershed is typical of the area. The canopy is primarily Douglas-fir in the 125-year age class (second-growth), 450-year age class (old-growth), or a combination of the two classes (Hawk and Dyrness, undated). In some locations, however, Western Red cedar and Hemlock are present. The geology of the watershed has been characterized as lava flows, welded and unwelded tuffs and pyroclastic flows, and water-worked volcanic sediments (Swanson and James, 1975). Almost all of the landslide activity is confined to the altered volcaniclastic rocks with little activity occurring in the lava flows (Swanson and Dyrness, 1975). Soils in this area are weathered from the underlying

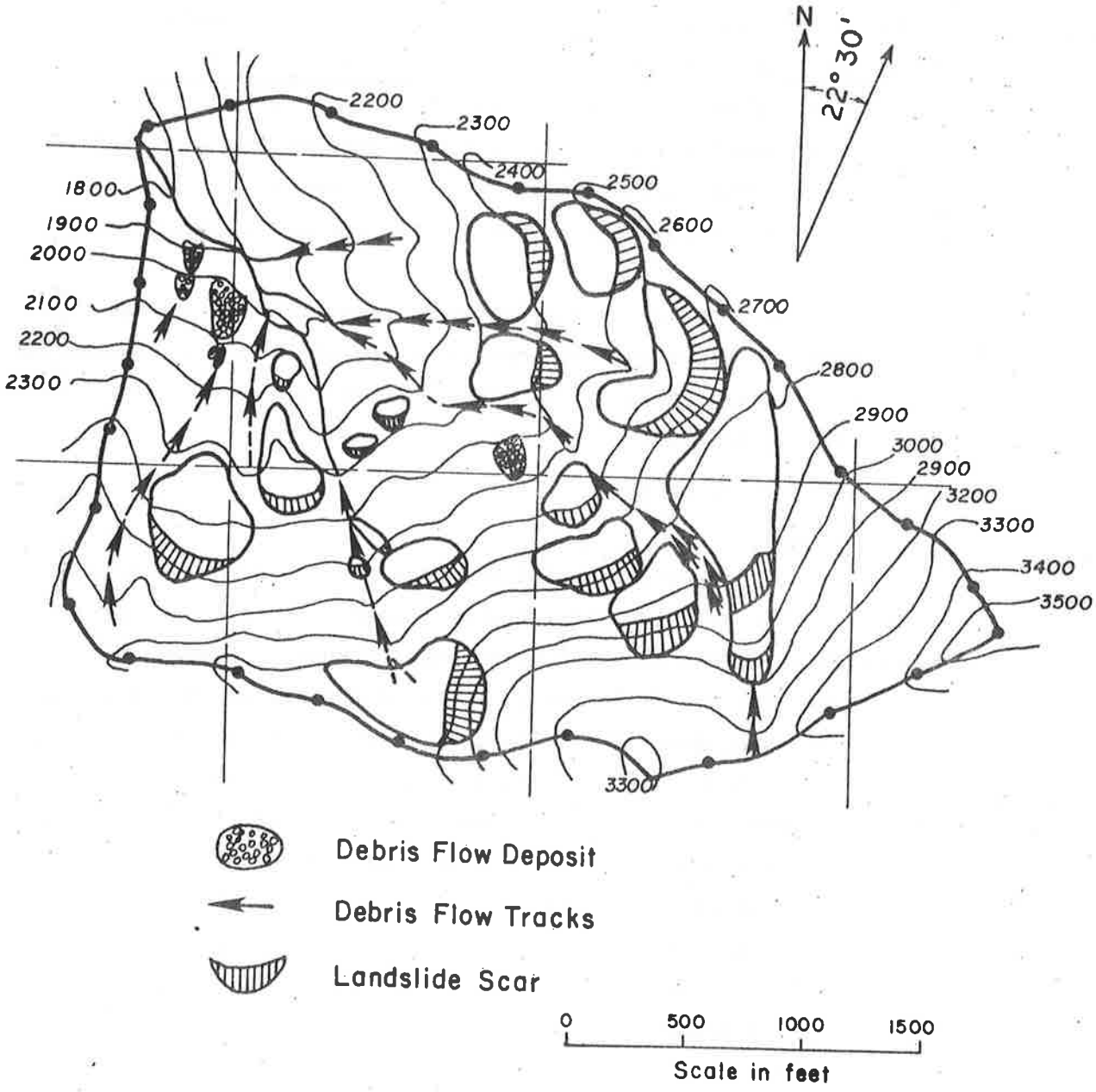

Figure 13.9 Topographic map of Watershed 2 showing landslide scars and deposits.

volcanic rocks (Dyrness, 1969; Hawk and Dyrness, undated, Paeth, et al., 1971) and can be grouped into five broad classes. Five groups were used to account for subtle but important variations in soil depth and relative stability that produced unrealistic results when only three groupings were used.

The estimated Unified Soil Classifications for the soils shown in Table 13.4 were ML, CL, and CH. These assumed classifications were used for initial estimates of soil strength parameters as outlined by Ward (1976). Distribution of these soils indicates that two groups predominate in the watershed (Figure 13.10).

A vegetation grouping was conducted on Watershed 2. Because the canopy is well developed, it was assumed the root system was also well developed. Therefore, classification of vegetation with respect to characteristic root strength was based on a combination of the canopy cover densities of the larger overstory trees and the smaller understory trees and brush. Cover percentages provided a method of classification for root strength. Most of Watershed 2 was characterized by vegetation groups of second and old growth plant communities (Figure 13.11).

Runoff from the watershed is controlled by groundwater discharge. Precipitation averages nearly 90 inches per year with about 90 percent of the total occurring as rainfall from October to April. Storms may last several days producing rainfall of several inches. Rainfall intensities are usually low and soil infiltration rates high, therefore, overland flow seldom occurs. Streamflow is fed primarily by saturated and unsaturated groundwater flow. Because of the importance of groundwater in slope stability, it was recognized that fluctuations in the groundwater table during a storm were important. Unfortunately, an acceptable, easily applied groundwater model was not available for use in this application, therefore, only selected levels were utilized for comparison.

The segmented watershed with the superimposed grid system is shown in Figure 13.12. Code values were input for the five soil classes and vegetation types along with elevations and cover densities. These codes start in the lower left corner and continue counterclockwise. For example, the vegetation code in Figure 13.8 is 1221.

In Watershed 2, 78.5 cells (0.5 cells for a cell near a stream channel) of 181 cells in the segmented watershed were denoted as having

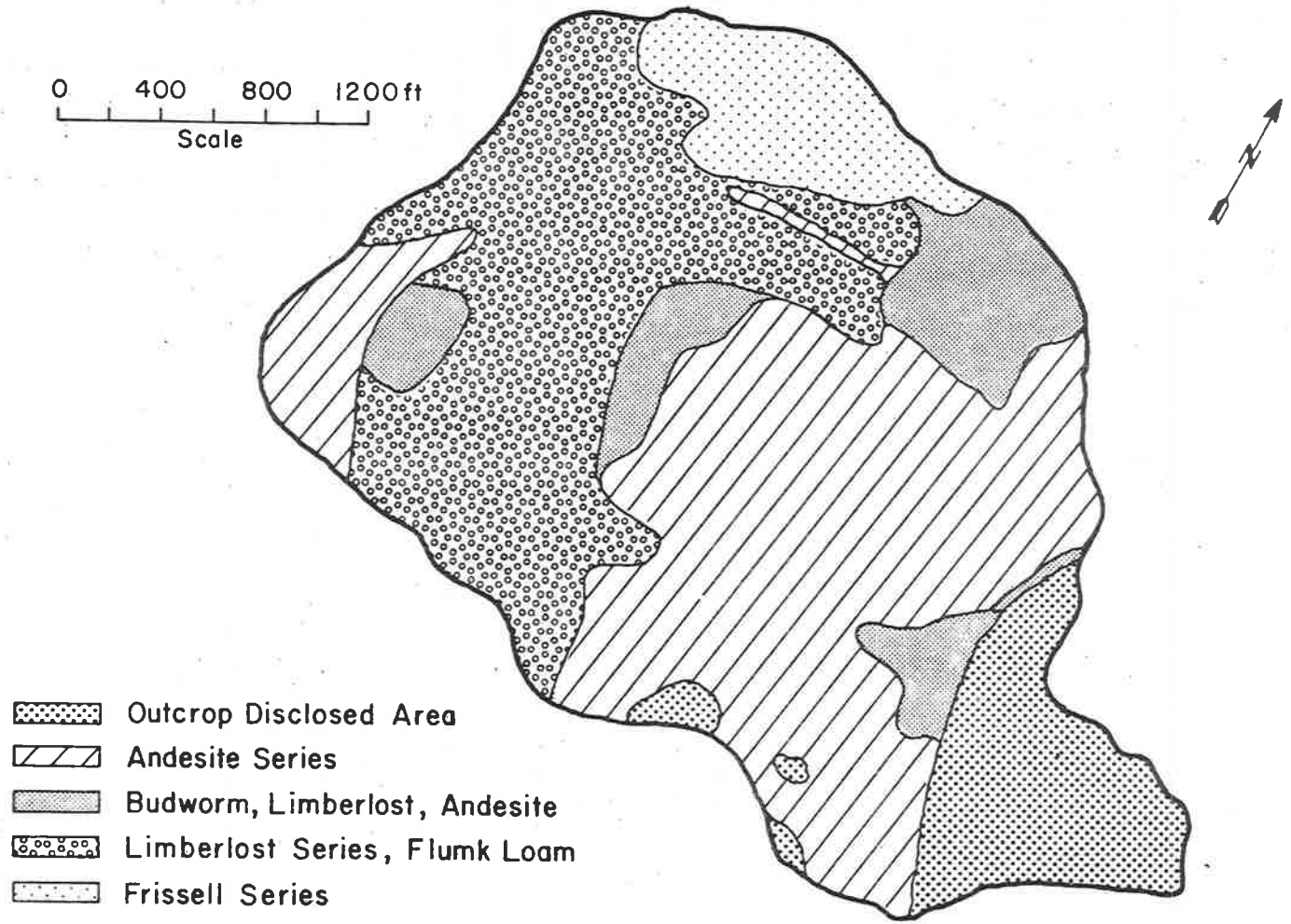

Figure 13.10 Soil classification map of Watershed 2 (after Hawk and Dyrness, undated).

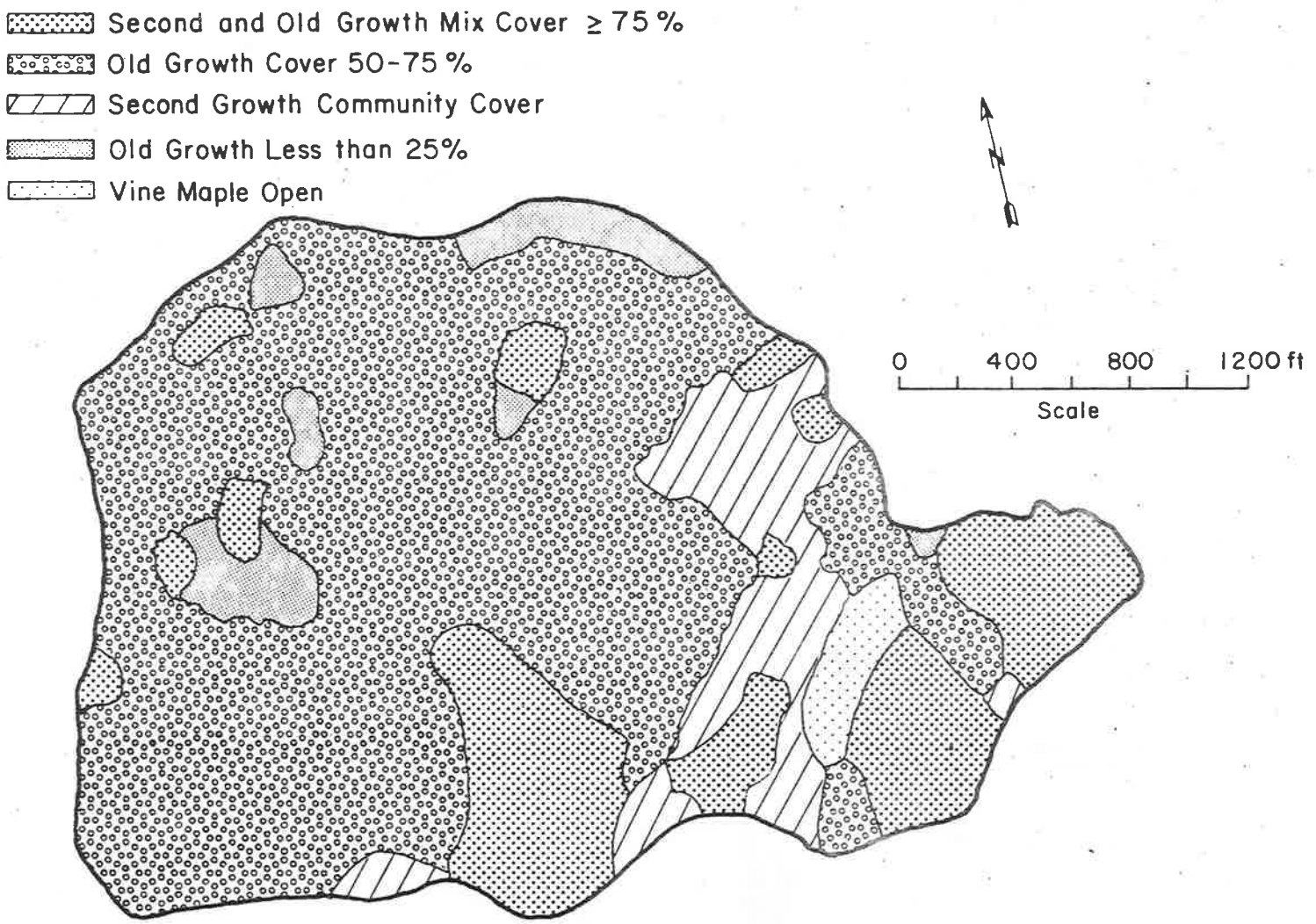

Figure 13.11 Vegetation map of Watershed 2 (after Hawk and Dyrness, undated).

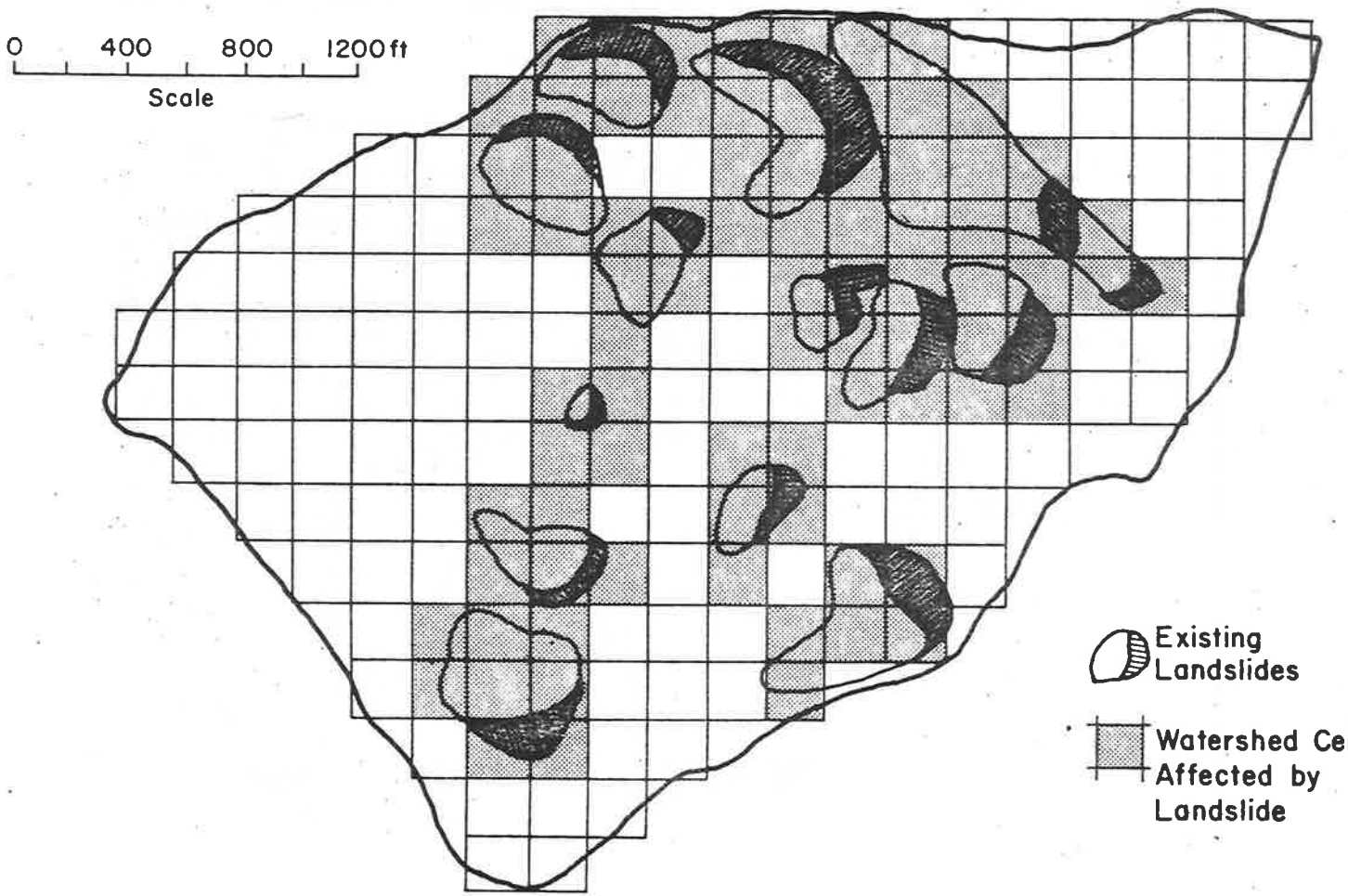

Figure 13.12 Watershed Number 2: existing landslides and watershed cell system.

mappable landslide scars and deposits. These hazard cells were used as a guide to model performance and adjustment. If the model predicted a potential landslide hazard in these cells, it is accepted as a correct result. Overestimation or underestimation of the number of hazardous cells indicates: a) some hazardous cells may have negative characteristics and consequently are mapped as nonhazardous, b) cells mapped as hazardous but not containing landslides may be near failure, or c) the model is incorrect due to erroneous data. Comparison of the number of correct classifications with incorrect classifications for initial runs indicated the physical process model reflected the correct slope stability conditions.

The model was adjusted through soil and root strength parameters to better match the observed data. Two criteria were established to this adjustment. First, under typical soil moisture conditions no cell should fail. Second, under saturated conditions all the landslide cells should fail. Although failure may occur in all the landslide cells before saturation, data does not indicate at what level failure occurred. Using these two criteria, the input values were adjusted over realistic ranges. These values plus others used in the model are listed in Table 13.6.

Low values of cohesion and friction angle for soil classes 2 and 3 were consistent with field observations of failures in these soils. Higher values for the other three soil classes reflect the relative stability associated with those groupings. Similar considerations were used when selecting proper ranges of root strengths. No formal methodology was used for arriving at the adjusted values in Table 13.6. The values do, however, reflect the relative stability of groups they represent.

The adjusted model indicated a total of 81.5 hazardous cells, 69 of which corresponded with the assumed hazardous cells, an 87.9 percent match. A total of 9.5 cells were classed as safer than assumed and 12.5 were classed as more hazardous. This is encouraging since it indicates the model represents the physical processes controlling landslide occurrence.

Table 13.6 Input values for LSMAP.

Soil porosity = 0.60
Dry unit weight of soil = 66.1 pounds per cubic foot
Saturated unit weight of soil = 103.6 pounds per cubic foot
Vegetative surcharge = 50 pounds per square foot

Soil Group (1)	Soil Names (2)	Cohesion Range, in pounds per square foot (3)	Friction Angle Range, in degrees (4)	Typical Depth in feet (5)
1	Rock outcrop	1000-2000	35-40	5
2	Andesite series	20-50	5-20	8
3	Budworm, Limberlost, Andesite (slope < 20%)	0-5	2-5	10
4	Limberlost, Flunky	150-200	25-28	5
5	Frissell	350-400	30-33	4

Vegetation Group (1)	Root Strength Range, in pounds per square foot (2)
1	290-360
2	220-260
3	5-25
4	100-125
5	15-65

The adjusted model was then used to study dynamic changes in the watershed. The first application showed the change in landslide hazards under varying groundwater conditions. The potentially hazardous landslide areas and their estimated failure probabilities for a relative groundwater level of 0.5 are shown in Figures 13.13 and 13.14. Even under these conditions there are numerous areas of high potential because of the overwhelming driving forces brought about by the steep terrain. As expected, rising groundwater levels increase landslide hazards (Figures 13.15 and 13.16). If a real-time groundwater level model were available, daily or seasonal fluctuations in landslide hazards could be determined. Use of the model in determining relative hazards with respect to groundwater levels is important in planning watershed activities. Based on model results, scheduling of activities may be better determined to coincide with lower landslide hazards. Roadways may also be better planned to avoid hazardous areas or indicate where stability enhancement is required.

Timbering is another dynamic watershed activity that can be assessed with the model. Landslide potential for a 50 percent clearing of the canopy cover is shown in Figure 13.17. Comparison of Figure 13.17 with Figure 13.13 shows adverse effects on slope stability produced by vegetation removal. Similarly, if the watershed is clear-cut, even more instability is produced (Figure 13.18). However, an instantaneous drop in root strength is assumed, which is incorrect. A more realistic approximation would be loss of strength with time. The model provides a method for assessing impact of this type of timbering activity on the watershed.

An important aspect of the model is estimating landslide probability. Use of both the potential and probability maps provides the land use manager with another means for analyzing impacts of watershed activities. In addition, the probability map aids interpretation of the potential map.

13.6 SUMMARY AND CONCLUSIONS

This chapter has presented the need for delineating the hazardous landslide areas and those factors which control landsliding. Delineation techniques were discussed and a mathematical modeling approach was

detailed. Application of the approach indicates its usefulness for determining landslide hazards in a watershed under varying natural and man caused conditions.

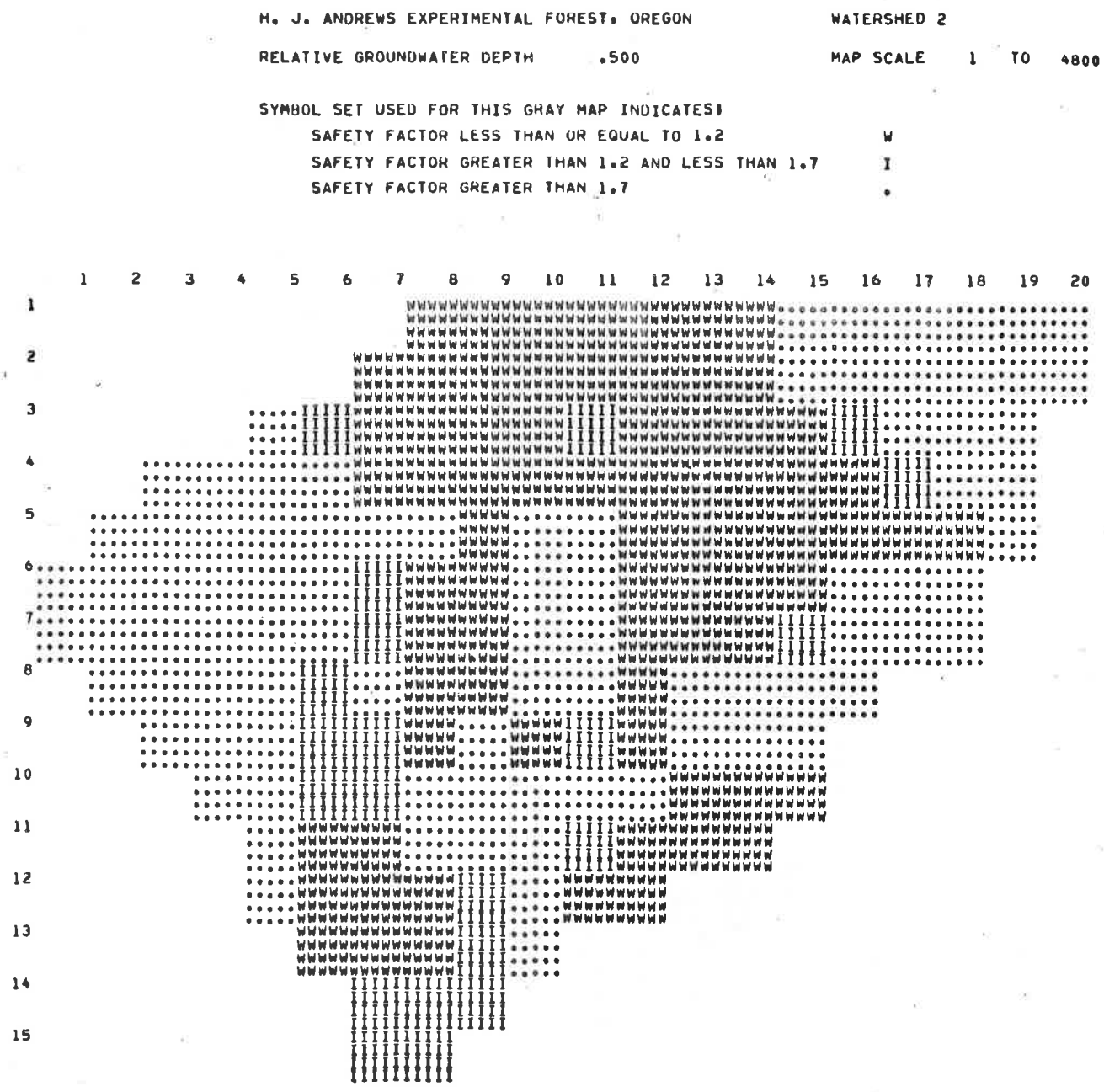

Figure 13.13 Gray map of potentially hazardous landslide areas for Watershed 2 with relative groundwater level of 0.5.

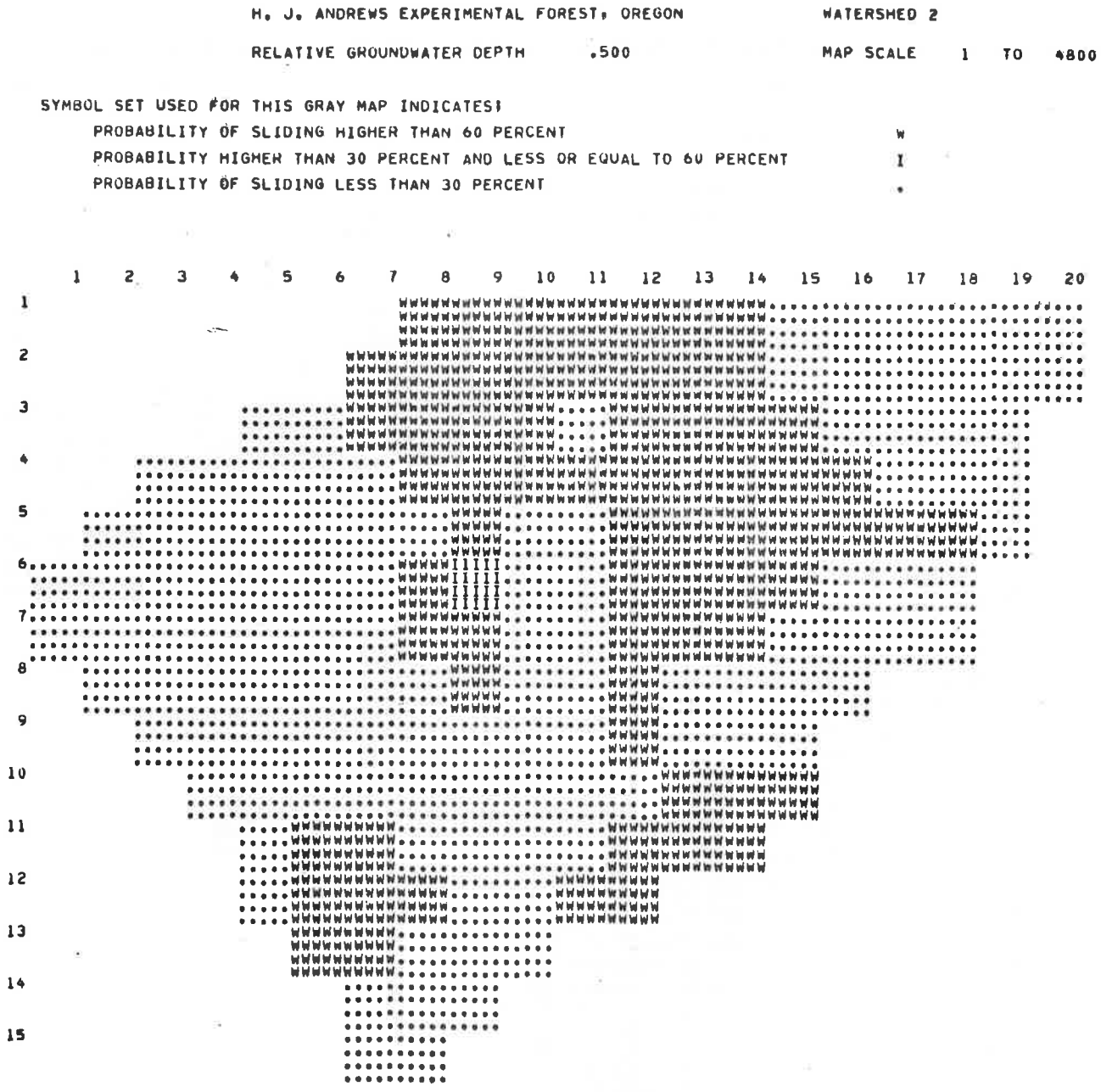

Figure 13.14 Gray map of estimated failure probabilities of landslide areas for Watershed 2 with relative groundwater level of 0.5.

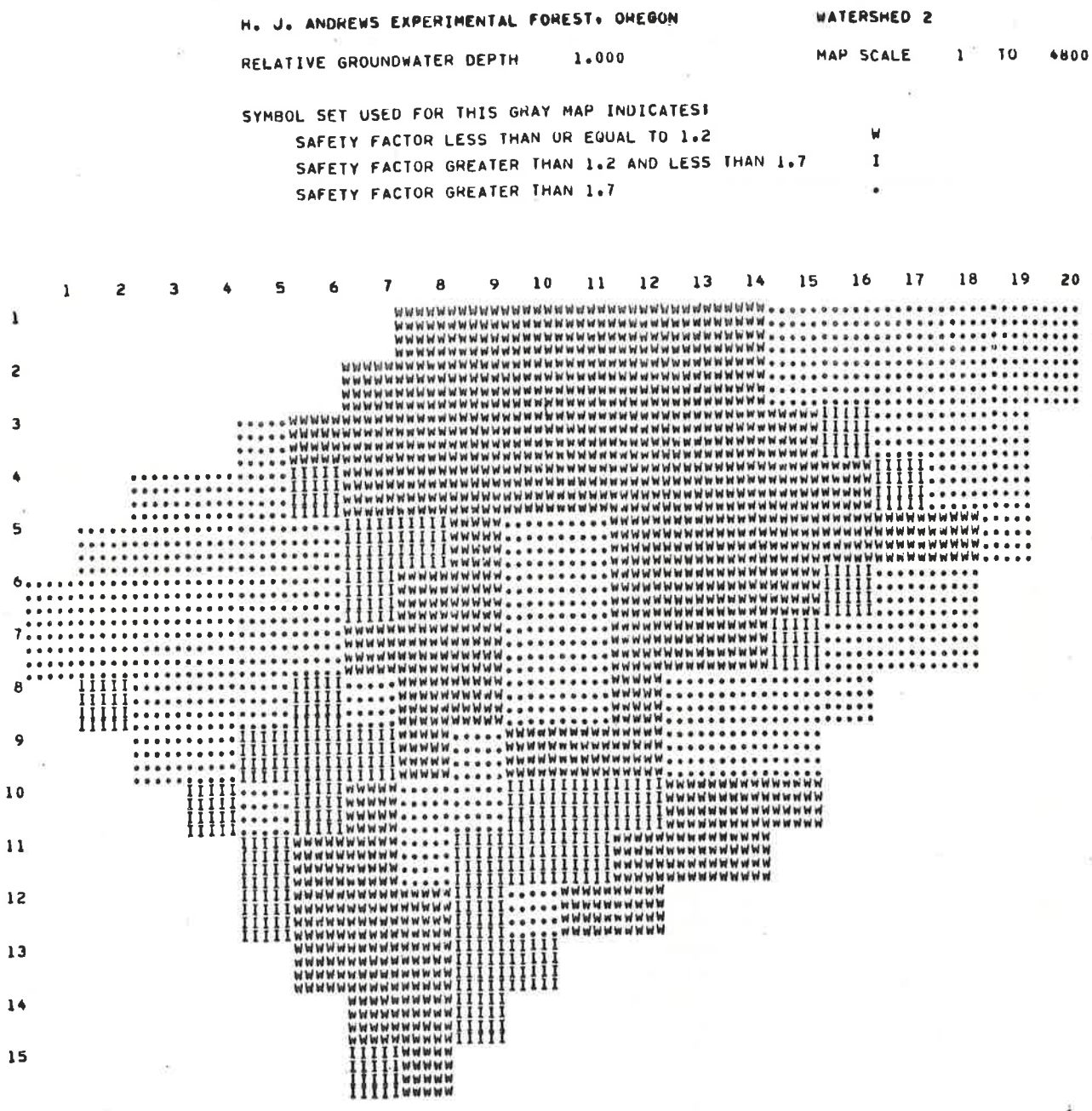

Figure 13.15 Gray map of potentially hazardous landslide areas for Watershed 2 with relative groundwater level of 1.0.

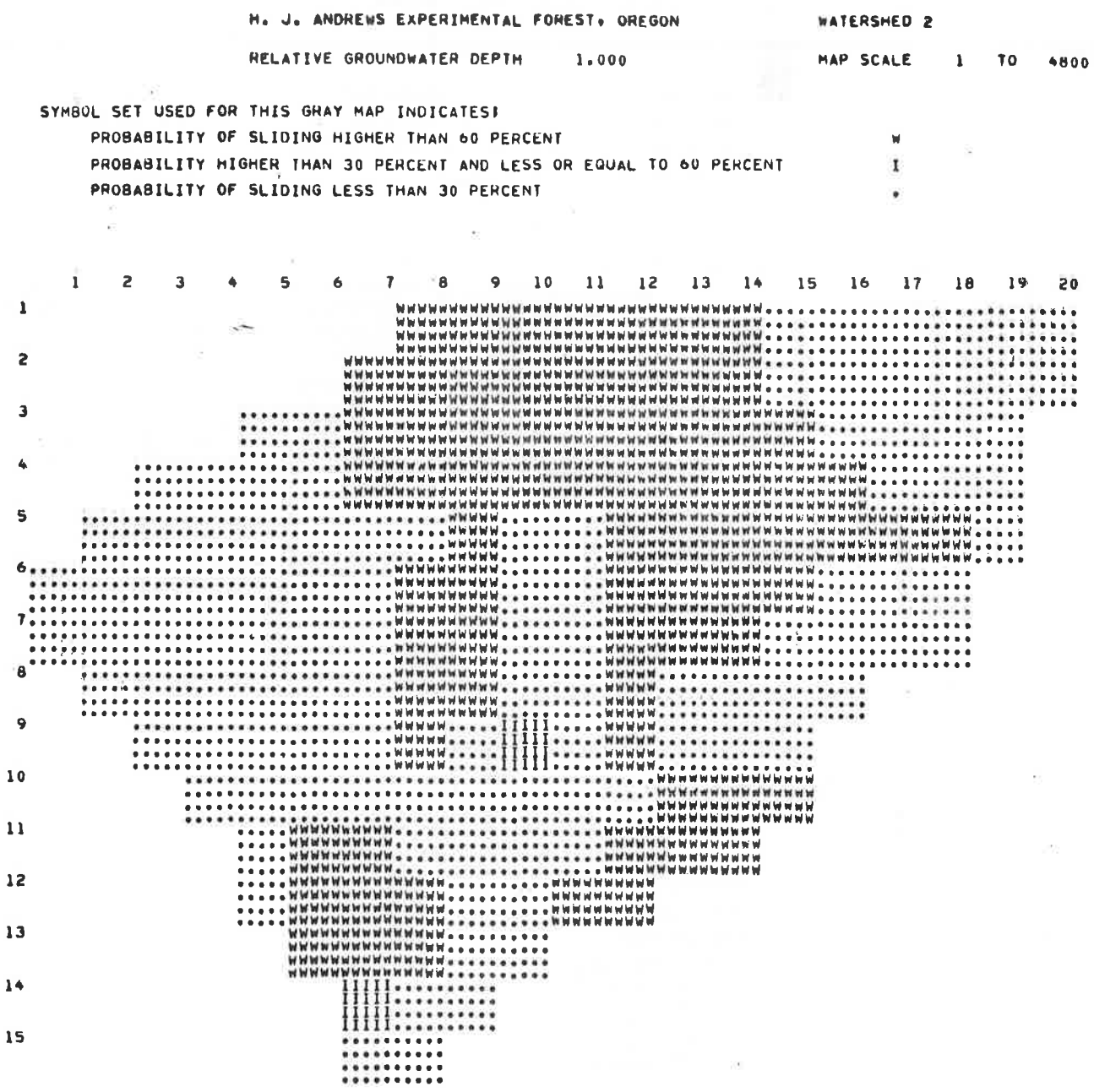

Figure 13.16 Gray map of estimated failure probabilities of landslide areas for Watershed 2 with relative groundwater level of 1.0.

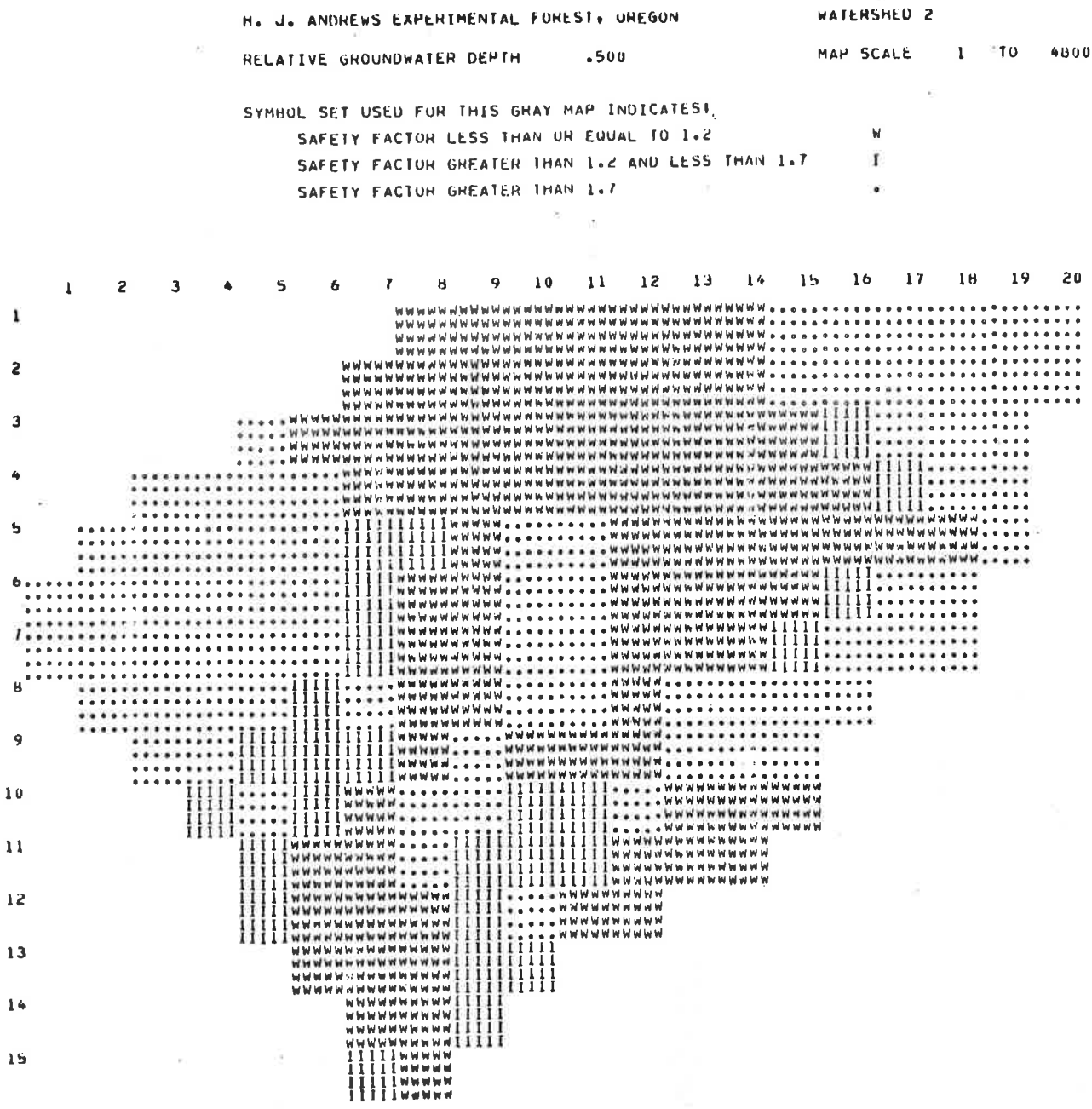

Figure 13.17 Gray map of potentially hazardous landslide areas for a 50 percent clearing of canopy cover with relative groundwater level of 0.5.

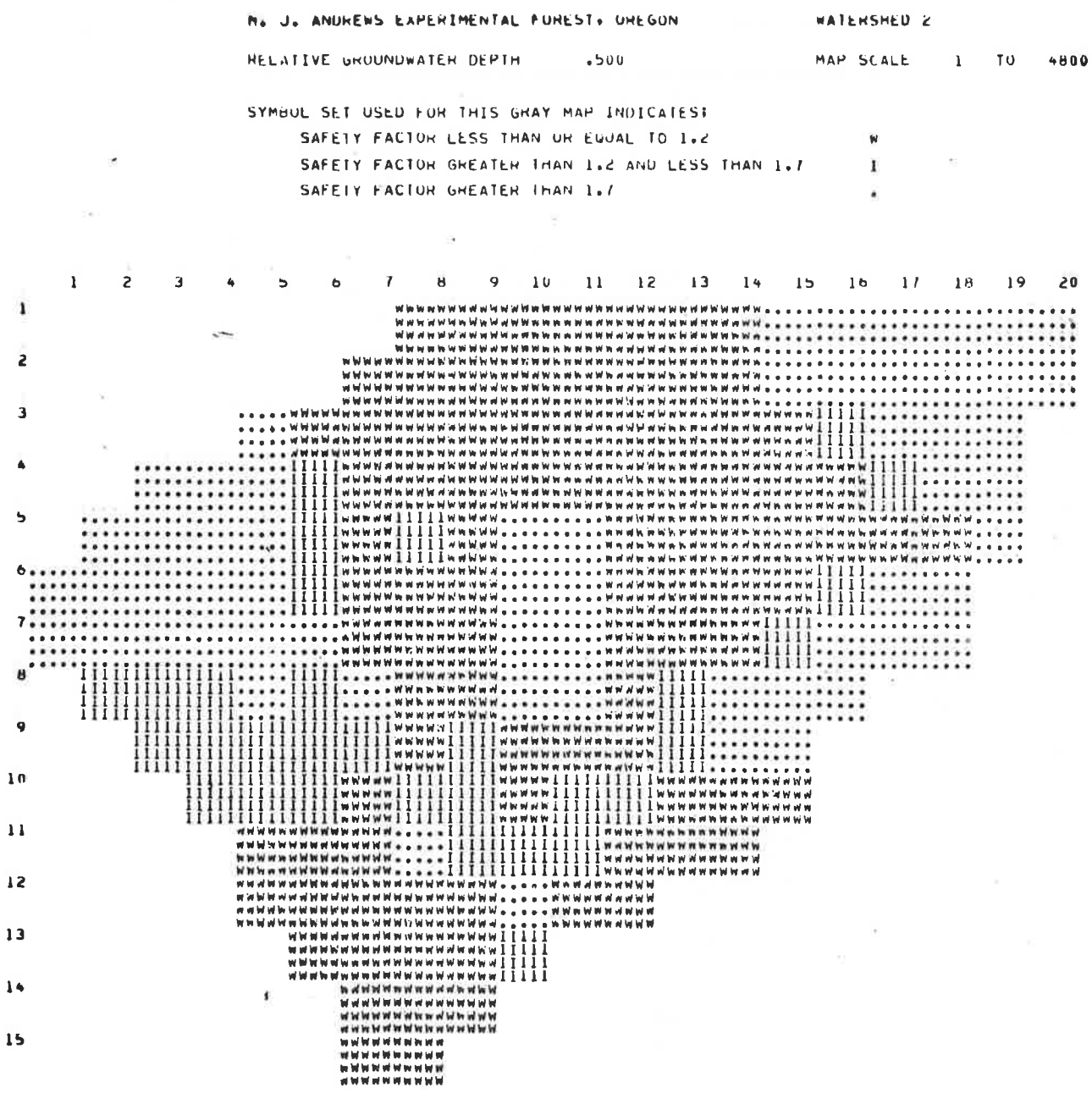

Figure 13.18 Gray map of potentially hazardous landslide areas for clear cut watershed with relative groundwater level of 0.5.

13.7 REFERENCES

Baker, R. F. and Chieruzzi, R., "Regional Concept of Landslide Occurrence," Bulletin No. 216, Highway Research Board, 1959, pp. 1-16.

Beaty, C. B., "Landslides and Slope Exposure," Journal of Geology, Vol. 64, No. 1, 1956.

Benjamin, J. R. and Cornell, C. A., Probability, Statistics, and Decision for Civil Engineers, McGraw-Hill, New York, N.Y., 1970, pp. 147-150.

Bethlahmy, N., "First Year Effects of Timber Removal on Soil Moisture," Bulletin of the International Association of Scientific Hydrology, Vol. 7, No. 2, 1962, pp. 34-38.

Blanc, R. P. and Cleveland, G. B., "Natural Slope Stability as Related to Geology, San Clemente Area, Orange, and San Diego Counties, California," Special Report 98, California Division of Mines and Geology, 1968.

Bolt, B. A., et al., Geological Hazards, Springer-Verlag, New York, 1975.

Brown, C. and Sheu, M. S., "Effects of Deforestation on Slopes," Journal of the Geotechnical Engineering Division, ASCE, Vol. 101, No. GT2, February, 1975, pp. 147-165.

Building Research Advisory Board, National Research Council, National Academy of Sciences, "Methodology for Delineating Mudslide Hazard Areas," 1974.

Burroughs, E. R. and Thomas, B. R., "Initial Report for the Identification of Landslide Hazard Areas in Tyee Sandstone with Slope Gradients Exceeding Sixty Percent," Draft Report, U.S. Forest Service, unpublished, undated.

California Division of Mines and Geology, "Urban Geology: Master Plan for California--The Nature, Magnitude, and Costs of Geologic Hazards in California and Recommendations for their Mitigation," California Division of Mines and Geology Bulletin 198, 1973.

Chang, T. P., "Landslide Investigation Techniques," Colorado State University, Science Series No. 1, Department of Watershed Sciences, 1971.

Cleveland, G. B., "Regional Landslide Prediction," Open File Release 72-73, California Division of Mines and Geology, Sacramento, California, 1971.

Cleveland, G. B., "Fire + Rain = Mudflows, Big Sur 1973," California Geology, Vol. 26, No. 6, June, 1973.

Conlon, R. J., "Landslide on the Goulnustoric River, Quebec," Canadian Geotechnical Journal, Vol. 3, No. 3, 1966.

Debano, L. F., et al., "Soil Wettability and Wetting Agents--Our Current Knowledge of the Problem," U.S. Forest Service Research Paper PSW-43, 1967.

Dyrness, C. T., "Hydrologic Properties of Soil on Three Small Watersheds in the Western Cascades of Oregon," Research Note PNW-111, U.S. Forest Service, September, 1969.

Endo, T. and Tsuruta, T., "On the Effect of Tree Roots Upon the Shearing Strength of Soil," Annual Report of the Hokkaido Branch Forest Experiment Station (In Japanese, English Summary), 1968.

Evans, J. R. and Gray, C. H., Jr., Eds., "Analysis of Mudslide Risk in Southern Ventura County, California," Open File Release 72-73, California Division of Mines and Geology, 1971.

Feld, J., "The Factor of Safety in Soil and Rock Mechanics," Proceedings, Sixth International Conference on Soil Mechanics and Foundation Engineering, Vol. 111, 1965, pp. 185-197.

Fife, D. L., "Soils of High Susceptibility to Mudslides and Development of Soils Maps," In: Analysis of Mudslide Risk in Southern Ventura County, California, edited by J. R. Evans and C. H. Gray, California Division of Mines and Geology, Sacramento, California, 1971.

Gaiser, R. N., "Root Channels and Roots in Forest Soils," Proceedings, Soil Science Society, Vol. 16, No. 1, 1952, pp. 62-65.

Gray, D. H., "Effects of Forest Clearcutting on the Stability of Natural Slopes," Association of Engineering Geologists Bulletin, Vol. 7, Nos. 1 and 2, 1970, pp. 45-65.

Gray, D. H., "The Role of Woody Vegetation in Reinforcing Soils and Stabilizing Slopes," Proceedings, Symposium on Soil Reinforcing and Stabilizing Techniques in Engineering Practice, Sydney, Australia, October 13-16, 1978.

Hammer, M. J. and Thompson, O. B., "Foundation Clay Shrinkage Caused by Large Trees," Journal of Soil Mechanics and Foundations Division, American Society of Civil Engineers, Vol. 92, No. SM6, 1966.

Hawk, G. and Dyrness, C. T., "Vegetation and Soils of Watershed 2 and 3," Internal Report 49, U.S. Department of Agriculture Forest Service, H. J. Andrews Experimental Forest, review copy, undated.

Hay, E., "What Really Makes Mud Roll," Forests, Vol. 81, No. 2, 1975.

Holtz, R. D. and Krizek, R. J., "Statistical Evaluation of Soils Test Data," Proceedings, First International Conference on Applications of Statistics and Probability to Soil and Structural Engineering, 1971, pp. 230-266.

Johnson, A. M., Physical Processes in Geology, Freeman, Cooper and Company, 1970.

Jones, F. O., Embody, D. R., and Peterson, W. L., "Landslides along the Columbia River Valley, Northeastern Washington," Survey Professional Paper 367, 1961.

Kiersch, G. A., "The Vaiont Reservoir Disaster," Civil Engineering Magazine, March, 1964.

Krynine, D. P. and Judd, W. R., Principles of Engineering Geology and Geotechnics, McGraw-Hill, New York, N.Y., 1975, p. 639.

Lambe, T. W. and Whitman, R. V., Soil Mechanics, John Wiley and Sons, New York, N.Y., 1969, pp. 352-373.

Liang, F. and Belcher, J. D., Air Photo Interpretation in Landslides and Engineering Practice," Highway Research Board, Special Report No. 29, Publication 544, 1958.

Lumb, P., "Safety Factors and the Probability Distribution of Soil Strength," Canadial Geotechnical Journal, Vol. 17, No. 3, 1970, pp. 225-242.

Martin, G. R., Finn, W. D., and Seed, H. B., "Fundamentals of Liquefaction Under Cyclic Loading," Journal of Geotechnical Engineering Division, American Society of Civil Engineers, Vol. 101, No. GT5, May, 1975.

McKean, J., "Density Slicing of Aerial Photography Applied to Slope Stability Studies," M.S. Thesis, Department of Earth Resources, Colorado State University, Fort Collins, Colorado, 1977.

Moore, H. C., "Engineering Interpretation of Soil Data," Proceedings, Seventh Annual Engineering Geology and Soils Engineering Symposium, Moscow, Idaho, 1969.

Nilsen, T. H. and Brabb, E. E., "Current Slope-Stability Studies in the San Francisco Bay Region," Journal of Research, U.S. Geological Survey, Vol. 1, No. 4, July-August, 1973, pp. 431-437.

Nilsen, T. H. and Turner, B. L., "Influence of Rainfall and Ancient Landslide Deposits on Recent Landslides (1950-1971) in Urban Areas of Contra Costa County, California," U.S. Geological Survey Bulletin 1388, 1975.

Okamoto, S., Introduction to Earthquake Engineering, John Wiley and Sons, New York, N.Y., 1973.

O'Loughlin, C., "The Effect of Timber Removal on the Stability of Forest Soils," Journal of Hydrology, Vol. 13, No. 2, New Zealand, 1974, pp. 121-134.

Olson, R. E., "Shearing Strengths of Kaolinite, Illite, and Montmorillonite," American Society of Civil Engineers, Journal of Geotechnical Engineering Division, Vol. 100, No. GT11, November, 1974.

Paeth, R. C., et al., "Factors Affecting Mass Movement of Four Soils in the Western Cascades of Oregon," Proceedings, Soil Science Society of America, Vol. 35, No. 6, 1971, pp. 943-947.

Perpith, W. M., Lukas, R. G., and Baker, C. N., Jr., "Dessication of Soil by Trees Related to Foundation Settlement," Canadian Geotechnical Journal, Vol. 2, No. 1, 1965.

Poole, D. H., "Slope Failure Forms: Their Identification, Characteristics and Distribution as Depicted by Selected Remote Sensor Returns," Proceedings, Sixth International Symposium on Remote Sensing of the Environment, Ann Arbor, Michigan, 1969.

Poole, D. H., "An Evaluation of the Utility of Remote Sensor Returns for a Study of Slope Failure Phenomena," Remote Sensing Institute Technical Report 14, East Tennessee State University, Johnson City, Tennessee, 1972.

Radburch, D. B. and Crowther, K. C., "Map Showing Areas of Relative Amounts of Landslides in California," U.S. Geological Survey Open File Map 1:500,000, 1970.

Radburch, D. B. and Weiler, L. M., "Preliminary Report on Landslides in a Part of the Orinda Formation, Contra Costa County, California," U.S. Geological Survey Open Report, 1963.

Rahn, P. H., "The Relationship Between Natural Forested Slopes and Angles of Repose for Sand and Gravel," Geological Society of American Bulletin, Vol. 80, No. 10, October, 1969.

Rogers, W. P., et al., "Guidelines and Criteria for Identification and Land-Use Controls of Geologic Hazard and Mineral Resource Areas," Publication No. 6, Colorado Geological Survey, Denver, Colorado, 1974.

Seed, H. B. and Wilson, S. D., "The Turnagain Heights Landslide, Anchorage, Alaska," Journal of Soil Mechanics and Foundations Division, American Society of Civil Engineers, Vol. 93, No. SM4, 1967.

Simons, D. B. and Li, R. M., "Watershed Segmentation by a Digital Computer for Mathematical Modeling of a Watershed," Draft Report, Rocky Mountain Forest and Range Experiment Station, Flagstaff, Arizona, December, 1975.

Simons, D. B. and Ward, T. J., "Landslide Potential Delineation," Civil Engineering Department, Engineering Research Center, Colorado State University, Fort Collins, Colorado, February, 1976.

Simons, D. B., Ward, T. J., and Li, R. M., "Computer Application in Mapping Potential Landslide Sites," Proceedings, Summer Computer Simulation Conference, Washington, D.C., 1976.

Singh, A., "How Reliable is the Safety Factor in Foundation Engineering?" Proceedings, First International Conference on Applications of Statistics and Probability to Soil and Structural Engineering, Hong Kong University Press, 1971, pp. 390-424.

Swanson, F. J. and Dyrness, C. T., "Impact of Clear-cutting and Road Construction on Soil Erosion by Landslides in the Western Cascade Range, Oregon," Geology, Vol. 3, No. 7, 1975, pp. 393-396.

Swanson, F. J. and James, M. E., "Geology and Geomorphology of the H. J. Andrews Experimental Forest, Western Cascades, Oregon," Research Paper PNW-188, U.S. Department of Agriculture Forest Service, 1975.

Swanson, F. J., et al., "A Conceptual Model of Soil Mass Movement, Surface Soil Erosion, and Stream Channel Erosion Processes," Internal Report 72, Erosion Modeling Group, 1973.

Swanston, D. N., "Debris Avalanching in Thin Soils Derived from Bedrock," U.S. Forest Service, Research Note PNW-64, 1967.

Swanston, D. N., "Mass Wasting in Coastal Alaska," U.S. Forest Service, Research Paper PNW-83, 1969.

Takada, Y., "A Geophysical Study of Landslides," Bulletin Disaster Prevention Research Institute, Kyoto University, Vol. 18, Part 2, No. 137, 1968.

Takeuchi, A., "Fractured Zone Type Landslide and Electrical Resistivity Survey - 1," Bulletin Disaster Prevention Research Institute, Kyoto University, Vol. 21, Part 1, No. 185, 1971.

Thompson, S., "The Leseur Landslide, A Failure in Upper Cretaceous Clay Shale," Proceedings, Ninth Annual Engineering Geology and Soils Engineering Symposium, Boise, Idaho, 1971.

Vandre, B. C., "A Case History of a Landslide Caused by Confined Groundwater," Association of Engineering Geologists Bulletin, Vol. 12, No. 4, 1975.

Varnes, D. J., "Landslide Types and Processes. Landslides and Engineering Practice," edited by E. B. Eckel, Highway Research Board, Special Report No. 29, 1958.

Voight, B., "The Mechanics of Retrogressive Block-Gliding, with Emphasis on the Evolution of the Turnagain Heights Landslide, Anchorage, Alaska," In Gravity and Tectonics, edited by Kecs De John and Robert Scholten, Wiley, 1973.

Wahlstrom, E. E. and Nichols, T. C., Jr., "The Morphology and Chronology of a Landslide near Dillon Dam, Dillon, Colorado," Engineering Geology, Vol. 3, No. 2, April, 1969.

Waltz, J. P., "An Analysis of Selected Landslides in Alameda and Contra Costa Counties, California," Association of Engineering Geologists Bulletin, Vol. 3, No. 2, 1971.

Ward, T. J., "Factor of Safety Approach to Landslide Potential Delineation," Thesis presented to Colorado State University, at Fort Collins, Colorado, in August, 1976, in partial fulfillment of the requirements for the degree of Doctor of Philosophy.

Ward, T. J., Li, R. M., and Simons, D. B., "Landslide Potential and Probability Considering Randomness of Controlling Factors," Proceedings, International Symposium on Risk and Reliability in Water Resources, University of Waterloo, Waterloo, Canada, June 26-28, 1978, pp. 592-608.

Wiggins Company, J. H., "Building Losses from Natural Hazards: Yesterday, Today and Tomorrow," prepared under National Science Foundation Grant No. ENV-77-08435, undated.

Williams, D. A. and Armstrong, J. E., "Investigation of a Large Landslide Associated with Construction of I-15 near Dillon, Montana," Proceedings, Eighth Annual Symposium Eng. Geology and Soils Engineering, 1970.

Woolley, R. R., "Cloudburst Floods in Utah 1850-1938," U.S. Geological Survey, Water Supply Paper 994, 1946.

Youd, T. L., "Liquefaction, Flow and Associated Ground Failure," U.S. Geological Survey Circular No. 688, 1973.

13.8 LIST OF SYMBOLS

Cr = root cohesion;
Cs = soil cohesion;
$\underline{c}$ = cohesion term;
$\bar{c}$ = effective cohesion;
D = driving forces;
E[] = expected value or mean of linear equation;
FS = factor of safety;
H = measure of soil depth;
H_u = unsaturated soil height;
H^w = saturated soil height or height to ground water table;
L_1 = dimensionless grouping of parameters;
L_2 = dimensionless grouping of parameters;
M = relative groundwater height;
n = number of soil layers;
p = cumulative probability;
P = probability of failure;
qo = vegetative surcharge;
R = resistive forces;
S = random variable;
Tsw = wind shear in trees;
U = nondimensional variate;
u = pore water pressure;
Var[] = variance;
$\underline{x}$ = variable;
$\bar{x}$ = mean of variable x;
Y = random variable;
Z = height above bedrock surface or random variable;
Z* = relative position above bedrock surface;
β = slope inclination;
γ = unit weight;
Δz = thickness;
Σ = summation sign;
$\underline{\sigma}$ = total normal stress;
$\bar{\sigma}$ - effective normal stress;
τ = overall shear resistance;
τ' = overall shear stress;
$\underline{\phi}$ = angle of internal friction;
$\bar{\phi}$ = effective angle of internal friction.

Subscripts

a = area; lower limit;
b = upper limit;
i = layer i;
sat = saturated;
w = water.

CHAPTER 14

APPLICATION OF KALMAN FILTERING IN WATERSHED AND RIVER ANALYSIS

by

Nguyen Duong, Assistant Professor, Department of Civil Engineering,
Colorado State University, Fort Collins, Colorado

14.1 INTRODUCTION

Much of the insight gained in other fields, expecially in systems engineering, is directly applicable to hydrology (Dawdy, 1969). Since state-space modeling and Kalman filtering techniques have been applied successfully to aerospace and industrial systems in the last two decades, and since there are many similarities between physical systems in these areas and hydrological systems (i.e., the models are not known precisely, the system under study is stochastic, and there are noises imbedded in the observed data), the application of these techniques to the analysis of watershed and river systems has been suggested in water resources literature. For instance, a number of papers have been published on the use of state-space techniques for watershed and rainfall-runoff modeling (i.e., Hino, 1973; Duong et al., 1973; Todini and Bouillot, 1975; Moore and Weiss, 1976), on-line river flow forecasting (i.e., Szöllösi-Nagy, Todini, and Wood, 1976; Kitanidis and Bras, 1978), raingauge network design (i.e., Bras and Rodriguez-Iturbe, 1975), or on-line prediction of consumption for water supply network control (Fallside and Perry, 1975).

The aim of this chapter is to give a short introduction to state-space modeling with particular reference to watershed and river channel systems, and discuss the applicability of Kalman filtering techniques to the identification of model parameters and the prediction of system's response.

The Motion of State, State-variable, State-space, and State Equations for Dynamic Systems

If the dynamics of a system are recorded, then the information obtained at each instant describes the instantaneous state of the system. We use a set of variables, called state variables, to identify a system and describe its dynamics. If a dynamic system is simple, then a single state variable will be sufficient to describe the state of the system completely. However, in most cases, a set of state variables, called a state vector, will be necessary to describe the state of a system completely at any instant. To be valid, all elements in a state vector must be independent. The n state-variables may be considered as associated with separate axes in an n-dimensional (Euclidian) space called the state-space.

The state concept is basically a mathematical description of the condition or "state" of a system as a function of time. In this respect it involves the conventional description of systems by differential equations; however, the algebra of the state-space approach is such as to enable the representation to be made in terms of groups of first-order equations only and in terms of state variables of direct significance to the analyst. The derived equations are called state equations.

Example 1 (Duong et al., 1973)

Direct runoff may be considered as the result of the transformation of rainfall excess by the basin. The physical process of this transformation is very complex, depending mainly upon the storage effects in the basin. To take into accout these effects, Kulandaiswamy (1964) derived the following general relation

$$S(t) = \sum_{n=0}^{N} a_n(Q,R) \frac{d^n Q}{dt^n} + \sum_{m=0}^{M} b_m(Q,R) \frac{d^m R}{dt^m} \qquad (14\text{-}1)$$

where S is the storage, t is time, N and M are integers, and $a_n(Q,R)$ and $b_m(Q,R)$ are parametric functions of the direct runoff Q and the excess rainfall R. To apply the storage relation 14-1 to the study of rainfall-runoff processes in a particular watershed, the values of N and M, and the form of $a_n(\cdot)$ and $b_m(\cdot)$ must be determined. Sometimes, this is not feasible in practice. A simplified version was therefore suggested by Prasad (1967):

$$S(t) = K_1 Q^N + K_2 \frac{dQ}{dt} \qquad (14\text{-}2)$$

in which K_2 may be a complicated function of several variables affecting the wedge-storage as well as the storage-discharge relationship. In his study, however, Prasad assumed that K_1, K_2, and N are constants for a particular hydrograph. Using continuity equation, the following differential equation for the rainfall-runoff process was obtained

$$K_2 \frac{d^2 Q}{dt^2} + K_1 N Q^{N-1} \frac{dQ}{dt} + Q = R. \qquad (14\text{-}3)$$

This can be written as

$$\frac{d^2 Q}{dt^2} = -\left(\frac{1}{K_2}\right) K_1 N Q^{N-1} \frac{dQ}{dt} - \left(\frac{1}{K_2}\right) Q + \left(\frac{1}{K_2}\right) R. \qquad (14\text{-}4)$$

By defining the following set of state variables

$$x_1(t) = Q(t)$$

$$x_2(t) = \frac{dQ(t)}{dt}$$

$$x_3(t) = K_1$$

$$x_4(t) = \frac{1}{K_2}$$

$$x_5(t) = N$$

and assuming that the model coefficients are time-invariant, Equation 14-4 becomes

$$\begin{bmatrix} \dot{x}_1(t) \\ \dot{x}_2(t) \\ \dot{x}_3(t) \\ \dot{x}_4(t) \\ \dot{x}_5(t) \end{bmatrix} = \begin{bmatrix} x_2(t) \\ -x_3(t)x_4(t)x_5(t)x_2(t)x_1(t)^{x_5(t)-1} + x_4(t)[R(t) - x_1(t)] \\ 0 \\ 0 \\ 0 \end{bmatrix} \quad (14\text{-}5)$$

or, in abbreviated notation,

$$\dot{\underline{x}}(t) = \underline{f}[\underline{x}(t), R(t)] . \quad (14\text{-}6)$$

Equation 14-6, or its original form 14-5, is a nonlinear state equation of the Prasad rainfall-runoff model. By choosing the direct runoff $Q(t)$ as the observed output from the system, one can write the observation equation in terms of the state variables as

$$y(t) = (1\ 0\ 0\ 0\ 0) \begin{bmatrix} x_1(t) \\ x_2(t) \\ x_3(t) \\ x_4(t) \\ x_5(t) \end{bmatrix} \quad (14\text{-}7)$$

or, like 14-6, in abbreviated notation as

$$y(t) = \underline{h}[\underline{x}(t)] . \quad (14\text{-}8)$$

The state equation 14-6 and the observation equation 14-8 constitute a complete representation of the rainfall-runoff process in state-space.

Remarks

(1) If one chooses $x_4(t) = K_2$ as a state variable, then the resulting state equation would be different from 14-5. Thus the set of state variables used to describe the state of a dynamic system is not unique. Choosing a convenient set of state variables for a system is, therefore, part of the art of engineering.

(2) Variables with no direct physical meaning can also be chosen as being state variables.

(3) The state equations constitute a set of first-order, simultaneous, differential equations which can be either linear or nonlinear.

(4) The observation equation can also be either linear or nonlinear with respect to the state variables.

(5) The state format, represented by Equations 14-6 and 14-8, is particularly attractive in the case of systems of large complexity when the use of computer or numerical methods of solution are likely to be required.

14.2 STATE EQUATIONS FOR LINEAR SYSTEMS

Continuous Case

The state equations for linear systems can be obtained as a special case of 14-6. The dynamic behavior of such a system can be modeled by a set of first-order linear differential equations of the form:

$$\dot{\underline{x}}(t) = \underline{F}(t)\underline{x}(t) + \underline{G}(t)\underline{u}(t) \qquad (14\text{-}9)$$

where $\underline{x}(t)$ is an n-vector of state variables of the system, $\underline{u}(t)$ is an m-vector of input variables, $\underline{F}(t)$ is an n x n matrix, and $\underline{G}(t)$ is an n x m matrix. The initial state is defined by $\underline{x}(0)$.

For this case, the observation Equation 14-8 is assumed to be degnerated to the following linear form:

$$\underline{y}(t) = \underline{H}(t)\underline{x}(t) \qquad (14\text{-}10)$$

where $\underline{y}(t)$ is an ℓ-vector of observed output variables, and $\underline{H}(t)$ is an ℓ x n matrix which relates the state variables to the outputs.

Example 2

Let us consider the Nash model of the rainfall-runoff process (Nash, 1960). In this model, the surface runoff is approximated by a series of n reservoirs each of which has the same storage coefficient K which is a dimensionless constant. It is assumed that the outflow from one reservoir is proportional by k to the content of the reservoir in question (Figure 14.1). Let $x_i(t)$, the i-th state variable, denote the content of the i-th reservoir at time t; then, by continuity, the following state equations are obtained

$$\begin{bmatrix} \dot{x}_1(t) \\ \dot{x}_2(t) \\ \dot{x}_3(t) \\ \vdots \\ \dot{x}_n(t) \end{bmatrix} = \begin{bmatrix} -k & & & & \\ k & -k & & & \\ & k & -k & & \\ & & \ddots & \ddots & \\ & & & k & -k \end{bmatrix} \begin{bmatrix} x_1(t) \\ x_2(t) \\ x_3(t) \\ \vdots \\ x_n(t) \end{bmatrix} + \begin{bmatrix} 1 \\ 0 \\ 0 \\ \vdots \\ 0 \end{bmatrix} u(t). \qquad (14\text{-}11)$$

This can be written in vector-matrix form as

$$\dot{\underline{x}}(t) = \underline{F}\,\underline{x}(t) + \underline{G}\,u(t). \qquad (14\text{-}12)$$

Since the outflow from the last reservoir is the observed output from the system, the observation equation is

$$y(t) = [0\ 0 \ldots k] \begin{bmatrix} x_1(t) \\ x_2(t) \\ \vdots \\ x_n(t) \end{bmatrix} \qquad (14\text{-}13)$$

or, in abbreviated notation,

$$y(t) = \underline{H}\,\underline{x}(t)\,. \qquad (14\text{-}14)$$

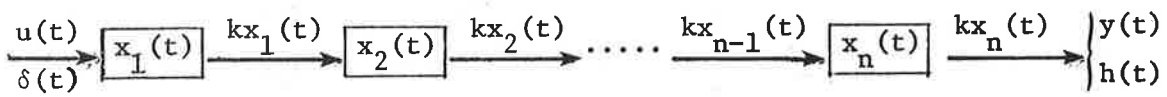

Figure 14.1 State representation of the Nash-model.

Remarks

(1) If the system is initially at rest and an input $u(t) = \delta(t)$, where $\delta(t)$ is the Dirac delta-function, is applied to it, then the output is the impulse response of the system, $y(t) = h(t)$, which is in fact the instantaneous unit hydrograph (I.U.H.).

(2) Replacing $u(t)$ by $\delta(t)$ and solving Equations 14-11 successively, one obtains:

$$\dot{x}_1(t) + kx_1(t) = \delta(t) \rightarrow x_1(t) = e^{-kt}$$

$$\dot{x}_2(t) + kx_2(t) = kx_1(t) \rightarrow x_2(t) = kte^{-kt}$$

$$\dot{x}_i(t) + kx_i(t) = kx_{i-1}(t) \rightarrow x_i(t) = \frac{(kt)^{i-1}}{(i-1)!} e^{-kt}$$

$$\dot{x}_n(t) + kx_n(t) = kx_{n-1}(t) \rightarrow x_n(t) = \frac{(kt)^{n-1}}{(n-1)!} e^{-kt}$$

Thus, from the observation equation 14-13, the impulse response of the system is

$$y(t) = kx_n(t) = k\frac{(kt)^{n-1}}{(n-1)!} e^{-kt} \quad . \tag{14-15}$$

which, by letting $k = \frac{1}{K}$, gives the well-known Nash I.U.H.

$$h(t) = \frac{1}{K}\left(\frac{t}{K}\right)^{n-1} \frac{1}{(n-1)!} e^{-\frac{t}{K}} \quad . \tag{14-16}$$

Discrete Case

In the case of the discrete form, the state vector is determinate only at specified instants within the range of a time interval such that successive values of $\underline{x}(t)$ are denoted by

$$\underline{x}(k) \quad \text{and} \quad \underline{x}(k+1)$$

which correspond to the instants

$$kh \quad \text{and} \quad (k+1)h \qquad , \; k = 0,1,2,3\ldots\text{etc.}$$

where h is the duration of the time interval between the values $\underline{x}(k)$ and $\underline{x}(k+1)$.

By analogy with Equation 14-9, the state equation for linear discrete processes has the general form

$$\underline{x}(k+1) = \underline{\phi}(k+1,k)\underline{x}(k) + \underline{\Gamma}(k)\underline{u}(k) \tag{14-17}$$

where $\underline{\phi}(k+1,k)$ is an n x n matrix, called the state transition matrix, which in the case of free systems maps the state at time k to the new state at time k+1 and $\underline{\Gamma}(k)$ is an n x m matrix having similar characteristics as $\underline{G}(t)$ in Equation 14-9.

Example 3 (Szöllösi-Nagy, 1976)

The simplified storage process of a reservoir having capacity V can be described by the following relations

$$x(k+1) = \begin{cases} 0 & \xi(k) + \phi(k+1,k)x(k) \leq D(k) \\ \phi(k+1,k)x(k) + \xi(k) - D(k) & \xi(k) + \phi(k+1,k)x(k) > D(k) \\ V & \xi(k) + \phi(k+1,k)x(k) \geq V + D(k) \end{cases} \quad (14\text{-}18)$$

where $\xi(k)$ denotes the inflow to the reservoir at instant k; D(k) is the water demand at the same time; $\phi(k+1,k)$ is a reducing factor to account for losses due to evaporation, seepage, etc., during the time interval (k,k+1); and $x(\cdot)$, the state variable, is the volume of stored water in the reservoir.

Letting $u(k) = \xi(k) - D(k)$ be the "net inflow" to the reservoir at instant k, the storage Equation 14-18 can be written as

$$x(k+1) = \phi(k+1,k)x(k) + u(k) \quad (14\text{-}19)$$

with the initial conditions x(o), u(o) given. It is clear that the range of variation of x is bounded by o and V.

Remarks

(1) In this example, if one assumes that $\phi(k+1,k)$ is time-invariant and equal to ϕ, then Equation 14-19 becomes

$$x(k+1) = \phi x(k) + u(k) . \quad (14\text{-}20)$$

For this case, the matrices $\underline{\phi}(k+1,k)$ and $\underline{\Gamma}(k)$ in the general Equation 14-17 reduce to simple scalar coefficients.

(2) Solving Equation 14-20 recursively, one obtains:

$$x(1) = \phi x(o) + u(o)$$
$$x(2) = \phi x(1) + u(1) = \phi^2 x(o) + u(1) + \phi u(o)$$
$$x(k) = \phi^k x(o) + \sum_{i=0}^{k-1} \phi^{k-i-1} u(i) \quad (14\text{-}21)$$

Thus, for the time-invariant discrete vector state Equation 14-17, the solution can be written as:

$$\underline{x}(k) = \underline{\phi}^{k}\underline{x}(o) + \sum_{i=0}^{k-1} \underline{\phi}^{k-i-1}\,\underline{\Gamma}\,\underline{u}(i)\,. \tag{14-22}$$

When the matrices $\underline{\phi}$ and $\underline{\Gamma}$ are time dependent, the solution becomes:

$$\underline{x}(k) = \prod_{i=0}^{k-1} \underline{\phi}(i+1,i)\underline{x}(o) + \sum_{j=0}^{k-2}\sum_{i=j+1}^{k-1} \underline{\phi}(i+1,i)\underline{\Gamma}(i)\underline{u}(i) + \underline{\Gamma}(k-1)\underline{u}(k-1) \tag{14-23}$$

State Transition Matrix

Consider the continuous state equation of an unforced linear system

$$\dot{\underline{x}}(t) = \underline{F}(t)\underline{x}(t)\,. \tag{14-24}$$

Assume that the solution of Equation 14-24 is known in the form

$$\underline{x}(t) = \underline{\phi}(t,o)\underline{x}(o), \tag{14-25}$$

where $\underline{x}(o)$ is the vector of initial states at $t_o = 0$, and $\underline{\phi}(t,o)$ is a state transition matrix since it maps the initial state into a state at any later time $t > 0$. Obviously,

$$\underline{\phi}(o,o) = I \tag{14-26}$$

where I is the identity matrix.

Taking derivatives of Equation 14-25 with respect to time, one obtains

$$\dot{\underline{x}}(t) = \frac{d}{dt}\,\underline{\phi}(t,o)\underline{x}(o) = \dot{\underline{\phi}}(t,o)\underline{x}(o)\,. \tag{14-27}$$

On the other hand, if one replaces $\underline{x}(t)$ in Equation 14-24 by its expression in Equation 14-25, a different expression for $\dot{\underline{x}}(t)$ is derived:

$$\dot{\underline{x}}(t) = \underline{F}(t)\underline{\phi}(t,o)\underline{x}(o)\,. \tag{14-28}$$

Thus, by comparing Equations 14-27 and 14-28, the following relationship must hold for the state transition matrix:

$$\dot{\underline{\phi}}(t,o) = \underline{F}(t)\underline{\phi}(t,o)\,. \tag{14-29}$$

For time-invariant systems, $\underline{F}(t) = \underline{F}$, the state transition matrix depends only on the time-lag between two instants, i.e., in our case on t only, $\underline{\phi}(t,o) = \underline{\phi}(t)$. The solution of Equation 14-29 for this case reduces to a simple matrix exponential:

$$\underline{\phi}(t) = \exp(\underline{F}t)\,. \tag{14-30}$$

Properties of the State Transition Matrix

The basic properties of the state transition matrix for time-varying and time-invariant systems can be summarized as follows:

(1) Time-varying systems:

$$\underline{\phi}(t_o,t_o) = I$$

$$\underline{\phi}(t_2,t_o) = \underline{\phi}(t_2,t_1) \cdot \underline{\phi}(t_1,t_o)$$

$$\underline{\phi}^{-1}(t_2,t_1) = \underline{\phi}(t_1,t_2)$$

(2) Time-invariant systems:

$$\exp[\underline{F}(t_o - t_o)] = \underline{I}$$

$$\exp[\underline{F}(t_2 - t_o)] = \exp[\underline{F}(t_2-t_1)] \cdot \exp[\underline{F}(t_1 - t_o)]$$

$$\left\{\exp[\underline{F}(t_2 - t_1)]\right\}^{-1} = \exp[-\underline{F}(t_2-t_1)] = \exp[\underline{F}(t_1 - t_2)]$$

Complete Solution for Continuous Linear Systems

To obtain the complete solution of the state equation of forced linear dynamical systems given by Equation 14-9, we use the Lagrangian method of variation of constants. According to this method, the constant $\underline{x}(o)$, which expresses the initial condition of the system in the solution 14-25 of the homogeneous state equation, is assumed to be a function of time, $\underline{c}(t)$, and is to be determined by forcing it to satisfy the condition 14-9.

From the assumed complete solution

$$\underline{x}(t) = \underline{\phi}(t,t_o)\underline{c}(t) , \tag{14-31}$$

and by taking the derivative with respect to t, one obtains:

$$\dot{\underline{x}}(t) = \dot{\underline{\phi}}(t,t_o)\underline{c}(t) + \underline{\phi}(t,t_o)\dot{\underline{c}}(t)$$

$$= \underline{F}(t)\underline{\phi}(t,t_o)\underline{c}(t) + \underline{\phi}(t,t_o)\dot{\underline{c}}(t) \tag{14-32}$$

On the other hand, by substituting the assumed solution 14-31 into the original differential Equation 14-9, one has:

$$\dot{\underline{x}}(t) = \underline{F}(t)\underline{\phi}(t,t_o)\underline{c}(t) = \underline{G}(t)\underline{u}(t) \tag{14-33}$$

which, combined with Equation 14-32, yields

$$\underline{\phi}(t,t_o)\dot{\underline{c}}(t) = \underline{G}(t)\underline{u}(t) \tag{14-34}$$

Equation 14-34 can be rewritten as

$$\dot{\underline{c}}(t) = \underline{\phi}^{-1}(t,t_o)\underline{G}(t)\underline{u}(t) \tag{14-35}$$

and, after integrating over $[t_o,t]$,

$$\underline{c}(t) = \underline{x}(t_o) + \int_{t_o}^{t} \underline{\phi}^{-1}(\tau,t_o)\underline{G}(\tau)\underline{u}(\tau)d\tau \tag{14-36}$$

This expression for $\underline{c}(t)$, when substituted into Equation 14-31, yields the complete solution for the state Equation 14-9 as

$$\underline{x}(t) = \underline{\phi}(t,t_o)\underline{x}(t_o) + \int_{t_o}^{t} \underline{\phi}(t,\tau)\underline{G}(\tau)\underline{u}(\tau)d\tau \tag{14-37}$$

Observation Equation 14-10 becomes:

$$\underline{y}(t) = \underline{H}(t)\underline{\phi}(t,t_o)\underline{x}(t_o) + \int_{t_o}^{t} \underline{H}(t)\underline{\phi}(t,\tau)\underline{G}(\tau)\underline{u}(\tau)d\tau \tag{14-38}$$

For time-invariant systems, Equations 14-37 and 14-38 reduce to:

$$\underline{x}(t) = e^{\underline{F}(t-t_o)}\underline{x}(t_o) + \int_{t_o}^{t} e^{\underline{F}(t-\tau)}\underline{G}\,\underline{u}(\tau)d\tau \tag{14-39}$$

and

$$\underline{y}(t) = \underline{H}\,e^{\underline{F}(t-t_o)}\underline{x}(t_o) + \int_{t_o}^{t} \underline{H}\,e^{\underline{F}(t-\tau)}\underline{G}\,\underline{u}(\tau)d\tau \tag{14-40}$$

Discrete State-space Formulation of a Continuous Linear Dynamic Process

Assume that $\underline{x}(k)$ is given and $\underline{u}(k)$ is constant within the time interval $[t_k, t_{k+1}]$; then according to Equation 14-37, one has

$$\underline{x}(k+1) = \underline{\phi}(k+1,k)\underline{x}(k) + \left[\int_{t_k}^{t_{k+1}} \underline{\phi}(k+1,\tau)\underline{G}(\tau)d\tau\right]\underline{u}(k) \tag{14-41}$$

By defining

$$\underline{\Gamma}(k) = \int_{t_k}^{t_{k+1}} \underline{\phi}(k+1,\tau)\underline{G}(\tau)d\tau \tag{14-42}$$

Equation 14-41 can be rewritten as

$$\underline{x}(k+1) = \underline{\phi}(k+1,k)\underline{x}(k) + \underline{\Gamma}(k)\underline{u}(k) \tag{14-43}$$

which is identical to Equation 14-17.

Example 4 (Szöllösi-Nagy, 1976)

The water quality of a river can be characterized by the dynamic interrelationship between the biochemical oxygen demand (BOD) and the dissolved oxygen (DO). In the Streeter-Phelps model, a first-order reaction kinetic for the BOD is assumed

$$\frac{dB(t)}{dt} = - K_r B(t) \tag{14-44}$$

where $B(t)$ is the BOD concentration in mg/ℓ and K_r is the BOD removal or decay coefficient in day^{-1}. By continuity

$$\frac{dD(t)}{dt} = - K_a D(t) - K_r B(t) + K_a D_s \tag{14-45}$$

where $D(t)$ is the DO concentration in mg/ℓ, K_a is the reaeration coefficient in day^{-1}, and D_s is the saturation level of the dissolved oxygen. Defining the state variables as

$$x_1(t) = B(t)$$

$$x_2(t) = D(t) - D_s$$

then the state equation for the Streeter-Phelps model has the form

$$\dot{\underline{x}}(t) = \underline{F}\,\underline{x}(t) \tag{14-46}$$

where

$$\underline{x}(t) = \begin{bmatrix} x_1(t) \\ x_2(t) \end{bmatrix} \quad \text{and} \quad \underline{F} = \begin{bmatrix} - K_r & 0 \\ - K_r & K_a \end{bmatrix} \tag{14-47}$$

If, in addition, $u_1(t)$ is the control of effluent dumping from the sewage treatment plant, and $u_2(t)$ is the artificial aeration carried out at the aeration facilities, the state equation for the continuous process model becomes

$$\dot{\underline{x}}(t) = \underline{F}\,\underline{x}(t) + \underline{G}\,\underline{u}(t) \tag{14-48}$$

where $\underline{u}(t) = \begin{bmatrix} u_1(t) \\ u_2(t) \end{bmatrix}$ and $\underline{G} = \begin{bmatrix} 1 & 0 \\ 0 & -1 \end{bmatrix}$

Assume that DO measurements are the only observed outputs available, the observation equation for the process can be written as

$$y(t) = \underline{H}\,\underline{x}(t) \tag{14-49}$$

where $\underline{H} = (0 \quad 1)$

If a digital computer is used to solve this problem, then a transformation of Equations 14-48 and 14-49 into discrete state-space formulation is required.

Assume that the process is time-invariant, i.e., $\underline{F}$ and $\underline{G}$ are constant, then from Equation 14-30, the state transition matrix between two successive instants k and $k+1$ has the form

$$\underline{\phi}(k+1,k) = \exp \underline{F} \tag{14-50}$$

Using the well-known Sylvester expansion theorem, the one-step state transition matrix is obtained as

$$\underline{\phi}(k+1,k) = \left[\begin{array}{c|c} \exp(-K_r) & 0 \\ \hline \dfrac{-K_r}{K_a - K_r}\left[\exp(-K_r) - \exp(-K_a)\right] & \exp(-K_a) \end{array}\right] \tag{14-51}$$

provided that $K_a \neq K_r$. The matrix $\underline{\Gamma}(k)$ in Equation 14-43 is obtained by evaluating Equation 14-42 in taking account of the time-invariant characteristic of $\underline{\phi}$ and $\underline{G}$. This matrix has the same form as $\underline{\phi}(k+1,k)$ given by Equation 14-51, except that the matrix element in the lower right-hand corner is negative. Thus, the discrete state-space-formulation of Equations 14-48 and 14-49 can be written as

$$\underline{x}(k+1) = \underline{\phi}(k+1,k)\underline{x}(k) + \underline{\Gamma}(k)\underline{u}(k) \tag{14-52}$$

and

$$y(k) = \underline{H}\,\underline{x}(k) \tag{14-53}$$

14.3 STATE EQUATIONS FOR LINEAR STOCHASTIC DYNAMIC SYSTEMS

Up until now we dealt with strict deterministic systems. However, as Yevjevich (1974) states, it is extremely difficult to find a pure deterministic hydrologic process in nature, because of uncertainties

in the environmental conditions. In addition, when using a model to simulate the dynamics of a hydrological system, uncertainties in the model structure, model parameters, and in the data will certainly affect the simulation results. Thus, hydrological systems should be considered as stochastic dynamical systems in which the system state is a random variable.

Let us first define some properties of random processes.

Random Sequences and the Markov Property

A random sequence is a collection of continuous-valued random variables (scalar or vector) indexed by a discrete-valued parameter such as

$$X(0),\ X(1),\ldots,X(k),\ldots,X(N)$$

A random sequence $X(k)$, $k = 0,1,2,\ldots N$ is said to be Markovian if

$$p[X(k+1)/X(k),X(k-1),\ldots,X(0)] = p[X(k+1)/X(k)] \qquad (14\text{-}54)$$

for all k; that is the probability density function of $X(k+1)$ depends only on the knowledge of $X(k)$ and not on the previous states. In other words, the Markov property implies that a knowledge of the present separates the past and the future. This property simplifies the calculation of the joint probability density function of a Markov random sequence, as can be seen by the following development:

$$\begin{aligned} p[X(N),X(N-1),\ldots,X(0)] &= p[X(N)/X(N-1),\ldots x(0)] \cdot p[X(N-1),\ldots,X(0)] \\ &= p[X(N)/X(N-1),\ldots X(0)] \cdot p[X(N-1)/X(N-2)\ldots, \\ &\quad X(0)]\ldots P[X(1)/X(0)]P[X(0)] \end{aligned} \qquad (14\text{-}55)$$

which may be reduced to

$$\begin{aligned} p[X(N),\ X(N-1),\ldots,X(0)] &= p[X(N)/X(N-1)] \cdot p[X(N-1)/X(N-2)]\ldots \\ &\quad \cdot p[X(1)/X(0)] \cdot p[X(0)] \end{aligned} \qquad (14\text{-}56)$$

Thus, the joint probability density function is equal to the product of the transition density functions, $p[X(k+1)/X(k)]$, and the initial density function $p[X(0)]$.

If $p[X(k+1)/X(k)] = p[X(k+1)]$ for all possible values of k, the sequence is said to be a purely random (or white noise) sequence.

The Generality of Markov Sequences

The Markov property is not as restrictive as it might seem. Suppose that we have a scalar second-order difference equation

$$X_1(k+1) = c_1(k)X_1(k) + c_2(k)X_1(k-1) + w(k), \qquad (14\text{-}57)$$

where $w(k)$ is a purely random Markov sequence and $c_1(k)$ and $c_2(k)$ are known sequences. Clearly the sequence $X_1(k)$ is not Markovian. However, we can make it into a component of a vector Markov sequence using the state vector $\begin{bmatrix} X_1(k) \\ X_2(k) \end{bmatrix}$, where $X_2(k+1) = X_1(k)$, since

$$\begin{bmatrix} X_1(k+1) \\ X_2(k+1) \end{bmatrix} = \begin{bmatrix} c_1(k) & c_2(k) \\ 1 & 0 \end{bmatrix} \begin{bmatrix} X_1(k) \\ X_2(k) \end{bmatrix} + \begin{bmatrix} 1 \\ 0 \end{bmatrix} w(k);$$

that is, the two-component vector $\begin{bmatrix} X_1(k+1) \\ X_2(k+1) \end{bmatrix}$ depends only on a knowledge of $\begin{bmatrix} X_1(k) \\ X_2(k) \end{bmatrix}$, the previous element in the sequence, and the purely random sequence $w(k)$.

Generalizing the above procedure, we see that, given any vector random sequence that depends on the finite past, in the sense of Equation 14-57, we can always convert it to an equivalent Markov random sequence by properly enlarging the state vector. Thus, Markov random sequences with finite dimensional state vectors include, in this sense, all random sequences between the two extreme cases, namely, the purely random sequence and the random sequence that depends on the infinite past. Consequently, Markov random sequences can be used to represent a great variety of physical phenomena.

Gauss-Markov Random Sequences

A Gauss-Markov random sequence is a Markov random sequence with the added restriction that $p[X(k)]$ and $p[X(k+1)/X(k)]$ are Gaussian probability density functions for all k.

The density function $p[X(k)]$ of a Gauss-Markov random sequence is, therefore, completely described by giving two deterministic sequences, the mean-value vector $\overline{X}(k) = E\{X(k)\}$ and the covariance matrix $P(k) = E\{[X(k) - \overline{X}(k)][X(k) - \overline{X}(k)]^T\}$.

Since linear transformations of a Gaussian vector preserve its Gaussian character, a Gauss-Markov random sequence can always be represented by the state vector of a multi-stage linear dynamic system forced by a Gaussian purely random sequence in which the initial state vector is Gaussian:

$$X(k+1) = \phi(k+1,k)X(k) + \Gamma(k)w(k) \tag{14-58}$$

where: X is an n-vector, w is an m-vector,

$$E\{w(k)\} = \overline{w}(k) \tag{14-59}$$

$$E\{[w(k) - \overline{w}(k)][w(\ell) - \overline{w}(\ell)]^T\} \tag{14-60}$$

$$E\{X(0)\} = \overline{X}(0) \tag{14-61}$$

$$E\{[X(0) - \overline{X}(0)][x(0) - \overline{X}(0)]^T\} = P(0) \tag{14-62}$$

$$E\{[X(0) - \overline{X}(0)][w(k) - \overline{w}(k)]^T\} = 0 \tag{14-63}$$

A block diagram representation of a Gauss-Markov sequence is given in Figure 14.2.

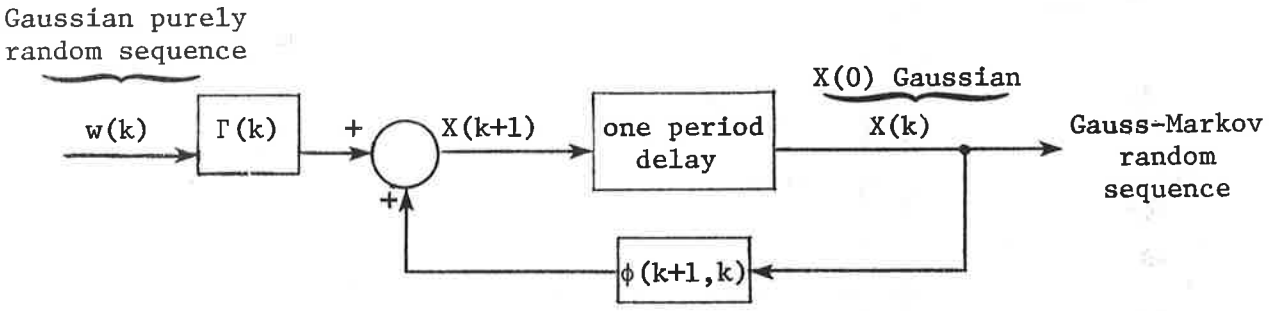

Figue 14.2 Representation of a Gauss-Markov sequence.

The relations for determining the sequence $\overline{X}(k)$ and $P(k)$ are readily found from the data of Equations 14-58 through 14-63. Taking the expected value of Equation 14-58, we have

$$\boxed{\overline{X}(k+1) = \phi(k+1,k)\overline{X}(k) + \Gamma(k)\overline{w}(k)} \tag{14-64}$$

where $\overline{X}(0)$ and $\overline{w}(k)$ are given.

Subtracting Equation 14-64 from Equation 14-58, we have

$$X(k+1) - \overline{X}(k+1) = \phi(k+1,k)[X(k) - \overline{X}(k)] + \Gamma(k)[w(k) - \overline{w}(k)] \tag{14-65}$$

Multiplying Equation 14-65 by its transpose and then taking the expected value of both sides yields

$$\boxed{P(k+1) = \phi(k+1,k)P(k)\phi^T(k+1,k) + \Gamma(k)Q(k)\Gamma^T(k)} \qquad (14\text{-}66)$$

where $P(0)$ and $Q(k)$ are given.

Equations 14-64 and 14-66 are linear difference equations for the mean value vector and covariance matrix. They completely specify the evolution of the density function $p[X(k)]$.

Example 5

Consider a discrete-time autoregressive (AR) model of order n of streamflow

$$y(k+1) = \phi_1 y(k) + \phi_2 y(k-1) + \ldots + \phi_n y(k-n+1) + w(k), \qquad (14\text{-}67)$$

where the ϕ's are the autoregressive coefficients, and $w(k)$ is a white Gaussian noise sequence with the usual properties. Defining the state variables as

$$x_1(k) = y(k-n+1)$$

$$x_2(k) = y(k-n+2)$$

$$x_n(k) = y(k) \ ,$$

that is,

$$\underline{x}(k) = [y(k-n+1),\ y(k-n+2),\ldots,y(k)]^T; \qquad (14\text{-}68)$$

then, Equation 14-67 can be written in the following form

$$\underline{x}(k+1) = \underline{\phi}\ \underline{x}(k) + \underline{\Gamma}\ w(k), \qquad (14\text{-}69)$$

where

$$\underline{\phi} = \begin{bmatrix} 0 & 1 & 0 & \ldots & 0 & 0 \\ 0 & 0 & 1 & \ldots & 0 & 0 \\ \cdot & \cdot & \cdot & & \cdot & \cdot \\ \cdot & \cdot & \cdot & & \cdot & \cdot \\ \cdot & \cdot & \cdot & & \cdot & \cdot \\ 0 & 0 & 0 & \ldots & 0 & 1 \\ \phi_n & \phi_{n-1} & \phi_{n-2} & & \phi_2 & \phi_1 \end{bmatrix}, \quad \underline{\Gamma} = \begin{bmatrix} 0 \\ 0 \\ \cdot \\ \cdot \\ \cdot \\ 0 \\ 1 \end{bmatrix} .$$

The observation equation is

$$y(k) = \underline{H}\ \underline{x}(k), \qquad (14\text{-}70)$$

where $H = [0, 0,\ldots,0 , 1]$.

Remarks

In the above model, the noise sequence plays the role of the input and the measurement uncertainty is not present. Other examples of stochastic state-space modeling in runoff can be found in Kontur (1975).

Random Processes and the Markov Property

A random process is a collection of continuous-valued random variables indexed by a continuous-valued parameter such as

$$X(t), \text{ for } t_o \leq t \leq t_f$$

In applications, the continuous-valued parameter (or independent variable), t, is often a time or distance measure. t_o and t_f are, respectively, the initial and final values of t.

All continuous dynamic processes that occur in natural and man-made systems are random processes, since the state of such systems can never be known exactly. Most random processes encountered in applications are Markovian, and a Markov process is completely specified by giving the joint density function $p[X(t), X(\tau)]$ for all t, τ in the interval (t_o, t_f).

Since we have $p[X(t), X(\tau)] = p[X(t)/X(\tau)] \cdot p[(X(\tau)]$, a Markov process is also completely specified by giving the density functions $p[X(t)/X(\tau)]$ and $p[X(\tau)]$ for all t, τ in the interval (t_o, t_f). If we have $p[X(t)/X(\tau)] = p[X(t)]$ for all t, τ in (t_o, t_f), then $X(t)$ is called a purely random (or white noise) process. It is an imaginary process and must be considered only as a limiting case, since, in any actual process, $X(t)$ and $X(\tau)$ will be dependent when $|t-\tau|$ is sufficiently small.

The Generality of Markov Processes

Suppose that we have a second-order differential equation for the scalar $x_1(t)$:

$$\ddot{x}_1 = c_1(t)\dot{x}_1 + c_2(t)x_1 + w(t)$$

where $w(t)$ is a scalar purely random Markov process and $c_1(t)$, $c_2(t)$ are known functions of time. Then $x_1(t)$ is not a Markov process. However, we can make it into a component of a vector Markov process using the state vector $\begin{bmatrix} x_1 \\ x_2 \end{bmatrix}$ where $x_2 = \dot{x}_1$ since

$$\frac{d}{dt}\begin{bmatrix} x_1 \\ x_2 \end{bmatrix} = \begin{bmatrix} 0 & 1 \\ c_2(t) & c_1(t) \end{bmatrix}\begin{bmatrix} x_1 \\ x_2 \end{bmatrix} + \begin{bmatrix} 0 \\ 1 \end{bmatrix} w(t)$$

Generalizing this procedure, we see that, given any random process involving a finite number of time derivatives, we can always convert it to an equivalent Markov random process by properly enlarging the state vector.

Gauss-Markov Random Processes

A Gauss-Markov random process is a Markov random process with the added restriction that $p[X(t)]$ and $p[X(t)/X(\tau)]$ are Gaussian density functions for all t, τ in the interval (t_o, t_f).

The density function $p[X(t)]$ of a Gauss-Markov process is, therefore, completely described by giving two deterministic functions, the mean value vector $\bar{X}(t) = E\{X(t)\}$ and the covariance matrix $P(t) = E\{[X(t) - \bar{X}(t)] \cdot [X(t) - \bar{X}(t)]^T\}$.

Since linear transformations of a Gaussian vector preserves its Gaussian character, a Gauss-Markov random process can always be represented by that state vector of a continuous linear dynamic system forced by a Gaussian purely random process where the initial state vector is Gaussian:

$$\dot{X} = F(t)X + G(t)w(t) \tag{14-71}$$

where

X is an n-vector, w is an m-vector

$$E\{X(t_o)\} = \bar{X}(t_o) \tag{14-72}$$

$$E\{[X(t_o) - \bar{X}(t_o)][X(t_o) - \bar{X}(t_o)]^T\} = P(t_o) \tag{14-73}$$

and $w(t)$ is a Gaussian purely random process with

$$E\{w(t)\} = \bar{w}(t) \tag{14-74}$$

Figure 14-3 shows a block diagram of the Gauss-Markov random process.

In Equations 14-71 through 14-74, we did not completely specify the purely random process $w(t)$. Let us see how $w(t)$ enters into the determination of the covariance matrix $P(t)$, where

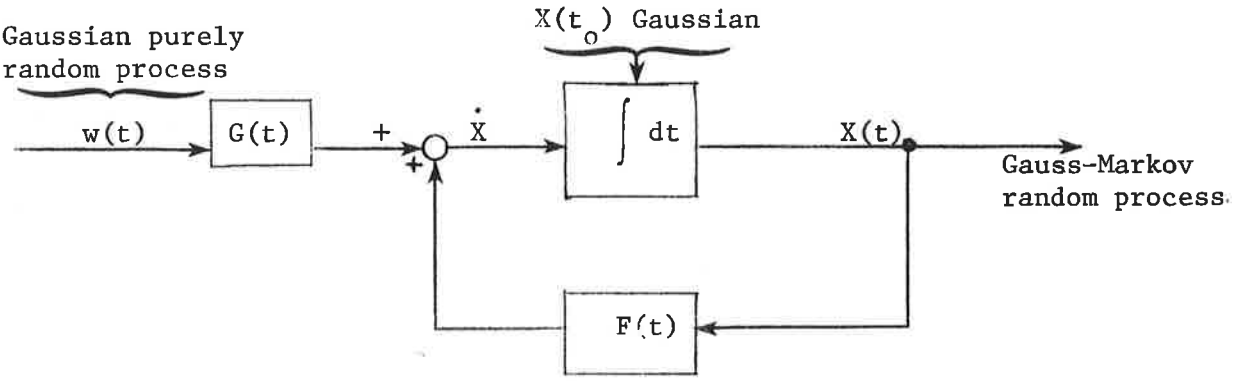

Figure 14.3 Representation of a Gauss-Markov process.

$$P(t) = E\{[X(t) - \bar{X}(t)][X(t) - \bar{X}(t)]^T\}$$

Clearly, the mean value of $X(t)$ is determined by considering the expected value of Equation 14-71:

$$\boxed{\frac{d}{dt}[\bar{X}(t)] = F(t)\bar{X}(t) + G(t)\bar{w}(t)} \tag{14-75}$$

where $\bar{X}(t_o)$ is given.

Subtracting Equation 14-75 from Equation 14-71 and postmultiplying the result by $[X(t) - \bar{X}(t)]^T$ yields

$$\left\{\frac{d}{dt}[X(t) - \bar{X}(t)]\right\}[X(t) - \bar{X}(t)]^T = F(t)[X(t) - \bar{X}(t)][X(t) - \bar{X}(t)]^T + G(t)[w(t) - \bar{w}(t)][X(t) - \bar{X}(t)]^T \tag{14-76}$$

Adding the transpose of Equation 14-76 to Equation 14-76 gives

$$\begin{aligned}\frac{d}{dt}\left\{[X(t) - \bar{X}(t)][X(t) - \bar{X}(t)]^T\right\} &= F(t)[X(t) - \bar{X}(t)][X(t) - \bar{X}(t)]^T \\ &+ [X(t) - \bar{X}(t)][X(t) - \bar{X}(t)]^T F^T(t) \\ &+ G(t)[w(t) - \bar{w}(t)][X(t) - \bar{X}(t)]^T \\ &+ [X(t) - \bar{X}(t)][w(t) - \bar{w}(t)]^T G^T(t)\end{aligned} \tag{14-77}$$

Taking the expected value of Equation 14-77 and using the definition of $P(t)$, gets

$$\begin{aligned}\dot{P} = F(t)P + PF^T(t) &+ G(t)E\left\{[w(t) - \bar{w}(t)][X(t) - \bar{X}(t)]^T\right\} \\ &+ E\left\{[X(t) - \bar{X}(t)][w(t) - \bar{w}(t)]^T\right\}G^T(t)\end{aligned} \tag{14-78}$$

From Equation 14-37, we have

$$X(t) - \bar{X}(t) = \phi(t,t_o)[X(t_o) - \bar{X}(t_o)] + \int_{t_o}^{t} \phi(t,\tau)G(\tau)[w(\tau) - \bar{w}(\tau)]d\tau \tag{14-79}$$

Assuming that

$$E\left\{[X(t_o) - \bar{X}(t_o)][w(t) - \bar{w}(t)]^T\right\} = 0; \tag{14-80}$$

that is, random deviations in initial conditions are uncorrelated with the random fluctuations of the forcing function, then we have

$$E\left\{[X(t) - \bar{X}(t)][w(t) - \bar{w}(t)]^T\right\} = \int_{t_o}^{t} \phi(t,\tau)G(\tau) \cdot E\left\{[w(\tau) - \bar{w}(\tau)][w(t) - \bar{w}(t)]^T\right\}d\tau \tag{14-81}$$

only knowledge of $[w(t) - \bar{w}(t)]$ needed to determine the covariance matrix $P(t)$ is a weighted integral of its autocorrelation:

$$E\left\{[w(t) - \bar{w}(t)][w(\tau) - \bar{w}(\tau)]^T\right\}. \tag{14-82}$$

Let $Q(t)$ be a non-negative definite matrix defined by

$$E\{[w(t) - \bar{w}(t)][w(\tau) - \bar{w}(\tau)]^T\} = Q(t)\delta(t-\tau) \tag{14-83}$$

where $\delta(t-\tau)$ is the Dirac delta function, then the following result is obtained (Bryson and Ho, 1969)

$$\boxed{\dot{P} = FP + PF^T + GQG^T} \tag{14-84}$$

where $P(t_o)$ is given.

When Q is a constant, $w(t)$ is called a stationary purely random process. In addition, if we have $F(t) = F$, a constant matrix, and $G(t) = G$, also a constant matrix, then it is possible that $P(t) \to P$, a constant matrix, as $t \to \infty$. For this case, $\dot{P} \to 0$ so that P may be determined from the linear relation

$$0 = FP + PF^T + GQG^T \tag{14-85}$$

Such a process is called statistically stationary.

State Variables and the Markov Property

There is a strong similarity between the state assumption for deterministic processes and the Markov assumption for stochastic processes. In fact, a Gauss-Markov sequence (process) can be represented by a white Gaussian random sequence (process) driving a linear discrete (continuous) dynamic system whose initial state is Gaussian. From the computational viewpoint, the state representation is far more convenient since we need only the mean and the covariances. In addition, Equations 14-75 and 14-76, which govern the state process, are deterministic and thus are amenable to deterministic treatment. As Bryson and Ho (1969) state, this is the key to the analysis of a stochastic process, namely, to characterize it by quantities which are themselves deterministically related and then operate on these quantities.

14.4 KALMAN FILTERING AND PREDICTION FOR LINEAR STOCHASTIC DYNAMIC SYSTEMS

In the real world, the individual state variables of a dynamic system cannot be determined exactly by direct measurements because we usually find that the measurements that can be made are functions of the state variables and that these measurements contain random errors. The system itself may also be subjected to random disturbances.

If we understand the dynamics of the ideal system (with perfect and complete measurements and no random disturbances) and we have some knowledge of the degree of uncertainty in the measurements and of the degree of intensity of the random disturbances to the system, then, on the basis of all the measurements up to the present time, we can determine the most likely values of the state variables. The process of determining these most likely values is called smoothing, filtering, or prediction, depending on whether we are finding past, present, or future values of the state variables, respectively. In this chapter, only the filtering and prediction problems are treated with particular reference to water resource systems. More information on optimal estimation techniques can be found in Lee (1964).

Estimation of Parameters using Weighted Least-squares

Suppose that we wish to estimate the n-component state vector X of a static system using the ℓ-component measurement vector, Y, containing random errors, v, which are independent of the state X, where

$$Y = HX + v \tag{14-86}$$

H is a known $(\ell \times n)$-matrix, and v has known statistics, i.e.,

$$E\{v\} = 0, \qquad E\{vv^T\} = R \text{ (a known } (\ell \times \ell)\text{-positive matrix).} \tag{14-87}$$

Assume that an estimate of the state, $\overline{X}$, could be obtained before the measurements were made, and that

$$E\{(X - \overline{X})(X - \overline{X})^T\} = P_{(-)}, \text{ a known } (n \times n)\text{-positive matrix.} \tag{14-88}$$

Let $\hat{X}$ be the weighted-least-squares estimate which minimizes the quadratic form

$$J = \frac{1}{2}[(X - \overline{X})^T P_{(-)}^{-1}(X - \overline{X}) + (Y - HX)^T R^{-1}(Y - HX)]. \tag{14-89}$$

Then, the values of $\hat{X}$ which make $dJ = 0$ are given by the following expression

$$\hat{X} = \bar{X} + P_{(+)}H^T R^{-1}(Y - H\bar{X}) \tag{14-90}$$

where

$$P_{(+)}^{-1} = P_{(-)}^{-1} + H^T R^{-1} H \tag{14-91}$$

$P_{(+)}$ in Equation 14-91 is the covariance matrix of the error in the estimate $\hat{X}$.

Remarks

1) Since $H^T R^{-1} H$ is at least a positive-semidefinite matrix, it is apparent from Equation 14-91 that $P_{(+)}$, the error covariance matrix <u>after</u> measurement is never larger than $P_{(-)}$, the error covariance matrix <u>before</u> measurement. Thus, the act of measurement, on the average, decreases the uncertainty in our knowledge of the state X.

2) The estimate and the error of the estimate are uncorrelated. In fact, we have

$$\hat{X} - X = (I - KH)(\bar{X} - X) + Kv$$

where $K = P_{(+)}H^T R^{-1}$

and

$$E\{(\hat{X} - X)\hat{X}^T\} = E\{[(I - KH)(\bar{X} - X) + Kv][\bar{X} - KH(\bar{X} - X) + Kv]^T\}$$

$$= -(I - KH)P_{(-)}H^T K^T + KRK^T = -P_{(+)}H^T K^T + KRK^T = 0 \tag{14-92}$$

(3) Since the prior knowledge of $P_{(-)}$ and R is sometimes vague and uncertain, a way to adjust their initial values is desirable and could be derived as follows (Bryson and Ho, 1969).

From Equation 14-89, the prior expected value of J is $(n + \ell)/2$. As a check, after the estimation process has been completed, the <u>actual</u> value of J in Equation 14-89 should be computed with $X = \hat{X}$; call it J^*. If J^* is not close to $(n + \ell)/2$ (its prior expected value), the elements of $P_{(-)}$ and R should be multiplied by the scale factor $J^*/[(n + \ell)/2]$, which adjusts the value of J^* to $(n + \ell)/2$.

<u>Optimal Filtering for Single-stage Linear Transitions</u>

Consider a system that makes a discrete transition from state 0 to state 1 according to the linear relation

$$X_1 = \phi_{1,0} X_0 + \Gamma_0 w_0, \tag{14-93}$$

where $\phi_{1,o}$ is a known $(n \times n)$ transition matrix, Γ_o is a known $(n \times n)$ matrix, and w_o is a random vector having the following statistics:

$$E\{w_o\} = \bar{w}_o \ , \qquad E\{(w_o - \bar{w}_o)(w_o - \bar{w}_o)^T\} = Q_o \tag{14-94}$$

The state X_o is also a random vector with mean $\hat{X}_o$ and covariance P_o, i.e.,

$$E\{X_o\} = \hat{X}_o \ , \qquad E\{(\hat{X}_o - X_o)(\hat{X}_o - X_o)^T\} = P_o \tag{14-95}$$

Furthermore, X_o and w_o are independent. From this information, it follows that X_1 is also a random vector, and, from Equation 14-64 and 14-66 it has a mean value $\bar{X}_1$ and a covariance $P_{1(-)}$ given by

$$\bar{X}_1 = \phi_{1,o}\hat{X}_o + \Gamma_o\bar{w}_o \tag{14-96}$$

$$P_{1(-)} = \phi_{1,o}P_o\phi_{1,o}^T + \Gamma_o Q_o \Gamma_o^T \tag{14-97}$$

Suppose that we make measurements <u>after</u> the transition to state 1. Then, from Equations 14-90 and 14-91, the best estimate of X_1 is given by

$$\hat{X}_1 = \bar{X}_1 + P_{1(+)}H_1^T R_1^{-1}(Y_1 - H_1\bar{X}_1) \tag{14-98}$$

where $P_{1(+)} = (P_{1(-)}^{-1} + H_1^T R^{-1} H_1)^{-1}$

$$= P_{1(-)} - P_{1(-)}H_1^T(H_1P_{1(-)}H_1^T + R_1)^{-1}H_1P_{1(-)} \ . \tag{14-99}$$

<u>Optimal Filtering for Linear Multi-stage Processes</u>

Consider the linear, stochastic, multi-stage process described by

$$X_{i+1} = \phi_{i+1,i}X_i + \Gamma_i w_i \ , \quad i = 0,1,\ldots,N-1 \tag{14-100}$$

where:

$$E\{X_o\} = \bar{X}_o \tag{14-101}$$

$$E\{w_i\} = \bar{w}_o \tag{14-102}$$

$$E\{(X_o - \bar{X}_o)(X_o - \bar{X}_o)^T\} = P_{o(-)} \tag{14-103}$$

$$E\{(w_i - \bar{w}_i)(w_j - \bar{w}_j)^T\} = Q_i\delta_{ij} \tag{14-104}$$

$$E\{(w_i - \bar{w}_i)(X_o - \bar{X}_o)^T\} = 0 \tag{14-105}$$

Measurements Y_i are made while the system is in stage i, and are linearly related to the state X_i by

$$Y_i = H_i X_i + v_i , \qquad i = 0,1,\ldots,N \tag{14-106}$$

where

$$E\{v_i\} = 0 \tag{14-107}$$

$$E\{v_i v_j^T\} = R_i \delta_{ij} \tag{14-108}$$

$$E\{(w_i - \bar{w}_i)v_j^T\} = 0 \text{ and } E\{(X_o - \bar{X}_o)v_i^T\} = 0 \tag{14-109}$$

From the derivations in the previous section, the weighted-least-squares or maximum-likelihood estimate of the state X_k, using only the measurements $Y_o, Y_1,\ldots,Y_k$, is given by the sequential use of the single-stage estimation procedure

$$\hat{X}_i = \bar{X}_i + K_i(Y_i - H_i\bar{X}_i) , \quad i = 0,1,\ldots,k, \text{ where } k \leq N \tag{14-110}$$

where

$$\bar{X}_{i+1} = \phi_{i+1,i}\hat{X}_i + \Gamma_i\bar{w}_i , \quad \bar{X}_o \text{ given} \tag{14-111}$$

$$K_i = P_{i(+)}H_i^T R_i^{-1} \tag{14-112}$$

$$P_{i(+)} = (P_{i(-)}^{-1} + H_i^T R_i^{-1} H_i)^{-1} =$$

$$P_{i(-)} - P_{i(-)}H_i^T(H_i P_{i(-)} H_i^T + R_i)^{-1} H_i P_{i(-)} \tag{14-113}$$

$$P_{i+1(-)} = \phi_{i+1,i} P_{i(+)} \phi_{i+1,i}^T + \Gamma_i Q_i \Gamma_i^T \tag{14-114}$$

Equations 14-110 through 14-114 constitute the Kalman filter (Kalman, 1960). The proportionality matrix K_i in Equation 14-112 is essentially the ratio between uncertainty in the state, $P_{i(+)}$, and the uncertainty in the measurements R_i; the matrix H_i is simply the state-to-measurement transformation matrix. K_i is called Kalman gain.

Remarks

1) The propagation of the covariance of the error of the estimate, Equations 14-113 and 14-114, is independent of the measurement Y_i.

Thus, the covariance matrix can be computed beforehand and stored if the parameters of the system and the observation equations are given.

2) The computation of the updated estimate, Equations 14-110 and 14-111, involve only the current measurement and error covariance. Thus, it can easily be carried out in real-time.

Optimal Predictions for Linear Multi-stage Processes

Given a linear, stochastic, multi-stage process described by Equation 14-100. The prediction of the system state beyond the stage where measurements are available, say stage m, can be done by repeated use of Equation 14-111, that is,

$$\hat{X}_{i+1} = \bar{X}_{i+1} = \phi_{i+1,i}\hat{X}_i + \Gamma_i \bar{w}_i \; ; \; i = m, m+1, \ldots . \qquad (14\text{-}115)$$

where $\hat{X}_m$ is obtained from the filter, Equations 14-110 through 14-114. In other words, the best prediction we can make uses the expected value of w_i, namely, $\bar{w}_i$, in the transition relations, Equation 14-100, starting, however, with the filtering estimate of $\hat{X}_m$.

Example 6 (Simons et al., 1978)

The dynamics of the streamflow and sediment discharge can be expressed by stochastic linear difference equations of multiple order. Based on the modeling concept suggested by Sinha and Sharma (1975) to deal with the interdependence of the state variables, the following models are used

i) Streamflow model

$$Q(t) = \sum_{i=1}^{p} a_i Q(t-i) + v_1(t) \qquad (14\text{-}116)$$

ii) Sediment discharge model

$$S(t) = \sum_{k=1}^{n} c_k Q(t-k) + \sum_{\ell=1}^{m} d_\ell S(t-\ell) + v_2(t) \qquad (14\text{-}117)$$

where $Q(t)$ and $S(t)$ are, respectively, the streamflow and sediment discharge at time t; a_i, $i = 1,\ldots,p$, c_k, $k = 1,\ldots,n$, d_ℓ, $\ell = 1,\ldots,m$ are the unknown parameters of the proposed models; $w_1(t)$ and $w_2(t)$ are the independent white Gaussian noise sequences which account for the modeling errors and are assumed to have the following statistics,

$$E\{v_j\} = 0 \; , \quad E\{(v_{jk} - \bar{v}_{jk})(v_{j\ell} - \bar{v}_{j\ell})^T\} = R_j \delta_{k\ell} ; \; j = 1,2. \qquad (14\text{-}118)$$

The structure of the above models is based on the fact that significant correlation exists between streamflow and sediment discharge, at least for a few days. Thus, the actual number of lags (i.e., days) to be included in the model can be determined by analyzing the autocorrelation and cross-correlation functions of the streamflow and sediment discharge time-series.

Using the following definitions

$$Y(t) \triangleq \begin{bmatrix} Q(t) \\ S(t) \end{bmatrix} \tag{14-119}$$

$$H(t) \triangleq \begin{bmatrix} Q(t-1)\ldots Q(t-p) & 0\ \ldots\ 0 & 0\ \ldots\ 0 \\ 0 & Q(t-1)\ldots Q(t-n) & S(t-1)\ldots S(t-m) \end{bmatrix} \tag{14-120}$$

$$X(t) \triangleq \begin{bmatrix} a_1 \ldots a_p & c_1 \ldots c_n & d_1 \ldots d_m \end{bmatrix}^T \tag{14-121}$$

and

$$v(t) \triangleq \begin{bmatrix} v_1(t) \\ v_2(t) \end{bmatrix} \tag{14-122}$$

model-equations 14-116 and 14-117 can then be combined in the state-space form

$$Y(t) = H(t)X(t) + v(t) \tag{14-123}$$

in which the covariance matrix R of the noise vector $v(t)$ has R_1 and R_2 as diagonal elements.

It remains to describe the way the states (i.e., the model coefficients) change. Since little is known about this, a priori, the simplest way to model the dynamics of the states is to express them by a "random walk" model

$$\theta_i(t) = \theta_i(t-1) + w_i \tag{14-124}$$

where $\theta_i(t)$ are the model coefficients and $w_i(t)$ are uncorrelated random Gaussian disturbances having constant means q_i and variances Q_i. The Q_i represents the square of the unknown average rates of change of the parameters θ_i.

Defining $\phi(t,t-1)$, the state-transition matrix, as a $(p+n+m)$ by $(p+n+m)$ unit matrix, the state equations 14-124 can be expressed as

$$X(t) = \phi(t,t-1)X(t-1) + w(t) \tag{14-125}$$

in which the covariance matrix Q of the noise vector $w(t)$ has Q_i as the diagonal elements. The following additional conditions are assumed to be satisfied.

$$E\{w_i - \bar{w}_i)v_j^T\} = 0 \tag{14-126}$$

$$E\{w_i - \bar{w}_i)(X_o - \bar{X}_o)^T\} = 0 \quad \text{and} \quad E\{(X_o - \bar{X}_o)v_i^T\} = 0 \tag{14-127}$$

The analysis problem associated with the system described by Equations 14-123 and 14-125 consists of:

i) estimating $X(t)$ when ϕ, H, R, Q, and Y are given, and

ii) predicting $Y(t)$ when ϕ, H, R, Q, and X are given.

The first task, also called model parameter identification, can be accomplished by the use of a Kalman filter, Equation 14-110 through Equation 14-114. The prediction of Y values when X values are known is based upon the Kalman predictor Equation 14-115.

Optimal Filtering for Continuous Linear Dynamic Systems with Continuous Measurements

The results of the previous section for multistage processes may be extended to continuous dynamic processes by formally letting the time between stages tend to zero. The difference Equation 14-100 becomes

$$\dot{X} = F(t)X + G(t)w(t) \tag{14-128}$$

where

$$F(t) = \lim_{\Delta t \to 0} \frac{\phi(t_i+\Delta t, t_i) - I}{\Delta t} \tag{14-129}$$

$$G(t) = \lim_{\Delta t \to 0} \frac{\Gamma(t_i)}{\Delta t} \tag{14-130}$$

If we let $R_i \Delta t \to R(t)$ (14-131)

and $Q_i \Delta t \to Q(t)$ as $\Delta t \to 0$, (14-132)

then we have $\hat{X}_i \to \bar{X}_i \to \hat{X}(t)$ (14-133)

$$P_{i(+)} \to P_{i(-)} \to P(t) \quad \text{as} \quad \Delta t \to 0 \tag{14-134}$$

and the following differential equations are obtained,

$$\dot{\hat{X}} = F\hat{X} + G\bar{w} + PH^T R^{-1}(Y - H\hat{X}), \quad \hat{X}(0) = 0 \tag{14-135}$$

$$\dot{P} = FP + PF^T + GQG^T - PH^T R^{-1} HP, \quad P(0) = P_o \tag{14-136}$$

The white-noise processes of the continuous system have the following statistics:

$$E\{[w(t) - \bar{w}(t)][w(t') - \bar{w}(t')]^T\} = Q(t)\delta(t-t') \tag{14-137}$$

$$E\{v(t)v^T(t')\} = R(t)\delta(t-t') \tag{14-138}$$

The approximation of the continuous Kalman-Bucy filter by a multistage filter when using a digital computer must be done with care, since R_i and Q_i in Equations 14-131 and 14-132 depend on the size of the time step Δt. More discussion on this subject can be found in Bryson and Ho (1969).

Correlated Process and Measurement Noises

Assume that the process and measurement noises are correlated, viz:

$$E\{w(t)v^T(\tau)\} = C(t)\delta(t-\tau) \tag{14-139}$$

One approach is to convert this problem to an equivalent problem with no correlation between process and measurement noises (Gelb, 1974). To do this, add zero to the right-side of Equation 14-128, in the form

$$\dot{X} = FX + Gw + D(Y - HX - v) \tag{14-140}$$

where $D = GCR^{-1}$. The filtering problem now under consideration is

$$\dot{X} = (F - DH)X + DY + Gw - Dv \tag{14-141}$$

$$Y = HX + v \tag{14-142}$$

where, in Equation 14-141, DY is treated as a known input and $(Gw - Dv)$ is treated as a process noise. By the choice of D specified above, $E\{(Gw - Dv)v^T\} = 0$, and thus the measurement and process noises in this equivalent problem are indeed uncorrelated.

14.5 KALMAN FILTERING FOR NONLINEAR DYNAMIC PROCESSES

Most of the dynamic systems and measurement systems encountered in practice are nonlinear. The Kalman filter developed in the previous section for linear systems may be applied to nonlinear systems with

additive white noise by linearizing about a nominal path or by continually (or occasionally) updating a linearization around the current estimates, starting with an initial guess. The three most common approximations are listed in Tables 14.1, 14.2, and 14.3, for the linearized Kalman filter, the extended Kalman filter, and the iterated extended Kalman filter. They are listed in terms of increasing computational loading and, probably, in increasing accuracy for any particular problem.

The linearized Kalman filter has the advantage that the measurement gains are independent of the state and can be computed a priori based on a nominal solution with the disadvantage that as time evolves the estimate may be quite removed from the nominal and nonlinearities become very important. The extended Kalman filter is linearized around the most recent estimate in an attempt to keep the estimate close to the actual state; here the gains must be calculated in real time. The iterated extended Kalman filter is an attempt to reduce the effect of measurement nonlinearities by iterating on the estimate at each measurement until there is little change in the estimate. An additional approach, the iterated extended Kalman filter/smoother discussed by Jazwinski (1970) is available for iteration between measurements to reduce the effect of system nonlinearities.

Table 14.1 Linearized Kalman filter algorithm.

System model:	$\dot{X} = f(X,t) + G(t)w(t)$	(1)
Observations:	$Y(t) = h(X) + v(t)$	(2)
Initial conditions:	$E\{X(0)\} = \hat{X}(0)$ $\text{Cov}[X(0) - \hat{X}(0)] = P(0)$ Nominal trajectory $\bar{X}(t)$ known	
Estimator between observations:	$\dot{\hat{X}} = f(\bar{X},t) + F(t)[\hat{X}(t) - \bar{X}(t)]$	(3)
	$\dot{P} = F(t)P + PF(t)^T + G(t)Q(t)G(t)^T$	(4)
where:	$F(t) = \left.\frac{\partial f}{\partial X}\right\|_{X = \bar{X}(t)}$	(5)
At an observation:	$\hat{X}(t)^+ = \hat{X}(t)^- + K(t)\{Y(t) - h(\bar{X}) - H(t)[\hat{X}(t)^- - \bar{X}(t)]\}$	(6)
	$K(t) = P(t)^-H(t)^T[H(t)P(t)^-H(t)^T + R(t)]^{-1}$	(7)
	$P(t)^+ = [I - K(t)H(t)]P(t)^-$	(8)
where:	$H(t) = \left.\frac{\partial h}{\partial X}\right\|_{X = \bar{X}(t)}$	(9)

Table 14.2 Extended Kalman filter algorithm.

System model:	$\dot{X} = f(X,t) + G(t)w(t)$	(1)
Observations:	$Y(t) = h(X) + v(t)$	(2)
Initial conditions:	$E\{X(0)\} = \hat{X}(0)$ $Cov[X(0) - \hat{X}(0)] = P(0)$	
Estimator between observations:	$\dot{\hat{X}} = f(\hat{X},t)$	(3)
	$\dot{P} = F(t)P + PF(t)^T + G(t)Q(t)G(t)^T$	(4)
where:	$F(t) = \left.\frac{\partial f}{\partial X}\right\vert X = \hat{X}(t)$	(5)
At an observation:	$\hat{X}(t)^+ = \hat{X}(t)^- + K(t)[Y(t) - h(\hat{X}(t)^-)]$	(6)
	$K(t) = P(t)^-H(t)^T[H(t)P(t)^-H(t)^T + R(t)]^{-1}$	(7)
	$P(t)^+ = [I - K(t)H(t)]P(t)^-$	(8)
where:	$H(t) = \left.\frac{\partial h}{\partial X}\right\vert X = \hat{X}(t)^-$	(9)

Table 14.3 Iterated extended Kalman filter algorithm.

System model:	Table 14.2, Equation 1
Observations:	Table 14.2, Equation 2
Initial conditions:	Table 14.2
Estimator between observations:	Table 14.2, Equation 3, Table 14.2, Equation 4, and Table 14.2, Equation 5
At an observation:	$\hat{X}(t)^{+}_{i+1} = \hat{X}(t)^{-} + K(t)_i\{Y(t) - h(\hat{X}(t)^{+}_{i}) - H(t)_i[\hat{X}(t)^{-} - \hat{X}(t)^{+}_{i}]\}$ (1)*
	$K(t)_i = P(t)^{+}_{i}H(t)^{T}_{i}\{H(t)_i P(t)^{+}_{i}H(t)^{T}_{i} + R(t)\}^{-1}$ (2)*
	$P(t)^{+}_{i+1} = [I - K(t)_i H(t)_i]P(t)^{+}_{i}$ (3)*
	$H(t)_i = \frac{\partial f}{\partial X}\Big\vert X = \hat{X}(t)^{+}_{i}$ (4)*
where:	$P(t)^{+}_{0} = P(t)^{-}$ (5)*
	$\hat{X}(t)^{+}_{0} = \hat{X}(t)^{-}$. (6)*

*Table 14.3, Equations 1 through 6 are iterated until little change is observed in the estimate.

Example 7 (Duong et al., 1979)

A catchment can be modeled as a cascade of storage reservoirs as illustrated in Figure 14.4. Two zones, aeration zone and saturation zone, are defined below the soil surface. Each zone is thought of as storing moisture in various storage reservoirs. Moisture movement from one reservoir to the other depends on the value of threshold element, the surrounding hydraulic conductivity, and the water deficiency rate of the storage.

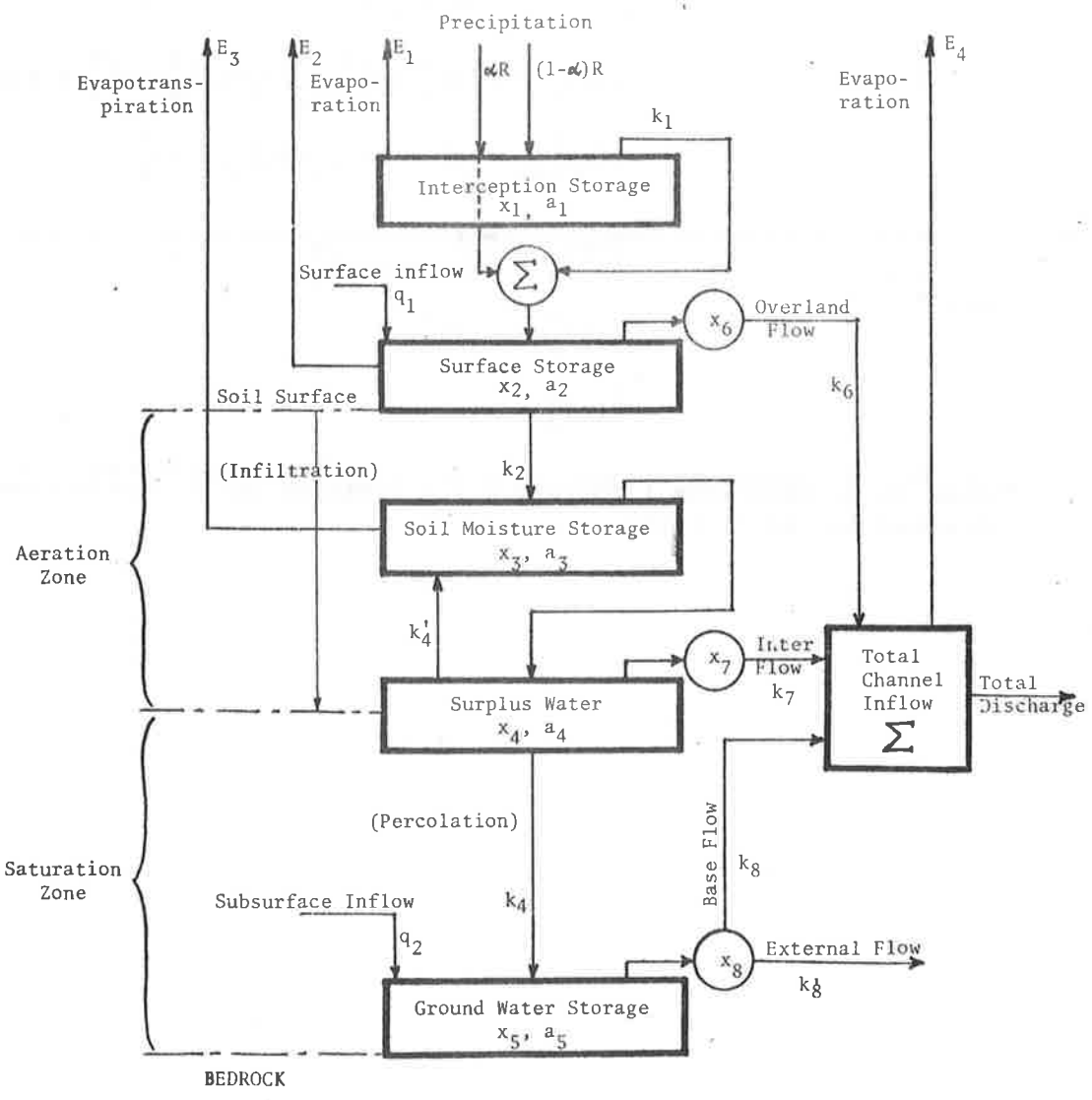

Figure 14.4 Schematic diagram of the proposed catchment model.

The vegetation canopy is considered as an interception storage. It receives a fraction of rainfall, $(1 - \alpha)R$, from the sky. The rest of the rainfall, αR, falls directly to the ground. A part of the water received by the canopy is lost through evaporation, E_1, and whenever the amount of stored water, x_1, reaches a threshold value a_1 (i.e., when the retaining capacity of the storage is full), the input water flows down directly to the soil surface. The change in the amount of water intercepted by the vegetation canopy over time can then be described by the following equation,

$$\frac{dx_1}{dt} = [(1 - \alpha)R - E_1][1 - k_1\eta(x_1 - a_1)] \tag{14-143}$$

where $\eta(\cdot)$ denotes a unit step function, and k_1 is a coefficient representing the flow of water from the canopy to the soil surface. Water on the soil surface comes from throughfall and surface inflow q_1. This amount of water is stored temporarily in the surface storage reservoir. A part of it will become overland flow if the retaining water x_2 is greater than a certain threshold value a_2, representing the maximum capacity of the storage. Another part of the surface water is lost through evaporation E_2, and the rest of it infiltrates to the soil moisture storage in the aeration zone. The infiltration process is assumed to progress proportionally to the amount of water available (x_2) on the soil surface and the water deficiency rate of the soil moisture storage. The following equation can then be used to describe the rate of change of the water content in the surface storage over time:

$$\frac{dx_2}{dt} = \{\alpha R + k_1[(1-\alpha)R - E_1]\eta(x_1-a_1) + q_1 - E_2 - k_2(1 + \frac{a_3-x_3}{a_3})x_2\} \cdot [1 - \eta(x_2-a_2)] \tag{14-144}$$

where k_2 is a coefficient representing the soil characteristics in the aeration zone, and the term

$$k_2(1 + \frac{a_3-x_3}{a_3})x_2 \tag{14-145}$$

represents the infiltration rate.

A part of soil moisture storage will be lost through evapotranspiration E_3. Soil moisture deficit can be replenished through capillary suction of free water in the lower soil layer. This feedback process is assumed to be proportional to the soil moisture deficiency rate $(a_3-x_3)/a_3$ and the amount of free water, x_4, available in the lower soil layer. If soil moisture storage x_3 attains the maximum storage capacity a_3, then added infiltrated water becomes free water which will be stored in a surplus water storage. The variation of soil moisture storage over time can be described by the following equation:

$$\frac{dx_3}{dt} = \{k_2(1 + \frac{a_3-x_3}{a_3})x_2 - E_3 + k_4'(\frac{a_3-x_3}{a_3})x_4\}[1 - \eta(x_3 - a_3)] \quad (14\text{-}146)$$

where k_4' is a coefficient representing the soil characteristics between the root zone and the lower soil layer, and the terms

$$k_4'(\frac{a_3-x_3}{a_3})x_4 \quad (14\text{-}147)$$

represent the capillary suction rate.

Surplus water starts to percolate through various lower soil layers to reach the groundwater storage. The percolation rate is again assumed to be proportional to the amount of free water, x_4, available and the water deficiency rate of the groundwater storage. If the amount of free water in storage reaches the maximum surplus water storage capacity, then added free water input will become interflow. The following equation is used to describe the variation of the amount of free water in storage over time,

$$\frac{dx_4}{dt} = \{[k_2(1 + \frac{a_3-x_3}{a_3})x_2 - E_3 + k_4'(\frac{a_3-x_3}{a_3})x_4]\eta(x_3 - a_3) - k_4'(\frac{a_3-x_3}{a_3})x_4 - k_4(1 + \frac{a_5-x_5}{a_5})x_4\}[1 - \eta(x_4 - a_4)] \quad (14\text{-}148)$$

where k_4 is a coefficient representing the soil characteristics in the saturation zone, and the term

$$k_4(1 + \frac{a_5 - x_5}{a_5})x_4 \tag{14-149}$$

represents the percolation rate of free water.

The groundwater in storage can be replenished by percolated water from upper soil layers and/or by subsurface inflow q_2. When the groundwater content x_5 reaches the maximum groundwater storage capacity a_5, added groundwater will become base flow. A part of this amount of water will be lost as external flow.

All the flows in this model are assumed to follow a certain law of recession, therefore the overland flow, interflow, and base flow can be described by the following dynamic equations, respectively, taking account of the free water available for each type of flow.

$$\frac{dx_6}{dt} = \{\alpha R + k_1[(1 - \alpha)R - E_1]\eta(x_1 - a_1) + q_1 - E_2$$

$$-k_2(1 + \frac{a_3 - x_3}{a_3})x_2\}\eta(x_2 - a_2) - k_6x_6 \tag{14-150}$$

$$\frac{dx_7}{dt} = \{[k_2(1 + \frac{a_3 - x_3}{a_3})x_2 - E_3 + k_4'(\frac{a_3 - x_3}{a_3})x_4]\eta(x_3 - a_3) - k_4'(\frac{a_3 - x_3}{a_3})x_4$$

$$- k_4(1 + \frac{a_5 - x_5}{a_5})x_4\}\eta(x_4 - a_4) - k_7x_7 \tag{14-151}$$

$$\frac{dx_8}{dt} = [k_4(1 + \frac{a_5 - x_5}{a_5})x_4 + q_2]\eta(x_5 - a_5) - k_8x_8 - k_8'x_8 \tag{14-152}$$

where x_6, x_7, and x_8 are the amount of water available for overland flow, interflow, and base flow, respectively; k_6, k_7, k_8, and k_8' are flow coefficients.

The total channel inflow, Q, will be the sum of the flow components described above, minus the amount of water lost through evaporation E_4. Thus,

$$Q = k_6x_6 + k_7x_7 + k_8x_8 - E_4 \tag{14-153}$$

E_1, E_2, and E_3 are assumed to be proportional to the water content in the corresponding storage, while E_4 is proportional to the surface area of the exposed water body. Equations 14-143 through 14-152 can be readily put into state-space form, whereas the model observation equation is given by Equation 14-153.

Example 8 (Muzik, 1975)

The unsteady flow due to rainfall over an impermeable uniformly sloping plane can be modeled as n elements in series (Figure 14.5). The elements are, for simplicity, of a unit width and of a length Δx. The state variables are chosen to be the average depths of flow, $y,\ldots,y_n$, within the elements. The output variables are the discharge rates from the elements, $q_1,\ldots,q_n$, and the input variables are the combined rates of precipitation over the elements $p_1,\ldots,p_n$, and the discharge rates from the immediately upstream elements.

For laminar flow

$$q = \frac{8gS_f y^3}{K\nu} \tag{14-154}$$

and for turbulent flow,

$$q = \frac{1.49}{n} y^{5/3} S_f^{1/2} \tag{14-155}$$

where g is the acceleration of gravity, S_f is the total energy line gradient, ν is the kinematic viscosity, n is the Manning's coefficient of roughness, and K is the laminar flow resistance parameter depending on the raindrop impact effect and the type of surface. For flow without rain and a smooth surface, $K = 24$.

Assuming a gradually varied flow and sufficiently short distance increment Δx, S_f can be approximated as

$$S_f = S_o + \frac{y_1 - y_2}{\Delta x} \tag{14-156}$$

where S_o is the slope of the runoff plane.

The state equations are the equations of continuity written for the n elements of the model. For example, the state equation of the 3rd element in Figure 14.5 is

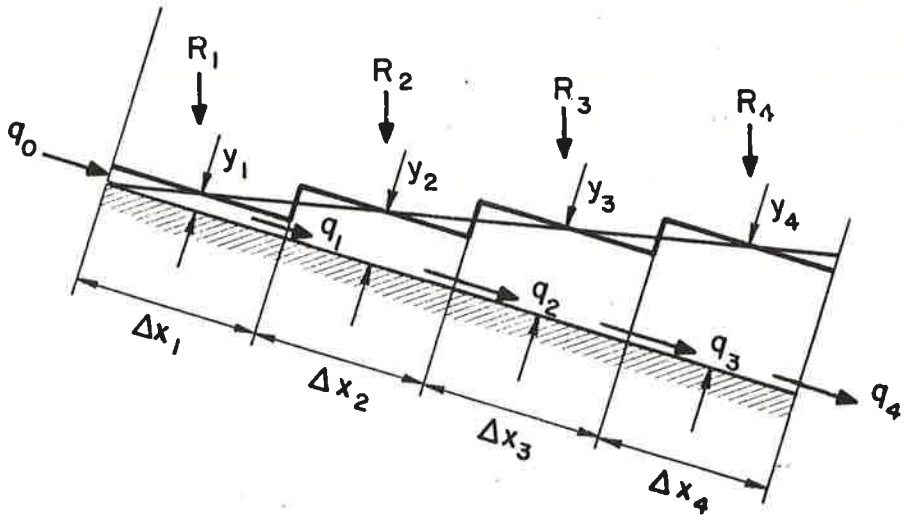

Figure 14.5 Simulation of unsteady flow by a series of interacting elements.

$$\dot{y}_3 = \frac{dy_3}{dt} = \frac{1}{\Delta x_3}\left[R_3 - (q_3 - q_2)\right] \tag{14-157}$$

The observation equations of the model may be written in a general form as:

$$q = \alpha y^m \tag{14-158}$$

Substitution for q_i in Equation 14-153, using Equation 14-154, gives

$$\dot{y}_3 = \frac{1}{\Delta x_3}(R_3 + \alpha y_2^m - \alpha y_3^m) \tag{14-159}$$

which is in the form of

$$\dot{y} = f(y,R,t) \tag{14-160}$$

14.6 CONCLUSIONS

Detailed analysis of watershed and river systems can be obtained through simulation with a complex physical process mathematical model. To increase the usefulness of this type of model when applied to the management and control of water resources systems, where uncertainty and adaptivity must be taken into account, a marriage between this type of modeling concept and systems engineering techniques is desirable.

The new stochastic conceptual hydrologic model retains all the advantages of the complex physical process mathematical model. In addition, it can handle uncertainty in the model and in the data. It is also easy to calibrate, and adaptable to changing environmental conditions. When formulated using state-space concept, model calibration and output prediction can be done on-line by a Kalman filter.

14.7 REFERENCES

Bras, R. L. and Rodriguez-Iturbe, L. 1975. Rainfall-Runoff as Spatial Stochastic Processes: Data Collection and Synthesis. Ralph M. Parsons Laboratory for Water Resources and Hydrodynamics, Department of Civil Engineering, MIT, TR#196.

Bryson, A. E., Jr., and Ho, Y. C. 1969. Applied Optimal Control. Blaisdell Publishing Co., Waltham, Massachusetts.

Dawdy, D. R. 1969. Mathematic Modeling in Hydrology. The Progress of Hydrology, in Proc. 1st Int. Seminar for Hydrology Professors.

Duong, N., Johnson, G. R., and Winn, C. B. 1973. An Application of Modern Control Concepts to Hydrology. Proc. of the Int. Conference on Systems and Control, Coimbatore, India.

Duong, N., Li, R. M., and Simons, D. B. 1979. A State-Variable Approach to Watershed Modeling and Control. Proc. of the XVIIIth Int. Congress of the IAHR, Italy.

Fallside, F., and Perry, F. P. 1975. On-Line Prediction of Consumption for Water Supply Network Control. Preprints, IFAC 6th Triennial World Congress, Boston, Massachusetts.

Gelb, A. (ed). 1974. Applied Optimal Estimation. MIT Press, Cambridge, Massachusetts.

Hino, M. 1973. On-Line Prediction of Hydrologic Systems. Proc., XVth Conference IAHR, Istanbul, Turkey.

Jazwinski, A. H. 1970. Stochastic Processes and Filtering Theory. Academic Press, New York.

Kalman, R. E. 1960. A New Approach to Linear Filtering and Prediction Problems. Journal of Basic Engineering, Trans. ASME, Vol. 82, No. 2, pp. 35-45.

Kitanidis, P. K., and Bras, R. L. 1978. Real-Time Forecasting of River Flows. Ralph M. Parsons Laboratory for Water Resources and Hydrodynamics, Department of Civil Engineering, MIT, TR#235.

Kontur, I. 1975. Some Stochastic Runoff Models. Proc. 2nd IWRA World Congress, V. 61-71, New Delhi, India.

Kulandaiswamy, V. C. 1964. A Basic Study of the Rainfall Excess Surface Runoff Relationship in a Basin System. Ph.D. Dissertation, University of Illinois, Urbana.

Lee, R. C. K. 1964. Optimal Estimation, Identification, and Control. Research Monograph No. 28, MIT Press, Cambridge, Massachusetts.

Moore, R., and Weiss, G. 1976. Real-Time Parameter Estimation of a Non-linear Catchment Model using Extended Kalman Filters. Presented at the Workshop on Recent Developments in Real-Time Forecasting/ Control of Water Resource Systems, IIASA, Laxenburg, Austria.

Nash, J. E. 1960. A Unit Hydrograph Study with Particular Reference to British Catchments. Inst. Civ. Eng. Proc., 17, 249-282.

Prasad, R. 1967. A Nonlinear Hydrologic System Response Model. Proc., ASCE J. Hyd. Div., 93, HY4, 201-221.

Simons, D. B., Duong, N., and Li, R. M. 1978. An Approach to Short-term Water and Sediment Discharge Prediction using Kalman Filter. Proc. AGU Chapman Conf. on Application of Kalman Filter to Hydrology, Hydraulics, and Water Resources, Pittsburgh, (Ed: Chao-Lin Chiu).

Szöllösi-Nagy, A., Todini, E., and Wood, E. F. 1976. A State-space Model for Real-Time Forecasting of Hydrological Time-Series. Journal of Hydrological Sciences.

Szöllösi-Nagy, A. 1978. Introductory Remarks on the State-space Modeling of Water Resource Systems, Research Memorandum RM-78-73.

Todini, E., and Bouillot, D. 1975. A Rainfall-Runoff Kalman Filter Model. System Simulation in Water Resources (ed. G. C. Vansteenkiste), North-Holland Publishing Co., Amsterdam.

Yevjevich, V. 1974. Determinism and Stochasticity in Hydrology. J. Hydrology, 22, 252-238.

CHAPTER 15

HANDHELD CALCULATOR PROGRAMS FOR ANALYSIS

by

Kenneth G. Eggert, Research Associate, Department of Civil Engineering, Colorado State University, Fort Collins, Colorado
Ruh-Ming Li, Associate Professor, Department of Civil Engineering, Colorado State University, Fort Collins, Colorado
Daryl B. Simons, Associate Dean of Engineering Research and Professor of Civil Engineering, Colorado State University, Fort Collins, Colorado

15.1 INTRODUCTION

This chapter presents several hand-held programmable calculator programs for watershed and river analysis. The program presented implement theory discussed previously in Chapters 4, 5, 6, 7, 10 and 12. Of course, many of the complex formulations presented in those chapters are inappropriate for use with these calculators. However, as will be shown in this section and the case study sections to follow, a wide range of engineering and prefeasibility studies may be addressed using the material presented in this chapter. The intent of this chapter is to provide a group of calculator programs that may be incorporated into an integrated approach analysis.

The programs provided are grouped into the following three packages: 1) a hydrology package; 2) a hydraulics package; and 3) a sedimentation package. The packages include the following programs:

A. Hydrology Package
   1. Rainfall hyetograph generation
   2. Green-Ampt infiltration
   3. Overland flow and finger-tip channel flow routing
   4. Overland flow routing parameter estimation
   5. Lognormal flood volume frequency analysis
   6. Gumbel flood peak frequency analysis

B. Hydraulics Package
   1. Normal depth calculation for trapezoidal channels
   2. Natural channel cross section properties
      a. Wetted perimeter--area relationship
      b. Area--depth relationship
      c. Area--top width relationship
   3. Normal depth in natural channels
   4. Backwater curve computation for natural channels
   5. Conversion of flow resistance parameters
   6. Muskingam-Cunge flood routing
   7. Super-elevation in bends

C. Sedimentation Package
   1. Particle size distribution
   2. Fall velocity
   3. Effective shear stress

4. Critical shear stress for Shields diagram
5. Sediment transport
   a. Lu's equation
   b. Meyer-Peter, Müller and suspended sediment
   c. C. T. Yang's equation
   d. H. Shen and C. Hung's equation
6. Aggradation-degradation analysis
7. Local scour
8. Riprap design

These programs individually may be used to facilitate many tedious calculations; however, when they are used in an integral analysis procedure, very complex problems may be solved.

The programs are written for two hand-held programmable calculators; the Texas Instrument TI-59 and Hewlett-Packard HP 97/67. These machines were selected both as the currently most powerful calculators available from two major manufacturers, and as examples of the two major program formats, i.e., algebraic entry and reverse Polish notation. Since the emphasis of this course is the analysis of watershed and river systems, no attempt has been made to provide either an encyclopedia of related programs or to break the provided programs down for use with calculators of lower capability. However, a user familiar with either of these program formats should be able to subdivide the provided programs into useful subunits. For additional programs in hydrology in hydraulics the reader is referred to Croley (1977).

The program description consists of a short description of the method implemented followed by a short example problem to verify the program entry. In addition to the short examples, two comprehensive examples are provided at the end of the chapter to illustrate the integrated analysis procedure. Examples of problems that may also be addressed with these programs will appear in Chapters 16 through 19.

15.2 PROGRAM DESCRIPTIONS AND EXAMPLES

This section presents a short description of each small calculator program. Due to differences in the calculators the user instructions are supplied separately for the Hewlett-Packard and Texas Instrument machines. The program listings and user instructions are provided in the separate volume, Small Calculator Programs for Analysis of Watersheds and River Systems.

Hydrology Package

The hydrology package includes programs for calculating hydrologic response from overland flow units. In addition, two programs for frequency analysis of flow data are provided. Rainfall hyetographs are estimated by an approach recommended by the Bureau of Reclamation or if there is sufficient data a rainfall pattern index method. An infiltration method that implements a time explicit formulation of the Green-Ampt infiltration equation is used to calculate the excess rainfall available for runoff. Overland flow runoff is routed using a method of characteristics solution for the kinematic wave approximation. An additional program is provided for estimating overland flow resistance as a function of ground cover density and also allows the calculation of overland flow depth for a known discharge per unit width. The two flood frequency programs allow the user to fit a Gumbel distribution to flood peak discharges and a lognormal distribution to flood volumes. These programs then provide for the calculation of return period corresponding to a given peak discharge or volume, or peak discharge or volume corresponding to a given return period.

Rainfall Hyetograph Generation Based upon Bureau of Reclamation Approach. The first method of rainfall hyetograph generation is that suggested by the U.S. Bureau of Reclamation (1974). This method divides the country into zones for which typical normalized six hour cumulative rainfall functions are presented. For the United States west of the 105^{0} meridian probable maximum 6-hour rainfall volumes may be read from a map such as Figure 15.1 from U.S. Bureau of Reclamation (1974). Since these rainfall volumes represent point maximums, they must be averaged out over the area of the watershed under consideration. This averaging may be accomplished by use of a plot such as Figure 15.2 from the same source. Finally, the corrected volume may be distributed over time to produce a representative hyetograph in the appropriate zone by the use of Figure 15.3 (USBR, 1974). Figures 15.2 and 15.3 have been programmed to facilitate the generation of these hyetographs.

The procedure is to find the appropriate rainfall point volume from Figure 15.1. Then that volume is scaled using Figure 15.2. The hyetograph is generated by computing the intensity every 30 minutes from the curves of Figure 15.3.

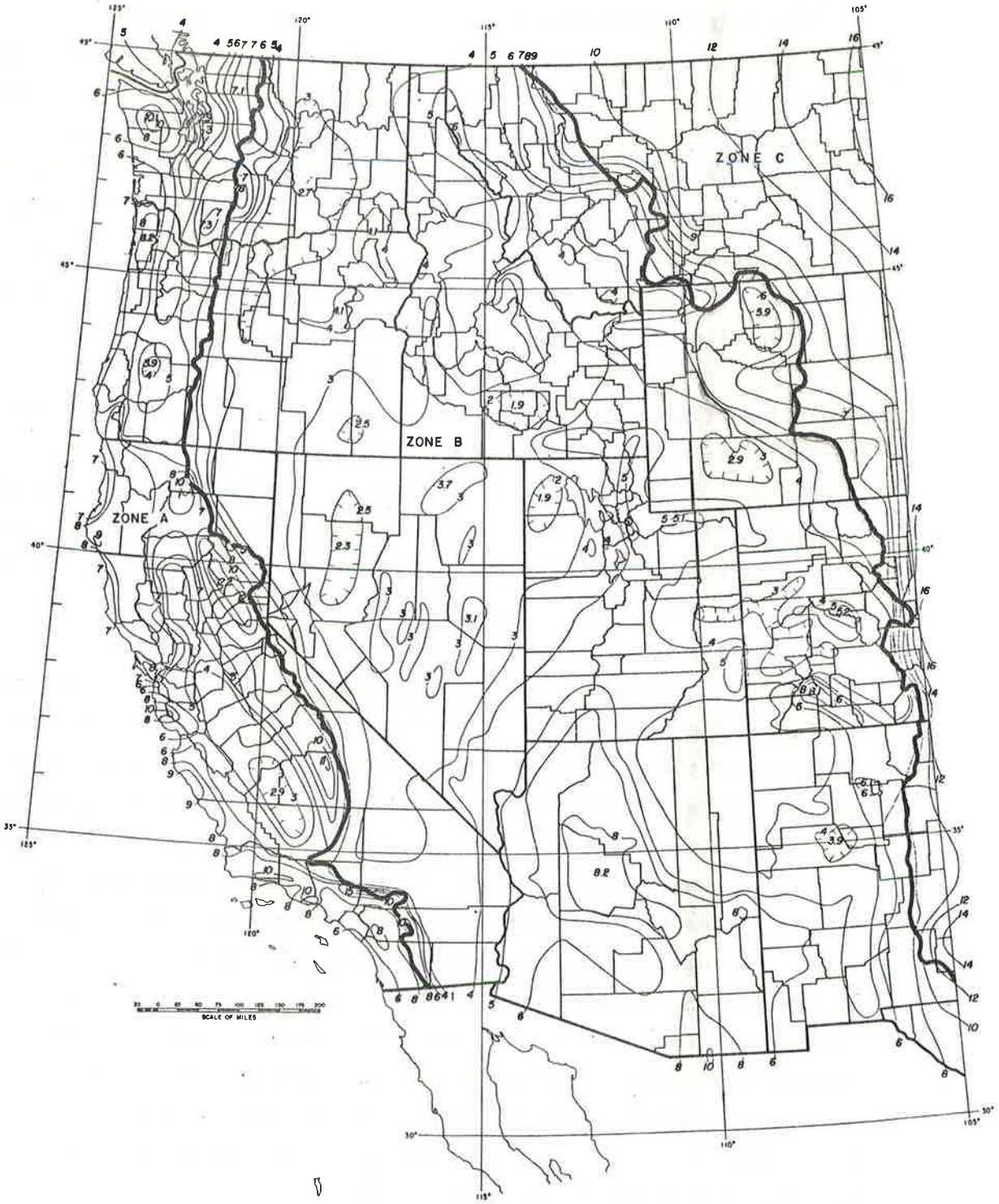

Figure 15.1 Probable maximum 6-hour point values in inches for general-type storms west of the 105° meridian (after USBR, 1974).

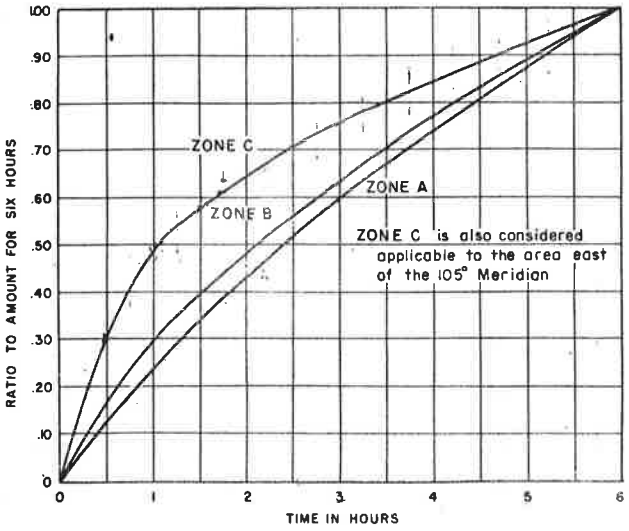

Figure 15.2 Distribution of 6-hour rainfall for area west of 105° meridian. See Figure 15.1 for area included within each zone (after USBR, 1974).

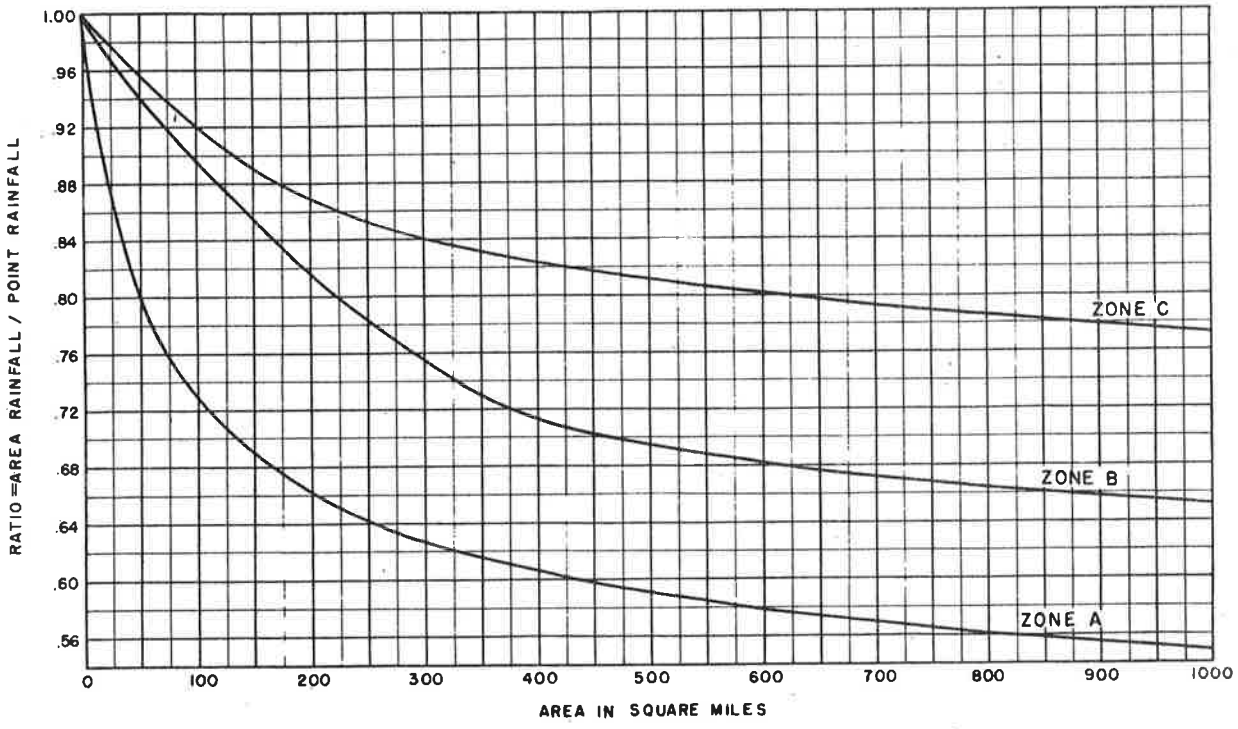

Figure 15.3 General storm: conversion ratio from 6-hour point rainfall to 6-hour area rainfall for area west of 105° meridian (after USBR, 1974).

Example: Bureau of Reclamation Hyetograph Synthesis

This example illustrates the use of two programs. The first program finds the reduction factor to be applied to the point rainfall volume to account for the size of the watershed.

Input: Zone C

Area = 100 mi^2

Output:

100.000

0.920

The reduction factor is .920 (for HP-97)

The second program distributes the volume of rainfall over a given time period. The factors used are based on a 6 hour storm so the program may not be applicable for all time periods.

Input: Zone C

Volume = 2.5 inches

Duration = 6 hours

Δt = 30 minutes

Reduction factor (r) = .920

Output hyetograph in minutes and inches/min:

2.3000+00

0.	300.0
0.0000+00	3.067-03
30.0	330.0
2.300-02	3.067-03
60.0	360.0
1.380-02	2.300-03
90.0	
6.900-03	
120.0	
5.367-03	
150.0	
5.367-03	
180.0	
3.833-03	
210.0	
3.833-03	
240.0	
3.067-03	
270.0	
3.067-03	

The output from the TI-59 is slightly different. From the point volume to area volume program, the scaled volume is printed.

2.5
100.

2.3

The rainfall hyetograph is output with intensities in inches/hour. Therefore the earlier storm has the following output.

1.38	0.23
30.	210.
0.828	0.184
60.	240.
0.414	0.184
90.	270.
0.322	0.184
120.	300.
0.322	0.184
150.	330.
0.23	0.138
180.	360.

Hyetograph Generation Based upon Pattern Index (T. J. Ward, 1979). Rainfall events may be described by the temporal variation of intensities during the rainfall duration. One method of describing such events is by using a dimensionless parameter called the pattern index. Pattern index is defined as

$$PI = \sum (p_i t_i) \qquad (15\text{-}1)$$

where PI = pattern index with a value ranging from 0 to 1

p_i = decimal equivalent of accumulated rainfall for period i of the event

t_i = decimal equivalent of accumulated time.

Conceptually, pattern index is the area under the curve of dimensionless accumulated time versus dimensionless accumulated rainfall amount (Figure 15.4).

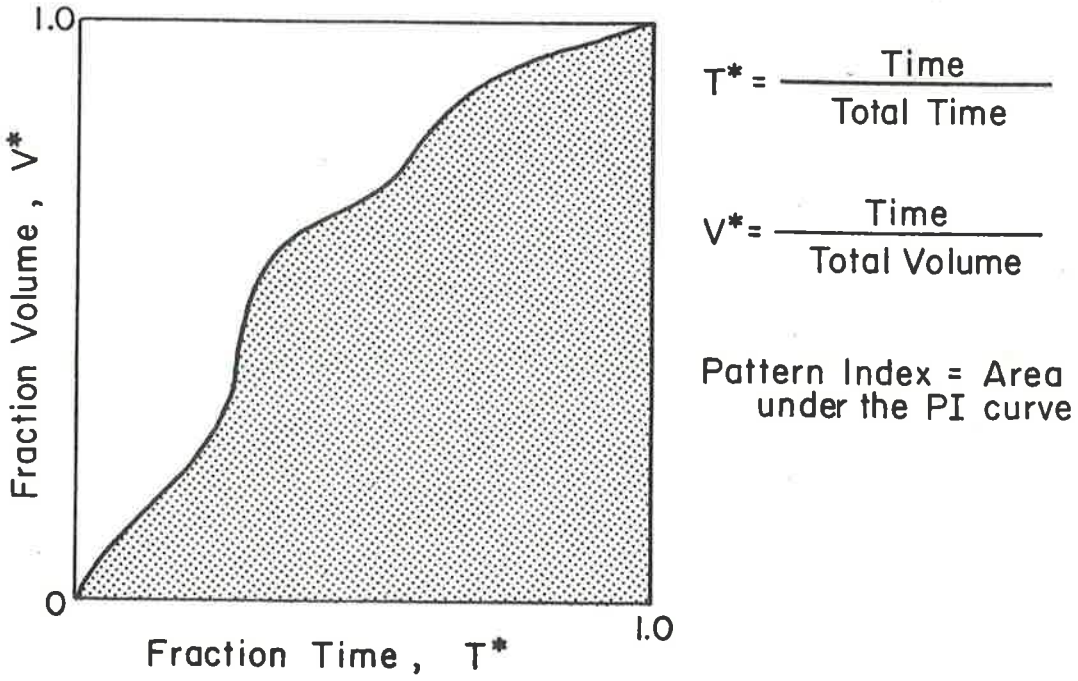

Figure 15.4 Pattern index.

Rainfall events may be quantitized by using pattern index as a numerical descriptor of the events. Three basic pattern types occur based upon pattern index. They are:

1) Delayed patterns: Events where a major portion of the total precipitation accumulation occurs during the latter half of the rainfall duration. Area under the curve ranges from greater than 0 to about 0.3 (Figure 15.5a).

2) Intermediate patterns: Events where temporal distribution of rainfall is relatively even throughout the duration. Area under the curve ranges from 0.3 to 0.7 (Figure 15.5b).

3) Advanced patterns: Events where a major portion of the total precipitation accumulation occurs during the first half of the rainfall duration. Area under the curve ranges from 0.7 to 1.0 (Figure 15.5c).

Two additional pattern types are possible which have pattern indices around 0.5. In these events a majority of the rainfall occurs during the middle of the duration or at both the beginning and end of the duration. These patterns are:

1) Advanced-delayed patterns: Events where a major portion of the rainfall falls within the first and last twenty-five percent of the duration. Area under the curve is about 0.5 (Figure 15.5d).

2) Delayed-advanced patterns: Events where a major portion of the rainfall occurs within the middle fifty percent of the duration. Area under the curve is about 0.5 (Figure 15.5e).

With the above rainfall patterns a number of storm events may be described by using either the pattern index or the amount of rainfall accumulation occurring within two twenty-five percent duration periods.

The pattern curves for advanced, intermediate, and delayed events may be approximated by the following equation:

$$V^* = T^{*b} \tag{15-2}$$

where

$$b = \frac{1}{PI} - 1.0 \tag{15-3}$$

Advanced-delayed and delayed-advanced curves are approximated by tangent and arctangent functions, respectively. The pattern index of these curves will always be 0.5 by definition, and therefore the pattern curves will be symmetical about the point $(T^*, V^*) = (.5, .5)$. The

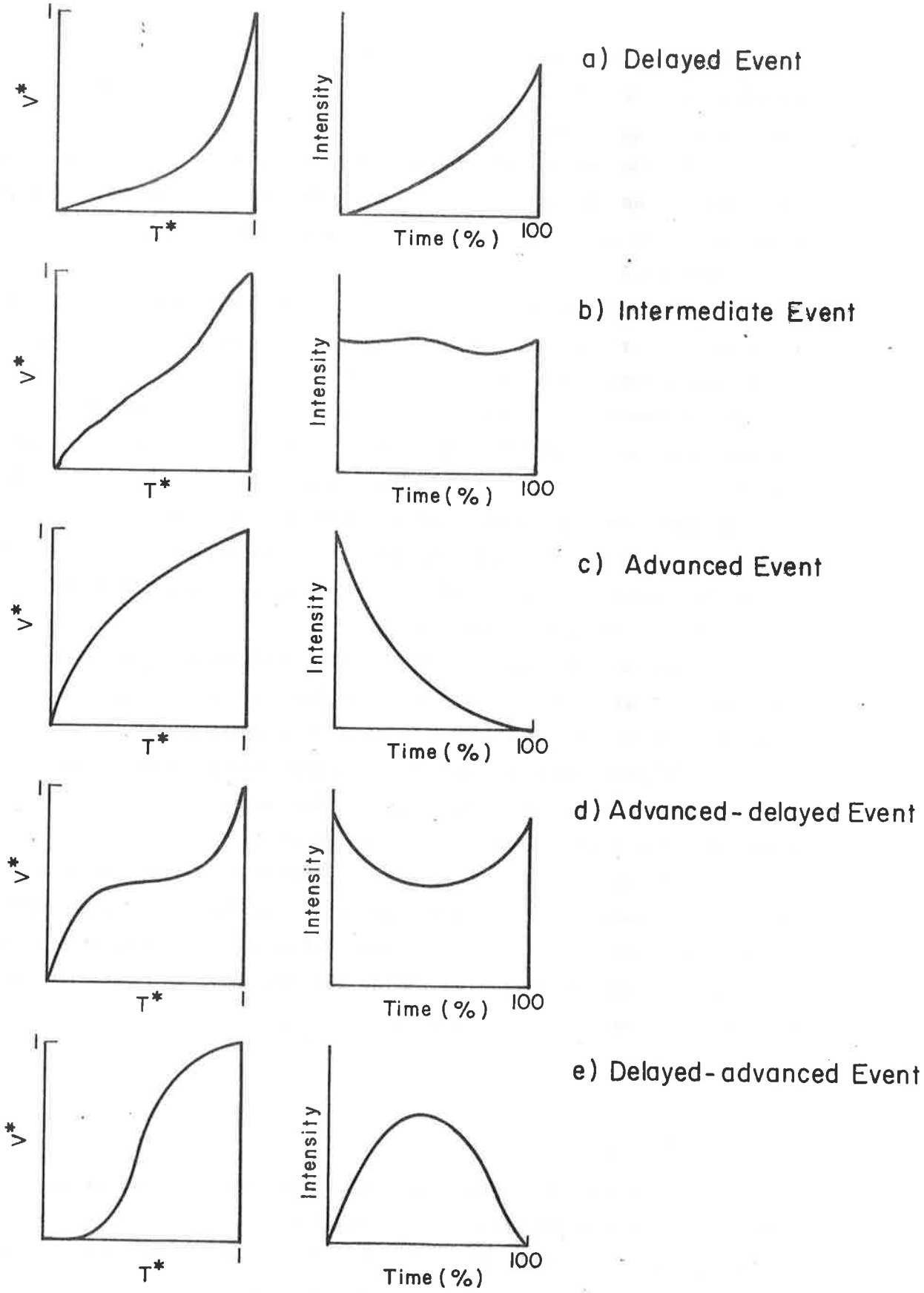

Figure 15.5 Rainfall event types.

pattern curves for advanced-delayed events are approximated by:

$$V^* = a_1 \text{Tan}[c_1(T^* - 0.5)] + 0.5 \qquad (15\text{-}4)$$

where a_1 and c_1 are variables. Likewise, pattern curves for delayed-advanced events are approximated by:

$$V^* = a_2 \text{Arctan}[c_2(T^* - o.5)] + 0.5 \qquad (15\text{-}5)$$

where a_2 and c_2 are variables.

By using Equations 15-2, 15-4 and 15-5, it is possible to create a calculator program which will generate rainfall events based upon pattern index. Two programs were developed for two separate groups of patterns. The first program is for the pattern curves for advanced, intermediate, and delayed events and the second program is for the advanced-delayed and delayed-advanced curves.

Example

Delayed Storm

Volume	1.2 inches
Time	50 minutes
Percent rain in first half of storm	15 percent
Number of Δt's in hyetograph	5

Hyetograph

Time (minutes)	Intensity (in./min)
10	0.09
20	0.50
30	1.19
40	2.13
50	3.29

Green-Ampt Infiltration: A time explicit formulation of the Green-Ampt equation is discussed in Chapter 7. These programs implement the homogeneous soil version for time varying rainfall as represented by a hyetograph. The principal equation used is Equation 7-11 for the change in infiltrated volume ΔF during time step t to $t + \Delta t$.

$$\Delta F = -\frac{(2F - K\Delta t)}{2} + \frac{[(2F - K\Delta t)^2 + 8K\Delta t(\delta + F)]^{1/2}}{2} \qquad (15\text{-}6)$$

vol of water

where F is the infiltrated volume, K is the hydraulic conductivity of the soil in the wetted zone, t is the time, δ is the potential head parameter and defines $\delta = (\theta_w - \theta_i)\psi_{ave}$, θ_w is the antecedent moisture content and ψ_{ave} is the average suction head across the wetting front. An average potential infiltration rate $\overline{f}$ for this time step is calculated by Equation 7-12.

$$\overline{f} = \frac{\Delta F}{\Delta t} \tag{15-7}$$

and compared to the current rainfall rate as entered by the user.

Based on the outcome of the comparison, the infiltrated volume is updated for the next time step by the potential calculated value if the rainfall rate r is greater than the average potential infiltration rate or by

$$\Delta F = r\Delta t \tag{15-8}$$

if $r < \overline{f}$. In the former case, a rainfall excess intensity will exist during that Δt; the excess is given by

$$e = r - \overline{f} \tag{15-9}$$

In the latter case, $e = 0$ the program continues in this manner until the end of the storm thereby supplying the user with an excess rainfall rate histogram for input to the overland flow routing program.

Example

$\delta = (\theta_w - \theta_i)\psi_{ave}$

$\theta_w = .419$

$\theta_i = .323$

$\psi_{ave} = 11.06$ in.

$\delta = 1.062$ in.

$K = 0.23$ in./hr

$K = .00383$ in./min

Storm			Excess	
Intensity (in./hr)	Time (min)		Time (min)	Excess Intensity (in./min)
0.070 .00117	18		18	.00117 .0000
0.013 .000217	85	67	85	.00022 .0000
1.200 .02	87	2	87	.02000 .0000
2.700 .045	89	2	89	.04500 .0057
4.800 .08	91	2	91	.08000 .0536
4.200 .07	92	1	92	.07000 .0475
7.200 .12	93	1	93	.12000 .0992
6.600 0.11	94	1	94	.11000 .0905
6.000 0.10	95	1	95	.10000 .0816
5.400 0.09	96	1	96	.09000 .0725
4.200 0.07	97	1	97	.07000 .0532
3.600 0.06	98	1	98	.06000 .0436
2.900 0.0483	99	1	99	.04000 .0327
1.800 0.03	100	1	100	.03000 .0149
0.900 0.015	106	6	106	.01500 .0013
2.400 0.04	107	1	107	.04000 .0273
0.400 .00667	110	3	110	.00667 .000
0.240 .0064	115	5	115	.00400 .000
0.970 0.161	121	6	121	.00783 .0040
0.300 .00500	125	4	125	.00500 .0000

Kinematic Wave Routing--Method of Characteristic Approach: The kinematic wave routing approximation was extensively discussed in Chapter 7. Since this program is probably the most complex of the group some of the theory will be discussed here as an aid to the user. This formulation may be used for routing for any channel or overland flow slope that a zero depth upstream boundary condition, that is, any slope such as a divide for which the depth of flow at the top is always zero. Slopes that have a non-zero upper boundary condition may not be routed using this program due to the possibility of kinematic shock.

The program formulation assumes that the lateral inflow may be represented as a histogram. The solution domain for the method is

illustrated in Figure 15.6. Here the time axis is shown vertical and the distance axis is horizontal. The downstream boundary, $x = L$, represents the end of the slope. The lateral inflow is shown distributed with respect to time up the upstream boundary of the domain, i.e., on the t axis. For overland flow, this function is the excess rainfall. For channel flow, the lateral inflow is the overland flow discharge per unit width. This discussion will be developed for overland flow but is directly analogous to channel flow by replacing depth y with area A, and discharge per unit width q with discharge Q.

As discussed in Chapter 7, this solution is valid along paths in the solution domain known as characteristic paths or characteristics. The effective meaning of this fact is that a characteristic defines a unique pair of points are on the upstream boundary $(0, t_o)$ and one on the downstream boundary (L, t_L). The object of the water routing is to know the discharge at the downstream boundary q_L for overland flow. We know from Chapter 7 that

$$q_L = \alpha' y_L^{\beta'} \tag{15-10}$$

where y_L is the depth of flow at the downstream boundary and α' and β' are determined by channel geometry, roughness and slope (see Chapter 7). Along a given characteristic

$$y_L = \int_{t_o}^{t_L} e(t)d\sigma \tag{15-11}$$

where e is the excess rainfall function. Therefore, if one selects a value of t_o, the uniqueness of the characteristics passing through $(0, t_o)$ allows the calculation of t_L; and since $e(t)$ is known, Equation 15-11 may be evaluated to give the depth of flow at the downstream boundary and then Equation 15-10 gives the discharge per unit width.

Equation 7-56 is the characteristic path through $(0, t_o)$ and (L, t_L) for a general lateral inflow $q_e(t)$. If the lateral inflow is in the form of a histogram such as the excess rainfall function, the equation may be evaluated piece by piece as illustrated by Equations 7-49 through 7-54 and Figure 7.8. This program performs the calculation of t_L corresponding to a selected t_o and the subsequent evaluation of Equations 15-11 and 15-10.

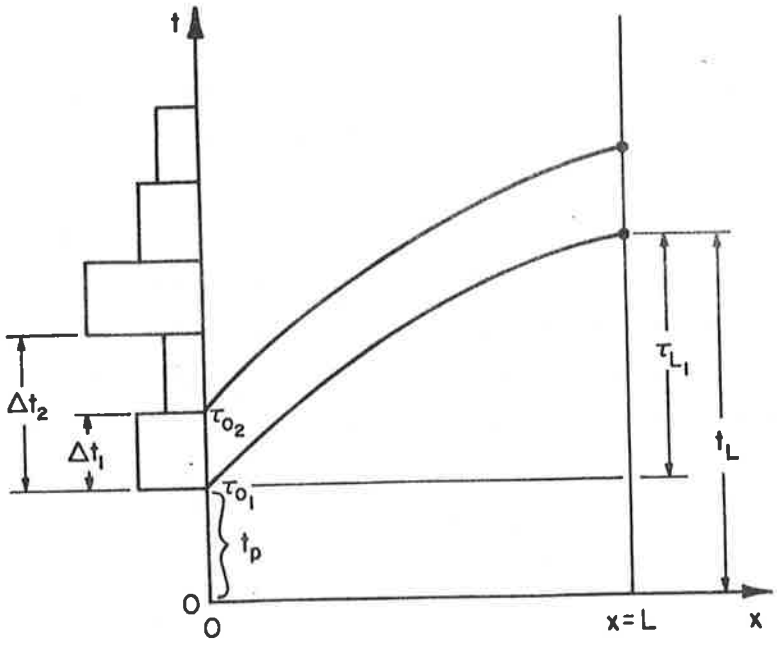

Figure 15.6

Using overland flow notations, Equations 7-50 and 7-51 become for $e_{i+1} > 0$

$$x_{i+1} = x_i + \frac{\alpha'}{e_{i+1}} \{[y_i + e_{i+1}(t_{i+1} - t_i)]^{\beta'} - y_i^{\beta'}\} \qquad (15\text{-}12)$$

for $e_{i+1} = 0$

$$x_{i+1} = x_i + \alpha'\beta' y_i^{\beta'-1} (t_{i+1} - t_i) \qquad (15\text{-}13)$$

With reference to Figures 7.8 and 15.6, a value of t_o is selected on the upstream boundary and the calculation begins by entering a value of e_{i+1} and t_{i+1}. The program selects either Equation 15-12 or 15-13 to evaluate x_{i+1}. This value of x is compared to the slope length and if $x_{i+1} < L$ the procedure is repeated with the next value of e and t. If $x \geq L$ the program braches to the calculation of t_L.

Based on current values of x_i, y_i, t_i, and e_{i+1}, t_L may be calculated from Equation 7-53 or 7-54 that is if $e_{i+1} > 0$ 0

$$t_L = t_j + \frac{1}{e_{i+1}} \left\{ \left[\frac{e_{i+1}(L-x_i)}{\alpha'} + y_j^{\beta'} \right]^{\frac{1}{\beta'}} - y_j^{\beta'} \right\} \qquad (15\text{-}14)$$

or if $e_{i+1} = 0$

$$t_L = \frac{L-x_i}{\alpha'\beta' y_i^{\beta'-1}} + t_i \qquad (15\text{-}15)$$

Knowing t_L, a point on the runoff hydrograph, (q_L, t_L) may be calculated by using Equations 15-11 and 15-10. Subsequent points on the hydrograph are calculated by selecting new t_o's and repeating the process. The usual method of using these programs is to select a t_o at the beginning of each change in excess intensity; however, further subdivision of the excess histogram yields higher resolution in the hydrograph calculation.

The first characteristic beginning at the time of ponding, $t_o = t_p$ in Figure 15.6, represents a special case in that it divides the solution domain into two regions. In the region above this characteristic, all calculations are as described above. Below this characteristic it is not necessary to calculate t_L as described above. This region is

populated by characteristics having their origin on the x axis. For all of these characteristics $t_o = t_p$. For any time along the downstream boundary less than the t_L of the time of ponding characteristic, there is a characteristic with $t_o = t_p$. Therefore for such times the q_L may be calculated immediately by integrating Equation 15-11 from t_p to t_L. The program supplied writes the values of q for each value of t_i along the first characteristic. Using Figure 15.6, values of q_i for times $t_p + \Delta t$, $t_p + \Delta t_L$, and so forth are output as the program steps along other first characteristics.

Recapitulating, using Figure 15.6 for the first characteristic, the program steps along the characteristic using Equation 15-12 or 15-13 as new values of e_{i+1} and $t_{i+1} = t_p + \Delta t_{i+1}$ are entered until a value of $x_{i+1} > L$ is calculated. At this time t_i is calculated using Equation 15-14 or 15-15, then q_L using Equation 15-11 and 15-10. Values of q_L at each t_i are output as this first characteristic is calculated. A new characteristic is then selected by picking a new t_o, say $t_p + \Delta t_1$, and repeating the procedure, except that q_L is not output since these subsequent characteristics do not begin on the x axis. A more detailed description of this programmable calculator program was given by Simons, Li and Eggert (1976).

Examples

The timing of the excess intensity timing is different for the two calculator programs, consequently examples are provided for each program. The basic difference is that the TI-59 program allows entry of times from the beginning of the rainfall event. The Hewlett-Packard 97/67 program requires the entry of time increments corresponding to the excess intensities; that is, with reference to Figure 15.6, $\Delta t_2 - \Delta t_1$, $\Delta t_3 - \Delta t_2$ and so forth. In addition, the units for excess and time inputs are different. The HP-97 requires input in seconds for time and ft/sec for excess intensity. The TI-59 requires input in minutes for time and in./min for intensity.

A. Kinematic Wave--Method of Characteristics Utilizing Hewlett-Packard Calculator HP-97

Given: $\alpha = 400$

$\beta = 3.0$

$L = 4000$ ft

$\alpha\beta = 1200$

time of ponding = 0

Excess Intensities:

Time (sec)	Excess (ft/sec)
600	$20. \times 10^{-6}$
900	$18. \times 10^{-6}$
1000	$30. \times 10^{-6}$
2000	$20. \times 10^{-6}$
2500	$15. \times 10^{-6}$
2700	$13. \times 10^{-6}$
3300	$21. \times 10^{-6}$
3700	$10. \times 10^{-6}$
4000	$1. \times 10^{-6}$

Output

```
                0.0000  ***
               34.5600  ***

           6.9120-04    ***
               34.5600  ***
              113.2272  ***

           2.1072-03    ***
              113.2272  ***
              156.1824  ***

           3.3855-03    ***
C_o →         156.1824  ***
             1305.1744  ***

           2.6376-02    ***
             1305.1744  ***
             2477.5284  ***

           4.3961-02    ***
             2477.5284  ***
             3056.6092  ***

           5.1515-02    ***
             3056.6092  ***

             2974.9735  ***
           7.1284-02    ***
             3059.6092  ***
```

```
                0.0000  ***
               3.4992   ***
               9.3024   ***
C_1 →        453.5744   ***
            1078.5604   ***
            1410.8172   ***
            2865.4116   ***

            3035.0899   ***
           6.4715-02    ***
            2865.4116   ***

               0.0000   ***
               0.3600   ***
             243.1600   ***
C_2 →        675.3100   ***
             916.1428   ***
            2045.3676   ***
            3138.1468   ***

            3085.0784   ***
           4.9967-02    ***
            3138.1468   ***

               0.0000   ***
             160.0000   ***
             501.2500   ***
C_3 →        700.4506   ***
            1663.5476   ***
            2623.6708   ***
            3413.8456   ***

            3221.1236   ***
           4.1529-02    ***
            3413.8456   ***
```

Results: The results interpretated from the output are:

Time (sec)	Discharge/unit width Excess (ft^3/sec-ft)
600	6.91×10^{-4}
900	2.11×10^{-3}
1000	3.40×10^{-3}
2000	2.64×10^{-2}
2500	4.40×10^{-2}
2700	5.15×10^{-2}
2975	7.13×10^{-2}
3639	6.47×10^{-2}
3839	5.00×10^{-2}
4221	4.15×10^{-2}

B. Kinematic Wave--Method of Characteristics Utilizing Texas Instrument TI-59

Given: $\alpha = 400$

$\beta = 3.0$

$L = 4000$ ft

time of ponding = 0

Excess Intensities:

Time (min)	Excess* (in./min)
10	.01440
15	.01296
16.67	.02160
33.33	.10441
41.67	.01080
45.	.00936
55.	.01512
61.67	.00720
66.67	.00072
↓	0.0

*Note that the unit of in./min is used due to the convenience in incorporating with the infiltration computation directly (see Green-Ampt infiltration program)

Output

```
          1.  01
 6.912-04

        1.5  01
 2.1072096-03

      1.667  01
 3.3988628-03

      3.333  01
 2.6371789-02

      4.167  01
 4.397191-02

        4.5  01
 5.1519335-02

 4.9581658  01
 7.1283671-02

 6.0650084  01
 6.4720981-02

 6.6482584  01
 4.9976469-02
```

Results: The results interpreted from the output are:

Time (min)	q (cfs/ft)
10	.00069
15	.00211
16.67	.00340
33.33	.02737
41.67	.04397
45.	.05152
49.58	.07128
60.65	.06472
66.48	.05000

Resistance to Overland Flow and Overland Flow Depth: The resistance to overland flow in natural watersheds may be regarded as a function of the ground cover density. Ground cover can include not only vegetation but rock and litter that contribute to flow resistance. The Darcy-Weisbach resistance equations may be expressed as

$$S_f = f \frac{q^2}{8gy^3} \tag{15-16}$$

where S_f is the friction slope, g is the acceleration due to gravity, q is the discharge per unit width and f is the Darcy-Weisbach resistance factor. Numerous authors, e.g., Chan, 1976, have used expressions for f of the form

$$f = \frac{K}{Nr} \tag{15-17}$$

where K is a constant related to ground cover and Nr is the flow Reynolds number. Normally this form is only used in the laminar flow range; however, extension of the expression well into the turbulent ranges are common in watershed simulation.

K has been shown to be a function of the fraction of ground cover. One possible fit is of the form

$$K = K_\ell + (K_h - K_\ell) C_g^2 \tag{15-18}$$

where K_ℓ and K_h are lower and upper bounds on K and C_g is the ground cover density. K_ℓ is usually regarded as the value of K associated with a smooth surface and is given the value of 100 in this program.

Equation 1 may be rewritten using Equation 2 and noting that $Nr = \frac{q}{\nu}$ where ν is the kinematic viscosity of water. This relation when solved for depth has the following form

$$y = \left(\frac{K \nu}{8 g S_f q} \right)^{1/3} \tag{15-19}$$

The kinematic wave theory discussed in Chapter 7 approximates S_f with the bed slope, S_o. This program uses Equation 15-18 to evaluate K and Equation 15-19 to give the depth of overland flow corresponding to a given discharge per unit width.

Example: Darcy-Weisbach Resistance Overland Flow Parameters

Given: $C_g = .50$ (50 percent)

$K_h = 40{,}000$

$K_\ell = 100$

$S_o = .01$

Find: α, β in $Q = \alpha y^{\beta}$

Results:

$K = 100$

$\alpha = 23.46$

$\beta = 3.00$

Lognormal for Flood Volume. Assuming that the flood volume Q has a lognormal distribution, this program allows the calculation of return period, T_r corresponding to a given flood volume Q and conversely, flood volume corresponding to a given return period. By definition the return period for a flood of volume Q = q is given by

$$T_r = \frac{1}{P[Q>q]} \tag{15-20}$$

where $P[Q>q]$ is the probability that flood volume Q is greater than q. From elementary probability

$$P[Q>q] = 1 - P[Q\leq q] \tag{15-21}$$

where $P[Q\leq q]$ is the cumulative probability distribution, cdf, of Q or $F_Q(q)$. Therefore, from Equations 15-20 and 15-21

$$T_r = \frac{1}{1-P[Q\leq q]} = \frac{1}{1-F_Q(q)} \tag{15-22}$$

Conversely,

$$q = F_Q^{-1}(1 - \frac{1}{T_r}) \tag{15-23}$$

where F_Q^{-1} is the inverse function of cdf F_Q. If F_Q is assumed lognormal then it is given by

$$F_Q(q) = \int_{-\infty}^{\ln q} \frac{1}{\sqrt{2\pi}\,\sigma} e^{-\frac{(\chi-\mu)^2}{2\sigma^2}} d\chi \tag{15-24}$$

where μ is the mean of lnq, and σ is the standard deviation of lnq. Therefore, $F_Q(q) = F_z((\ln q-\mu)/\sigma)$ where F_z is the cdf of a standard normal random variable. In addition,

$$F_Q^{-1}(q) = \exp[\sigma(F_z^{-1}(p) + \mu)] \tag{15-25}$$

By definition,

$$F_z(y) = \begin{cases} 0.5 + \int_0^z \frac{1}{\sqrt{2\pi}} e^{-x^2/2}\, dx & y \geq 0 \\ 0.5 - \int_0^z \frac{1}{\sqrt{2\pi}} e^{-x^2/2}\, dx & y < 0 \end{cases} \tag{15-26}$$

and $F_z^{-1}(y)$ may be found by solving Equation 15-26 for y given that $F_z(y) = P$ corresponding to some return period T_r. In this way Equations 15-26 are rewritten

$$P - 0.5 = \int_o^z \frac{1}{\sqrt{2\pi}} e^{-x^2/2}\, dx \qquad P \geq 0.5$$

$$0.5 - P = \int_o^{-z} \frac{1}{\sqrt{2\pi}} e^{-x^2/2}\, dx \qquad P < 0.5 \tag{15-27}$$

Equations 15-26 will be integrated using Simpson's Rule and Equations 15-27 will be solved using the Newlon method.

The sample mean discharge volume $\hat{\mu}_q$ and sample standard deviation $\hat{\sigma}_q$ are usually available from basic data. The estimation of μ and σ for Equation 15-24 can be made as follows.

$$\beta^2 = \ln\left(1 + \frac{\hat{\sigma}_q}{\hat{\mu}_q}\right)^2 \tag{15-28}$$

and

$$\alpha = \ln\hat{\mu}_q - \frac{\beta^2}{2} \tag{15-29}$$

Example

For $\hat{\mu}_q = 300$ acre-feet

$\hat{\sigma}_q = 100$ acre-feet

Find (a) q for $T_r = 10$ yr, and $T_r = 100$ yr

(b) T_r for $q = 50$ acre-feet, $q = 500$ acre-feet

(a)

T_r(yr	q(acre-feet)
10	431.418
100	605.146

(b)

q(acre-feet)	T_r(yr
50	1.000
500	24.226

Flood Frequency Analysis--Peak Annual Flow

The Gumbel distribution is often used in flood frequency analysis to fit peak and annual flow data. The cumulative distribution is given by

$$F(q) = P[Q_p \leq q] = e^{-e^{-(x-x_o)/\beta}} \tag{15-30}$$

This distribution contains two parameters, x_o and β that may be fitted by method of moments. The method allows the parameters to be evaluated thus

$$E[Q_p] = x_o + \gamma\beta, \gamma = 0.577216$$
$$\text{Var}\ [Q_p] = \frac{\pi^2\beta^2}{6} \tag{15-31}$$

Using the sample mean, $\hat{\mu}$ and sample variance, $\hat{\sigma}^2$ to estimate $E[Q_p]$ and Var $[Q_p]$, respectively, we have

$$\rho = \sqrt{\frac{6\sigma^2}{\pi^2}}$$
$$x_o = \hat{\mu} - \gamma\sqrt{\frac{6\sigma^2}{\pi^2}} \tag{15-32}$$

Therefore,

$$P[Q_p \leq q] = e^{-e^{-(q - \hat{\mu} + .45\hat{\sigma})\frac{1}{0.78\sigma}}} \tag{15-33}$$

This equation may be used to obtain the return period, T, as a function of peak discharge q since

$$T = \frac{1}{1 - P\ [Q_p \leq q]} \tag{15-34}$$

Conversely, the discharge corresponding to a given return period may be obtained from Equations 15-1 and 15-5 as

$$F(q) = 1 - \frac{1}{T}$$

Therefore,

$$q = F^{-1}(1 - \frac{1}{T}) \tag{15-35}$$

from Equation 15-30

$$F^{-1}\ (y) = \hat{\mu} - 0.45\ \hat{\sigma} - 0.78\ \hat{\sigma}m\ (\ln\ (y)^{-1})$$
$$y = 1 = \frac{1}{T} \tag{15-36}$$

<u>Example</u>: For $\bar{\mu}$ = 54971 cfs, and σ = 16,483 cfs

$$q = 76486.0$$
$$q_{100} = 106,696.6$$

Hydraulics Package

The hydraulics padkage includes programs for hydraulic computations in natural and trapezoidal channels. A set of programs is provided to fit power function relationship for area vs depth, wetted perimeter vs area, and top width vs depth to cross-section survey data. Two normal depth programs are included. The first calculates the normal depth in natural channels using the above cross-sectional relationships. The second computes the normal depth in trapezoidal channels. The Muskingham-Cunge method is programmed for routing floods through channels (see Chapter 6). A program is provided for the conversion between the Darcy-Weisbach, Mannings and Chezy friction parameters. The last program in this package provides for the calculation of super elevation of flow in bends.

Normal Depth in Trapezoidal Channels

The normal depth in trapezoidal channels may be calculated using Mannings equation

$$Q = \frac{1.486}{n} R^{2/3} AS^{1/2} \tag{15-37}$$

where n is the Mannings resistance parameter, R is the hydraulic radius, A is flow area, S is slope and Q is discharge. Hydraulic radius is given by

$$R = \frac{A}{P} \tag{15-38}$$

where P is wetted perimeter. Area and wetted perimeter for a trapezoidal channel may be expressed as function of depth as follows:

$$A = Z\ y^2 + by \tag{15-39}$$

where Z is the side slope angle or (horizontal to vertical), b is the bottom width and y is the depth. Wetted perimeter is given by

$$P = b + 2y\ (1 + Z)^{1/2} \tag{15-40}$$

Therefore,

$$Q = \frac{1.486}{n} \frac{[Z\ y^2 + by]^{5/3}\ S^{1/2}}{[b + 2y(1+Z)^{1/2}]^{2/3}} \tag{15-41}$$

This equation may be solved for y in terms of the other known parameters by use of Newtons method.

In addition, this program also provides the cross-sectional area, the mean velocity and the stream power.

Example

Normal Depth (Trapezoidal channel)

Given: $m = .5$ $(m = 1/2)$

$b = 10$

$Q = 2000$ cfs

$n = .020$

$S = .01$

Find: Normal depth, y_o, cross sectional area A, velocity V and stream power τV.

Initial guess: $y_o = 6$ feet

Results: $y_o = 5.614$

$A = 119.174$

$V = 16.782$

$\tau V = 35.548$

Channel Cross Section Properties

Hydraulic calculations in natural channels often require a functional expression of channel geometry. The most common of these relationships are wetted perimeter-flow area, flow area-depth, and top width-depth equations. These equations are usually given in the form of the power curves as

$$P = a_1 A^{b_1} \tag{15-42}$$

where A is area and P is wetted perimeter;

$$A = a_2 y^{b_2} \tag{15-43}$$

where y is depth of flow; and

$$T = a_3 y^{b_3} \tag{15-44}$$

where T is top width. The coefficients, a and exponents b are usually statistically fitted. The method usually proceeds by taking the logarithm of both sides of the equation. For example, the perimeter expression becomes

$$\ln P = \ln a_1 + b_1 \ln A \tag{15-45}$$

Using the logarithm of A as an independent variable and the logarithm of P as the dependent variable, a least squares fit may be calculated to provide values for a_1 and b_1. In order to provide a good fit, several values of the dependent and independent variables must be supplied from measurements of the channel cross section.

It is assumed that the cross-sectional geometry is known as a series of (x, z) points measured relative to some datum (see Figure 15-7). The programs supplied will calculate the values of a_1, b_1, a_2, b_2, a_3 and b_3 and present the correlation coefficient of the fit.

The TI-59 programs are as follows:

1. (x_i, z_i) data loading program
2. Area-wetted perimeter program
3. Area-depth program
4. Top width-depth program

The HP-97 programs are as follows:

1. Area-depth program
2. Wetted perimeter-depth program
3. Top width-depth program
4. Standard Pac program SD-03A (Curve Fitting)

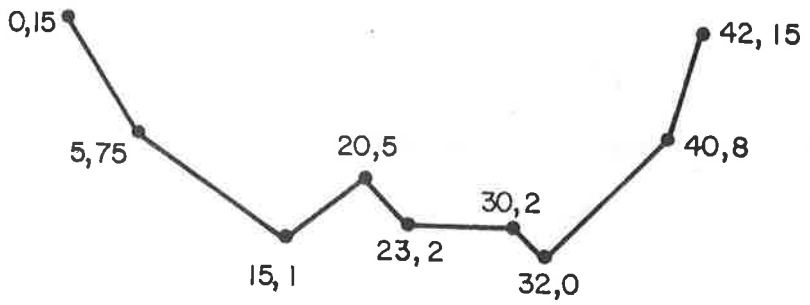

Figure 15.7

Example

For the following set of (x,z) survey coordaintes, determine the area-wetted perimeter, area-depth and top width-depth relationships

x	z
0	15
5	7.5
15	1
20	5
23	2
30	2
32	0
40	8
42	15

Wetted Perimeter = $4.89\ (\text{Area})^{0.43}$

Area = 2.15 (Depth) 1.66

Top width = $5.22\ (\text{Depth})^{0.86}$

Normal Depth in a Natural Channel

When the channel geometry is known through a series of functional expressions, the calculation of normal depth is straight-forward. This program is based on Manning's resistance equation. When the area wetted perimeter equation and the area depth equations given by

$$P = a_1 A^{b_1} \tag{15-46}$$

and

$$A = a_2 y^{b_2} \tag{15-47}$$

where P is wetted perimeter, A is area and y is flow depth are substituted into Manning's equation, the following expression for normal depth results

$$y_o = \left[\left(\frac{Qn}{1.49\ S^{1/2}}\right)^{3/2} \left(\frac{a_1}{a_2^{(5/2 - b_1)}}\right)\right]^{\frac{2}{(5b_2 - 2b_1b_2)}} \tag{15-48}$$

where y_o is normal depth, Q is discharge, n is Manning's resistance parameter, and S is slope.

Example

Discharge, $Q = 1000$ cfs

Manning's $n = 0.025$

slope $S = 0.005$

parameter $a_1 = 4.89$

parameter $b_1 = 0.43$

parameter $a_2 = 2.15$

parameter $b_2 = 1.66$

Normal depth $y_o = 10.907$ ft

Backwater Curve Computation in Natural Channels

Given channel cross sectional properties such as the wetted perimeter depth-area, area-depth, and top width-depth relations, the standard step method may be modified to provide backwater calculations in natural channels. Let

$$P = a_1 y^{b_1} \tag{15-49}$$

$$A = a_2 y^{b_2} \tag{15-50}$$

where P is wetted perimeter, A is cross sectional area and y is depth. Using Manning's equation

$$K = \frac{Q}{S^{1/2}} = \frac{1.486}{n} R^{2/3} A \tag{15-51}$$

where Q is discharge, n is Manning's resistance, S is slope and R is hydraulic radius and K is known as conveyance

$$K = \frac{1.486}{n} \left[\frac{(a_2 y^{b_2})}{a_1^{b_1} a_2^{b_2 b_1} y} \right]^{2/3} (a_2 y^{b_2}) S^{1/2} \tag{15-52}$$

$$K = \frac{1.486}{n} a_1^{-2/3} a_2^{-5/3} y^{(5/3\, b_2 - 2/3\, b_1)} \tag{15-53}$$

Therefore,

$$S = \left(\frac{Q}{K}\right)^2 \tag{15-54}$$

The total energy equation at a station may be written in terms of a known total head at another station.

$$y + z - \Delta x (2Q)^2 [K + C_1 y^{C_2}]^{-2} + \frac{Q^2}{2y} (a_2 y^{b_2})^{-2} = T_n 0 \tag{15-55}$$

where z is the bed elevation, $T_n 0$ is the known total head at another station and C_1 and C_2 are given by

$$C_1 = \frac{1.486}{n} a_2^{5/3} a_1^{-2/3} \tag{15-56}$$

$$C_2 = \frac{5}{3} b_2 - \frac{2}{3} b_1 \tag{15-57}$$

Equation 15-52 may be solved for depth y using Newton's method.

Example

Flow area vs relation depth	$A = 20 \cdot y^1$
Wetted perimeter vs depth relation	$P = 20 \cdot y^{0.5}$
Manning's	$n = 0.02$
Discharge	$Q = 10000$ cfs
Downstream depth	$y_1 = 35$ ft

Downstream bed elevation	$Z_1 = 100$ ft
Upstream bed elevation	$Z_2 = 105$ ft
Space increment	$\Delta x = 500$ ft
Total bed	$T_n = 138.17$ ft, and
Upstream depth	$y_2 = 31.18$ ft

```
   20.00 ENT1
     .50 ENT1
   20.00 ENT1
    1.00 GSBA
     .02 GSBE
10000.00 GSBC
   35.00 GSBE
  100.00 GSBE
         GSBo

  138.17  ***
170128.16  ***

  103.00 GSBE
  500.00 GSBe
         GSBb

   31.18  ***
```

Conversion of Resistance Coefficients

The need to convert from Manning's n, Chezy C or Darcy f to one of the other forms frequently arises in hydraulic calculations. The three resistance equations are given by

(Manning's)

$$S_f = \frac{n^2 Q^2}{2.22\, A^2 R^{4/3}} \tag{15-58}$$

where S_f is the friction slope; n is the Manning's resistance parameter, A is area, R is hydraulic radius and Q is discharge;

(Chezy)

$$S_f = \frac{Q^2}{C^2 A^2 R} \tag{15-59}$$

where C is the Chezy resistance parameter; and

(Darcy-Weisbach)

$$S_f = \frac{Q^2 f}{8 g A^2 R} \tag{15-60}$$

where f is the Darcy-Weisbach resistance parameter.

The conversion between resistance parameters is accomplished by equating the friction slope for the corresponding resistance laws or

$$C = \sqrt{8g/f} \tag{15-61}$$

$$f = 8g/C^2 \tag{15-62}$$

$$C = \frac{1.486}{n} R^{1/6} \tag{15-63}$$

$$n = \frac{1.486}{C} R^{1/6} \tag{15-64}$$

$$n = \sqrt{8g/f} \cdot 1.486 R^{1/6} \tag{15-65}$$

and

$$f = \frac{8g \cdot (1.486)^2 R^{2/6}}{n^2} \tag{15-66}$$

Example

For Darcy-Weisbach $f = 0.4$,
Chezy $C = 25.3772$.

For Chezy $C = 100$,
Darcy-Weisbach $f = 0.02576$.

For Darcy-Weisbach $f = 0.07$ and hydraulic radius $R = 3$ ft,
Manning's $n = 0.0295$.

For Manning's $n = 0.03$ and hydraulic radius $R = 3$ ft,
Darcy-Weisbach $f = 0.0723$.

For Chezy $C = 100$ and hydraulic radius $R = 3$ ft
Manning's $n = 0.0179$.

For Manning's $n = 0.02$ and hydraulic radius $R = 3$ ft,
Chezy $C = 89.47$.

Muskingum-Cunge Flood Routing

The Muskingum-Cunge flood routing was discussed in Chapter 6. For clarity some of the presentation is repeated here. The method is based on the assumption of a linear relationship between inflow I, outflow O, and volume of storage V in a channel reach, of the form

$$V = K[XI + (1-X)O] \tag{15-67}$$

in which K and X are the Muskingum parameters. Equation 15-67 leads to

$$Q_{j+1}^{n+1} = C_1 Q_j^n + C_2 Q_j^{n+1} + C_3 Q_{j+1}^n \tag{15-68}$$

from which the outflow discharge at the new time level Q_{j+1}^{n+1} can be calculated from a knowledge of the inflow discharge at the present level Q_j^n, the inflow discharge at the new time level Q_j^{n+1}, and the outflow discharge at the present level Q_{j+1}^n. The coefficients C_1, C_2, and C_3 are the Muskingum coefficients, defined as

$$C_1 = \frac{2X + \frac{\Delta t}{K}}{2(1-X) + \frac{\Delta t}{K}} \tag{15-69}$$

$$C_2 = \frac{-2X + \frac{\Delta t}{K}}{2(1-X) + \frac{\Delta t}{K}} \tag{15-70}$$

$$C_3 = \frac{2(1-X) - \frac{\Delta t}{K}}{2(1-X) + \frac{\Delta t}{K}} \tag{15-71}$$

in which Δt is the time step (also called time interval or routing period).

In the Muskingum-Cunge method, the parameter K is the propogation time of the flood wave, defined as

$$K = \frac{\Delta x}{c} \tag{15-72}$$

in which x is the computational reach length and c is the flood wave celerity. The parameter X is a measure of the amount of numerical diffusion, and can be calculated by

$$X = \frac{1}{2}\left(1 - \frac{q_r}{S_o c \Delta x}\right) \tag{15-73}$$

in which q_r is the reference discharge per unit width and S_o is the channel bed slope. The parameters K and X are assumed constant.

A method to estimate q follows.

$$q_r = \frac{Q_r}{T} \tag{15-74}$$

where Q_r is the reference discharge and T is the top width at the reference discharge.

The K and X are calculated based on a reference discharge Q_r. If

$$Q_r = \alpha' A_r^{\beta'} \tag{15-75}$$

then

$$A_r = \alpha Q_r^{\beta} \tag{15-76}$$

where $\alpha = (\frac{1}{\alpha_\omega})^{1/\beta'}$ and $\beta = \frac{1}{\beta'}$. The definitions of α, β, α', β', are given in Chapter 7.

The celerity of the flood wave c is given by

$$c = \alpha'\beta' A_r^{\beta'-1} \tag{15-77}$$

Example

Wetted perimeter vs. area relation

$$P = 5.8 \cdot A^{0.5}$$

Flow area vs. depth relation

$$A = 3.7 \cdot y^{2.4}$$

Top width vs. depth relation

$$T = 11.6 \cdot y^{1.2}$$

Reference Discharge

$$Q_r = 67 \text{ cfs}$$

Slope

$$S_o = 0.03$$

Manning's

$$n = 0.02$$

Space increment

$$\Delta x = 1000 \text{ ft}$$

At the upstream boundary:

Time t_i (min)	Discharge Q_1^i (cfs)
0	0
10	20
20	50
30	75
40	100
50	80
60	60
70	40
80	20
90	0

At the downstream boundary:

Time t_i (min)	Discharge Q_1^i (cfs)
0	0
10	14.64
20	45.87
30	71.32
40	95.44
50	88.28
60	59.32
70	45.85
80	21.04
90	4.56

Super Elevation in Bends

When water flows through a bend centrifugal forces cause the depth to be greater along the outside bank. By equating the gravity component to the centrifugal force the super elevation may be calculated (see Chapter 3) as

$$\Delta Z = \frac{V^2}{gr_c} \tag{15-78}$$

where ΔZ is the super elevation, V is the average velocity, g is the acceleration due to gravity and r_c is the radius of the bend measured to the channel centerline.

Example

Velocity V = 2 ft/sec

Radius of curvature r_c = 1000 ft

Top width = 100 ft

Super elevation ΔZ = 0.01242 ft

Sedimentation Package

The sedimentation package begins with a particle size distribution program. This program allows the user to fit a log normal distribution to particle size data. The next program allows for the calculation of particle fall velocity. Two short programs are included for calculating the critical and effective shear stress.

There are programs for four sediment transport equations. The first is the Meyer-Peter, Müller bed load equation (USBR, 1960). The user also has the option of computing the suspended load by the Einstein method based on estimated bed load from the Meyer-Peter, Müller equation. Programs for total sediment transport include Lu's (1973) equation, Yang's (1976) method, and Shen and Hung's (1971) equation. Degradation and aggradation analysis for long reaches is programmed using a simple finite difference formulation of the sediment continuity equation. An equation for local scour determination in a sand bed river is given. Finally, a program for the design of riprap bank protection is provided.

Log Normal Distribution for Sediment Size

The log normal distribution is often used to describe sediment size distribution. The cumulative distribution function (cdf) for the log normal distribution may be expressed as

$$F_D(d) = \int_{-\infty}^{\ell nd} \frac{1}{\sqrt{2\pi}\,\sigma} e^{\frac{-(x-\mu)^2}{2\sigma^2}} dx \qquad (15\text{-}79)$$

where d is the sediment particle diameter, μ is the mean of ℓnd, σ is the standard deviation of ℓnd, and ℓnd is the natural logrithm of sediment size d.

$$F_D(d) = F_Z\left(\frac{\ell nd - \mu}{\sigma}\right) \qquad (15\text{-}80)$$

where F_Z is the call of a standard normal distribution.

By definition,

$$F_Z(z) \begin{cases} = 0.5 + \int_0^z \frac{1}{\sqrt{2\pi}} e^{-\frac{x^2}{2}} dx, & z \geq 0 \\ = 0.5 - \int_0^{-z} \frac{1}{\sqrt{2\pi}} e^{-\frac{x^2}{2}} dx, & z < 0 \end{cases} \qquad (15\text{-}81)$$

Equation 15-81 is integrated using Simpson's Rule.

The mean μ and standard deviation σ of the ℓnd are usually calculated from the median sediment diameter, d_{50}, and the gradation coefficient, G, respectively. That is

$$\mu = \ell n\, d_{50} \qquad (15\text{-}82)$$

and

$$\sigma = \ell n\, G \qquad (15\text{-}83)$$

where

$$G = \sqrt{\frac{d_{84}}{d_{16}}} \qquad (15\text{-}84)$$

or

$$G = \frac{1}{2}\left(\frac{d_{84}}{d_{50}} + \frac{d_{50}}{d_{16}}\right) \qquad (15\text{-}85)$$

Therefore, with the parameters of the distribution estimated, the probabilies of any size interval, such as d_i and d_{i+1} may be determined.

Example

For sediment diameters:

$d_{15.9}$ = 0.119 mm

d_{50} = 0.163

$d_{84.1}$ = 0.222 mm

G = 1.366

Then for particles in the range d_i to d_{i+1} the probability of occurrence are tabulated below for the given d_i

i	d_i(min)	$P[d_i < d < d_{i+1}]$
1	.005	
2	.010	1.790×10^{-19}
3	.050	7.564×10^{-5}
4	.100	0.059
5	.200	0.685
6	.300	0.231
7	.400	0.023
8	.500	0.002
9	.600	1.483×10^{-4}
10	1.00	1.468×10^{-5}

Particle Fall Velocity

Particle fall velocities are a function of particle size and water properties that are represented by the kinematic viscosity. The fall velocity for sediment diameters less than 0.002 ft may be calculated from Stoke's Law. For larger sizes, Rubey's (ASCE, 1975) expression is used, or

$$w = \frac{2.9517\, d_s^2}{\nu} \quad ; \text{ for } d_s < 0.0002 \text{ ft} \qquad (15\text{-}86)$$

and

$$w = \frac{[36.064\, d_s^3 + 36\, \nu^2]^{1/2} - 6\nu}{d_s} \quad ; \text{ for } d_s \geq 1.002 \text{ ft} \qquad (15\text{-}87)$$

Example

For $d_s = 0.00052$ ft

$\nu = 1.16 \times 10^{-5}$ ft/sec

$w = 0.0576$ ft/sec

For $d_s = 0.00015$ ft

$\nu = 1.09 \times 10^{-5}$ ft/sec

$w = 0.0061$ ft/sec

Critical Shear Stress

The shear stress necessary to initiate sediment motion is known as the critical shear stress. The Shield's diagram (Figure 15.8) is

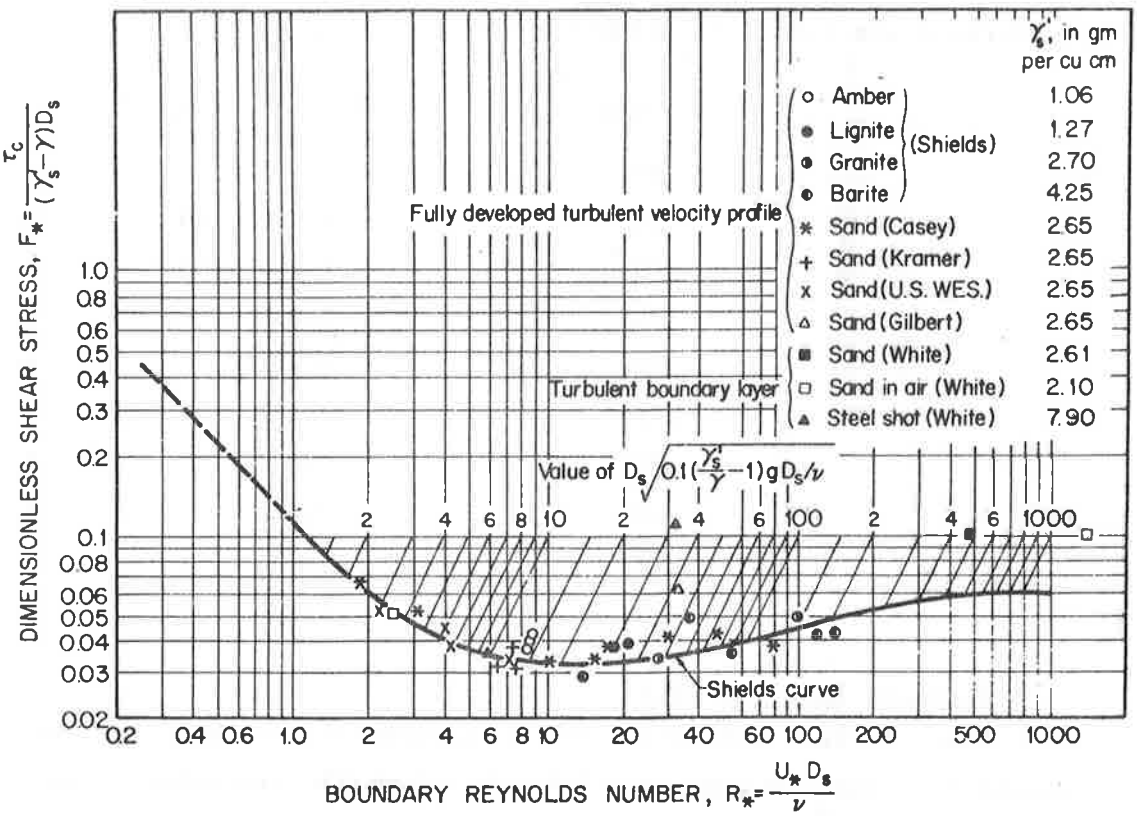

Figure 15.8 Shield's diagram: dimensionless critical shear stress (after Simons and Sentürk, 1977).

most often used to compute critical shear stress. The procedure is to determine either the boundary Reynolds number, $R_* = \frac{U_* D_s}{\gamma}$ or the parameter $\frac{D_s}{\nu}\ 0.1(\frac{\gamma_s}{\gamma} - 1)gD_s$ and finding the point of intersection with the dimensionless shear stress curve. The corresponding ordinate, F_*, is set equal to the Shield's parameter, that is

$$F_* = \frac{\tau_c}{(\gamma_s - \gamma)D_s} \tag{15-88}$$

For values of the boundary Reynolds number greater than 500, $F_* = 0.060$. However, Gessler (1965) suggested reducing $F_* = 0.047$ for Reynolds numbers greater than 500. The program allows the user to enter F_* or use a default value of $F_* = 0.047$.

Example

1. $D_s = 0.002$ ft

for $F_* = 0.047$ $\tau_c = 0.0001551$ lb/ft^2

2. $D_s = 0.002$

for $\frac{D_s}{\nu}\sqrt{0.1(\frac{\gamma'_s}{\gamma} - 1)gD'_s} = 2$

and $\frac{U * D_s}{\nu} = 11$

$F_* = 0.032$

$\tau_c = 0.0001056$ lb/ft^2

Effective Shear Stress

The effective boundary shear stress τ_e acting on the grain can be expressed as

$$\tau_e = \frac{1}{8} \rho f V^2 \qquad (15\text{-}89)$$

where ρ is the density of water, f is the Darcy-Weisbach friction factor and V is the average flow velocity.

Example

$f = 0.03$

$V = 2$ ft/sec

$\tau_e = 0.02$ lb/ft^2

Meyer-Peter, Müller sediment transport equation is discussed in Chapter 10, but is repeated again for clarity. Two programs are provided using this theory; one for bed load only and one that combines both bed load and Einstein's suspended load approximation. These programs may be used for only one representative sediment size; however, best results will be achieved by routing by size fractions.

The Meyer-Peter, Müller equation is a simple and commonly used bed load transport equation (see USBR, 1960). It is

$$q_b = \frac{12.85}{\sqrt{\rho}\ \gamma_s} (\tau_e - \tau_c)^{1.5} \qquad (15\text{-}90)$$

in which

$$\tau_c = \delta_s(\gamma_s - \gamma)d_s \tag{15-91}$$

For suspended sediment the sediment concentration profile which relates the sediment concentration with depth above the bed (Einstein, 1950) can be written as

$$\frac{C_\xi}{C_a} = \left(\frac{R-\xi}{\xi}\frac{a'}{R-a'}\right)^\eta \tag{15-92}$$

in which C_ξ is the sediment concentration at the idstance ξ from the bed, C_a is the known concentration at a distance a' above the bed, and w is a parameter defined as

$$\eta = \frac{w}{\kappa U_*} \tag{15-93}$$

In Equation 15-93 w is the settling velocity of the sediment particles, κ is the Karman constant (assumed 0.4), and U_* is the shear velocity of the flow defined as

$$U_* = \left(\frac{\tau_e}{\rho}\right)^{1/2} \tag{15-94}$$

Note that

$$\tau_e = \frac{1}{8}f\rho V^2 \tag{15-95}$$

where f is the overall Darcy-Weisbach resistance factor.

A logarithmic velocity profile is commonly adopted to describe velocity distribution in turbulent flows. A useful equation is

$$\frac{u_\xi}{U_*} = B + 2.5\ \ell n\left(\frac{\xi}{\eta s}\right) \tag{15-96}$$

in which u_ξ is the point mean velocity at the distance ξ from the bed, B is a constant dependent on roughness, and η_s is the roughness height.

The integral of suspended load above the a' level in the flow is obtained by combining Equations 15-92 and 15-96 or

$$q_s = \int_{a'}^{R} u_\xi C_\xi \xi = C_a U_* \int_{a'}^{R} \left[B + 2.5\ \ell n\left(\frac{\xi}{\eta_s}\right)\right]\left(\frac{R-\xi}{\xi}\frac{a'}{R-a'}\right)^\eta d\xi \tag{15-97}$$

Let

$$\sigma = \frac{\xi}{R} \tag{15-98}$$

and

$$G = \frac{a'}{R} \tag{15-99}$$

The equation becomes

$$q_s = \int_{a'}^{R} u_\xi C_\xi d\xi = C_a U_* \int_{a'}^{R} [B + 2.5 \ln(\frac{\xi}{\eta_s})](\frac{R-\xi}{\xi} \frac{a'}{R-a'})^\eta d\xi \tag{15-100}$$

If the bed load q_b from Meyer-Peter, Müller is used then

$$q_s = \frac{q_b}{11.6} \frac{G^{\eta-1}}{(1-G)^\eta} [(\frac{V}{U_*} + 2.5) I_1 + 2.5 I_2] \tag{15-101}$$

where the average flow velocity V is defined by the equation

$$V = \frac{\int_0^R u_\xi d\xi}{\int_0^R d\xi} \tag{15-102}$$

and

$$\frac{V}{U_*} = B + 2.5 \ln(\frac{R}{\eta_s}) - 2.5 \tag{15-103}$$

Einstein (1950) defined the two integrals in Equation 15-100 as

$$I_1 = \int_G^1 (\frac{1-\sigma}{\sigma})^\eta d\sigma \tag{15-104}$$

and

$$I_2 = \int_G^1 (\frac{1-\sigma}{\sigma})^\eta \ln\sigma \, d\sigma \tag{15-105}$$

The integrals I_1 and I_2 cannot be integrated in closed form for most values of w so a numerical integration is necessary. An efficient numerical method of determining I_1 and I_2 was developed by Li (1974).

The total load per unit width of channel is

$$q_t = q_b + q_s \qquad (15\text{-}106)$$

Equation 15-106 gives the total load per unit width of channel for a uniform size of sediment in the bed. A combined example appears at the end of the section on Shen and Hung's transport equation.

Lu's Sediment Transport Equation

Lu (1978) developed a transport equation based on experimental flume and river data. His equation was developed based on a nonlinear regression analysis. The results are summarized in the table below.

Table 5.1 Final results of nonlinear regression analysis.

Equation Form					$Y = P1 + P2 \cdot e^{P3 \cdot X1} + P4 \cdot X2 + P5 \cdot X3$					
in which					$Y = \log(C_t)$		$X2 = \log(\frac{w \cdot d}{\nu})$			
					$X1 = F = \frac{V}{\sqrt{g \cdot D}}$		$X3 = \log(\frac{D}{d})$			
Group	# of Data	F	log R	s^2	Corr. $(y,\hat{y})$	P1	P2	P3	P4	P5
(I)	104	<0.2	6.0 | 7.5	0.0553	0.883	1.0027	-4.0680	-15.041	-0.27675	0.46207
(II)	262	≥0.2	<5.0	0.0560	0.916	3.8651	-7.0711	-4.8363	-0.29139	0.02705
(III)	229	≥0.2	≥5.0	0.0555	0.885	2.5670	-4.9855	-4.0863	0.03739	0.41082
C_t : P.P.M., Sediment Concentration					F : Froude number = $\frac{V}{\sqrt{g \cdot D}}$					
w : fps, Fall Velocity of Particle					R : Reynolds number $\frac{V \cdot D}{\nu}$					
d : ft, Median Diameter of Particle					g : Gravitational Acceleration					
ν : ft^2/sec, Kinematic Viscosity					s^2 : Error Mean Square (from BMD07R)					
V : fps, Average Velocity					P1, P2, P3, P4, and P5: Coefficients					
D : ft, Hydraulic Depth										
Corr$(y,\hat{y})$: Correlation coefficient between measured value, y, and predicted value, $\hat{y}$										

Yang's Sediment Transport Equation

According to Yang (1976) the following stream power equation can be utilized for calculation and prediction of total bed material concentration transported in sand bed flumes and rivers:

$$\log C_t = 5.435 - 0.286 \log \frac{wD}{\nu} - 0.457 \log \frac{U_*}{w} + (1.799 - 0.409 \log \frac{wD}{\nu} - 0.314 \log \frac{U_*}{w}) \log(\frac{US}{w} - \frac{U_{cr}S}{w}) \quad (15\text{-}107)$$

where

C_t = total sediment concentration in parts per million by weight

D = median sieve diameter

S = water surface slope or energy slope

U_* = shear velocity

U = average water velocity

U_{cr} = critical average water velocity at incipient motion

ν = kinematic viscosity

w = terminal fall velocity

The term $\frac{U_{cr}}{w}$ can be calculated as

$$\frac{U_{cr}}{w} = \frac{2.5}{\log(\frac{U_*D}{\nu}) - 0.06} + 0.66 \quad \text{when } 1.2 < \frac{U_*D}{\nu} < 70 \quad (15\text{-}108)$$

and

$$\frac{U_{cr}}{w} = 2.05 \text{ when } 70 \leq \frac{U_*D}{\nu} \quad (15\text{-}109)$$

In this program the terminal fall velocity is calculated from the median grain size and the kinematic viscosity by the method presented in the fall velocity program.

Example

A combined example for sediment transport is provided after the program on Shen and Hung's method.

Shen and Hung (1971) began with the assumption that sediment transport is such a complex phenomenon that no single Reynolds number, Froude number, or combination of them can be found to describe sediment motion under all conditions. They recommended a regression method be used to develop a formula based on all available data for immediate engineering purposes. They selected the sediment concentration (bed material load) as the dependent variable and the fall velocity of the median sediment particle of the bed sample as well as the flow velocity and flow depth as the independent variables. The equation is

$$\log C = a_0 + a_1 X + a_2 X^2 + a_3 X^3 \qquad (15\text{-}110)$$

where

$$X = V^{a_4} S^{a_5} W^{a_6} D^{a_7} \qquad (15\text{-}111)$$

a_0 through a_7 are the parameters to be determined by regression technique, C is the sediment bed material load concentration by weight (wash load is arbitrarily taken to be less than 0.0625mm), V is the average flow velocity, S is the energy slope, W is the fall velocity of the median size sediment of the bed sample, and D is the flow depth. The sediment particle fall velocity was corrected to that of the actual measured water temperature and no attempt was made to include the effect of heavy sediment concentration (if exists).

With a total of 587 data points, the final results were $a_0 = -107404.45938164$, $a_1 = 324214.74734085$, $a_2 = -326309.58908739$, $a_3 = 109503.87232539$, $a_4 = 0.00750189$, $a_5 = 0.00428802$, $a_6 = -0.00239974$, and a_7 was very small as compared to a_4, a_5, and a_6 and subsequently was dropped for the final analysis.

Example for MPM, Lu's, Yang's, Shen and Hung

$Y = 0.51$ ft

$V = 2.89$ ft/sec

$Q = 11.79$ cfs

$\nu = 0.0000111$

$a_5 = 0.047$

$b_5 = 1.5$

$F_o = 0.025$

$S = 0.0017$

T_w = 8 ft

d_s = 0.19 mm

Lu's

```
.510 ENT↑
2.890 ENT↑
11.790 GSBA

.0000111 GSBB

.000623 GSBC

0.001  ***

3288.479  ***
0.015  ***
2.419  ***
```

C_t = 3288.479 PPM

= 0.015 cfs

= 2.419 lb/sec

MPM (Bed load)

```
.047 ENT↑
1.50 GSBA

.025 ENT↑
.0000111 GSBB

.51 ENT↑
.0017 ENT↑
2.89 ENT↑
8.00 GSBC

.000623 ENT↑
1.00 GSBD

6.230000000-04  ***
4.632062821-03  ***
0.77  ***
```

q_{sb} = 4.6 x 10^{-3} cfs

= 0.77 lb/sec

Yang's

```
.510 ENT↑
.0017 ENT↑
2.890 ENT↑
11.790 GSBA

.0000111 GSBB

.000623 GSBC

0.001  ***

2117.066  ***
0.009  ***
1.558  ***
```

C_t = 2117.066 PPM

= 0.009 cfs

= 1.558 lb/sec

Shen and Hung's

```
11.790 ENT↑
.0000111 GSBA

2.890 ENT↑
.0017 GSBB
.000623 GSBC

0.301  ***

2003.088  ***
0.009  ***
1.474  ***
```

C_t = 2003.088 PPM

= 0.009 cfs

= 1.474 lb/sec

Degradation-Aggradation Analysis

A simple calculation of degradation or aggradation may be obtained using a method based on the sediment continuity equation. Assuming no lateral inflow, the sediment continuity equation may be written as

$$\frac{\partial Q_s}{\partial x} + (1 - \lambda) \frac{\partial A_s}{\partial t} = 0 \qquad (15\text{-}112)$$

where Q_s is the volume sediment discharge, λ is the bed material porosity, A_s is the change in cross-sectional bed area, t it time and x is distance. In simple finite difference formulations

$$\frac{\Delta Q_s}{\Delta x} + (1 - \lambda) \frac{\Delta A_s}{\Delta t} = 0 \qquad (15\text{-}113)$$

Therefore, the change in area may be calculated as

$$\Delta A_s = - \frac{\Delta Q_s \, \Delta t}{\Delta x(1-\lambda)} \qquad (15\text{-}114)$$

The change in Q_s may be expressed as

$$q_{s_2} B_2 - q_{s_1} B_1 = \Delta Q_s \qquad (15\text{-}115)$$

where B_i is the channel width at Station i and q_{s_i} is the sediment volume discharge per unit width at Station i. In addition, ΔA_s may be expressed as

$$\Delta A_s = \frac{B_1+B_2}{2} \Delta z \qquad (15\text{-}116)$$

where Δz is the average change in bed elevation. Equating Equations 15-114 and 15-116 yields

$$\Delta z = - \frac{2Q_s \, \Delta t}{\Delta x(1-\lambda)(B_1+B_2)} \qquad (15\text{-}117)$$

or using Equation 15-115

$$\Delta z = - \frac{2\Delta t(B_2 q_{s_1} - B_1 q_{s_1})}{\Delta x(1-\lambda)(B_1+B_2)} \qquad (15\text{-}118)$$

This change in bed elevation is an average change over the entire Δx. If there is a control at the downstream end, the average change in bed elevation should be redistributed over Δx giving no change at the downstream end and $2\Delta z$ at the upstream end. Equation 15-118 may be used in conjunction with a transport equation to provide for dynamic

slope. That is, if the water hydrograph is subdivided into several Δts. The degradation-aggradation equation may be run for the first Δt and the slope updated by $2\Delta z$. Then the new slope may be used in the transport equation to calculate a new value of q_s. This q_s may then serve as input to the aggradation-degradation equation, and so forth.

Example

For $q_{s_1} = 300$ cfs

$q_{s_2} = 310$ cfs

$B_1 = 200$ feet

$B_2 = 20$ feet

$\Delta x = 200$ feet

$\Delta t = 60$ sec

$\lambda = 0.4$

$\Delta z = -5.0$

Local Scour Calculation

According to Liu et al. (1961), the equilibrium local scour may be estimated from

$$S = 1.1\, y\, \left(\frac{L_s}{y}\right)^{0.4} F_r^{0.33} \qquad (15\text{-}119)$$

where S is the depth of local scour, y is the upstream depth, L_s is a measure of the encroachment length and F_r is the Froude number.

Example

For $F_r = 2$

$y = 5$ feet

$L_s = 10$ feet

$S = 9.12$ feet

Design of Riprap

The common acceptable methods for sizing the riprap are discussed in Simons and Sentürk (1977). The method developed by Stevens and Simons (1971) is utilized in this analysis. The details are given in Simons and Sentürk (1977).

The safety factor for rock riprap in side slopes above the flow has a horizontal velocity vector is related to properties of the particle, side slope and flow by the following equation

$$SF = \frac{\cos\theta\tan\phi}{\eta'\tan\phi + \sin\theta\cos\beta} \tag{15-129}$$

where SF is the safety factor, θ is the side slope angle and ϕ is the angle of repose and β and η' are given below

$$\beta = \tan^{-1}\left(\frac{\eta\tan\phi}{\sin\theta}\right) \tag{15-121}$$

and

$$\eta' = \eta\left(\frac{1 + \sin\beta}{2}\right) \tag{15-122}$$

The parameter η is given by

$$\eta = \frac{21\tau_s}{(\gamma_s - \gamma)d_{50}} \tag{15-123}$$

Where γ_s is the specific weight of the rock, γ is the specific weight of water, d_{50} is the median diameter of the riprap and τ_s is given below.

$$\tau_s = r\,\tau_o \tag{15-124}$$

where

$$\tau_o = \gamma y_o S \tag{15-125}$$

where y_o is the normal flow depth and S is the friction slope. The ratio r is obtained from Figure 15.9. The angle of repose, ϕ may be obtained from Figure 15.10.

Example

Given design side slope 2.5 to 1, selected median riprap size of 2 ft, subject to a design shear stress of 4.66 lb/ft^2, find the safety factor.

From Figure 15.9, $r = 0.77$

From Figure 15.10, $\phi = 41°$ (for very angular rock)

Side slope $\theta = \tan^{-1}(\frac{1}{2.5}) = 21.8°$

Result: $SF = 1.43$

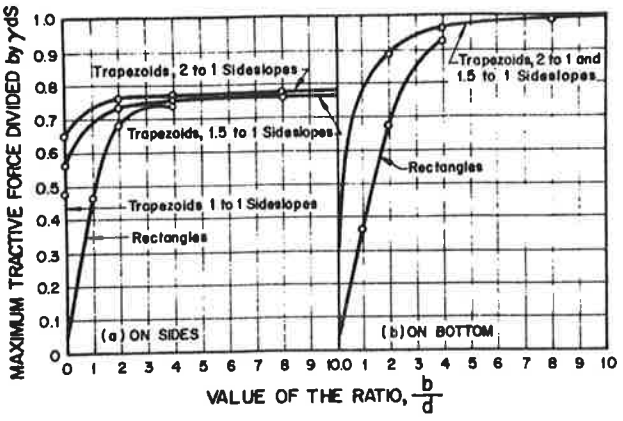

Figure 15.9 Variation of τ in a trapezoidal cross section.

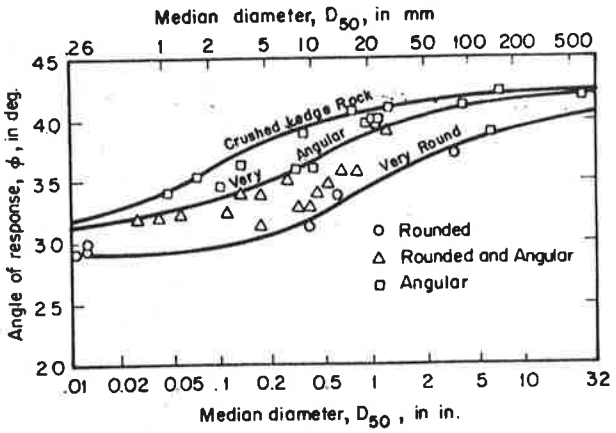

Figure 15.10 Angle or repose for dumped riprap (after Simons, 1957).

Note: Gravel filter or some other type of filter is always required if the bed material cannot provide adequate drainage.

15.3 COMPREHENSIVE EXAMPLE 1: DIVERSION DITCH DESIGN

HP-97

Problem Statement

A diversion ditch is needed to collect the runoff from an area of approximately 118 acres. The ditch must be designed to carry the runoff resulting from the expected 100-year six-hour precipitation. The ditch is to be earth-lined.

The following data is available or has been estimated. The watershed is approximated by a single plane with:

Length = 4664' and Width = 1100'

Overland slope = .025, Channel slope - .005

Overland resistance K_{high} = 20,000

Percentage of ground cover = 25%

The watershed is located near Casper, Wyoming.

Problem Solution Approach

The rainfall is determined through the Bureau of Reclamation method presented in USBR (1974). The value of rainfall during the six-hour period is determined from Hershfield (1961). The intensities are then determined by using the Hydrograph Synthesis program. From these intensities the excess intensities are determined using the Green-Ampt infiltration program. The q vs. y relationship is calculated using the resistance to overland flow program. The design hydrograph is then developed using the kinematic wave method of characteristics routing program. The peak discharge is selected and the channel designed using the normal depth for trapezoidal channels program making sure that the velocity of flow is kept low to prevent erosion.

Program Results

Hydrograph Synthesis Program. Input: 3.1 inches total value, six hour storm, zone C, r = 1.0 (note: since the area is so small, no reduction needs to be applied to the point rainfall).

Output:

```
3.100E+00  ***          180.0  ***
                     5.167-03  ***
       0.
0.000E+00  ***          210.0  ***
                     5.167-03  ***
     30.0  ***
 3.100-02  ***          240.0  ***
                     4.133-03  ***
     60.0  ***
 1.860-02  ***          270.0  ***
                     4.133-03  ***
     90.0  ***
 9.300-03  ***          300.0  ***
                     4.133-03  ***
    120.0  ***
 7.233-03  ***          330.0  ***
                     4.133-03  ***
    150.0  ***
 7.233-03  ***          360.0  ***
                     3.100-03  ***
```

Green-Ampt Infiltration Program. Input: Δt = 30 minutes. Intensities from previous program converted to inches/minute.

Converted Intensities

Time (min)	Intensity (in/min)
30	.0310
60	.0186
90	.0093
120	.0072
150	.0072
180	.0052
210	.0052
240	.0041
270	.0041
300	.0041
330	.0041
360	.0031

γ = .160; K_w = .00583 in/min.

Output:

0.0319	***	0.0072	***
30.0000	***	30.0000	***
1.9678-03	***	3.2734-04	***
30.0000	***	120.0000	***
0.0186	***	0.0072	***
30.0000	***	30.0000	***
1.0732-03	***	5.2039-04	***
60.0000	***	150.0000	***
0.0093	***	0.0052	***
30.0000	***	30.0000	***
2.1055-03	***	0.0000	
90.0000	***	180.0000	***
		0.0052	***
		30.0000	***
		0.0000	
		210.0000	***

Note: for the intensities less than K_w the excess is always zero. This is why the calculations are not carried out for the entire storm.

Overload Flow Resistance Program. Input: c_g = .25 (25%); K_h = 20,000; K_ℓ = 100; S_o = .025.
Output:

1342.75	***
439.68	***
3.00	***

Kinematic Wave-Method of Characteristics. Input:

α = 439.68

β = 3.0

L = 4664.09 ft

$\alpha\beta$ = 1319.04

Excess Intensities Converted to ft/sec

Time (min)	Intensity (ft/sec)
30	27.33×10^{-6}
60	14.91×10^{-6}
90	2.92×10^{-6}
120	0.45×10^{-6}
150	0.72×10^{-6}
180	0.0

For the first characteristic all excesses are input at 600-second intervals. The remaining characteristics are started 600 seconds after the preceeding characteristic. The first excess on these characteristics are input for the entire interval remaining (600, 1200 or 1800 seconds). The following excesses are input for their entire 1800 second interval.

Output:

x_i ⟶ 0.0000 ***
x_{i+1} ⟶ 70.9365 ***

q_L ⟶ 1.9387-03 ***
x_{L+1} ⟶ 70.9365 ***
567.4920 ***

1.5510-02 ***
567.4920 ***
1915.2854 ***

5.2345-02 ***
1915.2854 ***
4199.9809 ***

8.6410-02 ***
4199.9809 ***

C_0 Characteristic →
2501.4295 ***
5.3329-02 ***
4199.9805 ***

0.0000 ***
567.4920 ***

C_1 Characteristic →
2746.1096 ***
7.6590-02 ***
567.4920 ***

0.0000 ***
70.9365 ***
2324.3027 ***

C_2 Characteristic →
3293.6678 ***
4.2369-02 ***
2324.3027 ***

0.0000 ***
570.0455 ***
2636.9615 ***

C_3 Characteristic →
5061.8548 ***
1.5447-02 ***
2636.9615 ***

C_4 Characteristic →

x_1	0.0000	***
x_2	168.3824	***
x_3	1174.1039	***
x_4	2491.3464	***
x_5	3929.1941	***
t_L	7473.5856	***
q_L	7.8815-03	***
x_5	3929.1941	***

The resulting hydrograph is

Time (min)	Discharge (cfs/ft width)	Discharge* (cfs)
10.00	0.0019	2.09
20.00	0.0155	17.05
30.00	0.0523	57.53
40.00	0.0864	95.04
41.69	0.0933	102.63
55.77	0.0766	84.26
74.90	0.0424	46.64
114.36	0.0155	17.05
167.83	0.0071	7.81

*The values in Column 2 multiplied by the plane width of 1100 ft.

Normal Depth Program and Design. The peak discharge of 102.63 cfs is the design discharge. The channel will be built in a soil that is mostly fine and medium sands. From Chow (1959) the velocities should be 1 ft/sec or less (see graph below). The Manning's n for such a channel is around 0.025. The first design will be a triangular channel with 3:1 side slopes. The channel is to be built at a .5% slope.

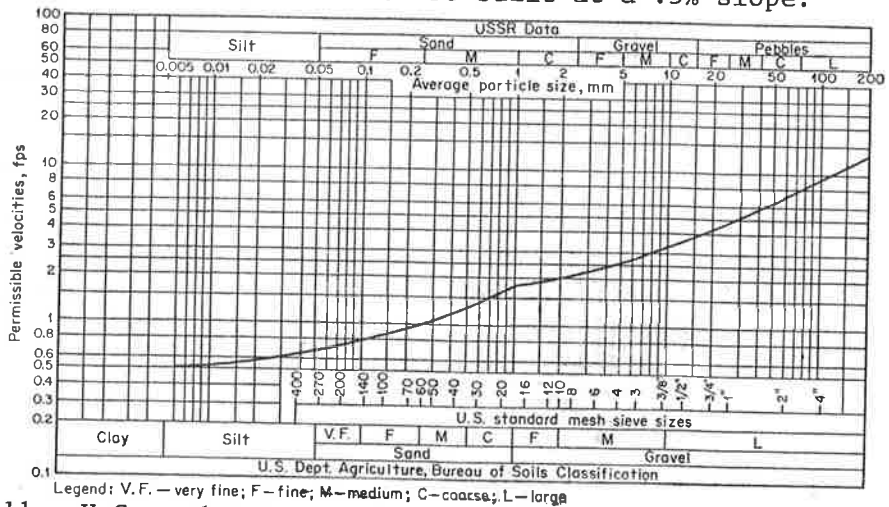

Figure 15.11 U.S. and U.S.S.R. data on permissible velocities for non-cohesive soils (after Chow, 1959).

Input: Z = 3 (bank slope 3:1)

b = 0

Q = 102.63 cfs

S = .005

n = .025

initial guess for y = 5'*

maximum number of iterations (N) = 20

*The guess should be made high since the program has no difficulty converging from a high guess. If the guess is low, sometimes an error message is printed. If so, make a higher guess.

```
2.80  ***
2.66  ***
2.65  ***
2.65  ***

2.65  ***
2.40-06  ***
4.  ***

20.99  ***
4.89  ***
```

The normal depth is 2.65 ft. However, the velocity of 4.89 ft/sec is too high. Another design with a wider channel might reduce the velocity.

Second design input: Z = 3

b = 10 ft

Q = 102.63 cfs

S = .005

n = .025

$y_{initial}$ = 3.0

N = 20

Output:

```
2.20  ***
1.69  ***
1.55  ***
1.53  ***
1.53  ***

1.53  ***
2.20-06  ***
5.  ***

22.41  ***
4.58  ***
```

The normal depth is 1.53 feet, but again the velocity of 4.58 ft/sec is too high. Since the slope cannot be changed and a reasonable geometry cannot be found which will reduce the velocity, the bank must be protected. For details on the procedure to protect the bank, see Example 2.

EXAMPLE 1 (TI-59): DIVERSION DITCH DESIGN

Problem Statement and Solution Approach

The problem statement and solution approach are the same as for the HP-97. However, because the TI-59 programs vary in the format of their input and output, the problem will be solved again using the programs available for the TI-59.

Program Results

Hydrograph Synthesis Program. Input: V = 3.1 inches
zone C

Output:

1.86 30.	0.31 210.
1.116 60.	0.248 240.
0.558 90.	0.248 270.
0.434 120.	0.248 300.
0.434 150.	0.248 330.
0.31 180.	0.186 360.

Green-Ampt Infiltration Program. Input: The time and rainfall intensities from the previous program (minutes and inches/hr).

γ = .160 inches

K_w = .35 in/hr

Output:

.0196732699
30.
.0107282769
60.
.0021019921
90.
.000357211
120.
.000550297
150.
0.
180.

Overload Flow Resistance Program. Input: C_g = .25 (25%)

K_h = 20,000

K_ℓ = 100

S_o = .025

Output:

439.684233

Kinematic Wave--Method of Characteristics Program. Input:

α = 439.68

β = 3.00

L = 4664.09

The times and intensities that were computed in the Green-Ampt Infiltration Program broken up into 10 minute blocks.

Time (min)	Intensity (in/min)
10	.01967
20	.01967
30	.01967
40	.01073
50	.01073
60	.01073
70	.00210
80	.00210

(continued)

Time (min)	Intensity (in/min)
90	.00210
100	.00036
110	.00036
120	.00036
130	.00055
140	.00055
150	.00055
160	0.0

Output:

```
            1. 01          55.7839952
1.9453227-03               .0765488134

           20.                7.4923053 01
.0155270595                   4.2318975-02

           30.                1.1437119 02
.0523639042                    1.552394-02

           40.              164.0781013
.0864169913                .0072121582

41.68454818
.0933088673
```

The resulting hydrograph is

Time (min)	Discharge (cfs/ft width)	Discharge* (cfs)
10	.00019	2.09
20	.0155	17.05
30	.0524	57.64
40	.0864	95.04
41.68	.0933	102.63
55.78	.0765	84.15
74.92	.0423	46.53
114.37	.0155	17.05
164.08	.0072	7.92

*The values in Column 2 are multiplied by the plane width of 1100 feet.

Normal Depth Program and Design (Trapezoidal Channel). The same procedure is followed as for the HP-97 example.

Input: z = 3

b = 0

Q = 102.63 cfs

n = .025

y_o initial guess = 3.0 ft

Output:

```
2.642472429
20.94800256
4.899273796
```

The normal depth is 2.64 feet. However, the velocity of 4.90 ft/sec is too high. Another design with a wider channel might reduce the velocity.

Second Design. Input: z = 3

b = 10 ft

Q = 102.63 cfs

S = .005

n = .025

$y_{initial}$ = 3.0 ft

Output:

```
1.53239303
22.36862254
4.588123377
```

The normal depth is 1.53 feet, but again the velocity of 4.59 ft/sec is too high. Since the slope is determined by the topography and cannot be changed, and a reasonable geometry cannot be found which will reduce the velocity, the bank must be protected. For details on the procedure to protect the bank, see Example 2.

15.4 COMPREHENSIVE EXAMPLE 2: FLOOD PROETECTION DESIGN

Problem Statement

A proposed building site is to be located adjacent to a natural stream (Figure 15.12). The planners have decided the site should be protected against a design storm of 100-year return period and six-hour duration occurring on the 30-square mile watershed above the site. The channel alignment must remain the same due to property constraints. Flooding is to be prevented only on the side of the channel on which the building site is located.

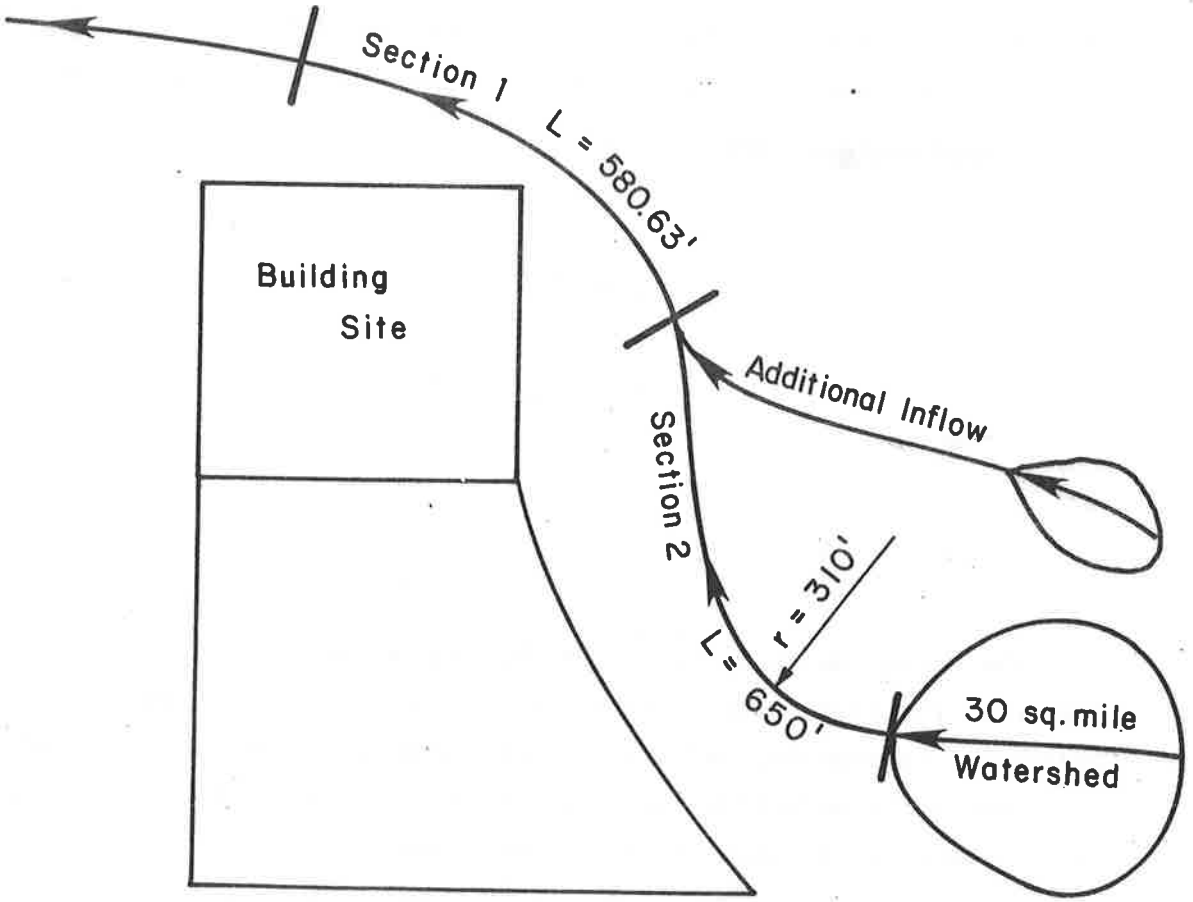

Figure 15.12 Plan view of channel and building site.

Solution Approach

The first portion of the solution is similar to design Example 1. The rainfall is determined in the same manner with the addition of a reduction factor to account for the difference between the predicted point rainfall and that for the 30-square mile watershed. The excesses are then determined as before using the Green-Ampt infiltration program. The watershed is approximated by an "Open Book" watershed of two planes and one channel. The channel is considered to be triangular with side-slopes of the same slope as the planes intersecting to form it. The runoff hydrograph is determined by implementation of the kinematic wave method of characteristics program three times, once for each plane and then for the channel.

The next step is the routing of the hydrograph from the watershed through the channel at the site. Due to the high discharges and alluvial material in the channel, a rigid boundary approach would not be applicable. A movable bed approach is employed. The first assumption is the channel flows in the upper regime with antidunes. This would indicate a lower Manning's n than would be predicted otherwise. To check this, the calculations are carried out with the lower n and then the flow regime checked.

To accomplish the routing, first the cross section geometric relationships are determined with the use of the channel cross section properties programs. Next, the hydrograph is routed through the channel which is divided into two sections. At the upstream end of the second channel section, an additional watershed flows in. The hydrograph for this watershed is given. The Muskingum-Cunge flood routing program is used to route the water through each reach. Next, the normal depth program is used to determine the flow conditions used later and to verify the assumption of upper regime flow.

The third set of calculations is concerned with the movable bed. The height of the antidunes is determined by calculating the flow conditions for the peak discharge in each section. The lognormal distribution for sediment size program is used to develop the sediment size distribution. The sediment transport rates for each size are determined using the Meyer-Peter Müller program. The change in the depth of the

bed for each reach due to general scour is computed through the degradation-aggradation program. The local scour program is then used.

The final step is the actual design of the bank. First, the riprap design program is used to size the riprap. Then the height to build the bank is evaluated from adding quantities from earlier analysis such as normal depth and antidune height. Likewise, the depth to bury the riprap is determined.

Results

Point Rainfall to Area Rainfall Conversion Program

Input: A = 30 mi^2

Zone C

Output:

30.000 ***
0.973 ***

Hyetograph Synthesis Program. Input: Zone C

v = 3.1 inches

r = .973

Output:

0.		210.0	***
0.0000+00	***	5.027-03	***
30.0	***	240.0	***
3.016-02	***	4.022-03	***
60.0	***	270.0	***
1.810-02	***	4.022-03	***
90.0	***	300.0	***
9.049-03	***	4.022-03	***
120.0	***	330.0	***
7.038-03	***	4.022-03	***
150.0	***	360.0	***
7.038-03	***	3.016-03	***
180.0	***		
5.027-03	***		

Green-Ampt Infiltration Program. Input: γ = .16 in.

K_w = .00583 in/min

Δt = 30 min

The following converted rainfall intensities.

Time (min)	Intensity (in/min)
30	.03016
60	.01810
90	.00905
120	.00704
150	.00704
180	.00503
210	.00503
240	.00402
270	.00402
300	.00402
330	.00402
360	.00302

Output:

```
   0.030160000  ***          0.007540000  ***
  30.00000000   ***         30.00000000   ***
1.383762673-02  ***      3.603942000-04   ***
  30.00000000   ***        150.0000000    ***

   0.018100000  ***          0.005030000  ***
  30.00000000   ***         30.00000000   ***
1.023194765-02  ***          0.000000000
  60.00000000   ***        180.0000000    ***

   0.009050000  ***          0.005030000  ***
  30.00000000   ***         30.00000000   ***
1.855519058-03  ***          0.000000000
  90.00000000   ***        210.0000000    ***

   0.007040000  ***
  30.00000000   ***
1.673424670-04  ***
 120.0000000    ***
```

Darcy-Weisbach Resistance Program. Input: for left plane

C_g = .30

K_h = 20,000

K_l = 100

S = .07

for right plane

$C_g = .30$

$K_h = 20{,}000$

$K_l = 100$

$S = .05$

Output:

Left		Right	
1891.00	***	1891.00	***
874.83	***	624.63	***
3.00	***	3.00	***

Kinematic Wave - Method of Characteristics Program (Left Plane).

Input: $\alpha = 874.83$

$\beta = 3.0$

$L = 30403.6$

$\alpha\beta = 2624.49$

The following converted excesses are used as input data.

Time (sec)	Excess (ft/sec)
1800	26.16×10^{-6}
3600	14.21×10^{-6}
5400	2.58×10^{-6}
7200	0.23×10^{-6}
9000	0.50×10^{-6}
10800	0.0

Output:

$x_o \longrightarrow$ 0.0000	***	1.5048-01 ***
$x_1 \longrightarrow$ 129.3162	***	7653.4265 ***
		13309.6453 ***
$q_L \longrightarrow$ 3.3929-03	***	
$x_1 \longrightarrow$ 129.3162	***	2.3004-01 ***
$x_2 \longrightarrow$ 1034.5295	***	13308.6453 ***
		20686.1310 ***
$q_L \longrightarrow$ 2.7063-02	***	
1034.5295	***	3.3567-01 ***
3491.5371	***	20686.1310 ***
		29179.4529 ***
9.1335-02	***	
3491.5371	***	3.5759-01 ***
7653.4265	***	29179.4529 ***

```
 4284.4389  ***
 3.6874-01  ***
29179.4529  ***

    0.0000  ***
 1034.5295  ***
10513.3068  ***
27129.5023  ***

 5128.2132  ***
 2.0538-01  ***
27129.5023  ***

    0.0000  ***
  129.3162  ***
 4219.9684  ***
13207.1019  ***
23257.7276  ***
```

```
 7251.4008  ***
 3.0582-02  ***
23257.7276  ***

    0.0000  ***
 1038.2185  ***
 4715.9814  ***
 9090.1900  ***
13655.5754  ***
18353.7661  ***
23051.9568  ***
27750.1475  ***

13616.6372  ***
 2.7437-02  ***
27750.1475  ***
```

Kinematic Wave - Method of Characteristics Program (Right Plane).

Input: α = 624.88

β = 3.00

L = 25353.2

$\alpha\beta$ = 1874.64

The same converted excesses and times that are used for the left plane are used as input data.

Output:

```
    0.0000  ***
 92.3689    ***

2.4164-03   ***
 92.3689    ***
738.9513    ***

1.9331-02   ***
738.9513    ***
2493.9608   ***

6.5242-02   ***
2493.9608   ***
5466.7457   ***

1.8749-01   ***
5466.7457   ***
9506.1969   ***

1.8489-01   ***
9506.1969   ***
14775.8416  ***
```

```
 2.3977-01  ***
14775.8416  ***
20842.5140  ***

 2.5542-01  ***
20842.5140  ***

4630.3988   ***
 2.6706-01  ***
20842.5140  ***

    0.0000  ***
 738.9513   ***
 7505.5220  ***
19378.2602  ***

5636.9523   ***
 1.4754-01  ***
19378.2602  ***
```

0.0000	***	0.0000	***
92.3609	***	735.8720	***
3614.2700	***	3366.5659	***
8433.6050	***	6493.0077	***
16612.7906	***	9754.0047	***
23997.8251	***	13109.8629	***
		16465.7211	***
8124.8761	***	19821.5793	***
6.5842-02	***	23177.4375	***
23997.9851	***		
		15567.8257	***
		1.9598-02	***
		23177.4375	***

Kinematic Wave - Method of Characteristics Program (Channel)

Input: Assume that the two planes intersect to form a triangular channel with the same side slopes as the planes. For the triangular case:

$\beta = 1.25$

$$\alpha = \left(\frac{8gS_o}{fa_1}\right)^{1/2}$$

where

$$a_1 = \left(\frac{2}{1/S_L + 1/S_R}\right)^{1/2} \left[\left(1 + \frac{1}{S_L^2}\right)^{1/2} + \left(1 + \frac{1}{S_R^2}\right)^{1/2}\right]$$

$S_L = .07, \quad S_R = .05$

$a_1 = 8.2953$

$f = .04$

therefore,

$\alpha = 3.9404$

$L = 15{,}000$ feet

Since the lateral inflows from the left and right planes do not occur at the same time after the C_o characteristic reaches the downstream boundary, the inflows must be put on a common time basis in order to be added together. Once added together, they serve as the excess input for the channel. First the times at which the inflows are to be taken are chosen. Then the lateral inflows for each plane are linearly interpolated to the specified time periods. The next step is to sum the inflows. Finally, the summed inflows are averaged between time periods to determine the average inflow over each time interval.

Results before interpolation:

RIGHT PLANE		LEFT PLANE	
Time (min)	q_ℓ (cfs/ft)	Time (min)	q_ℓ (cfs/ft)
10	3.3829×10^{-3}	10	2.4164×10^{-3}
20	2.7063×10^{-2}	20	1.9331×10^{-3}
30	9.1339×10^{-2}	30	6.5242×10^{-2}
40	1.5048×10^{-1}	40	1.0749×10^{-1}
50	2.3084×10^{-1}	50	1.6489×10^{-1}
60	3.3567×10^{-1}	60	2.3977×10^{-1}
70	3.5759×10^{-1}	70	2.5542×10^{-1}
71.41	3.6074×10^{-1}	77.17	2.6706×10^{-1}
95.47	2.0538×10^{-1}	103.95	1.4754×10^{-1}
140.86	9.0582×10^{-2}	155.40	6.5842×10^{-2}
256.94	2.7437×10^{-2}	289.45	1.9598×10^{-2}

Interpolation Results:

Time (min)	Discharges (ft^2/sec)			
	Left	Right	Left & Right	Average
0	0.0	0.0	0.0	
10	.0034	.0024	.0058	.0029
20	.0271	.0193	.0464	.0261
30	.0913	.0652	.1565	.1014
40	.1505	.1075	.2580	.2072
50	.2308	.1649	.3957	.3269
60	.3357	.2398	.5755	.4856
70	.3576	.2554	.6130	.5943
80	.3053	.2544	.5597	.5864
100	.1939	.1652	.3591	.4594
150	.0856	.0744	.1600	.2596
250	.0312	.0332	.0644	.1122

Output:

```
         0.0000  ***          1769.7885  ***
      2715.3691  ***          8.7225+02  ***
                              7778.8670  ***
      7.8746+00  ***
      2715.3691  ***             0.0000  ***
      7778.8670  ***          4703.1573  ***
                             12284.4086  ***
      1.4003+02  ***
      7778.8670  ***          1376.8865  ***
                              1.4542+03  ***
                             12284.4086  ***
```

```
     0.0000  ***          812.2554  ***
  6602.9630  ***       6.8772+03  ***
                       10273.7929  ***
  1124.2817  ***
  2.4094+03  ***          0.0000  ***
  6602.9630  ***       10239.4791  ***

     0.0000  ***          816.0238  ***
  7894.5397  ***       8.1914+03  ***
                       10239.4791  ***
   990.9222  ***
  3.9585+03  ***          0.0000  ***
  7894.5397  ***

                          855.0718  ***
     0.0000  ***       6.8910+03  ***
  8847.7553  ***          0.0000  ***

   908.5838  ***          0.0000  ***
  5.8799+03  ***
  8847.7553  ***          969.4725  ***
                       3.8940+03  ***
     0.0000  ***          0.0000  ***
  9767.8514  ***

                          0.0000  ***
   843.5443  ***
  7.8527+03  ***       1133.5535  ***
  9767.8514  ***       1.6830-03  ***
                          0.0000  ***
     0.0000  ***
 10273.7929  ***
```

Resulting Hydrograph:

Time min	Discharge cfs
10	8
20	140
29.5	872
39.95	1454
38.74	24094
46.52	3959
55.14	5880
64.06	7853
73.54	8877
83.60	8191
94.15	6891
115.98	3894
168.89	1683

Calculation of Channel Cross-Sectional Relationships. Given cross sections: The following cross section data are for the representative cross sections for three reaches; reach 0, which is upstream of the portion of the channel which flood protection is required, reach 1, which is the first half of the protected channel and reach 2, for the second half. The data listed below is in relative form. The elevations are from a zero datum being the lowest point in the representative cross section and the horizontal distance is measured from zero being the furthest point on the left side of the cross section looking upstream. See Figure 15.13.

Section 0		Section 1		Section 2	
X ft	Y ft	X ft	Y ft	X ft	Y ft
0	8	0	6	0	6
15	6	20	3	20	4
25	2	30	1	40	3
60	1.5	100	0	60	1
70	0	115	6	110	0
80	2			125	6
100	8				

Inputs: For all the cross-sectional relationships except the A-P the inputs are the same.

Section 0	Section 1	Section 2
Y_{max} = 8 ft	Y_{max} = 6 ft	Y_{max} = 6 ft
Y_{min} = 0 ft	Y_{min} = 0 ft	Y_{min} = 0 ft

and the coordinate data for the three sections.

The input for the A-P relationship consists of the areas and wetted perimeters for each depth increment taken from the AY and P-Y relationships. This data is just entered as ordered pairs into the H-P 97 standard Pack Curve Fitting program, SD-03A.

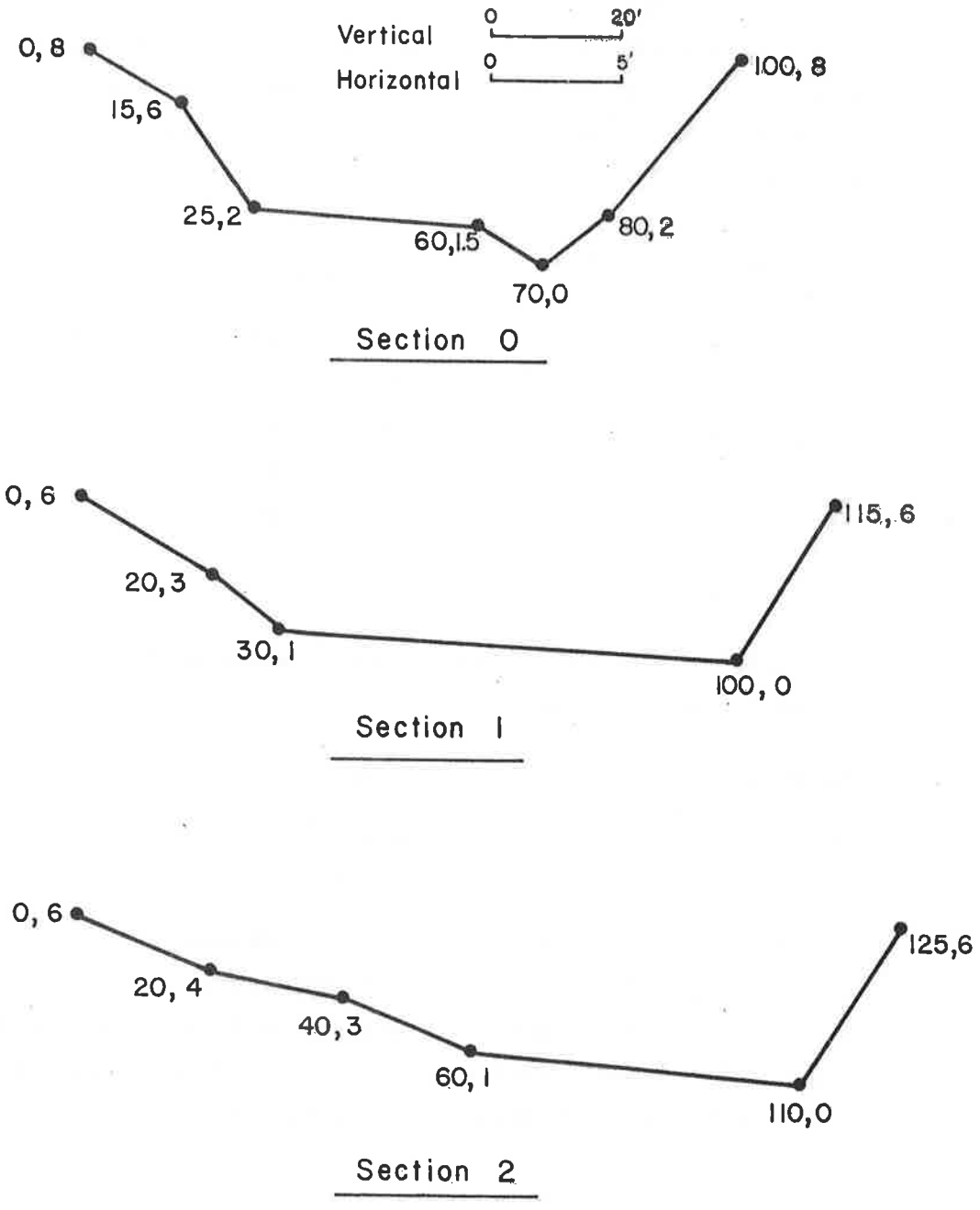

Figure 15.13 Representative cross sections.

A-P Data Input

(area is the x variable and wetted perimeter the y variable)

Section 0

Perimeter (ft_y)	Area (ft^2_x)
9.47	3.73
25.27	15.25
57.78	53.72
62.72	101.45
67.66	152.92
72.60	208.12
77.54	267.05
84.72	330.12
93.26	399.22
102.10	467.25

Section 1

Perimeter (ft_y)	Area (ft^2_x)
43.62	13.05
74.26	50.90
78.93	96.65
83.61	145.10
88.28	196.25
93.94	250.40
99.60	307.85
105.26	368.60
110.92	432.65
116.58	500.00

Section 2

Perimeter (ft_y)	Area (ft^2_x)
31.62	9.45
55.25	37.00
62.90	72.25
70.54	112.00
78.19	156.25
91.82	206.80
103.45	265.25
111.10	329.00
118.74	397.25
126,39	470.00

Output:

Section 0

Y-A			Y-T			Y-P			A-P		
8.00	***		8.00	***		8.00	***		6.95	***	r^2
0.00	***		0.00	***		0.00	***		6.69	***	a_1
6.00	***	Y	6.00	***	Y	6.00	***	Y	0.45	***	b_1
15.00	***	A	15.00	***	T	15.00	***	P			
2.00	***		2.00	***		2.00	***				
25.00	***		25.00	***		25.00	***				
1.50	***		1.50	***		1.50	***				
60.00	***		60.00	***		60.00	***				
0.00	***		0.00	***		0.00	***				
70.00	***		70.00	***		70.00	***				
2.00	***		2.00	***		2.00	***				
80.00	***		80.00	***		80.00	***				
8.00	***		8.00	***		8.00	***				
100.00	***		100.00	***		100.00	***				
3.73	***		9.33	***		9.47	***				
0.80	***		0.80	***		0.80	***				
15.25	***		25.00	***		25.27	***				
1.60	***		1.60	***		1.60	***				
53.72	***		57.33	***		57.78	***				
2.40	***		2.40	***		2.40	***				
101.45	***		62.00	***		62.72	***				
3.20	***		3.20	***		3.20	***				
152.92	***		66.67	***		67.66	***				
4.00	***		4.00	***		4.00	***				
208.12	***		71.33	***		72.60	***				
4.80	***		4.80	***		4.80	***				
267.85	***		76.00	***		77.54	***				
5.60	***		5.60	***		5.60	***				
330.12	***		82.67	***		84.42	***				
6.40	***		6.40	***		6.40	***				
399.72	***		91.33	***		93.26	***				
7.20	***		7.20	***		7.20	***				
476.25	***		100.00	***		102.10	***				
8.00	***		8.00	***		8.00	***				
0.99	***	r	0.95	***	r	0.95	***	r			
6.76	***	a_2	16.00	***	a_3	16.24	***	a_4			
2.13	***	b_2	0.95	***	b_3	0.95	***	b_4			

Output:

Section 1

Y-A			Y-T			Y-P			A-P		
6.00	***		6.00	***		6.00	***		0.97	***	r^2
0.00	***		0.00	***		0.00	***		24.95	***	a_1
									0.25	***	b_1
3.00	***	Y	3.00	***	Y	3.00	***	Y			
30.00	***	A	20.00	***	T	30.00	***	P			
1.00	***		1.00	***		1.00	***				
30.00	***		30.00	***		30.00	***				
0.00	***		0.00	***		0.00	***				
100.00	***		100.00	***		100.00	***				
6.00	***		6.00	***		6.00	***				
115.00	***		115.00	***		115.00	***				
13.85	***		43.50	***		43.62	***				
0.60	***		0.60	***		0.60	***				
50.90	***		74.00	***		74.26	***				
1.20	***		1.20	***		1.20	***				
96.65	***		78.50	***		78.93	***				
1.80	***		1.80	***		1.80	***				
145.10	***		83.00	***		83.61	***				
2.40	***		2.40	***		2.40	***				
195.25	***		87.50	***		88.28	***				
3.00	***		3.00	***		3.00	***				
250.40	***		93.00	***		93.94	***				
3.60	***		3.60	***		3.60	***				
307.85	***		98.50	***		99.60	***				
4.20	***		4.20	***		4.20	***				
368.60	***		104.00	***		105.26	***				
4.80	***		4.80	***		4.80	***				
432.65	***		109.50	***		110.92	***				
5.40	***		5.40	***		5.40	***				
500.00	***		115.00	***		116.58	***				
6.00	***		6.00	***		6.00	***				
1.00	***	r	0.97	***	r	0.97	***	r			
34.50	***	a_2	59.48	***	a_3	59.65	***	a_4			
1.54	***	b_2	0.37	***	b_3	0.37	***	a_4			

Output:

Section 2

Y-A			Y-T			Y-P			A-P		
6.00	***		6.00	***		6.00	***		0.99	***	r^2
0.00	***		0.00	***		0.00	***		14.53	***	a_1
									0.35	***	b_1
4.00	***	Y	4.00	***	Y	4.00	***	Y			
20.00	***	A	20.00	***	T	20.00	***	P			
3.00	***		3.00	***		3.00	***				
40.00	***		40.00	***		40.00	***				
1.00	***		1.00	***		1.00	***				
60.00	***		60.00	***		60.00	***				
0.00	***		0.00	***		0.00	***				
110.00	***		110.00	***		110.00	***				
5.00	***		6.00	***		6.00	***				
125.00	***		125.00	***		125.00	***				
9.45	***		31.50	***		31.62	***				
0.60	***		0.60	***		0.60	***				
37.00	***		55.00	***		55.25	***				
1.20	***		1.20	***		1.20	***				
72.25	***		62.50	***		62.90	***				
1.80	***		1.80	***		1.80	***				
112.00	***		70.00	***		70.54	***				
2.40	***		2.40	***		2.40	***				
156.25	***		77.50	***		78.19	***				
3.00	***		3.00	***		3.00	***				
206.80	***		91.00	***		91.82	***				
3.60	***		3.60	***		3.60	***				
265.25	***		102.50	***		103.45	***				
4.20	***		4.20	***		4.20	***				
329.00	***		110.00	***		111.10	***				
4.80	***		4.80	***		4.80	***				
397.25	***		117.50	***		118.74	***				
5.40	***		5.40	***		5.40	***				
470.00	***		125.00	***		126.39	***				
6.00	***		6.00	***		6.00	***				
1.00	***	r	0.99	***	r	0.99	***	r			
24.97	***	a_2	44.24	***	a_3	44.46	***	a_4			
1.66	***	b_2	0.57	***	b_3	0.58	***	b_4			

Summary of Results for Geometric Relationships.

	$A = a_1 y^{b_1}$	$P = a_2 A^{b_2}$	$T = a_e y^{b_3}$, $P = a_4 y^{b_4}$
	Section 0	Section 1	Section 2
a_1	6.78	34.50	24.97
b_1	2.13	1.54	1.66
a_2	6.69	24.95	14.53
b_2	0.45	0.25	0.35
a_3	16.08	59.48	44.24
b_3	0.95	0.37	0.57
a_4	16.24	56.69	44.76
b_4	0.95	0.37	0.58

Muskingum-Cunge Water Routing Program

The routing, in this case, need not be run since the channel reaches in question are short and the celerity of the flood is high, therefore little difference will show up in the hydrograph between the reaches. The program is run just as a matter of illustration.

Input:

Section 1

$a_1 = 24.95$, $b_1 = 0.25$

$a_2 = 34.50$, $b_2 = 1.54$

$a_3 = 59.48$, $b_3 = 0.37$

$\Lambda = 0.20$ $S = .012$

$\Delta X = 650$ ft

$\Delta t = 10$ min

$Q_{ref} = 2/3\ Q_{peak} = 2/3\ (8496) = 5664$ cfs

Input Hydrograph: (This is the hydrograph computed earlier at the downstream boundary of the watershed and linearly interpolated for a Δt of 10 minutes.

Time (min)	Discharge (cfs)
0	0
10	8
20	140
30	958
40	2667
50	4271
60	6954
70	8496
80	8436
90	7676
100	6094
110	4719
120	3727
130	3309
140	2891
150	2473
160	2055
170	1637

Output:

Section 1

```
650.0000  ***      Δx

  0.5792  ***      c1
  0.9206  ***      c2
 -0.8988  ***      c3

  0.0000
  0.0000  ***

 10.0000  ***      time (min)
  7.3646  ***      discharge (cfs)

 20.0000  ***
130.0967  ***

 30.0000  ***
901.9382  ***

 40.0000  ***
2581.6455  ***

 50.0000  ***
4652.9620  ***

 60.0000  ***
6857.3354  ***

 70.0000  ***
8460.4827  ***

 80.0000  ***
8472.7597  ***

 90.0000  ***
7703.3261  ***

100.0000  ***
6195.0943  ***

110.0000  ***
4737.3516  ***

120.0000  ***
3789.2981  ***

130.0000  ***
3286.2086  ***

140.0000  ***
2944.6851  ***

150.0000  ***
2457.9497  ***

160.0000  ***
2161.7275  ***

170.0000  ***
1628.2031  ***
```

Input:

Section 2

$a_1 = 14.53$, $b_1 = 0.35$

$a_2 = 24.97$, $b_2 = 1.66$

$a_3 = 44.24$, $b_3 = .57$

$n = .02$, $S = .012$

$\Delta X = 580.63$ ft

$\Delta t = 10$ min

$Q_{ref} = 2/3\ Q_{peak} = 2/3(10974) = 7316$ cfs

Given inflow hydrograph from small watershed

Time (min)	Q (cfs)
10	2
20	38
30	266
40	761
50	1373
60	2023
70	2496
80	2501
90	2273
100	1828
110	1398
120	1118
130	969
140	869
150	725
160	620
170	480

The inflow from the small watershed and the output hydrograph from Section 1 are combined to form the inflow hydrograph for Section 2 listed below.

Time (min)	Discharge (cfs)
0	0
10	9
20	168
30	1168
40	3343
50	6026
60	8880
70	10956
80	10974
90	9976
100	8023
110	6135
120	7907
130	4255
140	3814
150	3183
160	2722
170	2108

Output:

Section 2

```
  580.6300  ***     Δx (feet)

    0.9755  ***     c1
    0.9298  ***     c2
   -0.9053  ***     c3

    0.0000          t (time)
    0.0000  ***     Q (cfs)

   10.0000  ***
    8.3681  ***

   20.0000  ***
  157.4087  ***

   30.0000  ***
 1107.3788  ***

   40.0000  ***
 3245.1746  ***

   50.0000  ***
 5926.1890  ***

   60.0000  ***
 8769.9808  ***

   70.0000  ***
10909.8452  ***

   80.0000  ***
11814.5200  ***

   90.0000  ***
10009.3864  ***

  100.0000  ***
 8129.8944  ***

  110.0000  ***
 6170.7843  ***

  120.0000  ***
 4960.8217  ***

  130.0000  ***
 4252.0519  ***

  140.0000  ***
 3847.6312  ***

  150.0000  ***
 3196.8559  ***

  160.0000  ***
 2741.8228  ***

  170.0000  ***
 2133.1631  ***
```

Normal Depth (Natural Channel).

Input:

Section 0	Section 1	Section 2
$a_1 = 6.69$, $b_1 = 0.45$	$a_1 = 24.95$, $b_1 = 0.25$	$a_1 = 14.53$, $b_1 = 0.35$
$a_2 = 6.78$, $b_2 = 2.13$	$a_2 = 34.50$, $b_2 = 1.54$	$a_2 = 24.97$, $b_2 = 1.66$
$a_3 = 16.00$, $b_3 = 0.95$	$a_3 = 59.48$, $b_3 = 0.37$	$a_3 = 44.24$, $b_3 = .57$
$S = .02$, $n = .02$	$S = .012$, $\Lambda = .02$	$S = .012$, $\Lambda = .02$

Time (min)	Section 0	Section 1	Section 2
0- 50	1703	1654	2089
50-100	7531	7538	9766
100-170	2973	2992	3899

Output:

Section 0

1703 cfs			7531 cfs		2973 cfs	
1.92	***	Y_H	3.51	***	2.41	***
3.61	***	Y	6.62	***	4.38	***
54.48	***	T	88.51	***	65.35	***
104.59	***	A	310.46	***	157.24	***
16.28	***	V	24.26	***	18.91	***
39.19	***	Stream power	106.24	***	56.95	***

Section 1

1657 cfs		7538 cfs		2992 cfs	
1.72	***	3.71	***	2.32	***
2.53	***	4.89	***	3.27	***
83.90	***	106.97	***	92.25	***
144.40	***	396.92	***	214.38	***
11.45	***	18.99	***	13.96	***
14.32	***	50.68	***	23.47	***

Section 2

2089 cfs		9766 cfs		3899 cfs	
1.96	***	3.98	***	2.21	***
3.14	***	6.00	***	4.66	***
84.88	***	122.81	***	98.56	***
166.55	***	488.45	***	257.40	***
12.54	***	19.99	***	15.15	***
17.97	***	57.64	***	28.80	***

Check Upper Regime Assumption

This assumption is checked by using Figure 15.14. The stream power was computed in the normal depth program. For all the flows calculated the stream power is above 10 lb/sec-ft^2 which would indicate flow in the upper regime. Therefore the assumption of a Manning's n is valid

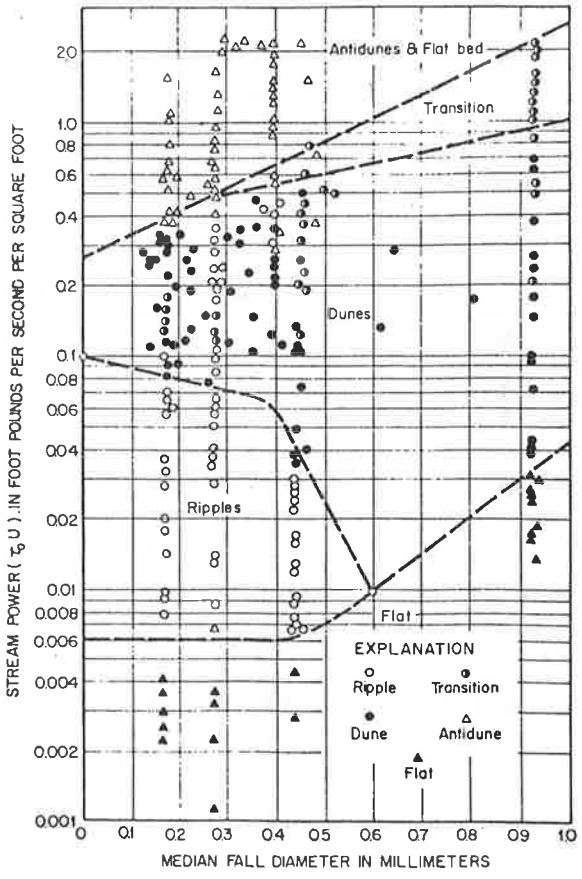

Figure 15.14 Bed form determination chart using stream power (Simons and Sentürk, 1977).

Particle Size Distribution Program.

Section 0

d_{50} = .2 mm

S = 2

Bounding grain sizes

001 → .1 → .3 → 3.0 mm

Input:

0.1 ***
1.0 ***

0.010 ***
0.159 ***

0.173 ***
0.562 ***

0.775 ***
0.279 ***

Meyer-Peter, Müller Program. (bed load only)

Input:

Section 0

d_{s_1} = .010 mm, p_1 = .159, f = .025
= 3.3×10^{-4} ft

d_{s_2} = .173 mm, p_2 = .562
= 5.7×10^{-3} ft

d_{s_3} = .279 mm, p_3 = .280
= 9.2×10^{-3} ft

The velocities are for the average discharges over the time increments

V_{0-50} = 16.28 ft/sec

V_{50-100} = 24.26 ft/sec

$V_{100-170}$ = 18.91

Output:

Section 0

3.300000000-04	***	0.006	***	0.009	***
0.016	***	0.062	***	0.031	***
0.060	***	0.205	***	0.103	***
0.028	***	0.098	***	0.048	***

Input:

Section 1

Sediment sizes the same as Section 0

f = 0.25

Velocities

$V_{0-50} = 11.45$

$V_{50-100} = 18.99$

$V_{100-170} = 13.96$

Output:

Section 1

3.300000000-04	***	0.006	***	0.009	***
0.006	***	0.021	***	0.015	***
0.029	***	0.099	***	0.049	***
0.011	***	0.035	***	0.019	***

Input:

Section 2

Sediment sizes the same as Section 0

f = .025

Velocities

$V_{0-50} = 12.54$

$V_{50-100} = 19.99$

$V_{100-170} = 15.15$

Output:

Section 2

3.300000000-04 ***	0.006 ***	0.003 ***
0.008 ***	0.026 ***	0.014 ***
0.033 ***	0.116 ***	0.057 ***
0.015 ***	0.056 ***	0.024 ***

Aggradation-Degradation Program.

Input:

Section 1

The upstream inputs are the previous calculated values for Section 0. The downstream inputs are the values from Section 1. The subscript 1 stands for downstream, 2 for upstream. B_1 and B_2 are the average width. For calculation the top width was assured to be an adequate approximation.

The q_s (sediment flow per foot width) are the sum of the sediment for all three sediment sizes for the Δt.

Δt sec	time min	q_{s_1} cfs/ft	q_{s_2} cfs/ft	B_1 ft	B_2 ft
3000	0-50	.111	.046	54.78	83.90
3000	50-100	.372	.177	88.51	106.97
7200	100-170	.174	.069	65.35	92.25

λ = .40

Output:

0.2432
1.1012
0.6841

total = + 2.03 ft (aggradation)

Input:

Section 2

Δt sec	time min	q_{s_1} cfs/ft	q_{s_2} cfs/ft	B_1 ft	B_2 ft
3000	0-50	.046	.050	83.90	84.88
3000	5-100	.177	.206	106.97	122.81
4200	100-170	.069	.089	92.25	98.56

λ = .4

Δx = 580.63

Input:

Section 2

-0.08392
-0.4771
-0.3041

total = - .82 ft (degradation)

Local Scour Program.

Input:

Section 1

$$Fr = \frac{V}{\sqrt{gy}} = \frac{19.75}{\sqrt{32.2\ (3.94)}} = 1.75$$

$y_o = 5.14$ ft

$L_s = 5.14\ (1.25) = 6.43$ ft

The 1.25 is derived by assuming the encroachment is half the distance the bank extends into the flow.

Output:

7.44 ft

Antidune Height Calculation.

Equations: H = antidune height (ft)
V = velocity of flow (ft/sec)
y_o = normal depth (ft)
g = acceleration of gravity (32.2 ft/sec^2)

$$H = 0.14\ \frac{(2)\pi V^2}{g}$$

This holds true if $H \leq y_o$

if $H > y_o$ then $H = y_o$

$\frac{2\pi}{g} V^2$ is the length of the dune. The .14 is the ratio of the height of the breaking wave to its length.

Calculations:

Section 1

The normal depth calculation must be made again this time on the maximum Q and not the average. The same parameters are used except Q = 8473 cfs as for previous Section 1 normal depth calculations.

Output:

```
  3.94  ***
  5.14  ***
108.99  ***
429.10  ***
 19.75  ***
 55.87  ***
```

y_o = 5.14

V = 19.75 ft/sec

H = 10.66 ft from the equation but 10.66 > y.

So, H = y_o = 5.14 ft.

Section 2: Normal Depth at Peak Flow

q_{peak} = 11015 cfs

All other parameters are the same as in previous normal depth calculations for this section.

Output

```
  4.20  ***
  6.31  ***
126.41  ***
531.24  ***
 20.73  ***
 63.13  ***
```

y_o = 6.31 ft

V = 20.73 ft/sec

H = 11.74 from the equation but 11.74 > y_o

So H = y_o = 6.31 ft.

Super Elevation.

Section 1: (Note: The curvature at Section 2 is such that the superelevation will lower the water on the side of the channel being protected. To be conservative, this will be ignored.)

Input: (Use maximum Q flow conditions)

r_c = 310' (radius of curvature at centerline)

T = 109 ft

V = 19.75 ft/sec

Output:

4.26 feet

Riprap Design Program.

The details of the method to design the riprap are found in Simons and Sentürk (1977). The method employs the use of a safety

factor. The riprap is sized until a suitable safety factor is found. The minimum allowable safety factor is chosen to be 1.3 for this design.

Input: First trial

Choose a d_{50} of 1.0 ft

The riprap is to be laid at a 2.5 to 1 slope

$\theta = \tan^{-1} 1/2.5 = 21.80$

$Q = 47°$ (from Figure 15.10 assuming angular)

Compute the bed shear stress

$\tau_o = \gamma y_o S = 62.4\ (6.31)\ (.012) = 4.72$

The depth of 6.31 ft is used since it is lb/st^2.

Determine the ratio of τ_s/τ_o y with the aid of Figure 15.9. The cross sections resemble trapezoidal channels enough to make the figure applicable. The ratio of b/d is quite large for all the sections. $\tau_s/\tau_o = .77$ (τ_s is for the slide slope).

Output: The program yields a safety factor of 1.0 which is too small.

Second Trial

Use a large d_{50}, try 1.5 ft

Input: Same as before except $d_{50} = 1.5$ ft

This size provides a safety factor of 1.3. Therefore use a 1.5 foot d_{50} riprap. For this large of riprap a filter should be used. For details of filter design see Chapter 17.

Calculation of Bank Height.

The bank must be designed to allow the maximum possible flow height to be obtained without being overtopped. This condition would include half the antidune height, the normal depth of flow, the aggradation height and half the super elevation height.

Section 1	y_o (ft)	1/2H (ft)	$1/2\Delta z_{el}$ (ft)	$1/2\Delta z_{ag}$ (ft)	freeboard (ft)	Total (ft)
Section 1	5.14	2.57	2.13	2.03	2	13.87
Section 2	6.31	3.16	0	0	2	11.47

For Section 1 use a design height of 14 feet above the bed. For Section 2 use a design height of 12.5 feet above the bed.

Calculation of Depth of Riprap Burial.

The toe of the riprap must be buried to a depth such that it will not be uncovered due to the combined effects of local scour, antidune formation and degradation due to general scour.

Section	1/2 H (ft)	$1/2\Delta z_{deg}$ (ft)	$1/2\Delta z_{LS}$ (ft)	Total with LS (ft)	Total without LS (ft)
Section 1	2.57	0	7.44	10.01	2.57
Section 2	3.16	.82	0	3.98	3.98

The first 50 feet of the riprap in Section 1 should be buried to a 10 foot depth to account for local scour due to the encroachment from the riprap bank. The rest of the riprap can be buried to 4 feet to accommodate the next severest condition.

15.5 SUMMARY

This chapter has presented several small calculator programs for use in an integrated approach to problem solving in watershed and river systems. The programs are grouped in three packages of related processes; hydrology, hydraulics and sedimentation. The programs are intended to complement one another and provide a means to follow complex basic problems in the sequence of determining the location hydrology, then hydraulic response and finally the sedimentation process impacts. To illustrate the approach, two comprehensive example problems have been provided. These programs will also provide means to solve many of the complex problems to be discussed in the case study chapters to follow.

15.6 REFERENCES

ASCE Task Committee on Sedimentation, 1975. Sedimentation Engineering, New York, 1975.

Chow, V. T., 1959. Open Channel Hydraulics, McGraw-Hill Book Company.

Croley, Thomas E., 1977. Hydrologic and Hydraulic Computations on Small Programmable Calculators, Iowa Institute of Hydraulic Research, University of Iowa, Iowa City.

Gessler, J., 1965. "The beginning of bedload movement of mixtures investigated as natural armoring in channels," W. M. Keck Lab. of Hydraulics and Water Resources, Calif. Inst. Techn., Pasadena.

Hershfield, D. M., 1961. Rainfall frequency atlas of the United States, for durations from 30 minutes to 24 hours and return periods from 1 to 100 years, U.S. Weather Bur. Tech. Rept. 40, May.

Lu, J. Y., 1978. "A sediment transport equation from nonlinear regression analysis," Colorado State University, Fort Collins.

Shen, H. W., and Hung, C. S., 1971. "An engineering approach to total bed material load by regression analysis," Proceedings, Sedimentation Sym., Berkeley.

Simons, D. B. and Sentürk, F., 1977. Sediment Transport Technology, Water Resources Publications, Fort Collins, Colorado.

Stevens, M. A. and Simons, D. B., 1971. "Stability analyses for coarse granular material on slopes," Ch. A., River Hydraulics, Vol. 1 (edited and published by H. W. Shen). Fort Collins, Colorado.

U.S. Bureau of Reclamation, 1960. Investigation of Meyer-Peter, Müller Bedload Formula. Sedimentation Section, Hydrology Branch, Division of Project Investigations, U.S. Department of the Interior, Bureau of Reclamation, June.

U.S. Bureau of Reclamation, 1974. Design of Small Dams, A Water Resources Technical Publication. U.S. Department of the Interior, Bureau of Reclamation.

Yang, C. T., 1976. "Minimum unit stream power and fluvial hydraulics," Journal of the Hydraulics Division, Proceedings, ASCE, Vol. 102, No. HY7, Paper 12238, pp. 919-934.

U.S. Weather Bureau, 1961. Rainfall frequency atlas of the United States for durations from 30 minutes to 24 hours and return periods from 1 to 100 years, U.S. Department of Commerce, Weather Bureau, May.

PROGRAM UNSTEDY

USER'S MANUAL

By D. B. Simons, Y. H. Chen and R. M. Li

INTRODUCTION

PROGRAM UNSTEDY was developed in the Engineering Research Center, Colorado State University, Fort Collins, Colorado in 1973 and subsequently modified to improve its applicabilities. The computer program simulates complex unsteady water and sediment movement considering inertia forces, friction, sediment transport, and degradation and aggradation. This program has the following applications:

1. River flood forecasting.
2. Unsteady flow generated by pumping and flood inflow to a storage and drainage tunnel system.
3. Study of a complex river system including tributaries, reservoirs, control structures, locks and dams, bifurcations, floodplain storage, etc.
4. Degradation and aggradation

During each computation, the water and sediment discharge, flow depth, flow velocity, water surface elevation, bed elevation changes and Froude number are determined. The program described in this user's manual has been simplified to consider only the water and sediment routing in a single channel with or without lateral inflow and with or without dams. Both MKS system and FPS system of units can be used. Super-critical flow and rapidly varied unsteady flow are beyond the scope of this program.

DATA INPUT

Data required to run PROGRAM UNSTEDY includes:

1. Channel cross-sectional geometries.
2. Manning's roughness coefficient at each cross section.
3. Boundary conditions:
   (1) Upstream boundary condition: discharge hydrograph Q(t).
   (2) Downstream boundary condition: stage hydrograph h(t) or stage-discharge relation h(Q).
4. Initial conditions defining Q at each cross section and h at the downstream section.
5. Sediment transport function if sediment routing is used.
6. Lateral water inflows.
7. Hydraulic characteristics of dams if they are presented in the model.

To show how to prepare the data deck, a test case is used. Figure 1 shows the modeled river reach. The river reach is represented by 11 cross sections. The length of reach is 30 km. River km of each cross section is also shown in Figure 1. The distance between cross sections can be varied. Each cross section is defined by (x,y) coordinate pairs. For example in Figure 1, cross section A-A is described by 15 (x,y) coordinate pairs.

Figure 2 shows a sample input. A detailed description of Figure 2 is given below:

Card 1 Unit system card, FORMAT (I2)

"1" indicates that MKS system of units is used.
"2" indicates that FPS (English) system is used.

Card 2 Sediment routing control, FORMAT (I2)

"0" indicates without sediment routing
"1" indicates with sediment routing

Card 3 Total number of cross sections, FORMAT (I2)

In the illustrated example, the total number of cross sections is 11 (See Figure 1). The number should not be larger than 50.

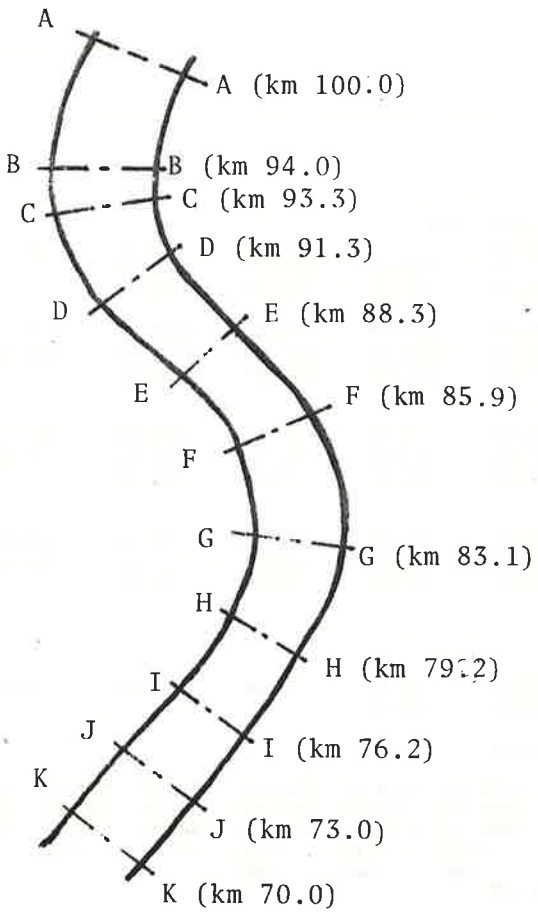

River Channel Plan View

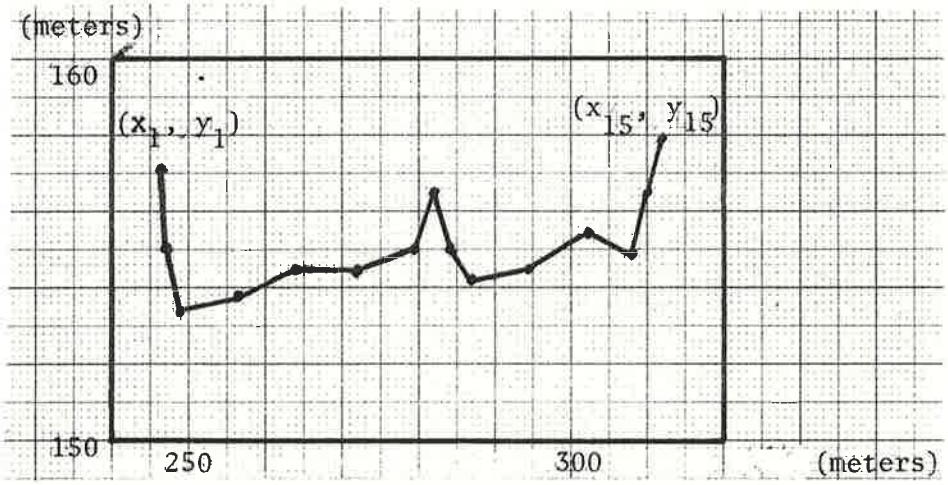

Cross Section A-A

Figure 1. The Test River Reach

Card

```
(1)------ 1
          1
         11
            1.000      0.050    40
(5)------   18.41      18.41      28.32      45.31      62.30      84.95      99.11     113.27
          135.92     147.25     169.90     155.74     141.58     118.93     113.27      99.11
           87.78      76.45      56.63      42.47      28.32
          1
           155.14     155.24     155.54     155.84     156.20     155.90     155.60     155.30
(10)------ 155.10     154.90     154.70     154.40     154.10     153.90     153.70     153.70
           153.90     154.20     154.50     154.80     155.10
         2
         2 3
             -10.00     -11.00     -12.00     -15.00     -20.00     -28.00     -33.00     -38.00
(15)------   -43.00     -49.00     -57.00     -52.00     -47.00     -39.00     -38.00     -33.00
             -29.00     -25.00     -20.00     -15.00     -10.00
               1.00
         6 7
            10.00      10.00      10.00      10.00      10.00      10.00      10.00      10.00
(20)------  20.00      20.00      20.00      20.00      20.00      20.00      30.00      30.00
            30.00      30.00      30.00      30.00      30.00
             1.00
          1
          4 1 3 711
(25)------  155.14
            18.41      18.41       8.41       8.41       8.41       8.41      18.41      18.41
            18.41      18.41      18.41
         2
        RANGE A-A      100.00
(30)------15
          193.54  157.09  194.15  154.92  198.11  153.37  213.35  153.76  228.59  154.53
          243.83  154.40  259.07  155.07  264.55  156.54  268.21  155.07  274.31  154.16
          289.55  154.43  304.79  154.43  316.67  154.92  320.02  156.45  324.60  157.88
(35)------  .180    .035    .035    .035    .035    .035    .035    .035    .035    .035
            .035    .035    .035    .180    .180
        RANGE B-B       94.00
        12
          640.05  158.88  655.29  158.40  658.34  158.31  670.53  156.57  675.40  155.81
          685.77  153.79  701.01  154.71  731.48  154.53  746.72  154.80  761.96  154.37
          768.36  158.18  777.20  158.52
            .180    .180    .180    .180    .035    .035    .035    .035    .035    .035
            .180    .180
        RANGE C-C       91.80
        17
          565.99  158.37  568.42  155.66  579.09  154.19  594.33  154.53  609.57  154.65
          624.81  154.77  640.05  155.20  655.29  155.17  670.53  155.56  676.93  155.81
          685.77  155.65  690.03  155.53  697.96  155.65  700.09  155.78  701.10  157.06
          711.67  157.57  713.50  157.82
            .180    .035    .035    .035    .035    .035    .035    .035    .035    .035
            .035    .035    .035    .180    .180    .180    .180
        RANGE D-D       91.30
        17
          457.18  157.03  464.80  156.57  465.41  155.64  466.02  155.59  472.42  155.04
          487.66  155.32  502.90  155.41  518.13  155.44  533.37  155.38  548.61  155.38
          563.85  155.17  579.09  155.20  594.33  153.61  602.86  155.59  605.91  157.09
          609.57  157.79  624.81  158.06
            .180    .180    .035    .035    .035    .035    .035    .035    .035    .035
            .035    .035    .035    .035    .180    .180    .180
        RANGE E-E       88.30
        21
          121.91  159.92  129.53  156.81  144.16  156.17  152.39  155.93  167.63  155.93
          174.34  156.17  182.87  156.29  198.11  156.45  205.73  156.35  209.39  155.47
          213.35  154.16  228.59  154.01  243.83  154.10  259.07  154.31  274.31  154.95
          289.55  154.68  304.79  155.47  320.02  155.78  333.43  156.02  335.26  157.24
          337.70  158.21
```

Figure 2. Data Input to Program UNSTEDY

Card

```
    .180    .180    .180    .180    .180    .180    .180    .180    .180    .035
    .035    .035    .035    .035    .035    .035    .035    .035    .035    .180
    .180
RANGE F-F       85.90
14
  380.98  157.73  396.22  157.06  407.50  157.12  411.46  155.84  426.70  155.78
  438.59  155.32  441.94  154.89  457.18  154.40  472.42  153.76  487.66  153.64
  500.15  155.32  501.68  157.85  502.90  157.88  518.13  158.06
    .180    .180    .180    .035    .035    .035    .035    .035    .035    .035
    .035    .180    .180    .180
RANGE G-G       81.00
17
  777.20  157.88  792.44  157.45  795.49  155.30  807.68  154.89  822.92  154.77
  838.16  154.40  853.40  154.40  868.64  153.19  874.73  153.43  880.83  155.30
  882.05  156.02  883.88  156.11  889.67  156.14  893.33  158.88  899.12  159.80
  914.36  164.49  929.59  169.61
    .180    .180    .035    .035    .035    .035    .035    .035    .035    .035
    .035    .035    .035    .035    .180    .180    .180
RANGE H-H       76.50
14
  563.85  157.79  579.09  157.63  591.59  156.84  593.72  155.78  594.33  155.47
  609.57  154.68  624.81  154.43  640.05  154.37  655.29  154.37  670.53  154.65
  685.77  154.95  701.11  155.23  716.25  155.68  731.48  155.75
    .180    .180    .180    .180    .035    .035    .035    .035    .035    .035
    .035    .035    .035    .035
RANGE I-I       76.20
15
  487.66  155.44  495.28  155.25  502.90  153.67  510.52  153.36  518.13  152.91
  525.75  153.18  533.37  153.00  540.99  153.36  548.61  153.52  556.23  153.12
  563.85  153.09  571.47  153.12  574.52  152.94  576.81  154.58  579.09  157.37
    .035    .035    .035    .035    .035    .035    .035    .035    .035    .035
    .035    .035    .035    .035    .035
RANGE J-J       73.00
25
  -48.77  167.63    0.00  158.79    4.88  155.14    9.14  153.40   21.33  151.78
   60.96  151.90   76.20  152.33   83.82  153.70   85.34  155.14   91.44  156.23
  106.67  156.23  121.91  154.25  144.77  153.95  152.39  153.58  182.87  153.92
  205.70  153.92  222.46  156.50  283.45  156.35  291.07  155.84  297.17  154.22
  301.74  155.14  304.79  155.38  335.26  155.44  505.94  155.75  573.00  167.63
    .180    .180    .160    .035    .035    .035    .035    .035    .160    .180
    .180    .060    .060    .060    .060    .060    .180    .180    .180    .120
    .160    .180    .180    .180    .180
RANGE K-K       70.00
25
  -48.77  167.63    0.00  158.79    4.88  155.14    9.14  153.40   21.33  151.78
   60.96  151.90   76.20  152.33   83.82  153.70   85.34  155.14   91.44  156.23
  106.67  156.23  121.91  154.25  144.77  153.95  152.39  153.58  182.87  153.92
  205.70  153.92  222.46  156.50  283.45  156.35  291.07  155.84  297.17  154.22
  301.74  155.14  304.79  155.38  335.26  155.44  505.94  155.75  573.00  167.63
    .180    .180    .160    .035    .035    .035    .035    .035    .160    .180
    .180    .060    .060    .060    .060    .060    .180    .180    .180    .120
    .160    .180    .180    .180    .180
(115)------
  0.000100  3.000000 -1.000000  1.000000
  0.000100  3.000000 -1.000000  1.000000
(120)------ 0.000100  3.000000 -1.000000  1.000000
  0.000100  3.000000 -1.000000  1.000000
  0.000100  3.000000 -1.000000  1.000000
  0.000100  3.000000 -1.000000  1.000000
  0.000100  3.000000 -1.000000  1.000000
(125)------ 0.000100  3.000000 -1.000000  1.000000
  0.000100  3.000000 -1.000000  1.000000
  0.000100  3.000000 -1.000000  1.000000
  0.000100  3.000000 -1.000000  1.000000
    2
(130)------   3    1      1.50    156.00    100.00      0.07
                4.00      3.50      3.00      2.75      2.50      2.25      2.00      1.75
                1.50      1.25      1.00      0.75      0.50      0.50      0.50      0.50
                0.50      0.50      0.50      0.50      0.50
                8    2      1.50    155.00    100.00      0.07
```

Figure 2. (continued)

Cards 4-7 Time period and discretization of inflow discharge hydrograph.

Three variables are read in Card 4 using FORMAT (2F10.3, I5). They are TØTALT, TØT, and NTØTAL, where TØTALT is the total routing time in days, TØT is the time increment in days between discretized values, and NTØTAL is the total number of routing steps. Figure 3 shows the inflow discharge hydrograph in this illustrated example. The length of the hydrograph is 1 day (TØTALT = 1.000), and the hydrograph is discretized into 21 values (NT = 21) with the time increment between discretized values equal to 0.05 days (TØT = 0.050 and NT = TØTALT/TØT + 1). These 21 values of discharges are input on Cards 5-7 with a FORMAT (8F10.2), in cubic meters per second (MKS system) or in cubic feet per second (FPS system). If the values of TØTALT and TØT are changed, then the number of discretized discharges and data cards should be changed accordingly. The values of NTØTAL and NT should be less than 200. The time increment between each computation step is equal to

$$DT = TØTALT/FLØAT\ (NTØTAL)$$

where NTOTALT should be a multiple of (NT-1). Since the numerical solution used in the program is based on an implicit scheme, there is no limitation on value of DT in terms of computation stability. However, a large DT may affect the accuracy of the computed results.

Card 8 Identification of types of downstream boundary conditions FORTRAN (I2).

"1" indicates that the downstream boundary condition is a stage hydrograph.

"2" indicates that the downstream boundary condition is a stage-discharge relation.

Cards 9-11 When the integer on Card 8 is 1, a known stage hydrograph in meters (MKS) or feet (FPS) should be used as the downstream boundary condition. A tidal cycle or stages controlled by dam operations are typical examples for this type of control. The stage hydrograph should be discretized following the same procedure for discretizing the inflow discharge hydrograph (Cards 4-7). Figure 4 shows an example. If the integer on Card 8 is 2, a stage-discharge relation should be used as the downstream boundary condition. This relation may be determined from the field data, using a normal flow condition or some other method. For flood routing in a river reach where the backwater effect is insignificant, a stage-discharge relation should be used as the downstream boundary condition. Figure 5 shows an example of the rating relation.

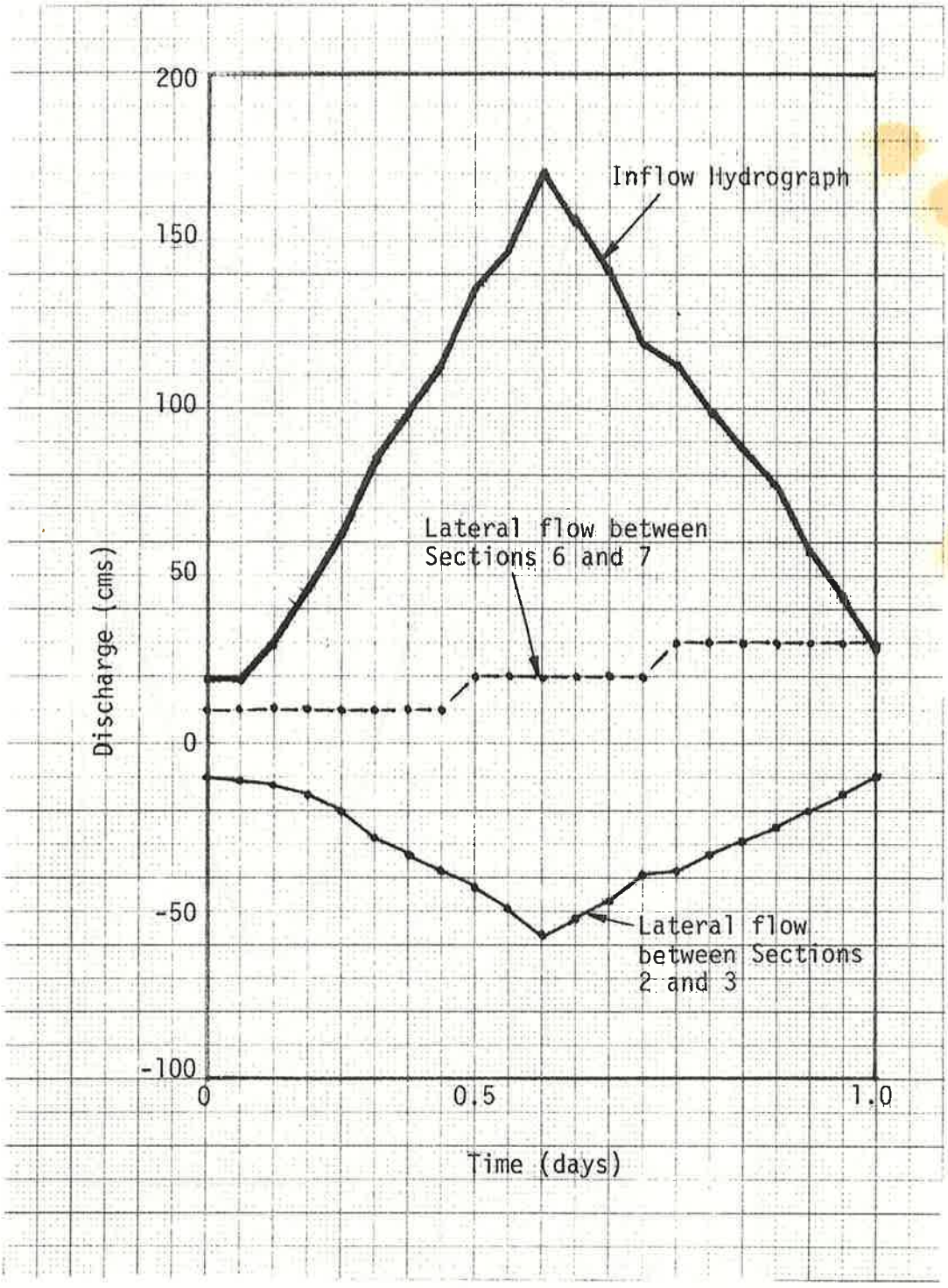

Figure 3. Inflow Discharge Hydrograph and Lateral Flow Hydrographs

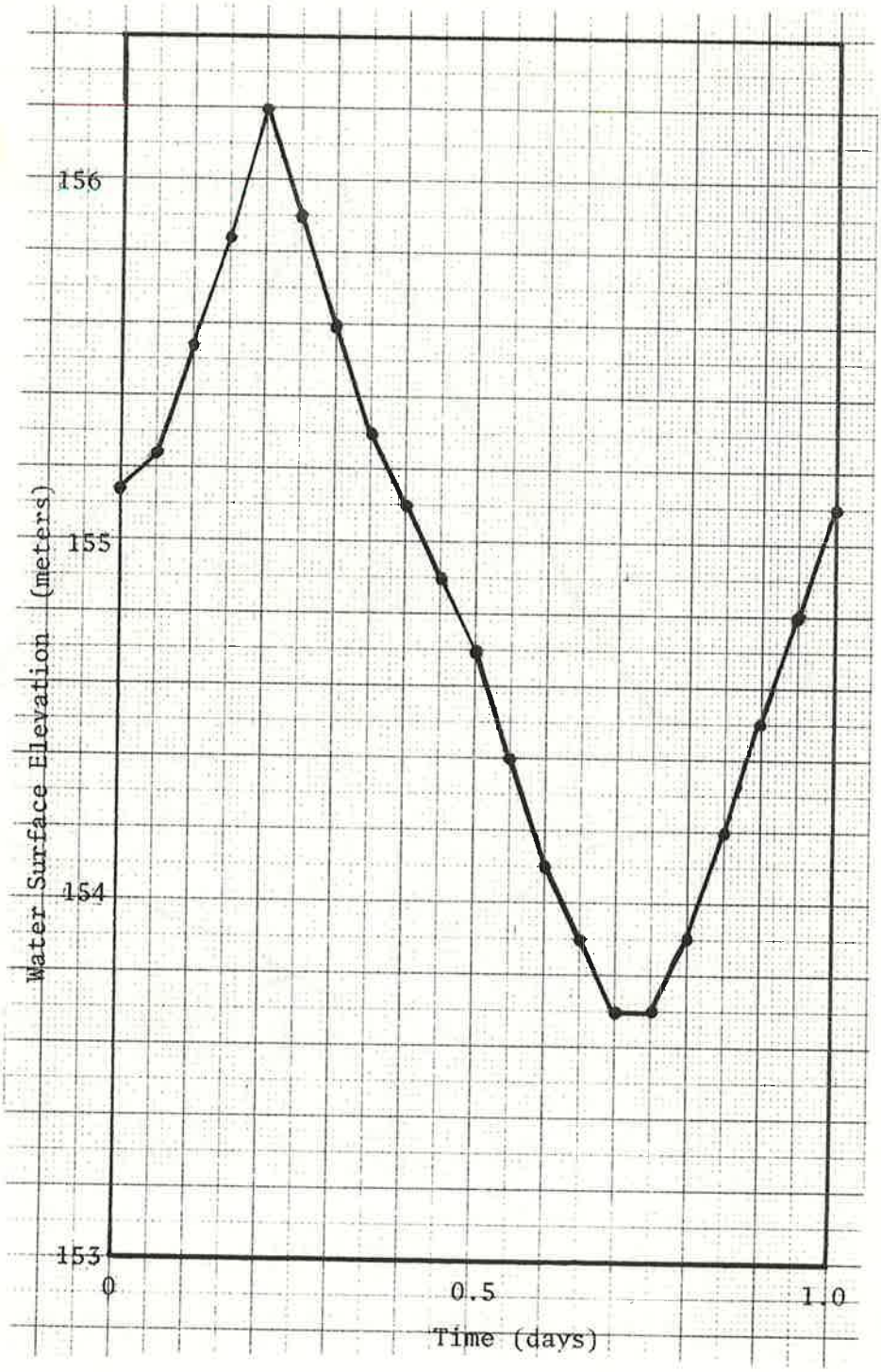

Figure 4. Water Stage Hydrograph at the Downstream Section

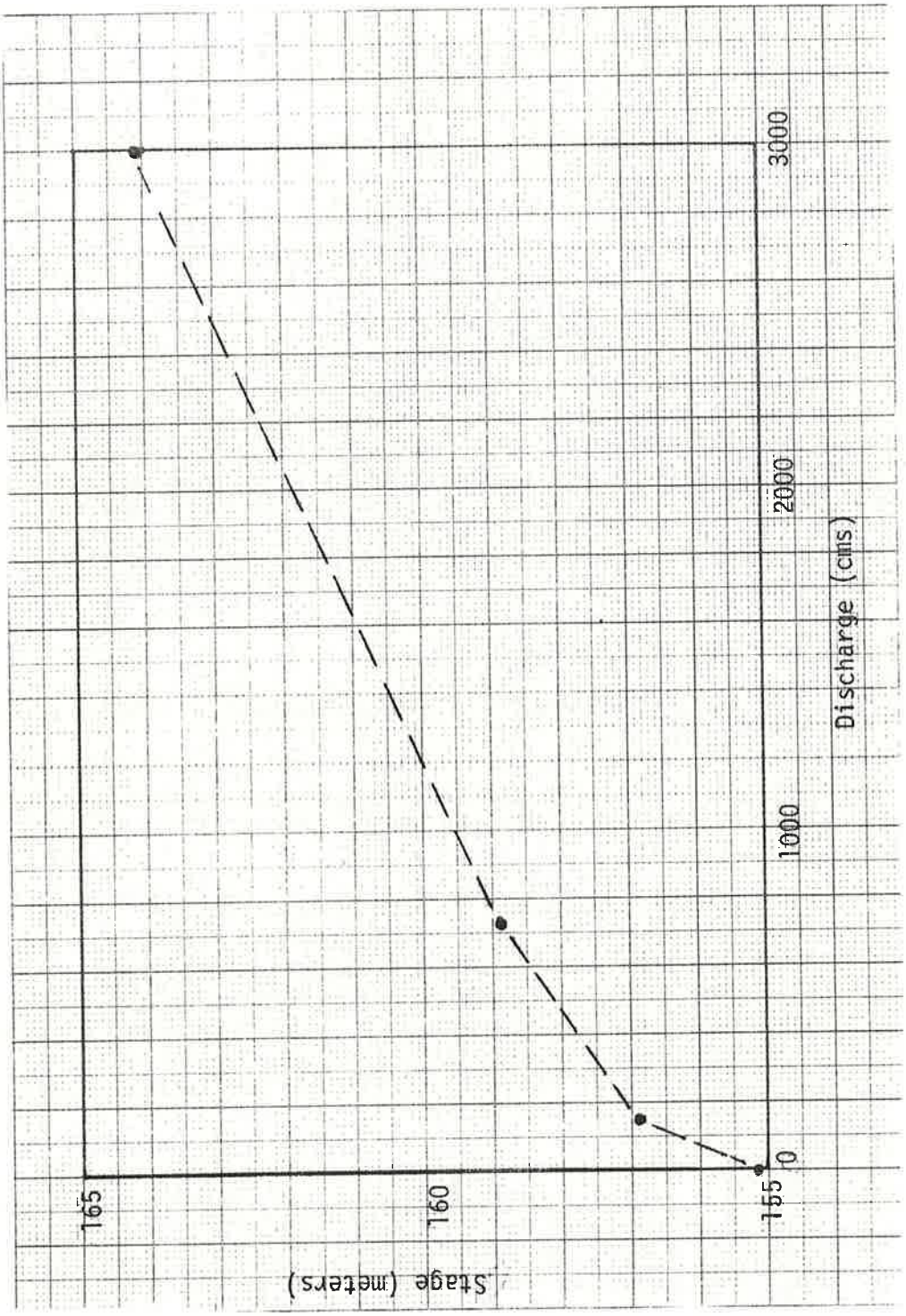

Figure 5. A Stage-Discharge Relation as the Downstream Boundary Condition

In this figure, the data points have the coordinates of

Discharge (cms)	Stage (meters)
0	155.13
150	156.88
730	158.88
3000	164.08

These data points are input to represent the original rating curve by assuming that the relation of stage to discharge is linear between points. For this type of downstream boundary condition, the cards shown on Figure 6 should be used to substitute the position of cards 9-11 in the original data deck. In Figure 6, card 1 shows the number of (discharge, stage) pairs used to represent the stage-discharge curve, input by a FORMAT (I2), the value of which should be smaller than 20. Card 2 gives the values of each pair. In the English (FPS unit system), cfs and ft should be used for the discharge and stage respectively.

Card 12-22 Input of lateral flows

A. Card 12 Input number of subreaches having lateral flows, FORMAT (I2)

B. Card 13 Input the upstream and downstream sections that bracket the first subreach having lateral flow, FORMAT (2I2).

C. Cards 14-16 Input the lateral water discharge in cms (MKS system) or cfs (FPS system), FORMAT (8F10.2). The lateral discharge hydrograph should be discretized following the same procedure for discretizing the inflow discharge hydrograph (Cards 4-7). Positive value of lateral discharge indicates lateral inflow and negative value of lateral discharge indicates outflow. The lateral flow hydrograph is plotted on Fig. 3.

D. Card 17 Proportion of lateral sediment flow, FORMAT (F10.2). If the lateral flow transports the same concentration of sediment as the main channel flow, its value should be 1.00. For water routing only (0 in Card 2), this card should be deleted.

E. Cards 18-22 Input the lateral flow into or out of the second subreach following the same format as Cards 13-17. This lateral flow hydrograph is also shown on Fig. 3.

If Card 12 is "0" (zero), cards 13-22 should be deleted.

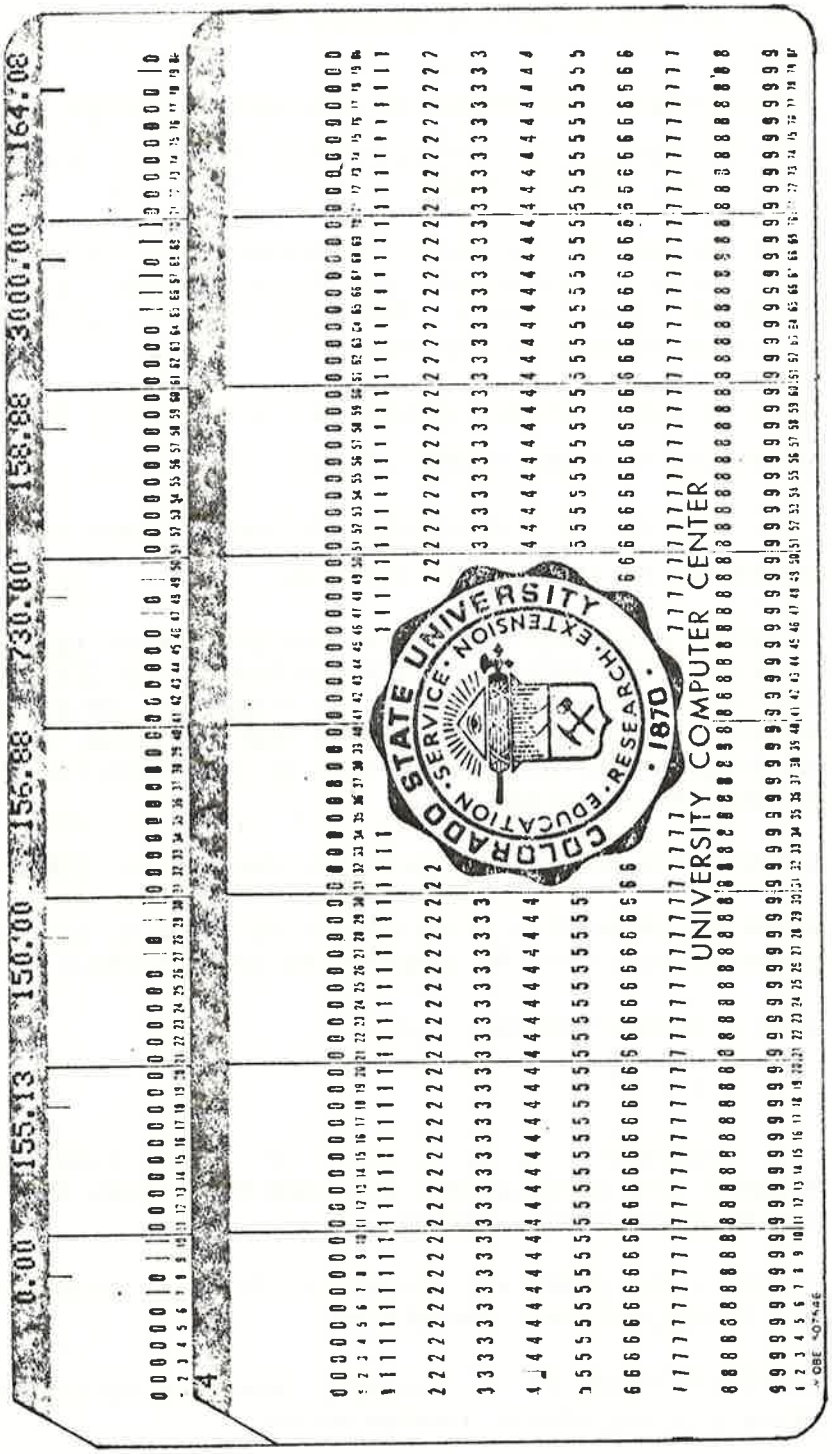

Figure 6. Data Input for Using a Stage-Discharge Relation as the Downstream Boundary Condition

Card 23 Output control variable NLIST, FORMAT (I2).

The computed results will be printed out once every NLIST time steps.

Card 24 Output control to print the computed discharge, depth, velocity hydrographs and bed elevation changes at the specified cross sections, FORMAT (40I2).

The first integer on this card defines how many cross sections where the computed hydrographs are to be printed. Its value should not be larger than 5. The other integers give the cross section identification number.

Card 25 Initial water surface elevations in meters or feet at the downstream section, FORMAT (F8.2).

Cards 26 - 27 Initial flow discharges defined at each cross section in cms or cfs, FORMAT (10F8.2).

These initial discharges should be assigned equal to the first value of the upstream discharge hydrograph (Card 5), less the lateral flows. The initial stages are determined from a backwater computation. It is important that the initial stage at the downstream section satisfies the downstream boundary condition.

Card 28 Computation control of geometric properties, FORMAT (I2)

The geometric preperties (cross-sectional area A, top width T, conveyance K, etc.) can be computed by three methods:

"1" uses a power relation, i.e.,

$$v = a\, y^{b}$$

where v represents A, T, K, etc., y is the flow depth, and a and b are coefficients obtained by fitting the v-y relation by least-square method.

"2" computes the geometric properties directly from the original cross-sectional geometries.

"3" tabulates value of v versus y and then determine v at a given y using linear interpolation.

The power relation is the simplest method among the three methods, but it may not always be applicable. The second method requires more computer time. The third method usually provides a good approximation to the original geometries.

Cards 29-35 Description of the geometric properties and roughness at cross section A-A, starting from the upstream cross section. Geometric properties of the other cross sections should be input sequentially in a downstream order following the same format of cards 29-35 as shown in Figure 2.

A. Card 29 Input the cross-section name, and the distance of the cross section in kilometers (MKS system) or miles (FPS system) upstream from a reference station. This format is (A10, F10.2).

B. Card 30 Input the number of (x,y) coordinate pairs FORMAT (I2) This number should not be larger than 99.

C. Cards 31-33 Input the (x,y) coordinate pairs with a FORMAT (10F8.2).

D. Cards 34-35 Input Manning's coefficient at each (x,y) coordinate of a cross section, FORMAT (10F8.3).

Cards 118-128 Input the sediment transport function, FORMAT (4F10.6)

```
C = CKT *  FC * U ** CMS * D ** CNS
```

where C is the concentration in volume of sediment per volume of water, U is the velocity, D is the hydraulic depth, and CKT, CMS, CNS, and FC are the coefficients evaluated from the field data and/or theories. The four values on each card are values of CKT, CMS, CNS, and FC respectively, for each cross section. For only water routing ("0" on Card 2), these cards can be deleted.

Cards 129-134 Input the hydraulic data for dam structures.

A. Card 129 Input the number of dams in the model reach. The format is (I2). If the input value is zero, then Cards 130-134 should be deleted.

B. Card 130 Input the hydraulic control data for dams, including the variables NL, NDIND, CG, ZW, WGATE, VFL where NL = the dam is located between Sections NL and NL+1.

NDIND = 1, Gated structure

= 2, closing dam (uncontrolled dam or weir)

CG, ZW, WGATE = discharge coefficient, sill height and width of gate or dam, respectively. The discharge equation is defined as

i) For uncontrolled dam, freefall flow

$$Q = CG * WGATE * (h_1 - ZW)^{3/2}$$

ii) For uncontrolled dam, submerged flow

$$Q = CG * WGATE * (h_1 - ZW)\,(h_1 - h_2)^{1/2}$$

iii) For gated dam, freefall flow
$Q = CG * WGATE * AG * (h_1 - ZW)^{1/2}$

iv) For gated dam, submerged flow
$Q = CG * WGATE * AG * (h_1 - h_2)^{1/2}$

in which h_1 and h_2 are the water surface elevations immediately upstream and downstream of the dam, respectively, and AG is the gate opening.

VFL = bed material fall velocity for sediment routing. Enter 0.00 for water routing.

C. Cards 131-133 On Card 130, NDIND is equal to 1, which indicates that a gated structure is used. Cards 131 to 133 input the prescribed gate opening heights descretized following the same way as descretizing the inflow hydrographs. If NDIND = 2, then these cards should be deleted.

D. Card 134 An uncontrolled dam (NDIND = 2) is located between computational sections 8 and 9.

PRINTOUT RESULTS

Figure 7 shows an example output of computed results, using a stage hydrograph (Fig. 4) as the downstream boundary condition. The variables shown in Fig. 7 are defined below:

TIME = routing time in days

RANGE = section number and river kilometers or miles

Q = flow discharge in cms or cfs

U = flow velocity in mps or fps

D = flow depth in meters or feet

Z = riverbed elevation in meters or feet

H = stage in meters or feet

QS = sediment transport rate in cms or cfs

DZ = bed elevation change from the initial value in meters or feet

DH = stage change from the initial value in meters or feet

A = cross-sectional area in square meters or square feet

T = top width in meters or feet

TIME		RANGE	Q	U	D	Z	H	WS	DZ	DH	A	I	FROUDE NO
0.000	1	100.00	18.41	.086	2.805	153.370	156.175	.663E-06	0.	0.	215.03	123.35	.0207
0.000	2	94.00	18.41	.132	2.362	153.790	156.152	.280E-05	0.	0.	139.30	91.75	.0342
0.000	3	91.80	8.41	.058	1.956	154.190	156.146	0.	0.	0.	144.61	132.40	.0178
0.000	4	91.30	8.41	.156	1.955	153.610	155.565	.804E-05	0.	0.	53.97	136.44	.0791
0.000	5	88.30	8.32	.084	1.514	154.010	155.524	.498E-06	0.	0.	98.54	98.26	.0269
0.000	6	85.90	8.22	.106	1.874	153.640	155.514	.841E-06	0.	0.	77.55	66.70	.0314
0.000	7	81.00	20.44	.233	2.257	153.190	155.447	.254E-04	0.	0.	87.64	85.80	.0737
0.000	8	76.50	17.60	.250	.972	154.370	155.342	0.	0.	0.	70.46	108.10	.0988
0.000	9	76.20	17.60	.119	2.239	152.910	155.149	.165E-05	0.	0.	147.66	81.51	.0283
0.000	10	73.00	17.37	.050	3.362	151.780	155.142	.120E-06	0.	0.	345.35	187.13	.0118
0.000	11	70.00	17.32	.050	3.360	151.780	155.140	.119E-06	0.	0.	345.01	187.06	.0118
.025	1	100.00	18.41	.086	2.805	153.370	156.175	.663E-06	0.	-.264E-06	215.03	123.35	.0207
.025	2	94.00	18.41	.132	2.362	153.790	156.152	.280E-05	-.147E-07	-.239E-06	139.30	91.75	.0342
.025	3	91.80	8.41	.058	1.956	154.190	156.146	0.	.190E-07	-.217E-06	144.61	132.40	.0178
.025	4	91.30	8.41	.156	1.955	153.610	155.565	.802E-05	-.509E-06	.281E-03	54.01	136.45	.0790
.025	5	88.30	8.40	.085	1.513	154.010	155.523	.520E-06	.903E-07	-.273E-03	98.51	98.24	.0272
.025	6	85.90	8.44	.109	1.874	153.640	155.514	.937E-06	-.722E-07	-.556E-03	77.51	66.68	.0322
.025	7	81.00	16.10	.179	2.282	153.190	155.472	.889E-05	-.757E-07	.245E-01	89.74	85.87	.0560
.025	8	76.50	16.76	.272	.889	154.370	155.259	0.	.159E-06	-.836E-01	61.61	103.68	.1126
.025	9	76.20	16.76	.114	2.236	152.910	155.146	.136E-05	-.266E-06	-.302E-02	147.41	81.49	.0270
.025	10	73.00	16.99	.049	3.361	151.780	155.141	.110E-06	.775E-08	-.349E-03	345.29	187.12	.0116
.025	11	70.00	17.03	.049	3.360	151.780	155.140	.111E-06	-.273E-11	0.	345.01	187.06	.0116
.050	1	100.00	18.41	.086	2.804	153.370	156.174	.663E-06	0.	-.353E-03	214.98	123.34	.0207
.050	2	94.00	18.61	.134	2.361	153.790	156.151	.293E-05	-.302E-07	-.111E-02	139.19	91.74	.0347
.050	3	91.80	8.27	.057	1.955	154.190	156.145	0.	.369E-07	-.161E-02	144.40	132.39	.0175
.050	4	91.30	8.27	.154	1.954	153.610	155.564	.760E-05	-.100E-05	-.932E-03	53.85	136.43	.0781
.050	5	88.30	8.43	.086	1.513	154.010	155.523	.529E-06	.178E-06	-.982E-03	98.44	98.20	.0273
.050	6	85.90	8.50	.110	1.873	153.640	155.513	.964E-06	-.162E-06	-.116E-02	77.47	66.67	.0325
.050	7	81.00	21.67	.249	2.250	153.190	155.440	.331E-04	-.171E-06	-.768E-02	86.98	85.77	.0790
.050	8	76.50	17.07	.236	.989	154.370	155.359	0.	.344E-06	.164E-01	72.23	108.97	.0927
.050	9	76.20	17.07	.112	2.302	152.910	155.212	.128E-05	-.497E-06	.633E-01	152.83	81.86	.0261
.050	10	73.00	7.49	.021	3.402	151.780	155.182	.383E-08	.147E-07	.399E-01	352.85	188.63	.0050
.050	11	70.00	-4.24	-.012	3.410	151.780	155.190	-.388E-09	.728E-11	.500E-01	354.41	188.94	-.0028
.075	1	100.00	23.36	.108	2.818	153.370	156.188	.167E-05	0.	.131E-01	216.64	123.46	.0260
.075	2	94.00	20.40	.146	2.366	153.790	156.156	.418E-05	-.470E-07	.413E-02	139.67	91.78	.0378
.075	3	91.80	8.76	.060	1.960	154.190	156.150	0.	.563E-07	.404E-02	145.15	132.40	.0184
.075	4	91.30	8.76	.162	1.956	153.610	155.566	.938E-05	-.154E-05	.928E-03	54.10	136.46	.0821
.075	5	88.30	8.80	.090	1.510	154.010	155.520	.632E-06	.272E-06	-.407E-02	98.14	98.04	.0286
.075	6	85.90	9.11	.118	1.869	153.640	155.509	.129E-05	-.263E-06	-.516E-02	77.20	66.56	.0350
.075	7	81.00	17.87	.202	2.266	153.190	155.456	.144E-04	-.278E-06	.823E-02	88.34	85.82	.0636
.075	8	76.50	15.16	.214	.976	154.370	155.346	0.	.554E-06	.317E-02	70.80	108.27	.0845
.075	9	76.20	15.16	.098	2.363	152.910	155.273	.706E-06	-.669E-06	.124E+00	157.80	83.01	.0222
.075	10	73.00	3.63	.010	3.458	151.780	155.238	.190E-09	.202E-07	.961E-01	363.52	190.74	.0023
.075	11	70.00	-10.29	-.028	3.460	151.780	155.240	-.122E-07	.691E-10	.100E+00	363.90	190.82	-.0065
.100	1	100.00	28.32	.129	2.838	153.370	156.208	.349E-05	0.	.336E-01	219.17	123.64	.0310
.100	2	94.00	23.09	.164	2.380	153.790	156.170	.663E-05	-.655E-07	.176E-01	140.91	91.89	.0423
.100	3	91.80	9.98	.068	1.974	154.190	156.164	0.	.874E-07	.177E-01	146.96	132.43	.0206
.100	4	91.30	9.98	.181	1.964	153.610	155.574	.146E-04	-.230E-05	.927E-02	55.24	136.59	.0907
.100	5	88.30	9.11	.093	1.511	154.010	155.521	.725E-06	.408E-06	-.290E-02	98.25	98.10	.0296
.100	6	85.90	9.05	.117	1.869	153.640	155.509	.125E-05	-.362E-06	-.514E-02	77.20	66.56	.0347
.100	7	81.00	21.33	.247	2.242	153.190	155.432	.320E-04	-.381E-06	-.153E-01	86.33	85.75	.0786
.100	8	76.50	11.53	.134	1.110	154.370	155.480	0.	.747E-06	.138E+00	85.86	115.22	.0497
.100	9	76.20	11.53	.067	2.541	152.910	155.451	.176E-06	-.740E-06	.302E+00	173.23	89.86	.0153

Figure 7. Sample of Printout Results

FROUDE NO. = Froude number defined by $U/\sqrt{gA/T}$, where g is the gravitational acceleration.

The computed discharge hydrograph Q(t), depth D(t), velocity U(t), and DZ(t) at a cross section can be obtained by plotting Q, D, U, DZ at that cross section versus TIME, or can be obtained from the hydrograph output controlled by Card 24. Two computed discharge hydrographs at the downstream section are shown in Fig. 8. These two hydrographs clearly show the effects of the downstream boundary condition.

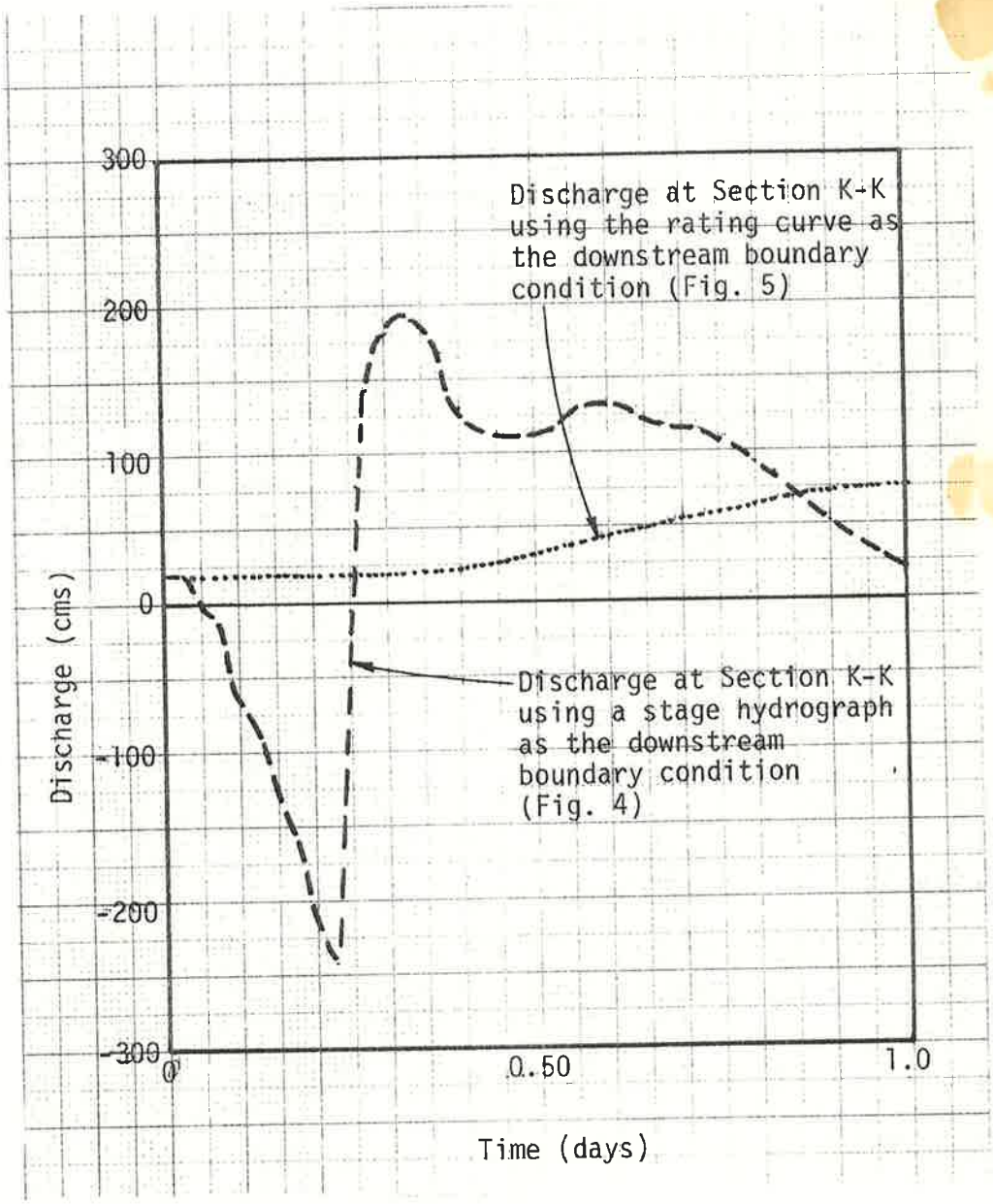

Figure 8. Computed Discharge Hydrograph at the Downstream Section

CHAPTER 16

OVERVIEW OF CASE STUDIES AND DATA MANAGEMENT

by

Daryl B. Simons, Associate Dean for Engineering Research and
Professor of Civil Engineering,
Colorado State University, Fort Collins, Colorado
Ruh-Ming Li, Associate Professor, Department of Civil Engineering,
Colorado State University, Fort Collins, Colorado
Nguen Duong, Assistant Professor, Department of Civil Engineering,
Colorado State University, Fort Collins, Colorado

16.1 INTRODUCTION

In the previous chapters (Chapters 2-15) the basic theory and fundamental tools for analysis of watershed and river systems were discussed. The analytical tools for analysis range from simple geomorphic analysis, hand-held calculator analysis, simplified computer models, and complicated computer models. In addition, the data needs for specific models were also presented. In this chapter, an overview of some case studies is presented to illustrate types of problems that are often encountered in the analysis of watershed and river systems. General data needs for analysis are discussed and an effective system for data management is presented. Then, a general approach to determine the required level of analysis is recommended.

Following this chapter, Chapters 17 to 20 will present in detail various case studies to further demonstrate practical applications of the analytical tools to solve real world problems.

16.2 OVERVIEW OF SOME CASE STUDIES

General

The following describes several case histories that illustrate the complexity of water and river systems, the associated development and utilization of mathematical modeling techniques to achieve improved planning, analysis and design.

Variation of a Canal Cross Section with Time

A canal was constructed to carry a discharge of approximately 2,000 cu ft per second. The canal cross section was approximately 80 ft wide and had an average depth of approximately 10 ft. The side slopes were originally constructed at 1½:1 (see Figure 16.1). The segment of this particular canal was constructed through a sand hill area. The bank material is very erodible. When a canal is constructed with banks consisting of such material, large width-to-depth ratios result as the channel adjusts. This can be illustrated by looking at wetted perimeter versus discharge relationships for channels with different types of bank materials ranging from highly erodible sands that will yield wide channels to cohesive materials that tend to resist erosion and may be quite narrow. When flow was introduced into this sand bank channel, rapid erosion of the banks occurred. This caused the

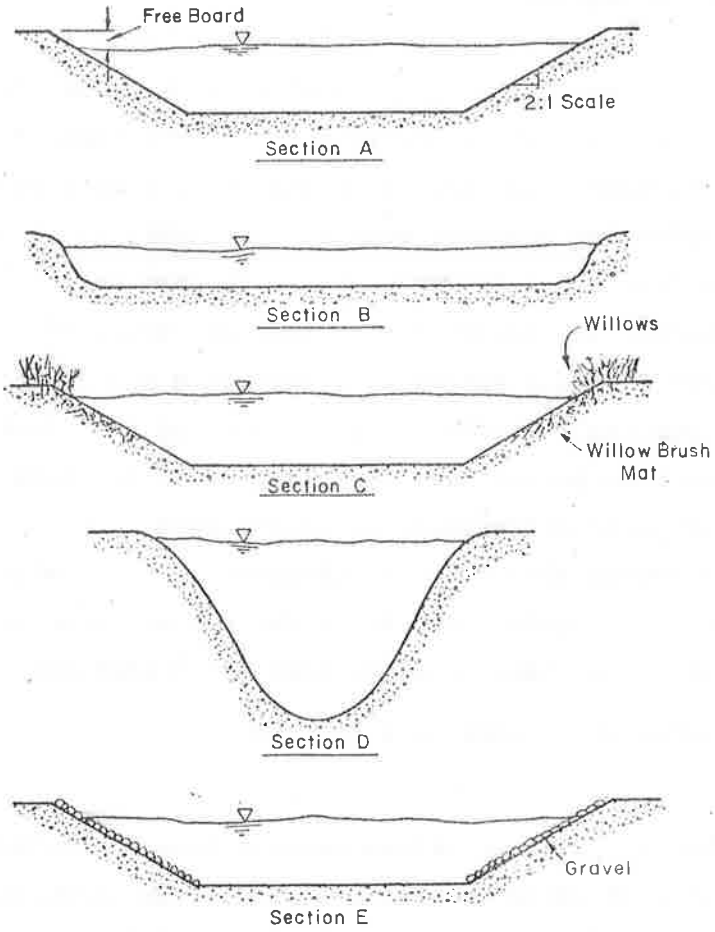

A. Original channel constructed in sand hills area

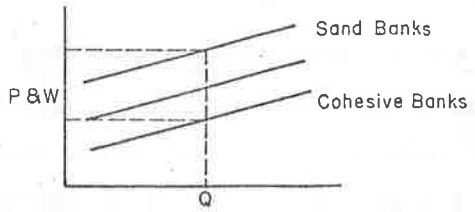

B. With sandy erodible banks the channel widened, and encroached on the right-of-way.

C. Channel was reconstructed to its original dimensions. A willow brush mat was placed on the bank and willows were planted.

D. Willow growth developed rapidly, the banks were reinforced with roots extending into the flow. The roots slowed the local velocity and trapped fine sediment particles that were being carried in suspension. The deposition of fine sediment caused the canal to develop a narrow and deep cross section which restricted the flow causing a backwater upstream that reduced freeboard and caused local flooding.

E. The channel was once more reconstructed to its original dimensions and the banks were riprapped with local river gravel. The gravel armor has done an excellent job of stabilizing the channel cross section. The Lane, Simons, Shields, etc. methods can be used to determine the size, gradation and thickness of gravel blankets to stabilize the channel and river banks, and reduce the supply of sediment downstream.

Figure 16.1 Variation of a channel cross section with time.

channel to widen from its original width of 80 ft to a width on the order of 150-200 ft. There was a corresponding reduction in depth. The widening of the channel encroached on the right-of-way and introduced numerous other problems. Hence, it was decided to reconstruct the canal cross section to its original dimensions and stabilize the banks into that position, using willow mattresses. At the same time the growth of willows in the banks was encouraged. Willow growth developed rapidly. Roots from the willows extended into the flow. The roots from the willows slowed the local velocity and trapped the fine sediments consisting of silts and clays that were transported in the flow. The result was deposition of fine sediments on the banks. As deposition occurred, the root system continued to extend itself from there into the channel. The net result was the development of a very narrow, deep channel that restricted the flow to such an extent that backwater effects caused serious encroachment on the freeboard and the canal upstream. In some instances, the backwater caused overflow and bank failure. Because of these problems it was decided to reconstruct the canal once more to its original dimensions. This was done and the banks were riprapped with local river gravel to provide protection from erosion of the flowing water. The gravel armor has done an excellent job of stabilizing the canal cross section. Furthermore, the water losses introduced by extensive growths of vegetation along the bank line have been eliminated. This type of problem can be easily handled in terms of designing the size of riprap required. Reference can be made to Simons and Sentürk (1977) that outlines the Lane method and other methods, including those recently developed at Colorado State University, to determine the size, gradation and thickness of gravel bank cuts required to stabilize such systems.

The importance of the effects of silts and clays, or the so-called wash load, on river and canal geometry cannot be over-stressed. Back in the early 1900's when irrigation systems were being developed in the Imperial Valley of California the water diverted from the Colorado River to these systems carried large quantities of wash load. The channels were sized according to current engineering knowledge. The concentrations of silts and clays in the flowing water diverted to the canals was such that berming occurred in the canals. The berms consisted of

materials that held water well, were fairly fertile and encouraged rapid growth of vegetation and grasses. As in the foregoing case, the channel narrowed dramatically with time as a consequence of the growth of vegetation at the water line, the extension of roots into the water and the trapping of fine sediments. In some instances these channels became almost pipe-like. The berms would grow out over the flowing water partly covering the channel. This change in channel geometry constricted the water cross section and increased the resistance to flow. Hence, it was necessary to regularly restore these channels to their original dimensions in order for them to convey the required quantities of water to the irrigation system.

In subsequent years there has been a rapid development of large storage facilities on the Colorado River. More and more of the sediments that normally flowed downstream are now trapped in upstream reservoirs. As a consequence, the irrigation system alluded to that originally received large quantities of silts and clays with the water diverted to it no longer does so. In fact, the upstream reservoirs trap the majority of the sediments and most of these canal systems now operate with almost a clear water environment. That is, the water diverted from the river system and its reservoirs is largely free of sediment. This change in the quality of the water brought about by upstream storage and control caused the reverse of the situation to occur in these canals. With the removal of silts and clays the water entering the canals had an opportunity to attack the banks and bed, eroding them. Where the materials were sufficiently erodible, the channels widened, depths reduced, and another set of adverse conditions developed. In this case it was possible to reconstruct these canals to desirable dimensions and armor them with properly sized gravel or riprap. This type of protection has very effectively held the channels in the desired location with the desired cross-sectional dimensions. Again, design of stabilization works for such systems can be handled as was cited above.

To further illustrate the possible effects of silts and clays on channel geometry, let us refer to a river system in the western United States that up until the early 1900's carried relatively large quantities of silts and clays during periods of high flow while the channel was actively changing form. At that particular time the channel was

relatively stable, there was vigorous growth of vegetation on bars and on the bank line and, for a significant part of the year, the channel was reasonably stable. Major channel changes only occurred during major flow events. In the early 1900's a major earthquake in the area caused a large landslide to form a dam of considerable size across the river valley. This resulted in a lake. The lake is of sufficient size that it has essentially removed the silts and clays that normally flow in the river at high stages. In the absence of silts and clays downstream, during high flow events the banks and bars were attacked and new bars were formed, but these new bars and new bank lines had little silts and clays in them as a consequence of the desilting upstream and they were unable to hold moisture for a sufficiently long period to allow the growth of vegetation. Consequently, in recent decades the bank lines have changed, new bank lines have formed, but without silts and clays in the newly deposited material, and no new vegetation has been able to grow. The end result has been the elimination of a significant amount of riparian vegetation along the stream line, greatly reducing the beauty of the stream system and in many ways deteriorating it from the viewpoint of recreational use, fisheries habitat, etc. Once again, the potential for change exists when the wash load concentrations flowing in either canals or rivers are altered.

As a final example of the importance of wash loads on river and canal morphology, a study was conducted by Colorado State University in Venezuela that extended over a period of years. This study dealt primarily with the geomorphology and the hydraulics of rivers and the relationship of these river systems to the watersheds. It was found that vegetation developed and grew along certain segments of the bank line and floodplain. In other sections or locations it could be identified that vegetation sometimes started growing but died before a root system could be developed due to an inadequate supply of water and nutrients. Conducting extensive soil sampling along the banks and in the floodplains of these rivers showed that in every case where a substantial growth of vegetation was occurring, there was a significant percentage of silts and clays. Hence, where a river system experiences natural cutoffs that subsequently fill with finer sediments, an environment is developed that can support rapid and vigorous growth of

vegetation. In those segments of the floodplain that consist largely of gravels and sands, the area drains so rapidly that significant vegetation usually does not develop.

Degradation Analysis of a Small Dam

There are many small dams that are built for a single purpose including flood control, low head hydropower generation, erosion control, irrigation, etc. The major impacts include the aggradation in the upstream and the degradation (local scour and general scour) in the downstream reach (see Figure 16.2). Baffled chute spillways are often utilized as the emergency spillways for these small dams to dissipate the energy associated with the design of freeboard discharge. The required analysis involves the determination of the magnitude of degradation to be expected downstream from the emergency spillway chute during passage of the design hydrograph. Such an analysis is required to determine how far the baffled outlet end of the chute must extend below the present channel grade. In order to provide enough information for an adequate design, different conditions that depict the future water and sediment inflows to the dam prior to the occurrence of the design hydrograph are required. Examples of cases that could be considered follow.

Case I considers that the reservoir is 90 percent filled with sediment resulting from a series of small floods, prior to the occurrence of the design hydrograph. These small floods pass all of the flow through the principal spillway. The degradation due to the design hydrograph would be negligible and the total expected scour depth below the structure is equal to the general scour depth resulting from the flows through the principal spillway. Case II assumes that immediately following the closure of the dam the water storage has reached the top of the dam and the sediment storage capacity has enough room for the sediment yield associated with the design hydrograph. Under this condition, the emergency spillway chute would pass the freeboard hydrograph with essentially clear water. This is because nearly all of the sediment will be trapped upstream of the dam. The third condition, Case III, may represent the worst possible condition which assumes that after a long period of operation, two 50-year floods and one 100-year flood occur prior to the passing of the design hydrograph. The total expected scour

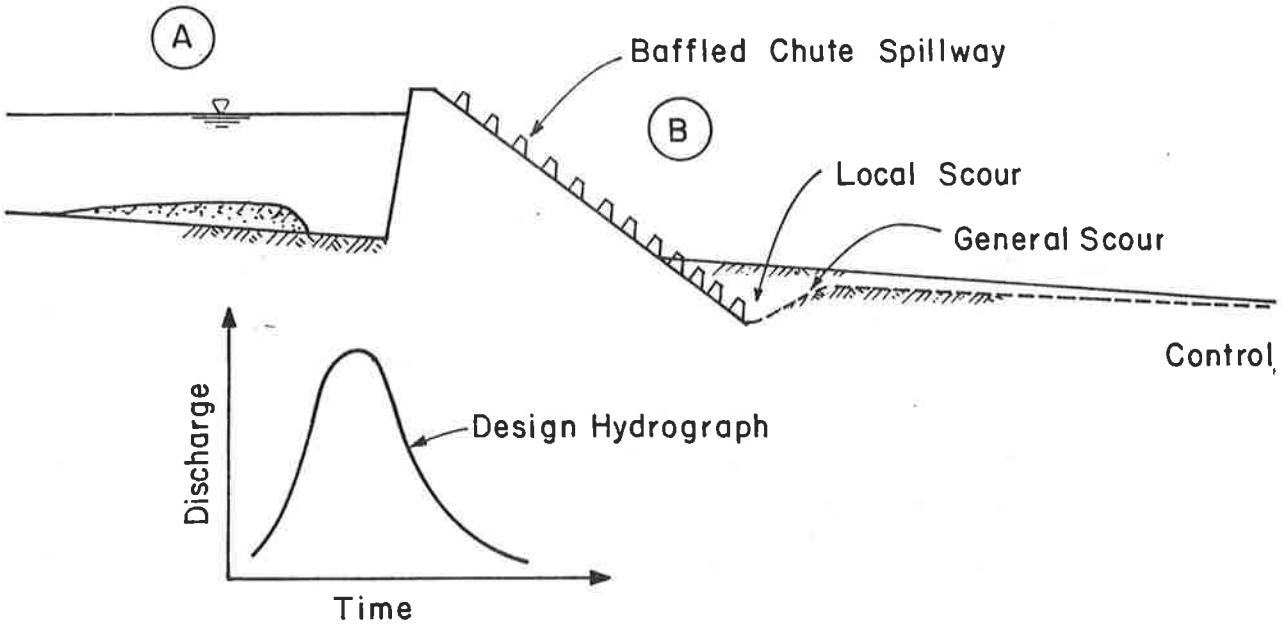

A. Major upstream effects of small reservoir

   1. Aggradation

   2. Decreased capacity

B. Major downstream effects of small reservoir

   1. Degradation (local scour and general scour)

   2. Bank erosion

Figure 16.2 Impact of construction of a small dam.

is the sum of the general scour due to flows through the principal spillway for a long period of operation and the general and local scour resulting from a sequence of two 50-year floods, one 100-year flood and the freeboard hydrograph. This condition is very unlikely to occur yet constitutes the worst possible condition in determining the degradation below the emergency spillway structure. The determination of the change in sediment storage is vital for the evaluation of both Case I and III. This requires the estimation of the annual sediment yield and sediment yields resulting from various sizes of storms from the watershed. The magnitude of scour can be determined utilizing a sediment routing procedure and considering the size fractions of bed material. This computational procedure will involve use of a sediment transport equation, the sediment continuity equation, the armoring effect of coarse materials, and the channel geometry equation. An example of this design case will be presented in Chapter 18.

Gravel Mining Impact in Streams

Gravels are important natural resources that are required for construction. As population grows, the acquisition of gravels is steadily increasing. Removal of gravels from streams may induce either positive or negative impacts on the stability of stream morphology. Unwise gravel mining activities often result in significant adverse impacts on the river environment. Figure 16.3 illustrates such a case history. Since 1969 a gravel mining company has excavated approximately 6,500,000 tons of gravel and sand in the San Juan Creek, Orange County, California. This gravel and sand mining activity resulted in a vertical cut of approximately 55 ft of the stream bed near the Casper regional park before the end of 1977. Three storms in early 1978 induced a series of significant stream morphology changes. Measured profiles before and after each of the storms are plotted in Figure 16.3. The deepest erosion depth was about 30 ft and extended approximately 3,500 ft upstream of the park boundary. A major effort to rehabilitate the Casper park was required. In order to evaluate various alternatives, a mathematical model for routing sediment by size fraction was developed and utilized (see Chapter 18). Four engineering alternatives were evaluated. Alternative I is a "do nothing" plan terminating the mining of sand and gravel. This alternative would allow natural healing processes in the

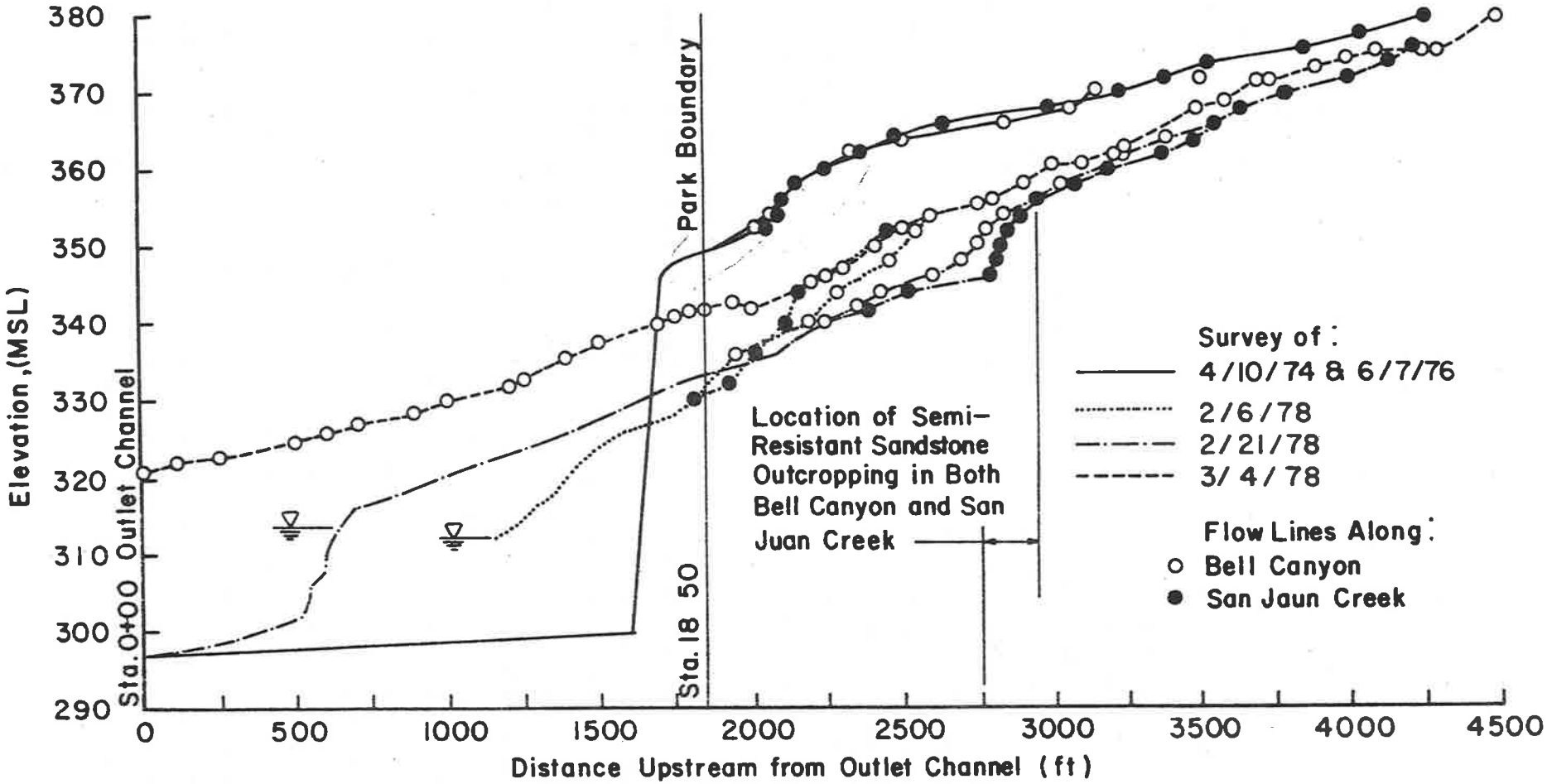

Figure 16.3 Measured bed profiles.

form of aggradation to take place. No mitigation measure would be imposed on the existing stream. Alternative II is essentially the same as Alternative I except it permits regular mining of sand and gravel. Alternative III proposes construction of a drop structure located near the upstream end of the gravel pit. Alternative IV proposes construction of a series of small gabion check dams near and upstream of the gravel pit boundary coupled with regular gravel mining.

Removal of Dams from River Systems

Many dams are in existence in the United States and the world. The removal of dams from river systems happens from time to time either by man or by other causes such as natural disasters. The potential impacts on the downstream reach caused by the removal of a dam are illustrated in Figure 16.4. The impacts resulting from a released wave of sediment include: 1) sediment migrates downstream, 2) conversion of gravel bed stream to sand bed stream, and 3) the sand wave will form sand bars, dunes, etc. that may increase or decrease resistance to flow, velocity, sediment transport, stage, flood, etc. A careful environmental impact analysis is often required to assess the short- and long-term effects of the downstream system. The movement of a sand wave through a river system as results from removal of a dam is a complicated problem. This problem includes the rate of sand wave movement, the degradation upstream of the old dam site, the deposition of the material along the upstream channel, the possible changes in water surface elevations and velocities and the possible effects on the channel stability and flood potential. Simple but realistic assumptions are needed to obtain a solution to this problem in a practical and economical way. The dominant physical processes considered in the analysis should include: the flow of water, sediment transport, sediment routing, degradation, aggradation, and bed control due to the presence of an armor layer at small to intermediate discharges. The governing equations include the continuity equations for water and sediment, the momentum equation and the energy equation. The processes governing water and sediment movement are unsteady in nature, therefore a routing procedure is needed. In order to simplify the problem, a known discharge assumption (Chapter 12) can be used if the study reach is not too long and the primary objective of analysis is

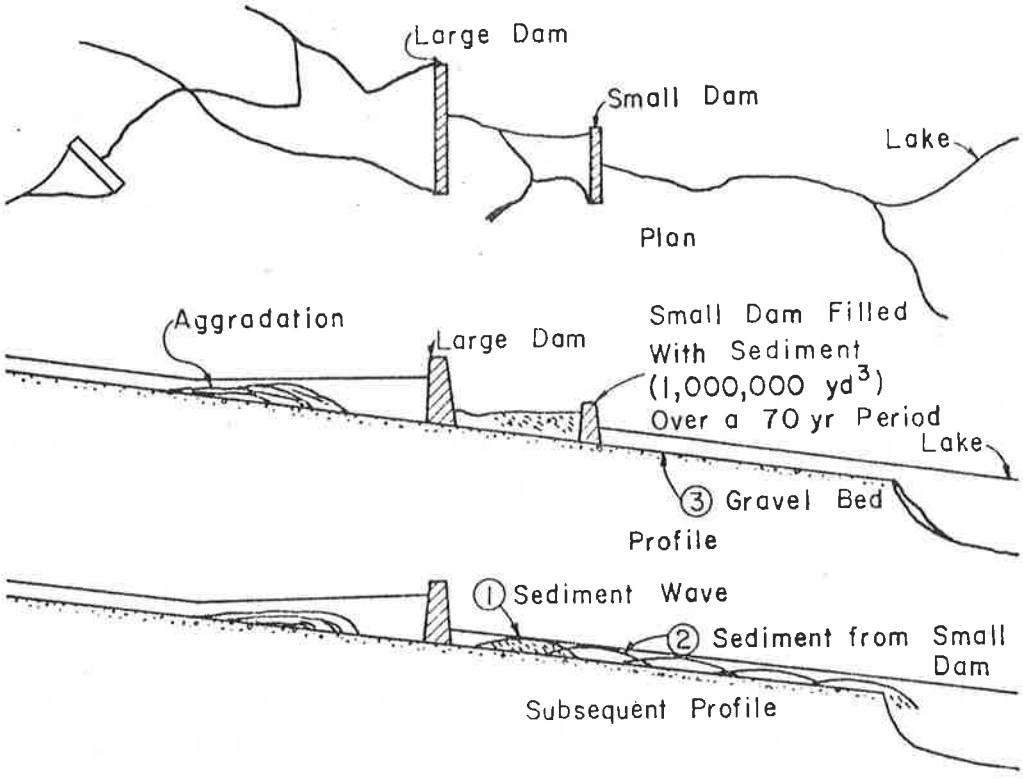

1. Released wave of sediment (1,000,000 yd^3)

2. Sediment wave moved downstream

3. Converted gravel bed stream to sand bed stream

4. The sand wave will form sand bars, dunes, etc. that may increase or decrease resistance to flow, velocity, sediment transport, stage, flooding, etc.

5. It is necessary to eliminate the rate at which the wave of sediment will move downstream and what will be the short- and long-term effects?

Figure 16.4 Response of river to removal of small dam.

to analyze the movement of sand waves. An example of analysis associated with the dam removal will be given in Chapter 18.

Flood Hydrograph from a Watershed with a Series of Cascade Sub-basins

Most of the conventional methods for determining the flood hydrographs from watersheds are based on the average basin characteristics. The resulting hydrographs usually are nearly symmetrical in shape and fairly short in duration (see Figure 16.5b). An inspection of the basin characteristics including shape and topography (Figure 16.5a) will suggest that the hydrograph shape is questionable. The topography of the watershed should be approximated by a series of cascade sub-basins when a large variation of slopes exists. The multiple watershed model presented in Chapter 7 would yield a more reasonable hydrograph shape similar to Figure 16-5c. When determining a probable maximum flood, a large discrepancy can result between these two approaches (see Chapter 19).

Flow Around a Sharp Bend

Because of restriction due to space and other reasons, it is sometimes necessary to divert a large flow around a sharp bend with a short radius. Figure 16.6 introduces a system of sharp bends with breaking bed slopes. If the design flow is large, such as a probable maximum flood, the hydraulic design is difficult. To assess the adequacy of the system shown in Figure 16.6, it is necessary to evaluate the hydraulic characteristics, hydraulic performance and stability of the system. The major hydraulic considerations require determination of: 1) Depth of flow, 2) velocity of the flow, 3) regime of flow, 4) super-elevation of the water surface in the bend, 5) the depth of aggradation near the bend, 6) the increase in depth of flow caused by separation in the bend, and 7) riprap requirements along the bend.

The depth of flow and velocity can be determined utilizing the slope of the system and a proper Manning's resistance coefficient. With this system the stream power (the product of average velocity and boundary shear stress) will be sufficiently large that the flow will be in upper regime with antidunes. These antidunes occur in the form of unstable surface waves that have a maximum amplitude approximately equal to the depth of flow. As the water and sediment traverse the bend,

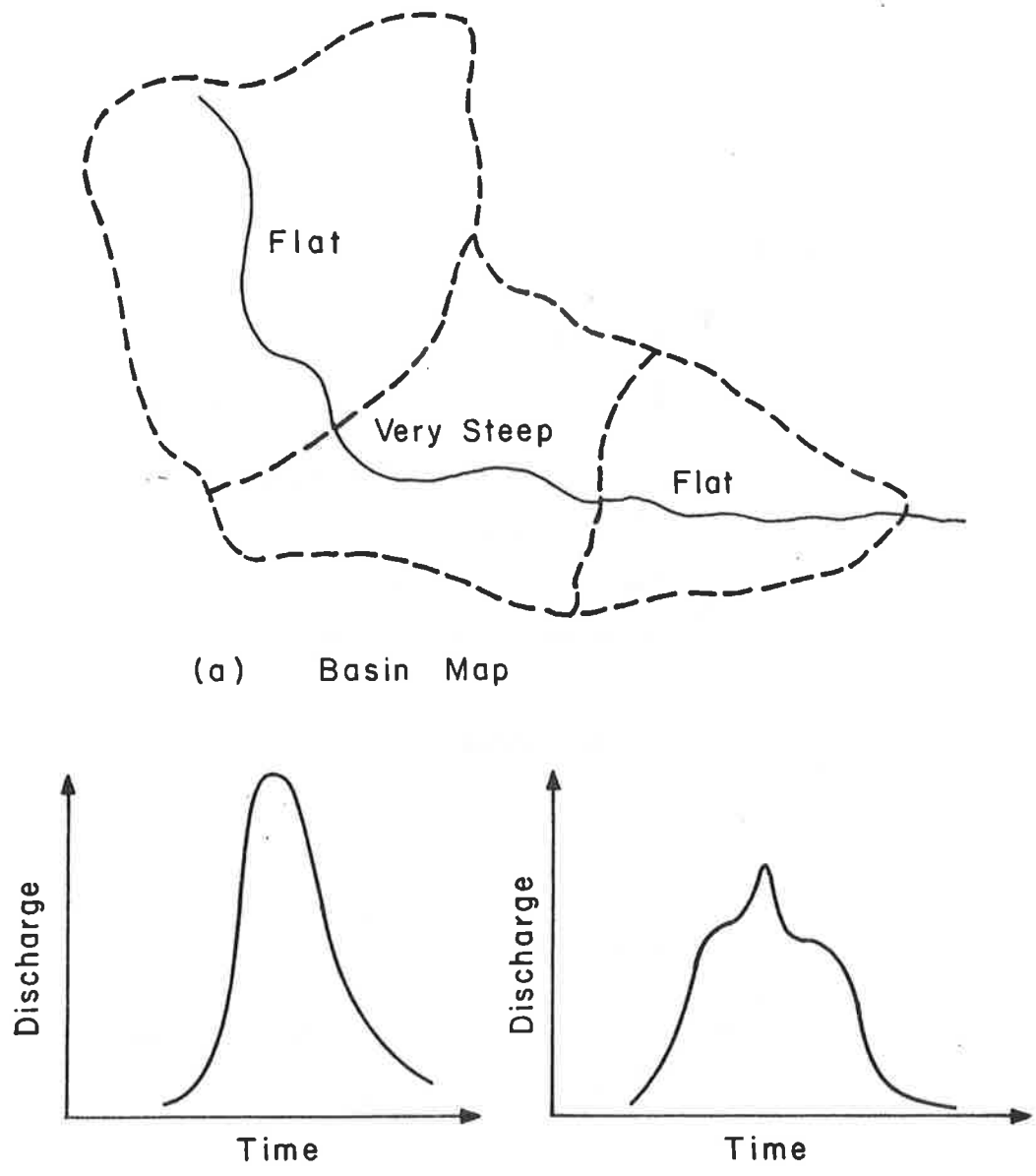

Figure 16.5 Flood hydrographs.

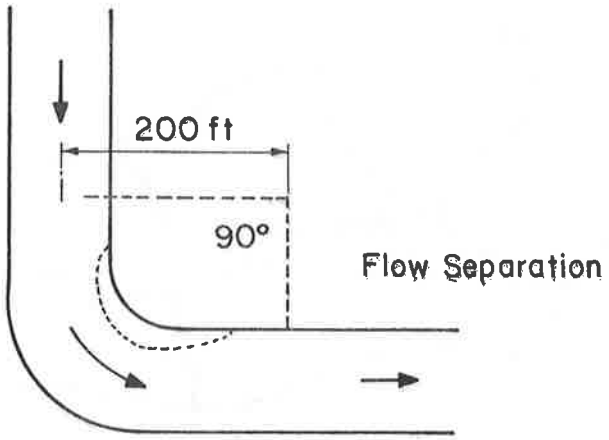

(a) Plan View

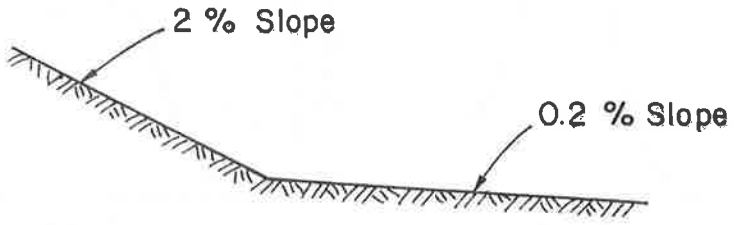

(b) Bed Profile

Figure 16.6 Flow around a bend with breaking slopes.

the water is superelevated on the outside of the channel. The channel will carry both water and sediment and because of nonuniformity of sediment transport caused by variations in channel slope and cross-sectional geometry, it will experience local aggradation and degradation which will affect the channel's capacity to transport water and sediment. Also, the high velocity flow will cause separation of the flow from the boundary resulting in a reduction in the effective cross-sectional area, deposition of a point bar and an increase in depth of flow. The relatively large bed material load and the variation in the sediment transporting capacity of each element of the system will induce local aggradation and degradation until the system adjusts to a new equilibrium.

Flow Diversion Problems

Flow diversion problems frequently occur in the urbanized areas. The flow diversion would cause unbalanced sediment distribution in the channel system, which may cause aggradation in some reaches and degradation in other reaches. Figure 16.7 illustrates an example of potential problems. If the degree of urbanization is increased, more serious problems associated with degradation, aggradation and channel bank erosion will be introduced. The flood protection project for the school should be evaluated according to short- and long-term response of the system.

Evaluation of Data Collection Program

Data is the key element for monitoring and studying the system response of a watershed or river. The increasing use of mathematical models for evaluating proposed land-use practices has verified the necessity of obtaining good sets of data for development, modification, calibration, verification, sensitivity analysis, and successful application of models. Unfortunately, many existing data sets are neither accurate nor adequate for detailed system analysis utilizing mathematical models. When a data collection network has been improperly designed and operated it often provides inaccurate and inadequate information that is neither spatially or temporally consistent. In other situations data is collected that is unnecessary considering the purposes of study. In addition, poor data sets are not usually identified, resulting in a waste of considerable time and effort in their collection and analysis. It is very important that a clearly-defined methodology be developed for

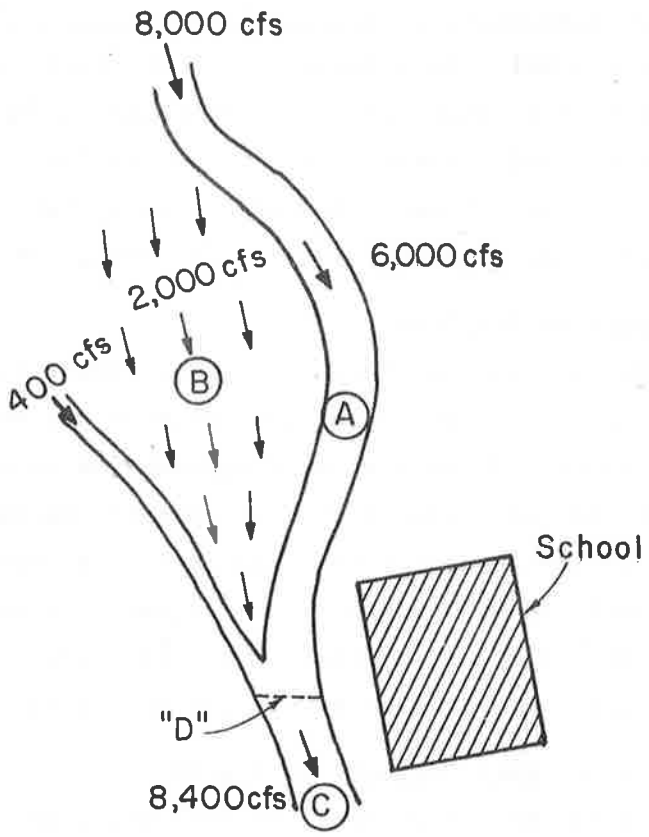

A. Reach above "D"

   1. Aggradation

   2. Increase stage

B. Flow diversion area

   1. Aggradation or degradation depending on physical environment

   2. Aggradation if highly urbanized

C. Reach below "D"

   1. Degradation

   2. Bank erosion

Figure 16.7 Flow diversion problems.

evaluating and/or designing data monitoring and collection programs of existing and proposed data collection networks. With an adequate data collection, evaluation, and design scheme it will be possible to efficiently and economically collect useful data. There are many cases in which hydrologists or hydraulic engineers are requested to evaluate a specific data collection program.

The data collection methodology adopted should be dependent on the type of data required, the frequency and accuracy of sampling, the manpower requirement, and economic constraints. The measurements can be automatic or man-operated depending on instruments. For evaluating and/or designing a data collection program, the spatial and temporal designs of the data collection network are the most important items. For example, typical questions are: "How many gaging stations are required?", "Where should they be located?", "When should they be operated?". The adequacy of spatial and temporal designs is dependent on the purpose of the study, the spatial and temporal variability of a physical environment, and the desired accuracy of analysis. A systematic approach to the solution of this problem should be developed. This approach will include identification of the problems, the survey and evaluation of the current data base, the application of available mathematical models to determine the sensitivity and hence the importance of each element of data and to evaluate the adequacy of the spatial and temporal designs of the data collection program. Often available data do not adequately describe the spatial and temporal variations in the system. Application of physical process simulation models calibrated by utilizing available data to generate the spatial and temporal variations is the most feasible way to examine the temporal and spatial data requirements. An example of the evaluation of a data collection program will be given in Chapter 19.

Floodway Analysis and Flood Insurance Program

The conventional flood level analysis relies on the HEC-2 program developed by the U.S. Army Corps of Engineers. For a realistic flood analysis the impacts of sediment and debris on the flood level should be determined. The proposed analysis should be different from the conventional HEC-2 analysis. It should recognize that the channel bed is movable and adjustable, responding to scour and deposition. The

analysis should consider both aggradation and degradation of the channel and provide the necessary information to: 1) evaluate the potential for blockage at bridges and channel restrictions resulting from aggradation, 2) determine the potential local scour downstream of structures, 3) determine possible flow diversions, and 4) estimate the effect of sediment aggradation on the water surface profile. In addition to the erosion and sedimentation analysis, potential problems associated with vegetative debris are studied, particularly in relation to possible blocking of the channel at bridges. An example of floodway analysis will be given in Chapter 17.

Bunay-Barry Canal Design

A general layout of the Wadi Canal system, Yemen Arab Republic, is given in Figure 16.8. Because the canal system intakes water from the river draining a steep watershed in the arid area, the problems encountered in the Wadi Canal system are unique in many respects compared to usual canal design problems. The unsteady input of water and sediment to the canals, the high sediment load of the Wadi and the heterogeneous distribution of bed and transported material all contribute to the difficulty of the problems involved.

The source of water for the canals is the flood flows of the Wadi Zabid which fluctuates to a great extent considering both the discharge and the sediment. In the past the water has been diverted by a temporary earth dike constructed across the Wadi. When a large flow occurred in the Wadi, the dike was destroyed and it was usually impossible to rebuild the dike until the next dry season. Concrete diversion weirs are being constructed to command the remodeled canal system. The canal should be designed either to transport the sediment through it or to have both stable banks and bed for the design discharge. If the primary objective is to transport the sediment inflow, the canal design bed slope must be fairly steep since the banks would erode unless stabilized. Conversely, if the primary objective of the design is to have both stable banks and bed, the design bed slope must be flatter. This would greatly reduce the capability of the canal to transport any measurable bed material load. This design alternative would be attractive if the sediment concentration in the water supplied to the canal was relatively small.

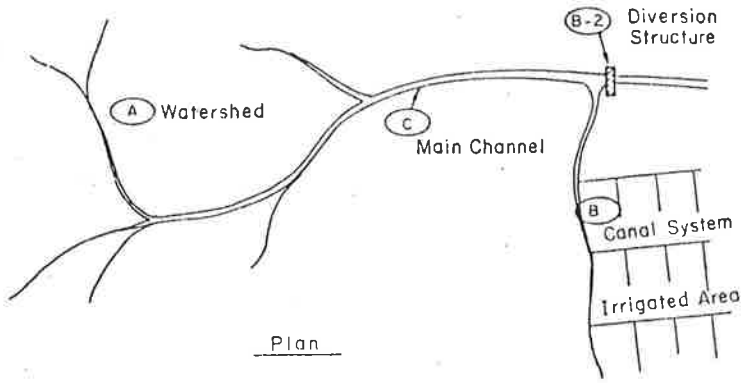

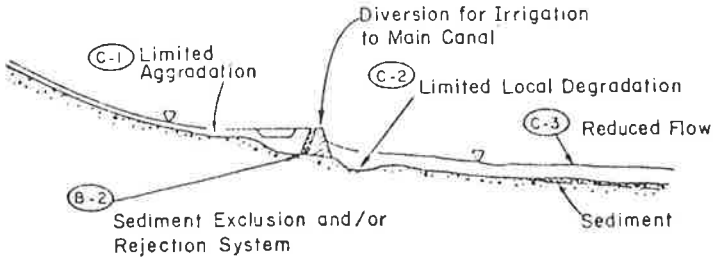

Profile

A. Watershed Characteristics

1. Steep slopes
2. Small flows
3. Large velocities
4. Relatively coarse bed and bank materials
5. Large sediment transport rates

B. Canal System Characteristics

1. Designed to operate on a flat gradient to assure stability of banks and beds of the canal system
2. Sediment delivered to the canal system has been reduced by use of sediment excluders at the diversion dam. Even so, it is difficult to reduce the sediment load to the point where the canal system can carry the sediment without depositing part of it in the canals, laterals, ditches, etc.

C. Effect on Main Channel

1. Limited aggradation upstream of diversion dam
2. Limited local degradation downstream of diversion dam
3. Downstream flow reduced due to diversion for irrigation. This reach will receive more sediment than it normally would from upstream, after the small reservoir upstream of the diversion dam is filled with sediment. Hence, significant aggradation may occur over time downstream of the diversion structure.

Conclusion

In this type of system it is virtually impossible to design a system that will not experience aggradation and require maintenance. However, with a detailed analysis of the systems the problems can be minimized.

Figure 16.8 Watershed, river and irrigation systems.

Impact of Construction of a Large Dam on a River System Upstream of a Diversion to an Irrigated Area

A particular river system and its watershed was of such a nature that during most of the year the water flowing in the river channel carried significant percentages of fine sediments comprised of silts and clays. An irrigation system was developed that diverted water from this river long before there was any construction of dams upstream of the diversion structure (see Figure 16.9). The main canal diverts water from the river system to the irrigated area at a diversion structure. Thereafter, it flows around the side hill comprised of rather permeable materials including sands and gravels, passes through a city area where there is relatively dense development along both sides of the channel and then continues downstream to serve the distant irrigated area.

Recently, a large storage dam was constructed on a river immediately upstream of the diversion structure that serves the irrigation system. The reservoir is in effect a desilting basin, and water released from there is essentially clear. This clear water released from the dam flows down the short reach of river channel and is then diverted by means of the diversion dam to the irrigation canal. This release of clear water may cause some degradation immediately downstream of the dam as one would anticipate. Then the essentially clear water enters the canal. There has been some degradation in the main channel and bank erosion that has exposed more permeable bed and bank materials. This has increased seepage losses. There are several major detrimental factors as a consequence of the increased seepage from the canal.

1. A significant decrease in the amount of water that can be delivered to the farm units for irrigation.
2. The seepage from the canal system has the potential to cause a rise in the water table. The increase in the level of the water table may cause extensive damage to adjacent buildings by filling the basement levels with water.

There are, of course, other potentially detrimental factors that can adversely affect the irrigation system. For example, with clear water in the canal system it will be an ideal environment for the growth of aquatic plants. With these plants choking the channels, there will

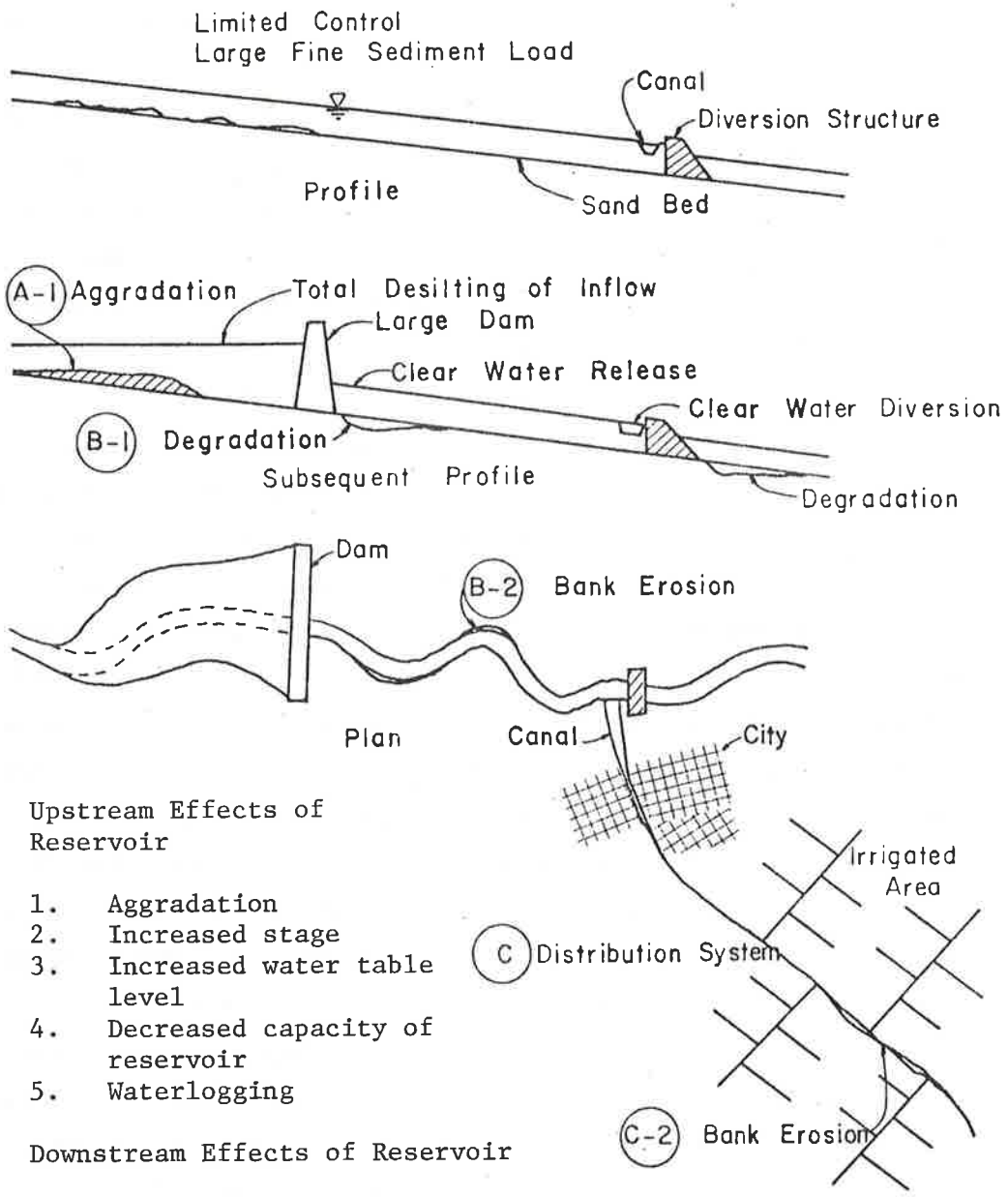

A. Upstream Effects of Reservoir

1. Aggradation
2. Increased stage
3. Increased water table level
4. Decreased capacity of reservoir
5. Waterlogging

B. Downstream Effects of Reservoir

1. Degradation
2. Bank erosion

C. Effects on Distribution System

1. Degradation
2. Bank erosion
3. Increase seepage losses
4. Growth of aquatic plants
5. Reduce efficiency of irrigation system requiring redesign

Figure 16.9 Impact of construction of a large dam on a river system upstream of a diversion to an irrigated area.

be added water losses and it will be difficult to convey the water required to the irrigation systems. Therefore, some type of periodic treatment will be required to keep the channels free of vegetation. There is another important issue on the farm units. Where land has been irrigated by diversions from head ditches into furrows, the head ditches were spaced so that a fairly efficient application of water could be made with water containing silts and clays. With silt and clay in the water, relatively long runs were possible. When one attempts to use these same lengths of runs with clear water there are excess seepage losses and, in fact, before the water reaches the ends of the furrows, all of it is infiltrated thus building up the groundwater level. This means that the distribution systems on the farm units must be dramatically changed. Length of runs may have to be cut in productive space. The numerous ditches may also add to problems of harvesting.

As referred to previously, the clear water tends to scour the banks and degrade the bed of the canal system. If the attack is sufficiently severe, channel stabilization of some nature may be required or, as another possibility, some type of lining may be required to minimize the losses of water and to provide stability to the system.

In summary, it is important to stress than canals and river systems develop in accordance with the forces to which they are subjected. When conditions are altered, a variety of responses is initiated in rivers, canals and watersheds that supply water to the river systems. It is necessary, then, in carrying out these developments to utilize methods of analysis such as mathematical models to investigate the potential for change and to help identify both the favorable and adverse factors that may result from the development and subsequent changes to the system. In addition, it should be stressed that systems are continually being subjected to changes and once one has an operational model for the system one can periodically evaluate long-term response resulting from changes in upstream and downstream developments in the basin. The necessity for overall basin planning cannot be over emphasized. To carry out a meaningful investigation for basins and sub-basins the mathematical approaches utilizing process models and management models are essential.

The Response of a River System and Intervening Reaches of Channel to the Construction of Major Reservoirs

In the analysis of river systems it is usual to find water resources development projects that involve the construction and use of major reservoirs. Such a case is outlined in Figure 16.10. The reservoir, identified as "A", has been constructed on a major river. Reservoir "B", further downstream, is planned for subsequent development. At location "C", there is a city that will be affected by the backwater from reservoir "B". With this general background, consider the responses of the system to the development. To begin with, reservoir "A" is large. It stores on the order of 10,000,000 acre/ft of water. However, even though it is large, it only stores a small percent of the flow that is discharged from its watershed annually. This is illustrated by the small inserted hydrograph. This particular hydrograph points out that approximately five times the volume of the reservoir runs down the river system each year. Literally all of the sediment carried into the reservoir is trapped and the quantity of water that is desilted is approximately equal to five times the volume of the reservoir, about 50,000,000 acre/ft per year. The sediment load carried by the river is average to large. This means that desilting of such a large volume of water causes a large volume of sediment to be deposited within reservoir "A" each year. This deposition can significantly decrease the storage capacity of the reservoir for hydropower, irrigation, and flood control in a relatively short time. Furthermore, essentially clear water is released downstream of the dam. The channel is comprised of materials ranging from fine sand, silts and clays, to coarse gravel. The fact that there are coarser materials in the bed of the stream will tend to limit the degradation induced downstream of the dam by the release of clear water. Nevertheless, it is essential not only to evaluate the rate at which the loss of live storage will occur in the reservoir, but also to document the rate and magnitude of ultimate degradation so that the structure's safety can be adequately considered.

Next, consider reservoir "B". This particular reservoir has approximately the same storage capacity as reservoir "A". The waters released into this particular reservoir will be essentially clear insofar as the water coming through reservoir "A" is concerned. On the other

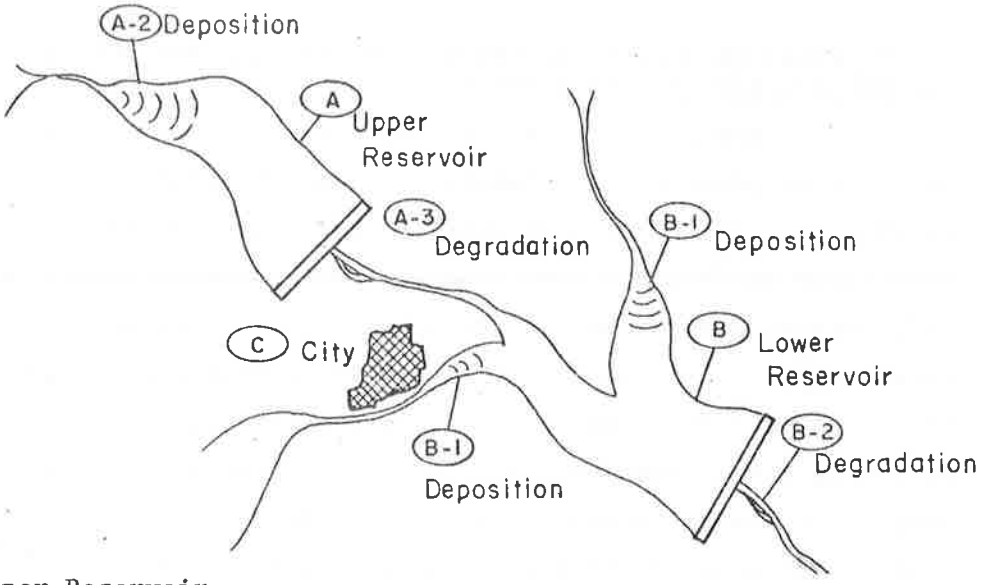

A. Upper Reservoir

1. Large volume of runoff
2. Desilting of 5-6 times the storage capacity of the reservoir, hence rapid filling with sediment
3. Downstream degradation limited to armoring of bed, lateral movement and bank erosion

B. Lower Reservoir

1. Deposition in upper reaches, including below reservoir "A" after it has filled with sediment
2. Degradation downstream of the structure

C. Effects on City

1. Backwater of reservoir
2. Deposition of sediment
3. Increase in river stage
4. Flooding
5. Increase in groundwater level
6. Flood protection required. Designed to consider changing stage with time

D. Conclusion

Analysis should consider routing sediment through the second major reservoir by releasing first part of runoff through reservoir and storing last part

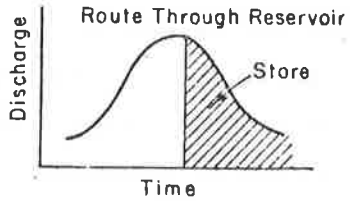

Figure 16.10 The response of a river system and intervening reaches of channel to the construction of major reservoirs.

hand, in the vicinity of city "C" and on the upper side of Figure 16.10 two other river systems that flow into the reservoir can be seen. These are not desilted and, consequently, will carry significant quantities of sediment into the reservoir. Once again it is necessary to consider the rate of loss of live storage as a consequence of inflowing sediments. It should also be recognized that ultimately reservoir "A" will lose its capacity to store sediment and sediments may be discharged from reservoir "A" to reservoir "B". On the other hand, there is the possibility that other reservoirs upstream of reservoir "A" will be constructed over the next decade or two. This type of activity can significantly increase the lifetime of reservoirs such as "A" and "B". This is very typical of what has happened to downstream reservoirs due to the construction of upstream reservoirs along the Colorado River.

Because of the importance of sediment in terms of the economics of operation of the reservoirs over long periods of time, an interesting problem with respect to reservoir "B" is to attempt to construct it in such a way that relatively large quantities of sediment can be discharged annually from it instead of being stored within it. This would involve building a large gated structure, put together in such a way that reservoir "B" could essentially run as an open river during those periods of high flow when water could be passed through the system. Then, toward the end of the runoff period, it would be necessary to close the gates in sufficient time to allow filling of the reservoir. With this type of operation it would be necessary to empty the reservoir annually. Otherwise, it would not be possible to pass excess sediments through the reservoir system. Hence, it can be seen that there are many trade-offs that have to be considered when determining the economics of these systems as well as the response of the rivers and impacts that may result.

Next, refer to location "C" on Figure 16.10. Here a city is located on a river discharging into an arm of the reservoir. The backwater from the reservoir may require construction of flood protection works for the city. In addition, just determining water levels in the vicinity of the city is not adequate. It is necessary to route the water and sediment down the river system into the reservoir to determine the rates of deposition, the locations of deposition, and how these deposits of sediment may increase river stage, aggravate the flooding

situation, increase the groundwater level, and perhaps cause other adverse responses. Once again it is stressed that the response of these systems is complicated and the best possible way of evaluating the response of the river systems involving rates of deposition in the reservoirs, aggradation upstream of the reservoirs, degradation downstream of the reservoirs, the lifetime of the reservoirs, and the economic production of water for irrigation, hydropower, and municipal use, is by comprehensive model studies such as those identified earlier.

In order to carry out these comprehensive model studies involving reservoirs and the responses of river systems and watersheds, it is essential that there be an adequate data base. In most instances the data base is probably inadequate. There are various alternatives that can be utilized to help alleviate this problem. One is to involve the use of physical models with the mathematical models where detailed information on the performance of portions of the structure or short river reaches is desired. It is, in fact, entirely feasible to produce how the system will respond using physical models. However, certain field data are necessary in order to validate the physical model. Consequently, whether it is a physical model, a mathematical model, or a combination of both, it is necessary to carefully overview the system, determine those data which exist, and conduct a study to determine how important actual data are to obtain accurate results. With this knowledge, a data base can be formulated. It is recognized that to obtain an adequate data base of all the hydrologic and climatological variables may require years. Hence, in most instances river development proceeds without all of the desired data. This makes the physical process model more applicable to the analysis. With properly constituted physical process models, one can minimize the amount of data required and can arrive at logical conclusions regarding evaluation of river development. Note that it is feasible to gather the existing data, synthesize missing data, formulate process models and analyze the system to gain a better answer in terms of the design, the long range planning, and the spatial and temporal response of the system using physical process models, than by any other methodology presently available. Furthermore, these models, since they are based upon physical processes, can be used

continuously through the construction of the project, and after implementation of it, to predict and adjust methodologies related to operation of the system to obtain optimum economic results.

Conceptual Distribution of the Ganges River Water and Associated Problems

Record low flows occurred on the Ganges River during the dry seasons of 1975, 1976 and 1977 causing grave concern that upstream development and diversions could seriously alter an important natural resource and reduce an important part of the downstream water supply which could in turn adversely affect the economic development of the nation. Again, this is a type of problem (see Figure 16.11) that is amenable to mathematical analysis coupled perhaps with physical models of segments where complexities of the system are such that detailed information is required. The problem of the diversion of the Ganges River flows encompasses many facets, including environmental and ecological considerations, groundwater development, irrigation, water for municipal supplies, saltwater intrusions and the actual fate of spill rivers. In many instances only limited data are available with the exception that relatively long flow records in terms of river stage have been gathered. However, the accuracy of these records needs to be verified. In connection with the analysis of the Ganges River problem, sediment-related problems should be evaluated. A quick survey of the river system and the use of the river's waters verifies that sediment is a major problem affecting diversion structures, spill channels and navigation. The Ganges River is subjected to a wide range of flow conditions and it reacts accordingly. The river channel has characteristics that are transitional between that of a meandering and braided river. Low flow gradients and low discharges fall in a range where meandering occurs and the characteristics of a meandering river develop. The low flow meandering channel is destroyed and replaced by a transitional condition at intermediate and higher flow stages. The velocity and sediment transport in the channel are large and the system is quite unstable as indicated by rapid channel changes, bed erosion, and formation of new bars and fresh bank erosion.

The bed material consists of a small percent of clay, some silt, and predominantly fine sand with a median diameter ranging from 0.15 to 0.30 mm depending upon sampling techniques. This material is highly susceptible to erosion and transport at intermediate and high flows.

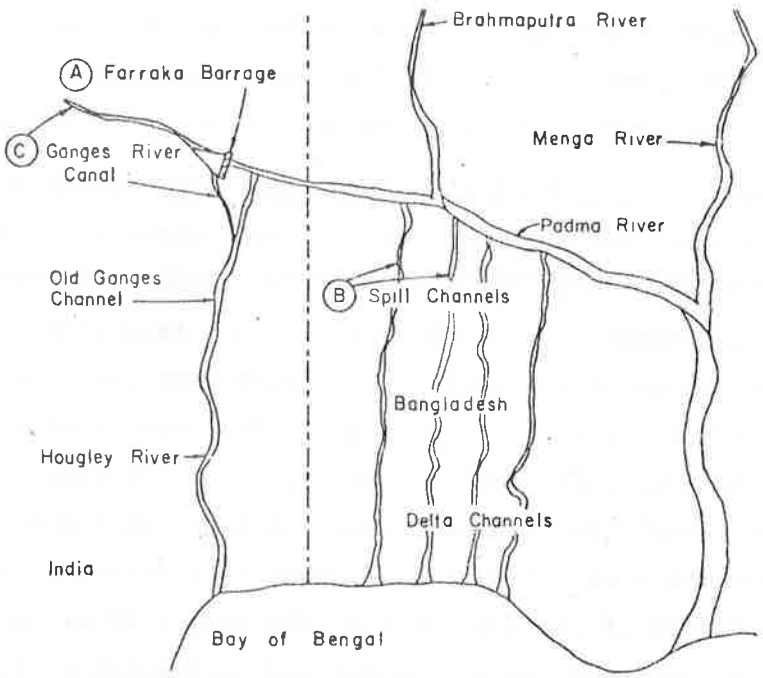

A. Low Flow in the Ganges River will:

1. Reduce river stage
2. Reduce depth
3. Adversely affect:
   a. Navigation
   b. Irrigation diversions
   c. Spill channels

B. Farraka Barrage

1. Canal diverts water to the Hougly River channel
2. Slope of canal is about 0.2 ft/mi
3. Low flow diversion is 15,000-20,000 cfs
4. High flow diversion is 40,000 cfs
5. Possibility of sediment deposition in the canal

C. Spill Channels

1. Flow varies with conditions on the Ganges
2. Flow affected by alignment of the Ganges
3. Diversions from the Ganges must consider:
   a. Headworks
   b. Canal design
   c. Barrage, etc.

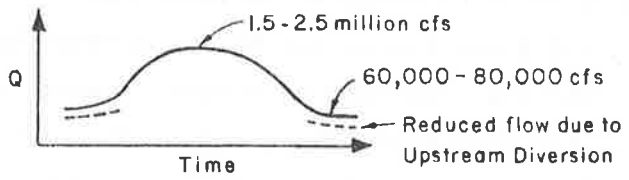

Figure 16.11 Distribution of the Ganges River water and associated problems.

The bank material consists of lenses of sands and mixtures of clay, silt and sand. This material is easily eroded at all stages of flow but in particular during intermediate and high stages. Segments of banks often slide into the channel during periods of falling stage.

The river can rapidly shift laterally, cutting out old sand bar deposits, forming new ones, changing the flow alignment and channel geometry. There are few, if any, segments of channel banks that are relatively stable unless protected by riprap or training works. The bed profile of the Ganges River is quite flat and on the order of 0.2 ft per mile. This slope is approximately equal to the slope of the delta toward the bay. The flatness of the total delta makes it difficult to design distribution channels that are sufficiently steep to transport the sediment carried into them by the river water. This is mainly a problem that arises during periods of intermediate and high flow. The smaller sediment loads in the river at low flow confine river sediments to the channels provided by the river. This is an important factor seriously affecting the design, construction and operation of supply channels for irrigation and for redistribution of other flows. More specifically, the flow of water is accompanied by the transport of sediment. When the water discharge is small, the corresponding transport is also very small, when the water discharge is large, the transport of sediment in such systems as the Ganges is correspondingly large. Some of the major problems associated with sediment are:

1. Major changes in channel alignment and dimensions with varying discharge in time.
2. Local scour and deposition endangering control structures and training works.
3. Aggradation and/or degradation.
4. Major changes in the location of sand bars that can affect flow patterns, discharge, and sediment transport into irrigation, inlets and spill channels.

Records show that flow in the Ganges ranges from minimums on the order of 60,000 cfs to maximums on the order of 2.6 million cfs. Presently upstream diversions may reduce the minimum flows on the order of 20,000-25,000 cfs and may reduce peak flows on the order of 40,000 cfs. If upstream diversion channels can accommodate this discharge, downstream

users must consider the possibility of increased future diversions that will result in further reduction in available water.

The reduction in water discharge and the corresponding changes in sediment discharge can cause several specific responses that are tentatively identified. Such responses must be considered in future water resources planning and development. The most significant possible responses follow:

1. Lower stages during the low flow season and possibly minor reductions in stage at high flow if upstream diversions are made during the high flow season.
2. A significant reduction in capacity to transport sediment during the low flow season. However, this effect would be partly offset by storage of part of the low flow sediment discharge in the pools formed by upstream diversion works.
3. Increased potential for bank erosion during the low flow period due to shallow depths, higher banks, and increased seepage forces where adjacent floodplain lands drain into the river channel.
4. An increased lateral shifting of the main channel of the river during the low flow season.
5. Possible releases of sediment in waves from upstream barrage pools when control gates are opened to pass flood flows. This may affect both river stage and channel stability.
6. Increased flow of sediment from minor tributaries of the main channel due to the reduction in river stage in the main channel and the resulting steeper gradient in the tributary channels.
7. Adverse effects of water level and entrance conditions at spill channels.
8. Reduced depth of flow in both pools and crossings that will adversely affect navigation during the low flow season.
9. Possibly increased intrusion of brackish and saline water in the delta channels and adjacent areas.
10. Require construction of distribution channels to improve availablity of water for irrigation, industry, etc.

Other possible adverse effects related to agriculture, fisheries, forests, navigation and ecology could be alluded to here, but because of limited time and space, must be eliminated.

The foregoing paragraphs simply attempt to identify some of the possible responses within this river system and some of the impacts. Once again, this type of problem can be best approached using process type mathematical models.

Yazoo Basin Sedimentation Study

The Yazoo River Basin occupies nearly one quarter of the state of Mississippi. The river basin is composed of a main stem, 31 tributaries and four major reservoirs. The study involves a systems analysis of the main channel and its tributaries in such a way that water and sediment is routed from the watershed and through the main channel to determine the effectiveness of the system considering flood control, navigation and the location of aggradation and degradation in the main channel and its tributaries and methods of minimizing these and related problems. The analysis provides a means of evaluating various design alternatives to determine the best plan for development. The first alternative considered involves dredging sediments from the main channel. From the model one could determine the effects of channel enlargement on the flow line, on reduced velocities, on sediment deposition rates, etc. Since the first alternative may not be the most satisfactory one and since developing the channel as indicated in the first alternative may lower the flow line and cause additional sediment flow to the main channel from the tributary system, the next alternative involves an analysis of the system with control structures located on the tributaries just upstream of the point where major tributaries enter the Yazoo main stem. These structures would prevent head cutting and the discharge of excess sediments into the main channel. Another alternative is to utilize various techniques to further minimize sediments contributed from the watershed to the main channel. For example, control structures such as check dams could be designed, spaced and located to further reduce the sediment inflow from the tributaries to the main channel. The analysis could be carried out to determine the optimum design considering control structures and dredging to minimize maintenance problems in the main channel after it has been modified to meet the requirements dictated by

flood control needs, and navigation requirement. Details of the study will be presented in Chapter 20.

Geomorphological Response of Rivers Entering the Terai Region, Nepal

General: the major river systems of Nepal drain southward from the mountains through the hills, the inner Terai and the Terai. As the water flows southward climatic conditions change from alpine to temperate to tropical. Simultaneously, elevations change from a maximum of 29,000 ft to a minimum at the Nepal-Indian border on the order of 500 ft. The great change in altitude within Nepal is reflected in very steep channels formed of coarse material supported by geologic controls in the steepest portions of the system. In contrast, the lower ends of the rivers, though still relatively steep, are braided, overloaded with sediments derived from the upstream channels and watershed, and are rapidly aggrading in some reaches.

Referring to a simplified profile of the rivers, note that the slope of the channels decreases with distance (Figure 16.2). Simultaneously, the size of bed material reduces from large rock in the headwaters to sand and gravel in the lower reaches of the rivers. Note that the assumed size distribution curves (A), (B) and (C) may have little or no overlap, i.e., these locations may have very few bed material sizes in common.

The reduction in size of bed material with distance is similar for all alluvial rivers, even canals. This condition results primarily from 1) hydraulic sorting that occurs as a part of the sediment transport processes, and 2) secondarily, as a consequence of abrasion and fracturing of the particles as they are acted upon by climatic, chemical and hydraulic forces.

The geomorphic processes in such systems are very active. These systems are further complicated by land and water resources utilization and development. Again, referring to the schematic diagram of the river profile, note that the size of the bed material at any one location is a function of the velocity of the flow, the duration and turbulence of the flow and other less significant variables such as concentration of suspended sediment, temperature of the water, geologic controls, etc., that have acted historically to produce present conditions. In those reaches of the channels where their transporting capacities have exceeded

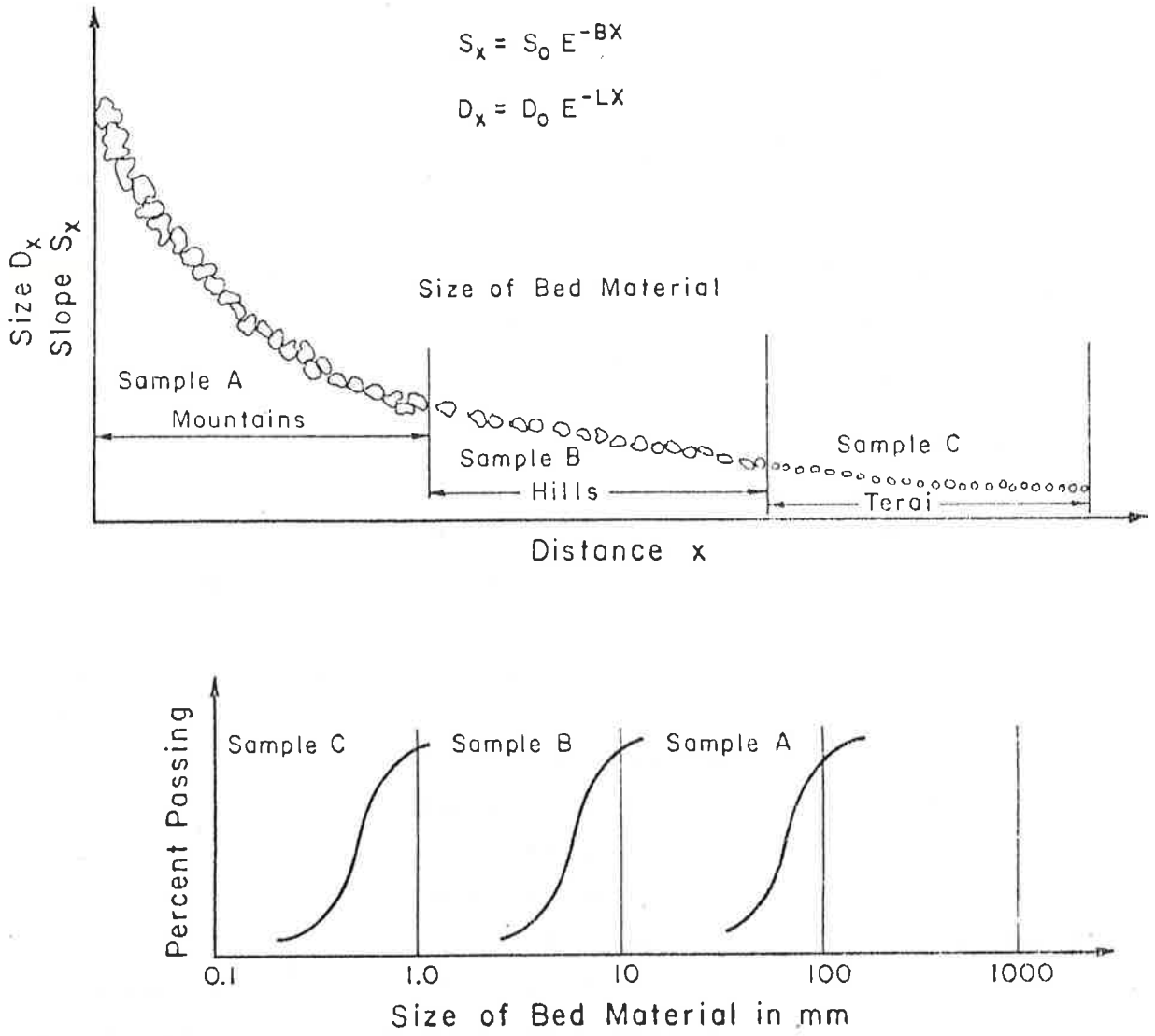

Figure 16.12 Variation of bed material.

the available supply of sediment the bed is swept clean and the exposed material is composed of larger particles that have been able to resist transport. Further down the river systems a point is reached where the supply of sediment to the channels exceeds the transporting capacity of the channel and aggradation occurs. This may cause the channel to fill with sediment and change its course. Accordingly, in the rivers of Nepal the upper ends have degraded and armored themselves. In contrast, the lower ends of the catchments are experiencing aggradation, channel changes and the building of broad alluvial fans. The lower Kosi River

is an extreme example of an overloaded, aggrading, unstable river that is difficult to control and utilize effectively.

The rivers in the Terai are braided relatively flat, overloaded with sediments and aggrading. This is a difficult environment for implementation of water resources development and flood control projects. Consequently, consider some of the major responses of such rivers to water resources development of various types that must be numerically evaluated.

Impacts of Hydropower and Flood Control Dams: Dams constructed for such purposes have relatively high heads and store large volumes of water. Major responses of the system within the reservoir and in the upstream channel affected by the reservoir include:

1. Storage of the inflowing sediment in the reservoir (a large percent in the live storage volume)
2. Aggradation of the upstream channel affected by backwater caused by the reservoir
3. Increase in river stage resulting in a possible increase in flood damage
4. Increase in water table level
5. Increased mass wasting on the periphery of the reservoir--potentially a very serious problem
6. Loss of some riparian land and vegetation.

Changes in the system downstream of the dam include:

1. Reduction of peak flows except under unusual circumstances
2. Degradation of the channel below the dam caused by the release of clear water (may provide additional flood protection)
3. Increased bank erosion and mass wasting
4. Increase in the gradient of tributaries that may render them less stable resulting in the production of additional sediment (may tend to offset the degradation caused by the clear water release)
5. Increased damages to hydraulic structures, bridges and roads.

Impact of Barrages: This includes

1. Barrages increase river stage
2. Impose flow conditions that encourage the deposition of sediment upstream of the barrage
3. The initial storage of sediment upstream causes scour and degradation downstream

4. The potential for flood damage is increased upstream
5. Dikes may be required to confine the higher stages resulting from channel aggradation upstream
6. The water table level is increased upstream
7. After the initial deposition above the barrage, the sediment load normally increases below the barrage as a consequence of the clearer water diverted at the barrage. This ultimately results in aggradation of the downstream channel.
8. Bank erosion can result both upstream and downstream requiring river control and bank stabilization works to protect riparian land and the barrage.

Construction of Embankments for Flood Control on the Terai: Prior to river development, the aggrading river systems of the Terai had the freedom to move laterally and build broad alluvial fans. When this lateral movement is restricted by construction of embankments and bank stabilization works, the following river responses are initiated:

1. The river channel aggrades
2. The effectiveness of the levees for flood protection diminishes with time
3. Ultimately a perched river condition develops that is impossible to confine during major floods
4. The land between the levels and the channel are subjected to greater flood damage
5. The channels aggrade to such an extent that bridges do not have adequate waterways and may fail.
6. Costly river training works are required to confine the river between the levees.

Canals: Irrigation and/or power canals can only be allowed to receive a relatively small percentage of the sediment transported by the river and even then only the smaller fractions. This is necessary to:

1. Avoid filling the canals with sediment, resulting in high maintenance costs or even total failure
2. Limit the damage to hydraulic machinery

The quantity and quality of sediment that a canal can accommodate must be determined by calculations and/or model studies as described earlier in this report.

General Design Procedures: From the preceding discussions it is noted that the river systems are complex and difficult to control. In addition, water resources development adds to the complexity and alters the behavior of these systems. The analysis and design of water resources development projects can be evaluated using various types and levels of analysis as follows:

1. Quantitative geomorphic, hydrologic and hydraulic analysis. This method gives approximate values useful for planning. Also, this method provides an important check on more comprehensive methods of analysis and design.
2. Conventional analysis coupled with the inputs and checks provided by method (1).
3. Comprehensive analyses utilizing data storage and retrieval systems coupled with mathematical models. This approach is identical to (2) but additionally provides a means of looking in more detail at a larger number of alternatives. Also this method more effectively utilizes the total data base available. For a state of the art review of the utilization of mathematical modeling techniques, refer to Chapters 6-12.

16.3 DATA NEEDS FOR ANALYSIS

General

Evaluating the adequacy of available data for supporting various phases of a river system study is an essential element of the analysis. Consideration must be given to gaps in the available data and related supplemental data collection requirements as well as techniques for data synthesis and data sensitivity analysis.

Data needs are, of course, dependent on the complexity of the system being analyzed and the methods of analysis employed. The data requirements for a basin-wide study to include both watershed and channel modeling are presented in Tables 16.1 and 16.2, which outline, respectively, the data necessary to support channel and tributary modeling and that required for watershed modeling. These tables are arranged in matrix form and include a description of the data and an assessment of its degree of importance to the particular phase of the study.

Table 16.1 Basic data needs for channel modeling.

	Description of Data	Degree of Importance
A.	Maps and Charts	
	Topographic map of river environment	Primary
	Geologic map of river environment	Secondary
	Hydrographic charts	Primary
B.	Aerial and Other Photos	
	Large scale photos of river and surrounding terrain	Secondary
	Small scale aerial photos of river and surrounding terrain	Primary
	Color infrared photos for flow patterns, scour zones, and vegetation	Secondary
C.	Hydraulic Structures (existing and planned structures)	
	Plans and design details	Primary
	Alterations and repairs	Secondary
	Scour	Primary
	Operation procedure	Primary
D.	Hydrology and Hydraulics	
	Discharge records	Primary
	Flow velocity records	Primary
	Stage records	Primary
	Flood frequency curves	Secondary
	Sediment discharge records (bed material and wash load)	Primary
	Resistance to flow	Primary
E.	Channel Geometry	
	Cross-sections	Primary
	Islands	Primary
	Flood plain	Primary
	Bed slope	Primary
	Water surface slope	Primary
	Bars	Primary
	Sinuosity	Secondary
	Controls (falls, rapids, restriction, rock outcropping, dams, diversions)	Primary

Table 16.1 (Continued)

	Description of Data	Degree of Importance
F.	Hydrography	
	Water hydrograph	Primary
	Sediment hydrograph (bed material and wash load)	Primary
G.	Sediment size	
	Bed material size distribution	Primary
	Bank material size distribution	Primary
H.	Environmental data	
	Riparian community	Secondary
	Salinity of water	Primary
	Turbidity	Secondary
	Water temperature	Secondary
	Fish habitat	Secondary
	Chemical quality	Secondary
I.	Climatologic data	
	Precipitation	Secondary
	Wind	Secondary
	Air temperature	Secondary

Table 16.2 Basic data needs for watershed modeling.

	Description of Data	Degree of Importance
A.	Maps and Charts	
	Topographic maps of watersheds	Primary
	Soil maps of watersheds	Primary
	Geologic maps of watersheds	Primary
	Vegetation maps of watersheds	Primary
	Land use maps of watersheds	Primary
B.	Aerial and Other Photos	
	Aerial photos	Primary
	Color infrared photos of watersheds	Primary
C.	Soil and Geologic Data	
	Hydraulic conductivity	Primary
	Capillary section	Primary
	Soil porosity	Primary
	Particle size distribution	Primary
	Soil moisture	Primary
	Rock outcropping	Primary
	Armoring size and distribution	Primary
D.	Forest Inventory Data	
	Total vegetation volume	Secondary
	Total litter volume	Secondary
	Canopy cover density	Secondary
	Ground cover density	Secondary
	Interception storage capacity of a typical canopy	Secondary
	Evapotranspiration of a typical canopy	Secondary
E.	Hydrology and Hydraulics in Water System	
	Flow discharge records	Primary
	Flow velocity records	Primary
	Flow stage records	Primary
	Resistance to flow	Primary
	Sediment discharge records (bed material and wash load)	Primary

Table 16.2 (Continued)

Description of Data	Degree of Importance
F. Climatological Data	
Precipitation	Primary
Wind	Primary
Radiation	Primary
Air temperature	Primary
Humidity	Secondary
Precipitation frequency curves	Secondary
G. Hydrographic Data	
Water hydrographs	Primary
Sediment hydrographs	Primary
H. Environmental Data	
Wildlife	Secondary
Fish habitat	Secondary
Turbidity	Secondary
Chemical quality	Secondary
Water temperature	Secondary
I. Land Use Data (historical and present records)	
Forested areas	Primary
Urban areas	Primary
Industrial areas	Primary
Recreational areas	Secondary
Agricultural areas	Primary

It must be noted that certain categories of data including hydrologic, hydraulic, channel geometry, and hydrographic, are extremely dynamic in nature and strongly a function of past and present conditions. Therefore, available data should be validated against today's river system conditions to determine their acceptability for the analysis.

The Importance of Data as Related to Model Sensitivity

Model sensitivity is a measure of the effect of change in a parameter on the model response. A sensitive parameter may converge quickly while the converse applies to an insensitive parameter. The most common form of a model sensitivity analysis is by parameter perturbation. One parameter is varied while the others are held constant and the response to this change is recorded.

The results of a model sensitivity analysis of the following six watershed parameters for a simple basin illustrate the approach: channel resistance, ground cover, canopy cover, hydraulic conductivity, temperature, and rilling ratio. The simple basin consists of one subwatershed unit, one channel unit and two plane units located in the Walnut Gulch, Arizona, watershed. The parameters were fitted by calibrating the results of the model to the recorded hydrographs for two storms--one large event (1.22 inches of rainfall) and one small event (0.50 inches of rainfall). These calibrated parameters were perturbated individually for both the large and small storm events. The effects of varying the parameters were measured by the change in peak discharge, peak time and total water volume.

The results of a sensitivity analysis will vary for different watersheds depending on the characteristics of the watershed. In general, an increase in any given parameter will decrease the peak discharge and water volume and increase the time to peak. In this case, an exception to this rule was the effect of the rilling ratio on peak time, but it was found that the sensitivity for all of the parameters increased as the size of the storm decreased. Hydraulic conductivity was the most sensitive parameter for the model in determining water volume and peak discharge. Channel resistance and ground cover which determine the overland resistance were the key parameters in determining the peak time of the outflow hydrograph. Because the watershed tested for the model sensitivity analysis has very little canopy cover and a very low rilling ratio, these two parameters were quite insensitive, but this would not be the case on a watershed where there is a significant amount of canopy cover or a high rilling ratio. Temperature was a very sensitive parameter because of the effect temperature has in changing the hydraulic conductivity and thereby changing the infiltration. Thus, for a given

response, a sensitivity analysis reveals which variables have a dominant influence. Data gaps associated with the less sensitive parameters are only of secondary importance and data gathering or data synthesis can be concentrated on the dominant parameters (see Chapter 7).

16.4 DATA STORAGE AND RETRIEVAL SYSTEM

General

Historical records are the most important source of data in studies of physical systems. This is particularly true in the case of river basin studies where a river is composed of numerous interacting natural and man-influenced physical processes. A river in turn influences the social and economic base of its river basin community by serving as a transportation route, providing water for domestic, agricultural and industrial uses, serving as a recreation site, providing hydropower generation, and functioning as a flood water drainage. The value of historical data depends a great deal on the availability of data management techniques for extracting the largest amount of useful information for solving particular problems. A river basin manager and planner dealing with complex systems and their associated problems must view data management as a set of interacting components such as data acquisition, data storage, data retrieval, and data processing and analysis. This appendix is limited to the discussion of an efficient approach to data management for river basin system analysis.

There are many ways to store historical data including charts, maps, microfilm and microfiche, computer cards, and magnetic recording devices. Because of the large volume of data that is required to describe a river system, a data storage and retrieval methodology is needed that will minimize the effort of creating, accessing, and updating such a large data bank. Table 16.3 gives a comparison of some data storage devices that are available for use. The first approach of providing digitized information for the computer is to record and store data on punched cards. A second approach is the combined use of magnetic tape and permanent files. The third approach is the use of disc-pack storage units. Table 16.3 gives a brief comparison of cards and combined magnetic tape-permanent file storage devices. As Table 16.3 indicates, the use of the magnetic tape-permanent file devices is less costly, more reliable, and easier to use than the card storage approach.

Table 16.3 Comparison of cards, magnetic tape--permanent file data storage devices.

System of Storage	Storage per 2000 card images	Cost per 2000 card images	Reliability	Updating	Retrieval/ Processing
Cards	Poor: 1 box = 160,000 characters	Poor: $3.75 per 2000 card box, or $375. per 100 boxes Hard to store	Poor: Cards deteriorate with time and use. Possibility of unauthorized, or incorrect changes in data	Poor: Manual updating requires large amounts of man hours, with the possibility of errors	Poor: Time consuming. Manual retrieval of data with no provision for processing
Tape	1 tape = 120 boxes of cards	Tape: $12.00 per tape Easy to store	Good: Limit access to master tape. More than one tape can be created as a backup	Excellent: System allows for quickly updating data directly	Excellent: Both human and computer time efficient retrieval, with provisions for processing data in a number of ways. Data tape can be quickly searched for necessary data. Small computer storage requirement. Five times faster than reading cards

If large amounts of storage are needed beyond that provided by a magnetic tape-permanent file system, a disc-pack storage device may be the best approach. Table 16.4 lists comparisons and approximate costs of magnetic tape-permanent file devices and disc-pack storage devices. As the table indicates, if a large, heavily-used data base is needed, then the disc-storage device is probably the best approach to data storage. Until that time the magnetic tape-permanent file approach is the best.

By combining the magnetic tape-permanent file or disc-pack storage devices with interactive program routines, a data bank can be created that has many useful attributes. After the data base is encoded and transferred to the specified magnetic storage device, it can be accessed by a large number of users for updating data, checking for data errors, creating data files for analysis, and retrieving information for specific requests. All of these operations can be carried out by a single person at an interactive console. By using an interactive system, the access to the data bank is rapid and need not rely on variable input-output time associated with batch job processing through a typical card reader input. An interactive system also allows for the rapid correction of mistakes in requesting data as well as providing rapid answers to specific questions.

The advantages of data storage on magnetic devices managed through interactive terminals far exceed those associated with card storage and typical input-output terminals. The application of interactive-magnetic device data bank storage and retrieval systems to river basin data storage problems represents the current state of the art.

Data Storage and Retrieval System for River Basin Analysis

The data storage and retrieval system should be capable of storing and managing all information obtained from the data acquisition phase and the data analysis phase. The efficiency of a data storage and retrieval system is important since it affects the availability and the quality of the input data for any level and type of analysis required in the basin. Therefore, the specific data base scheme for each data category should be worked out to ease access, retrieval, and updating of data. A data management system should be established along with the data base to assist users in the retrieval and reformatting of the data

Table 16.4 Magnetic tape permanent file and disc storage comparison.

	Storage	Cost	Access	Remarks
Magnetic tape-Permanent file	19 million characters per tape	$12 per tape plus mounting	Unlimited when placed on permanent file	Good for data bases with limited users
Disc Pack	1) Single Density 126 million characters	Lease - ~ $8800/year	Unlimited multiaccess unlimited	Best for data bases with many users that require that information be stored on the more accessible discs and not on the lesser accessible tapes
	2) Double Density 224 million characters	Lease - ~ $10,000/year	Unlimited multiaccess	
		Limited Access ~ $4-$5/hour both single and double density	1 to 4 hour time blocks per day as contracted	

to obtain the desired information for the simulation and analysis of all or any part of the river basin under study. The data management system should be of modular type and set up in an overlay structure to increase its flexibility in changing component elements and to reduce computer memory requirements.

The primary objective of such a data storage and retrieval system is to support multiple levels and types of analysis. The specific tasks involved in the development of the system are:

1. Identify general data needs for various levels and types of analysis considering water supply, flood control, sediment control, drainage and irrigation requirements, stream bank erosion, water quality, reservoir operation, and environmental impacts.
2. Assemble and evaluate all of the available data from various agencies relating to climatology, hydrology, hydraulics, geomorphology, geology, water quality, land use, and such activities of man as hydraulic structures and river engineering works.
3. Standardize the time and space designation of data and develop a unified classification of data categories.
4. Establish the structure of the comprehensive data storage and retrieval system to include all data categories that are needed for multiple levels and various types of analyses.
5. Define a complete node system for location identification of all required data collection stations along the river channel system (including major tributaries) and in the watersheds.
6. Develop a data analysis package for incorporation into the data management system for extracting the maximum amount of information from the collected data.

A Case Study: The Yazoo Data Storage and Retrieval System

The following sections outline the application of the data storage and retrieval system for the Yazoo River Basin study conducted by Colorado State University for the Vicksburg District, U.S. Army Corps of Engineers. Although many of the specific technical details of the data base management system are omitted, the general workings and capabilities of the system are presented through discussion and examples.

Characteristic Features of the Yazoo River Data Base Management System Structure: The Yazoo data base is set up to reflect the logical structure of the watershed and the river channel system under study. This hierarchical structure is coded by a node system, which is described in the next section, to ease the data identification and retrieval task. The data base schema for the Yazoo River system is presented in Figure 16.13, which shows various data categories and their corresponding keys.

The data management system is a set of operating computer programs, established along with the data base to assist users in the retrieval and reformatting of the data to obtain the desired information for simulation and analysis of the river basin system. The overall package is of modular type and set up in overlay (layered) to increase its flexibility in changing component elements and to reduce computer memory requirements. The structure of the Yazoo River data management system is presented in Figure 16.14.

Query Language: To help users who are not familiar with computer systems, a simple query language for data retrieval and processing is developed. It consists of four groups of command statements, written in ordinary language, to guide the operations of the four-layered programs (i.e., GETDATA, PROCESS, OUTPUT, and UPDATE). The command language specifications for the Yazoo River data management system are presented in Simons, Li and Duong (1978).

To ensure an understanding of the use of various command statements for data retrieval and processing, samples of test cases are presented in the last section of this chapter. Each output is headed by a corresponding bloc of command statements.

Data Processing Capability: At the present time, the following data processing options are available in the Yazoo data base management system:

1. Retrieve information at a gaging station.
2. Retrieve data at a gaging station by five different alternatives (station number, station name, station coordinates, node + river mile, river name + river mile).
3. Retrieve data for a particular date, year, or water year.
4. Retrieve data for a particular time period (i.e., from date (x) to (y); from water year (x) to (y)).

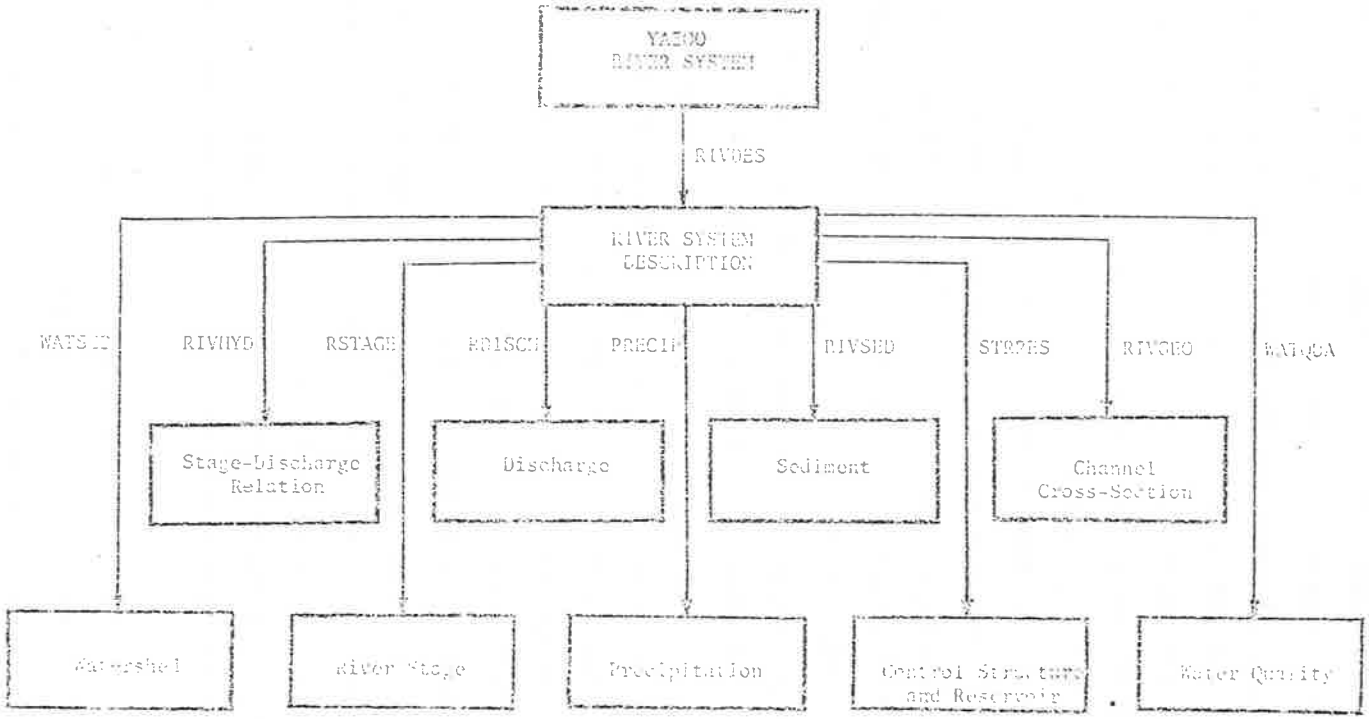

Figure 16.13 Overall structure of the Yazoo data base.

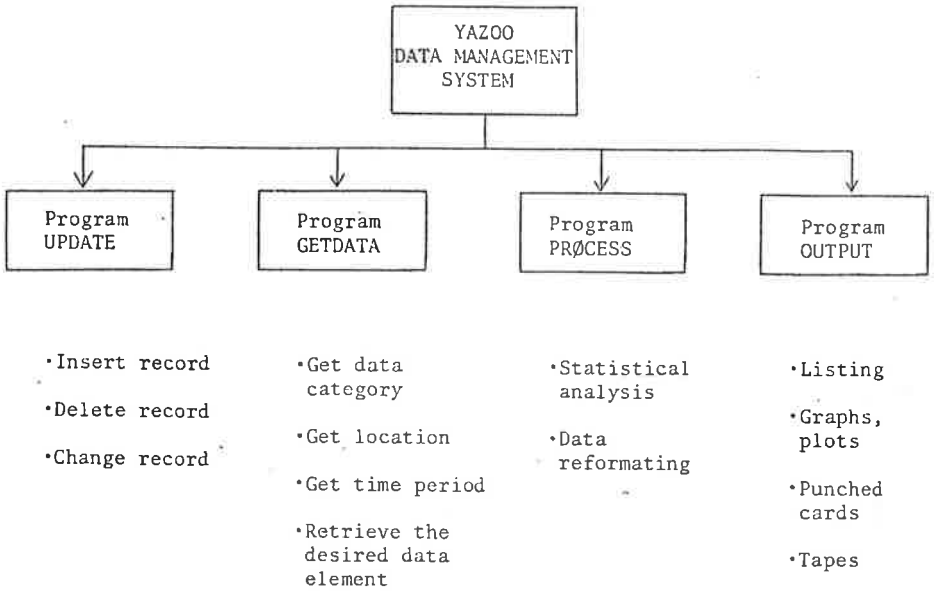

Figure 16.14 Overall structure of the Yazoo data management system.

5. Print or plot output results on paper or CRT tube.
6. Carry out elementary operations on data analysis, such as:
   - Flood frequency plot for a particular station (x)
   - Flow duration analysis for a particular station (x)
   - Stage-discharge plot for a particular station (x)
   - Cross section overlay plot for a particular station (x)
   - Discharge-hydrograph plot at a station (x)
   - Stage-hydrograph plot at a station (x)
   - Changing river stage with constant discharge
   - Rainfall cumulative plot for a particular station (x)
   - Thalweg level plot for a river or a segment of a river
   - Basic statistics analysis
   - Regression analysis
   - Correlation analysis

Other options for extracting additional useful information from the data can be added to the basic Yazoo data base management system.

The Node-System for Location Identification in the Yazoo River Basin

In order to speed access to information at specific stations, a uniform numbering system was developed. A group of four pairs of numbers is used to describe a node in the Yazoo River system starting at

Vicksburg as node 00000000 and increasing going upstream. From right to left, the first pair indicates successive node numbers in the main stem of the river system; the next pair indicates the first-order tributary from the main stem, starting at the node defined by the pair on the right; and so on. The structure of the node-system for the Yazoo River system is presented in Figure 16.15. Thus, using a node-system, a particular gaging station can be defined by a downstream node and a stream-mile from that node. This makes the retrieval of data of a particular river segment or sub-basin simpler.

Data Categories in the Yazoo River Data Bank

Data stored in the Yazoo River data bank are separated into various categories and reside in various tape files for ease of maintenance and to minimize the operating cost. Each data file contains all the gaging station information and the corresponding data elements. In the present version of the Yazoo River data bank, portions of the following data categories have been processed and put in storage for selected locations:

- Stage-discharge data
- Daily discharge data
- Suspended sediment data
- Bed material data
- River cross-section information
- River control structure characteristics
- Reservoir characteristics
- Stage readings
- Meteorological information

Watershed data will also be included in the Yazoo River data bank as soon as the data preparation and verification is completed.

Sample Test Cases

This section contains illustrative examples of control statements and corresponding outputs from the Yazoo data base management system for some sample analyses related to needs of field personnel, engineers, and planners when dealing with a large, complex river basin system.

1. When designing a hydraulic structure, one of the first pieces of information needed is a flood frequency analysis. Figures 16.16a,b provide an example of flood frequency analysis

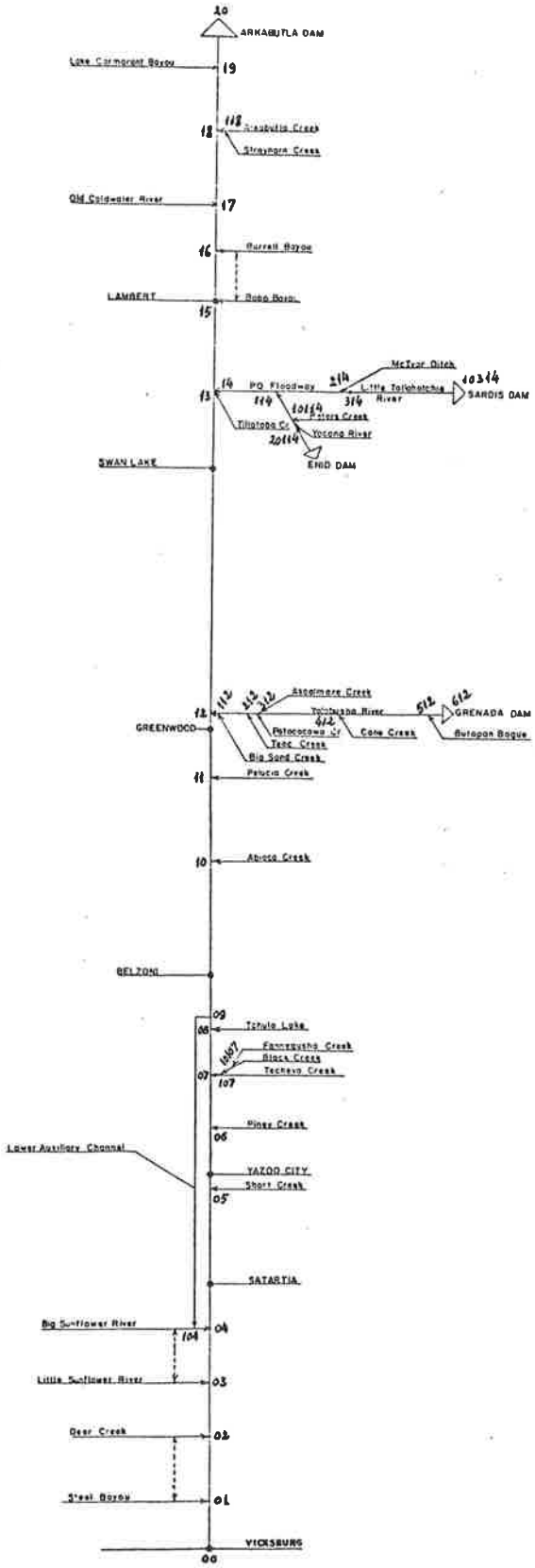

Figure 16.15 Node-system for the Yazoo River system.

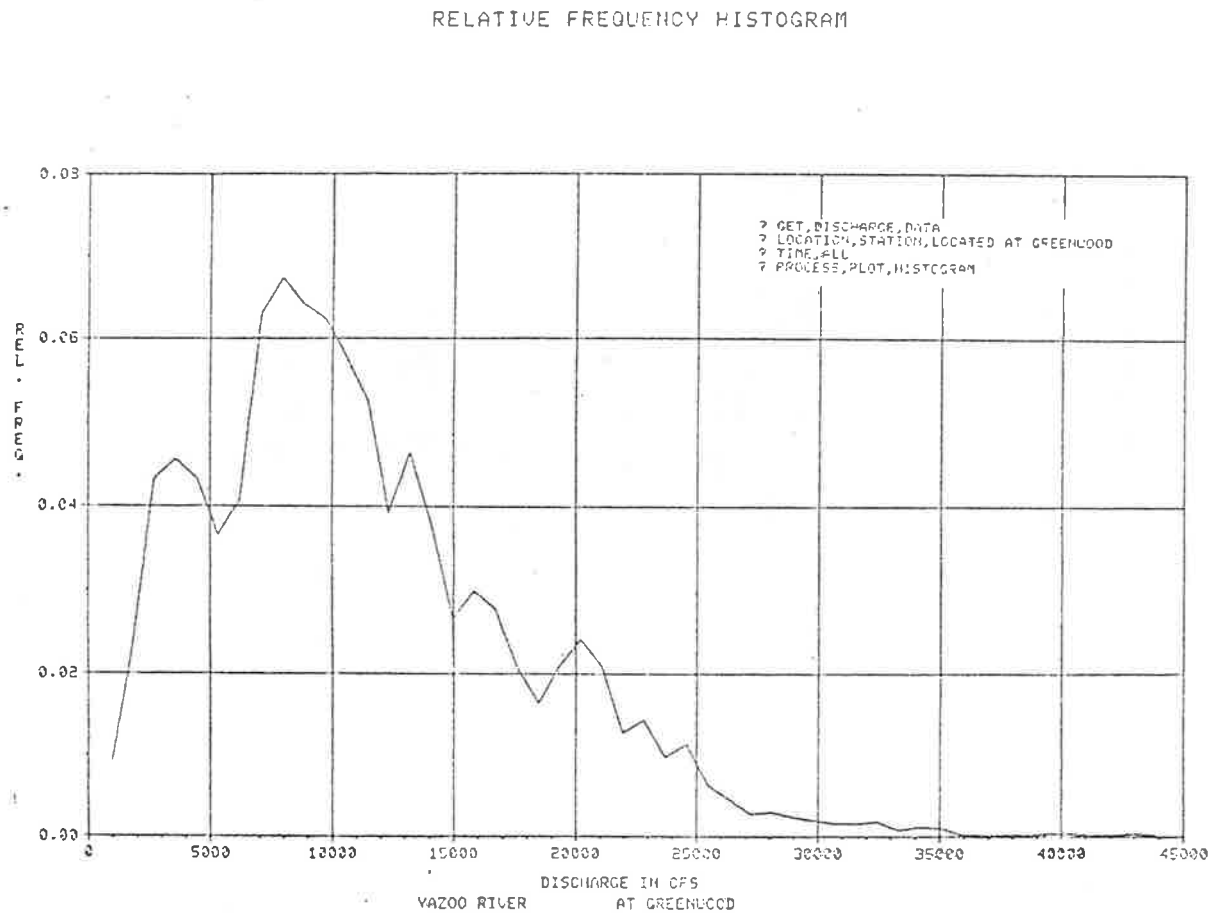

Figure 16.16a Plot of relative frequency histogram for discharge at Greenwood.

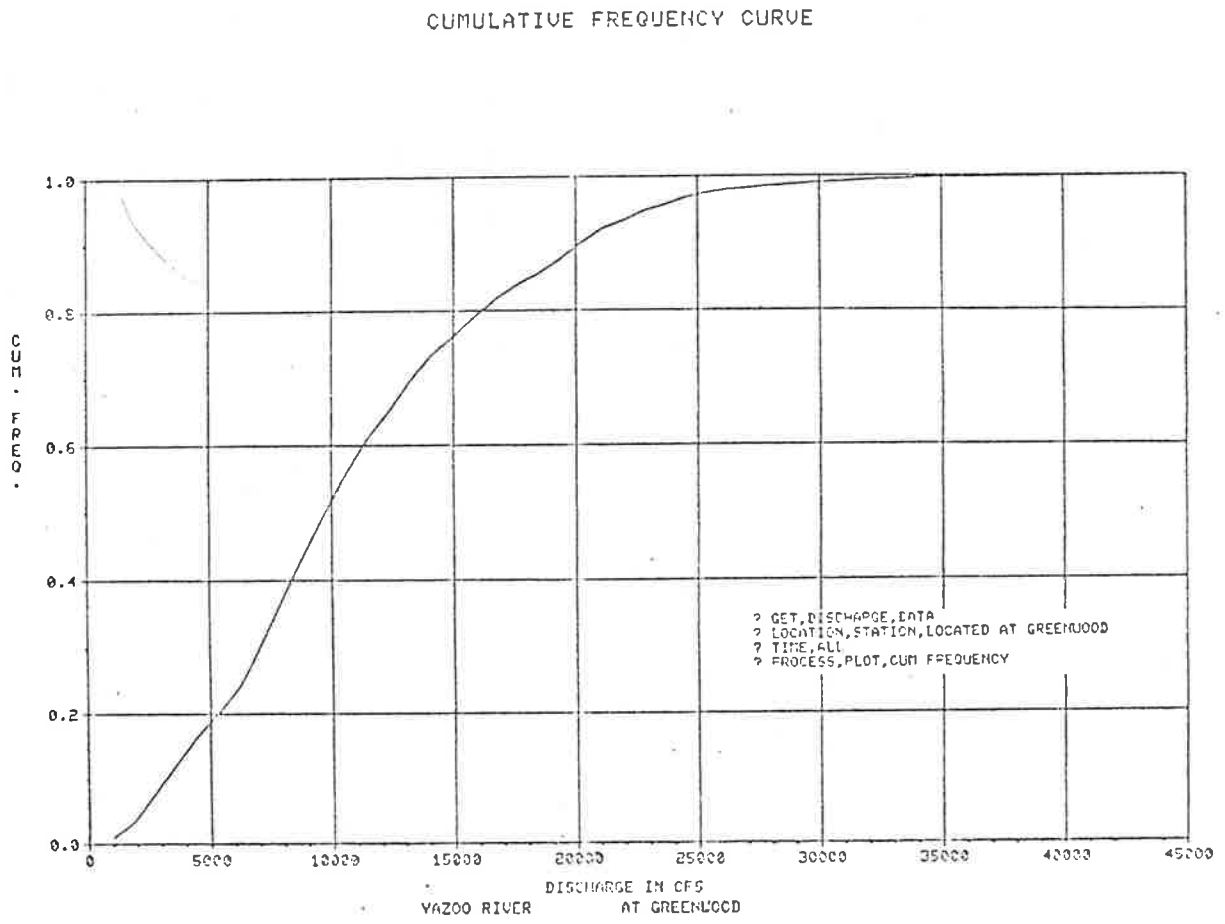

Figure 16.16b Plot of cumulative frequency distribution for discharge at Greenwood.

carried out on the historical data of the Yazoo River at Greenwood, Mississippi.

2. The determination of the stage for a design discharge at a cross section is usually necessary for determining flood hazard and for hydraulic structure design. Figure 16.17 shows the stage-discharge curves of the Yazoo River at Belzoni for year 1973.

3. The trend of changing stage-discharge relations over time usually provides valuable information about the dynamics of a river at a particular location. Figure 16.18 is an overlay plot of stage-discharge curves of the Yazoo River at Belzoni for three consecutive years: 1973/1974/1975.

4. Regression analysis is a simple, but very useful, technique used to derive the relationship between two sets of data. The computed analytical expression could then be used for short-term record extension. Figure 16.19 shows the derivation of the power function for stage-discharge data for the Tallahatchie River near Swan Lake for several years.

5. The change in river stage over time for some given discharge, Q, at one particular station could give some information concerning channel cross-section geometry and the aggradation or degradation at that location. Figure 16.20a shows a plot of changing stage over time for Q of 5000 cfs for the Tallahatchie River near Swan Lake for several years. Figure 16.20b lists the corresponding values of the river stage for each year for Q of 5000 cfs for the same station.

6. In order to check the dynamics of aggradation or degradation it is always useful to plot the change in cross-sectional shape over time. Figure 16.21a,b,c are overlay plots of cross-sectional data at three different stations on the Yocana and Yazoo Rivers.

7. Discharge data are needed to calibrate river system models which are used for the study of future behavior of the system. Thus, stage and discharge hydrography are desired pieces of information for engineers and planners. In Figure 16.22 plots

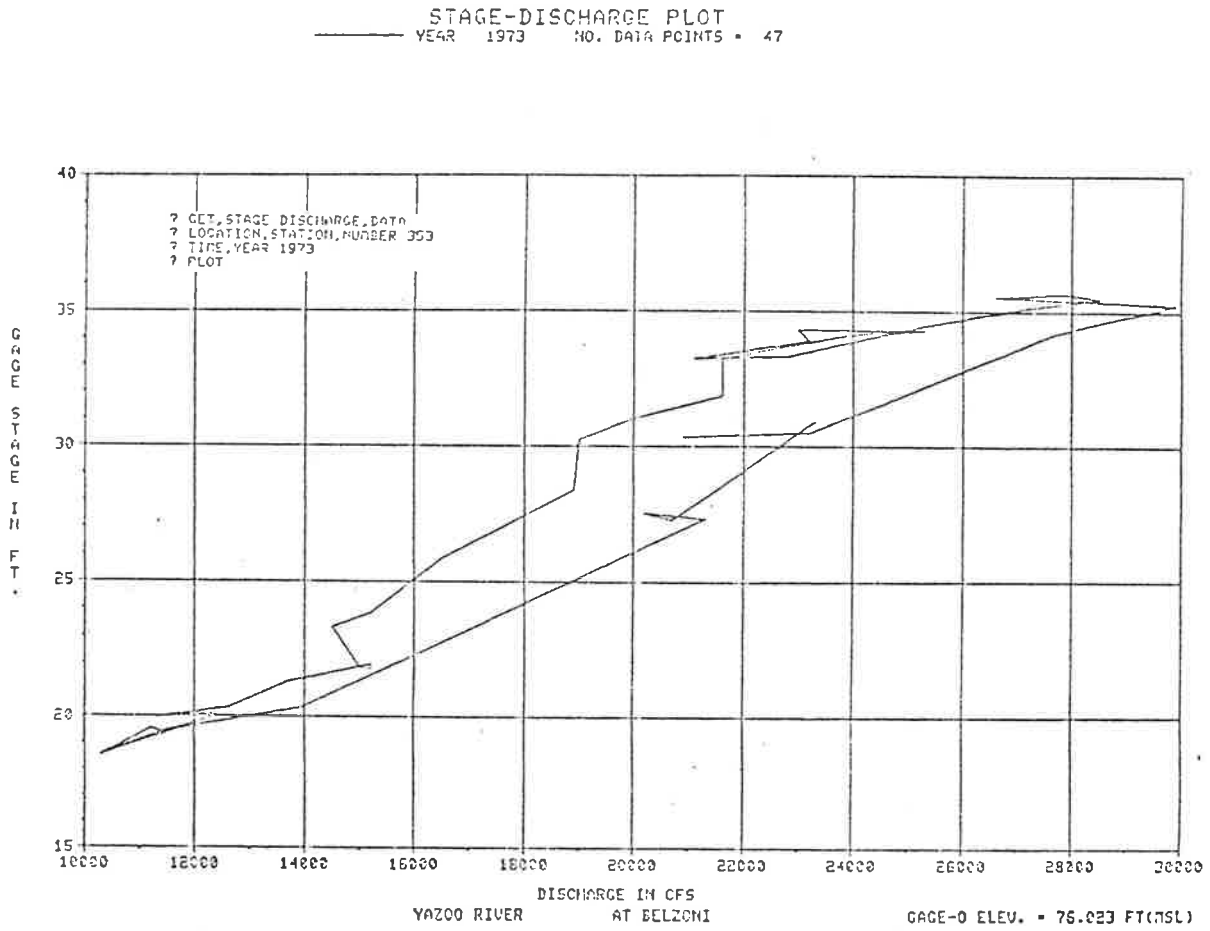

Figure 16.17 Plot of stage-discharge relationship for year 1973 at Belzoni.

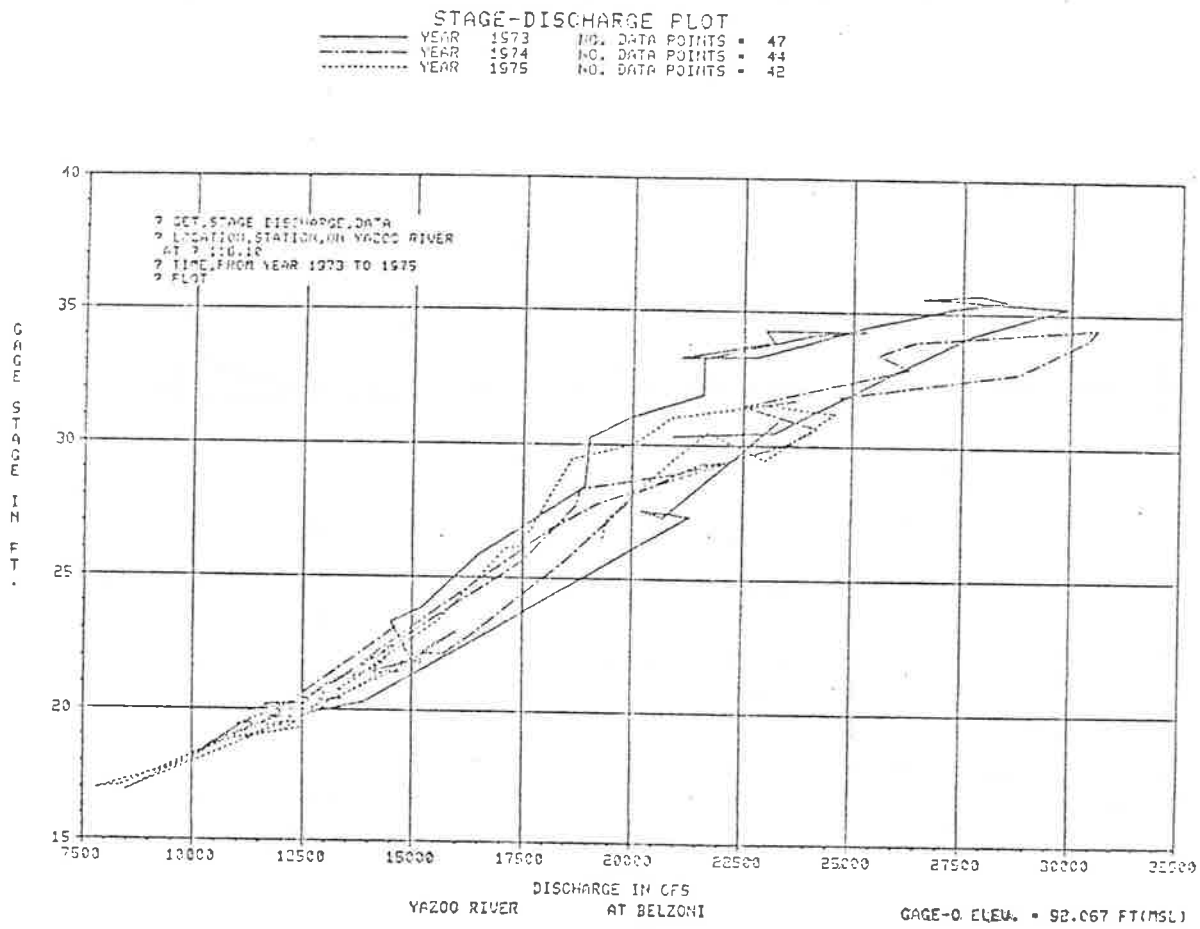

Figure 16.18 Plot of stage-discharge relationship for three consecutive years at Belzoni.

```
? GET,STAGE DISCHARGE,DATA
? LOCATION,STATION,LOCATED NR SWAN LAKE
? TIME,FROM YEAR 1972 TO 1974
? PROCESS,LIST,REGRESSION ANALYSIS


                                YEAR = 1972
            REGRESSION EQUATION IS     Q =  54.39603((S).EXP( 1.7053))
CORRELATION COEFFICIENT =   .9894              STANDARD ERROR =   .091329

                                YEAR = 1973
            REGRESSION EQUATION IS     Q =  13.98061((S).EXP( 2.1633))
CORRELATION COEFFICIENT =   .9524              STANDARD ERROR =   .141689

                                YEAR = 1974
            REGRESSION EQUATION IS     Q =  14.39231((S).EXP( 2.1442))

CORRELATION COEFFICIENT =   .9965              STANDARD ERROR =   .090748
```

Figure 16.19 Regression analysis of stage-discharge data near Swan Lake.

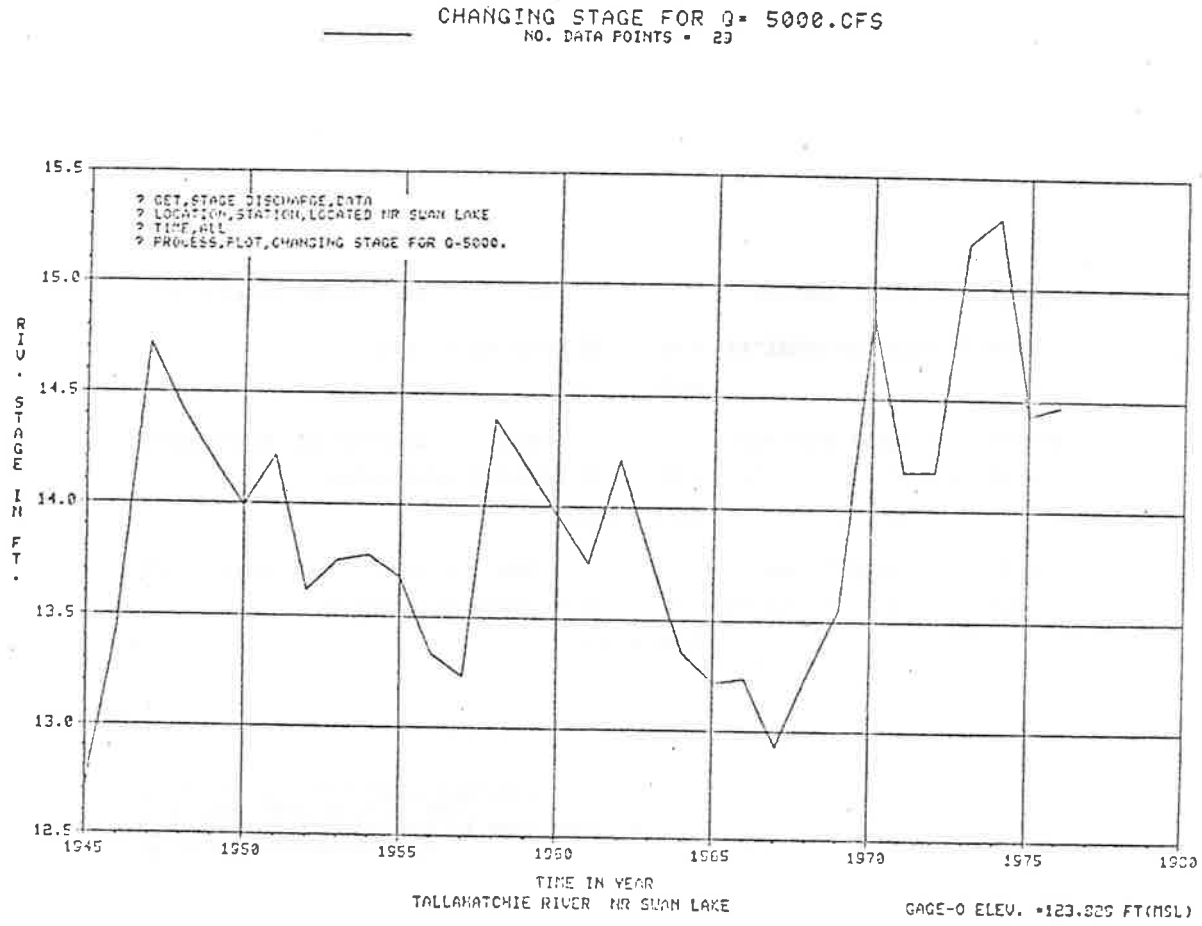

Figure 16.20a Plot of yearly average values of flood stage for a given discharge near Swan Lake.

```
? GET,STAGE DISCHARGE,DATA
? LOCATION,STATION,NUMBER 1320
? TIME,ALL
? PROCESS,LIST,CHANGING STAGE FOR Q=5000.
```

CHANGING RIVER STAGE FOR Q = 5000. CFS

TALLAHATCHIE RIVER NR SWAN LAKE

(GAGE-0 ELEV. = 123.829 FT(MSL))

YEAR	RIVER-STAGE IN FT
1945	12.70
1946	13.45
1947	14.72
1948	14.44
1949	14.20
1950	13.99
1951	14.21
1952	13.61
1953	13.75
1954	13.77
1955	13.67
1956	13.33
1957	13.23
1958	14.39
1961	13.75
1962	14.21
1964	13.35
1965	13.22
1966	13.24
1967	12.93
1968	13.25
1969	13.55
1970	14.86
1971	14.17
1972	14.17
1973	15.19
1974	15.31
1975	14.43
1976	14.47

Figure 16.20b Listing of yearly average values of flood stage for a given discharge near Swan Lake.

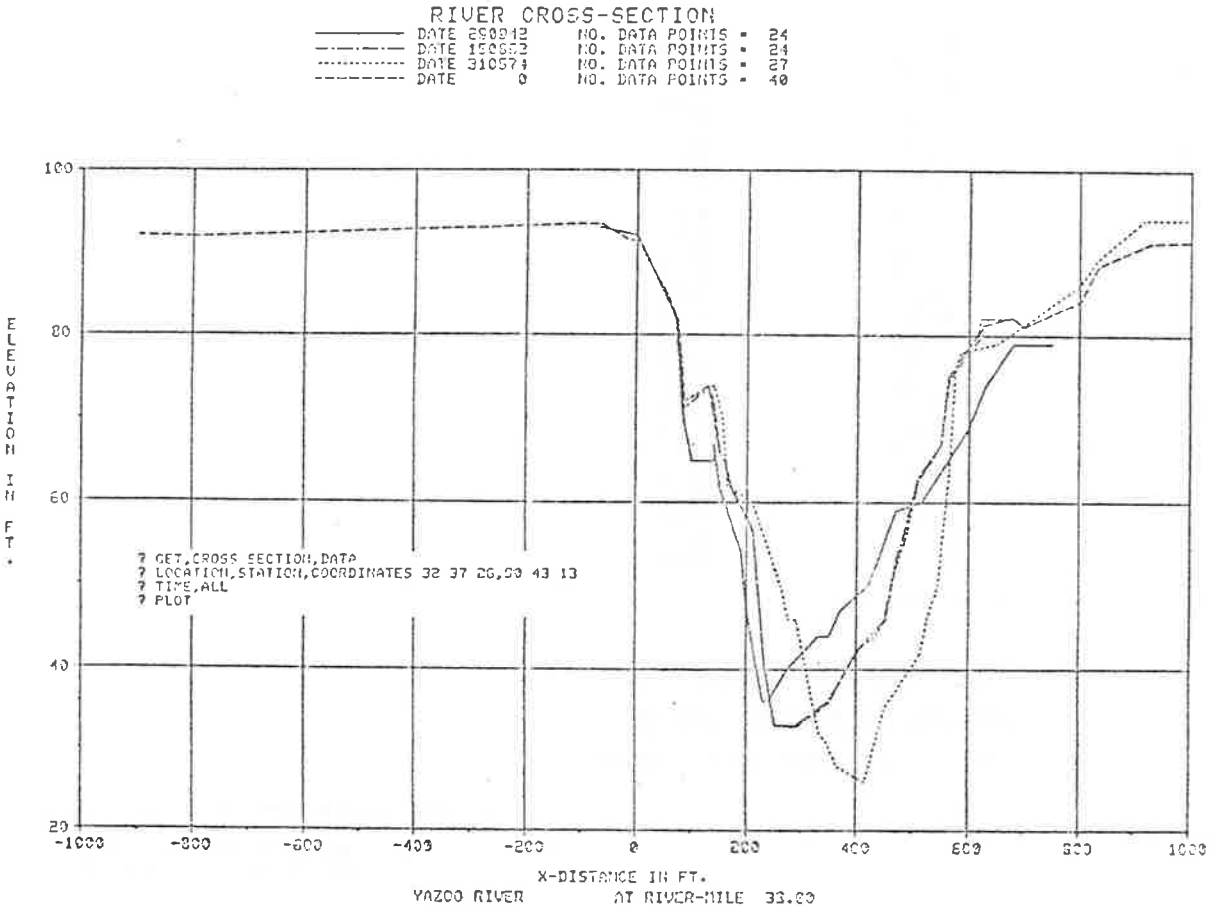

Figure 16.21a Plot of channel cross sections of the Yazoo River at RM 33.00 for different dates.

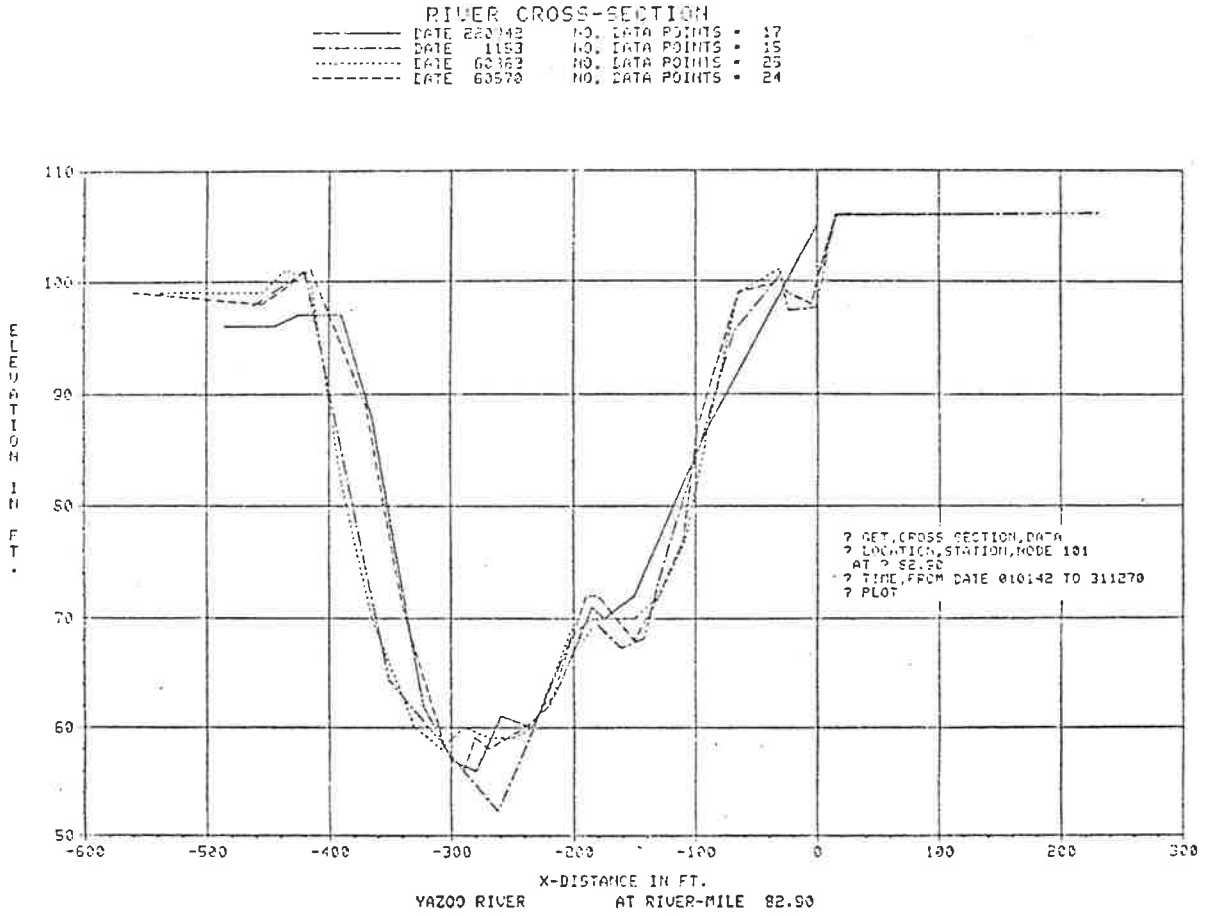

Figure 16.21b Plot of channel cross sections of the Yazoo River at RM 82.90 for different dates.

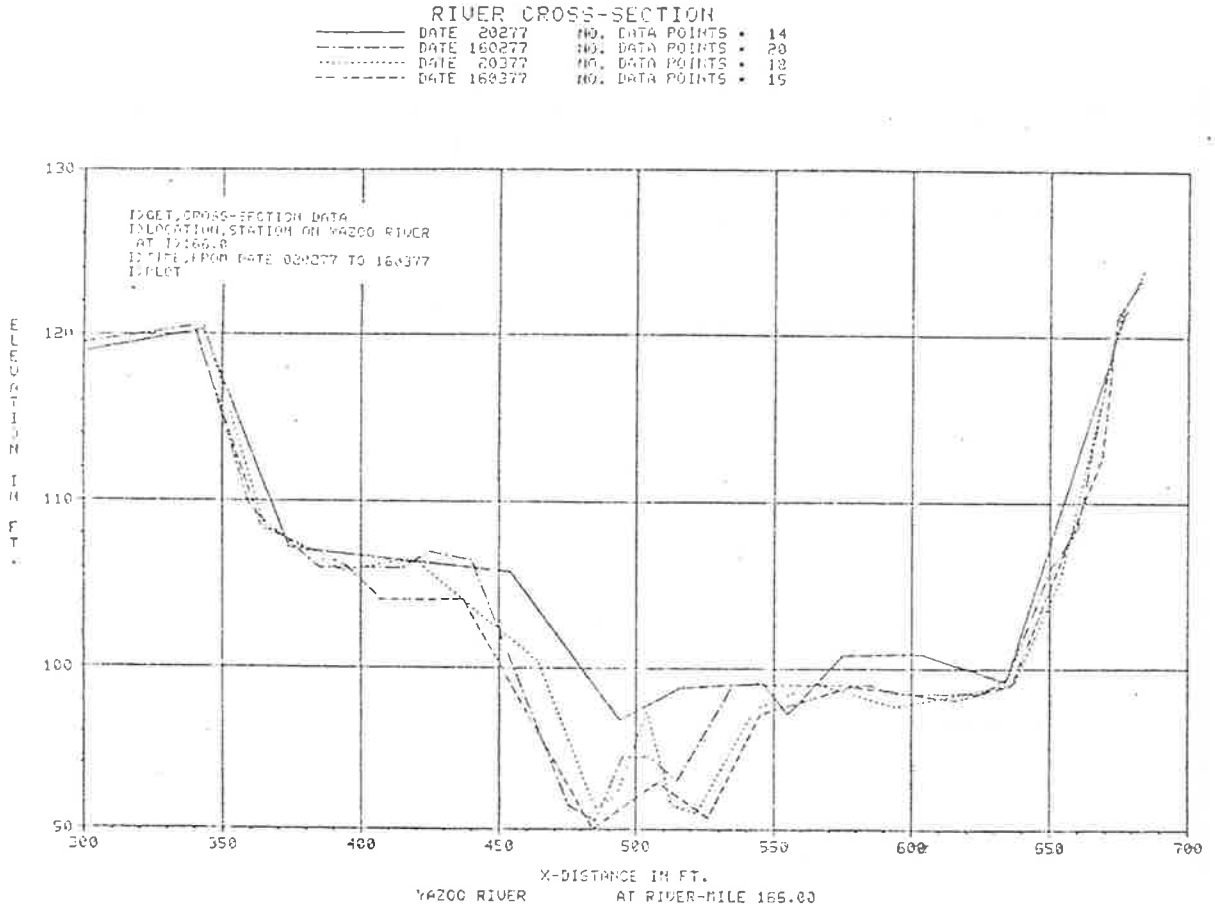

Figure 16.21c Plot of channel cross sections of the Yazoo River at RM 166.0 for different dates.

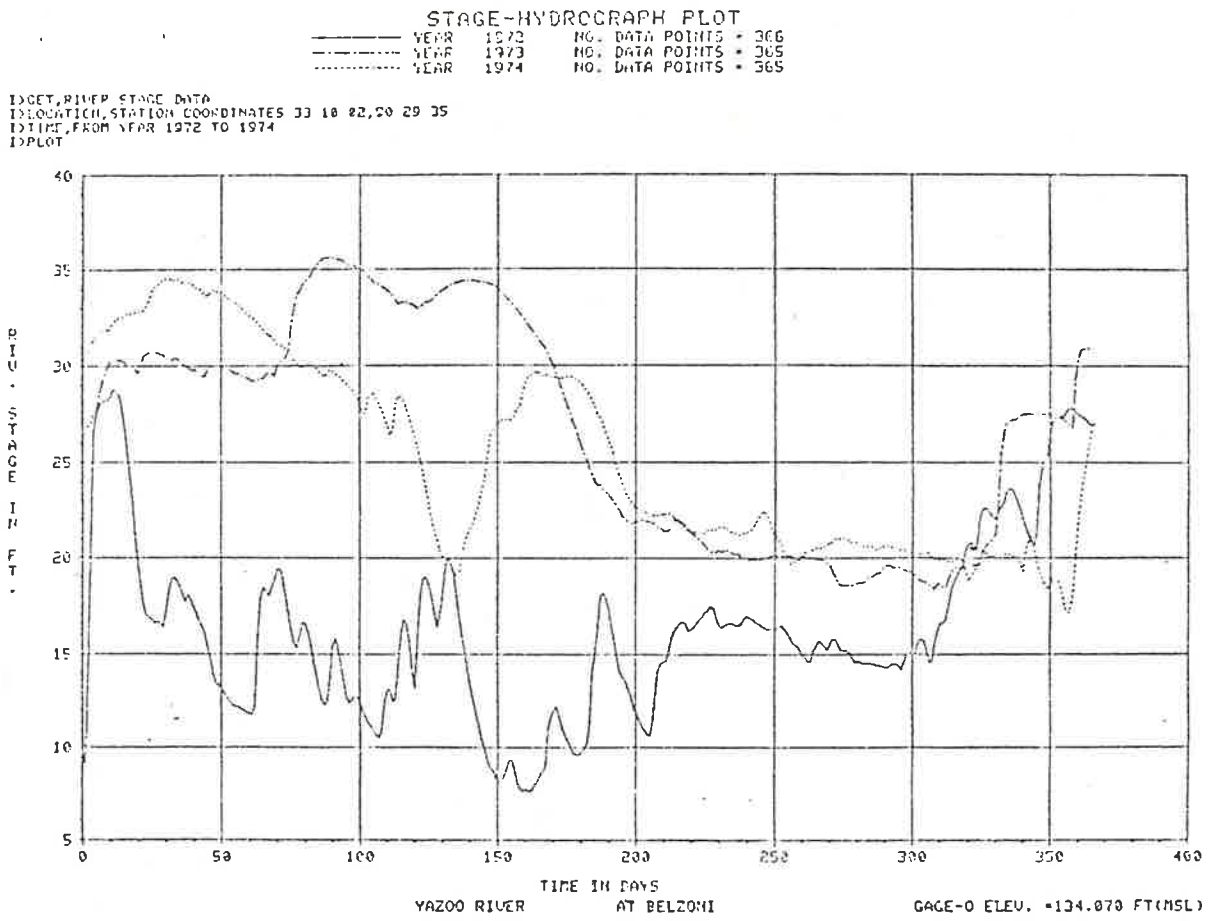

Figure 16.22 Plot of stage-hydrographs at Belzoni for three consecutive years.

of hydrographs for the Yazoo River at Belzoni for the calendar years 1972, 1973 and 1974 are presented.

8. Similar examples as (7) above with outputs in a tabular format, suitable for periodic reporting purposes, for calendar year 1973 and water year 1973 at Lambert and Belzoni respectively are presented in Figures 16.23 and 16.24.

9. Basic statistics are needed to understand the extreme events or for forecasting purposes. Thus, a way to get this useful information directly from historical data which are stored in the data bank is desirable. Figure 16.25 shows some typical outputs for basic statistics analysis.

10. Rainfall data are needed for water resources planning and also to operate watershed simulation models for basin system analysis. An example of the retrieval and listing of daily rainfall data at Byhalia for calendar year 1973 is shown in Figure 16.26. The result of data processing of the retrieved data set to obtain cumulative rainfall is given by a plot in Figure 16.26.

11. Thalweg level plots can give engineers and planners some useful information on variation of bed slope of a river or a segment of a river. This final example shows a plot of thalweg level for a segment of the Yazoo River (from river mile 3. to river mile 100.) in August 1962 (Figure 16.27).

16.5 LEVEL OF ANALYSIS

Chapters 2 to 15 have introduced various levels of analytical tools for analyzing watershed and river systems.

Various levels of analysis can be formulated, verified and utilized depending on level of accuracy required, available data, constraints, magnitude of projected watershed and river changes, rate of changes, whether or not the watershed or channel is on the threshold of a major change considering its geometry, hydraulics, hydrology, and sediment transport.

Level 1--office work and limited field investigations to estimate if significant watershed and river response may occur. This would need hand-held calculator applications.

```
? GET,DISCHARGE,ALL INFORMATION
? LOCATION,STATION,LOCATED AT LAMBERT
? TIME,YEAR 1973
? DISPLAY
```

YAZOO RIVER SYSTEM DATA BANK

RIVER DISCHARGE DATA CATEGORY

STATION NAME	STATN NO	DIST FR MOUTH	LATITUDE	LONGITUDE	GAGE ZERO(MSL)	DATA TYPE	NO YEARS
TALLAHATCHIE RIVER AT LAMBERT	1320	253.2(MI)			123.829(FT)	CONTI	14

DAILY DISCHARGE FOR 1973

COMPUTED DAILY DISCHARGE IN CUBIC FEET PER SECOND

DAY	JAN	FEB	MAR	APR	MAY	JUN	JUL	AUG	SEP	OCT	NOV	DEC
1	9480.	5380.	4550.	4820.	14300.	6550.	2330.	2230.	2060.	747.	449.	9700.
2	9260.	6780.	4560.	3930.	14000.	5090.	2150.	2060.	2020.	724.	413.	9080.
3	8970.	6730.	7730.	3870.	15100.	5010.	2130.	2030.	2050.	693.	359.	7930.
4	9350.	6530.	7550.	2610.	15000.	5220.	2430.	2010.	2038.	646.	352.	6975.
5	9290.	6330.	7230.	2000.	14700.	5540.	2490.	2123.	2403.	800.	320.	7830.
6	9120.	6210.	6702.	2710.	14400.	5310.	2023.	1980.	6530.	940.	341.	6830.
7	9490.	6223.	8020.	2720.	14100.	5120.	2030.	2100.	2000.	1090.	225.	6140.
8	9360.	7020.	8300.	3000.	14100.	5002.	2300.	2270.	2100.	1233.	250.	6350.
9	9250.	8370.	8760.	3350.	13870.	4470.	2033.	2240.	2020.	1340.	289.	5840.
10	9310.	9100.	8400.	3240.	13520.	3000.	2480.	2210.	2150.	1400.	256.	5700.
25	7950.	4020.	6700.	14020.	4900.	2530.	2423.	2210.	1020.	1050.	1670.	7070.
27	7530.	4700.	6210.	14000.	5370.	2480.	2400.	2190.	870.	1130.	7370.	7220.
28	7020.	4985.	4740.	14010.	6710.	2550.	2150.	2170.	826.	1030.	9710.	7320.
29	6410.	0.	3550.	14020.	6700.	2500.	2100.	2410.	794.	917.	10000.	6960.
30	5870.	0.	3820.	14300.	6900.	2410.	2160.	2000.	768.	788.	10400.	5720.
31	5200.	0.	3500.	0.	6100.	0.	2170.	2000.	0.	624.	0.	4910.

MONTHLY STATISTICS

MEAN	7620.	7324.	8432.	6639.	13018.	3567.	2476.	2543.	1972.	1337.	3038.	6825.
MAX.	9560.	9310.	13720.	14320.	15100.	6900.	2397.	4030.	2690.	2050.	10300.	9760.
MIN.	4630.	4650.	3500.	2720.	4020.	1910.	2150.	1990.	768.	624.	188.	4040.

TOTAL DISCHARGE FOR YEAR WAS 1823331. MEAN DISCHARGE FOR YEAR WAS 4995.4

HIGHEST DISCHARGE VALUE WAS 15100.CFS, OCCURRED ON MAY 3
LOWEST DISCHARGE VALUE WAS 188.CFS, OCCURRED ON NOV 14

Figure 16.23 Display of discharge data at Lambert for calendar year 1973.

```
? GET,RIVER STAGE,ALL INFORMATION
? LOCATION,STATION,LOCATED AT BELZONI
? DIST,WATER YEAR 1973
? ELEVATION
```

YAZOO RIVER SYSTEM DATA BANK

RIVER STAGE DATA CATEGORY

STATION NAME		STATN NO	DIST FR MOUTH	LATITUDE	LONGITUDE	GAGE ZERO(MSL)	DATA TYPE	NO YEARS
YAZOO RIVER	AT BELZONI	353	116.2(MI)			76.02(FT)	CONTI	11

DAILY RIVER STAGE FOR WATER YEAR 1973

COMPUTED DAILY RIVER STAGE IN FEET ABOVE GAGE ZERO ELEVATION

DAY	OCT	NOV	DEC	JAN	FEB	MAR	APR	MAY	JUN	JUL	AUG	SEP
1	18.60	18.70	27.10	30.80	34.50	32.60	29.80	25.70	27.20	28.70	22.20	22.00
2	18.60	18.60	27.20	30.70	34.40	32.50	29.50	25.10	27.20	28.50	22.10	22.30
3	18.60	18.50	27.20	31.00	34.50	32.40	29.40	24.40	27.20	28.20	21.90	22.40
4	18.50	18.40	27.30	31.40	34.40	32.20	29.20	23.60	27.20	27.90	21.90	22.30
5	18.60	18.70	27.40	31.50	34.30	32.00	29.10	22.70	27.40	27.50	21.70	21.90
6	18.50	18.60	27.50	31.60	34.20	31.90	28.90	22.20	27.80	27.30	21.50	21.40
7	18.70	18.50	27.50	31.80	34.30	31.70	28.80	21.40	27.90	26.90	21.40	21.20
8	18.70	18.50	27.50	31.90	34.30	31.60	28.70	21.20	28.60	26.50	21.40	21.30
9	18.70	18.50	27.50	31.80	34.10	31.50	28.30	20.40	29.10	26.10	21.40	20.80
10	18.80	19.30	27.50	32.00	34.00	31.30	28.10	20.00	29.40	25.80	21.30	20.20
26	19.30	21.20	30.30	34.10	33.80	29.70	28.20	24.50	29.40	22.20	21.20	20.70
27	19.20	22.60	30.60	34.20	32.00	29.60	27.60	26.10	29.30	22.20	21.30	20.50
28	17.10	25.50	30.50	34.30	32.70	29.40	27.40	26.60	29.20	22.30	21.30	20.60
29	19.50	26.50	30.50	34.50	0.00	29.60	26.90	26.90	29.10	22.20	21.40	21.00
30	19.80	27.30	30.70	34.50	0.00	29.60	26.70	27.00	28.90	22.30	21.50	21.00
31	18.80	0.00	30.80	34.50	0.00	29.70	0.00	27.10	0.00	22.30	21.80	0.00

MONTHLY STATISTICS

MEAN	32.06	33.80	30.74	28.08	22.57	28.80	24.33	21.50	28.75	19.06	22.27	26.80
MAX.	34.50	34.50	32.00	29.00	27.10	29.70	28.70	22.20	22.40	0.00	0.00	0.00
MIN.	30.70	32.70	29.40	26.30	19.20	27.20	22.20	21.20	19.70	0.00	0.00	30.90

MEAN RIVER STAGE FOR YEAR WAS 25.84

HIGHEST RIVER STAGE VALUE WAS 34.50FT. ABOVE GAGE ZERO ELEVATION, OCCURRED ON JAN 25
LOWEST RIVER STAGE VALUE WAS 18.40FT. ABOVE GAGE ZERO ELEVATION, OCCURRED ON NOV 4

Figure 16.24 Display of flood stage data at Belzoni for water year 1973.

```
? GET,DISCHARGE,DATA
? LOCATION,STATION,LOCATED NR SWAN LAKE
? TIME,FROM DATE 101272 TO 100273
? LIST
```

DISCHARGE VALUES (CFS) FOR THAT PERIOD ARE

1972	22								
12100.	13200.	13300.	14200.	14500.	15200.	15600.	15900.	16100.	16200.
16300.	16400.	16400.	16400.	16300.	16200.	16200.	16100.	16000.	15900.
15800.	15900.								
1973	41								
16000.	16000.	16100.	16200.	16600.	17100.	17500.	17500.	18000.	18000.
17600.	17200.	16700.	16200.	15700.	15200.	14700.	14200.	13800.	13400.
14000.	14800.	15400.	15800.	16200.	16000.	15800.	15500.	15000.	14500.
14000.	13700.	13600.	13500.	13400.	13300.	13200.	13200.	14000.	14600.
15000.									

```
? GET,DISCHARGE,DATA
? LOCATION,STATION,LOCATED NR SWAN LAKE
? TIME,FROM DATE 101272 TO 100273
? PROCESS,LIST,MIN VALUE

        THE MINIMUM VALUE IS   12100.00  WHICH OCCURRED ON DEC 10,1972

? GET,DISCHARGE,DATA
? LOCATION,STATION,NUMBER 132D
? TIME,FROM DATE 101272 TO 100273
? PROCESS,LIST,MAX VALUE

        THE MAXIMUM VALUE IS   18000.00  WHICH OCCURRED ON JAN  9,1973

? GET,DISCHARGE,DATA
? LOCATION,STATION,NUMBER 132D
? TIME,FROM DATE 101272 TO 100273
? PROCESS,LIST,BASIC STAT

        MINIMUM VALUE =  12100.00          MAXIMUM VALUE =  18000.00
        MEAN VALUE =  15382.54          STANDARD DEVIATION =   1365.89
```

Figure 16.25 Example of basic statistics calculation from the retrieved data.

```
? GET,PRECIPITATION DATA,DAILY
? LOCATION,STATION,NUMBER 1262
? TIME,YEAR 1973
? LIST
```

RAINFALL DATA FOR YEAR 1973

DAILY TOTAL RAINFALL IN INCH

DAY	JAN	FEB	MAR	APR	MAY	JUN	JUL	AUG	SEP	OCT	NOV	DEC
1	0.00	0.00	.10	0.00	.77	0.00	0.00	0.00	0.00	0.00	0.00	0.00
2	0.00	0.00	.05	0.00	1.31	0.00	.28	0.00	.23	2.28	2.00	0.00
3	.70	0.00	0.00	.08	.04	0.00	0.00	0.00	0.00	1.24	0.00	.24
4	0.00	0.00	.33	0.00	0.00	0.00	.08	0.00	0.00	.35	.40	.55
5	0.00	0.00	0.00	0.00	0.00	.20	0.00	0.00	.05	0.00	0.00	0.00
6	0.00	0.00	1.34	0.00	0.00	0.00	0.00	0.00	.37	0.00	0.00	0.00
7	0.00	1.48	0.00	.05	1.70	0.00	0.00	0.00	0.00	2.78	.11	0.00
8	0.00	.07	0.00	0.00	0.00	0.00	0.00	0.00	0.00	0.00	0.00	0.00
9	0.00	0.00	0.00	.38	0.00	0.00	0.00	0.00	0.00	0.00	0.00	0.00
10	0.00	0.00	1.82	0.00	0.00	0.00	.05	0.00	0.00	0.00	0.00	0.00
11	0.00	0.00	.02	0.00	.55	0.00	0.00	0.00	0.00	0.00	0.00	0.00
12	0.00	.18	0.00	0.00	0.00	0.00	0.00	0.00	0.00	0.00	0.00	0.00
13	0.00	1.11	0.00	0.00	0.00	0.00	0.00	.04	.33	.55	0.00	0.00
14	0.00	.11	0.00	0.00	0.00	0.00	0.00	.41	0.00	0.00	0.00	0.00
15	0.00	0.00	0.00	.02	0.00	0.00	0.00	0.00	0.00	0.00	.07	0.00
16	0.00	0.00	0.00	.52	0.00	0.00	1.58	0.00	0.00	0.00	0.00	0.00
17	0.00	0.00	0.00	.30	0.00	0.00	0.00	0.00	0.00	0.00	0.00	0.00
18	.05	0.00	0.00	.93	0.00	0.00	0.00	0.00	0.00	0.00	.65	0.00
19	0.00	0.00	.00	2.85	.14	0.00	.10	0.00	0.00	0.00	0.00	0.00
20	0.00	0.00	.05	0.00	0.00	0.00	0.00	0.00	0.00	0.00	1.55	0.00
21	2.52	0.00	0.00	0.00	0.00	0.00	0.00	0.00	0.00	0.00	0.00	0.00
22	2.00	2.00	0.00	.62	0.00	0.00	0.00	0.00	0.00	0.00	0.00	0.00
23	0.00	0.00	0.00	1.54	.38	0.00	0.00	0.00	0.00	0.00	0.00	0.00
24	0.00	0.00	.00	.93	0.00	0.00	0.00	0.00	0.00	0.00	.54	0.00
25	0.00	0.00	.11	0.00	0.00	0.00	0.00	0.00	0.00	0.00	.02	0.00
26	0.00	0.00	0.00	.10	0.00	0.00	.55	0.00	0.00	0.00	0.00	0.00
27	.07	0.00	0.00	0.00	2.35	0.00	0.00	0.00	0.00	.40	0.00	0.00
28	.55	0.00	0.00	0.00	0.00	.55	0.00	0.00	0.00	.21	0.00	0.00
29	0.00	0.00	.25	0.00	0.00	0.00	0.00	.10	0.00	0.00	0.00	0.00
30	0.00	0.00	.35	0.00	0.00	.10	0.00	.05	0.00	0.00	0.00	0.00
31	0.00	0.00	.20	0.00	0.00	0.00	.15	0.00	0.00	0.00	0.00	0.00
MONTHLY SUMMARY												
MON.TOT	3.79	3.31	5.21	8.69	7.00	1.15	2.79	1.51	1.63	4.23	3.54	.80

```
DO YOU WANT TO CONTINUE WORKING WITH THE RETRIEVED DATA SET
? YES
? PROCESS,LIST,SUM RAINFALL
```

Figure 16.26a Example of data conversion and display of daily rainfall at Byhalia.

Input:

```
I>GET,PRECIPITATION DATA,DAILY
I>LOCATION,STATION NUMBER 1262
I>TIME,YEAR 1973
I>PROCESS,PLOT,CUM RAINFALL
```

Output:

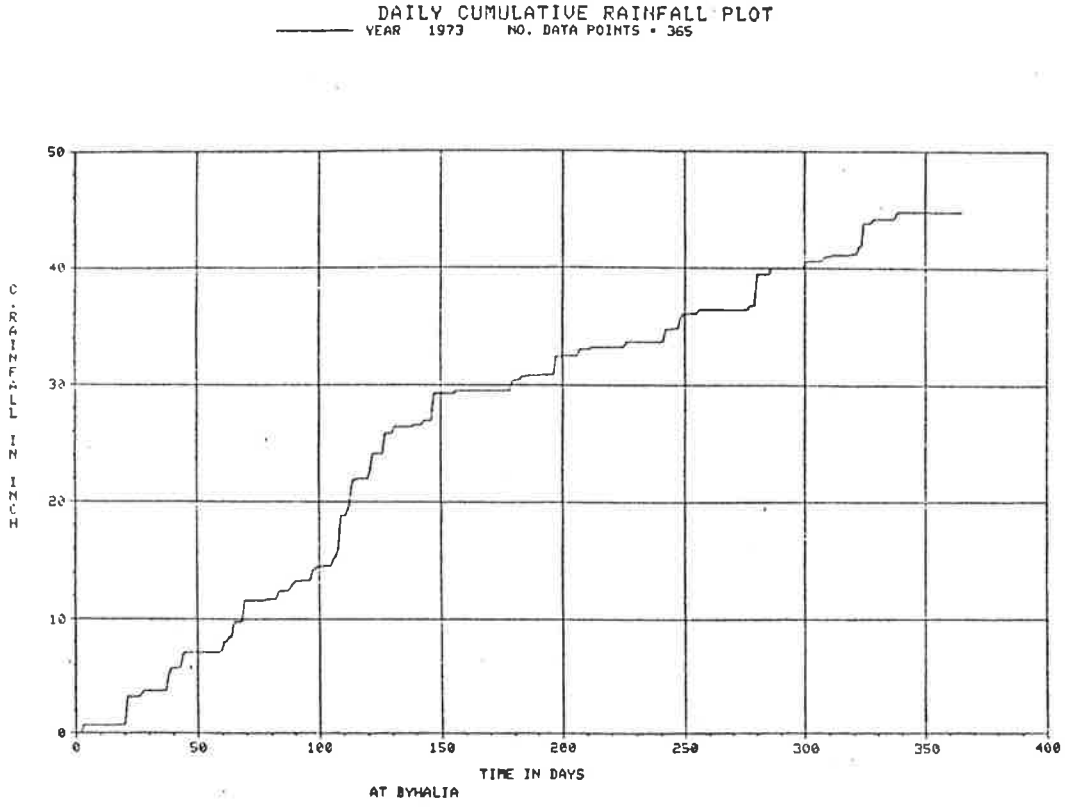

Figure 16.26b Example of data conversion and plot of cumulative rainfall at Byhalia.

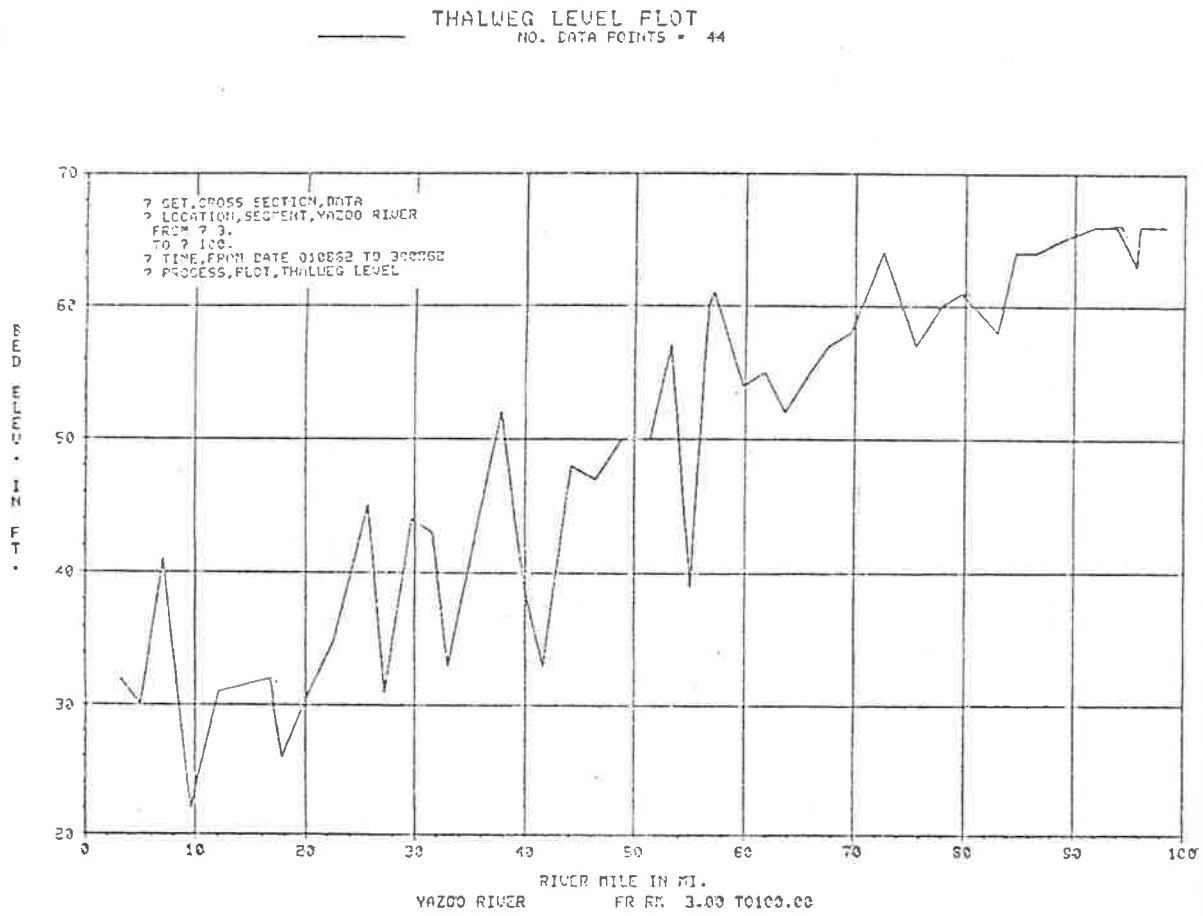

Figure 16.27 Example of channel cross section data processing for thalweg level plot.

Level 2--conduct field work to establish baseline data (present conditions) and project changes that will result from alterations in flow, etc. Either hand-held calculator applications or simple computer models could be used in this level of analysis.

Level 3--obtain additional data (some data could be synthesized) to utilize the present state-of-the-art methods to simulate changes continuously and/or for major events. This level would require computer application of either simple or complicated state-of-the-art models.

Level 4--research to develop and/or modify state-of-the-art technology to improve Level 3 analysis. This might incorporate sediment routing by size fraction. This approach would utilize an interactive data storage and retrieval system and could include data essential for the analysis of water quality, biology, recreation, etc.

Level 5--incorporate the management model with Level 3 and/or Level 4 analysis as one component of the comprehensive system of models.

All levels of analysis should be capable of evaluating watershed and river responses to all levels of watershed management and streamflow alteration. The methods of analysis must include the stream system and the watershed. The data required and recommended level of analysis for various levels of analysis follow.

Level 1

Needs	Data Required	Method of Analysis
Knowledge of present system	Recorded data: climatic hydrologic hydraulic Maps Aerial photos Field data: type of river bank erosion stability bed and bank material vegetation channel geometry watershed characteristics riffle and pool sequence velocity geology control structures Proposed structures, water rights, etc.	Geomorphic, transport, hydrologic and hydraulic relations required for a qualitative analysis. An example is to use Lane relation (Simons and Sentürk, 1977) hydraulic geometric equations, etc.

Level 2

Needs	Data Required	Method of Analysis
Requires more accurate and detailed data. Also needs more information on changes in above as function of space and time	All data for Level 1 plus: detail data on study subreaches, cross sections in the subreaches, stage-discharge relations, suspended sediment, bed material, channel slope, etc.	Conduct Level 1 type study supported with additional data on sediment transport, geomorphic relations, stage duration, flow distribution, peak flows, minimum flows, etc. Determine more precise values of the system response
	Information on: verticals at a cross section, engineering and natural controls, land-use changes, and watershed impacts. Decide whether to treat river as rigid or alluvial system.	If results indicate: 1. Large changes in time and space 2. Thresholds 3. High costs 4. Need for greater accuracy 5. Cannot satisfy legal, etc., constraints then go on to Level 3 analysis

Level 3

Use the current state-of-the-art models and techniques to route water and sediment for major runoff events or simulate continuously if necessary. Generally, a known discharge model will provide sufficient accuracy.

Develop methodologies to accommodate all interests including water resources development, water quality, recreation, biology, river mechanics, etc.

Develop and utilize a common data storage and retrieval system. Such an approach is necessary to conduct an accurate, economical, efficient and sufficient analysis.

Level 4

Use the current models to identify short- and long-term data needs and research needs. Then conduct research to improve Level 3 type models and analysis. Also, could proceed with a higher level of sophistication involving water quality, sediment routing by size fraction, two-dimensional modeling, improve watershed modeling components, etc.

Level 5

Incorporate the management models such as linear programming, dynamic programming, screening, direct search, and/or nonlinear programming optimization techniques with Level 3 and/or Level 4 model as one component of the comprehensive system of models.

16.6 SUMMARY

In this chapter, an overview of some case studies is made to illustrate types of problems that are often encountered in the analysis of watershed and river systems. General data needs for analysis are discussed and an effective system for data management is presented. Then, a general approach to determine the required level of analysis is recommended.

16.7 REFERENCES

Simons, D. B. and Senturk, F., Sediment Transport Technology, Water Resources Publications, Fort Collins, Colorado, 1977.

Simons, D. B., Li, R. M. and Duong, N., "Sedimentation Study of the Yazoo River Basin," prepared for U.S. Army Corps of Engineers, Vicksburg District, Vicksburg, Mississippi, October, 1978.

CHAPTER 17

CANAL AND CHANNEL DESIGN AND RIVER RESPONSE ANALYSIS

by

Daryl B. Simons, Associate Dean for Engineering Research and
Professor of Civil Engineering,
Colorado State University, Fort Collins, Colorado
Ruh-Ming Li, Associate Professor of Civil Engineering,
Colorado State University, Fort Collins, Colorado
Yung-Hai Chen, Assistant Professor of Civil Engineering,
Colorado State University, Fort Collins, Colorado

17.1 INTRODUCTION

The hydraulic engineer is frequently required to design channels, canals, floodways, and navigable waterways. In the past, most designs were conducted by assuming a rigid boundary channel system. The river is a dynamic system, and a realistic analysis must consider the channel as a movable bed system. The assessment of sediment movement and stream morphology are certainly of vital importance for a proper channel design. Quite often, the bank protection measures are required to protect the area that is particularly vulnerable to bank erosion. The basic analytical tools required to conduct an analysis are discussed in Chapters 2 to 15. For a preliminary assessment, the programmable calculator programs presented in Chapter 15 are especially useful. This chapter presents four selected studies specific to the design of channels, canals, floodways, and navigable waterways. The first study presented is a design of channel bank protection associated with Bijou Creek, Colorado (Simons, 1975). The second example is a canal design considering a large fluctuation of water and sediment inflow (Simons and Li, 1978). The third problem is an erosion, sedimentation and debris analysis of proposed Boulder Creek Floodway, Boulder, Colorado, (Simons and Li, 1979), and the last case study is an investigation of the effects of Chippewa River erosion and silt reduction measures, (Simons and Chen, 1978). These four examples provide a good overview of hydraulic analysis required for channel design.

17.2 CHANNEL BANK PROTECTION PROBLEM-BIJOU CREEK, COLORADO

General

Presented in this section is a hydrologic and hydraulic analysis of Bijou Creek, a tributary to the Narrows Unit near Fort Morgan, Colorado. The proposed location of the Union Pacific Railroad is approximately 1500 ft north of the creek (see Figure 17.1). A hydrologic and hydraulic analysis of the safety of the proposed railroad location is presented.

The analysis identifies three design floods and corresponding water surface elevations with return periods of 50, 100, and 200 years. Bank protection is specified for each of the design floods and for six different channel design alternatives. The design floods were estimated using the Gumbel Method of frequency analysis and all of the available hydrologic data. The design of riprap bank protection considers the design flood discharge,

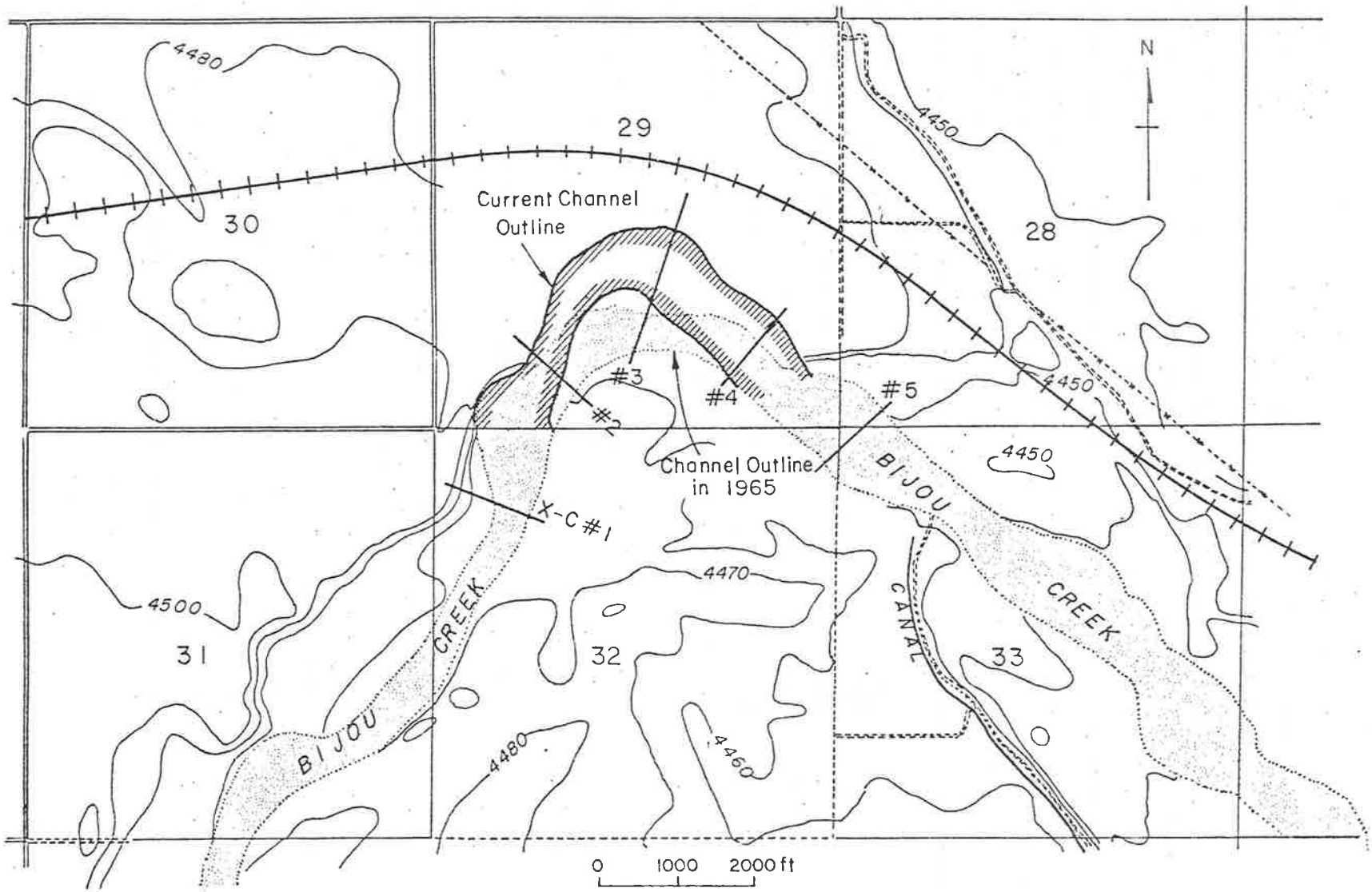

Figure 17.1 Topographic map of the study area.

superelevation in the bend, antidune height, local scour, bed material size, and stability of riprap materials.

Flood Frequency Analysis

According to the USBR report (1965), the analysis of streamflow data for the period 1939 to 1946 by the Corps of Engineers and A. Hansen of their Project Office, established that the maximum recorded mean daily flow is 30,900 cfs. This flow was assigned a frequency of once in 200 years. Based on the available streamflow data for Bijou Creek for the six-year period 1951 through 1956 and consultation with H. Grout of the Flood Hydrology Section, the recurrence rate of this maximum daily flow was subsequently changed into once in 50 years. The historical records show that there were two extreme flood events 282,900 cfs and 466,000 cfs observed at the stream-flow gauging station of Bijou Creek near Wiggins, Colorado. According to Matthai (1969) of the USGS, these two extreme flood events are respectively 5.5 and 9.0 times the 50-year flood. In other words, the 50-year flood estimated by USGS is about 51,600 cfs. This value has been confirmed by utilizing the earlier publication by Matthai (1968). Taking into consider-ation the two extreme floods that have occurred, the flood with a return period of 50 years is determined to be 51,600 cfs.

Following the procedures given by Matthai (1968), floods and their return periods are as follows:

Return Period	Flood Discharge
5 years	13,400 cfs
10 years	23,000 cfs
20 years	33,000 cfs
30 years	41,400 cfs
40 years	47,100 cfs
50 years	51,600 cfs

The above estimated floods were plotted in Figure 17.2 using a Gumbel probability paper. From Figure 17.2, the floods with various return periods can be interpolated or extrapolated. The estimated design floods with return periods of 100 and 200 years are respectively 62,000 cfs and 72,500 cfs. The three design floods used in the following analysis are the 50-year, 100-year, and 200-year floods respectively.

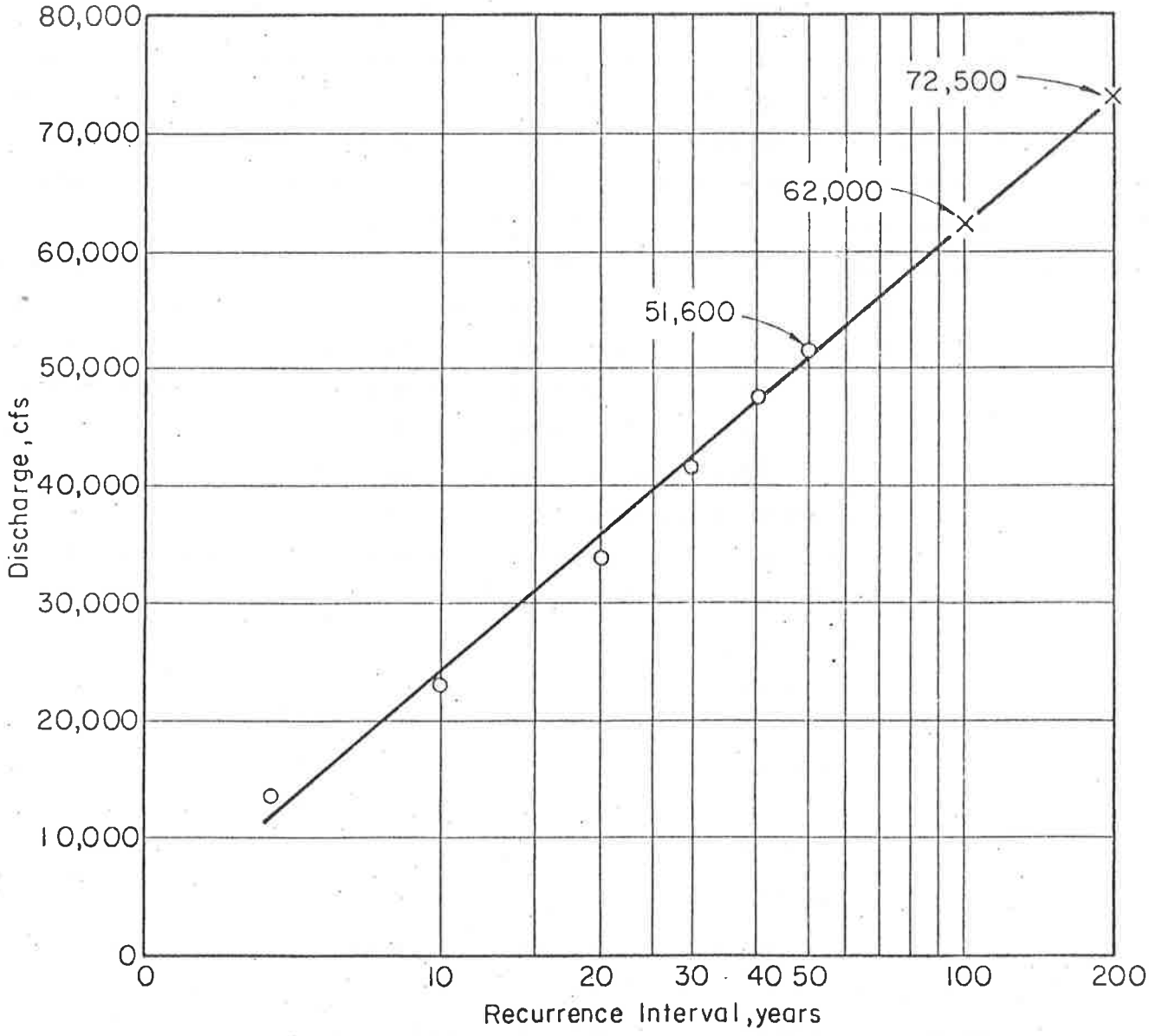

Figure 17.2 Gumbel's method frequency analysis. Annual floods on Bijou Creek near Wiggins, Colorado.

Channel Morphology

A field study was conducted to obtain morphologic data for the hydraulic analysis. The information utilized in the analysis includes the representative cross section of the channel, the representative bed material size, and the energy slope. With these data, the flow resistance coefficient was estimated.

Representative Cross Section: The representative cross section in the vicinity of the study site was developed by considering the channel cross sections established by the field study. Five selected cross sections were surveyed. Among them only two cross sections were similar in shape. They are representatives of the cross section of the study reach. The dimensions of the representative cross section were established by averaging these two cross sections. The results of this analysis are shown in Figures 17.3 and 17.4.

Figure 17.3 shows the relationship between cross-sectional areas and the flow depth as follows,

$$A = 242.6\ y_n^{1.52} \qquad (17\text{-}1)$$

in which A is the cross-sectional area, and y_n is the normal depth of flow measured from the thalweg level.

Figure 17.4 gives the following relationship between the wetted perimeter and the flow depth,

$$P = 682.0\ y_n^{0.31} \qquad (17\text{-}2)$$

The average top width of channel as estimated by field survey and topographic maps is 1,700 ft.

Representative Bed Material Size: The results of sieve analysis of the bed material samples taken at cross sections are shown in Figure 17.5. The average median bed material size, D_{50}, is 0.45 mm. The average D_{16} size (the size for which 16 percent is finer by weight) is 0.22 mm, and the average D_{84} size (the size for which 84 percent is finer by weight) is 0.91 mm. The bank material has nearly the same distribution as that of the bed material, but contains lenses of silt and clay. The bank is highly stratified and can be easily eroded.

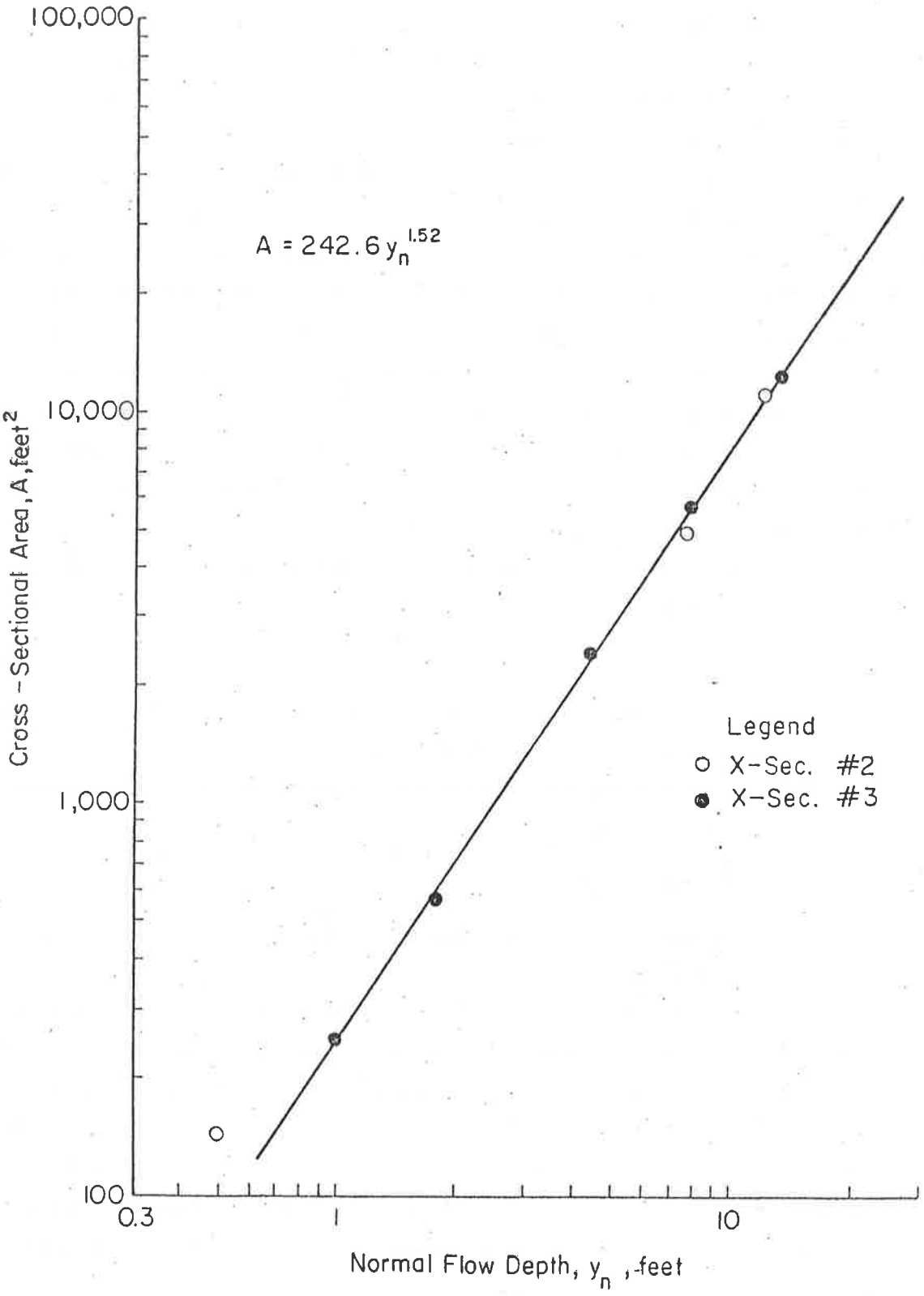

Figure 17.3 Cross-sectional area versus flow depth relation.

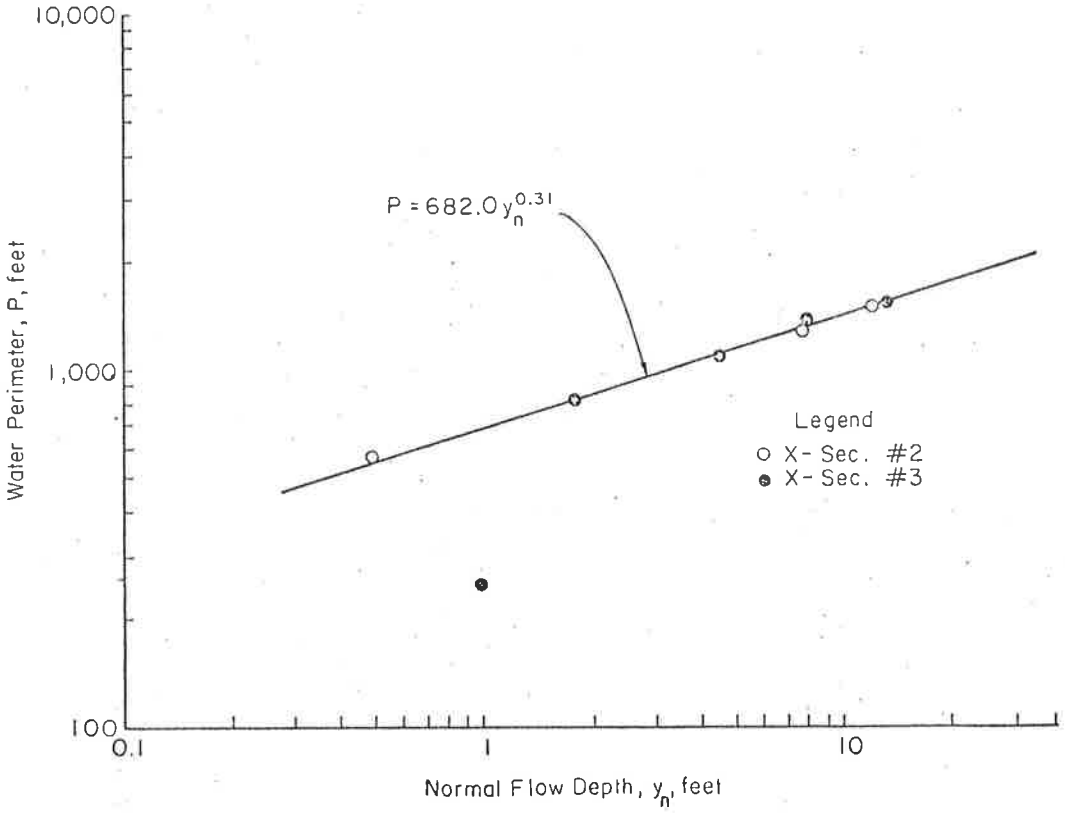

Figure 17.4 Wetted perimeter versus flow depth relation.

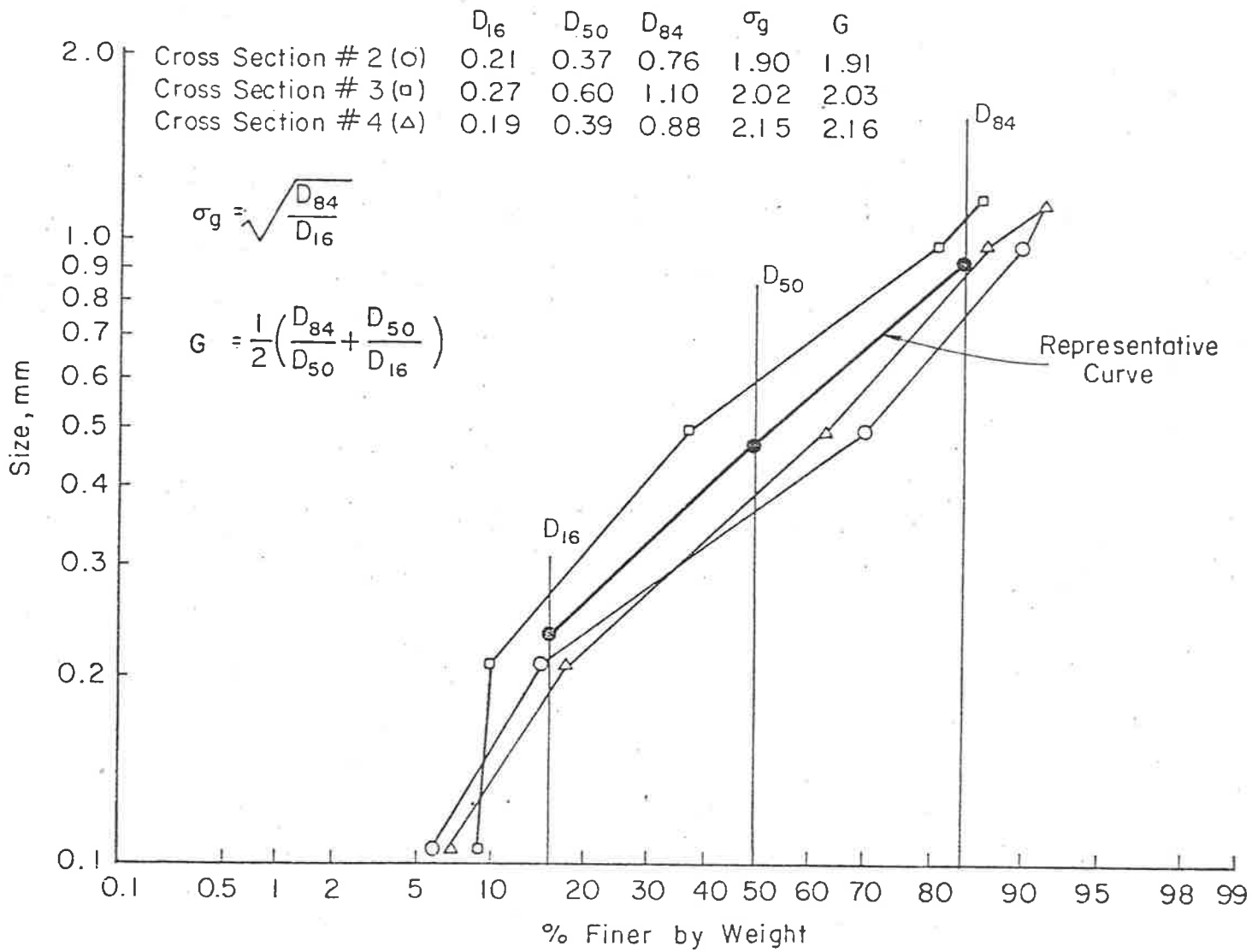

Figure 17.5 Analysis of bed material size of Bijou Creek.

Energy Slope: The energy slope may be less than the channel bed slope. However, for a safer design, it is assumed that the energy slope is equal to the channel bed slope. The average channel bed slope from field surveys is 0.00252. This slope is adopted as the design energy slope.

Flow Resistance Coefficient: Matthai (1969) showed that during the floods of June 1965 in South Platte River Basin, Bijou Creek was in upper regime having antidunes with breaking waves. Similarly, computations show that the bed forms of Bijou Creek (D_{50} = 0.45 mm) will be antidunes or standing waves during floods. Resistance to flow associated with antidunes depends on how often the antidunes form, the area of the reach which they occupy, and the violence and frequency of their breaking. According to Simons and Richardson (1971), if the antidunes do not break, resistance to flow is about the same as for a plane sand bed, and the discharge coefficient, $C/\sqrt{g}$, (where C is the Chezy resistance coefficient, and g is the gravitational acceleration) ranges from 14 to 23 (Manning's coefficient, n, is about 0.017 to 0.027 for the flow depths being considered). The acceleration and deceleration of the flow through the nonbreaking antidunes (frequently called standing waves) causes resistance to flow to be slightly more than that for flow over a plane bed. If many antidunes break, resistance to flow can be very large because the breaking waves dissipate a considerable amount of energy. With breaking waves, $C/\sqrt{g}$ may range from 10 to 20, and Manning's coefficient, n, ranges from about 0.019 to 0.038 for the flow depths being considered.

From available data on the stage-discharge relation at the stream gauging station (see Matthai (1968) and (1969)), it is estimated that the Manning roughness coefficient, n, during the design floods is about 0.023. This value of Manning's n gives a computed mean flow velocity of 18.7 fps in Bijou Creek for the extreme flood event of June 1965 (discharge 466,000 cfs). This computed mean flow velocity is comparable with the maximum mean flow velocity of 20 to 22 fps in Plum Creek near Louviers, reported by Matthai (1969).

Hydraulic Analysis

The information on hydraulic conditions needed for designing bank protection includes the normal depth of flow, the cross-sectional area of flow, the mean flow velocity, the Froude number, the antidune height, the local scour depth, the superelevation of the flow in bend, the local depth,

and the local velocity. Moreover, different design alternatives will result in different hydraulic conditions. In this study, six design alternatives were proposed; the first alternative was to protect the existing outer bank with riprap (see Figure 17.6), the second alternative was to realign the bend to its plan geometry before 1965 and to protect the outer bank with riprap (see Figure 17.7), and the third alternative was to realign the bend to that of a mild bend relative to the existing channel alignment and to protect the outer bank with riprap, (see Figure 17.8). The fourth, fifth, and sixth alternatives were: 1) to determine the necessary buffer strip distance between the railroad and the present north river bank if bank protection is not utilized, 2) to use rock riprap spur dikes to protect the existing river bank, and 3) to substitute soil-cement riprap for rock riprap utilized in Design Alternatives 1, 2, and 3.

The fifth alternative is to construct a series of rock riprapped spur dikes to guide the flow away from the existing north bank, (see Figure 17.9). The flow alignment is the same as that of the second alternative (see Figure 17.7).

A summary of computed hydraulic conditions in the first three basic alternatives is given in Table 17.1. The calculations pertaining to determination of riprap size are briefly described.

Normal Depth, Cross-Sectional Area, Mean Flow Velocity, and Froude Number: The following normal depth-discharge relation is determined by using Manning's equation, Equations 17-1 and 17-2 , the slope of energy gradient $S = 0.00252$ and Manning's roughness coefficient $n = 0.023$.

$$Q = 395.02\ y_n^{2.32} \tag{17-3}$$

In this relation Q is the design discharge and y_n is the normal depth of flow measured from the thalweg level.

For design floods with return periods of 50, 100, and 200 years, the normal depths from thalweg level are determined by Equation 17-3. Then, the cross-sectional area and the wetted perimeter can be computed using Equations 17-1 and 17-2 , respectively. Then, the mean flow velocity, the hydraulic radius, and the Froude number are calculated. The Froude number is

$$F = \frac{V}{\sqrt{gR}} \tag{17-4}$$

in which F is the Froude number, V is the mean flow velocity, and R is the hydraulic radius.

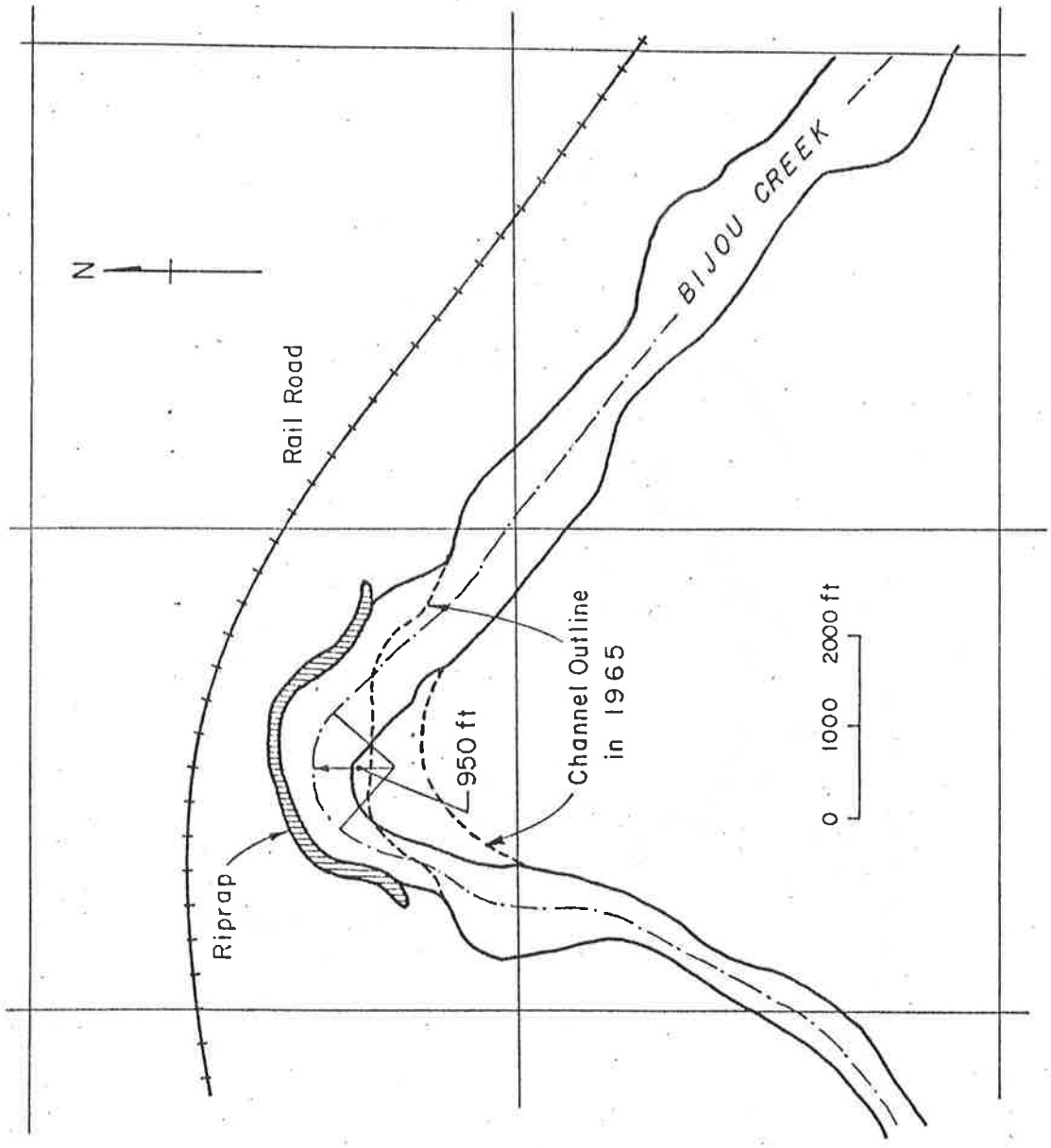

Figure 17.6 The proposed first alternative.

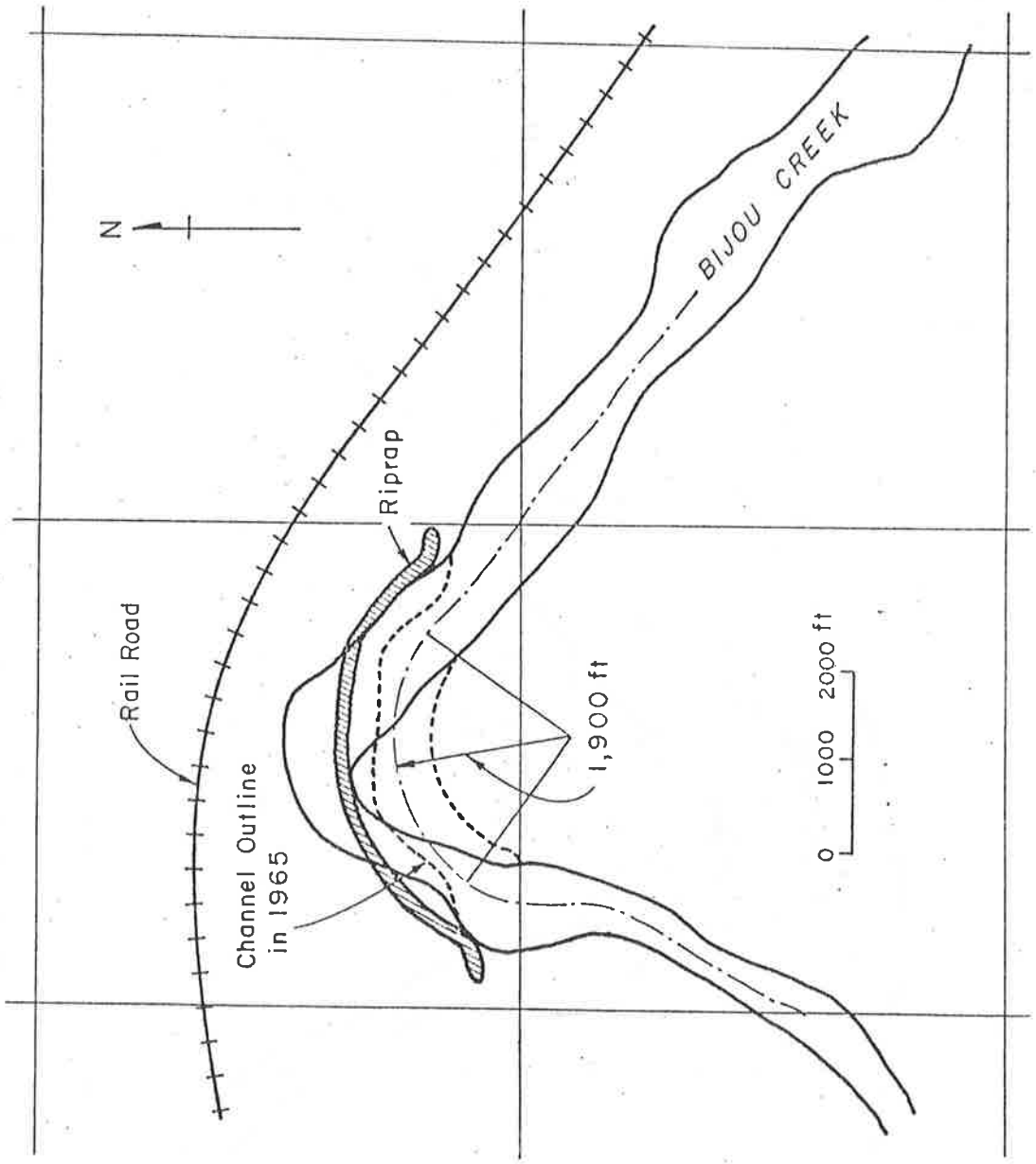

Figure 17.7 The proposed second alternative.

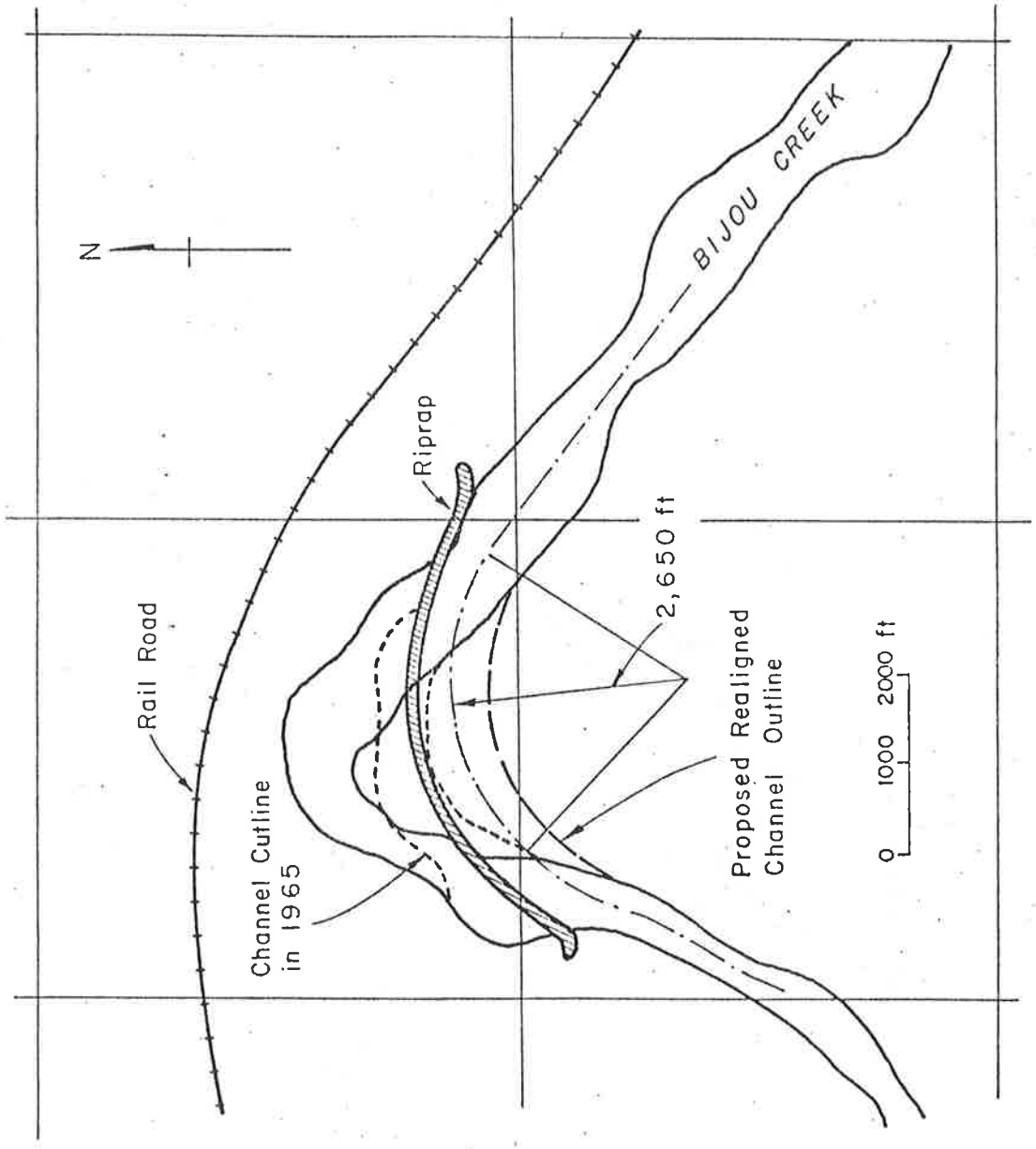

Figure 17.8 The proposed third alternative.

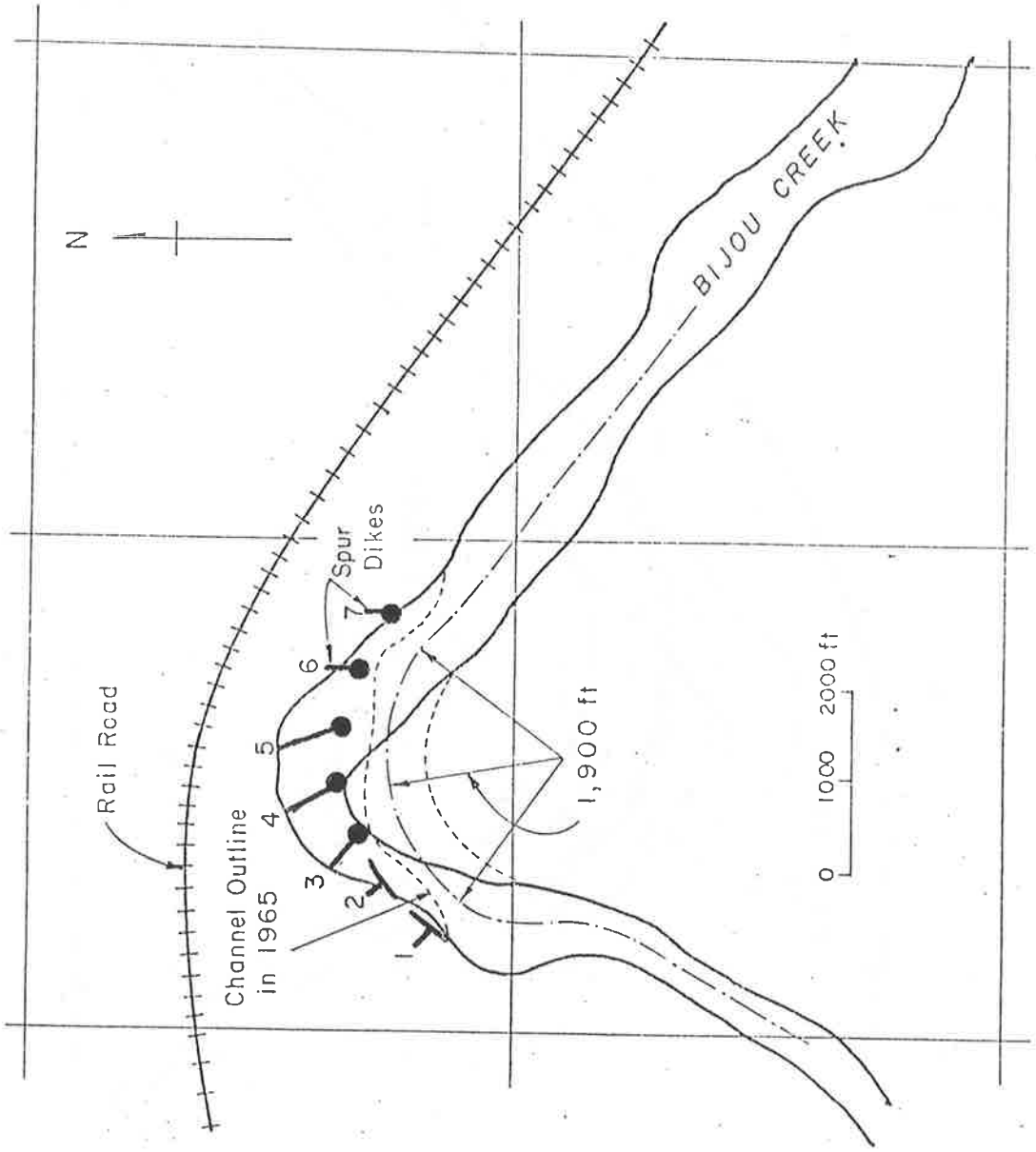

Figure 17.9 The proposed fifth alternative.

Table 17.1 Summary of computed hydraulic conditions.

T years	Q cfs	y_n ft	A ft^2	V ft/sec	F	H ft	d_s ft	A_ℓ	r_c ft	Δz ft	y_o ft	V_o ft/sec
								1	950	4.25	12.40	17.37
50	51,600	8.17	5,904	8.74	0.72	2.09	8.82	2	1,900	2.12	10.28	15.30
								3	2,650	1.52	9.69	14.70
								1	950	4.82	13.65	18.50
100	62,000	8.84	6,660	9.31	0.74	2.37	9.63	2	1,900	2.41	11.20	16.20
								2	2,650	1.73	10.57	15.60
								1	950	5.36	14.82	19.50
200	72,500	9.46	7,379	9.82	0.75	2.64	10.33	2	1,900	2.68	12.14	17.11
								3	2,650	1.92	11.38	16.40

Note: T is the return period, Q is the design discharge, y_n is the normal depth from the thalweg level, A is the cross-sectional area of flow, V is the mean flow velocity, F is the Froude number, H is the antidune height, d_s is the scour depth at the leading portion of riprap bank protection, A_ℓ is the alternative of designs, r_c is the radius at the center of a bend, Δz is the superelavation, and Y_o and V_o are respectively the depth and velocity for designing riprap sizes.

As shown in Table 17.1, the Froude numbers are approximately 0.74, which implies the maximum Froude numbers are on the order of 1.0 to 1.6. According to Simons and Richardson (1971), these flow conditions should be in the upper regime with either standing waves (nonbreaking antidunes) or antidunes with breaking waves. The estimated Manning's coefficient of 0.023 is correct for these flow conditions. In addition, the backwater effects are negligible because the flows are in the upper regime. The normal depth as computed by Equation 17-3 should be satisfactory for design purposes.

Antidune Height: Antidunes form as a series or train of inphase (coupled) symmetrical sand and water waves. The height and length of these waves depend on the shape of the channel and the characteristics of the fluid and the bed material.

Kennedy (1961) made a detailed study of antidune flow. He recommended that the wave length is generally given by $2\pi V^2/g$ and two-dimensional waves break when the ratio of wave height to wave length reaches a value of approximately 0.14. For a conservative estimation, the antidune height is estimated by the following equation:

$$H = 0.14 \frac{2\pi V^2}{g} = 0.027\ V^2 \qquad (17\text{-}5)$$

in which H is the antidune height.

Local Scour Depth: Local scour occurs in the bed of the channel around embankments due to the action of vortex systems induced by the obstructions to the flow. The basic mechanism causing local scour is the vortex of fluid resulting from the pile-up of water on the upstream edge of an obstruction and subsequent acceleration of flow in the contracted reach. In this study, the proposed bank protection structure is a continuous riprap revetment, the local scour only expected to occur at the leading portion of the revetment.

Detailed studies of scour around embankments have been made mostly in laboratories. There are very few case studies for scour at field installations, especially for the continuous revetment. According to the studies of Liu et al. (1961), the equilibrium scour depth for local scour around a spur nose is determined by

$$\frac{d_s}{y_1} = 1.1 \left(\frac{L_s}{y_1}\right)^{0.4} F_1^{0.33} \qquad (17\text{-}6)$$

in which L_s is the spur length, y_1 is the upstream depth, d_s is the depth of scour measured from mean streambed elevation, and F_1 is the upstream Froude number.

Assuming that Equation 17-6 is applicable in the leading portion of the continuous riprap revetment, the local scour depths for different design floods are estimated and given in Table 17.1. The ratio of L_s to y_1 is assumed to be 1.25 because the design side slope of the riprapped bank is 2.5:1 (horizontal to vertical distance).

Superelevation: Because of the change in flow direction in the bend, there is a centrifugal force that causes superelevation of the water surface. That is, the water surface is higher at the concave bank (outer bank) than at the convex bank (inner bank). There are many equations for evaluating the superelevation and the differences in superelevation that are obtained by using the different equations are small (see Richardson et al., (1975)). The following equation for computing the superelevation was recommended by Richardson et al., (1975) and is used in this report:

$$\Delta z = \frac{V^2}{gr_c} W \qquad (17\text{-}7)$$

whre Δz is the superelevation, r_c is the radius at the center of a bend, and W is the top width of the channel.

Flow Conditions Used to Estimate Riprap Size: There are many methods for determining riprap size (Simons and Sentürk, 1977). Among them, the method developed by Stevens et al. (1974) may be the most comprehensive and appropriate method to use. In applying their method, the depth of flow, the flow velocity and the angle between the horizontal and the velocity vector in the plane of the side slope are necessary.

As mentioned earlier, the forms of antidunes or standing waves constitute a series of inphase symmetrical sand and water waves. For steady flows, the depths and velocities are nearly the same at wave troughs or peaks. In this report, the flow depth for designing riprap sizes is determined to be the sum of the normal depth from thalweg level and the superelevation, i.e.,

$$y_o = y_n + \Delta z \qquad (17\text{-}8)$$

and the flow velocity for designing riprap size is computed by utilizing Manning's equation as follows,

$$V_o = \frac{1.486}{n} S^{1/2} y_o^{2/3} \qquad (17\text{-}9)$$

in which S is the energy slope.

The angle between the horizontal and the velocity vector in the plane of the side slope is assumed to be negligible.

Hydraulic Design

Three design alternatives are considered in this study. Different hydraulic designs result for each of the three design alternatives and the three different design floods. The hydraulic design includes the determination of the total length of bank protection, the minimum buffer strip distance between the railraod and the river bank, the estimated volume of earth work, the side slope of riprapped bank, the sizes of riprap material, the thickness of riprap, the size of the gravel filters, the thickness of the gravel filters, the height of riprap protection above the existing bed level, and the depth the riprap should extend below thalweg level. Using the hydraulic data, the foregoing values can be determined. Table 17.2 provides a summary of the hydraulic designs for different design conditions. The methods of design are briefly described.

Length of Bank Protection, Minimum Buffer Strip, and Excavation Volumes: From Figures 17.6, 17.7 and 17.8, the length of bank protection, minimum buffer strip distance between the railroad and the river bank, and the excavation volumes for three different design alternatives can be estimated. The minimum buffer strip distance is a measure of how far the river bank must migrate due to bank erosion to endanger the railroad. A wider minimum buffer strip distance between Bijou Creek and the railroad will provide a larger factor of safety for the railroad. However, the length of bank protection and excavation volumes increase accordingly, which in turn increases the cost of construction.

Side Slope of Riprap Bank: The side slope of the riprapped bank should be less than the angle of repose of the bank material. Analysis shows that the angle of side slope should be at least five degrees less than the angle of repose of the bank material. The bank material is medium sand with some clay and silt with average D_{50} of about 0.35-0.45 mm. Its angle of repose is about 29° (see Simons (1957). A side slope 2.5:1 (horizontal to vertical distance) is utilized and the corresponding angle of side slope is 21° - 48' (see Figure 17.10).

Table 17.2 Summary of hydraulic designs.

T Years	Q cfs	A_ℓ	L ft	B_m ft	E x 10^5 yd^3	Z	K_{50} ft	G_K	t_r ft	f_{50}^1 mm	G_f^1	t_f^1 in.	f_{50}^2 mm	G_f^2	t_f^2 in.	h_a ft	h_b^ℓ ft	h_b ft
		1	4,700	700	--	2.5	1.5	1.3	3.3	6.0	3.0	10.0	60.0	2.0	10.0	14.5	10.0	5.0
50	51,600	2	5,700	1,250	6.26	2.5	1.1	1.3	2.4	6.0	3.0	8.0	60.0	2.0	7.0	12.5	10.0	5.0
		3	6,250	1,500	9.42	2.5	1.0	1.3	2.2	6.0	3.0	7.0	60.0	2.0	7.0	12.0	10.0	5.0
		1	4,700	700	--	2.5	1.7	1.3	3.7	6.0	3.0	12.0	60.0	2.0	11.0	16.0	11.0	5.0
100	62,000	2	5,700	1,250	7.04	2.5	1.3	1.3	2.9	6.0	3.0	9.0	60.0	2.0	9.0	13.5	11.0	5.0
		3	6,250	1,500	10.64	2.5	1.2	1.3	2.6	6.0	3.0	8.0	60.0	2.0	8.0	13.0	11.0	5.0
		1	4,700	700	--	2.5	2.0	1.3	4.4	6.0	3.0	14.0	60.0	2.0	13.0	17.5	12.0	5.0
200	72,500	2	5,700	1,250	7.85	2.5	1.4	1.3	3.1	6.0	3.0	10.0	60.0	2.0	9.0	14.5	12.0	5.0
		3	6,250	1,500	11.91	2.5	1.3	1.3	2.9	6.0	3.0	9.0	60.0	2.0	9.0	14.0	12.0	5.0

Note: T is the return period in years, Q is the design discharge, A_ℓ is the alternative of designs, L is the total length of riprap bank protection, B_m is the minimum buffer strip distance between the railroad and the riverbank, E is the estimated excavation volumes, Z is the ratio of the horizontal distance to the vertical distance for the side slope of riprap bank, K_{50} is the design riprap size for which 50 percent is finer by weight, G_K is the gradation coefficient of riprap, t_r is the thickness of riprap, f_{50}^1, G_f^1, and t_f^1 are respectively the gravel size for which 50 percent is finer by weight, the gradation coefficient and the thickness of the first layer of gravel filter, f_{50}^2, G_{50}^2, and t_f^2 are respectively the gravel size for which 50 percent is finer by weight, the gradation coefficient and the thickness of the second layer of gravel filter, h_a is the design height of riprap protection above the existing bed level, and h_b^ℓ and h_b are respectively design riprap depths in and not in the leading portion of the bank protection.

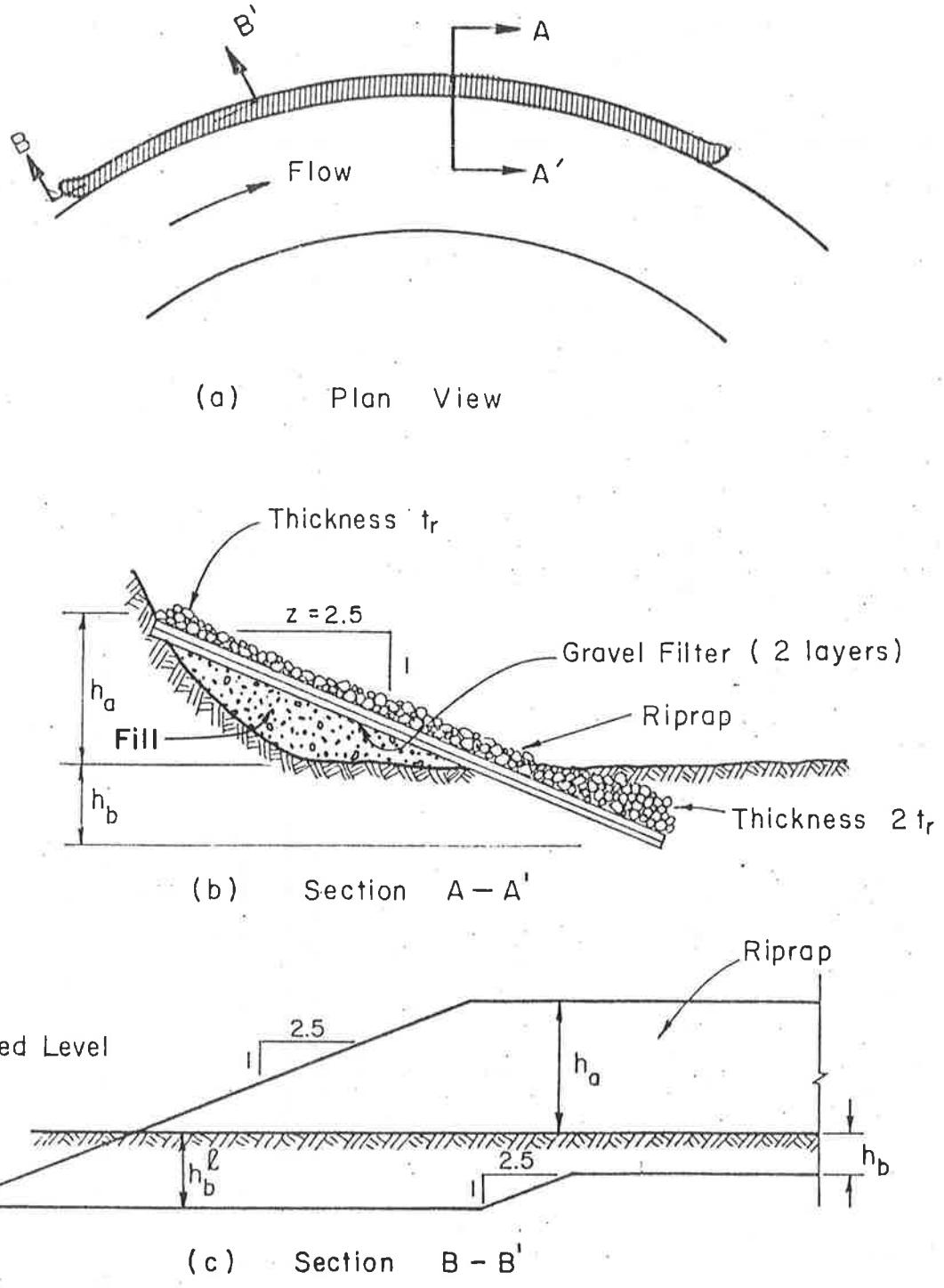

Figure 17.10 The sketch of proposed riprap design.

Riprap Design: The size of riprap is determined using the method proposed by Stevens et al., (1974). This is judged to be the most comprehensive and appropriate method to use. Also, the method developed by the Bureau of Reclamation (1958) to determine the maximum rock size in a riprap mixture is used for comparison. The flow conditions required for designing riprap sizes were discussed earlier and were given in Table 17.1.

Using a safety factor of 1.3 and an angle of repose of riprap material of 41° (from Simons (1957)), the required riprap sizes with a uniform gradation are determined. The results are shown in Table 17.3.

Generally, it is not economical or feasible to riprap a bank with uniform size rock, especially when large rock is required. Therefore, it is advisable to design a riprap mixture. That includes an adequate range of sizes. In addition, the safety factor for determining the D_{50} of rock riprap mixture can be lower than if uniform size rock is utilized. This is because there are stronger interlocking effects in the riprap mixture than for riprap of uniform size. In this study, the D_{50} of the riprap mixture is determined using the method proposed by Stevens et al., (1974) and by assuming the safety factor of 1.1. According to Richardson et al, (1975), riprap gradation should follow a smooth size distribution curve with gradation coefficient of about 13. If the size distribution is assumed to be lognormally distributed, this gradation coefficient establishes that the ratio of maximum size rock to medium size rock is about 2.2. The proposed riprap values are given in Table 17.3.

The Bureau of Reclamation (1958) developed a figure to determine the maximum rock size in a riprap mixture downstream from stilling basins. If the bottom velocity is assumed equal to the reference velocity on the top of the rock (see Stevens et al., (1974)), the maximum rock sizes in the riprap mixtures for different design conditions can be estimated. The results utilizing both methods are given in Table 17.3 for comparison. From Table 17.3 it is concluded that the riprap sizes established by the Stevens et al., (1974) method are adequate and are recommended.

The thickness of riprap should be sufficient to accommodate the largest rock in the riprap material. With a well-graded riprap with minimum voids, a thickness of the size of the maximum size stone should be adequate. In order to provide extra protection of the riprap against

Table 17.3 Design of riprap size.

Return Period (years)	Discharge (cfs)	Design Alternative	Uniform Size by Stevens et al.,(1974) (ft)	Riprap Mixture by Stevens et al.,(1974) Median Diameter (ft)	Riprap Mixture by Stevens et al.,(1974) Maximum Size (ft)	Maximum Size by USBR (1958) (ft)
50	51,600	1	2.6	1.5	3.3	2.6
		2	2.0	1.1	2.4	2.0
		3	1.8	1.0	2.2	1.8
100	62,000	1	3.0	1.7	3.7	3.1
		2	2.2	1.3	2.9	2.2
		3	2.0	1.2	2.6	2.0
200	72,500	1	3.4	2.0	4.4	3.5
		2	2.5	1.4	3.1	2.5
		3	2.2	1.3	2.9	2.3

local scour, the thickness of the riprap should be doubled for that part located below the existing bed level (see Figure 17.10).

Gravel Filter Design: Filters should be placed under the rock unless the material forming the core of the structure is coarse gravel or of such a mixture that it forms a natural filter. Two types of filters are commonly used: gravel filters and plastic filter clothes. Because the riprap sizes are quite large in the designs presented, gravel filters are recommended.

The sizes of gravel in the filter layer should meet the following two basic requirements: 1) stability requirement--fine enough to prevent the base material from entering, and 2) permeability requirement--much more permeable than the base material (see Winkley (1971)). Following the suggested specifications for gradation by Winkley (1971), the gravel filters were determined and are given in Table 17.2. Two layers of filter material are required because the riprap sizes are large.

Thickness of the filters may vary depending on the riprap thickness, but should not be less than six to nine inches. Filters that are one-half the thickness of the riprap are satisfactory and provide a great degree of safety.

Height and Depth of Riprap: The design height of riprap protection above the existing bed level (see Figure 17.10) must provide for freeboard, water depth, superelevation and wave height. The normal depth from the thalweg level and the superelevation were determined earlier. Because the forms of antidunes are a series of inphase symmetrical sand and water waves, the wave height at the water surface can be assumed equal to the antidune height. The minimum height required for riprap protection above the existing bed level can be determined by considering normal depth, superelevation, and antidune height. In order to provide additional protection against the breaking waves, an extra foot of freeboard is added to the required minimum height of riprap above bed level.

The riprap (see Figure 17.10) must extend some distance below thalweg level to provide safety against possible local scour, general degradation, and troughs of passing sand waves. The general degradation is assumed to be negligible because the proposed structures do not significantly contract the flow. Some local scour is expected at the leading portion of the riprap

revetment. Hence, a larger depth of riprap is required at this location. The minimum depth of riprap below thalweg level can be determined by considering the potential scour and the antidune height.

In general, the riprap should extend at least five feet below thalweg level in order to protect against possible long-term degradation of the river reach. If the computed depth of riprap protection below thalweg level is less than five feet, the design depth is set at five feet.

Additional Design Alternatives

Three additional design alternatives are proposed by modifying Alternative 1, 2, and 3. Data is of the fourth, fifth, and sixth alternatives which follow.

The Fourth Alternative: The fourth alternative is simply to provide sufficient buffer strip distance between the railroad and the existing river bank so that bank protection may not be required. The distances the north bank will migrate under different design flood conditions can be evaluated by utilizing sediment transport rates and the migration history of the 1965 flood. The estimated bank migration distances for the design floods are given in Table 17.4.

In order to provide extra protection against slope failures and long-term bank migration due to smaller sizes of floods, the design buffer strip distances should be at least twice the computed migration distances (factor of safety - 2.0) because the accumulated bank migration distance due to smaller sizes of floods can be very significant. The proposed buffer strip widths of the design floods are given in Table 17.4.

Table 17.4 Bank migration.

Return Period (years)	Discharge (cfs)	Bank Migration Distance (ft)	Design Buffer Strip Distance*(ft)
50	51,600	562	1124
100	62,000	629	1258
200	72,500	715	1430

*The eroded bank should be restored to its present alignment after each flood to maintain an adequate buffer zone.

The Fifth Alternative: The fifth alternative is to construct a series of rock riprapped spur dikes to guide the flow away from the existing north bank, (see Figure 17.9). The design of the spurs include: the form of spurs, the angle of spurs to the bank, the length of spurs, the spacing between spurs, the height or elevation of spurs, the construction materials, the crest width and slopes, and the local scour. The design of spurs is summarized in Tables 17.5, 17.6, and 17.7. Table 17.5 gives a summary of spur dike designs for different design floods including buffer strip distance, number of spurs, spacing of spurs, height of spur above the existing thalweg level, depth of spur at the spur nose below the existing thalweg level, riprap size at the spur nose, and riprap size in the spur shank. Table 17.6 provides the suggested design dimension of spurs including spur form, spur length, angle of spur to bank, the portion requiring riprap the same size as used on the nose, and length requiring shank protection. Table 17.7 summarizes the size of riprap and filter design at the nose of the spurs and for the spur shanks.

Figure 17.11 shows the suggested spur dike design. The methods of design are briefly described.

As shown in Figure 17.9, spurs No. 1 and 2 are T-head spurs, and the others are round-head spurs. The angle of spur to the bank is usually 60° to 120°. The available literature shows that the angle for T-head spurs is normally 90° but the angles for round spurs varies. Mamak (1964) states that the best results for deflecting flow and trapping sediment load are obtained with spurs inclined upstream for 100° to 110°. However, the study by Franco (1967) showed that for channelization, the normal or angled downstream spurs (60°) performed better than the angled upstream spurs. Judging from the purpose of spurs and flow conditions being considered, it is determined that the angles of round spurs should be constructed about 70° to the bank angled downstream as shown.

The length of a spur depends on its location, amount of contraction of stream width, and purpose of the spur. The purpose of the spurs considered in this study is to guide the flow away from the bank and to provide a flow alignment similar to that of 1965. The lengths of spurs are determined to serve this purpose. (see Figure 17.9 and Table 17.7)

The spacing between spurs is primarily related to the length of the spur. In general, the recommended spacing is from one and one-half to

Table 17.5 Summary of spur dike design.

T years	Q cfs	B_m ft	N_s	S_d ft	h_a ft	h_b^{ℓ} ft	K_{50}^n ft	K_{50}^s ft
50	51,600	1,250	7	600	12.5	10.0	1.1	0.6
100	62,000	1,250	7	600	13.5	11.0	1.3	0.7
200	72,500	1,250	7	600	14.5	12.0	1.4	0.7

Note: T is the flood return period in years, Q is the design discharge, B_m is the minimum buffer strip distance between the railroad and the spur nose, N_s is the number of spurs, S_d is the spur spacing, h_a is the design height of spur above the existing thalweg level, h_b^{ℓ} is the design depth of spur at the spur nose below the existing thalweg level, K_{50}^n is the median size of riprap at the spur nose, and K_{50}^s is the size of riprap for the spur shank.

Table 17.6 Dimensions of spur dikes.

Spur Number	Spur Form	Spur Length (ft)	T-Head Length (ft)	Angle of Spur to Bank	Length Requiring Nose Riprap Size (ft)	Length Requiring Shank Protection (ft)
1	T-head	200	400	90	20	180
2	T-head	200	400	90	20	180
3	Round head	500	N/A	70	200	300
4	Round head	750	N/A	70	200	550
5	Round head	750	N/A	70	200	550
6	Round head	400	N/A	70	200	200
7	Round head	200	N/A	70	200	0

Table 17.7 Size and filter design for riprap at spur noses and spur shanks.

(a) at spur noses

T years	Q cfs	K_{50} ft	G_K	t_r ft	f_{50}^1 mm	G_f^1	t_f^1	f_{50}^2	G_f^2	f_f^2 in.
50	51,600	1.1	1.3	2.4	6.0	3.0	8.0	60.0	2.0	7.0
100	62,000	1.3	1.3	2.9	6.0	3.0	9.0	60.0	2.0	9.0
200	72,500	1.4	1.3	3.1	6.0	3.0	10.0	60.0	2.0	9.0

(b) at spur shank

T year	Q cfs	K_{50} ft	G_K	t_r ft	f_{50}^1 mm	G_f^1	t_f^1	f_{50}^2	G_f^2	t_f^2 in.
50	51,600	0.6	1.3	1.3	6.0	3.0	6.0	20.0	2.0	6.0
100	62,000	0.7	1.3	1.5	6.0	3.0	6.0	20.0	2.0	6.0
200	72,500	0.7	1.3	1.5	6.0	3.0	6.0	20.0	2.0	6.0

Note: T is the return period, Q is the design discharge, K_{50} is the design riprap size for which 50 percent is finer by weight, G_K is the gradation coefficient of riprap, t_r is the thickness of riprap, f_{50}^1, G_f^1, and t_f^1 are respectively the gravel size for which 50 percent is finer by weight, the gradation coefficient and the thickness of the first layer of gravel filter, and f_{50}^2, G_f^2, and t_f^2 are respectively the gravel size for which 50 percent is finer by weight, the gradation coefficient, and the thickness of the second layer of gravel filter.

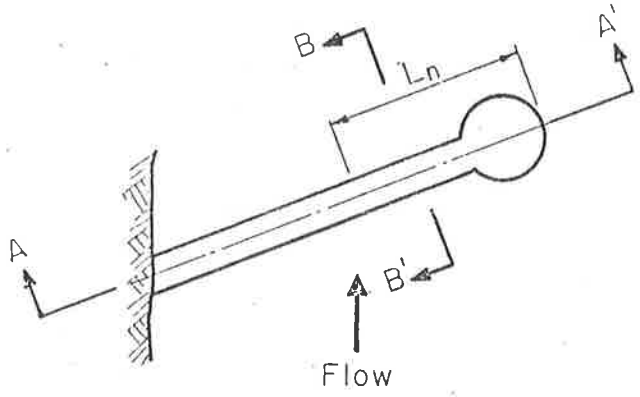

(a) Plan View

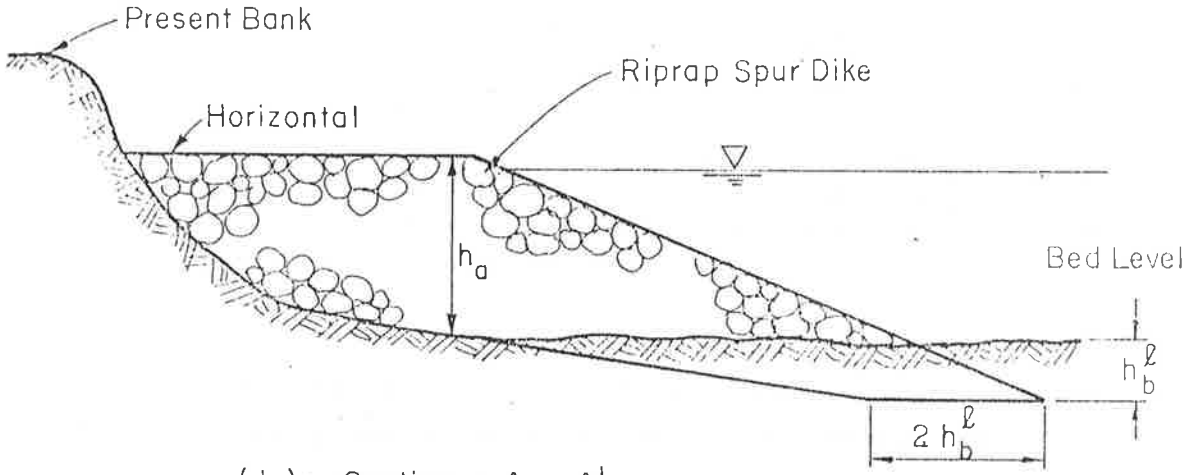

(b) Section A – A'

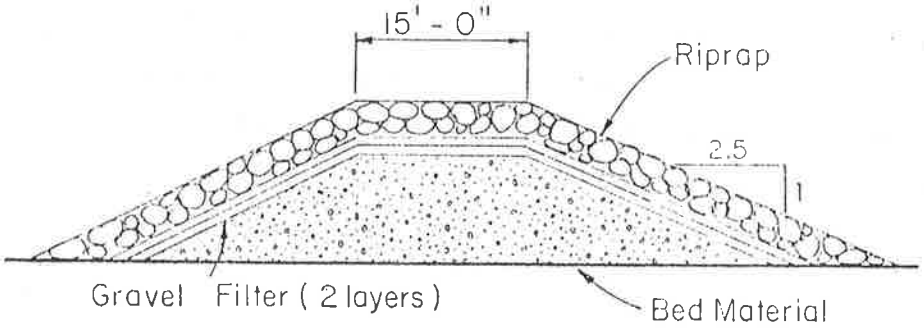

(c) Section B – B'

Figure 17.11 Sketch of spur dike design.

six times that of the upstream projected spur length into the flow. For bank protection in a sharp bend, a smaller spacing should be used. For the design conditions, the spacing of spurs is determined to be 600 ft.

The height or elevation of spur is determined by considering the maximum flow depth above thalweg level. In order to provide additional protection against the breaking waves, an extra foot of freeboard was added to the design height of each spur above the existing thalweg level.

The local scour depth at the spur nose is the same as that at the leading portion of the continuous riprap revetment. The computed local scour depths for different design floods are given in Table 17.2. The minimum depth of riprap below thalweg level is determined by considering the local scour depth and the antidune height, which also gives the design depth of spur at the spur nose below the existing thalweg level.

The construction materials are shown in Figure 17.11. The riprap design and the gravel filter design at spur nose are the same as those used in the continuous revetment (see Table 17.2 and 17.7). The length requiring nose riprap size can be estimated by considering the flow separation zone. The riprap size in the shank inside this zone may use a smaller rock size. A reduction of fifty percent in rock size is determined by considering the decrease in flow velocity. The riprap at the downstream side of shank may be eliminated if a larger risk is accepted. This is because the downstream side of shank is not expected to be subjected to a strong velocity. However, it may subject to scour due to overtopping.

The crest width of rock riprap spurs usually ranges from 3-20 ft. and the side slope from 1.25:1 to 5:1. Considering the convenienve in hauling and placing the rock ripraps, the crest width of spurs is determined to be 15 ft. The side slope was determined to 2.5:1.

The Sixth Alternative: This alternative is to replace the rock riprap with soil-cement riprap, design alternatives 1, 2, and 3. This alternative may be of interest because large rocks are ususally very difficult to obtain and soil-cement riprap can be manufactured at the site without too much difficulty.

The design procedure for soil-cement riprap is the same as those described earlier. Table 17.8 provides a summary of the riprap designs for different design floods.

Table 17.8 Soil-cement riprap design.

T years	Q cfs	A_ℓ	Z	K_{50} ft	G_K	t_r ft	f_{50}^1 mm	G_f^1	t_f^1 in.	f_{50}^2 mm	G_f^2	t_t^2 in.
		1	3.0	4.2	1.1	5.6	10.0	2.5	17	160.0	2.0	17
50	51,600	2	3.0	3.0	1.1	4.0	10.0	2.5	12	160.0	2.0	12
		3	3.0	2.8	1.1	3.7	10.0	2.5	11	160.0	2.0	11
		1	3.0	5.0	1.1	6.7	10.0	2.5	20	160.0	2.0	20
100	62,000	2	3.0	3.5	1.1	4.7	10.0	2.5	14	160.0	2.0	14
		3	3.0	3.2	1.1	4.3	10.0	2.5	13	160.0	2.0	13
		1	3.0	5.8	1.1	7.7	10.0	2.5	23	160.0	2.0	23
200	72,500	2	3.0	4.0	1.1	5.3	10.0	2.5	16	160.0	2.0	16
		3	3.0	3.7	1.1	4.9	10.0	2.5	15	160.0	2.0	15

Note: T is the return period in years, Q is the design discharge, A_ℓ is the alternative of designs, Z is the ratio of the horizontal distance to the vertical distance for the side slope of riprap bank, K_{50} is the design riprap size for which 50 percent is finer by weight, G_K is the gradation coefficient of riprap, t_r is the thickness of riprap, f_{50}^1, G_f^1, and t_f^1 are respectively the gravel size for which 50 percent is finer by weight, the gradation coefficient and the thickness of the first layer of gravel filter, and f_{50}^2, G_f^2 and t_f^2 are respectively the gravel size for which 50 percent is finer by weight, the gradation coefficient and the thickness of the second layer of gravel filter.

The comparison of Tables 17.2 and 17.9 shows that the required riprap sizes using soil-cement are much larger than those using rock. This is because the specific gravity of soil-cement (1.78) is smaller than that of rock (2.65), which makes the submerged weight of soil-cement only half that of the submerged weight of the rock. This alternative may not be practical because the size of soil-cement riprap is too large to handle. In addition, the soil-cement is subject to some weathering and erosion.

Summary and Recommendations

A hydrologic and hydraulic analysis of the Bijou Creek on the Narrows Unit near Fort Morgan, Colorado is presented. The analysis identifies the design floods with different return periods (50, 100, and 200 years) and three design alternatives of bank protection for each design flood condition.

The estimation of design floods utilizes the Gumbel Method of frequency analysis using all of available data. It is estimated that the design floods with return periods of 50, 100, and 200 years are respectively 51,000 cfs, 62,000 cfs, and 72,500 cfs.

The design of bank protection is determined considering design flood discharge, superelevation in the bend, antidune height, depth of flow above thalweg level, local scour, bed material size, and stability of riprap materials.

Considering the two extreme flood events that have occurred at the study site, it is recommended that the 200-year flood (72,500 cfs) should be adopted as the design flood. However, if a larger level of risk can be allowed, a smaller design flood can be used.

The six design alternatives to protect the river bank were evaluated. Without providing bank protection, the bank migration distances are on the order of 600 ft, which indicate that the proposed railroad will be in some danger for design conditions if bank protection is not provided.

The construction of spurs (the fifth alternative)is an acceptable method to protect the bank. However, a further economic analysis should be made before the selection of such an alternative.

To replace rock riprap with soil-cement riprap may not be practical because the sizes of soil-cement riprap may be too large to handle.

Table 17.9 Distribution of water in percent of flow in the Wadi Mawr.

MONTH	LOCATION			
	Structure NO. 1		Structure NO. 2	
	North	South	North	South
January	28	50	0	0
February	28	50	0	0
March	28	50	0	0
April	17	18	25	40
May	17	18	25	40
June	17	18	25	40
July	17	18	25	40
August	17	18	25	40
September	17	18	25	40
October	17	18	25	40
November	22	31	15	23
December	28	50	0	0

In order to save some costs on earth work, the continuous riprap revetment in the second and third alternatives may be changed into a continuous riprap dike without filling the current channel bend behind the dike line. This constitutes a seventh possible alternative.

Different design alternatives result in different design dimensions, different levels of risk, and different costs of construction. The selection from design alternatives should be made considering the level of risk, the cost of construction, and the availability of construction material.

17.3 CANAL DESIGN PROBLEM - WADI MAWR, YEMEN REPUBLIC

General

Presented in this section are the designs of longitudinal slopes and the cross sections of four canals of the Wadi Mawr Canal System, Yemen Arab Republic. The four canals considered are the North Supply Canal No. 1 and the South Supply Canal No. 1 which takes off from Diversion Structure No. 1 and the North Supply Canal No. 2 and the South Supply Canal No. 2 which takes off from Diversion Structure No. 2 (see Figure 17.12).

Diversion Structure No. 1 would be located across the Wadi Mawr near Nahal Rashid. This is approximately 11.3 km downstream from the Wadi Mawr gage. A north supply canal having a length of 14.6 km and a south canal having a length of 11.2 km would command the existing canals and serve a total area of approximately 8,400 hectares. Diversion Structure No. 2 would be located near Al Lejam approximately 25.1 km downstream from the Wadi Mawr gage. A north supply canal having a length of 10.3 km and a south supply canal having a length of 13.0 km would command the existing canals. The total area served by Diversion Structure No. 2 is approximately 5,500 hectares. The distribution of water is dependent on the month of the year and the amount of water in the Wadi Mawr.

In this analysis, sediment routing and bank stability evaluations only relate to the head reach of each canal for the preliminary design.

Flow Distribution Analysis

The flood waters of the Wadi Mawr fluctuate significantly. The four canals considered in this study will divert approximately 78 percent to 100 percent of the water in the Wadi Mawr most of the

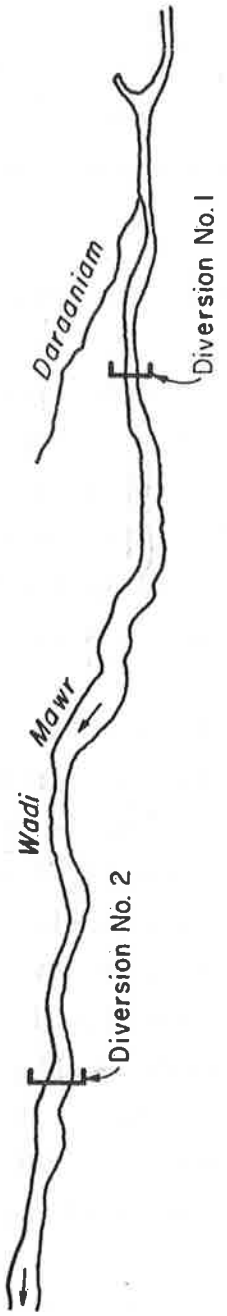

Figure 17.12 Location of diversion structures and canals.

time except during very large flood events. During periods of large flow, some of the excess water will pass Structure No. 2. It is known that the canals will not operate at their design capacities, except for very short intermittent periods. The unsteady water supply to the canals introduces a new type of canal design problem. In order to account for the unsteadiness of the water supply in the canal design, it is necessary to route the sediment through the canal system in real time. Because of lack of long-term records, a typical annual hydrograph is used. The 1977 daily flow hydrograph is selected because it is considered to be a typical annual hydrograph. The available daily flow record in 1977 ends November 5, 1977.

The distribution of water into the four canals was made according to the percentages for the particular months of the year as specified in Table 17.9. As indicated in this table, the summation of percentages for the months of January, February, March, November and December are not equal to 100 percent. The remaining water would divert to the Daraanish Canal.

The amount of water that would be diverted into a specific canal is not only dependent on the distribution shown in Table 17.9, but it is also a function of canal capacity. The discharge in a canal for a particular time period is the smaller of the following two quantities: a) the rate that would be distributed according to Table 17.9 prorated from the discharge in the Wadi Mawr and b) the canal capacity. Based on the above mentioned regulation rules, the water that would be diverted to each canal using the 1977 annual hydrograph is given in Figures 17.13 to 17.17.

Initial Designs by Tipton and Kalmbach, Inc.

The initial designs of the four canals considered in this study were provided by Tipton and Kalmbach, Inc. The initial design of the head reach for each canal is summarized in Table 17.10. The typical cross-sectional shape of the canals is trapezoidal with side slopes of 1.5:1 (horizontal to vertical).

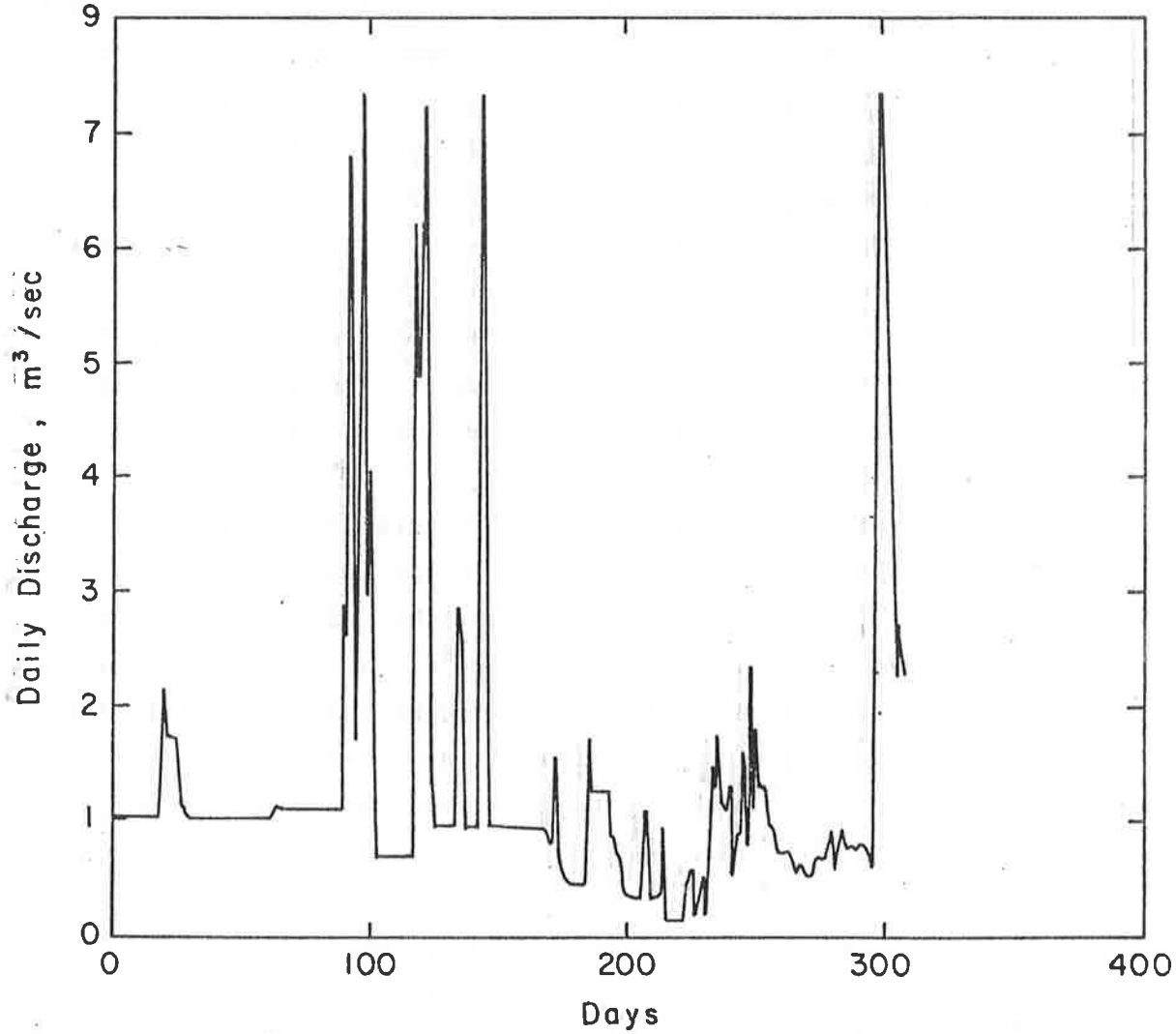

Figure 17.13 Discharge of canal 1N.

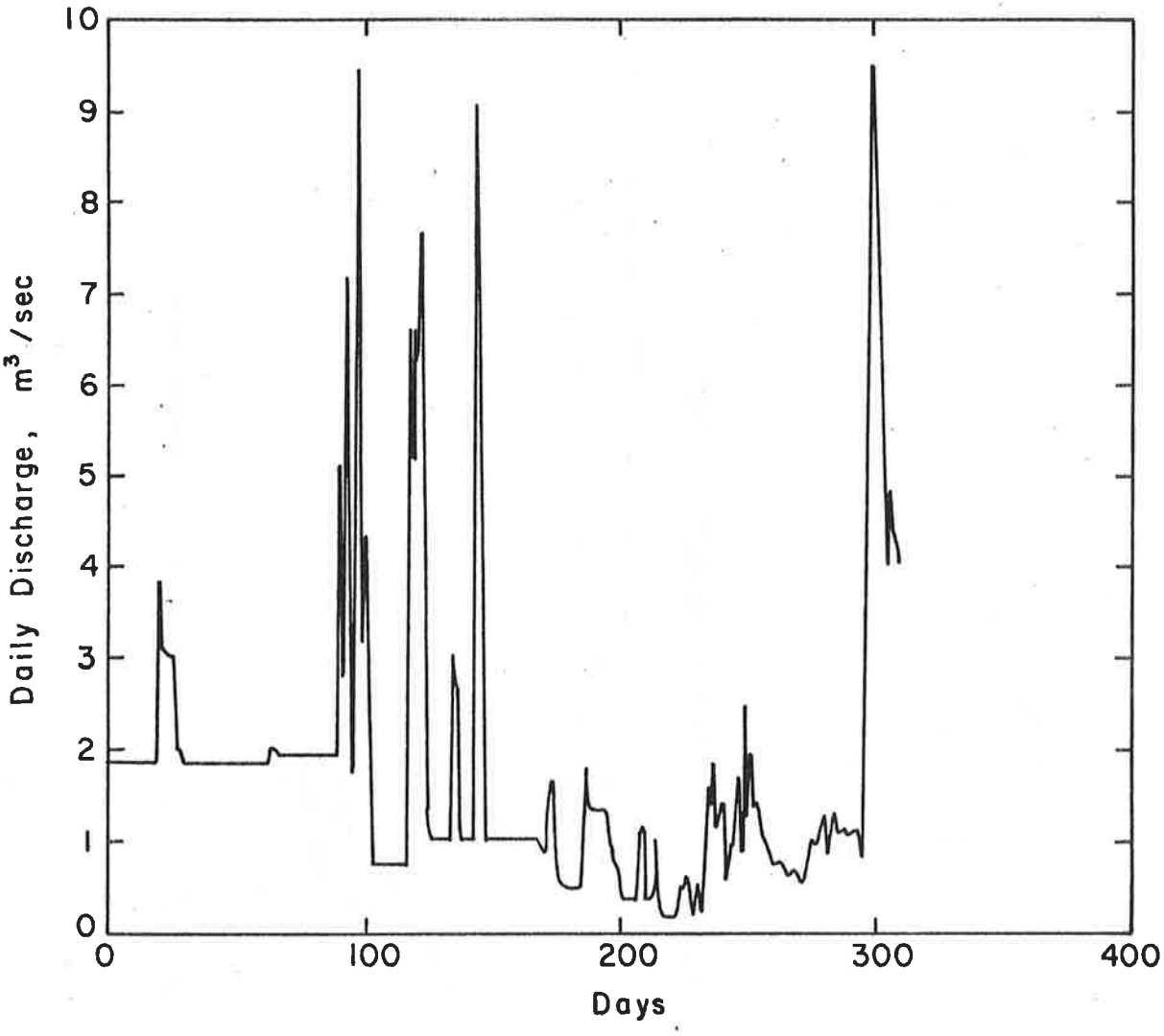

Figure 17.14 Discharge of canal 1S.

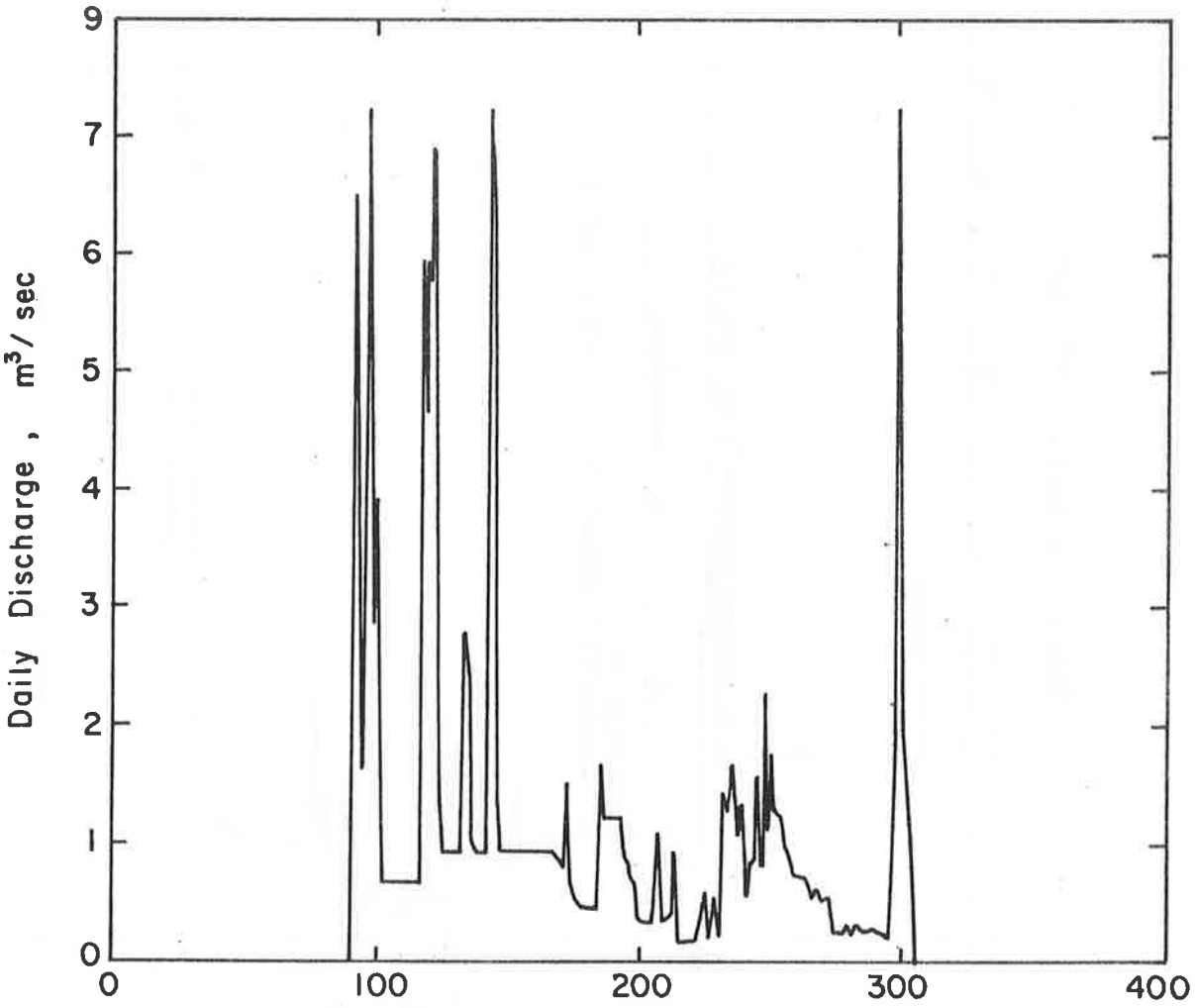

Figure 17.15 Discharge of canal 2N.

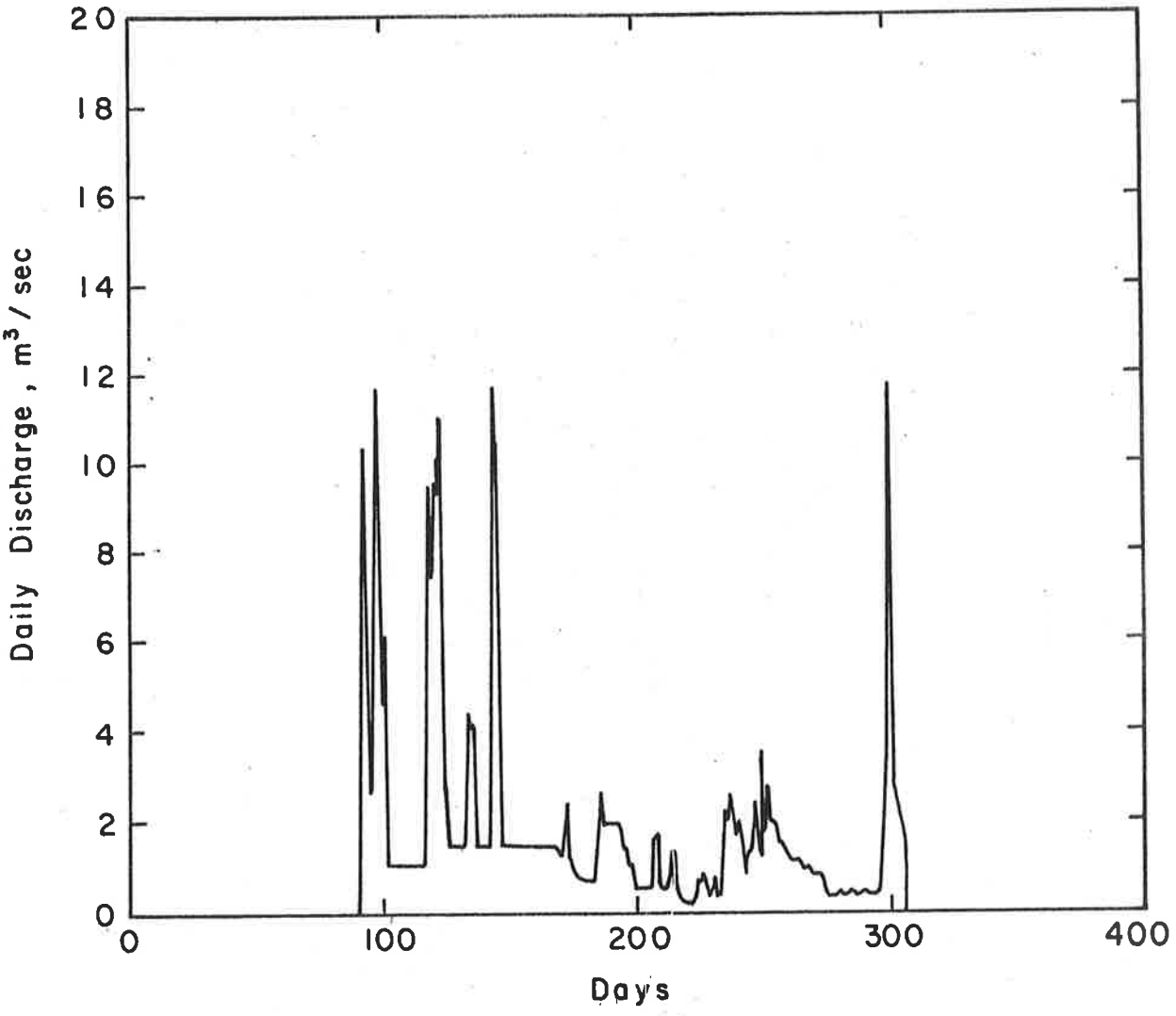

Figure 17.16 Discharge of canal 2S.

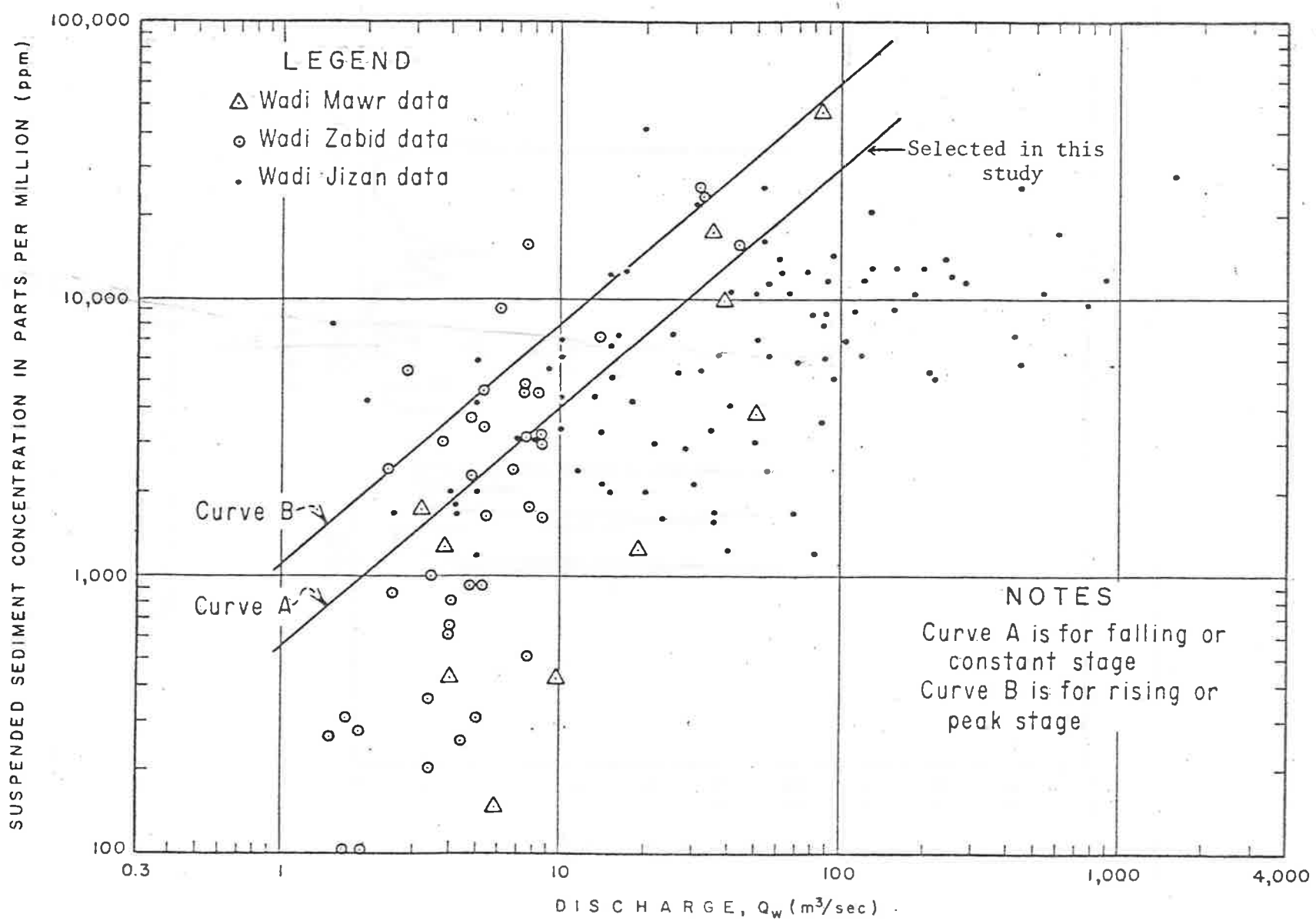

Figure 17.17 Available suspended sediment concentration data for the general study area.

Table 17.10 Initial design dimensions of canal head reaches by Tipton and Kalmback, Inc.

Canal	Design Capacity (m^3/sec)	Bottom Width (m)	Side Slope horizontal :vertical	Bed Slope	Manning's Roughness Coefficient
1-N	7.34	4.70	1.5:1	0.0007	0.02
1-S	9.47	5.50	1.5:1	0.0006	0.02
2-N	7.25	4.80	1.5:1	0.0007	0.02
2-S	11.69	6.00	1.5:1	0.0005	0.02

The Manning's coefficient was estimated by Tipton and Kalmback, Inc. based on experience with existing canals. This value was used in the design of the Wadi Zabid Canal System (see Simons and Li, 1977).

Sediment Transport Rates

Suspended Load. The sediment transport rates are very important for estimating the erosional and/or depositional potential of canals. The following describes the development of a sediment rating relation useful for estimating the transporting capacity of the canal system in the Wadi Mawr.

Sediment samples from the Wadi Mawr were obtained at the gaging station at Shat Al Erge. During high discharge conditions, the samples were obtained from the cableway across the river. During low discharge periods, the Wadi was waded to obtain samples. Suspended sediment samples were taken with a U.S. Federal Inter-Agency DH-59 sampler, and with a series of single-stage samples collected at the gaging station. Also, the sediment data from Wadi Zabid and Wadi Jigan were used to establish general relations (Sabol, 1977). The measured suspended sediment concentration and adopted suspended sediment rating curve of the Wadi Mawr used in this study is described as follows;

$$Q_{ss} = 1.98\ Q_w^{1.85} \qquad (17\text{-}10)$$

where Q_{ss} is the suspended sediment load in metric tons per hour and Q_w is the water discharge in m^3/sec.

Bed Load. The bed of Wadi Mawr above the gaging station is predominantly composed of gravel and coarse sand. The majority of bed material load will be transported by rolling and sliding in contact with the river bed. Only a small portion of the bed material will be transported in suspension. Only a small portion of the bed material will not be sampled by the DH-59 suspended sediment sampler used in the Wadi Mawr. Hence, an estimation of the bed load is necessary to provide an adequate analysis. Sabol (1977) selected the Meyer-Peter, Müller equation (see Simons and Sentürk, 1977) to estimate the bed load for this study. A recent model study of steep channel sediment transport rates with gravel bed material conducted at Colorado State University indicates that the Meyer-Peter, Müller equation is applicable for this condition. The Meyer-Peter, Müller equation is based on the water discharge, the hydraulic geometry, width and depth of flow, the bed slope, channel roughness, and the size distribution of the bed material. The size distribution was determined from sieve analysis of samples from Wadi Zabid and from visual and photographic surveys of samples from Wadi Zabid and from visual and photographic surveys of the Wadi Mawr Channel (Sabol, 1977).

Measured hydraulic data show that the top width varies with discharge for discharges less than 50 m^3/sec. Utilizing the measured hydraulic data and the Meyer-Peter,Müller equation. The following bed load

$$Q_{sb} = 9.01\ Q_w^{0.8} \quad \text{for} \quad Q_w \leq 50\ m^3/sec \tag{17-11}$$

and

$$Q_{sb} = 5.2\ Q_w \quad \text{for} \quad Q_w > 50\ m^3/sec \tag{17-12}$$

Equation 17-12 were recommended by Sabol (1977).

Total Sediment Load. The total sediment load is the sum of suspended and bed loads. Thus, the total sediment transport rate in the Wadi Mawr can be expressed as

$$Q_s = 1.98\ Q_w^{1.85} + 9.01\ Q_w^{0.8} \quad \text{for} \quad Q_w \leq 50\ m^3/sec \tag{17-13}$$

and

$$Q_s = 1.98\ Q_w^{1.85} + 5.2\ Q_w \quad \text{for} \quad Q_w > 750\ m^3/sec \tag{17-14}$$

Equations 17-13 and 17-14 relate sediment transport rates to the discharge in the Wadi Mawr and cannot be directly used for canal design due to being insensitive to the design parameters such as bed slope and cross-sectional shape. A change in bed slope and cross-sectional shape would result in changes in velocity and top width. According to Simons and Sentürk (1977), a common sediment rating relation can be made by correlating the unit width sediment transport rate with velocity. This relation was adopted in this study. Utilizing the available data, the resultant sediment transport equation for the Wadi Mawr system follows (see Figure 17.18):

$$q_s = 9.36\ V^{2.83} \qquad (17\text{-}15)$$

where q_s is the sediment transport rate per unit width of channel in metric tons/hr/m and V is the average velocity in m/sec.

As a check on Equation 17-15 the computed results utilizing Equation 17-15 were compared with those determined by Equations 17-13 and 17-14. The check is satisfactory (see Figure 17.19). Hence, Equation 17-15 is used for canal design.

Sediment Discharge into Canals. The sediment inflow rate for each canal is dependent on the discharge rate, the sediment concentration in the Wadi Mawr, and the elevation of the intake. For simplicity, it is assumed that 70 percent of the concentration of sediment in the Wadi Mawr will enter the canal. With known water discharge, the sediment inflow rates for the four canals and the 1977 daily hydrograph can be estimated.

Evaluation of Canal Design

The canals should be designed either to transport the sediment through the canal or to have stable banks and bed for the design discharge. If the primary objective is to transport the sediment inflow through the canals, the slope of energy gradient must be fairly steep and the banks would erode unless stabilized. Conversely, if the primary objective of the design is to have both stable banks and bed, the design bed slope must be flatter. This would greatly reduce the capability of the canal to transport a significant bed material load. This design alternative would be attractive if the sediment concentration in the canal was relatively small.

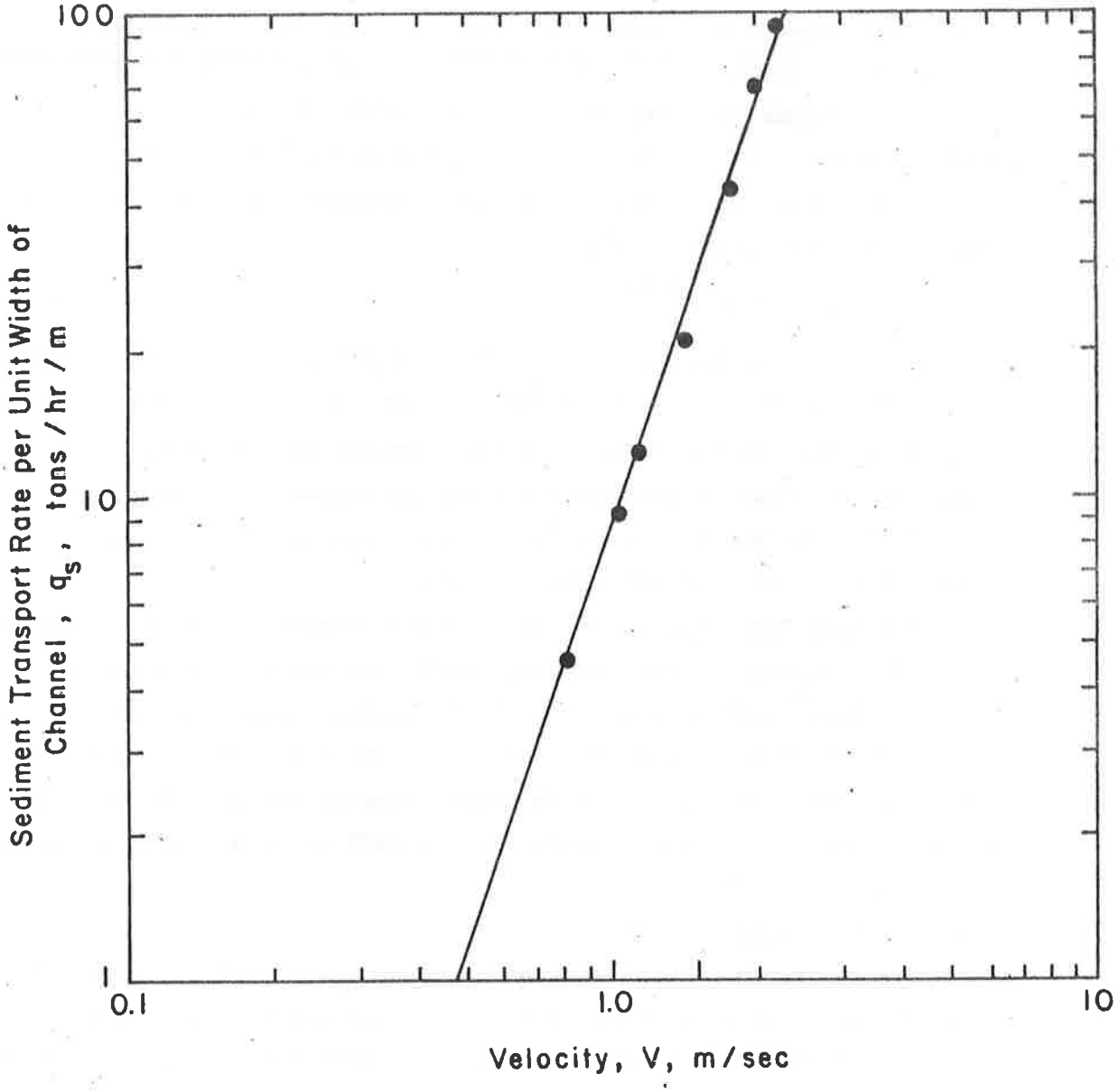

Figure 17.18 Sediment transport capacity.

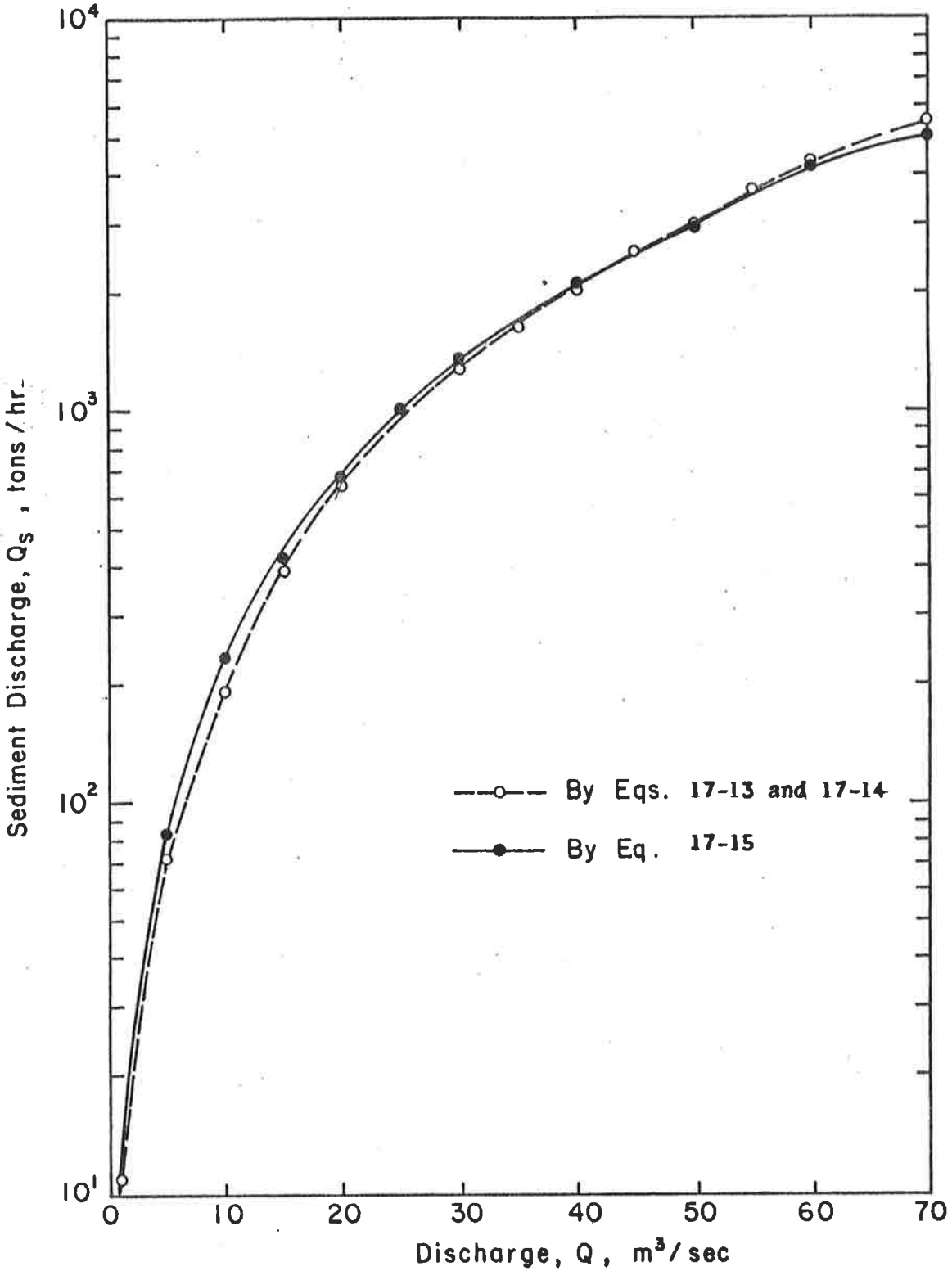

Figure 17.19 Validation of the sediment transport capacity.

As mentioned earlier, the water and sediment inflows to the canal fluctuate greatly with time. Conventional canal design methods using the design discharge only are not valid, especially if the primary objective is to transport the sediment load introduced at the head works through the canal. This section describes canal design considering the different alternatives. The design parameters such as cross section, design discharge, longitudinal slope and side slope were given in Table 17.10.

Canal Design Considering Sediment Transport. If the primary concern is to design a bed slope steep enough to transport the sediment inflow, the design slopes for different discharges (with the corresponding sediment inflows) can be determined using Manning's equation and the sediment transport equation. Since the inflow of water to the canals is highly variable, the conventional method considering only the design discharge is not valid. Hence, a new method of design that accounts for the variation of inflows and the long term sediment degradation and aggradation cycle is developed and utilized. This method is derived using Manning's equation, the sediment transport equation, the continuity equation for sediment and the typical annual hydrograph. The design bed slope which would minimize the net degradation and aggradation of the channel bed is determined by solving the following minimization problem,

$$\underset{S}{\text{Min}} \sum_{i=1}^{N} (C_i - I_i) \qquad (17\text{-}16)$$

where N is the number of days of a typical hydrograph, C_i is the canal sediment transport capacity during the ith day, I_i is the sediment inflow rate during the ith day, and S is the bed slope. A computer program was developed to solve the above problem. The optimum bed slopes of flow and velocity at the design discharges are given in Table 17.11.

It is important to point out that the above design would minimize the net degradation and aggradation on an annual basis but would not eliminate canal maintenance. It is expected that some aggradation of coarser particles in the head reach and at the intake would tend to plug the system and increase the bed slope locally near the head works requiring maintenance dredging. The prediction of the local response of the canal in the head reach could be made by conducting a more

Table 17.11 Hydraulic design conditions of optimum bed slopes considering sediment transport.

Canal	Design Discharge (m^3/sec)	Optimum Bed Slope	Flow Depth (m)	Mean Velocity (m/sec)
IN	7.34	0.00108	0.868	1.314
IS	9.47	0.000997	0.955	1.338
2N	11.69	0.000984	0.877	1.262
2S	7.34	0.000943	1.046	1.382

detailed analysis involving routing sediment through the canals by size fractions.

Also, Table 17.11 indicates that high velocities are expected for these design conditions. Undoubtedly, the banks would be fairly unstable if no stabilization measures are used. The banks of both canals would be stable if they were protected by armoring them with particles having a size of 5.0 mm or larger. This size of bank protection material was determined using the method recommended by E. W. Lane and the U.S. Bureau of Reclamation (see Simons and Sentürk, 1977).

The comparison of Table 17.11 with Table 17.10 indicates that the longitudinal bed slopes for the initial designs by Tipton and Kalmbach are smaller than those determined by Equation 17-16 but results are sufficiently close.

Canal Design Considering Bank Stability Without Treatment. The bank stability is dependent on the size of armor material that would develop as a natural consequence of erosion on the banks. Judging from the parent soil condition (mostly clay and silt) and the transported material in the Wadi, it is very conservative to assume an armor size of at least 1.0 mm. However, in reality an armor size of 5 mm could be developed on the banks considering the characteristics of the transported material. The armor size is often assumed to be the d_{75} (75% finer by weight) of the bank material.

Considering canal bank stability, it is desirable to use the design discharge because it is the largest and most erosive discharge that would flow in the system. Applying the same method recommended by E. W. Lane and the U.S. Bureau of Reclamation (Simons and Sentürk,

1977), and Manning's equation, the appropriate bed slopes that would assure stable banks for design capacities and armor sizes are determined. Table 17.12 shows the hydraulic design conditions considering bank stability, bed slope, and armor size.

According to Table 17.12 the initial design developed by Tipton and Kalmback, Inc., as indicated in Table 17.10, is equivalent to the case assuming that the armor size of bank material is between 1.0 mm and 5.0 mm for all of the canals. This assumption is reasonable. As mentioned earlier, the flat bed slopes required to assure bank stability would induce a large amount of deposition because of low sediment transport capacity.

Table 17.12 Bed slopes considering bank stability with various armor sizes.

Canal	Bed Slopes for Various Armor Sizes			
	0.5 mm	1.0 mm	5.0 mm	70.0 mm
IN	0.0003	0.00035	0.0014	0.0074
1S	0.00027	0.00031	0.0013	0.0068
2N	0.00027	0.00031	0.0014	0.0076
2S	0.00024	0.00028	0.0012	0.0061

Evaluation of the Initial Design by Tipton and Kalmbach, Inc.

Comparison of the initial design presented in Table 17.10 with the design considering sediment transport (Table 17.11) and with the design considering bank stability (Table 17.12), it is concluded that the initial design by Tipton and Kalmback, Inc. is feasible if maintenance work is conducted. It was determined in this study that the designs would induce an annual deposition of 43,000 m^3 of sediment in the North Supply Canal No. 1, 30,100 m^3 in the South Supply Canal No. 1, 36,100 m^3 in the North Supply Canal No. 2, and 13,200 m^3 in the South Supply Canal No. 2. The above estimations were made assuming a sediment bulk rate of 1.5. This analysis does not account for the adjustment of bed gradient during the depositional process. The actual volumes of deposited sediment would be somewhat less than the above estimated values.

Nevertheless, the estimated deposition volume is large enough to indicate the difficulty of maintaining the canals. Such a design approach is feasible only if sediment excluders, ejectors and/or sediment traps are utilized to remove excess sediments at the diversion works or in the head reaches of the canals. If sediment traps are employed, the design volumes should be approximately 28,000 m^3 for the North Supply Canal No. 1, 20,000 m^3 for the South Supply Canal No. 1, 24,000 m^3 for the North Supply Canal No. 2, and 8,800 m^3 for the South Supply Canal No. 2.

In order to estimate the size of material that would most likely deposit in the head reach an estimation of the maximum particle size that would be in motion for the design capacity is made. Table 17.13 shows the results.

Table 17.13 Incipient motion of particle sizes.

Canal	Design Discharge (m^3/sec)	Maximum Particle Size (mm)
1-N	7.34	9.4
1-S	9.47	9.1
2-N	7.25	9.3
2-S	11.69	8.6

The quantities indicated in Table 17.13 were estimated by Shield's criteria of incipient motion (Simons and Sentürk, 1977). The particular sizes of sediment that would enter the North Supply Canal No. 1 and the South Supply Canal No. 1, would be much coarser than those diverting to the North Supply Canal No. 2 and the South Supply Canal No. 2. Hence, the deposition problem is more serious for the canals that divert from Structure No. 1. In addition, because the assumed armor size of about 3.00 mm is not a certainty, it is suggested that the head reach should be armored. An armor size of about 10 mm or larger should be considered.

The bed slopes of the initial design are flatter than those determined considering sediment transport (Table 17.11) and those designed assuming a 5.0 mm armor size (Table 17.12), but are steeper than those designed so that the banks would be stable if protected with 1.0 mm armor material. The initial design is feasible if the prescribed maintenance measures are implemented. The longitudinal slope would be gradually increased due to deposition and the bank stability would be enhanced by growth of grass and development of a layer of armor particle on the bank. Thus, the initial design by Tipton and Kalmback, Inc. (Table 17.10) is an adequate design.

Summary and Conclusions

In this example an initial design of Wadi Mawr Canal System by Tipton and Kalmbach, Inc. was evaluated. Also, other design alternatives were considered. Two primary design objectives were analyzed for a range of flows. One objective was to design a system capable of transporting sediment to minimize the net degradation and aggradation. In this system, stabilization of the banks is required. The other objective was to design canals that would not require bank stabilization. This design would require considerable maintenance work to remove excess sediment that would deposit in the canals. Considering the optimum canal design it is advisable to select an alternative that would minimize changes in the present design and minimize future maintenance. Because the bank material is predominantly formed of silt and clay, the banks would be highly unstable if a steep slope without bank stabilization was used. Riprapping the banks for the entire channel system is probably not economically feasible. Thus, an important consideration is the stability of the canals. The initial design by Tipton and Kalmbach, Inc. is feasible considering both the sediment transport and the bank stability. However, sediment traps are required to remove excessive sediment in the head reaches of the canals. The design volumes of these traps should be approximately 28,000 m^3 for the North Supply Canal No. 1, 20,000 m^3 for the South Supply Canal No. 1, 20,000 m^3 for the South Supply Canal No. 1, 24,000 m^3 for the North Supply Canal No. 2 and 8,800 m^3 for the South Supply Canal No. 2. Because the assumed armor size of 1.00 mm to 5.00 mm is not a certainty,

it is strongly suggested that riprapping the head reach, using an armor size of about 10 mm or larger should be considered. This size of material can be easily obtained from the Wadi bed since the canal head reaches parallel the Wadi for some distance downstream of the diversions.

The problems encountered in the Wadi Mawr Canal system are unique in many aspects compared to usual canal design problems. The unsteady input of water and sediment to the canals, the high sediment load of the Wadi and the heterogeneous distribution of bed and transported material all contribute to the difficulty of canal design. It is highly recommended that a comprehensive system analysis capable of routing water and sediment by size fraction through the Wadi and the entire canal system be made to improve knowledge of the response of the system, considering both short and long term time periods.

17.4 FLOOD CHANNEL DESIGN - BOULDER CREEK, COLORADO

General

The city of Boulder is located at the mouth of Boulder Canyon which concentrates and discharges flow from a 130 square mile drainage basin. This makes Boulder, Colorado particularly vulnerable to flash flooding. The Corps of Engineers has been working with the citizens of Boulder to develop a flood protection measure. Three alternative plans have been developed and initially evaluated. The plan involving excavated floodway and physical improvements along Boulder Creek, has been tentatively selected as the most viable design. This plan includes an excavated floodway from 6th Street downstream to 17th Street, to reduce damages for the 100-year and lesser floods. Boulder Creek is a relatively stable alluvial stream during low flow periods due to an armor layer of large particles that protect the river bed. For an extreme event such as a 100-year flood, most of the armor layer would be ruptured and the sediment supply at the canyon mouth would be large. Sediment movement will significantly alter the channel geometries by the processes of erosion and sedimentation. A realistic flood analysis must consider the channel as a movable bed system when considering an extreme event. The assessment of sediment and debris impacts on the proposed plan is certainly of vital importance for evaluating the response of channel and adequacy of the designs.

This section summarizes the principle findings and recommendations resulting from a two-phase study of the erosion, sedimentation, and

debris analysis of Boulder Creek Floodway associated with the 100-year flood. The Phase I study analyzed the problems from 6th Street downstream to 17th Street associated with the Plan II design (excavated floodway) and the 100-year flood. The Phase II study dealt with the current channel without further modification (do-nothing plan). The analysis is different from the conventional HEC-2 analysis (1976). It recognizes that the channel bed is movable and adjustable responding to scour and deposition. The analysis considers both aggradation and degradation of the channel and provides the necessary information to: 1) evaluate the potential for blockage at bridges and channel restrictions resulting from aggradation, 2) determine the potential local scour downstream of structures, 3) determine possible flow diversions, and, 4) estimate the effect of sediment aggradation on the water surface profile. In addition to the erosion and sedimentation analysis, potential problems associated with vegetative debris were studied, particularly in relation to possible blocking of the channel at bridges.

The proposed excavated floodway (Plan II) will provide significant flood protection for the City of Boulder and will not increase potential problems associated with sediment and vegetative debris. These conclusions were drawn from a thorough comparison of the responses of the "do-nothing plan" and the proposed floodway plan. However, the proposed floodway plan will not totally eliminate the potential sediment problem and the debris problems are significant.

Watershed and River

Watershed

Boulder Creek is a steep mountain stream draining a portion of the eastern slope of the Rocky Mountains in Boulder County, Colorado. The creek extends 22 miles eastward from the Continental Divide to the mouth of the Canyon at Boulder. The watershed above the mouth of Boulder Creek concentrates and discharges the flow from a 130 square-mile drainage basin. Barker Reservoir, located about 12 miles upstream from Boulder, provides only incidental flood storage, and the effects of this structure on downstream peak flows diminishes rapidly with distance from the dam. The basin map is shown in Figure 17.20. The upstream watershed is steep and forested, and there is high potential for the production of sediment and vegetative debris.

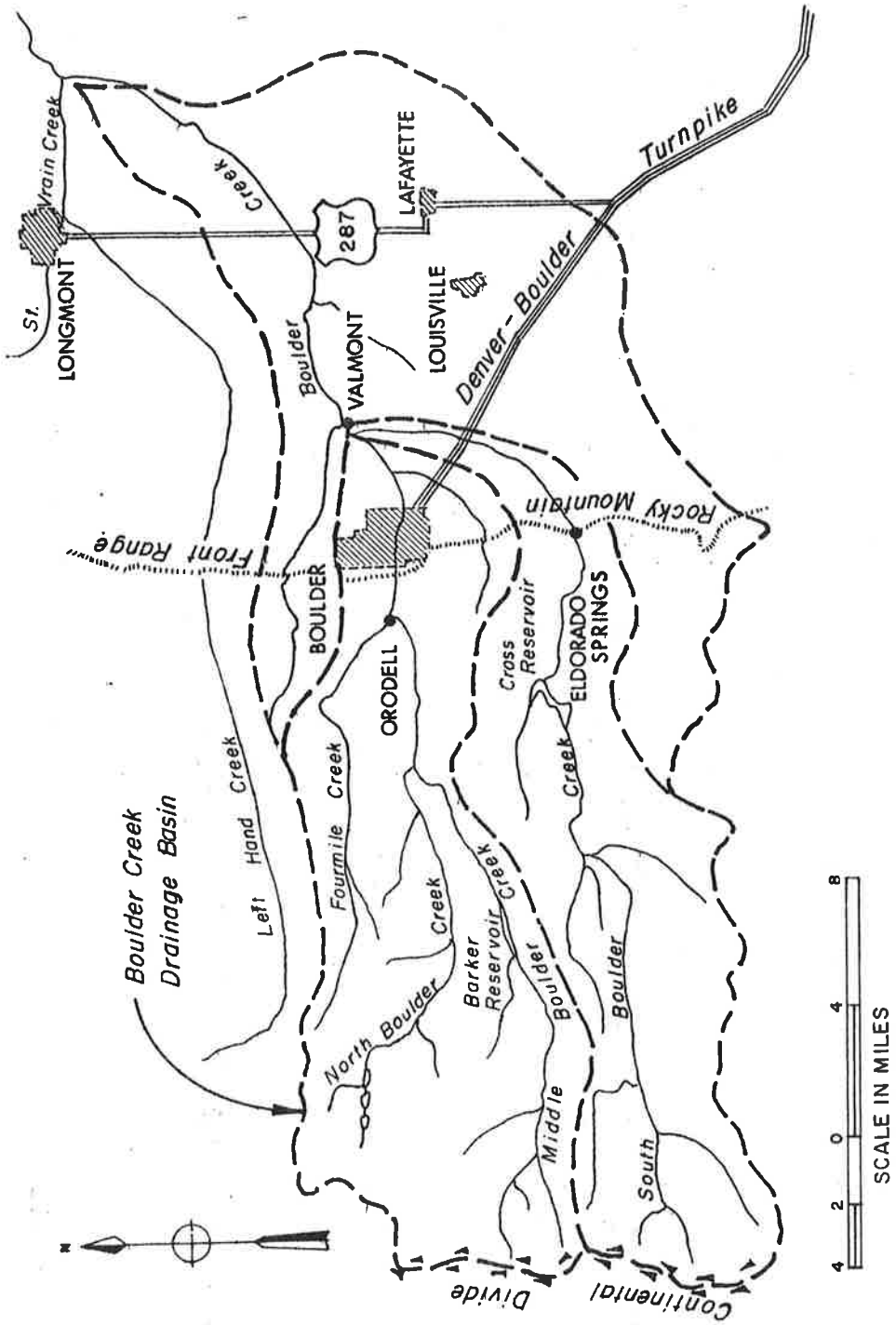

Figure 17.20 Basin map.

Hydrology

The steep stream gradient and the large drainage area above the city makes Boulder particularly vulnerable to flash flooding. Stream gaging stations have been maintained on Boulder Creek near Ordell, Colorado since 1906, and on South Boulder Creek near Eldorado Springs since 1888, with only minor interuptions in the record. In addition to these two stations, there is a short record (1889-1909) available from a former gaging station located in Boulder. Peak discharge estimates are available at this site for the historic major floods of 1894, 1914 and 1969. This fragmentary gaging record for Boulder Creek at Boulder was considered too short to be reliable for estimating the flood frequency. Three methods were utilized in the "Water and Related Land Resources Management Study" (1977) to estimate the flood frequency. These methods include: (1) Environmental Protection Agency Storm Water Management Model, (2) Regional criteria presented in Technical Manual No. 1, a manual for estimating flood characteristics of natural streams in Colorado, prepared by the U.S. Geological Survey for the Colorado Water Conservation Board, and (3) Determination from estimated values for the 1894, 1914 and 1909 events. The discharge-probability curves determined by these three methods are shown in Figure 17.21 for comparison. In addition, the 100-year hydrographs at the west edge of Boulder (drainage above the mouth of the canyon) are given in Figure 17.22.

Channel Geometry

The index maps showing the location of cross sections and reaches are for both the proposed floodway and the do-nothing condition as given in Figures 17.23 and 17.24. The channel gradient is about 0.015 and is fairly steep. Detailed cross-sectional data are available and utilized. The number of intervals in a cross section is often more than 50. This makes the sedimentation analysis very difficult. To define reaches is therefore necessary for determining erosion and deposition. Nine reaches are defined for both the proposed and the do-nothing condition. In the proposed floodway, reaches No. 6 and No. 8 will have man-made sediment deposition areas.

Bed Material Size Distribution

Bed material samples have been taken at three sites. Approximate sampling locations were given in Figures 17.23 and 17.24. Fifteen samples from both surface and subsurface layers were analyzed. Ten

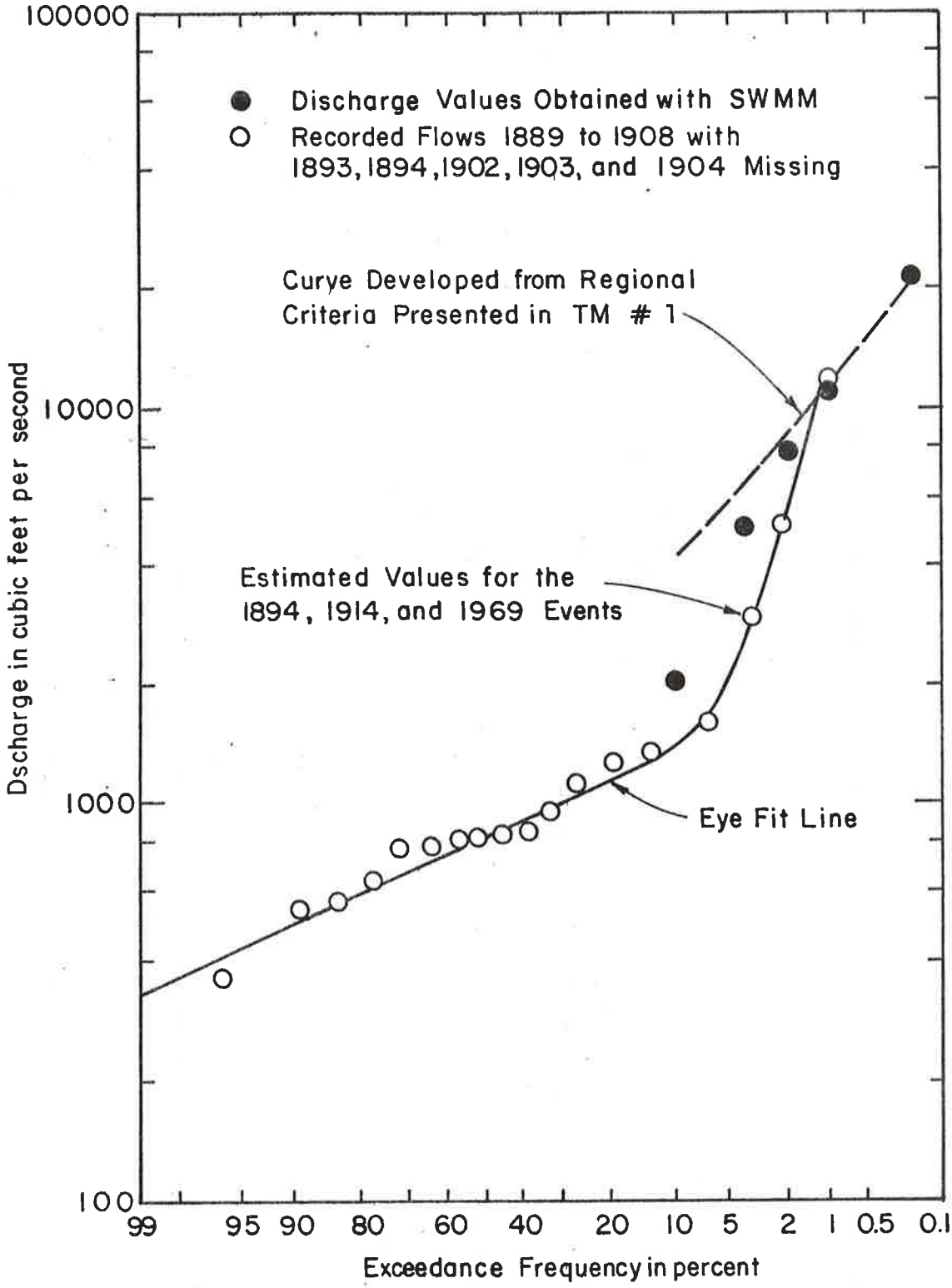

Figure 17.21 Discharge-probability curves.

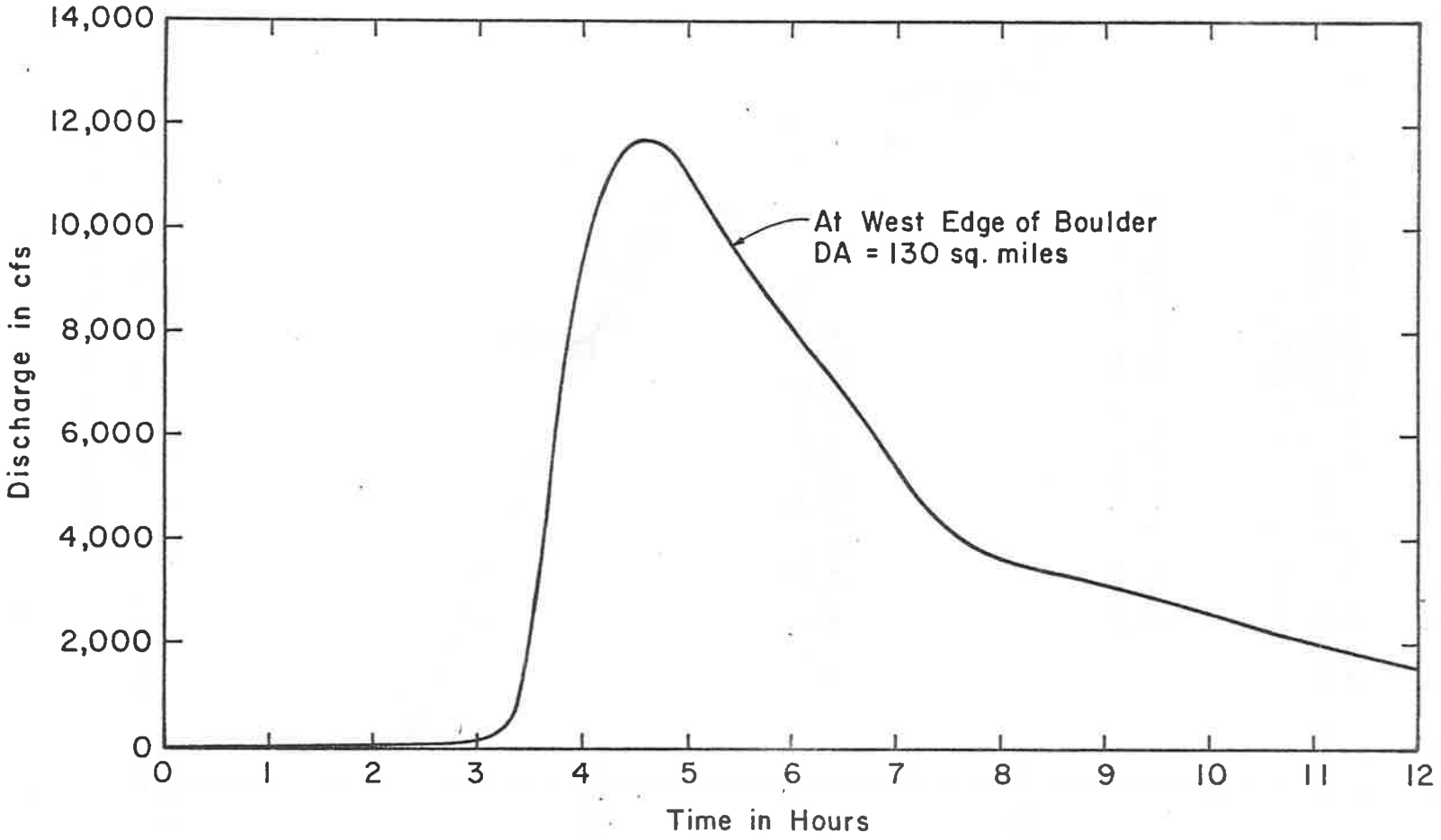

Figure 17.22 100-year hydrographs at west edge of Boulder (drainage above the mouth of the canyon).

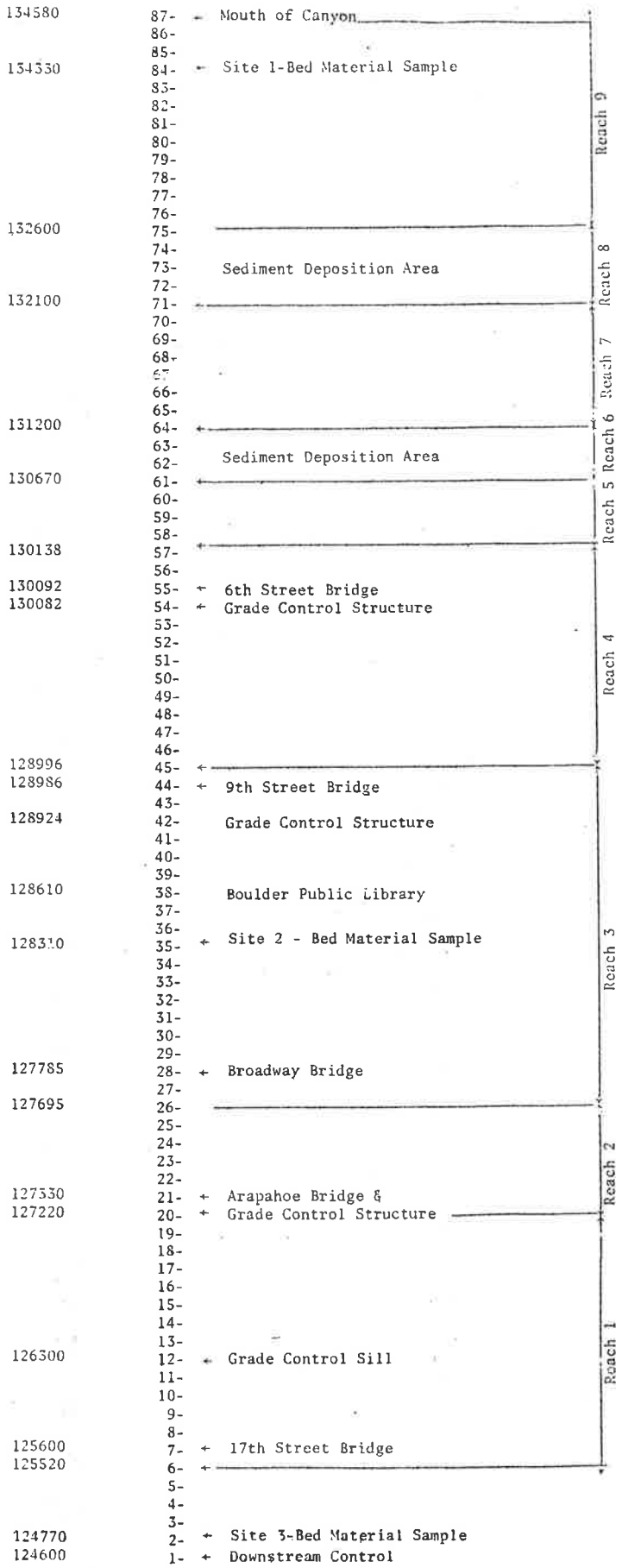

Figure 17.23 Index map of cross sections and reaches (proposed floodway).

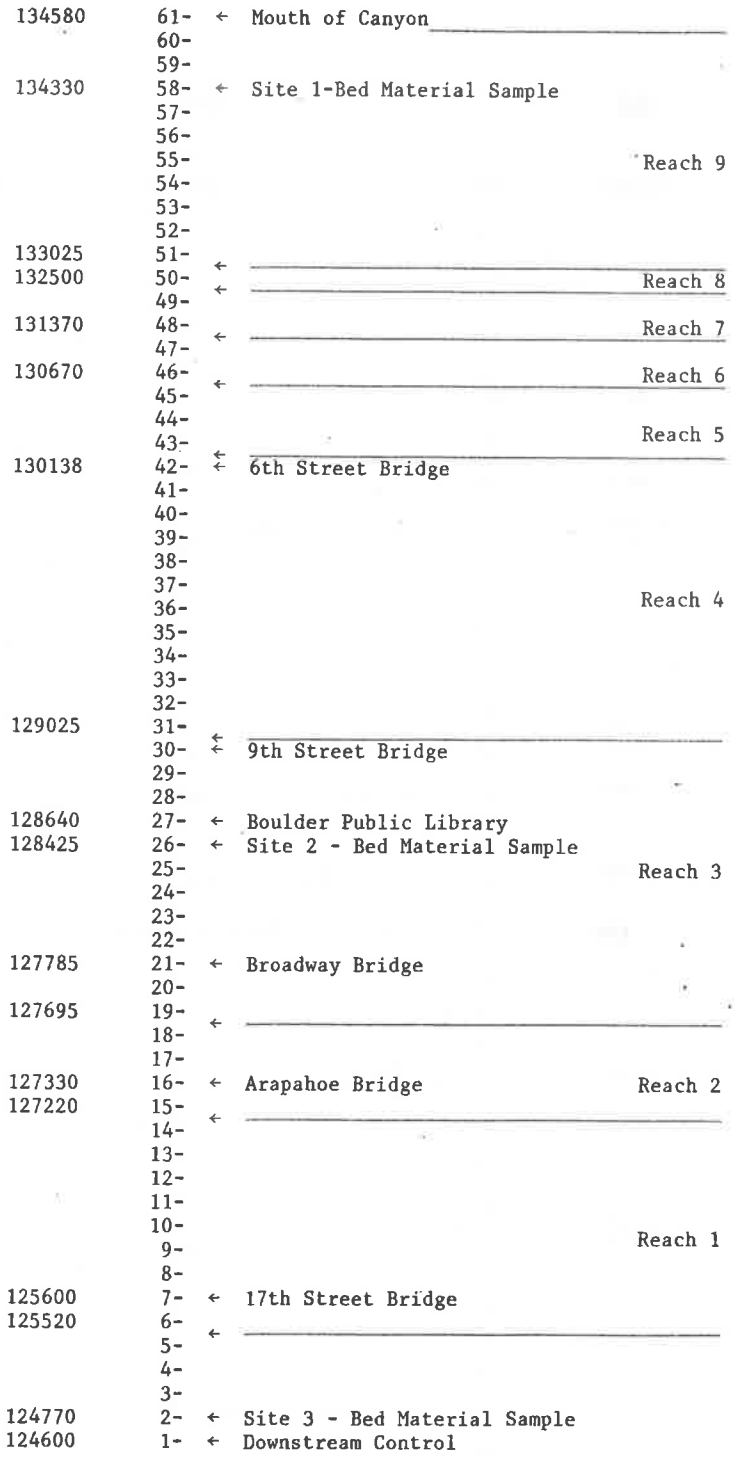

Figure 17.24 Index map of cross sections and reaches (do-nothing condition).

samples were from the surface layer (armor layer) and five samples from the subsurface layer.

For the surface layer (armor layer), the distribution was obtained by hand sieving for sizes less than three inches and by measurement, weighing and counting for sizes larger than three inches. Much finer material exists in the subsurface layer. The subsurface layer samples were split by sieving into two fractions (one larger than one inch and another smaller than one inch). Then, the sample consisting of particles smaller than one inch was dried and its size distribution was determined by sieve analysis. The size distribution of particles larger than one inch was determined by hand sieving, measuring, weighing and counting.

Field observations verify that it is difficult to collect representative samples of bed material in Boulder Creek. For simplicity, the following characteristics of the bed material were adopted. The surface layer at site 1 has a D_{50} of 200 mm and a σ of 2.0. Site 2 has a D_{50} of 130 mm and a σ of 2.0, and site 3 has a D_{50} of 105 mm and a σ of 2.0. The subsurface layer is fairly uniform for the three sites sampled. The estimated properties are a D_{50} of 25 mm and a σ of 8.0. Since the estimated bed materials distributions are subject to a certain level of uncertainty, two other bed material distributions, 1) with D_{50} 25 percent larger and, 2) with D_{50} 25 percent smaller were utilized to examine the sensitivity of the sediment analysis to the size and gradation of the sediment.

Hydraulic Structures

There are six bridges and four grade control structures existing and/or planned in the study area extending from 6th Street downstream to 17th Street for the proposed floodway. Three of these grade control structures are located at bridge sites to reduce the channel bed gradient sufficiently to ensure that the Froude number of the flow is less than or equal to 0.8 for the 100-year flood. The burial depth of these structures should be sufficient to prevent failure due to local scour.

Riparian Vegetative Information

The tree size distribution was determined in the riparian zone of the study reach and provided valuable information for debris analysis.

The information on tree weight is required for the evaluation of forces on the structure caused by impact of vegetative debris. The

strength of trees may affect the quantity of vegetative debris. However, in general, the production of vegetative debris is the result of bank erosion.

Most trees (80 to 90 percent) on the study areas are Plains Cottonwood, Narrowleaf Cottonwood, or Peachleaf Willow. Cottonwoods have a specific gravity of about 0.33, that is, a unit weight of 20.6 lbs/ft^3. Assuming (1) the trunk of the tree has a shape of a frustrum of a cone, (2) the weight of the branches is about equal to the trunk weight, and (3) the root weight is about 0.3 times the trunk weight, the approximate weights of typical trees, brahcnes, and roots were estimated.

The strength of a tree is a function of tree type, water content, and density among other factors. For example, air dry wood can be on the order of 1.50 to 2.00 times stronger than green wood. Strength values for three types of Cottonwoods for green, clean, straight grain lumber were estimated.

Resistance to Flow

It is difficult to accurately estimate resistance flow for a boulder bed channel. The relative roughness can change greatly during a flood. According to Chow (1959) the normal value of Manning's roughness coefficient n is 0.05 for a mountain stream with no vegetation in the channel, banks usually steep, trees and brush along banks submerged at high stages and channel bottom consisting of cobbles with large boulders. This description seems to fit Boulder Creek very well. This value of Manning's n is close to that computed by the method presented by Golubtsov (1969) which yields a value of 0.057. A rough estimate of Manning's n using the measured time of travel for a discharge of 175 cfs yields a value of approximately 0.06. In addition, Strickler's Formula is often used to estimate the grain resistance (Simons and Sentürk, 1977). Assuming that d_{50} is 200 mm, the Manning's n is 0.049 according to Strickler's Formula. A recent study at Colorado State University by Simons, Al-Shaikh-Ali, and Li (1978) indicated that the passage of sediment wave during the flood can significantly reduce the resistance to flow. The assumed value of Manning's n of 0.048 in the main channel by URS Company is somewhat conservative in the sediment analysis but would slightly underestimate the flood potential. Since the major objective of this analysis is to deal with sedimentation and debris problems, a conservative Manning's n value of 0.048 is utilized for the analysis of the main channel.

Sediment Transport Rates

The rate of sediment transport as related to channel aggradation and degradation is perhaps the most important factor when conducting the sedimentation analysis.

Existing data on sediment transport rates collected in both laboratory flumes and in the field have been in relatively flat channel systems and with a uniform sediment. Hence, most of the available sediment transport equations are not applicable for the Boulder Creek study conditions. However, recent laboratory studies at Colorado State University by Li, et al. (1977), utilizing a steep channel (5% to 25% bed slope) and gravel and boulder bed sediment indicated that a form of Meyer-Peter, Müller sediment transport equation (USBR, 1960) is applicable for steep gravel and boulder bed streams. For practical application, the coefficients should be calibrated using measured field data but since there were no pertinent data available, the original coefficients were used. Also, the Meyer-Peter, Müller type equation accounts for the bed load only, so the suspended portion of the bed material load was computed by the Einstein procedure (Simons and Sentürk, 1977).

The Meyer-Peter, Müller equation as applied was developed utilizing data from gravel bed flumes and the Shield's incipient motion criteria. The equation was modified to properly account for the armoring effect of coarser particle sizes. Past experience verifies that the Meyer-Peter-Müller equation and the Einstein suspended sediment procedure provide the best estimate of sediment transport for field situations such as Boulder Creek.

Method of Analysis

The degradation and aggradation problem is very complicated. Simplifying assumptions are needed to obtain solutions in a practical and economical way. The dominant physical processes include water runoff, sediment transport, sediment routing, degradation, aggradation, breaking and forming of the armor layer, etc. These processes are unsteady in nature. In order to simplify the solution and to make the results of the analysis compatible with the HEC-2 flood level analysis, a known discharge assumption was used. The known discharge solution is appropriate in this study because of the short distances involved in the analysis. In addition, to save computer time, the degradation and aggradation analysis was conducted on a reach basis utilizing the average hydraulic parameters in the reaches. The amount of predicted aggradation and degradation was distributed to the verticals of a cross

section according to the channel conveyance to yield a set of new cross sections.

The developed mathematical model routes the sediment by size fractions. The transporting capacity of each reach was determined utilizing the average hydraulic conditions of the reach and the sediment transport equation described earlier. The sediment routing procedure was accomplished by applying the sediment continuity equation and considering the size distribution of the upstream sediment supply and the bed material for both the surface and subsurface layers. Reach No. 6 and No. 8 of the proposed floodway will have man-made sediment deposition areas. Each sediment deposition area will create a large-scale roller which will cause sediment deposition. These depositional areas require special attention to account for the sediment extracted from the main channel and to simulate deposition in these areas. For simplicity the velocity of the current entering this deposition area was assumed to be 0.5 that of the main channel. The sediment concentration of the flow into these areas is determined using the Einstein Procedure.[6] In addition, the deposition shape of this area was assumed to vary with sediment settling rates.

Due to lack of detailed information on the upland watershed, experience was utilized to estimate debris yield. Accordingly, the vegetative debris yield was assumed equal to one percent by volume of the sediment yield. The hydraulic forces on different size trees were determined and compared to the strength of trees. It is concluded that the debris generated by the bending and shear failures caused by the hydraulic forces acting on the bank line trees is minimal. Major contributions of trees from within the study area would result from bank erosion.

From the erosion and sedimentation analysis, the sediment yield and the associated erosion and deposition in the reaches were determined. Then, the amount of potential vegetative debris was estimated. In addition, the probability of debris plugging and the extent of potential blockage of debris at bridges were determined.

Results of Analysis

Figure 17.25 shows the comparison of water surface profiles (assumed rigid boundary channels) of the 100-year flood for the "do-nothing plan" (natural) and the proposed floodway. The proposed excavated floodway (Plan II) would provide significant flood protection

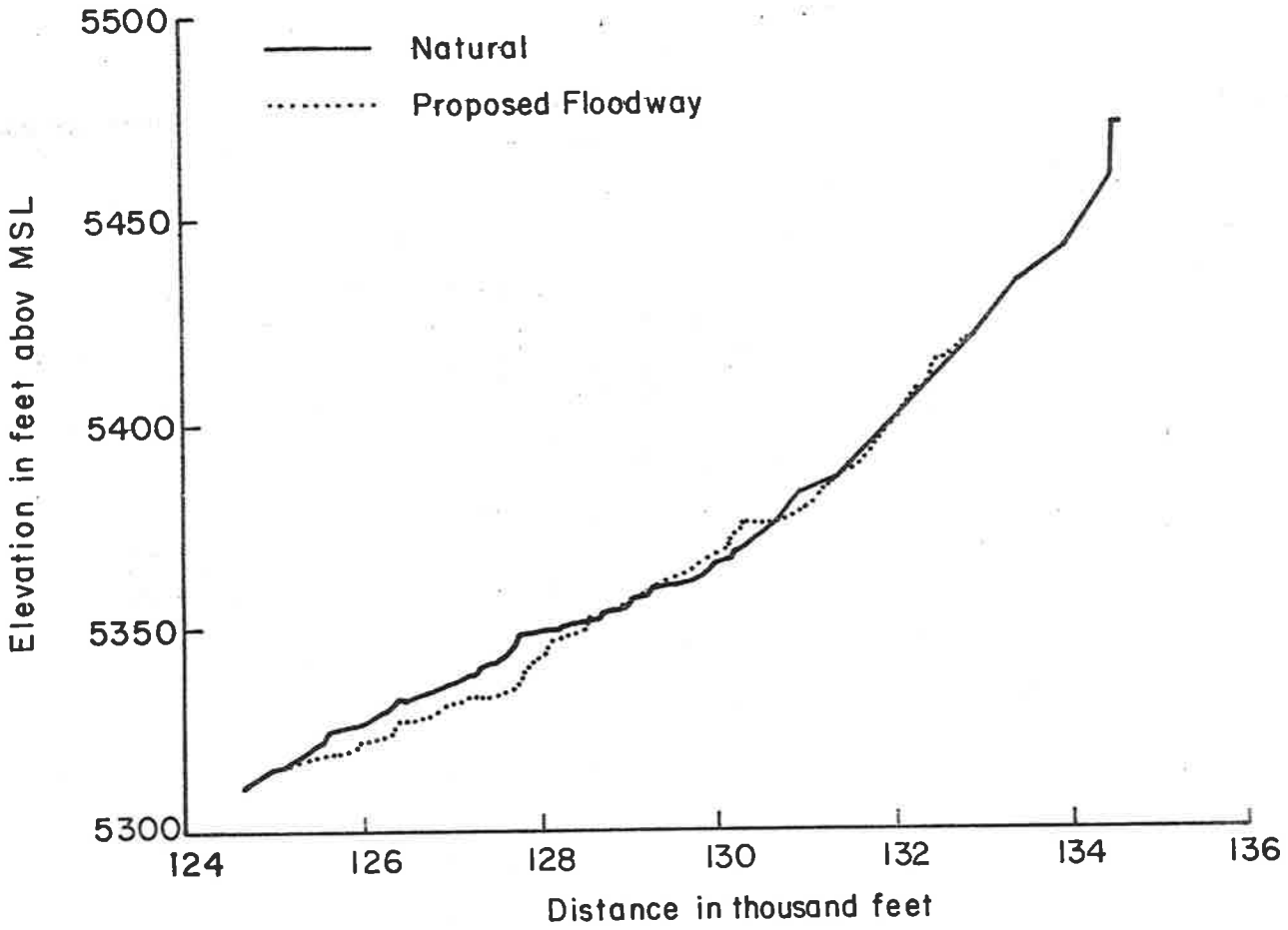

Figure 17.25 Water surface profiles for 100-year flood.

for the areas from 6th Street downstream to 17th Street. The average flood stage reduction is about 4.0 ft. The maximum reduction in stage is 9.3 ft. This occurs at river distance 127,640 ft. Other comparisons between the "do-nothing plan" and the proposed floodway are given in Table 17.14. This table only gives the general and qualitative comparison of the two conditions examined. Detailed comparisons are given in the Phase I and the Phase II reports (Simons and Li, 1979a and 1979b).

The sedimentation and debris problems associated with the "do-nothing" condition are relatively worse than those associated with the proposed floodway. For both the "do-nothing plan" and the proposed floodway, the effect of sediment movement on the flowline is only significant for reaches upstream of the 6th Street Bridge, where most of the anticipated aggradation and degradation occurs. (See Figures 17.26-17.31). Figure 17.26 compares the initial design profile of the proposed floodway and the final bed profile after a 100-year flood. Most of the study reaches are aggrading. However, Reach No. 7 experiences significant degradation due to the channel contraction. Most areas experiencing degradation and aggradation are located upstream of the 6th Street Bridge (river distance 130,092). The accumulated degradation and aggradation for each reach during the 100-year flood is shown in Figure 17.27. This figure indicates that the rate of degradation and/or aggradation is generally decreasing with time due to bed adjustment. With the new cross-sectional data adjusted for aggradation and degradation, a HEC-2 water surface profile for a discharge of 12,000 cfs was determined. A comparison of water surface profiles for the initial boundary condition and the condition after routing the 100-year flood is given in Figure 17.28. This figure shows that the effect of sediment movement on the flowline is only significant upstream of the 6th Street Bridge. The maximum increase in river stage is about 2.6 ft. This anticipated maximum effect on the flowline is located near river Station 133,430 ft.

Figure 17.29 shows the comparison of the initial bed profile and the final bed profile after a 100-year flood for a do-nothing condition. The majority of the study reaches are aggrading. Most areas experiencing degradation and aggradation are located upstream of the 6th Street Bridge (river distance 130,138 ft). The accumulated degradation and aggradation for each reach during the 100-year flood is shown in Figure

Table 17.14 General comparison of do-nothing and Plan II floodway.

Item	Description	Do-Nothing Plan	Proposed Floodway (Plan II)
1.	Average flood stage reduction from 6th Street downstream to 17th Street	-	4.0 ft
2.	Maximum flood stage reduction at a particular location	-	9.3 ft
3.	Number of bridges that the low chord elevation is lower than the estimated 100-year flood level	4	1
4.	Flow diversion (overflow to flood plains)	significant	negligible
5.	Estimated sediment supply supply at the mouth of canyon	23,900 cubic yards	22,300 cubic yards
6.	Percent of sediment from the mouth of canyon that passes 17th Street Bridge	23 percent	20 percent
7.	Maximum aggradation volume per unit length of channel	281 ft^3/ft from river distance 130,670 ft to 132,600 ft	307 ft^3/ft from river distance 132,100 ft to 132,600 ft
8.	Maximum degradation volume per unit length of channel	116 ft^3/ft from river distance 132,100 ft to 132,600 ft	253 ft^3/ft from river distance 131,200 ft to 132,100 ft
9.	Maximum effect of sediment deposition on flood level predication (comparison of flood levels with and without sediment routing)	2.3 ft	2.6 ft
10.	Maximum potential blockage at bridges due to sediment aggradation	3 percent	4 percent
11.	Maximum size of sediment that will move in the system during the 100-year flood	1.7 ft	2.5 ft
12.	Local scour problems	insignificant	small
13.	Estimated number of equivalent trees in the system	47	53
14.	Prob. of partial blockage* due to vegetative debris at the 6th Street Bridge	0.99993	0.993
15.	Estimated percent of blockage at bridges due to vegetative debris	50 percent	30 percent
16.	Potential pressure caused by blockage due to vegetative debris	256 lb/ft	200 lb/ft

*Probability of partial blockage is the probability of trapping of at least one element of debris by the bridge.

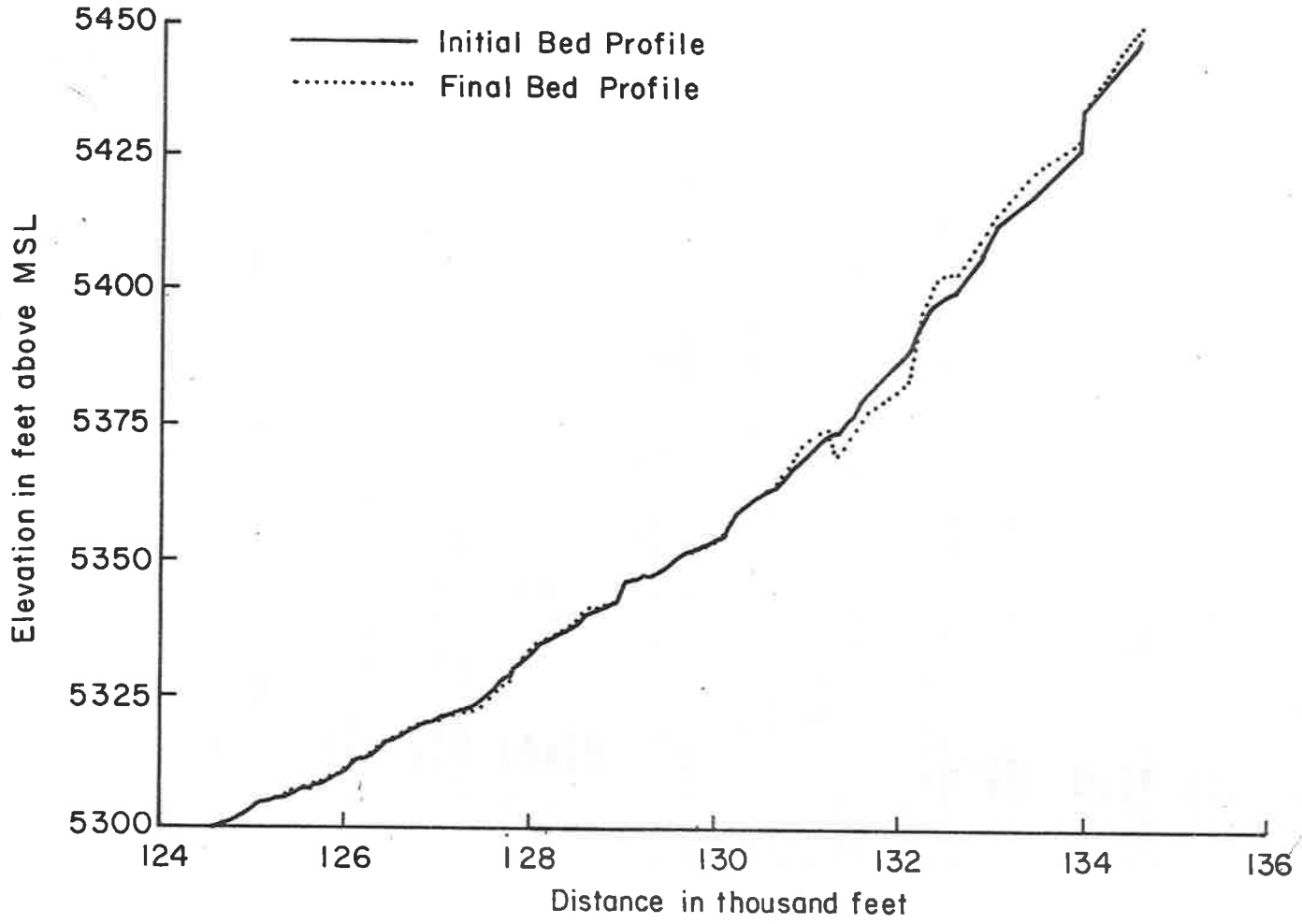

Figure 17.26 Comparison of initial design profile and final bed profile after 100-year flood for the proposed floodway (Plan II).

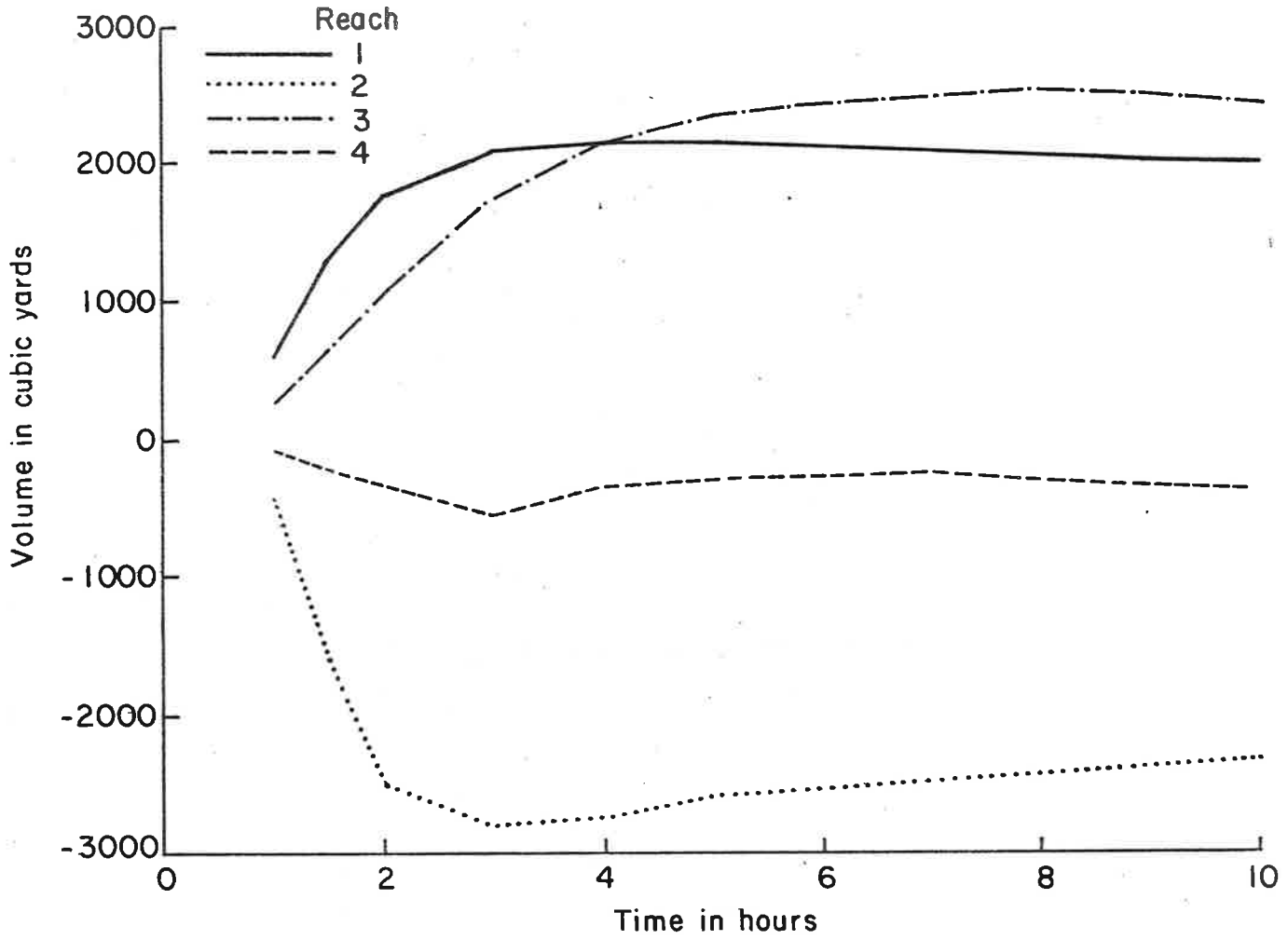

Figure 17.27a Aggradation and degradation in reaches during the 100-year flood for the proposed floodway.

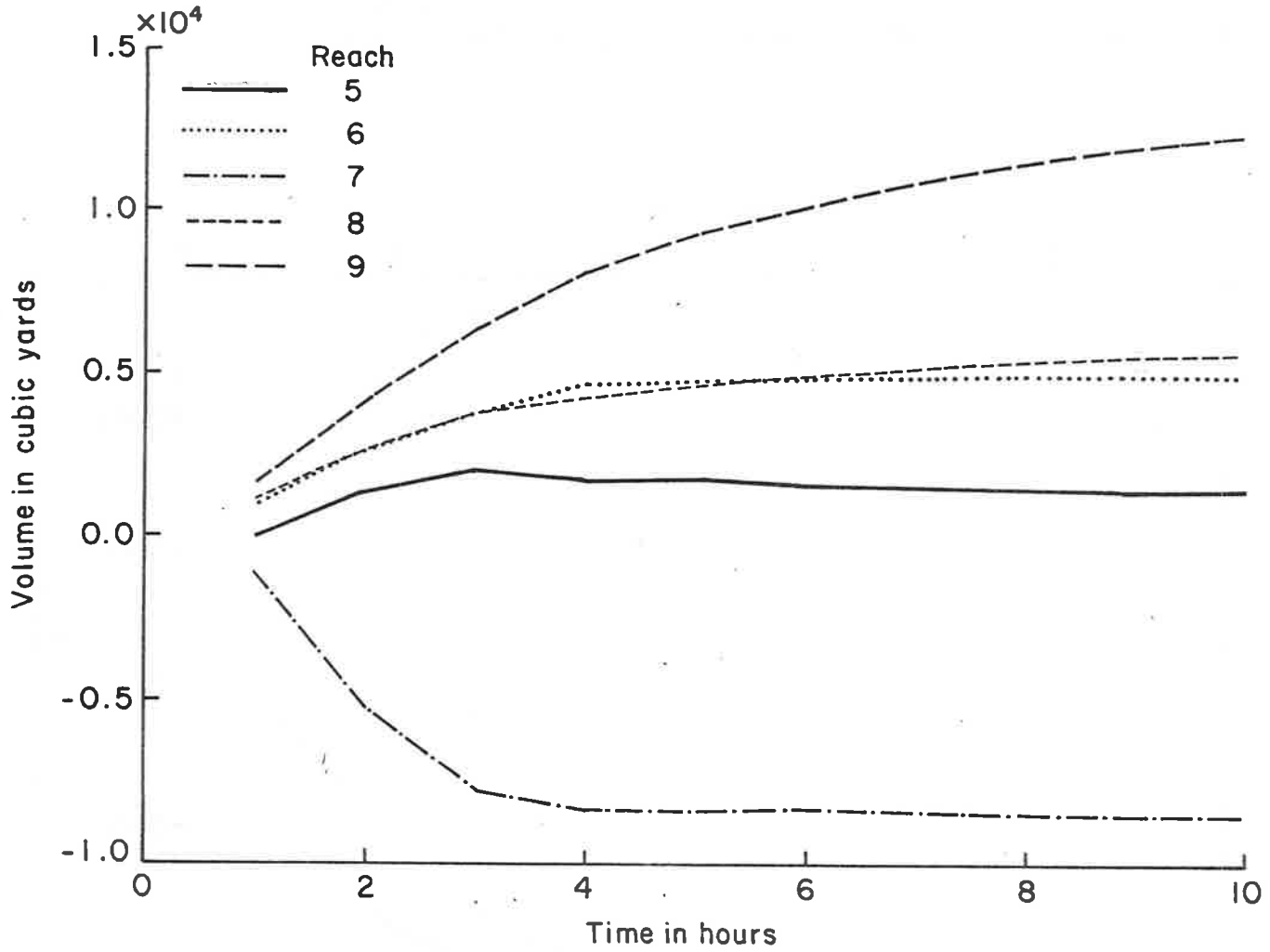

Figure 17.27b Aggradation and degradation in reaches during the 100-year flood of the proposed floodway.

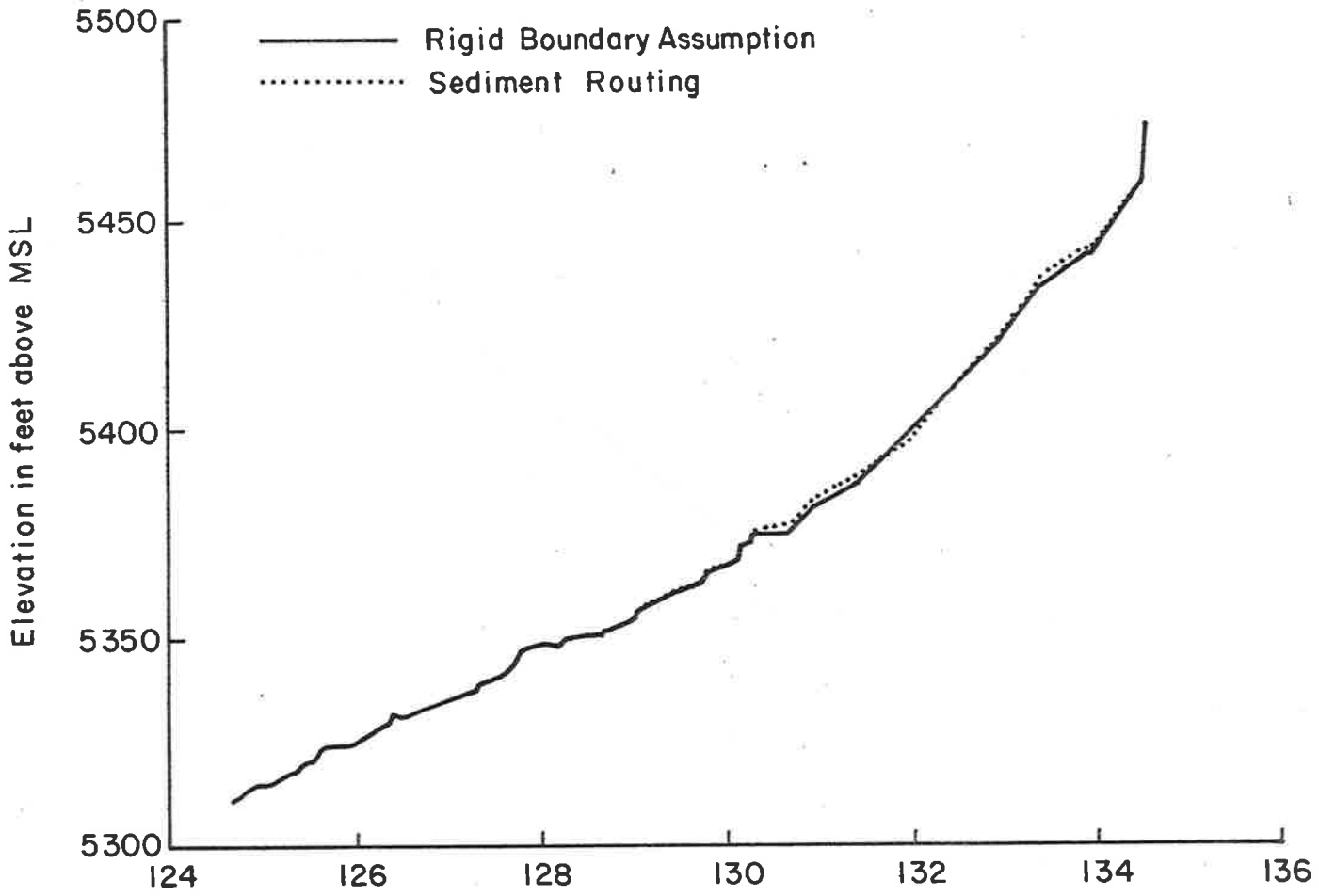

Figure 17.28 Comparison of water surface profiles of rigid boundary assumption and condition after routing the 100-year flood for the proposed floodway (Plan II).

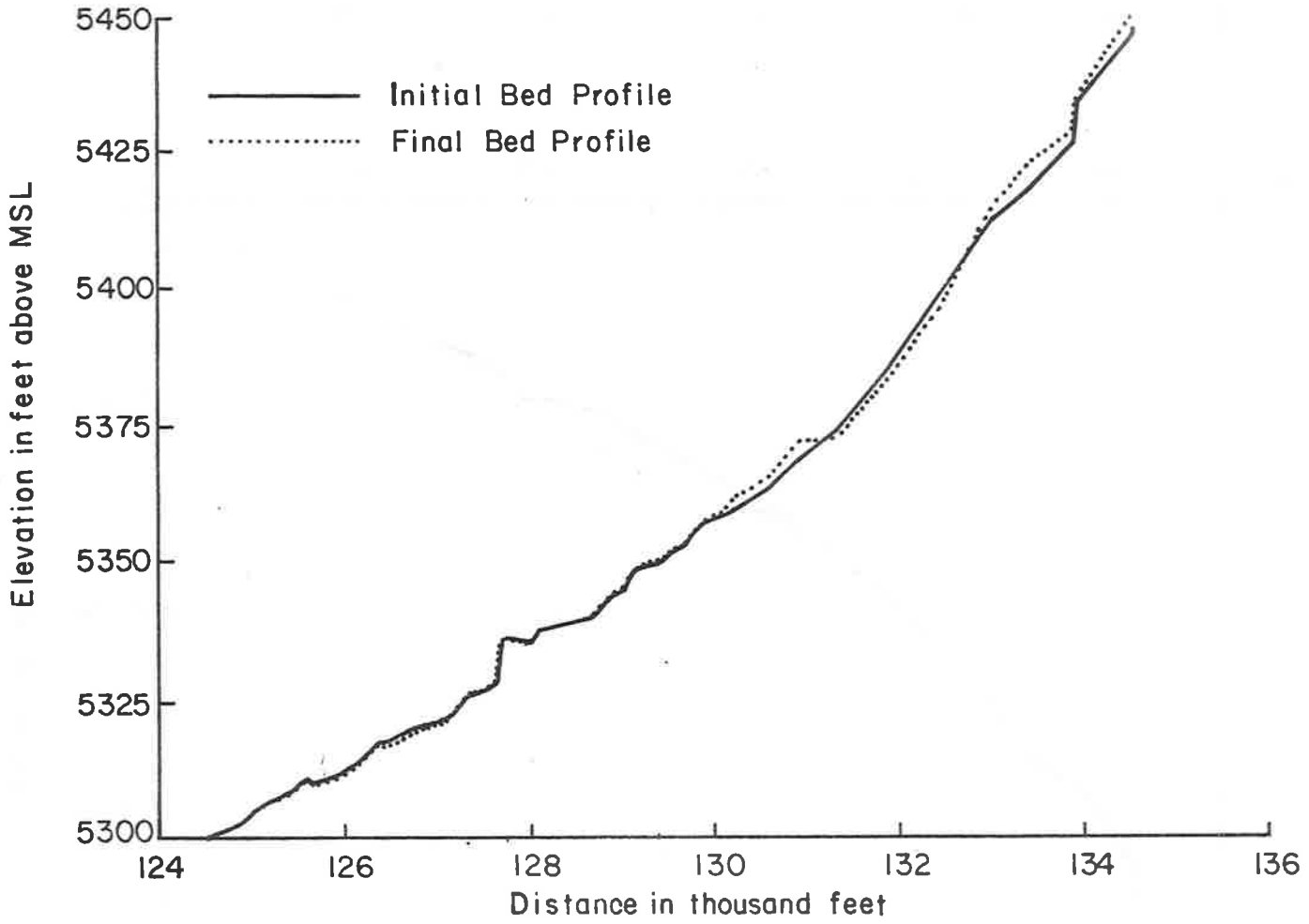

Figure 17.29 Comparison of initial design profile and final bed profile after the 100-year flood for the do-nothing plan.

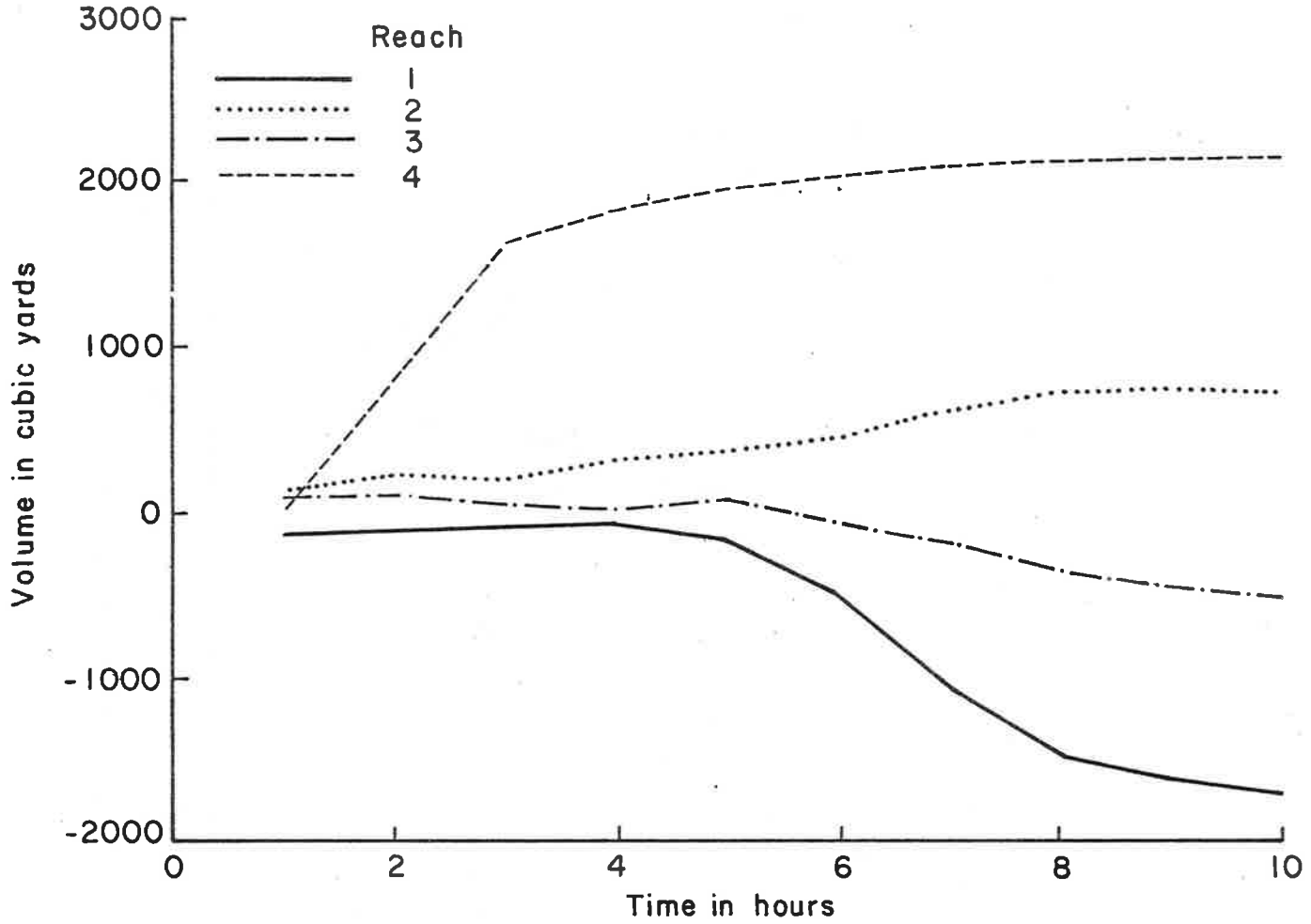

Figure 17.30a Aggradation and degradation in specified reaches during the 100-year flood (do-nothing plan).

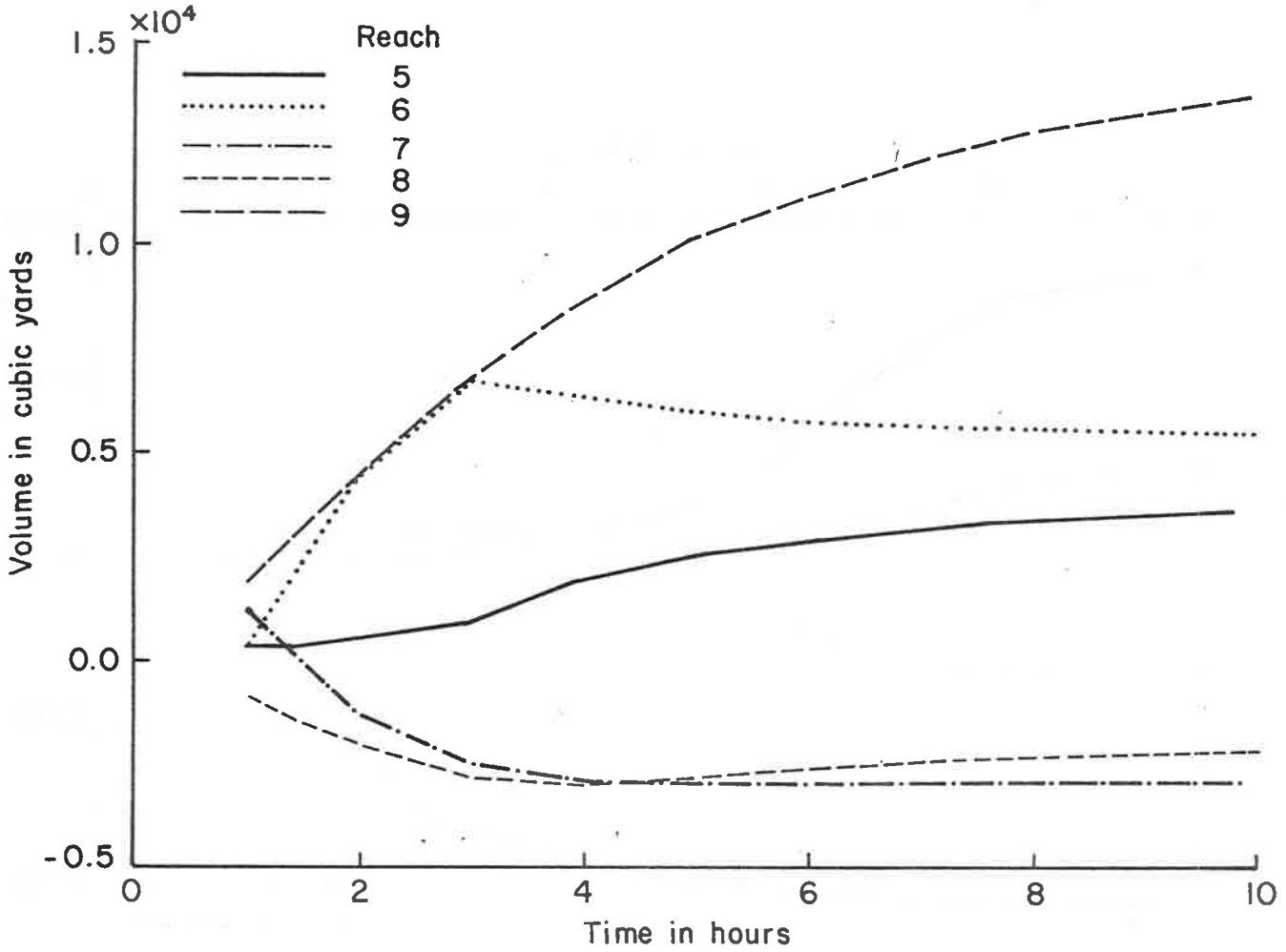

Figure 17.30b Aggradation and degradation in specified reaches during the 100-year flood ("do-nothing" plan).

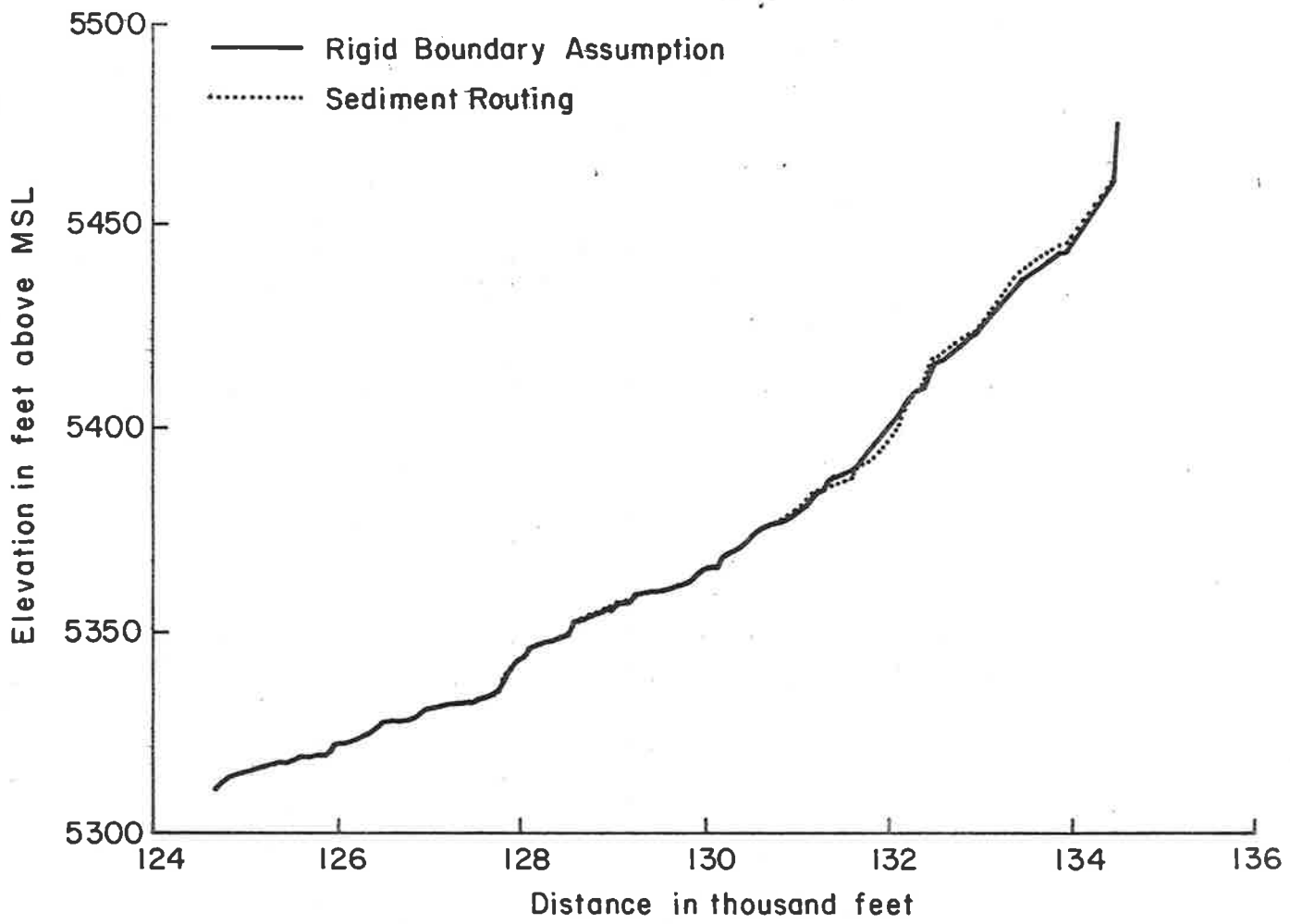

Figure 17.31 Comparison of water surface profiles considering the rigid-boundary assumption and the condition after routing the 100-year flood ("do-nothing" plan).

17.30. This figure indicates that the rate of degradation and/or aggradation is generally decreasing with time due to bed level adjustment. The volumes of degradation and aggradation for this "do-nothing" condition are comparable to those expected for the proposed excavated floodway. With the new cross-sectional data adjusted for aggradation and degradation, a HEC-2 water surface profile for a discharge of 12,000 cfs was determined. A comparison of water surface profiles for the initial boundary condition and the condition after routing the 100-year flood is given in Figure 17.31. This figure shows that the effect of sediment on the flowline is only significant upstream of the 6th Street Bridge. The maximum increase in river stage is about 2.3 ft. This anticipated maximum effect is located near river Station 133,430 ft.

The potential blockage at bridges due to high stages is much more serious in the "do-nothing plan." These potential blockage problems are very serious at Broadway (river distance 127,785 ft), Arapahoe (river distance 127,300 ft), and 17th Street (river distance 125,000 ft) bridges. In addition, there are flow diversion problems in the areas downstream of river distance 128,425 ft. The sediment movement does not contribute significantly to potential blockage due to sediment aggradation, local scour and possible flow diversions. However, the transport of vegetative debris may cause additional blockage and possible failure of bridges, significant flow retardation due to backwater and ponding effects, flow diversion, and even channel avulsions. Because of the higher water surface elevations for the "do-nothing plan", the potential for flow blockage at bridges is increased. This, in turn, increases the trapping opportunities and worsens the debris problems.

Summary and Conclusions

The proposed floodway plan will not result in significant erosion and sedimentation problem if the proposed channel is restored to its former dimensions after each major flood. The effect of sediment movement on the flowline is only significant for the areas upstream of 6th Street Bridge. Within the reach from 6th Street downstream to 17th Street, the sedimentation problem is minimal if the design channel is

maintained. There are practically no problems associated with potential blockage due to sediment aggradation, local scour and possible flow diversions. However, the potential problems associated with vegetative debris are unavoidable. The presence of a large amount of vegetative debris may cause blockage and possible failure of bridges, significant flow retardation due to backwater and ponding effects, flow diversions, and even channel avulsions. The best solution to the debris problem requires limiting the supply of debris. This involves appropriate zoning of trailer courts and riverine home areas, the clearance of trees and other debris from immediate debris-producing areas, and installation of debris traps and the construction of check dams. Such measures can provide solutions that will limit the debris supply and debris induced problems.

For limiting the supply of sediment and debris, it is recommended that the channel within the reach from river distance 131,200 ft to 132,100 ft be widened to reduce the velocity and hence, to decrease the supply of sediment and debris from this reach. In addition, the reliability of the proposed floodway would be significantly enhanced if a different bridge design was used. A possible modification is to permit the bridge deck structures to be washed off the abutments in the event of excessive hydraulic pressure caused by debris plugging. The design clearance of bridges are generally inadequate except for the 6th Street and Boulder Library Bridges. The condition at Arapahoe is particularly adverse. In addition, significant lowering of the thalweg level may result following the excavation required by the proposed floodway plan. Every effort should be made to place the original armor layer back on the bed of the excavated floodway to eliminate locate scour problems that may otherwise occur.

17.5 EROSION AND SILT REDUCTION MEASURES - CHIPPEWA RIVER, UPPER MISSISSIPPI BASIN

General

The Upper Mississippi River is part of the main riverine artery of the United States (see Figure 17.32). Its utilization both commercially and recreationally is an important aspect of the national economy. Improvement of the Upper Mississippi River for navigation channel depth

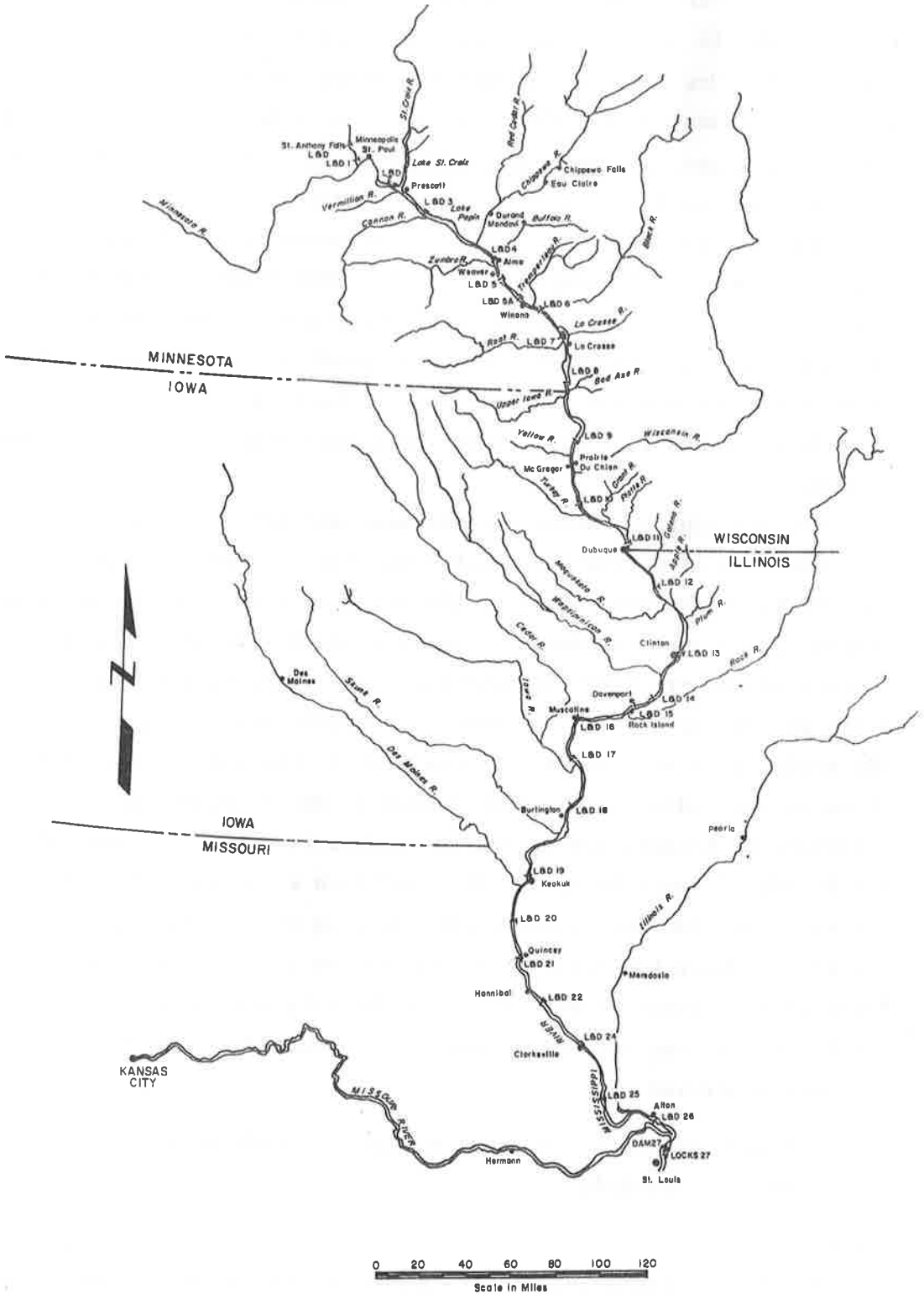

Figure 17.32 The Upper Mississippi river system.

was increased to 9 feet by constructing a series of locks and dams in the Upper Mississippi River. Since that time the navigation channel has been maintained by these structures and supplemental dredging.

Pool 4 between Locks and Dams 3 and 4 is 44.1 miles long, the longest pool in the St. Paul District. Lake Pepin, a natural river lake formed by the Chippewa delta, comprises over one-half the length of Pool 4. Prior to the creation of the 9-foot navigation channel, the floodplain land below Lake Pepin adjacent to the Upper Mississippi River was heavily forested. Lakes, ponds and deep sloughs were scattered through the forested area. Much of the floodplain area was changed following the construction of the navigation pool. The relatively stable water levels in the navigation pool converted the lower portion of the floodplain from wooded islands and dry marshes into excellent marsh and aquatic habitat.

Both the navigation channel and backwater areas have sedimentation problems. Ninety percent of the total amount of sediment entering Pool 4 is trapped by Lake Pepin. This deposition is slowly reducing the capacity of the lake. The Great River Environmental Action Team (GREAT I) is investigating the significance of shoaling in Lake Pepin. The sediment which is discharged from Lake Pepin is very fine and causes little or no dredging problems in the navigation channel downstream but some of this fine sediment is deposited in backwater areas. In contrast, the Chippewa River, transports a large amount of coarse sediment to the Mississippi River which contributes to dredging requirements as far downstream as Pool 5A.

The Chippewa River Basin extends 175 miles from Upper Michigan through northwestern Wisconsin. The Chippewa River drains 9,435 square miles and enters the Mississippi River just below Lake Pepin (Figure 17.33). The basin comprises 17 percent of the State of Wisconsin. Major land uses in the basin are recreation, forest management, and agriculture. The topography was formed by glacial activity which left thick sedimentary deposits in the lower portion of the basin that thin out toward the northeast. The glacial drift forms an almost

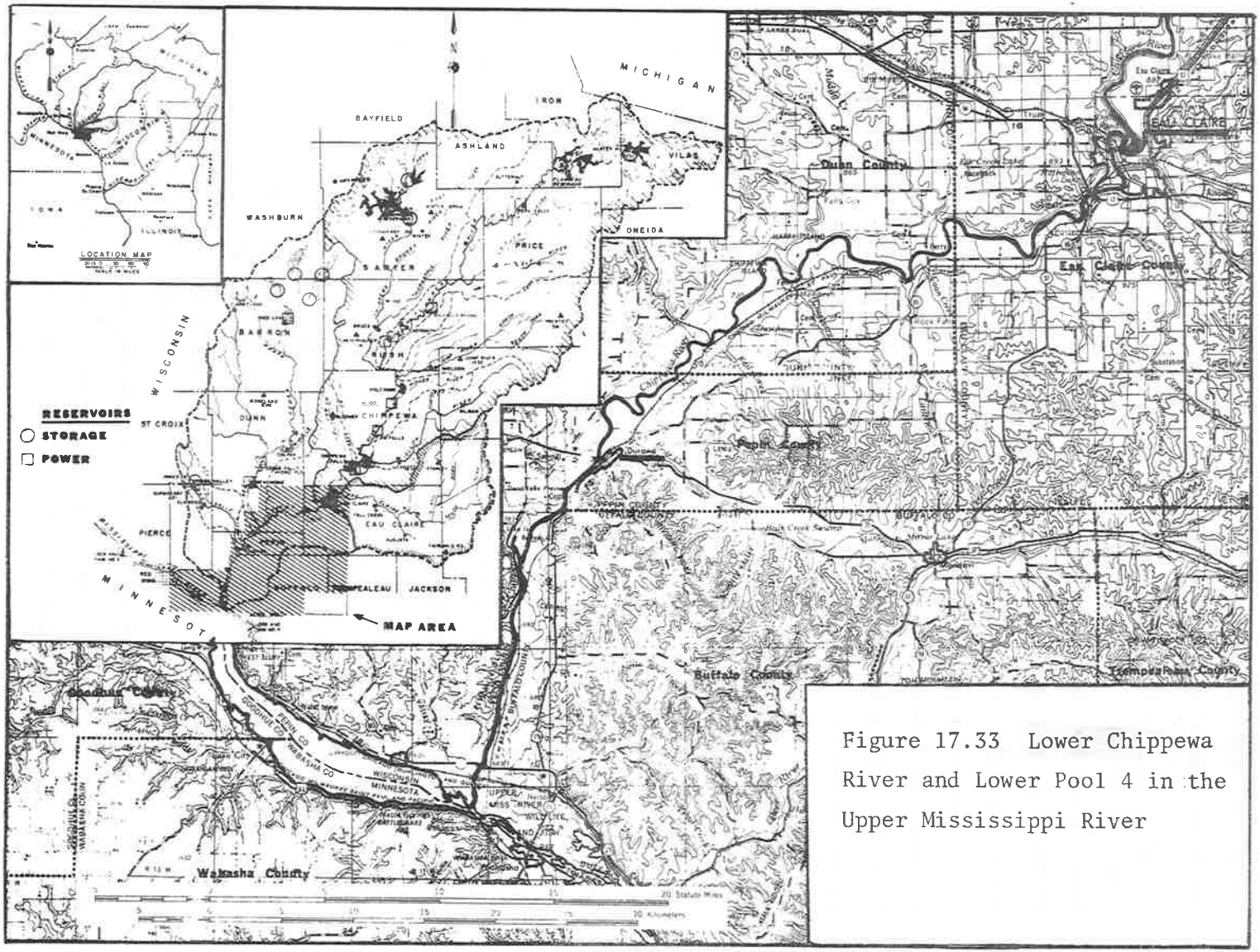

Figure 17.33 Lower Chippewa River and Lower Pool 4 in the Upper Mississippi River

continuous mantle, as thick as 150 feet over the bedrock. Drift in the basin is composed of ground moraines, and outwash materials. Permeable sand and fine gravel outwash, which was deposited by meltwater streams from stagnating glaciers, forms the valley bottom on the Lower Chippewa River, making its banks highly erodible.

From its confluence with the Mississippi River to the town of Durand 16 miles up the valley, the Chippewa River is essentially a braided river with a sinuosity of 1.06. The main channel is characteristically broad and shallow and contains shifting sandbars and sand islands. The average channel width is 700 feet and the average depth is about 3 feet. The bank full width is approximately 1,000 feet. Channel slope for this river reach is 1.76 feet per mile. Upstream from Durand to Eau Claire at river mile 61, the Chippewa River has a meandering configuration with sinuosity of 1.49. This reach is characterized by eroding sand and gravel banks. The channel width is somewhat less than that below Durand, averaging about 600 feet. The channel slope for this reach is about 1.5 feet per mile.

A geomorphic study of the Chippewa River indicates that erosion has long been a severe problem along the Chippewa River especially below Eau Claire. Several steep high banks (more than 100 feet in height) are being eroded at their toes which causes the sandy bank material to slide into the channel resulting in failure of the flat surfaces at the toe of the bluffs. Also, many of the sandy banks averaging 10 to 15 feet in height above average low water level are being eroded, resulting in some loss of floodplain. Much of this sediment is ultimately transported to the Mississippi River. The amount of sediment delivered exceeds the transport capacity of the Mississippi River, causing aggradation. It is necessary to dredge the deposits of excess sediment to provide adequate water depth for navigation. The Chippewa sediment is estimated to be responsible for about 20 percent of all maintenance dredging along the Mississippi River within the St. Paul District (U.S. Army Engineer District, St. Paul, 1974). The dredging activities and disposal of dredged material are environmental and economic issues. If the sediment from the Chippewa River can be reduced to the extent that the Mississippi River can transport the

remainder and maintain a navigable thalweg, then dredging requirements in Pools 4 and 5 can be significantly reduced. The primary objectives of this study are: 1) to identify alternatives and determine how effectively they reduce sediment supply from the Chippewa River to the Mississippi River navigation channel and backwater areas, and 2) to assess the impact of each identified alternative on the river environment in the Lower Chippewa and Upper Mississippi River systems.

Selected Alternative Measures

The alternatives investigated include (Figure 17.34):

a. Increase storage of existing flood control dams in the Chippewa River Basin to reduce downstream flood discharges.
b. Dredge a sedimentation trap at the lower end of the Chippewa River.
c. Establish a meander pattern in the Chippewa River below Durand.
d. Divert a portion of the Chippewa River flow into Lake Pepin with and without dredging.
e. Divert a portion of the Chippewa River into a sedimentation basin formed by the backwater of Pool 4 with and without dredging.
f. Construct a low-head dam at the lower end of the Chippewa River.
g. Construct a series of low-head dams on the lower Chippewa to reduce channel gradient.
h. Establish stream erosion controls and dredge a sedimentation trap at the Chippewa mouth.
i. Establish stream erosion controls and construct a low-head dam at the Chippewa mouth.

Evaluation of Alternative Measures

Evaluation of alternatives was accomplished as follows. The hydrologic, hydraulic, geologic, geomorphic and dredging data and aerial photographs were analyzed to identify the most promising alternative measures. Then a one-dimensional water and sediment routing model for Pool 4 in the Upper Mississippi River and the Lower Chippewa River, described in Chapters 8 and 11 was used to evaluate each alternative.

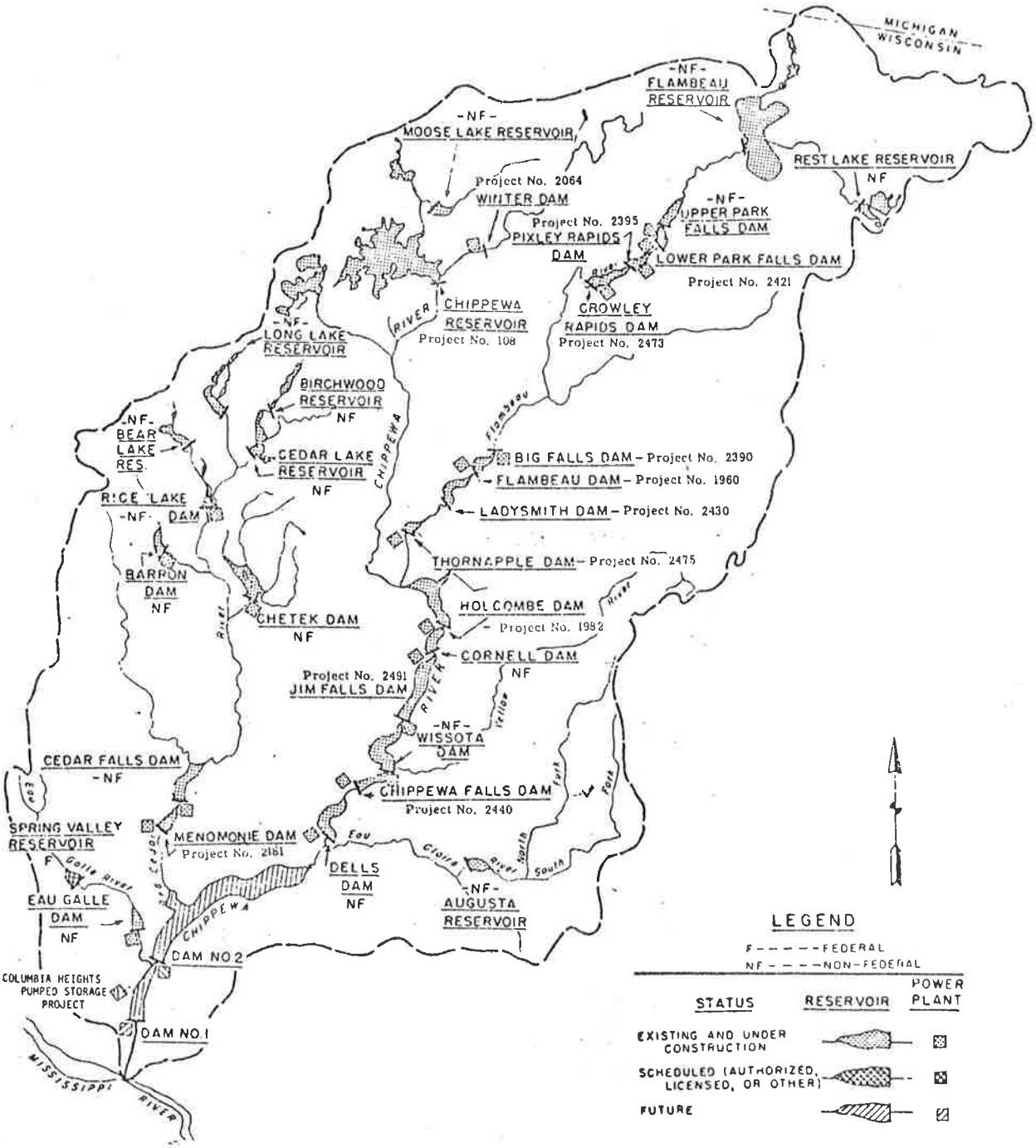

Figure 17.34a Reservoirs in the Chippewa River Basin.

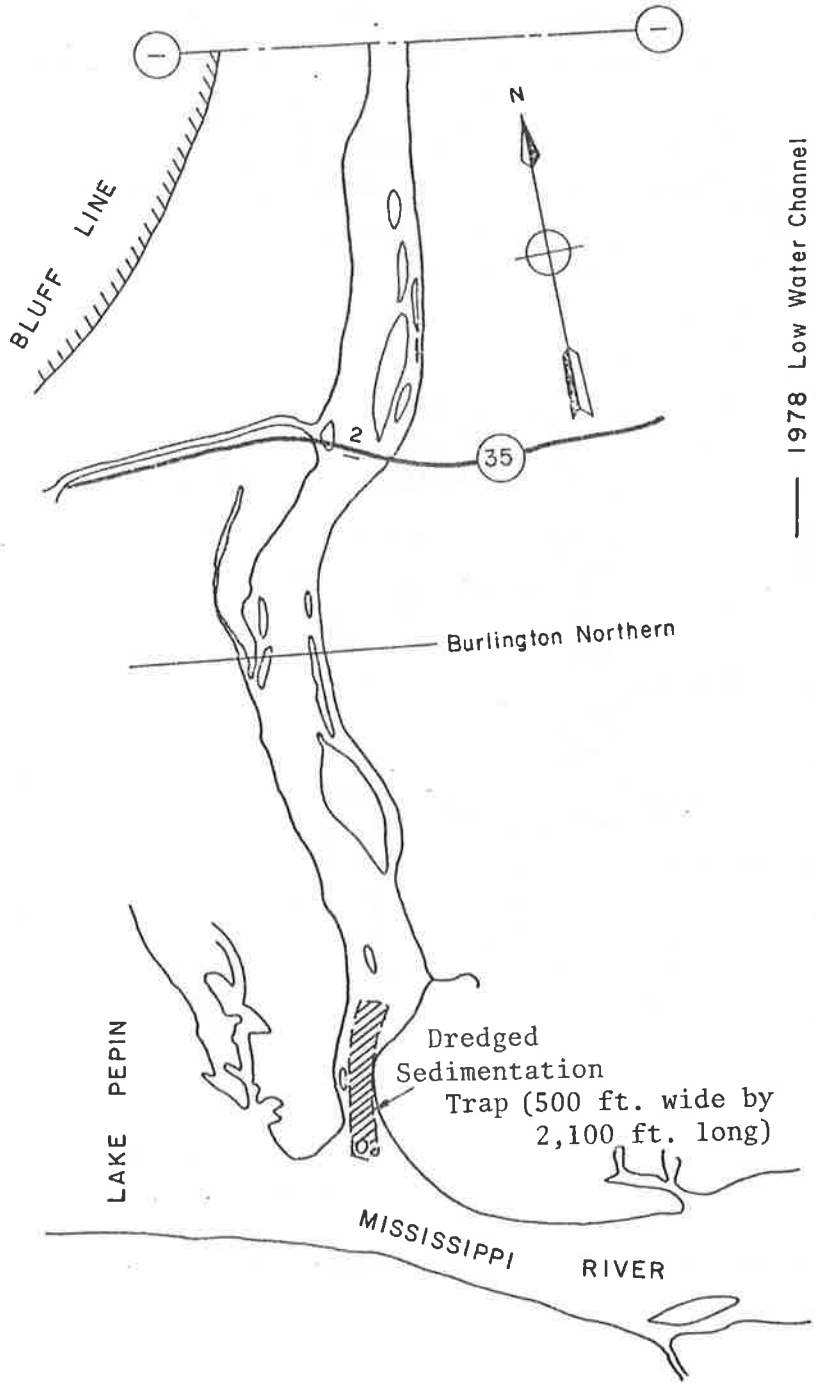

Figure 17.34b Location of Alternative 2: Dredge a sedimentation trap at the lower end of Chippewa River.

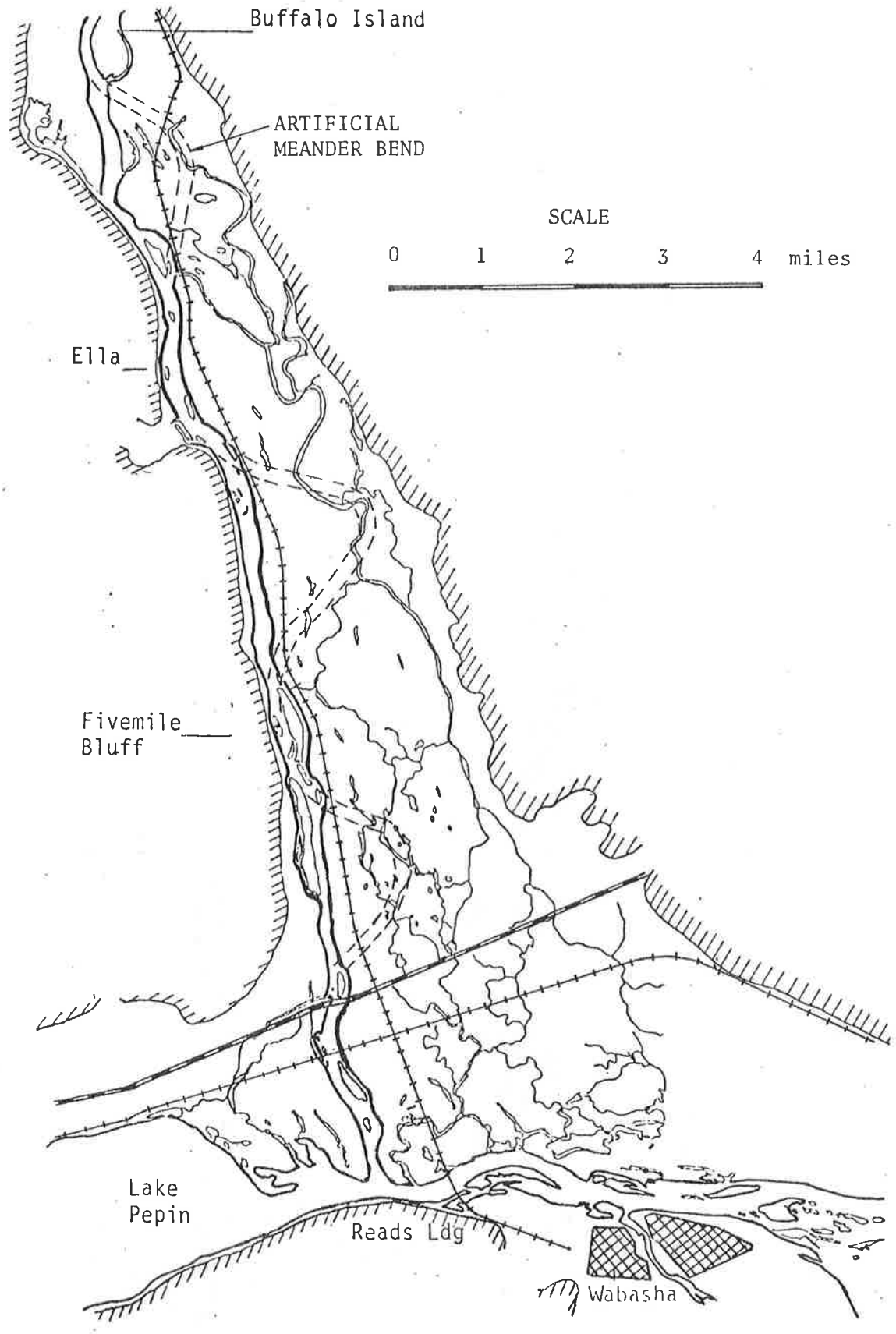

Figure 17.34c Location of Alternative 3: Establish a meander pattern in the Chippewa River below Durand.

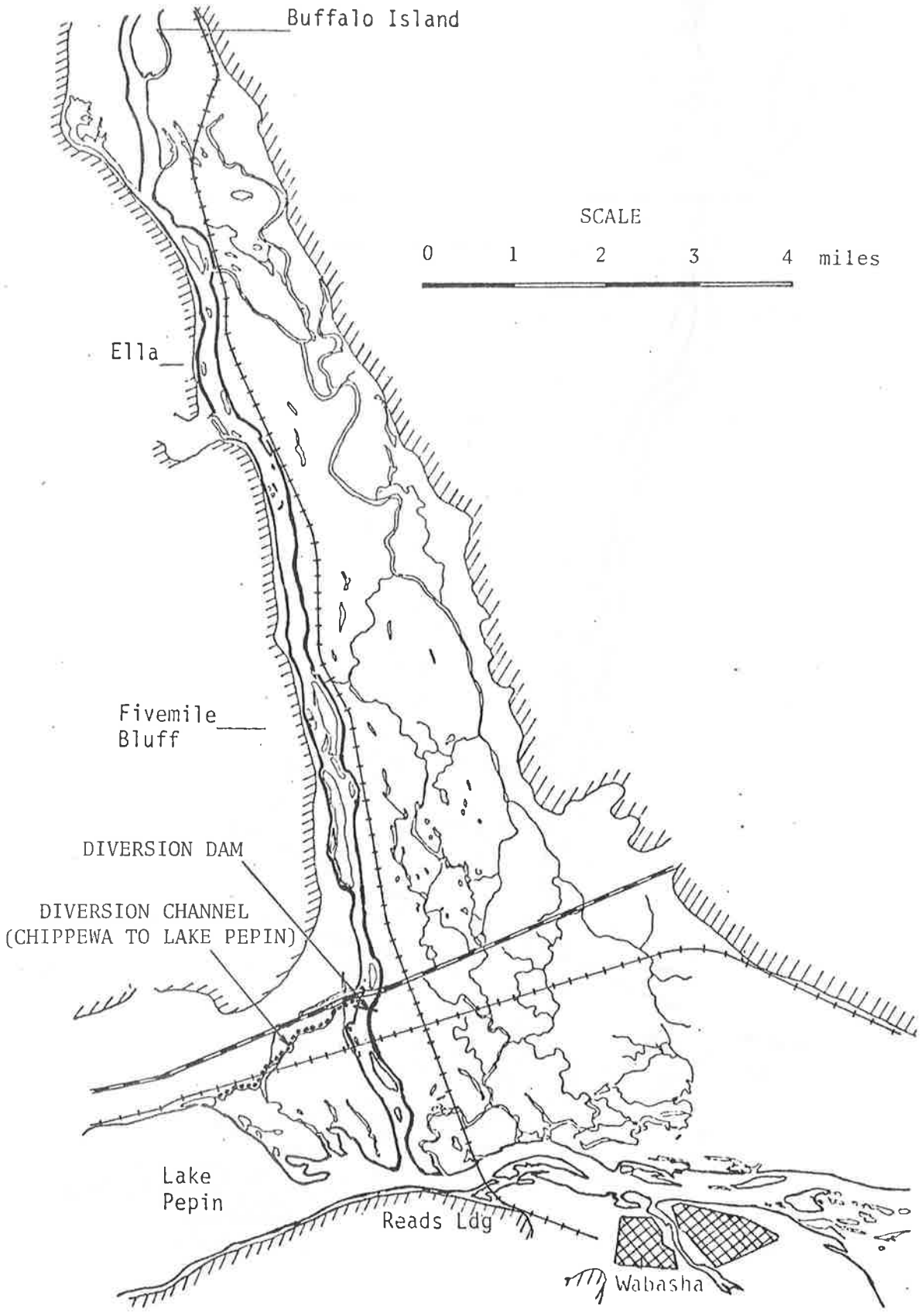

Figure 17.34d Location of Alternative 4: Divert a portion of the Chippewa flow into Lake Pepin.

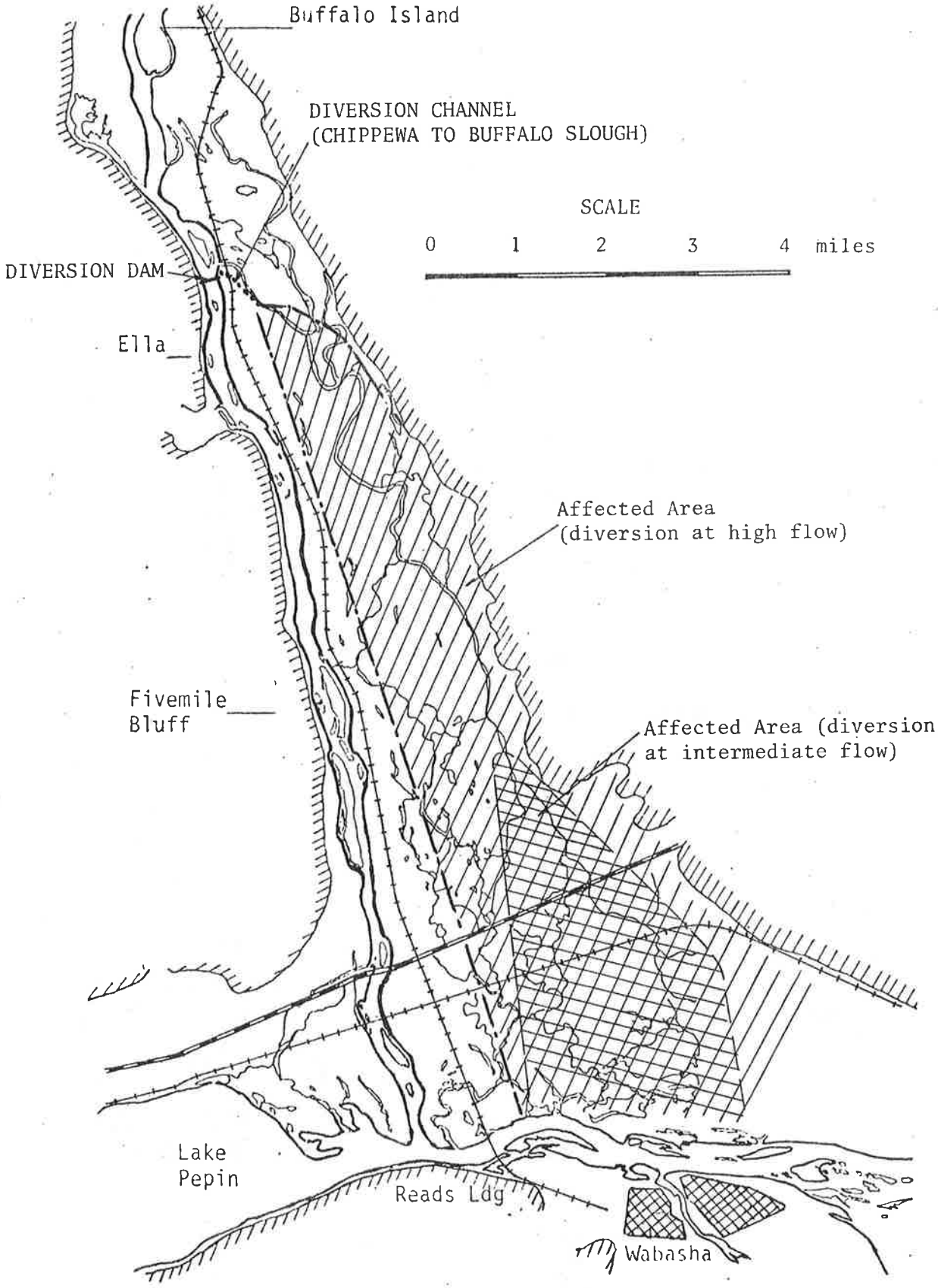

Figure 17.34e Locations of Alternative 4: Divert a portion of the Chippewa flow into a sedimentation basin through Buffalo slough.

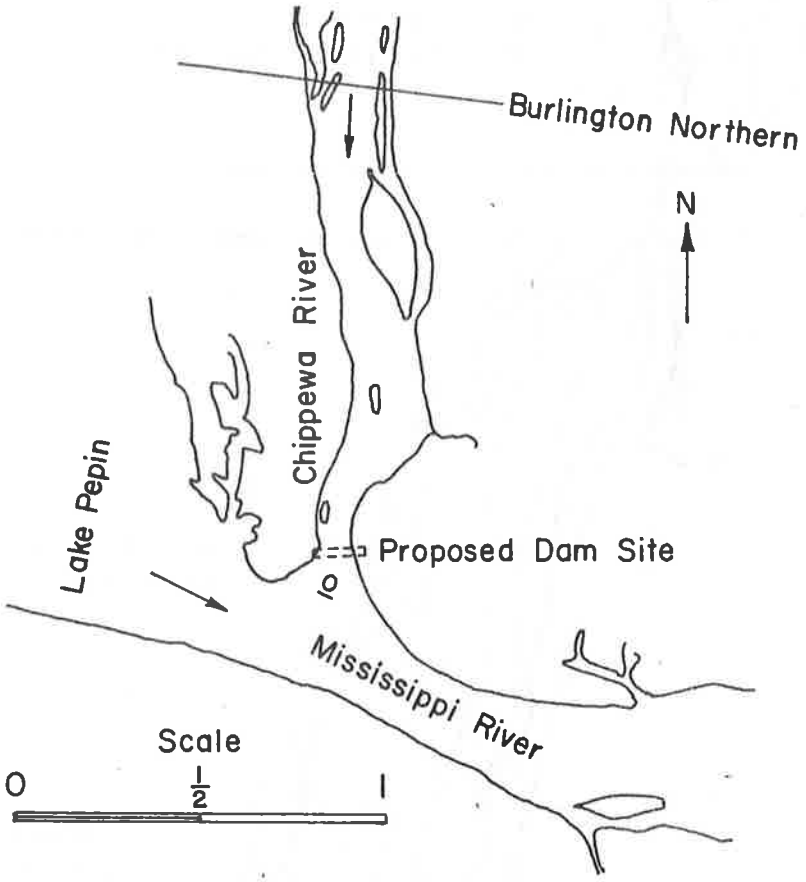

(a) Location of Low-Head Dam

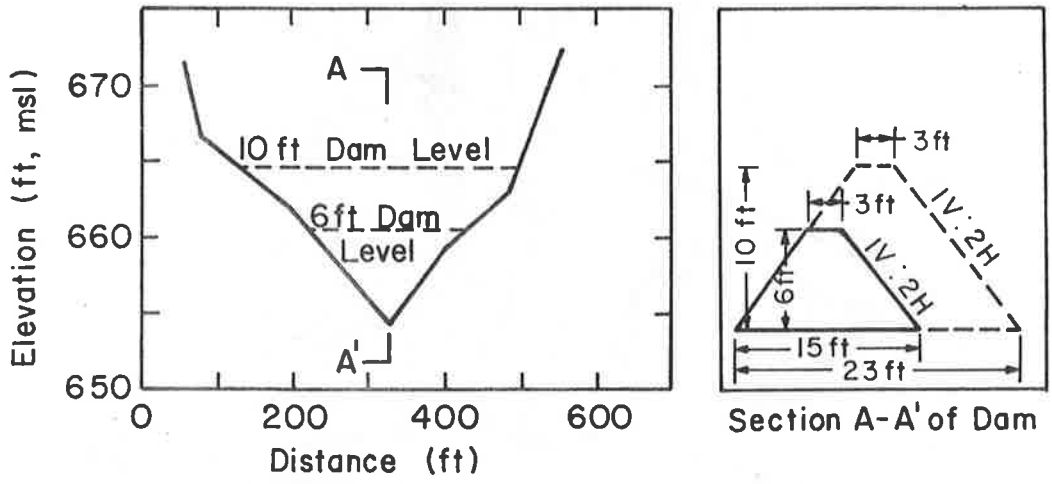

(b) Cross-Sectional Shape at the Dam Site

Figure 17.34f Alternative 6: Construct a low-head dam at the lower end of the Chippewa River.

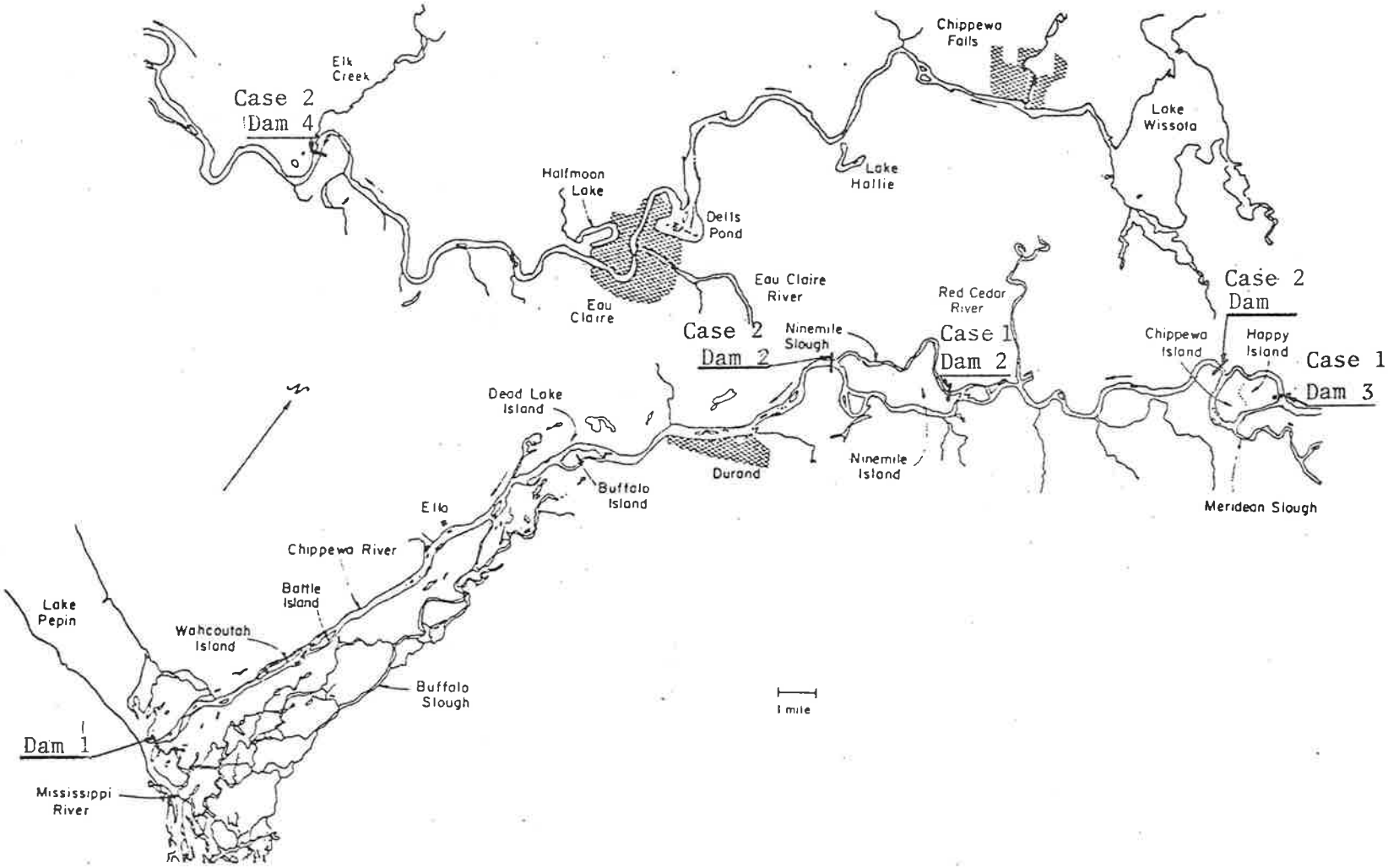

Figure 17.34g Location of Alternative 7: Construct a series of low-head dams.

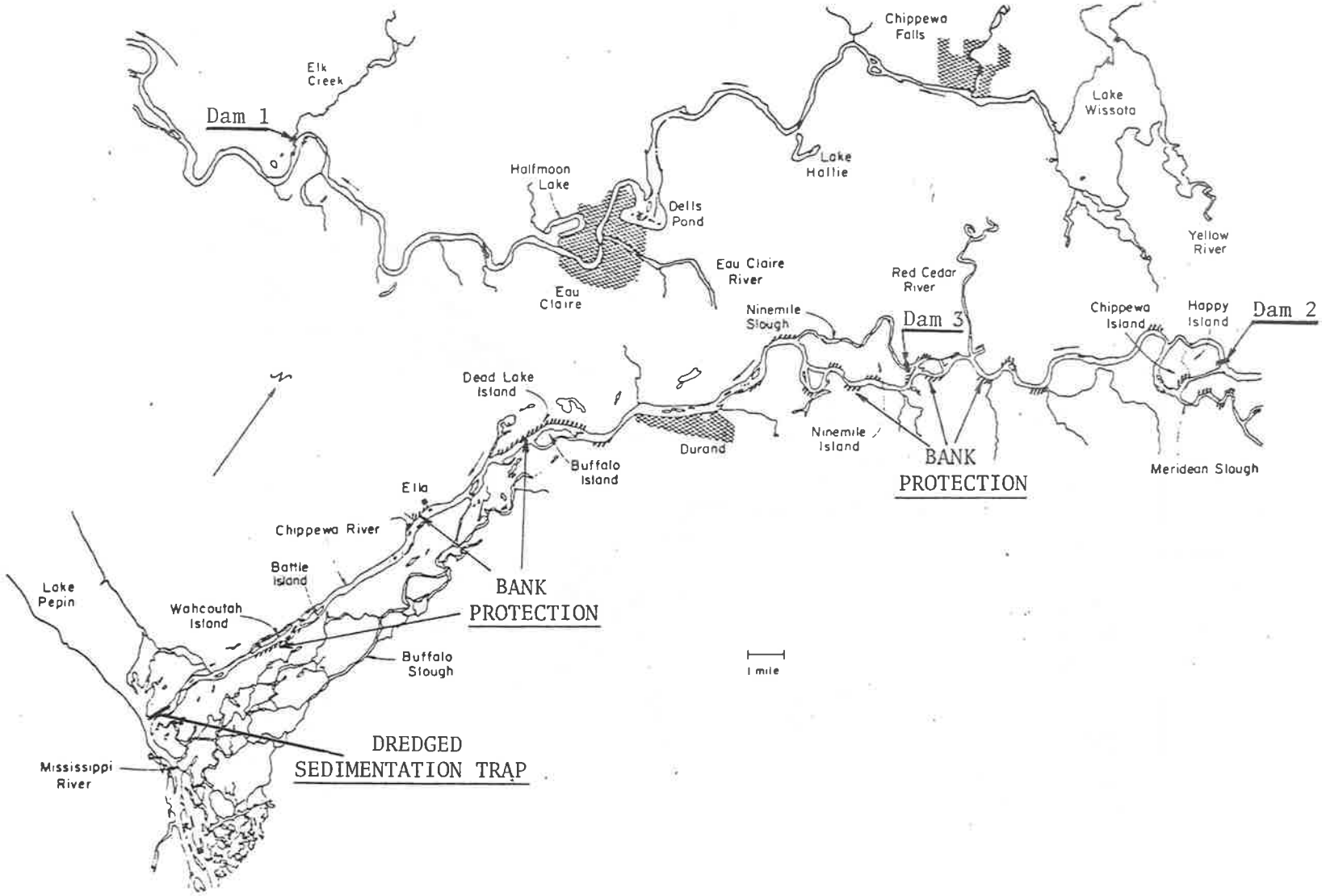

Figure 17.34h Some locations of Alternative 8: Establish Streambank Erosion Controls and dredge a sedimentation trap at the lower end of the Chippewa River.

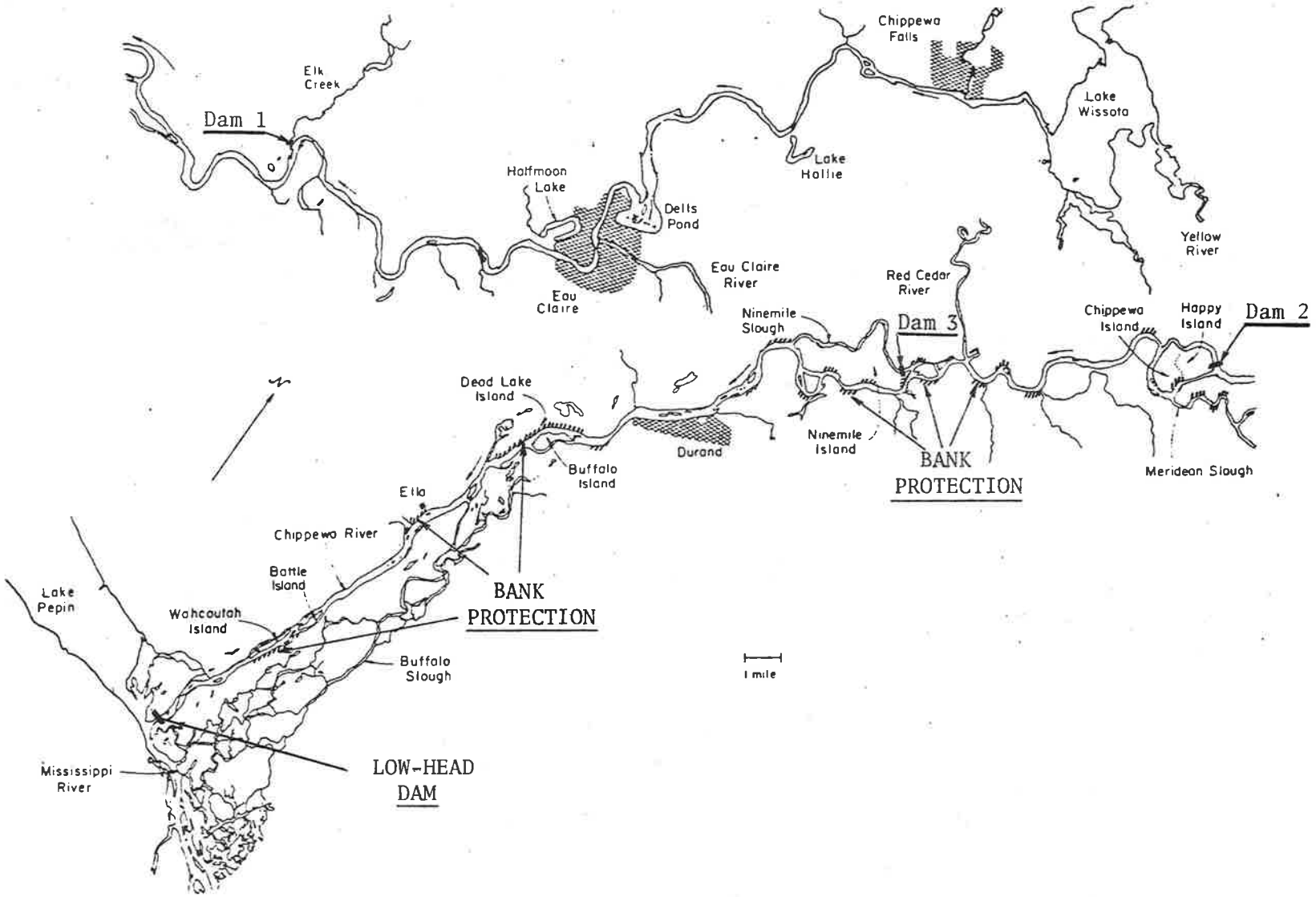

Figure 17.34i Some locations of Alternative 9: Establish streambank erosion controls and supplemental sediment controls and construct a low-head dam at the lower end of the Chippewa River.

The impacts of the alternative measures studied on the physical environment of the Mississippi and Chippewa Rivers are summarized in Table 17.15. The factors considered include: sediment reduction, time required to achieve the reduction, bank stability, geomorphic changes, hydrologic changes, affected areas and dredging requirements. Considering the objectives of development in the Lower Chippewa Basin, the selected alternative measure should decrease bank erosion, decrease sediment supply to the Mississippi, and improve the river basin for recreation, navigation, fish and wildlife resources, agriculture, municipal and industrial purposes. Among the nine alternative measures evaluated, Alternatives 3 (establish a meander pattern below Durand) and 4 (divert a portion of Chippewa flow into Lake Pepin) are considered to be impractical based on the summary information in Tables 17.15 and 17.16. Table 17.16 gives the criteria for evaluation of each alternative. Alternative 1 (increase storage of existing flood control dam) has limited efficiency. Alternative 5 (divert a portion of Chippewa flow into a sedimentation basin) would significantly alter the floodplain characteristics in the Lower Chippewa River Basin and could adversely affect the river environment. Alternative 2 (dredge a sedimentation trap at the Chippewa mouth), 6 (constructs a low-head dam at the Chippewa mouth), 8 (establish stream bank erosion controls and dredge a sedimentation trap at the Chippewa mouth), and 9 (establish streambank erosion controls and construct a low-head dam at the Chippewa mouth) are identified to be technically feasible and warrant further study to assess environmental impacts, and costs and benefits of implementing these alternative measures. The cost derived from the construction and maintenance of the structures and adverse impact on the river environment, against the benefits derived from the reduction in bank erosion, better usage of the river for recreation and navigation, floodplain development, and reduction in the dredging requirement in Pool 4 would be the major factors requiring detailed consideration in finalization of the adopted development plan.

Table 17.15 Summary of impacts of the alternative measures on the physical environment.

Alternative	When Effective	Hydrologic Changes	Affected Area in Chippewa	Sediment Reduction	Dredging Requirement	Channel Stability and Geomorphic Changes	Construction Requirement
Without-Project Condition	N/A	Flow distributions through divided channels would be changed due to changes in channel dimensions. However, these changes should not significantly affect flood stage.	N/A	Because of the increase in channel dimension due to erosion, the sediment supply from the Chippewa River to Pool 4 would be reduced by 12 percent in the next 50 years on the average. This would be a reduction of about 60,000 tons in an average year.	The dredging requirement in Pool 4 would be reduced by 15 percent in the next 50 years, or about 40,000 cu yd in an average year.	1) There would be a 0.7 ft overall aggradation within the main channel of Pool 4 below Lake Pepin during the next ten years; 2) the natural levee along the Pool 4 banks, on the island and near the mouths of backwater areas would grow about 0.3 ft in ten years; 3) Sedimentation in the backwater areas would continue to accumulate at an overall averaged rate of about 0.1 inch per year; 4) Erosion of the Chippewa River would continue. In the next 50 years, the Chippewa flow would erode about 180 acres of floodplain, and the riverbed would degrade about 0.7 ft. This would result in a decrease in channel slope of about 2 percent.	None

Table 17.15 (continued).

Alternative	When Effective	Hydrologic Changes	Affected Area in Chippewa	Sediment Reduction	Dredging Requirement	Channel Stability and Geomorphic Changes	Construction Requirement
Alternative 1: Increase storage of existing flood control dam	Within one year after implementation of the alternative	Reduces the flood peak discharge by 6,000 cfs and flood stage by about 1.5 ft with additional 5-ft storage	Reduces the flood inundated area	15-20% (additional 5-ft storage) 10-15% (additional 2.5-ft storage)	The dredging requirement in Pool 4 would be reduced by 25% in the next 50 years	1)Bank erosion and sediment supply would be reduced; 2) Effect of the reduction would propagate downstream in the Mississippi River at about one mile per year; 3) Dredging requirements and growth of natural levees in the Mississippi River would be reduced proportional to sediment reduction. The sediment reduction from the Chippewa River would become fully effective in the entire Lower Pool 4 reach below Lake Pepin in about 15 years and this would reduce the dredging requirement by about two-thirds of the sediment reduction rate from the Chippewa River; 4) Sedimentation in the backwater areas (mainly Robinson Lake and Bid Lake) would not be significantly reduced except near offtake from the Mississippi	None

Table 17.15 (continued).

Alternative	When Effective	Hydrologic Changes	Affected Area in Chippewa	Sediment Reduction	Dredging Requirement	Channel Stability and Geomorphic Changes	Construction Requirement
Alternative 2: Dredge a sedimentation trap at the lower end of the Chippewa River	Within one year after implementation of the alternate	Not significant	Mainly the disposal site	The annual reduction in the Chippewa sediment supply would approximately equal the weight of the dredged material from the sedimentation trap. A sedimentation trap of 3 ft x 500 ft x 2000 ft (a volume of 117,000 cu yds) would reduce the sediment supply by 218,000 tone in an average year, or by about 43 percent of the present sediment supply	Considering the long-term effect if the sedimentation trap was maintained every year, the dredging requirement in Pool 4 would be reduced about 90 % of the Chippewa sediment reduction. A trap of 3 ft x 500 ft x 200 ft would reduce the requirement by 145,000 cu yds in an average year or about 54% of the present average dredging requirement	1)The deposition in the mainstem of Pool 4 would be reduced depending upon the Chippewa sediment reduction; 2) Sedimentation rates in the backwater areas of Pool 4 would not be significantly affected; 3) Reduction in the Chippewa sediment supply would not significantly affect Pools 5 and 5A unless the reduction was more than 70% of the original supply rate; 4) This alternative would not reduce erosion problems in the Chippewa River	The sediment trap should be maintained yearly

Table 17.15 (continued).

Alternative	When Effective	Hydrologic Changes	Affected Area in Chippewa	Sediment Reduction	Dredging Requirement	Channel Stability and Geomorphic Changes	Construction Requirement
Alternative 3: Establish a meander pattern in the Chippewa River below Durand (Figure 10)	Slowly develop	Minor	Affect the flood-plain area along the new channel	15% reduction	The dredging requirement in Pool 4 would be reduced by about 25 percent in the next 50 years	1) Sinuosity of the new river reach would increase from 1.06 to 1.2 and the slope would decrease from 1.76 to 1.55 feet/mile; 2) Impact on the Mississippi River would be minor	The Chippewa River at the upper end of the proposed meander channel should be dredged to form a meander loop. Also the meander channel during developing period should be carefully monitored and maintained

Table 17.15 (continued).

Alternative	When Effective	Hydrologic Changes	Affected Area in Chippewa	Sediment Reduction	Dredging Requirement	Channel Stability and Geomorphic Changes	Construction Requirement
Alternative 4: Divert a portion of the Chippewa River flow into Lake Pepin]	Within one year after implementation of the alternative	Reduce flow downstream of diversion and increase flow in Lower Lake Pepin	Affect about 100 acres of forest and wetland along the diversion channel	Twice the sediment diversion rate in 1st year but reduce to the diversion rate in about the 7th year	The dredging requirement in Pool 4 would be reduced by about 90% of the Chippewa sediment reduction	1) The floodplain along the diversion channel would be affected; 2)Aggradation would occur upstream of dam and near the lower end of the Chippewa at a rate of about 0.2 ft/year; 3) degradation would occur immediately below the dam; 4)Deposition would occur in the diversion channel and in Lake Pepin near the channel mouth; 5) Changes in the Mississippi River would be similar to Alt. 1; 5) Provide minor bank protection in the Chippewa River below the diversion dam	A diversion dam and diversion channel should be constructed and maintained
Alternative 5: Divert a portion of the Chippewa River flow into a sedimentation basin (Figure 14)	Within one year after implementation of the alternative	Reduce flow downstream of diversion and increase flow in Buffalo Slough	Immediate about 3,000 acres of forest land along Buffalo Slough below river mile 4 at intermediate flow if 30% was diverted. At high flow about 8,000 acres along Buffalo Slough would be inundated	Twice the sediment diversion rate in 1st year but reduce to the diversion rate in about the 7th year	The dredging requirement in Pool 4 would be reduced by about 90% of the Chippewa sediment reduction	1) Buffalo Slough would become active; 2) Excess water could refresh the affected area initially but the area could deteriorate as the sediment inflow continued; 3) Other changes would be similar to Alt. 1, and 1, 2, and 5 of Alternative 4	A diversion dam and diversion channel should be constructed and maintained

Table 17.15 (continued).

Alternative	When Effective	Hydrologic Changes	Affected Area in Chippewa	Sediment Reduction	Dredging Requirement	Channel Stability and Geomorphic Changes	Construction Requirement
Alternative 6: Construct a low-head dam at the lower end of the Chippewa River.	Within one year after construction.	With a 10-ft dam in place, the flood peak would be raised 2.2 ft for an average flood and 3.5 ft for a 100-year flood.	The increase in flood stage would extend to river mile 6 upstream of dam and inundate an additional 1,100 acres of forest and marsh land. In the long term, the effect could extend upstream to Durand due to sediment deposition upstream of the dam.	A 10-ft dam would reduce the Chippewa sediment supply by 55 percent while a 6 ft dam would reduce the supply by 40 percent for a short period after construction of the dam. The effectiveness of the low-head dam would be reduced by half over 40 years compared to the without project condition, if the sediment deposited upstream of the dam was not removed. This would result in a reduction of about 170,000 tons/yr for the 10 ft dam compared to the present sediment supply in an average year. This is about 34 percent of the present sediment supply in an average year.	In the long-term the dredging requirement in Pool 4 would be reduced by about 90 percent of the amount of Chippewa sediment reduction. For example, a 10 ft dam would reduce the dredging requirement by about 113,000 cu yds. This is about 43 percent of present dredging if the sediment deposited upstream of the dam was not removed.	1) The deposition in Pool 4 would be reduced due to decreases in the Chippewa sediment supply, while Pool 5 and 5A would not be significantly affected by this alternative; 2) Floodplain erosion in the Chippewa River basin below river mile 9 would be reduced by 22 percent or by about 40 acres compared to the without project condition; 3) the Chippewa River upstream of mile 9 would remain essentially the same as the without project condition; 4) Deposition would occur behind the dam. The height of sediment deposition would be about 6/10 of the dam height.	Natural crushed rock at least 8 inches or soil-cement rocks at least 1 ft in size could be utilized to construct the low-head dam. The material required for constructing a 6 ft dam and a 10 ft dam would be approximately 500 cu yds and 2000 cu yds respectively. The dam should be maintained and the sediment deposited above the dam should be removed in order to maintain the original efficiency of this alternative.

Table 17.15 (continued).

Alternative	When Effective	Hydrologic Changes	Affected Area in Chippewa	Sediment Reduction	Dredging Requirement	Channel Stability and Geomorphic Changes	Construction Requirement
Alternative 7: Construct a series of low-head dams on the lower Chippewa River.	Within one year after construction.	The proposed dams would block about one-half of the bank-full area at dam sites, and in turn would raise flood stage 2-3 ft above the normal flood stage for an average flood and 3-4 ft for a 100 year flood. Because of the erosion and deposition sequence caused by dams, the channel slope would be reduced by about 20 percent in 40 years. This would reduce local velocity by about 10 percent and could affect propagation of flood water.	The increase in flood stage would inundate an additional 2,430 acres of the lower Chippewa floodplain including about 2,100 acres of forest land and 330 acres of farmland.	The sediment reduction caused by the four dam case would be about 3 percent more than that caused by Alt. 6.	The reduction in dredging requirement caused by the four dam case would be about 3 percent more than that for Alt. 6.	1) Effects on geomorphology of the Mississippi River would be similar to that caused by Alt. 6; 2) the dams would reduce erosion upstream of the dams but would increase erosion downstream of dams. The overall decrease in floodplain erosion would be about 25 percent or about 45 acres; 3) the erosion and deposition sequence caused by dams would reduce the channel slope by about 25 percent in 40 years.	Dams could be constructed using 8-inch natural crushed rock or 1-ft soil-cement rock. The material required for construction would be 2,000--4,000 cu yds for the series of dam studied. The dams should be maintained and the sediment deposited above the dam should be removed in order to maintain the original effectiveness of this alternative.

Table 17.15 (continued).

Alternative	When Effective	Hydrologic Changes	Affected Area in Chippewa	Sediment Reduction	Dredging Requirement	Channel Stability and Geomorphic Changes	Construction Requirement
Alternative 8: Establish streambank erosion controls and dredge a sedimentation trap at the lower end of the Chippewa River	Within one year after construction.	Depends on the type of erosion control structures. The dredged sedimentation trap would not significantly affect hydrologic variables. However, the dredged bed material disposed on the floodplain would affect the adjacent floodplain area.	Depends on the type of erosion control structures. The dredged sedimentation trap would not significantly affect hydrologic variables. However, the dredged bed material disposed on the floodplain would affect the adjacent floodplain area.	If the protective works and the sedimentation trap were maintained every year, this alternative would reduce the Chippewa sediment supply by about 15 percent plus an amount equal to the weight of dredged material from the sedimentation trap, compared to the without project conditions. For example, a cut 500 ft wide, 2,100 ft long and 3 ft deep would reduce the sediment supply by 275,000 tons/yr or by about 55 percent of the present supply.	In the long term, the dredging requirement in Pool 4 caused by dredging a 500 ft, 2,100 ft x 3 ft sedimentation trap at the lower end of the Chippewa River would be 247,000 tons/yr. This is a reduction of about 69 percent of the current dredging quantity.	1) Effects on geomorphology of the Miss. River would be similar to that caused by Alt. 2 but to a larger degree; 2) Protection of the nine identified erosion sites would save 60 acres of the Chippewa floodplain from erosion, or about 30% of the total floodplain areas to be eroded in the next 50 years if river banks were not protected; 3) The Chippewa River would degrade about 1.1 ft in the next 50 years. This would cause a reduction in bed slope of about 0.06 ft/mile or a reduction in slope of 3%.	The erosion control structures should be properly designed, constructed and maintained. Also, the sedimentation trap should be redredged periodically.

Table 17.15 (continued).

Alternative	When Effective	Hydrologic Changes	Affected Area in Chippewa	Sediment Reduction	Dredging Requirement	Channel Stability and Geomorphic Changes	Construction Requirement
Alternative 9: Establish stream-bank erosion controls and construct a 10-ft low-head dam at the lower end of the Chippewa River	Within one year after implementation of the alternative.	Similar to Alt. 6.	Similar to Alt 6.	In the long term, the Chippewa sediment supply would be reduced by 40 percent compared to the without-project conditions if the deposited sediment upstream of dam was not removed. The reduction would total about 260,000 tons/yr or about 52 percent of the present sediment supply.	In the long term, the dredging requirement would be reduced by 173,000 cu yds/yr, or about 65 percent of the original dredging requirement.	1) Effects on geomorphology of the Miss. River would be similar to that caused by Alt. 6; 2) Protection of the nine identified erosion sites would save 60 acres from erosion; 3) the Chippewa River would degrade about 1 ft in the next 50 years, except immediately upstream of the dam where the deposition height would be about 6 ft.	Bank erosion control structures and the low-head dam should be properly designed, constructed and maintained.

Table 17.16 Criteria for evaluation of alternative measures.

		ALTERNATIVE								
		1	2	3	4	5	6	7	8	9
Efficiency on reduction in sediment supply and dredging requirement	Good		✓		✓	✓	✓	✓	✓	✓
	Fair	✓								
	Poor			✓						
When effective	Immed.	✓	✓		✓	✓	✓	✓	✓	✓
	Slowly			✓						
Bank erosion improvement	Major								✓	✓
	Fair	✓								
	Minor			✓	✓	✓	✓			
	No		✓							
	Incr.			✓			✓	✓		✓
	No		✓						✓	
	Decr.	✓								
Affected area	Large			✓		✓	✓	✓		✓
	Small	✓	✓		✓				✓	
Recommendations on future study	Yes		✓				✓		✓	✓
	No	✓		✓	✓	✓		✓		

17.6 REFERENCES

Chow, V. T., 1959. Open Channel Hydraulics, McGraw Hill Book Company.

Franco, J. J., 1967, "Research for River Regulation Dike Design," Journal of Waterways and Harbors Division, ASCE, Vol. 93, No. WW3, August, pp. 71-87.

Golubtsov, V. V., 1969, "Hydraulic Resistance and Formula for Computing the Average Flow Velocity of Mountain Rivers," Soviet Hydrology: Selected papers, Issue No. 5.

Kennedy, J. F., 1961, "Stationary Waves and Antidunes in Alluvial Channels," California Institute of Technology Report KH-R-2, Pasadena, California.

Li, R. M.; Simons, D. B.; Ward, T. J.; and Steele, K. S., 1977, "Hydraulic Model Study of Flow Control Structures, Phase I Report," prepared for USDA Forest Service, Angeles National Forest, Pasadena, California and Rocky Mountain Forest and Range Experiment Station, Flagstaff, Arizona.

Liu, M. K.; Chang, F. M.; and Skinner, M. M., 1961, "Effect of Bridge Construction on Scour and Backwater," Department of Civil Engineering, Colorado State University, Report No. CER60MKL22, February.

Mamak, W., 1964, "River Regulation," Dept. of the Interior and the National Science Foundation, Washington, D.C.

Matthai, H. F., 1968, "Magnitude and Frequency of Floods in the United States," Part 6-B, Missouri River Basin below Sioux City, Iowa, U.S. Geological Survey Water-Supply Paper 1680.

Matthai, H. F., 1969, "Floods of June 1965 in South Platte River Basin, Colorado," U.S. Geological Survey Water-Supply Paper 1850-B.

Richardson, E. V.; Simons, D. B.; Karaki, S.; Mahmood, K.; and Stevens, M. A., 1975, "Highways in the River Environment--Hydraulic and Environmental Design Considerations," Training and Design Manual prepared for U.S. Department of Transportation, Federal Highway Administration, Department of Civil Engineering, Colorado State University, Fort Collins, Colorado.

Simons, D. B., 1957, "Theory and Design of Stable Channels in Alluvial Material," Ph.D. Dissertation, Department of Civil Engineering, Colorado State University, Fort Collins, Colorado.

Simons, D. B., 1975, "Study of Bijou Creeek on the Narrows Unit near Fort Morgan, Colorado," prepared for USDI Bureau of Reclamation.

Simons, D. B., Al-Shaikh-Ali, K. S., and Li, R. M., 1979, "Flow Resistance in Cobble and Boulder Riverbeds," Journal of the Hydraulics Division, Proceedings of the American Society of Civil Engineering, Vol. 105, No. HY5.

Simons, D. B. and Chen, Y. H., 1978, "Erosion Control Measures for the Erosion Demonstration Program," Lower Chippewa River Basin, for U.S. Army Engineering District, St. Paul, Minnesota, March.

Simons, D. B. and Li, R. M., 1978, "Design of Supply Canals of Diversion Structure Nos. 1 and 2 of Wadi Mawr Canal System," prepared for Tipton and Kalmbach, Inc., Denver, Colorado.

Simons, D. B. and Li, R. M., 1979, "Erosion, Sedimentation and Debris Analysis of Proposed Boulder Creek Floodway," URS Company, Denver, Colorado.

Simons, D. B. and Li, R. M., 1979, "Erosion, Sedimentation and Debris Analysis of Do-Nothing Condition, Boulder Creek," URS Company, Denver, Colorado, March.

Simons, D. B. and Richardson, E. V., 1971, "Flow in Alluvial Sand Channels," Chapter 9, River Mechanics, edited and published by H. W. Shen, Colorado State University, Fort Collins, Colorado.

Simons, D. B. and Sentürk, F., 1977, "Sediment Transport Technology," Water Resource Publications.

Stevens, M. A.; Simons, D. B.; and Lewis, G. L., 1974, "Safety Factors for Riprap Protection," paper presented at the 1974 ASCE Meeting in Montreal, Canada, July 15-19.

U.S. Army Corps of Engineers, 1976, "HEC-2 Water Surface Profiles," Programmers Manual. Hydroligic Engineering Center.

U.S. Army Corps of Engineers, 1976, "HEC-6 Scour and Deposition in Rivers and Reservoirs," Users Manual, Hydrologic Engineering Center.

U.S. Army Corps of Engineers, 1977, "Water and Related Land Resources Management Study Metropolitan Denver and South Platte River and Tributaries, Colorado, Wyoming and Nebraska," Vol. V Supporting Technical Reports Appendices, Appendix H-Hydrology.

U.S. Bureau of Reclamation, 1958, "Hydraulic Design of Stilling Basins and Energy Dissipations," Engineering Monograph No. 25, Technical Information Branch, Denver, Colorado.

U.S. Bureau of Reclamation, 1965, "Sediment Study without Bijou Creek Diversion into Narrows Reservoir," Narrows Unit, Colorado, MRBP.

U.S. Department of the Interior, Bureau of Reclamation, 1960, "Investigation of Meyer-Peter, Müller Bedload Formula," Sedimentation Section, Hydrology Branch, Division of Project Investigations.

Winkley, B. R., 1971, "Practical Aspects of River Regulation and Control," Chapter 19, River Mechanics, edited and published by H. W. Shen, Colorado State University, Fort Collins, Colorado.

CHAPTER 18

DEGRADATION AND AGGRADATION ANALYSIS

by

Ruh-Ming Li, Associate Professor, Department of Civil Engineering, Colorado State University, Fort Collins, Colorado
Daryl B. Simons, Associate Dean for Engineering Research and Professor of Civil Engineering, Colorado State University, Fort Collins, Colorado

18.1 INTRODUCTION

The river is a dynamic ecological system and its boundary is subjected to change due to processes of aggradation and degradation. The degradation and aggradation may alter the stream form and pattern, cause additional flood hazards, loss of primary farmland, endanger fish, reduce recreational value, and induce other environmentally adverse impacts. The degradation and aggradation is an integral part of stream channel response to precipitation, flow, and man's activities. The basic tools required to conduct an analysis are discussed in Chapters 2 to 15. This chapter presents four selected studies specific to the degradation and aggradation problems. The first study presented is a degradation analysis below a dam located in the T or C, Williamsburg Watershed, New Mexico (Simons and Li, 1978a). The second study is an erosion and sedimentation analysis of San Juan Creek near Conrock Gravel Pit, Orange County, California (Simons and Li, 1978b). The third example deals with a degradation analysis associated with the pipeline crossings at the Jim River, Alaska (Water and Environment Consultants, Inc., 1974), and the fourth example is an analysis of sediment movement in the Muskegon River following the removal of Newaygo Dam (Water and Environment Consultants, Inc., 1978). These four examples illustrate an array of degradation and aggradation problems that hydraulic engineers often encounter.

18.2 DEGRADATION BELOW A DAM--T OR C, WILLIAMSBURG WATERSHED, NEW MEXICO

General

Presented in this section is an analysis of degradation below the emergency spillway chute of the Site 8C,T or C, Williamsburg Watershed, New Mexico. The structure proposed by the Soil Conservation Service is a single-purpose flood retarding structure. The dam will be located in Mud Springs Canyon about one mile upstream from Williamsburg and about one and one-half miles from its confluence with the Rio Grande (USDA Soil Conservation Service, 1977).

The analysis involves the determination of the magnitude of degradation to be expected downstream from the emergency spillway chute during passage of the design hydrograph. Such an analysis is required to determine how far the baffled outlet end of the chute must extend

below the present channel grade to accommodate degradation. In order to provide enough information for an adequate design three different conditions that depict the future water and sediment inflows to the dam prior to the occurrence of the freeboard hydrograph were considered in this study.

Case I considers that the reservoir is 90 percent filled with sediment resulting from a series of small floods, prior to the occurrence of the freeboard hydrograph. These small floods pass all of the flow through the principal spillway. The degradation due to the freeboard hydrograph would be negligible and the total expected scour depth below the structure is equal to the general scour depth resulting from the flows through the principal spillway.

Case II assumes that immediately following the closure of the dam, the water storage has reached the top of the dam (EL.4880.5') and the sediment storage capacity has enough room for the sediment yield associated with the freeboard hydrograph. Under this condition, the emergency spillway chute would pass the freeboard hydrograph with essentially clear water. This is because nearly all of the sediment will be trapped upstream of the flood retarding structure.

The third condition, Case III, represents the worst possible condition which assumes that after 85 years of operation, two 50-year floods and one 100-year flood occur prior to the passing of the freeboard hydrograph. The total expected scour is the sum of the general scour due to flows through the principal spillway for 85 years of operation and the general and local scour resulting from a sequence of two 50-year floods, one 100-year flood and the freeboard hydrograph. This condition is very unlikely to occur, yet constitutes the worst possible condition in determining the degradation below the emergency spillway structure.

The determination of the change in sediment storage is vital for the evaluation of both Case I and Case III. This requires the estimation of the annual sediment yield and sediment yields resulting from various sizes of storms on the watershed. The sediment yield is determined by a combination of the Universal Soil Loss Equation modified by Williams (1975) and the Meyer-Peter, Müller bedload equation (USBR, 1960).

The magnitude of scour is determined utilizing a sediment routing procedure that considers the size fractions of bed material. This computational procedure involves use of a sediment transport equation, the sediment continuity equation, the armoring effect of coarse materials, and channel geometry equations. Hence, the mathematical model is developed according to physical principles governing water and sediment transport, degradation and armoring processes. Both the local scour immediately below the structure and the general scour pivoting from a downstream control point are considered in the analysis.

Assuming the downstream control is located at the confluence with the Rio Grande (Station 161 + 70), a scour depth from the present level of 15.1 ft. is expected for the Case I condition. Under Case II, the total scour depth from the present level is 18.9 ft. For the worst condition of Case III, the estimated scour depth from the present bed level is 34.7 ft. In this case, the lowest bed elevation after experiencing the design floods is 4352.3 ft.

Mathematical Model

Spatial Designation: The general layout and topographic map of the study site is given in Figure 18.1. The dam will be constructed of clayey sand and gravel and will be about 88 feet high with a 20 foot top width and a crest length of approximately 1920 feet. This would provide storage that would extend at least 3100 ft. upstream of the dam. With this length of reservoir and noting that the median bed material diameter is 10 mm, nearly all of the incoming sediment will deposit upstream of the structure, unless the reservoir is filled with sediment. The principal spillway as planned is a 3'-0" x 4'-0" reinforced concrete box conduit, without control gates. The principal spillway is designed to pass a maximum flow rate of 400 cfs. If the structure functions properly, floodwater resulting from a 100-year flood would be stored in the reservoir temporally and would slowly pass through the principal spillway. The emergency spillway consists of a concrete baffled chute having a width of 200 feet, a depth of 12.1 feet, and a crest elevation of 4468.4 feet. The side walls of the baffled chute were designed to accommodate a freeboard hydrograph discharge of 25,057 cfs, and the blocks designed for two-thirds of the freeboard discharge, 16,700 cfs (USDA Soil Conservation Service, 1977).

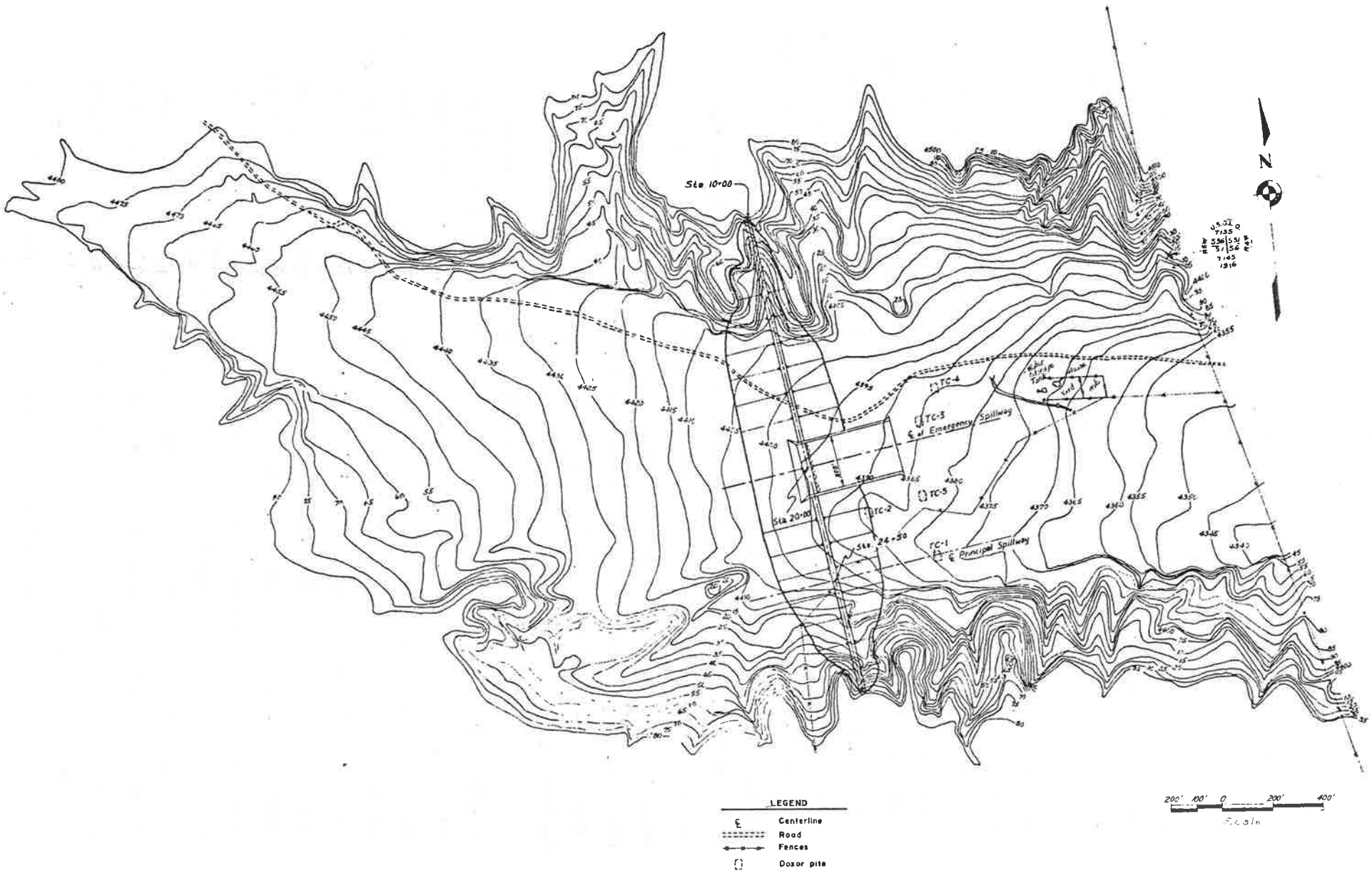

Figure 18.1 General layout and topographic map.

The proposed reservoir has a storage capacity of 2297 ac-ft. Of this, 830 ac-ft are provided to store 100 years of sediment supply and 1467 ac-ft are for the flood water storage for the 100-year flood with 24 hours duration. Assuming 90 percent trapping efficiency of the reservoir, a maximum sediment storage capacity of 2067 ac-ft can occur.

The stability of the emergency spillway baffled chute requires that it be designed so that the ultimate scour during the passage of the freeboard hydrograph does not cause the failure of the structure. The purpose of the degradation study is to determine the ultimate scour below the baffled chute for the freeboard discharges so that proper design measures can be taken to assure the stability of the structure. This requires estimating both the local scour immediately below the structure and the general scour pivoting from a downstream control point. A mathematical model was developed to simulate these scour processes. The spatial arrangement of the structure for analysis utilizing the mathematical model is given in Figure 18.2.

Temporal Representation: In order to provide enough information for an adequate design, three conditions representing different sequences of water and sediment inflows to the dam prior to the occurrence of the freeboard hydrograph were considered. These three conditions are outlined in Section 18.2. For determining sediment inflow rates, an analysis of sediment yield is necessary.

The estimated annual sediment yield utilizing the procedure recommended by Agricultural Research Service (1976) is 8.4 acre-feet which is close to 8.3 acre-feet estimated by USDA Soil Conservation Service. However, the total sediment yield consists of both wash load and bed material load. The procedure recommended by Agricultural Research Service (1976) gives the estimation of sediment yield for particles smaller than 2.0 mm. This size of particle is essentially the upper bound of the wash load considering the measured material size distribution for the watershed under investigation. Therefore, the total annual sediment yield should exceed 8.4 acre-feet.

The sediment yields from floods of various return periods were estimated using a combination of the Universal Soil Loss Equation Modified by Williams (1975) and the Meyer-Peter, Müller bedload sediment transport equation. The former relation determined the washload yield and the latter estimated bed material load. The computed results

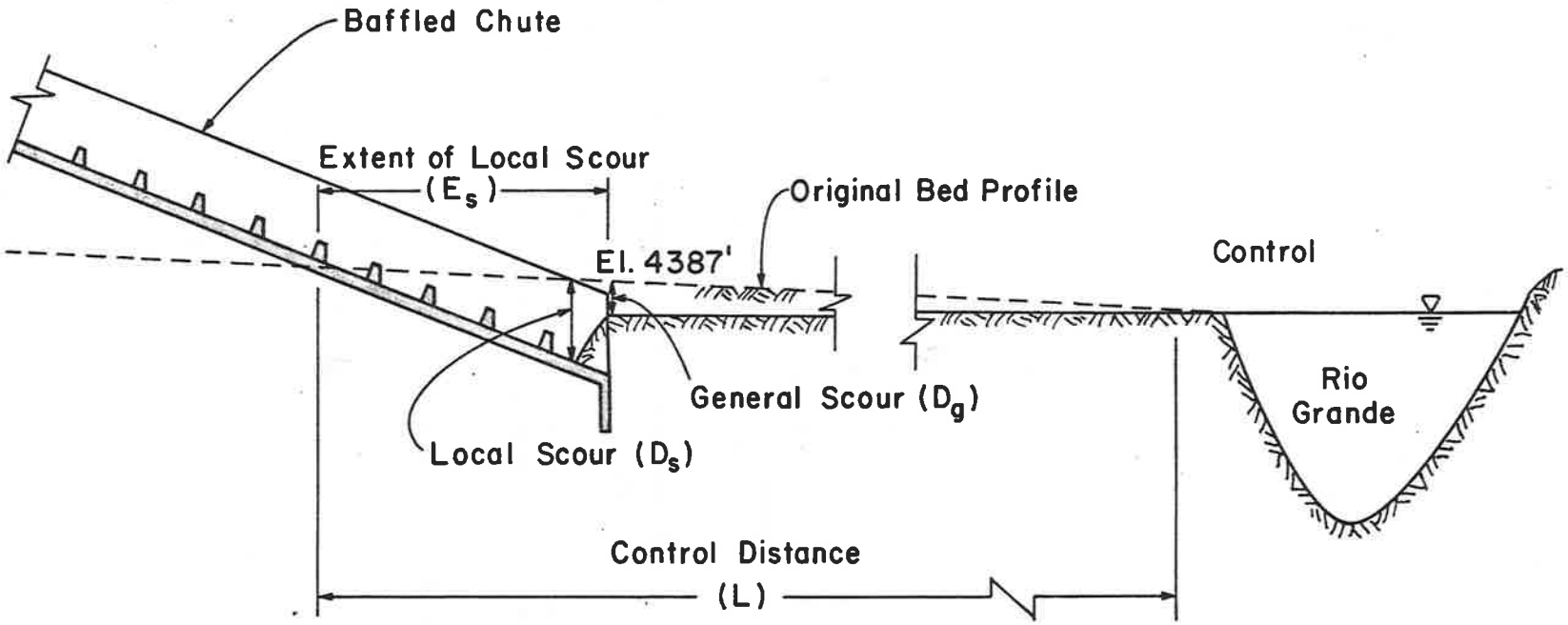

Figure 18.2 Spatial designation of the scour.

are tabulated in Table 18.1. The average ratio of the washload sediment yield to the bed material load sediment yield is 2.24, which is close to 1.78 determined by the ratio of availability of the washload to the bed material load indicated in the New Mexico Agricultural Experiment Stateion Research Report AES-RP-233.

Table 18.1 Sediment yield computation.

Return Period (Yr.)	Runoff Volume* (Ac-Ft)	Runoff Peak** (cfs)	Washload (Ac-Ft)	Bed Material Load (Ac-Ft)	Total Yield (Ac-Ft)
2	279.3	704.5	6.4	4.3	10.7
5	633.7	1598.5	15.9	9.7	25.6
10	913.0	2303.1	23.9	14.0	37.9
25	1310.4	3305.5	35.9	20.0	55.9
50	1621.9	4091.3	45.6	24.7	70.3
100	1976.4	4985.6	56.9	29.9	86.8
Design Storm Inflow Hydrograph	12265.0	30939.1	439.4	176.0	615.4

Note:

*Runoff volumes for the various return periods are 24 hr. design storms.

**Runoff peaks are estimated by scaling runoff volumes according to the ratio of the peak flow to the runoff volume of the design storm inflow hydrograph.

The median size of flood was determined to have a return period of 2 years. Assuming that the annual rainfall in the watershed is 10 inches, and that 4.2% of the rainfall becomes direct runoff considering the weighted mean of various sizes of storms, the annual runoff volume can be estimated as 451 ac-ft. Therefore, on the average, there will be approximately 1.61 floods equivalent to the median size flood within a year. Thus, the annual sediment yield can be estimated to be 17.2 ac-ft. With the above information, the temporal design of Case I, II, and III can be made.

Case I considers that the reservoir has filled with sediment to the maximum storage capacity prior to the occurrence of the freeboard

hydrograph. It would take approximately 120 years to trap about 2067 ac-ft sediment in the reservoir. During this period, all flows pass through the principal spillway and are capable of inducing general scour only. When passing the freeboard hydrograph, the magnitude of scour would not be significantly increased because the sediment would also be delivered through the emergency spillway. This case would cause the smallest scour depth below the structure.

Case II assumes that immediately following the closure of the dam, the water storage has reached the top of the dam (EL.4480.5') and the sediment storage capacity has enough room for the sediment yield associated with the freeboard hydrograph. The potential sediment yield for the freeboard hydrograph is 615 ac-ft which is smaller than the reservoir sediment storage capacity of 2067 ac-ft. In this case, the temporal representation is limited to passing the freeboard flood. The design flood has a peak discharge of 25,057 cfs and a duration of 18 hours.

The third condition, Case III, simulates the worst condition which may occur. This assumes that after accumulating approximately 1462 ac-ft of sediment for a period of 85 years, two 50-year floods and one 100-year flood occur prior to the passing of the freeboard hydrograph. These two 50-year floods, one 100-year flood plus the design storm inflow hydrograph would reach the sediment storage capacity of 2067 ac-ft. The total expected scour depth is the sum of the general scour due to flows through the principal spillway for the 85-year period and the general and local scour resulting from a sequence of two 50-year floods, one 100-year flood and the freeboard hydrograph. This condition is very unlikely to occur, yet constitutes the worst possible condition in determining the magnitude of the degradation below the emergency spillway structure.

Governing Processes: The scour below a hydraulic structure is a complex problem. The dominant physical processes include water discharge, sediment transport, sediment routing, degradation, and armoring by sorting the smaller sizes of sediment from the coarse material. These processes are unsteady in nature. In order to simplify the problem, a known discharge model is used (see Chapters 6 and 12). The known discharge solution is appropriate in this study because of the

short distance considered in the spatial arrangement of the structure and the channel.

The estimation of scour is made utilizing a procedure that routes sediment considering size fractions. This procedure includes the use of a bedload sediment transport equation for gravel streams (Meyer-Peter, Müller Bedload Formula, USBR, 1960), the sediment continuity equation, the sediment supply equation, and the channel geometry equation (see Chapter 10). Only the bed load transport is considered. For flow through the principal spillway, only general scour is considered. For flow past the emergency spillway both local and general scour must be determined. The local scour and the general scour are simulated interactively in a sequential manner within a time step. The time step used in the simulation is 15 minutes.

The baffled chute is usually designed to achieve an exit velocity less than the critical velocity (Peterka, 1963). For a conservative estimation, a critical flow velocity is assumed for the terminal velocity. Because the current downstream channel is fairly steep (S = 0.026), the flow will reach normal depth in a short distance. If the downstream channel is eroded sufficiently flat, the flow from the baffled chute will join the downstream tailwater with approximately the normal flow depth as the water level.

Channel Morphology

Based on the available information, the following information on channel morphology is derived for use in the mathematical model.

Representative Downstream Channel Cross Section: The representative cross section in the vicinity of the study site was developed by considering the surveyed channel cross sections which are upstream of the crossing of I-25 near Station 125 + 70. The channel cross sections below this point are too wide and shallow. For a simple and conservative analysis, it is expedient to use the data upstream of the intersection of I-25.

Figure 18.3 shows the relationship between the wetted perimeter, P, and the cross-sectional area, A, for the five sections. The representative relation considering these five cross sections is

$$P = 12.7\ A^{0.48} \qquad (18\text{-}1)$$

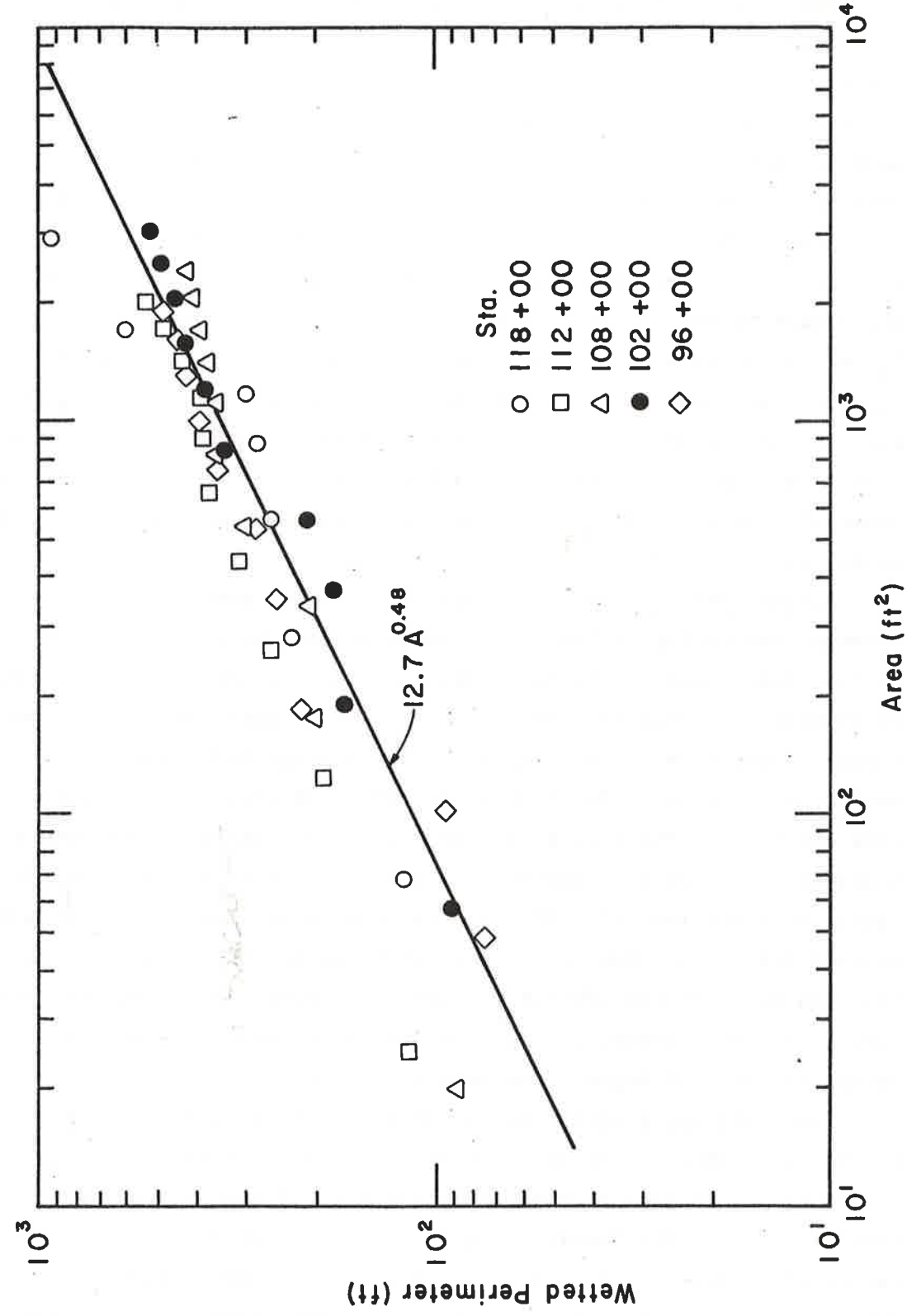

Figure 18.3 Wetted perimeter versus flow cross-sectional area relation.

Representative Bed Material Size: The bed material samples were collected upstream of the crossing of I-25 near 125 + 70 and within the potential scour area. The measured samples verified a highly heterogeneous distribution of bed material with respect to channel location and soil depth. Judging from the location of samples, sampling depth, and the range of sizes of bed material, it is concluded that Sample No. TC-3.1 taken at Pit TC-3 is the most logical choice for the representative bed material size because the median diameter and gradation coefficient for sample No. TC-3.1 are respectively D_{50} = 6.0 mm and σ = 5.9, which are very close to the average of D_{50} = 6.4 mm and σ = 5.8 considering all samples. Figure 18.4 gives the representative bed material size distribution. The maximum particle size is assumed to be 100 mm. The field investigation confirmed that the above size distribution is a conservative estimate for determining scour potential.

Channel Bed Slope and Control: The current slopes of channel between consecutive stations were computed and the present channel bed profile downstream of the dam found to be fairly uniform to the crossing of Highway I-25 near Station 125 + 70. The channel bed slope becomes flatter downstream of this station. The average bed slope for the entire study reach (from 92+00 to 161+70) is 0.024. For a conservative estimation, the representative channel bed slope before general degradation occurs is assumed to be 0.026. This is the average slope upstream of station 127 + 70. The friction slope may be less than the channel bed slope. However, for a safer design, it is assumed that the friction slope of the downstream channel is equal to the channel bed slope. In other words, the friction slope of the downstream channel before the general degradation occurs is 0.026.

Flow Resistance Coefficient: Considering the stream power and the median diameter, the bed form of the channel is likely to be in the upper regime having essentially a plane bed (see Simons and Sentürk, 1977). The Manning roughness coefficient for a plane bed ranges from about 0.017 to 0.027. According to Chow (1959), the Manning roughness coefficient is 0.025 for the channel pattern and bed material sizes presented in the study reach. Furthermore, the Manning roughness coefficient is about 0.024 using the Strickler Formula (Simons

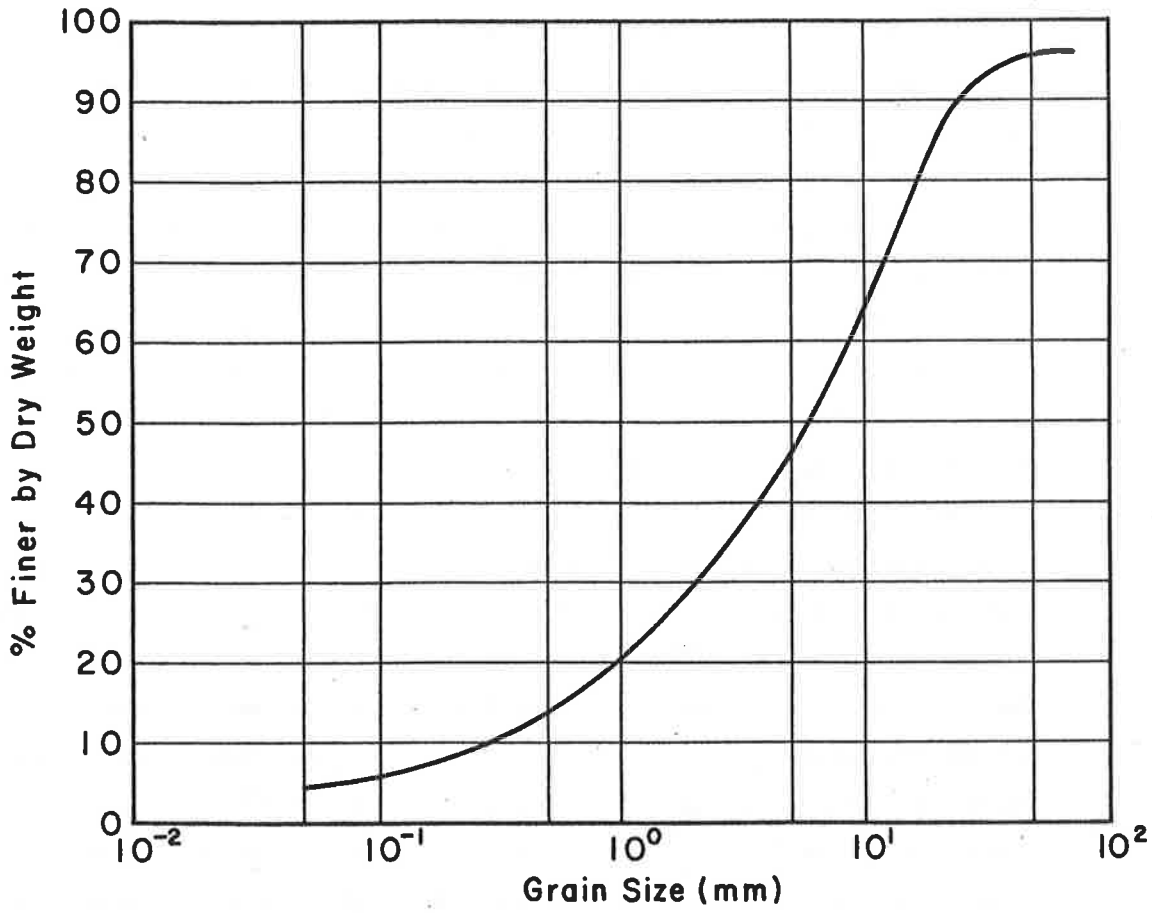

Figure 18.4 Representative bed material size distribution.

and Sentürk, 1977). It is determined that a Manning roughness coefficient of 0.025 is satisfactory for analysis.

Results of Analysis

The analysis shows that the ultimate scour depth is dependent on the water and sediment inflows to the reservoir prior to the occurrence of the freeboard hydrograph. Three cases defined in the temporal design were studied. The results demonstrate that the total scour depth for Case I is 15.1 ft after about 120 years of operation. For Case II, the passage of the freeboard hydrograph will cause a local scour of D_s = 18.9 ft below the present bed level (EL. 4387), and the corresponding length E_s of local scour will be 85.2 ft (see Figure 18.2). Considering the effect of the assumed control at Station 161 + 70 (6970 ft. from the structure), the general scour depth will be D_g = 6.5 ft. The resultant mean particle sizes in the local scour hole and in the downstream channel will be about 25 mm and 11 mm, respectively. The final channel bed gradient indicated is 0.025.

Figure 18.5 shows the time-lapse change of local and general scour. Note that the local scour depth defined in this study is measured from the present bed level. This local scour depth represents a combination of general scour and local scour according to definitions presented in some publications. Thus, the lowest expected bed level resulting from the spillway design flood is 4368.1 ft. This condition is not the worst condition considering scour potential.

The worst possible condition assumes that after 85 years of reservoir operation, two 50-year floods and one 100-year flood occur prior to the passing of the freeboard hydrograph. The 50-year floods and 100-year floods passing the spillway were scaled according to the design freeboard hydrograph utilizing runoff volumes. The assumed sequence of hydrographs after 85 years of operation is shown in Figure 18.6. The general scour due to an 85 year operation is determined to be 12.0 ft. The local scour depth resulting from the assumed sequence of hydrographs will be 22.7 ft, and the corresponding length of local scour will be 102.0 ft. The ultimate scour depth for this worst condition will be 34.7 ft. In this case, the lowest bed elevation after experiencing the design floods is 4352.3 ft. If the control of local scour is desired, an armor layer of rocks with size larger than 1.5 ft and with a thickness of two rock diameters is required to pave an area approximately 100 ft long downstream of the structure and 12 ft below the present bed level. This size of riprap was determined using the Shield's criterion of incipient motion (Simons and Sentürk, 1977) and considering a safety factor of 1.5. The determination was based on the peak flow rate of the freeboard hydrograph. This peak flow rate will induce a tractive force of 5.02 lb/ft^2, which will cause motion of sediment particles smaller than 1.04 ft. If a safety factor of 1.5 is employed, the design armor layer rock size should be about 1.5 ft. If a soil cement is used, the size required would be about 3.3 ft, which is much larger than for rocks. This is because the specific gravity of soil cement (1.78) is smaller than that of rock (2.65), which makes the submerged weight of soil cement only half that of the submerged weight of the rock. Usually a riprap protection requires a properly designed and placed gravel filter. The bed material in the current river bed has an acceptable gradation for the filter.

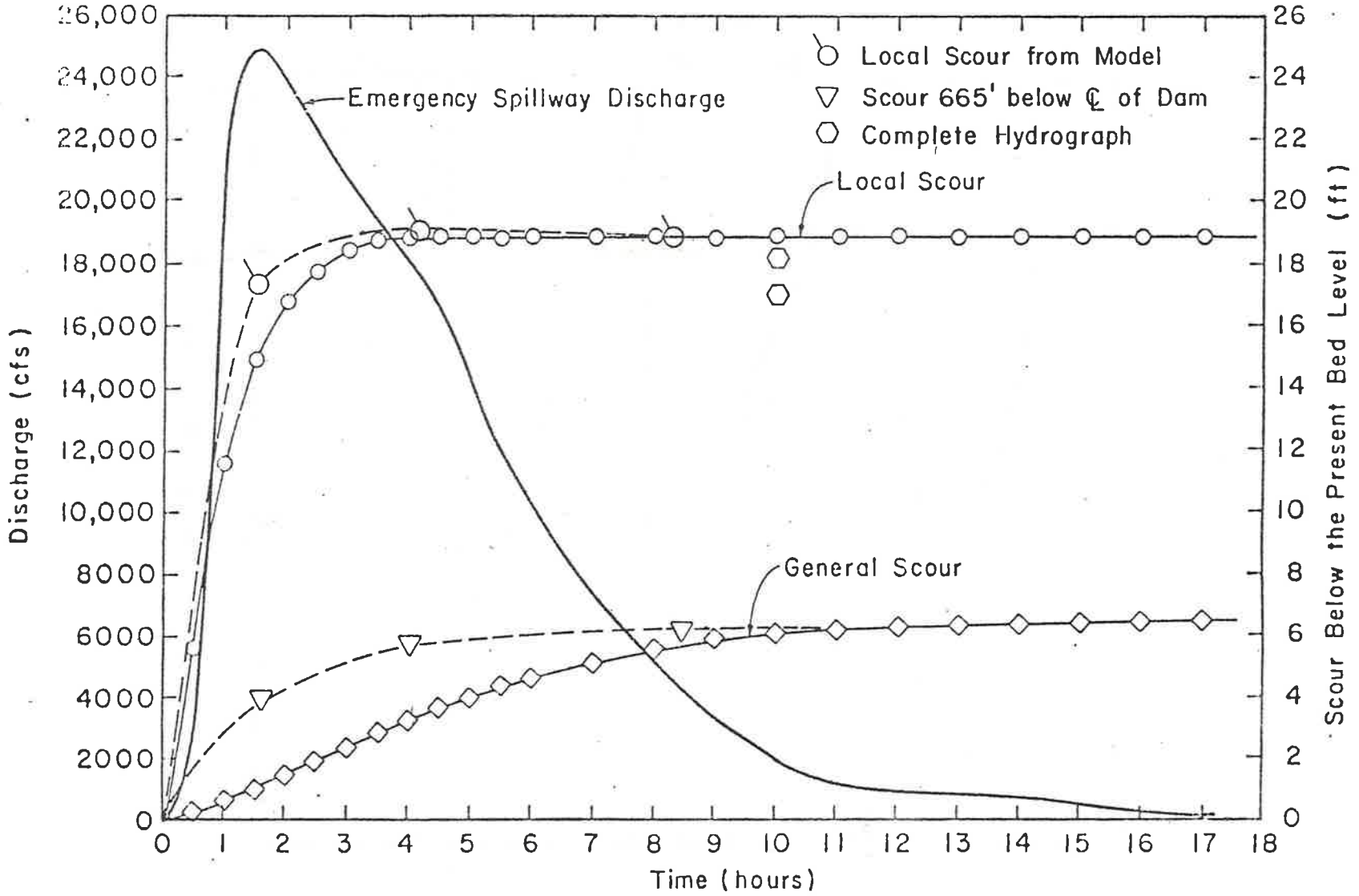

Figure 18.5 Local and general scour with the existing downstream control (6970 ft from the structure).

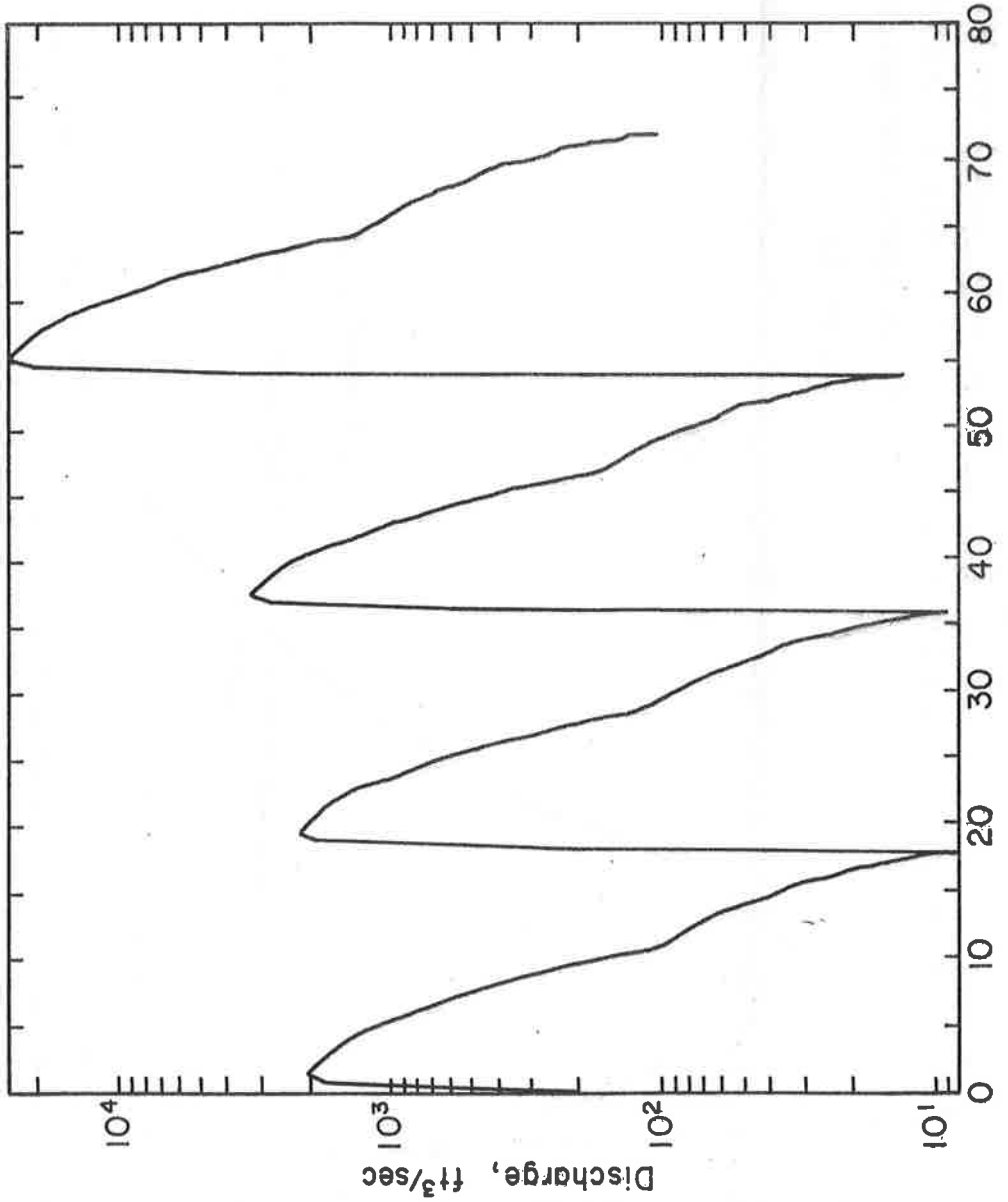

Figure 18.6 The assumed sequence of hydrograph after 85 years of operation.

No additional effort is needed to prepare the gravel filter. The recommended design of the pavement control below the spillway is given in Figure 18.7.

In order to check the applicability of the mathematical model, a large-scale physical model (model scale 1:30) was utilized by a Federal agency to estimate the local and general scour for the design freeboard hydrograph (Case II). The results from both totally independent model approaches were extremely close (see Figure 18.5), demonstrating a successful application of the mathematical model.

Summary and Conclusions

The analysis presented herein involves the determination of the degradation to be expected downstream from the emergency spillway chute during passage of the design hydrograph. Three cases of water and sediment inflow to the reservoir prior to the occurrence of the freeboard hydrograph were studied. The scour depth was determined utilizing a mathematical model that simulates the general and local scour considering the routing of sediment by size fractions. The results of the analysis show that considering the worst possible condition, the lowest expected bed level with the existing control will be 4352.3 ft, a scour depth of 34.7 ft below the present bed level. If the control of the local scour is desired, an armor layer of rock with size larger than 1.5 ft having a thickness of two rock diameters is required to pave an area approximately 100 ft long downstream of the structure and 12 ft below the present bed level.

The mathematical model was developed utilizing physical principles that govern water and sediment discharge, degradation, and armoring processes. Thus, it is applicable to a wide range of physiographic conditions when adjusted accordingly. The degree of confidence in this analysis is very much dependent on the quality of data provided by the Soil Conservation Service. If the quality of data is good, the results presented in this study should provide a reasonable and conservative estimation of scour totally acceptable for design purposes.

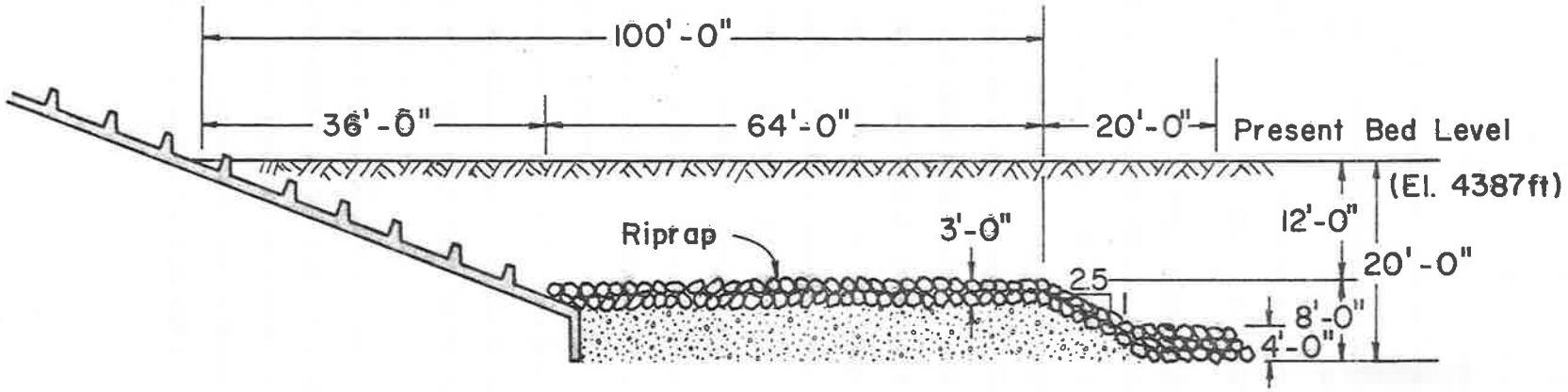

Figure 18.7 Sketch of the recommended design of control pavement.

18.3 DEGRADATION AND AGGRADATION ASSOCIATED WITH GRAVEL MINING-- SAN JUAN CREEK, CALIFORNIA

General

Presented in this section is an analysis of erosion and deposition problems in the San Juan Creek and Bell Canyon associated with Conrock gravel mining operations. A mathematical model for routing sediment by size fraction was developed and is utilized to estimate the erosion and deposition response of the stream and gravel pit subject to different hydrologic inputs and operational alternatives. Four engineering alternatives that consider rehabilitation of the Casper Regional Park and allow mining of sand and gravel are evaluated. Alternative I is a "do nothing" plan terminating the mining of sand and gravel. This alternative would allow natural healing processes in the form of aggradation to take place. No mitigation measure would be imposed on the existing stream. Alternative II is essentially the same as Alternative I except it permits regular mining of sand and gravel. Alternative III proposes construction of a drop structure located near the upstream end of the gravel pit. Alternative IV proposes construction of a series of small gabion check dams near and upstream of the gravel pit boundary coupled with regular gravel mining.

The developed mathematical model has been calibrated using 1969 floods (January 25 and February 25, 1969) and validated utilizing the recent three storms (January 15-16, February 9-10 and March 4, 1978). The validation results are excellent. The evaluation of alternatives indicates that Alternative IV (a series of check dams) is the most feasible design for meeting the objectives.

Hydrology

Flood Frequency: Utilizing the available flow records at the U.S. Geological Survey gaging station near San Juan Capistrano, California, a flood frequency analysis was made. The available records at this station are from October, 1928, to present. The drainage area above this point is 106 square miles. Because the drainage area above the Conrock gravel pit is only 77 square miles, the flows entering the gravel pit are assumed to be proportional to the drainage areas above the two sites. According to Leopold, Wolman, and Miller (p. 251, 1964),

the flood or bankfull discharge can be expressed as a power function of drainage area and the exponent of the equation varies from 0.65 to 0.8. For mean annual flow in humid regions, the exponent is about 1.0. In this study, a value of 1.0 was assumed. This assumption was also adopted by Camp, Dresser, and McKee (January, 1978). Figure 18.8 shows the plot of the flood frequency of peak flows for the two locations on San Juan Creek noted on the inset map on the figure. Location 1 is along San Juan Creek approximately at the upper edge of the gravel pit, and downstream of the Verdugo Canyon. Location 2 is at the U.S.G.S. gaging station. Our results are very close to those of Camp, Dresser and McKee (January, 1978).

Design Storms: The comparison of the 1969 flood hydrographs with the theoretical 100-year hydrographs by Camp, Dresser and McKee for San Juan Creek immediately above the Conrock gravel pit was made by Camp, Dresser and McKee (January, 1978) and is shown in Figure 18.9. As pointed out by Camp, Dresser, and McKee, the natural flood hydrographs may be of substantially longer duration than the classical hydrographs estimated by usual theoretical methods (Soil Conservation Service and Orange County Flood Control District). These floods may be capable of transporting considerably more sediment than the shorter duration floods utilizing the identified theoretical methods. For an adequate analysis of erosion and sedimentation, a better estimation of hydrograph shape is essential.

The best way to predict the flood hydrographs for the study site is to employ a more advanced theoretical approach involving rainfall-runoff relationships and numerical modeling techniques, such as the one developed by Simons et al. (1977). However, due to time and money constraints, a more practical means is used for estimating the hydrograph shapes for floods with various return periods. This method involves the development of a typical hydrograph normalized with respect to the flood peak. Figure 18.10 shows that the normalized hydrographs based on the available data are sufficiently close and the hydrograph of January 25, 1969, is selected as the typical hydrograph. The design storms with different return periods are then estimated based on peak flow determined by Figure 18.8 and the typical hydrograph shown in Figure 18.10. The storm hydrograph on March 4, 1978, was

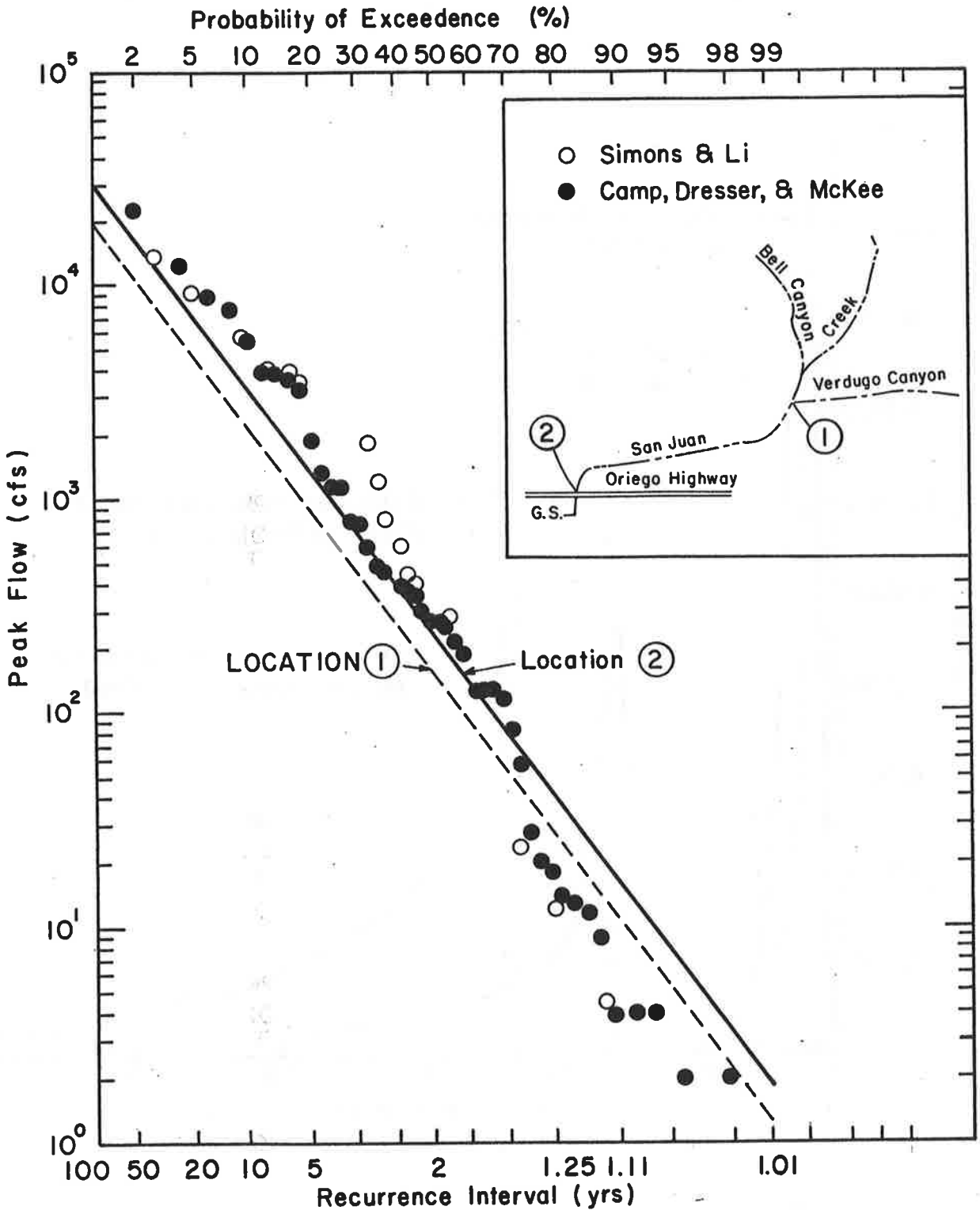

Figure 18.8 Frequency discharge relationship for San Juan Creek (after Camp, Dresser & McKee).

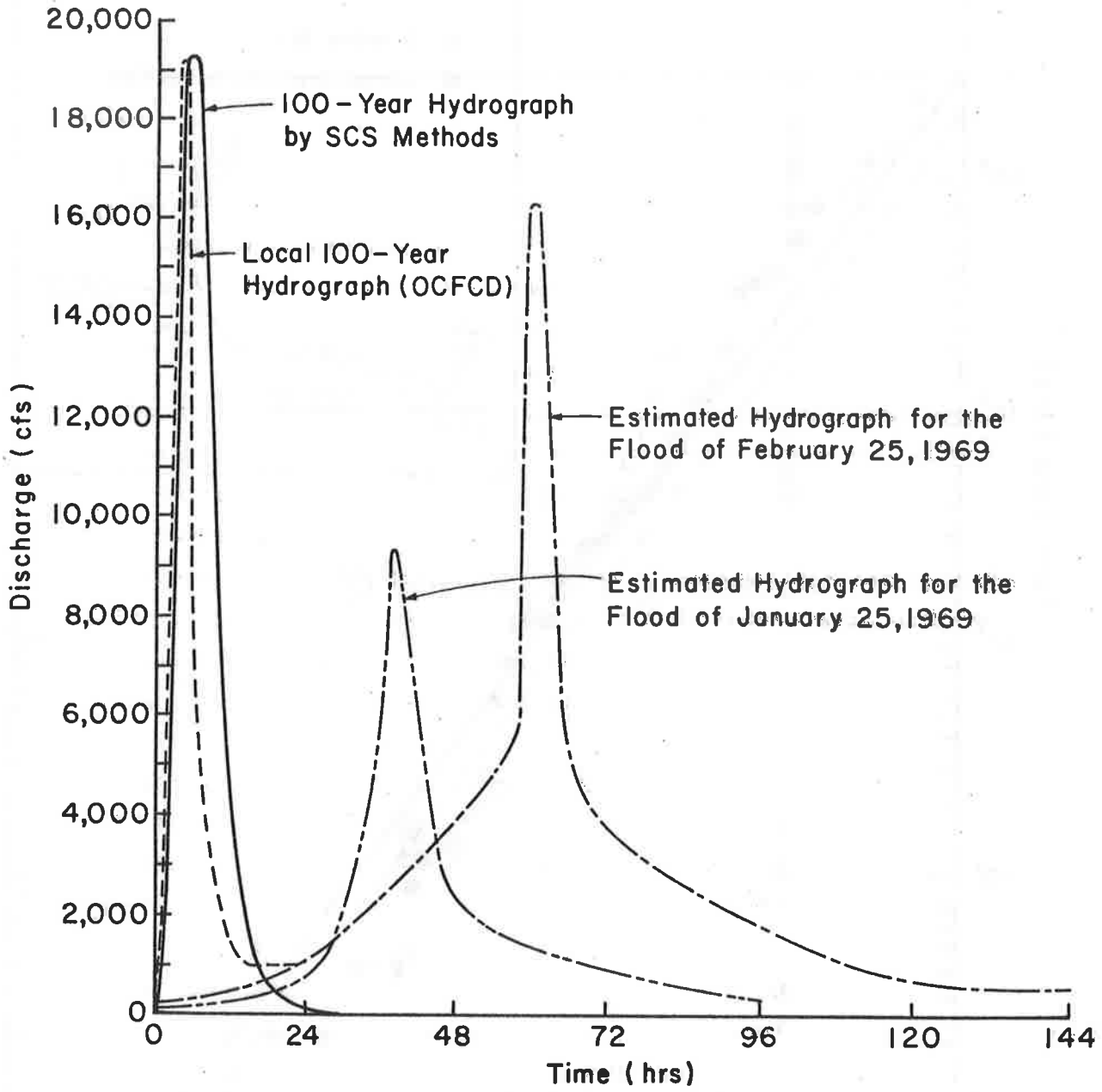

Figure 18.9 Comparison of the 1969 flood hydrographs with the theoretical 100-year hydrographs for San Juan Creek at its confluence with Bell and Verdugo Canyons (after Camp, Dresser & McKee, January 1978).

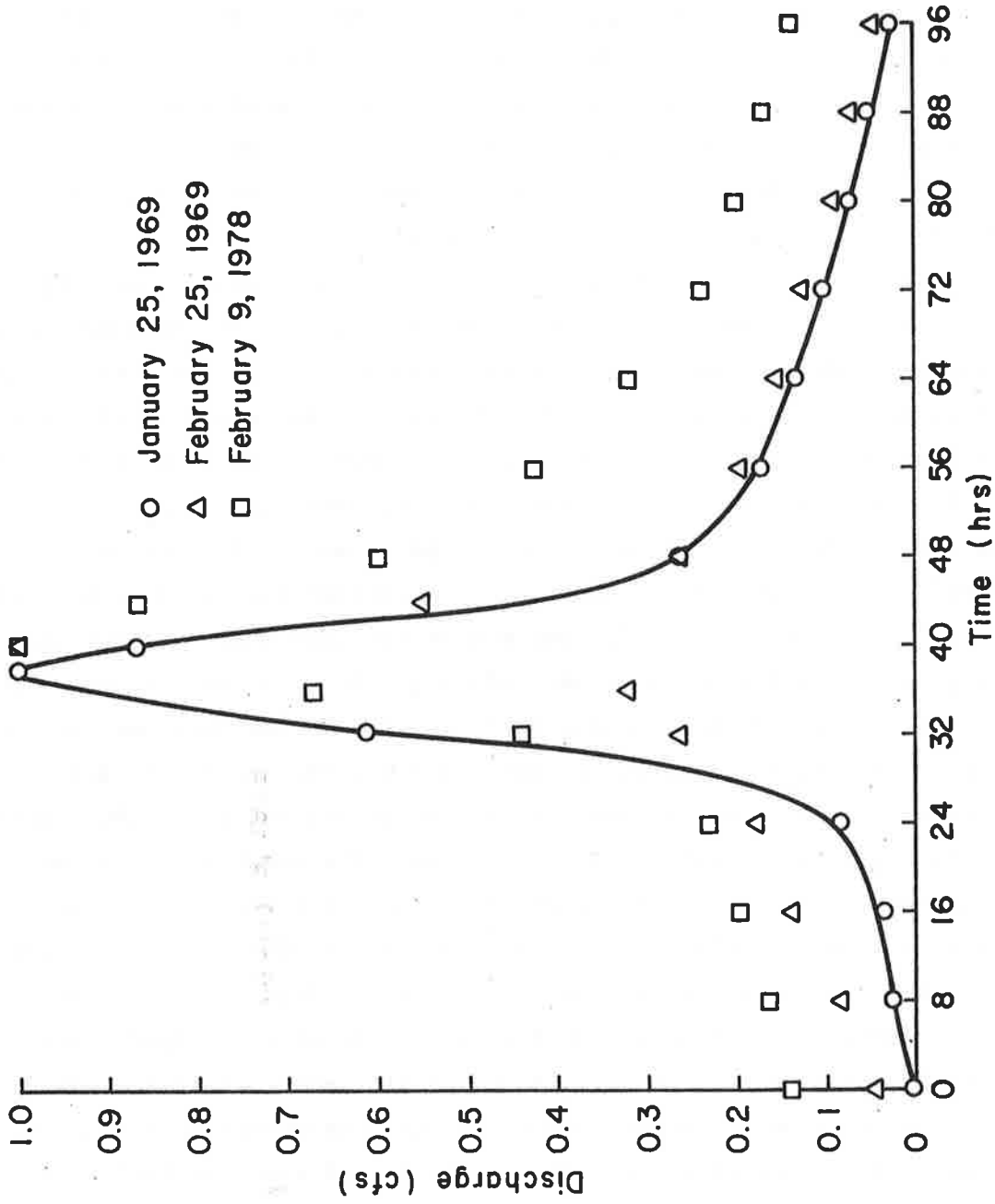

Figure 18.10 Normalized hydrographs.

not reported by the U.S.G.S. Only the peak discharge at Capistrano was given and it was estimated to be 12,000 cfs utilizing the slope-area method. The above-mentioned method was also used to obtain a hydrograph for the flood event of March 4, 1978.

Storm Events of January, February, and March, 1978: The storms of January, February, and March, 1978, have induced significant degradation along the San Juan Creek and Bell Canyon upstream of the Conrock gravel pit. These storms have provided considerable valuable data which should be used to test any suggested methodology for analyzing the stream and gravel pit response.

The storm of January 15 and 16, 1978, lasted about three days. It started on January 14 and ended on January 17. The measured hydrographs at the San Juan gage near Capistrano indicated very small discharges. The peak flow was only 210 cfs. It is suspected that the records were not accurate. An indirect check of the peak flow based on the material deposited in the gravel pit was made. This method utilized Shields Criterion of the incipient motion (Simons and Sentürk, 1977) with the assumption of a channel bed slope of 0.1 (the local bed slope immediately upstream of the gravel pit), a Manning's roughness of 0.03, and a channel width of 400 ft. The critical discharges large enough to move a specific size of sediment were determined. According to Camp, Dresser and McKee (March, 1978), the coarsest particle of the material in the gravel pit after the January, 1978, storm was between 75 mm and 100 mm. The theoretical evaluation indicates that the critical discharges to move the particle sizes between 75 mm and 100 mm range from 200 cfs to 300 cfs. These values are close to those measured near Capistrano. Thus, the measured hydrographs near Capistrano were used to determine the hydrographs for the gravel pit. The small quantity of runoff resulting from large quantities of rain may be due to dry anticedent moisture conditions. A further study to relate rainfall and runoff relation is needed to develop more accurate information.

The storm of February 9-10, 1978, started on February 8, 1978, and ended on February 15, 1978. This storm was of a very long duration with two flow peaks. The hydrographs just upstream of the gravel pit were directly scaled from those measured near Capistrano utilizing the ratio of drainage areas.

The storm hydrograph of March 4, 1978 was unavailable. The estimated flow peak near Capistrano was between 10,000 to 13,500 cfs. A value of 10,500 cfs was adopted for this study (the peak flow entering the gravel pit is 7,600 cfs). Having the peak flow identified, the hydrograph was estimated by normalizing the hydrograph as described earlier.

The storm hydrographs of January, February, and March 1978 are given in Figures 18.11, 18.12, and 18.13. These hydrographs were used in the validation of the developed mathematical model.

Stream and Gravel Pit Geometry

Detailed discussions of stream and gravel pit geometry have been presented by Camp, Dresser and McKee (January and March 1978). Measured profiles before and after each of the storms that occurred in early 1978 are plotted in Figure 18.14. For evaluation, a simplified geometry was assumed for the condition prior to the 1978 storms. The simplified geometry is given in Figure 18.15. This simplified geometry is very close to the actual conditions. The assumption of a 650 ft width in the gravel pit is consistent with the estimated volume of 6,500,000 tons of gravel and sand excavated since 1969. The assumption of a 400 ft width in San Juan Creek is consistent with the degradation width after the February 1978 storm. The width of channel usually increases during the degradation process, especially if there is erosion-resistance material and heavy armor on the bed. Dr. Mostafa (1978) even assumed that the final channel width could reach 600.0 ft. The assumption of 400.0 ft width is appropriate for an average condition. In reality, the channel is divided into three branches; San Juan Creek, Bell Canyon, and Verdugo Canyon shortly upstream of the Casper Regional Park boundary. The Verdugo Canyon contributes only about 5% of total flow and is also limited in degradation due to a culvert that serves as a control. For all practical purpose, Verdugo Canyon can be omitted from the analysis. The 400.0 ft width channel above the confluence of Bell Canyon and San Juan Creek implies that the sum of the widths of these two creeks is 400.0 ft.

Based on the report by Camp, Dresser, and McKee (March, 1978) and the information provided by Dames and Moore, the channel and pit geometry after each of the storms occurring in early 1978 were compiled. Figure 18.14 showed the profile after each storm. The elevations at the original pit

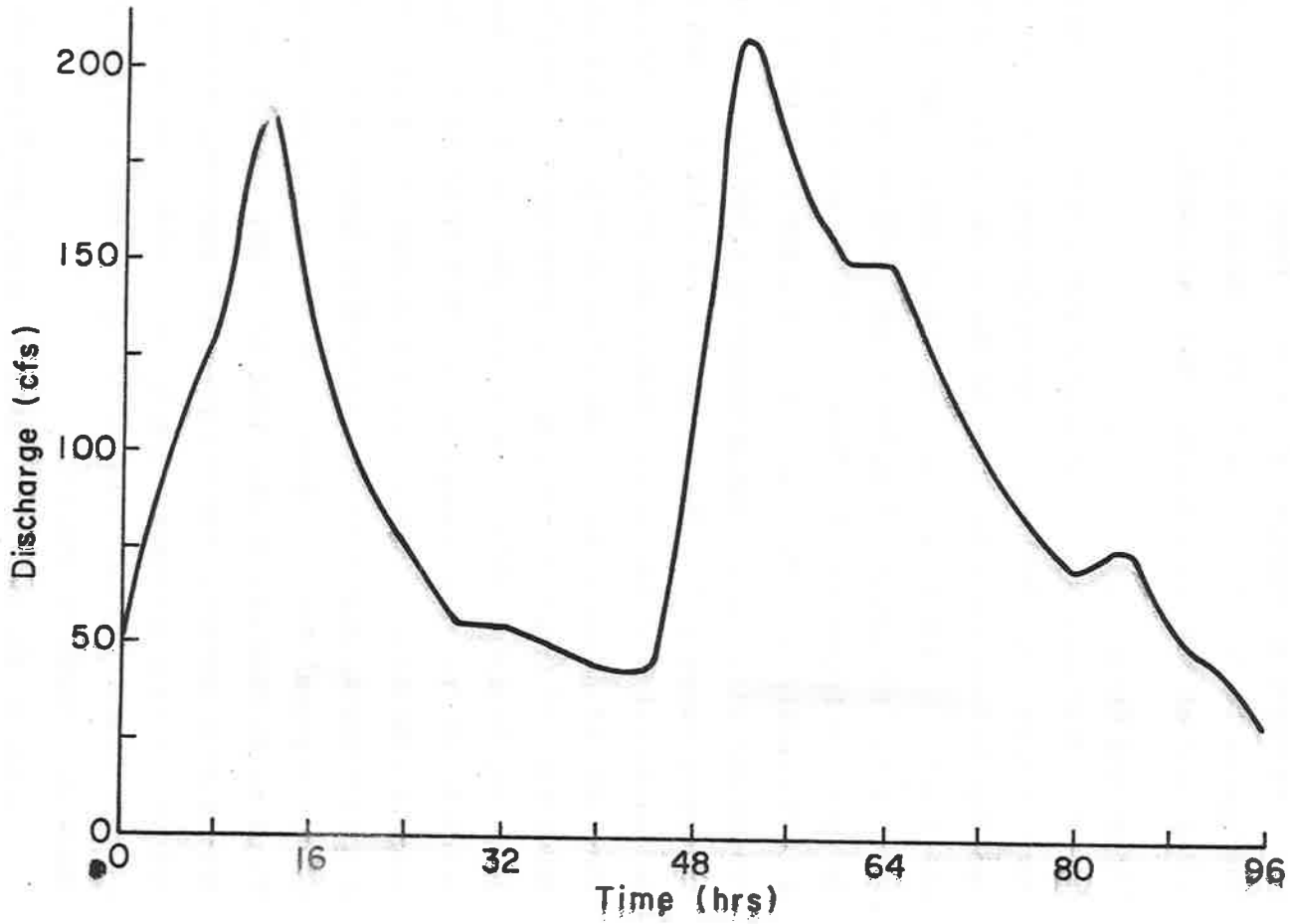

Figure 18.11 Storm hydrograph of January 1978.

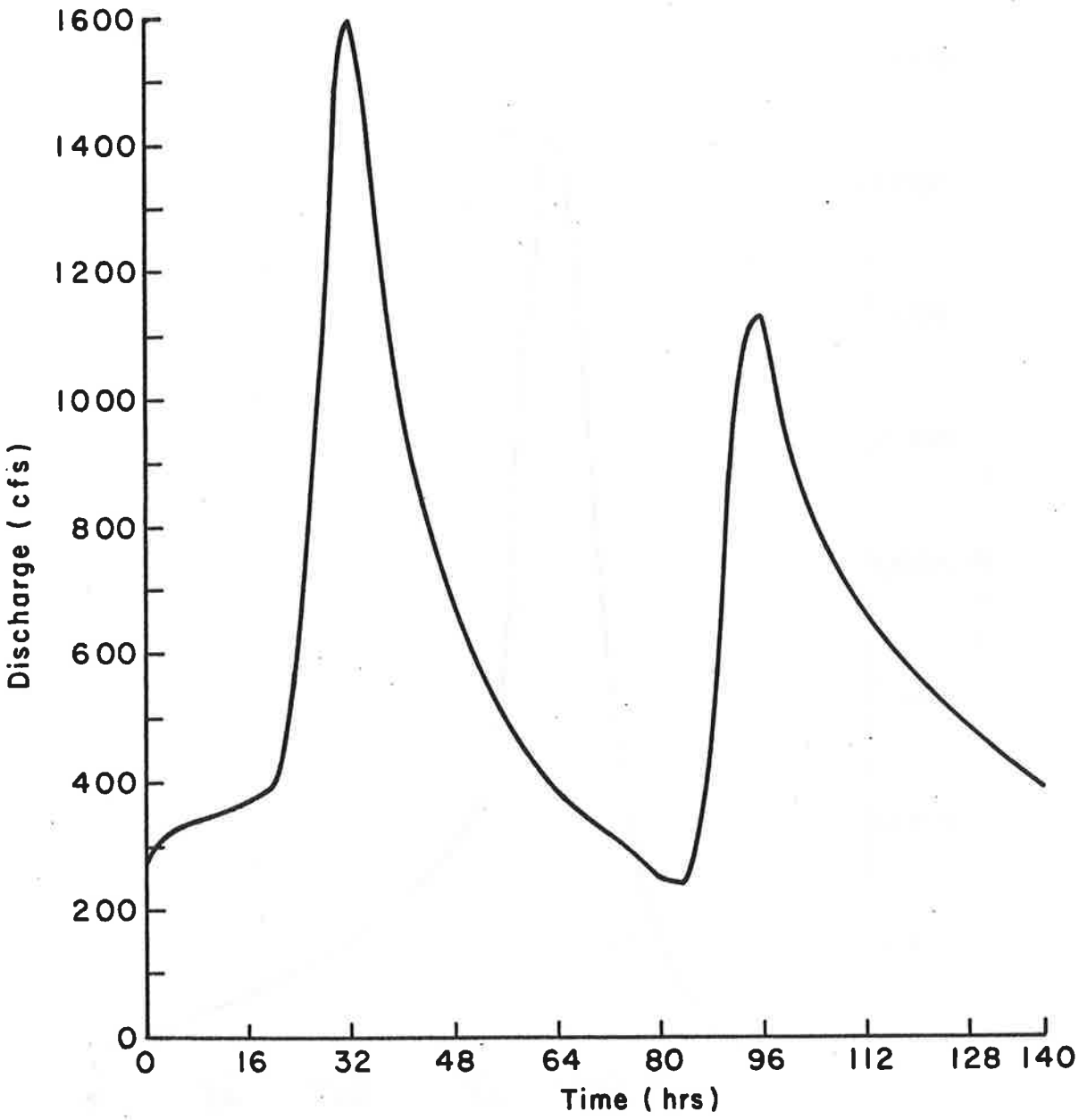

Figure 18.12 Storm hydrograph of February 1978.

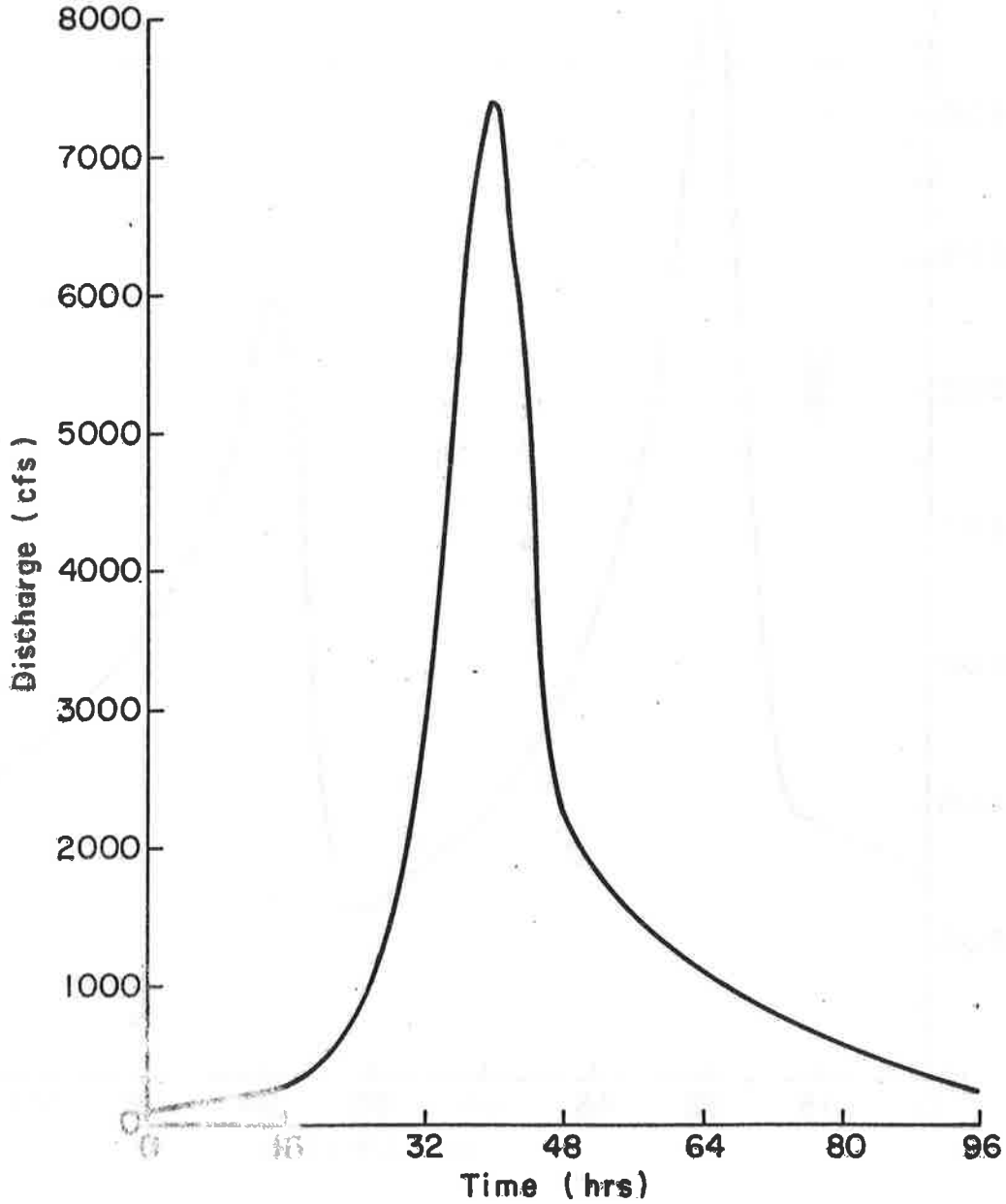

Figure 18.13 Storm hydrograph of March 1978.

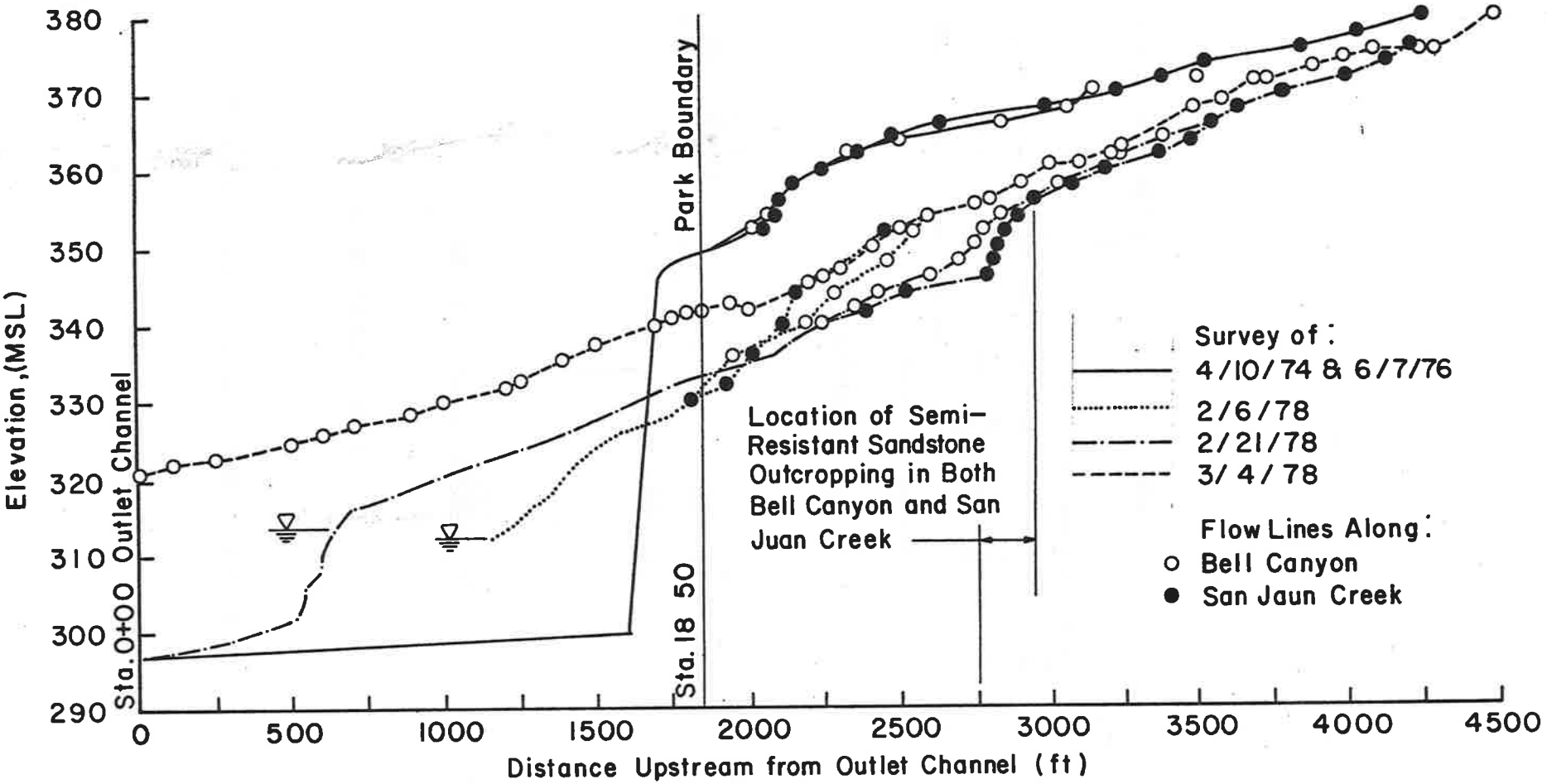

Figure 18.14 Measured bed profiles.

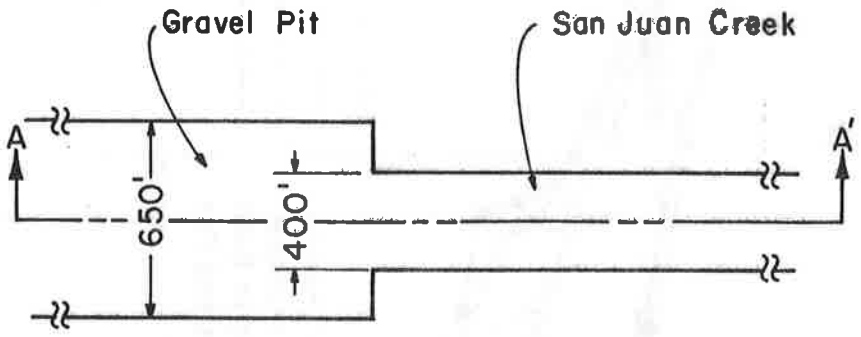

(a) Plan

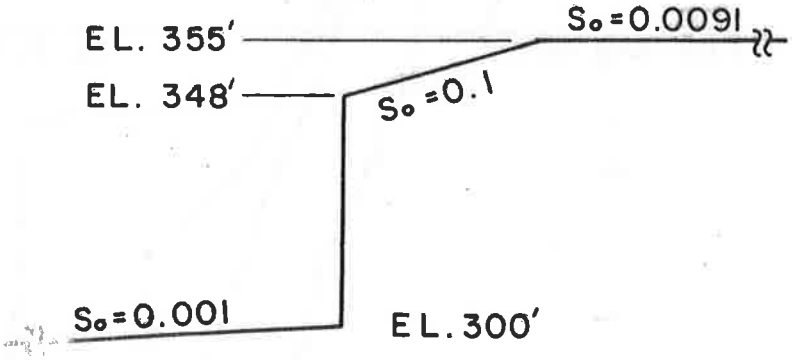

(b) Section A-A'

Figure 18.15 Simplified geometry before 1978 storms.

boundary and bed slopes are tabulated in Table 18.2. The measured data show that the elevation at the original pit boundary (station 16+00) was 327.0 ft after the January 1978 storm, 331.0 ft after the February 1978 storm, and 338.0 ft after the March 1978 storm.

Table 18.2 Geometry after 1978 storms.

Storms	Elevation at the Original Pit Boundary (Station 16+00) (ft)	Average Bed Slope
January 1978	327.0	0.0310
February 1978	331.0	0.0150
March 1978	338.0	0.0118

Flow Resistance Coefficient

It is difficult to accurately estimate resistance to flow for a gravel channel. The size of gravel forming the stream bed can change greatly as a consequence of degradation and aggradation processes. The resistance to flow changes accordingly. Considering the stream power and the median diameter of bed material, the bed form of the channel is likely to be in upper regime with a plane bed (see Simons and Sentürk, 1977). The Manning roughness coefficient for a plane bed ranges from 0.017 to 0.027 depending on particle size. According to Chow (1959), the Manning roughness coefficient is 0.03 for the channel pattern and bed material sizes presented in the study reach. Furthermore, the Manning roughness coefficient is about 0.029 based on the Strickler Formula (Simons and Sentürk, 1977). It is determined that a Manning roughness coefficient of 0.03 is satisfactory for the analysis.

Sediment Transport and Yield

The determination of sediment discharge is a difficult task but is the most important step in the fluvial analysis of streams. Due to the highly heterogeneous distribution of bed material, application of a transport

highly heterogeneous distribution of bed material, application of a transport equation by size fraction is necessary for an adequate analyis.

Representative Bed Material Size: The bed material samples of San Juan Creek were collected and analyzed by Dames and Moore. The size distributions of surface material was very uniform. Figure 18.16 shows that the distribution of three composite samples is similar. The composite Sample A was selected as the typical bed material along the San Juan and Bell Canyon channels upstream of the gravel pit. The median diameter and gradation coefficient of the composite Sample A are very close to those averaged from the individual samples. The size distributions of transported material during two 1969 floods were determined from the samples in the gravel pit collected in 1976. The size distribution curve is shown in Figure 18.17.

Sediment Transport Rates: The available data on sediment transport rates either in the laboratory flumes or in the field have been collected in relatively flat channel systems and with a uniform sediment. Most of the available sediment transport equations are applicable for these conditions. Recent laboratory studies at Colorado State University by Li et al. (1977) on steep channel (5 percent to 25 percent bed slope) and gravel bed sediment transport indicated that a form of Meyer-Peter, Müller sediment transport equation is applicable for steep gravel bed streams. However, the coefficients should be calibrated using measured data. The original Meyer-Peter, Müller equation accounts for the bed load only. The suspended portion of the bed material load plus the washload delivered from upland area makes the coefficient of the transport equation larger than that originally proposed by Meyer-Peter, Müller.

According to Camp, Dresser, and McKee (January 1978) report to [illegible] furnished by [illegible]ock showed that in the three years 1966 to 1969, [illegible] tons of sand and gravel were produced and sold. During these years, the records of the U.S. Geological Survey at Highway 74 showed that the runoff was modest. It was assumed that the volume of the pits before the 1969 floods (see Figure 18.15) represented the 1,204,000 tons of sediment; thus ignoring the amount deposited by the flows of 1967 and 1978. The above assumption of sediment yield produced by two 1969 floods was used to calibrate the sediment transport equation. The bulk rate of sediment was assumed to be 1.5. The calibrated results were then

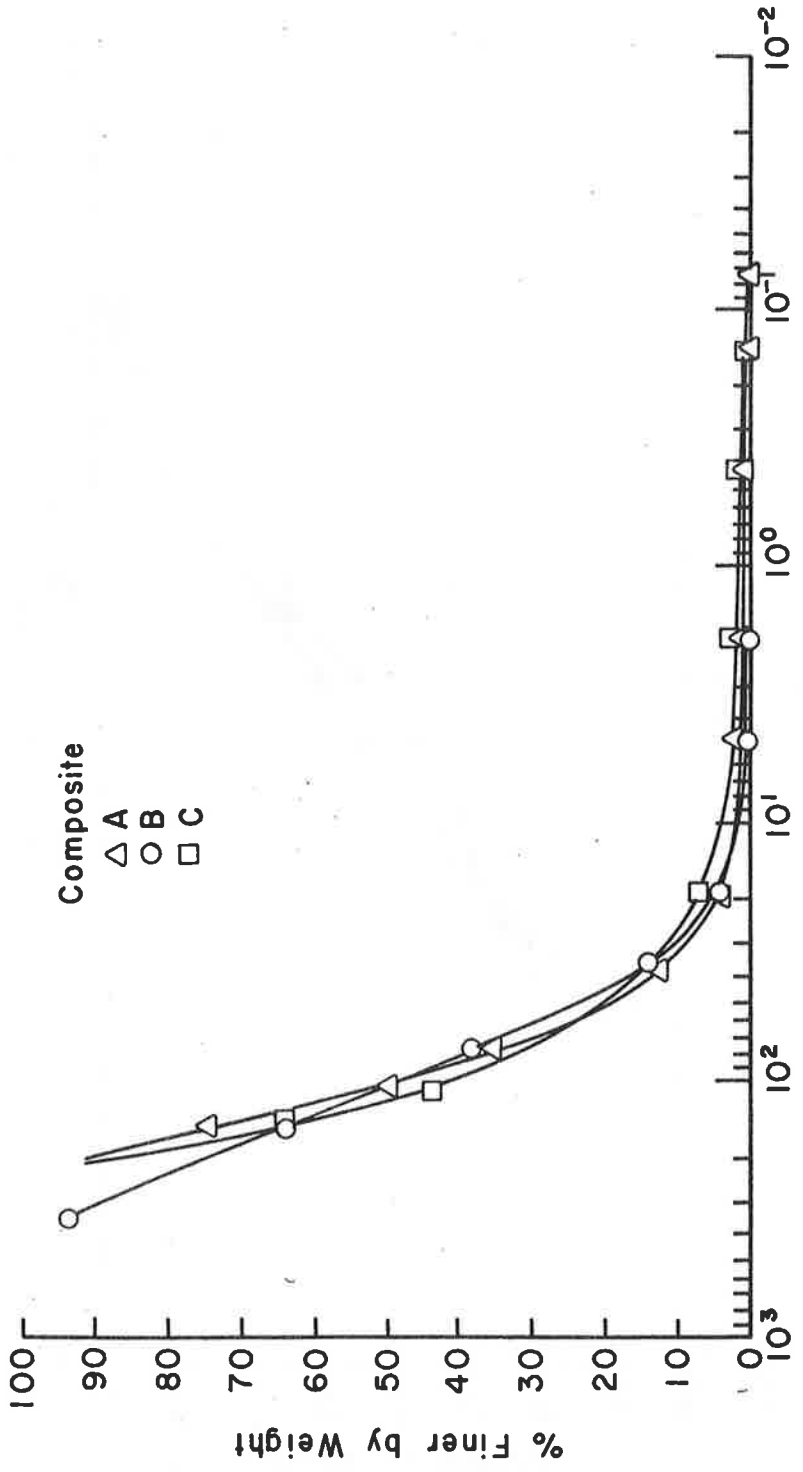

Figure 18.16 Size distribution of bed material in San Juan Creek.

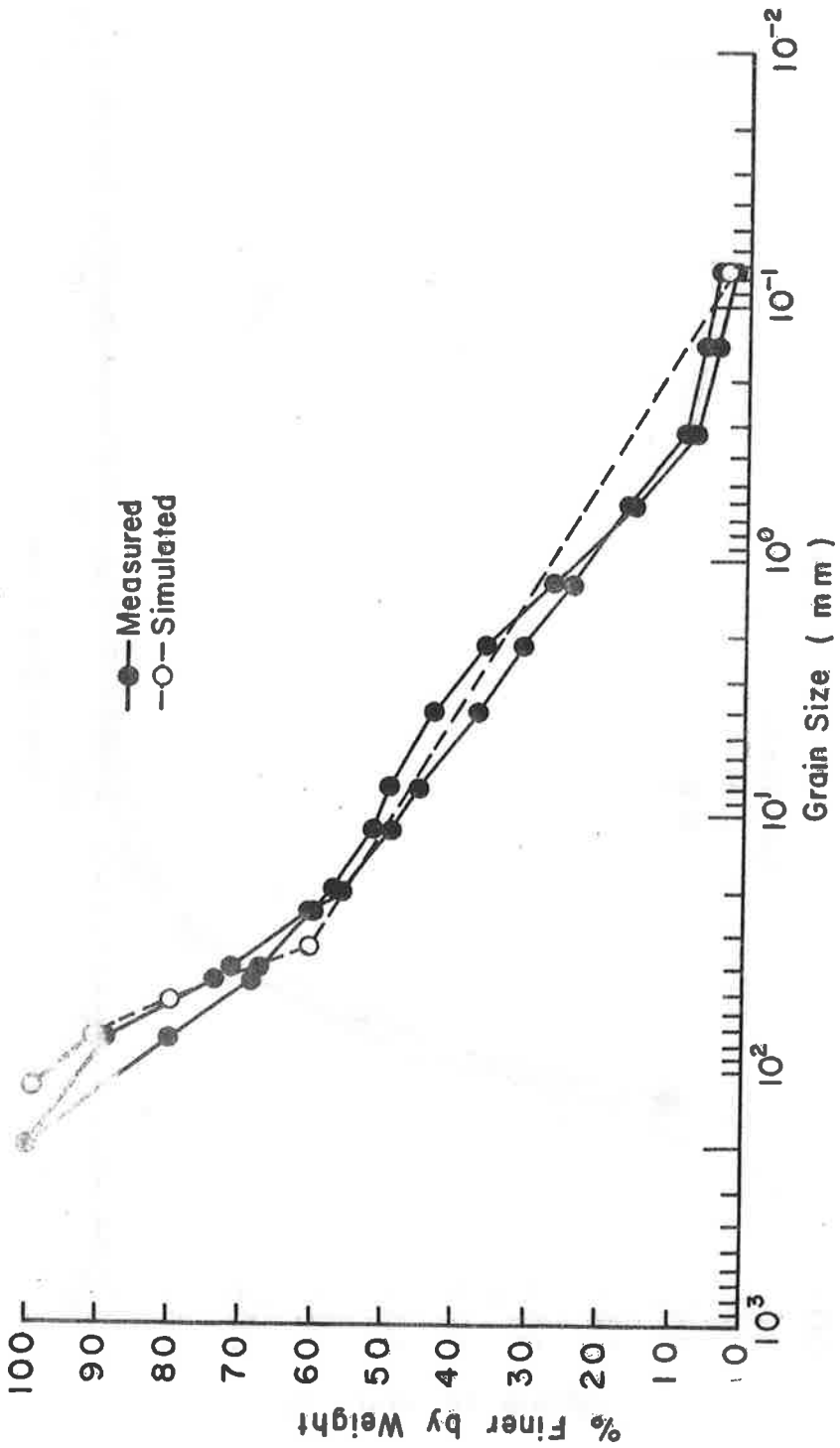

Figure 18.17 Size distribution of material in the gravel pit collected in 1976.

used later to validate the mathematical model using the 1978 floods. Figure 18.16 shows that the estimated size distribution of transported material is very close to that measured. As a further check of the validity of the developed discharge-sediment rating relation, a comparison of the computed total sediment discharges with those determined by USGS (1969) was made. Figure 18.18 verifies a good comparison of sediment discharge rates except the computed values are consistently higher than those determined by the USGS. Note that the sediment discharges computed in this study are the total bed material loads upstream of the Conrock pit using a bed slope of 0.0091, width of 400 ft and the bed material size as shown in Figure 18.16, while the sediment discharge rates determined by the USGS were made at the bridge on Highway 74 using measured suspended data.

Sediment Yields: The method of determining sediment transport developed in this study requires an additional assumption of a very large sediment supply from the upland area in order to determine the sediment yield. According to the reports by Converse Davis Dixon Associates, Inc. (February and March 1978), ample sediment is available from the upland watersheds due to landslides and fire based on past records and geological information. Thus, the assumption of a large amount of sediment supply from upland area is reasonable. Hence, the sediment yield during flood events is only limited to the channel carrying capacity.

The estimated sediment yields for floods with frequencies of 2, 5, 10, 15, 20, 25, 50, and 100 years are given in Table 18.3. The median size of flood has a return period of two years. For 42 years of records (1928 to 1969), the average water yield upstream of the gravel pit is 7300 ac-ft. Thus, the average number of median size floods is 22.7 per year, the average annual sediment yield is 80,000 tons per year.

Mathematical Model

Governing Processes: The degradation or head-cut upstream of the pit and the deposition of the material in the pit occur simultaneously. This problem is very complicated. Simplifying assumptions are needed to obtain the solutions in a practical and economical way. The dominant physical processes include water runoff, sediment transport, sediment routing, degradation, aggradation, breaking and forming of the

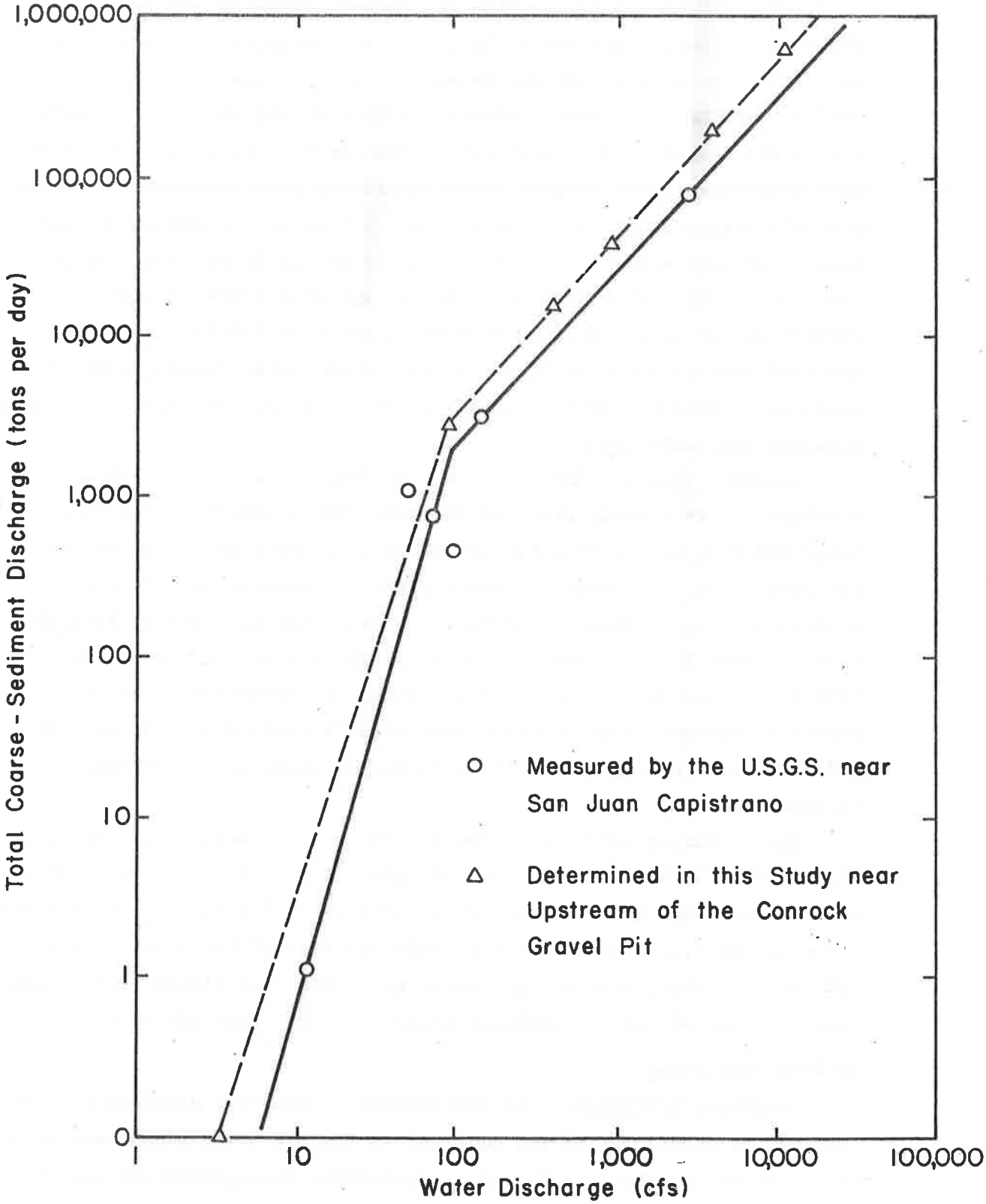

Figure 18.18 Relation between water discharge and total coarse-sediment discharge, San Juan Creek near San Juan Capistrano, California (after USGS, 1969).

Table 18.3 Summary of sediment yield for San Juan Creek near Casper Park boundary.

Flood Frequency (Return Period) (yr)	Peak Discharge (cfs)	Flow Volume (ac-ft)	Sediment Yield(tons)
2	174	322	3,510
5	1,017	1,880	26,300
10	2,542	4,700	67,700
15	3,632	6,716	100,700
20	5,085	9,397	150,300
25	8,354	15,448	285,100
50	12,712	23,506	509,100
100	21,792	40,296	1,110,800

armor layer, etc. These processes are unsteady in nature. In order to simplify the problem, a known discharge assumption is used. The known discharge solution is appropriate in this study because of the short distance considered in the space. As mentioned earlier, for simplicity a simplified geometry representation as shown in Figure 18.15 was used.

Referring to Figure 18.19, the temporal resolution of the degradation and aggradation processes considered in this study was treated in two separate conditions. For condition a) the transport rate in Zone II is much larger than in Zone I due to the local steep gradient (assuming a slope of 0.1 estimated from the bed profile prior to 1978 storms) and the destruction of the armor layer on the bed of the channel. Degradation occurs in this reach. The bed material size of Zone II is assumed to be a mixture of the surface size distribution (Figure 18.16) and the size distribution described in the pit (Figure 18.17). The deposition and forming of a delta takes place in Zone I due to its negligible transporting capacity. The difference in sediment transport rates in Zones I and II for an increment of time would determine the new elevation of the downstream end of channel assuming a bed slope of 0.10. The growth of the delta can be determined as the amount of material transported into the pit. For simplicity, the slope of delta is assumed to be 0.10 based upon the slope from the head of delta or shown after the February 9-10, 1978 storm. No lateral slope was assumed. As soon as the elevations of the degrading and aggrading reaches meet, the bed slope flattens as shown for conditions. b) with this condition, the delta will grow both upstream and downstream, and the degradation should continue as evidenced by conditions after the February 1978 and March 1978 floods. The slope becomes flatter and flatter and the degree of degradation is reduced but it still proceeds slowly. The new slope and extent of degradation and/or aggradation were computed based on the difference in sediment transporting capacities in different zones. The sediment transport rate in Zone II changes with the change in the bed slope. Eventually, the pit should fill with new material if gravel mining is discontinued.

The simulation was made using time steps of four hours. The time lapse changes of elevation at the original gravel pit boundary (Station 16+00) are given in Figure 18.20. The simulation results are

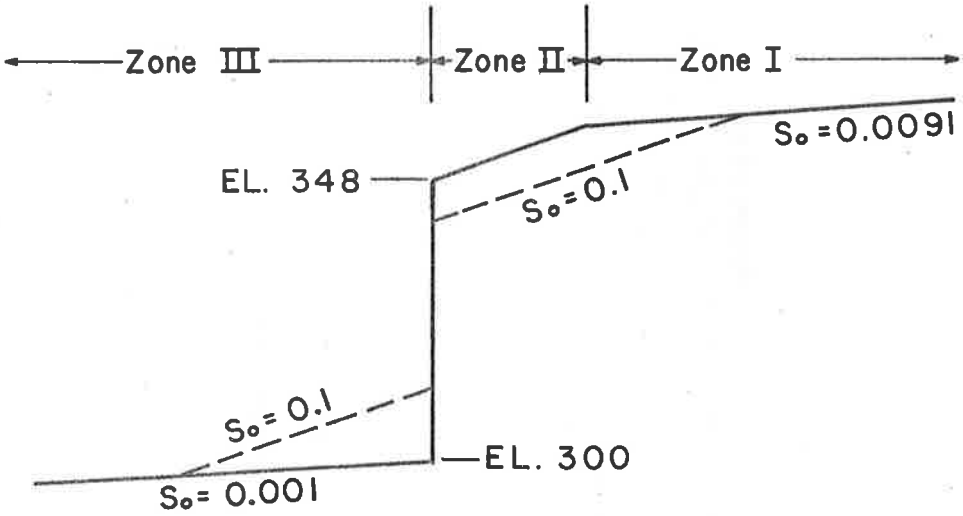

(a) Before the Joining of the Reaches Experiencing Degradation and Aggradation.

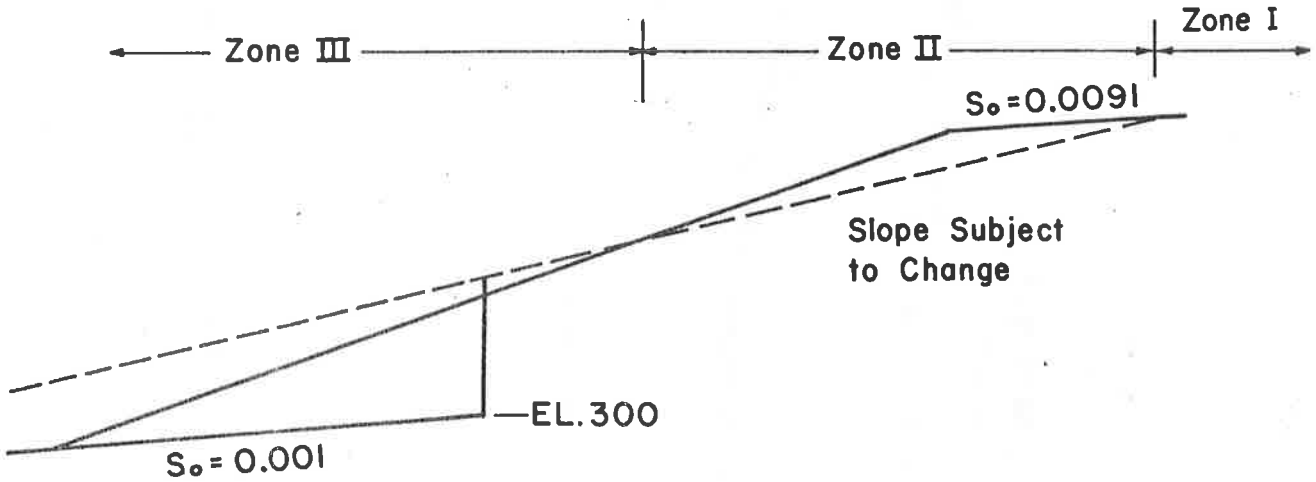

(b) After the Joining of the Reaches Experiencing Degradation and Aggradation.

Figure 18.19 Sketch of degradation and aggradation processes.

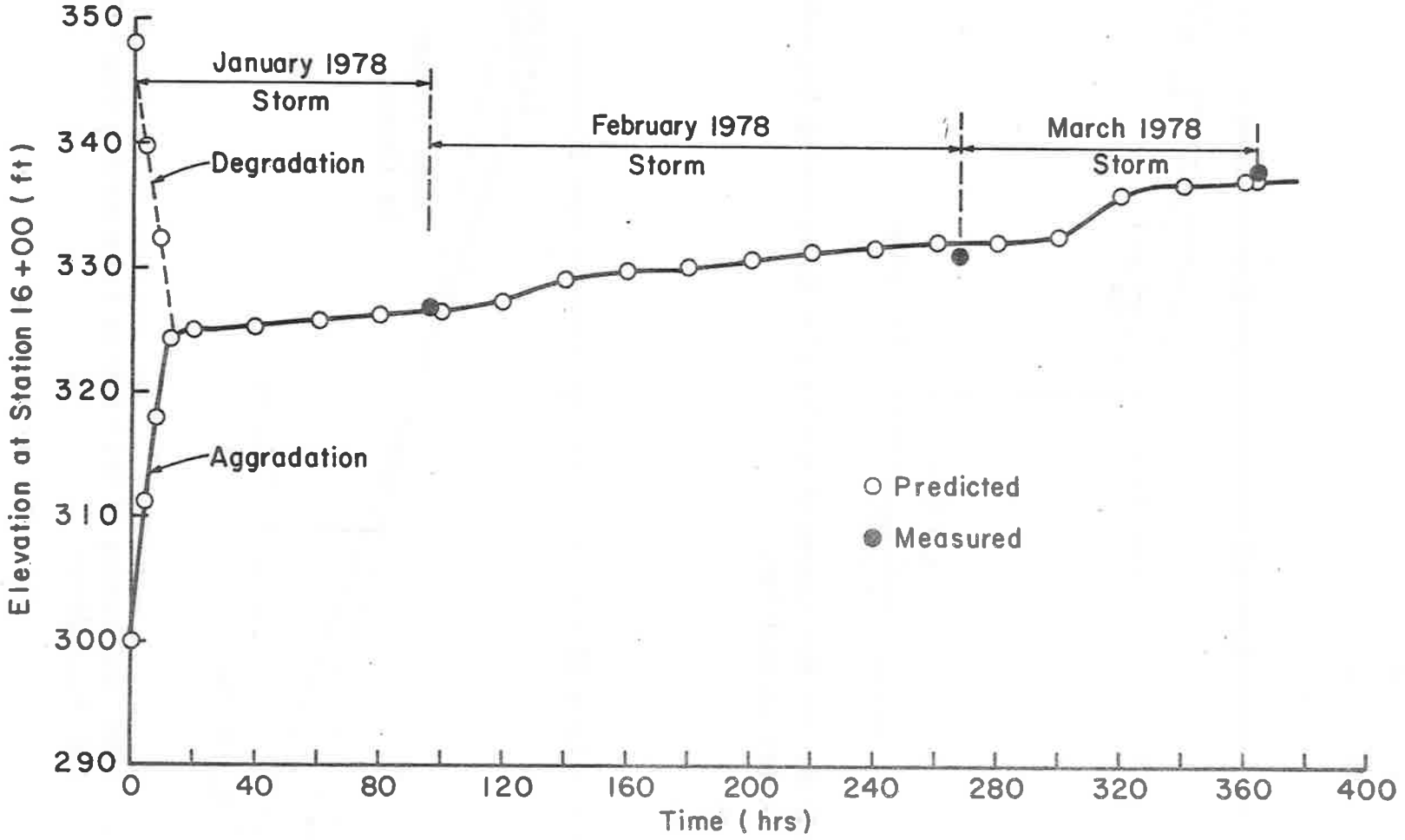

Figure 18.20 Time lapse changes of elevation at the original gravel pit boundary (Station 16+00).

excellent when compared with field measurements. The comparison of simulated elevations and bed slopes with measured data (see Table 18.2) are given in Table 18.4. Again, the results are excellent. One point worth mentioning is that the simulated results are the predicted results utilizing the calibrated sediment transport parameters based on the data of two 1969 storms.

Table 18.4 Comparison of simulated and measured results

Storms	Elevation at the Original Pit Boundary (Station 16+00) ft			Average Bed Slope		
	Simulated	Measured	Error %	Simulated	Measured	Error %
January 1978	326.4	327.0	0.2	0.0339	0.0310	9.4
February 1978	332.2	331.0	0.4	0.0138	0.0150	8.0
March 1978	337.3	338.0	0.2	0.0110	0.0118	7.0

Evaluation of Design Alternatives

With the validated sediment transport equation and the mathematical model, four engineering alternatives that consider rehabilitation of the Casper Regional Park and allow mining of sand and gravel are evaluated. The analysis in this study is simply to identify the most feasible solution, no attempt is made to provide detailed hydraulic design of the proposed structure. The results of the evaluation follow.

Alternative I: This is a "do nothing" and without gravel mining alternative. Under this alternative, the gravel pit would be gradually filled up, the delta will continue to grow and aggradation will complete restoration of grades to approximately original slopes in 75 years, under average conditions. The above estimation was made by assuming an average annual sediment yield of 80,000 tons to fill the available space of 6,000,000 tons. The elevations at station 16+00 after occurrence of individual storms with different return periods are given in

Table 18.5. The available space for gravel is so large that it even requires approximately six 100-year floods to fill it up. The restoration of Casper Regional Park by natural processes requires a long period of time unless some large flood events occur in the future.

Table 18.5 Alternative I subject to floods with various return periods.

Flood Frequency (Return Period) (yr)	Peak Discharge (cfs)	Flow Volume (ac-ft)	Elevation at the** Original Gravel Pit Boundary (Station 16+00)(ft)
2	174	322	337.3
5	1,017	1,880	337.7
10	2,542	4,700	338.3
15	3,632	6,716	338.7
20	5,632	9,397	339.3
25	8,354	15,448	340.8
50	12,712	23,506	342.6
100	21,792	40,296	346.1

*Without gravel mining operation.
**Start with computed elevation at 337.3

Alternative II: This alternative would allow the continuation of gravel mining while providing the opportunity to heal the degradation in the Casper Regional Park naturally. The expected rate of gravel and sand mining is 1,000,000 tons per year. If the additional supply after the March 4, 1978 storm is negligible, the gravel pit would be excavated within approximately three years to the geometry similar to that prior to the 1978 storms. The aggradation rate in the Casper Regional Park would be very slow, because the annual excavation rate is close to that produced by a 100-year flood event. Furthermore, some additional head cut should be expected along the current bed profile. Assuming that gravel pit dimensions after the removal of sand and gravel are similar to those prior to 1978 storms, the new head cut elevations at station 16+00 for various sizes of storms are given in Table 18.6. This alternative would induce worse problems that the Alternative I and certainly require a much longer period of time to restore the Casper Park.

Table 18.6 Alternative II and subject to floods with various return periods.

Flood Frequency (yr)	Peak Discharge (cfs)	Flow Volume (ac-ft)	Elevation at the* original gravel pit boundary (Station 16+00)(ft)
2	174	322	317.8
5	1,017	1,880	320.3
10	2,542	4,700	322.9
15	3,632	6,716	324.4
20	5,085	9,397	326.1
25	8,354	15,448	329.3
50	12,712	23,506	332.5
100	21,792	20,296	336.5

*With gravel operation.
**Start with computed elevation at 337.3.

Alternative III: This alternative would construct a drop structure near station 16+00, approximately 250 ft downstream of the Conrock property line. The proposed structure would be a gabion check dam with crest elevation of approximately 355 ft. The equilibrium slope upstream of the dam would be close to the original gradient. If an equilibrium slope of 0.91 percent is assumed, it would provide a space for trapping approximately 1,870,000 tons of sediment and would take approximately 23 years, under average conditions, or two 100-year floods to fill up the degraded area completely. If the crest elevation of the drop structure is set at 348 ft it would take approximately 9 years under an average rate to fill the sediment behind the structure. Although this alternative would allow continued gravel mining and provide the opportunity to heal the San Juan Creek and Bell Canyon gradually, the rate of restoration is still too slow. This would also terminate the gravel and sand supply to the gravel pit for a long time. This alternative is not attractive for the above reasons. A series of small dams to restore the park locally and control any further degradation may be a better alternative.

Alternative IV: This alternative would construct a series of small gabion check dams across San Juan Creek and Bell Canyon at space intervals. This arrangement would allow the stream to restore from degradation locally and to control any further head cutting. The proposed engineering plan is shown in Figure 18.21. The three check dams are 2.5 feet high, approximately 1,400 ft apart, and each would trap approximately 37,300 tons of sediment if an equilibrium slope of 0.91 is assumed. This amount of sediment is close to one-half of the average annual sediment yield, thus, on the average, these three check dams would be filled up after approximately one and one-half years. This would be prior to the depletion of the sand and gravel in the pit and would continue to provide sand and gravel to the Conrock Pit. Of course, if any flood events larger than a 15-year return period occurs, the check dams would be filled up and the Conrock Pit would receive a supply of gravel and sand. After the Conrock Pit receives enough sand and gravel supply for another one and one-half years of operation, then the check dams can be built approximately 2.5 ft higher until the grade of the most downstream check dam has an elevation of about 355 ft. This requires the construction of 21 check dams over seven time periods. This scheme would first allow the stream to restore from degradation locally and to control any further head cutting and would eventually restore the degradated reach. In the meantime, the scheme still provides the supply of sand and gravel. Furthermore, this alternative would spread the capital cost of construction over a period of at least 30 years. This is the most feasible alternative.

The construction of the access road crossing in San Juan Creek is required for the park usage. This access road can be designed in such a way that it will also serve as a check structure. In addition, a low check structure can be implemented near the mouth of Bell Canyon to restore the canyon. The check dams for the access road and near the mouth of Bell Canyon would be approximately 10'0" high. In order to stabilize the gravel pit, an additional low check structure is required near station 16+00. The available space upstream of the access road will trap approximately 600,000 tons of sediment. It will take about 7.5 years to restore the creek and the canyon, or one flood event with a return period longer than 50 years. In order to prevent further

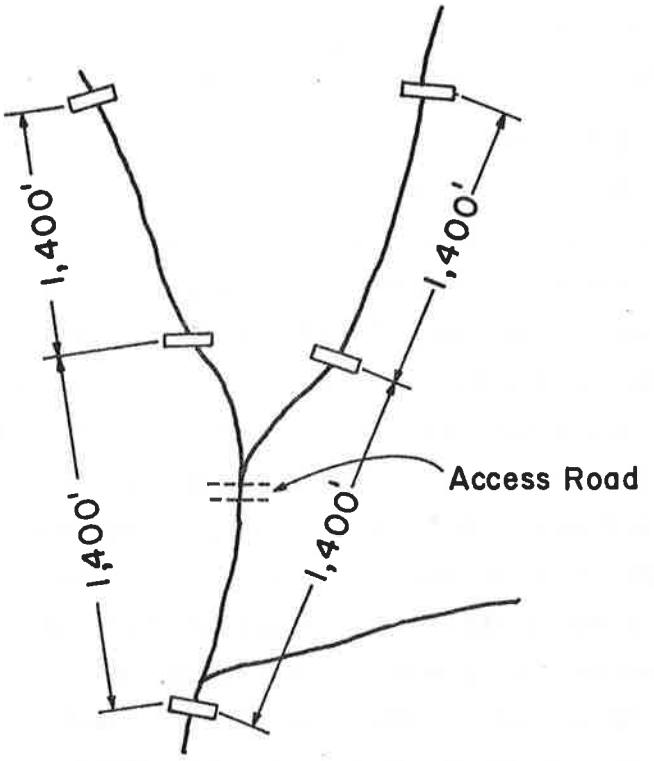

(a) Plan

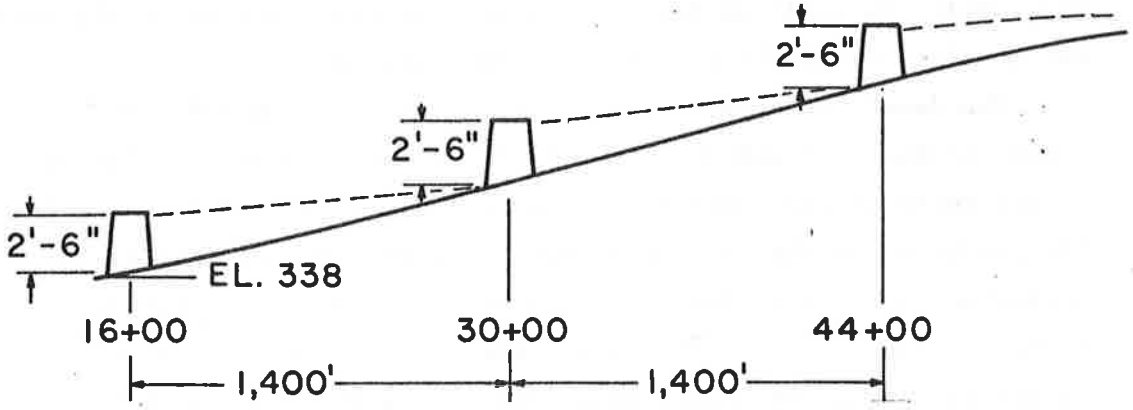

(b) Profile

Figure 18.21 Proposed engineering plan for Alternative IV.

cutting, slope protection in the form of riprap would be required on the sharp bends in Bell Canyon and San Juan Canyon. Again, this scheme would allow the protection of the channel from further cutting and the restoration of the park in a reasonable period of time.

Summary and Conclusions

This section presents an analysis of erosion and deposition problems in the San Juan Creek and Bell Canyon associated with the Conrock gravel mining operation. A mathematical model for routing sediment by size fraction was successfully developed and is utilized to estimate the erosion and deposition response of the stream and gravel pit subject to different hydrologic inputs and operational alternatives. Four engineering alternatives that consider rehabilitation of the Casper Regional Park and mining of sand and gravel were evaluated. Alternative I is a "do nothing" plan terminating the mining of sand and gravel. This alternative would allow natural healing processes in the form of aggradation to take place. No mitigation measure would be imposed on the existing stream. Alternative II is essentially the same as the Alternative I except it permits regular mining of sand and gravel. Alternative III proposes construction of a drop structure located near the upstream end of the gravel pit. Alternative IV proposes construction of a series of small gabion check dams near and upstream of the gravel pit boundary coupled with regular gravel mining.

The developed mathematical model was calibrated using two 1969 floods (January 25 and February 25, 1969) and validated utilizing the recent three storms (January 15-16, February 9-10, and March 4, 1978). The predicted results are excellent and have been verified by field measurements. The evaluation of alternatives indicate that Alternatives I and II require a long period of time to allow the healing of the creek by natural processes unless some large flood events occur in the future. Alternative III is a feasible engineering solution but unattractive, and Alternative IV proposing construction of a series of small check dams is the most feasible and attractive engineering plan for meeting the objectives.

18.4 DEGRADATION ANALYSIS FOR PIPELINE CROSSING DESIGN--JIM RIVER, ALASKA

General

The Kim River in Alaska is a meandering, coarse bed stream. There are six degrees of freedom for it to adjust its channel geometry during high flows. They are width, depth, slope, meander wavelength, amplitude, and radius of curvature. In this study, all these variables are treated as time-dependent. The proposed pipeline crossing site has been analyzed for the lowest bed levels and also for the possible extremities of river course that can occur during the economic life of the project. The analysis shows that the lowest expected bed level at the crossing site for the design flood (200 hr duration and 30,300 cfs flood peak) will be 1057.3 MSL. This represents a scour from present bed level of 7.0 ft. This scour is the expected maximum and is conservative in that it considers only a negligible amount of sediment transport into the reach from upstream and does not consider the cobble layer that exists five feet below present bed. Clear water scour (no transport from upstream) gives a scour depth of 7.5 ft.

The scour is determined by a sediment routing procedure which involves the use of sediment transport equations, the sediment continuity equation, armoring effect of coarse materials, and local channel geometry equations. Depth-discharge relations are synthesized in a time-dependent manner which generates a looped rating curve similar to those of many alluvial rivers. The tendencies of lateral migration are deduced and the limits of possible river migration are determined.

Channel Morphology

It is expected that the general properties such as geometry and alignment of the river will be changed by the passage of floods during the lifetime of the project. It is therefore necessary to establish information on the river morphology to estimate these changes. The representative cross section in the vicinity of the proposed crossing is developed by averaging the nearby seven cross sections where the channel geometries have been surveyed (September 1973)(see Figure 18.22).

From this representative cross section the following channel geometry relations are established (see Figure 18.23):

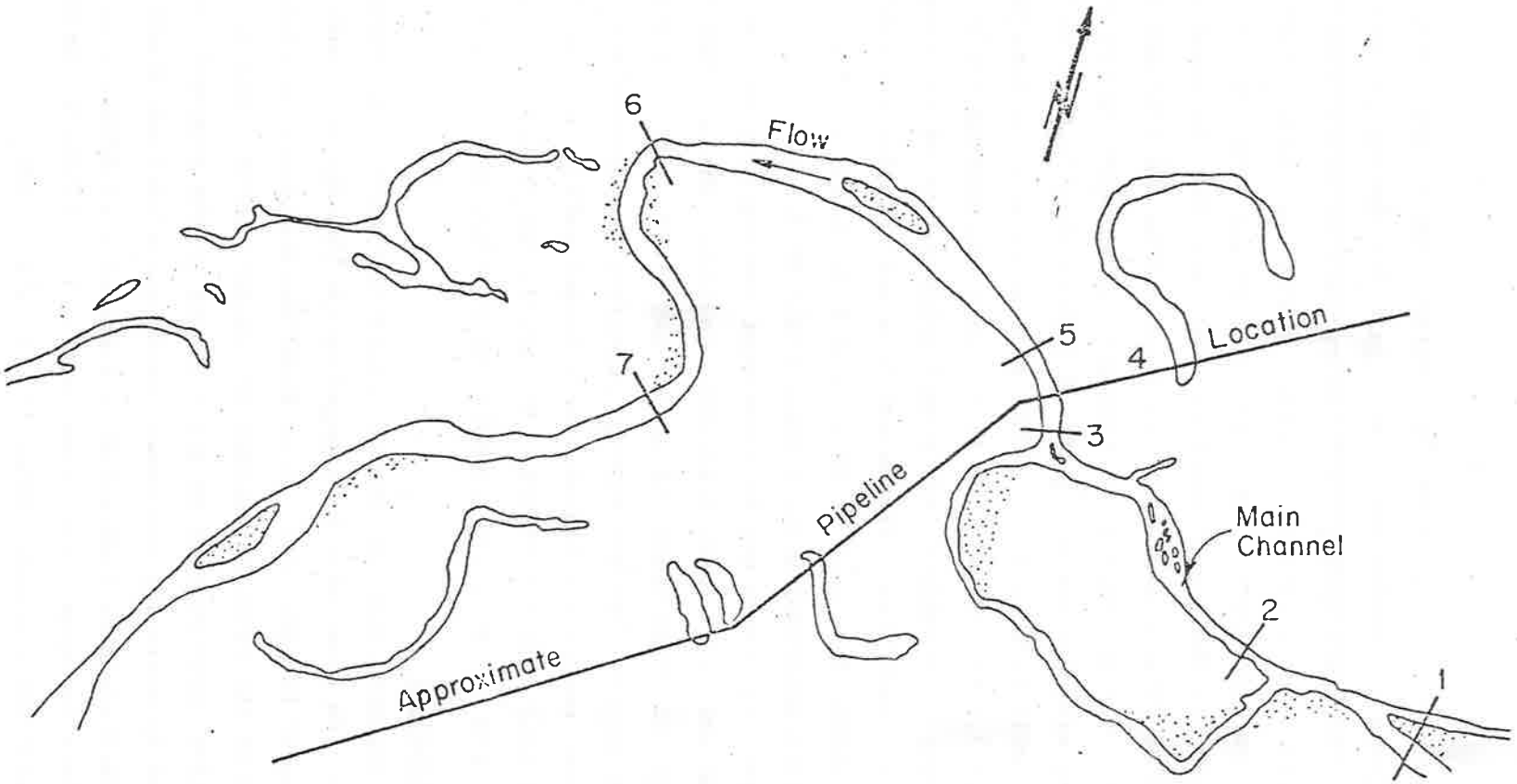

Figure 18.22 Location of cross sections taken near Jim River Crossing, Alaska.

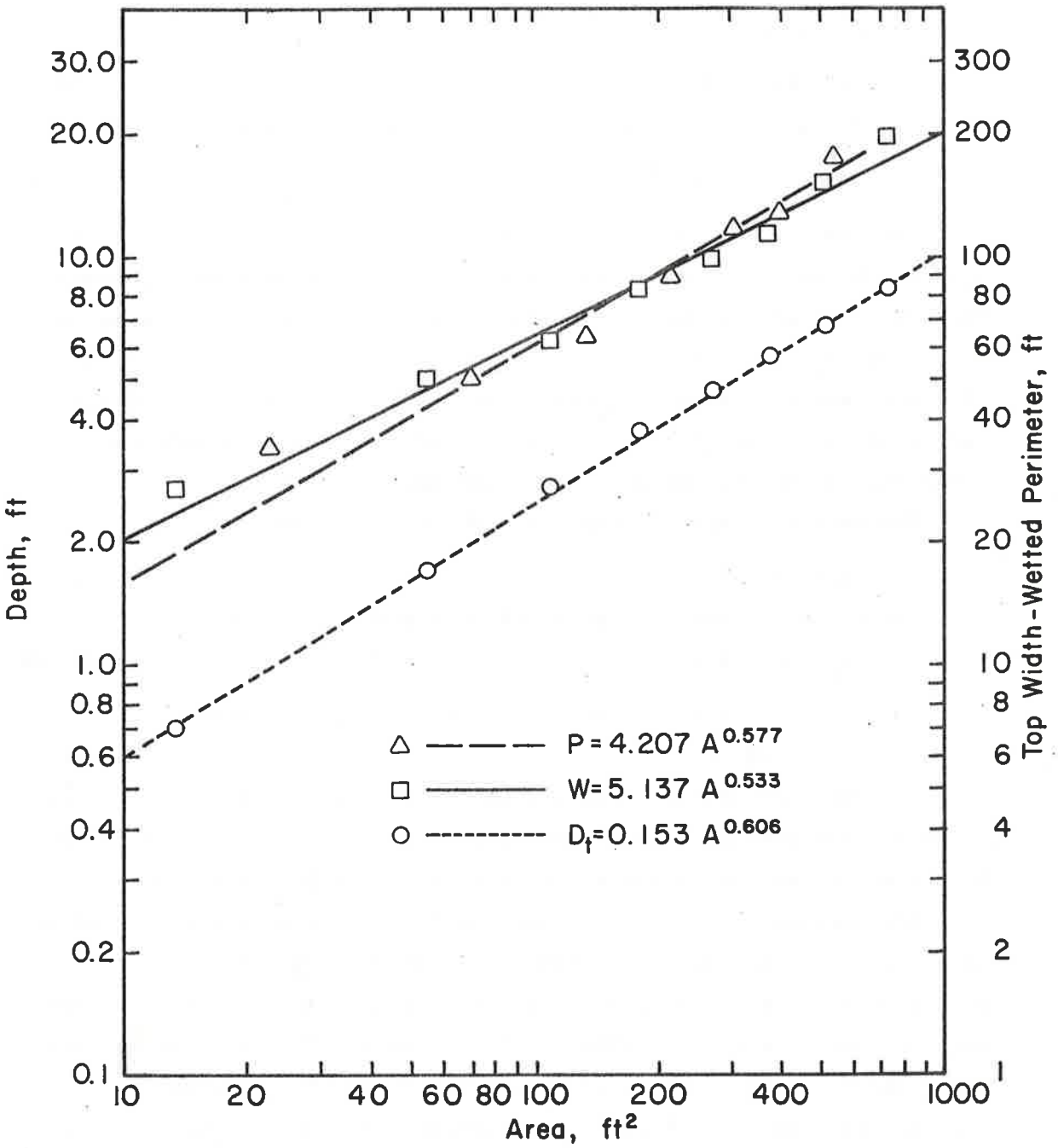

Figure 18.23 Channel geometry relations.

The wetted perimeter, P, versus flow area, A

$$P = 4.027\ A^{0.577} \tag{18.2}$$

The top width, W, versus flow area

$$W = 5.137\ A^{0.533} \tag{18.3}$$

The depth from thalweg level, D_t, versus flow area

$$D_t = 0.153\ A^{0.606} \tag{18.4}$$

The analysis of 13 meander loops located in the reach six miles upstream to about 20 miles downstream of the proposed crossing shows that the average meander wavelength, L, is 2460 feet. The average wave amplitude, A_m, is 1250 feet, the average radius of curvature, r, is 607 feet, and the average sinuosity is 1.70. The sharpest bend has a radius of curvature of about 200 feet, and the relations between meandering dimension parameters are estimated as follows:

The meander length to channel width relation is

$$L = 13.667\ W \tag{18.5}$$

The meander amplitude to the channel width relation is

$$A_m = 6.944\ W \tag{18.6}$$

The meander length to the radius of curvature relation is

$$L = 4.053\ r \tag{18.7}$$

By averaging meander belt widths at 10 locations near the proposed crossing, the average meander belt width is 2,922 feet and the meander belt width in the immediate vicinity of the crossing is 2,700 feet.

The average water surface slope or the approximate energy gradient in a 6,200-ft reach near the proposed crossing is 0.00319. The channel bed slope for a 1,800 ft reach immediately downstream the proposed crossing is about 0.00389, and the reach 1,950 ft upstream from this site has a slope of 0.00128 (see Figure 18.24). The average channel bed slope as taken from USGS topographical maps is 0.00419 for a 4.59-mile reach near the crossing (see Figure 18.25).

The energy slope is usually less than the channel bed slope. For a safer design, it is reasonable to assume the energy slope to be equal to channel bed slope. The design bed slope of 0.004 which was adopted by Pipe Line Technologists for computing design flood is satisfactory for design purpose.

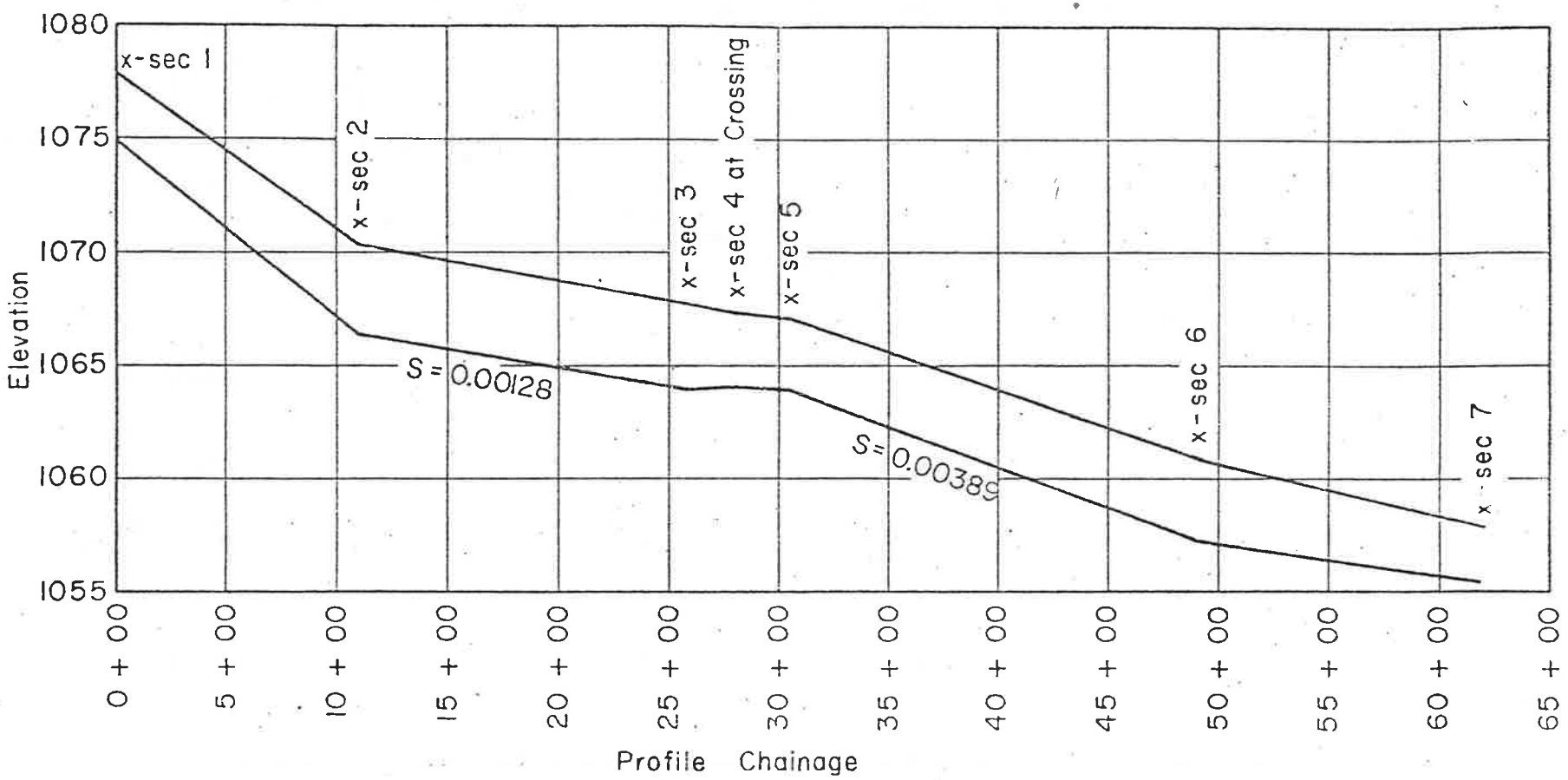

Figure 18.24 Bed and water surface profiles.

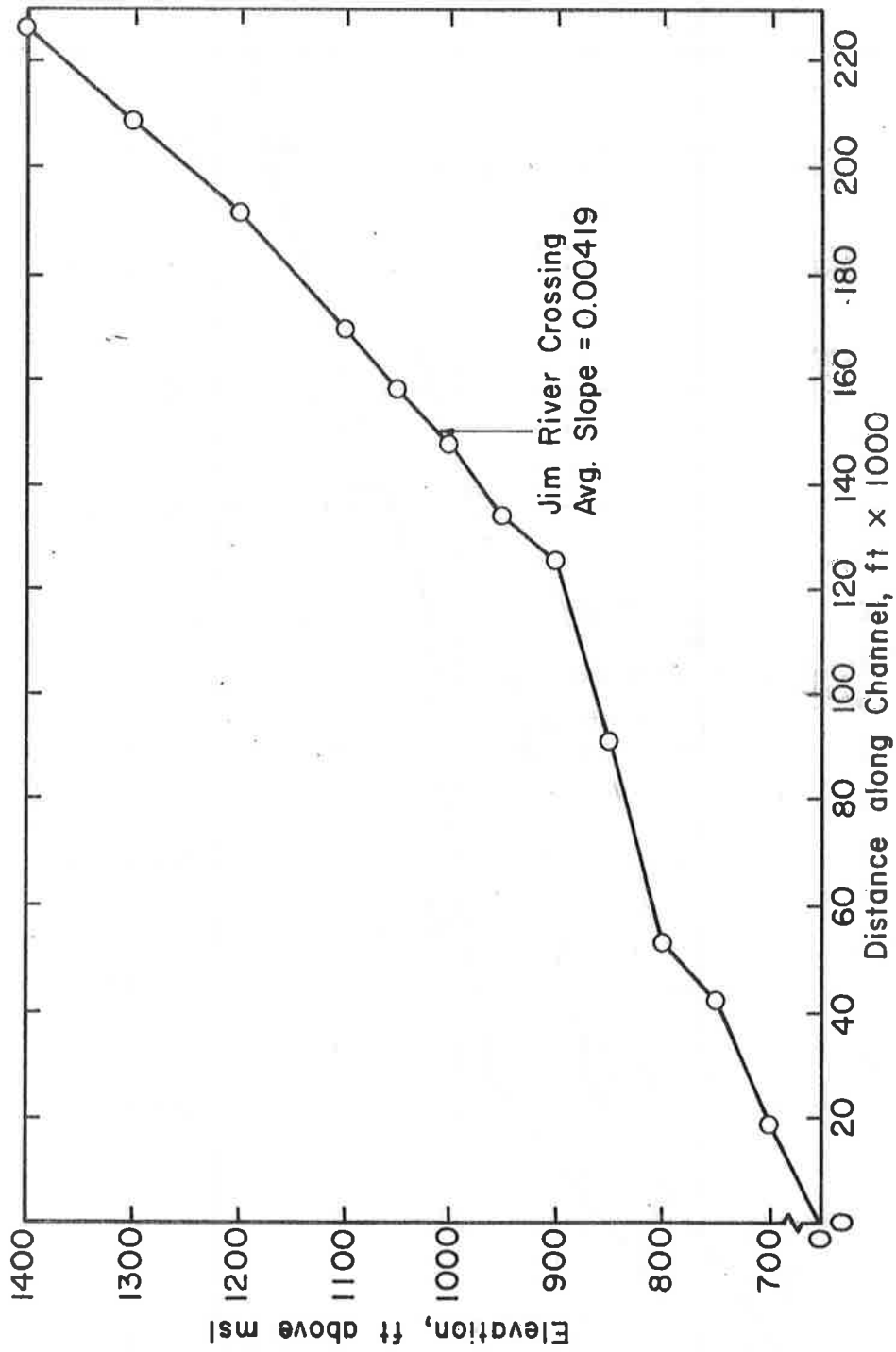

Figure 18.25 Average channel bed slopes.

The median bed material size, D_{50}, is 0.256 ft (78.03 mm) and the gradation coefficient, σ, is 1.54. The data from the boring log in the vicinity of the crossing shows that there is a cobble layer approximately 5 feet below the riverbed and this layer is about 4.5 feet to 8.5 feet thick. To assume the same particle distribution for this cobble layer will yield a conservative estimation of values. This assumption is necessary because the size distribution of this cobble layer is not known. The Manning's roughness values, n, are assumed to be the same values as those adopted by Pipe Line Technologists (1973). They are n = 0.09 for the left overbank flow, n - 004 for the channel flow, and n - 0.09 for the right overbank flow. The Manning's n with a value of 0.04 for the channel flow portion was checked by the Strickler formula and was found to be consistent with the bed material sampled near the crossing site.

Depth-Discharge Relations

A straight alluvial river has three degrees of freedom in adjusting its geometry during the degradation or aggradation processes, i.e., width, depth, and bed slope may change with time. These three degrees of freedom are considered in the analysis. Since this information is unavailable, the depth-discharge relations are established for a straight rigid channel and for a straight alluvial channel respectively.

The depth-discharge relations for a straight rigid channel are synthesized by Manning's equation with the assumption of fixed channel geometry; or the bank-full top width, the bank-full depth from the thalweg level, and the channel bed slope are time-invariant. The current channel shape is approximated in Figure 18.26 which was provided by Pipe Line Technologists (1973). The hydraulic inputs for this synthesis are the channel geometry equations, the channel bed slope, and Manning's n, which were described previously. The established depth-discharge relations for a rigid bed are given in Figure 18.27 which gives the comparison to the case of an alluvial bed.

The depth-discharge relations for a straight alluvial river are synthesized by a method similar to that for a rigid bed channel. The main difference is that the channel shape is no longer constant (see Figure 18.26). The bank-full top width, the bank-full depth from thalweg level, and the channel bed slope are time dependent and are

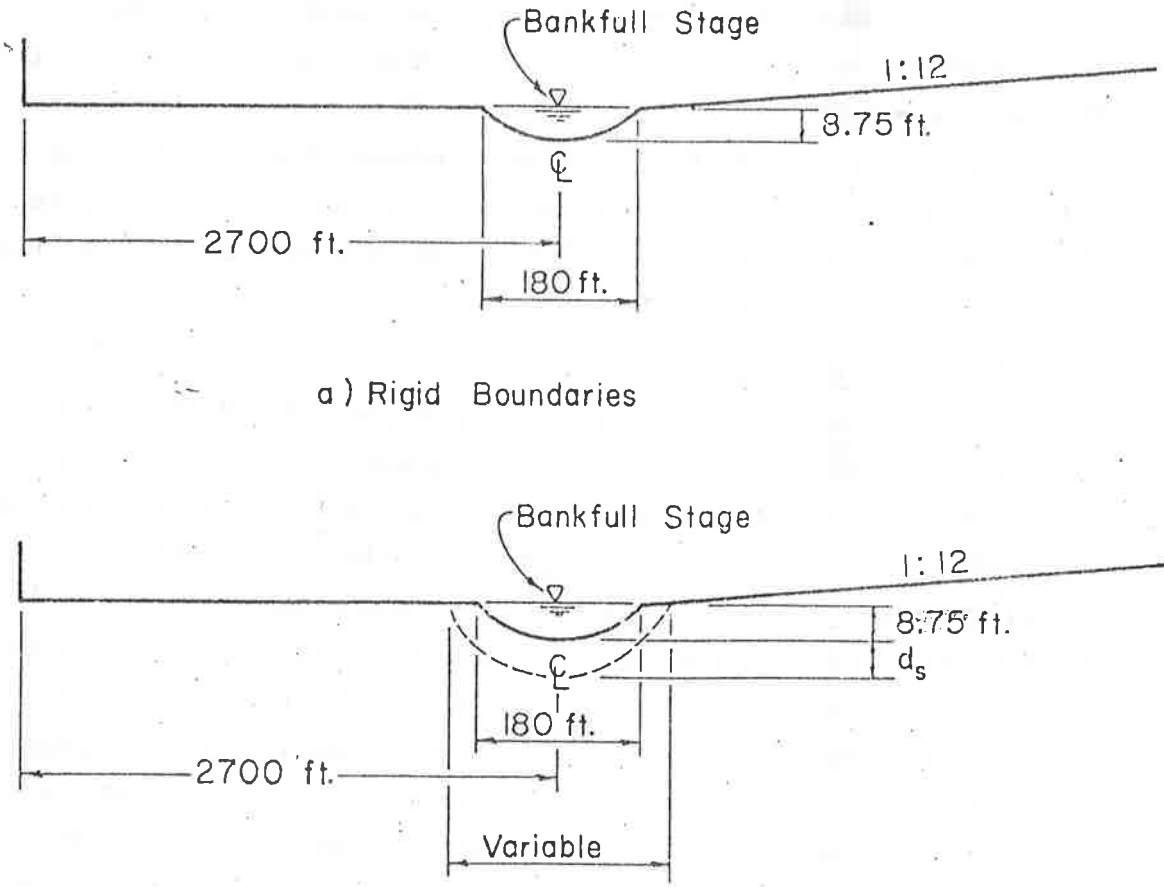

Figure 18.26 Channel geometry for Jim River.

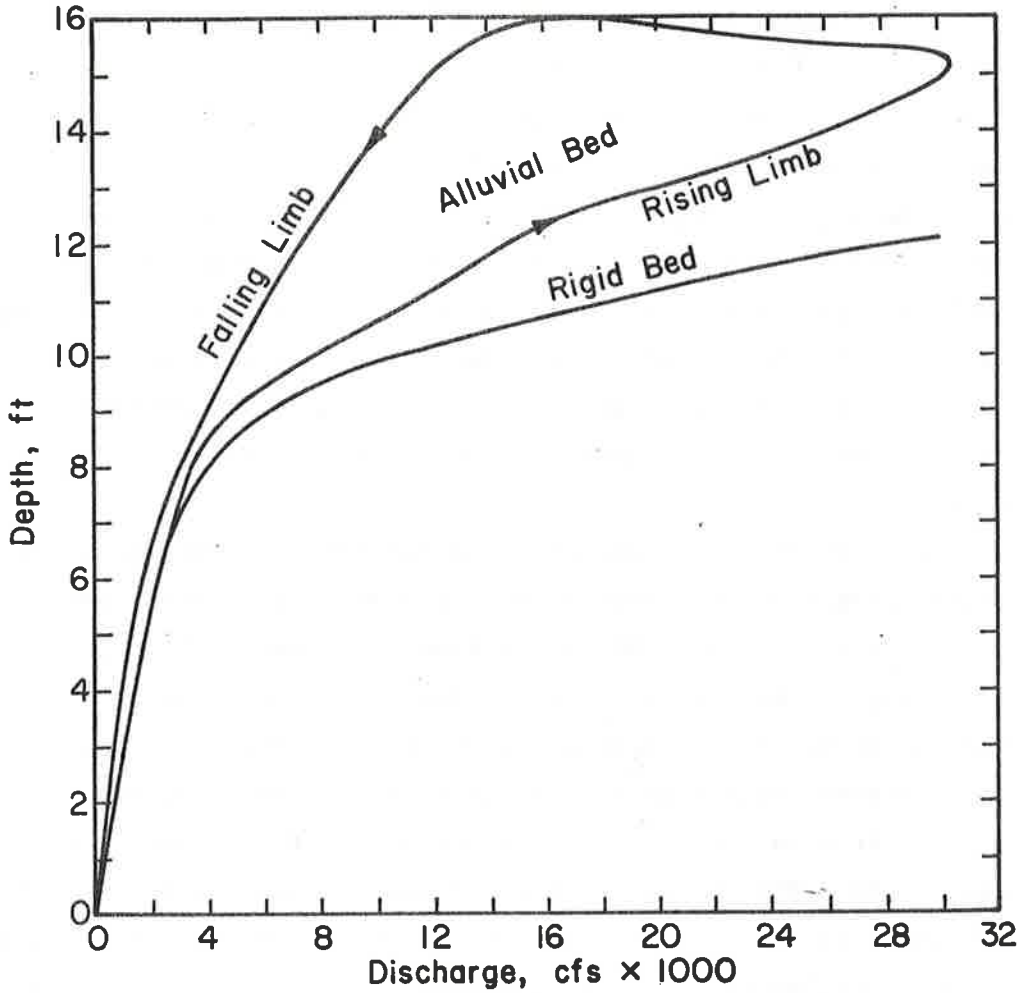

Figure 18.27 Depth-discharge relationships for straight channels (assuming clear water scouring).

consequently adjusted in accordance with the successive lowering of the thalweg level due to the passage of floods. The synthesized depth-discharge relations for the period of the design flood are shown in Figure 18.27 which indicates a looped rating-curve similar to those measured in many alluvial rivers.

Determination of the Lowest Thalweg Level

The thalweg level at the crossing site was measured in September, 1973 as 1061.3 MSL. During the economic life of the pipeline project, the thalweg at the crossing may fall below this level due to the passage of floods. The possible minimum level is expected to be experienced during the design flood. The lowering of the thalweg may be due to one or a combination of reasons: 1) general lowering at the thalweg during high flows, 2) additional lowering of the thalweg in bends due to the curvature of flow, 3) potential local lowering of thalweg due to the passage of bed forms, and 4) development of impending cutoff upstream of the site and shortening of flow path during high flows.

In this study the possible minimum level is determined by considering the above four reasons individually. The general lowering of the thalweg during the design flood is computed by a procedure involving sediment routing in a straight reach. This procedure includes the use of bed load sediment transport equations for gravel streams (Meyer-Peter, Müller Bedload Formula, see Chapter 4), the sediment continuity equation, and the channel geometry equations established in this study. The channel geometry variables are treated as being time-dependent and the armoring effect of coarser bed material due to unequal sediment transport rates of different size fractions is considered. The hydraulic inputs for this computation are the design flood hydrograph (200-hour flood duration and a peak flow of 30, 300 cfs), the current particle distribution, the current bed slope, the current channel geometry, and all the other inputs required for determination of the depth-discharge relation. Since the channel bed slope is only 0.00128 for a reach of 1,950 ft upstream from the proposed crossing, the upstream sediment inflows are practically negligible. This is because the effective particle size prevents motion except during a short period of the flood peak (30,300 cfs). The effect of upstream

sediment supply will be discussed later. The length of channel reach used for computation is assumed to be 5,000 ft, since it gives the maximum depth of general scour for the design flood. The computed cumulative scour depth during the design flood for a straight reach is shown in Figure 18.28, and the corresponding water surface levels and the thalweg levels are given in Figure 18.29.

In curved reaches there will be an additional lowering of the thalweg. At this crossing there is little or no curvature of flow. The pipeline crossing is located in a relatively straight reach and additional scour due to curvature of the flow is not expected.

The Froude number at the time of peak flow is around 0.6 and the stream power is 10.3 lb/ft/sec. From these values it is found that the river bed form will most likely be in the plane bed. Therefore, no appreciable bed forms are expected, and hence Manning's n as determined only by grain resistance is adequate for design. Also, there will not be additional lowering of the bed because of bed material moving through the reach.

The main effect of the development of a cutoff upstream of the site, a shortening of the flow path during high flows, is to increase the channel bed slope. Since an extreme energy slope of 0.004 is used in this analysis, no additional considerations of this effect are necessary.

The main effect of sediment supplies from an upstream reach is to decrease the scour depth, and these sediment supplies may be estimated by the sediment transport equation using the upstream bed slope. The resultant scour-depth for different upstream bed slopes due to the passage of the design flood are as follows:

Upstream Bed Slope	Resultant Scour Depth
(no supply)	7.46 ft
0.00128 (current slope)	7.06 ft
0.002	5.99 ft
0.003	3.38 ft
0.004	0.00 ft

The current upstream bed slope is 0.00128 and the corresponding scour depth is 7.06.

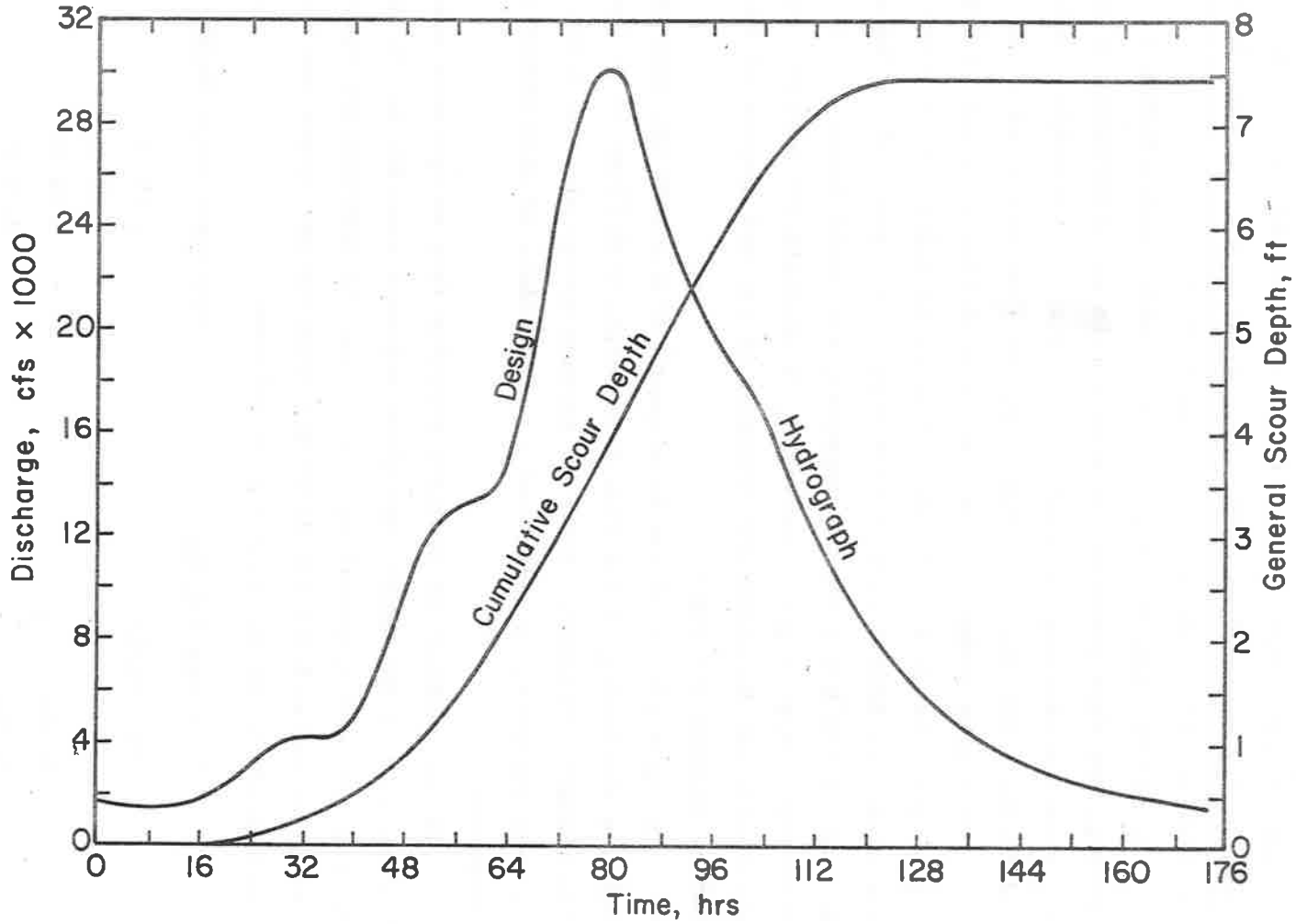

Figure 18.28 Design flood hydrograph and resulting scour depth (assuming clear water scour).

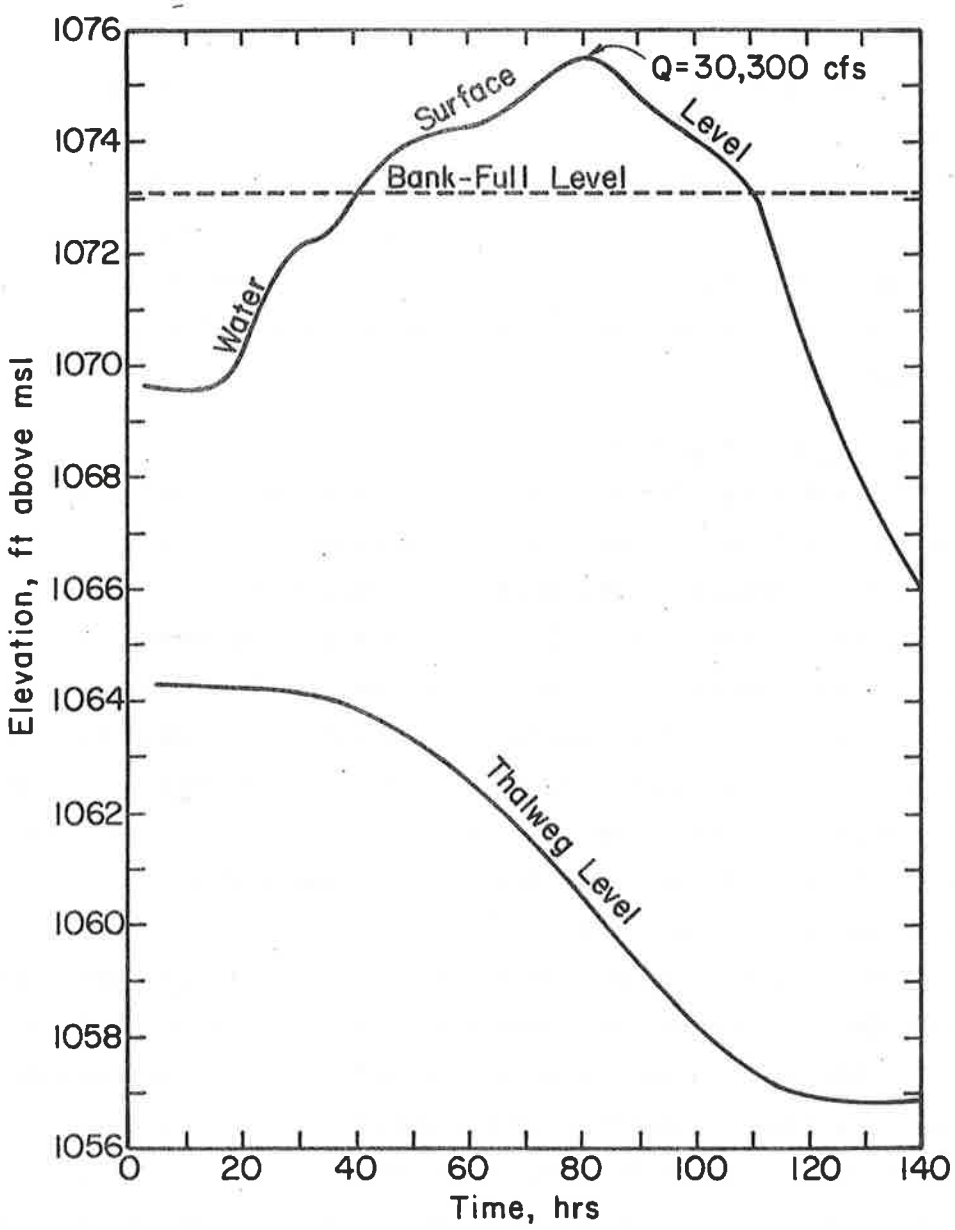

Figure 18.29 Thalweg and water surface elevations (assuming clear water scour).

The computation results show that the mean diameter of bed material becomes coarser as scour proceeds. As mentioned previously, a thick cobble layer (4.5' - 8.5' thick) is laying five feet underneath the surface layer. If the particle distribution of this cobble layer were available, the sediment transport equations would yield a smaller scour depth. This is because the armor plating of these cobbles will further retard scouring.

In summary, the expected lowest bed level at the pipeline crossing is 1057.3 ft. This is seven feet below the present bed elevation of 1064.3. This elevation is believed conservative in that it allows for a modest inflow of sediment from the upstream reach, (clear water scour gives an elevation of 1056.8 ft, 7.5 ft below present bed), and the cobble layer five feet underneath the present bed was not included in the analysis.

Lateral Channel Migration

A meandering alluvial river has three additional degrees of freedom to adjust its geometry beyond those for a straight alluvial river, i.e., meander wavelength, wave amplitude, and radius of curvature may all change with time. The Jim River is a meandering river, therefore these three degrees of freedom should be considered in estimating possible lateral channel migrations. The extent of possible lateral channel migration depends upon: 1) the meander belt width, 2) the rate and direction of the channel's lateral migration, and 3) the possible change of channel alignment due to the development of cutoffs upstream and downstream of the site.

The probable maximum meander wavelength, the probable maximum wave amplitude, and the probable maximum radius of curvature during the project's lifetime are estimated by the relations between meander dimension parameters (Equations 18-5, 18-6, and 18-7). The input is the probable maximum bank-full width which is determined for the design flood. The estimated extremities of these three quantities are as follows: the meander wavelength is 4,220 ft, the wave amplitude is 2,150 ft, and the radius of curvature is 1.040 ft. The sinuosity estimated from the above quantities is 1.49, which is less than the current average value of 1.7. This indicates a current tendency to straighten the channel reach.

The average meander belt width near the crossing site is 2,922 ft and has a value of 2,700 ft in the immediate vicinity of the crossing (see Figure 18.30). From Figure 18.30 it can be seen that the proposed crossing is near the center of the meander belt. The estimated probable maximum wave amplitude during high flows is 2,149 ft and is less than the local meander belt width. Hence, the probability of the river moving the entire meander belt distance during the project's lifetime is very small.

The channel may migrate in a direction along the axis of the meander belt. This is shown by the studies of the crossings by James Brice. A change of 125 ft has occurred in the direction of the pipeline over a 14-year period. Continued migration in this direction at a similar rate would definitely jeopardize the pipeline during its economic lifetime. The meander wavelength of the loop in the crossing vicinity before the development of cutoff is about 3,000 ft, and the probable maximum wavelength as deduced in this study is 4,223 ft. This shows the possibility for channel migration in the direction along the axis of the meander belt, but the development of a cutoff upstream of the site in the past 10 years has largely reduced this possibility. It is clearly shown in the 1973 survey that the flow has concentrated in this cutoff path (see Figure 18.30). However, for a safer and more economical design, riverbank protection works are recommended for the left bank (looking downstream) near the crossing to prevent possible migration (Figure 18.30).

Judging from the information on the extremities of meander size parameters and available aerial photos, the probable limits of bank lines during the lifetime of the project have been estimated. They are shown as dashed lines in Figure 18.30. Sag points would require a pipe deep-burial distance of 650 ft.

With bank protection or with close surveillance so bank protection could be installed in the event channel migration endangers the crossing, sag points can be located 150 ft to the left of the left bank and 100 ft to the right of the right bank. The total deep burial distance would be about 350 ft. The right bank appears fairly stable and probably will not require bank protection during the life of the pipeline. The left bank upstream of the crossing is unstable and probably will

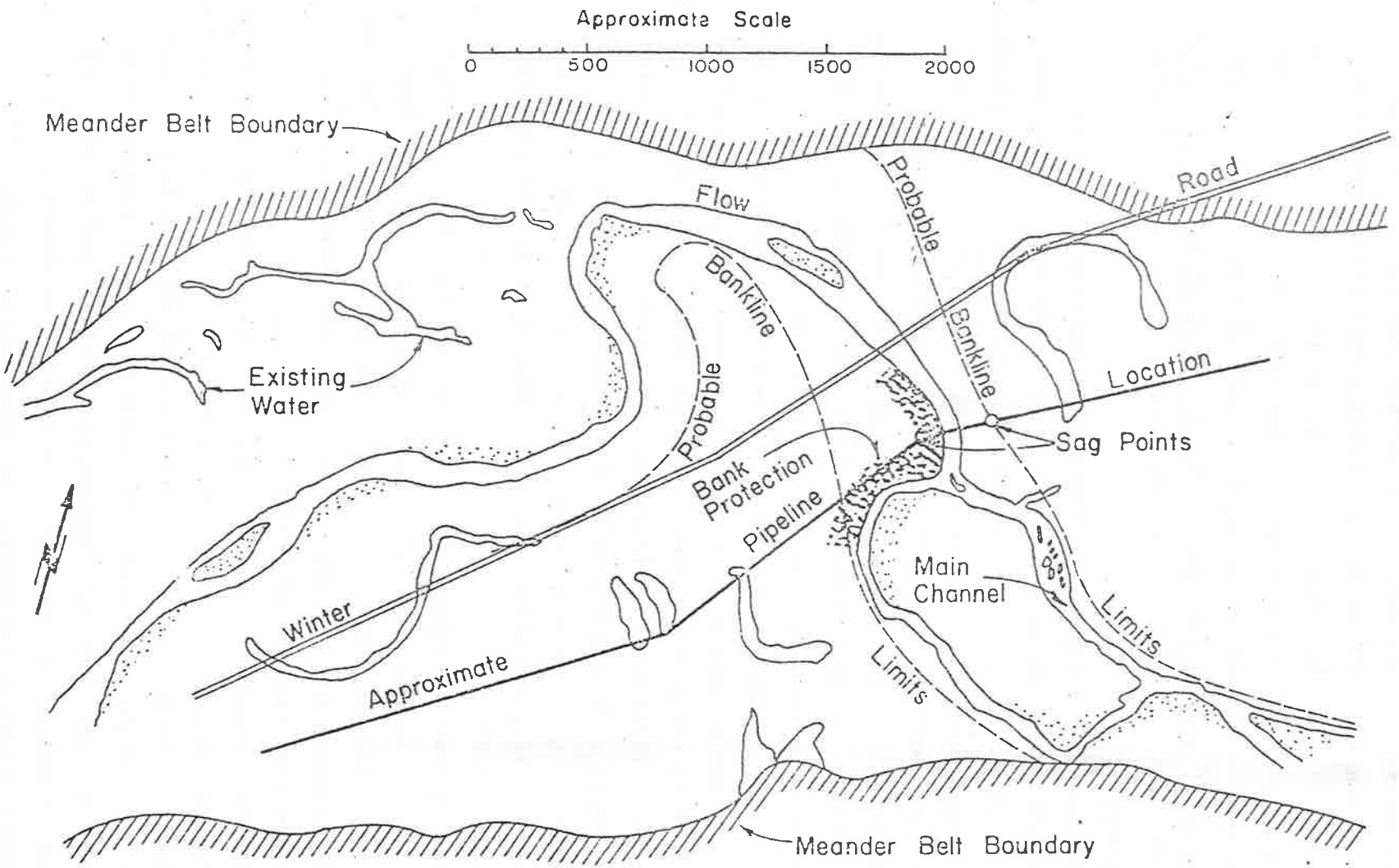

Figure 18.30 Probable limits of Jim River banklines.

need bank protection. Plugs in the left channel upstream of the crossing would probably eliminate the need for bank protection works on the left side. These plugs would also improve the flow of the river through the crossing.

18.5 SEDIMENT PROBLEMS ASSOCIATED WITH DAM REMOVAL--MUSKEGON RIVER, MICHIGAN

General

Presented in this section is an analysis of sediment movement in the Muskegon River following the removal of Newaygo Dam, Michigan. A mathematical model capable of routing water and sediment was utilized to show both how the sediment wave has moved to date and how they will move in the future. This model was applied between Bridgeton Bridge and a location six miles upstream of the old dam site.

The model utilized is a physical process simulation model capable of predicting sediment movement. This model has been widely used to solve many real world problems. Also, it has been verified for the Muskegon River, utilizing collected data.

The results of analysis indicate that the sand wave has advanced at approximately one mile per year for the first nine years and will move more slowly in the future. The flushing rate of the sand wave at the tail end is slower than the rate of advancement of the wave. The flushing rate has been about 0.25 miles per year for the first nine years and will be slower in the future. The differential rates of advancement and flushing elongate the sand wave. This phenomenon was verified both by field observation and with tests conducted in a small laboratory flume. The presence of sand on the bed of the channel at any one location is temporary and transient. The sediment released by removal of the Newaygo Dam is moving through and will move out of the system eventually. Part of the sediment stored behind the dam was wash load (silt and clay) and most of it flushed through the system immediately; the sand wave will ultimately flush through the system. This will require on the order of 50-80 years, depending on the magnitude of future hydrologic events. The presence of sand in the system has caused negligible change in local stage and a slight increase in the flow velocity. Effects of the sand wave will be eliminated as the sand moves through the system.

Study Reach Description

The study reach extends from Bridgeton Bridge to a point 6.5 miles above Old Newaygo Dam. The Muskegon River meanders. It has a sand, gravel, and cobble bed that was formed by the river. From the aerial photos of the river one can see that it has occupied various positions throughout geological time and as such is a dynamic system. In the study reach, the bed is armored and it is anticipated that this armor will not be eliminated except during periods of extremely high flow.

Within the reach, the river banks all exhibit a depositional structure. In some locations the banks are reasonably unstable and at some locations the banks are heavily vegetated. There are locations upstream of Newaygo where mass wasting is occurring. This intermittently added some sediment to the river. Downstream of Newaygo the topography flattens, but with some high banks. In general, the lower end of the river is relatively flat in comparison to the upper reaches.

Based on observations made during two field trips and field data, it is known that only small amounts of sediment will be transported except during intermediate and large flow events.

The New Newaygo Dam was in existence until November 1968, when dismantling commenced. Removal was completed in July, 1969. The removal of the dam resulted in the release of deposited sediment that is now migrating through the system. The volume of the sand wave is computed to be approximately 60 percent of the 930,000 cubic yards of sediment stored in the reservoir prior to removal of the dam. This figure is a reasonable estimate considering the sediment transported from the reservoir during the two-year period prior to removal of the dam during which the spillway gates were totally open. Also, a significant part of the deposited sediment consists of clay, silt, fine sand and organic material that was readily transported through the system causing no aggradation of the bed of the river.

The Mathematical Model

Governing Physical Process: The movement of a sand wave through a river system as results from removal of a dam is a complicated problem. This problem includes the rate of sand wave movement, the degradation upstream of the old dam site, the deposition of the material along upstream channel, the possible changes in water surface elevation and

velocities and the possible effects on channel stability and flood potential. Simplistic but realistic assumptions are needed to obtain a solution to this problem in a practical and economical way. The dominant physical processes considered in the model include: the flow of water, sediment transport, sediment routing, degradation, aggradation, and bed control due to the presence of an armor layer at small to intermediate discharges. The governing equations include the continuity equations for water and sediment, the momentum equation and the energy equation. The processes governing water and sediment movement are unsteady in nature, therefore, a routing procedure is needed. In order to simplify the problem, a known discharge assumption is used. The lnown discharge sediment routing is appropriate in this study because of the short reach of river considered.

The known discharge assumption is that during any one time period, water discharge is constant along a reach of river, except where lateral inflow or outflow occurs. Though a model of this type cannot predict dynamic effects that an unsteady model can, it requires considerably less computer time. Also, the model is still able to accurately calculate velocities and flood stages. This model can be utilized to route sediment movement over long time periods. The time increment utilized in the input hydrographs may vary from a few hours to a month or longer, depending on the flow conditions and the required accuracy of the results. It should be noted that the known discharge model can simulate unsteady flow profiles if they are coupled to an unsteady flow water routing model. Details of the known discharge model are presented in Chapter 12.

Data Development: The data base for this model requires a cross section file, discharge file, and input-output control file. Each of the files were kept separate and were generated to allow ease of accessibility of data.

The discharge file was generated from the daily discharge readings at the USGS gaging station at Newaygo, downstream of the old dam site. The records from November 15, 1968 to December 18, 1977 were used. Due to the large number of discharge readings and the direct proportionality of this number to computer time required for routing, the discharge file was reduced in magnitude. Each of the time increments consisted

the average flow for each seven-day period, a reasonable assumption since the average deviation over each period was less than ten percent. For prediction in the future, the discharge file was extended to cover an additional 18 years simply by adding the record from 1968 to 1977 twice in a row.

In order to evaluate the response of the study reach under flood conditions, the information on flood frequency is required. The estimate of flood frequency discharges was made by Michigan Department of Natural Resources and the magnitudes of floods with different return periods are given in Table 18.7, following.

Table 18.7 Discharge with various return periods.

Return Period (years)	Discharge (cfs)
2	6,300
5	8,510
10	10,060
25	12,130
50	13,750
100	15,440
200	17,210

A stage-discharge relation was used as the downstream control. This control is located at Bridgeton Bridge. This is not an unreasonable procedure since the stage-discharge relation at Maple Island Rd., downstream of Bridgeton, is quite similar to that at Bridgeton, which only consists of four points (Figure 18.31).

Since pre-dam removal conditions were not known, the cross section file was generated from the data furnished by the Michigan Department of Natural Resources and by interpolating 1968 conditions from the estimated 1977 position of the sediment wave, its volume, and the armored bed of the river. The position of the sediment wave at the time extended from approximately five miles above Bridgeton Bridge to three miles below Newaygo Dam. The volume of sediment was estimated to be 60 percent or the original volume (560,000 cubic years) of impounded sediment. This reduction in volume results from considering the fine sediment and the organic material being flushed downstream as wash load.

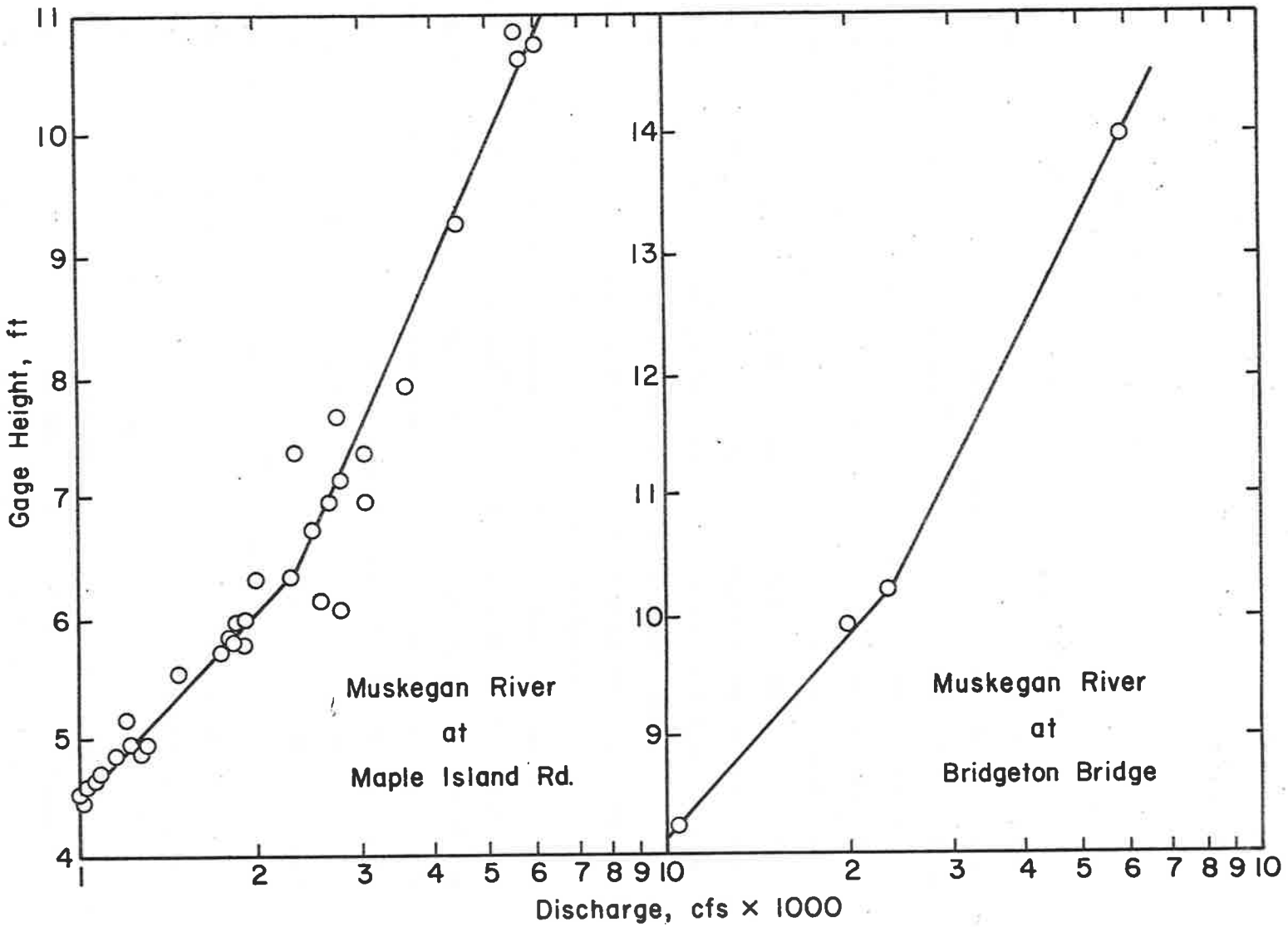

Figure 18.31 Stage discharge relations at Maple Island Road and Bridgeton Bridge.

The median diameter of the sand forming the wave was determined to be 0.25 mm. This was arrived at by examining the bed material distribution for the study reach from the USGS sediment information and from the sediment grade scale recommended by Simons and Sentürk (1977).

The resistance to flow of the movable bed is a function of bed material size, hydraulic parameters, and bed roughness. The Manning's n for the main channel as furnished by the Michigan Department of Natural Resources ranges from 0.023 to 0.035 along the study reach with an average of 0.03. This range of Manning's roughness coefficient is valid for lower regime sand bed channels when ripples and dunes form on the bed. The examination of the flow discharge from November 15, 1968 to December 31, 1977 indicated that this period was essentially a low flow period with a peak flow of 10,800 cubic feet (approximate return period of 14 years). Thus, the Manning's roughness coefficient furnished by the Michigan Department of Natural Resources is correct for the conditions with the presence of the sand wave. In order to account for the high resistance in the overbank area due to vegetation and housing, a Manning's n value of 0.15 was used in the overbank area.

In order to evaluate the response of the study reach under pre- and post-dam removal conditions it is necessary to estimate Manning's roughness more accurately. Recent studies at Colorado State University by Simons, Al-Shaikh-Ali, and Li (1979) indicated that the passage of sand wave could reduce the resistance to flow and slightly increase the velocity. For the Muskegon River, the presence of sand wave currently along the channel after the removal of the dam is evident as shown in Figure 18.32. This figure gives the variation of D_{75}, bed material size 75 percent finer by weight, with the distance. The areas with small D_{75} are the areas temporarily covered by sand waves. In order to evaluate the effects of dam removal on water surface elevation and velocity three sets of cross-sectional conditions 1) representing the pre-dam removal (1968), 2) the present (1977), and 3) the future (1995) were used. Different Manning's roughness coefficients existed for the 1968 pre-dam removal conditions. The Manning's roughness for 1968 conditions should be higher than those for 1977 and 1995. Prior to removal of the dam, the bed of the study reach predominantly consisted of gravels and cobbles due to armoring resulting from long-term

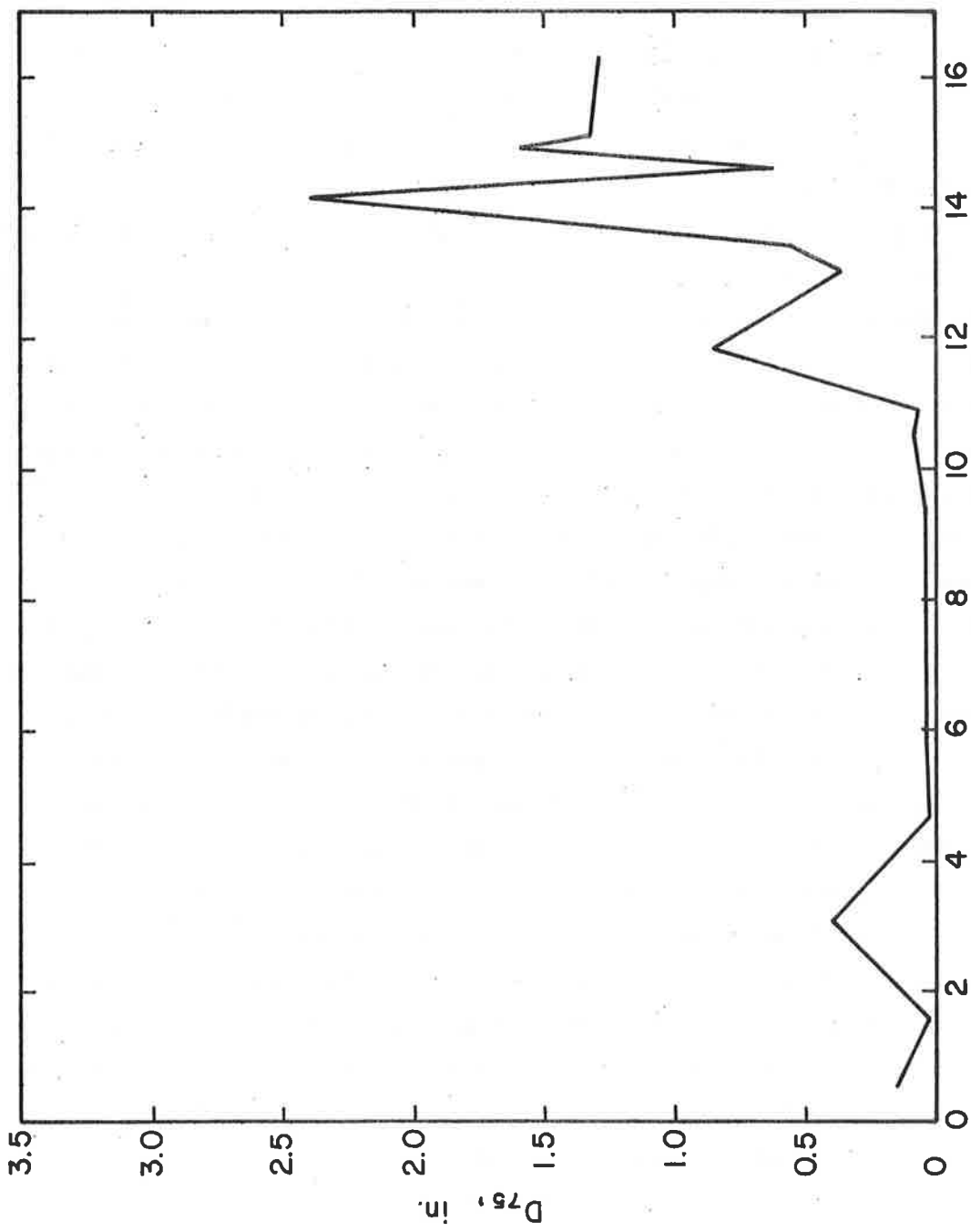

Figure 18.32 Spatial distribution of bed material size, 75% finer by weight.

degradation. According to Chow (1959), the normal value of Manning's roughness coefficient for streams of this type is 0.04 and the minimum value for major streams with irregular and rough section is 0.035. Based upon values of Manning's n suggested by Chow and others, Manning's roughness coefficient of 0.036 was adopted for the 1968 channel conditions for all cross sections, except in the Old Woman Bend area. Here, due to extreme sinuosity and other factors, the n value was increased 23 percent utilizing the local physical and hydraulic conditions (see Chow, 1959).

Model Verification: Before attempting to use a mathematical model, both model calibration and verification are necessary. Manning's roughness and sediment transport parameters are the common model parameters that need to be calibrated. Manning's roughness coefficients used in the HEC-2 program were provided by the Michigan Department of Natural Resources. A specific sediment transport equation could not be specifically established for the Muskegon River due to lack of enough field measurement data. The equation developed by Li (1978) was applied. In order to check the applicability of the model, a verification run was made. This simulation run covers the period from November 15, 1968 to December 31, 1977. The calculated 1968 cross section data and the weekly hydrograph (491 time periods) were used to verify the model. The 1977 bed profile that was predicted compared very well with the measured profiles as shown in Figure 18.33. Also, the cross section at Old Woman's Bend (river mile 10.57) was predicted with excellent accuracy (Figure 18.34). The simulated average rate of sand wave movement for the first nine years is one mile per year which is close to that observed in the field and the rate as determined from a small physical model study of the system that was conducted in the hydraulic laboratory at Colorado State University. A brief description of this physical model follows.

A small flume was utilized to model the sediment impounded by Newaygo Dam, and the sand wave movement after removal of the dam. Using time lapse photography and normal flow conditions, the location of the sediment wave was documented as it migrated downstream (Figure 18.35). This physical simulation helped verify that the sand wave was traveling at approximately one mile per year and that as the sand wave elongated and diminshed in amplitude, the velocity of the sand wave decreased.

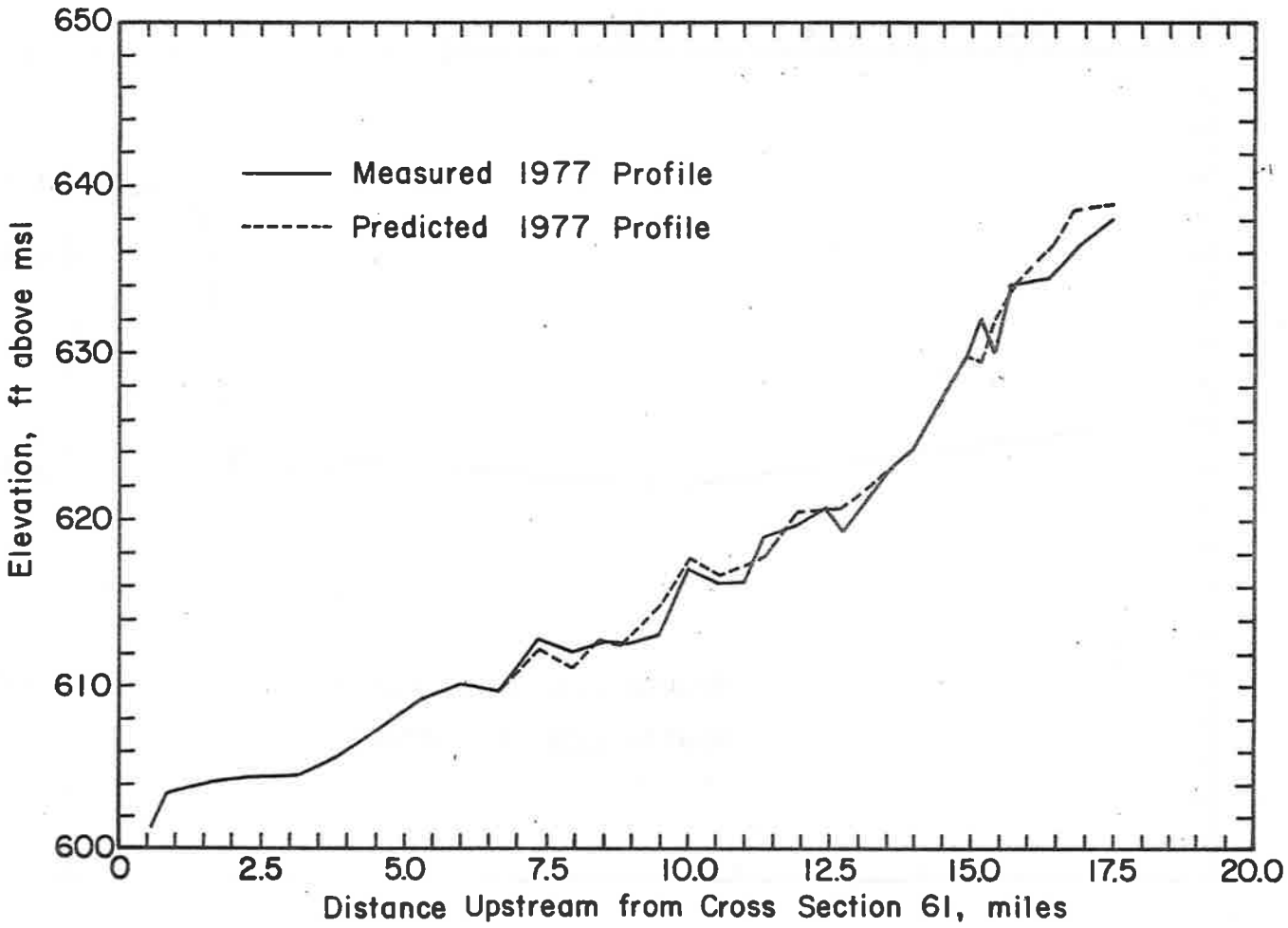

Figure 18.33 Comparative bed profiles for the Muskegon River.

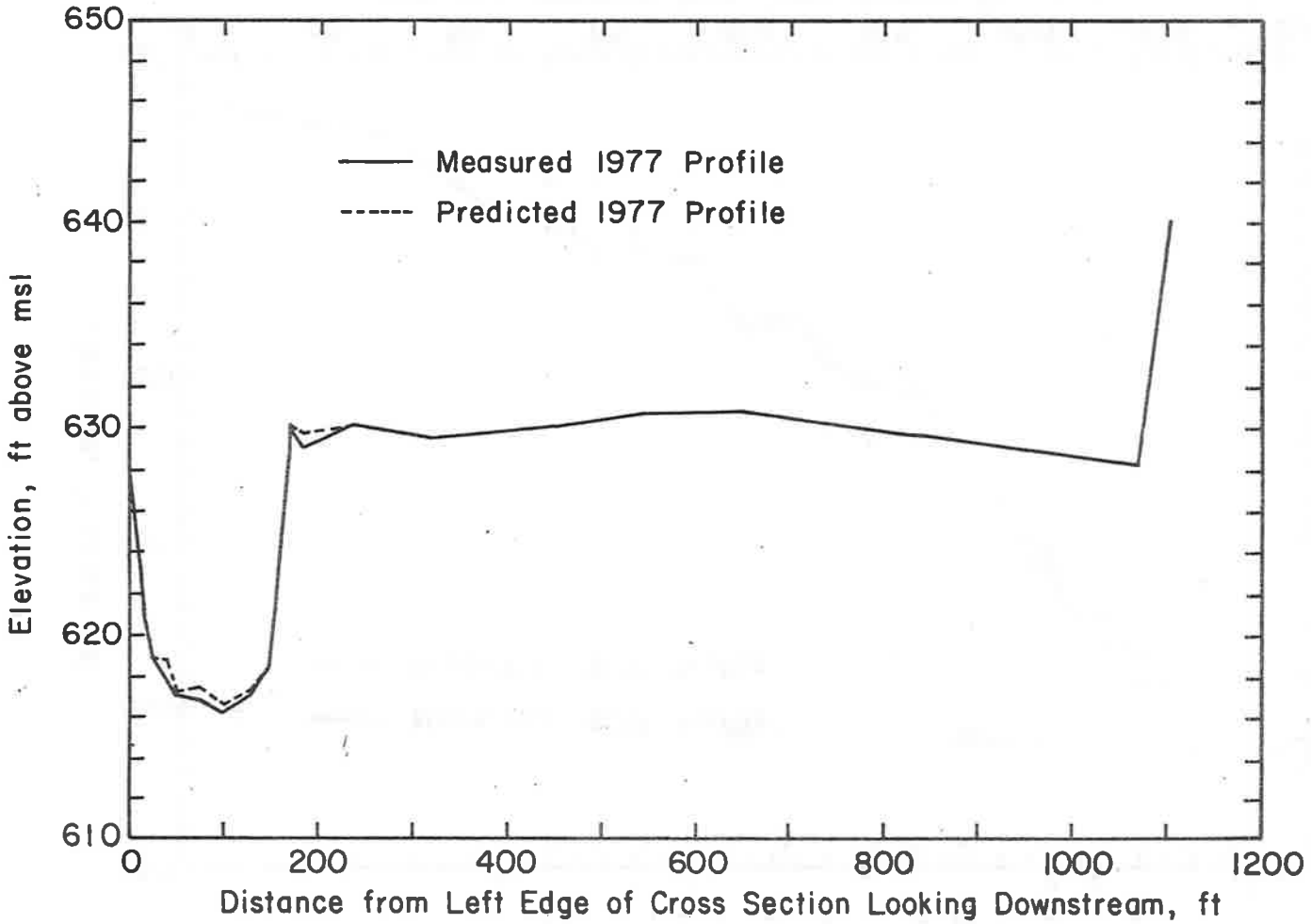

Figure 18.34 Comparative cross sections at Old Woman Bend.

(a) Initial condition, t = 0

(b) t = 1 sec.

(c) t = 10 sec.

(d) t = 2 min.

(e) t = 3 min.

Figure 18.35 Experimental study of water and sediment wave movements after removal of a dam in a 3-inch flume.

Results of Analysis

The Muskegon River model has been verified with field data and laboratory flume data both quantitatively and qualitatively. This verification demonstrates the applicability of this method of analyzing the sediment movement in the Muskegon River. To evaluate the effect of the movement of the sand wave through the Muskegon River system, a weekly hydrograph with a total time period of 27 years was routed through the system. This routing commenced on November 15, 1968 (beginning at the time of the dam removal) and ended in 1995. Bed elevations, stages and velocities were computed and compared to determine the impact of the moving and elongating sand wave on the hydraulics of the river.

Figures 18.36 and 18.37 show the overlays of the bed profiles for different years. The material originally deposited behind the old dam site has been eroded from this area and is moving downstream. The rate of sand wave movement was much faster in the beginning than at present. As the wave of sediment has slowed down and elongated the river has adjusted accordingly. In order to illustrate the sand wave movement more explicitly it is expedient to show the change of channel thalweg elevation with time. Figure 18.38 shows how the sand wave is moving through the system with time and space. The average rate of advancement of the sand wave for the first nine years (1968 to 1977) was about one mile per year. The rate at which the trailing end of the sand wave moves through the system is much slower than the rate of advancement. The flushing rate (rate which the trailing end of the sand wave has moved) as estimated from 1972 to 1977 was about 0.25 miles per year. The differential rates of advancement of the two ends of the sand wave elongates the wave with time as shown in Figure 18.38. This phenomenon is in accordance with the field data (see Figure 18.32) and with the observations of movement of the sand wave in the small laboratory flume (Figure 18.35). The rates of movement of both ends of the sand wave are slowing down with time because of reduced shear stress on the bed as the sand wave elongates. As shown in Figure 18.38, the average rate at which the leading edge of the sand wave will advance during the next 18 years (after 1977) is approximately 0.28 miles per year and the corresponding average rate of movement of the trailing edge of the sand wave is about 0.14 miles per year. Figure 18.38 also shows that by 1995,

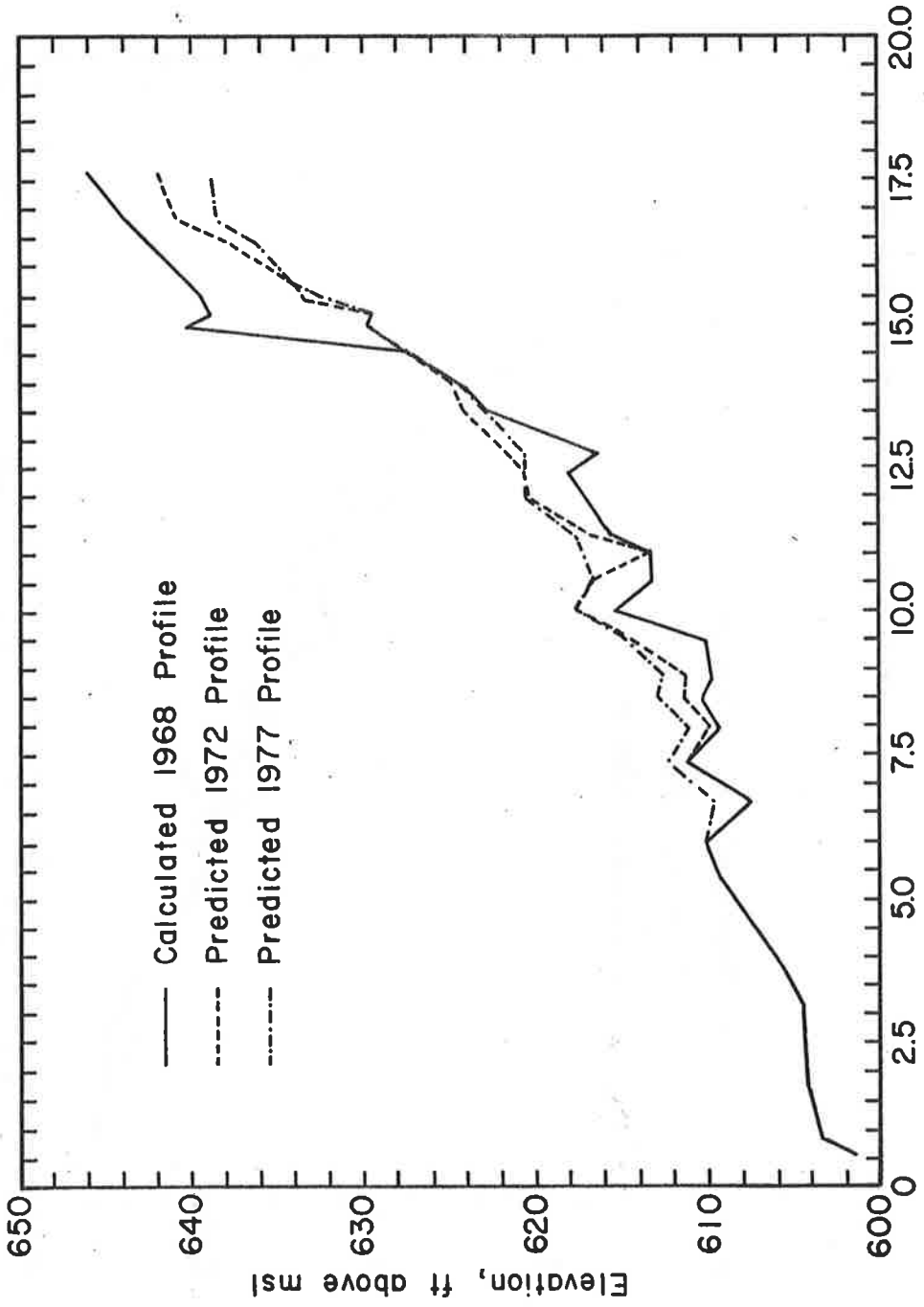

Figure 18.36 Comparative bed profiles for the Muskegon River.

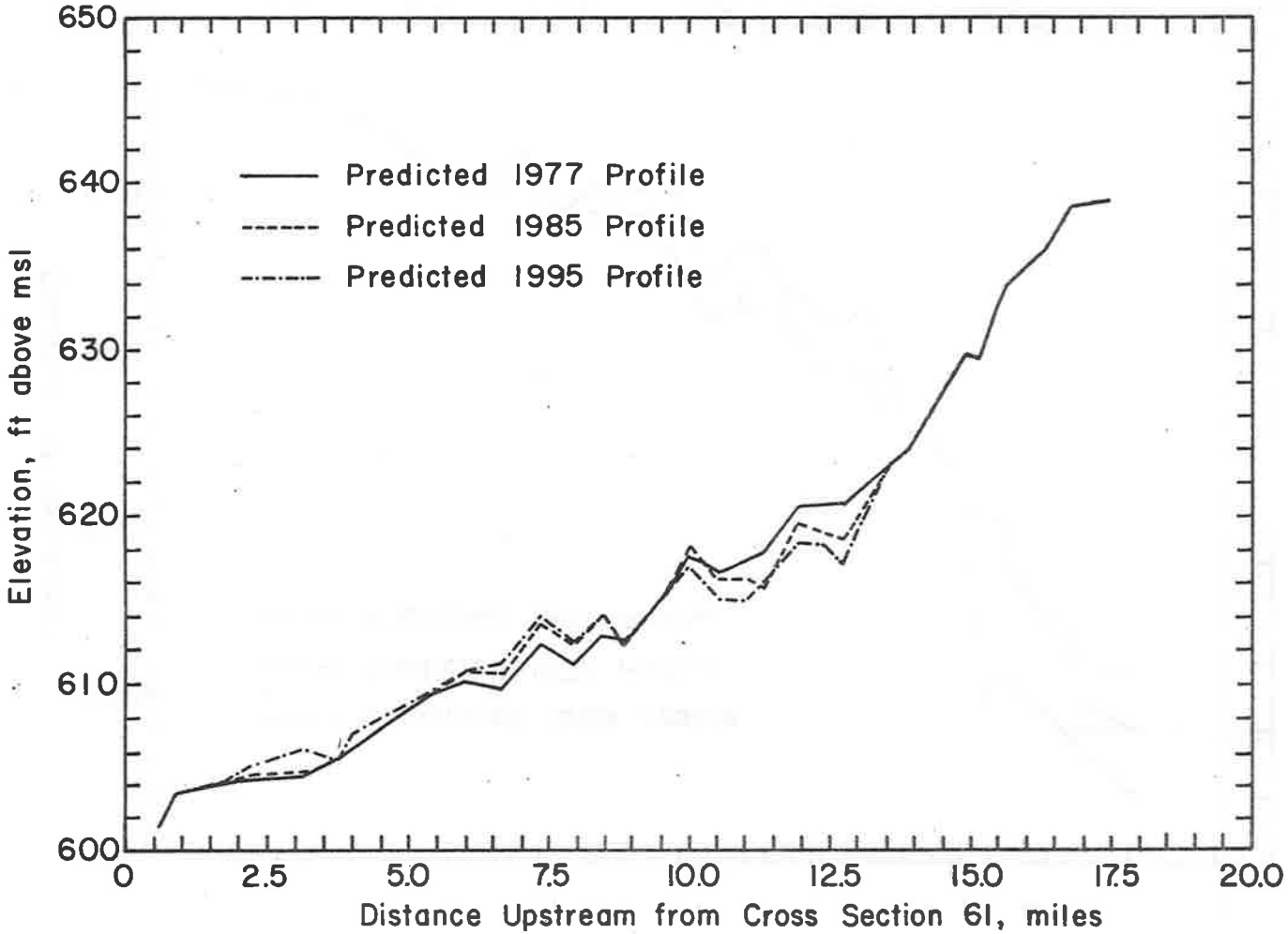

Figure 18.37 Comparative bed profiles for the Muskegon River.

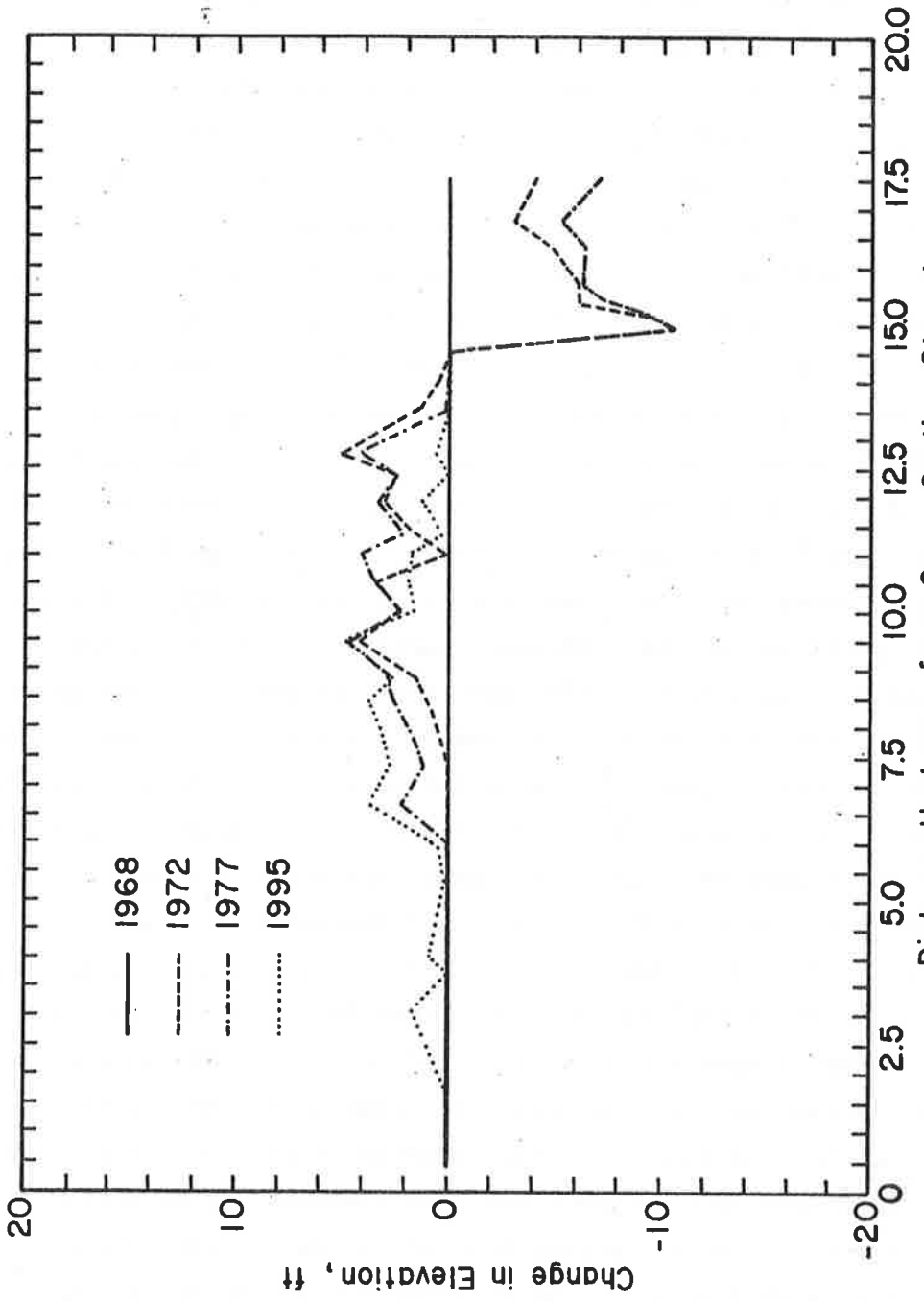

Figure 18.38 Sand wave movement depicted by delta-z of the river bed.

the sand wave will have moved past Old Woman's Bend (river mile 10.57). The presence of sand on the bed at any one location is temporary and transient. Figure 18.39 demonstrates this point by showing the simulated thalweg level at the cross section below the Newaygo Dam (river mile 14.44). This figure shows that the sand wave had moved past this USGS gaging station in approximately 180 weeks. Considering assumed normal low flow conditions (the flow from 1968 to 1977), the sand wave will have moved through the Bridgeton Bridge in approximately 80 years. However, should a series of large flood events occur in succession, the sand wave would move through the system much faster due to the high discharge and low resistance to flow. It is estimated that the sand will flush through the Bridgeton Bridge reach in the order of 50 to 80 years depending on the magnitude of future hydrologic events.

The sand wave has slightly altered the river stages as it has migrated downstream. The presence of sand in the system may cause small increases in local stage at low flows but not at high flows. Figure 18.40 shows that for a two year flood event (6,300 cfs) the water surface profiles for 1977 (present conditions) are approximately one-half foot higher than that for 1968 conditions for reaches upstream of river mile 9.0. The river mile is defined as a distance upstream of cross section No. 61. Figure 18.40 also indicates that only a slight increase in river stage is expected by 1995 for the reach upstream of river mile 7.0. Figure 18.41 gives the water surface profiles for 1968, 1977 and 1995 for a 25-year flood event, and Figure 18.42 compares the water surface profiles for 1968, 1977 and 1995 for a 100-year flood event. These two figures confirm that sand waves have not significantly changed river stages for high flows and could even decrease river stage in some instances. This reduction in stage is due to the decrease in resistance to flow because of the presence of sand in the river bed which can result in a smoother boundary condition at high flows.

Sediment and water routing has been conducted over the entire study reach from a point 6.5 miles above Newaygo to Bridgeton Bridge. The model has been calibrated for the average hydraolgic, hydraulic, and sediment conditions for the entire reach. However, at the specific study site, Old Woman's Bend, the extreme sinuosity acts as a pseudo control within the study reach. As such, the average Manning's friction

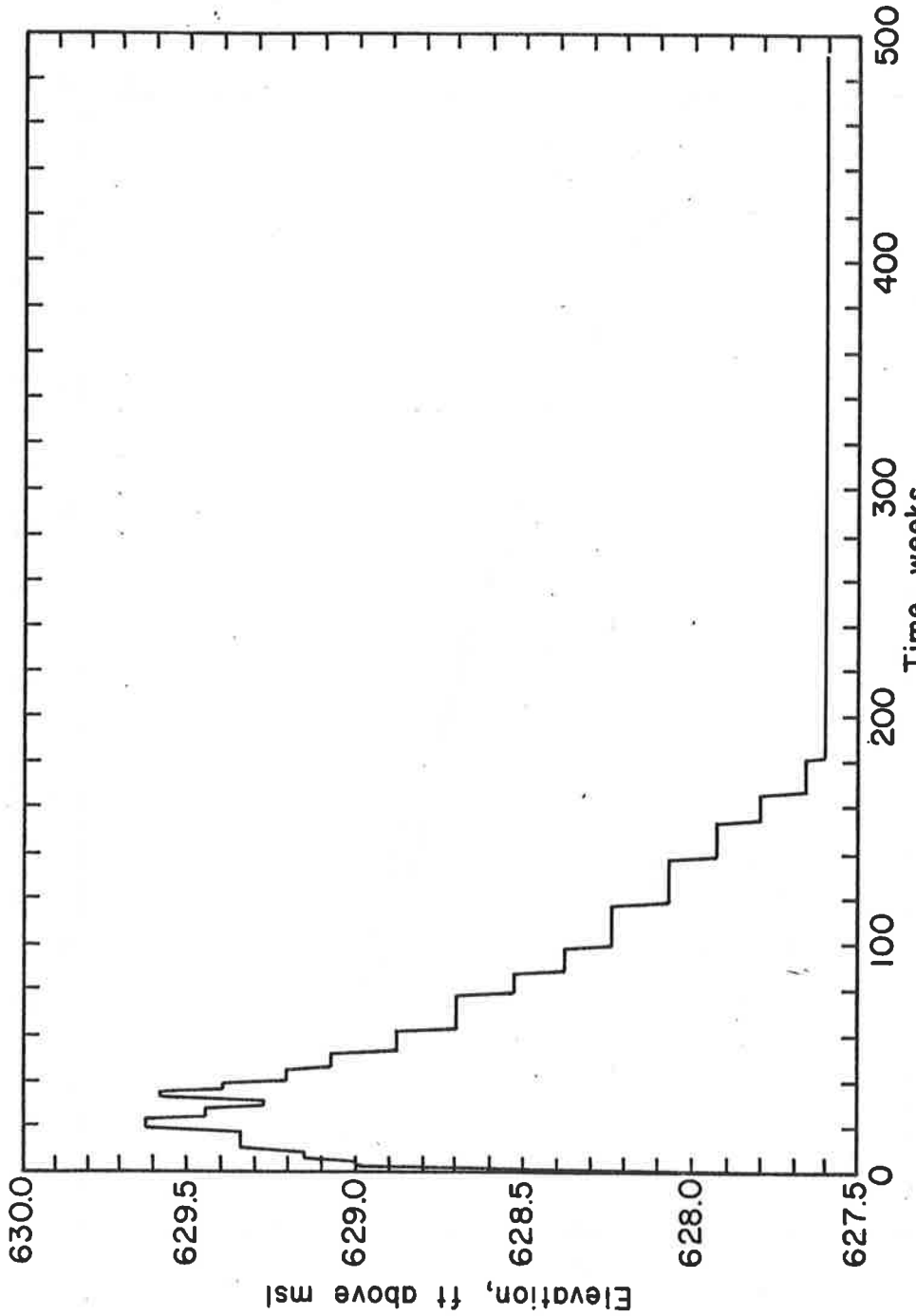

Figure 18.39 Minimum bed elevation below old dam site.

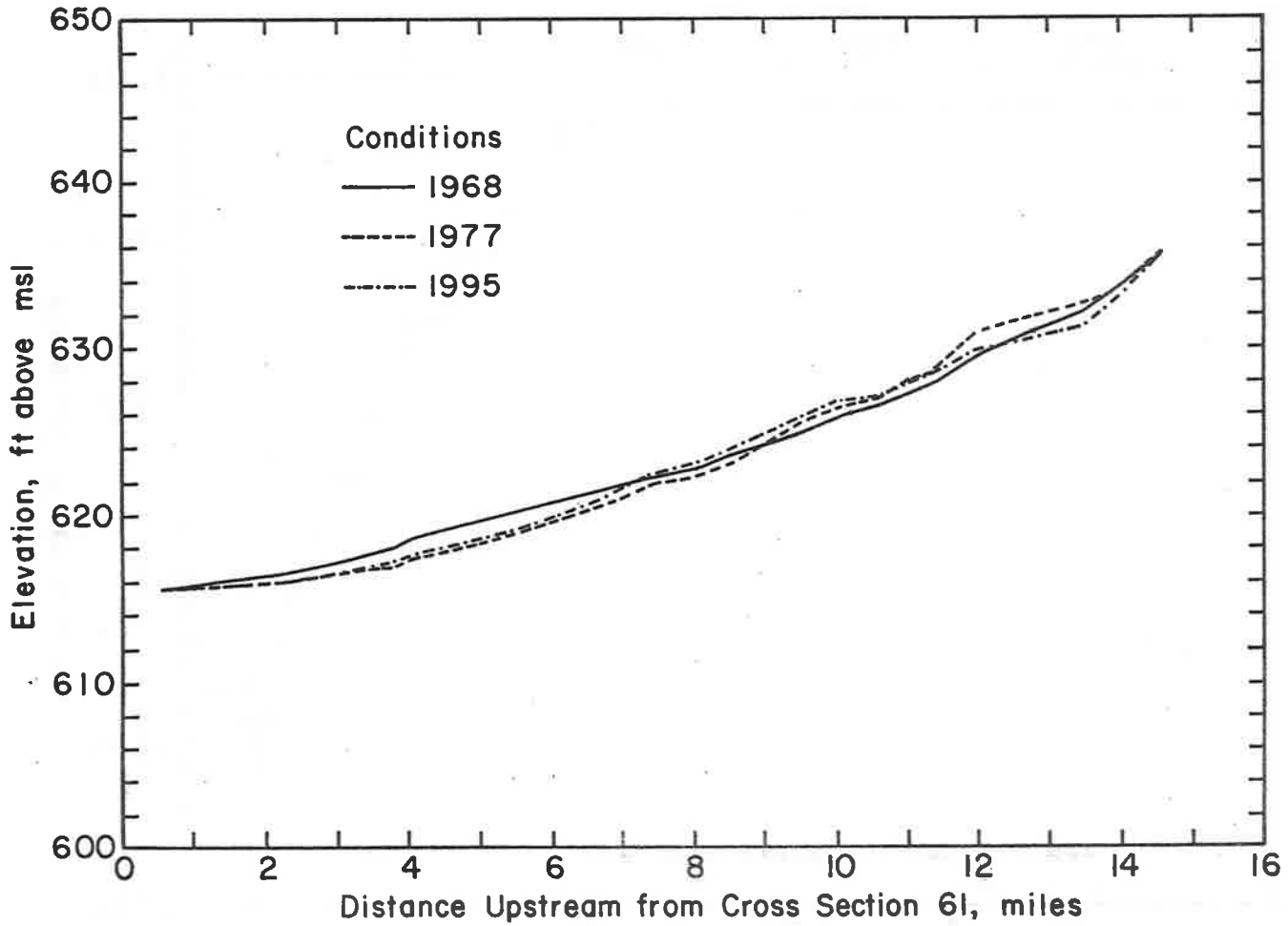

Figure 18.40 Comparative water surface profiles for a 2-year flood event.

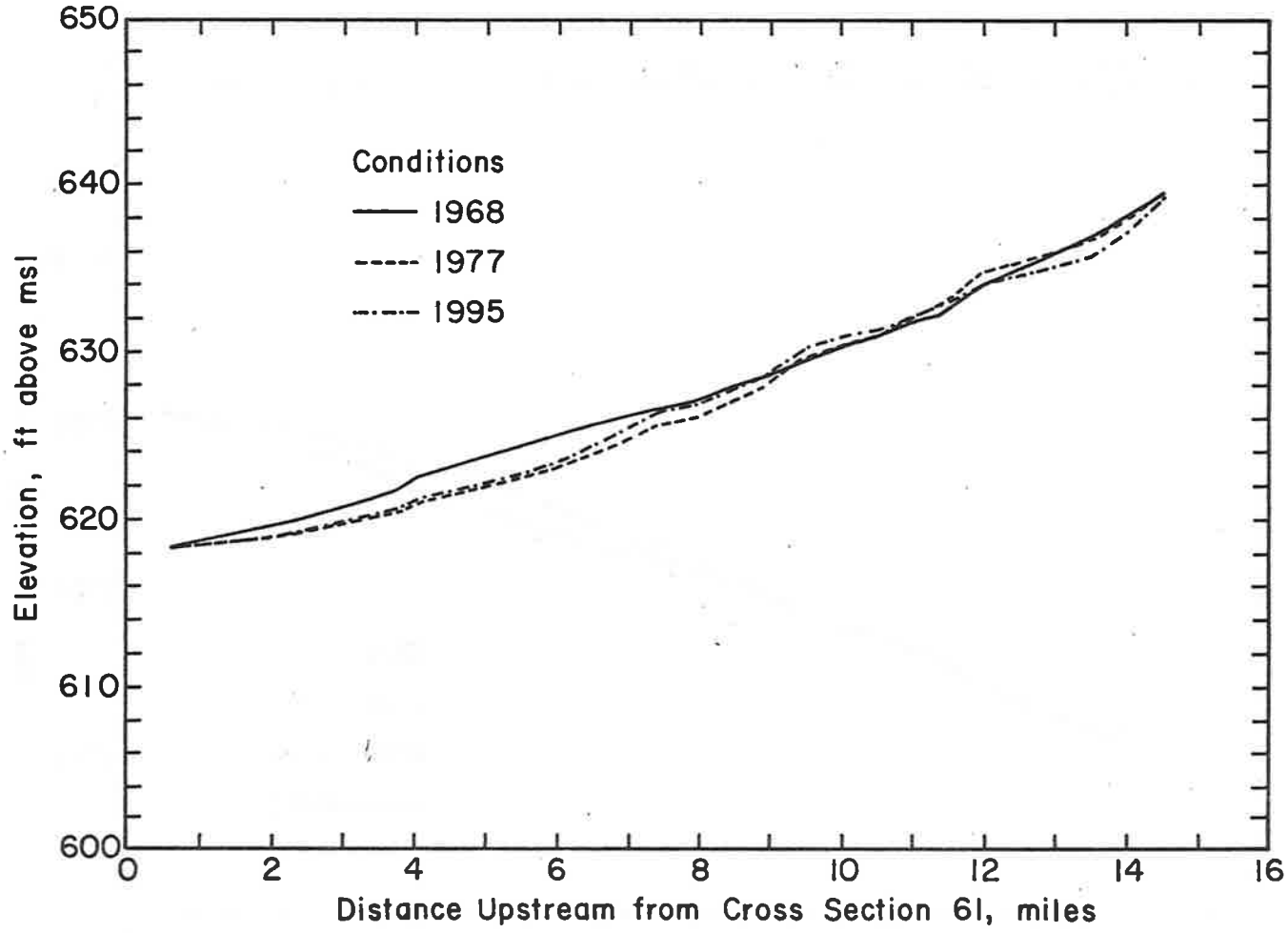

Figure 18.41 Comparative water surface profiles for a 25 year flood event.

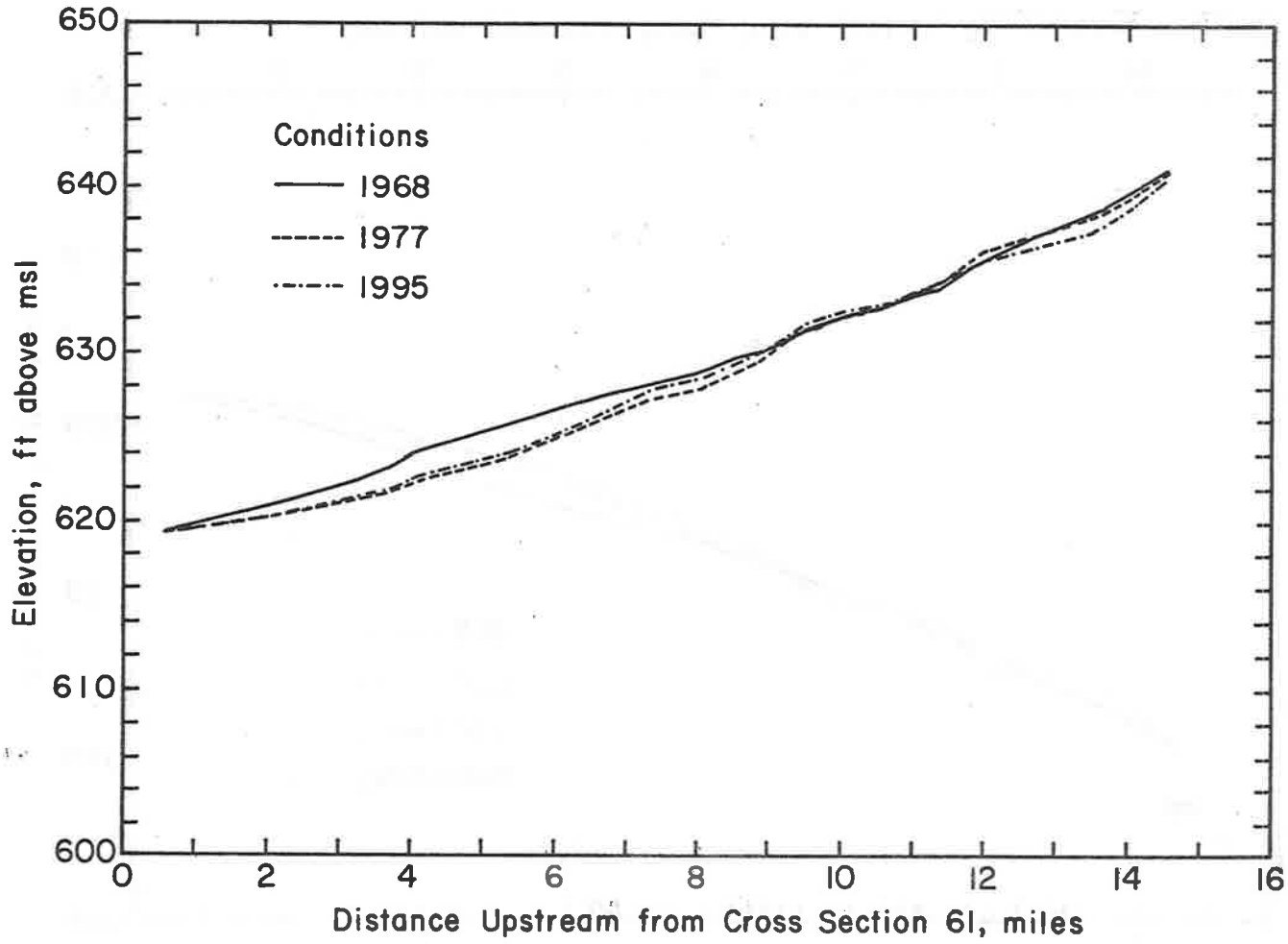

Figure 18.42 Comparative water surface profiles for a 100-year flood event.

coefficient (n) will not represent the actual conditions without including corrections for sinuosity, local velocity perturbations, superelevation across the individual cross sections, and the occurrence of divided flow through the neck of the bend.

To correct for these conditions the Manning's n value has been increased 23 percent through Old Woman's Bend. The resulting stage-discharge relation is given in Figure 18.43. The analysis yields a computed river stage of 631.95 feet for a return period of 14 years. The indirectly observed stage for this discharge in the Old Woman's Bend area has been estimated as 631.9 feet--a very close agreement considering the complexity of the hydraulics in the bend area. It must be emphasized that the natural variation of river stage with time for a given discharge is on the order of 1-2 feet. The flooding potential is practically unchanged due to sediment movement. Considering the total system, the temporary effect of the sand wave will be eliminated as the sand wave moves further downstream. This point is illustrated by examining the stage-discharge relation just below the dam (river mile 14.44). Figures 18.44 and 18.45 show that the stage-discharge relations at this location have changed with time. As the sand wave moved into this reach, there was a corresponding increase in stage. Then by 1977, the sand wave had moved through this location and river stage returned to approximately the same relation that was utilized by the USGS prior to removal of the dam. The simulated stage-discharge relations very closely corresponds to the USGS stage-discharge relation as determined by 1971 data.

The velocity is an important factor for evaluating the stability of the channel (see Simons and Sentürk, 1977). In general, the velocity is not significantly affected due to the sand wave even at relatively high discharges, except at local constrictions where the bed and banks of the river are most resistant to erosion. Figures 18.46 and 18.47 show that the local velocity could increase due to sand wave migration during high flows such as the 25- and 100-year events. The maximum increase in velocity is on the order of 1.0 ft/sec. However, the average velocities for the entire study reach are only slightly affected by the sediment movement. Table 18.8 summarizes average flow velocities for the entire study reach for various flow conditions. This table

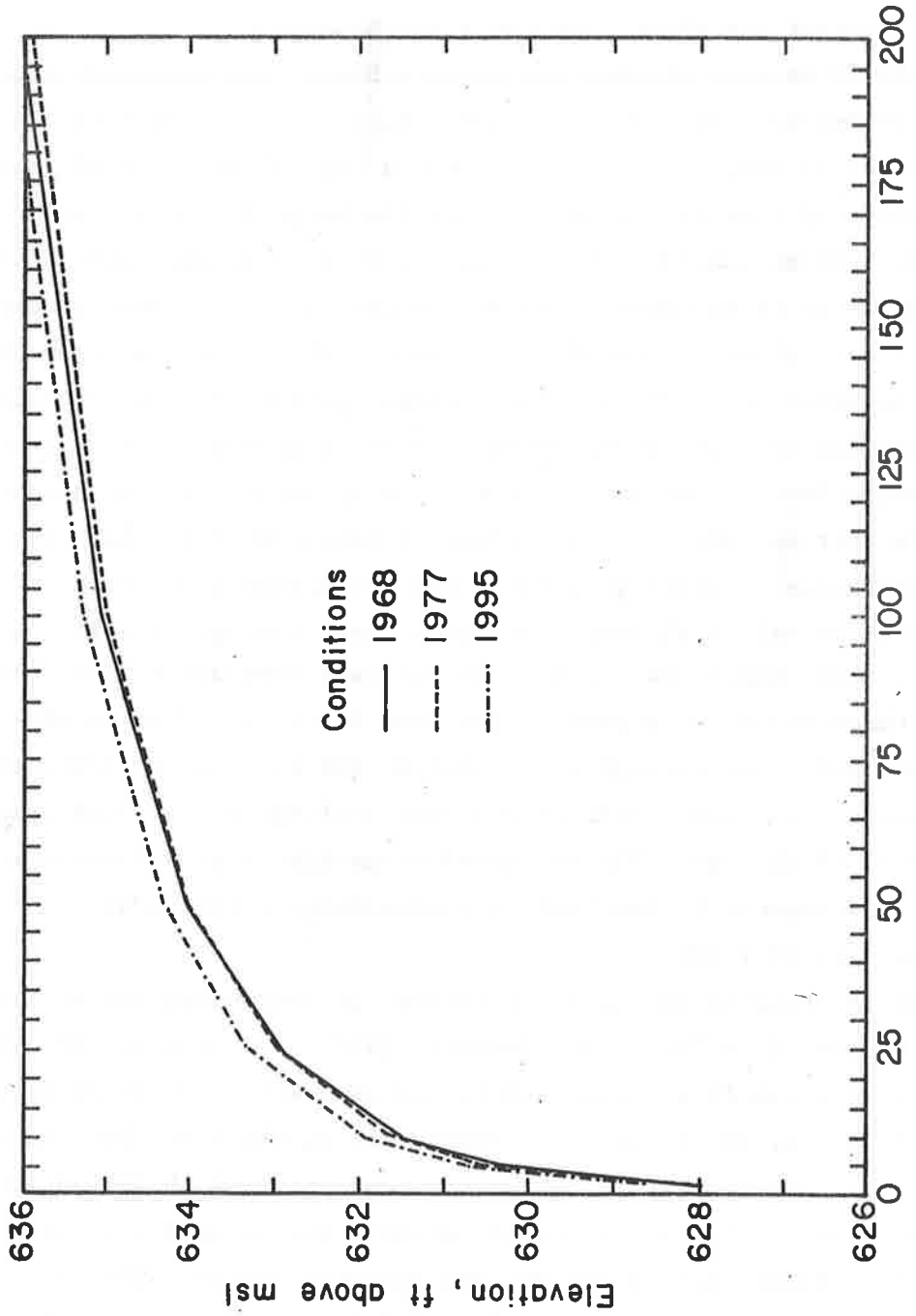

Figure 18.43 Comparative water surface elevations at Old Woman's Bend.

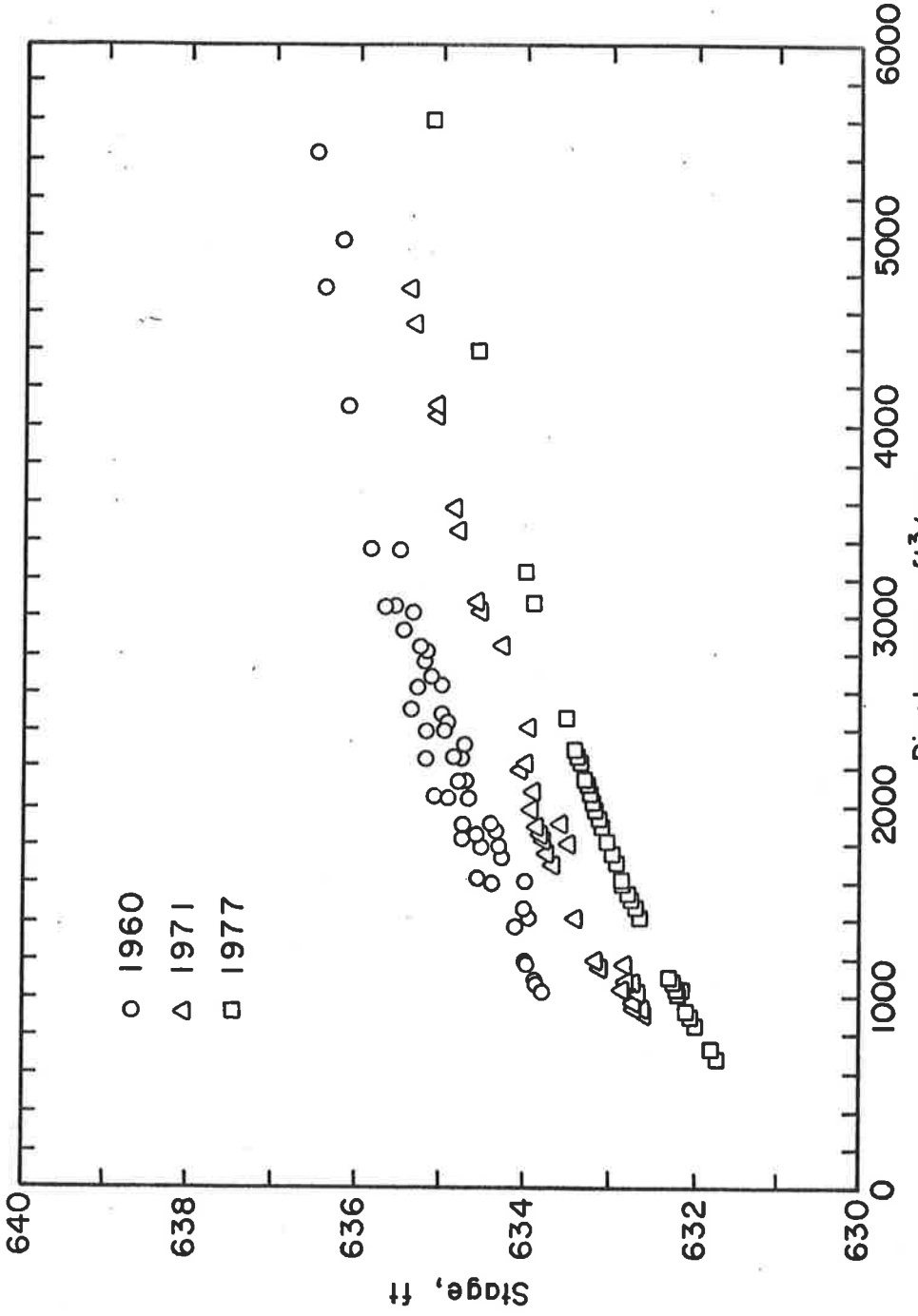

Figure 18.44 Stage discharge relationship below old dam site.

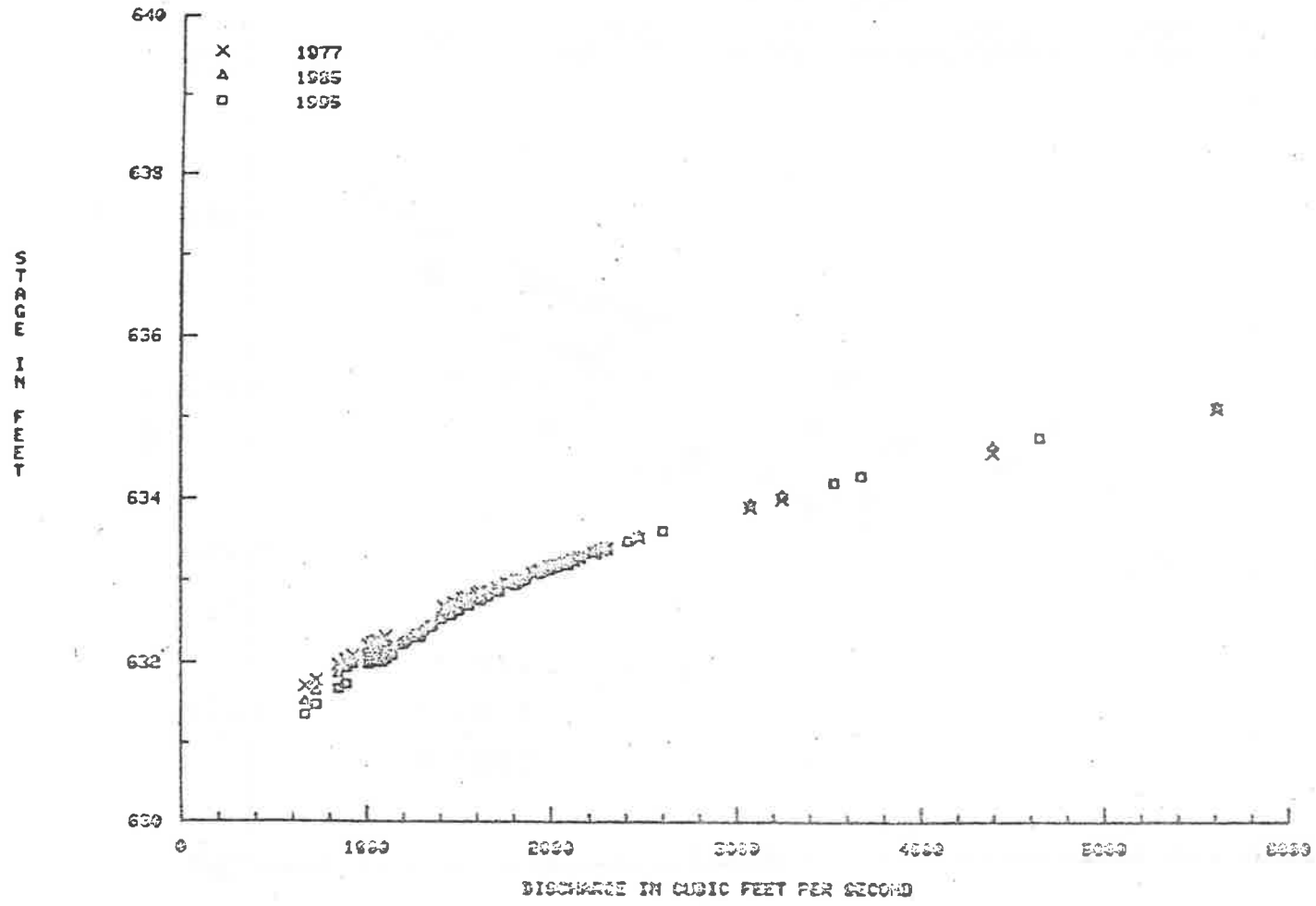

Figure 18.45 Stage discharge relationship just below old dam site.

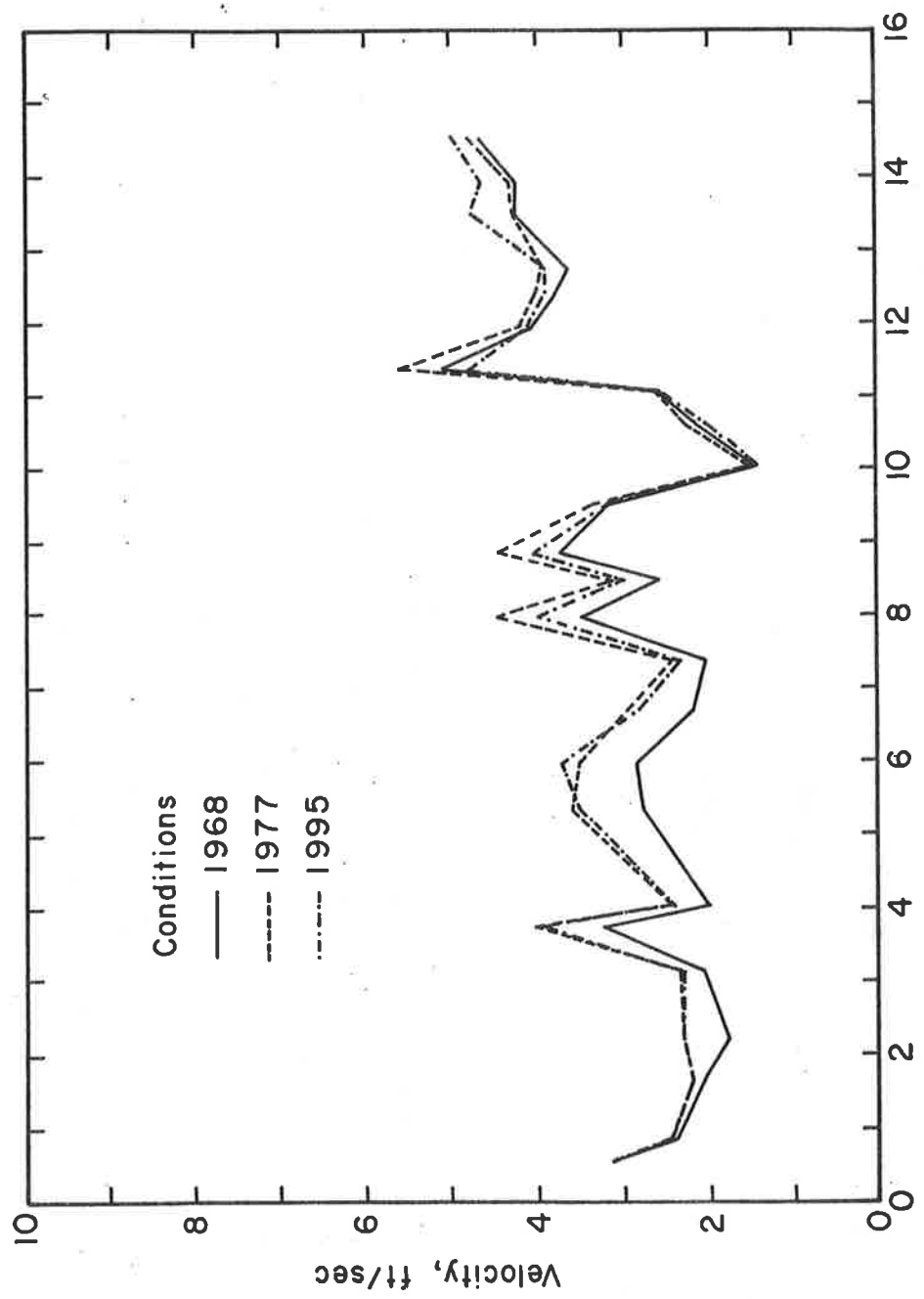

Figure 18.46 Comparative velocities for a 25-year flood event.

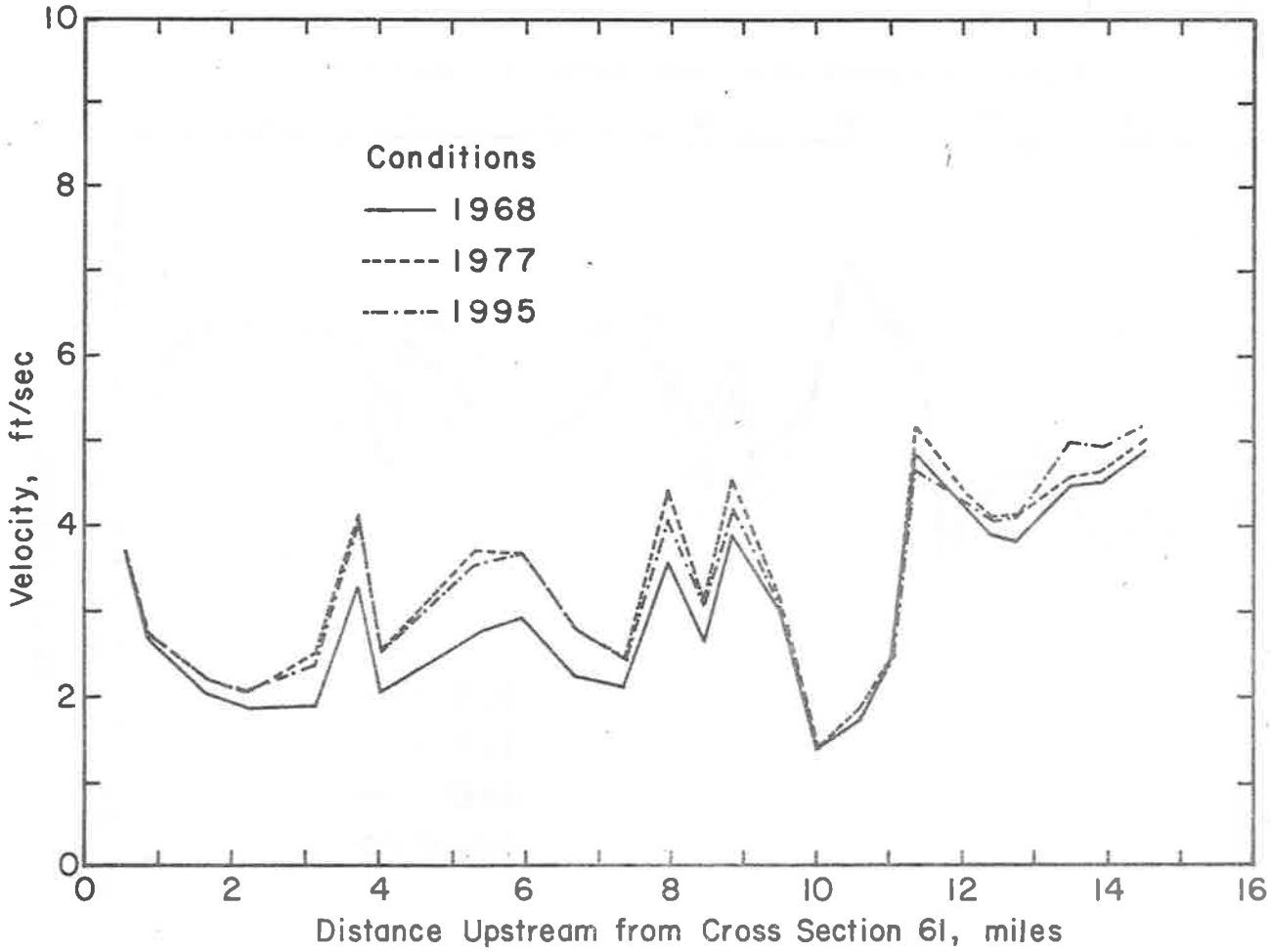

Figure 18.47 Comparative velocities for a 100-year flood event.

shows that the average increase in flow velocity considering the present condition (1977) over the pre-dam removal conditions (1968) is about 12 percent. The average velocity of flow in 1995 is estimated to be about 9 percent longer than for 1968 conditions. It should be emphasized that the accuracy with which velocities can be measured in the field is limited. An error on the order of 3-10 percent is to be expected depending on equipment, flow conditions and methodologies used. Hence, the anticipated change in velocities caused by the sand wave are on the order of expected errors in velocity measurement. This increase in velocity caused by the sand wave has not and will not significantly increase the rate of bank erosion. The river has changed from time to time in the past forming Old Woman's Bend before the removal of Newaygo Dam. With the Croton Dam in place, no significant sediment is supplied from upstream. Hence, natural erosion will continue to erode the Old Woman's Bend. This phenomenon would exist with or without Newaygo Dam. This erosion can only be controlled by bank protection.

Table 18.8 Average flow velocity in ft/sec along the study reach.

Return Period (years)	Average Flow Velocity		
	1968	1977	1995
2	2.79	3.25	3.09
5	2.97	3.27	3.15
10	2.98	3.30	3.21
25	3.02	3.38	3.30
50	3.05	3.41	3.34
100	3.09	3.44	3.38
200	3.13	3.45	3.42

Summary and Conclusions

The results of analysis indicate that the sand wave has advanced at approximately one mile per year for the first nine years and will move slowly in the future. The rate of flushing at the tail end of the sand wave is slower than the rate of advancement of the wave. The flushing rate has been about 0.25 miles per year for the first nine years and will be slower in the future. The differential rates of advancement and flushing elongate the sand wave. This phenomenon was verified both by field observation and with tests conducted in a small

laboratory flume. The presence of sand on the bed of the channel at any one location is temporary and transient. The sediment released by removal of the Newaygo Dam is moving through and will move out of the system eventually. Part of the sediment stored behind the dam was wash load (silt and clay) and most of it flushed through the system immediately. The sand wave will ultimately flush through the system. This will require on the order of 50 to 80 years depending on the magnitude of future hydrologic events. The sand wave has slightly altered river stages as it has migrated downstream. The presence of the sand wave has caused negligible increases in river stages at all flows. Flow velocity is related to bank stability. In general, the velocity is not significantly affected due to the sand wave except at local constrictions. The average velocity has not been significantly increased within the Old Woman Bend and hence the sand wave has not caused measurable changes in bank erosion.

The temporary effect of the sand wave will be eliminated as the sand wave moves farther downstream. This point is supported by the stage-discharge relations just below the dam (river mile 14.44). As the sand wave moved into this reach, there was a corresponding increase in stage. Then by 1977, the sand wave had moved through this location and river stage returned to approximately the same relation established by the U.S.G.S. prior to removal of the dam. In general, the effects on river stage, velocity and bank stability due to the presence of the sand wave in the Muskegon River system are within the range of expected variation for the nature system.

18.6 REFERENCES

Agricultural Research Service. 1976. Control of Water Pollution from Cropland. Volumes I & II, Agricultural Research Service and Environmental Protection Agency, June.

Brice, J. 1971. Measurement of Lateral Erosion at Proposed River Crossing Sites of the Alaska Pipeline. USGS Water Resources Division, Alaska District.

Camp, Dresser, and McKee. 1978. Preliminary Analysis of Flood Hazards Resulting from an Intermediate Regional Flood Upstream from Conrock Gravel Pit, San Juan Creek, Orange County, California. Pasadena, California, January 6.

Camp, Dresser, and McKee. 1978. Supplemental Report on Erosion and Deposition Processes in and above Conrock Gravel Pit, San Juan Creek, Orange County, California. Consolidated Rock Company, Pasadena, California, March 20.

Chow, V. T. 1959. Open Channel Hydraulics. McGraw-Hill Book Company.

Converse Davis Dixon Associates, Inc. 1978. Geologic Investigation of Erosion Sedimentation Factors in Upper San Juan Creek, Orange and Riverside Counties, California. February 1 and March 20.

Leopold, L. B., Wolman, M. G., and Miller, J. P. 1964. Fluvial Processes in Geomorphology. San Francisco, W. H. Freeman and Company, 522 p.

Li, R. M., Simons, D. B., Ward, T. J., and Steele, K. S. 1977. Hydraulic Model Study of Flow Control Structures. Phase I Report, prepared for USDA Forest Service, Arizona.

Mastafa, M. D. 1978. Erosion of San Juan Creek in the Vicinity of Casper Regional Park. Environmental Management Agency (EMA), Orange County Design Division, Consulting Engineer, Huntington Beach, California.

Peterka, J. A. 1963. Hydraulic Design of Stilling Basins and Energy Dissipators. USDI Bureau of Reclamation, July.

Pipe Line Technologists, Inc. 1973. Design Flood Model. July.

Simons, D. B., and Li, R. M. 1978a. Degradation below the Emergency Chute of the Site 8C. Prepared for USDA Soil Conservation Service, T or C, Williamsburg Watershed, Albuquerque, New Mexico.

Simons, D. B. and Li, R. M. 1978b. Erosion and Sedimentation Analysis of San Juan Creek near Conrock Gravel Pit, Orange County, California. Prepared for Dames & Moore, Denver, Colorado, June.

Simons, D. B., Al-Shaikh-Ali, K. S., and Li, R. M. 1979. Flow Resistance in Cobble and Boulder Riverbeds. Journal of the Hydraulics Division, Proceedings of the American Society of Civil Engineering, Vol. 105, No. HY5.

Simons, D. B., and Sentürk, F. 1977. Sediment Transport Technology. Water Resources Publication, Fort Collins, Colorado.

U.S. Bureau of Reclamation. 1960. Investigation of Meyer-Peter, Müller Bedload Formula. Sedimentation Section, Hydrology Branch, Division of Project Investigations, U.S. Department of the Interior, Bureau of Reclamation, June.

USDA Soil Conservation Service. 1977. Design Engineers Report - T or C, Williamsburg Watershed, Site 8C. Albuquerque, New Mexico, June.

USGS. 1969. Preliminary Determinations of Sediment Discharge San Juan Drainage Basin, Orange and Riverside Counties, California. Open-file Report, Menlo Park, California, by C. G. Kroll and G. Porterfield, December 16.

Water and Environment Consultants, Inc. 1978. Analysis of Sediment Movement in the Muskegon River following the Removal of Newaygo Dam. Prepared for Michigan Department of Natural Resources.

Water and Environment Consultants, Inc. 1974. Fluvial Analysis of Jim River Crossing Number 1.

Williams, J. R. 1975. Agricultural Research Service Report ARS-S-40. June.

CHAPTER 19

WATERSHED BEST MANAGEMENT ANALYSIS

Ruh-Ming Li, Associate Professor, Department of Civil Engineering, Colorado State University, Fort Collins, Colorado

Timothy J. Ward, Assistant Professor, Department of Civil Engineering, Colorado State University, Fort Collins, Colorado

Daryl B. Simons, Associate Dean for Engineering Research and Professor of Civil Engineering, Colorado State University, Fort Collins, Colorado

19.1 INTRODUCTION

Throughout the previous chapters it has been stressed that physical process models can aid the land use manager in decisions about watershed activities. Chapter 3 discussed controlling processes in watersheds. Chapters 7 and 10 presented governing equations and selected physical process models for routing water and sediment and determining their yields. These models were applied to a wide range of watersheds under varying conditions. Chapter 13 added a new dimension and introduced another significant watershed characteristic, mass wasting, into modeling of watersheds.

The previous chapters dealt mostly with selected applications to demonstrate each model. In this chapter specific models or concepts will be used for analysis of watersheds in terms of best management practices. A best management practice, loosely defined, is one that meets social, economic, political, and environmental goals all at once. Since this is usually impractical or impossible, goals must be weighted or modified in order to arrive at the practice that is acceptable to all concerns. Often, however, some goals are fulfilled or addressed by qualitative data that is insufficient when subjected to close scrutiny. In fact, the judicial system these days is giving less weight to learned opinions and more attention to the so-called "state-of-the-art" quantitative evaluations. This emphasis alone has enticed more consultants, researchers, government agencies, and expert witnesses into using those approaches which will stand up to scrutiny and testing while at the same time providing realistic solutions to complex answers.

Quantitative approaches are extremely important to the land use planner. No longer is a planner able to say yes or no if asked if a watershed activity will increase sediment yield. The questions now, to stretch the point, are, "If I cut this amount of trees, what will my sediment yield be next runoff season?". Although a bit overstated, this type of quantitative question must be answered, and usually before planned development can take place. Quantitative analyses can provide information that can prove or disprove a stated position, like clear cutting causes increased sedimentation. This is a gross overgeneralization that does not truly consider all of the other factors that control sediment yield. The land use planner must also answer questions that

may cover wide areas or long time spans. This need for spatial and temporal resolution of solutions has led planners away from techniques were developed on data specific to particular areas or collection periods and to those that are not dependent on measured data for development.

In short, there is a growing awareness on the part of planners to rely more heavily on those techniques that provide reasonable answers and are accepted by the public. Physical process models represent this group of techniques that are becoming more in vogue with technical and lay people alike. In this chapter, model applications showing how management practices can be quantified in terms of water and sediment yields. As an interesting addition, evaluation of data collection systems using model simulation is also presented. Three model applications to actual watersheds are given. These are: 1) SEDWAT (Chapter 10) to Watershed 17 in the Beaver Creek Watershed, Flagstaff, Arizona, 2) MULTWAT (Chapter 7) to an arid, southwest drainage for determining a probable maximum flood, and 3) a generalized planning level model (Chapter 10) for assessing sediment yield changes in a watershed caused by management activities. This last model is applied to a test watershed in the Arapahoe-Roosevelt National Forest as part of the U.S. Forest Service lead forest program. The evaluation of a data collection system is described using information from the Four-Mile Creek Watershed near Traer, Iowa. This watershed is maintained by Iowa State University on contract with the Environmental Protection Agency. These four examples aptly illustrate the usefulness of physical process models.

19.2 APPLICATION OF SEDWAT TO WATERSHED 17

General

In this first example the water and sediment yield model (SEDWAT) developed by Simons, Li, Shiao, and Eggert (1977) is used to assess changes in streamflow and sediment yield from different watershed practices. These practices are mechanical site preparation, timber harvesting, and grazing.

Watershed 17 is a relatively rocky, sparsely vegetated drainage in the Beaver Creek Watershed near Flagstaff, Arizona. The watershed has an area of about 265 acres. Overland slopes average about eight percent and the main channel slope is about four percent. Initial canopy cover was 10 percent and ground cover was 34 percent. Hydraulic conductivity was 0.05 in./hr. The base event was the "Labor Day" storm of September 5, 1970. Peak recorded discharge was about 345 cfs and runoff volume was about 3.98 inches. Sediment production was 0.30 tons per acre. After adjustments, model simulations produced a peak of 363 cfs, a water yield of 3.75 inches and sediment yield of 0.30 tons per acre. Comparative hydrographs were previously presented in Chapter 7. All three of these simulated values are quite good because the controlling processes are correctly incorporated in the model. Because the simulated measured responses are comparable, the simulated results will be used as initial conditions.

Application

To demonstrate the use of SEDWAT for analyzing future management activities, four planning alternatives were simulated in the model. The four management alternatives are:

Alternative 1. Mechanical Site Preparation

The major modification to the watershed is compaction of the soil. The percent of area with ground and canopy remains the same but the hydraulic conductivity is reduced to 0.01 in./hr. It should be noted that this response is the yield which would be expected after the loose material had been flushed out of the system during an earlier storm.

Alternative 2. Clear-Cut Timbering

While economical, clear-cut timbering practices are often accompanied by high erosion rates and subsequently higher sediment yields. The increase in sediment yield is simulated by combining the

effects of mechanical site preparation from Alternative 1 with all canopy cover. Here the hydraulic conductivity is again .01 and the percent of area covered by ground cover and canopy cover is zero.

Alternative 3. Removal of Trees with Less Ground Disturbance

If care is taken to minimize the disturbance of ground cover, the canopy can be removed with considerably lower sediment yield. This result may be seen by reducing the ground cover percent to one-half the original level and the hydraulic conductivity to .04 in./hr. The canopy is completely removed.

Alternative 4. Overgrazing

Livestock or large populations of native animals can often cause severe damage to the ground cover by overgrazing. The effects of overgrazing can be simulated by removal of the ground cover and reduction of the hydraulic conductivity through compaction by trampling. In this example the conductivity is reduced to .03 in./hr and the ground cover is zero.

These alternatives are summarized in Table 19.1.

Table 19.1 Parameters used in SEDWAT simulation of management alternatives.

	Baseline and Alternative Parameters		
Alternative	Hydraulic Conductivity	Canopy Cover	Ground Cover
Baseline Condition	0.05 (in./hr)	10 (percent)	34 (percent)
1	.01	10	34
2	.01	0.0	0.0
3	.04	0.0	17
4	.03	10	0.0

The results of model simulation of the baseline condition and all four alternatives are listed in Table 19.2. Simulated hydrographs for the undisturbed (Figure 19.1) and four land use alternative responses are shown in Figures 19.1-19.5. The undisturbed response is shown as a solid line in Figures 19.1-19.5 and the response to the land use changes is shown as a dashed line. Obviously land use Alternative 2

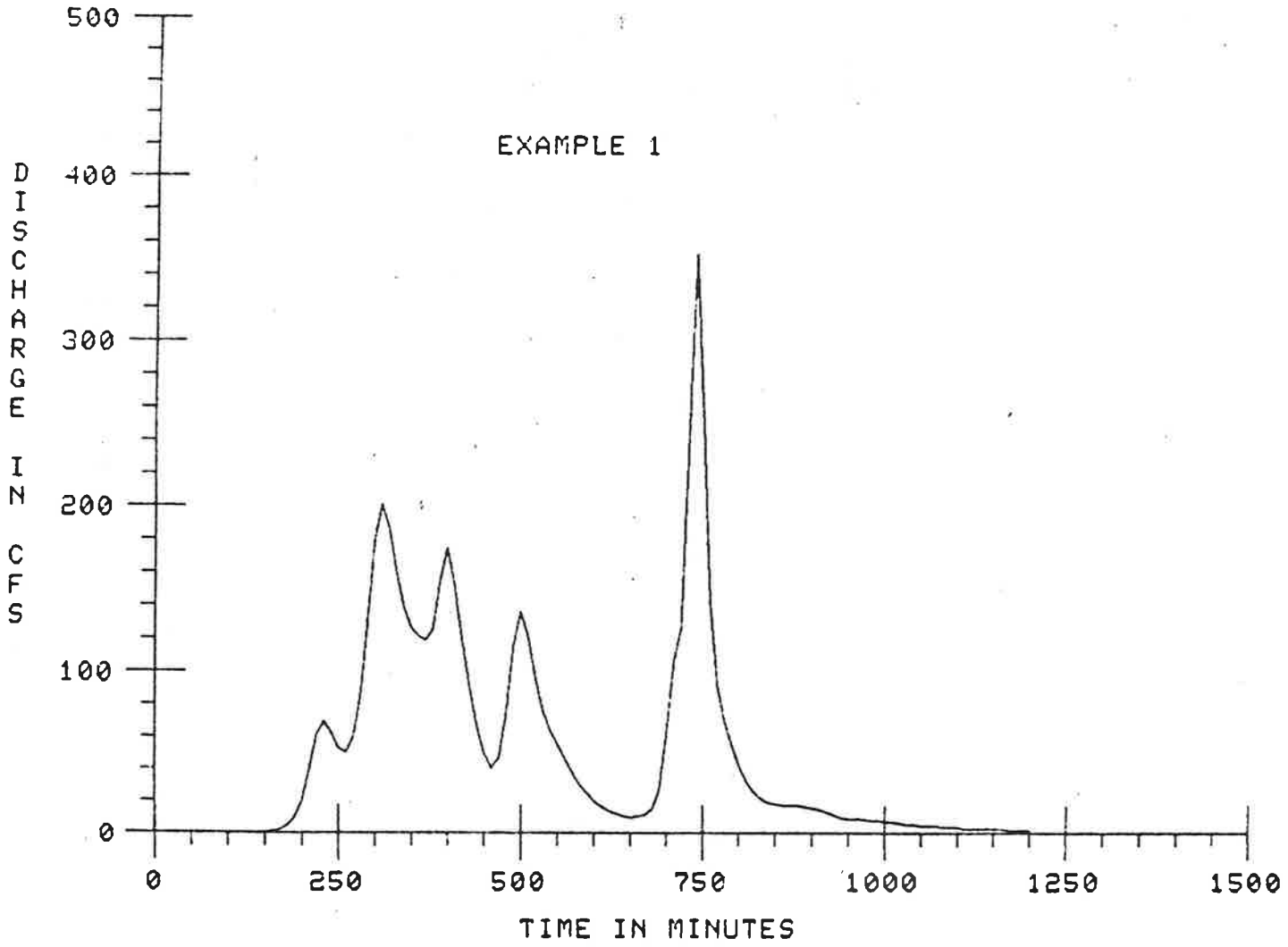

Figure 19.1 Undisturbed response, Watershed 17 for storm of September 5, 1970.

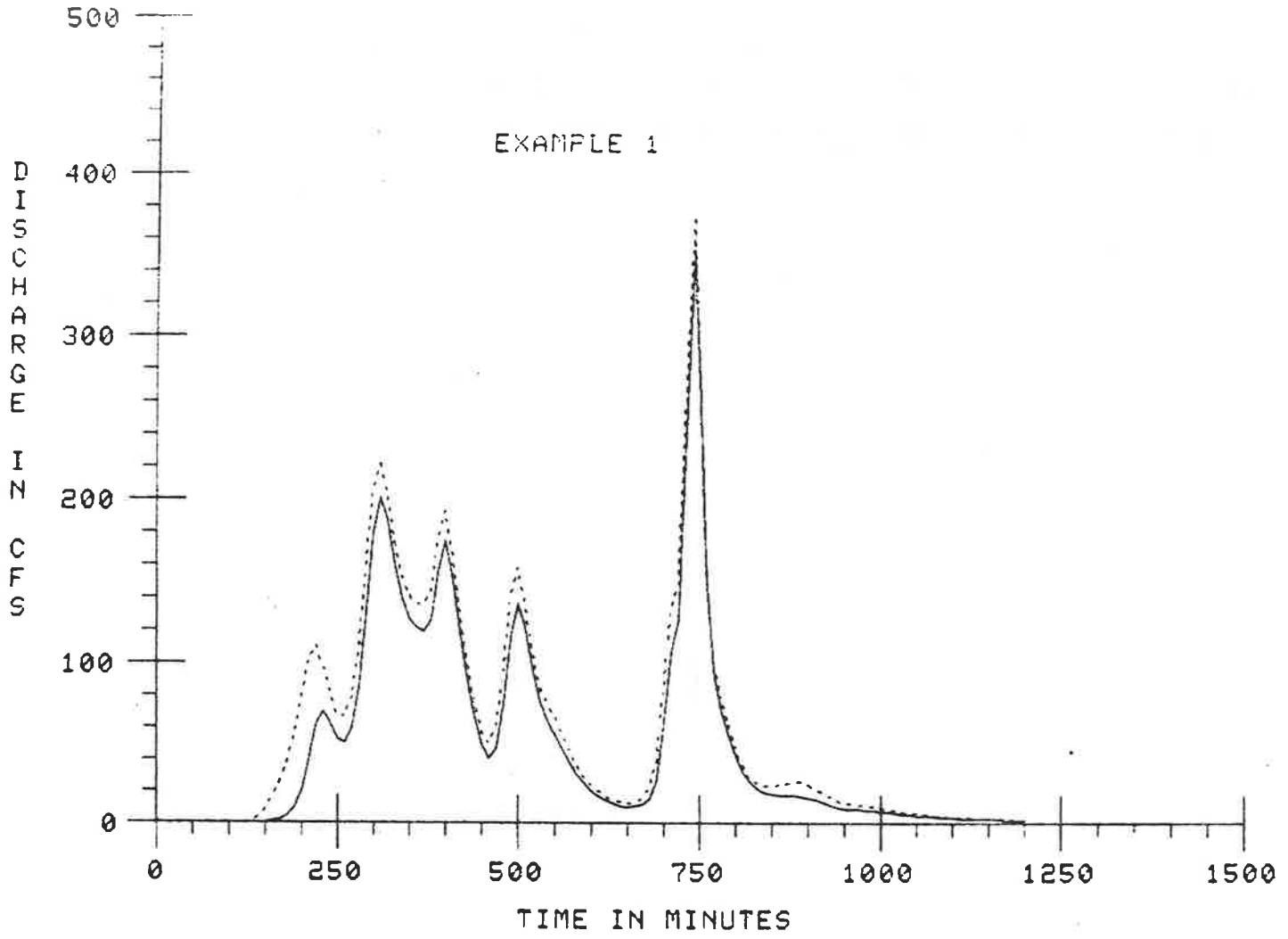

Figure 19.2 Effects of mechanical site preparation on Watershed 17 for storm of September 5, 1970.

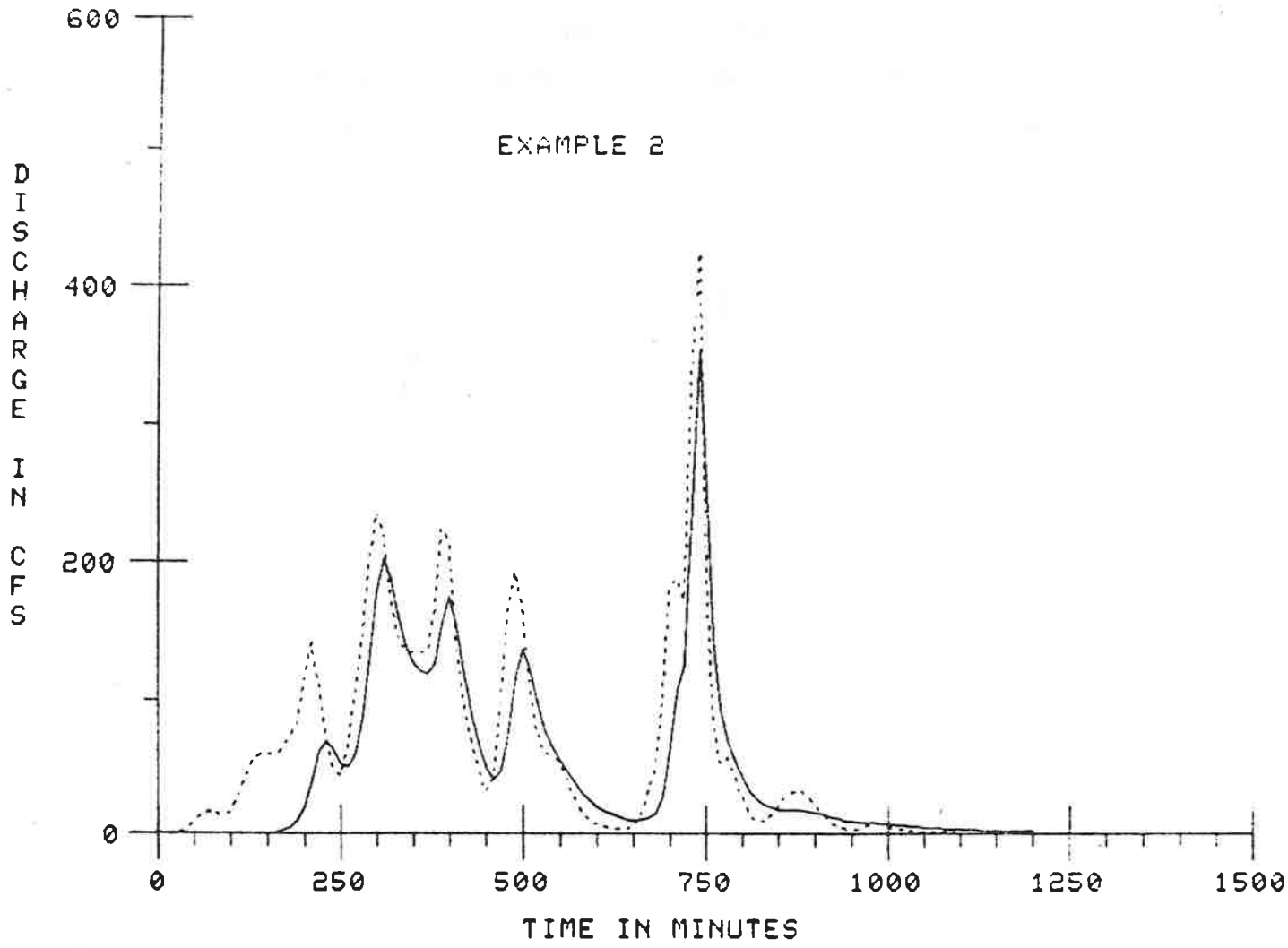

Figure 19.3 Effects of clear-cut timbering on Watershed 17 for storm of September 5, 1970.

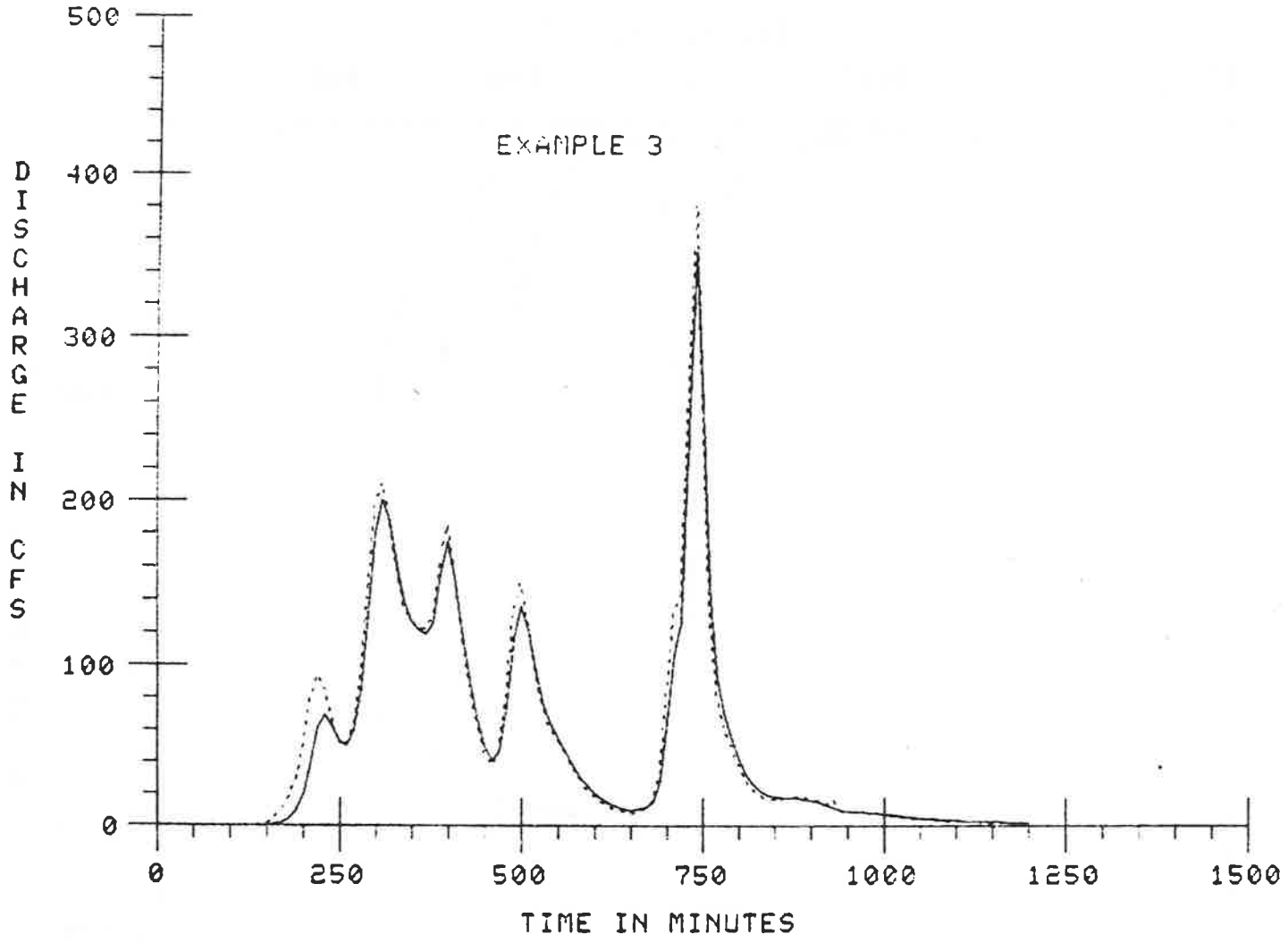

Figure 19.4 Effects of timbering with care to preserve ground cover on Watershed 17 for storm of September 5, 1970.

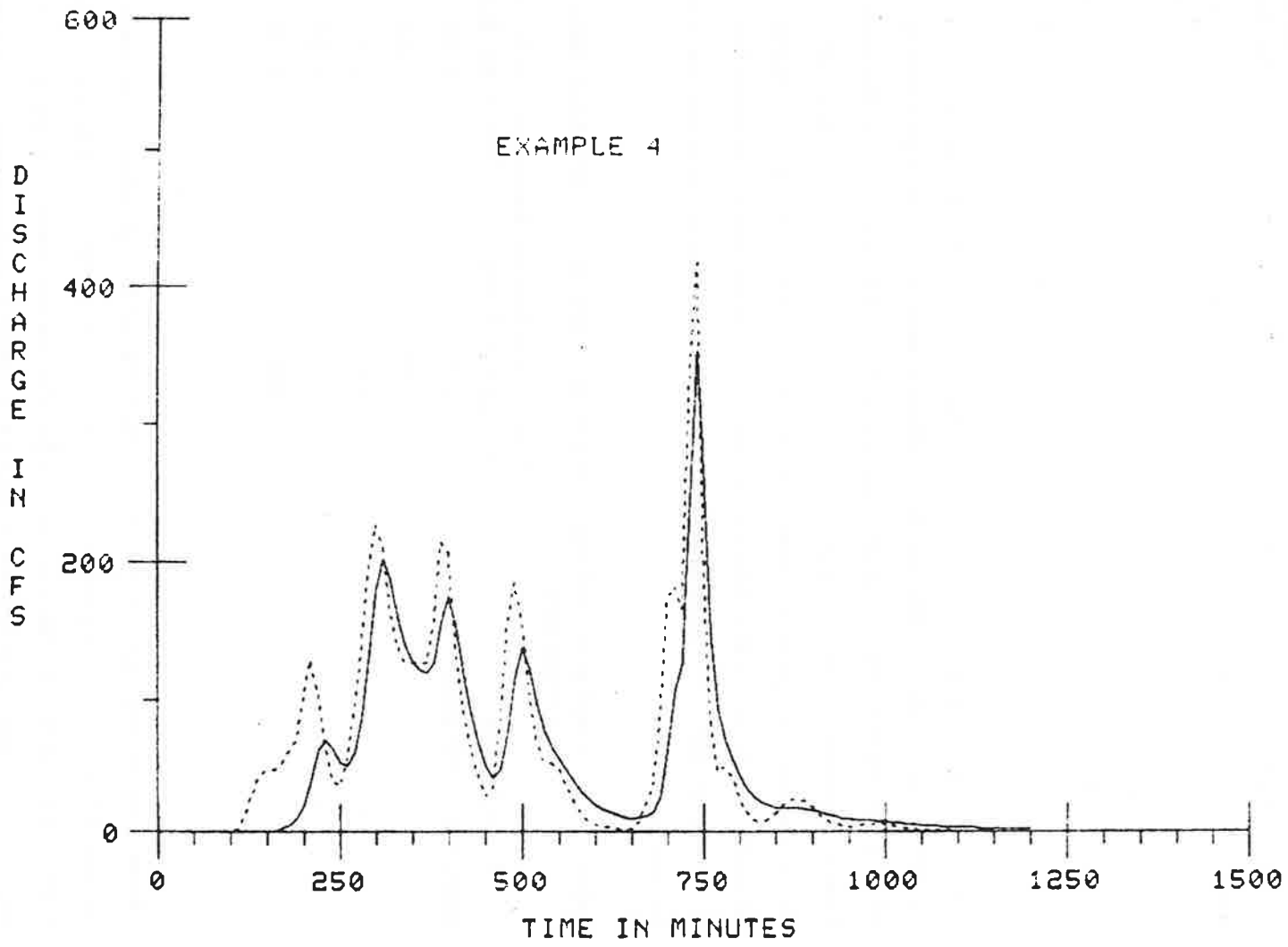

Figure 19.5 Effects of overgrazing on Watershed 17 for storm of September 5, 1970.

Table 19.2 Simulated watershed responses using SEDWAT for four land use alternatives.

Alternative	Ratio of Simulated Result to Baseline Condition: Peak Discharge	Water Yield	Sediment Production
Baseline Condition	363 cfs	3.75 in.	0.30 T/ac
1	1.17	1.21	1.06
2	1.17	1.21	3.25
3	1.13	1.04	1.62
4	1.15	1.09	2.79

creates conditions allowing the highest sediment production. In every alternative the peak discharge was increased primarily because of a drop in hydraulic conductivity and partially from a decrease in flow resistance. Water yield also increased in every alternative because of decreases in interception and infiltration. One more comparison can be made to demonstrate the relative effects of each alternative. This is the average concentration of the sediment-water mixture as listed in Table 19.3.

Table 19.3 Simulated sediment-water concentration for four land use alternatives.

Alternative	Concentration of Sediment in Mixture: Part per million	Ratio to Baseline
Baseline Conditions	706	1.00
1	619	.88
2	1897	2.69
3	1100	1.56
4	1808	2.56

These comparisons present a key point in terms of assessing management alternatives. If increases in water and sediment yields were the criteria then alternative two would be the worst case. However, as Table 19.3 shows, if water quality in terms of sediment concentrations is used then alternative four is just as undesirable.

It should be noted that the parameters chosen in all of the above examples reflect particular response to land use. These numbers were arbitrarily chosen and could reflect, in some instances, the most severe impact. One of the strengths of using a simulation model such as SEDWAT is that effects of different levels of land use may be examined. By selecting appropriate changes in canopy and ground cover, soil properties, and flow resistance, the manager can carefully and rapidly compare relative effects of many alternatives.

19.3 PEAK FLOOD PREDICTION FOR AN ARID WATERSHED

General

This second example diverges a little bit from the concept of best management analysis, but it does tie in with overall watershed planning. In the arid and semi-arid west, normally low flowing or ephemeral streams can become raging torrents when swollen by runoff from intense thunderstorms. Because of the intermittency and random nature of such events, they cannot be analyzed using conventional flood frequency analyses as applied to larger streams or rivers. Instead the concept of probable maximum flood (PMF) is applied to estimate the absolutely largest event that could occur based on present knowledge. Such a runoff does not coincide with what is termed the 100-year flood. It is usually many times larger. The PMF can be estimated utilizing several different techniques including analysis of the largest floods recorded. Here again such an approach is data dependent and may not completely represent the long-term system response. Another approach is to use the probably maximum precipitation (PMP) to generate a PMF. This generation can be from observed hydrograph similarities, such as a unit hydrograph, or through use of a rainfall-runoff simulation model. The similation model is preferred if it is based on physical principles. In this example, the multiple watershed model (MULTWAT) developed by Simons, Li, and Spronk (1978) was used to determine the validity of a PMF hydrograph computed using other techniques. The primary purpose was for design of a diversion. Selection of a realistic PMF hydrograph is necessary in order to avoid high costs but provide the necessary safety in design. More details of this application are considered in the following segments.

Model Application

Background

On-site inspection of the waterhsed suggested that the PMF as calculated using an initial approach based on the average basin characteristics (Bureau of Reclamation, 1974) may be too large. The reasons for this were:

1) The upper half of the watershed is quite stable. It is armored with small rock and pebbles and shows no tendency to develop rills of gullies. Also, this part of the watershed is quite well protected with trees, shrubs, and in particular a good growth of grass.

2) Topography of the watershed can be approximated by a series of three cascade sub-basins. The upper part of the basin is relatively flat with a ground cover density of approximately 70 percent and a canopy cover density of 15 percent. The middle sub-basin is very steep with 50 percent canopy cover density and 70 percent ground cover density and the lower sub-basin is relatively flat with a canopy cover density of 15 percent and a low ground cover density of approximately 40 percent. The shape and characteristics of the watershed indicate that the PMF hydrograph determined by the method given in "Design of Small Dams" is apt to be quite different from the one that considers the shape of the watershed and physical processes. It is anticipated that the peak flow will be smaller than the 31,800 cfs computed for the drainage area.

3) Observation of the dimensions of existing channels suggests that flows from the watersheds are not large. Observing the geometry of the channels at bends, it is possible to determine where maximum flow depths have undercut the vertical embankments at a height on the order of a few feet above the existing channel bank. Recent historic flows have probably not exceeded 4,000 cfs on the watershed. The maximum recorded flood of a nearby watershed (approximately 1,000 square miles) was 32,000 cfs.

Floods near the site are almost always the results of rainstorm rather than snowmelt. The prediction of flood hydrographs involves the consideration of such factors as: 1) amount, intensity, duration and temporal distribution of rainfall, 2) size, slope, and shape of the watershed, 3) soil conditions and vegetation, 4) channel size and shape, and 5) resistance to flow in watersheds and channels. The flood estimate in this example included the theoretical determination of peak flow, volume of flow, and the hydrograph at the site resulting from the probable maximum precipitation (PMP). The PMF that results from applying the PMP to the watershed was estimated by assuming a flood equivalent to about 40 percent of the PMF and the antecedent rainfalls three to five days prior to the occurrence of the main flood. This required an assumption that the antecedent moisture condition is approximately equal to the field capacity that describes the moisture condition at which surface drainage is completed.

The PMP area rainfall correction and direct runoff were determined.

by methods currently employed by the Bureau of Reclamation (1974). Due to the distinct changes in slope from sub-basin to sub-basin, and because of the long, narrow-shaped watershed, the simplified procedure for obtaining the hydrograph developed by the Soil Conservation Service (U.S. Bureau of Reclamation, 1974) does not result in an acceptable hydrograph. A method that is based upon the governing physical processes was applied to obtain a more realistic answer.

Watershed Sedmentation

The drainage basin of the watershed has an area of about 11.2 square miles. Approximately 0.6 square mile in the upper portion drains to a closed basin and does not contribute runoff. It is assumed that the discharge from this basin would not contribute runoff to the project site even during the PMF. The highest elevation on the watershed approximates 8,700 ft. with the lowest elevation near the proposed diversion dam approximating 6,500 ft. Typical average drainage basin slope for the watershed is approxiamtely 5 percent. However, due to the distinct changes in slope from sub-basin to sub-basin, the average basin slope cannot represent the topographic features of the watershed adequately. There is a necessity to divide the watershed into sub-units. The watershed was divided into three subwatersheds, eight plan units, and six channel units (Figure 19-6). Each geometrical component of the subwatershed can be represented as an "open book" watershed. For subwatersheds and planes, analytical infiltration and water routing methods were utilized to obtain hydrographs. Hydrographs simulated on each of these units are combined by a numerical kinematic wave channel routing technique to form the total hydrograph for the watershed (see Chapter 7). The length, width, and slopes of the segmented units are given in Table 19-4.

Probable Maximum Precipitation

Following the Bureau of Reclamation (1974) methodology for determining the PMP (page 53), the point rainfall of one-hour PMP was determined to be 11.0 inches. The ratio of area rainfall to point rainfall was estimated to be 0.8 (page 54). Thus, the area rainfall of the one hour PMP is 8.8 inches. The one-hour thunderstorm PMF was selected over the 6-hour general storm because the one-hour thunderstorm would produce a high design peak flow.

Table 19.4 Geometry of the studied watershed.

UNIT	LENGTH (ft.)	WIDTH (ft.)	SLOPE
WS-1L	2,342.72	4,760	0.0639
WS-1R	4,216.90	4,760	0.0404
WS-1CH	4,760.00		0.0546
WS-2L	3,914.43	2,920	0.0523
WS-2R	1,814.01	2,920	0.0899
WS-2CH	2,920.00		0.0685
WS-3L	2,444.25	19,960	0.0440
WS-3R	4,120.31	19,960	0.0394
WS-3CH	19,960.00		0.0200
PL-1	1,434.92	8,160	0.0458
PL-2	2,289.04	8,160	0.0784
CH-1	8,160.00		0.0287
PL-3	2,761.12	6,260	0.261
PL-4	4,364.35	6,260	0.207
CH-2	6,260.00		0.0446
CH-3	5,520.00		0.189
PL-5	5,369.17	4,050	0.273
PL-6	2,271.57	4,050	0.315
CH-4	4,050.00		0.0778
CH-5	2,360.00		0.292
PL-7	885.03	5,040	0.400
PL-8	1,216.91	5,040	0.361
CH-6	5,040.00		0.137

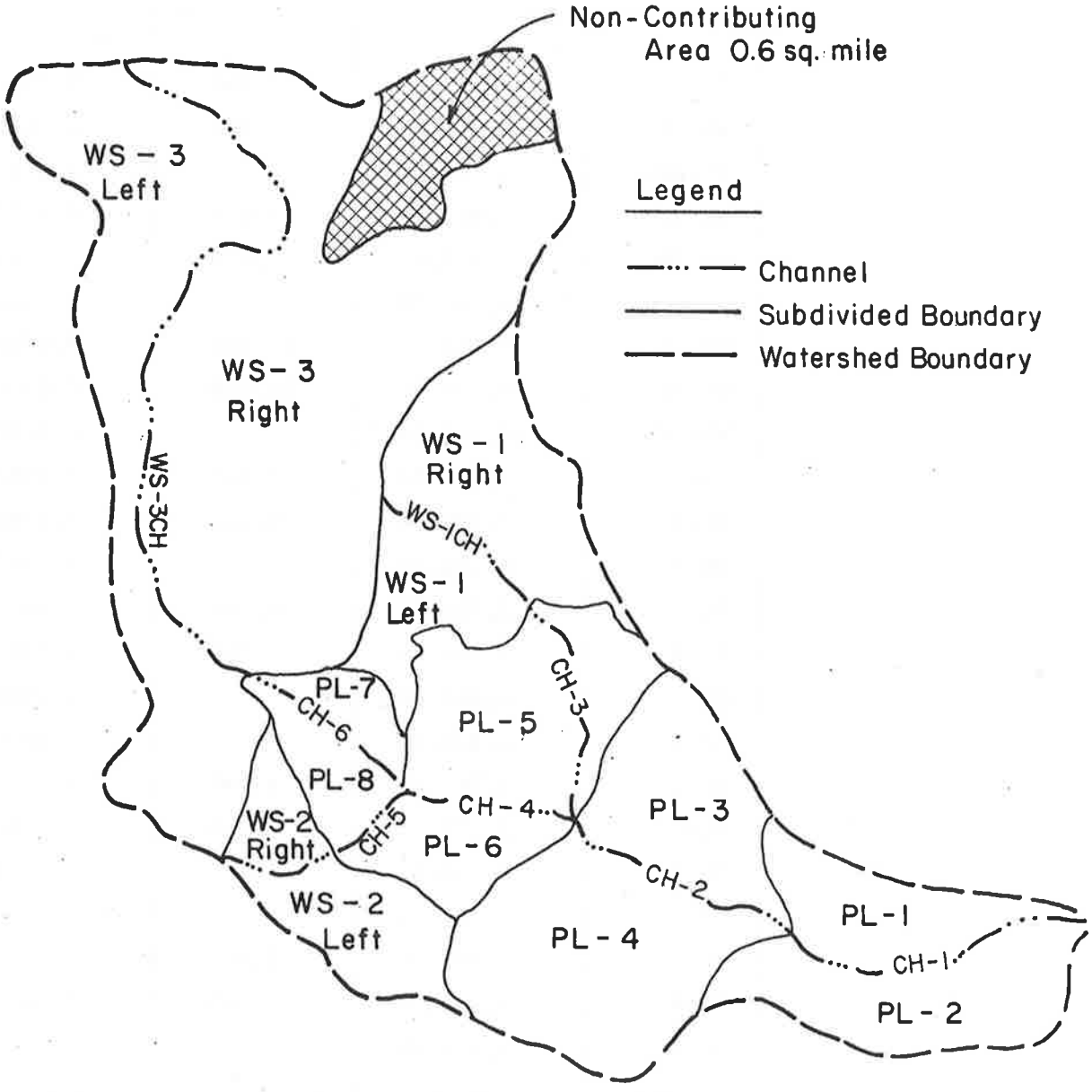

Figure 19.6 Watershed segmentation of the application area.

The temporal distribution of the one-hour thunderstorm was based on the procedure suggested in the "Design of Small Dams" (page 543). The 15-minute intensities for the one-hour PMP are given in Table 19.5.

Table 19.5 15-minute rainfall intensities for one-hour probable maximum area rainfall.

Time Minutes	Intensities in/hr
15	10.56
30	7.04
45	3.52
60	14.08

Direct Runoff

Peak rates of runoff are estimated to range from approximately 50 cubic feet per second (CF per square mile for the mean annual flood) to 500 cfs per square mile for the 50-year flood. The soils at the project site fall into Soil Conservation Service Hydrologic Groupings B and C. This hydrologic soil grouping is a four step rating indicating how much of a given rainfall will enter the soil profile and not run off. The hydrologic cover complex, (vegetative cover) falls into the juniper-grass category. The vegetative cover is mixed consisting of varying amounts of juniper, pinon, grass and cholla cover, or may be predominantly one of these types. Grass cover at the project site is generally heavier than that of desert grasses due to higher annual precipitation. Juniper-grass is typical of mountain slopes and mesas of intermediate elevations. Based on the above hydrologic soil cover complexes, the associated runoff curve numbers selected for use in the flood hydrograph computations approximated 85 for the one-hour, probable maximum precipitation occurrence. With this runoff curve number and the total rainfall of 8.8 inches, the direct runoff volume of the PMF is 7.0 inches (page 541 of "Design of Small Dams," 1974). Using the following soil parameters in the multiple watershed model:

hydraulic conductivities in the wetted zone 1.0 in/hr for upper and middle sub-drainages, 0.5 in/hr for the lowest sub-drainage, porosity 0.4, initial degree of saturation 0.65, final degree of saturation 1.0, average suction head 2 inches, the estimated total water volume for the PMF over the duration of 6 hours is 6.96 inches. This value is very close to that determined by the runoff curve number.

Channel Characteristics

The channel cross sectional data was utilized to determine the relationship between wetted perimeter and flow area. The channel resistance factors were estimated utilizing the information provided by Chow (1959) and Simons and Senturk (1977). The estimated values of the Manning roughness coefficient n are: 0.025 for the channel in the lowest sub-basin and 0.07 for the channels in the middle and upper sub-basins. There are trees, grass, cobbles and debris in the channel bottoms and banks of the middle and upper sub-basins.

Probable Maximum Flood Hydrographs

The computed PMF hydrograph based on the multiple watershed model is given in Figure 19.7. The peak flow of the PMF is 22,700 cfs and the duration of the flood is 6 hours. The shape of the determined hydrograph reflects the topographic features of the basin. The multiple peaks are very reasonable considering the series of three sub-basins. For quick comparison, the 100-year and probable maximum floods previously determined by the Soil Conservation Service method are given in Figure 19.8. The previous hydrographs are symmetrical in shape and fairly short in duration very different than that presented in Figure 19.7.

SUMMARY

This PMF was determined by a physical process simulation model that routes water from subwatersheds and planes to channel networks. The rainfall input to the model was the one-hour PMP. The total PMF runoff volume was equal to 7.0 inches of runoff from watershed. The simulated peak flow (PMF) is 22,700 cfs and the duration is about 6 hours. The shape of this second hydrograph is very reasonable, and is based on the analysis of three sub-basins. This 29 percent reduction in estimated flood peak could significantly reduce the diversion channel requirements. Also, there is little evidence of significant historical

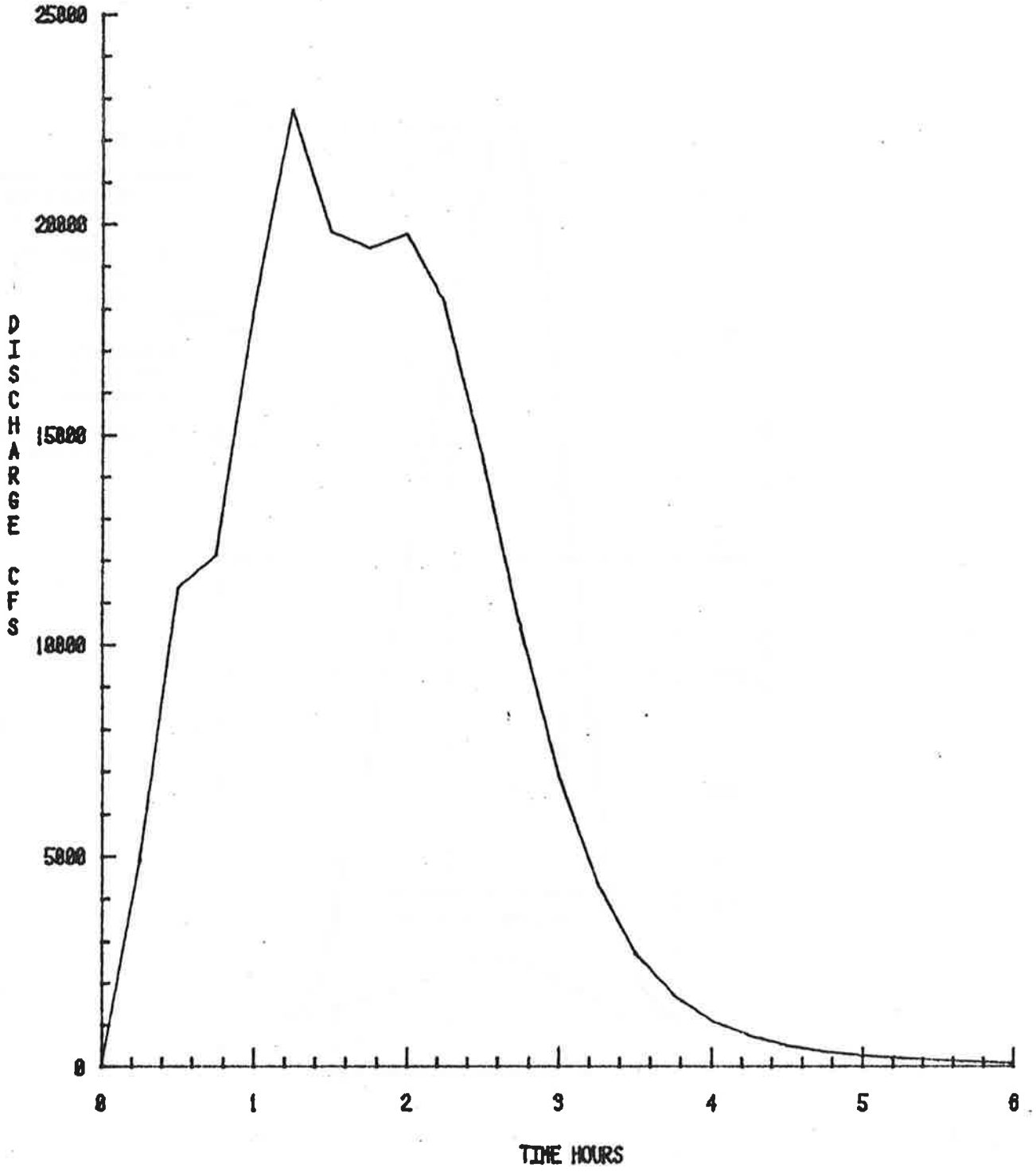

Figure 19.7 Hydrograph determined by MULTWAT.

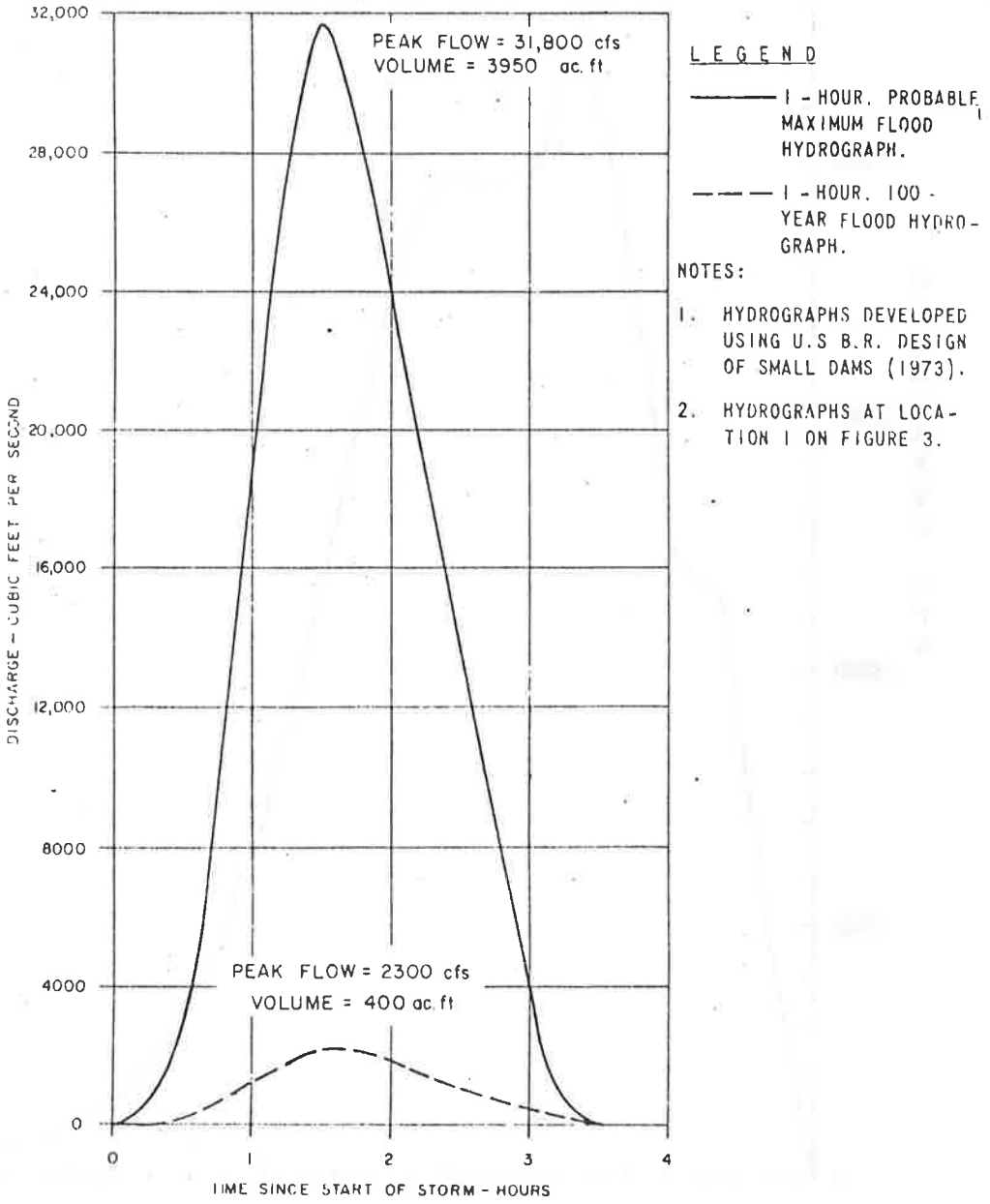

Figure 19.8 PMF as previously determined.

runoff from the upper 50 percent of the basin. If this observation was utilized in the analysis, the computed PMF would be even smaller than the reported value of 22,700 cfs. The general conclusion was that a large factor of safety (regarding peak flow) exists in the design of the diversion channel.

As this above example indicates, use of old methods may not always provide the best analysis of a problem. Better analysis may be obtained from current knowledge.

19.4 GENERALIZED PLANNING MODEL FOR ASSESSING FOREST PRACTICE ON WATER AND SEDIMENT YIELDS

General

In this application, the generalized watershed model described in Chapter 10 is applied to a selected site in the Arapahoe-Roosevelt National Forest. The Arapahoe-Roosevelt is a lead forest. In lead forests, technolgoies for assessing land use changes are being developed. The Arapahoe-Roosevelt National Forest has embarked upon a program to develop a methodology via computer modeling to utilize data from several sources - timber, soils, hydrology - in order to estimate sediment yields from land use changes. The demonstration watershed selected for application is Cabin Creek, a 10.5 square mile watershed located about eight miles north of Hot Sulphur Springs, Colorado. Figure 19.9 shows a sketch of the watershed. There are six gaged sites in the watershed where discharge, sediment transport, and water quality measurements have been collected. The vegetation of the area is characterized by lodge pole pine and spruce-fir conifer types. Soils are typically loams and sandy loams, with mixes of clay and gravel. They are characterized as being well drained. For this planning level model, the watershed was subdivided into cells forty acres in size. This large size is acceptable since only a rough estimate of sediment yield is needed for the analysis of watershed management practices. A finer resolution is only used, along with a more detailed model, if more information is necessary for planning decisions. Rainfall records from a nearby climatically similar site were used to portray the summer precipitation felt responsible for producing sediment loading to the stream. Synthetic outflow hydrographs based on measured data were used to represent the four month snowmelt period. Six day average flow values were used. Peak discharge for a six day period was about 62 cfs at the basin outlet. Discharge for each of 44 channel segments (217 overland flow planes) was apportioned from the gaging sites representing the segment. The watershed has been logged and these effects are noted in vegetation and soil values. Sediment tranport relations for the channel were calibrated from measured data. Bedload transport is very well correlated with water discharge, but suspended sediment is not. Each channel is described by the characteristics of the most immediate downstream channel. Values for other parameters needed in the physical process model were derived using methods presented in Chapter 7 and 10.

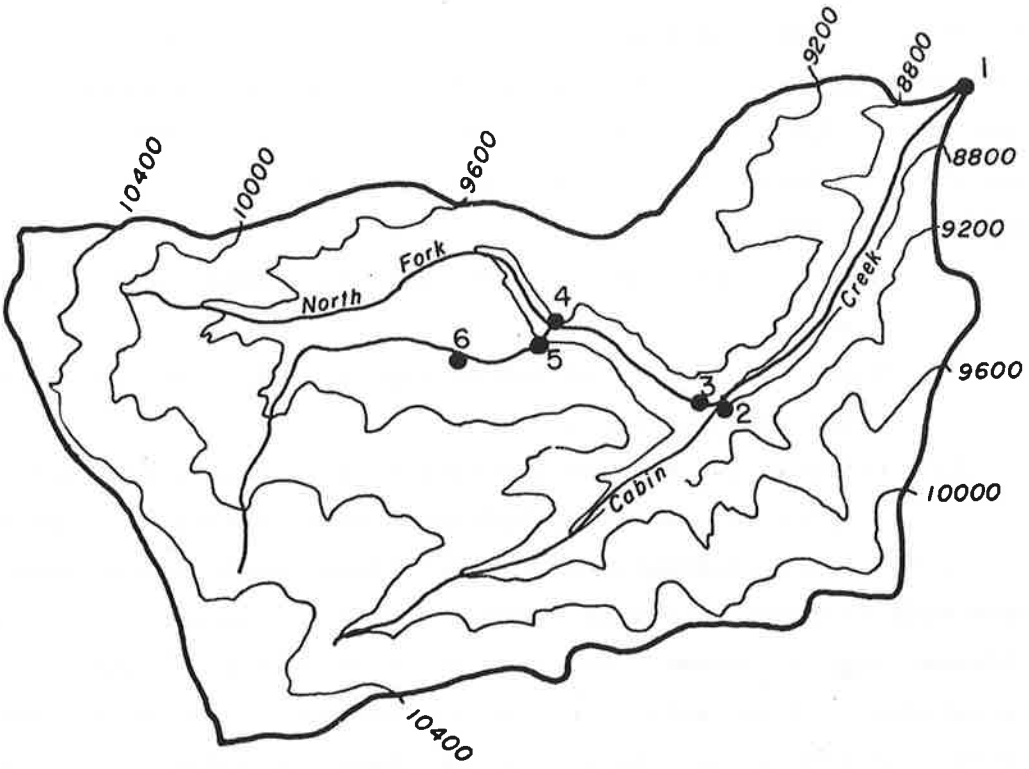

Figure 19.9 Topographic map of Cabin Creek watershed (1 inch = 1 mile).

Application

Alternative Evaluation

The model was applied to the watershed using the initial data to represent base line conditions. Because running the model for about 70 storms per summer is very prohibitive in terms of time and the information gained from numerous runs is not that much more useful, only selected representative storms are used. Sediment yields are then scaled upwards using the rainfall volume. Minor model adjustment was needed to produce representative simulated yields for the base line conditions. Model adjustment on calibration is inherent in all modelling efforts. After model adjustment, four selected watershed modifications were simulated to assess the relative impacts of each. The three alternative modifications are:

1) Clearcut one side of subdrainage 2, ground cover remains the same,
2) Clearcut one side of subdrainage 2 with reduction of ground cover to 25 percent,
3) Clearcut one side of subdrainage 2, reduce ground cover to 25 percent, and lower hydraulic conductivity by 30 percent.

In all three alternatives, channel flows remain at the same levels. These modifications represent changes that might normally occur under a different logging scheme. One with little disturbance, one with some disturbance, and one with extensive disturbance to the soil-plant-water system. Of particular interest is the change in sediment yield at different points in the watershed. For this reason only one subdrainage was affected by logging, a common situation in many watersheds. The results of these simulations is shown in Table 19.6.

Table 19.6 Relative sediment yields at selected subdrainages showing effects of isolated logging.

Site	Baseline Conditions yield in tons	Ratio of yield from alternative to yield from base line conditions		
		Alternative		
		1	2	3
1	12.43	1.05	1.37	1.37
2	4.66	1.12	2.01	2.01
3	2.42	1.0	1.0	1.0
4	1.06	1.0	1.0	1.0
5	0.64	1.0	1.0	1.0
6	1.01	1.0	1.0	1.0

As these simulated yields show, watershed modifications in one part of the drainage can create impacts that are manifested elsewhere in the basin. The other nonchanging values for the rest of the subdrainages are shown for comparison only in Table 19.6.

Discussion of Simulations

An interesting result stems from these simulations, one that must be accounted for by close inspection. Comparison of alternatives 2 and 3 indicate that there is no difference in sediment yield at the outlets for these two cases. However, sediment yields at the stream outlets do not fully depict the processes occurring in the watershed. Examination of channel aggradation and degradation, and comparison of supply to each channel segment with transport capacity helps explain the identical results for alternatives 2 and 3. This is best depicted by comparing the total sediment deposited in the channels in subdrainges. There are eleven channel segments above Site 2. In the base line conditions there was a net 0.61 tons of aggradation in these channels. In alternative 1 this jumped by 24 percent. The change in aggradation between alternative 2 and base line conditions was 2700 percent, and between alternative 3 and base line was 3020 percent. An increase in aggradation of 11 percent between modifications 2 and 3 has effectively halted an increase in sediment yield by reducing hydraulic conductivity. What this result indicates is that transport capacity controls sediment outflow from subdrainage 2 and that under these channel flow conditions aggradation and channel storage occurs. However, if flow conditions were to change, such as increased snowmelt runoff, the stored channel sediments may "flush out" and tremendously increase sediment yields at the downstream sites. For example, if streamflow were to increase 15 percent as a result of more snow or faster melting, the sediment yields would be increased because of the higher transport capacities (assuming sediment supply from overland flow remains the same). Such a streamflow change was made for the conditions in alternative 3 as listed in Table 19.7.

Table 19.7 Increase in sediment yield caused by alternative 3 modifications and 15 percent rise in streamflow.

Site	Base Line Conditions Sediment Yield in Tons	Ratio of Sediment Yield with Modification in Watershed to Base Line Conditions	
		Alternative 3	Alternative 3 with Increased Stream Flow
1	12.43	1.37	1.55
2	4.66	2.01	2.44
3	2.42	1.0	1.07
4	1.06	1.0	1.01
5	0.64	1.0	1.28
6	1.01	1.0	1.19

These results indicate that an increased flow will move some of the aggraded sediments out of subdrainage 2. Increased sediment yields also occur from the other subdrainages. Of particular interest in the increases in yields from subdrainages 5 and 6 where the increased flows have again flushed out otherwise transported sediments or caused channel scour.

Valuable information is provided by examining the changes in channel aggradation and degradation at each channel segment. Of particular interest are those sites where increased aggradation may affect aquatic habitat for fisheries and may lead to channel changes and flooding of surrounding areas. Use of this generalized planning model can help the forest manager in quantitizing the relative effects of different alternatives in a rapid manner.

19.5 EVALUATION OF A WATERSHED DATA COLLECTION NETWORK USING PHYSICAL PROCESS MODELS.

General

This application of physical process models to best management practices differs a bit from the response type analyses previously presented. In this example, the concept of data collection networks is discussed with special emphasis placed on one role that physical process models can have in evaluation. The procedures are applied to an agricultural watershed, Four-Mile Creek, near Traer, Iowa. This watershed is maintained by Iowa State University under contract to the Environmental Protection Agency. Data are being collected to calibrate and test models that describe water, sediment, nutrient, and pesticide yields from agricultural watersheds. The watershed is 19.51 square miles in size including several smaller sized subwatersheds. Six recording raingages monitor rainfall precipitation. Eight gaging sites (three of the U.S. Geological Survey Sites) record streamflow. Three of the eight are on field sized watersheds where intensive soil and water measurements are taken.

Objectives of Application

This application had two objectives. First, to develop a generalized procedure for designing and evaluating a data collection system. This procedure included analysis techniques, used of mathematical models, available data and common sense. The other objective was to apply the developed procedure to the selected agricultural drainage. Both of the objectives are detailed in the following sections.

Approach of Application

Data Needs

This application presents a systematic approach to designing or evaluating a data collection system. The first task is identification of data needs. These needs are directed towards monitoring system response or towards development of a data base for applying mathematical models. In this study, the adequacy and completeness of the data collection network is assessed relative to mathematical modeling of the system being measured. In turn, a selected mathematical model is used to demonstrate its usefulness as an evaluation technique. Data needs

are categorized and information delineated under each category. Needs are compared with available information in order to identify and assess any gaps that may limit the applicability of the data base.

Spatial and Temporal Designs

Spatial and temporal designs of a data collection network are important items to be delineated. Spatial design covers the location, number, and spacing of measurement points. Temporal design assesses sampling frequency and instrument timing connected with collection of specific data. Adequacy of spatial and temporal designs is dependent on the purpose of the study, spatial and temporal variability of a physical environment, and desired accuracy of analysis. A systematic approach to this problem was developed. This approach includes a survey and evaluation of the current data base, application of selected mathematical models to determine the model sensitivity to data, and an evaluation of the adequacy of spatial and temporal requirements of specific data. Spatial and temporal design of the collection network can be determined through statistical analysis of autocorrelation and space correlation. If a realistic value is set for the correlation coefficient for spatial and temporal data, measurement site spacing and sampling interval requirements can be determined. Mathematical models aid spatial and temporal assessment by depicting the watershed in terms of response timing and magnitude at various locations. These responses help in selection of instrument timing and size of measurement devices. If no data or inadequate data are available, the data base for the study area or from nearby sites can be used to provide supplementary information about the site.

Quality of Data

Quantity is an insufficient measure of a data collection network. Data quality is equally important. The quality of data can be assessed by simple comparisons of timing between sampling sites, by relative magnitude of measurements, by trends in the data, and by model sensitivity to good and bad data. Data quality, must be considered in evaluation of a data collection network with respect to measurement techniques and instruments, accuracy of the model being used, and the size of the area being modeled.

Application of Procedures

Procedures for evaluation are better illustrated by examples. Techniques are applied to the data base. Although all methods are not applied, a sufficient amount of information is obtained from modeling efforts to help evaluate the data collection system.

Data Needs

General

Data for modeling runoff from agricultural lands can be subdivided into several broad groups. These groups include watershed and channel geometry, soil, vegetation, climate and meteorology, hydrology, hydraulics, and man's influence. As models vary so do the specific inputs in each group. Specific needs will be discussed in following subsections. Typical data requirements for modeling are listed in Table 19.8.

Although general, this list shows that there are numerous needs to be considered when designing a data collection system. There are different methods for collecting data, some are listed in Table 19.9. As the list indicates there are a number of measuring devices that are needed in data collection.

Data needs should be approached deliberately because of the time, money, and instrumentation needs related to collection of each piece of information. Needs must be carefully considered and each piece of requested information justified and prioritized with respect to other data. Modeling needs are usually dictated by model inputs. Therefore, the person using the model must know the importance of each model input and how necessary it is for successful operation.

Modeling of rainfall, runoff, sediment yield, dissolved oxygen, and nutrient transport in agricultural drainages requires complex collection networks. Seldom, is enough data collected to meet the needs of most users. Therefore, some models may be untested or unverified. It is important then to define data needs, data priorities, and data availability to pinpoint weaknesses in the link between data collection and data use. The first step is definition of specific data needs. This is detailed in the model application section.

Spatial and Temporal Design

Design or evaluation of a data collection system must consider the spatial and temporal variability of the measured data. Because physical

Table 19.8 Input parameters for modeling of water and sediment yield from watershed.

I. Watershed and Channel Geometry Data

1. Area of watershed
2. Slopes and lengths of channels and land surfaces
3. Channel cross sections

II. Soil Characteristics

1. Soil type
2. Distribution of types
3. Porosity
4. Grain size distribution
5. Infiltration characteristics

III. Vegetative Cover Data

1. Density or coverage
   a. Canopy cover
   b. Ground cover
2. Cover interception of rainfall
   a. Canopy cover
   b. Ground cover

IV. Climatic Data

1. Rainfall hyetographs
2. Snowmelt rate
3. Evaporation rate
4. Air temperature

V. Hydrologic and Hydraulic Data

1. Water discharge hydrographs showing timing, peak, and volume of runoff
2. Resistance to flow parameters
3. Sediment yield
4. Grain size analysis of transported sediment

Table 19.9 Typical data collection methods.

Type of Data	Methodology
Rainfall	Measured by automatic recording rain gauge or meteorological radar
Evaporation	Measured by evaporation pan
Infiltration	Measured by infiltrometer
Flow Discharge	Measured by weir, current meter or rating table for a calibrated section
Water Surface Elevation	Measured by an automatic recording bubble gauge or in a stilling well
Flow Velocity	Measured by current meter or dye dilution method
Sediment Discharge	Measured by automatic pump sampler or standard depth-integrating samplers
Flow Resistance Parameter	Manning's equation
Location of the Channel	Measured by plane surveys or from USGS maps or aerial photographs
Channel Cross Section Geometry	Measured by hand level-survey rod, sag tape, or transit-stadia rod
Channel Bed Profile	Measured by sonic soundings and transit-stadia rod
Rock Outcrop and Manmade Control	Measured by geological survey or from available geological maps
Bed and Bank Samples	Determined by composite soil samples
Watershed Geometry	Determined from topographic maps
Vegetation Distribution	Determined from aerial photographs or a vegetation map
Soil Type Distribution	Determined from soil survey maps and field investigations
Sediment Source 5	Color infrared or black and white photographs

processes, or their measurable characteristics, are usually complex, continuous, and random, they vary markedly from area to area and over short time spans. This variability must be considered in the data collection network. For existing networks, previously measured data is analyzed for cross-correlation, autocorrelation, trends, patterns, order of magnitude, and spatial representativeness. For networks design, data usually does not exist which makes it difficult to determine necessary sampling points and sampling frequency. However, the advent of computer based physical process models has aided in design by allowing the designer to develop hypothetical events and resultant synthetic system response characteristics at presumed sampling sites. These response characteristics, if reasonably realistic, serve as "data" to be analyzed the same in an existing collection network. Approaches for evaluating an existing system are presented first, followed by an application, using a physical process models, for system evaluation.

Spatial and Temporal Analyses of Data

Temporal Correlations

When analyzing the spatial variability of sameness of time variant data, a common time increment should be chosen. If the time increment is very long, the lag cross correlation (see Yevjevich, 1972) between two stations is usually higher than if the increment is short. For example, stream gages ten miles apart on the same river probably have high cross correlation of yearly, monthly and even average daily discharge. However, as the time interval becomes less, such as minutes, the cross correlation usually drops. Such a situation is shown in Figure 19.10. As the sketch shows, there is a sampling time interval, Wt* , such that a correlation, p_t (for example 0.8), exists between the stations. Greater time intervals indicate greater cross correlations or redundancy in the data, smaller intervals are associated with a gain in information by using both gages.

If all the gages in the network are correlated above the selected value, there is a redundancy in the data for those measurements at that time period and a reassessment of sampling frequency and number of sites is needed. However as the measurement interval decreases, for example, from daily to hourly data, correlations may drop indicating that the present network needs to be expanded. Changes in sampling interval is

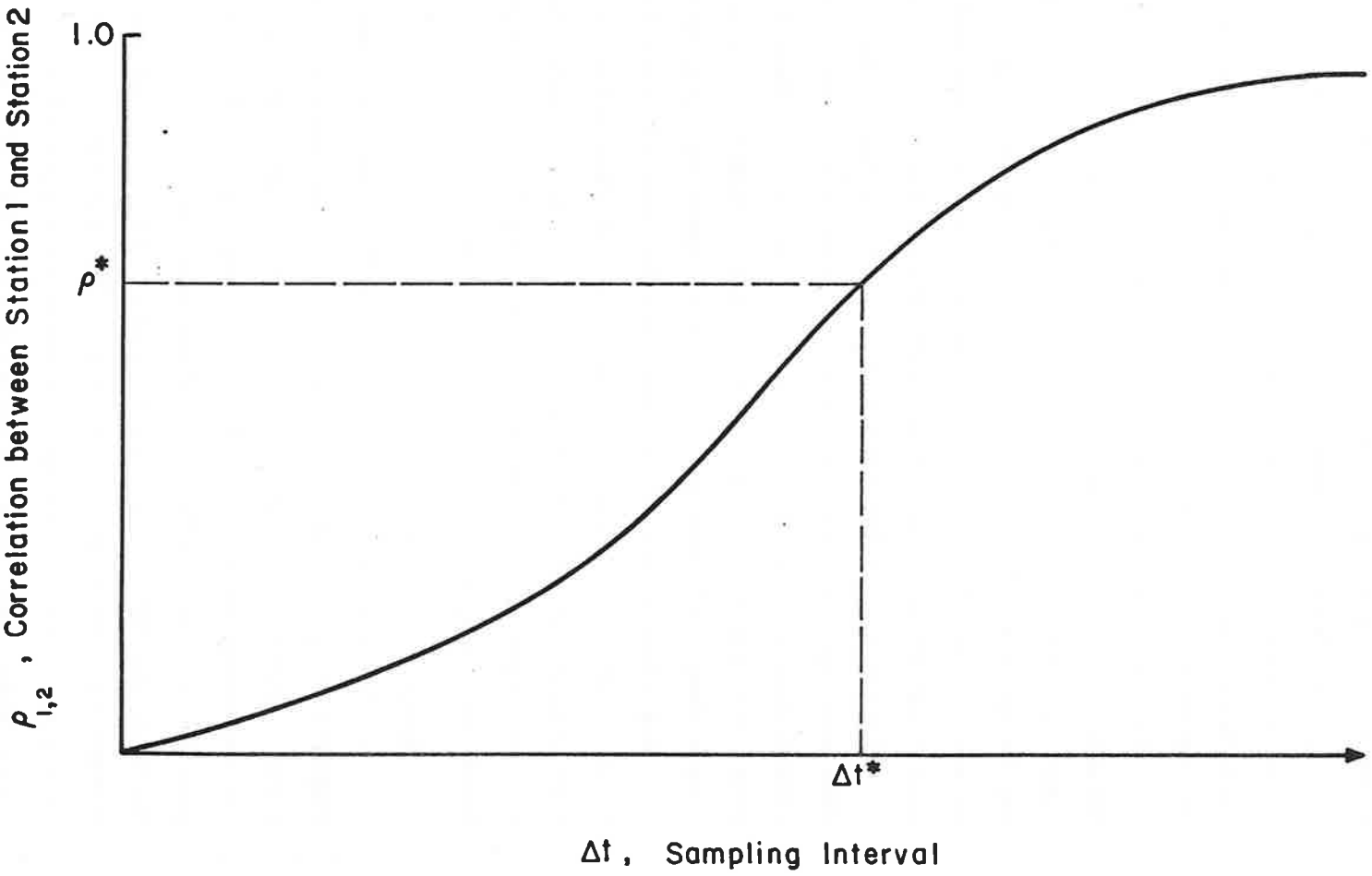

Figure 19.10 Increase in cross correlation between measurements with increase in time for separate stations. Constant distance between stations.

an important concept in system design since it helps determine the adequacy and efficiency of the collection network. Establishment of the temporal interval corresponding to data needs aids this analysis. For example, if data for a simple water balance model is needed, daily precipitation may be adequate. However, if a storm event model is to be used, a shorter collection interval is needed. If the model being considered requires both long interval and short interval data, a dual system should be established.

Autocorrelation of data at stations and lag cross correlations between stations are other information useful for temporal analysis. If sampling intervals at a station are quite short then a measured value may be quite close to the previous measurement (Figure 19.11). If the values are highly correlated at a certain Δt then the sampling frequency can be reduced without information loss. However, if the autocorrelation is too low then the sampling frequency may not be adequate thus missing important information. Redundancy and lost information are illustrated in Figure 19.12 by Δt^* and $\Delta t'$. Sampling intervals less than Δt^* are too short and redundant information results. Intervals longer than $\Delta t'$ result in a loss of important information.

Lag cross correlation between sites may indicate that a sampled value at one site occurs at some time interval before or after another site (Figure 19.13). Passage of a flood wave between two stations with a travel time of Δt^* between gaging stations or movement of a storm front are examples of this type of occurrence.

Spatial Correlations

If for a given time interval, such as one day, measurements are compared at different sites, a situation as shown in Figure 19.13 might arise. Similar to Figure 19.13, there may be a distance Δx^* corresponding to a selected correlation, p_x^*. As Δx increases, the gain in information for a constant sampling interval decreases. High correlations between stations indicate the stations are too close to one another for the sampling interval. The concepts of spatial and temporal correlation can be combined as shown in Figure 19.14. This generalized figure shows the types of relationships that are derived from a data loss to aid in evaluation.

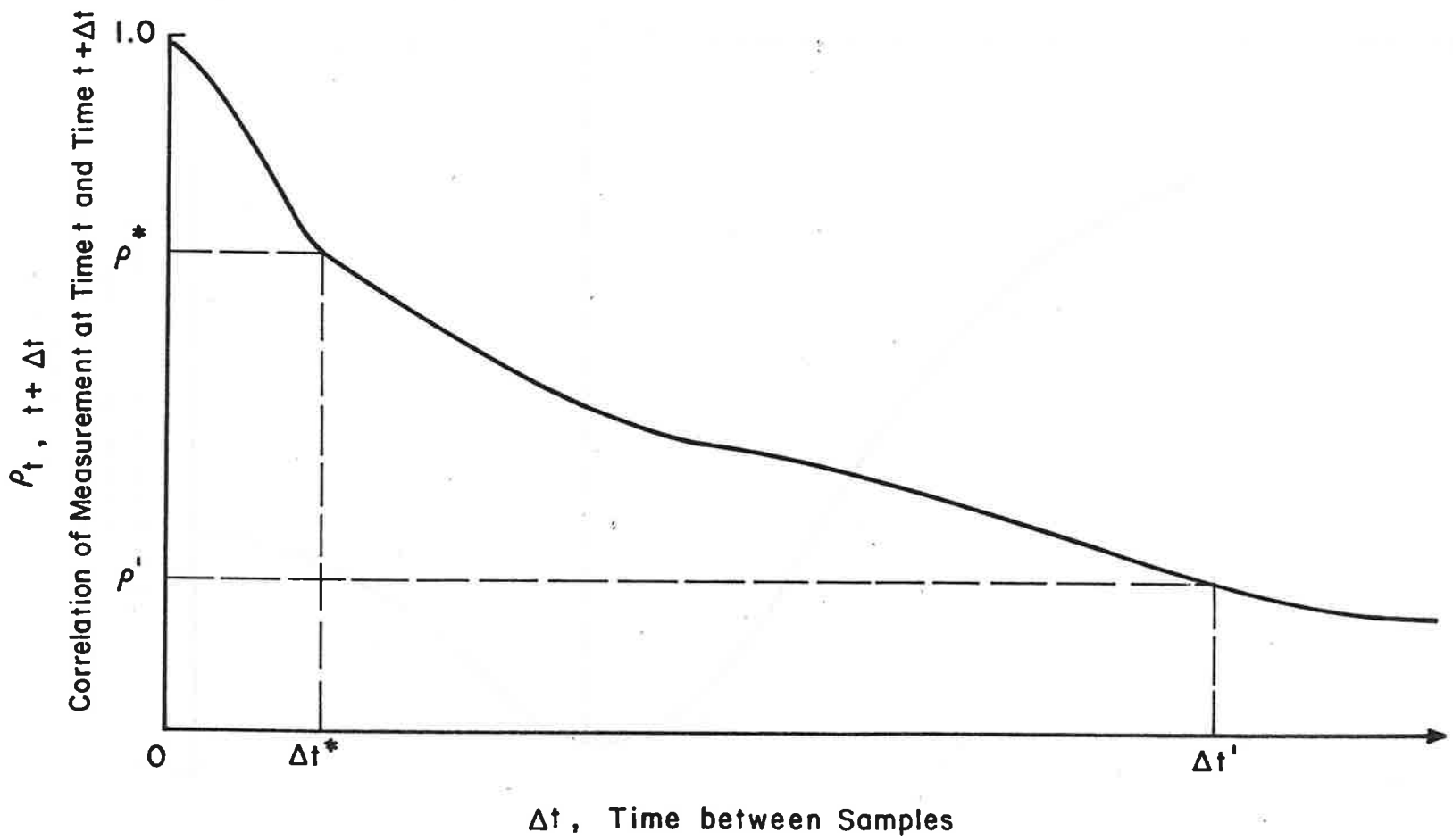

Figure 19.11 Autocorrelation of samples at one station.

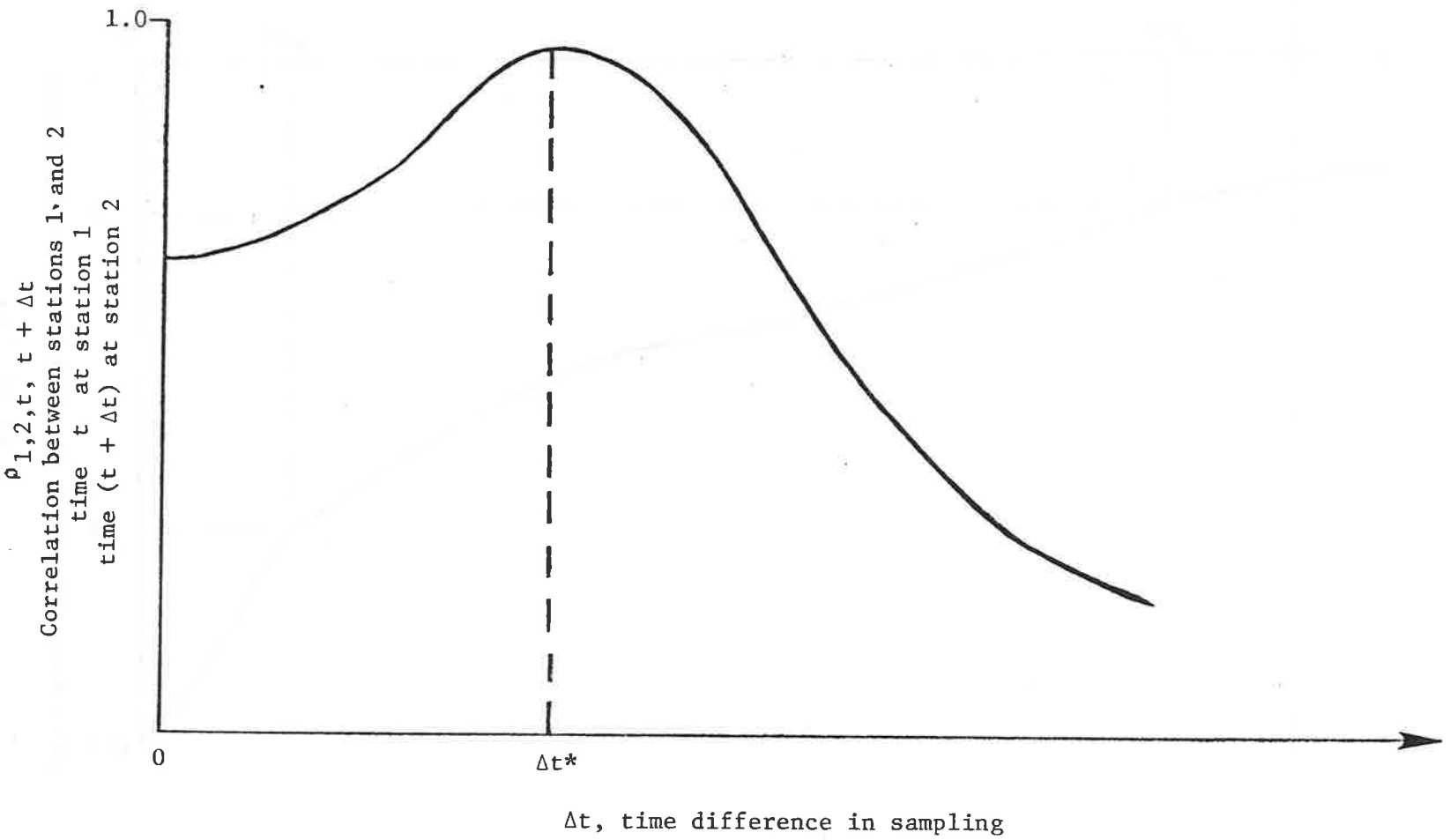

Figure 19.12 Cross correlation of measurements at two different stations with changes in sampling times on same time base.

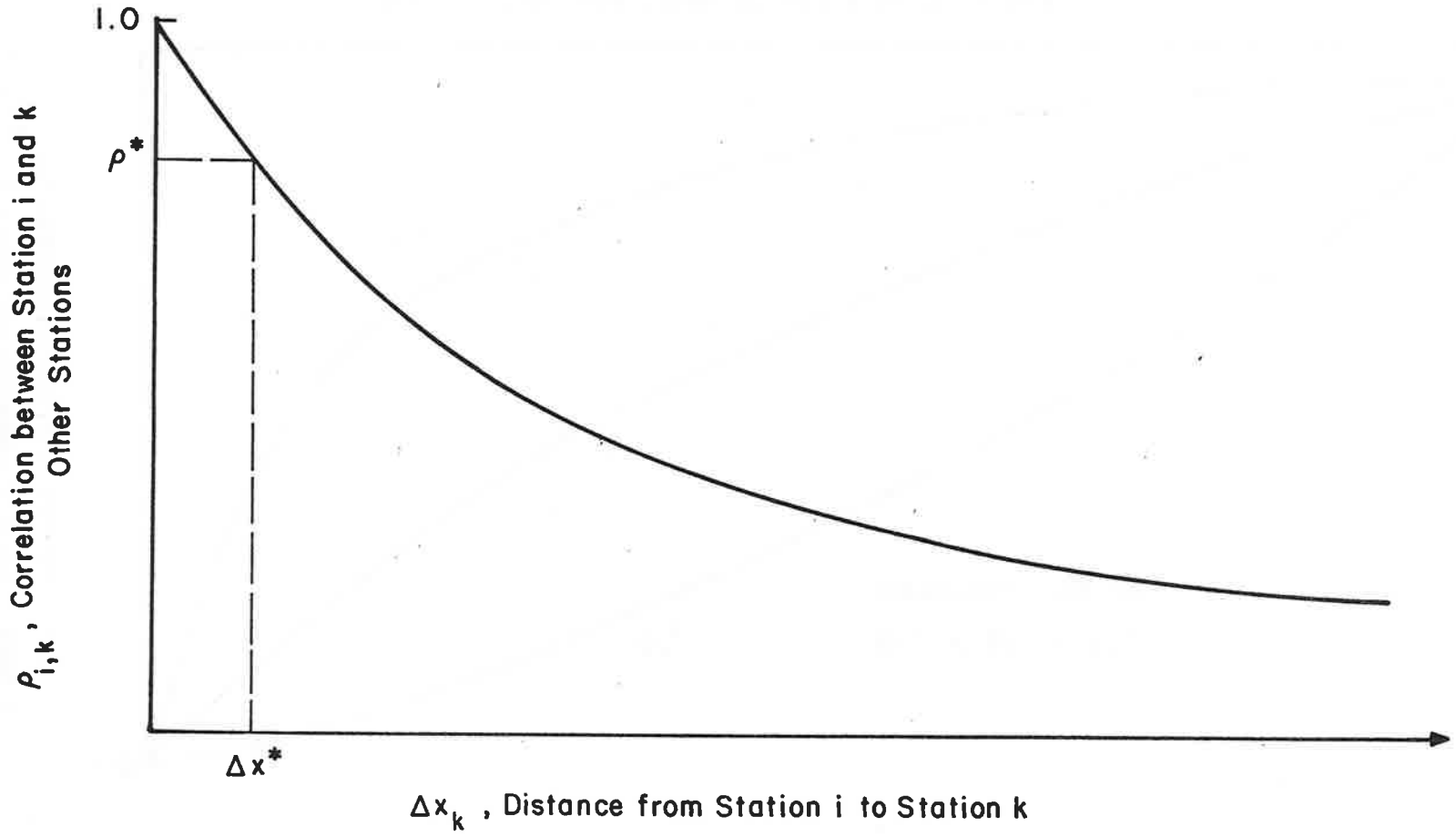

Figure 19.13 General decrease in correlation of measurements with increase in distance between separate stations. Constant sampling interval.

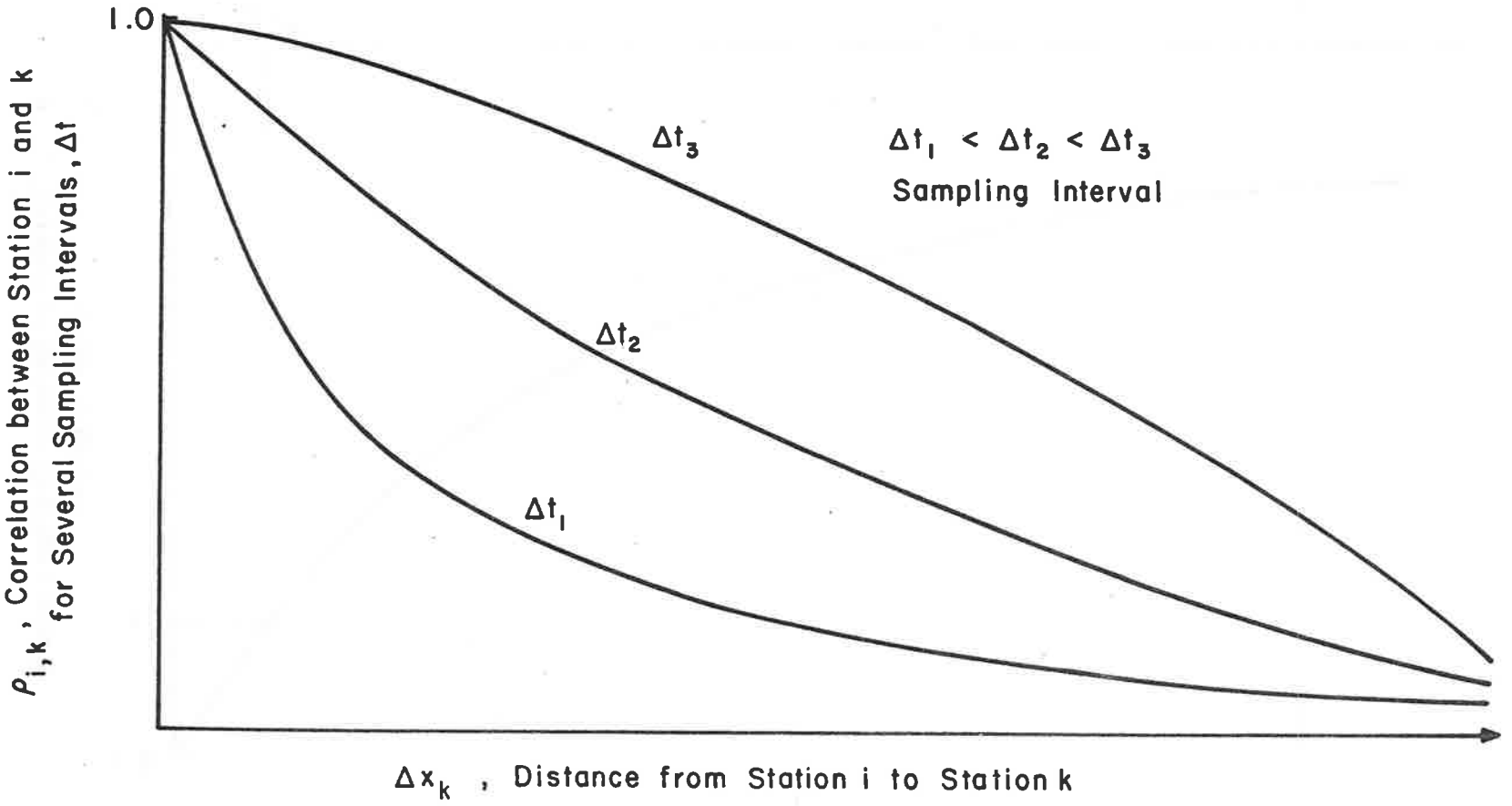

Figure 19.14 Combination of spatial and temporal correlations of measured data at different stations.

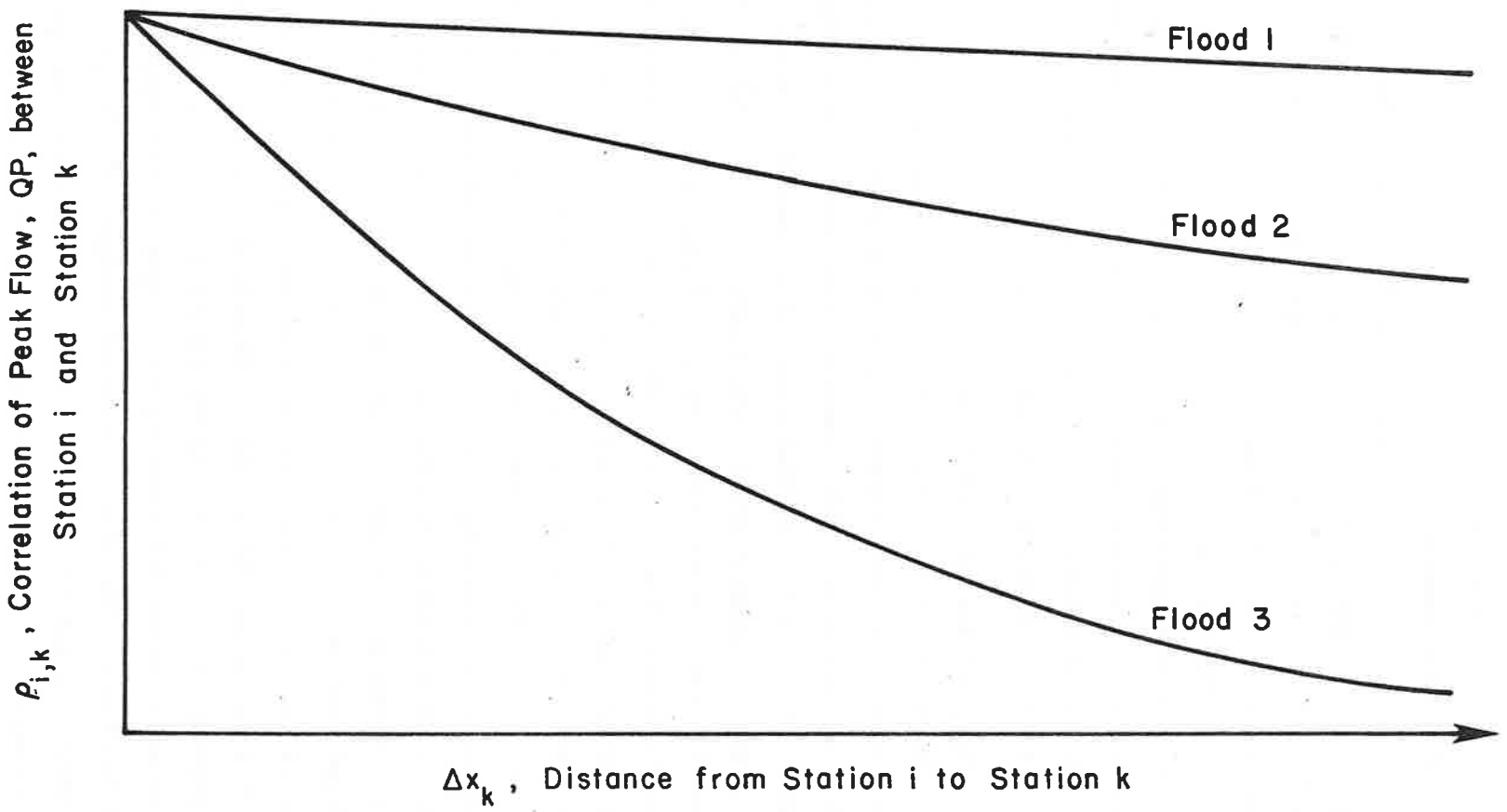

Figure 19.15 Spatial correlation of samples of time independent measurements.

There are data that are independent of time and can be analyzed using spatial correlation. A good example is peak flow of a flood wave as it moves down a channel. The flood peak may increase, decrease, or stay about the same magnitude as it traverses a channel (Figure 19.15). If the peak remains constant, or fairly so, then the channel system may experience a combination of resistance effects and lateral inflows that counteract the frictional damping and storage effects, or attenuation, usually experienced by channel flood flows. A change in flood peak with distance indicates that the peak is either increasing or decreasing as a result of these processes. A true picture of flood behavior is derived after examining several levels of floods. If high correlations persist for all flood levels, then the gaging stations may be placed too closely. Lower correlations indicate the opposite.

Temporal and Spatial Trends

Temporal trends in data at a site and comparisons of trends between sites assist in understanding the time behavior of the system. An important analysis is the dimensionless mass accumulation curve in Figure 19.16. For some dimensionless accumulated quantity, V*, there is a corresponding dimensionless time, T*, so that a characteristic curve for the sampled event exists. Examples are rainfall at a site or runoff volume. For rainfall, the characteristic curve is described by the pattern index, PI, which is the area beneath the curve and is always less than one. Five generalized types of patterns exist as shown in Figure 19.17. The advanced type is indicative of a storm of high intensities followed by lower intensities and the delayed type is a storm with intensitieis late in the period. The intermediate type possesses three general shapes and can be referred to as constant, advanced-delayed, and delayed-advanced. The constant type occurs as a fairly uniform intensity rain. Advanced-delayed type has high intensities at the beginning and end of the storm period, and delayed-advanced has high intensities midway in the storm duration. Each of these storm pattern types will create different system responses for equal rainfall volumes and durations. Therefore a careful analyses of the predominant storm patterns can aid in evaluating sampling intervals and gage placement. For example, if storms are characterized by high intensity-short duration rain bursts, such as advanced or delayed types, then the sampling interval

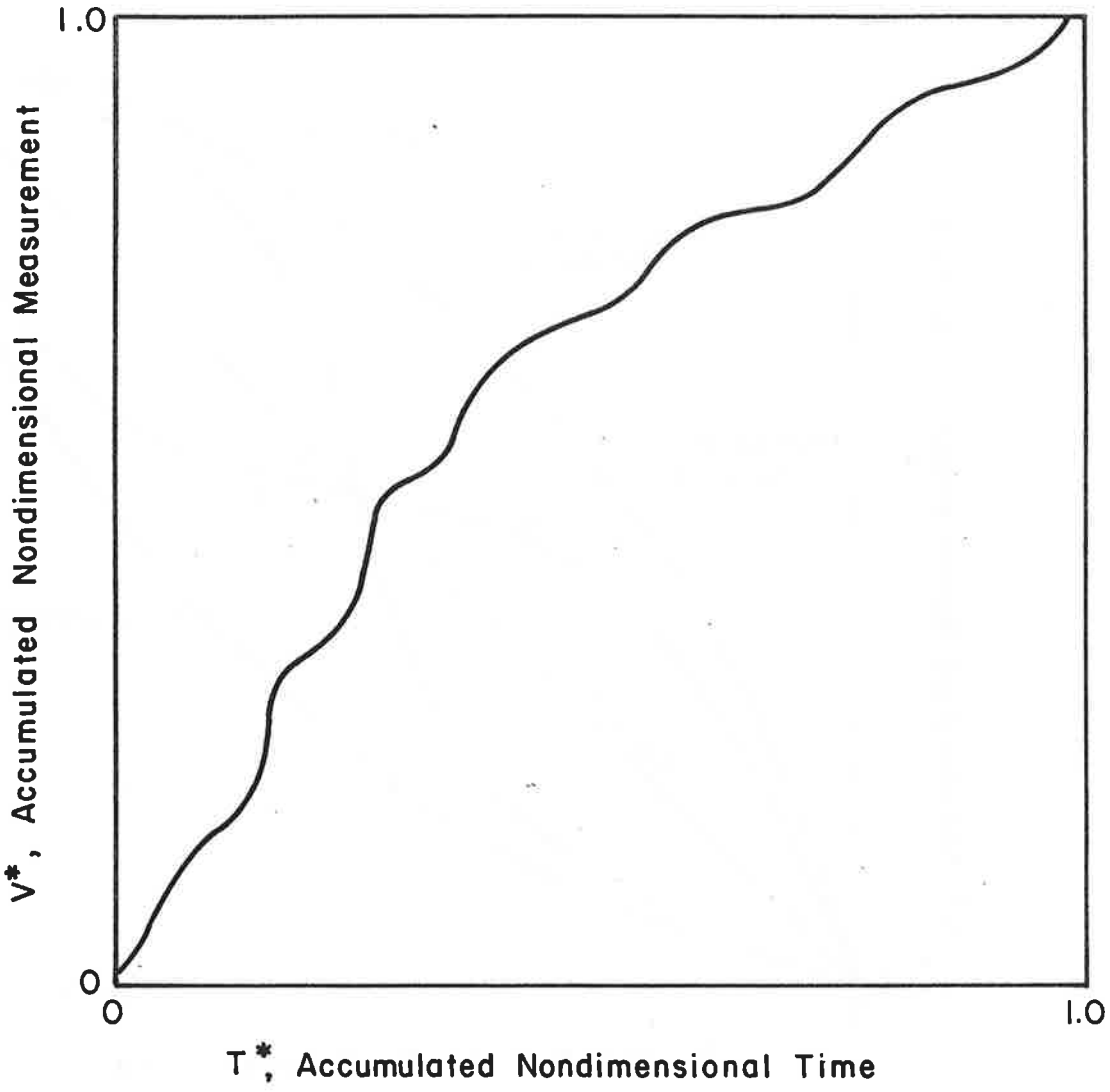

Figure 19.16 Dimensionless mass accumulation curve.

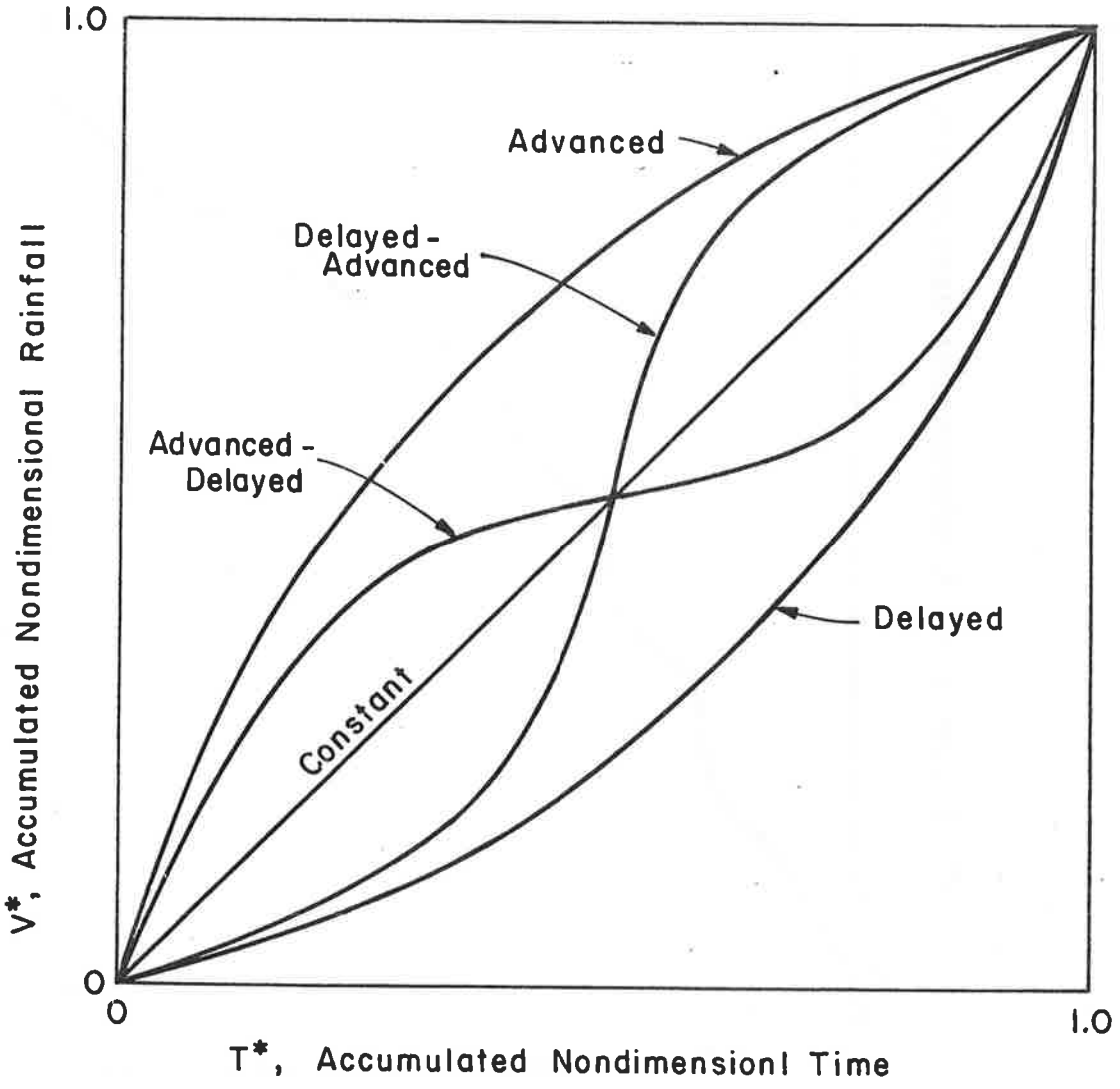

Figure 19.17 Nondimensional mass rainfall curve showing different pattern types.

on the recording mechanism needs to be shortened to provide a finer resolution of time.

Comparison of patterns between gages helps identify the homogeneity of a storm as it moves across an area. If a storm is fairly uniform over an area, then the patterns at the gages should be similar. However, if the storm is fairly localized then the patterns can be quite different (Figure 19.18). Consistently similar patterns between gages for all types of storms (advanced, delayed, etc.) indicate that there is an overabundance of recording sites and some recorders could be replaced by nonrecording gages. Conversely, consistently different patterns indicate the opposite and therefore a need for additional recording gages.

Another type of temporal analysis involves considering the change in a measured value over a day, a season, or a year. The classic example is the daily discharge hydrograph. A hydrograph indicates when the majority of runoff occurs, the rapidity of rise and fall identifies the response characteristic of the watershed, and the peaks portray the magnitudes of flows that may be expected. Individual storm runoff hydrographs also provide substantial information about the temporal distribution of flows. Steepness of the rising limb, shape of the recission limb, duration of flow, and peak discharge are all important. Comparison of hydrographs at different gaging sites for the same runoff event combines temporal and spatial aspects. The loss of nutrients or pesticides from soil with time is another temporal analysis that can aid modeling of chemical yields from watersheds.

Comparisons of temporal and spatial trends provide valuable information. One example is comparison of the decay ratio of applied pesticides between two different watersheds. The difference in decay rates could be caused by differences in soil properties, types of crops, moisture conditions, or slight changes in microclimate. Spatial and temporal comparisons would indicate that certain areas require special attention to data collection for accurate modeling. Another example of temporal and spatial trend comparison occurs through the subtle and sometimes major changes in mobile bed channel geometry: such comparisons as channel location movement, and changes in width, depth, wetted perimeter, or area of a cross section with time and between locations. Section to

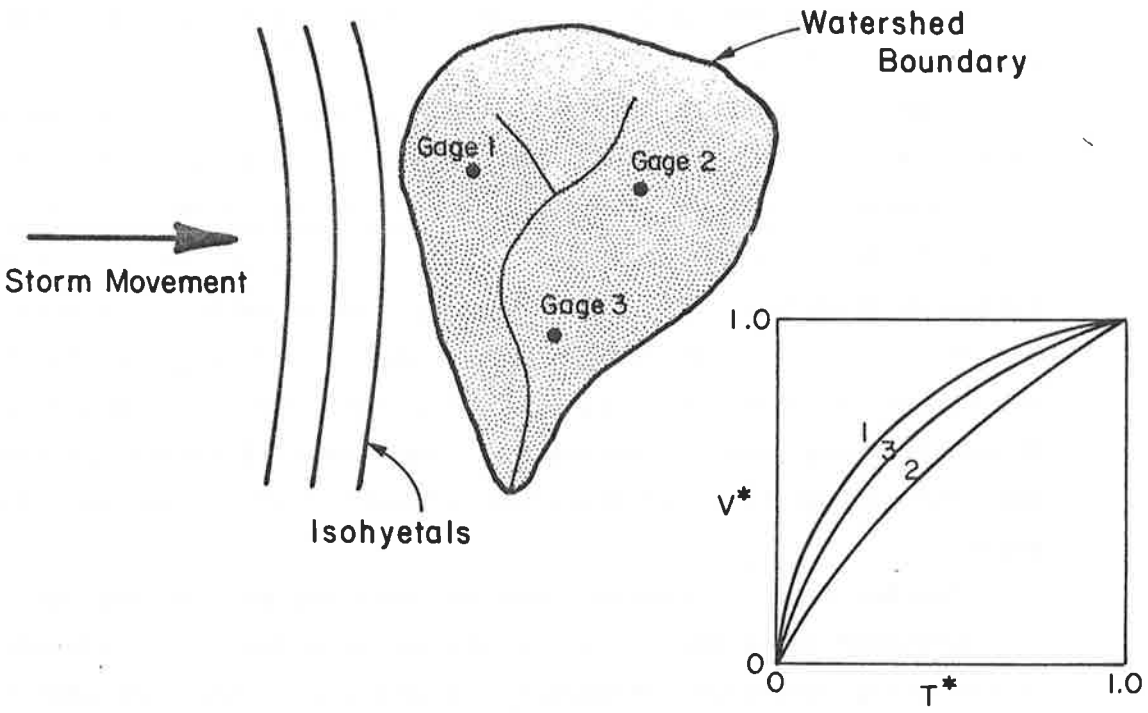

General Storm - Similar Patterns

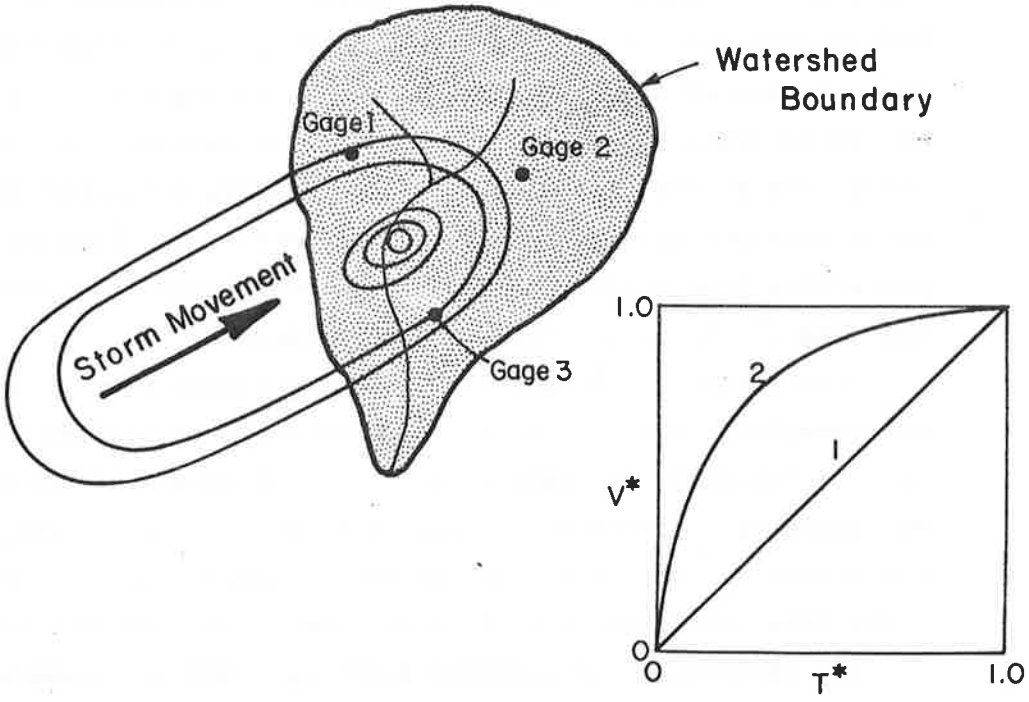

Localized Storm - Dissimilar Patterns

Figure 19.18 Storms over a watershed with three gages and effects on patterns.

section changes for one year can be compared with another year to see if certain sections may be subject to rapid changes with time while others remain relatively stable. These rapidly changing areas may require increased surveillance or more measurement sites.

Spatial and temporal comparisons of data at and between sites aid analyses of a data collection system effectiveness. Unfortunately, these types of analyses are usually reserved for existing systems. However, modeling technology helps solve this problem.

Use of Physical Process Models

Physical process models of watersheds can be effectively used to analyze existing or proposed data collection network designs. These models can provide information on water, sediment, and chemical movement in a watershed as well as where and how frequently samples should be collected to adequately access such movements

Existing Systems

Physical process models, in this case those that describe water, sediment, and chemical movement in watersheds, can be used to evaluate the design of an operating data collection system. Such models are useful in data checking, data synthesis and selection of new sampling locations.

Because physical process models are developed based on governing phenomena, they can be used to check the validity of collected data. For example, models used to estimate solar radiation for water balance studies can be applied to a collected set of solar and other climatic variables to check the accuracy of the solar measurements. If the computed and measured values are in serious disagreement then: 1) the data is wrong, 2) the model is wrong, or 3) both are wrong. Whatever the case, the climatic data base should be checked to assure that the measured information is accurate. Similarly, rainfall runoff models, once calibrated, can be used to verify that the measured rainfall would likely produce the measured hydrograph. Because physical process models represent the rainfall runoff phenomenon very well, discrepencies between input and runoff output usually indicate data problems. A final example is use of water routing models to check the acceptability of automatic measuring devices with respect to time span between samples. Models provide insight into how much information is lost or gained between sample times.

If data are found to be erroneous or certain data were uncollectible or instruments failed, process models help simulate data to fill the gaps. For example, if a water level recorder failed to operate properly so the runoff event record was incomplete, a physical process model, if calibrated, could be used to fill in the missing data. This could be particularly important if corresponding water quality samples were taken during runoff. Conversely, if the runoff hydrograph is believed to be acceptable, it can be used to quantify the rainfall event that created it. Similarly, if solar radiation measurements are suspect, they may be replaced by model generated values.

Sometimes an existing data collection system is not spatially adequate so new sites may need to be added and older sites removed. Physical process models can aid in site selection. If a new site is to be added, physical process models, because of their ability to utilize spatially diverse data can be applied to pinpoint sites where additional collection of data is needed. An example would be the selection of a new stream gaging station. The physical process model can ascertain characteristics about timing and magnitude for different runoff events at several points on a stream channel. This would aid site selection by indicating those sites where hydrograph characteristics are dissimilar with those measured at other sites. For example, if a new station is to be placed between two existing stations, at what site will the measured values differ sufficiently from the other two stations to justify such an installation? This varies according to channel characteristics, water discharge, and overland flow contributions, but all of these effects can be incorporated and considered in the physical process model. Physical process models can be used to eliminate sampling sites following the same approach. An example of site elimination is when rain gages are removed or converted from one type to another. Process models are repeatedly operated with input information from an artificially decreasing number of gages until a number is reached that just adequately represents the rainfall related to the runoff from an area.

There are other uses of physical models for analyzing data collection systems that have not been detailed here. However, the basic concept is that these models can provide useful information about the spatial and temporal design of an adequate data collection system.

Proposed Systems

What physical models do for an existing system can be done for a proposed system. Often times, however, data used to develop model parameters are not available for a specific site. In such cases, data from similar nearby sites is used to help develop the necessary model parameters and input variables. Process models, once adjusted, can be used to delineate key sampling sites, determine frequency measurements, indicate important variables, and transfer data from sites with longer or more complete records to new collection sites.

Delineation of key sampling sites was previously discussed for existing systems. For proposed systems the task is similar except simulated measurements, such as hydrographs, are compared for all sites and hydrographs that are not simulated are compared to measured data. If the model is truly representative, the comparisons should establish an adequate site selection process. Model outputs also help determine the size of sampling equipment. For example, if the model indicates the 100 year flood is 500 cfs, the gaging site should be designed (if economically feasible) to accommodate such a discharge for a long term project.

Similarly, a sediment and water hydrograph could be simulated showing how often samples must be taken to truly represent the sampled variable.

Process models can be used to ascertain which variables are most important in modeling of watershed response. Use of sensitivity analyses helps determine those variables that must be accurately measured or collected because of their importance in modeling. For instance, small plots where runoff response is very rapid and directly linked to rainfall input, flow resistance factors are overwhelmed by those related to infiltration. However, in larger systems, flow resistance plays a more important role in terms of hydrograph shape. Sensitivity analyses cannot be conducted using only one set of input conditions but must consider large and small events, large and small watersheds, and a wide but realistic range of variables. Using this approach, an appreciation of tolerable measurement errors and recording accuracy of key variables can be gained.

Another application of process models is data transfer or synthesis between measured and unmeasured sites. An example of this is transfer of hydrographic information between adjacent watersheds in order to reconstruct past events. If one watershed had an adequate data base acceptable for simulation, then information on model parameters and inputs can be used for data synthesis in the nearby watershed. This type of transferability allows for a more realistic representation than do other methods based on contributing area because it accounts for soils, topographic, and vegetation effects.

Use of physical process models can provide valuable insights about the spatial and temporal variability of existing or proposed systems. Insights and quantitative information provided by the models allow intelligent evaluation and design of data collected systems.

Specific Model Application

General

A significant part of evaluation requires use of physical process models. Since the core of the primary model is rainfall-runoff simulation, this part of the simulation is selected for this example application. The processes that simulate the production of sediment and nonpoint source pollutants are heavily dependent on the results of rainfall-runoff. In order for the former to provide good results, the latter must provide realistic results.

This evaluation uses the multiple watershed rainfall-runoff simulation model (MULTWAT) to help analyze the data collection system at Four-Mile Creek. MULTWAT is used in three areas. First, a comparison is made of recorded and simulated hydrographs obtained from the available data to determine the adequacy of the data collected. Simulations are carried out on two sizes of watersheds within Four-Mile Creek, small and medium size subwatersheds with areas of 13.83 acres and 369.6 acres, respectively. Next, the model is tested for sensitivity to the various input parameters to determine the quality of the data being collected to reduce the errors in the simulation results and to help with the calibration of the model. Finally, the creation of hydrographs utilizing the model for storms of specified duration and return periods, which are not available from recorded data, are then used in the determination of the

spatial and temporal design of the system. These simulations are considered for the two previously mentioned watersheds within the total Four Mile Creek watershed. This analyses has been conducted with capable assistance from William Fullerton.

Data Needs

The physical process model MULTWAT, requires data which represent the phenomena being simulated. To entirely model the processes would be impractical due to the immense amount of data required and the resulting complexity of the model. Simplifying assumptions must be made to make the model manageable. Necessary assumptions were delineated and listed in Chapters 7 and 10. The physical processes modelled are interception, infiltration, overland flow and channel flow. Thus, with the model formulated, the data needs are known. For MULTWAT the data needs are given in Table 19.10.

Available Data and Gaps

Iowa State University has listed collected data at Four-Mile Creek for the period 1976-1978 in a report to the EPA. From this source and several supplemental sources, such as United States Geological Survey topographic maps and United States Weather Service records, most of the data needs listed in Table 19.10 are satisfied. However, several data gaps which exist are listed in Table 19.11.

Data gaps in some groups can be filled in by a calibration process. This is accomplished by varying the parameter in question until the simulated hydrographs differ from the recorded hydrographs as little as possible. The data gaps under soil characteristics are filled in by this method along with the gaps in resistance parameters. This procedure is used for the Four-Mile Creek watershed. However, the technique requires detailed recorded hydrographs which are available for the small and medium sized watersheds, but not for the entire watershed. Therefore, the parameters calibrated in the two smaller watersheds were extended to cover the whole watershed. The validity of this procedure cannot be tested due to the absence of the recorded hydrographs.

Model Results Using Collected Data

General

Before the model may be run, the watershed must be divided into subwatershed units, plane units and channel units. A schematic map of

Table 19.10 Input data for MULTWAT Program.

I. Geometry
   1. Number of subdivisions
   2. Slope, length, and area for each plane and subwatershed unit
   3. Slope and length for channel units
   4. Relationships of: a) wetted vs. cross-sectional area and b) top width vs. cross-sectional area for each of the channel units

II. Soil Characteristics
   1. Effective hydraulic conductivity
   2. Porosity
   3. Initial and final soil moisture
   4. Average suction head
   5. Temperature
   6. Rilling ratio

III. Vegetative Cover
   1. Density
      a. Percent canopy cover
      b. Percent ground cover
   2. Cover storage
      a. Canopy cover
      b. Ground cover

IV. Rainfall Data
   1. Rainfall hyetographs that are spatially consistant over each subdivision

V. Overland Flow and Channel Flow Data
   1. Resistance to flow for each channel unit
   2. Resistance to flow for each subwatershed channel

VI. Outflow Hydrograph Criteria
   1. Duration of hydrograph
   2. Time increment used for the calculation of the hydrograph

Table 19.11 Data gaps identified for MULTWAT.

I. Geometry
   1. No gaps, good quality

II. Soil Characteristics
   1. Effective hydraulic conductivity
   2. Porosity
   3. Initial and final soil moisture
   4. Average suction head

III. Vegetative Cover
   1. Data are present, but they are not given for the entire watershed and extrapolation methods must be utilized.

IV. Rainfall Data
   1. No gaps

V. Overland Flow and Channel Flow Data
   1. Resistance for channel units
   2. Resistance to flow for overland units

the Four-Mile Creek watershed is presented in Figure 19.19. The simplified geometry data are presented in Table 19.12.

Small Watershed Simulation

The small watershed selected was ISU site 1 with an area of 13.83 acres. The site was picked because of a recording raingage located near it, available cover data, and a recording discharge measurement device located on its outlet. Representative storms during 1977 and 1978 which produced measureable runoff were chosen for simulation. The storms, their respective rainfall volumes, and durations are listed below:

Date	Volume (inches)	Duration (minutes)
August 15, 1977	1.48	413
September, 17, 1977	1.10	232
April 17, 1978	2.56	1390
May 12, 1978	1.43	670
May 27, 1978	1.12	50
June 20, 1978	1.19	240

The soil parameters were adjusted in an attempt to match the recorded hydrographs. The results are listed in Table 19.13. Several of the events did not model well. These events have a minimal amount of runoff. It was very difficult to calibrate these events and still produce good results with the larger events. Since the larger events are more significant, they are used for parameter calibration.

Medium Watershed Simulation

The medium sized watershed selected was ISU site 8 with an area of 369.6 acres. It was chosen for the same reasons as site 1. In addition site 1 lies within its boundaries so that the parameters calibrate for site 1 may be utilized. No calibration was done on the simulations for site 8; the parameters from site 1 were directly applied. The same events of those for site 1 were also used. The results are presented in Table 19.14. The events that cannot be modelled well are those with little runoff. The amount of runoff being produced is smaller than the resolution capability of the model, but for larger events the results do show that the model can simulate the rainfall-runoff response adequately with the data available.

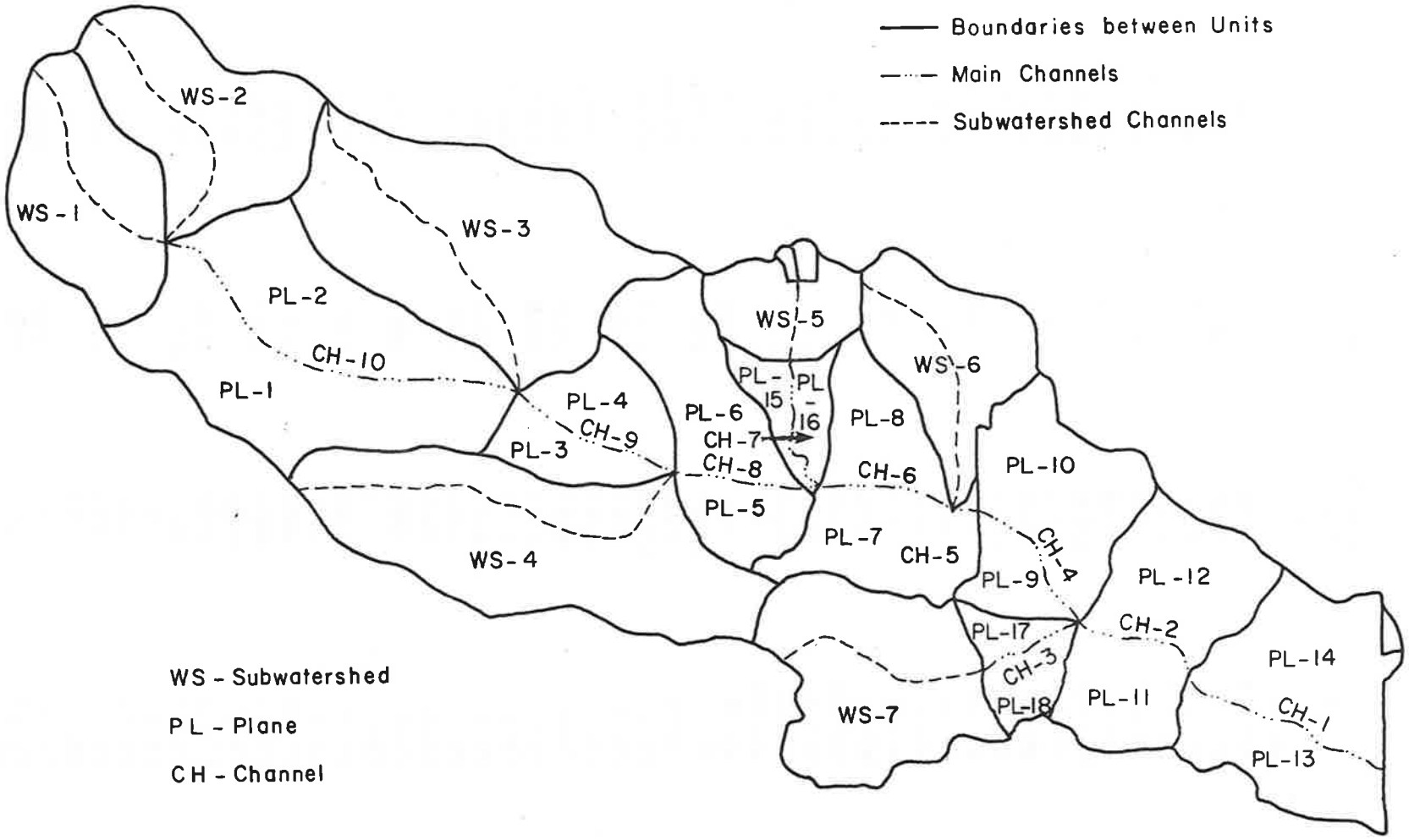

Figure 19.19 Four-Mile Creek map.

Table 19.12 Watershed geometry for Four-Mile Creek.

Unit	Length Feet	Width Feet	Slope	Area Acres
WS-1L	6200	3131	.0147	446
WS-1CH	6200		.00629	
WS-1R	6200	1890	.0123	269
WS-2L	7200	1768	.0162	292
WS-2CH	7200		.00542	
WS-2R	7200	2869	.0170	474
WS-3L	11000	1611	.0278	407
WS-3CH	11000		.00691	
WS-3R	11000	3508	.0253	886
WS-4L	13000	3553	.0266	1061
WS-4CH	13000		.00623	
WS-4R	13000	1388	.0277	414
WS-5L	3000	2645	.0330	182
WS-5CH	3000		.0183	
WS-5R	3000	2282	.0326	157
WS-6L	9000	1199	.0455	248
WS-6CH	9000		.0122	
WS-6R	9000	1781	.0440	368
WS-7L	7400	3184	.0355	541
WS-7CH	7400		.0115	
WS-7R	7400	1970	.0381	335
PL-1	12500	2961	.0322	850
CH-10	12500		.00264	
PL-2	12500	2294	.0239	658
PL-3	6267	1395	.0412	201
CH-9	6267		.00303	
PL-4	6267	1626	.0316	234
PL-5	4133	2056	.0367	195
CH-8	4133		.00218	
PL-6	4133	4970	.0242	472
PL-7	7066	2890	.0388	469
CH-6	7066		.00170	
PL-8	7066	1887	.0431	306
CH-5	1		1.0	
PL-9	5400	1335	.0573	166
CH-4	5400		.00148	
PL-10	5400	3677	.0488	456
PL-11	4800	2769	.0534	305
CH-2	4800		.00146	
PL-12	4800	3406	.0454	375
PL-13	7400	2253	.0653	383
CH-1	7400		.00135	
PL-14	7400	4523	.0495	768
PL-15	2933	1318	.0557	89
CH-7	2933		.0443	
PL-16	2933	948	.0400	64
PL-17	3467	1034	.0652	82
CH-3	3467		.0433	
PL-18	3467	1580	.0488	126

Table 19.12 Continued.

Unit	Length Feet	Width Feet	Slope	Area Acre
ISU-Site 1L	574.50	494.21	.0453	6.52
ISU-Site 1CH	574.50		.0174	
ISU-Site 1R	574.50	554.50	.0456	7.31

Note: 1) Channel 5 is a "Dummy Unit" provided so that the discharge from WS-6 is added in before the hydrograph is established at this point.
2) WS-5 is also called "ISU-Site 8".

Abbreviations:
PL - Plane
CH - Channel
WS - Subwatershed
L - Left
R - Right

Table 19.13 Comparison of simulated and recorded hydrographs for the small watershed.

Date	Peak Discharge (cfs)		Volume (Acre Ft.)		Time to Peak (Min.)	
	Recorded	Sim.	Recorded	Sim.	Recorded	Sim.
8/15/77	10.1	10.1	.22	.36	20:28	22:30
9/17/77	.34	.39	.01	.09	20:06	20:24
4/17/78	.31	1.4	.06	.10	23:15	23:20
5/12/78	Negligible recorded runoff - no simulated runoff					
5/27/78	2.01	7.06	.05	.25	16:49	16:48
6/20/78	2.15	1.67	.16	.14	9:12	1:14

Table 19.14 Comparison of simulated and recorded hydrographs for the medium sized watershed.

Date	Peak Discharge (cfs)		Volume (Acre Ft.)		Time to Peak (Min.)	
	Recorded	Sim.	Recorded	Sim.	Recorded	Sim.
8/15/77	51.40	100.70	4.12	8.43	22:38	22:45
9/17/77	23.60	8.40	1.42	2.10	20:32	22:33
4/17/78	14.50	1.56	5.61	1.28	23:24	23:29
5/12/78	0.93	No runoff	0.30	No runoff	4:07	No runoff
5/27/78	108.40	95.28	3.32	5.94	16:55	16:59
6/20/78	18.84	17.23	2.25	3.21	1:55	2:24

Use of the Model in Data Synthesis and Evaluation

Time of Concentration Determination

The time of concentration is an important factor when designing a gaging system since it helps determine at what intervals readings should be taken by providing insight into the watershed's response to a given rainfall. Rainfalls with specified return periods are calculated using a regression method developed from information in United States Weather Service Technical Paper No. 40. The equation and results are provided in Table 19.15.

In order to reach a time of concentration, it is expedient to assume a constant rainfall excess. Since interest is in time it takes for the water to travel from the furthest point of the watershed to the outlet, the infiltration and interception for the time of concentration runs are set at zero. To account for infiltration and interception the actual rainfall rate is multiplied by a factor ranging from 0.1 to 0.4 to account for losses. The 0.1 factor is used for the one year storm and the 0.4 factor is used for the 100 year storm. The factors for storms with return periods between these values are calculated by linearly interpolating between the one and 100 year volumes according to the storms actual volume. For example, if the one year actual storm has a volume of 1 inch and the 100 year storm has a volume of 2 inches, a 50 year storm with a rainfall volume of 1.5 inches will have a factor of 0.25 to determine its excess. The results of the runs for ISU site 1 and site 8 are presented in Table 19.16. Considering the entire watershed, the rainfall intensities are such that the time of concentration is never reached for any of the durations or return periods.

The time of concentration for site 1 varies between 16 and 112 minutes and for site 8 between 28 and 200 minutes depending on the storm's return period. An estimate of the time it takes the watershed to completely respond to a rainfall input is important. Depending on the number of intermediate points desired between the start of rainfall and the time of concentration an idea of the time interval and when discharge readings that should be taken are provided.

Table 19.15 Four-Mile Creek watershed synthetic rainfalls using the regression method developed from "TP-40".

Duration (Hour)	Return Period (years)						
	1	2	5	10	25	50	100
.5*	1.01	1.22	1.50	1.72	2.00	2.22	2.43
1.0	1.29	1.57	1.94	2.22	2.59	2.87	3.15
1.5	1.45	1.77	2.19	2.51	2.93	3.25	3.57
2.0	1.57	1.91	2.37	2.72	3.17	3.52	3.86
2.5	1.66	2.02	2.51	2.88	3.36	3.73	4.09
3.0	1.73	2.12	2.62	3.01	3.51	3.90	4.28
3.5	1.79	2.19	2.72	3.12	3.64	4.04	4.44
4.0	1.85	2.26	2.80	3.21	3.76	4.17	4.58
4.5	1.90	2.32	2.88	3.30	3.86	4.28	4.70
5.0	1.94	2.37	2.94	3.37	3.94	4.38	4.81
6.0	2.01	2.46	3.06	3.50	4.10	4.55	5.00
9.0	2.18	2.66	3.31	3.80	4.44	4.93	5.41
12.0	2.29	2.81	3.49	4.00	4.68	5.20	5.71
24.0	2.58	3.15	3.92	4.50	5.27	5.85	6.43

*Rainfall in inches

$$PPT = 1.2870 + .4053\ (PnY) + (.4040 + .1360\ (PnY))\ PnT$$

PPT = precipitation
Y = storm duration in hours
T = return period in years

Table 19.16 Time of concentration results, Four-Mile Creek.

	Return Period (yr)	Duration (min)	Rainfall Intensity (in/hr)	Time of Concentration (min)
Site 1				
	100	30	1.94	16
	50	30	1.58	18
	25	30	1.24	20
	20	30	0.86	24
	5	30	0.61	30
	5	60	0.40	39
	2	60	0.23	57
	1	120	0.079	112
Site 8				
	100	30	1.94	23
	50	60	1.02	43
	25	60	0.80	51
	10	60	0.56	60
	10	120	0.341	79
	5	120	0.243	96
	2	120	0.138	120
	2	180	0.103	162
	1	180	0.058	200

Sensitivity Analysis

A sensitivity analysis is necessary for two reasons. The analysis is important in determining the quality of the various data needed in order to keep errors within acceptable limits. It is also a useful aid in the calibration process in that it gives the user an idea regarding how the simulated hydrographs respond to changes in the parameters being calibrated.

The sensitivity analysis was carried out on a the medium sized watershed (ISU site 8) for two storms. The storms occurred on May 27, 1978 and August 15, 1977. These storms are used since they represent two distinct types of rainfalls that occur at the site. The first being of short duration, high intensity and the second of long duration, low intensity.

In the analysis, the parameters required as input to the model are varied one at a time at various percentages of their original values while leaving all other parameters constant. The results are graphed in Figures 19.20 and 19.21 for peak flows only. Volume and duration are similarly affected. The results show that the most sensitive parameters are the soil characteristics and the overland flow resistance which is governed by the percentage of ground cover and the resistance factor. This could be significant since these two areas have little data collected. However, the calibration process can fill in these gaps and still produce reasonable simulations as was noted earlier.

Correlation in Simulated Runs

To help assess the required spatial and temporal design for the water discharge gaging stations in the entire watershed, correlations to determine how the discharge varies in space and time were determined. The available discharge records along the main channel are such that they are inadequate in providing the data necessary to make such correlations on a basis any finer than hourly. Since most of the events are less than a day in length, this information is important. Thus, in order to provide information for such correlations, the runoff results from the 100 year storm for the entire watershed are substituted for actual data. These hydrographs are simulated for the downstream end of the watershed (channel 1) and a point further upstream (channel 5). These points correspond to the USGS gaging station at Traer and Lincoln, respectively. The hydrographs are presented in Figures 19.22 to 19.25.

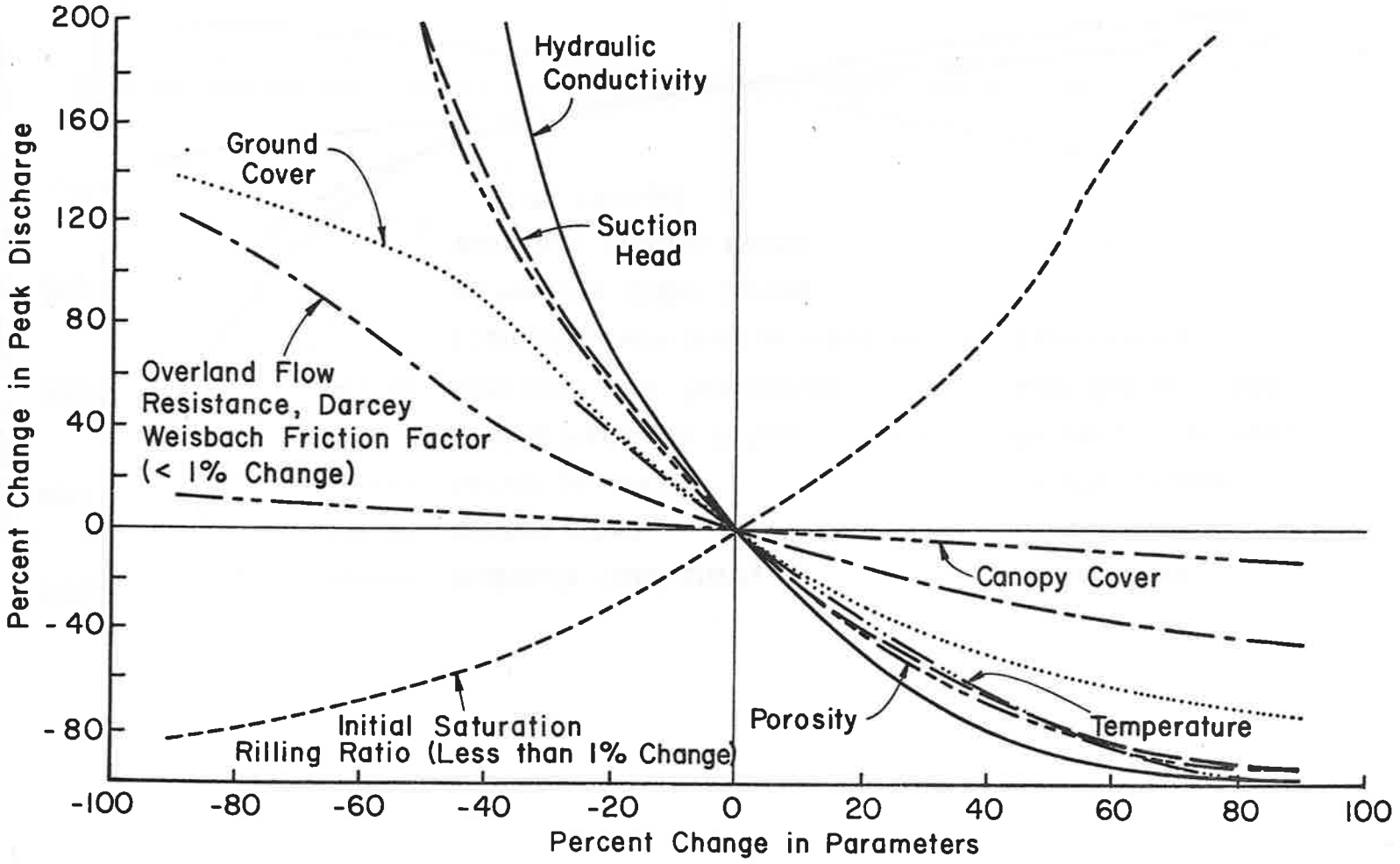

Figure 19.20 Peak discharge sensitivity analysis for watershed ISU8, storm of May 27, 1978.

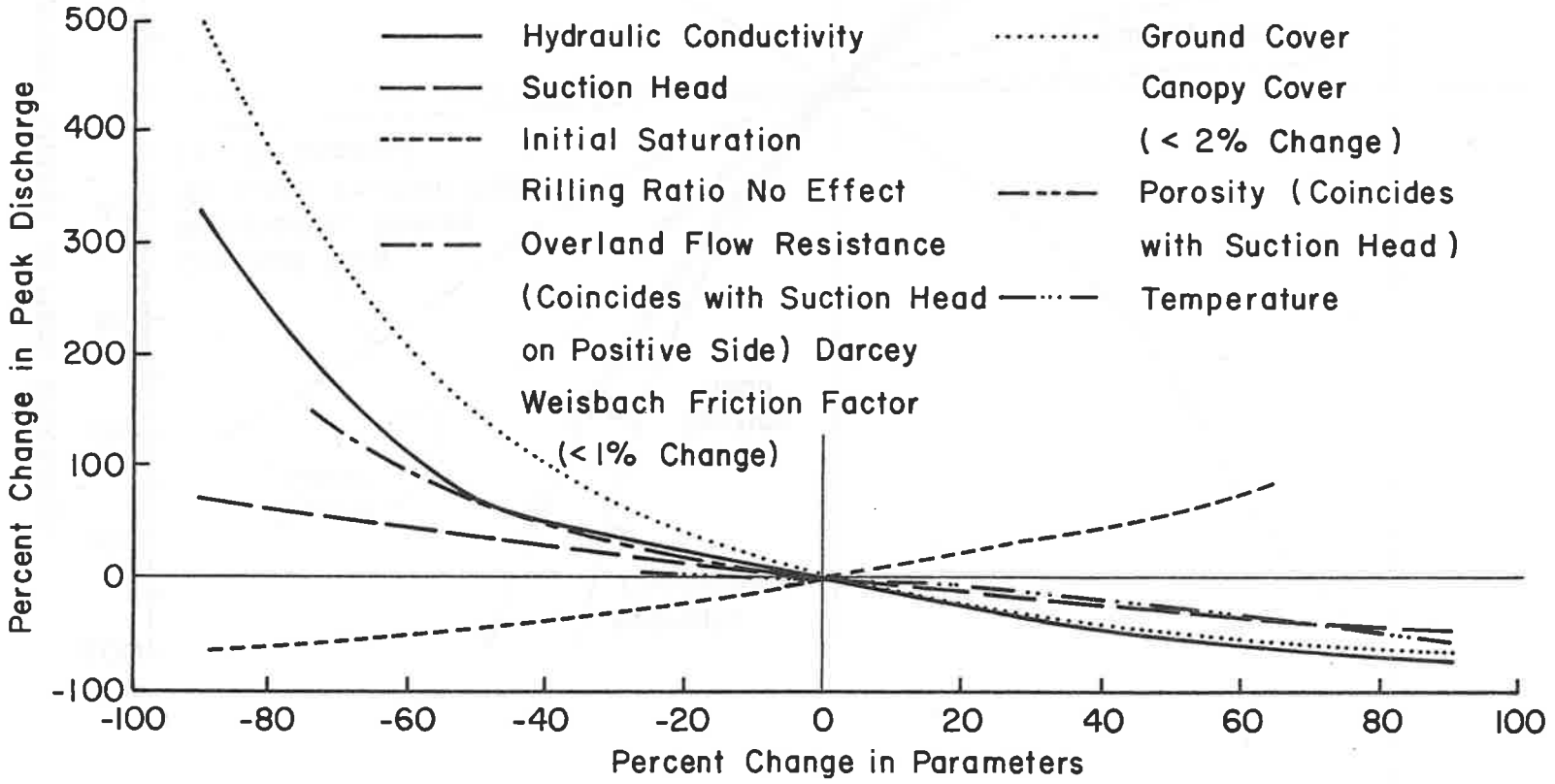

Figure 19.21 Peak discharge sensitivity analysis for watershed ISU8, storm of August 15, 1977.

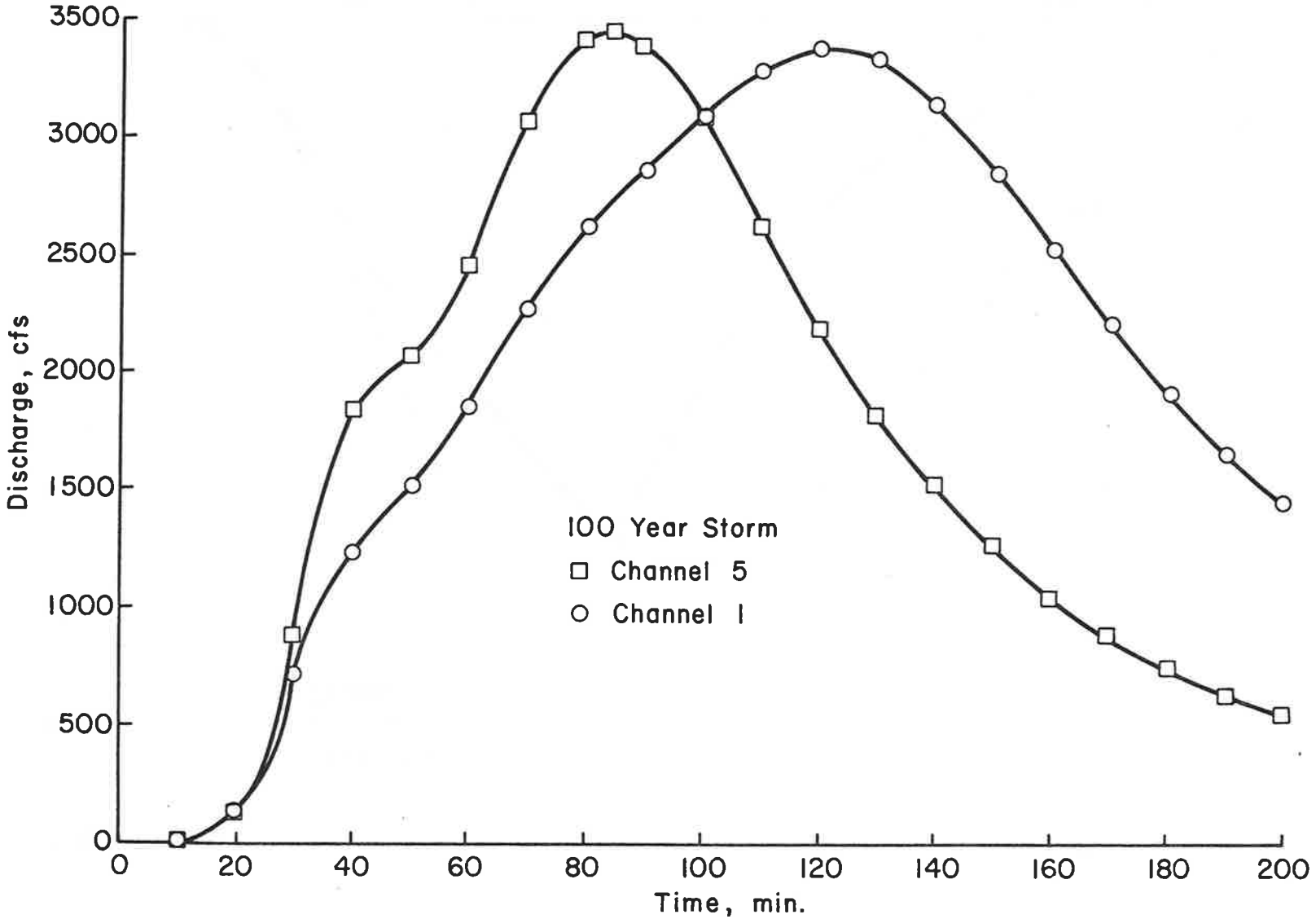

Figure 19.22 Simulated hydrographs for 30 minute, 100 year storm. (Time is real time)

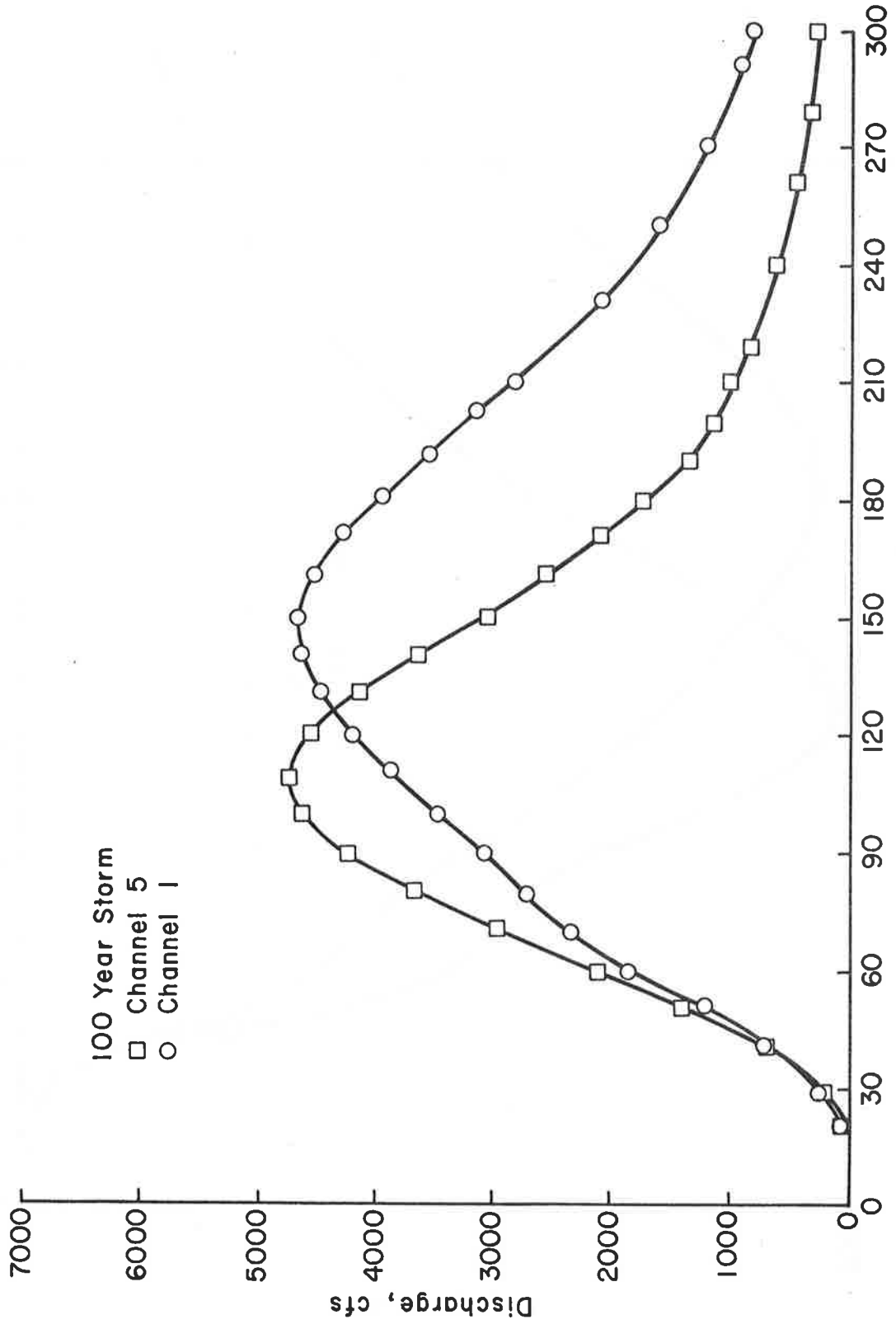

Figure 19.23 Simulated hydrographs for 1 hour, 100 year storm.
(Time is real time)

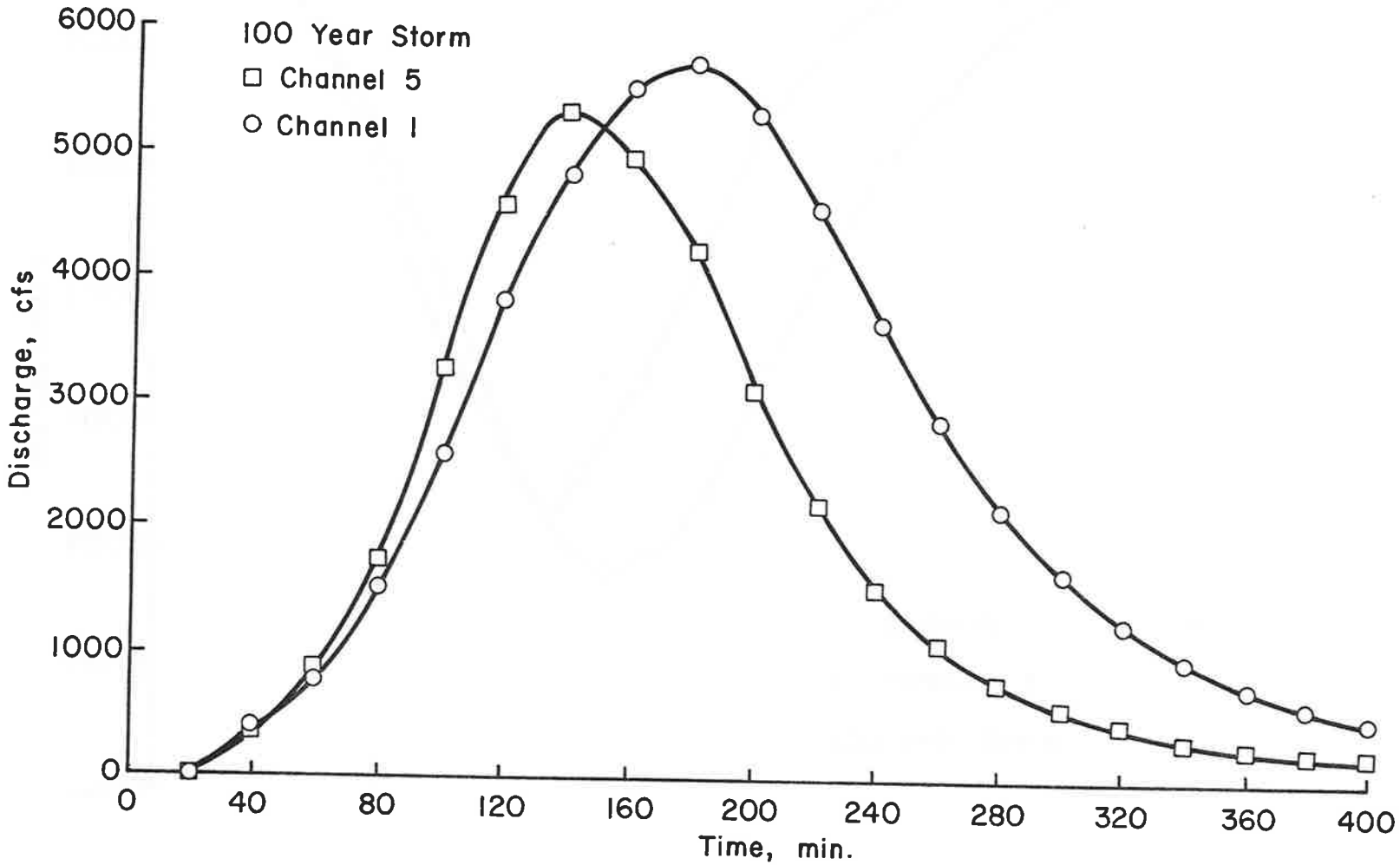

Figure 19.24 Simulated hydrographs for 2 hour, 100 year storm. (Time is real time)

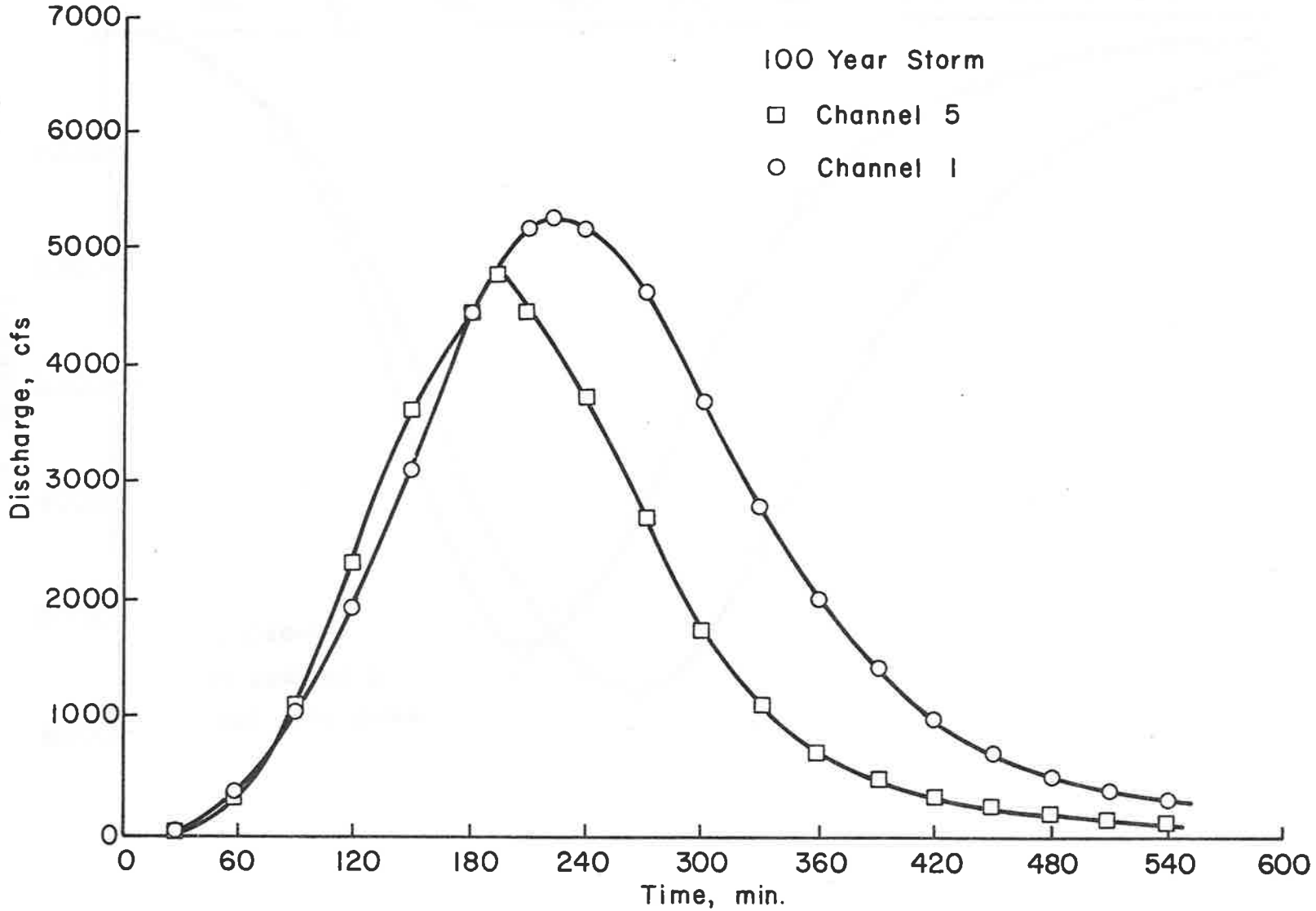

Figure 19.25 Simulated hydrographs for 3 hour, 100 year storm.
(Time is real time)

An autocorrelation is made for each hydrograph at both stations. The time between discharge samples is varied to determine how the discharge at different time intervals is correlated. This is done to help assess the time increment that would be most useful for taking readings. For example, if readings are taken at highly correlated time intervals, little information is gained by each and excessive data is taken. However, if the readings are recorded at intervals that have very little correlation, the data is too sparse and of little use. The results of the autocorrelations are given in Figures 19.26 and 19.27.

A cross-correlation was made between gaging stations for each storm. The length of time between discharge samples at channel 1 and channel 2 is varied. This correlation helps with the spatial design. The spatial design can be evaluated by the extent of correlation existing between the stations for the various time lags. If the correlation is always high or if it is always low the stations are not spaced properly for the same reasons given in the preceding paragraph. The results are shown in Figure 19.28.

As stated previously there should be an upper and lower "correlation land" where sample timing and station spacing occurs. The upper correlation may be about 0.8. The lower correlation can be estimated using statistical techniques. Using a "t" test the value of correlation below which there is no significance can be calculated. At the 95% level of significance the limiting values of the correlation coefficients range between 0.44 for the 30 minute storm with ten time lags and 0.31 for the three hour storm with no time lag. To maintain correlation in the readings they should be taken at some increment that provides a correlation greater than 0.44. The 30 minute storm provides a good basis for design of the system with since this type of short duration high intensity storm causes high discharges which in turn result in large sediment and nonpoint pollutant yield. This will result in extra data being taken for longer storms, but it would not be wise to design the system for longer storms and then collect poor data for short storms. The system should be designed with more correlation than the lower limit calculated so that bad data can be identified using nearby stations or data gaps filled in a station malfunctions.

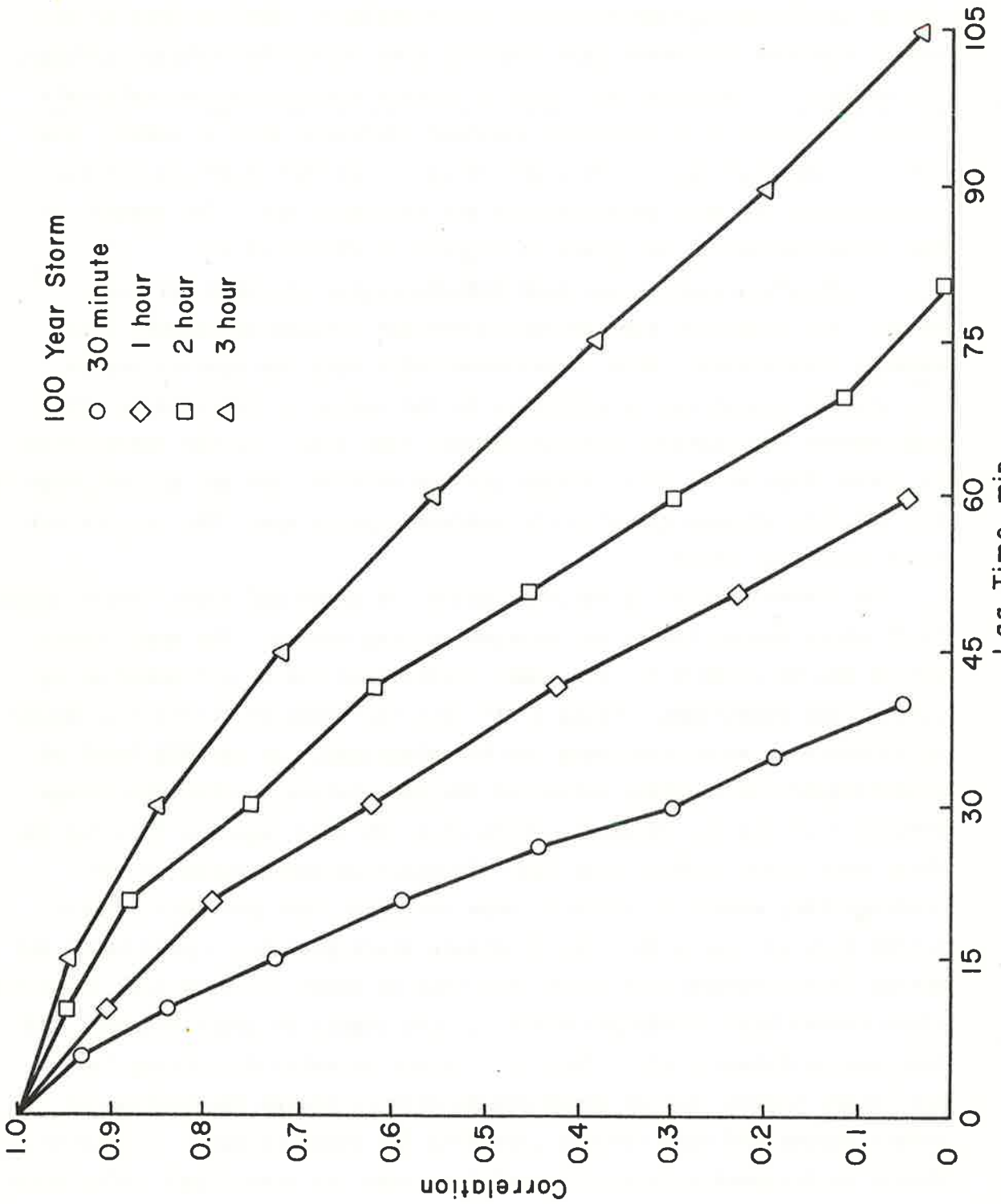

Figure 19.26 Autocorrelation for channel 5.

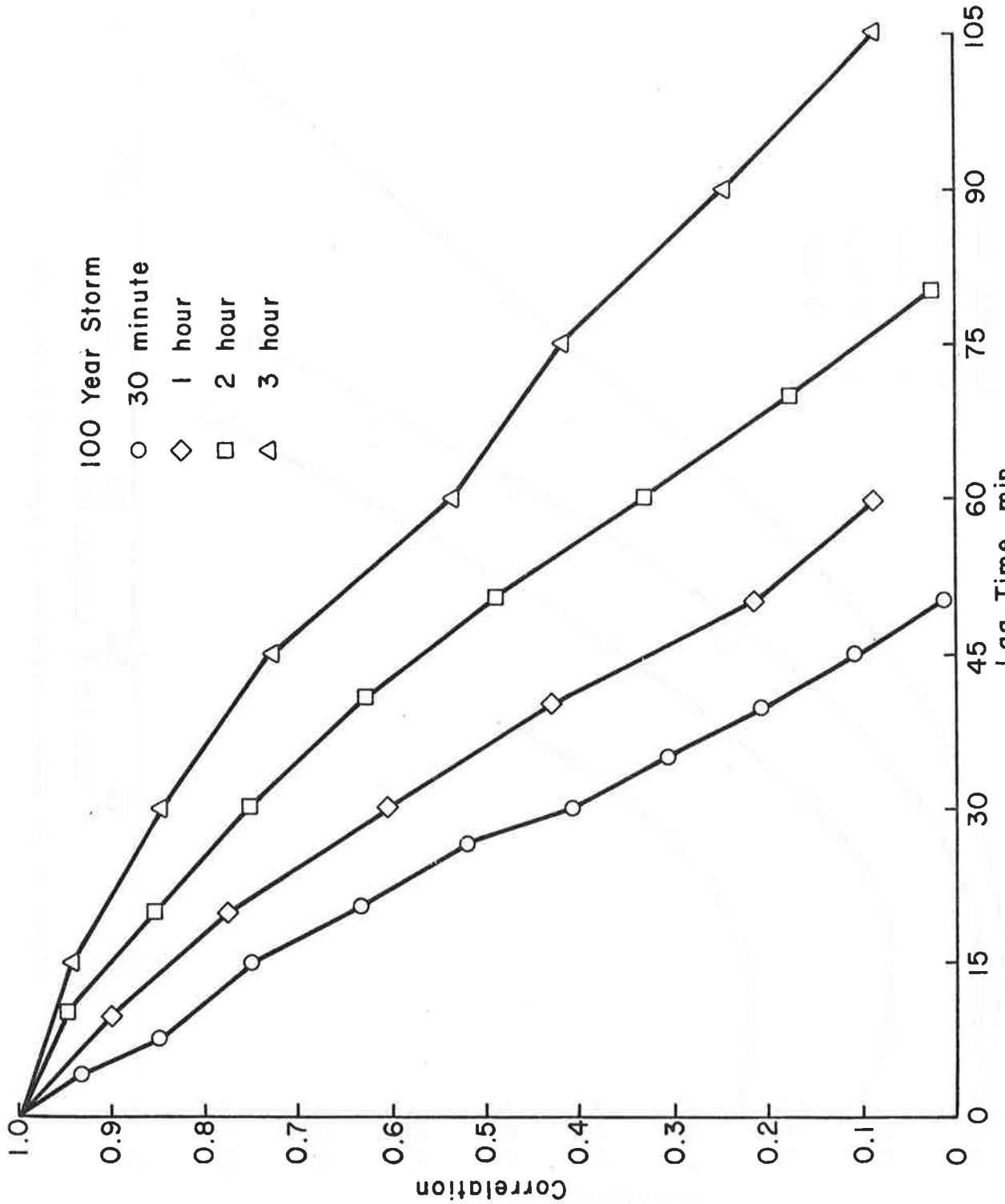

Figure 19.27 Autocorrelation for channel 1.

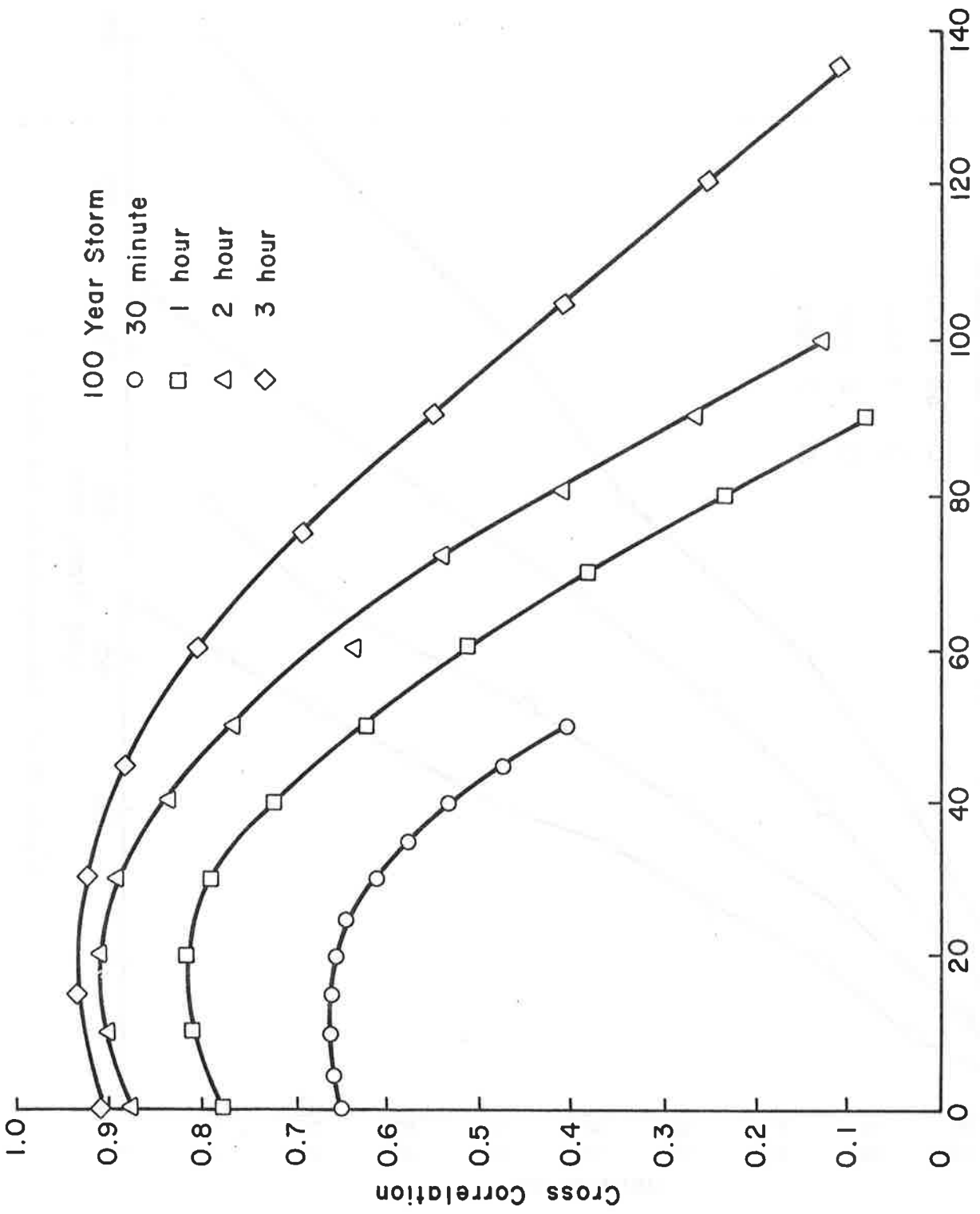

Figure 19.28 Cross-correlation of simulated hydrographs.

Summary

Use of physical process models can aid in the design and analysis of data collection systems. Process models can be used as a basis for identifying data gaps and checking data quality. They can also be used to simulate data that can be utilized in correlation analyses and design modification. Use of models in this fashion allows a more efficient, better conceived collection network.

19.6 SUMMARY

A primary goal of physical process modeling is to provide methodologies for analyzing the response of watersheds to proposed or anticipated land use modifications. In this chapter, three different model applications were described. In the first application a rainfall-runoff model for a small watershed that could be represented by two planes and a channel was presented. This application showed the capability of that model to estimate changes resulting from a variety of land use modifications. The second example demonstrated the use of a multiple watershed model for estimating a design peak flow from an arid watershed. This approach was compared to another methodology to show that the second methodology was overestimating the peaks flow and incorrectly displaying the hydrograph shape. These discrepencies occurred because the second methodology was fully considering watershed geometry and flow characteristics. The third application was a generalized planning model that was used to estimate sediment yields from a large watershed of complex geometry. This model is used for a general estimate of watershed response because it considers overland flow units of large dimensions (smaller dimensions could be used but with increases in cost). Large units are used because of the resolution of data used as input. Even with the coarseness in the watershed segmentation, the model provides realistic values for different alternatives that can be compared. As an interesting addition, use of physical process models for evaluating data collection networks on watersheds was presented. In this example, models were shown to be useful in filling data gaps and providing information that can be incorporated into design and evaluation decisions.

These examples demonstrate the utility of physical process models. They can be used for relative comparisons of land use alternatives, in checking other methodologies, or for evaluating proposed or existing data collection systems.

19.7 REFERENCES

Chow, V. T., Open Channel Hydraulics, McGraw-Hill Book Company, New York, 1959.

Simons, D. B. and Sentürk, F., Sediment Transport Technology, Water Resources Publication, Fort Collins, Colorado, 1977.

Simons, D. B., Li, R. M., Shiao, L. Y., and Eggert, K. G., "Storm Water and Sediment Runoff Simulation for Upland Watersheds using Analytical Routing Technique," Volume I--Water Routing and Yield, Colorado State University Report CER77-78DBS-RML-LYS-DGE16, prepared for USDA Forest Service, Rocky Mountain Forest and Range Experiment Station, Flagstaff, Arizona, April 1977.

Simons, D. B., Li, R. M., and Spronk, B. E., "Storm Water and Sediment Runoff Simulation for a System of Multiple Watersheds," Vol. I, Water Routing and Yield, Draft report prepared for USDA Forest Service, Rocky Mountain Forest and Range Experiment Station, April 1978.

Yevjevich, V., "Determinism and Stochasticity in Hydrology," J. Hydrology, 22, 1974, pp. 252-238.

U.S. Bureau of Reclamation, "Design of Small Dams," 1974.

CHAPTER 20

LARGE RIVER BASIN ANALYSIS--YAZOO RIVER SEDIMENTATION STUDY

by

Daryl B. Simons, Associate Dean for Engineering Research and Professor of Civil Engineering, Colorado State University, Fort Collins, Colorado

Ruh-Ming Li, Associate Professor of Civil Engineering, Colorado State University, Fort Collins, Colorado

20.1 INTRODUCTION

As presented in Chapters 2 through 19, there are many analytical tools available for use in predicting the response of a watershed and river system. One of the shortcomings of most analytical systems developed to date for analyzing the watershed and river system is that they are too limited in scope. Most watersheds that are subject to planning and legal requirements for water resources management, flood control, and environmental quality are quite large and often encompass complete river basins or sub-basins. Man's activities usually have short- and long-term effects on the environment, and the short-term projects may have prolonged effects. An integral analytical system is required to deal with a large river basin and to predict the response for both short- and long-terms. This chapter illustrates in detail the analysis of a large basin, the Yazoo River Basin, Mississippi for the U.S. Army Corps of Engineers.

The Yazoo River Basin includes approximately 13,400 square miles in the northwest portion of Mississippi, U.S.A. About 6,600 square miles are in the alluvial valley of the Mississippi River, while the remaining 6,800 square miles are hill watersheds. According to overflow characteristics, the Yazoo Basin is divided into backwater and headwater areas. The Yazoo headwater area is the portion above Yazoo City comprising about 2,300 square miles of alluvial lands and 6,600 square miles of rolling and rugged hill watersheds (Figure 20.1). The Upper Yazoo Project is a complex flood control system located upstream of Yazoo City. The project provides for approximately 178 miles of channel enlargement of the main river, about 203 miles of levees, and 109 floodgate structures.

The Yazoo Basin Sedimentation Study involves a system analysis of the main channel and 31 tributaries from which water and sediment is routed through the main channel. The total cost of the proposed flood control project is about $169,000,000 and the benefit cost ratio is 1.8. Initial engineering for the project by the Vicksburg District revealed that over $2,000,000 would be required for annual operation and maintenance as a project (most of which would be for removal of sediment deposition). The primary purpose of this study is to provide additional information regarding anticipated sediment depositional rates and to develop alternate

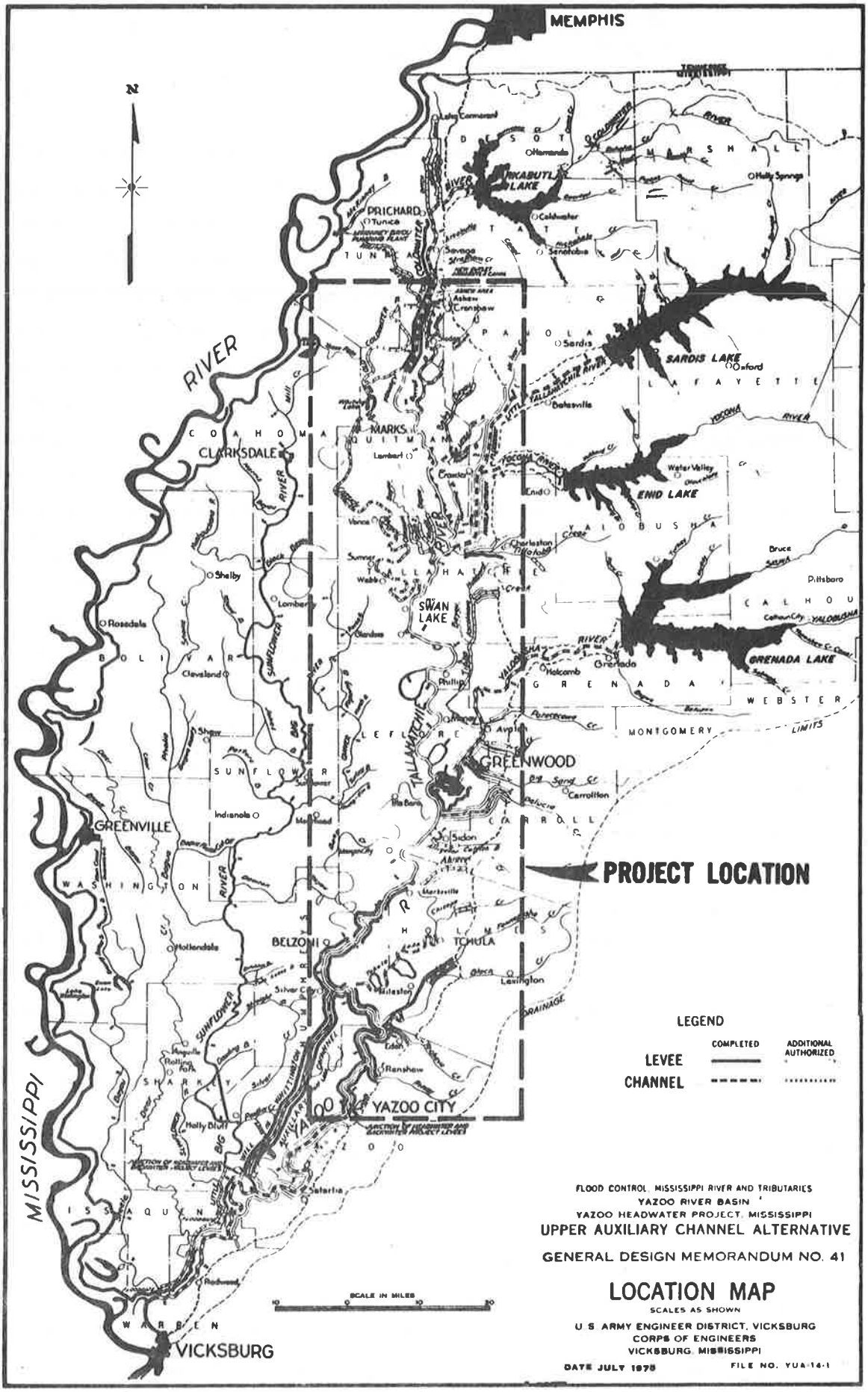

Figure 20.1 Project location map.

channel designs, tributary controls, or stabilization required to reduce anticipated deposition and thereby reduce operation and maintenance costs for the project. This analysis provided a method for evaluating the Upper Yazoo Project system and the various design alternatives outlined by the U.S. Army Corps of Engineers.

For analyzing a complicated system like the Yazoo River Basin, different levels of resolution in the analysis are needed to achieve different objectives. Two mathematical models were developed for different levels of resolutions. One is for simulating the flood and sediment movement in short time resolutions (less than a day) which involves the use of an unsteady flow model (see Chapters 8 and 11). This model is particularly useful in predicting flood movement in the Yazoo River system. Another model simulates the sediment movement only and assumes the water hydrographs are known. This simplified model involves use of the discharge synthesized technique and the known discharge uncoupled model for sediment routing (see Chapter 12). This model can be utilized to evaluate the response of the system using a larger time increment such as one or two days, or even longer. In this study a seven-day time increment for simulation was used since this is the approximate time required for water to travel through the system being analyzed. The closeness of weekly and daily flow statistics further validate the selection of a seven-day time increment for simulation. The primary objective of this study was to identify and analyze the sedimentation problems. Consequently, the known discharge model was used extensively in the analysis.

After calibration, the model was utilized to evaluate design alternatives, to identify the extent of sediment problems in the main stem and principal tributaries, and to suggest possible remedies. These alternative study runs were conducted by routing water and sediment through the tributaries and the Yazoo River main stem for a selected long-term hydrograph utilizing the various alternative plans. For evaluating the long-term effect a 50-year hydrograph was utilized. A total of 15 alternative study runs were made. The alternative study runs considered the natural conditions of the system, the recommended channel dimensions, the effects of land use, the effects of channelization, the effects of construction scheduling, various plans for reducing sediment supply

from the tributaries, different dredging schedules and proposed navigation channels.

20.2 THE PROBLEMS FOR ANALYSIS

Design Alternative Plans

According to General Design Memorandum No. 41, Upper Auxiliary Channel Alternative, Yazoo River Basin Headwater Project by the U.S. Army Corps of Engineers, Vicksburg District, the following structural alternatives were considered:

Plan A (Cross Country)

Major features of this plan include an overland auxiliary channel and channel modifications on the Yazoo-Tallahatchie-Coldwater River system. This plan considers channel modification or enlargement on 177.7 miles of river, 72.3 miles of new channel and 233 miles of levees.

Channel size on the main stem varies as follows: Yazoo City to Greenwood, 150-foot bottom; Greenwood to Swan Lake, 110-foot bottom; Swan Lake to the mouth of the P-Q Floodway, 100-foot bottom; from the mouth of the P-Q to the mouth of the Old Little Tallahatchie, 85-foot bottom; and from the Old Little Tallahatchie to the mouth of the Old Coldwater, a 50-foot bottom. On the auxiliary channel, bottom width is 100 feet from Swan Lake to Greenwood where it increases to 160 feet, and remains the same to its confluence with the Yazoo at Tchula Lake.

Plan B (Big Channel)

This plan omits the overland auxiliary channel and provides the same flood reduction as Plan A. Flood protection is achieved through increasing channel capacity by enlarging the Yazoo-Tallahatchie-Coldwater River system. This plan includes 177.7 miles of channel enlargement, 1.3 miles of new channel, 142 miles of levees, and a structure to allow the controlled diversion of some flows through Tchula Lake.

Channel size on the main stem differs from Plan A due to the 150-foot bottom from Yazoo City to Tchula Lake, a 310-foot bottom from Tchula Lake to Greenwood, and a 210-foot bottom from Greenwood to Swan Lake. Above Swan Lake, channel dimensions are similar to Plan A.

Plan C (Small Channel)

This plan follows the same channel alignment as Plan B but utilizes a smaller channel and higher levees. It includes 177.7 miles of channel

enlargement, 1.3 miles of new channel, 202.8 miles of levees, 0.2 mile of floodwall, and a diversion of some flows through Tchula Lake. Channel size is the same as Plan A except there is no auxiliary channel.

Plan D (Low Levee)

This alternative utilizes the same channel alignment as Plans B and C but would allow overtopping of the levees along the main stem by floods of greater than a 10-year frequency. The physical features include 177.7 miles of channel enlargement, 1.3 miles of new channel, 156 miles of levees, and diversion of flows through Tchula Lake. Channel size in Plan D is identical to Plan C.

Plan E (Recommended)

The recommended plan is a combination of features of Plans B and C. It includes a larger channel north of Greenwood than Plan C. Physical features include 177.7 miles of channel enlargement, 1.3 miles of new channel, 202.8 miles of levees, 0.2 mile of floodwall, and diversion of flows through Tchula Lake. Channel bottom width is 150 feet between Yazoo City and Greenwood, 130 feet between Greenwood to the mouth of the P-Q Floodway, 100 feet from the mouth of the P-Q Floodway to the mouth of the Little Tallahatchie River, and 75 feet from the Old Little Tallahatchie to the mouth of the Old Coldwater River.

Plan E was recommended after evaluation of different alternatives with respect to environmental impacts, social aspects, economic constraints, engineering problems, and trade-off analysis. The layout is shown in Figure 20.2. The potential sedimentation problems and possible remedies associated with this alternative plan were analyzed in this study.

Other Structural Alternatives

Several other structural alternatives that were considered include: the diversion of Coldwater River flows to the Mississippi River, various alignments for a cross-country channel, a Quiver River diversion, other combinations of auxiliary channel and river enlargement, additional reservoirs, and a floodway alternative. These alternatives were eliminated by the U.S. Army Corps of Engineers (Design Memorandum No. 41) due to excessive costs or inability to provide the necessary channel capacity to accommodate reservoir emptying without channel modifications.

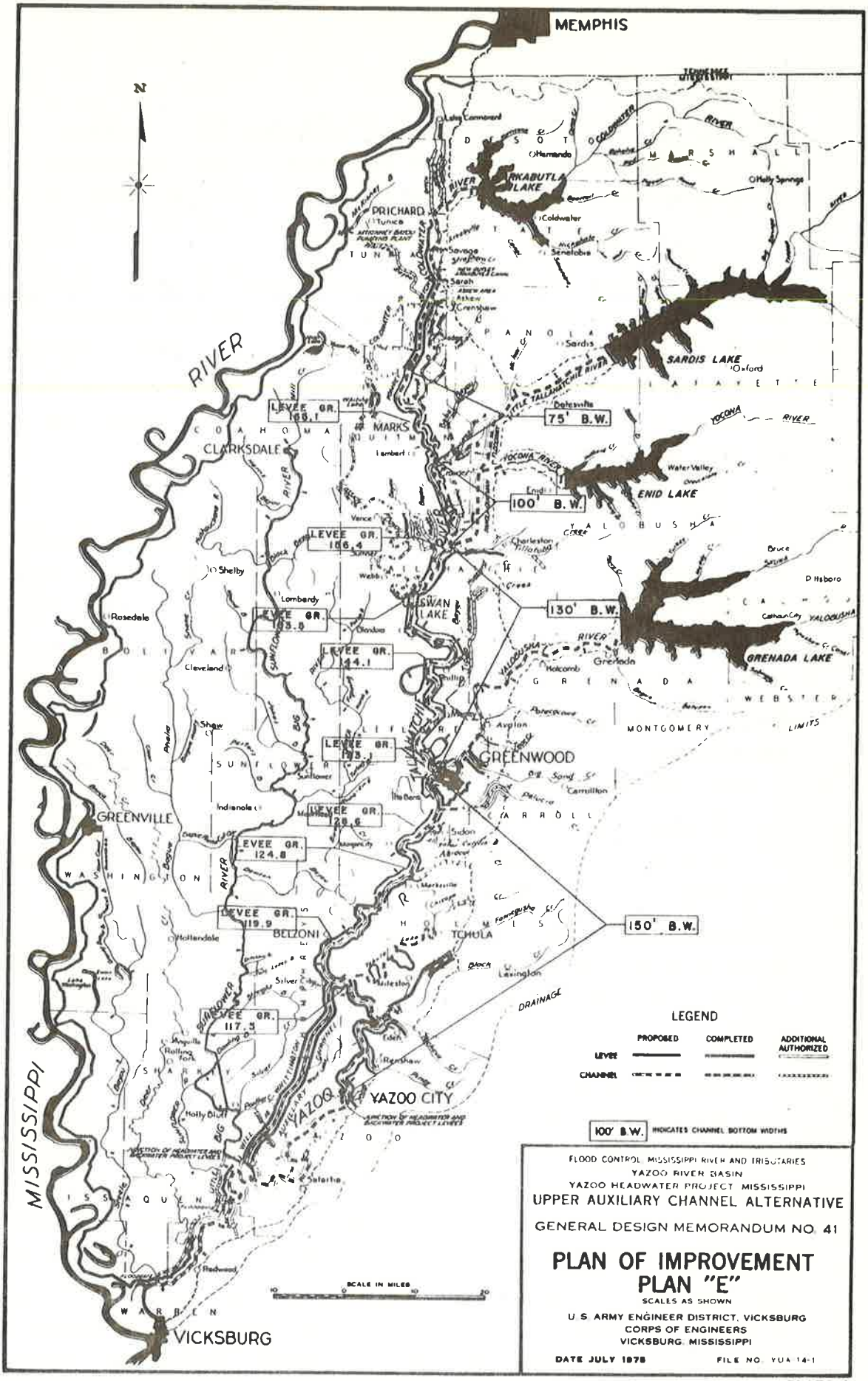

Figure 20.2 Layout of Plan E.

Alternative Study Runs

A large portion of the Yazoo River Basin delta will receive substantial flood control benefits from construction of the proposed project as a result of the increased flow-carrying capacity of the main stem river system. Major problems currently existing in the Yazoo Basin include not only flooding but deposition and erosion of sediment that affects many of the tributary streams and the main stem river system.

During the design of the proposed project, emphasis was placed on creating a channel system that would minimize effects of the project work on sedimentation problems in the Yazoo Basin. It is recognized the proposed work will not alleviate all sedimentation problems in the basin streams, and in some cases existing problems could be increased. It is anticipated that developing the channel as proposed will lower the flowline and may cause additional sediment flow to the main channel from the tributary system. Consequently, a plan should be studied that utilizes control structures on the tributaries just upstream of the point where major tributaries enter the Yazoo main stem. These structures would prevent head cutting and the discharge of excess sediments into the main channel.

Another alternative considers utilizing other techniques to further minimize sediment contributed from the watershed to the main channel. For example, control structures such as check dams could be designed, spaced and located on major tributaries to further reduce sediment inflow to the main channel. Also, an analysis could be executed to determine the optimum design utilizing control structures and dredging to minimize maintenance problems in the main channel after it has been modified to meet the requirements dictated by flood control needs and navigation requirements.

In order to identify the extent of sedimentation problems in the main stem and principal tributaries, and the possible remedies, 15 alternative study runs were made. These alternative study runs were conducted by routing water and sediment through the tributaries and the Yazoo River main stem for a selected hydrograph utilizing the various alternative plans. The alternative study runs follow.

Run No. 1

Simulation run utilizing a 50-year synthetic hydrograph (11 years of recorded data and 39 years of generated data) with natural (existing) river conditions. Greenwood Cutoff was assumed closed for flows less than 25,000 cfs and open for flows greater than 25,000 cfs. It was further assumed that Abiaca Creek would only deliver about 20 percent of the sediment inflow at the hill line to the Yazoo River.

Run No. 2

Simulation run utilizing a 50-year synthetic hydrograph with Plan E conditions and Greenwood Cutoff operated as in Run No. 1. It was assumed that Abiaca Creek would be a leveed floodway that would likely deliver most of the sediment contributed at the hill line to the Yazoo River.

Run No. 3

Simulation run utilizing a 50-year synthetic hydrograph with Plan E conditions, and the Greenwood channel operated as in Run No. 1. The sediment contributing to the main stem from selected tributaries was reduced to near that observed considering the existing conditions identified in Run No. 1.

Run No. 4

Simulation run the same as Run No. 2 but with a reduction of sediment load for the tributaries determined after results were obtained from Run No. 3. This determined whether an additional reduction in sediment load to the main stem could be justifiable in lieu of maintenance dredging.

Run No. 5

Simulation run the same as Run No. 2 except all peak flows were assumed increased 15 percent on both the tributaries and the main stem. This determined the effect of channelization on the tributaries and the main channel.

Run No. 6

Simulation run the same as Run No. 5 except peak flows were increased on the tributaries by an additional 15 percent; however, flows on the main stem were determined by the model. This evaluated the effect of future land use changes on the system.

Run No. 7

Simulation run the same as Run No. 2 except it was assumed the river was dredged to the original Plan E channel configuration after each year. This run determined the practicality of annual dredging. Additionally, the amount of deposition with annual dredging was compared with allowing sediment to accumulate during the 50-year life of the project.

Run No. 8

Simulation run of a 50-year synthetic hydrograph with completion of the construction schedule for the Upper Yazoo Project. The purpose of the run was to identify problems that could occur in the future as construction continues and dredging proceeds upstream.

Run No. 9

Simulation run assuming natural conditions and utilizing the unsteady flow model for 1973 and 1974 with the Greenwood Cutoff open.

Run No. 10

Simulation run of Plan E using the unsteady flow models for 1973 and 1974 assuming the Greenwood Cutoff is open. This run determined increases in peak flow rates on the main stem.

Run No. 11

Simulation run determining the sediment deposition rate on the lower reach of the Yazoo River from Belzoni to Vicksburg for the identical conditions in Run No. 2.

Run No. 12

Simulation run the same as Run No. 2 except it was assumed the river was dredged to the original Plan E channel every five years. The purpose of this run was to determine if a five-year dredging interval is practical and to compare it with the amount of sediment deposition if sediment is allowed to accumulate for the 50-year life of the project.

Run No. 13

Simulation run similar to Run No. 3 except the main stem channel design was modified.

Run No. 14

Simulation run that combines Runs No. 4 and 13. This was the best alternative design considered without maintenance dredging.

Run No. 15

Simulation run the same as Run No. 11 except a minimum pool with a water surface elevation of 65 feet was assumed maintained at the proposed lock and dam near Vicksburg. Results of this evaluation indicated whether or not required nine-foot navigation depths could be maintained with the proposed Upper Auxiliary Alternative Plan and the Yazoo River Navigation Project in operation. The design channel dimensions were modified from the original Plan E to accommodate navigation.

Model Development

The development of a large river basin model involves the following steps: data assembly and inventory, data evaluation, development of a data storage and retrieval system, collection of required data that cannot be synthesized, identification of data gaps and synthesis of additional data required for analysis, overall system design including spatial and temporal design, subsystem model development such as the main stem model and tributary models, validation and linking of the subsystem models, development of application data files, model calibration and verification, and application of the models to evaluate system response for different design alternatives. Figure 20.3 summarizes these procedures of model development schematically. The data requirements and the data storage and retrieval system were discussed in Chapter 16. The subsystem models were presented in Chapters 8, 11, and 12. This chapter presents the system design and the application to evaluate system response for different design alternatives.

20.3 SYSTEM DESIGN

Overall System Design

As mentioned previously, the Yazoo River Basin is composed of a main stem and numerous tributaries (refer to Figure 20.1). Analysis of the Basin simulates the river system as a whole rather than only selected areas.

In the Yazoo River Basin, tributaries to the main stem were divided into controlled, uncontrolled, and point source type streams. Controlled tributaries, for example, the Yalobusha River, are regulated by

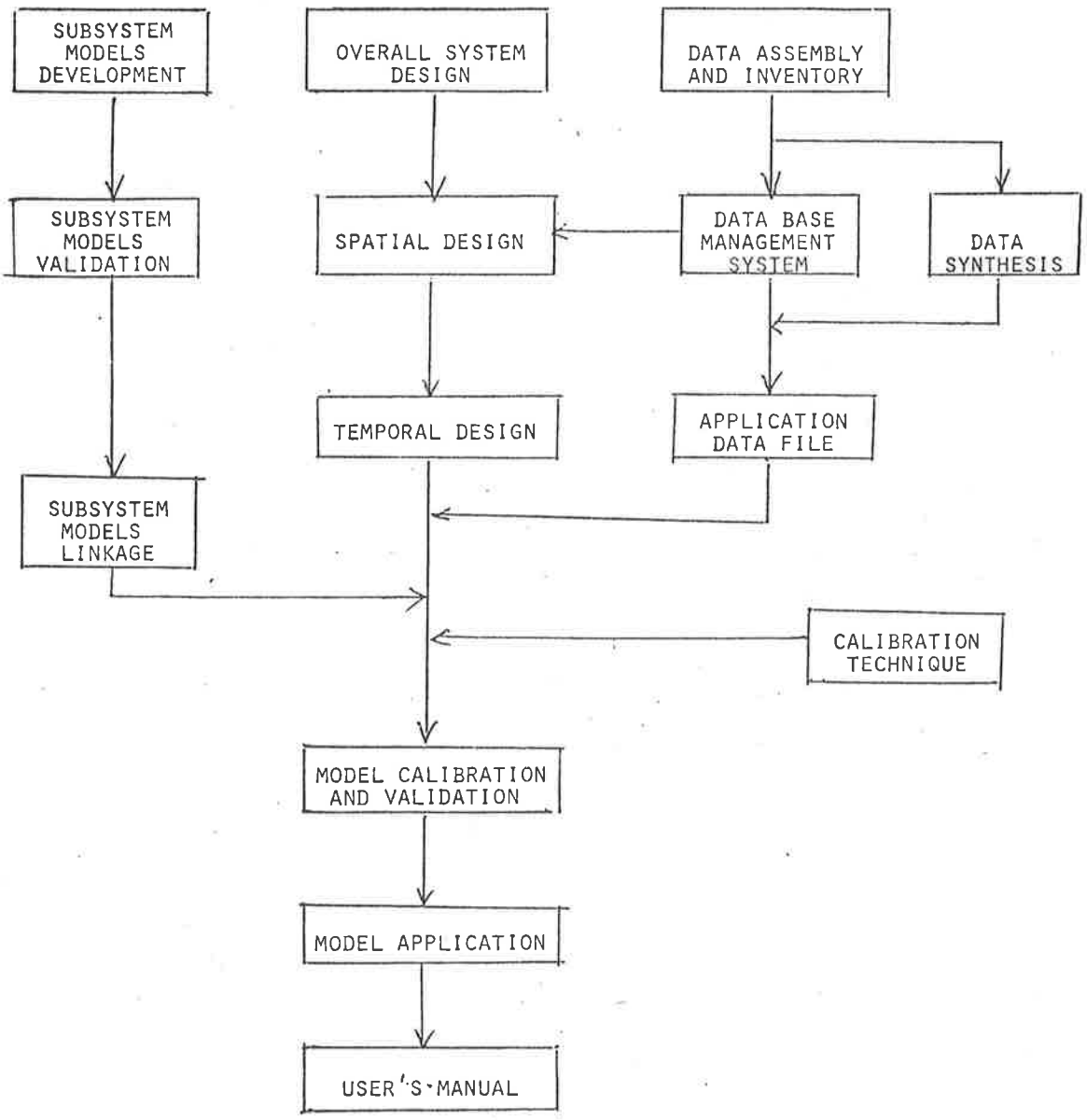

Figure 20.3 Flow diagram of model development.

large storage reservoirs including Arkabutla, Sardis, Enid, and Grenada. The controlled tributaries significantly effect the response of the Basin. Uncontrolled tributaries are generally smaller than controlled ones and do not have large storage reservoirs; however, they are important in analysis. An example of this type of tributary is Big Sand Creek. The third type of tributary is referred to as a point source and is generally smaller than the other two types. Point source tributaries are considered as a single point input. The potential impact of sediment inflow from point source tributaries to the main stem is small. However, in order to conserve flow continuity, these tributaries were included in the analysis of the Yazoo system as point source inputs. An example of this type of tributary is Piney Creek.

Classification of tributaries is based upon examining system response which is described in the next section. Controlled, uncontrolled, and point source tributaries are shown schematically in Figure 20.4. This figure also shows the relation of the tributaries to the main stem system. In addition, the nonpoint source contribution from additional uncontrolled areas was considered in order to conserve flow continuity in the total system.

The computer model developed to analyze the system is a physical process model based on the physical environment. Information provided by the model for the main stem includes: water discharge, water level, sediment discharge, and aggradation or degradation of the channel. These outputs were simulated for different alternatives and operating conditions of the river system development as previously identified. The input required was provided from output of the controlled and uncontrolled tributaries, and other point or nonpoint contributions from tributaries. Input for these types of models consists of water and sediment discharges from primary input sources, and lateral inflows or outflows from land surfaces. Reliable methods are needed to synthesize these required input data if measured data are not available. Because of a limited data base for the analysis, discharges from ungaged tributaries and nonpoint sources were synthesized utilizing watershed area and continuity. Sediment versus discharge rating relations for tributaries were estimated by assuming that a dynamic equilibrium condition is reached on the natural channel utilizing a 50-year hydrograph.

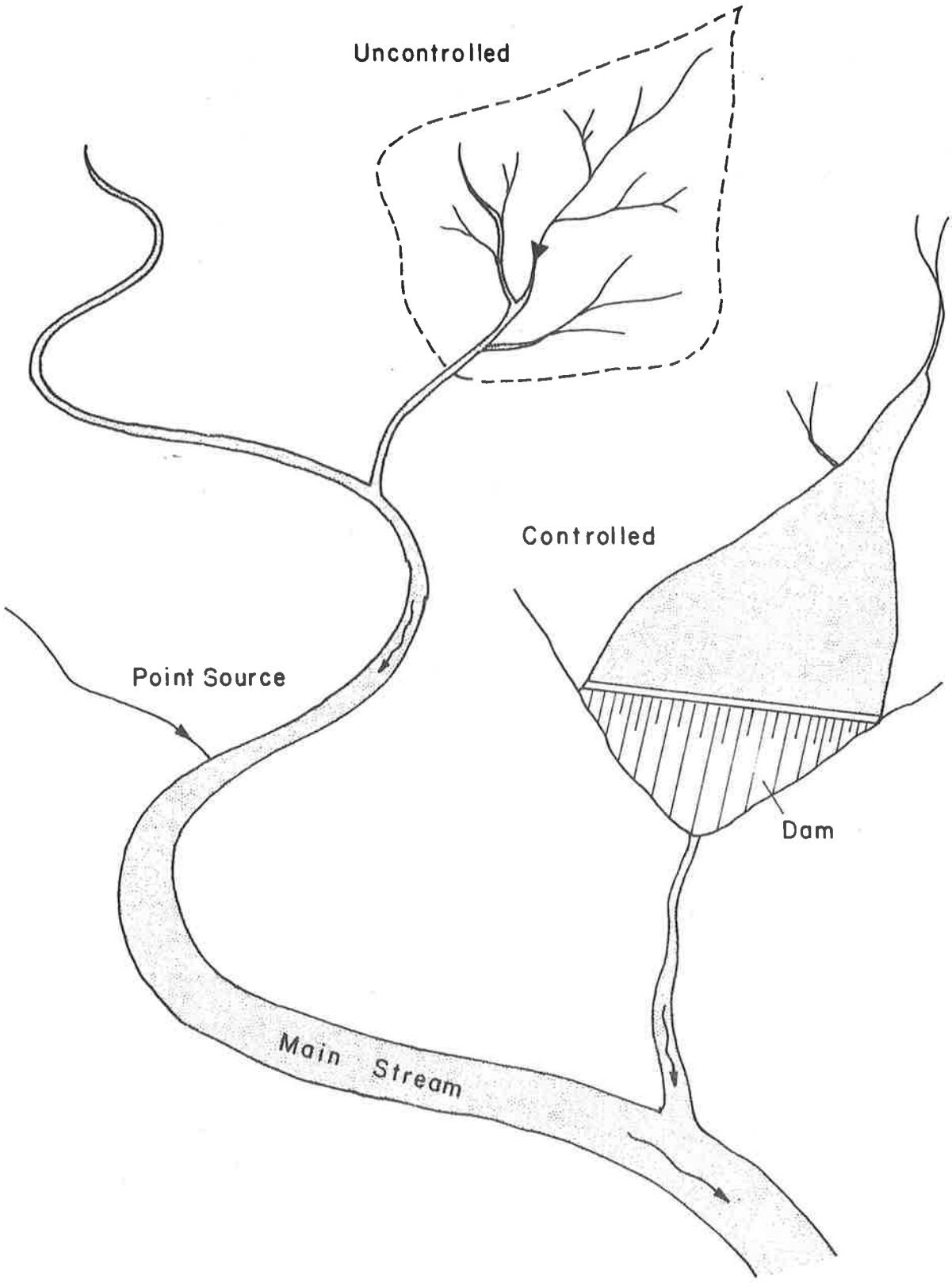

Figure 20.4 Schematic of river system.

Subsequent problems encountered in the conceptual system design included determination of locations of main tributaries and other sources, and generation of hydrographs for the simulation of future channel response.

Spatial Design

Spatial and temporal designs of the Yazoo River system are necessary to provide a realistic representation of the space-time structure for accurate simulation of the system. The location of rivers and tributaries and the location of all pertinent gaging stations, structures, and confluences are included in the spatial design. The spatial design was based on the potential contribution of all sediment sources to the bed elevation changes.

By applying the sediment continuity equation, a sediment transport equation, and a set of typical flow conditions, the bed elevation changes along the main stem between each two neighboring confluences were determined. Also, the percentage changes contributed by the tributaries were determined considering the ratio of sediment transport rates between the main stem and its tributaries. By summing all changes in the sediment storage volume (product of bed elevation change, wetted perimeter, and the space increment between two neighboring confluences) and relating this total change to the individual change, the percentage of sediment from each tributary contributing to changes in bed elevations in the main stem was determined.

After ranking the potential contributions of sediment according to the computed percentages, the determination of important tributaries (either controlled or uncontrolled) and point source inputs were delineated. The abstracted system of the Yazoo River system is given in Figure 20.5. There are 31 tributaries to the Yazoo Basin. Only 12 of the tributaries were identified important for the analysis: Arkabutla Creek, Little Tallahatchie River, P-Q Floodway, Yocona River, Tillatoba Creek, Yalobusha River, Potococowa Creek, Teoc Creek, Big Sand Creek, Abiaca Creek, Pelucia Creek, and Techeva Creek. Other inputs could be considered as point source inputs. Old Coldwater River, Bobo Bayou, Burell Bayou, and all the tributaries in the Sunflower Basin such as Big Sunflower River, Little Sunflower River, Deer Creek, and Steele Bayou were excluded from analysis.

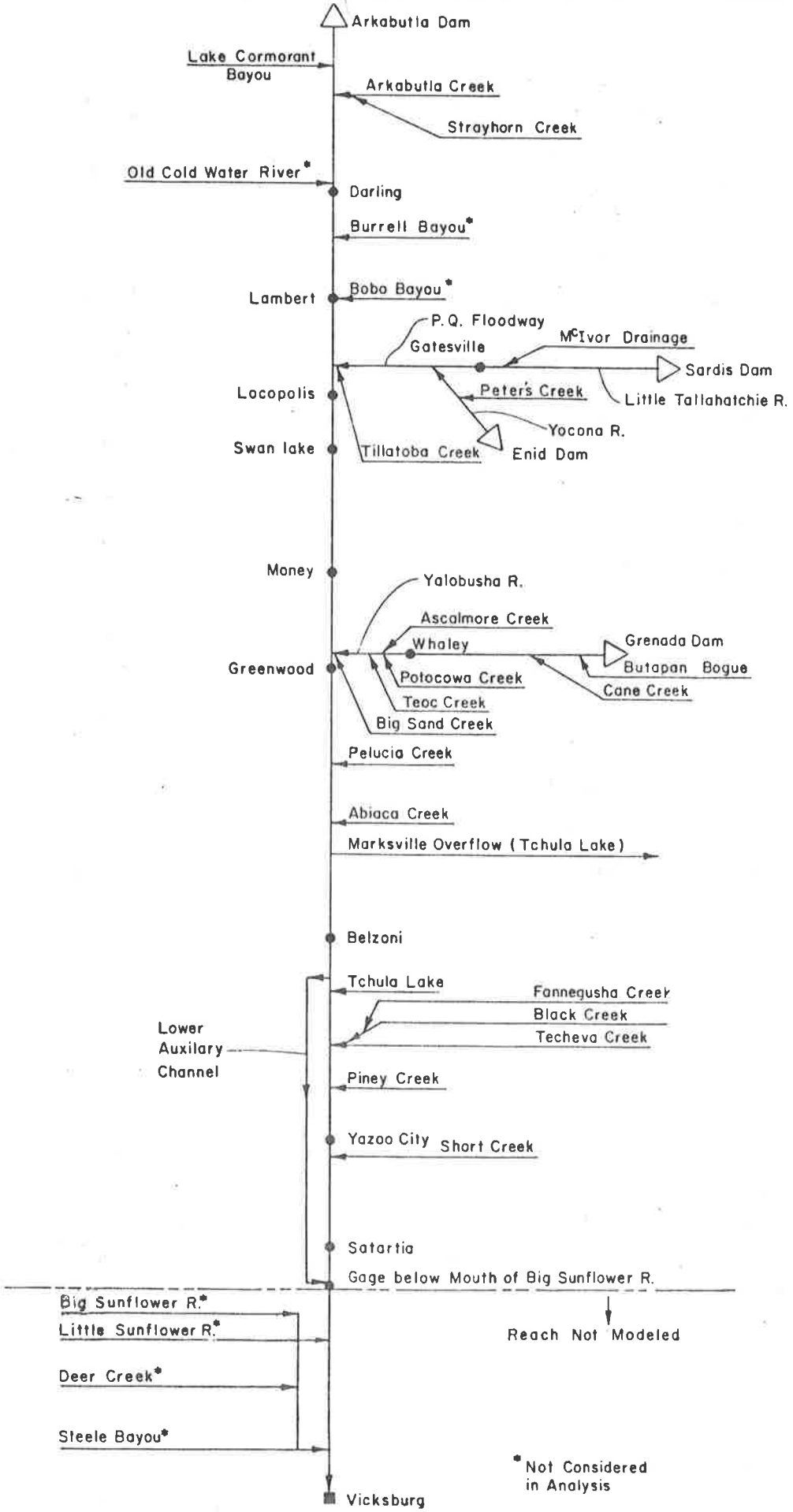

Figure 20.5 Spatial representation of the existing conditions (Run No. 1).

Spatial representation of Alternative Run No. 1 was the same as shown in Figure 20.5. The proposed Plan E is the basic spatial design for other alternative runs. Run No. 2 is Plan E as proposed by the U.S. Army Corps of Engineers (Figure 20.2) and represented in Figure 20.6. Alternative study Runs No. 3, 4, 5, 6, 7, 11, and 12 have the same spatial design as Run No. 2 except channel cross section data for Runs No. 7 and 12 were changed to conform with the original cross sections after a specified period in lieu of maintenance dredging.

For simplicity, Plan E and its modified channels would have channel bottom elevations as specified in the design, even when the original bed elevation is lower than the design bed. It was tentatively determined that the construction schedule proceed upstream in two-year intervals. At the end of the eighth year, construction would proceed from Yazoo City to Greenwood, and construction would be complete to the mouth of the P-Q Floodway at the end of the 14th year. The total Upper Yazoo project would be completed at the end of the 18th year after start of construction. Run No. 8 considers the effect of construction. Spatial representation for study runs (No. 9 and 10) utilizing the unsteady flow water and sediment routing model includes a smaller area. The spatial design is shown in Figure 20.7. The first modifications to Plan E were evaluated in Runs No. 13 and 14 and the impact of the Upper Yazoo Project on the lower reach and the feasibility of a nine-foot navigable channel with lock and dam near Vicksburg were studied in Runs No. 11 and 15.

Temporal Design

General Description

A primary component of the analysis of the Yazoo River Basin is realistic water discharge records. These records were developed from existing discharge and water stage data. Sixty-two sets of discharge records were developed for this study including 30 sites with existing discharge or stage records, 14 ungaged tributary sites, and 18 nonpoint sources as outlined in Figure 20.8. Two sets of discharge records were developed for each site. The first set was composed of 4,018 average daily flow values for January 1, 1964 to December 31, 1974. This period was used because of the availability of discharge or water stage measurements. The second set was composed of 2,609 weekly average flow values,

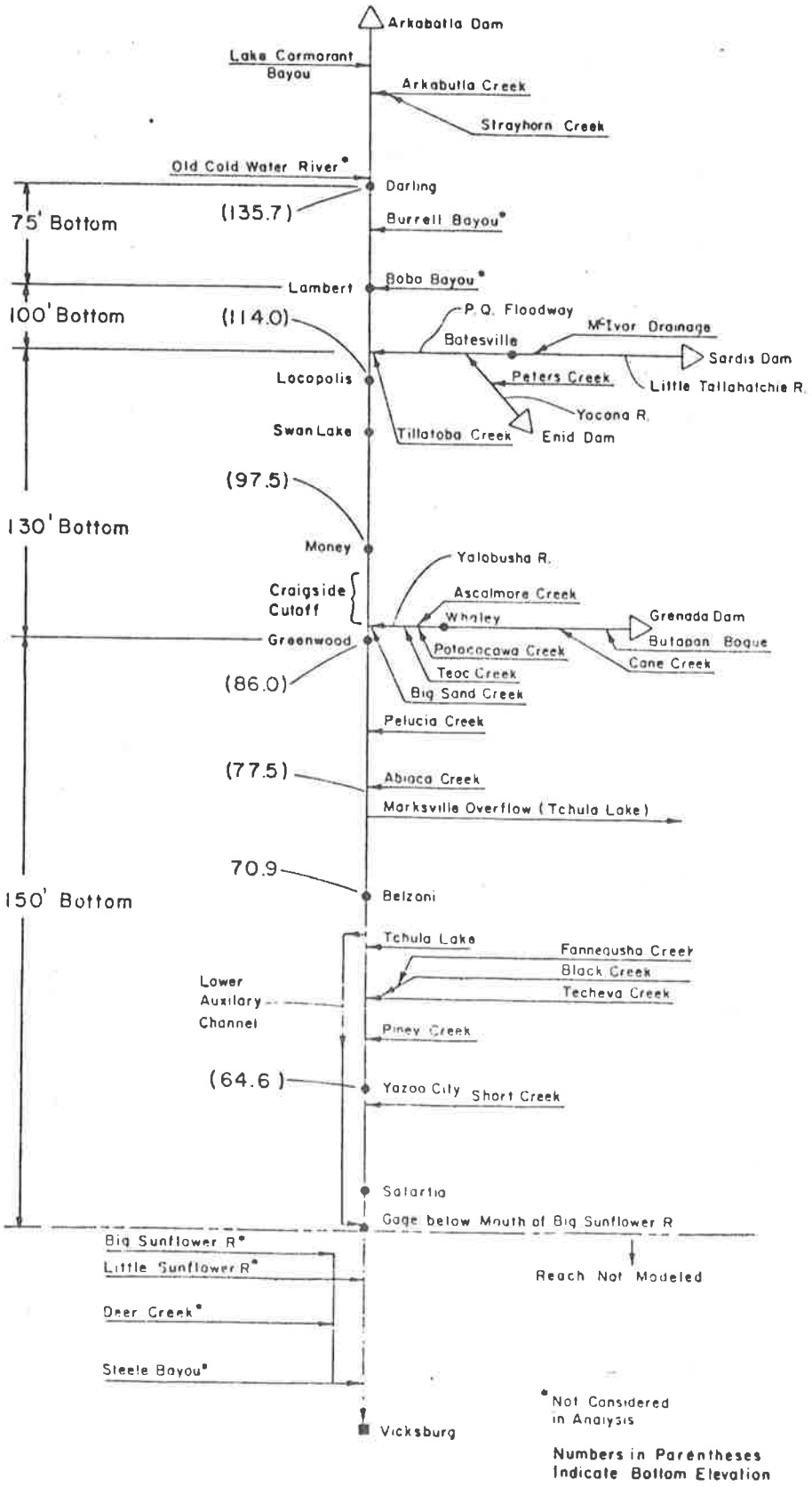

Figure 20.6 Spatial representation of Plan E conditions (Runs No. 2, 3, 4, 5, 6, 7, 11, and 12).

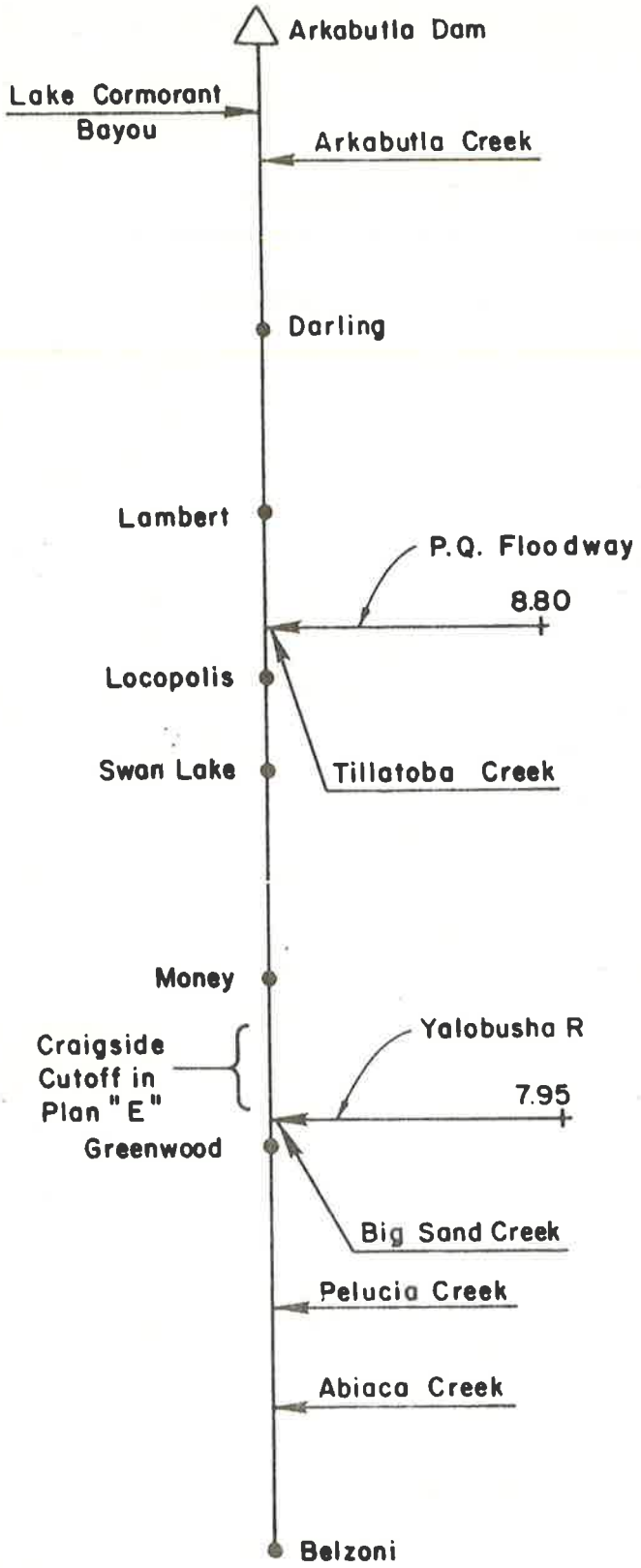

Figure 20.7 Spatial representation of the unsteady flow model (Runs No. 9 and 10).

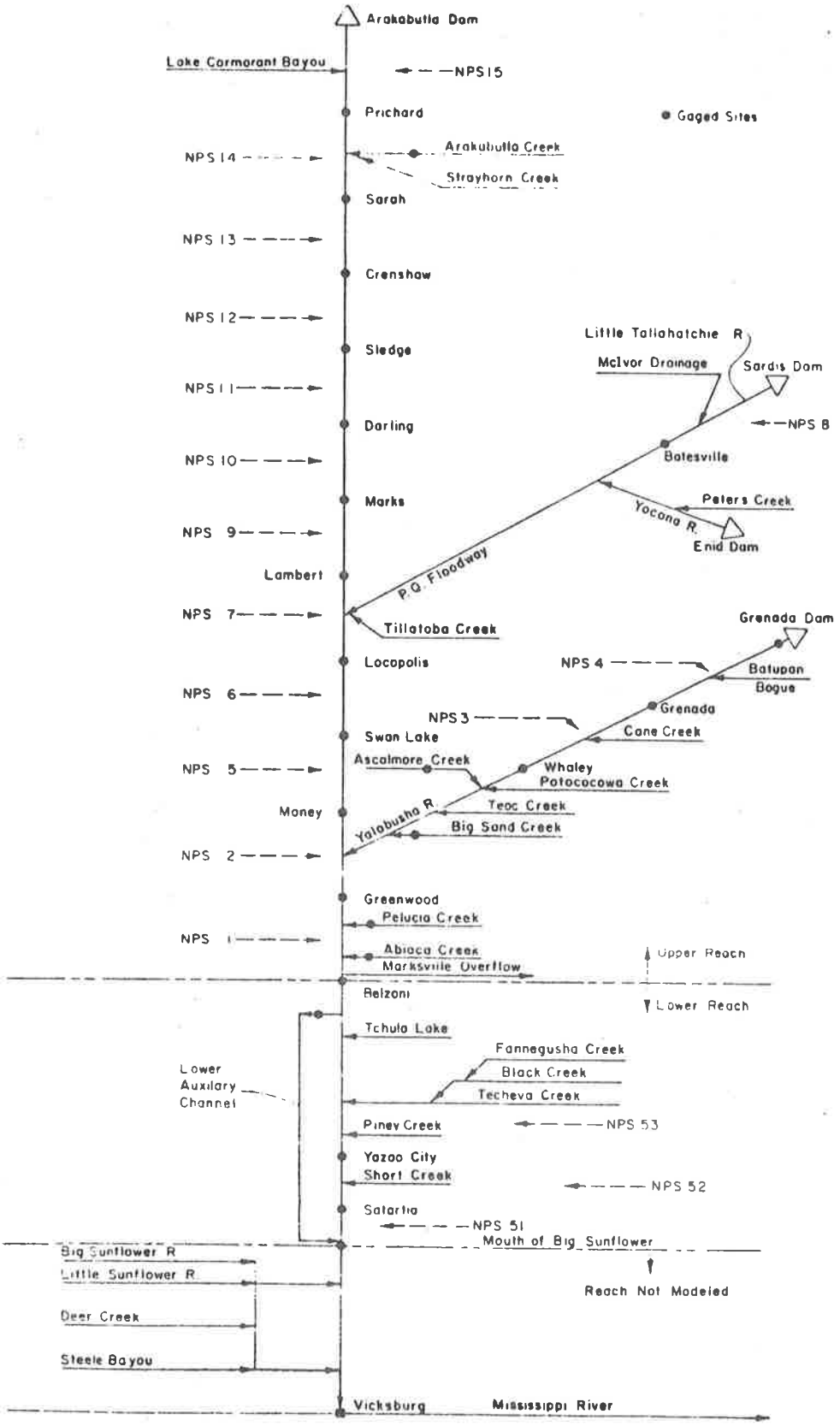

Figure 20.8 Spatial representation of gaged sites, ungaged sources, and nonpoint sources.

i.e., the average daily flow for a seven-day time span. This time period included 574 discharge values for the 11 years from 1964 through 1974 plus 2,035 synthesized values of discharge for the next 39 years. Weekly flow records were developed from pre-existing average daily flow records.

Development of Average Daily Flow Records

Average daily flow records for seven sites were obtained from the U.S. Geological Survey Water Resources Division. These sites included outflows from the four major reservoirs and the three river sites of Lambert, Swan Lake, and Greenwood. Records for the other 23 gaged sites were developed from U.S. Army Corps of Engineers stage records supplied on magnetic tape. Stage-discharge rating curves were developed either from observed stages and discharges or supplied by personnel from the U.S. Army Corps of Engineers.

Stage readings taken at 8 A.M. were converted to discharges and were used to develop average daily discharges by linear interpolation. Existing average daily discharges and the interpolated discharges provided the flow records for gaged sites. Ungaged sites such as Teoc Creek required data synthesis using nearby sites. The approach used in this synthesis involved computed representative discharge per square mile for a nearby similar site or pair of sites. The area of the synthesized site was multiplied by discharge per square mile. When applicable, an average discharge per unit area for two nearby gaged stations was used for synthesis of discharge. For some sites, the discharge per unit area was found as the difference in flow between two river or major tributary sites.

After all gaged and ungaged sites were determined, nonpoint sources were computed. Nonpoint sources for a river reach were computed as the difference between outflow and inflow in the reach. Using this flow continuity approach, all water is accounted for by gaged, ungaged, and nonpoint sources. Use of daily flow continuity is reasonable since flow travel times between any two stations in a reach is usually less than one day.

Development of Weekly Flow Values

Weekly flow values were developed using an approach similar to that used to estimate daily flow values but includes additional simulation of

extended records. Generation of synthetic streamflow sequences that are sufficiently long so they can be expected to simulate typical flow conditions was an important task. This record allowed realistic input to the mathematical simulation models of the Yazoo River Basin system to evaluate effects of various flows on structures and environmental conditions along the river. To accomplish this task, several stochastic models were constructed to preserve the mean, variance, and autocorrelation structure of the historical flow record.

Time series models are often fitted to the autocorrelation function or equivalently its Fourier transform. The stationary component of the time series is then removed. Research has shown the best method is to synthesize logarithms of the flows using an Auto-Regressive Moving Average Scheme (ARMA) with time varying auto-regressive (AR) coefficients that preserve long range dependence of the hydrologic series. This approach employs Kalman filtering to improve the fitting of an AR (2) (auto-regressive lagged two-time periods) model to the historic data. (See Chapter 14) This model was then used to extend the 11-year record an additional 39 years to a total of 50 years.

Trend elements were approximated by polynomial equations, while a cyclical component with variations resulting from seasonal flow patterns was represented by harmonic functions. Removal of the trend and cyclical components facilitated ARMA simulation of the time series. In this application, an AR (2) model was fitted to the standardized time series. A sixth order harmonic model was used to fit the time variant AR (2) coefficients. The harmonic model was then used to extend the AR (2) coefficients forward in time. These coefficients were used to create a new standardized series. The operations are summarized as follows:

(a) Compute the average discharge for each seven-day period.

(b) Take the logarithm of the average discharge data.

(c) Detect the trend and cyclical components of the discharge series and subtract them from the historical data.

(d) Standardize the residual time-series.

(e) Fit an AR (2) model to this series by Kalman Filtering.

(f) Fit a sixth order harmonic model to the coefficients of the AR (2) model.

(g) Calculate the mean and standard deviation of the fitting errors of the AR (2) model. These statistics generated random noise which was added to the generated data from the AR (2) model when synthesized data was desired.

Synthesized streamflow data was obtained through the following inverse operations:

(a) Generate the coefficients for the AR (2) model with the sixth order harmonic model.

(b) Generate the residual time-series by adding in normally distributed random errors.

(c) De-standardize the data to return to a residual time-series.

(d) Add the trend and cyclical components to the residual time-series.

(e) Take the exponential of the generated data.

(f) Check with the lower and upper bounds on the generated values.

(g) Check the simulated with the historical flow characteristics, such as frequency of peak flow and flow volume distribution.

If the flows were realistic and consistent the flow series was accepted for use.

After the weekly flow values for the gaged sites were extended to 50 years, ungaged and nonpoint sources were computed the same as daily flow values. A seven-day average was used because flow rates indicate that water can move through the system from Arkabutla Dam to Vicksburg in about seven days.

Comparison of the Results

A summary of daily and weekly flow values at key gaging stations is given in Table 20.1. As Table 20.1 shows, the simulated record retains the characteristics of the actual record particularly for the gaged stations. Flow frequency for four key main stem gaging stations are shown in Figure 20.9. The shapes of the frequency curves are very similar. However, the 50-year synthesized hydrograph has lower frequencies than the 11-year observed hydrograph for similar discharges. This shows that the 50-year synthesized hydrograph is statistically comparable to the original statistics. This similarity can be seen by comparing the observed and synthesized hydrographs near Lambert as shown in Figures 20.10a and 20.10b. These figures indicate the time series analysis retains the cyclical nature and relative magnitude of the observed data.

Table 20.1 Comparison of flow statistics for 11 years daily, 11 years weekly, and 50 years of weekly flows.

Upper River

Station	Statistic	11 Years Daily	11 Years Weekly	50 Years Weekly
Belzoni	Max	28158.76	28114.91	28114.91
	Min	1339.75	1466.92	1466.92
	Mean	11335.60	11335.60	12183.22
	Std.Dev.	5777.74	5734.42	4436.44
Greenwood	Max	43800.00	40857.14	40857.14
	Min	971.00	1065.71	1065.71
	Mean	11727.19	11727.19	12674.57
	Std.Dev.	6513.29	6426.53	4924.74
Money	Max	22830.88	22419.91	22419.91
	Min	516.73	561.00	561.57
	Mean	8145.13	8145.13	9183.14
	Std.Dev.	4785.18	4731.65	3860.66
Swan Lake	Max	44900.00	36428.57	36428.57
	Min	612.00	774.14	774.14
	Mean	7929.28	7929.28	8917.06
	Std.Dev.	4857.45	4750.23	3842.77
Locopolis	Max	33753.37	29802.49	29802.49
	Min	650.53	713.15	713.15
	Mean	7291.47	7291.47	8260.64
	Std.Dev.	4767.61	4685.40	3641.99
Lambert	Max	15100.00	14571.43	14571.43
	Min	85.00	116.43	116.43
	Mean	2843.12	2843.12	3400.68
	Std.Dev.	2785.66	2670.86	2681.66
Yazoo City	Max	19656.32	19605.04	19605.04
	Min	2000.00	2086.55	2086.55
	Mean	9229.60	9229.60	9709.58
	Std.Dev.	3929.38	3895.01	3078.39
Satartia	Max	20142.66	20122.68	20122.68
	Min	2000.00	2000.00	2000.00
	Mean	9410.73	9410.73	9891.98
	Std.Dev.	4218.92	4184.54	3499.55
Yazoo River at Mouth Big Sunflower	Max	44171.82	44155.87	44155.87
	Min	2245.98	2411.04	2411.04
	Mean	18816.81	18816.81	19723.91
	Std.Dev.	9563.75	9496.20	8098.45

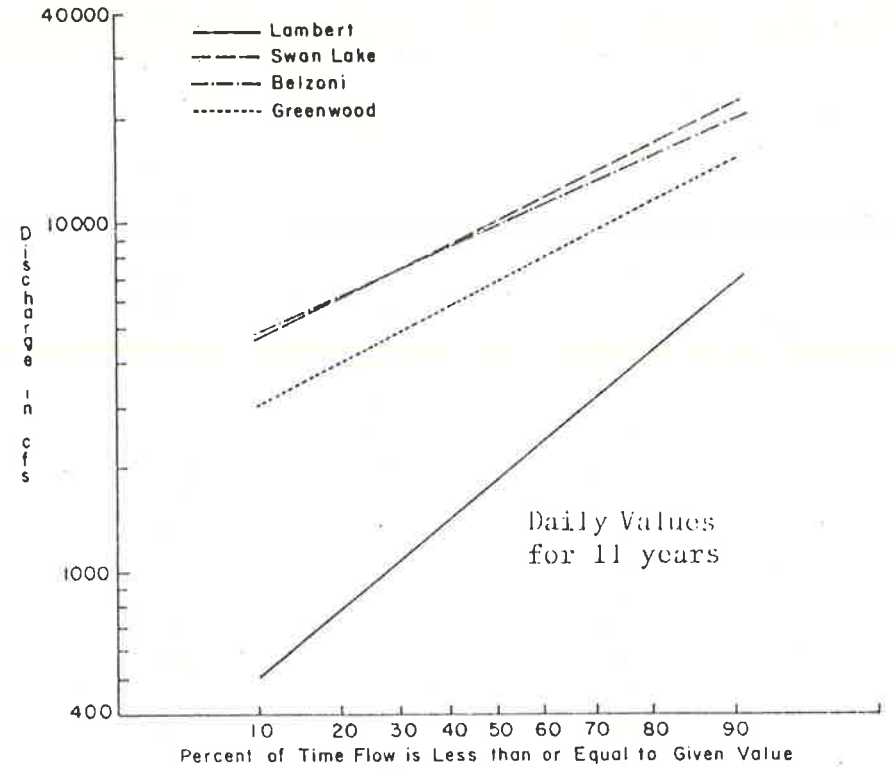

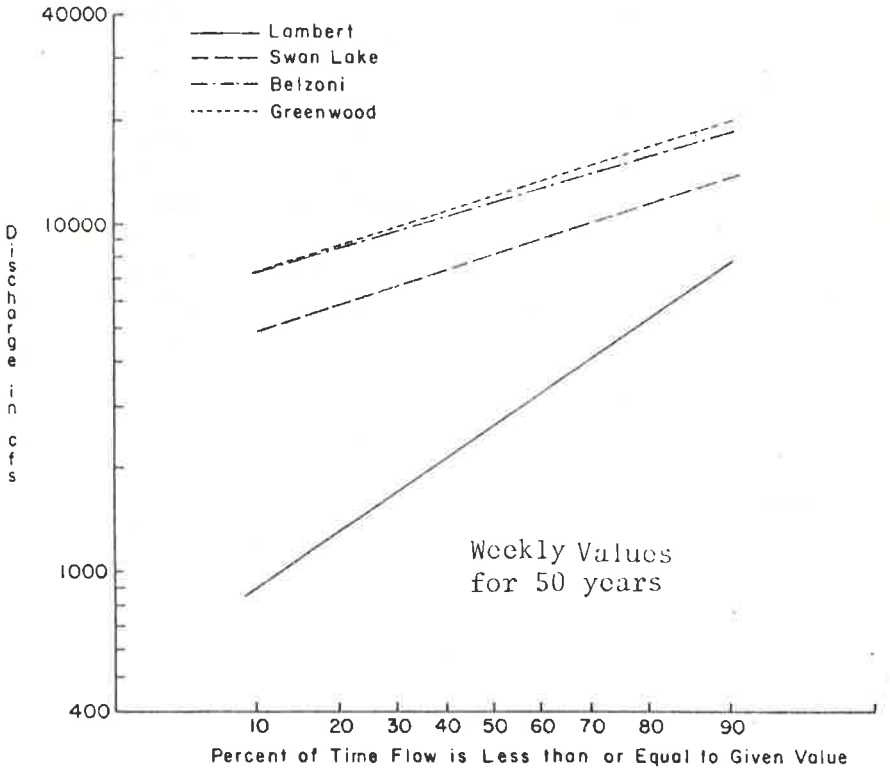

Figure 20.9 Flow frequencies for four main stem gages.

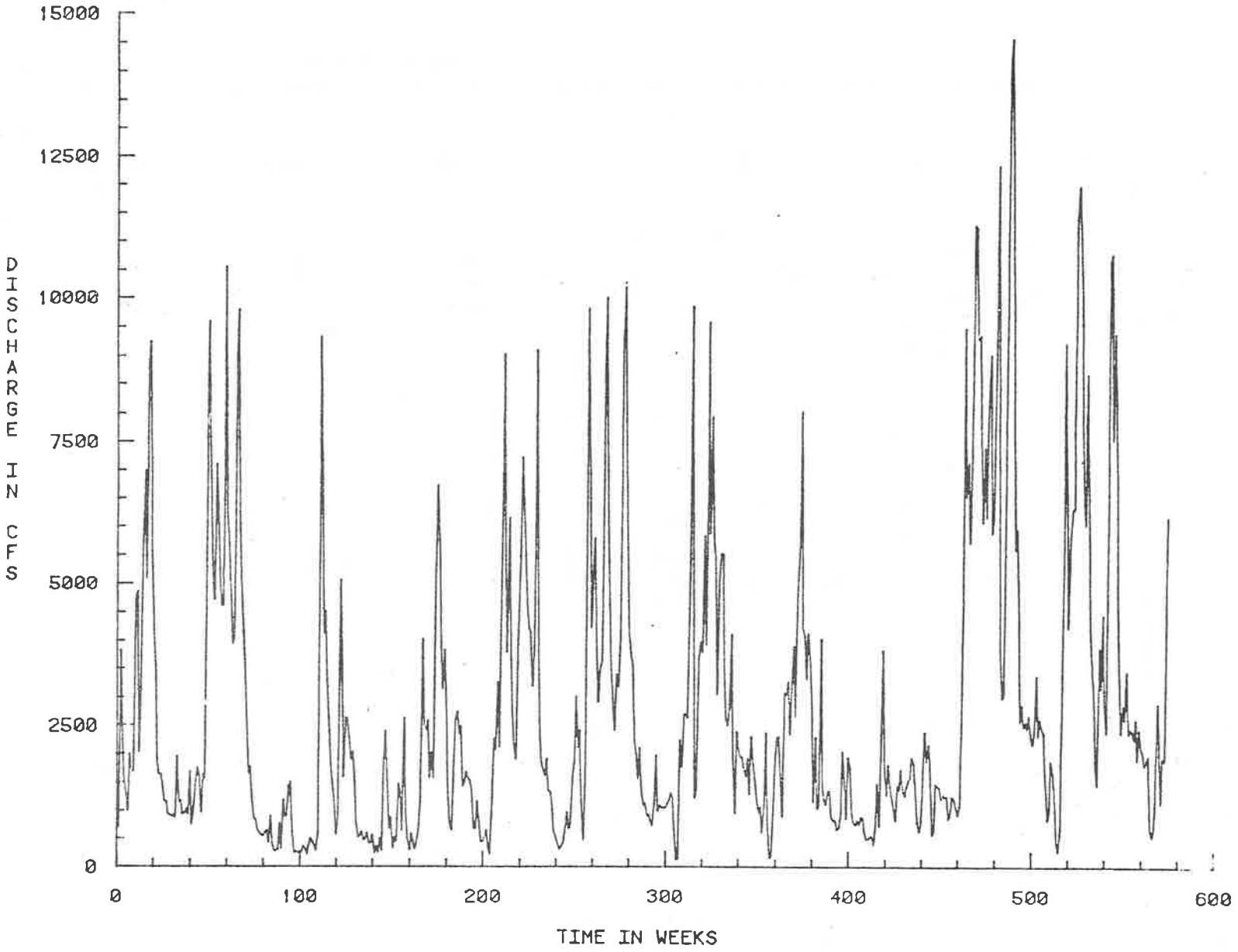

Figure 20.10a Seven-day average discharge for Tallahatchie River near Lambert observed at station No. 405.

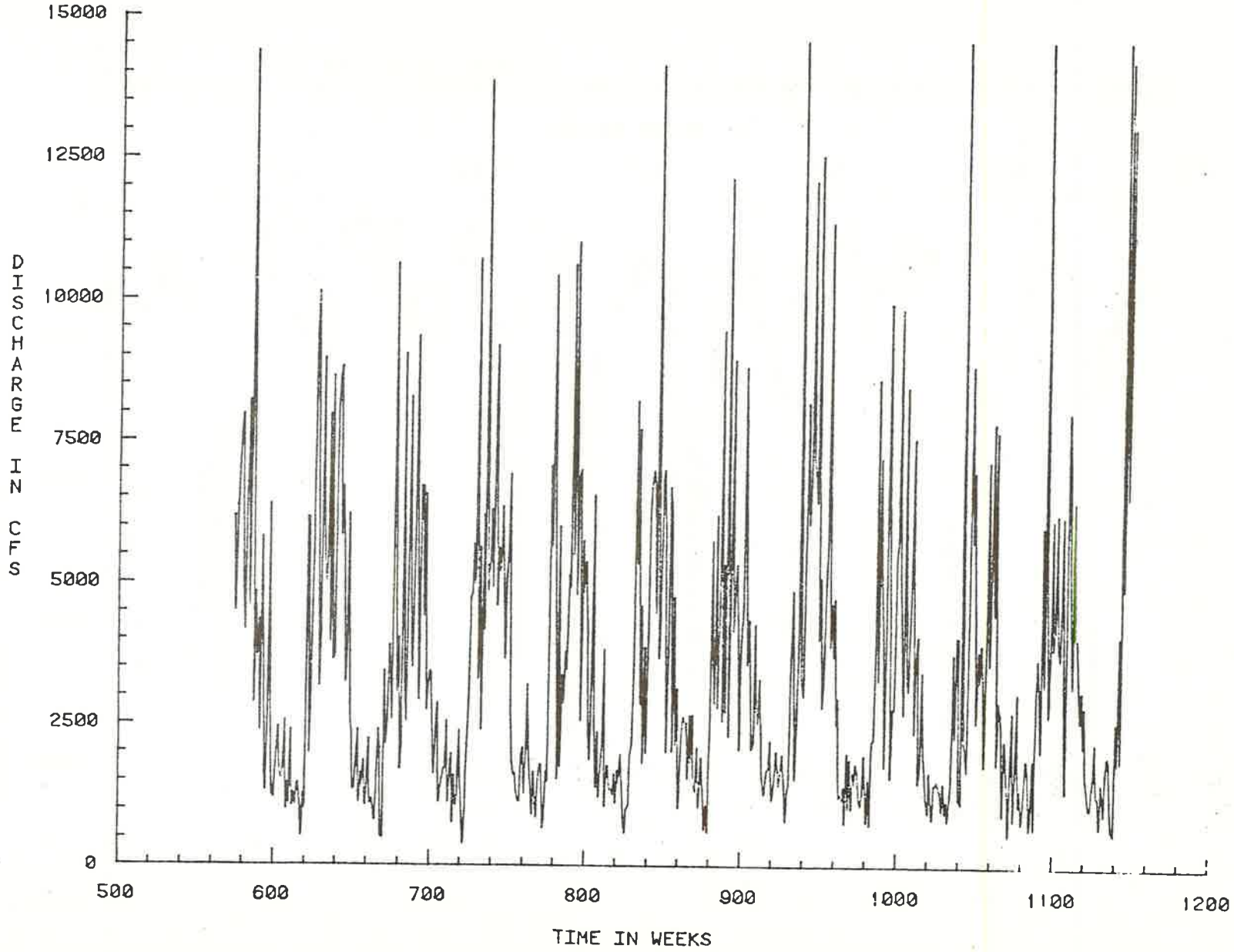

Figure 20.10b Seven-day average discharge for Tallahatchie River near Lambert generated for station No. 405.

20.4 RESULTS OF ANALYSIS

Both unsteady flow and known discharge models were calibrated and verified for two separate reaches of the river with good results. The two reaches of the mainstream river that were tested included the Ft. Pemberton Cutoff at Greenwood Bendway, and a reach on the Tallahatchie from Swan Lake to Locopolis. Results of both models are acceptable and comparable. This verifies that the known discharge model can be used to analyze the Yazoo River system.

Both the unsteady flow and the known discharge models were applied to evaluate river response to specified design alternatives. The details of the models were given in Chapters 8, 11, and 12. The alternative study runs were specified by the U.S. Army Corps of Engineers and were described in Section 20.2. Runs No. 9 and 10 were analyzed by applying the unsteady flow model. The other 13 runs were completed utilizing the known discharge model (Chapter 12). Spatial representations of each study run were discussed in Section 20.3.

Application of the Unsteady Flow Model

To evaluate the effectiveness of Plan E in passing the flood flow, a two-year hydrograph (1973 and 1974) was routed through the natural Yazoo River and the proposed Plan E channel system utilizing the unsteady flow model (Runs No. 9 and 10, respectively). The Greenwood Cutoff was assumed open for these two runs. Discharges, stages, and bed elevations were computed and compared to evaluate the impact of Plan E. The enlargement of channel cross sections and the introduction of the Craigside Cutoff affects the propagation of the flood wave. Comparison between the flood discharges of Runs No. 9 and 10 shows that the peak discharge after implementing Plan E increased less than two percent at Greenwood and two percent at Belzoni for floods similar to the one in 1973. Also, due to the cutoff upstream of Ft. Pemberton, the flood wave from the Tallahatchie River peaked near Greenwood about two hours earlier. This alteration may or may not help reduce the flood potential in the Greenwood area. This river response depends on the flood wave introduced by the Yalobusha River. An assumption of 15 percent increase in discharge due to channelization adopted by the U.S. Army Corps of Engineers (Run No. 5) is certainly conservative.

Generally, for the two-year simulation period, Plan E would lower the local river stages. Effects would be more significant at low flow (11,000 cfs at Belzoni) than high flow (28,000 cfs at Belzoni) as shown in Figure 20.11. In this figure, changes in stages in the Yazoo main stem at low flow and high flow after implementation of Plan E are plotted. Negative values indicate that the stage in the Plan E channel is lower than in the natural channel. Maximum decreases in stage would occur near the Craigside Cutoff and between Swan Lake and Locopolis where the bankfill cross-sectional area was increased significantly for Plan E. Some increase in stage would also occur after implementing the recommended plan. The efficiency in flood stage reduction would be greatly impaired if the Plan E channel is not maintained for a long period, as described later in this section.

Geomorphic changes computed by the unsteady model indicates there would be more sediment deposition in the Yazoo River main stem two years after implementing Plan E than in the natural channel (Figure 20.12). The deposited sediment volume in the Plan E channel from Belzoni to just below the Greenwood Bendway would be 3,055,000 cubic yards, compared to 1,399,000 cubic yards in the natural channel. This results from the enlargement of the channel section for Plan E plus the increase of sediment inflow from Abiaca Creek. The Greenwood Bendway downstream of the mouth of the Yalobusha River would continue filling if the Ft. Pemberton Cutoff is opened. The estimated deposition volume in the Greenwood Bendway is 838,000 and 784,000 cubic yards in the Plan E channel and the natural channel, respectively. Because of the enlargement of the channel in the Tallahatchie River for Plan E, more sediment would deposit in the Tallahatchie and less sediment would be transported downstream. This would result in erosion immediately upstream of and at the Ft. Pemberton Cutoff as shown in Figure 20.12.

Application of the Known Discharge Model

General

Applicability of the known discharge model in the Yazoo River System was examined and established by comparing it to the unsteady flow model. As mentioned earlier, the primary purpose of this study was to identify sedimentation problems and evaluate possible remedies. The known discharge simulation model is adequate for this purpose. The simplicity in application, the tremendous savings in computer time, plus

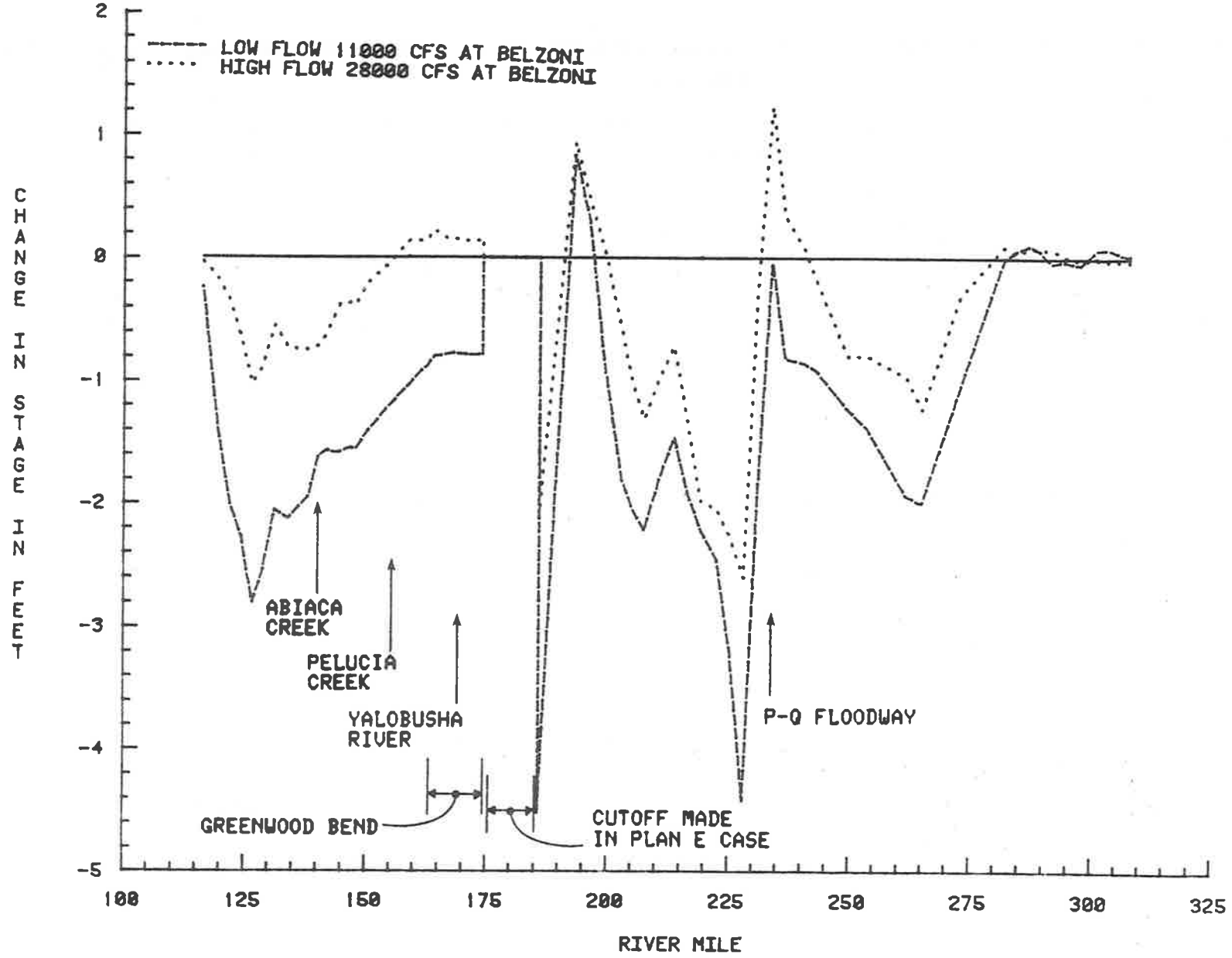

Figure 20.11 Stage changes from the natural channel case to the Plan E case (unsteady flow model).

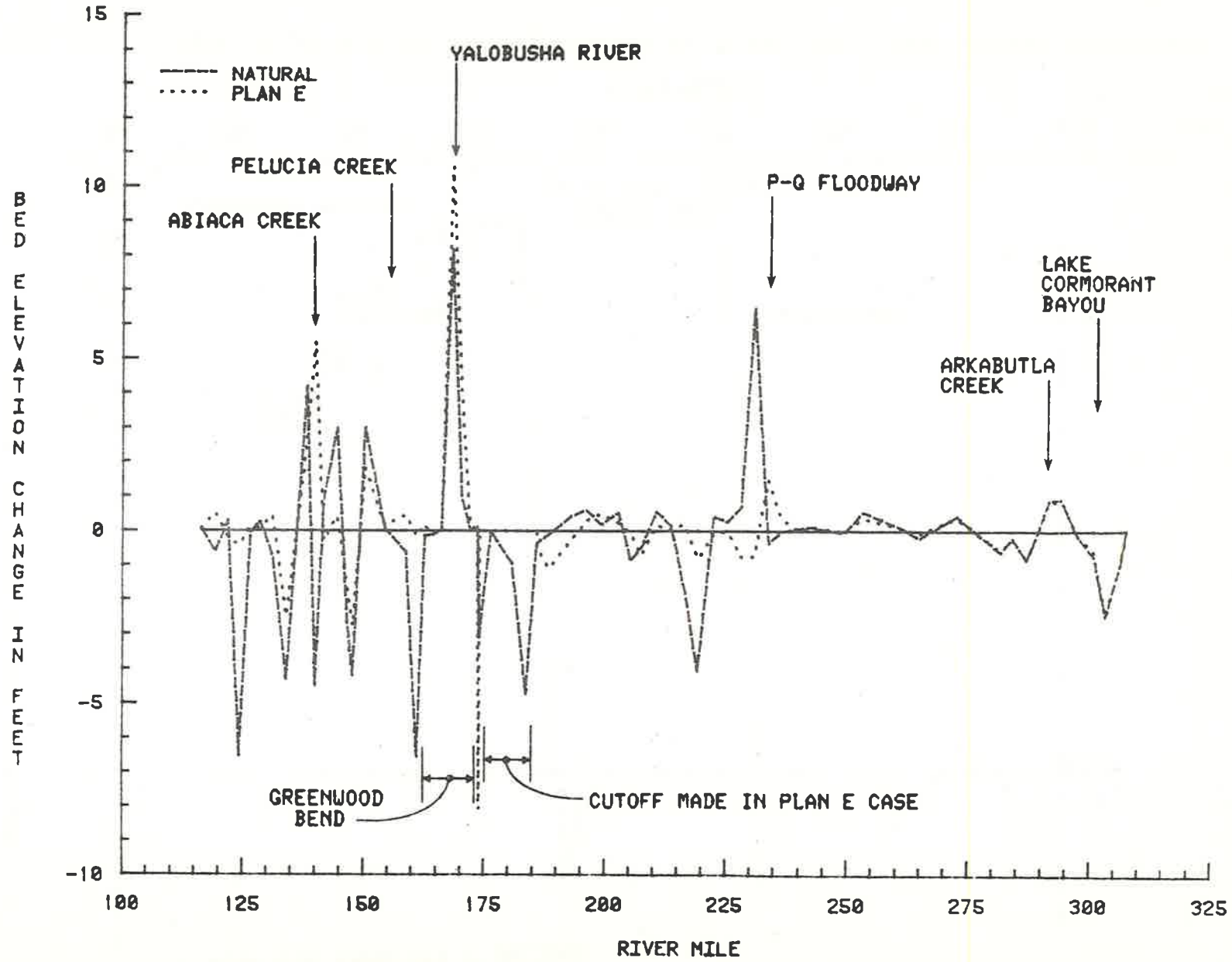

Figure 20.12 Bed elevation changes in the Yazoo main stem after two years (unsteady flow model).

the accuracy achieved verifies the known discharge model as an excellent tool for evaluating alternatives.

As mentioned in Section 20.3, the spatial representation of the known discharge model covered a much larger study area. The spatial designs for various study runs differed. Nevertheless, it is worthwhile to identify the river segments utilizing the same designation system. Hence, referring back to Figure 20.5, River Segment No. 1 extends from the mouth of Big Sunflower to Belzoni. River Segment No. 2 extends from Belzoni to just below the Greenwood Bendway. River Segment No. 3 includes the Greenwood Bendway, and River Segment No. 4 extends from immediately upstream of the Greenwood Bendway to Arkabutla Dam. The Yalobusha River is identified as River Segment No. 5. River Segment No. 6 includes the Little Tallahatchie and the P-Q Floodway. The Yocona River is defined as River Segment No. 7 and the Greenwood Cutoff is identified as River Segment No. 8. Simulated results for different river conditions for a 50-year synthetic hydrograph are summarized in Table 20.2. The summary of dredging volume for Runs No. 7 and 12 are given in Table 20.3. The net degradation and aggradation volumes in the main stem above Belzoni (sum of River Segments No. 2, 3, 4, and 8) are given in Table 20.4. For Runs No. 7 and 12, total dredging volumes were included in Table 20.4.

Run No. 1 (Natural Conditions)

For the main stem from Belzoni to Arkabutla Dam (River Segments No. 2, 3, 4, and 8), the estimated rate of net filling (net degradation and aggradation) is about 210,000 cubic yards per year with natural conditions. Figure 20.13 shows the beginning and final bed profiles after 50 years under natural conditions.

The maximum water surface elevations at each cross section are also plotted in Figure 20.13. These maximum water surface elevations are the maximum values at each cross section considering the 50-year simulation period. These values do not necessarily occur at the same time for all of the cross sections and may not take place during the period of maximum discharge. The downstream water surface elevations and the long-term sediment movement in the system will dictate local water surface elevations.

The cumulative net degradation and aggradation volumes in the main stem for the 50 years of simulation are shown in Figure 20.14. Generally,

Table 20.2 Summary of net degradation and aggradation for 50 years under different design conditions.

Alternative Runs No.	Net Degradation and Aggradation in 10^3 cubic yards Reaches							
	1	2	3	4	5	6	7	8
1	--	1,941	445	8,097	1,242	-2,078	908	- 48
2	--	22,075	2,846	16,909	4,181	-2,809	658	3
3	--	14,683	2,112	15,186	3,226	-3,750	518	- 14
4	--	13,422	1,323	14,038	2,142	-4,002	454	- 22
5	--	25,209	3,484	18,717	7,023	-1,405	859	-109
6	--	30,829	5,143	20,319	11,171	-275	955	-128
7	--	2,944	-1,278	-7,212	-121	-10,613	-890	- 81
8	--	19,832	2,250	12,127	3,157	-3,893	608	- 21
11	5,313	23,228	2,742	16,665	3,990	-2,863	233	- 39
12	--	6,464	-992	-2,849	457	-9,203	-625	- 76
13	--	15,889	1,488	12,385	2,418	-3,121	587	- 36
14	--	14,510	726	11,117	1,408	-3,359	613	- 49
15	9,446	26,388	3,960	19,520	6,018	-2,709	222	-15

Table 20.3 Summary of total dredging volumes.

Alternative Runs No.	Cumulative Dredging Volumes for 50 Years in 103 Cubic Yards Reach					
	1	2	3	4	8	Total
7		36,568	4,509	29,582	687	71,346
12	--	35,100	2,199	25,910	399	63,608

Table 20.4 Summary of net degradation and aggradation in the main stem above Belzoni.

Alternative Runs No.	Total Degradation and Aggradation Volume in 50 years 10^3 Cubic Yards	Ratio to Natural Condition	Ratio to Plan E Condition
1	10,435	1.0	0.25
2	41,833	4.01	1.0
3	31,967	3.06	0.76
4	28,761	2.76	0.69
5	47,301	4.53	1.13
6	56,163	5.38	1.34
7*	65,719	6.30	1.57
8	34,188	3.28	0.82
12*	57,981	5.56	1.39
13	29,726	2.85	0.71
14	26,304	2.52	0.63

*Dredging volumes are included.

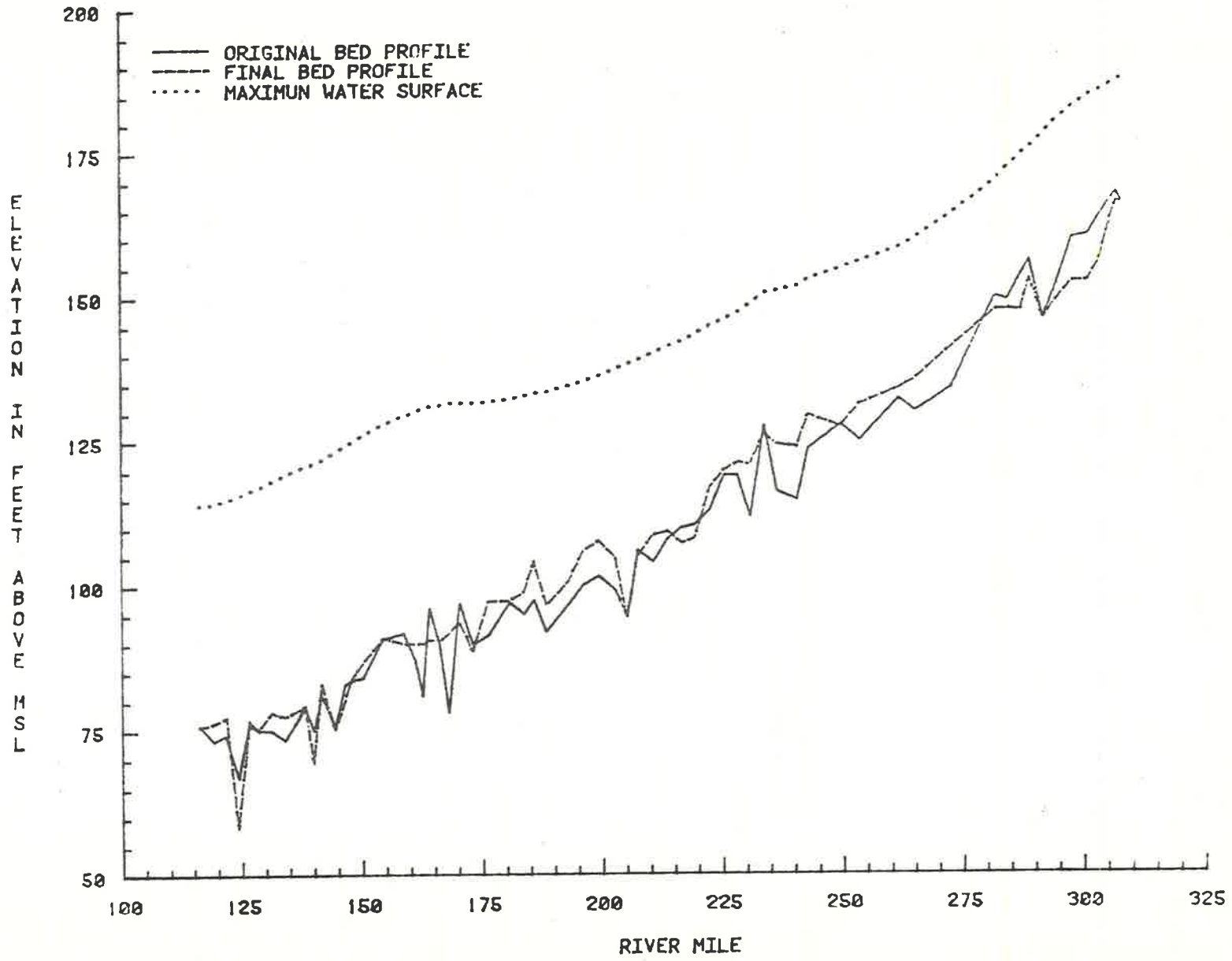

Figure 20.13 Beginning and final bed profiles and maximum water surface elevations for natural conditions (Run No. 1).

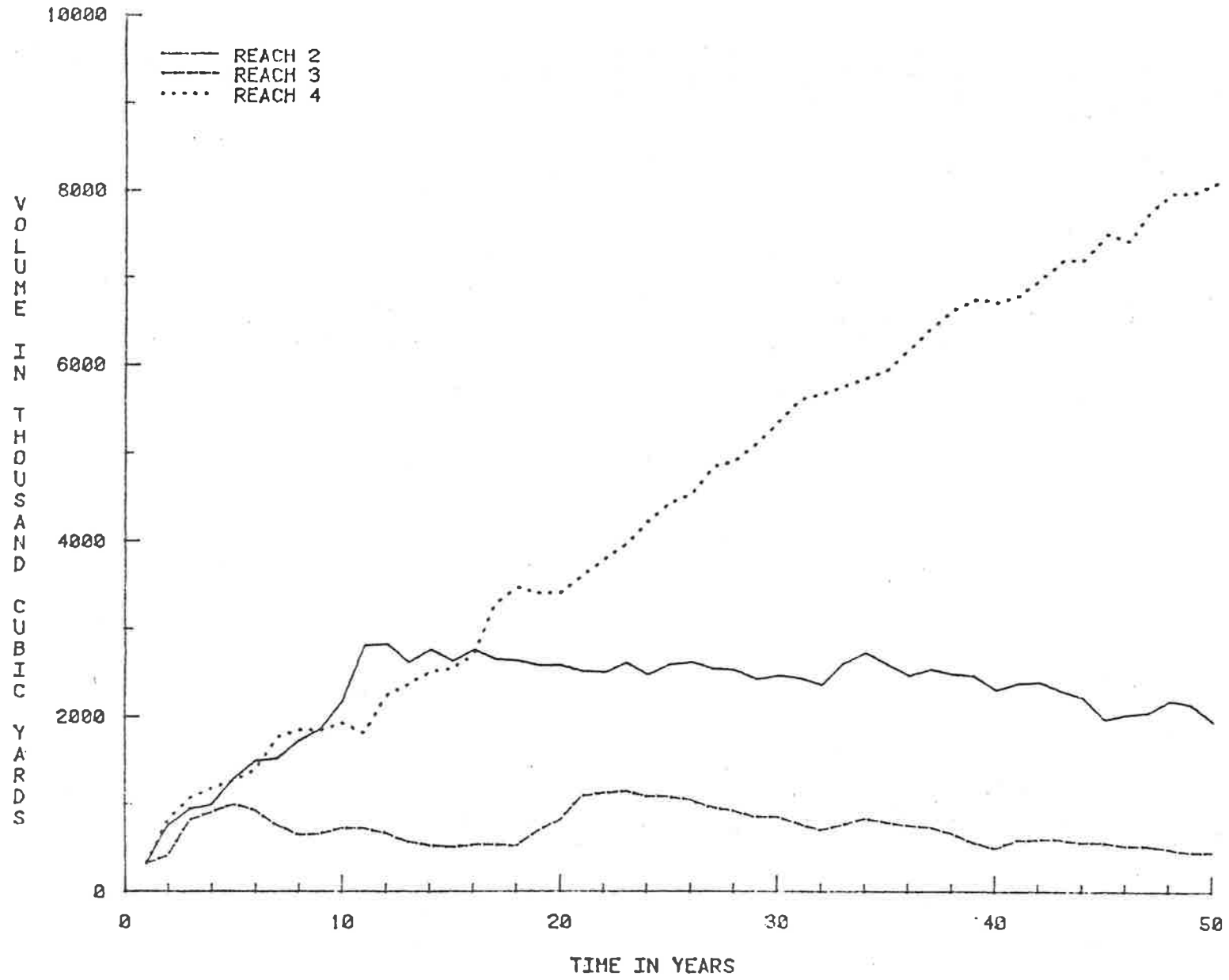

Figure 20.14 Cumulative degradation and aggradation volumes in the main stem for natural conditions (Run No. 1).

the main stem segments, except the Greenwood Cutoff, are depositing for the 50-year simulation cycle. River Segment No. 4 (from Greenwood to Arkabutla Dam) is filling, particularly below the P-Q Floodway. This is due to severe degradation in the P-Q Floodway.

The cumulative degradation and aggradation in the major tributaries (River Segments No. 5, 6, and 7) is shown in Figure 20.15. As indicated by model results, the Yalobusha River (River Segment No. 5) is aggrading, which agrees with observations by the U.S. Army Corps of Engineers (Design Memorandum No. 41). This river has been filling with sediment since the enlargement of the channel cross section in 1954. River Segment No. 6 (P-Q Floodway and the Little Tallahatchie River) is degrading according to model calculations. This also agrees with observations by the U.S. Army Corps of Engineers. The river bed gradient of the Little Tallahatchie River is about four times that of the main stem river due to construction of the P-Q Floodway. Degradation in the P-Q Floodway was so severe that extensive emergency dredging was required to maintain the Tallahatchie River below the mouth of the P-Q Floodway. The Yocona River (River Segment No. 7) is sensitive to the water surface in the P-Q Floodway. The simulated results show that the Yocona River is almost in a state of equilibrium.

Examples of the stage-discharge relationship just below Greenwood Bendway (river mile 162.5) during the first year, 10th year, 30th year, and 47th year are displayed in Figures 20.16. The 47th year was selected because it closely approximated the 1973 flood. These figures indicate the stage-discharge relationship at the station is consistent with time for the natural condition.

Run No. 2 (Plan E)

The net rate of sediment deposition in the main stem utilizing Plan E conditions increased approximately 400 percent. That is, the net depositional rate in the main stem is about 840,000 cubic yards per year. This is due to the enlargement of the channel, the increase in the sediment supply from Abiaca Creek (about 500 percent), and the increase in the degradation along the P-Q Floodway (about 40 percent). Lowering the water surface levels in the Tallahatchie enhances degradation in the P-Q Floodway.

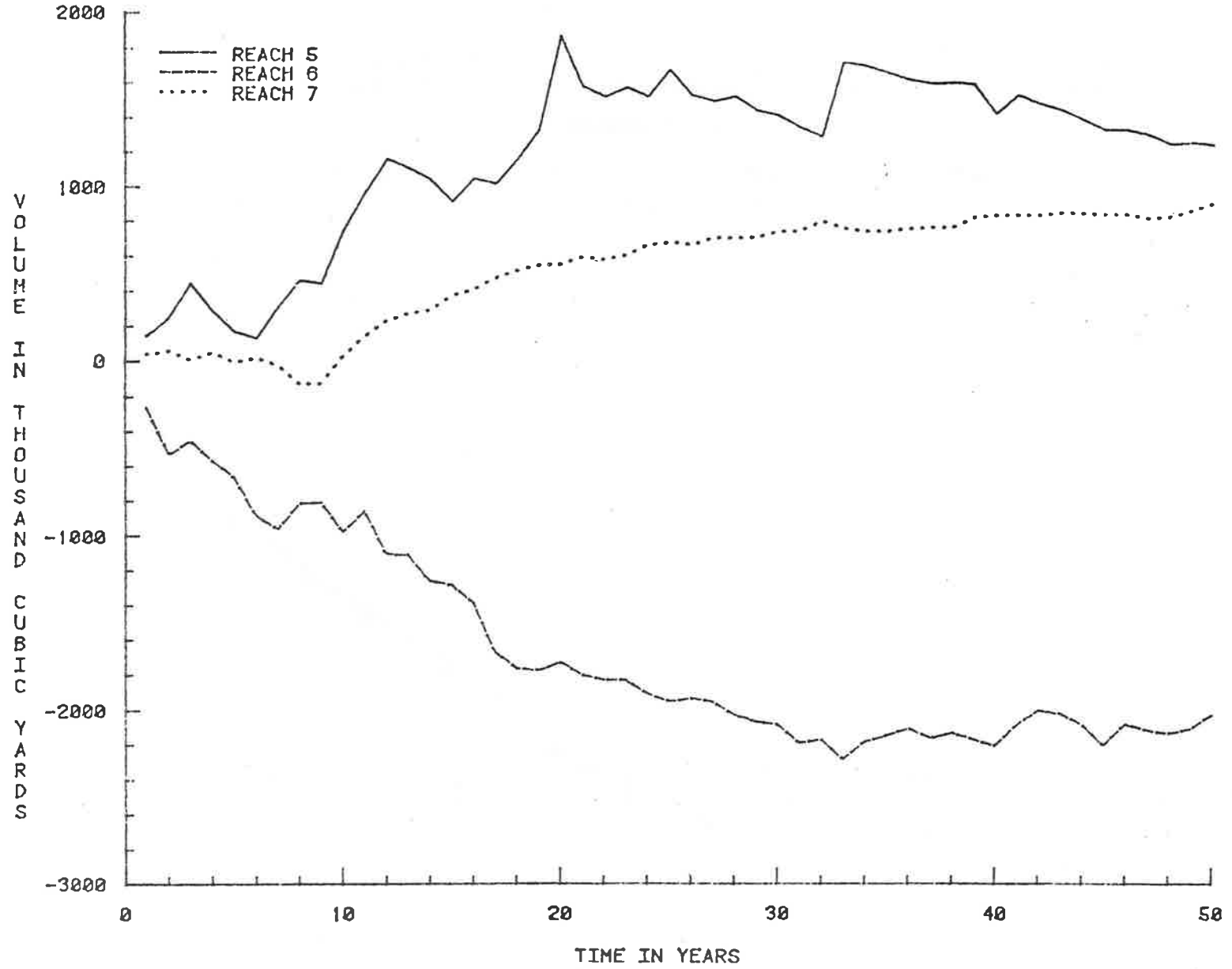

Figure 20.15 Cumulative degration and aggradation volumes in the major tributaries for natural conditions (Run No. 1).

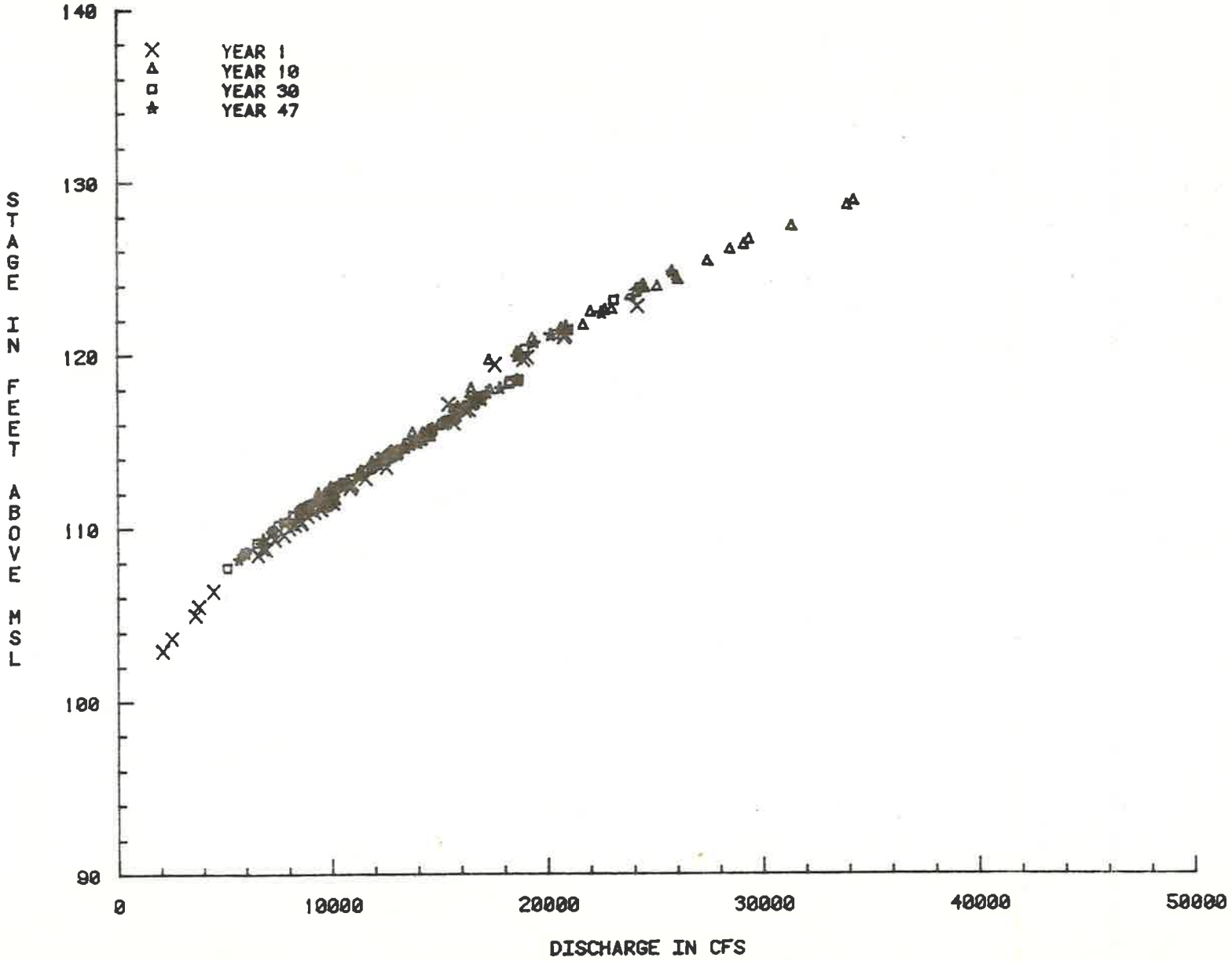

Figure 20.16 Stage discharge relationship downstream of the Greenwood Bendway (river mile 162.5) for natural conditions.

Figure 20.17 shows the beginning and final bed profiles as well as the maximum water surface elevations along the main stem under Plan E conditions considering 50 years of simulation. This figure clearly indicates that the most important areas causing maintenance problems are the reaches below Abiaca Creek and below the mouth of the P-Q Floodway. The maximum water surface levels are generally higher than those under natural conditions for reaches downstream of Money. Cumulative aggradation volumes in the main stem for 50 years are shown in Figure 20.18. The study shows that deposition rates of Plan E are much larger than those for natural river conditions. The computed average rate of deposition for Plan E decreases with time, which is consistent with changes in hydraulic conditions.

For a detailed examination of Plan E, Figure 20.19 provides the maximum water surface elevations under both the natural and Plan E conditions for the 50-year simulation period. Generally, the maximum water surface elevations are higher for Plan E in the main stem except in the reach near the upstream of Swan Lake (river mile 219.08). The higher water surface elevations in the reach downstream of river mile 200.0 are due to accumulation of sediment for 50 years without maintenance, and the significant increase of sediment supply to the main stem from Abiaca and the P-Q Floodway. The reduction in stage near and upstream of Swan Lake is primarily the result of the Craigside Cutoff.

It is important to mention that if the Plan E channel is allowed to accumulate sediment for 50 years without maintenance, the efficiency of flood stage reduction of Plan E would be significantly decreased. This is further demonstrated in Figure 20.20. In this figure, the annual maximum water surface elevations just below the Greenwood Bendway (river mile 162.5) for both natural and Plan E conditions are plotted. The river stage reduction by implementation of Plan E is only good in the first two years at river mile 162.5. After the channel fills with sufficient sediment, river stage reduction is significantly decreased and finally terminated in some reaches. The stage frequency curves just below the Greenwood Bendway for natural and Plan E conditions are shown in Figure 20.21. These curves indicate that the proposed Plan E can only be effective if maintenance measures such as dredging and/or control of sediment inflows from major sediment contributing tributaries are implemented. This is particularly true for the reach downstream of Money.

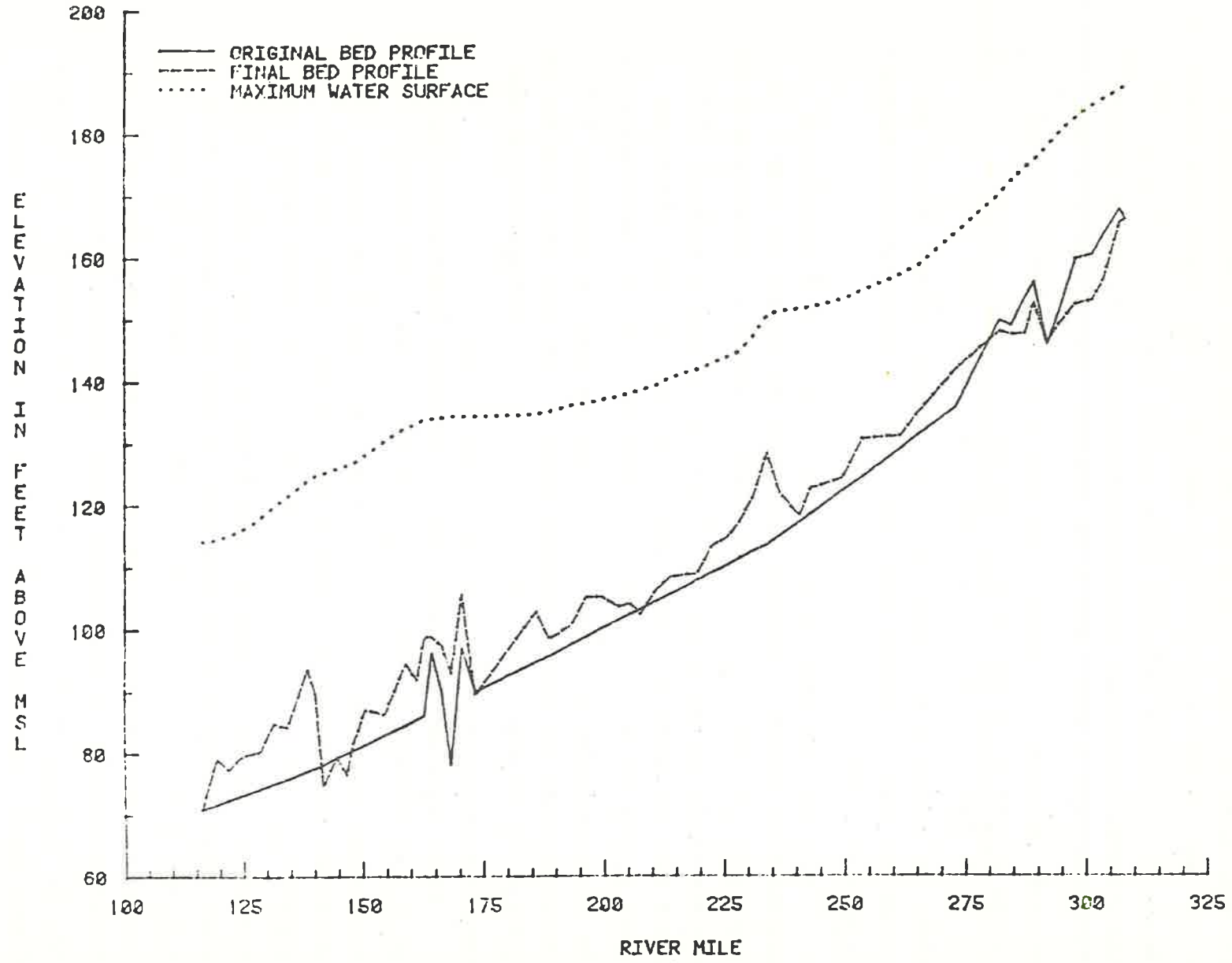

Figure 20.17 Beginning and final bed profiles and maximum water surface elevations for Plan E conditions (Run No. 2).

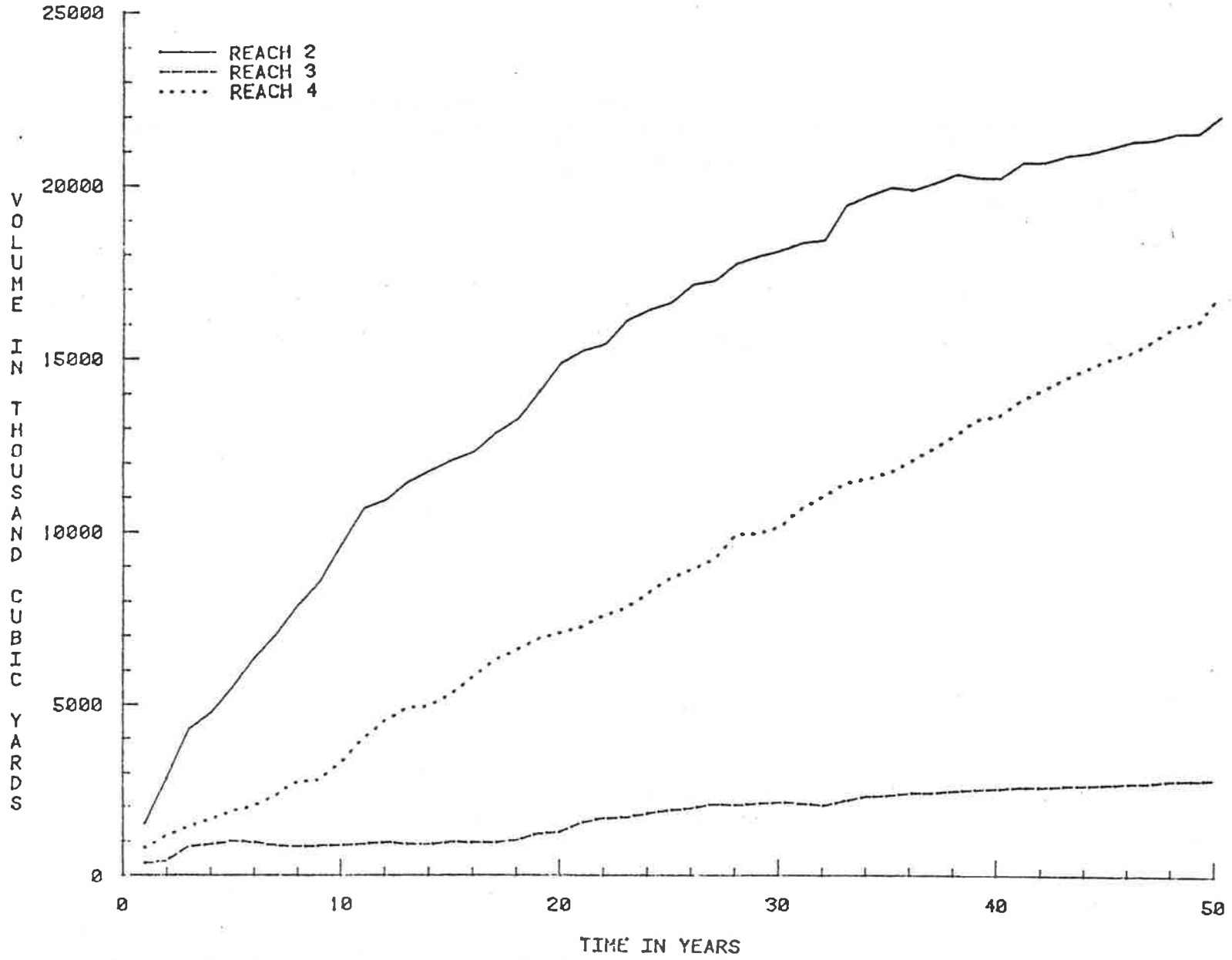

Figure 20.18 Cumulative degradation and aggradation volumes in the main stem for Plan E conditions (Run No. 2).

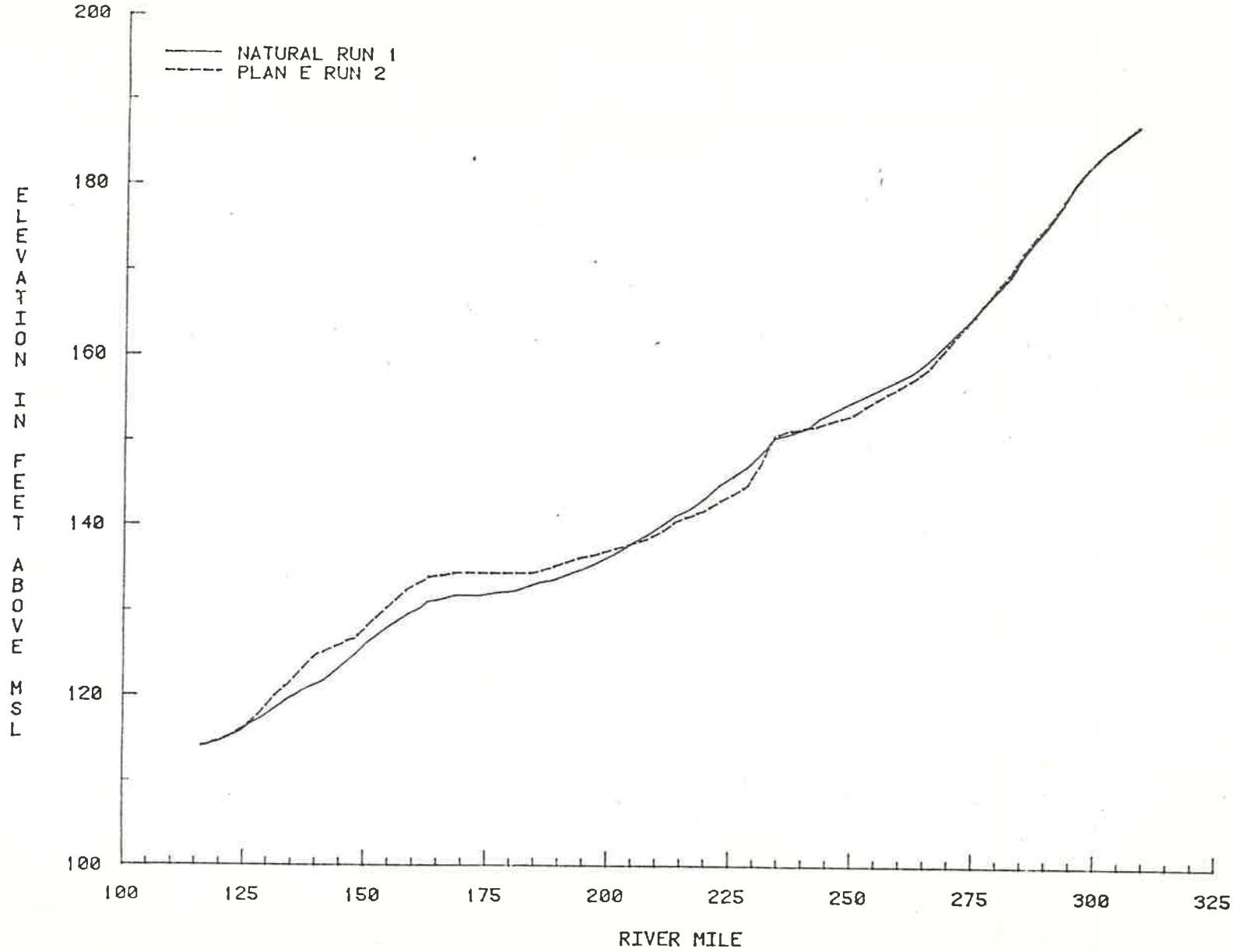

Figure 20.19 Comparison of maximum water surface elevations between natural and Plan E conditions (Runs No. 1 and 2).

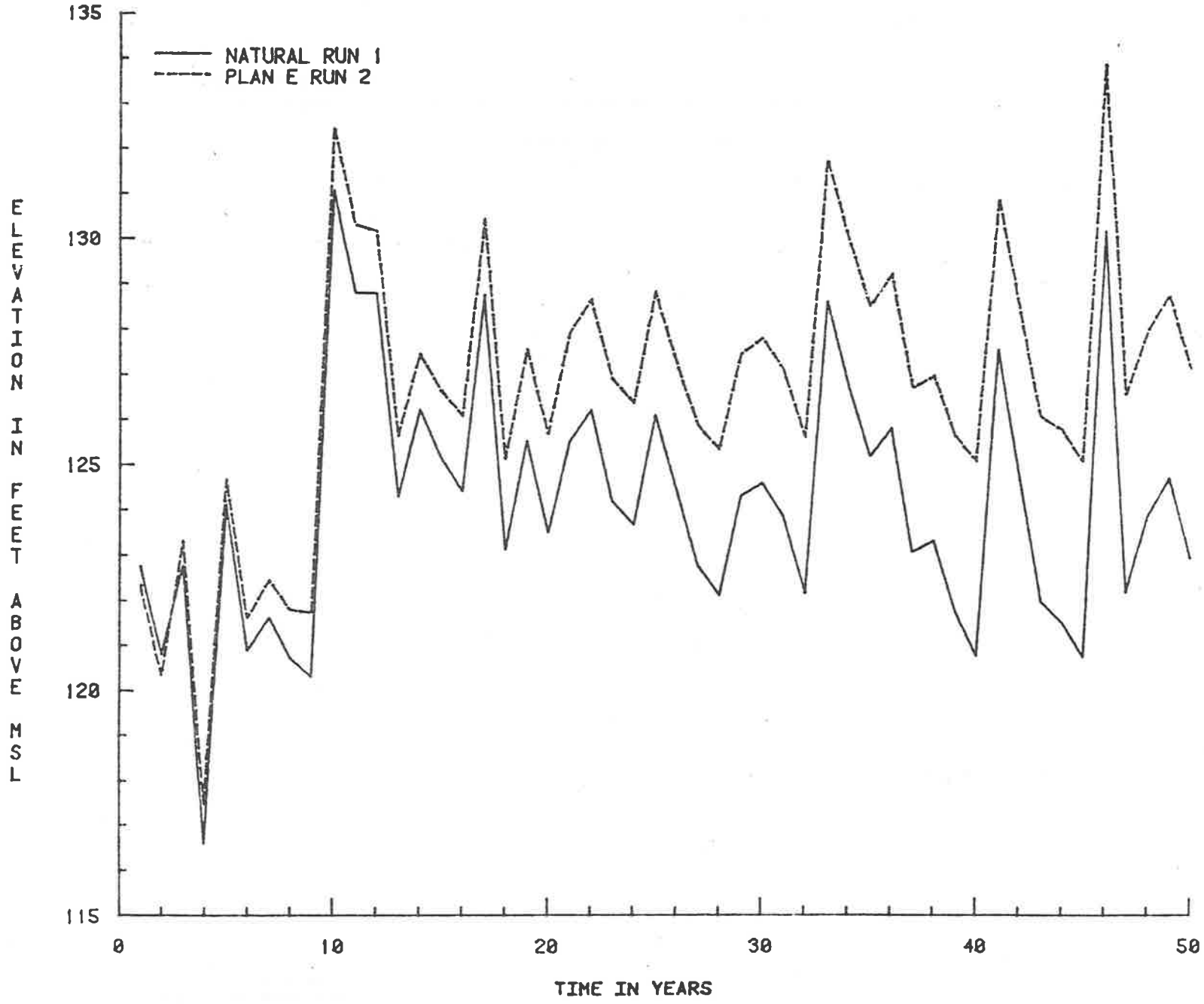

Figure 20.20 Annual maximum water surface elevations just downstream of the Greewood Bendway (river mile 162.5) for natural and Plan E conditions.

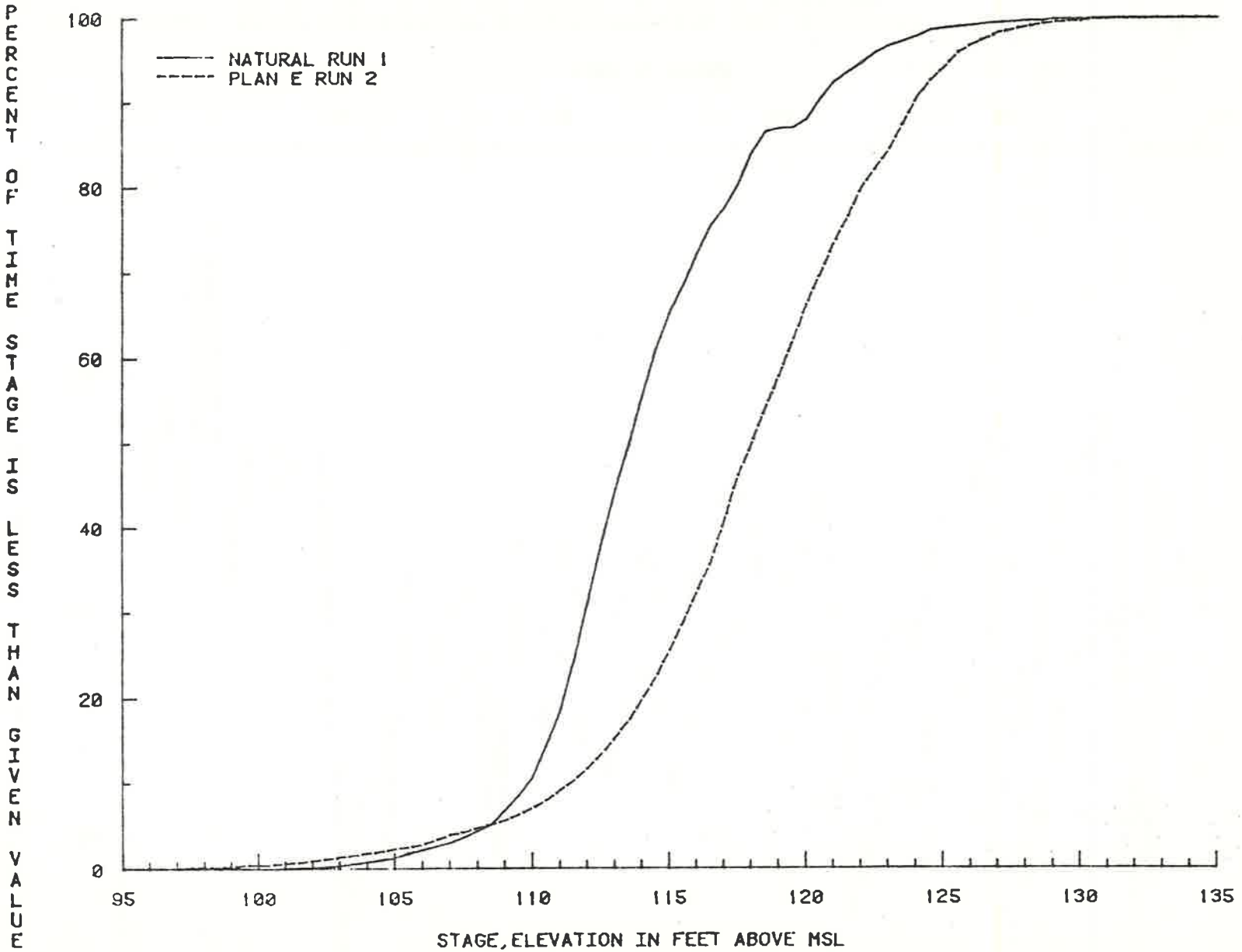

Figure 20.21 Stage frequency curve just below the Greenwood Bendway (river mile 162.5) for natural and Plan E conditions.

The stage-discharge relationship below Greenwood Bendway (river mile 162.5) for different time periods is shown in Figure 20.22. Again, this figure indicates that the proposed Plan E can only be effective for flood control if maintenance dredging, control of sediment supply from tributaries, or other means of maintenance are implemented.

Runs No. 3 and 4 (Control of the Sediment from Tributaries)

Comparison of the responses of Plan E and natural conditions show that reduction of sediment from Abiaca and Tillatoba is necessary. With a 50 percent reduction in sediment inflow from Abiaca and Tillatoba (Run No. 3), a 24 percent reduction in net filling rate along the main stem is achieved. A further control in tributary sediment inflow with a 50 percent reduction of sediment from Abiaca, Pelucia, Big Sand, and Tillatoba Creeks (Run No. 4), results in a 31 percent reduction in the net filling rate along the main stem. Figure 20.23 shows the cumulative degradation and aggradation volumes in the main stem (sum of River Segments No. 2, 3, 4, and 8) for Runs No. 2, 3, and 4. Figure 20.24 demonstrates that the maximum water surface elevations are smaller for Run No. 4 compared to Run No. 2. These figures illustrate the effectiveness of maintaining the main stem by controlling the sediment from major contributing tributaries.

Runs No. 5 and 6 (Effect of Channelization and/or Land Use)

The effect of channelization on the system response was evaluated by assuming a 15 percent increase in peak flows on tributaries and the main stem (Run No. 5). In addition, the effect of future land use changes on the river system was evaluated by assuming that peak flows would be increased on tributaries by an additional 15 percent. Flows on the main stem were determined by the model (Run No. 6). Results of evaluation are presented in Figure 20.25 with regards to cumulative net filling volumes. This figure shows that if all peak flows are increased 15 percent on both tributaries and the main stem, the rate of net filling in the main stem would increase about 13 percent. If an additional 15 percent increase in peak flows on the tributaries is imposed, an additional 19 percent increase in the net filling rate in the main stem would result.

The maximum water surface elevations along the main stem for the 50-year simulation under Runs No. 2, 5, and 6 are shown in Figure 20.26.

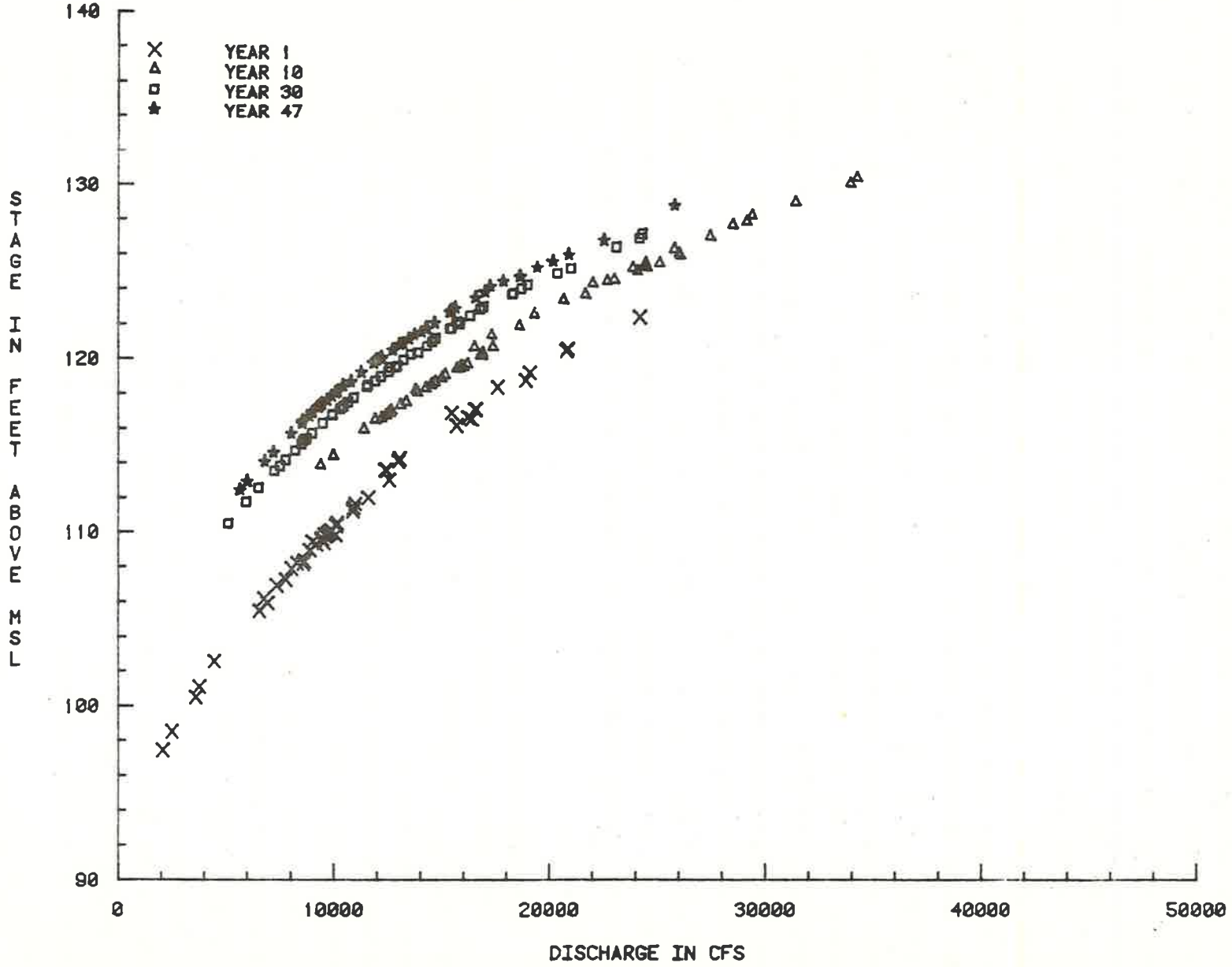

Figure 20.22 Stage discharge relationship at Greenwood Bendway (river mile 162.5) for Plan E.

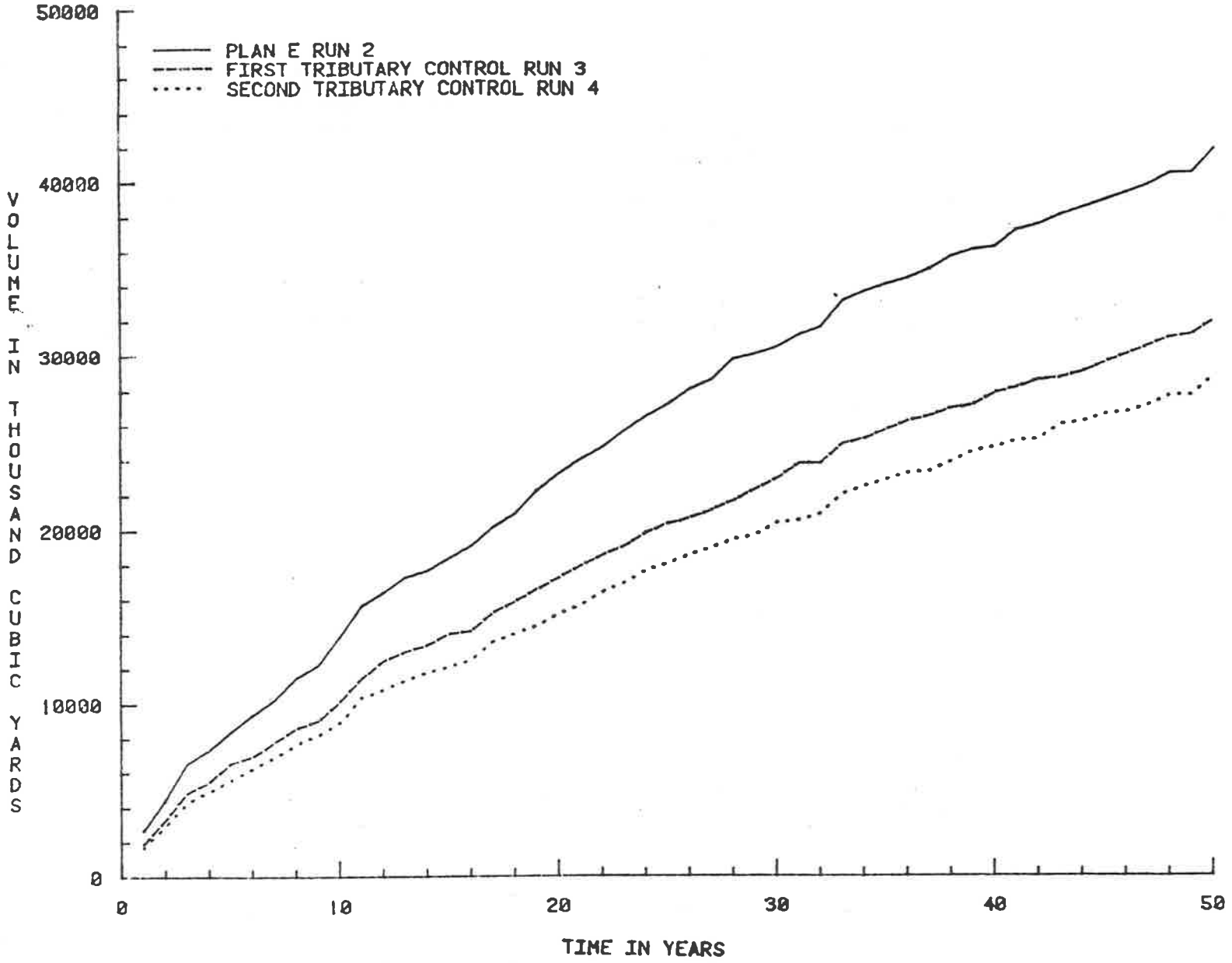

Figure 20.23 Cumulative degradation and aggradation volumes in main stem for Runs No. 2, 3, and 4 (control of tributary sediment inflow).

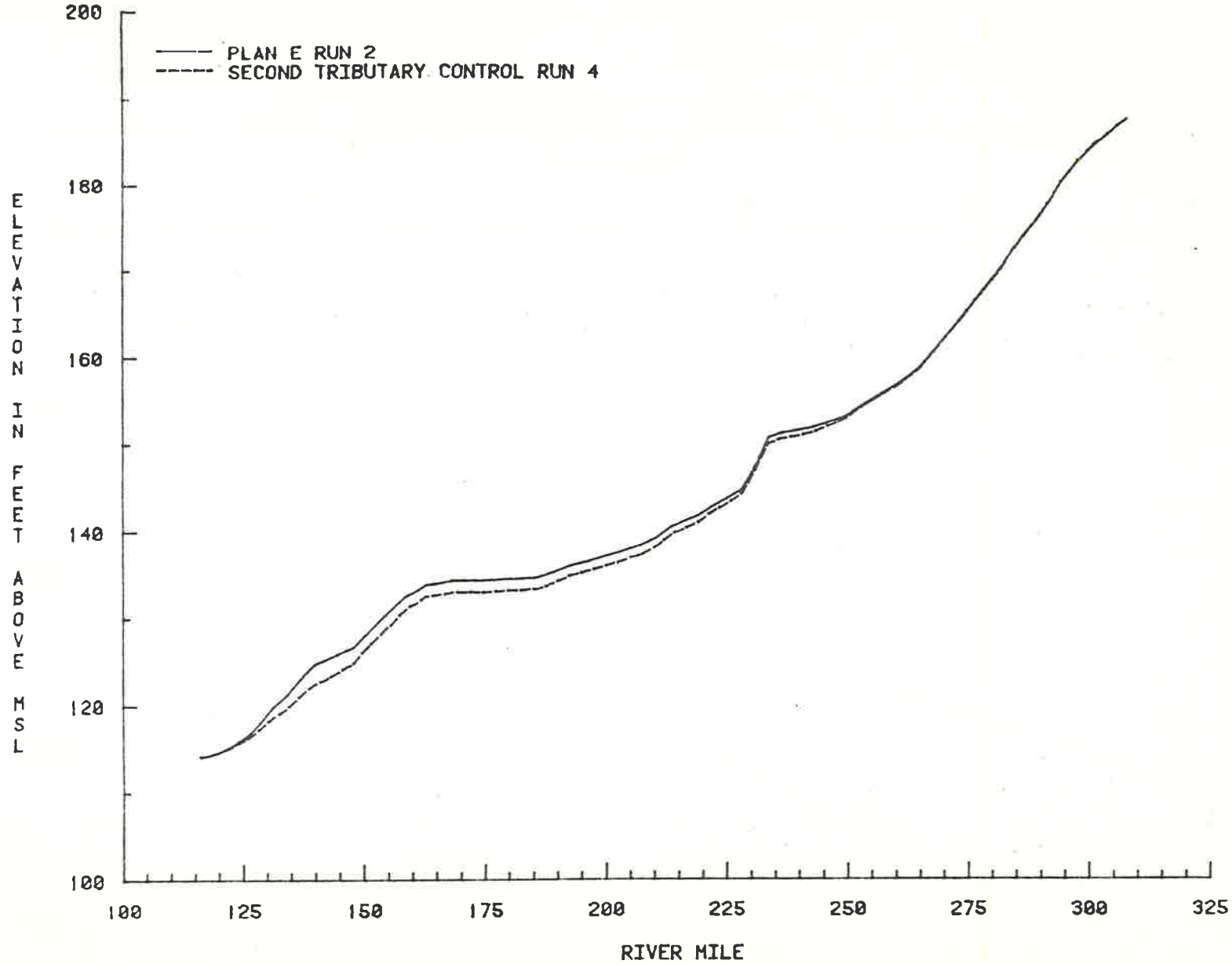

Figure 20.24 Maximum water surface elevations for Runs No. 2 and 4 (control of tributary sediment inflow).

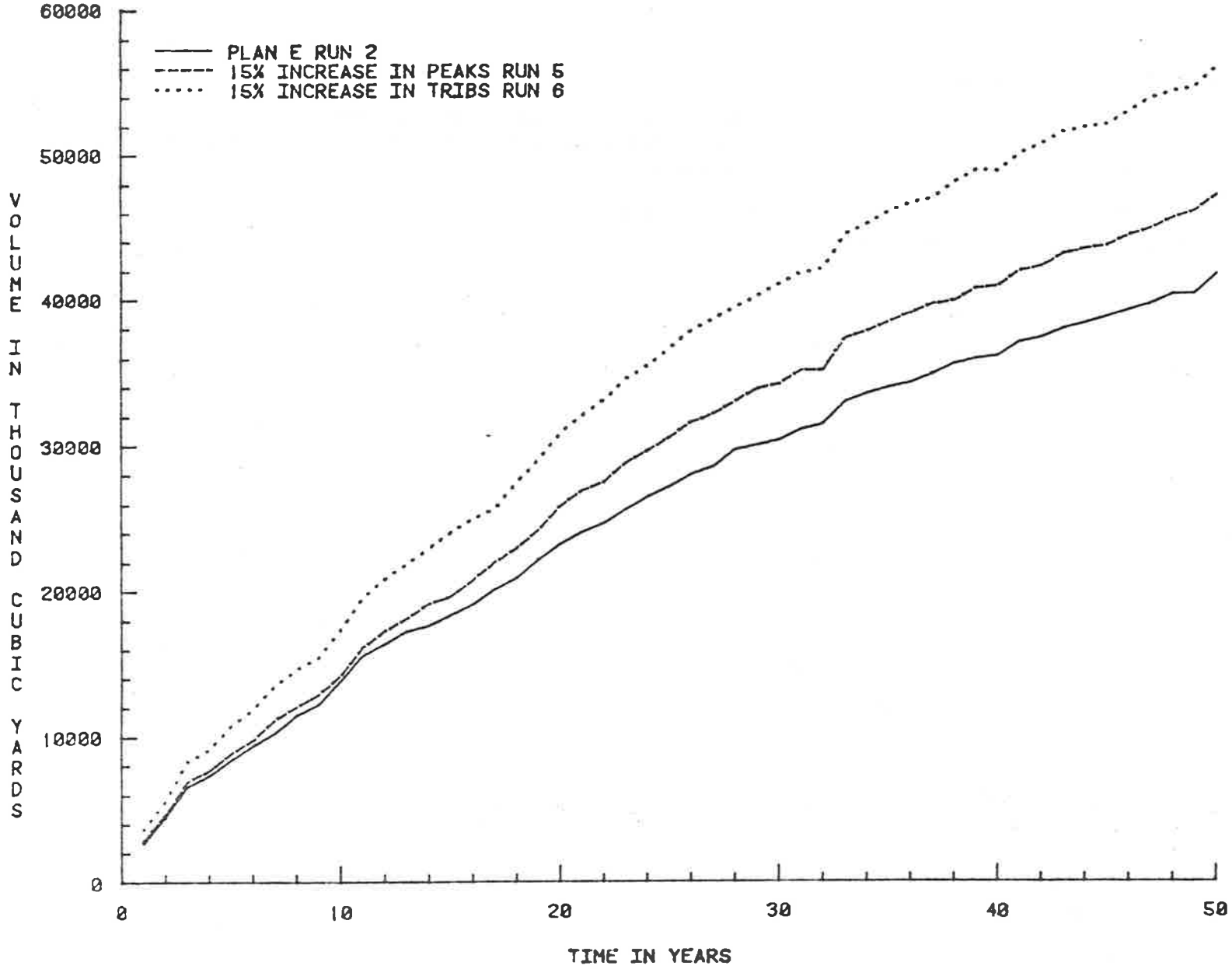

Figure 20.25 Cumulative degradation and aggradation volumes in the main stem for Runs No. 2, 5, and 6 (effect of channelization and land use changes).

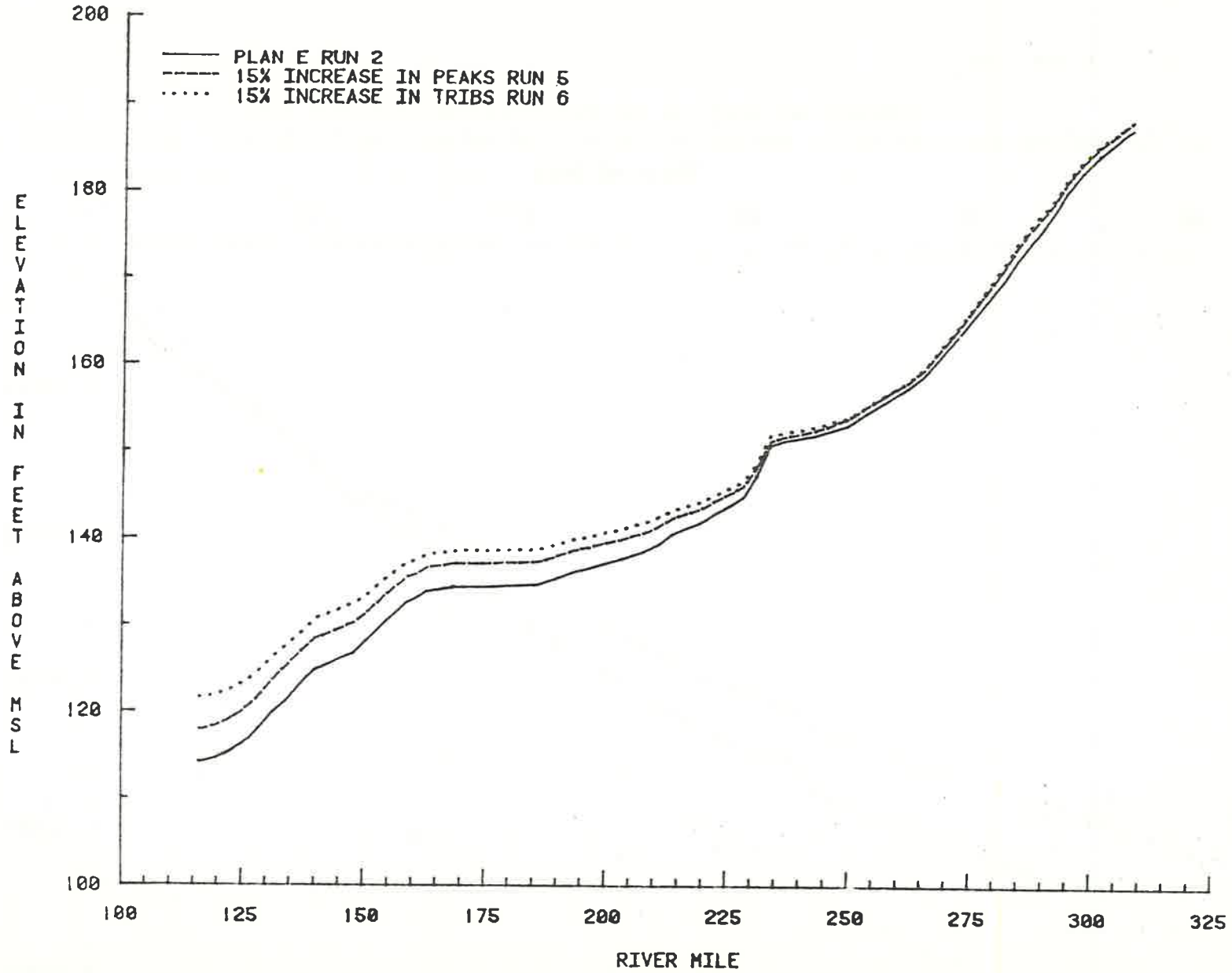

Figure 20.26 Maximum water surface elevations for Runs No. 2, 5, and 6 (effect of channelization and land use changes).

In general, both the channelization and the land use change would induce the increase in the river stage.

Runs No. 7 and 12 (Annual and Every 5-year Dredging)

In addition to controlling the inflow of the tributary sediment, another effective means of maintaining the main stem is to utilize maintenance dredging. In this study, two time intervals (annual and every five years) of dredging were examined. The cumulative maintenance dredging volume of the two time intervals, listed in Table 20.3, is shown in Figure 20.27. If annual dredging is implemented, the total amount of maintenance dredging for 50 years is 71,346,000 cubic yards (or 1,426,000 cubic yards annually). If every five years the total amount of dredging is 63,608,000 cubic yards (or 1,272,000 cubic yards annually), the dredging quantity decreases 11 percent over the annual dredging.

The maximum water surface elevations along the main stem under Plan E, annual dredging, and every five years dredging (Runs No. 2, 7, and 12) for the 50-year simulation are presented in Figure 20.28. This figure shows that the river stages with dredging are much lower than those with no maintenance dredging. The proposed plan of flood reduction can only be effective with maintenance in the main stem. In addition, the maintenance dredging every five years would practically provide the same level of flood reduction as with annual dredging. A comparison of maximum water surface elevations for both natural and Plan E with every five-year dredging (Runs No. 1 and 12) is given in Figure 20.29. This figure shows that the Plan E channel with a dredging interval every five years will provide good flood protection. This is further demonstrated in Figures 20.30. The figure shows that the stage-discharge relationship at river miles 162.5 is not significantly changing with time. In addition, it is important to mention that both annual and every five-year dredging, as shown in Table 20.2, would substantially increase the degradation in the P-Q Floodway. A refined analysis to obtain an optimum dredging schedule is necessary.

Run No. 8 (Construction Scheduling)

In reality, the construction of Plan E cannot be completed immediately. On the average, the rate of construction would be approximately 10 miles per year. The construction schedule was tentatively

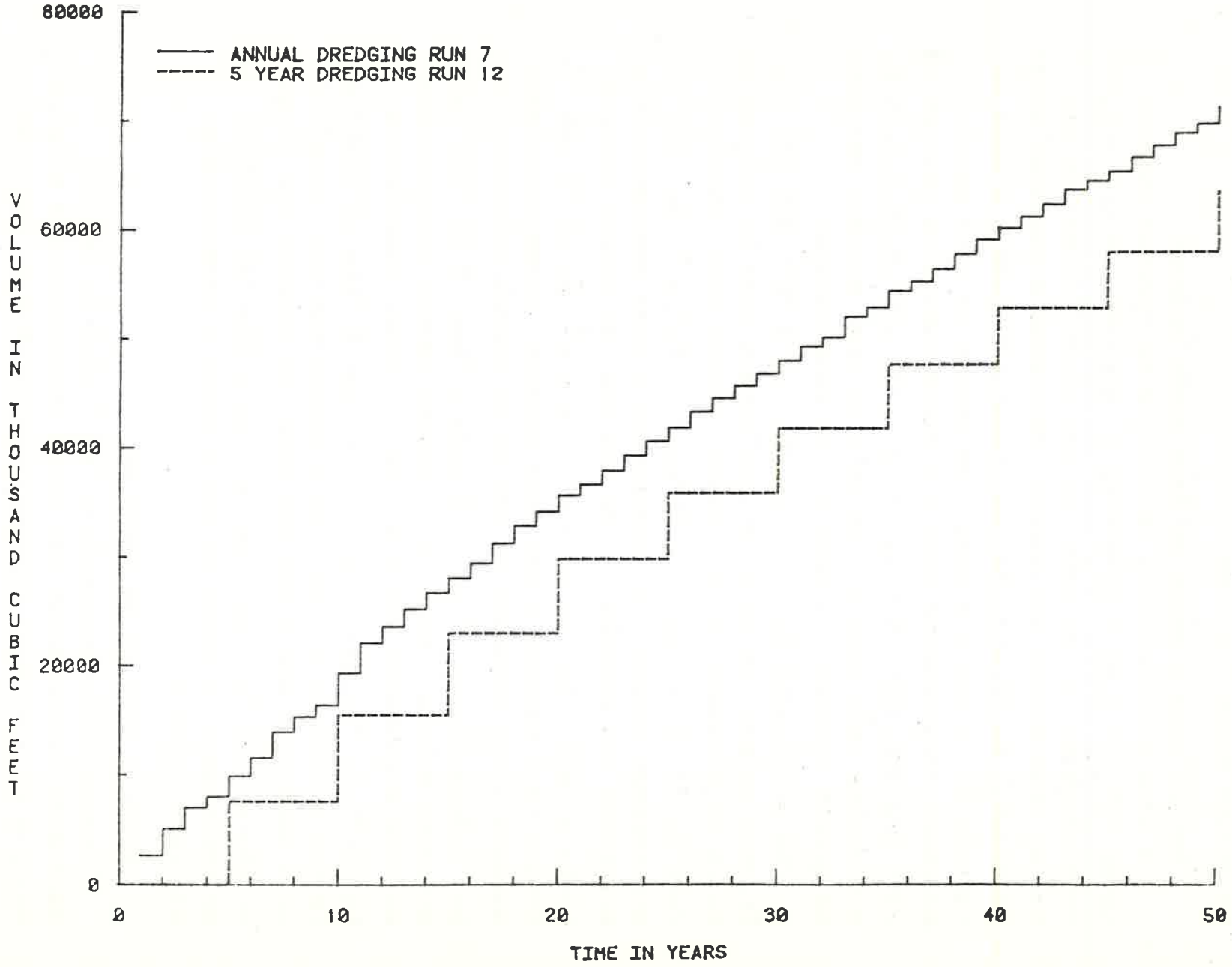

Figure 20.27 Cumulative dredging volumes in the main stem for annual dredging and every 5-year dredging (Runs No. 7 and 12).

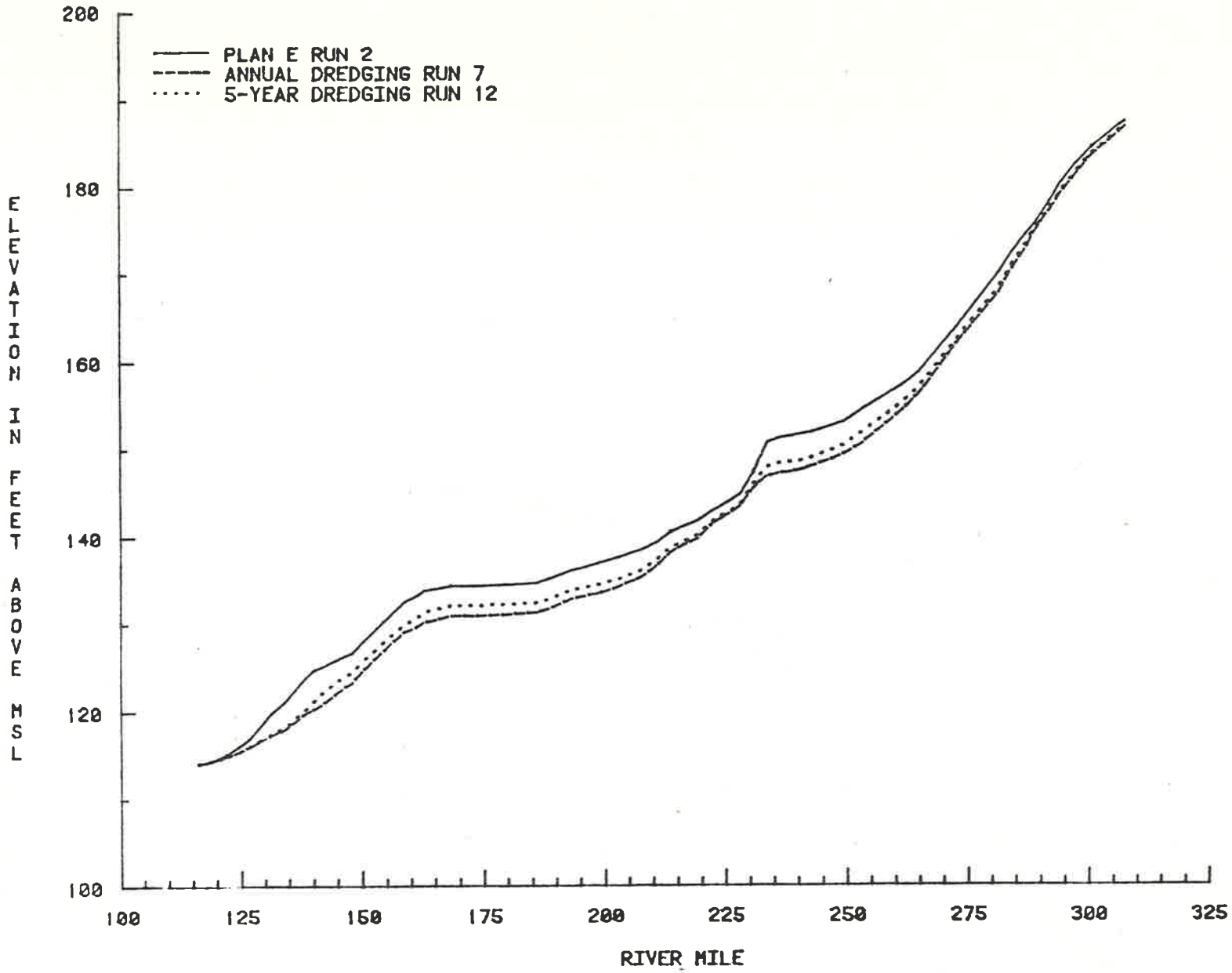

Figure 20.28 Maximum water surface elevations for Runs No. 2, 7, and 12 (effectiveness of dredging).

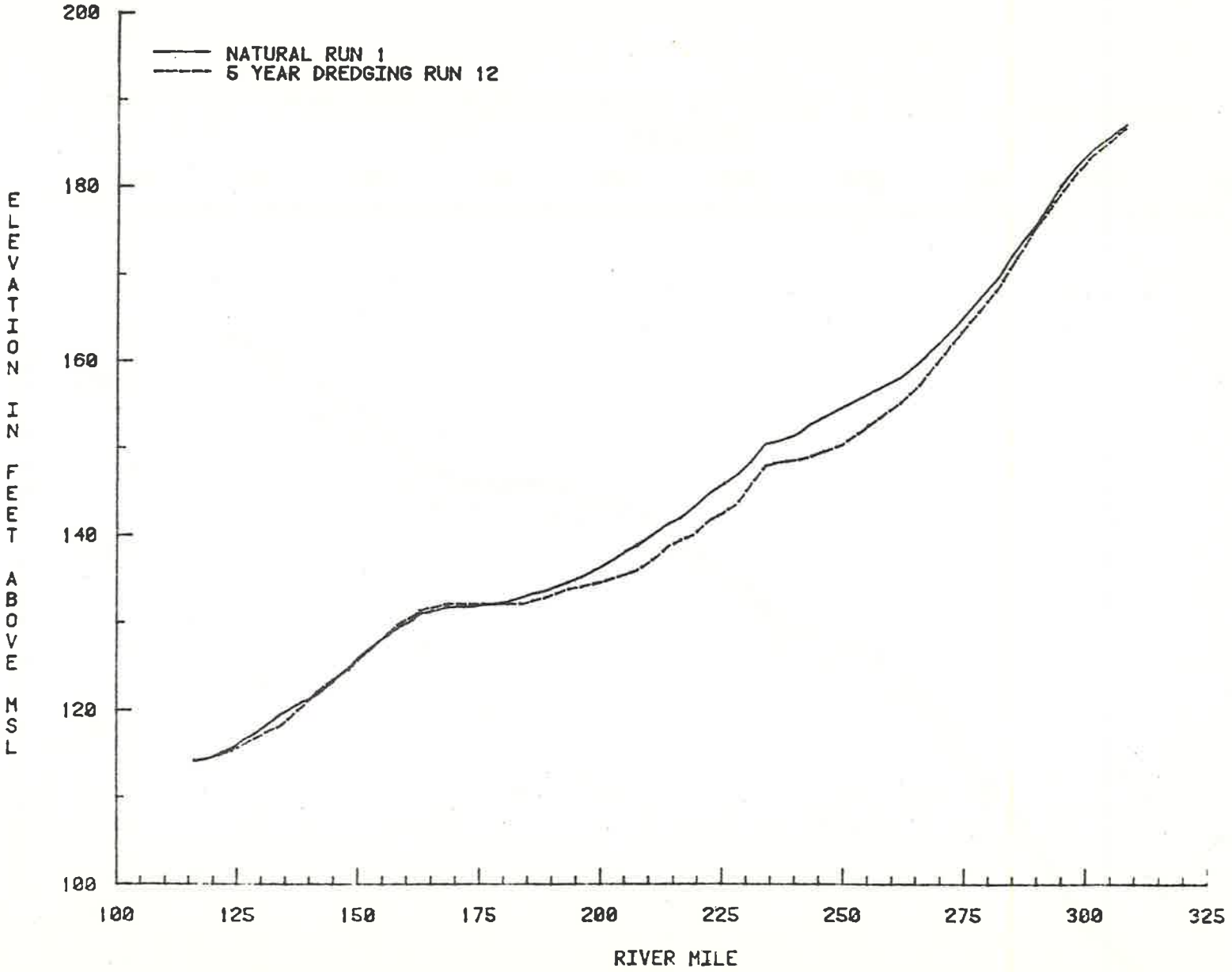

Figure 20.29 Maximum water surface elevations for Runs No. 1 and 12.

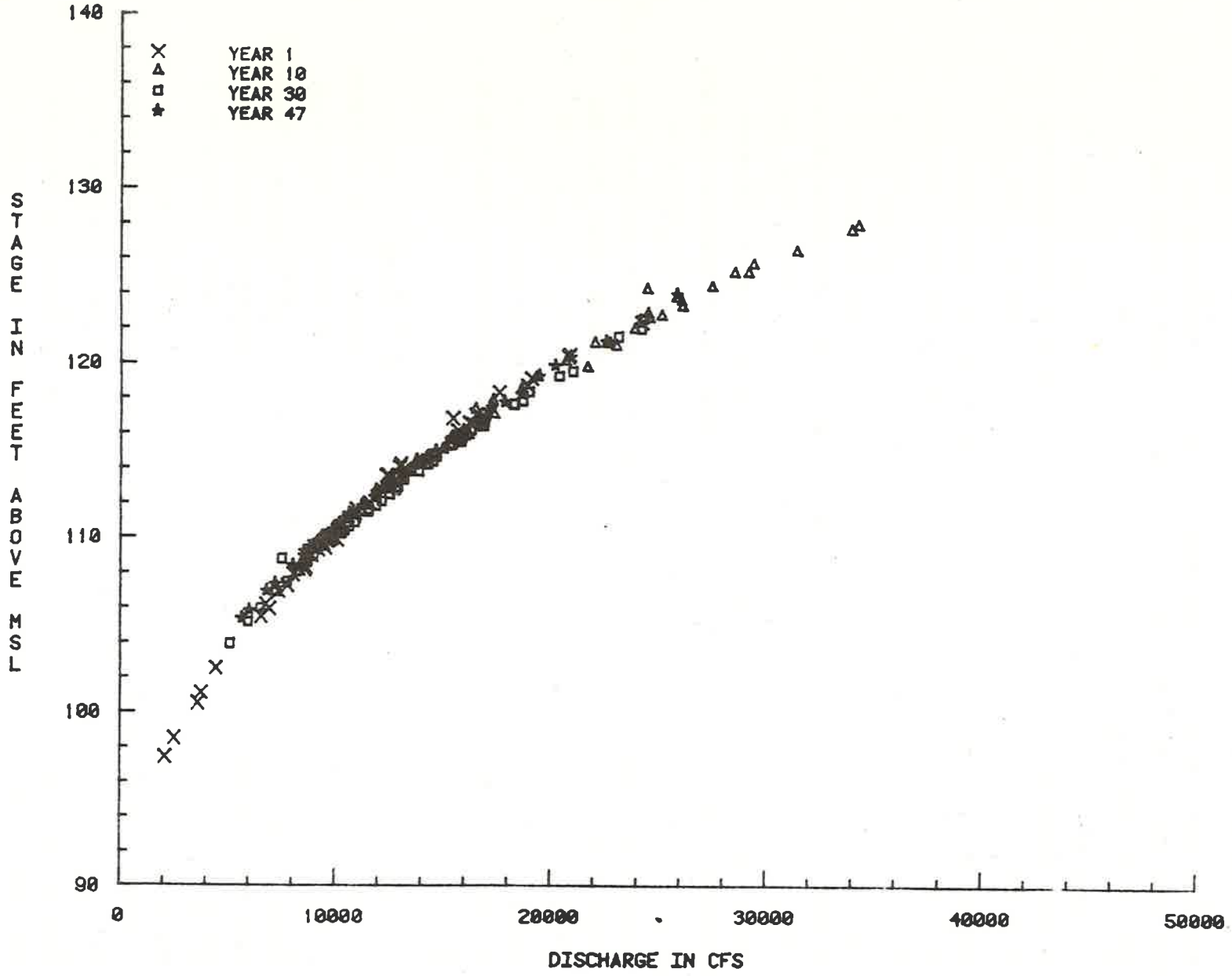

Figure 20.30 Stage discharge relationship at Greenwood Bendway (river mile 162.5) for every 5-year dredging.

determined by the U.S. Army Corps of Engineers to proceed upstream from Yazoo City in two-year increments. At the end of eight years, construction would have proceeded from Yazoo City to Greenwood. The construction would be completed to the mouth of the P-Q Floodway at the end of the 14th year. The total Upper Yazoo Project would be completed at the end of the 18th year after initiation of construction.

Run No. 8 studied the effect of construction on the system. Results of cumulative degradation and aggradation in the main stem are shown in Figure 20.31. This figure shows that at the beginning of construction, the net depositional rate in the main stem is smaller than that for Plan E. The rates of filling are close to one another after approximately 20 years. The total volume of degradation and aggradation is smaller for Run No. 8 as compared to the original Plan E (Run No. 2) because of the gradual rate of channelization. This justifies the assumption that immediate channelization is more conservative than construction scheduling if sedimentation is the major concern. However, considering the flooding potential, the assumption of immediate completion of Plan E is less conservative than the case with construction scheduling. Figure 20.32 gives the annual maximum stages at Swan Lake (river mile 219.08) for Runs No. 2 and 8. This figure shows that the flood stages, with the proposed construction schedule, are generally higher during the first 12 years. A refined analysis considering construction scheduling is important for the implementation of the Plan E channel.

Runs No. 13 and 14 (Modification of the Plan E Channel)

Because of severe degradation in the P-Q Floodway, it is desirable to raise the base level near the mouth of the P-Q Floodway. The large amount of deposition in the reach between Belzoni and Greenwood indicates that improved sediment transporting capacity is needed in this reach. The modification of the Plan E channel design as assumed in Run No. 13 would cause a higher base level from Greenwood to Darling, and an increase in the sediment transporting capacity from Belzoni to Greenwood. This would be achieved by narrowing the channel width. The original plan for modification in the reach from Belzoni to Greenwood considers the lowering of the channel bottom at Belzoni about two feet. However, it was decided not to make this change after it was identified that the sediment transport capacity is decreased by deepening the channel.

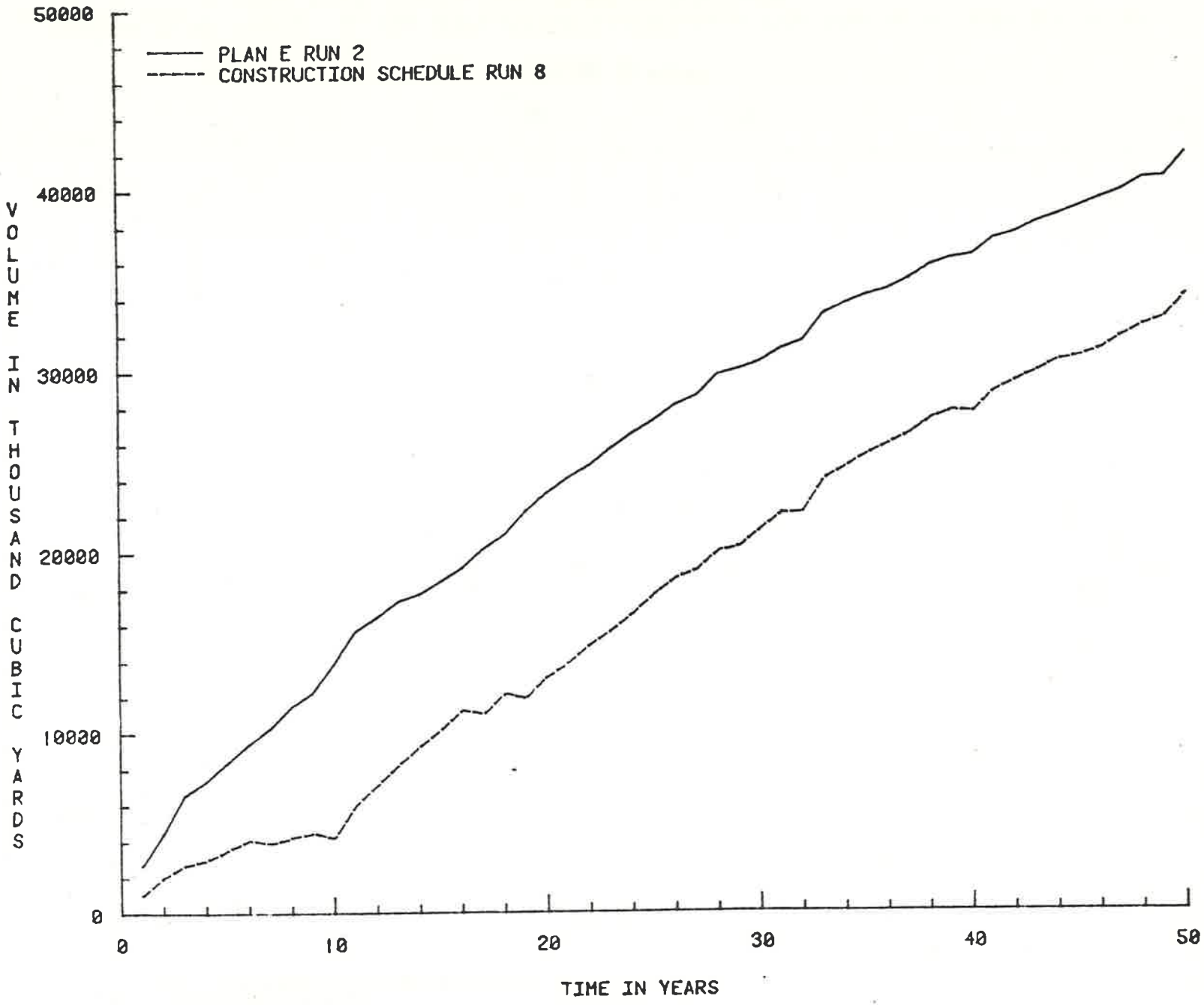

Figure 20.31 Cumulative degradation and aggradation volumes in the main stem for Runs No. 2 and 8 (effect of construction scheduling).

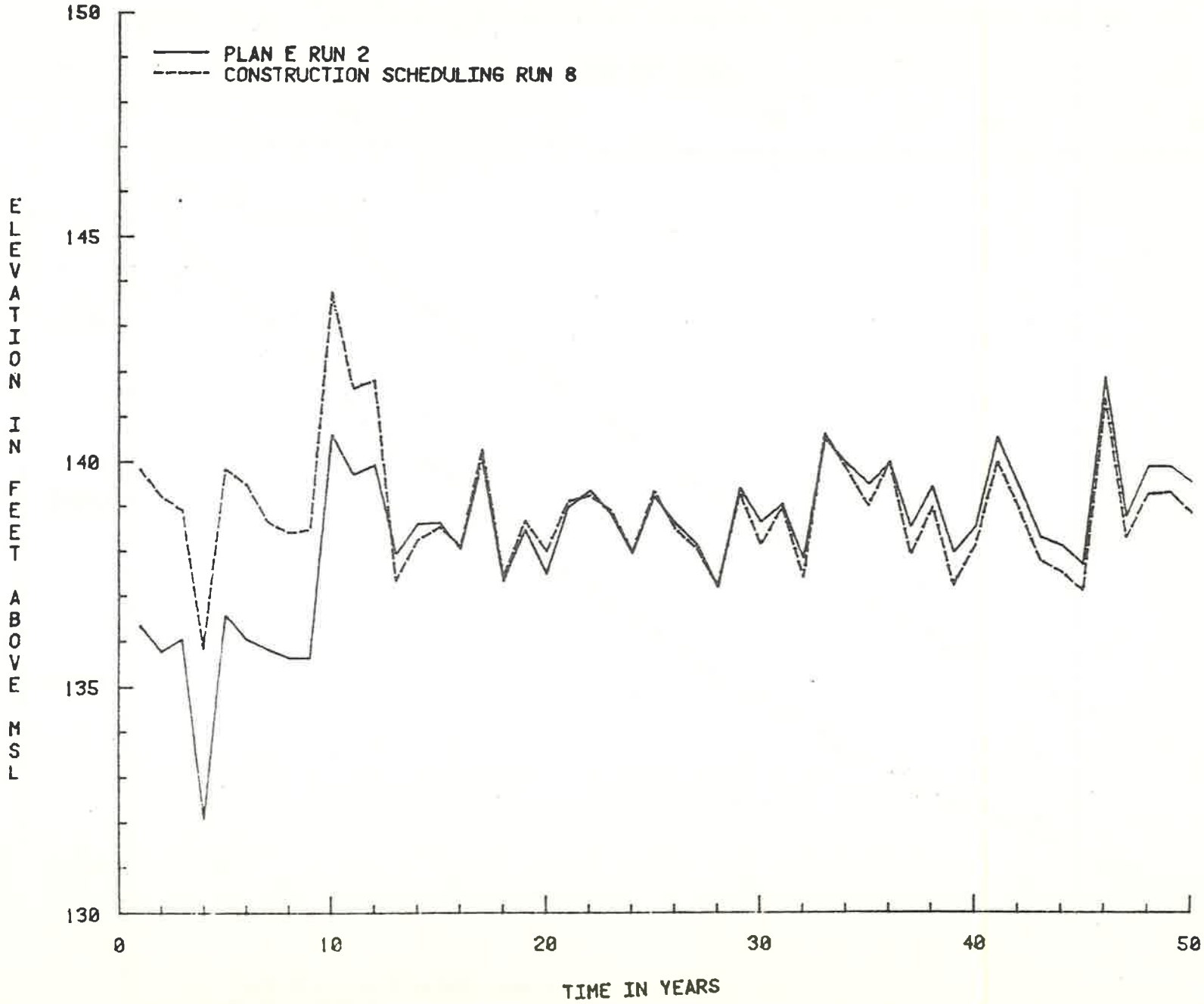

Figure 20.32 Annual maximum water surface elevations at Swan Lake (river mile 219.08) for Plan E and construction scheduling conditions.

Figure 20.33 compares the cumulative aggradation volumes in the main stem for Runs No. 3 and 13. This comparison indicates that channel modification will reduce the net filling rate by approximately seven percent. Reduction of the net degradation and aggradation compared to the original Plan E is about 29 percent.

The best alternative plan without maintenance dredging is assumed to be a combination of controlling tributary sediment (Run No. 4) and the channel modification (Run No. 13). This alternative study run is called Run No. 14. Figure 20.34 shows the cumulative aggradation volume in the main stem for Runs No. 2 (original Plan E) and 14 (the best alternative). As shown in Table 20.2 and Figure 20.34, the best alternative plan without maintenance dredging would reduce the net filling rate in the main stem about 37 percent. A comparison of the maximum water surface elevations along the main stem between the original Plan E and the best modified Plan E is given in Figure 20.35. Comparison indicates the best alternative would also provide a better level of flood protection compared to the original Plan E. However, the maintenance dredging is still required to provide adequate flood protection. The requirement for maintenance dredging is strongly indicated in Figure 20.36. This figure shows the change in the stage-discharge relationship at Greenwood and Swan Lake over 50 years of simulation for Run No. 14. As can be seen, both locations experienced an increase in the stage for a given discharge over a period of time. This is particularly true for reaches downstream of Money.

Runs No. 11 and 15 (Impact on the Lower Reach and the Proposed 9-Foot Navigation Channel)

The majority of study runs were conducted for the river system above Belzoni. The sediment deposition rate caused by the Upper Yazoo Project on the lower reach, from Belzoni to Vicksburg, was evaluated in Run No. 11. As presented in Table 20.2, the net deposition and aggradation volumes above Belzoni are very close for Runs No. 2 and 11. This indicates that the assumption of Belzoni being a downstream control for evaluating the response of the Plan E channel is reasonable.

The feasibility analysis of the proposed nine-foot navigation channel was studied in Run No. 15. This study run assumed that a minimum pool with a water surface elevation of 65 feet exists at the proposed lock and dam near Vicksburg (for simplicity it was assumed to exist

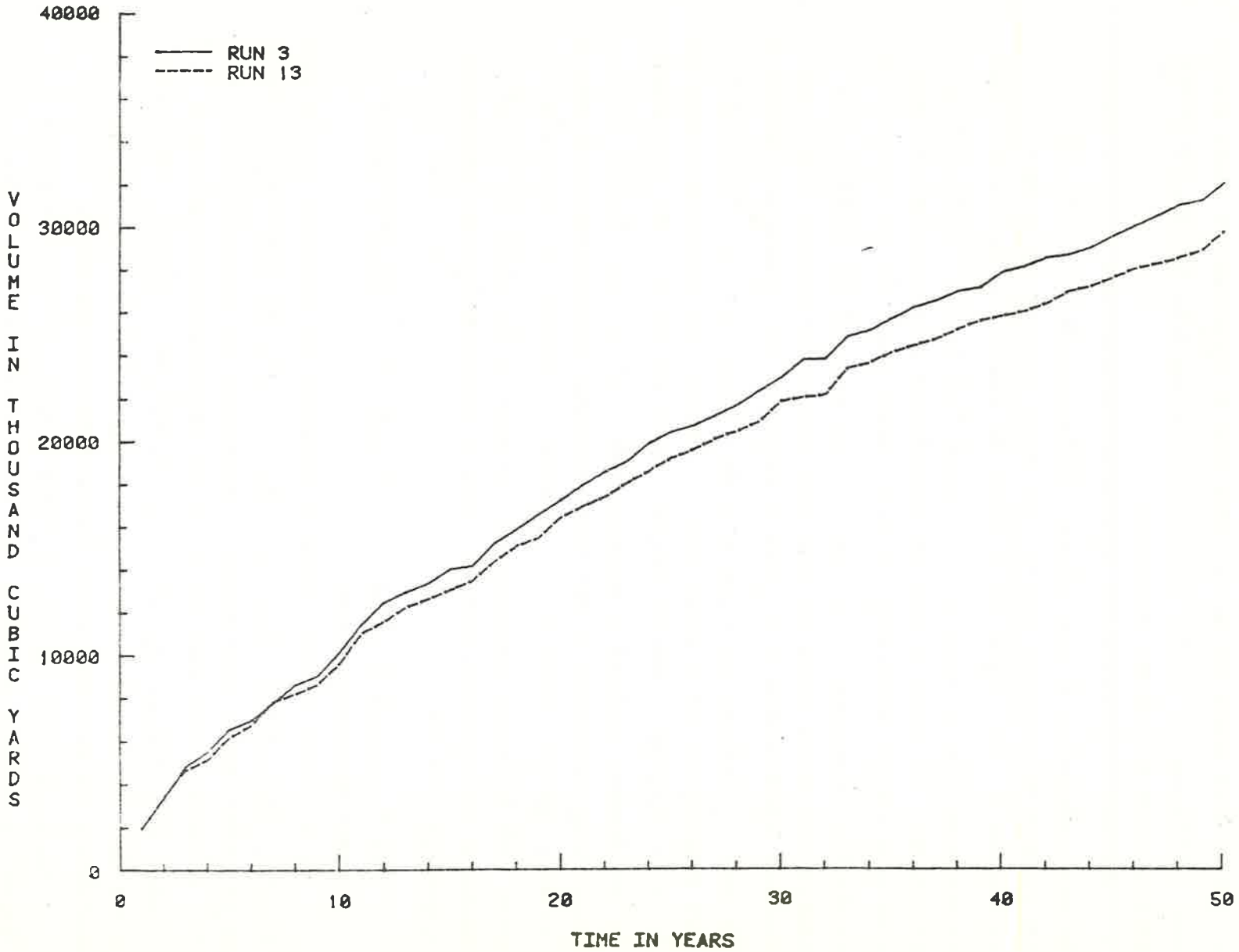

Figure 20.33 Cumulative degradation and aggradation volumes in the main stem for Runs No. 3 and 13 (effectiveness of channel modification).

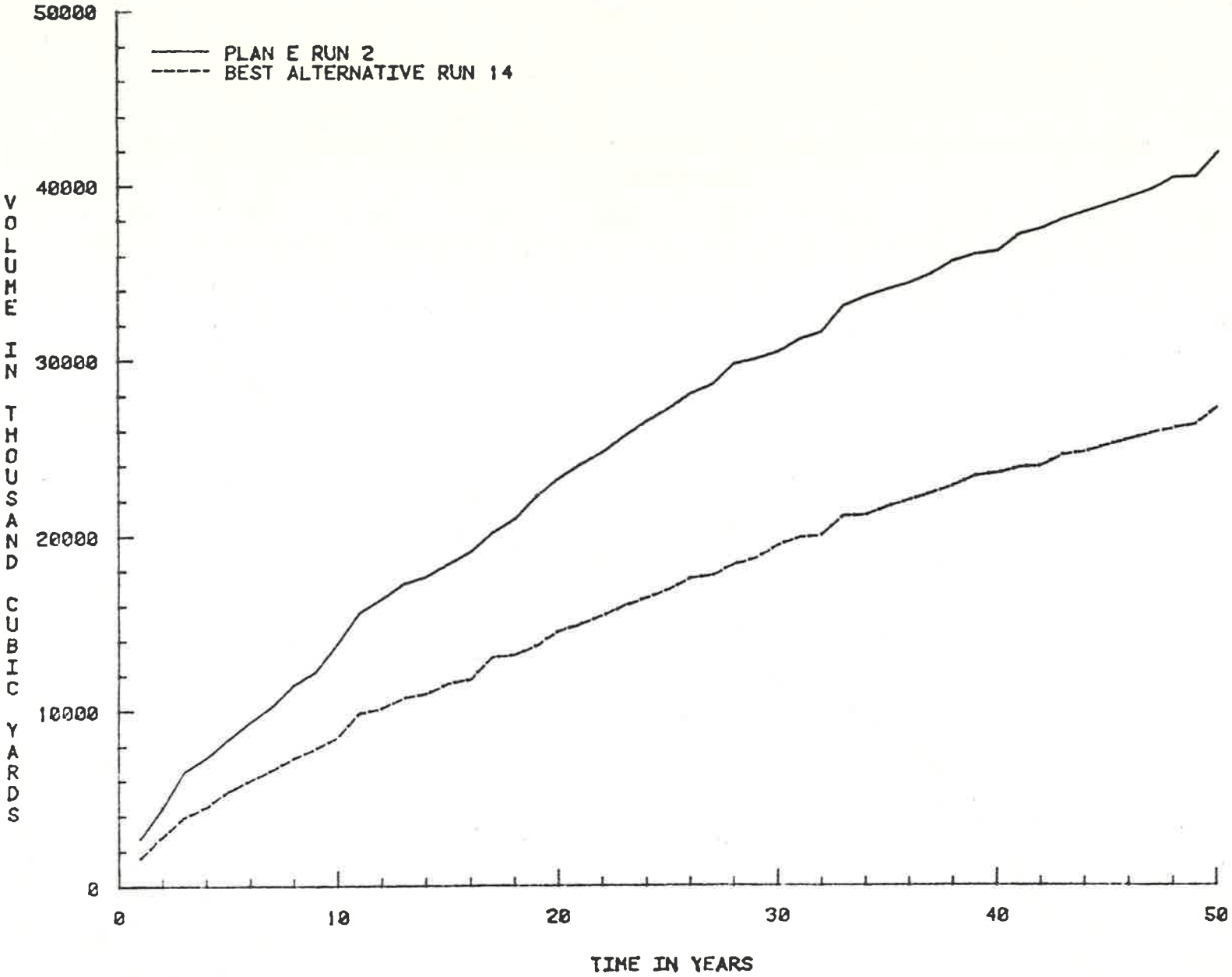

Figure 20.34 Cumulative degradation and aggradation volumes in the main stem for Plan E and the best alternative (Runs 2 and 14).

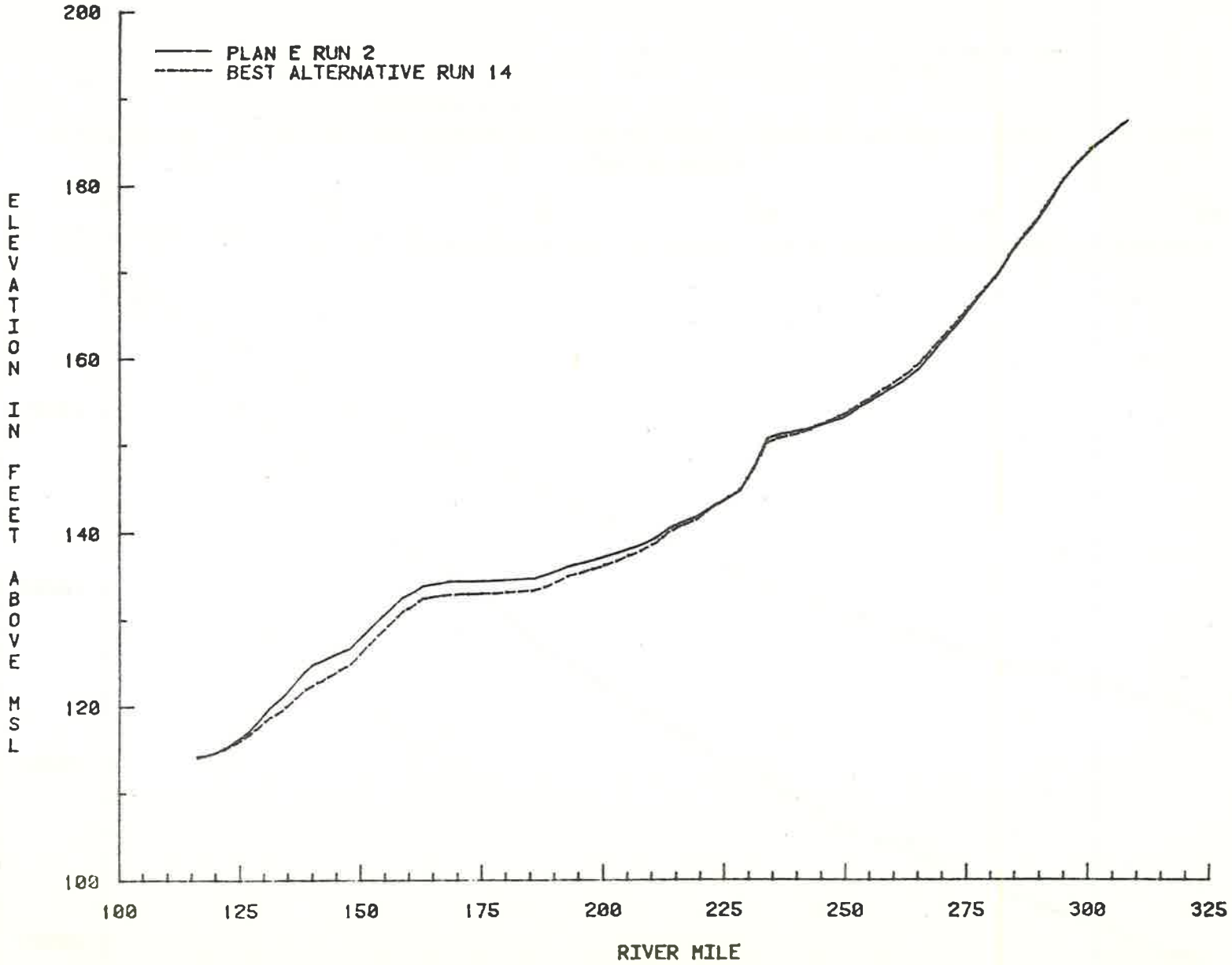

Figure 20.35 Maximum water surface elevations for Plan E and the best alternative (Runs No. 2 and 14).

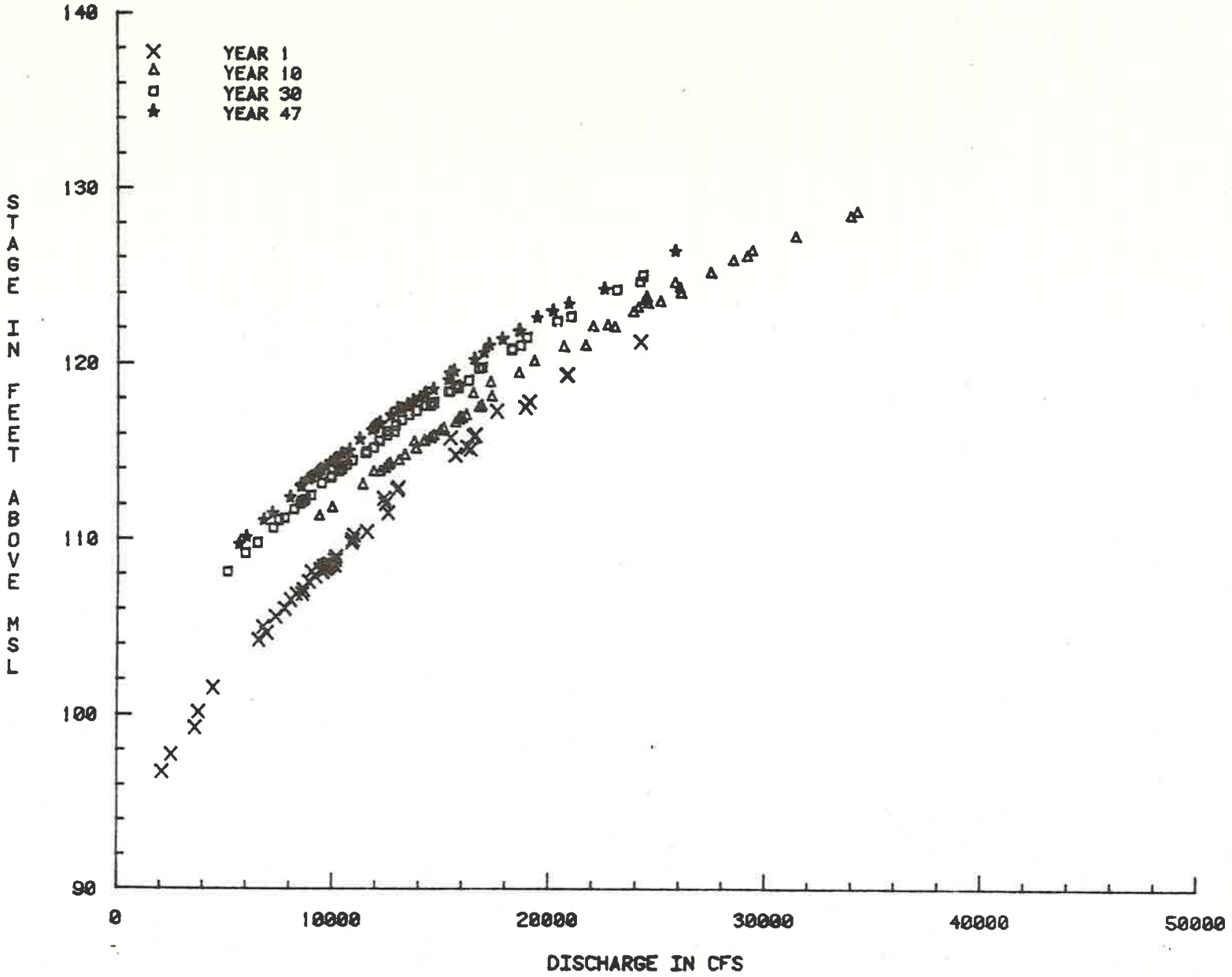

Figure 20.36 Stage discharge relationship at Greenwood Bendway (river mile 162.5) for the best alternative.

at the mouth of the Big Sunflower), and the channel has a 200-foot bottom width from Vicksburg to Greenwood. The sediment filling rate in the lower reach is 78 percent larger than that without development of a navigable channel. In addition, this development would increase the quantity of deposition in the upper main stem reach. The cumulative degradation and aggradation volumes in the lower reach (River Segment No. 1) for both Plan E and navigation conditions are presented in Figure 20.37. This figure shows that the impact of the navigation channel on the lower reach is not too significant.

Figure 20.38 shows that minimum thalweg depths along the main stem from the mouth of the Big Sunflower to Greenwood for the 50-year simulation are generally larger than nine feet except in the Greenwood Bendway and downstream of Abiaca Creek. Therefore, the proposed nine-foot navigation channel with a lock and dam near Vicksburg is a feasible development alternative if the Plan E channel is maintained, particularly in the reach between Belzoni and Greenwood. However, a more detailed analysis is needed for designing, implementing, and maintaining the nine-foot navigation channel.

20.5 SUMMARY

In summary, the proposed Plan E would slightly increase the peak discharge, generally reduce the flood stages if the channel is maintained, and significantly increase the amount of deposition in the main stem. The proposed Plan E can provide adequate flood protection for the upper headwater areas if the Plan E channel is maintained by the reduction of sediment inflows from major contributing tributaries and/or providing maintenance dredging about every five years. Furthermore, the necessity of maintenance dredging is more critical below Money.

Results of the analysis in this study are primarily based on the known discharge model. For the main stem, the estimated rate of net filling (considering degradation and aggradation) is about 210,000 cubic yards per year under the natural condition. The rate of net filling with Plan E conditions increased deposition 400 percent, or the net filling rate in the main stem is about 840,400 cubic yards per year. If all peak flows are increased 15 percent on the tributaries and main stem (effect of channelization), the rate of net filling in the main stem

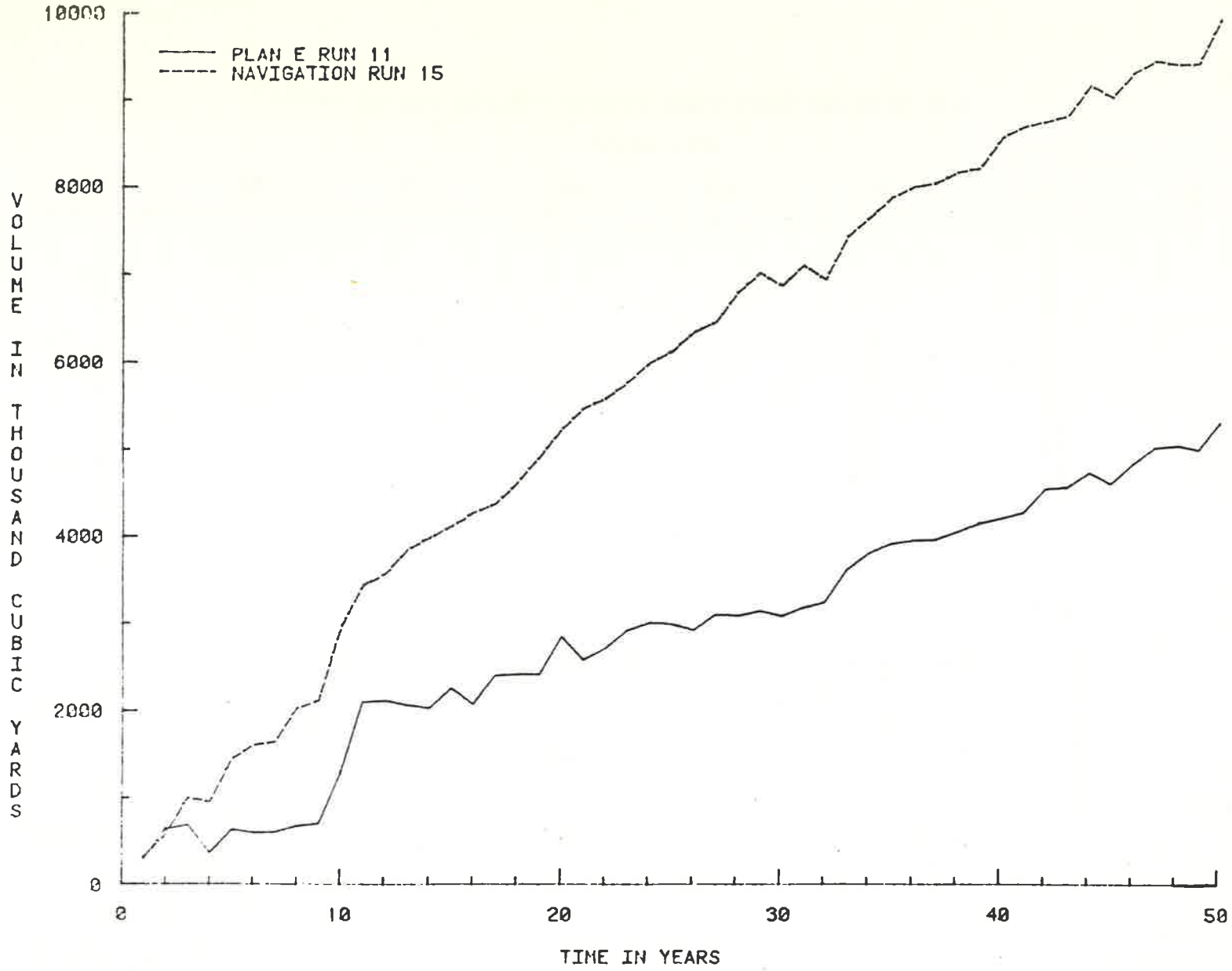

Figure 20.37 Cumulative degradation and aggradation volumes in the lower reach for both Plan E and navigation channels (Runs No. 11 and 15).

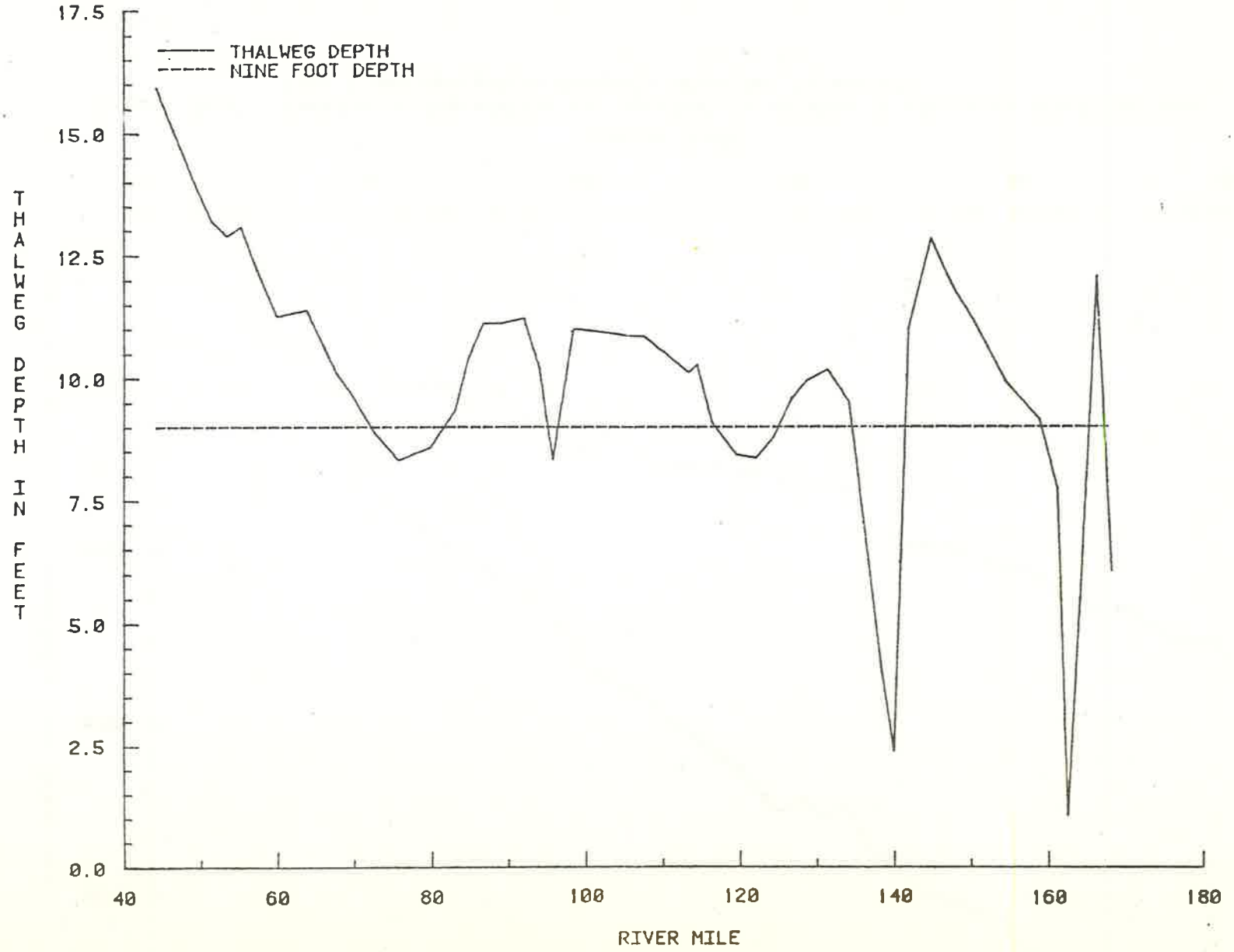

Figure 20.38 Minimum thalweg depth along the main stem.